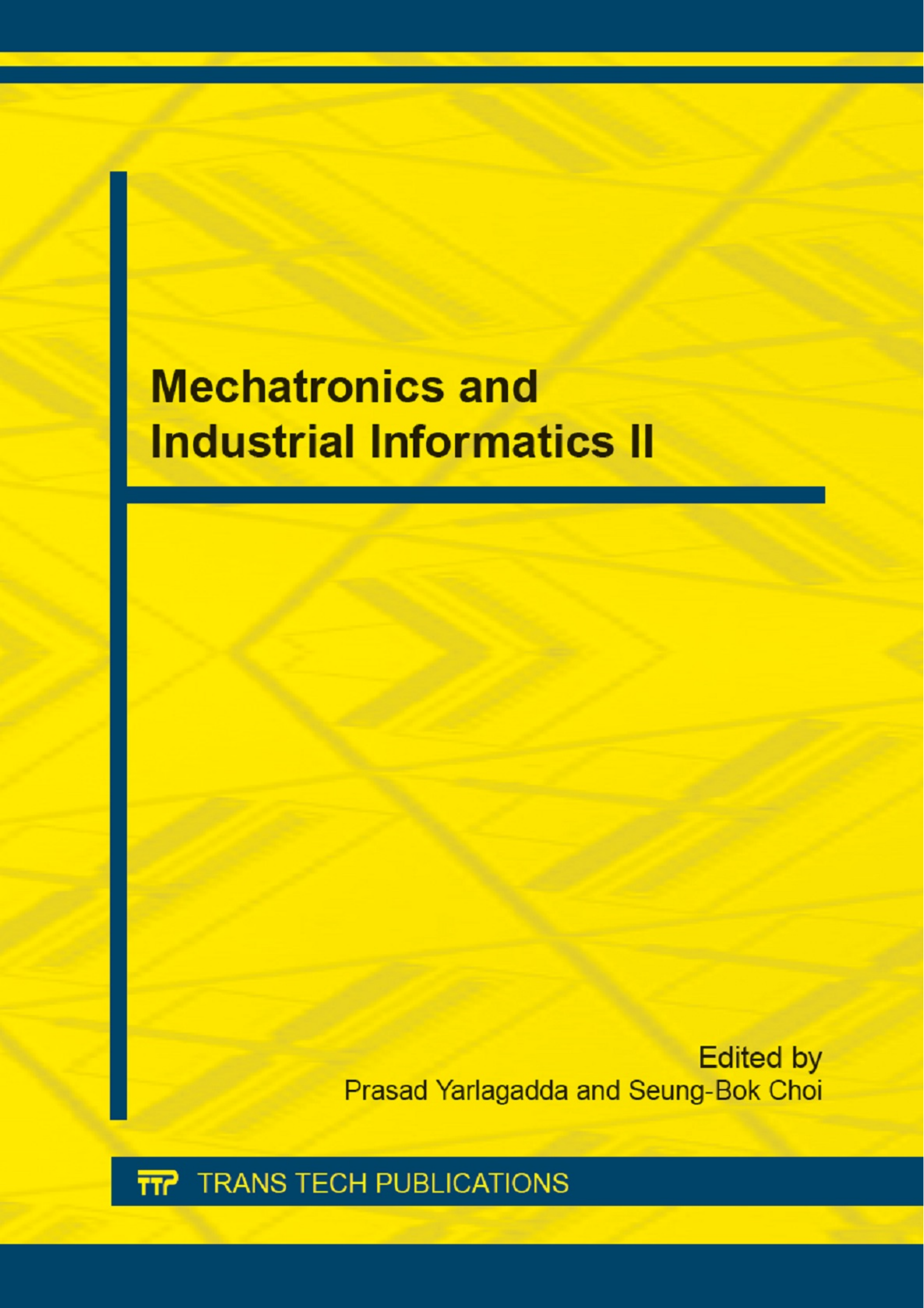

Mechatronics and Industrial Informatics II

Edited by
Prasad Yarlagadda and Seung-Bok Choi

TTP TRANS TECH PUBLICATIONS

VISIT…

LANZAROTE
Caliente.COM

Mechatronics and Industrial Informatics II

Edited by
Prasad Yarlagadda
Seung-Bok Choi

Mechatronics and Industrial Informatics II

Selected, peer reviewed papers from the
2014 2nd International Conference on
Mechatronics and Industrial Informatics
(ICMII 2014),
May 30-31, 2014, Guangzhou, China

Edited by

Prasad Yarlagadda and Seung-Bok Choi

Copyright © 2014 Trans Tech Publications Ltd, Switzerland

All rights reserved. No part of the contents of this publication may be reproduced or transmitted in any form or by any means without the written permission of the publisher.

Trans Tech Publications Ltd
Churerstrasse 20
CH-8808 Pfaffikon
Switzerland
http://www.ttp.net

Volume 596 of
Applied Mechanics and Materials
ISSN print 1660-9336
ISSN cd 1660-9336
ISSN web 1662-7482

Full text available online at *http://www.scientific.net*

***Distributed** worldwide by*

Trans Tech Publications Ltd
Churerstrasse 20
CH-8808 Pfaffikon
Switzerland

Fax: +41 (44) 922 10 33
e-mail: sales@ttp.net

and in the Americas by

Trans Tech Publications Inc.
PO Box 699, May Street
Enfield, NH 03748
USA

Phone: +1 (603) 632-7377
Fax: +1 (603) 632-5611
e-mail: sales-usa@ttp.net

Preface

This volume records the accepted papers of 2014 2nd International Conference on Mechatronics and Industrial Informatics (ICMII 2014) which took place in Guangzhou, China between 30-31 March, 2014. This conference brought together leading researchers and scientists in the domain of mechatronics and industrial informatics from across the nation. The experience of various researchers was intended to be brought to an audience comprising of young researchers, so that they get to know the state of the art in the field.

We are grateful to the program committee members and the external reviewers for their hard work and expertise in selecting the program. Our special thanks go to many people worked together in organizing ICMII 2014 and ensuring its success. We hope that they found their involvement just as interesting and fun as we did.

The Committee of ICMII 2014

2014 2nd International Conference on
Mechatronics and Industrial Informatics
(ICMII 2014)

Conference Organization

Co-Chairmen

Prof. Seung-Bok Choi, Inha University

Prof. Yun-Hae Kim, Korea Maritime University, Korea

Prof. Prasad Yarlagadda, Queensland University of Technology, Australia

Technical and Organizing Committee

Prof. Yi-Sheng Huang, National Ilan University, Taiwan

Prof. Chen-Chien Hsu, National Taiwan Normal University, Taiwan

Prof. Zhong Wende, Nanyang Technological University, Singapore

Prof. Jiankun Hu, University of South Wales, Australia

Prof. Yong Guan, Iowa State University, USA

Prof. Yao-Wen Chang, National Taiwan University, Taiwan

Prof. Wenjun Meng, Taiyuan University of Sci. and Tech., China

Prof. Haoran Geng, University of Jinan, China

Prof. Nabil Gindy, University of Nottingham, UK

Prof. Toshio Haga, Osaka Institute of Technology, Japan

Prof. Jong Kook Lee, Chosun University, Korea

Prof. Yong-Lin Kuo, National Taiwan Univ. of Sci. and Tech., Taiwan

Prof. Mao-Hsiung Chiang, National Taiwan University, Taiwan

Prof. Qiang Wang, Jinan University, China

Prof. Sihai Jiao, Research Institute, Baosteel, China

Prof. Xiaoping Zhou, Hubei University Of Technology, China

Prof. Jian Gao, Guangdong University of Technology, China

Prof. Xiaobo Zhou, University of Colorado at Colorado Springs, USA

Prof. Yun-Hae Kim, Korea Maritime University, Korea

Prof. Carlos Caceres, The University of Queensland, Australia

Prof. Shahrum Abdullah, University Kebangsaan Malaysia

Dr. Xiangping Bu, Wayne State University, USA

Prof. Sagar Kamarthi, Northeastern University, USA

Prof. Heinz-Gunter, Brokmeier, Technische Universitat Clausthal

Prof. Zhengyi Jiang, University of Wollongong, AU

Prof. Niels Bay, University of Denmark, Denmark

Prof. Viktor P. Astakhov,General Motor Business Unit of PSMi

Prof. Cesar de Sa, Jose, University of Porto, Portugal

Prof. Phil Koshy, Mcmaster University, Hamilton,Ontario, Canada

Prof. Kambakar P Rajurka University of Nebraska-Lincoln, USA

Prof. Kaiming Wu, Wuhan University of Science and Technology, China

Prof. Shaohui Yin, Hunan University, China

Prof. Jinglong Bu, Hebei United University, China

Prof. Wenlei Sun, Xinjiang University, China

Prof. Jun Wang, Northeastern University, China

Prof. Jeng-Haur Horng, National Formosa University, Taiwan

Prof. Jiwei Cai, Hebei United University, China

Prof. Wu-Shiung Feng, Chang Gung University, Taiwan

Prof. Keon Myung Lee, Chungbuk National University, Korea

Table of Contents

Preface and Conference Organization

Chapter 1: Applied Mechanics, Mechanisms and Dynamics

Experimental Study on the Transverse Stiffness of WJ-8 Rail Fastening
C. Liu, Z.P. Zeng, B. Wu, J.Y. Yuan and X.F. He 3

Research on Modeling and Characteristics of Two-Stage Pressure Hydro-Pneumatic Spring
Z.X. Li, Z.L. Ma, H. Jiang and X. Xu 7

Study on the Mechanism of Detecting Flaws in the Transmission Tower Foundation by the Finite Element Method
X.M. Shi, Q. Gao, J.J. Liu, J.G. Zhang, D.B. Cheng and N.L. Zhang 12

Study on Torsion-Eliminating Performance of Laterally Interconnected Air Suspension
Z.X. Li, L.Y. Ju, H. Jiang and X. Xu 17

SVR Based Modeling Method to Structures Finite Element Uncertainty Propagation Analysis
Y. Zhu and S.H. Zhu 22

Hopf Bifurcation Analysis of Digital Hydraulic Cylinder
J. Chen, J.F. Xing and B.J. Lv 27

Simulation on Kinetic Characteristics of Moving Mooring Marine Current Turbine System
Y.Y. Tian, J. Yu, S.C. Sun and X.T. Li 32

Chapter 2: Materials Processing and Advanced Manufacturing Technology

Situation of Natural Gas Hydrate Research
Z. Li, M.H. Kun, Z.L. Ming and Z.S. Yang 39

Study on the Stainless Steel 1Cr18Ni9Ti Micro-Hole Drilling Experiment
B.H. Li, Z. Liu, H. Wang and Z.S. Zhong 43

The Influence of Electric Parameters on the Surface Quality of Ceramic in Internal Grinding Using the Ultrasonic and ELID Composite Grinding
Y.Y. Zheng, H. Pang, Q. You and X.F. Jia 47

Equipment Modification for Friction Stir Joining Based on PLC
L. Ji 52

Research on Galvanized Layer Uniformity Detecting Technology of Transmission Angle Steel Tower Materials
J.Y. Jiang 56

The Improved Design of Embedded CNC Milling Machine
H.Y. Zhang and Y.F. Shu 60

Chapter 3: Product Design, Manufacturing and Industrial Informatics Applications

Simulation Research on the Magnetic Field of the Positioning Permanent Magnet for MEMS inside Human Body Based on Ansoft
X.Q. Liu and Y.H. Li 67

The Design and Calculation of Fur Material Cleaning Machine
Y. Su, Z.F. Li and S.Q. Huang 72

The Semi-Automatic Restoration of Regular Paper Fragments
Z.Q. Ding 79

Development of Computer-Aided Manufacturing System for a Jewelry-Making CNC Machine
Y. Miao, K. He, H.T. Fang, Z.M. Zhou and R.X. Du 83

Analysis of the Ceramic Pattern Modelling Based on Primitives
J.F. Hu and B.S. Li 90

Research and Application of Adaptive Technology in Equipment Installation
B. Luo and L. Ye 94

The Design and Manufacture of the Wireless Power Transmission System in the Cardiac Pacemaker
X.Q. Liu, Y.H. Li, L. Min and H. Ping 100

Regarding Calculation of Cross Section of Elevator Conductor and Rated Capacity of Switch
G.M. Huang 104

Design of Mine Ventilator Fault Diagnosis System
B.T. Zhao, X.F. Jia and Y. He 110

Nonlinear Econometric Model of Electronic Products and its Application
H.Y. Zhou 114

Study on the Transformation of Military Logistical of Internet of Things Era
Y. Lu, C. Xie and L. Shang 119

The Research on Cloud Mobile Office System Development for Enterprise Application
F. Wu, Z.M. Wang, G. Yao and Z.M. Miao 123

An Execution Framework for Domain-Oriented QoS Evaluation of Manufacturing Cloud Services
H. Jin, X.F. Yao and J. Zhang 127

Using Verification Planner to Track the Verification Process
X. Huang, D. Jun, L.T. Liu and L.C. Liu 131

Comprehensive Evaluation of the Development Level of Shanxi's Real Estate Industry Based on Factor Analysis and Cluster Analysis
X.L. Tang and Z.L. Tan 136

Research of Refined Oil Emergency Reserve Monitoring System Construction Scheme
N. Chen, Q.M. Zhang and D.D. Tang 141

Chapter 4: Computer Information Processing Technology, Artificial Intelligence and Intelligent Algorithms

An Algorithm for Representing Planar Curves in B-Splines
Z.Z. Lin and S.H. Shu 149

Dynamic Pricing and Inventory Temperature Decisions for Fresh Foods with Variable Demands
L. Tang 154

Forecasting High Frequency Data: An ARMA-Soft RBF Network Model for Time Series
D. Marcek 160

Fuzzy Comprehensive Assessment of Air Material Suppliers
Z. Lv 164

Mixed NMF Blind Source Separation Algorithm
Z.J. Zhao and Z.J. Liu 169

Natural Gas Consumption Forecasting Based on Combinatorial Optimization Model
J.Q. Wang, L. Chen, L. Li and Y.X. Wang 174

Rough Match Function Based on Topological Structure
Y.L. Zheng 179

The Effect of Empathic Technology on Artificial Intelligence
J.G. Liu and Q. Li 183

Research of Smart Home System Based on Handheld Device
B. Li, H.Y. Dai and H.F. Cheng 188

A Self-Adaptive Harmony Search Algorithm for Unconstrained Optimization Problems
P. Zhang, P. Sun, Y.N. Zhang and G.J. Li 192

Ceph CRUSH Data Distribution Algorithms
X.Y. Liang and Z.C. Guan 196

Forecasting Consumer Confidence Index Based on Radial Basis Function Neural Network
H.Y. Xie, G.Y. Chen, Z. He and D.P. Zhao 200

Performance Comparison of Energy-Aware Task Scheduling with GA and CRO Algorithms in Cloud Environment
L. Wu, Y.J. Wang and C.K. Yan 204

Rapidly Analyze the Fault Tree with Numerical Methods
B. Wu, Z.H. Zhao and Y.H. Ren 209

Research of Differential Evolution Algorithm for Motor Control
Z.F. Wu 216

An Improved RFID Tag Collision Algorithm
T.B. Ran and X.S. Wu 222

Targets Detection Based on Multifractal Method
F. Liu 226

Hybrid Intelligent Optimization Approach for RFID Network Planning
D.L. Guo, Q. Xiang and Z.H. Li 230

Optimization of Multitask in Real-Time Control Based on Artificial Bee Colony Algorithm
S.M. Chen, Y.T. Xu, Q.X. Hu and Z.T. Wang 234

Research for Wind Power System Reactive Power Optimization Based on Improved Artificial Fish Swarm Algorithm
S.H. Zhang 241

The Prediction of Grounding Grid Corrosion Rate Using Optimized RBF Network
C.F. Song, Y.B. Hou and J.Y. Du 245

Research on Multi-Agent Formation's Obstacle Avoidance Problem Based on Three-Dimensional Vectorial Artificial Potential Field Method
J.Y. Dai, L.F. Yin, C. Peng, B.J. Yang and C.S. Wang 251

A Evaluation Model for Valid Prediction of Cabs' Number Change from Urban Cabs Trajectories
W.B. Ma, S. Deng and H.B. Huang 259

A Method of Building Chinese Sentiment Lexicon Based on Semantics
J.N. Yang, A.M. Yang and Y.M. Zhou 263

A Model of Predicting Corrosion Rate for Substation Grounding Grid Based on the Similarity and Support Vector Regression
J.Y. Du, J. Han, Y.J. Zhao and W.H. Liu 271

Efficient Graph Component Labeling on Hybrid CPU and GPU Platforms
X.H. Pan 276

Evaluation Research on Agricultural Informatization Level in Tropical Areas of China Based on Entropy Method
L. Ye, Y.P. Li, X.L. Qin, Y.Q. Liu, W.H. Liang and Q.D. Song 280

The Generalized Fuzzy Time Series Model for Forecasting Base on the Optimization of the Length of Intervals
Y.H. Wang and W.R. Qiu 286

Web Page Ranking Algorithm Based on the Meta-Information
X.L. Li 292

E-Bayes Estimation of Burr Distribution Parameter under Square Loss Function
H.B. Liu, T. Yin and C. Wang 297

E-Bayes Estimation of Laplace Distribution Parameter under Q-Symmetric Entropy Loss Function
H.B. Liu, T. Yin and C. Wang 301

E-Bayes Estimation of Rayleigh Distribution Parameter
H.B. Liu, T. Yin and C. Wang 305

Chapter 5: Sound, Image, Signal and Video Processing and Technologies

2D(PC)2A Based Dimensionality Reduction of Textural Feature for Face Recognition with a Single Training Sample
W.H. Sun 311

A Local Optical Flow Constraint Target Extracting Algorithm of Kalman Filter Based on Background Modeling
Y.N. Wang 316

A Novel HOG Descriptor with Spatial Multi-Scale Feature for FER
Y. Tong, L.B. Jiao and X.H. Cao 322

An Animation Video Resource Conversion System Based on Supercomputers
K.H. Zhong, Y.W. Chen, L.F. Liu and J. Zhang 328

An Image De-Noising Algorithm Based on K-SVD and BM3D
L. Jun 333

An Image Retrieval Algorithm Based on Region Segmentation
X.M. Xiong and Y.L. Liu 337

Combined Filter Method Based on Terrain Factors
M. Yan and Y.Q. Liang 342

Design and Implementation of Safety Lock Based on Face Recognition
C.X. Qi, L. Zhao and Q.L. Dong 346

Image Quality Assessment Based on Region of Interest
Y. Wang, Z.G. Lin and Z.C. Liao 350

Lane Mark Identifying and Tracking Base on Edge Enhancement
Y.Y. Xing, B. Yu and F.Q. Yang 355

Mathematical Morphology Based Moving Object Detection Algorithm under Complicated Background
J. Zhou 361

Removing the Stripe Noises Interference on the Hα Full-Disk Solar Image Based on Multiscale Transform
S. He, S. Zheng and Y. Huang 365

Research on Scene Organize Algorithm Based on BVH with Dynamic Rendering Tree
L. Xu and M.Z. Liu 370

Study of Video Object Detection and Shadow Suppression Algorithms
Q.L. Gai and G.Q. Wang 374

Video Time-Space Body Filtering Based on Dual-Directional Markov Chain Monte Carlo Particle Filter
J.B. Song, L. Ye and Q. Zhang 379

Voice Assistant — Application of Speech Recognition Technology in the Android System
G. Liu and H.B. Zhang 384

A Content Based Image Retrieval Model Using Feature Space Dividing
G. Huang 388

A Statistical Model for Real-Time Video Moving Target Detection Based on Bayesian Statistics
Z.H. Zhang, S.L. Zhang, B. Yang and X. Bai 394

An Improved Moving Object Tracking Method Based on Graph Cuts
M.J. Zhang and B.S. Kang 398

Compact Wake-Up Word Speech Recognition on Embedded Platforms
A.H. Xing, T. Li, J.L. Pan and Y.H. Yan 402

Research on Lossless Predictive Coding Methods for Stereo Images
S.G. Li 406

Research on the Transmission Characteristics of FitzHugh-Nagumo Neuron
G.P. Wang, W.X. Yang and S. Yang 413

Classified Quantization Research on Dot Gain Characteristic
Q. Wang, Q. Wang, X.L. Qiu and T.M. Wang 417

A Recognition Method of License Plate Number Based on BP Neural Network
B.X. Liu, Y.H. Huang, X.D. Wu and Y.X. Li 422

Based on Fractional Brownian Motion and Fourier Descriptors of the Side Face Recognition Algorithm
H. Wu, G.X. Tang, T. Han and B.H. Jie 427

Pitch Detection Method Based on Morphological Filtering
Y.Q. Wang, X.P. Wang and L.C. Wang 433

Rolling Bearing Fault Diagnosis with EMD-Based Fault Characteristic Frequency Difference Analysis
Y.P. Guo, Y. Xiong and G.C. Song 437

LED-Based 3-DMD Volumetric 3D Display
C.L. Jing, Q.B. Feng, Y.S. Zhang, G.L. Yang, Z.G. Song, Z.Q. Pei and G.Q. Lv 442

Chapter 6: Measurement Technology, Instruments and Sensors, Detection Technologies

An Improved Gaussian Fitting Method Used in Light-Trap Center Acquiring
Z.Y. Xu, H.Y. Zheng and H.Y. Yang 449

Computer Vision Application and Research on the One-Dimensional Body Mass Precision Measuring Device
S.Y. Nie and C.Q. Yang 453

Hydrocarbon Micro-Seepage Anomalies Detection Algorithm Based on FPCS for Hyperspectral Remote Sensing Data
Z.L. He, X.L. Deng and S.M. Ai 457

Landing Point Predicting Method in Target Re-Entry Measurement
X.Y. Li, W.K. Zhu, J.B. Zhou, G.M. Chen, L. Yang and H.H. Wu 463

Study of Velocity Measurement Error Analysis and Improving Velocity Measurement Accuracy on High-Speed Train
T. Hou, D.W. Fan and H.X. Niu 468

Study on Architecture of Measurement of Multi-Points Strain of Hinge Sleeve of Cubic Press under Super-High Pressure
X. Sun, J.X. Shi, Z.X. Zhong and H. Zhao 472

Continuous Blood Pressure Measurement Method Based on the Pulse Image Sensor and BP Neural Network
A.H. Zhang, X.Z. Zhou, L.M. Yang, R. Shen and Z. Wei 476

Measuring Device for the Moment of Human Aspects
H.C. Zeng and C.Q. Yang 480

Change Detection in SAR Images Based on Semi-Supervised Learning
S. Tian, J.S. Song, S.B. Tian and W. Gong 484

Road Roughness Measurement and Analysis for Vehicle Bench Test
J.W. Yu, N. Liu and B. Wang 490

An Improved of Extended Kalman Filtering Method on Tracking Accuracy of Bistatic Sonar System
Y. Sun and J.W. Zhao 494

Application of Mobile Data Acquisition Technology in Highway Lightning Protection
Y.H. Zhang, X. Jiao, Y.Y. Zhong, J.C. Zhou and J. Yuan 498

The Detection of Concealed Targets Based on NQR of Nitrogen-14
X.Y. Huang, G.G. Xu and F.L. Hao 505

Anti-Bias Association Algorithm for AIS and Radar Tracks Based on Centroid Reference Topological Characteristics
L. Qi, H.P. Wang, Y. Liu and C. Wang 511

Trusted Data Aggregation with Low Energy in Wireless Sensor Networks
T.D. Engouang, Y. Liu and Z.J. Zhang 519

The Research on Sensor Fault Diagnosis Based on the SVM Prediction Model
Y.J. Zhu, X.M. Yu and B.H. Yang 528

Review of MEMS Techniques and Applications in Aerodynamics Research
L.T. Fan 532

Design and Applications of Embedded System in Video Surveillance
Z.C. Yan and P.X. Fen 536

Analysis and Design of a Capacitive Sensor for Measuring Thickness
J.H. Lei 540

Chapter 7: Automation Technology, Control System Modeling and Simulation Technology

Application of the Flexible Brake on Wind Driven Generator
H.F. Zhou and Q. Li 547

Fast Finite-Time Consensus Tracking of First-Order Multi-Agent Systems with a Virtual Leader
Q.Y. Xiao, Z.H. Wu and L. Peng 552

Global Robust Output Regulation of a Class of Nonlinear Systems with Nonlinear Exosystems and its Application
S.M. Liu, Y. Jiang and J.Y. Dai 560

Research on Attenuating Variable-Rate Reaching Sliding Mode Control Strategy for Three-Phase Current Source Inverter
J. Bai, S.Q. Lu, X. Dong and J. Liu 565

Research on Spacecraft Attitude Control Simulation Technology Based on Multidisciplinary Integration
Y.B. Zhang, C.F. Wei, X.Q. Li and X.L. Shi 572

The Facilities Vegetables Warning and Control System Based on Mobile Phone SMS
L. Yan, D.J. Hao and H. Zhang 576

The Research of Furnace Temperature Control Technology Based on Model Free Adaptive Control System
J. Chen and X. Han 580

The Sliding Mode Variable Structure Control Method for Brushless DC Motors
X.J. Yin and J.G. Xu 584

Time Domain Simulation for a 6 DOF Tanker Model in Presence of Waves
Q.M. Sun and J.G. Chen 590

The Approach for Analyzing Motion Mode of High-Order Control Systems
S.G. Zhang, K. Wang and X.P. Dang 594

The Design of Valve Block of Megawatt Wind Turbine Hydraulic Yaw System and AMESim Simulation Model
J. Gao, L.W. Yan, C.J. Ai and H. Xie 598

Modeling for the Flow Coupled Secondary Hydraulic Lifting System of the Excavator Bucket
F.Y. Zang, Y. Wang and X.Z. Kong 602

3D Geometric Modeling of Francis Turbine Blades Based on Wooden Patterns and UG Software
L. Lu and L.D. Zhang 606

Power Spectra Density Replication Control Strategy for 2-Axis Hydraulic Shaker Based on HV Estimator
Y. Chen, Q.L. Luan, Z.W. Chen and H.N. He 610

Numerical Simulation of Seismic Wave Propagation in Different Media
Z.R. Feng 616

Design of Salt In-Bags Incasing Control Management System Based on Dual Closed-Loop Fuzzy Controller
Y.B. Hui, Y.G. Wang, L. Wang and Q.F. Niu 620

New Control Topology for Railway Static Power Conditioner
Y. Pan and J. Bao 625

Triangle Formation Control of Multi-AUVs with Communication Constraints
G.N. Li, H.Y. Dong and H.L. Xu 631

The Integrated Automation Solutions Research of Zhengzhou North Station
Z. Chang, H.P. Zhu and X.C. Zhang 636

Motion Simulation and Finite Element Analysis of the Manipulator Based on SolidWorks
P. Lu, D.L. Cheng, G. Shi, Z.H. Zhou and N.K. Li 640

Chapter 8: Power Engineering and Control, Power Electronics

Dynamic Economic Dispatch Based on Improved Particle Swarm Optimization
Y.G. Li and L. Han 649

Electric Power Communication Network Optimization Algorithm Based on the Equivalent Network
N.Z. Xing, J.Q. Guo and R. Yu 653

Fault Location Scheme for Transmission Lines Using Kaiser Self-Convolution Windowed FFT Phase Comparison
G.C. Fan, Y.L. Zhu, H.W. Yan and Y.F. Gao 659

Optimal Assignment of Emergency Power Considering V2G
X.Y. An, J.C. Liu, Y.X. Wu, J.Y. Li, L.Z. Zhang, C. He, H.H. Chen and X.L. Zheng 664

Optimal Reserve Distribution Model for Power System with Large Scale Wind Power Integration
C. He, J.C. Liu, J.Y. Li, Y.X. Wu, X. Li, X.Y. An, H.H. Chen and X.L. Zheng 669

Realization of FCB Function in 350MW Subcritical Units with 35% Capacity Bypass
L. Wang, G. Li, C.Y. Zhang, L. Zhang and D.Z. Bi 674

Research on Microgrid System in the DC-Building
Y.N. Yuan and M. Meng 678

Suggestions on Implementing Energy-Saving Diagnosis Technologies and Services of Power Grid Enterprises
Y.H. Li, L.F. Cheng, L. Xi, G.H. Xu and T. Yu 682

Unbalanced Power Allocation Method to the Research of the Influence of the Power System Trend
H. Wang, N. Wang and D.H. Xue 687

User-Defined Governor Model Based on PSCAD and Analysis of Low Frequency Oscillation Mechanism
S.W. Xiao and C. Wang 692

Methods to Establish the Fault Tree of Substation Automation System Based on HAZOP
B.B. Han, Y. Wang and F.Y. Guo 696

Research for Short-Term Load Forecasting Based on Linearization Meteorological Factors
S.H. Zhang 700

A Transducer Matching Method with Signal Frequency and Inductor Adjustment Combined for Submerged Structure Ultrasonic Cleaning
Y.Z. Yin, C.P. Zhu, B. Wang, Q. Wu, C. Yao, B.Y. Chen, Q.G. Ren, Q.B. Han, Y.B. Tang, Z.B. He, G.C. Chen and Z.X. Li 704

Design of Active Filter Based on the Active Power Balance
L. Ji 709

Identification of Lightning Strike and Short-Circuit Fault Based on Wavelet Energy Spectrum and Transient Waveform Characteristics
Y.F. Gao, Y.L. Zhu, H.Y. Yan and H.W. Yan 713

Application Research on the Intellectual Inspection System of Transmission Line Based on the "Mobile Information Platform"
Z.W. Yang, W. Yi and Y. Jin 719

Design and Simulation Analysis of the Mirror Current Source Circuit Based on Multisim10
H. Wang, W. Yang, B.H. Li, X.C. Liu and Q.P. He 723

Chapter 9: Vehicle Control Systems and Intelligent Traffic

Performance Analysis of Simulation of Pedestrian Traffic inside the Hub
B. Li and M. Li 729

Design of Intelligent Public Transportation Vehicle Terminal Based on S5PV210
H.P. Sun, Z.G. Gao and L.N. Chen 735

Research Based on Fuzzy Control of Electric Power Steering System
Y.L. Cao and Z.B. Yang 739

Research on Traffic Behaviors and Psychological Characteristics of Pedestrians within the Comprehensive Hub
B. Li and M. Li 743

Apply the Damaged Road Data for Driving Simulator
A.L.M.J. Yiming and R.Z.W. Maimaiti 747

Modeling and Design of Fuzzy-Neural Network Controller of Electric Power Steering System
G.Q. Geng 751

Simulation Study for Mixing Characteristics of NH3 and Automobile Exhaust in the SSCR System
D.W. Qu, K. Zhang, L.Y. Fan and H.B. Gao 755

Coordinated Charging of EVs Based on Demand-Side Management
Y.K. Li, H. Ouyang, J.K. Zhao, X.K. Rong and Y. Dong 760

A New State Machine Optimization Method in the Protocol Conversion System
Q. Li 766

Chapter 10: Communications Technology and Materials

Design and Implementation of USB Coordinator Based on Z-Stack
Z.C. Jiang, S.D. Lee, J.Y. Chen, Z.J. Qin and R.F. Yu 773

Design of Intelligent Underground Sound Bird Repellent System Based on Wireless Communication Network
X.J. Yin, J. Lin and Z.Z. Shao 782

Loss Characteristics Analysis and Optimization of an Off-Axis Rotary Optical Fiber Communication System
X.H. Wang, Q. Zhao, L. Li, J. Ding, Q.X. Zheng and L. Liu 788

Simulation on PAPR Suppression Algorithm for Multicarrier System
R. Zhang and Z.B. Zeng 794

Theory Analysis and Simulation of Optical 90° Hybrid without Intersection
W.H. Liu and G.J. Wu 799

Two Analog Transmission Schemes for Distributed Detection
X.Y. Liu, P.S. Zhu and W. Liu 803

Mode Conversion Models Based on Spatial Spectral Matching for Mode Division Multiplexing in Optical Fibers
M.Y. Lan, S. Nie, L. Gao, S.Y. Cai, C.X. Ma, X.L. Qi and Z.C. Du 807

Reference Signals Design and Evaluation on Radio-Interface Based Synchronization of LTE Base Station System
R.H. Zeng, D.S. Miao, N.Z. Zheng and H.W. Yang 811

Electromagnetic Coupling Reduction in Microstrip Antenna Arrays Using Single-Negative Electric Waveguided Metamaterials
L.Z. Hu, G.M. Wang and G.C. Wu 816

Equivalent Electromagnetic Properties of Composite Media
X.F. Pang 822

Research on Coupler of Single Mode Fiber with Photonic Crystal Fiber
Q.S. Wei, Z. Chen, Y.H. Luo, Y. Ma, X.L. He and Z. Che 826

Chapter 11: Computer Network and Information Security

An Evolving GPSR Protocol in Urban Roundabout Scenario
H.Y. Yu, H.M. Yang, X.Q. Di and L.D. Qu 833

CNC Network of Research and Development
B.J. Zhang 838

Complex Network Evolution Model Based on Node Attraction
R. Sun 843

Fundamental Considerations on New Technology Evolution in Latest Network Development
Y.J. Luo 847

Intrusion Detection Systems
G.G. Liu 852

QoS Routing Protocol Based on Resource Optimization for Aerospace Networks
W.Q. Wu, B.N. Luo, P.P. Chen and Q.Y. Zhang 856

Research on Composite Web Services Selection Based on Dijkstra Algorithm
Y.Q. Li, Y.W. Li and L. Che 861

Rumor Propagation Model for Complex Network with Non-Uniform Propagation Rates
R. Sun and W.B. Luo 868

A New Method for High Speed CAN Protocol Conversion Circuit
Q. Li, Y.F. Liu, D.C. Luo and J.J. Yang 873

A NHPP-Based Reliability Model of Wireless Sensor Networks
B. Zhao, J.F. Yang, M. Zhao, Q. Li and Y. Liu 877

Implementation of USB in Embedded Systems Based on ARM Microprocessor
X.L. Li 883

The Network Security System Research Based on Intrusion Detection
J. Qian, Y.P. Wang and H.X. Li 888

The Design and Implementation of Fast-Path Architecture for IPv6 Control Router
G. Wang 892

Chapter 12: Database Systems and Software Development

A Pushlet System Optimization Method Based on Servlet
Y.L. Liu and X.M. Xiong 899

A Refinement of Hierarchical Databases
Q. Li, J.G. Liu and B. Wang 903

Design and Implementation of University Parking Query System
X.W. Zhang and B. Yu 909

SQL Server Access Methods Based on LabVIEW
Z.W. Zhu, J.X. Chen and Z.C. Sun 914

A Discussion on the Electromagnetic Compatibility of Data Center
X.E. Zhao 918

Design of a Mobile Client Application Based on Android Platform
C.X. Qi 923

Multi-Domain Modeling and Co-Simulation Based on Modelica and Simulink
G.S. Tian and L.C. Zhang 927

The Design and Implementation of a Cross Platform Multimedia NetWork Classroom
M.L. Shao 931

A Positioning System of Book Based on QR Code in Library
S.D. Lee, W.Q. Liu, W. Zeng, X. Gao and C.S. Zhang 936

Design and Implementation of a New CNG Dispenser Control Platform
X. Zhang, X.D. You, Q. Luo and X.J. Zou 944

Chapter 13: E-Commerce, E-Government, Internet Technologies, WEB Design

Applying Improved Clustering Algorithm into EC Environment Data Mining
Y.P. Ma, B. Ma and T.H. Jiang 951

Applying Modeling Technique Optimize Business for E-Government Based on Big Data
W.J. Luo, F. Yuan and X.D. Tian 960

Modeling Software Architecture Evolution for Electronic Commerce System Based on Graph Representation
H.W. Jiang and G.J. Kuang 966

Study on E-Government Virtual Information Service Center Model Based on Cloud Computing
D. Li and X.L. Liu 971

The Research of Digital Challenge to Tourism Destination Brand
W.Y. Zhang 976

IOT Application Research between Digital Publishing and Traditional Publishing
Z.W. Chen 981

uKeMa: An Ultra-Lightweight Key Management and Authentication Scheme for Wearable Ad Hoc Networks Based on Body Language
Y.H. Xie 986

Analysis on Development and Application of Online Customized Tour
X.J. Wang and X.K. Li 990

Advances in Online Authority Research
B. Wu and C.Y. Zhang 994

Interaction Representation and Application of Flash Animation in Webpage Design
S.S. Yang 998

Application and Thinking of “Jiangcheng Culture” Elements in Web Design
Z. Xin 1003

Chapter 14: Engineering Education and Engineering Management

Micro Lesson in Microera under the Background of Video Resources
L. Zhang and X.H. Wang 1009

Research and Implementation of Curriculum-Oriented Knowledge Learning Platform
J.W. Xue, S.H. Xu and Y.Y. Yu 1013

Second Time Development of Coal Quality Management System
B. Qian and H.Y. Zhang 1018

The Research on Construction of Open Hierarchical Practical Teaching System
Z.Y. Wang, L.G. Li and Y.G. Wang 1022

Application of Multimedia Technology in Experiment Teaching of Environmental Engineering Microbiology
S. Liu and L.N. Sun 1026

Optimal Model of Tutor Selection in Graduation Thesis Guidance for Undergraduate
C.J. Rao and Q.Q. Liu 1030

Research of Neuroergonomics Experimental Teaching System in Industrial Engineering
J. Wu and W.M. Han 1034

Research of the Model to Foster Engineering Students’ Ability and the Assistant Analyzing System
Y.Z. Fang, Z.F. Liu, D.F. Zhao and Z.F. You 1040

Study on Innovative Researching Project Management for the Computering Software-Based Enterprises
Q. Li 1044

Analysis of the Way to Enhance the Professional Core Competence of Engineering Students of New University
X.Q. Zhao 1048

Construct the Virtual Gram Stain Experiment Platform Based on 3DMax and VRP
S. Liu and L.N. Sun 1052

Supplier Selection Model of College Materials Procurement
C.J. Rao and L. Yu 1056

Research on the End-to-End Modularity Process for Manufacturing Enterprise
H.J. Wang, T.T. Zhao and H.F. Sun 1060

SWOT Analysis of Chinese Rural Information Society Policies
P. Zhou 1065

CHAPTER 1:

Applied Mechanics, Mechanisms and Dynamics

Applied Mechanics and Materials Vol. 596 (2014) pp 3-6
© (2014) Trans Tech Publications, Switzerland
doi:10.4028/www.scientific.net/AMM.596.3

Experimental study on the transverse stiffness of WJ-8 rail fastening

Can Liu[1,a], Zhiping Zeng[2,b*], Bin Wu[1], Jiayu Yuan[1] and Xianfeng He[1]

[1]School of Civil Engineering, Central South University, Changsha 410075, China

[2]National Engineering Laboratory for High-Speed Railway Construction, Changsha 410075, China

[a]liucan35@163.com; [b]996710155@ qq.com

Keywords: Lateral horizontal force; Lateral displacement; Transverse stiffness; Bolt torque

Abstract: The study of WJ-8 rail fastening is about the relationship between lateral horizontal force and rail's lateral displacement, and the rail fastening's transverse stiffness was obtained since the rail slipped. The rail lateral displacement was measured by using the loading device of rail's lateral horizontal force which was changed as needed. Moreover, when the lateral horizontal force changes, it was analyzed that how it affected rail's lateral displacement and rail fastening's transverse stiffness under different bolt torque conditions. Therefore, the recommended value of transverse stiffness is acquired which is based on analyzing the test results.

Introduction

With the speeding up of high speed railway, the interaction force between wheel and rail is growing, and it will generate lateral displacement. But excessive lateral displacement of the rail will make the rail gauge larger and change the track geometry, and then affecting the wheel-rail contacting state. As a result, it affects the safety and comfort of train[1]. So it is important to research the relationship between lateral displacement of rail and lateral horizontal force through specific tests.

Rail fastening is an important coupling part of track, and its role is to maintain the rail gauge, to impede the rail moving from sleepers, to prevent the rail overturning and to provide the necessary flexibility[2]. Rail fastening's lateral stiffness is an important parameters of rail. Through full-scale model test, the size of transverse stiffness is investigated under different sizes of bolt torque conditions. Moreover, the results are based on the analysis for lateral horizontal force affecting the lateral displacement of rail.

Test Methods

In previous studies, the relationship between lateral displacement of rail and lateral horizontal force is often analyzed by using finite element analysis software to build the track static model. However, the finite element mode is objective and idealized. There is deviation between the calculated results and the actual situation's results. For this reason, a indoor full-scale model tests is experimented on CRTS II slab track rail of the roadbed.

When the test starts. First, two segments(symmetrical) of rail are selected between two rail fastenings and the bolt torque of two rail fastenings is fixed to the required size by using rail torque wrench. Then, the measuring device of lateral displacement is placed in the middle of the two segments, and to be perpendicular to the rail. The ultra-thin hydraulic jack and force sensor are placed in a steel tank, and the face of ultra-thin hydraulic jack is close to the underside of force sensor. And then, the two connecting sticks are set into the sleeve. It should be noted that the inner end of connecting sticks must be close to the ultra-thin hydraulic jack or the force sensor, and the outer end of connecting sticks are connected with the linkers through fixing hole. At the same time, the outside of the linkers are closed to the inner face of rail. Then again, indicators are fixed by the steadies on the outside of rail. In addition, the probe of indicators must be perpendicular to the outer surface of rail. At last, The ultra-thin hydraulic jack is linked to hydraulic hand pump with a complete set, so does the link between force sensor and the reader of force sensor. The mounting method of measuring device is shown in Figure 1 and Figure 2.

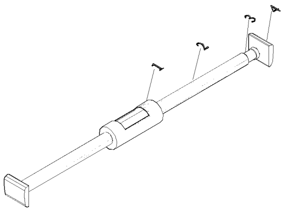

1-steel tank 2-sleeve 3-connecting sticks 4-linkers

Fig.1 Measuring device of fastener's lateral stiffness

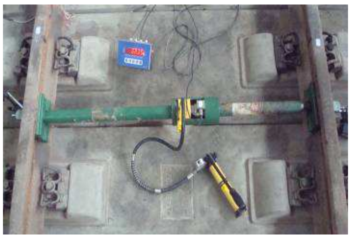

Fig.2 The photo of fastener's lateral stiffness test

When the measurements are conducting. The ultra-thin hydraulic jack produce lateral force on both sides of rail, with equal size and opposite direction, and the size of lateral horizontal force is shown in the reader of force sensor. Meanwhile, the magnitude of rail's displacement is reflected by the indicators on both sides of rail. To analysis more conveniently and reduce experimental error, the test is performed three times under each bolt torque of rail fastener[3].

The test results and analysis

While the size of rail fastenings' bolt torque are respectively taken as 140, 160 and 200N·m, the rail's displacement is measured under the conditions of changing the size of the lateral horizontal force. The test results are shown in Table 1 and the curves of lateral horizontal force - average displacement are shown in Figure 3. These following conclusions from test: (1) The left rail's displacement are almost equal to the right and the growth rate of them are also equal under the same horizontal force. (2) The rail's displacement and lateral force are not fully rendered as proportional relationship. While the lateral force is smaller, the growth of rail's displacement is also slower, and the relationship between them is proportional analogously. But while the lateral force exceeds a predetermined value, the displacement grow rapidly and the rate of it becomes larger, and the rails slipped. (3) there is a "turning point" in the curve of lateral force-displacement, and two curves about the "Turning point" can be approached by linear interpolating function. (4) Under the conditions of the "turning point" appearing in the curve, the larger fastener's bolt torque is, the greater corresponding lateral force is. But the corresponding displacement of the rail does not exhibit as simple regularity. That is, when the torque is taken as 140N·m, the size of corresponding lateral force and rail's lateral displacement each are 30kN and 90um; when the torque is taken as 160N·m, the size of them respectively change into 35kN and 80um; however, when the torque is taken as 200N·m, the size of them separately turn into 45kN and 100um.

Table 1. Rail's displacement [um]

Fastening's torque140N·m											
First time				Second time				Third time			
Lateral force [N]	The left rail [um]	The right rail[um]	Average value [um]	Lateral force [N]	The left rail [um]	The right rail[um]	Average value [um]	Lateral force [N]	The left rail [um]	The right rail[um]	Average value [um]
0	0	0	0	0	0	0	0	0	0	0	0
4747	10	8	9	4908	8	9	8.5	4713	8	8	8
9686	21	18	19.5	9269	18	21	19.5	9819	18	18	18
15321	36	31	33.5	14620	30	35	32.5	14552	28	27	27.5
19330	50	43	46.5	20108	46	53	49.5	19766	41	40	40.5
24200	66	63	64.5	24459	56	64	60	24264	54	56	55
29453	96	91	93.5	29359	77	89	83	29193	75	83	79
39126	173	172	172.5	39061	132	151	141.5	38954	143	155	149
47152	288	282	285	49194	257	299	278	49009	251	278	264.5
56540	445	436	440.5	55368	355	410	382.5	58603	412	449	430.5

Continued table 1. Rail’s displacement [um]

Fastening’s torque160N·m											
First time				Second time				Third time			
Lateral force [N]	The left rail [um]]	The right rail[um]	Average value [um]	Lateral force[N]	The left rail [um]	The right rail[um]	Average value [um]	Lateral force [N]	The left rail [um]	The right rail[um]	Average value [um]
0	0	0	0	0	0	0	0	0	0	0	0
10001	13	14	13.5	9760	15	16	15.5	10094	17	16	16.5
15097	21	22	21.5	14699	24	23	23.5	14808	26	26	26
19811	30	32	31	19570	34	32	33	19688	37	39	38
24946	41	44	42.5	24597	52	41	46.5	24745	48	53	50.5
29581	52	57	54.5	29781	61	56	58.5	30341	64	74	69
34393	67	74	70.5	34299	73	70	71.5	34575	78	91	84.5
39803	91	101	96	39287	106	104	105	38779	99	117	108
49544	168	190	179	49087	199	191	195	48128	149	172	160.5
54042	219	245	232	53850	281	269	275	52949	192	205	198.5
Fastening’s torque200N·m											
First time				Second time				Third time			
Lateral force [N]	The left rail [um]	The right rail[um]	Average value [um]	Lateral force [N]	The left rail [um]	The right rail[um]	Average value [um]	Lateral force [N]	The left rail [um]	The right rail[um]	Average value [um]
0	0	0	0	0	0	0	0	0	0	0	0
10303	13	11	12	9741	11	13	12	9183	11	11	11
14919	20	17	18.5	14700	19	20	19.5	13220	17	18	17.5
20073	30	28	29	19669	29	31	30	19698	28	35	31.5
24503	41	38	39.5	24833	40	44	42	24755	37	49	43
29795	57	53	55	29508	51	55	53	28430	44	59	51.5
34411	72	69	70.5	34418	65	68	66.5	35809	59	83	71
39448	89	85	87	39357	81	83	82	38916	68	95	81.5
44466	108	103	105.5	45580	106	107	106.5	42150	78	107	92.5
49219	131	124	127.5	50941	131	133	132	47099	92	126	109
53942	158	152	155	55292	151	155	153	55370	127	163	145
59175	191	188	189.5	59025	171	176	173.5	60466	156	195	175.5
63889	228	223	225.5	64014	211	214	212.5	65758	191	231	211

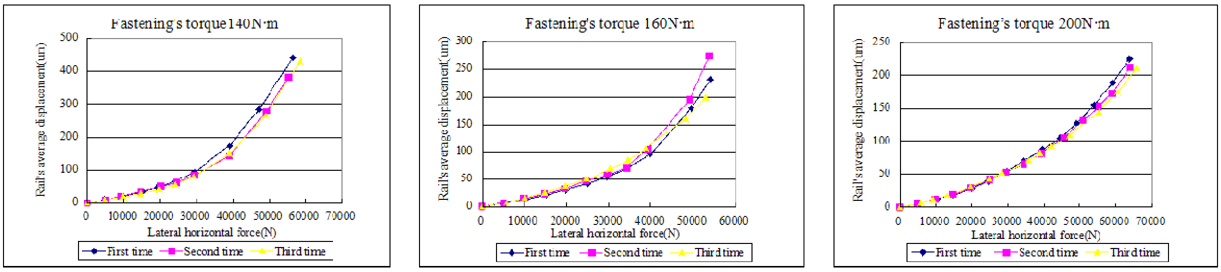

(a)Fastening’s torque 140N·m **(b) Fastening’s torque 160N·m** **(c) Fastening’s torque 200N·m**

Fig.3 The curves of lateral horizontal force - average displacement

The measured rail supports the transverse horizontal force which is assigned to the four groups of rail fastenings, which is located on the left and right of the measured rail. So the single fastener shares a quarter of lateral force. According to the test data of lateral force and rail’s displacement, the size of transverse stiffness can be calculated under the conditions of rail slipping, and the results are shown in Table 2. It can be drawn that: the size of left and right sides transverse stiffness are almost equal; the larger fastener’ s bolt torque is, the greater corresponding transverse stiffness is. Especially, when the torque is taken as 160N·m[4](Standard value), the size of transverse stiffness is

45.3kN/mm. However, the standard value is 35±5kN/mm[5], the followings may cause that the test results are larger. (1) As rail sliding, the transverse horizontal force is great. In addition, the test results of rail displacement are smaller than actual size. Therefore, even a slight error of lateral displacement will bring about a great error of fastener stiffness's values. (2) The rail suffered static friction before slipping. Since the maximum of static friction is greater than sliding friction, the measurements of lateral force is bigger in this moment. (3) As rail sliding, the lateral force is taken as the magnitude after loading. Without a doubt, it is bigger than the actual value while rail slipped.

Table 2 .The size of rail fastening's lateral stiffness when rail slipping[kN/mm]

Fastening torque [N·m]	140			160			200		
Lateral force [N]	29453	29359	29193	34393	34299	34575	44466	45580	47099
The left fastening	34.4	44.1	39.9	56.4	37.8	50.0	51.7	53.6	59.1
The right fastening	33.4	39.1	36.8	50.1	36.7	40.4	56.6	51.5	55.9
Average value	38.0			45.2			54.7		

Conclusions

(1) The relationship between rail's displacement and lateral forces is not fully rendered as proportional relationship[6]. There is a "turning point" in the entire curve of displacement, and the two curves about the "Turning point" can be approached by linear interpolating function.

(2) As the rail slipping, the size of the lateral force is connected with the fastener's bolt torque.

(3) The measured value of WJ-8 rail fastening's transverse stiffness is larger than the theoretical value, and the recommended value of rail fastening's transverse stiffness is respectively taken as 38, 45 and 55kN/mm, under the conditions of that the corresponding torque is 140, 160 and 200N·m.

Acknowledgements

The research described in this paper was financially supported by the Joint Funds of the National Natural Science Foundation of China (Grant Nos. U1361204, U1334203, U1134209); the National Natural Science Foundation of China (Grant Nos. 51378513, 50908236); the National Key Technology R&D Program (Grant No. 2013BAG20BH00); the Teacher Research Fund of Central South University of China (Grant No. 2013JSJJ021); the Science and Technology Foundation of Chinese Railway Corporation (Grant Nos. 2013G003-A-3, 2012G013-B, 2013G008-E, 2012G011-A-2); the Open Fund Project of Hunan Provincial University Innovation Platform of China (Grant No. 12K007).

References

[1] Miao Cai-xia, Lian Liang-song. Dynamic analysis of track structure's elasticity and lateral displacement. East China Jiaotong University Journal, 2004,21(4) 22-25.(In Chinese)

[2] Chen Xiu-Fang. Rail engineering, China Building Industry Publishing House, Beijing, 2005. (In Chinese)

[3] China Academy of Railway Sciences. Temporary technical conditions of passenger dedicated line's fastening systems. China Academy of Railway Sciences, Beijing, 2006. (In Chinese)

[4] Ministry of Railways, Science and Technology Division. The interim technical conditions of WJ-8 type rail fastening, China Railway Publishing House, Beijing, 2009. (In Chinese)

[5] China Academy of Railway Sciences. WJ-8 fasteners technical tests. China Academy of Railway Sciences, 2009. (In Chinese)

[6] Feng Shu-qin, Li Rui. Analysis of high-speed railway's fastening for lateral deformation of rail. Shanxi Architecture, 2007,33(31) 267-269. (In Chinese)

Applied Mechanics and Materials Vol. 596 (2014) pp 7-11
© (2014) Trans Tech Publications, Switzerland
doi:10.4028/www.scientific.net/AMM.596.7

Research on Modeling and Characteristics of Two-stage Pressure Hydro-pneumatic Spring

Zhongxing Li [1, a], Zili Ma [1,b], Hong Jiang [2,c], Xing Xu [1,d]

[1] School of Automotive and Traffic Engineering, Jiangsu University, Zhenjiang, 212013, China

[2] School of Mechanical Engineering, Jiangsu University, Zhenjiang, 212013, China

[a] zhxli@mail.ujs.edu.cn, [b] aliemstar@163.com, [c]99998888@126.com, [d]xuxing@mail.ujs.edu.cn

Keywords: Hydro-pneumatic spring; AMESim; Two-stage pressure; Stiffness characteristics

Abstract: The structure and principle of the two-stage pressure hydro-pneumatic spring were introduced. the physical and dynamic vehicle models with it were established under AMESim environment. Static characteristic curves of the two-stage pressure hydro-pneumatic spring were drawn. A single chamber hydro-pneumatic spring was used to compare the suspension dynamic travel and body vertical acceleration of the vehicles equipped with two-stage pressure hydro-pneumatic spring. The results show that two-stage pressure hydro-pneumatic spring can effectively enhance the vehicle riding comfort by decreasing body vibration.

Introduction

Hydro-pneumatic spring serves as a core component of hydro-pneumatic suspension. It is equipped with both variable elastic and damping components, so it presents nonlinear stiffness and damping characteristics [1,2].

Single chamber hydro-pneumatic springs are widely used in engineering vehicles, military vehicles and trucks [3,4], but the nonlinear stiffness for this kind of hydro-pneumatic spring is limited [5], heavy vehicles often load with actual mass change in a wide range. It is cannot meet the changing stiffness range when full loaded, so riding comfort will be affected.

To solve problems, this paper presents a two-stage pressure hydro-pneumatic spring with novel structure. The pre-charge pressure in the second pressure chamber is higher than the first chamber. When the vehicle is fully loaded, two air chambers work together to reduce the suspension stiffness.

Structure and Working Principle of Two-stage Pressure Hydro-pneumatic Spring

Its structure diagram was shown in Fig. 1. The hydro-pneumatic spring was mainly composed of working cylinder, tube piston, damping valve, first-stage pressure cylinder and second-stage pressure cylinder. damping valves were consisted of orifices, rebound valves and, compression valves. In order to prevent the phenomenon of emulsification, a rubber diaphragm was installed in each pressure cylinder to separate the oil and gas.

During the compression stroke, the upward movement of the cylinder lead to pressure increment in the cavity of the tube piston, the oil flowed through the main channel damping valve into the first stage pressure chamber. If the load or external stimulus exceeded the pre-charge pressure in the second stage pressure chamber, both chambers worked simultaneously. During the stretching stroke, the increased working cylinder volume resulted in the oil pressure decreasing.Oil returned the working cylinder through the damping valve.

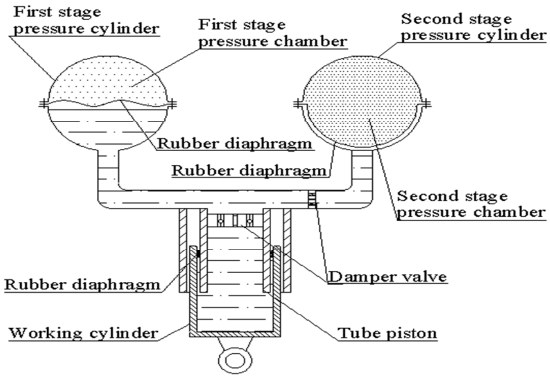
First stage pressure cylinder
First stage pressure chamber
Second stage pressure cylinder
Rubber diaphragm
Rubber diaphragm
Second stage pressure chamber
Rubber diaphragm
Damper valve
Working cylinder
Tube piston

Fig.1 Structure of two-stage pressure hydro-pneumatic spring

The Mathematical Model of Two-stage pressure hydro-pneumatic spring

The output force of the cylinder can be calculated by

$$F = P_4 A_1 \tag{1}$$

where F is the output force of working cylinder (N); P_4 is the chamber pressure of working cylinder(Pa); A_1 is the Cross-sectional area of the piston tube(m^2).

The rate of volumetric change is equal to the fluid flow into or out of the first stage and second stage pressure cylinder, when fluid compressibility is ignored.

$$A_1 \dot{x} = Q = Q_1 + Q_2 \tag{2}$$

where $\dot{x}$ is the relative velocity of the tube piston cylinder $(\mathrm{m/s})$; Q is the oil flow, the summing inflow or outflow of cylinder (m^3/s); Q_1,Q_2 $(\mathrm{m}^3/\mathrm{s})$ are the inflow or outflow for the first and the second stage pressure cylinder respectively.

Also consider relative motion direction of the tube piston and the working cylinder, the flow equation should be:

$$P_4 - P_3 = \frac{1}{2}\rho \times \left[\frac{Q}{C_d\left(A_d + n_c A_c\left(\frac{1}{2}+\frac{1}{2}sign(\dot{x})\right)\right)}\right]^2 \mathrm{sign}(\dot{z}) \tag{3}$$

where P_3 (Pa) is the pressure in the branch; $\rho(\mathrm{kg/m}^3)$ is the hydraulic oil density; C_d is the coefficient of orifice flow; $A_d(\mathrm{m}^2)$ is the area of orifice flow; n_c is the number of check valve; $A_c(\mathrm{m}^2)$ is the effective flow area of orifice valve.

The integral of flow Q_1 and Q_2 as a function of time t, volume changes of each gas pressure chamber can be obtain respectively.

$$V_1 = V_{10} - \int_0^t Q_1 \, \mathrm{d}t \tag{4}$$

$$V_2 = V_{20} - \int_0^t Q_2 \, \mathrm{d}t \tag{5}$$

where V_1, $V_2(\mathrm{m}^3)$represent the instantaneous volume of gas in the first stage and the second stage gas chamber respectively; V_{10},$V_{20}(\mathrm{m}^3)$ represent the gas volume in the first stage and the second stage gas chamber respectively at the static equilibrium position.

At the static equilibrium position, the first and the second stage pressure of the air chambers pressure are defined as P_{10},P_{20}.

Nitrogen is usually prefilled in the gas chamber as the inert gas. Using the ideal gas equation to establish the mathematical model of the changing process of certain state:

$$P_1V_1^r = P_{10}V_{10}^r \tag{6}$$

$$P_2V_2^r = P_{20}V_{20}^r \tag{7}$$

where P_1, P_{10}(Pa) represent the instantaneous pressure and equilibrium position pressure of the first stage pressure chamber respectively;P_2, P_{20}(Pa) represent the instantaneous pressure and equilibrium position pressure of the second stage pressure chamber respectively; r is the gas polytropic exponent.

(1) - (7) is the mathematical model of the two-stage pressure hydro-pneumatic spring.

Modeling and simulation of two-stage pressure hydro-pneumatic spring

Dynamic model of novel hydro-pneumatic spring is established under AMEsim software， as shown in Fig. 2. Main parameters are listed in Tab. 1. Static characteristics shown in Fig. 3

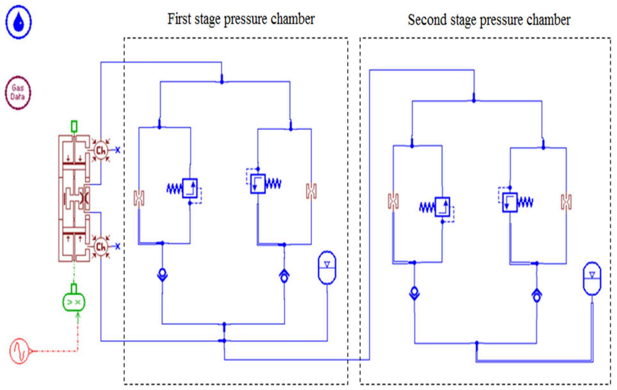

Fig.2 AMESim model of hydro-pneumatic spring

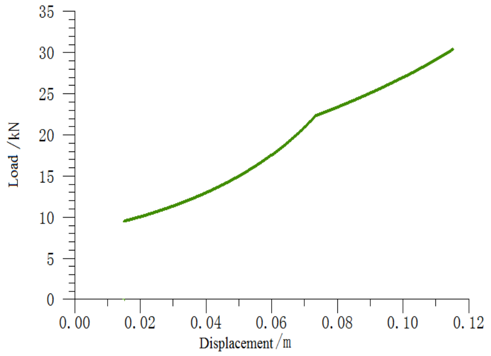

Fig.3 Static characteristic curve

Tab.1Simulation Parameter of Hydro-Pneumatic Spring

Parameters	Values	Parameters	Values
Tube piston diameter (mm)	90	Gas polytropic exponent	1.7
Piston stroke (mm)	120	Oil density (kg/m3)	865
Chambers volume (L)	0.4	Hydraulic oil dynamic viscosity (Pa·s)	0.050
The first chamber initial pressure (MPa)	1.3	The second chamber initial pressure (MPa)	4.7
Elasticity modulus(MPa)	1700		

The influence of two-stage pressure hydro-pneumatic spring on vehicle riding performance

The 1/4 model of a heavy off-road vehicle was built with AMEsim, and its parameters are listed: sprung mass is 1262.5kg (empty load) or 2262.5kg (full load), unsprung mass is 856kg, the tire stiffness is 1.3×10^6N/m.Step excitation as input signal, amplitude is 0.05m. The simulation time is 10s, while the step size is 0.001s.

Under empty load driving condition, suspension dynamic displacement d_1 and body acceleration a from simulation shown in Fig.4 and Fig.5.

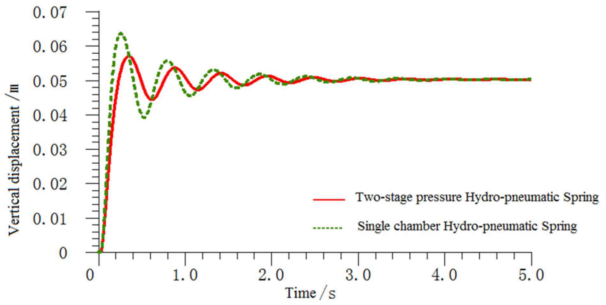

Fig.4 Comparison of suspension dynamic displacement response with empty load

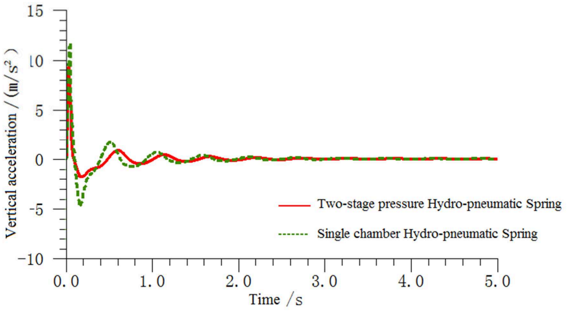

Fig.5 Comparison of body acceleration response with empty load

As shown in Fig.4, maximum overshoot of two-stage pressure hydro-pneumatic spring suspension dynamic displacement has diminished, and the amplitude of vibrations decreased. Fig.5 shows that body vertical acceleration peak value of two-stage pressure hydro-pneumatic spring suspension is significantly suppressed, although with empty load, the generated pressure has reached the second air chamber working pressure, thus produces a significantly inhibitory effect on the peak, and all acceleration response amplitudes are less than the former.

When fully loaded, the simulation results in Fig.6 and Fig.7. Suspension dynamic displacement and body acceleration response of two-stage pressure hydro-pneumatic spring suspension has greatly improved than single chamber hydro-pneumatic spring suspension, and the inhibitory effect of body acceleration peak is very obvious.

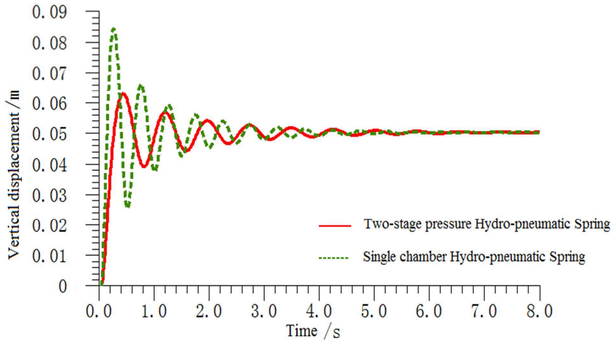

Fig.6 Comparison of suspension dynamic displacement response with full-loads

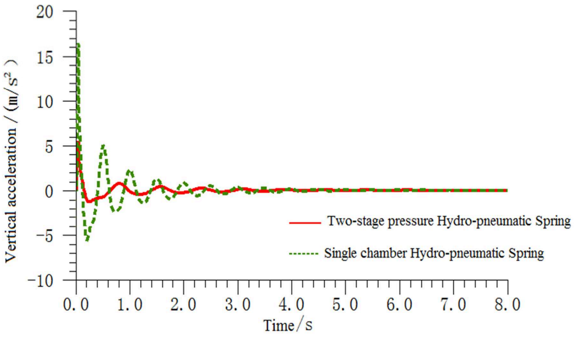

Fig.7 Comparison of body acceleration response with full-loads

Due to the second stage pressure chamber, the decreasing suspension stiffness makes car body natural frequency lower under the same load.

Conclusions

1) Compare to single chamber hydro-pneumatic spring suspension with different loading mass, the two-stage pressure hydro-pneumatic spring suspension can keep the natural frequency remain unchanged basically.

2) For the dynamic response process of the external excitation, suspension system equipped with the two-stage pressure hydro-pneumatic spring. That is to find out suspension dynamic travel and car body vertical acceleration are both well improved, so that the vehicle ride comfort improved significantly.

Acknowledgements

This work was financially supported by the National Natural Science Foundation of China (51075190 and 51305111), Six Talents Peak Foundation of Jiangsu Province (2012-ZBZZ-030) and the Natural Science Foundation of Jiangsu Province (BK20131255).

References

[1] Longxin Zhen, Wenming Zhang: submitted to Journal of Mechanical Engineering(2009), In Chinese
[2] Dejun Zhang, Jiang Liu, Fan Yu: submitted to Journal of Shanghai Jiao Tong University(2005) , In Chinese
[3] Longxin Zhen, Wenming Zhang, Guobiao Wang: submitted to Mining & Processing Equipment(2004) , In Chinese
[4] Jianmin Sun: submitted to Construction Machinery(2007) , In Chinese
[5] Jun Zuo, Shuping Cao, Menglin Yi. Control.Sci.Forum Vol.64-68(2000),p.208, In Chinese

Applied Mechanics and Materials Vol. 596 (2014) pp 12-16
© (2014) Trans Tech Publications, Switzerland
doi:10.4028/www.scientific.net/AMM.596.12

Study on the mechanism of detecting flaws in the transmission tower foundation by the finite element method

Xiaomin Shi[1,a], Qiang Gao[2,b*],Jianjun Liu[3,c],Jianguo Zhang[4,d]

Dabing Cheng[5,e],Nailong Zhang[6,f]

[1]Undergraduate of Mechanical Engineering, Soochow University, China 215021
[2]School of Mechanical Engineering, Soochow University, China 215021
[3]Jiangsu Electric Power Company Research Institute, China 211103
[4]Jiangsu Electric Power Company Research Institute, China 211103
[5]Jiangsu Electric Power Company Research Institute, China 211103
[6]Jiangsu Electric Power Company Research Institute, China 211103
[a]sudashixiaomin@sina.com,[b]gaoqiang@suda.edu.cn,[c]esuoting@163.com
[d]zjg197108@sina.com,[e]15105168882@163.com,[f]nlzhang10@163.com
Corresponding author:gaoqiang@suda.edu.cn

Keywords: impact-echo, transmission tower foundation, flaw, finite element

Introduction

Power transmission towers are major equipment of State Grid, the towers are usually a statically indeterminate truss structure system composed of angle iron or steel tubes, the foundation of the tower is a reinforced concrete structure. The safety of the tower foundation is very important to the power system. The perennial wind loads on the tower caused pulling and pressure stresses occur in the towers all the time and leads to appearing of new flaws and expansions of those existed flaws easily. In the other hand, tower foundations are easily affected by surroundings and geological activity because they are buried undergrounds, the circumstances lead to aging and cracking of concrete. Power transmission lines are usually very long, nondestructive testing to foundations is necessary when excavation is impossible. At present, methods of detecting flaws in concrete mainly include ultrasonic testing, electromagnetic pulse and impact-echo method. Ultrasonic testing needs smooth surfaces and the depth available is limited. Electromagnetic waves scatter violently because the rebar frame in reinforced concrete, this phenomenon makes testing results inexact. The impact-echo method was proposed by Dr M.Sansalone of America in 1984[1].The iTECS is developed in Japan, the practicality has been achieved in 2000[2]. Researchers have carried out a lot of researches on detecting flaws in concrete with impact-echo method[3-5].Study on detecting flaws in power transmission tower foundation using the impact-echo method has not been seen published so far. In this paper, the dynamic response analysis of the impact-echo method for power transmission tower foundation with flaws is solved based on finite element method; the result of numerical analysis is consistent with the depth of the setting flaw, which shows the feasibility of detecting flaws in transmission tower foundations with the impact-echo method.

Model of finite element method

In this paper, we chose the reinforced concrete numbered C20 which is widely used in power transmission tower foundations, material properties are shown (Table.1).

Table.1Material properties

Material	Elasticity modulus[Pa]	Poisson's ratio	Density [Kg/m^3]
Concrete	2.8e10	0.2	2400
Rebar	2.1e11	0.3	7850

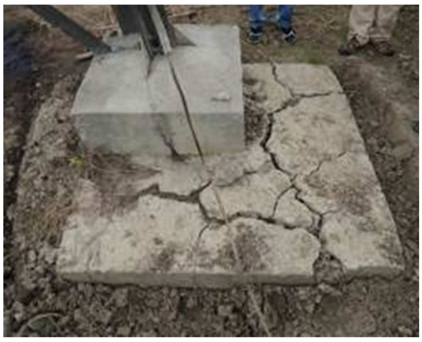

Fig.1 Flaws of a transmission tower foundation

Impact loads. Impact loads can be approximately set as a sine function of force in relationship to time

$$F = F_{max} \sin(\pi \cdot t/t_c) \qquad (1)$$

WhereF_{max} is set as 1N, the load step is divided into 20 parts;t_c is the duration of the impact load. There should not be incident waves and reflected waves at the input terminal at the same time; this means the propagation length of the impact wave must be less than double thickness of the component during the duration of impact load, that is:

$$t_c < 2D/V \qquad (2)$$

D is the depth of the component; V is the propagation speed of waves, the speed of longitudinal frequency can be calculated by the function below

$$V_p = \sqrt{E(1-\mu)/[\rho(1+\mu)(1-2\mu)]} \qquad (3)$$

E is Elasticity modulus, μ is Poisson's ratio, ρ is density.V_p can be calculated to be 3600m/s. Plug this into Eq.2 we can get the maximum of the duration of impact loads as 200μs. Some accurate instrument can detect flaws between 0.1m to 5m, the maximum of duration is 53μs when detecting 0.1m deep flaws.

In this model, t_c is set as 40μs, the interval between load steps is set as 2μs according to real instruments. The final impact load is shown in Fig.2

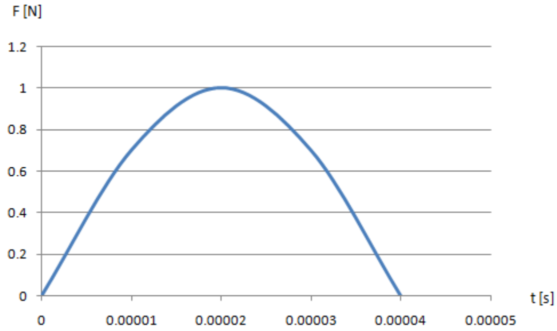

Fig.2The impact load

Date processing and results analysis. After finishing calculating, pick a node around the impact point on the surface, output its displacement diagram in the direction of impact load, we can get the spectrogram after Fast Fourier Transform (FFT). Some special peaks can be seen in the spectrogram, their frequencies are decided by the thickness of the model and the depth of flaws. According to the principle of impact-echo method, we can calculate the depth of flaws with the function below

$$D = C_p/2f. \tag{4}$$

D: the depth of flaws; C_p: speed of longitudinal wave; f: frequencies associated with flaws

Numerical analysis with real sizes

In this paper, we tried to solve the numerical analysis with the size of a real transmission tower foundation (Fig.3).The structure of a real tower foundation is very complex, after consulting with relevant departments we know that flaws mostly appear in the top tier of a foundation. We can simplify the numerical model as a model of the top tier. Finally the model was built as a block and its size is 1m×1m×1.6m, the flaw is set at the depth of 1m.

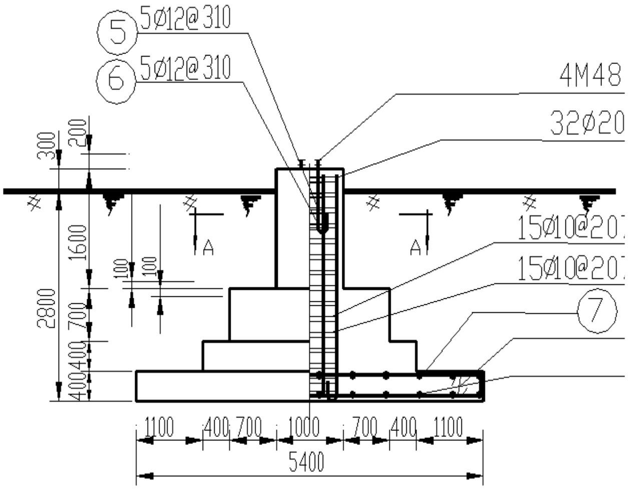

Fig.3Atransmission tower foundation

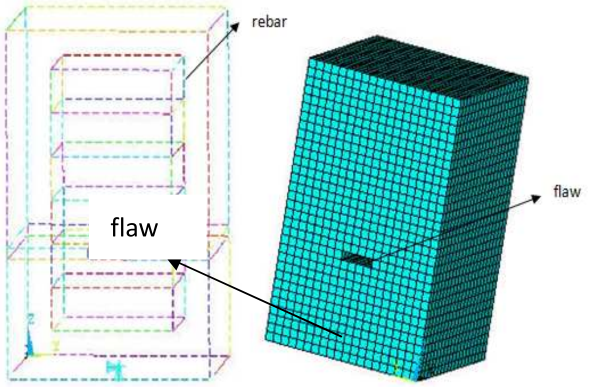

Fig.4AFEM model of a transmission tower foundation with a flaw

Analysis result

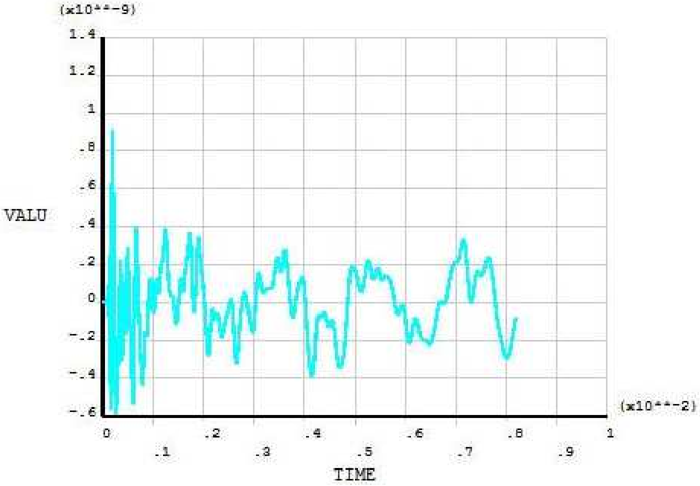

Fig.5 Displacement diagram

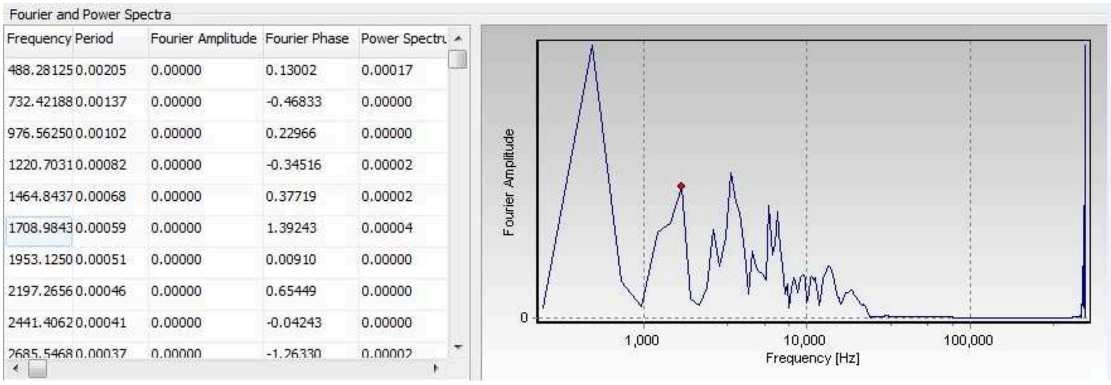

Fourier and Power Spectra

Frequency	Period	Fourier Amplitude	Fourier Phase	Power Spectru
488.28125	0.00205	0.00000	0.13002	0.00017
732.42188	0.00137	0.00000	-0.46833	0.00000
976.56250	0.00102	0.00000	0.22966	0.00000
1220.7031	0.00082	0.00000	-0.34516	0.00002
1464.8437	0.00068	0.00000	0.37719	0.00002
1708.9843	0.00059	0.00000	1.39243	0.00004
1953.1250	0.00051	0.00000	0.00910	0.00000
2197.2656	0.00046	0.00000	0.65449	0.00000
2441.4062	0.00041	0.00000	-0.04243	0.00000
2685.5468	0.00037	0.00000	-1.26330	0.00002

Fig.6 Spectrogram

The frequency of the first peak is decided by the thickness of model (Fig.6), the frequency of the second peak is associated with the depth of the flaw, results analysis is shown in Table.2.

Table.2 Results analysis

Model	Size[m]	Depth of the flaw[m]	Corresponding frequency[Hz]	Depth calculated[m]	Error between the actual and calculated date
1	1.00×1.00×1.60	1.00	1708.98	1.05	5%

Conclusion

The dynamic response analysis of the impact-echo method for probing transmission tower foundation with flaws is solved based on finite element method in this paper. The results shows that we can accurately simulate the process of detecting flaws in concrete with the impact-echo method, results analysis verifies the feasibility of detecting flaws in transmission tower foundation with the impact-echo method.

References

[1]LIN Weizheng: Non-destructive Testing techniques for Civilengineering Quality .Beijing: China Electric Power Press,2008.(in Chinese)

[2]Iwano, Satoshi: Study on the Detection Method of Crack of theConcrete Structures by iTECS//62nd Annual Scientific Conference of the Japan Society of Civil Engineers,2007.(in Japanese)

[3]Chiamen Hsiao, Chia-Chi Cheng, TzunghaoLiou and YuantingJuang: DetectingFlaws in Concrete Blocks Using the Impact-echo Method,NDT&International 41 (2008) 98-107.

[4]XU Lianghuan:Research on the First Wave of the Phase Reversal.Exploration Engineering,2005,17(6):4-5.

[5]Li Jie,SHAOweiyue: Applied Research on iTECS. Transportation world, 2011(16):126-127.

Applied Mechanics and Materials Vol. 596 (2014) pp 17-21
© (2014) Trans Tech Publications, Switzerland
doi:10.4028/www.scientific.net/AMM.596.17

Study on Torsion-eliminating Performance of Laterally Interconnected Air Suspension

Zhongxing Li[1, a], Longyu Ju[1,b], Hong Jiang[2,c], Xing Xu[1,d]

[1] School of Automotive and Traffic Engineering, Jiangsu University, Zhenjiang, 212013, China

[2] School of Mechanical Engineering, Jiangsu University, Zhenjiang, 212013, China

[a] zhxli@mail.ujs.edu.cn,[b] julongyu@126.com, [c]99998888@126.com, [d] xuxing@mail.ujs.edu.cn

Keywords: Laterally interconnected; Torsion-elimination; Air suspension; Simulation and experimental study

Abstract: Laterally interconnected air suspension combines the right and left air springs with pneumatic pipes, which can protect the auto-body parts from fatigue damage and increase the service life of vehicles. The mathematical model of full vehicle with laterally interconnected air suspension was established based on the analysis of its working principle, and a test bench was built. The simulation and experimental results show that, laterally interconnected air suspension can reduce the peak of dynamic body torsion load effectively, especially for steady state conditions, in which the body torsion load caused by the spring force can be nearly eliminated.

Introduction

As the dynamic vertical load of wheels is distributed unevenly when driving on uneven roads, a large torsion load will be generated on the vehicle body. In order to reduce the body torsion load and improve the dynamic vertical load sharing performance, interconnected suspensions are widely used in vehicle suspension systems.

The earliest interconnected suspension applied in manufacture field was mechanical interconnected suspension, which was installed on Citroen 2CV in 1949 [1]. Afterwards, different kinds of interconnected suspensions which use oil, oil & gas, air as transmission medium were developed [2]. In 1961, William W. Higginbotham proposed interconnected air suspension [3].

Interconnected air suspensions can be divided into two types: laterally interconnected and longitudinally interconnected. Sedans and SUVs prefer laterally interconnected air suspension because long and thick pipes are hard to be filled in the chassis space. This paper presents the mathematical model of full vehicle with laterally interconnected air suspension, and a test bench was also built to examine its torsion-eliminating performance.

Torsion-elimination Principle

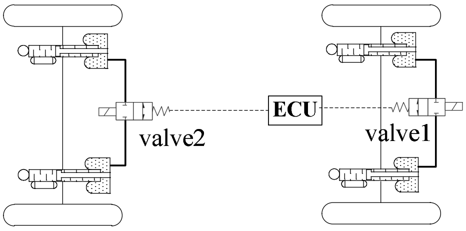

Fig. 1 Structure of laterally interconnected air suspension

Laterally interconnected air suspension combines the left and right air springs with pneumatic pipes, and the electromagnetic valves are installed in the gas lines. As is shown in Fig. 1, ECU (electronic control unit) controls electromagnetic valves to achieve connection or disconnection between the left and right air springs, according to vehicle's real riding condition.

When suspension is deformed, car body will subjected to a torsion load around the longitudinal axis of the body, T_X , which is caused by air springs, dampers and the anti-roll bars.

$$T_X=\left[A_e(P_1-P_2)+c\left(\dot{Z}_{s1}-\dot{Z}_{s2}\right)\right]\frac{T_f}{2}-\left[A_e(P_3-P_4)+c\left(\dot{Z}_{s3}-\dot{Z}_{s4}\right)\right]\frac{T_r}{2}+T_{bar} \qquad (1)$$

In the equation, F_1, F_2, F_3, F_4 are suspension forces (corresponding to the front left, front right, rear left, rear right, the same below); T_f, T_r are the front and rear track; A_e is the effective area of air spring; P_1, P_2, P_3, P_4 are air pressures inside 4 air springs; c is the damping coefficient; Z_{s1}, Z_{s2}, Z_{s3}, Z_{s4} are the 4 suspension dynamic trave; T_{bar} is torsional load caused by transverse stability rod.

On uneven roads, ECU activates electromagnetic valves to connect the left and right air springs. Then the discrepancy of air springs pressure, P_1 and P_2, P_3 and P_4, will gradually decrease, resulting in the decreasing of body torsional load T_X. In order to reflect the torsion-elimination mechanism of interconnected air suspension more clearly, the torsional load for vehicle caused by transverse stability rod is neglected in the following research.

The Vehicle Model

The vehicle is simplified as a 7 DOF model: the vertical, roll and pitch movement of the body and vertical movement of 4 wheels. The structure of vehicle physical model is shown in Fig. 2.

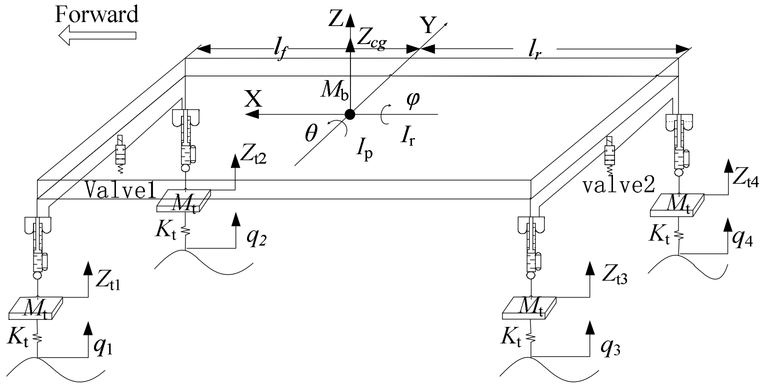

Fig. 2 Physical model of vehicle body and wheels for vertical vibration

In Fig. 2, M_b is body mass; M_t is tire mass; I_r is the rotational inertia of the body around the X axis; Φ is body roll angle, which is assumed positive when the body rolls toward the right side; I_p is the rotational inertia of the body around Y axis; θ is body pitch angle, which is assumed positive when the body bends forward; q_i is vertical displacement excitations of 4 wheels; Z_{ti} are vertical displacements of 4 wheels; K_t is vertical tire stiffness; T_f, T_r are respectively front and rear wheel treads; l_f, l_r are respectively distance from front and rear axle to the centroid.

7 DOF mathematical model of vehicle can be simplified as follows:

$$\begin{cases} M_{\mathrm{b}}\ddot{Z}_{\mathrm{cg}} = F_1 + F_2 + F_3 + F_4 - M_{\mathrm{b}} \cdot g \\ I_{\mathrm{r}}\ddot{\phi} = \dfrac{T_{\mathrm{f}}}{2}(F_1 - F_2) + \dfrac{T_{\mathrm{r}}}{2}(F_3 - F_4) \\ I_{\mathrm{p}}\ddot{\theta} = l_{\mathrm{r}}(F_3 + F_4) - l_{\mathrm{f}}(F_1 + F_2) \\ M_{\mathrm{t}}\ddot{Z}_{\mathrm{t}i} = K_{\mathrm{t}}(q_i - Z_{\mathrm{t}i}) - F_i + M_{\mathrm{bf}} \cdot g/2 \quad (i\text{=1, 2}) \\ M_{\mathrm{t}}\ddot{Z}_{\mathrm{t}i} = K_{\mathrm{t}}(q_i - Z_{\mathrm{t}i}) - F_i + M_{\mathrm{br}} \cdot g/2 \quad (i\text{=3, 4}) \end{cases} \tag{2}$$

where, M_{bf}, M_{br} represent the sprung mass of front and rear suspensions respectively.

Supposing the air spring is an adiabatic system, internal gas motion equation can be described as

$$P(\frac{V}{m})^{\kappa} = \mathrm{const} \tag{3}$$

where, P represents absolute gas pressure in air spring; V is air spring volume; m is the mass of gas inside the air spring; k is the isentropic exponent, which is 1.4 for air.

On the premise of meeting the engineering application, throttling effect of pipeline can be equivalent to orifices. Mass flow rate through the holes can be described as follows [4]

$$q_{\mathrm{m}} = \begin{cases} AP_{\mathrm{up}}\sqrt{\dfrac{1}{RT_{\mathrm{up}}}\dfrac{2k}{k-1}\left[\left(\dfrac{P_{\mathrm{dn}}}{P_{\mathrm{up}}}\right)^{\frac{2}{k}} - \left(\dfrac{P_{\mathrm{dn}}}{P_{\mathrm{up}}}\right)^{\frac{k+1}{k}}\right]} & \dfrac{P_{\mathrm{dn}}}{P_{\mathrm{up}}} \geqslant 0.528 \\ AP_{\mathrm{up}}\left(\dfrac{2}{k+1}\right)^{\frac{1}{k-1}}\sqrt{\dfrac{1}{RT_{\mathrm{up}}}\dfrac{2k}{k+1}} & \dfrac{P_{\mathrm{dn}}}{P_{\mathrm{up}}} < 0.528 \end{cases} \tag{4}$$

where, P_{up} is absolute upstream gas pressure, P_{dn} is absolute downstream gas pressure, T_{up} is upstream gas temperature, A is effective circulation area of the orifice.

Simulation of Torsion-eliminating Performance

The parameters of simulation model under Matlab/Simulink environment are listed in table 1

Tab. 1 Values of parameters for full car model

Parameter	Value	Parameter	Value
Body mass M_{b} (kg)	1396	X axis rotational inertial I_{r} (kg·m^2)	606
Wheel mass M_{t} (kg)	40	Y axis rotational inertial I_{p} (kg·m^2)	4192
Front/ rear wheel track $T_{\mathrm{f}}/T_{\mathrm{r}}$ (m)	1.55	Tire stiffness K_{t} (kN/m)	250
Distance from centroid to front axle l_{f} (m)	1.3	Distance from centroid to rear axle l_{r} (m)	1.4
Original volume of air spring V_0 (m^3)	0.0024	Effective area of air suspension A_{e} (m^2)	0.009

In order to examine the torsion-eliminating performance of laterally interconnected air suspension, step excitations are imposed on front-left and rear-right wheels. Fig. 3 and Fig. 4 shows the comparison of peak value and steady value of torsional body load.

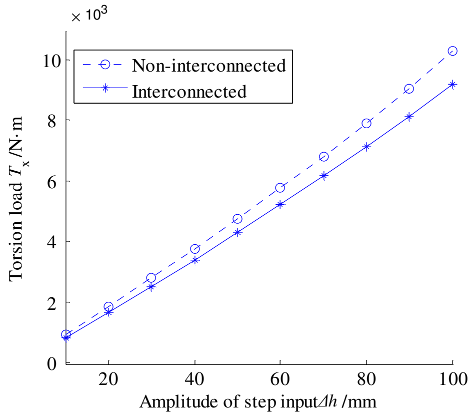

Fig. 3 Comparison of peak torsional body load

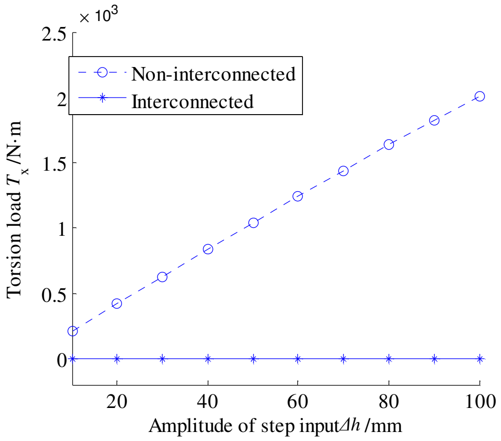

Fig. 4 Comparison of steady torsional body load

As is shown in Fig. 3, the peak value of vehicle body torsional load was reduced by 9.3%~12% by using laterally interconnected air suspension. Fig.4 shows that for unconnected air suspension, body torsion load in steady state conditions becomes larger with the increase of excitation's amplitude; while the value is almost zero for interconnected one.

Experiment of Torsion-eliminating Performance

In order to verify the simulation results, a full car model and a testing system of laterally interconnected air suspension are established. Excitations imposed on the vehicle by MTS320 Four Channel Hydraulic Servo Vibration Platform are the same as the simulation process. Considering the measuring range of sensors, excitation amplitude is set to 10~50 mm, with an interval of 10 mm.

Fig. 5 shows the vehicle body torsional load of laterally interconnected air suspension vehicle always remains in a low level, and the reduction percentage reaches even more than 91.7%, which indicates effective improvement for torsional load.

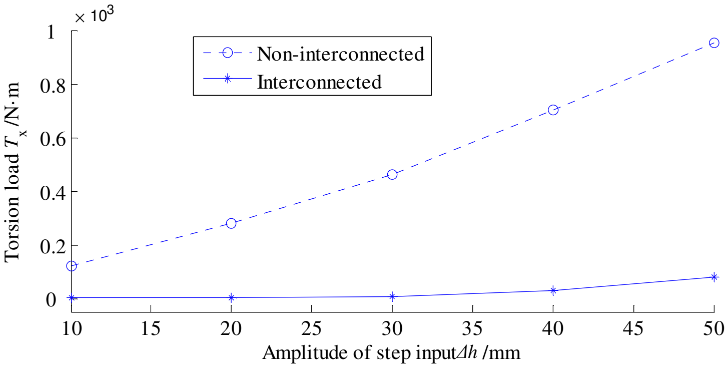

Fig. 5 Steady state body torsional load in experiment

Conclusions

The basic structure and working principle of laterally interconnected air suspension were presented, and the effectiveness of air spring interconnection on the vehicle body torsion load was examined by simulation and experimental study.

1) Simulation results showed that laterally interconnected air suspension decreased the peak of the body torsion load by 9.3%~12% under the step excitation imposed on the front-left and right-rear wheels. In steady state conditions, body torsion load caused by the spring force can be nearly eliminated.

2) Experimental results also demonstrated the torsion-elimination of laterally interconnected air suspension. The body torsion load caused by the spring force was reduced by over 91.7%.

Acknowledgements

This work was financially supported by the National Natural Science Foundation of China (51075190 and 51305111), Six Talents Peak Foundation of Jiangsu Province (2012-ZBZZ-030) and the Natural Science Foundation of Jiangsu Province (BK20131255).

References

[1] Fei Ding and Nong Zhang: submitted to Journal of Mechanical Engineering (2012), In Chinese
[2] M.C. Smith, G.W. Walker: submitted to Journal of Automobile Engineering (2005)
[3] W.W. Higginbotham, U.S. Patent 2,988,332. (1961)
[4] Maolin. Cai: submitted to Hydraulics Pneumatics & Seals (2007), In Chinese

Applied Mechanics and Materials Vol. 596 (2014) pp 22-26
© (2014) Trans Tech Publications, Switzerland
doi:10.4028/www.scientific.net/AMM.596.22

SVR based modeling method to structures finite element uncertainty propagation analysis

Yue Zhu [1, a *], Sihong Zhu [2,b]

[1] College of Engineering, Nanjing Agricultural University, Nanjing, 210031, China

[2] College of Engineering, Nanjing Agricultural University, Nanjing, 210031, China

[a]zhuyue_jin@163.com, [b]zhushon@njau.edu.cn

Keywords: Model uncertainty quantization analysis, Model validation,SVR,GARTEUR model Confidence interval

Abstract. Aiming at the uncertainty propagation analysis in modeling of FE model for structure, supported Vector Regression (SVR) method was presented to construct the implicit mapping between structure response and uncertainty parameters. The computational process of forward transfer of uncertainty parameters has been clarified. Three level testing criteria was used to evaluate extensively precision and generalization ability of RSM(Response Surface Modeling)based SVR. The super parameters in RSM were clarified through graded cross-validation. Uncertainty quantization analysis of GARTEUR model prove that the RSM based SVR has higher accuracy. Confidence level 95% finite element model was built because the confidence interval of nature frequency mean-value and variance were computed.

Introduction

In order to exactly predict the structural response of the whole space design error confidence, the three major national laboratory in recent years provide the techniques of model validation and model validation technology personnel, hope to fully solve the problem of structural dynamics modeling accuracy. At present, the technology of the model validation is still in its early stage of development, facing many challenges [1].Sandia national laboratories (SNL) published many reports about modern model validation methodology[2-4]and elaborated the basic ideas, concepts, methods and process.

In this paper, the finite element model validation[5] uncertainty transmitted and to study the quantitative process, analyzes the uncertainty factors (e.g., variance) in forward transfer process in the model, the calculation input parameter uncertainty on the response characteristics of uncertainty of statistics.

Based on bayesian statistical learning theory [6] of Support Vector machine Regression (Support Vector Regression) method [7], the first use of orthogonal experimental design method to produce the sample space, using *Support Vector machine* regression method in the sample space response surface model is established, and interpolation and extrapolation laboratories, through three level test precision of the response surface model is established, using cross validation method to choose the kernel width σ and super parameter C in Support Vector machine, finally using a *monte carlo sampling* input to establish the response surface model, the calculation results are quantitative uncertainty analysis, the results proved that *SVR* has excellent modeling capabilities, finite element model can well solve the uncertainty analysis and calculation in the process of practical problems such as small sample, nonlinear, high dimension, and accuracy of finite element initial model from the angle of probability is evaluated.

Theoretical basis

Given the training sample set $\{(x_j, y_j); j=1,2,\cdots l\}, x_j \in R^n, y_i \in R$, the corresponding target value y_i, defines linear insensitive loss function ε Eq. 1.If the target y has learned, and construct the difference between the regression estimate function $f(x)$ is less than ε ,the loss is equal to zero

$$\left|y-f(x)\right|_{\varepsilon}=\begin{cases} 0 & \left|y-f(x)\right|\le\varepsilon \\ \left|y-f(x)\right|-\varepsilon & \left|y-f(x)\right|>\varepsilon \end{cases} \tag{1}$$

Assumed that the nonlinear case regression estimate function is: $f(x)=w^{T}\varphi(x)+b, w\in R^{nh}, b\in R$; this optimization problem (2):

$$\begin{cases} \text{Min} & \frac{1}{2}w^{T}w+C\sum_{i=1}^{l}(\zeta_i+\zeta_i^{*}) \\ s.t. & y_i-w\varphi(x_i)-b\le\varepsilon+\zeta_i \\ & w\varphi(x_i)+b-y_i\le\varepsilon+\zeta_i^{*} \\ & \zeta_i^{*}\ge 0 \\ & \zeta_i\ge 0 \end{cases} \tag{2}$$

C as penalty factor, $i=1,2......l$ The dual optimization problem for

Thus regression estimate function is obtained through the study:

$$f(x)=\sum_{x_i\in SV}(\alpha_i-\alpha_i^{*})K(x_i,x) \tag{3}$$

Due to the radial basis kernel has better statistical performance, this paper chooses the kernel function is the form of a gaussian radial basis kernel:

$$K(x,x_j)=\exp\left(-\left\|x-x_j\right\|^{2}/\sigma^{2}\right) \tag{4}$$

Based on analysis of SVR uncertainty propagation

Use MC-SVR method for finite element model uncertainty propagation generally calculate through the following steps:

Significance test for sample points. Normal distribution fitting and confidence interval estimates: overall, for a single set has to confidence $(1-\alpha)$, $\alpha=0.05$, Degree of confidence is 0.95, The overall sample is X, estimation item of an overall mean and variance, respectively is $\mu=\bar{X};\sigma^{2}=S^{2}$. The confidence interval of the mean estimate:

$$\bar{X}\pm\frac{S}{\sqrt{n}}t_{\alpha/2}(n-1) \tag{5}$$

The confidence interval estimates of variance:

$$\left(\sqrt{n-1}S^{2}\Big/\chi^{2}_{\alpha/2}(n-1),\ \sqrt{n-1}S^{2}\Big/\chi^{2}_{1-\alpha/2}(n-1)\right) \tag{6}$$

t do not rely on any parameters of distribution, χ^{2} distribution is the look-up table.

Assumes that the sample data of the minimum value of the first order modal frequency is $f_{\min}^{i}$, the maximum value is $f_{\max}^{i}$, on the sample data of the order modal frequency can be according to the formula (7) for processing:

$$f_i^{j*}=2*(f_i^{j}-f_{\min}^{j}\Big/f_{\max}^{j}-f_{\min}^{j})-1 \tag{7}$$

After transformation, the size of different modal frequencies can be between [-1, 1].

$$RMSE=\frac{1}{N_{grid}\bar{y}}*\sqrt{\sum_{grid}(y-y_{reg})^{2}} \tag{8}$$

$$R^2 = 1 - \frac{\sum_{j=1}^{N_{grid}} (y_{reg}(j) - y(j))^2}{\sum_{j=1}^{N_{grid}} \left(y(j) - \bar{y}\right)^2} \tag{9}$$

The case study

France's national institute of aeronautics and astronautics, designed and manufactured in the 1990 s GARTEUR [8] plane model (Fig. 1). The model by the European aviation science and technology as the evaluation test analysis technology and model correction of the benchmark model. Model plane a wingspan of 2 m, 1.5 m long, fuselage main structure for aluminum, wing surface has a layer of viscoelastic damping materials containing constraint, the total quality of 44 kg. The model simulation of the actual aircraft main vibration modal characteristics, contains a number of intensive mode.

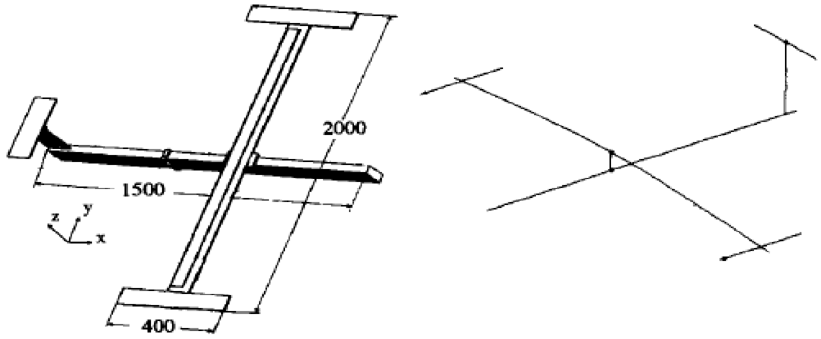

Fig. 1 *GARTEUR model diagram*

Using PATRAN built finite element model .Finite element model containing 74 beam element, a total of 76 nodes and 76 degrees of freedom. (refer with: Table 1)

Table 1 Selection of uncertain parameters

Serial number	Design parameters	Statistical characteristics parameters	
		μ	σ
1	Density of material	2.70E+03	2.70E+02
2	Rotational stiffness	3.12E-08	3.12E-09
3	I section inertia	8.33E-08	8.33E-09
4	II section inertia	8.33E-09	8.33E-10
5	III section inertia	1.56E-06	1.56E-07
6	IV section inertia	7.20E+10	7.20E+9

Learning sample points in accordance with the laws of 3σ design, consider the difficulty of parameter value range of the size of function approximation, the influence of sample points are uncertain parameters on the normalization of the sample space, so the sample points scheme design space can be used for different sizes of physical parameters. In the sample space of normalization, mean and variance of sample points according to the type Eq. 5, Eq. 6 to carry on the test of significance. Then the sample points according to the uncertain parameters in five levels: $\{m_i - 3\sigma, m_i - 1.5\sigma, m_i, m_i + 1.5\sigma, m_i + 3\sigma\}$. Respectively calculated GARTEUR model 1 to 5 order natural frequency as the learning samples.

MC simulation randomly generated 300 samples of normal distribution points, the input to the response surface model, obtained by natural frequency, the inherent frequency distribution fitting.

Table 2 The SVM response surface level I, II, III inspection results

Frequency order	parameter		SVM inspection		SVM inspection		SVM inspection	
	σ	C	$RMSE$	R^2	$RMSE$	R^2	$RMSE$	R^2
1	7	5.0×105	7.7460E-5	1.0000	4.7460E-3	0.9821	0.2820	0.722
2	6	2.5×105	6.9460E-5	1.0000	2.9460E-3	0.9901	0.3895	0.732
3	6	3.5×105	5.7460E-5	1.0000	7.7360E-3	0.9996	0.3143	0.716
4	7	4.0×105	8.7460E-6	1.0000	5.7160E-3	0.9827	0.2632	0.743
5	6	4.0×104	5.7960E-5	1.0000	3.2960E-3	1.0000	0.2529	0.812
Average value			5.4200E-5	1.0000	4.8880E-3	0.9909	0.3004	0.745

Fittingresult is shown in Fig. 2

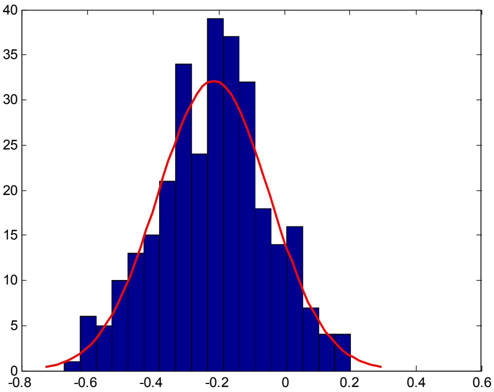

Fig. 2 The inherent frequency distribution fitting

Summary

1, Based on support vector machine (SVM) regression method to establish the response surface model, the structural finite element model, this paper analyzes the uncertainty propagation problem, calculate the mean and variance of structural response of the confidence interval, the uncertainty of the finite element model for the quantitative.

2, Level 3 inspection standards are introduced to establish the comprehensive evaluation on the response surface model precision and generalization ability, through the classification of cross validation method to determine the super parameter vector machine (SVM) model of C and kernel width.

3, Support vector machine (SVM) method in structural uncertainty modeling the successful application of the finite element model for model validation in the establishment of the prediction error model opens a new route.

References

[1] Trucano T，Oberkampf W，Pilch M. V&V Principles and Challenges. SAND2006-6435C, 2006.

[2] Oberkampf W L, Trucano T G. Verification and Validation in Computational Fluid Dynamics. SAND2002-0529, 2002.

[3] Oberkampf W L, Trucano T G,Hirsch C. Verification, Validation, and Predictive Capability in Computational Engineering and Physics. SAND2003-3769, 2003.

[4] Trucano T G, Pilch M, Oberkampf W L. General Concepts for Experimental Validation of ASCI Code Applications. SAND2002-0341, 2002.

[5] Guo Qintao．Structural dynamics finite element model validation studies several key problems [D]．Nanjing: nanjing university of aeronautics and astronautics, 2005.

[6] VAPNIK V N．Statistical learning theory[M]．NewYork：Wiky，1998．

[7] SUYKENS J A K，VANDEWAL I E J．Least squares support vector machines classifiers[J]. Neural Network Letters, 1999. 19(3): 293-300．

[8] Balmes E．GARTEUR group on ground vibration testing，Results from the test of a single structure by 12 laboratories in Europe [A]．Proceedings of15th IMAC [C]．USA，1997．I346-1352．

Applied Mechanics and Materials Vol. 596 (2014) pp 27-31
© (2014) Trans Tech Publications, Switzerland
doi:10.4028/www.scientific.net/AMM.596.27

Hopf Bifurcation Analysis of Digital Hydraulic Cylinder

Jia Chen[1, a], Jifeng Xing[1] and Bangjun Lv[1]

[1]College of Power Engineering, Naval University of Engineering, Wuhan 430033, China

[a]jiachen815@aliyun.com

Keywords: digital hydraulic cylinder; Hopf bifurcation; Limit cycle; MATCONT.

Abstract. A dimensionless nonlinear state-space model was established considering the structural particularities of digital hydraulic cylinder, and dynamic bifurcation characteristics of the system were analyzed and validated based on MATCONT. The results show that, when the piston diameter, valve orifice area gradient, ball-screw pitch and the maximum desired speed are not designed appropriately, digital hydraulic cylinder is prone to Hopf bifurcation. Limit cycles that the stable and the unstable neutralize each other at subcritical Hopf bifurcation points, causing the system tracking outputs divergence from continuous oscillation to increasing oscillation. Losing synchronism of stepper motor is essentially a form of the instability caused by system supercritical Hopf bifurcation.

Introduction

Digital hydraulic cylinder is an integrated electromechanical-hydraulic servo mechanism. The inherent nonlinearities and coupled actions of each individual component make the system behaviors more complex. When parameters are not designed appropriately, bad phenomena like dynamic impact, oscillation and creeping, happen easily. Hopf bifurcation is an important sort of dynamic bifurcation, which could interpret some self-excited vibrations in dynamical systems. Application of bifurcation theory makes it easy to analyze the impact of parameter variation on system structural stability effectively, and system dynamic behavior around unstable equilibrium points could also be investigated conveniently. In [1], based on bifurcation theory, the stability of valve controlled asymmetric cylinder system had been analyzed and designed considering the impact of pipeline. The influences of nonlinear factors that time lag and dead zone of control valve on the dynamics characteristics and bifurcation boundaries were analyzed for a simplified hydraulic position regulating system in [2]. Literature [3] studied the roles of geometric characteristics of the oil return orifices and stiffness of the valve spring in system stability of a four-way valve controlled symmetrical cylinder system, and noted that the system is unstable at the bifurcation equilibrium point and generates a stable limit cycle. This paper takes full account of the particularities of digital cylinder structure, and based on the nonlinear dynamics model in [4], investigates the impacts of system parameters on structural stability and analyzes the dynamic bifurcation characteristics to guide parameter design and utilization of the actual system.

Hopf Bifurcation

For nonlinear system containing parameters, $\dot{x} = f(x,\mu)$, $x \in R^n$ is the state vector, and $\mu \in R^m$ is the system parameter vector. According to bifurcation theory, a Hopf bifurcation occurs, when the parameter μ varies continuously through μ_*, and following conditions are met: (1) $f(x_*,\mu_*) = 0$; (2) except the one pair of purely imaginary eigenvalues $\lambda = \pm j\omega$ for system Jacobi matrix $J = \partial f(x,\mu)/\partial x$ at point (x_*,μ_*), there are no any other eigenvalues with zero real part; (3) $[d\,\mathrm{Re}(\lambda)/d\mu]|_{\mu=\mu_*} \neq 0$. Near the bifurcation point (x_*,μ_*), limit cycles exist. Hopf bifurcation could be divided into the supercritical and the subcritical by the bifurcation direction and limit cycle stability. The foregoing bifurcation conditions could be only used to determine whether a Hopf bifurcation occurs, whereas the Hopf bifurcation type must be judged by calculating the first Lyapunov coefficient [5] l_1 at the bifurcation point. If $l_1 < 0$, the bifurcation is supercritical; while $l_1 > 0$, the bifurcation is subcritical. The formula is

$$l_1(\mu_*) = \mathrm{Re}\left[\left\langle p, C(q,q,\bar{q})\right\rangle - 2\left\langle p, B\left(q, A^{-1}B(q,\bar{q})\right)\right\rangle + \left\langle p, B\left(\bar{q}, (2i\omega E - A)^{-1}B(q,q)\right)\right\rangle\right] \Big/ (2\omega) . \tag{1}$$

Where, p and q are the left and right eigenvectors of Jacobi matrix $A = J(\mu_*)\big|_{x_*}$ at the bifurcation point, and satisfy $Aq = j\omega q,\ q \in C^n$, $A^T p = -j\omega p,\ p \in C^n$. And normalization conditions that $\langle q,q\rangle = q^H q = \bar{q}^T q = 1$, $\langle p,q\rangle = p^H q = 1$ are also fulfilled. $B(x,y)$ and $C(x,y,z)$ are the bilinear function and three linear function.

Dimensionless Nonlinear State-space Model of Digital Hydraulic Cylinder

Digital hydraulic cylinder is essentially a class of mechanical hydraulic servo mechanism driven by stepper motor working as the input translation unit from the electrical to the mechanical. System working principle has been elaborated explicitly in [4], and a perfect nonlinear mathematical model was also deduced based on the comprehensive analysis of each components. Through the analysis in [4], if assume that digital cylinder is uniformly passing the desired displacement x_d with the desired speed v_d , and the actual output displacement is x_p , the output displacement error and deviation angles of ball-screw and stepper motor will be $x_e = x_d - x_p$, $\theta_{be} = 2\pi x_p / t_2 - \theta_b$, $\theta_e = 2\pi i_s x_d / (i_r t_2) - \theta$. The differential forms are written as $\dot{x}_e = v_d - \dot{x}_p$, $\dot{\theta}_{be} = 2\pi \dot{x}_p / t_2 - \dot{\theta}_b$, $\dot{\theta}_e = 2\pi i_s v_d / (i_r t_2) - \dot{\theta}$. Here, t_2 is the ball-screw pitch, θ_b is the angular displacement and i_r is the reducer transmission ratio of ball screw, while θ is the angular displacement and i_s is the reducer transmission ratio of stepper motor.

Since the system physical quantities of digital hydraulic cylinder differ greatly on magnitude order and change rate, the nonlinear model obtained by direct modeling is too ill-conditioned to solving the bifurcation problems accurately. So dimensionless method is applied to better the model condition number. According to the principle of dimensional homogeneity, set valve orifice area gradient w , oil density ρ and supply pressure p_s as the basic quantities, then get dimensionless state vector and time that $[x_e', x_v', z']^T = [x_e, x_v, z]^T / w$, $[\dot{x}_p', \dot{x}_v']^T = [\dot{x}_p, \dot{x}_v]^T \sqrt{\rho / p_s}$, $[\theta_{be}', \theta_e']^T = [\theta_{be}, \theta_e]^T$, $[\dot{\theta}_b', \dot{\theta}']^T = [\dot{\theta}_b, \dot{\theta}]^T w\sqrt{\rho / p_s}$, $[p_1', p_2']^T = [p_1, p_2]^T / p_s$, $t' = t\sqrt{p_s/\rho}\big/ w$. Where, x_v is the axial displacement of the spool, z is average bristle deformation of the friction contact, p_1, p_2 are the pressures in rod chamber and non-rod chamber. Define state vector $x = [x_1, x_2, \cdots, x_{11}]^T = [x_e', \dot{x}_p', p_1', p_2', x_v', \dot{x}_v', \theta_{be}', \dot{\theta}_b', \theta_e', \dot{\theta}', z']^T$, then get a dimensionless nonlinear state-space model as,

$$\begin{cases} \dot{x}_1 = v_d\sqrt{\rho/p_s} - x_2 \\ \dot{x}_2 = [A_1 p_s x_3 - A_2 p_s x_4 - (B_p + \sigma_2 + \sigma_1)\sqrt{p_s/\rho}\,x_2 - (\sigma_0 - \sigma_1\sqrt{p_s/\rho}\,|x_2| \big/ g(x_2))w x_{11} - 2\pi x_7 K_T(x_1)/(\eta t_2) - F_e] w\rho \big/ (p_s M) \\ \dot{x}_3 = [C_i p_s(x_4 - x_3) - A_1\sqrt{p_s/\rho}\,x_2 + q_{sv1}(x_3, x_5) - q_{sv3}(x_3, x_5)] K w\sqrt{\rho/p_s^3} \big/ [V_{10} + A_1(x_d - w x_1)] \\ \dot{x}_4 = [C_i p_s(x_3 - x_4) - C_e p_s x_4 + A_2\sqrt{p_s/\rho}\,x_2 - q_{sv4}(x_4, x_5) + q_{sv2}(x_4, x_5)] K w\sqrt{\rho/p_s^3} \big/ [V_{20} - A_2(x_d - w x_1)] \\ \dot{x}_5 = x_6 \\ \dot{x}_6 = [F_v(x_1, x_5, x_6, x_7, x_8, x_9, x_{10}) - F_s(x_3, x_4, x_5) - F_t(x_3, x_4, x_6) - B_m\sqrt{p_s/\rho}\,x_6 - F_{fv}] w\rho \big/ (p_s m_v) \\ \dot{x}_7 = 2\pi w x_2 / t_2 - x_8 \\ \dot{x}_8 = [i_r d_2 F_a(x_1, x_5, x_6, x_7, x_8, x_9, x_{10})/2 + x_7 K_T(x_1) - B_b x_8\sqrt{p_s/\rho} \big/ w - T_{fb}] w^2\rho \big/ (p_s J_b) \\ \dot{x}_9 = 2\pi i_s v_d w\sqrt{\rho/p_s} \big/ (i_r t_2) - x_{10} \\ \dot{x}_{10} = [T_m \sin(Z_r x_9) - B x_{10}\sqrt{p_s/\rho} \big/ w - d_2 F_a(x_1, x_5, x_6, x_7, x_8, x_9, x_{10})/(2 i_s)] w^2\rho \big/ (p_s J) \\ \dot{x}_{11} = x_2 - w|x_2|\,x_{11} \big/ g(x_2) \end{cases} , \tag{2}$$

$$g(x_2) = [F_c + (F_{sc} - F_c)\exp(-p_s x_2^2 / (\rho v_{sk}^2))] \big/ \sigma_0 , \tag{3}$$

$$1/K_T(x_1) = 4\pi^2 \big/ (\eta t_2^2)[4 l_s(x_d - w x_1, L) \big/ (\pi d_s^2 E) + 1/K_n + 1/K_b] + 32 L_s(L) \big/ (\pi d_s^4 G) + 1/K_{c\theta} , \tag{4}$$

$$q_{svi} = \begin{cases} C_d w_i (x_{0i} + \bar{\Delta}_i)\sqrt{2\triangle p_{svi}/\rho}, & \bar{\Delta}_i \ge 0 \\ C_d w_i\, x_{0i}^2 \big/ x_{0i} - k_{li}\bar{\Delta}_i\sqrt{2\triangle p_{svi}/\rho}, & \bar{\Delta}_i < 0 \end{cases},\ i = 1,2,3,4,\ \triangle p_{svi} = \begin{cases} p_s(1 - x_3), & i = 1 \\ p_s(1 - x_4), & i = 2 \\ p_s x_3 - p_0, & i = 3 \\ p_s x_4 - p_0, & i = 4 \end{cases},\ \bar{\Delta}_i = \begin{cases} w x_5 - \Delta_i, & i = 1,4 \\ -w x_5 - \Delta_i, & i = 2,3 \end{cases}, \tag{5}$$

$$F_s(x_3,x_4,x_5)=\begin{cases}0.43w_1p_s(1-x_3)\sqrt{(wx_5-\Delta_1)^2+r_c^2}+0.43w_4(p_sx_4-p_0)\sqrt{(wx_5-\Delta_4)^2+r_c^2}, & x_5\ge 0\\ -0.43w_2p_s(1-x_4)\sqrt{(wx_5+\Delta_2)^2+r_c^2}-0.43w_3(p_sx_3-p_0)\sqrt{(wx_5+\Delta_3)^2+r_c^2}, & x_5<0\end{cases},$$

$$F_t(x_3,x_4,x_6)=\begin{cases}C_dx_6\sqrt{2\rho p_s}[w_1L_1\operatorname{sgn}(1-x_3)\sqrt{|1-x_3|}-w_4L_2\operatorname{sgn}(x_4-p_0/p_s)\sqrt{2\rho|x_4-p_0/p_s|}], & x_5\ge 0\\ C_dx_6\sqrt{2\rho p_s}[w_2L_1\operatorname{sgn}(1-x_4)\sqrt{|1-x_4|}-w_3L_2\operatorname{sgn}(x_3-p_0/p_s)\sqrt{2\rho|x_3-p_0/p_s|}], & x_5<0\end{cases} \tag{6}$$

$$\begin{aligned}F_v(x_1,x_5,x_6,x_7,x_8,x_9,x_{10})&=F_N\cos\psi-|F_N|\operatorname{sgn}((x_{10}/i_s-x_8/i_r)d_2/2\cos\psi-wx_6\sin\psi)\tan\rho_v\sin\psi\\ F_a(x_1,x_5,x_6,x_7,x_8,x_9,x_{10})&=F_N\sin\psi+|F_N|\operatorname{sgn}((x_{10}/i_s-x_8/i_r)d_2/2\cos\psi-wx_6\sin\psi)\tan\rho_v\cos\psi\end{aligned},$$

$$F_N=\begin{cases}K_N(\triangle x_N-x_c)+B_N\triangle\dot{x}_N, & \triangle x_N>x_c\\ 0, & |\triangle x_N|\le x_c\\ K_N(\triangle x_N+x_c)+B_N\triangle\dot{x}_N, & \triangle x_N<-x_c\end{cases},\quad \begin{cases}\triangle x_N=[2\pi wx_1/(i_rt_2)-x_9/i_s+x_7/i_r]d_2/2\sin\psi-wx_5\cos\psi\\ \triangle\dot{x}_N=[(x_{10}/i_s-x_8/i_r)d_2/2\sin\psi-wx_6\cos\psi]\sqrt{p_s/\rho}/w\end{cases}, \tag{7}$$

where A_1, A_2, V_{10} and V_{20} are the effective areas and initial volumes of the two chambers respectively, determined by design parameters such as the diameters of piston, rod and ball-screw D_1, D_2, d_s, and the effective piston stroke L. F_e is the external load, and M is the effective mass. C_i, C_e are the internal and external coefficients of hydraulic cylinder. K is the oil bulk modulus. F_c is the moving Coulomb friction of hydraulic cylinder, F_{sc} is the maximum static friction, v_{sk} is the Stribeck velocity. $l_s(x_p,L)$ is the ball-screw mounting distance, relating to L and x_p. $L_s(L)$ is the total length of ball screw. p_0 is the oil return pressure, C_d is the valve port flow coefficient. Ignore the differences between each valve port, area gradient w_i, initial overlap Δ_i, leakage coefficient k_{li} and opening correction x_{0i}, can be expressed uniformly as w, Δ, k_l and x_0. d_2 is the pitch diameter of screw drive mechanism, and x_c is the unilateral gap width. Meaning of the other notations, see details in [4].

Bifurcation Calculation and Analysis

The bifurcation calculation essence is to solve the nonlinear algebraic equations satisfying the conditions of equilibrium and bifurcation. Continuation algorithm has a capacity to converge in large range to be the most effective solution method for nonlinear equations. MATCONT is continuation algorithm based bifurcation calculation software developed in MATLAB. It facilitates the calculation of equilibrium solution and the detection and identification of bifurcation for nonlinear dynamic system [6]. Meanwhile, the function of numerical integration is convenient for further validation and analysis of system bifurcation characteristics. Therefore, MATCONT is used in bifurcation calculation and analysis to investigate the dynamic behavior of digital hydraulic cylinder. Here set the equilibrium state of single direction uniform motion as the origin, and focus on analyzing the impact of structural parameters and operating parameters on system dynamic stability. Assume $v_d>0$, $x_v>0$, namely, locate the equilibrium state of steady tracking for the positive input. Set each parameter as the free parameter in turn, while value the remaining as the fixed referring [4], and execute single-parameter bifurcation analyses successively. Only when take continuous samples from each feasible region for parameter D_1, w, t_2 and v_d, Hopf bifurcation can be detected. The calculation results of Hopf bifurcation are shown in Table 1.

Table 1 Calculation results of Hopf bifurcation

Free parameter	D_1 [m]	w [m]	t_2 [m]	v_d [m/s]
Feasible region	[0.09,0.40]	[0.015,0.095]	[0.001,0.05]	[0,0.04]
Bifurcation point	0.106	0.091	3.63×10^{-3}	0.024
First Lyapunov coefficient	735.138	2.61×10^{3}	-46.690	52.496

Value the free parameter in the left and right small neighborhoods of the bifurcation point, and simulate the model in time domain respectively, then get the phase diagrams and time-domain curves of state variables. The following only shows the simulations around bifurcation points $D_1=0.106\text{m}$ and $t_2=3.63\times10^{-3}\text{m}$ as an example to interpret, and other calculation results can also be validated in this way. Fig. 1 and 2 are the time domain simulations when $D_1=0.106\text{m}$, $D_1=0.104\text{m}$, and Fig. 3 and 4 are the simulations when $t_2 = 3.63\times10^{-3}\mathrm{m}$, $t_2 = 3.43\times10^{-3}\mathrm{m}$. Moreover, to benefit comparison and analysis, the dimensionless quantities have been transformed to the actual ones.

Seen from Fig. 1(a) tracking output phase diagram, the response trace converges to a stable limit cycle when $D_1 = 0.106\mathrm{m}$, that is to say, the actual output of digital hydraulic cylinder follows the desired output steadily, but the tracking displacement error and velocity fluctuate in each fixed range continuously. As shown in Fig. 1(b) and 1(c), the corresponding time-domain curves show periodic oscillations with constant amplitudes. While known from Fig. 2, when $D_1 = 0.104\mathrm{m}$, the output can no longer follow the input steadily, the periodic oscillations become increasing oscillations and diverge over time. In Fig. 2(a), the tracking output trajectory of digital hydraulic cylinder neither converges to a fixed point, nor forms a closed curve, but continuously spiral outward after passing through a dense orbit region. Further analysis shows that, two limit cycles with distinct stability simultaneously exist in the system output phase plane when $D_1 \ge 0.106\mathrm{m}$, besides, the stable limit cycle is located inside the unstable one, therefore, the system output tracks the input stably with periodic oscillations, and with D_1 increasing, the amplitude decreases and the system stability is enhanced; whereas when D_1 diminishes, the stable limit cycle expands, while the unstable limit cycle contracts, and finally the two cycles encounter and neutralize each other at the bifurcation point and only leave an unstable equilibrium point, so the system response oscillates to divergence when $D_1 < 0.106\mathrm{m}$. At this time, the subcritical bifurcation occurs, which is consistent with the calculated first Lyapunov coefficient $l_1 = 735.138 > 0$ when $D_1 = 0.106\mathrm{m}$. So in actual design, D_1 should be selected larger and away from the bifurcation point to avoid the response oscillation or divergence.

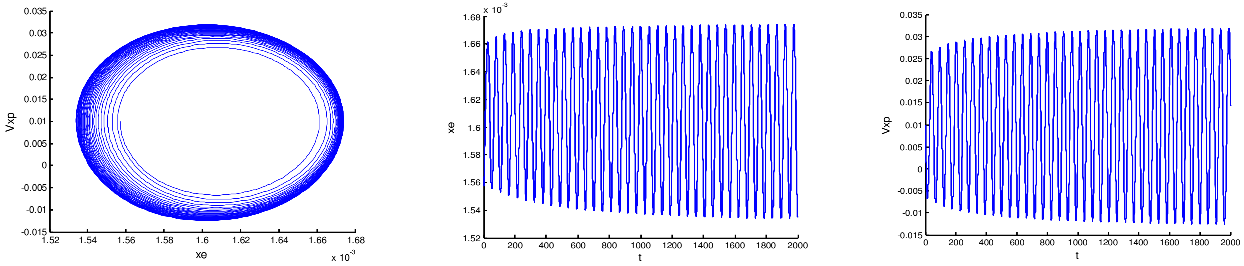

(a) Tracking Output phase diagram (b) Tracking displacement error (c) Tracking velocity

Fig. 1 Simulation in time domain when $D_1 = 0.106\mathrm{m}$

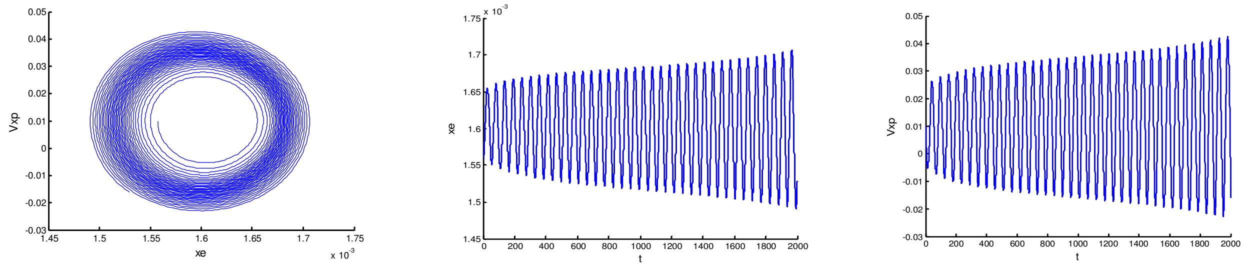

(a) Tracking Output phase diagram (b) Tracking displacement error (c) Tracking velocity

Fig. 2 Simulation in time domain when $D_1 = 0.104\mathrm{m}$

Fig.3 and 4 show that, the system output response is complex when t_2 is minor, and there is no standard limit cycle in system output phase plane. In Fig. 3(a), the tracking output locus converges inward asymptotically, and the stepper motor output (or digital spool rotation) is convergent in phase diagram as well. In Fig. 3(c), after chattering for a period of time, stepper motor could steadily drive the digital spool rotating at a low speed to form a fixed opening, consequently, the system output can eventually track the input stably when $t_2 = 3.63\times10^{-3}\mathrm{m}$. But at that time $t_2 = 2.63\times10^{-3}\mathrm{m}$, as shown in 4(a), the output trajectory stretch along the axis x_e ceaselessly to not form a closed orbit in a certain area, and the velocity Vx_p of hydraulic cylinder oscillates close to zero. That is to say, the digital hydraulic cylinder couldn't trace the input normally, the actual output is close to zero, and the tracking error is increasing with the input. Seen from Fig. 4(b) and 4(c), the stepper motor falls out step to jitter lastingly in a small region near zero position, and could not drive the digital spool running with the input as usual. Since at the bifurcation point $t_2 = 3.63\times10^{-3}\mathrm{m}$, the first Lyapunov coefficient

$l_1 = -46.690 < 0$, so it can be understood that, the stepper motor oscillates to instability and generates a supercritical bifurcation. A limit cycle appears near zero position, which makes the motor output no effective rotational displacement. The axial displacement of digital spool is mostly zero and uncontrolled, making digital hydraulic cylinder no output. Therefore, in order to ensure the normal operation of the system, ball-screw pitch should not be too small.

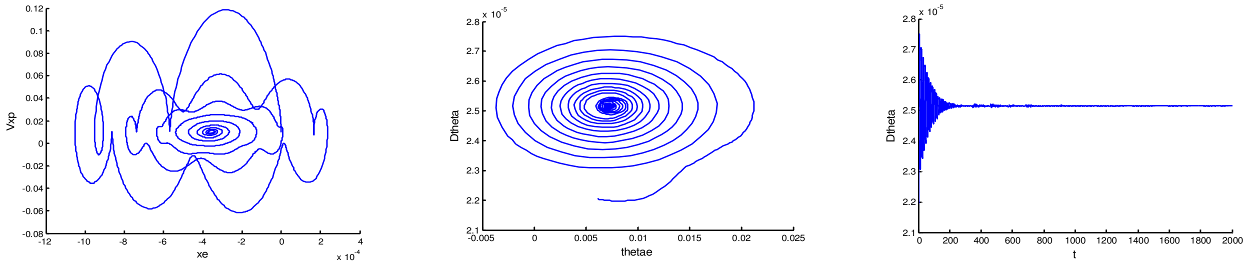

(a) Tracking Output phase diagram (b) Stepper motor phase diagram (c) Stepper motor angular speed

Fig. 3 Simulation in time domain when $t_2 = 3.63\times10^{-3}\mathrm{m}$

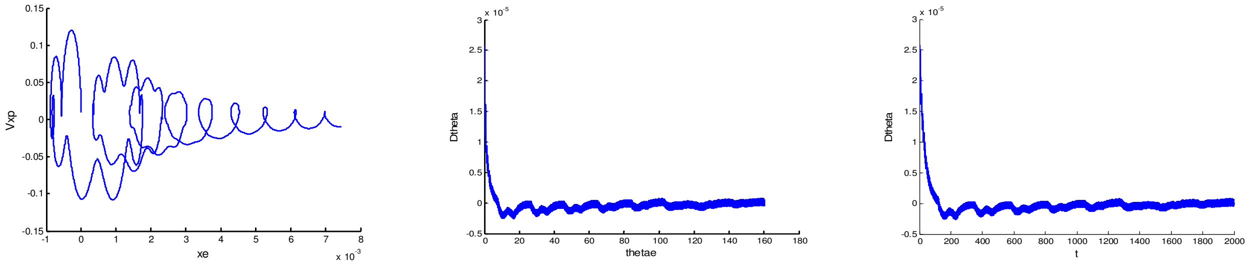

(a) Tracking Output phase diagram (b) Stepper motor phase diagram (c) Stepper motor angular speed

Fig. 4 Simulation in time domain when $t_2 = 2.63\times10^{-3}\mathrm{m}$

Conclusions

From the perspective of nonlinear dynamics, it's this paper proved in that, improper designs and selections of the parameters that piston diameter D_1, valve orifice area gradient w, ball-screw pitch t_2 and maximum desired velocity v_d, will result in Hopf bifurcation in the dynamic response of digital hydraulic cylinder, which block the stable system output following the input. Both stable limit cycle and unstable limit cycle exist in digital hydraulic cylinder tracking output phase plane, and the two cancel each other at the bifurcation point resulting in subcritical Hopf bifurcation. When closing to the bifurcation point, the system stability region diminishes, and the output flutters intensively, so the design parameters and operating parameters should be arranged away from the bifurcation points. Falling out of step for stepper motor is actually the occurrence of supercritical Hopf bifurcation and the birth of limit cycle near zero position, making it unable to control the digital valve opening and hydraulic cylinder output effectively, which maybe another form of dynamic instability.

References

[1] Junhong Yang, Shengyi Li, Yifan Dai: Mechanical Science and Technology for Aerospace Engineering, Vol. 26, No. 12(2007), p. 1625-1629. (In Chinese)

[2] B. Magyar, C. Hos, G. Stepan: Mathematical Problems in Engineering, Vol. 2010, p. 1-15.

[3] Shusen Zhang: Journal of Dynamic Systems, Measurement, and Control, Vol. 135 (2013), p. 1-10.

[4] Jia Chen, Jifeng Xing, Xiaohua Zeng, et al, in: Proceedings of the 3rd IEEE International Conference on Computer Science and Automation Engineering/IEEE, Guangzhou, China (2013), p. 1702-1706.

[5] Y. A. Kuznetsov: *Elements of Applied Bifurcation Theory* (Springer-Verlag, New York 2004).

[6] W. Govaerts, Y. A. Kuznetsov, V. De Witte, et al: MATCONT and CL_MATCONT: Continuation toolboxes in matlab, http://www.sourceforge.com/, (2011).

Applied Mechanics and Materials Vol. 596 (2014) pp 32-36
© (2014) Trans Tech Publications, Switzerland
doi:10.4028/www.scientific.net/AMM.596.32

Simulation on Kinetic Characteristics of Moving Mooring Marine Current Turbine System

Yingyuan Tian, Jian Yu , Shanchun Sun, Xiaotao Li

Yichang Testing Technology Research Institute
58 Shenglisan Road, Yichang, Hubei, China
yytian1980@126.com

Keywords: Simulation, kinetic characteristic, mooring, marine current turbine.

Abstract. This paper aims to get the kinematic performance and control parameters of moving mooring marine current turbine system such as velocity, period of motion, speed increasing ratio, motion trail, tension of cable, steerage and timing of control, strength of the platform and etc. This article first gets the hydrodynamic parameters with CFD and then builds the equations of motion, and the system simulation test was carried out with Matlab and Adams. The result shows that this moving mooring marine current turbine system can move on a designed trajectory by steering in flow environment. The velocity of the platform is about six to eight times to the current speed. The simulation lays a foundation for the development of engineering prototype. There have been plenty of information proved the theoretical breakthrough but we still need to face great challenge in the project practice in the coming future.

Introduction

Recently the marine current turbine has been identified as an important potential prototype for ocean renewable energy development. Especially the moving mooring marine current turbine system is one of the best choices due to its high efficiency.

Moving mooring marine current turbine is an advanced electricity generating system with moving platform and high strength cable, which moored at the sea bed as the mooring system, figure 1. When the velocity of marine current is large enough, the rudder is steered by automatic control. The platform moved at planned path with high speed times to the current velocity. The system flies underwater in the sea like a kite. The speed of the platform is about six to eight times to the current velocity, so the moving platform is much smaller compared to the traditional electricity generating system. For example, the turbine moves along the planning path with speed of 16m/s in flow with speed of 2m/s. The blade size of this system is about twentieth of the blade in traditional turbine. Therefore, the cost about manufacturing, installing, and maintenance is decreased dramatically. Thus the moving mooring marine current turbine has chance to be commercially operation in the coming future. The relationship between movement track and steering is in figure 2.

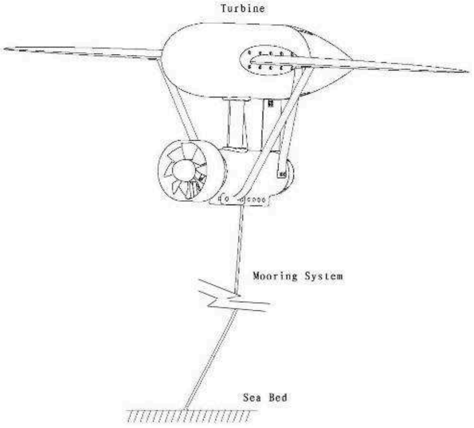

Fig1. The moving mooring marine current turbine system

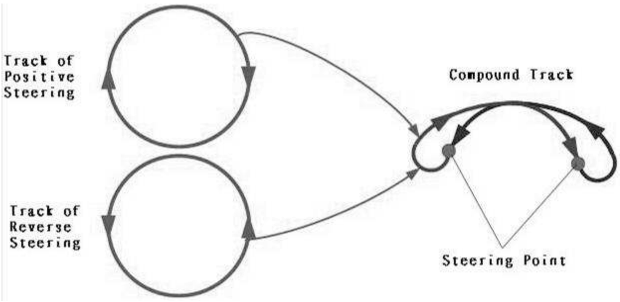
Track of Positive Steering
Compound Track
Track of Reverse Steering
Steering Point

Fig.2 The relationship between movement track and steering

Moving platform design

The design principle of the moving mooring marine current turbine system is that the platform is close to zero buoyancy underwater. The wings generate enough lift in the relatively low flow rate. The platform moves fast when steering the rudder because of the changing of force. The general parameters of platform include mass, center of mass, buoyancy, center of buoyancy, moment of inertia and so on. Design considerations also consist of the strength, the motion attitude and the maneuverability of the platform. As an experimental prototype, some necessary test equipments have to be equipped in the platform, see figure 3.

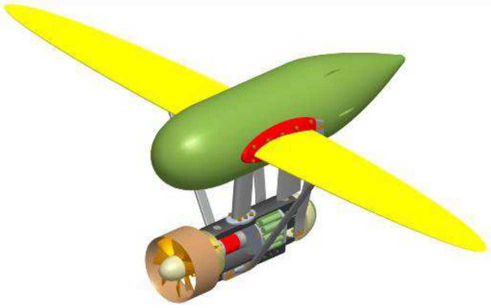

Fig3. The platform of the moving turbine

Numerical simulation of hydrodynamic parameters

The hydrodynamic parameters of the system are obtained from CFD. The steady and rotary force derivatives of the platform are based on numerical tunnel test with Fluent. The typical flow field is shown in figure 4.

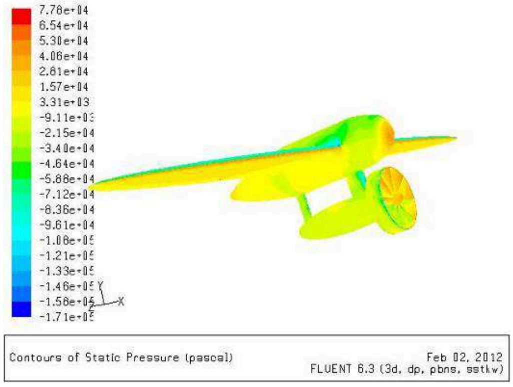
7.78e+04
6.54e+04
5.30e+04
4.06e+04
2.81e+04
1.57e+04
3.31e+03
-9.11e+03
-2.15e+04
-3.40e+04
-4.64e+04
-5.88e+04
-7.12e+04
-8.36e+04
-9.61e+04
-1.08e+05
-1.21e+05
-1.33e+05
-1.46e+05
-1.58e+05
-1.71e+05
Y
X
Z
Contours of Static Pressure (pascal)
Feb 02, 2012
FLUENT 6.3 (3d, dp, pbns, sstkw)

Fig.4 Simulation on flow field in numerical tunnel

The resistance characteristics vary with angle of attack and sideslip angle due to the only one symmetry plane of the platform. The drag coefficient with angle of attack and sideslip angle is shown in figure 5.

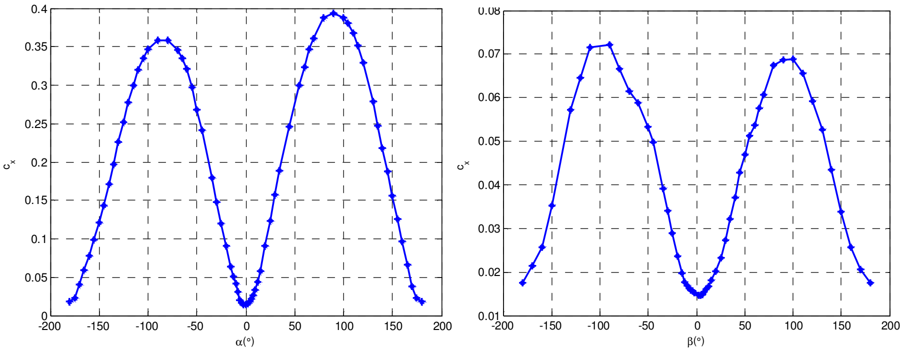

Fig.5 Drag coefficient curve with angle of attack and sideslip angle

Movement modeling of the system

Study the motion characteristics of the system by building and analyzing the mathematical model. The mathematical models of the platform underwater include dynamical equations and kinematics equations. The dynamical equations are based on momentum equations of space rigid. The kinematics equations are based on transforming between fixed coordinates and moving coordinates. The dynamic characteristic of the whole system is described as follows,

$$\frac{d(m\vec{V}_C)}{dt} = \vec{F} \tag{1}$$

$$C_{eb} = C_1(\varphi)C_3(\theta)C_2(\psi) \tag{2}$$

The mathematical model of the cable is a multi-body dynamics model taking into account the hydrodynamics. The platform is as an end node to provide the boundary conditions. Continuous cable is dispersed as a series of hinged cable segments and analyzed with multi-body dynamics separately. We divide the cable into 100 segments considering the computational accuracy and calculation speed.

In this paper the mathematical model of the cable is build with programming languages of Adams, see figure 6.

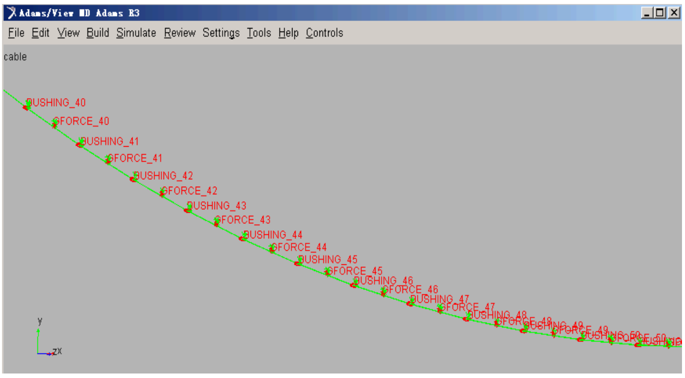
Adams/View MD Adams R3
File Edit View Build Simulate Review Settings Tools Help Controls
cable
BUSHING_40
GFORCE_40
BUSHING_41
GFORCE_41
BUSHING_42
GFORCE_42
BUSHING_43
GFORCE_43
BUSHING_44
GFORCE_44
BUSHING_45
GFORCE_45
BUSHING_46
GFORCE_46
BUSHING_47
GFORCE_47
BUSHING_48
y
zx

Fig.6 Mathematical model of the cable with Adams

Simulation and test of the system

The aim of the simulation is to get the system features, in order to verify and optimize the design. The following below is a system-level multidisciplinary collaborative simulation schematic. The collaborative simulation based on Matlab and Adams includes structure, fluid mechanics, multi-body dynamics and control disciplines, see figure 7.

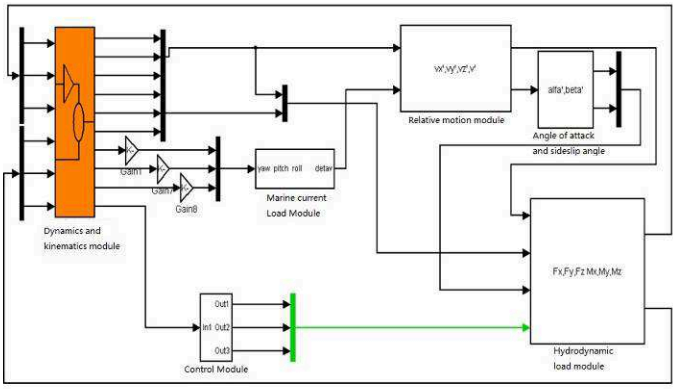
vx',vy',vz',v'
Relative motion module
alfa',beta'
Angle of attack and sideslip angle
Gain1
Gain7
Gain8
yaw pitch roll detav
Marine current Load Module
Dynamics and kinematics module
Fx,Fy,Fz Mx,My,Mz
Out1
In1 Out2
Out3
Control Module
Hydrodynamic load module

Fig.7 Co-simulation model diagram of the system

From the schematic we can see the co-simulation model include kinematics and dynamics module, marine current load module, relative motion module, angle of attack and sideslip angle solving module, hydrodynamic loads module and control module. The scaled model simulation results under 1m/s flow speed are shown below, figure 8 and figure 9.

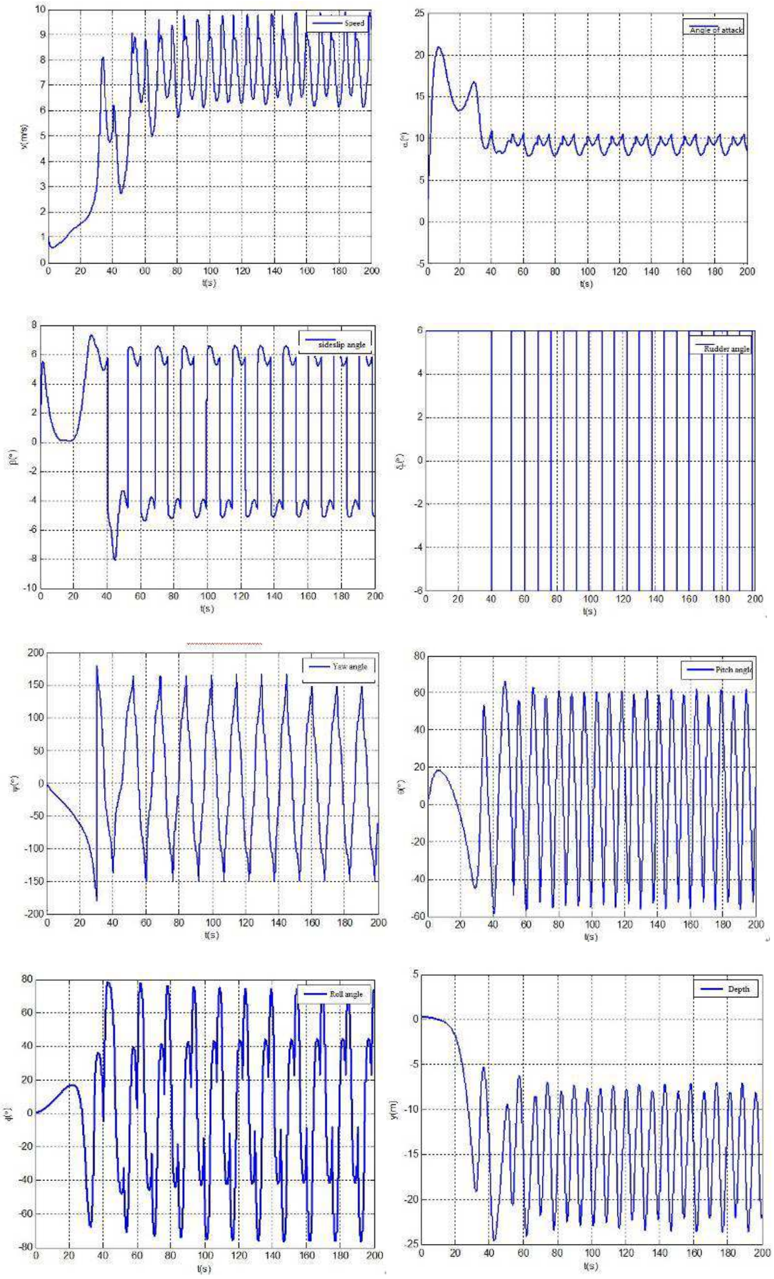

Fig.8 Attitude, rudder angle, depth and speed curve

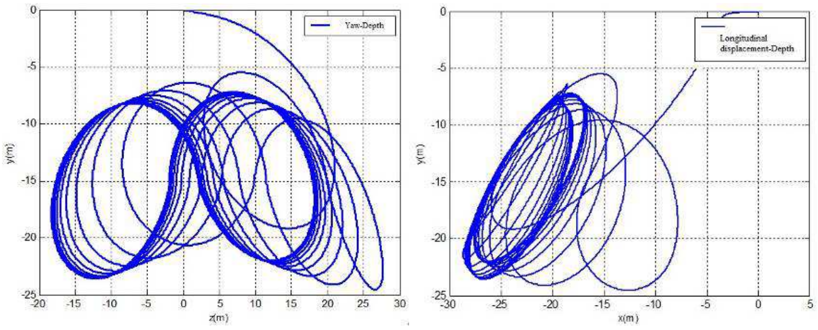

Fig.9 Trajectory of the platform

Conclusions

The simulation results show that the moving mooring current turbine is a high efficient prototype to be applied in developing ocean energy, although further work is necessary to prove the performance and reliability in real ocean environment. The system has large speed increasing ratio and can move along the designed track under automatic control.

Acknowledgement

Authors gratefully acknowledge Yichang Testing Technique Research Institute for its technical and financial support.

References

[1] Van Zwieten, J.H. : Florida's Center for Ocean Energy Technology, OCEANS, 2008

[2] Lisa A. Levin, Ron J. Etter,2Michael A. Rex, Andrew J. Gooday, Craig R. Smith, Jesu´ s Pineda, Carol T. Stuart, Robert R. Hessler, and David Pawson: Environmental influences on regional deep-sea species diversity, Annu. Rev. Ecol. Syst. 2001. 32:51–93

[3] Hill F A, Havel T F and Livermore C: Modeling mechanical energy storage in springs based on carbon nanotubes, Nanotechnology. 2009

[4] Chesnokov S A, Nalimova V A, Rinzler A G, Smalley R E and Fischer J E: Mechanical energy storage in carbon nanotube springs Phys. Rev. Lett. 1999

[5] O. Sulaiman & A.H. Saharuddin: Power integrity requirement of new generation of ROV for deep sea operation, Global Journals Inc, 2012

[6] Information on http://www. minesto.com/

[7] Information on http://www.emec.org.uk/

CHAPTER 2:

Materials Processing and Advanced Manufacturing Technology

Applied Mechanics and Materials Vol. 596 (2014) pp 39-42
© (2014) Trans Tech Publications, Switzerland
doi:10.4028/www.scientific.net/AMM.596.39

Situation of Natural Gas Hydrate Research

Zhang Li [a], Men Hong Kun [a], Zhuli Ming Ming [b], Zhang Shu Yang [a]

[a] School of Energy, China University of Geosciences, Beijing 100083, China

[b] Society of Petroleum Engineers, University of Southern California, Los Angeles CA 90089-0911, America

leahor@foxmail.com

Keywords: Natural Gas Hydrate; Environmental problems; Research situation

Abstract. Natural Gas Hydrate has become a research focus at home and abroad at present. This paper expounds the concept of natural gas hydrate and its types. Analyze its study process and research situation, and make a brief description of its distribution, mining and related environmental problems by tracking the discovery history of gas hydrates. Then put forward the problems in instant need of solving and the key research contents.

Introduction

Gas Hydrate is solid crystalline compounds which is formed by Methane gas molecule that is naturally enclosed in water molecules expands crystal lattice at particular pressure and temperature. It is also known as frozen methane, methane hydrates. Sometimes ethane, propane, butane, carbon dioxide and hydrogen sulfide and methane can also be mixed together to form a solid gas hydrate. Gas hydrate is a new type of clean energy and mineral resources which is discovered and valued in 20th century. It is estimated that the amount of its resources is twice the total amount of world's coal, oil, natural gas resources, and it is the largest unknown untapped energy libraries on the planet. In 1810, gas hydrates was first discovered in the laboratory. The early 1960s , the former Soviet scholars found natural gas hydrate output Siberian permafrost by seismic geophysical methods, but it did not draw attention . In 1964 ,when drilling in Merisel Jaca gas field in Siberia in Russia , first discovered the presence of gas hydrates in nature .As an important type of energy it gained worldwide attention and research.

Gas as Hydrate Research Status

Gas hydrate crystalline lattice is mainly composed by water molecules, and at low pressure and different conditions, crystallization water molecules may form different types of polyhedral cage structure. Its basic feature is its high gas concentrate ability that is 1 cubic meter of gas hydrate can release 164 cubic meters of natural gas and 0.8 cubic meters of fresh water at normal temperature and pressure, which is determined by the empty space of the crystal structure and lattice frame. According to the lattice structure, the gas hydrate can be divided into type Ⅰ, Ⅱ and H. Type Ⅰ lattice cage pile arrangement as each cage body-centered forming a cubic crystal structure. The lattice cage has sufficient space to accommodate methane, ethane, and other gases with similar molecules (such as carbon dioxide, hydrogen sulfide, etc). Type Ⅱ lattice cage is larger, forming diamond-type crystal structure. It can accommodate not only the gas molecules such as methane and ethane, but also can accommodate molecules larger size such as propane, isobutene, butane gas. Type H is hexagonal crystal structure. Type Ⅰ gas hydrates is the most widely distributed in nature, while the type Ⅱ and H is more stable. Methane - methane hydrate water stable system temperature and pressure, not only depending on the gas mixture (in addition to other methane gas) components, but also on other gases and components of ionic impurities in the water. Adding methane carbon dioxide, hydrogen sulfide, and other components of ethane and propane hydrate equilibrium curve shifts to the right, the hydrate stability field area will be expanded; contrast, in the water by adding sodium chloride salt, hydrate equilibrium curve move to the left, an area of narrow hydrate stability field (Fig.1).

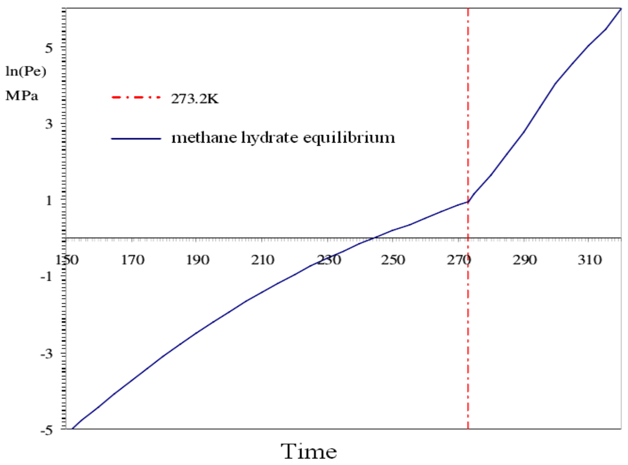

Figure.1 Methane hydrate phase-equilibrium curve in pure water

As the world oil and gas resources increasingly depleted, scientists from countries are working to find new energy to succeed. Meanwhile, with the increasing amount of gas hydrate found in tundra and marine. Its potential strategic significance and considerable economic attracted great attention of many governments.

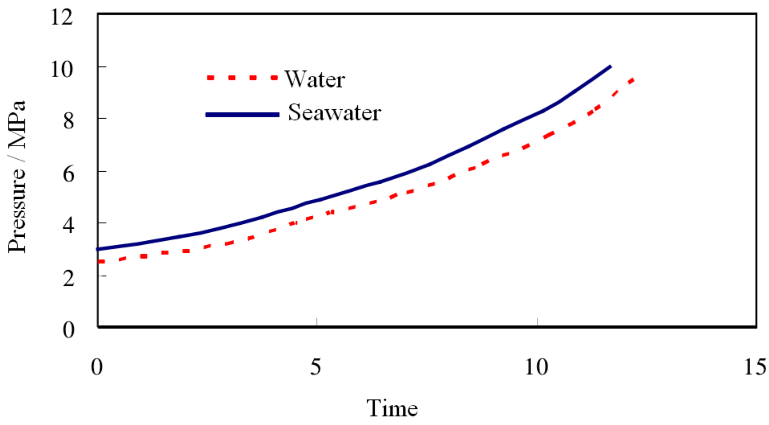

Figure.2 Methane hydrate phase-equilibrium curve in water and seawater

They have invested heavily in the establishment of specialized agencies to research to become the new hot spot in the 21st century potential new energy research. Until now, we has directly or indirectly discovered gas hydrates in more than 60 waters in the world, where we saw 18 gas hydrate drilling cores and 42 signs of gas hydrate BSR earthquake. Currently, gas hydrate research focused on the following aspects: the determination and assessment of gas hydrate resources, environmental issues and their development prospects the gas hydrate facing, and gas hydrate storage and use of technology.

Distribution of Gas Hydrates. The world has been found the evidence the existence of gas hydrates in more than 40 waters. Preliminary estimates of global reserves of natural gas hydrate resources : the methane gas is about 1×1015～1×1017 m 3 (average 21×1015 m 3), methane carbon is about 10000Gt. In the world gas hydrate resources, if only 1 to 2 % of the economically recoverable reserves are also a great source of energy. Gas hydrate resources distributed as follows : the amount of natural gas hydrate prospective resources estimated from north to Alaska, Bering Sea , offshore California , Central America Trench, Panama Basin , Columbia Basin , Gulf of Mexico , a Bach Ma Hailing Blake , Baltimore Canyon, to the Eastern Canada offshore may be more than (760～2 915)×1012ft3 .

Gas Hydrates Production. At present gas hydrate mining that has invested in the international are in the tundra Messoyakh field in western Siberia and the Canadian Beaufort Sea Mackenzie Delta edges. The methods used are thermal stimulation, decompression, mixed mining and injecting inhibitors.

With gas hydrate exploration, its related environmental problems and geological disasters also need attention. In land coastal areas the amount of methane the gas hydrates archived may be 3000 times of the amount of methane in the atmosphere. Dimensionless permeability with increasing hydrate saturation decreases, when the lower hydrate saturation, dimensionless permeability decreases faster when higher hydrate saturation, dimensionless permeability decreases more slowly. Corresponding to a different type of porous media regression parameters, different dimensionless penetration rate of decline, while Fig.3 shows the take different values corresponding to N different dimensionless permeability curves can be seen that the more experienced index large, dimensionless permeability decreases faster.

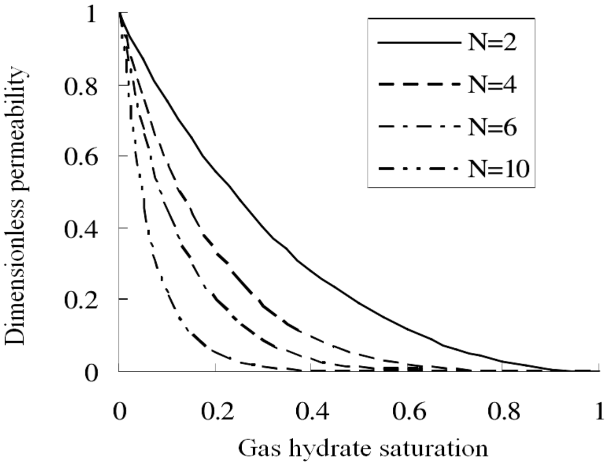

Figure.3 Dimensionless permeability as a function of NGH saturation

These areas release large amounts of methane which significantly affect the atmospheric composition and thermal radiation properties of the atmosphere thus affecting the global climate. During the exploitation of gas hydrates, if large amounts of methane gas is emitted into the atmosphere, which is bound to further aggravate global warming. In addition, gas hydrate exploration is also very likely lead to collapse. Continuous deposition leads to gas hydrates burring deeper, eventually the burial depth is enough to change the temperature of stability bottom zone, so that the state is no longer stable gas hydrate. Therefore, the consolidation of the gas hydrate bottom zone reduced and the gas releasing formed overpressure. The gravity load or seismic disturbances caused the collapse of the fragile trigger zone (or low shear strength band) and submarine landslides

Gas Hydrate Research in China. In the late 1980s, we began to focus on the studies of gas hydrates. In 1999, the Guangzhou Marine Geological Survey carried out preliminary investigation of gas hydrate resources in the Xisha Trough, which kicked off a large survey of marine gas hydrates work. In recent years, leaders and MLR Science and Technology, Ministry of Finance, the State Planning Commission and other ministries attach great importance to the investigation and study of gas hydrates. In 863 Plan, supported by the National Science Foundation to carry out individual projects such as collecting research techniques, physical modeling and numerical simulation techniques, seismic recognition technology, to preliminary forecast the amount of marine gas hydrate resources. Lanzhou Institute of Geology, Chinese Academy of Sciences, Guangzhou Institute of Geochemistry, Cold and Arid Regions Environmental and Engineering Research Institute and other units have carried out geological, geochemical and experimental research related to simulation.

Petroleum University, Daqing Petroleum Institute and other units has achieved important results in the development of gas hydrates in the laboratory simulation technology ,pipeline detection and clearance studies of natural gas hydrate technology. Commissioned by the China Geological Survey Bureau, China Nonferrous Geological Exploration Institute of Gansu taked the “gas hydrates in permafrost regions of the pre- geochemical exploration research" project. In 2005, the exploration taked the “Qinghai-Tibet Railway remote sensing identification of gas hydrate research" project.

National Natural Science Fund Committee also set up a " formation conditions of gas hydrates in permafrost regions of discussion " of the project, which is undertaken by the CAS Cold and Arid Regions Environmental and Engineering Research Area.

Conclusion

Gas hydrate is an important alternative energy in "post-oil era". With the thorough of the research, the urgent problems faced as the following main points: look for the most efficient production methods; affect the development of gas hydrates on the climate; drilling problems; energy status of gas hydrates. In addition, research should focus on how to obtain useful information (such as logging, core and drilling records), improve the geological model and geophysical exploration methods and improve production technology. Since the hydrate reservoir in the development process, the saturation degree of change is much greater than the hydrate dissolution and fouling occurs in the reservoir, and the synthesis and decomposition of hydrate obviously accompanied by the exothermic and endothermic phenomenon hydrate reservoir temperature changes will be more significant, these factors do not exactly lead to changes in the relationship between permeability and saturation hydrate reservoir and hydrocarbon reservoirs, therefore, also need to do more research in this area.

Reference

[1] S.X. Liu, P. Guo and J.F. Du. Natural Gas Industry. Vol 25(2005), p. 121.

[2] K. Wu. Northern Economy and Trade. Vol 11(2008), p. 135.

[3] Y.M. Yuan. Science and technology information. Vol 4(2006), p. 370.

[4] Y. Song and S.B. Liu. Petroleum & Petrochemical Today. Vol 14(2006), p.17.

[5] G.C. Huang: The Process of Resource Exploration and Estimate for Submarine Gas Hydrate(MS, China University of Geosciences, China, 2008).

[6] K.L. Pan. Stability Study of Natural Gas Hydrate Reservior (MS, China University of Petroleum (East China),2009)

[7] X.Y. Long, Z.M. Yuan and J. Ni. Progress in Exploration Geophysics. Vol 29(2009), p. 170.

[8] H.Xu, J.Q. Huang and B. Xia. Natural Gas Industry. Vol25(2005), p. 21.

[9] Buffett B A, Zatsepina O Y. Formation of gas hydrate from dissolved gas in natural porous media[J]. Marine Geology, 2000, 164(11): 69-77.

[10] Handa Y P, Stupin D. Thermodynamic properties and dissociation characteristics of methane and propane hydrates in 70 A radius silicagel pores[J]. J. Phys. Chem. 1992, 96(8): 599-603.

[11] Clennell M B, Hovland M, Booth J S, Henry P, Winters W J. Formation of natural gas hydrate in marine sediments. Part l: Conceptual model of gas hydrate growth conditioned by host sediment properties[J]. J. Geophys. Res. 1999, 104(22): 985-1003.

[12] Yousif, M. H.. Experimental and theoretical investigation of methane—gas-hydrate dissociation in porous media[C]. SPE Reservoir Engineering(Society of Petroleum Engineers), 1991, 6(1): 69-76.

[13] Laura A Stem. Stephen H Kirby. Peculiarities of methane clathrate hydrate formation and solid-state deformation, Including Possible Superheating of Water Ice. Science, 1996, 7(1): 843-848.

[14] Kvenvolden K A. A review of geochemistry of methane in nature gas hydrate[J]. Organic Geochemistry, 1995, 12(11/12): 997-1008.

Applied Mechanics and Materials Vol. 596 (2014) pp 43-46
© (2014) Trans Tech Publications, Switzerland
doi:10.4028/www.scientific.net/AMM.596.43

Study on the stainless steel 1Cr18Ni9Ti micro-hole drilling experiment

Benhong Li[1,a] , Zhi Liu[2,b], Hao Wang[3,c], Zaosheng Zhong[4,d]

[1,2,3,4]Foshan Professional & Technical College, Foshan 528137, China

[a]lbh_1974@163.com, [b]lzchhuyy@163.com, [c]gdwanghao@sina.cn, [d]zhongzaoshen@163.com

Keywords: 1Cr18Ni9Ti, Micro-hole, Drilling Force, Simulation analysis, Empirical formula.

Abstract. Stainless steel is difficult to machine, especially micro-hole machining. In order to obtain the effect of drilling force by tool material and cutting parameters, the drilling experiments on stainless steel 1Cr18Ni9Ti have been done by diameter of 1.2 mm containing cobalt high speed steel and carbide drill. According to the experimental results, analysising the reason of drilling force change under different parameters and establishing a carbide drill drilling force empirical formula which combined with the regression analysis method.

Introduction

As the advantages of acid and alkali resistant ability, high mechanical property, glossy and beautiful surface, etc, stainless steel 1Cr18Ni9Ti is widely applied to the fields of spaceflight, aviation, chemistry, medicine, architecture and so on. But its high plasticity, high toughness, small thermal conductivity, high cutting temperature and good cohesiveness result in bad machinability, the shorten life of cutters [1]. Micro-hole machining, although many global experts have done a large amount of experiments and researches for this machining of stainless steel material, is still a big difficulty in holes machining [2,3].

Based on the structure and operating principle of drilling template, Peifei Yang has concluded some experience of tolerance matching and selection in tiny bite's guide sleeve, deduced some critical influencing factors of tolerance matching and selection by optimized calculation[4]. Lanying Xu and some experts have found this theory is consistent with the actual through analyzing the variation of drilling force in stainless steel 1Cr18Ni9Ti drilling process by finite element software and comparing with actual data [5]. Other experts like Jian Wu also has affirmed the unworkability of stainless steel from drilling experiments, comparing 1Cr18Ni9Ti with 45 steel, and made a sequential conclusion on its influencing factors [6].

The aim of this essay, using cobalt high speed steel and hard alloy drill bit, 1.2mm in diameter, for drilling experiments on stainless steel 1Cr18Ni9Ti, is to explore the variational rule of drilling force, caused by tool material and cutting parameters, and establish an empirical formula based on cutting force F and torque M of hard alloy cutter.

Drilling experiment

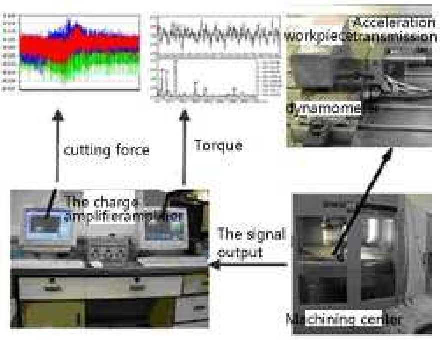

Fig 1 Drilling Experiment Equipment

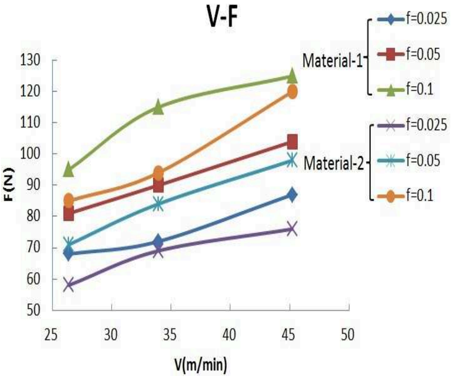

Fig 2 Force Result Data

Trial equipment. This drilling experiment was done on Germanic CNC machining center. Equipment is shown in Figure 1, it includes DMU60T CNC machining center, acceleration sensor, computer, YDM-III99 dynamometer and charge amplifier. Through data collection in specialized integrated software, the cutting force of cutter in X, Y and Z three directions can be measured by YDM-III99 dynamometer.

Parameter setup. Cobalt high speed steel and hard alloy drill bit, 1.2mm in diameter, and trial material 1Cr18Ni9Ti, 3mm thick, were applied to the experiment. Parameters of experiment as shown in Table 1.

Table 1 Experiment Parameter

Drill material	Spindle speed n(r/min)	The amount of feed f(mm/r)	Drilling spee V（m/min）
High speed steel with cobalt	7000	0.025	24
	9000	0.05	34
	12000	0.1	45

Experimental data. We choose the single factor experiment method, in which one of drill material, speed, the amount of feed and drilling speed is variables, the others are fixed quantity. The datas obtained from experiment as show ed in Table 2:

Table 2 Experiment Result

Drill material	Spindle speed n(r/min)	The amount of feed f(mm/r)	Drilling spee V（m/min）	The cutting force $F(N)_{Max}$
High speed steel with cobalt drill	7000	0.025	26	68
	7000	0.05	26	81
	7000	0.1	26	95
	9000	0.025	34	72
	9000	0.05	34	90
	9000	0.1	34	115
	12000	0.025	45	87
	12000	0.05	45	104
	12000	0.1	45	125
Carbide drill	7000	0.025	26	58
	7000	0.05	26	71
	7000	0.1	26	85
	9000	0.025	34	69
	9000	0.05	34	84
	9000	0.1	34	94
	12000	0.025	45	76
	12000	0.05	45	98
	12000	0.1	45	120

Analysis of experimental result

Material of drill bit. A trend graph, figure 2, was made and a relationship between V and F was got from two drill bits with different materials in the same conditions according to the trial data. As shown in figure 2, the cutting force F of cobalt high speed steel drill bit is obvious higher, approximate 4% to 17%, in the same conditions than hard alloy's throughout the cutting experiment. And its torque is higher than hard alloy's as well. Cause analysis: Resulted from material, the thermal conductivity and heat resistance of hard alloy drill bit is higher. And in the same conditions, higher thermal conductivity and heat resistance are good for heat dissipation, resulting in lower operating temperature and smaller deformation, when it's drilling. Therefore, it ensures smaller cutting force, going after better cutting ability.

The amount of feed. As shown in Figure 2, the cutting force F of cobalt high speed steel and hard alloy drill bits, when it's drilling, is proportional to their drilling feed f, and increases accordingly. Similar to the effects of material, the cutting force F of cobalt high speed steel drill bit is also higher, about 4% to 17%, in the same conditions. Cause analysis: As the drilling feed f increases, the cutting quantity per unit time will increase as well. Hence, it means that the cutting force is higher as the result of more energy input.

Drilling speed. the cutting force F will increase accordingly as the speed of mainshaft become faster and faster, especially when V>35m/min. The reason is: Because of higher drilling speed, the cutting quantity per unit time increases and scrap iron can't be discharged well, so it causes an rapid increase in F as the drill bit and scrap iron bound together. It could be worse when drilling feed increases at the same time. Figure 3 is about the cutting effect when drilling speed V=34m/min and drilling feed f=0.1mm/r. At that time, the scrap iron is too much to be discharged, and this problem could lead to lots of burr and flash when the hole is drilled.

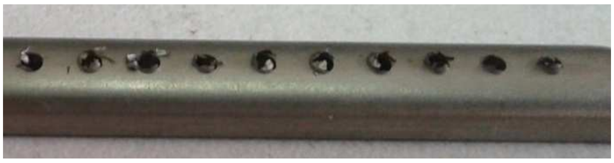

Fig.3 Drilling Glitch

Formula derivation

Table 3 Regression analysis

The serial number	lgf	lgV	lgF(y)
1	-1.6051	1.4148	1.7630
2	-1.3005	1.4155	1.8517
3	-1.0000	1.4153	1.9295
4	-1.6021	1.5317	1.8377
5	-1.3013	1.5312	1.9245
6	-1.0000	1.5317	1.9730
7	-1.6022	1.6533	1.8807
8	-1.3008	1.6535	1.9944
9	-1.0000	1.6534	2.0790

Establish formula. An empirical formula, about the cutting F of stainless steel 1Cr18Ni9Ti when using 1.2mm in diameter hard alloy drill bit to drill, was established by regression analysis method, drilling speed V and feed f as underlying variables, according to the trial data. And the essay has verified its feasibility [7]. On the basis of "Mechanical processing craft manual", an assumption of the formula as follow:

$$F = A\mathrm{f}^{\mathrm{a}} v^{b} . \tag{1}$$

A, a, b as three coefficients need to be solved among this non-linear relationship formula. In order to use least square method, formula (1) should be linearized：

$$\lg F = \lg A + a \lg f + b \lg v . \tag{2}$$

$$y = \lg F, c = \lg A, x_1 = \lg f, x_2 = \lg v .$$

$$\Rightarrow y = c + ax_1 + bx_2 \ . \tag{3}$$

The computations, based on the principle of least square method and combined with table 2, are shown in table 3, the derivation of the formula (4) as following :

$$\hat{y} = 1.4001 + 0.276x_1 + 0.5698x_2 . \tag{4}$$

$$\mathrm{c} = 1.4001, a = 0.2761, b = 0.5698$$

$$\Rightarrow F = 25.1246\mathrm{f}^{0.2761} v^{0.5698} . \tag{5}$$

Analysis of formular feasibility. The visibility and feasibility of this formula, combined with all the derivation and data, are shown in Table 4:

Table 4 Calculating Data

Source	Sum of squares	DOF	Variance	F	Significance
Return Value	U=0.0688	M=2	U/M=0.0348	150.34	α=0.01
Residual Value	Q=0.0013	N-M-1=6	σ^2=0.00027		
Sum	S=0.0705	8			

As shown in Table 4, $F = 150.43 > F_{0.01}(2,6) = 10.92$， the formula is visible when α=0.01. The regression of this formula, regression sum of squares are far greater than residual sum of squares, is visible by examining F. And the cutting formula is recognized as feasible.

Conclusions

An experimental result was got by using cobalt high speed steel and hard alloy drill bit, 1.2mm in diameter, for drilling experiments on stainless steel 1Cr18Ni9Ti. Besides, a cutting formula, drilling speed V and feed f as underlying variables, was established through analyzing the reason for changing cutting force from drill bit's material, drilling feed and speed. It can provide an reference for setting parameter when using 1.2mm in diameter hard alloy drill bit on stainless steel drilling.

Literature References

[1] Jun Xu, Gang Cao. Technological improvement on stainless steel drilling [J]. Equipment Manufacturing Technology, 2009(5): 158-159.

[2] Jun Cheng, Feng Jiao. Research status on micro-hole drilling process [J]. Mechanical Engineer, 2007(11): 9-11.

[3] Zhirong Huang. Research and optimization on micro-hole machining technological parameter[D]. Northeastern University, 2005, 2.

[4] Peifei Yang. Design method of drill fence plate [J]. Textile Machinery, 2005(1): 42-44.

[5] Lanying Xu, Bangyan Ye, Qiang Wu. Simulation and experimental research on stainless steel 1Cr18Ni9Ti hole drilling [J]. Proceedings on the 13th annual seminar from the national manufacturing automation research institute of high universities, 2008: 27-30.

[6] Jian Wu, Yongdi Han. Drilling trial research on austenitic stainless steel 1Cr18Ni9Ti [J]. Tool Engineering, 2008（42）： 12-15.

[7] Houde Peng. Analysis of dependence from spring oscillator's empirical formula [J]. Journal of Chongqing liberal arts Institute, 2012, 8（4）： 50-54.

Applied Mechanics and Materials Vol. 596 (2014) pp 47-51
© (2014) Trans Tech Publications, Switzerland
doi:10.4028/www.scientific.net/AMM.596.47

The influence of electric parameters on the surface quality of ceramic in internal grinding using the ultrasonic and ELID composite grinding

You Yi Zheng[1,a*], Hao Pang[2,b], Qi You[3,c],and Xiao Feng Jia[4,d]

[1,2,3,4]School of Powere and Mechanical Engineering,Henan Polytechnic University,Jiaozuo

[a,b,c,d]hpuph@126.com

Keywords: Ultrasonic Grinding;ELID grinding;Electrical parameters;Oxide film;Ceramics;Surface quality

Abstract: Analyzed the relationship between electrical parameters of the ultrasonic and electrolytic in-process dressing (ELID) composite grinding and the surface quality of the ceramic through the experiment. The value of the voltage and the current were recored by labview and the surface quality of the ceramic was tested using Talysurf CCI 6000 In the experiment. The results show that the selection of electrical parameters affects the electrolysis speed of diamond grinding wheel and the speed of the oxide film formed and the quality of the oxide film, and then affects the grinding performance of the grinding wheel and the grinding quality of workpiece.

Ceramics is a kind of typical hard -brittle materials with high hardness,is becoming more and more people's attention with the widely application . Efficient mirror processing technology is an important branch of ultra-precision machining technology of hard and brittle materials, which has important implications for the development of aerospace, microelectronics, information, defense and optoelectronics and other advanced technology[1,2]. Currently, the study of conventional technology of mirror finishing of hard-brittle materials is more mature and perfect, but the prominent disadvantages are low efficiency and high cost. Ultrasonic machining is suitable for processing a variety of hard and brittle materials and complex cavity with high precision, but low efficiency [3,4], while ELID grinding has high precision ,high efficiency and conducives to the promotion, but difficults to discharge debris[5]. Therefore, the authors proposed combining ELID grinding and Ultrasonic grinding to study the effects of electrical parameters of composite grinding on the surface quality. At present,The domestic research of ELID grinding is concentrated in the process,Mainly is the electrolytic generation and control of the thickness of the oxide film is not easy to be achieved[6], the surface quality is not very good after grinding,while the ultrasonic vibration conducive to the smooth discharge of debris with Cavitation, Pump suction effect and Eddy current effect , the surface quality improved significantly after processing[7].

Basic principle of the ultrasonic and ELID composite grinding technology

In the ultrasonic and ELID composite grinding， the electric signal generated by the ultrasonic power source was converted into magnetic energy in the first coil via a wireless transmission device, in the second coil, the magnetic energy was converted into electrical energy in turn,and then the electrical signal was converted into mechanical vibrations by the transducer, which cannot be used for processing because its frequency is large and the amplitude is small, Then amplified mechanical vibration by horn to work through the tool wheel. For ELID grinding, The metal-bond (iron-based) diamond abrasive wheel was connected to positive terminal of a power supply via electrical contact, Copper as the negative terminal of the power supply for good conductivity can be fixed by adjusting bolts and complete insulation with other objects, there is a certain clearance between the negative power and the grinding wheel that can be adjusted by the adjusting screw, when the specific grinding liquid with electrolysis through the gap, The iron-based metal binder on the surface of the grinding wheel can be sustained electrolysis so that the new sharp diamond grit being exposed gradually to realize the role of wheel dressing. While a layer of dense, non-conductive oxide film is formed on the surface of the grinding wheel to suppress the wheel excessive electrolysis and prevent the wheel transition loss ,The bare diamond abrasive of the grinding wheel is always in a state of sharp to grinding process continuously. Using the wireless transmission device can effectively prevent the wire winding caused by the spindle during rotation.When the abrasive on the surface of wheel worn down due to the continuous grinding, the oxide film on the surface will be scratched and removed by the workpiece material, and then the electrolytic process continues, the same to the truing of the wheel.

Efficient grinding experiment of ceramic using the ultrasonic and ELID composite grinding

2.1 The effect of the supply voltage on the surface quality

Test parameters:ultrasonic frequency:34.435KHz, spindle revolution:1000r/min, electrode gap :0.2mm, duty ratio: 50%, ultrasonic amplitude: 8.2μm. Test in three different voltage 60V, 90V, 120V without change of other parameters, respectively.

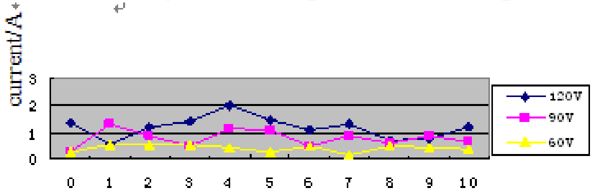

Fig.1 Relationship between electrolytic current and time

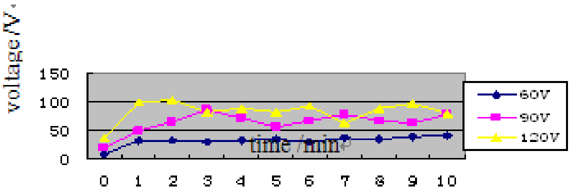

Fig.2 Relationship between electrolytic voltage and time

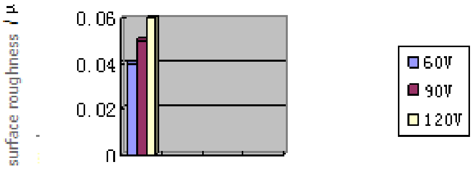

Fig.3 The surface quality of ceramic under different voltage

Fig.1 shows The curve of the current change with time measured in the test every minute during the 10 minutes from the start with 120V, 90V, 60V three voltages, respectively.

Fig.2 shows The curve of the voltage change with time measured in the test every minute during the 10 minutes from the start with 120V, 90V, 60V three voltages, respectively.

Fig.3 shows The surface quality of the ceramic measured after test in 120V, 90V, 60V three voltages, respectively.

The test results and analysis: As can be seen from Figure1, 2, the electrolytic current into a decreasing trend with time increasing, while the electrolytic voltage rise. The higher the electrolytic voltage, the faster the current decreases, because the electrolytic voltage is high , the electrolytic current generatied is big, So that the faster the speed of forming the oxide film, but the oxide film is not conductive, so the electrolytic current rapidly decreases. High voltage and high current speed up the process of electrolysis of grinding wheel , Lead to grinding wheel loss too rapidly.

In the case of the other parameters do not change, the surface quality of the ceramic increases with the increase of the electrolysis voltage in three different voltages 60V, 90V, 120V ,respectively.

Because the electrolytic voltage is large ,the electrolytic current is also relatively large, and the rate of decline is fast,electrolytic corrosion on the wheel is also fast. Electrolytic capacity is strong, the insulation of the oxide film is relatively weak and the thickness of the oxide film is thickening, the height of grit protrusion is large, the surface quality is relatively large when grinding. While the voltage is low, the thickness of the oxide film is relatively thin, the height of grit protrusion is small, it can work out a smooth surface, The surface quality is relatively small compared with the high voltage.

2.3.2 The effects of the duty ratio on the surface quality

Duty ratio is the ratio of Pulse takes up time and the total time in a continuous working period, The size of the duty ratio affects the time to participate in the electrolysis directly, then affects the electrolytic rate of the grinding wheel.

Test parameters: ultrasonic frequency 34.435KHz, spindle revolution 1000r/min, electrode gap 0.2mm, supply voltage 60v , ultrasonic amplitude 8.2μm. Test in four different duty ratio 0.25, 0.5, 0.67,0.75without change of other parameters, respectively.

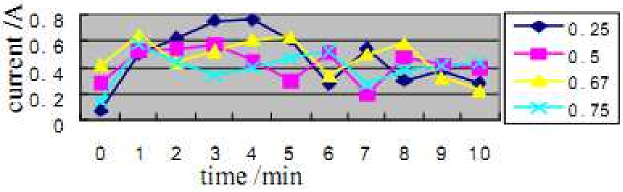

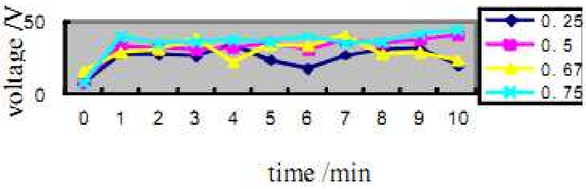

Fig.4 Relationship between duty ratio and electrolytic current

Fig.5 Relationship between duty ratio and electrolytic voltage

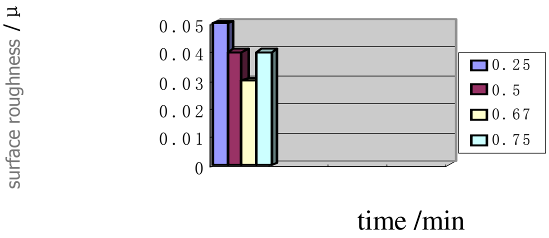

Fig.6 Relationship between duty ratio and the surface quality

Fig.4 shows The curve of the current change with time measured in the test during the 10 minutes from the start when duty ratio were0.25, 0.5, 0.67, 0.75,respectively.

Fig.5 shows The curve of the voltage change with time measured in the test during the 10 minutes from the start when duty ratio were 0.25, 0.5, 0.67, 0.75,respectively.

Fig.6 shows The surface quality of the ceramic measured after test when duty ratio were 0.25, 0.5, 0.67, 0.75,respectively.

The test results and analysis: It can be seen from the data of the figure 4, figure 5and figure 6 the surface quality of the ceramic increases with the increase of the duty ratio. the roughness is opposite bigger when the duty ratio was 25%, while the roughness is the best and the surface is the most smooth when the duty ratio was 67%. This is because electrolytic capacity is stronger with the increase of duty ratio, then the electrolytic current increases, and then electrolytic speed increases, the greater the thickness of the oxide film formed. However the duty ratio is so large that the generated oxide film electrolysis for a long time, so the insulation is poor. The larger the duty ratio, the more serious the electrolytic corrosion for grinding wheel, and the more the diamond grits bared,the larger the height of grit protrusion. on the contrary, The smaller the duty ratio, the less serious the electrolytic corrosion for grinding wheel and the fewer the diamond grits bared,the smaller the height of grit protrusion. But the size of the height of the grit protrusion directly decides the size of the grinding force and the surface roughness.

The ultrasonic vibration conducive to the smooth discharge of debris with Cavitation, Pump suction effect and Eddy current effect; And because joined the vibration,it makes the locus of grinding is a curve, which is also conductive to the discharge of debris. So it can solve the fatal flaw of the ELID grinding is not easy to discharge, and make the surface quality improve greatly.

2.3.3 The effects of the electrode gap on the surface quality

Test parameters: ultrasonic frequency 34.435KHz, spindle revolution 1000r/min, duty ratio 5μs：5μs, supply voltage 60v , ultrasonic amplitude 8.2μm. Test in three different electrode gap 0.2mm, 0.5mm, 0.7mm without change of other parameters, respectively.

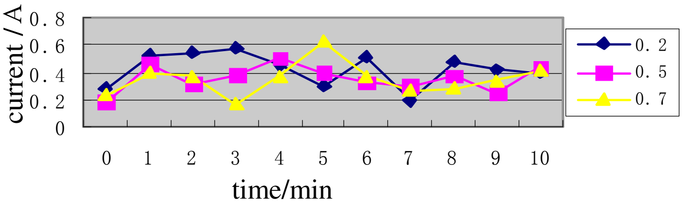

Fig.7. The relationship between the electrode gap and the electrolytic current

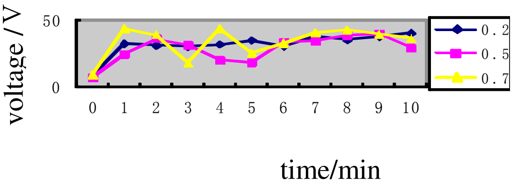

Fig.8. The relationship between the electrode gap and the electrolytic voltage

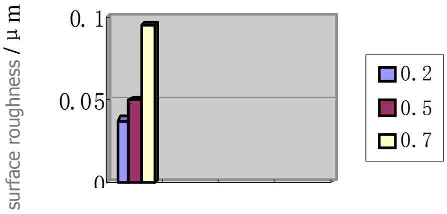

Fig.9.The surface quality of the ceramic under different electrode gap

Fig.7 shows the curve of the current chang with time measured in the test during the 10 minutes from the start when taking the electrode gap with0.2 mm, 0.5 mm and 0.7 mm.

Fig.8 shows the curve of the voltage chang with time measured in the test during the 10 minutes from the start when taking the electrode gap with0.2 mm, 0.5 mm and 0.7 mm.

Fig.9 shows The surface quality of the ceramic measured after the test, when taking the electrode gap with 0.2 mm, 0.5 mm and 0.7 mm.

The test results and analysis: As can be seen from figure 7, 8 , 9 that the electrolytic current decreases with the increase of electrode gap, while the change of the voltage is not obvious. The electrolytic current has a downward trend with the increase of electrolytic time, The electrolytic voltage increases with the increase of electrolytic time, but the change is very gentle. These are because that the unit of electric current density decreases with the increase of the electrode gap, and the thickness of the oxide film increases with the increase of the electrolytic time, and the electrical conductivity becoming worse than before which lead to the decrease of the current while the increase of the voltage.

The surface quality of the ceramic increases with the increase of the electrode gap After grinding. When the electrode gap is larger, the shocking of the surface quality of ceramic is larger. In the case of other conditions unchanged, the size of the electrode gap directly affects the current density, the smaller the electrode gap, the stronger the electrolytic capacity ,so current density is large. The quality of the oxide film formed is closely related to the current density, Current density can not be too high nor too low. Current density is too low to make the grinding wheel electrolysis and sharp, thus it lose the significance of ELID grinding, and become a general grinding. If current density too high, the oxide film generated fast and thick, But the density drops ,Not only affects the height of grit protrusion and make the wheel electrolytic losses too fast . therefore, it should ensure that there is always grits protrusion of micro blade for cutting in the process of grinding for ceramic , So it need stable current density .When the electrode gap is small, the Current density change is also small, it will make the surface quality high.

Conclusion

In the ultrasonic and ELID composite grinding test,Analysis the rule of the influence of the electrical parameters of the composite processing on the surface quality of ceramic, thereby ,accorded to the requirements of the different grinding to change electric parameters to control the thickness of the oxide film, thus affect the surface quality.The test results show that the different electrical parameters directly affect the thickness of the oxide film generated by electrolysis, which affects the surface quality.The following conclusions from this experiment:

Electrolytic current is large and and it’s faster to fall and the thickness of the oxide film is also thicker under the high electrolytic voltage and the different time.therefore, it suitable for the coarse grinding during the machining of the initial stage with the large grinding depth Under the 120 v voltage,while it suitable for fine grinding of the workpiece under the 60V voltage.

It is suitable to choose a small voltage If the requirement for the surface quality of the workpiece is relatively high; but choose the high electrolytic voltage if the requirement for the surface quality of the workpiece is not too high and high machining efficiency.

The ultrasonic vibration conducive to the smooth discharge of debris with Cavitation, Pump suction effect and Eddy current effect; And because joined the vibration,it makes the locus of grinding is a curve, which is also conductive to the discharge of debris. So it can solve the fatal flaw of the ELID grinding is not easy to discharge, and make the surface quality improve greatly. he surface quality of the ceramic increases with the increase of the duty ratio. the surface is the most when the duty ratio was 67%.

The smaller the electrode gap, the smaller the float of the current density, the surface quality of the workpiece machined.Therefore is more ideal, in order to obtain the high quality surface of the workpiece machined as possible as using a small electrode gap.

Reference:

[1]Yan Yan Yan. Research on [D]. ultrasonic assisted grinding of ceramics.Jiaozuo: Henan Polytechnic University, 2005 (6)

[2]Qiu loyal. Mechanism of precision mirror surface grinding of hard and brittle materials and technology. Master Thesis of Beijing University of Technology, 2008.05

[3] Cao Fengguo. Ultrasonic machining technology. Beijing: Chemical Industry Press, 2005

[4] Zhang Liaoyuan. Modern processing technology. Beijing: Mechanical Industry Press, 2002

[5] ELID Wang Zhiqiang. Research on control of electric spark truinggrinding wheel, master's thesis of Tianjin University, 2007.01

[6] Wang Yinxia, Ma Bao Ji, Wang Dang Li, study on the measurement method of grinding oxide film thickness of.ELID Ning. The new technology and new process, 2011,1:45-47

[7]T.B.Thoe,D.K.Aspinwall,M.L.H.Wise.Review on Ultrasonic Machining[J]. InternationalJournal of Machine Tools and Manufacturing. 1988，38(4)：239-255.

Applied Mechanics and Materials Vol. 596 (2014) pp 52-55
© (2014) Trans Tech Publications, Switzerland
doi:10.4028/www.scientific.net/AMM.596.52

Equipment Modification for Friction Stir Joining based on PLC

Ling Ji

College of media, Linyi University, Linyi ,China

jnjllhy@163.com

Keywords: equipment modification; Programmable Logic Controller(PLC); numerical control;FSJ

Abstract: In order to achieve the common drilling and milling machine for friction stir joining(FSJ) , A model ZXTM-40 equipment is modified., it's workstation transmission mode and axial direction press mode are mechanical transmission, through the modification, install stepper motors and drives , write program code ， PLC control the motor ,it can work to achieve Longitudinal automatic movement . the speed of workstation can input through the Interactive panel, the control system operate parameters to achieve semi-automated operation of equipment and overtravel protection.. In the vertical direction， install a sleeve on the handle, the sleeve has scale and recesses, it can control the pressure measurement of friction stir pin. weights hanged on the sleeve, research proves the optimum parameters are 3KG weights and 40CM away from the center, Workbench moving speed of 125mm/min, rotation speed of 730r/min, it can join 1mm thick 2024 aluminum by FSJ, appearance of bead is good.

Introduction

With the development of numerical control technology, the old machine can not meet the needs of modern industry, FSJ is an efficient, solid-phase connection, it is a new green technology that has come out of twenty years. The domestic and foreign scholars have done a lot of research in many aspects, such as the base material, the shape of the stir tool, the rotation speed, the welding speed, the down press depth, numerical simulation, some researchers analyze the performance of the mechanical properties ,corrosion, microstructure [1-5]. The scope in the thickness of the base material from 3 to 15mm, due to different thickness have different down pressure, the stiffness requirements of the machine are different, in this work, A drilling and milling machine is modified to a Semi-automatic machine, it can join two sheet metal by FSJ, the thickness of the board is under 3mm.

Equipment modification

The machine model is ZXTM-40, motor power is 1.5KW, workbench adopts mechanical transmission, Displacement accuracy of the system is mainly determined by the accuracy of the angular displacement of the stepper motor, precision ball screw,, the side workbench is enough space to install the motor and accessories, the answer is suitable motor and corresponding accessories can achieve this functionality.

Control system is the core of the machine, the choice should be taken into account for its performance, economy and maintenance services. Control systems are mainly three types [6]: open loop stepper motor drive system; induction motor or direct current(DC) motor drag, closed loop consecutive number control (CNC) measuring systems grating feedback; AC / DC servo motor drive, encoder feedback and a half closed loop CNC system. Which open loop stepper motor drive system, the controller sends a pulse feed command, control and drive circuits after the power amplifier, the stepper motor rotation, ball screw driven by the execution unit. the system is simple,it is convenient debugging maintenance, reliable, low cost, easy modification success.

Stepper motor is controlled using pulsed digital signals, each step the error automatically becomes to zero, it is easy to control, the key is to determine the parameters.

Since the device is used for FSJ, the experimental material is 2024 aluminum alloy, 0.5-3mm thickness, welding speed range is 50-300mm/min, Fig.1 shows force between stir pin and welded material

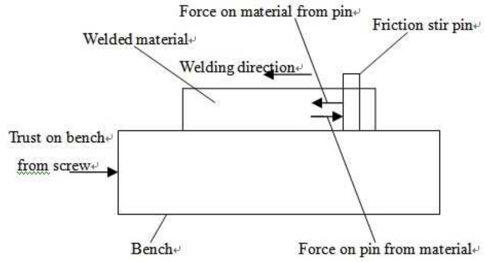
Force on material from pin
Friction stir pin
Welded material
Welding direction
Trust on bench from screw
Bench
Force on pin from material

Fig.1 Force between stir pin and welded material

Wang Xijing [7] obtained by measuring, 3mm thick aluminum plate, when the welding speed is 190mm/min, the table motor force F is 17KN, so that the sheet of 3mm or less, calculated according to the maximum 20KN, the motor power P' is

$$P' = F \times V = 20 \times 10^{3} \times 300 \times 10^{(-3)}/60 = 100W \tag{1}$$

Taking into account the loss of the motor during operation, the power P is actually needed

$$P = 1.2 \times P' = 120W \tag{2}$$

Because T = 9550P / n (n is the rotational speed), the ball screw lead is 5mm, because the motor revolution a circle is a ball screw lead, so we can obtain the speed is n

$$n = 300/5 = 60r/min \tag{3}$$

then

$$T = 9550 \times 120 \times 10^{(-3)}/60 = 19.1N \cdot m \tag{4}$$

Reference motor model table, select the motor model is 110BYG250-150, the maximum motor torque is 19.5Nm.

According to the actual space of the machine, determine the installation of the motor, usually with flange type, base type, with a base flange, this machine with a base flange mounting method.

Programmable Logic Controller (PLC) is an application designed for automatic control in industrial environments, which has a strong industrial processes connected with the interface, PLC has many function, such as logic control, timing control, stepper control, strong features.

PLC model is Wuxi Xinjie XC3-14T-E, which has X0 and X1 two pulse outputs, pulse number can output settings according to the set speed, in order to achieve a given distance control and a constant speed. The ladder diagram is shown in Fig.2, Compiled into assembly language by the ladder, and then converted into machine language, the corresponding code is executed by PLC.

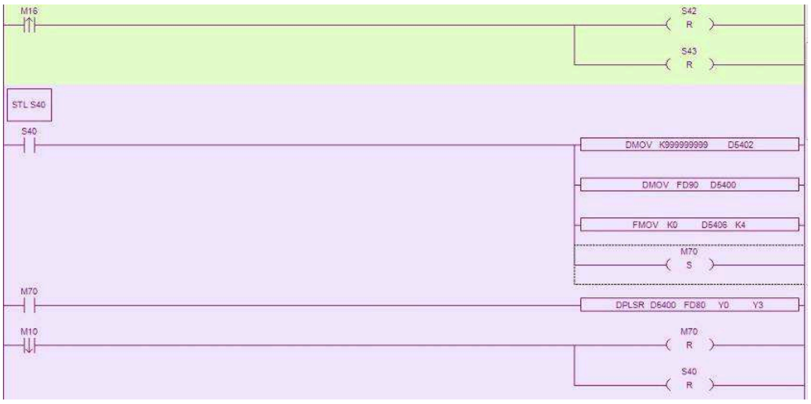

Fig.2 The ladder diagram of PLC

The man-machine interface model is Wuxi Xinjie OP320-A, it is cheap, easy to operate.

Stepper motor drive can transform the electrical pulse into the angular displacement. When a pulse signal is received, it will drive the stepping motor to set the direction of rotation of a fixed angle (referred to as "step angle"), which is fixed to the rotational angle of the step by step operation. The number of pulses can be controlled by controlling the amount of angular displacement, so as to achieve accurate positioning; through control pulse frequency ,the motor rotation speed and acceleration can be controlled, and the speed can be adjusted.

According to the stepper motor model, select the matching drive models as 2HA1180, the maximum phase current is 8.0A, 256 segments. The motor affiliates are shown in Fig.3.

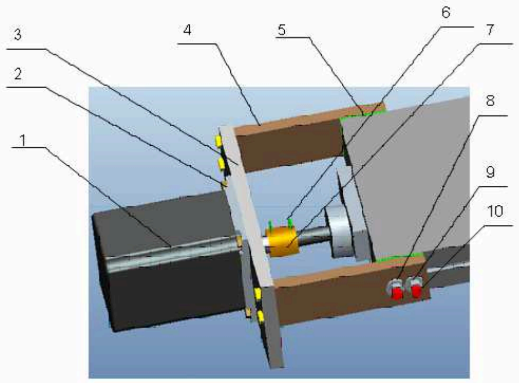

1-step motor; 2-screw; 3-connecting board; 4-supporting board
5-shim;6-holding screw;7-coupling;8-shim;9-nut;10;T type screw

Fig.3 Motor and affiliates installation diagram

Experimental

Rose A, Mehta M, Davis TA [8-10] studied the method about fixed depth, if the thickness is 3mm,the depth is around 2.8mm, so that the metal can be sufficient stirred , the connection after the process is stable, the pressure is constant , so this mechanism installs a sleeve on the handle, the sleeve hanging weights to achieve automatic control pressure. this surface appearance is obtained at a 3KG weights and 40CM torque arm, After tensile testing, fracture location in the connection area and base metal junction, breaking a 45-degree angle, the maximum tensile strength is 92Mpa, accounting for 71% of the base material. The results are shown in Fig.4 and Fig.5.

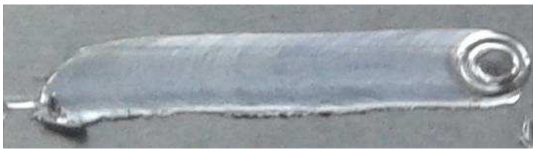

Fig.4 Surface appearance of Aluminum joint prepared by FSW

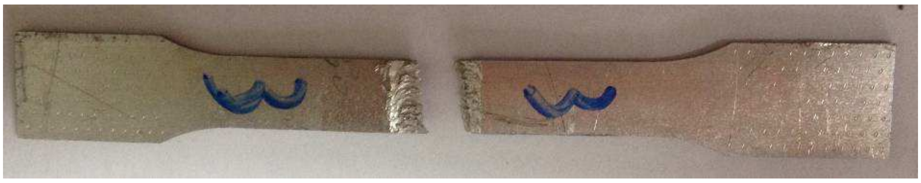

Fig5. The specimen and tensile fracture location

Conclusions

According to the stress analysis workbench , choose the appropriate stepper motors and drives, to achieve uniform motion in the horizontal direction bench by PLC controlled stepper motor , continuously variable transmission can be achieved , and from the control panel can choose the number buttons any data for running speed , emergency stop function can be achieved , the movement distance is set to 0.1m automatically stop, to prevent the machine from destoryed.

Two pieces of 2024 aluminum alloy are jointed successfully through FSJ with modified equipment under a tool rotation rate of 730 r/min and a traverse speed of 125mm/min, 3KG weights and 40CM torque arm, the maximum tensile strength is 71% of the base material.

Acknowledgements

This work was performed as a part of National Natural Science Foundation of China‘‘Aviation magnesium alloy FSJ connection integrity and milling deformation mechanism and prediction”(Foundation No. 51175255). The authors wish to thank Dunwen Zuo , Precision and Micro Manufacturing Technology Laboratory and Nanjing University of Aeronautics and Astronautics.

References

[1] Mishra R S, Ma Z Y. Materials Science and Engineering: R: Reports, 2005, 50(1): 1-78.

[2] Mandal S, Rice J, Hou G, et al. Journal of materials engineering and performance, 2013, 22(6): 1558-1564.

[3] Upadhyay P, Reynolds A. Metallurgical and Materials Transactions A, 2013: 1-10.

[4] Rajakumar S, Muralidharan C, Balasubramanian V. Materials & Design, 2011, 32(2): 535-549.

[5]Elangovan K, Balasubramanian V, Valliappan M. The International Journal of Advanced Manufacturing Technology, 2008, 38(3-4): 285-295.

[6] LIU Ya-dong, LI Cong-xin,WANG Xiao-xin. Journal of Shanghai Jiaotong University. 2001, 35(10): 1517-1520. In China.

[7] WANG Xijing, ZHANG Zhongke, HAN Daobin, ZHANG Changqing. Journal of Lanzhou University o f Technology,2010,1- 4. In China.

[8]Meng wusheng, Gao qing, Li junlin . Mechanotronics, 2013 (5): 46-49. In China.

[9] Rose A, Manisekar K, Balasubramanian V. Transactions of the Nonferrous Metals Society of China, 2011, 21(5): 974-984.

[10]Mehta M, Chatterjee K, De A. Science and Technology of Welding and Joining, 2013, 18(3): 191-197.

Applied Mechanics and Materials Vol. 596 (2014) pp 56-59
© (2014) Trans Tech Publications, Switzerland
doi:10.4028/www.scientific.net/AMM.596.56

Research on Galvanized Layer Uniformity Detecting Technology of Transmission Angle Steel Tower Materials

Jiayin Jiang

College of Energy and Electrical Engineering, Hohai University, Nanjing 211100, China

jiayin0027@163.com

Keywords: angle steel tower materials; galvanized layer uniformity; test point arrangement form; control chart; detection

Abstract. Combined with the actual working condition and related standards, the galvanized layer uniformity detection of transmission tower materials is studied and the sampling scheme of galvanized layer uniformity detecting is formulated. With the help of the diagonal test point arrangement form which is used in flatness error detection, a double cross shaped test point arrangement form was established for the galvanized layer uniformity detecting of angle steel tower materials. In order to quantitatively evaluate the thickness uniformity of the galvanized layer and realize information management, the X-Rs control chart was applied in the galvanized layer uniformity detecting.

Introduction

Transmission tower provides important guarantee to the transmission lines' safety [1]. As the tower works in the wilderness, anticorrosion treatment becomes especially important. As an important anticorrosion method for the tower, hot dip galvanizing is wildly used. The galvanized layer uniformity which is an important indicator that impacts the quality of the galvanized layer has received much concern. The galvanized layer thickness differs at different places of the angle steel. As the anodic coating, places where the galvanized layer is thin will generate base corrosion first. To guarantee the quality of the tower materials, enterprises often take the method of increasing the average galvanized layer thickness to guarantee the quality of the tower materials [2]. This method will lead to the increase of plating costs. Thus, the study of the galvanized layer uniformity detecting has great significance.

Angle steel tower materials sampling and detecting policy for galvanized layer uniformity

Angle steel tower materials sampling scheme for galvanized layer uniformity. In order to evaluate the galvanized layer uniformity of the angle steel tower materials, the length of the angle steel will be divided into four types: from 0 to 3 meters, from 3 to 5 meters, from 5 to 8 meters and more than 8 meters, according to the "angle steel tower sampling specifications" and the common sizes of the angle steel tower materials [3]. A sampling scheme was formulated as shown in Table 1.

Table 1 The sampling scheme for galvanized layer thickness uniformity detecting (Unit: One)

Length[m]	Sample size	Estimating array	
		Ac	Re
(0 3]	3	0	1
(3 5]	3	0	1
(5 8]	2	0	1
＞8	1	0	1

Note Ac—Acceptance number Re—Rejection number.

Galvanized layer uniformity detecting policy and scheme. According to the requirement of the galvanized layer uniformity in the “angle steel tower material sampling specifications”, the angle steel tower material is qualified through 4 times copper sulfate test without exposing the base. Though this method is simple and effective, but it is just qualitative detect and it can’t make quantitative judgment for galvanized layer uniformity. Besides, this method is lack of data support for the process improvement of galvanized layer.

As shown in Fig.1, the galvanized layer thickness of the sampled angle steels will be detected at the test points and the values will be depicted in the X control chart. The thickness uniformity of the galvanized layer will be judged through the fluctuations of the thickness.

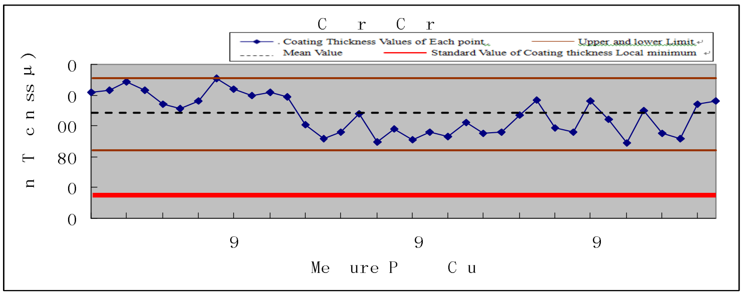

Fig.1 The x control chart for galvanized layer thickness uniformity

The moving range is the difference of galvanized layer thickness between two adjacent points in the figure. The moving range is depicted in Fig.2 with dots. The fluctuation of the moving range reflects the fluctuation of the galvanized layer thickness to some extent. The lower the moving range fluctuates, the better the galvanized layer thickness uniformity will be.

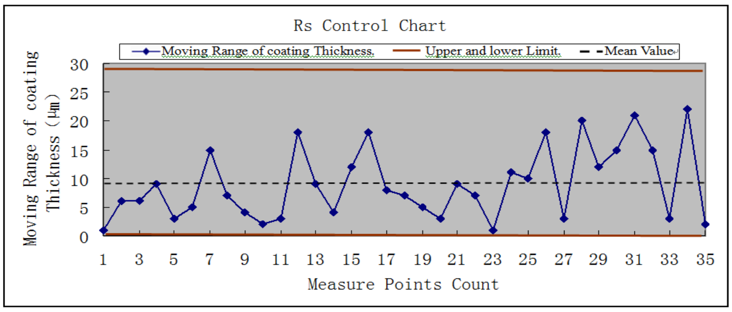

Fig.2 The Rs control chart for galvanized layer thickness uniformity

Test points arrangement form of the galvanized layer thickness uniformity detecting

According to the theory of mathematical statistics, there must be sufficient data to make the measuring results true and reliable. The feasibility of data collection methods must be fully considered in practical work and the data collection methods shouldn’t be too complicated. With reference of the diagonal test point arrangement form which is used in flatness error detecting [4], a double cross shaped test point arrangement form is proposed. The double cross shaped test point arrangement form is shown in Fig.3. Several test points will be selected from the cross lines. The points, from a1 to e5 in Fig.3, are the test points selected. The galvanized layer thickness at these points could comprehensively reflect the entire angle steel’s galvanized layer thickness uniformity.

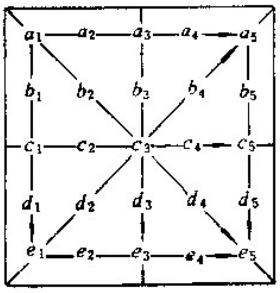

Fig.3 The double cross shaped test points arrangement form

As the angle steel’s length is much larger than its width and taking feasibility of actual operation into account, the angle steel’s surfaces are imaginarily expanded to the same plane. As shown in Fig.4, the double cross lines will be drawn and this pattern will be taken as the unit pattern. Considering the detecting efficiency, the above test point arrangement form is simplified and a total 10 points will be selected as the test points from each unit pattern. Adjacent test points’ galvanized

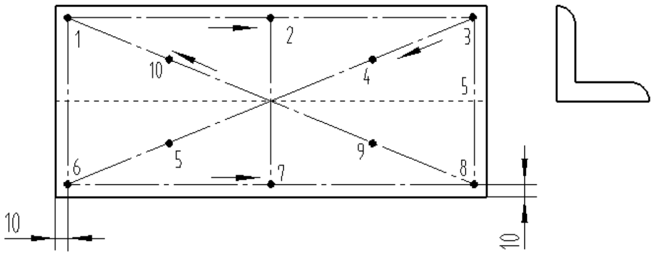

Fig.4 The simplified test point arrangement diagram

layer thickness differences need to be computed in the Rs control chart. The adjacent test points are selected according to the detecting sequence in this paper. As shown in Fig.4, the first point was selected from the top left corner and the second to the tenth point was selected following the direction of the arrows. The periphery test points are 10mm from the edges of the angle steel.

Angle steels of different lengths will be carried out unit division based on the pitch method for flatness error measuring and the segmented sampling program for length sampling. Angle steel whose length is from 0 to 3 meters will be divided to 2 unit segments. Those whose length are from 3 to 5 meters, from 5 to 8 meters and above 8 meters will respectively be divided to 3 unit segments, 4 unit segments and 5 unit segments. The galvanized layer thickness will be detected at each unit segment's test points. Fig.5 is the test point arrangement diagram for angle steel whose length is from 0 to 3 meters.

With the number of test points on each unit segment's single side, the test point amount of angle steels in different lengths can be calculated. The test point amount of angle steel whose length are from 0 to 3 meters, from 3 to 5 meters, from 5 to 8 meters and above 8 meters respectively are 36, 52, 68 and 84.

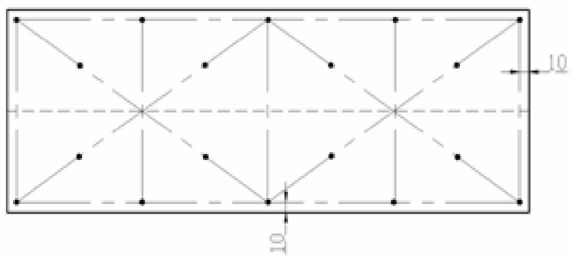

Fig.5 Test point arrangement for angle steel with the length from 0 to 3 meters

Case analysis about galvanized layer thickness uniformity detecting

With the above sampling standard and test point arrangement form, a number of angle steel's galvanized layer thickness uniformity was detected. Fig.1 is the X control chart for the galvanized layer thickness uniformity of angle steel with the length of 3.2m and thickness of 4 mm. Fig.2 is the Rs control chart for the galvanized layer thickness uniformity.

As Fig.1 shows, the average galvanized layer thickness at the 52 test points is bigger than the minimum standard thickness value which is 55μm. The average galvanized layer thickness of multi-points is 69μm which is bigger than the standard thickness value 65μm [5]. The galvanized layer thicknesses at all the 52 test points are within the upper and lower control limits and the fluctuation is normal. The galvanized layer thickness of this angle steel is in accordance with the galvanized layer thickness standard.

The moving range is calculated as follows:

$$R_{si} = |X_i - X_{i+1}|, i = 1,2...,n-1 \tag{1}$$

The moving range is depicted in Fig.2. It can be seen from the distribution of the moving range that all the points are within the upper and lower control limits. The fluctuation of the moving range ranges from 0 to 20μm and the average moving range is about 10μm. These show that the galvanized layer thickness uniformity of this angle steel is good.

According to the determination rules of the x-Rs control chart, the sampled angle steel's galvanized layer thickness uniformity is satisfactory. A certain number of angle steels from this batch of angle steels were extracted based on the sampling scheme shown in Table 1. With the above galvanized layer thickness testing method, galvanized layer thickness at these test points will be detected and the eligibility of this batch angle steels' galvanized layer thickness uniformity will be judged.

If the number of samples is increased to 25, the processed detection data can be used to evaluate galvanized layer thickness while it can be used to quantitatively evaluate the uniformity of the galvanized layer thickness at the same time.

Summary

This paper conducted a research on the uniformity detecting of the galvanized layer thickness which is used for angle steel anticorrosion. Combining with the relevant standards and the actual working conditions of the angle steel, a sampling scheme was established. With reference of the diagonal test point arrangement form which is used in flatness error detection, a double cross shaped test point arrangement form was proposed and this provides a basis for the quantitative evaluation of the established uniformity. The x-Rs control chart is used in the galvanized layer thickness uniformity detecting which makes the evaluation of the galvanized layer thickness uniformity quantitative and intuitive. This detecting method overcomes the lack of destructive copper detecting and provides data support for the relevant process improvement. A vision was proposed that the galvanized layer thickness detecting and galvanized layer thickness uniformity detecting share the detection data. This vision improves the efficiency of the galvanized layer quality detecting. This vision also lays the foundation for the galvanized layer quality detection's information management and standardized operation.

References

[1] Y. Chen: Electric Power Construction Vol.31no.8 (2010), p.55-58

[2] S.P. Yuan: Electric Power Construction Vol.28no.3 (2009), p.44-48

[3] Angle steel tower sampling operation specification, china power press, 2011

[4] GB/T 11337-2004, Measurement of departures from flatness

[5] Angle steel tower manufacturing operation specification, china power press, 2011

Applied Mechanics and Materials Vol. 596 (2014) pp 60-63
© (2014) Trans Tech Publications, Switzerland
doi:10.4028/www.scientific.net/AMM.596.60

The improved design of embedded CNC milling machine

HaiYing Zhang ，YuFeng Shu

DongGuan Polytechnic No.3 University Road ,Songshan Lake Sci.&Tech.Industry Park,
Dongguan, Guangdong Province, China 523808

Keywords: Embedded; milling machine; improved design

Abstract: The machining of complex shape workpiece embedded NC milling machine is suitable for all kinds of hard, brittle, thin products. This paper embedded CNC grinding machine design requirements, through the transmission gear, the workpiece clamping and buffering mechanism to improve the design, CNC system and abrasion resistant materials were optimized, so as to meet the requirements of high performance precision grinding machine.

Microprocessor based on ARM embedded technology with a small, low -power , low-cost , high-performance features, which determine that it has good prospects for development in the field of NC . High-precision Embedded CNC milling machine for machining complex geometries that grinding glass, silicon wafers and other brittle , hard, very thin products have advantages , such as mobile phones that require high precision glass processing , processing difficulty , shape error are required in 0.02mm within requires milling, chamfering, edge and so on. Microcontroller based on Embedded CNC milling machine development and design will become the development trend of the new generation of numerical control technology , has broad prospects for development , and can greatly improve efficiency and reduce costs. Through conventional cam milling machine (also known by imitating molding machine) to control the shape of the product to be ground , which uses the product template positioning, shaped glass grinding straight edge, round edge, OG , bevel etc. . In shaped by imitating machine, work-piece rotation axis by using a three-phase AC motor drives the drive shaft clamp the work-piece is rotated around the work-piece to achieve grinding . The traditional way by mold processing before processing products need to produce specialized products templates when producing more varieties, templates to create and manage the high cost of replacing the template trouble. Develop the Automatic High-precision Embedded milling machine to meet the needs of variety, volume, high precision glass processing .

The overall design

The system has the structure of main-base. Upper PC with S3C2410 ARM9 controller as the core , porting Linux systems, and QT / Embedded graphical library , Mainly to act the function of G-code file processing, display processing location , and other interactive features manual control . The lower PC with S3C44BOX ARM7 controller core, Si Maidi the SM5004 FPGA chip for the movement controller, motor driver , coolant switch, emergency stop and other machine control functions. Upper and lower computer via CAN bus communication.

The improved design of the mechanical parts

Variety of designs optimized design methods is widely used in the design of High-precision Embedded automatic milling machine, in particular the use of mechanical systems engineering principles and fuzzy optimization method to solve a large number of design challenges and reliability issues. Mechanical parts design, many design parameters are often given a range , designers need to determine the exact value of the design parameters under uncertain information , which contains design ideas IF-THEN logic. The transmission of High-precision milling machine is mainly by copying gear , transmission reliability is directly related to the success or failure of the whole gear design , taking full account of the gear design parameters fuzziness and randomness based on the combination of traditional optimization method , discusses the fuzzy optimization method with fuzzy reliability constraints gear , according to the number of intervals in fuzzy theory algorithms , the result set generated by all the conditions set analyzed and calculated , and the results are fully discussed . This method provides machinery parts products theoretical for the design and evaluation of products, for improving product quality and reliability have great significance .

Various existing profiling milling machine using a fixed drive shaft fixed to the eccentric roller shaft grinding wheel profiling mother round workpiece clamping shaft, thus boosting the grinding and wheel movement , and thus realize the workpiece processing requirements. Generally use the dovetail slot and slide between the grinding bodies and grinding pan rack , to do translational and positioning. This translation agency's installation is complicated, energy consumption, easy to wear, easy to affect accuracy. High-precision Embedded CNC milling machine uses a new translation agencies that compact, high-precision and easy to install. High-precision Embedded CNC milling machine table and wheel frame are installed self-developed cross- roller guides positioning device guide-ways do to solve the problem guiding and positioning table and the wheel frame translation . Rolling linear guide rail is placed between the slider and a special roller , so that the sliding friction between the slider and the rail into rolling friction , greatly reducing friction between the two sports to gain : the difference between the move and static friction is small, with excellent mobility , which the interval of time between the driving signal and the lag action of mechanical is very short, beneficial to improve the response speed and sensitivity of CNC system.

High precision automatic control milling machine the work-piece clamping mechanism is divided into three parts, including the collet assembly , gear assembly and feed control lever assembly . Around the work-piece chuck body are mounted on the left and right spindle, spindle mounted in the left and right the sleeve through bearings, the sleeve has the right bottom feed alveolar , and feed gear with the completion of the feed movement , gripping and releasing the work-piece. High precision automatic milling machine has two work-piece chuck body , one is the mosquito clamp plate screw directly connected to the end face around the spindle , the connection is simple, but bad reliability, suitable for precision shape and edge down high product, another is specially designed quick installation chuck, spindle and chuck using conical seat fit chucks with high-precision taper spindle is mounted on the left and right , making the collet seat accurate positioning of the work-piece by a metal splint plywood and plastic or nylon plate combined composition, metal plates with screws installed in the collet seat, plywood after improvements, made of metal and plastic or nylon, plywood panels , both to ensure a certain degree of rigidity, but also to ensure work-piece clamping needed flexibility.

High-precision automatic milling machine due to improved movement methods, increasing the pressure buffer device, exercise machine is very stable and reliable, essentially eliminating the common quality defects of the ordinary copying milling machines , greatly reducing the work breakdown shape allowed, accuracy unqualified, crooked edges , uneven edges down , etc. , to ensure the reliability of the work-piece shape and grinding , improve product quality and production efficiency

CNC system hardware design

S3C2410 core board, S3C44BOX intermediate plate and SM5004 FPGA motion control chip , constitute the core of the control section embedded CNC system. In the selection of the development board, we used the Shenzhen excellent company FS44BOX and FS2410 development board kit. Taking into account the need for a larger panel of the CNC system effective display area, with a 10.1 inch Sharp TFT LCD screen , supporting a maximum resolution of 640 * 480 , CNC system can achieve a good graphical user interface (GUI) development board in two on the integration of the necessary SDRAM, Flash, serial , USB interface , 10M Ethernet interface and LCD display interfaces , in addition to an SD expansion card interface and the necessary matrix keyboard . Rich peripheral interfaces favor communication between devices , and reduces hardware development effort. Especially in the study of the early prototype trial process and shorten the development time , be able to develop products faster , carry out the necessary tests for further research experience, shorten the development cycle.

CNC system software design

Using Windows operating system , using VC++ language development system control software. According to the actual production requirement, mainly achieve the following functions:

1) Manual control. Achieved manually move each control axis ; rotating the work-piece position ; each axis back to zero control ; start and stop grinding , coolant and other functions.

2) Processing program management. By entering the coordinates of a point system input parts graphics, but also simulate the machining trajectory. Parts can be designed as a file pattern stored in the machine; but also on the part pattern shape and process modifications.

3) Automatic processing. Press to enter the parts diagram automatically grind. The system can process a variety of complex -shaped parts of lines, arcs and ellipses graphic composition, such as: linear polygon , polygon with arbitrary arc , complete oval .

4) Parameter setting, fault diagnosis.

A reasonable choice of wearing material

Embedded PLC based control milling machine for the study, studied six different carbon and silicon content of the steel milling machine hardness, impact toughness , tensile strength, elongation and reduction of area , and analyze the friction and wear properties . The results showed that with increasing carbon content and silicon content, milling machine gradually increasing the wear resistance of steel.

As the milling machine takes a long time in the course of friction with wear and stainless steel, copper, aluminum and other metals happen, so the research and development of timber milling machine has become an important factor in high-performance embedded applications, milling machine, with high strength and high wear resistance of timber milling machine milling machine can reduce friction loss , and extend the life of milling machines.

Conclusion

Through two years of prototype experiments, embedded CNC milling machine basically completed the requirements to complete the design of the main technical indicators. FM-A series automatic profiling milling machine grinding improved chassis and body translation agency, designed a new pressurized buffer device, while the design of the quick installation chuck , effectively improve the grinding accuracy and reliability of the product. Based on Embedded PLC control milling machine for the study, studied six different carbon contents and impact of the silicon content of the steel milling machine, with the increase of carbon and silicon content, milling machine wear-resistant steel resistance gradually increased. Mobile phone glass, window glass and other clocks glass need to be squaring and chamfering, strong demand for milling machine, now replaced by a large part machining precision engraving machine, production efficiency is not high. Therefore, the development of embedded CNC milling machine has a very important significance.

Author: Haiying Zhang, male, Birthday：1968.12, professor, Mechanical engineering teaching and researching
Address: College of Electrical and Mechanical, DongGuan Polytechnic ,No.3 University Road ,Songshan Lake Sci.&Tech.Industry Park, Dongguan, Guangdong Province, China 523808
Tel: 15876468160

References

[1] Haiying Zhang. Profiling die by computer design, Equipment manufacturing [M] .2009.

[2] ShiGuo Li. Light Industry Machinery CAD [M] Beijing: China Light Industry Press, 1998.

[3] liangGui Pu. Mechanical design [M] Beijing: Higher Education Press, 2005.

[4] Dong Xueqin, Guilin Wang. Austempering temperature on the influence of microstructure and properties of low alloy wear-resistant steel [J]. Casting technology, 2013, 34 (8) :991-993.

[5] ZhongQi Cui, BeiXing Liu. Metallurgy and Heat Treatment Principles [M]. Harbin Institute of Technology Press, 1998.

[6] J Liu, H. C Wang. Effects of rare earths in borax salt bath immersion vanadium carbide coating process on steel substrate[J]. Surface＆Coatings Technology. 2008: 4788-4792.

CHAPTER 3:

Product Design, Manufacturing and Industrial Informatics Applications

Applied Mechanics and Materials Vol. 596 (2014) pp 67-71
© (2014) Trans Tech Publications, Switzerland
doi:10.4028/www.scientific.net/AMM.596.67

Simulation research on the magnetic field of the positioning permanent magnet for MEMS inside human body based on Ansoft

Xiuquan Liu [a] *, Yanhong Li [b]

School of Mechanical and Electronic, Guangzhou Panyu Polytechnic, Guangzhou, China

[a]liuxiuquan1@126.com, [b]liyh@gzpyp.edu.cn

Keywords: magnetic positioning; permanent magnet; Ansoft.

Abstract. the magnetic dipole model of the cylindrical permanent magnet was introduced. Then, based on Ansoft software, the simulation model of the cylindrical permanent magnet was established, and the influence of some parameters, such as the height, radius and magnetization direction on the magnetic induction intensity ,were studied; at the same time, under these two models the calculation was compared, the result shows the the magnetic dipole model is applied on condition that distance is nine times greater than the cylindrical permanent magnet size.

Introduction

The capsule endoscope MEMS inside human body is mostly used for the measurement of physiological and biochemical parameters and the diagnosis and treatment of diseases, which embodies the concept of minimally invasive and noninvasive medical, becomes one of the main directions of medical development in the 21st century. The problem of location and orientation of the capsule MEMS inside human body has been one of the key technologies. X-ray or the ultrasonic may be determined the location and orientation， but the two methods have some side effects for patients and doctors, which can't be used for a long time. The permanent magnet magnetic field has no harmful to the human body, so many scholars use the permanent magnet for magnetic positioning, when the size of the permanent magnet is far less than the external measuring distance, it can be seen as a magnetic dipole [1-3]. The magnetic induction intensity of the permanent magnet is collected by the array sensor in the plane and the position parameters are calculated by the magnetic dipole equations [4]. The equivalent magnetic charge and equivalent electric current model were used for calculating the magnetic induction intensity of the permanent magnet, and the former is more simple and effective [5]. The magnetic dipole and the equivalent magnetic charge model were applied for the simulation of the permanent magnet, when the distance was far bigger than its size， the calculation results were consistent [6].

The above analysis and calculation of the magnetic field of the permanent magnet is complex very much, and the finite element software Ansoft is especially suitable for the modeling and simulation of permanent magnet, it could convert complicated actual engineering into a simple solving problem.

In this paper, based on Ansoft software the three dimensional simulation model of the cylindrical permanent magnet is established, the influence of some parameters, such as the height, radius and magnetization direction on the magnetic induction intensity, are analyzed, and the calculation is compared with the magnetic dipole model and the simulation model.

The models of the cylindrical permanent magnet

A the magnetic dipole model

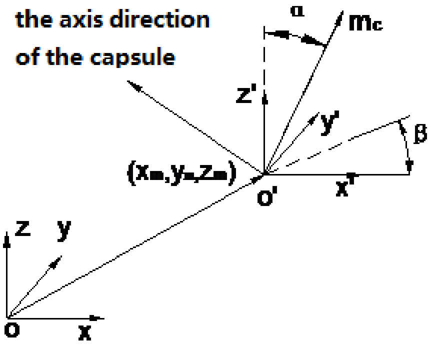

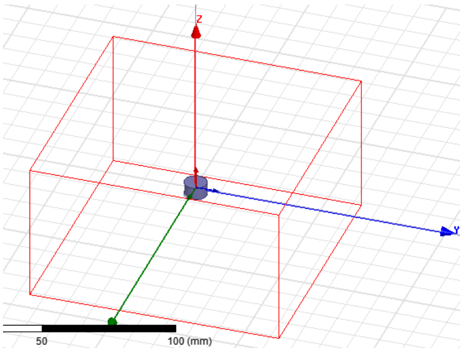

Fig.1 The position of the capsule MEMS inside human body[7]

Fig.2 The simulation model of the cylindrical permanent magnet based on Ansoft

Inside human body, the capsule MEMS could be regarded as rigid body. The position of the rigid body in the space is determined by the coordinates of an internal arbitrary point (x_m, y_m, z_m) and the two angles(α , β), shown in Fig.1. Capsule magnetic moment is mc， vetor(x_m, y_m, z_m, α , β) is used for the capsule magnetization posture, here (x_m, y_m, z_m) is the capsule center coordinates, (α , β) is the cylindrical coordinates angle. So in the global coordinate system, the magnetic field density B at a arbitrary point in the space by the magnetic dipole is:

$$B_x = \frac{\mu_0 m_c}{4\pi r^5}[(2X^2 - Y^2 - Z^2)\sin\alpha\cos\beta + 3XY\sin\alpha\sin\beta + 3XZ\cos\alpha]$$

$$B_y = \frac{\mu_0 m_c}{4\pi r^5}[(2Y^2 - X^2 - Z^2)\sin\alpha\sin\beta + 3XY\sin\alpha\cos\beta + 3YZ\cos\alpha]$$

$$B_z = \frac{\mu_0 m_c}{4\pi r^5}[(2Z^2 - X^2 - Y^2)\cos\alpha + 3XZ\sin\alpha\cos\beta + 3YZ\sin\alpha\sin\beta]$$

$$X = x_s - x_m$$

$$Y = y_s - y_m$$

$$Z = z_s - z_m$$

B The simulation model of the cylindrical permanent magnet based on Ansoft

The simulation model is shown in Fig.2, the parameters of the cylindrical permanent magnet are shown in Table 1, Here H is its height, R is its radius, Hc is its coercive force, S is the electrical conductivity, Br is the remanence. its material is NdFeB, the size of the solving area is defined, which is filled with vacuum, and the magnetization direction is Z axis. Then the magnetic induction intensity is calculated and analyzed with the three dimensional static magnetic field solver based on Ansoft [8].

Table 1 The parameters of the cylindrical permanent magnet

Parameter Name	Symbol	Value	Unit
Radius	R	4.5	mm
Heiht	H	3	mm
coercive force	H_c	-880	kA/m
electrical conductivity	S	625000	S/m
remanence	Br	1.18	T

The calculation and analysis of the magnetic induction intensity

A The influence of the structure parameters such as height and radius on the magnetic induction intensity

Because the cylindrical permanent magnet is placed within the capsule, the geometric size of the permanent magnet is restricted, generally the radius is no bigger than 5mm, and the height is not too much. The magnetic induction intensity of the permanent magnet is measured by magnetic sensors, for example HMC1023, which is a three orthogonal magneto-resistive sensors, the field range is wide, ± 6 Gauss; the minimum detectable field is 85ugauss[9].

The radius is 4.5mm, the height is varied from 2mm to 5mm, the relation between the permanent magnet height and the magnetic induction intensity of Z-axis is shown in Fig.3. With the height increasing, the B of Z-axis become bigger, and when the height kept constant, with the increasing of the distance, it decreases, approximately handstand cubic curve. When the distance ranges from 60 to 100mm, the height is 2mm, the B range is 0.7-0.07Gs, the height is 3mm, the B range is 0.8-0.17Gs, the height is 5mm, the B range is 1.6-0.46Gs, all are within the± 6Gs scope, a much greater than the minimum detectable field 85uGs.

The height is 3mm, the radius is varied from 2mm to 5mm, the relation between the radius and the magnetic induction intensity of Z-axis is shown in Fig.4. With the radius increasing, the B of Z-axis become bigger.

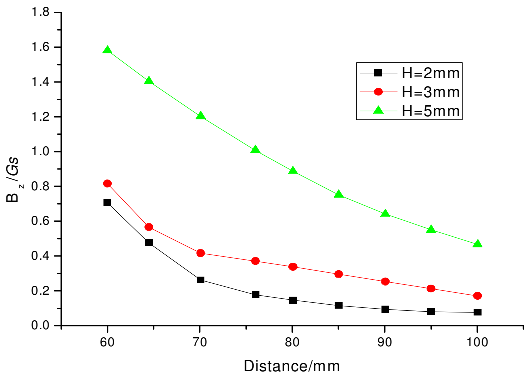

Fig.3 The relation between the height and B of Z-axis

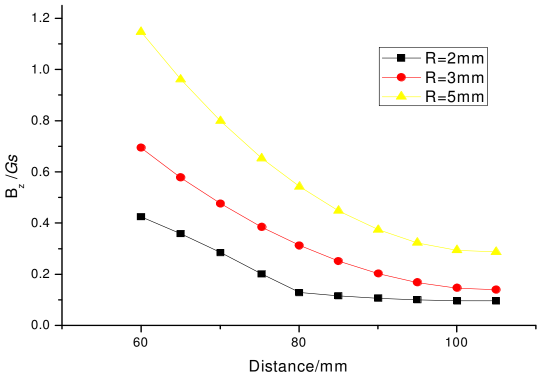

Fig.4 The relation between the radius and B of Z-axis

B The influence of permanent magnet magnetization direction on the magnetic induction intensity

The polarity of the cylindrical permanent magnet has three direction, X or Y or Z axis, X and Y axis are symmetrical, and the effect is the same, so the polarity of Y or Z axis is discussed.

A path in the XY or XZ or YZ plane is built, which is a ring, and the radius is 150mm. the relation between the magnetic induction intensity and the angel along the ring in the XY plane is shown in Fig.5. The magnet magnetization directions is Y or Z axis, the magnetic induction intensity and Angle is approximately sinusoid, and the amplitude of B is bigger in the direction of Y-axis than in the direction of Z-axis, the former minimum is up to 72mGs, the other is only 0.2mGs. The relation between the magnetic induction intensity and the angel along the ring in the XZ plane is shown in Fig.6.Tthe magnetic induction intensity and angle is approximately sinusoid, and the amplitude of B is bigger in the direction of z-axis than in the direction of Y-axis, the minimum respectively is 68mGs and 22mGS. The relation between the magnetic induction intensity and the angel along the ring in the YZ plane is shown in Fig.7. The magnetic induction intensity and angle is approximately sinusoid, and the amplitude of B is bigger in the direction of z-axis than in the direction of Y-axis, the minimum respectively is 65mGs and 42mGS. from the perspective of the minimum, under Y axis the magnetizing direction B is better than Z axis.

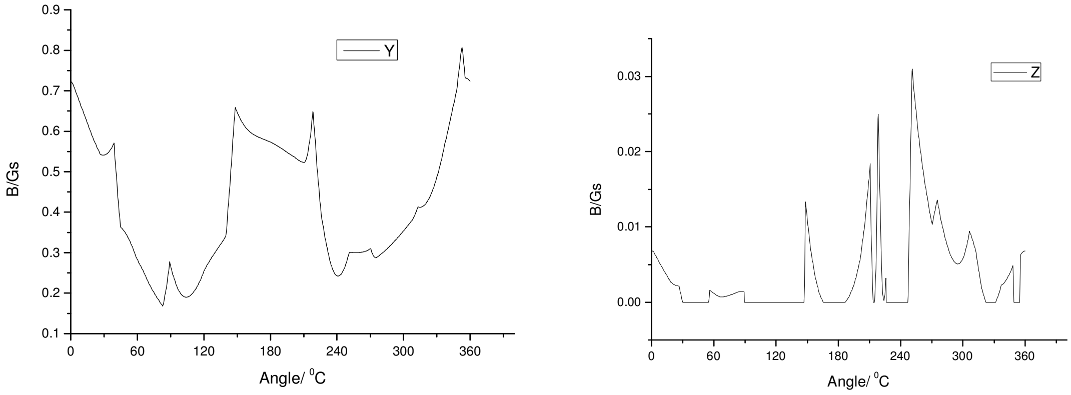

Fig.5 The relation between B and angels along the ring in the XY plane

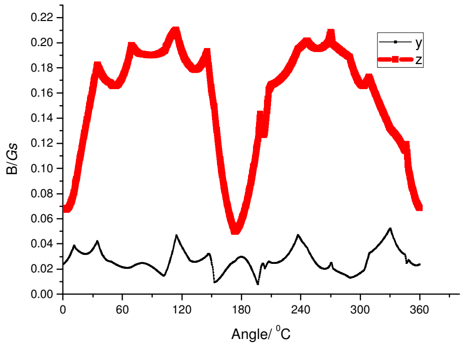

Fig.6 The relation between B and angels angels along the ring in the XZ plane

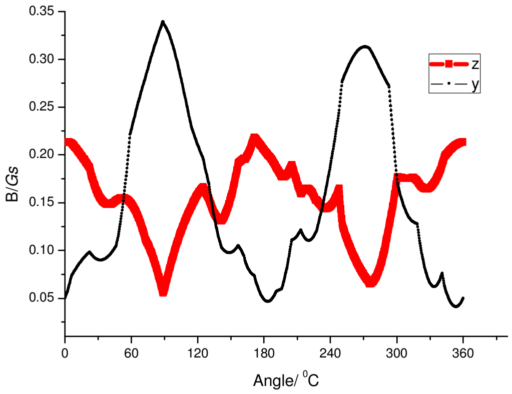

Fig.7 The relation between B and along the ring in the YZ plane

C The comparison of the magnetic dipole and simulation model base on Ansoft

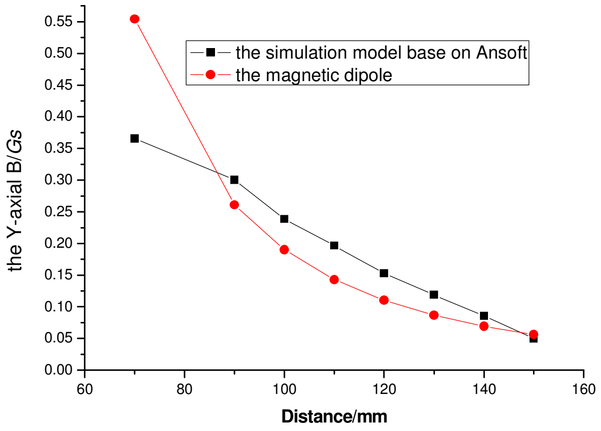

Fig.8 The comparison of B with two models

With the magnetic dipole and the simulation model base on Ansoft, the Y-axial B is calculated, shown in Fig.8. When the distance is less than 80mm, the error of the magnetic induction intensity is very large, when the distance ranges from 80-150mm, the error is smaller. The size of the cylindrical permanent magnet is Φ9×3, the magnetic dipole model is applied on condition that distance is greater than the cylindrical permanent magnet size, From the simulation above, the distance is about 9 times bigger than its size.

Conclusions

The three-dimensional simulation model of the cylindrical permanent magnet is established base on Ansoft, the influence of some parameters on the magnetic induction intensity were analyzed, The greater the permanent magnet height and radius, the bigger the magnetic induction intensity, it also influenced by the magnetization direction, from the perspective of the minimum, under X or Y axis magnetizing direction B is better. the magnetic dipole model is applied on condition that the distance is about 9 times bigger than its size.

Acknowledgements

This research is financially Supported by State Key Laboratory of Robotics and System (HIT)（SKLRS-2012-MS-03, the Ram City scholars project of Guangzhou bureau(10B009G) and and the science and technology plan project of Panyu, Guangzhou（2012-Z-03-64).

References

[1] Chao Hu , Wanan Yang , Dongmei Chen , Max Q.-H. Meng , Houde Dai. An Improved Magnetic Localization and Orientation Algorithm for Wireless Capsule Endoscope[C]. 30th Annual International IEEE EMBS Conference, (2008).p.2055-2058

[2]Johannessen, E. A., Wang, L., Cui, L., et al. Implementation of multichannel sensors for remote biomedical measurements in a microsystems format[C]. IEEE Transactions on Biomedical Engineering, (2004). p.525-535

[3] Wenhui, H., Guozheng, Y. Pingping, J, et al.. High Technology Letters,12(2006),p. 255-259.

[4] Wang, X., Meng, M. Q.-H., Chan, Y. A low-cost tracking method based on magnetic marker for capsule endoscope[C]. in 2004 International Conference on Information Acquisition,(2004),p. 524-526

[5] TANG Shuangqing , CHEN Xikun , TANG Bo.. COLLEGE PHYSICS，24(2005),p.32-36

[6] LI Jin, ZHENG Xiao-lin, HOU Wen-sheng, HE Jin, FANG Xing. Journal of System Simulation，21(2009),p.5919-5922 in Chinese

[7] Zhang Wei，Theoretical and Experimental Study on Driving and Controlling a Capsule MEMs by an Outer Magnetic Field, edtied by School of Mechanical and Automotive Engineering, South China University of Technology, Guangzhou(2007) in Chinese

[8] Zhao Bo,Zhang Hongliang. Ansoft 12 application in engineering field, edtied by China WaterPower Press (2010),in Chinese

[9] Honeywell hmc1023 instructions, http://wenku.baidu.com/link?url=31iYzd4H1I7IYSbNQPmTbCz1A6us78i-rCg-lInlu5d4Ns5e0HwlesVY7nRT6igZMXDrTA3xCOMFZ9Fy8zo5cmVk3qgvmYiYlnwRsO1TUZG, in Chinese

Applied Mechanics and Materials Vol. 596 (2014) pp 72-78
© (2014) Trans Tech Publications, Switzerland
doi:10.4028/www.scientific.net/AMM.596.72

The design and calculation of fur material cleaning machine

Yi Su[1a] ,Zhengfeng Li[1a]， Shuqin Huang[2b]

[1] School of Mechanical and Electrical Engineering, Wuxi Institute of Commerce, Wuxi Jiangsu, 214153, China

[2] School of Mechanical and Electrical Engineering,Tai zhou Polytechnic College.Tai zhou Jiang su. 225300,China

E-mail: [a:] cyddlzhf@163.com, [b:] hsq_1965@163.com

Keywords: fur material; Cleaning machine; Incomplete gear; design

Abstract: In order to improve dyeing capacity of the fur material, a fur material cleaning machine is designed; This paper Introduces the structure and working principle of the machine, The paper also discusses the design process of incomplete gear mechanism, introduces the problems that should be paid attention, elaborates relevant calculation steps. The use of incomplete gear mechanism realize the alternation of rotary movement time and idle time ,The machine has the advantages of gas-electric combination, program control, high production efficiency, convenient operation, etc.

The introduction

In order to reduce the tension of the fur material, make dye into the fur material easily and enhance the dyeing properties, cleaning process should be done in earlier stage.At present some small businesses are still adopt the method of artificial cleaning which is high labor intensity and low production efficiency, In order to improve the productivity, we designed a fur material cleaning machine with high degree of automation.

Structure and working principle

2.1 Structure

The fur material cleaning mechanism structure is shown in figure 1, the motor is connected by the coupling and the worm gear reducer, the driving gear is installed on the output shaft of the worm gear and worm reducer, the driving gear and driven gear make up of incomplete gear mechanism. the driven gear is installed on the lower end of the transmission shaft, the upper end of the transmission shaftis linked with the turntable, the cylinder is installed on turntable.Cylinder rotate with rotary table.

2.2 Working principle

Spray water to the cylinder during putting the fur material into it ,the cylinder rotating movement and the rammer up-and-down movement should meet the requirement in the time and order.So the the cylinder movement should be intermittent. piece of inductor are installed on Cylinder symmetrically , when the inductor on cylinder rotate to proximity switch, switch signal to make the air cylinder move, driving the rammer move down ,the rammer contact with the fur material and squeeze it by impact force to achieve the purpose of sufficient lubrication and cleaning;When rammer rises, the cylinder began to rotate ;the rammer up-and-down movement and the cylinder rotating movement coordinated, which can not only avoid rammer broken from the torsional moment, but also make rammer contact with the fur material sufficiently[1].

According to the requirement, ordinary cylinder is at 0.5 ~ 1 m/s, rotary table work speed should be at 20 ~ 30 r/min, the stroke of air cylinder which drives rammer is commonly 200 ~ 400 mm, so the calculated time that air cylinder reciprocate one time is 0.4 ~ 1.6 s.

Incomplete gear mechanism design

3.1 Structure characteristics

In order to achieve alternation change of the turntable movement time and idle time, we adopt incomplete gear mechanism.

Incomplete gear mechanism is involute gear mechanism and its gear tooth is not full of the entire circumference.as shown in figure 2.Driving gear do continuous rotary motion , driven gear does intermittent motion.Driving gear convex locking arc match with driven gear concave locking arc to ensure the gear stop .On the driven gear,the gear which concave locking arc is on is called thick tooth, is the first gear to participate in mesh on the driven teeth.Driving gear rotate a week , the times of driven gear intermittent movement N is equal to the number of tooth gear on the driven gear.

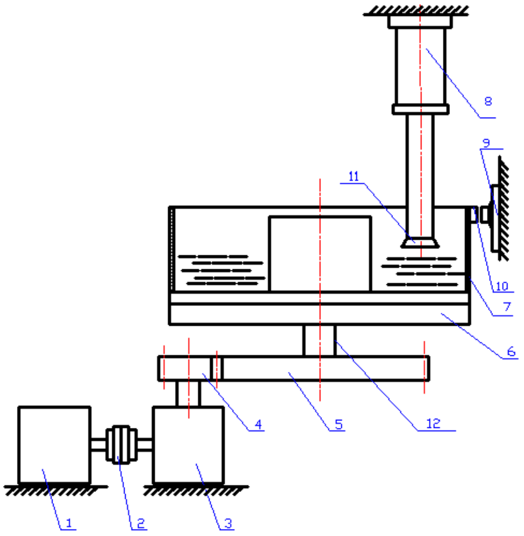

1.motor,2.coupling,3.worm gear reducer,
4. driving gear, 5. driven gear, 6.turntable,
7. cylinder, 8. air cylinder , 9. switch ,
10. inductor,11. rammer

Figure 1 Fur material cleaning machine

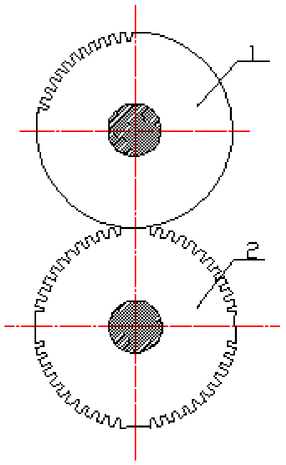

1. driving gear, 2.driven gear

Figure 2 Incomplete gear mechanism

3.2 Points for attention

The following four aspects of problems should be considered in incomplete gear mechanism design.

1) motion-stand ratio K The driven and driving gear movement time than rest time, namely motion-stand ratio should meet the design requirements.

2)The determination of coefficient about the first and the last gear tooth on the driving gear h^*_{as} and h^*_{am} The intermediary gear tooth on driving gear and addendum of driven gear are the same as the ordinary gears. Usually take the addendum coefficient $h^*_{a1} = h^*_{a2} = 1$, but the coefficient of the first and the last gear tooth on the driving gear h^*_{as} , h^*_{am} are different. In general, $h^*_{am} \prec 1$, often take $h^*_{as} \prec h^*_{am}$.

3)Continuous transmission performance Due to the addendum coefficient of the first tooth reduced, in order to make the contact ratio after the first tooth addendum reduced meets $\varepsilon \succ 1$, when the first tooth left before the point B_1 on the constant speed ratio transmitted and actual meshing line $\overline{B_1 B_2}$,shown in figure 3,the second pair of gear tooth should enter to mesh on point B_2.

4)Locking arc configuration problems When the driving gear first time to enter to mesh ,the locking arc endpoint E should be in the center line of the two gears, as shown in figure 3.When the last gear tooth left meshing, the locking arc start point S should also be in the centerline of the two gears, as shown in figure 4. [2]

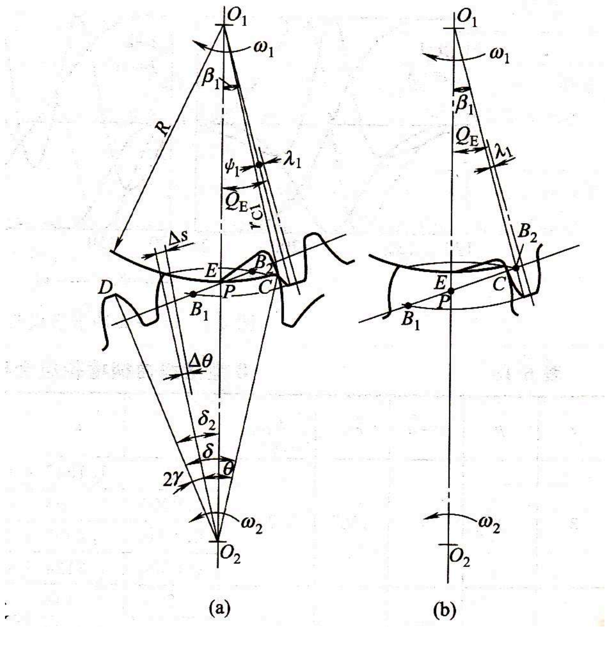
O_1
ω_1
β_1
R
φ_1
λ_1
Q_E
r_{C1}
Δs
E
B_2
D
P
C
B_1
$\Delta\theta$
δ_2
δ
2γ
θ
ω_2
O_2
(a)
O_1
ω_1
β_1
Q_E
λ_1
B_2
E
C
P
B_1
ω_2
O_2
(b)

Figure 3 The first teeth into engagement position

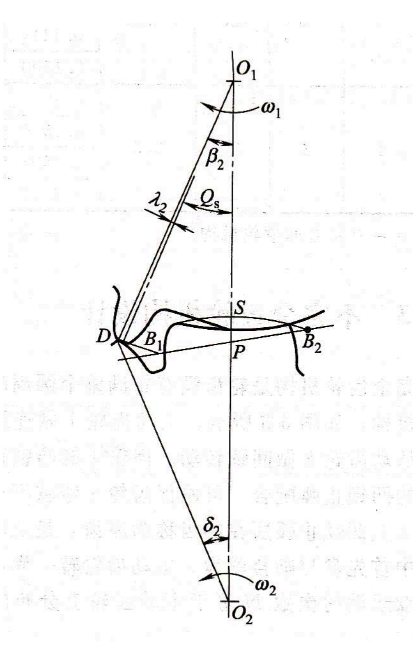
O_1
ω_1
β_2
λ_2
Q_s
S
D
B_1
P
B_2
δ_2
ω_2
O_2

Figure 4 End teeth disengage position

3.3 Calculation example

Below a fur material washing machine which its turntable diameter is 1200mm can be calculated as an example. Select motor model Y132s-6(P=3KW, n=960r/min), and select worm reducer which is wpo120-40. Because the worm gear ratio is i = 40, so the active speed gear is n_1=24r/min, and so select the speed driven gear which is n_2 = 24r/min. The Design requires when each revolution of the driving gear, and the driven gear revolts and then stop for a quarter week.

The symbols used in the formula show in Figure 3 and Figure 4, the following calculation steps:

(1) Determine the modulus m, center distance and a number of teeth z.

The driven gear run every turn by a quarter, select $z_2 = 13$, $z_2' = 52$, then take $z_1' = z_2' = 52$.

Known from reference [2] Table 6-19 $K = 3$, then the locking teeth arc which is between the two adjacent active gears is:

$$z_1 = z_2 + 1 - K = 13 + 1 - 3 = 11$$

The number of modulo is $m = 5$ mm, so the center distance can be:

$$a = \frac{m}{2}(z_1' + z_2') = \frac{5}{2}(52 + 52) = 260(mm)$$

(2) Pressure angle α and the coefficient of addendum is $h^*{}_a$ .Take

$$\alpha = 20^\circ\text{;}\quad h^*{}_{a1} = h^*{}_{a2} = 1$$

(3) Addendum pressure angle α_a

$$\alpha_{a1} = \arccos\frac{z_1'\cos\alpha}{z_1' + 2} = \arccos\frac{52\cos 20^\circ}{52 + 2} = 25^\circ 11'$$

$$\alpha_{a2} = \arccos\frac{z_2'\cos\alpha}{z_2' + 2} = \arccos\frac{52\cos 20^\circ}{52 + 2} = 25^\circ 11'$$

(4) In an intermittent motion，the angle of the driven gear δ' is:

$$\delta = \frac{2\pi}{z_2'}K = \frac{360^\circ}{52}\times 3 = 20^\circ 46' \qquad (\text{when } z_1 = 1)$$

$$\delta' = \frac{2\pi}{z_2'}z_2 = \frac{360^\circ}{52}\times 13 = 90^\circ \qquad (\text{when } z_1 = 11 \succ 1)$$

(5) At the end of the driving gear tooth out of meshing position, driven gear tooth vertex position Angle δ_2 :

$$2\gamma = \frac{\pi}{z_2'} + 2(inv\alpha_{a2} - inv\alpha) = \frac{\pi}{52} + 2(inv25^\circ 11' - inv20^\circ) = 5^\circ 16'$$

$$\delta_2 = \frac{\pi}{z_2'}K + \gamma = \frac{180^\circ}{52}\times 3 + 2^\circ 38' = 13^\circ 1'$$

(6)The first and the end of the driving gear teeth and the teeth of the top pressure angle are α_{as} and α_{am}

$$L = \frac{z_2'(z_1'+z_2') + 2(1+z_2') - (z_1'+z_2')(2+z_2')\cos\delta_2}{2} = \frac{52\times 104 + 2\times 53 - 104\times 54\cos 13^\circ 1'}{2}$$
$$= 21.1997$$

$$h^*{}_{am} = \frac{-z_1' + \sqrt{z_1'^2 + 4L}}{2} = \frac{-52 + \sqrt{52^2 + 4\times 21.1997}}{2} = 0.4045$$

Take $h^*{}_{as} = 0.35$ （Should make $h^*{}_{as} \prec h^*{}_{am}$ ）, get

$$\alpha_{as} = \arccos\frac{z_1'\cos\alpha}{z_1' + 2h^*{}_{as}} = \arccos\frac{52\cos 20^\circ}{52 + 2\times 0.35} = 22^\circ$$

$$\alpha_{am} = \arccos\frac{z_1'\cos\alpha}{z_1' + 2h^*{}_{am}} = \arccos\frac{52\cos 20^\circ}{52 + 2\times 0.4045} = 22^\circ 17'$$

(7) The first tooth contact ratio ε

$$\varepsilon = \frac{z_1'}{2\pi}(\tan\alpha_{as} - \tan\alpha) + \frac{z_2'}{2\pi}(\tan\alpha_{a2} - \tan\alpha)$$
$$= \frac{52}{360^\circ}(\tan 22^\circ - \tan 20^\circ) + \frac{52}{360^\circ}(\tan 25^\circ 11' - \tan 20^\circ) = 1.2115 \succ 1$$

(8) Two perspectives on the driven gear locking arc are θ and $\Delta\theta$

$$\theta = \delta - 2\gamma = 20^\circ 46' - 2\times 2^\circ 38' = 15^\circ 30';\quad \Delta\theta = \frac{1}{z_2' + 2} = \frac{1}{52+2} = 1^\circ 4'$$

(9) Locking arc radius R

$$R = \frac{m}{2}\sqrt{(z_2'+2)^2 + (z_1'+z_2')^2 - 2(z_2'+2)(z_1'+z_2')\cos(\frac{\theta}{2} - \Delta\theta)}$$

$$= \frac{5}{2}\sqrt{(52+2)^2 + (52+52)^2 - 2(52+2)(52+52)\cos(\frac{15^\circ 30'}{2} - 1^\circ 4')} = 126.8960(mm)$$

(10) When the driving gear into engagement with the first position, then the vertex angle of tooth is β_1

$$\frac{\theta}{2} = 7^\circ 45' \succ \alpha_{a2} - \alpha = 5^\circ 12'$$

$$r_{c1} = \frac{m}{2}\sqrt{(z_2'+2)^2 + (z_1'+z_2')^2 - 2(z_2'+2)(z_1'+z_2')\cos\frac{\theta}{2}}$$

$$=\frac{5}{2}\sqrt{(52+2)^2+(52+52)^2-2(52+2)(52+52)\cos\frac{15°30'}{2}}=127.5380(mm)$$

$$\alpha_{c1}=\arccos\frac{mz_1'\cos\alpha}{2r_{c1}}=\arccos\frac{5\times52\cos20°}{2\times127.54}=16°42'$$

$$\psi_1=inv\alpha_{as}-inv\alpha_{c1}=inv22°-inv16°42'=40'$$

$$\beta_1=\arctan\frac{(z_2'+2)\sin\frac{\theta}{2}}{z_1'+z_2'-(z_2'+2)\cos\frac{\theta}{2}}+\psi_1$$

$$=\arctan\frac{(52+2)\sin\frac{15°30'}{2}}{52+52-(52+2)\sin\frac{15°30'}{2}}+40'\quad=9°52'$$

(11)When the driving gear is disengaged from the end position, then the location of the vertex angle of tooth is β_2:

$$\beta_2=\arcsin\frac{(z_2'+2)\sin\delta}{z_2'+2h^*_{am}}\quad=\arcsin\frac{(52+2)\sin13°1'}{52+2\times0.404}=13°19'$$

(12) Over the end of the pinion gear E convex arc angle to the path $\overline{O_1E}$, then the angle which is between the first tooth and the midline is Q_E.

$$\lambda_1=\frac{\pi}{2z_1'}-inv\alpha_{as}+inv\alpha\quad=\frac{180°}{2\times52}-inv22°+inv20°=1°26'$$

$$Q_E=\beta_1+\lambda_1=8°52'+1°26'=10°18'$$

(13) And the angle Q_S which is between the end of the pinion gear teeth midline and over the starting point of a convex arc S to Trail $\overline{O_1S}$

$$\lambda_2=\frac{\pi}{2z_1'}-inv\alpha_{am}+inv\alpha\quad=\frac{180°}{2\times52}-inv22°17'+inv20°=1°6'$$

$$Q_S=\beta_2+\lambda_2=13°19'-1°6'=12°13'$$

(14) Angular motion of the pinion gear β

$$\beta=Q_E+Q_S+2\pi\times\frac{z_1-1}{z_1'}\quad=10°18'+12°13'+360°\times\frac{11-1}{52}=91°45'$$

(15) Stop time and moving time ratio is k and sporting coefficient is τ

$$k=\frac{\beta N}{2\pi-\beta N}=\frac{91°45'\times 1}{360°-91°45'\times 1}=0.3421\text{；}\quad \tau=\frac{\beta N}{2\pi}=\frac{91°45'\times 1}{360°}=0.2549$$ [2]

(16) Exercise time t_2 and Stop time $t_2^{'}$

The driving gear sets for constant rotation , then Angular velocity $\omega_1=\frac{\pi n_1}{30}$.The time required per revolution $t_1=\frac{2\pi}{\omega_1}$, and the movement time of the driven gear t_2 and stop time $t_2^{'}$ can be expressed as: $t_2=\frac{\beta}{360^0}t_1$, $t_2^{'}=(1-\frac{\beta}{360^0})t_1$ [3]

Because $n_1=24$ r/min, then $t_1=2.5s$, $t_2=0.637s$, $t_2^{'}=1.863s$ can be calculated. Stop time $t_2^{'}$ is greater than the time required for one cylinder reciprocating 1.6S, which meets the requirements.

Conclusions

Design of fur material cleaning machine has simple structure, high degree of automation, it can improve the production efficiency, reduce the labor intensity of workers.

References

[1] Shuqin.Huang. a punching machine[p]China:CN201220676105.5.2013.06.12

[2] datong Qin , Liyang Xie .Modern mechanical design manual singles (mechanical design) [M]. Beijing: chemical industry press, 2013:159-160

[3] Shuliang Zou ,Conggui Chen , Anbing Li. Designof Partial Gear Meehanism in Automatie Turntable [J]. Journal of hengyang institute of technology, 1994, 8 (2) : 99-102

Applied Mechanics and Materials Vol. 596 (2014) pp 79-82
© (2014) Trans Tech Publications, Switzerland
doi:10.4028/www.scientific.net/AMM.596.79

The semi-automatic restoration of regular paper fragments

ZhongQiu Ding

Shandong University(weihai)，Electromechanical and Information Engineering,264209 weihai,China

347717832@qq.com

Keywords: Binarization Edge contrast matrix Q cluster Manual intervention

Abstract. The restoration of regular paper fragments can be solved by edge matching. Edge matching is based primarily on the length and location of the break in writing, however, it is possible that the edges of some regular paper fragments are blank. And so the error of restoration is the inevitable. In this case, it needs manual intervention based on the article content and then eliminate errors. Prior to the establishment of a mathematical model, there is a need for binarization of regular paper fragments with Matlab, then establish vector space model and construct edge contrast matrix, get the order after the Q cluster analysis of fragments. Finally the original picture can be obtained through splicing and restoring in the order.

Introduction

The restoring of crushed files has an important application in judicial evidence recovery, restoration of historical documents and the access to military intelligence and other areas have important applications.Traditionally, splicing restoration work required to be completed manually, which has high accuracy .But the artificial splicing restoration has some shortcomings for its low speed and limit of application on area.With the development of computer technology, the auto restoration of fragments is gradually come into view. Through the efforts of experts and scholars at home and abroad, the auto restoration of fragments has made great progress. This paper is aimed primarily at feature extraction for regular paper fragments data from the China Undergraduate Mathematical Contest in Modeling. Feature extraction is a very important step in the splicing and restoring of paper fragments which determines the accuracy and efficiency. The conventional stitching approach of document fragment is always based on the geometric characteristics of the borders, thus search out the fragment which can match with it. However, the edge of regular paper fragment is trim, which reduces the feature information and increases the difficulty of splicing and restoring. The stitching approach based on the geometric characteristics of the border can not be applied to the regular paper fragment of similar edges. The method proposed in this paper mainly takes advantage of similarities between adjacent fragments of document and the geometric characteristics of text line, for example, the height of text line, the distance of text lines and other information. But with the increase of fragments' quantity, there will be more manual intervention and errors, cluster analysis can improve this situation.

Binarization of regular paper fragments

The picture of paper fragments can be transformed into the gray matrix by taking advantage of the imread function in Matlab, in which the size of matrix matches with the size of paper fragments. Then dealing with the gray matrix in order to get the binarized matrix, in which 1 represents a blank and 0 represents black. The method is shown as follows:

$$P(i,j)=\begin{cases}0, X(i,j)\geq T\\255, X(i,j)<T\end{cases} \tag{1}$$

In which *X(i,j)* refers to the gray matrix of the fragment, *P(i,j)* refers to the binarized matrix, *i* refers to the line number in matrix, *j* refers to the column number in matrix, *T* refers to the given threshold.

Stitching and restoring of vertical cutting paper fragments

The edge information of vertical cutting paper fragments exists in both left and right edges that belong to Annex I and Annex II. Therefore the point is the similarity between the vertical edges of each paper fragment, the greater the degree of similarity is, the higher the degree of matching between two vertical edges is.

First , transform the paper fragments into the binarized matrix, and obtain a matrix of 1980*72. Then take the first column and the last column of each matrix as the edges of paper fragment, and obtain a edge contrast matrix of 1980*38 which refers to A. Cosine similarity of the text is the cosine of the angle between the text feature vectors in space. The calculation is shown as follows:

$$\sum_{j=1}^{19}\sum_{k=1}^{19}C(j,k)=\frac{\sum_{i=1}^{19}a_i\times a_{i+19}}{\sqrt{\sum_{i=1}^{19}a_i{}^{\wedge}2}\times\sqrt{\sum_{i=1}^{19}a_{i+19}{}^{\wedge}2}} \tag{2}$$

In which *C(j,k)* refers to the cosine of the angle formed between the first column of the j-th paper fragment and the last column of the k-th paper fragment, *ai* refers to the i-th column of the matrix *A*.

Through analyzing the data of *C(j,k)* and comparing the similarity between two vertical edges, get the order of stitching and restoring. According to the page margins of printed text, the piece on the most left side of the page can be selected from lots of regular pieces. On the basis of similarity between two vertical edges, we can join together the pieces horizontally from the ensured piece.

Stitching and restoring of paper fragments cut both horizontally and vertically

The edge information of each paper fragments in Annex III and Annex IV exists in its top edge, bottom edge, left edge and right edge. The binarized datas that extracted from the first and the last column of each fragment's binarized matrix are regarded as the matching basis between left edges and right edges. According to this, make the first round of matching by the way in the first question, and get the transverse stitching ans restoring of fragments. After the operation,there are some horizontal strips. Then, make the second round of matching based on the first round, that is extracting the first and the last row of each horizontal strip's binarized matrix and regarding them as the matching basis between top edges and bottom edges. During the process, the manual intervention is required that screening out the first picture on the left and eliminating splicing errors.

Improved stitching and restoring of paper fragments cut both horizontally and vertically based on cluster analysis

There are some differences between English typography and Chinese typography: The alphabets printed in English are case-sensitive and have different height, but the Chinese characters are of square feature and have the same height. Taking account of these differences, the stitching of paper fragments printed in Chinese in a more simple way. The idea is shown as follows:

The text lines in most documents are parallel, if the text line is fractured in the edge of a piece, then its adjacent fragments must have the same text line in the same position, according to this feature, it it easy to select its adjacent fragments among all the paper fragments.

After transforming the paper fragments into the binarized matrix, If a line contains 0 ,then turn all the elements of this line into 0. In this way, we can avoid the influence of the blank which exists in typeface's break on edge information, and let the position of each text line in the fragment become the basis of clustering. Extract a column for each matrix to form a new matrix, and find its transposed matrix *a(i,j)*. Find the absolute distance between any two row vector among this transposed matrix with the absolute distance formula:

$$D_{(m,n)} = \sum_{j=1}^{180} \left| a_{(m,j)} - a_{(n,j)} \right| \qquad (3)$$

Find the square of the absolute distance between the m-th row and the n-th row:

$$d_{(m,n)} = \sum_{j=1}^{180} \left[a_{(m,j)} - a_{(n,j)} \right]^{\wedge} 2 \qquad (4)$$

（m=1,2,3……209，n=1,2,3……209，m≠n）

Q cluster analysis is the study about classification problem of the multifactor things. It's principle is making use of sample's own properties and using mathematical method to determine the affinity-disaffinity relationship between samples according to some similarity or diversity index and quantitatively , and clustering samples ,according to the degree of the affinity-disaffinity relationship. Therefore, determine the closeness between samples with Q cluster analysis quantitatively, cluster these samples according to the degree of closeness. With this approach, the fragments that in the same original line are clustered into a category. We can divide these fragments into N categories, N is determined by experiment and cutting method. And here, N=25. During this process, error is still inevitable, but the manual intervention is less.

Within each category, matching edges by the way in the first question and obtain 11 complete picture in a horizontal direction. Next, splice these 11 pictures in a vertical direction with the same method. Finally, it makes up a complete and correct image.

The results and analysis

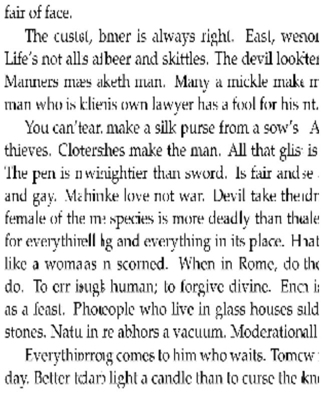

fair of face.
The custst, bmer is always right. East, wenoı
Life's not alls albeer and skittles. The devil lookter
Manners mæs aketh man. Many a mickle make m
man who is klienis own lawyer has a fool for his nt.
You can'tear. make a silk purse from a sow's A
thieves. Clotershes make the man. All that glis: is
The pen is nwinightier than sword. Is fair and se
and gay. Mahinke love not war. Devil take theidr
female of the me species is more deadly than thale
for everythirell hg and everything in its place. Hat
like a womaas n scorned. When in Rome, do the
do. To err isugh human; to forgive divine. Enca i:
as a feast. Phoeople who live in glass houses sild
stones. Natu in re abhors a vacuum. Moderationall
Everythinrroig comes to him who waits. Tomcw
day. Better tdan light a candle than to curse the kn

Fig.1 The result of vertical cutting fragments

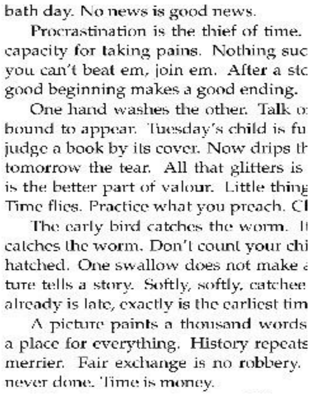

bath day. No news is good news.
Procrastination is the thief of time.
capacity for taking pains. Nothing suc
you can't beat em, join em. After a stc
good beginning makes a good ending.
One hand washes the other. Talk o:
bound to appear. Tuesday's child is fu
judge a book by its cover. Now drips tł
tomorrow the tear. All that glitters is
is the better part of valour. Little thing
Time flies. Practice what you preach. Cl
The early bird catches the worm. It
catches the worm. Don't count your chi
hatched. One swallow does not make a
ture tells a story. Softly, softly, catchee
already is late, exactly is the earliest tim
A picture paints a thousand words
a place for everything. History repeats
merrier. Fair exchange is no robbery.
never done. Time is money.

Fig.2 The result of fragments cut both and horizontally and vertically

According to Fig.1 and Fig.2, the recovery is excellent, so the algorithm design is reliable.

Conclusions

In this paper, the method of edge information extraction combined with cluster analysis is accurate and reliable. Though it needs manual intervention, the stitching and restoring has a high correct rate. According to the experimental results, the method presented in this paper is feasible, and can be applied to the archaeology and military.

References

[1] Hun Yu, ZaiKe Hou and XuLi He. Design and implementation of image stitching algorithm based on contour feature[J].SHIYOU UNIVERSITY(Natural Science Edition),Vol.2 No.27 (2003) p114-p118 In Chinese.

[2]DongMei Li and YanJie Wang. Image stitching technology based on feature matching[J].Image processing,Vol.53 No.24 (2008) p296-298 In Chinese.

[3]QiYuan Jiang, JinXing Xie and Jun Ye. Mathematical Model[M].High Education Press, 2011 In Chinese.

[4]ZhenYa Zhang, Jin Wang, HongMei Cheng and XvFa Wang. Text space index method based on cosine similarity[J]. Computer Science. No.09(2005) In Chinese.

Applied Mechanics and Materials Vol. 596 (2014) pp 83-89
© (2014) Trans Tech Publications, Switzerland
doi:10.4028/www.scientific.net/AMM.596.83

Development of Computer-aided Manufacturing System for a Jewelry-making CNC Machine

Ya Miao[1,2,4,a], Kai He[1,2,b,*], Haitao Fang[1,2,c], Zhimin Zhou[1,2,d] and Ruxu Du[3,e]

[1]Shenzhen Institutes of Advanced Technology, Chinese Academy of Sciences, Shenzhen, China

[2]Shenzhen Key Laboratory of Precision Engineering, Shenzhen, China

[3]The Chinese University of Hong Kong, Shatin, N.T, Hong Kong

[4]University of Science and Technology of China, Hefei, China

[a]ya.miao@siat.ac.cn, [b]kai.he@siat.ac.cn, [c]ht.fang@siat.ac.cn, [d]1413303695@qq.com,
[e]rdu@mae.cuhk.edu.hk

*corresponding author

Keywords: Jewelry-making CNC Machine, CAM, NC Program, Simulation.

Abstract. This paper designs a CAM system for a jewelry-making CNC machine. The CAM system not only provides a human-computer interface for setting machining parameters, but also can generate special NC programs automatically and realize the simulation for the machining process. In addition, the paper gives an efficient application for machining an ellipsoidal gold bead. The basic design of the jewelry-making CAM system and the experimental results are presented.

Introduction

Generally, the special CAM system generates suitable NC program according to each workpiece's shape and the special CNC machine's system. For the jewelry-making CNC machine, there are many well-known jewelry CAD/CAM softwares on the market, such as Artcam Jewelsmith, Jewelcad, MasterCAM ART, etc. All have mature CAD jewelry modeling function, but their CAM post processor hardly could produce suitable NC program for 5 or more axises special NC machine tools actually used. In addition, on account of the high cost of the oversea CAD/CAM copyrighted software, these softwares are not proper choices in jewelry industry applications in china. Thus, it is necessary to develop the special CAM system for jewelry-making CNC machines.

With the improvement of people's living standard, more and more beautiful jewelry is required, especially a kind of ellipsoidal gold bead jewelry named lucky bead with simple patterns on its surface. At present, the jewelry-making CNC machines used for machining a pattern on a bead surface have a similar machine structure. It usually has 5 axises or more but lacks a matched special CAM module.

In the jewelry industry, manual trial cutting on a bead to get a perfect pattern is the main production mode, which is dependent on the proficiency and experience of operators and results in many problems like poor levels of automation, low production efficiency, low product accuracy and consistency. In order to overcome the shortcoming of manual operation, CAM system of jewelry is needed to develop to improve pattern's quality and machining efficiency, which also reduces the demand of operator's knowledge and experience[1].

In this paper, a simple CAM system is designed for a jewelry-making CNC machine, which is used to cut patterns on the surface of ellipsoidal beads in order to explore a method of quickly developing a CAM system for special jewelry-making CNC machines.

Jewelry-making CNC Machine's Structure

The designed CAM system is adapted to the our designed jewelry CNC machine shown in the Fig.1. The CNC machine has 9 axises, A, B, C, D, E, X, Z, M01, M02, to coordinate to cut patterns, where X, D, Z are translational axises and C, E, A, B are rotational axises. Axis A, B, D, E, X, M01, and M02 control tool's motion. Axis C, and Z axis control the workpiece's motion. Axis X, and D can drive the tool move horizontally forward and backward, whereas Axis A, and E can make tools rotate about Axis X and D respectively. Axis B can rotate X-D table horizontally. The ellipsoidal workpiece is clamped by the air cylinder, and Axis Z can drive workpiece to move forward and backward perpendicularly to X-D orientation, and Axis C axis can rotate workpieces around Axis Z. Axis M01 and M02 are the tools' self-rotating axises.

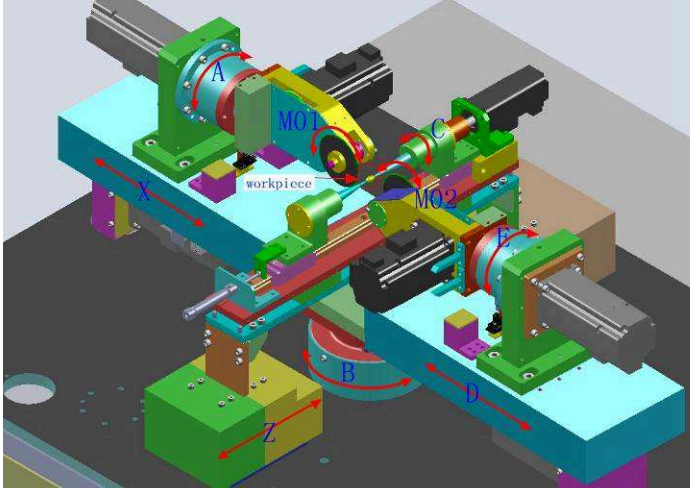

Fig. 1. The jewelry-making CNC machine

CAM System Design

The CAM system should include three main functions: it must have a human-computer interface to help operators set technological parameters. In the meantime, it should assist operators with calculation and generate NC program by itself. In addition, it can also realize process simulation, which makes operators a better understand of the process results. Based on the above points, the CAM system is divided into 5 modules, including the workpiece definition module, the machining parameters module, the tool path planning module, the NC program generation module and the process simulation module. In consideration of software implementation, the software development kits are MFC Dialog framework in VC++ and OpenGL graph lib, which put friendly interface and graph process into practice. The design of every module of CAM system are introduced in next sections.

Workpiece Definition Module. The workpiece is an ellipsoidal bead, and the designed CAM system must provide a graphic interface to guide users to set workpiece's dimensions, then CAM system software automatically models the workpiece.

The ellipsoid surface is gridded into limited numbers of small rectangles to render model by OpenGL drawing functions. According to the small rectangles' sum and equation (1) , it can easily calculate the vertexs of gridded rectangles.

$$\begin{cases} x = a\sin\theta\cos\varphi \\ y = a\sin\theta\sin\varphi \\ z = c\cos\theta \end{cases}, \quad 0 \le \theta \le \pi, 0 \le \varphi \le 2\pi. \tag{1}$$

Machining Parameters Module. Process design is mainly based on the analysis and processing of large amounts of information by selection(processing method, machine tool, cutting tool and machining sequence, etc.), computing (machining allowance, dimensions, tolerances, cutting parameters and time quota, etc.), drawing (process chart), as well as by process documents, etc. In general, the process parameters are chosen according to the size and shape of the parts and processing content [2].

During the process planning of the jewelry CAM system, three main parameters shown in Fig. 2 should be considered. The CAM system offers users system parameters and NC code related parameters setting as well as a patterns library. In the patterns library, operators could choose needed elementary patterns and set elementary patterns' parameters, which include shape parameters and position parameters on the bead's surface.

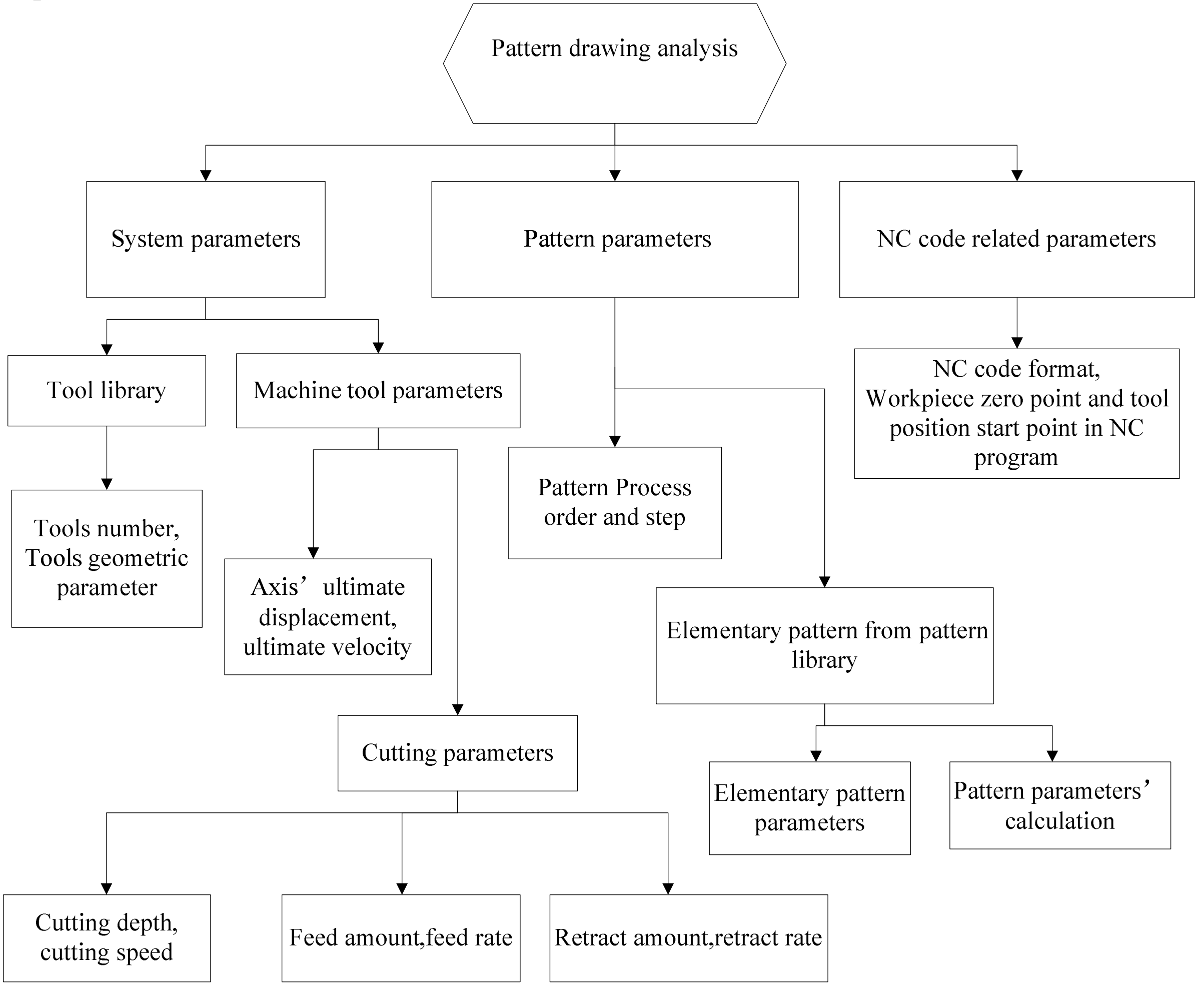
Pattern drawing analysis
System parameters
Pattern parameters
NC code related parameters
Tool library
Machine tool parameters
NC code format, Workpiece zero point and tool position start point in NC program
Tools number, Tools geometric parameter
Axis' ultimate displacement, ultimate velocity
Pattern Process order and step
Elementary pattern from pattern library
Cutting parameters
Elementary pattern parameters
Pattern parameters' calculation
Cutting depth, cutting speed
Feed amount,feed rate
Retract amount,retract rate

Fig. 2. Technological parameters needed

Tool Path Planning Module and NC Program Generation Module. In order to generate NC program , the CAM system needs to plan the tool path, and calculate the cutter location point according to the designed patterns and workpiece' s shape feature, then transform the location point which is in the workpiece coordinate system to the machine tool' s coordinate system to get the nine axises' relative vector displacements simultaneously.

Inverse Solution to Axises' Relative Vector Displacements. When calculating every axis' relative vector displacement from origin state, the CNC machine configuration shown can be considered simply as 5 axises configuration like other jewelry-making CNC machine. Because Axis X, A, and M01 are symmetry with Axis D, E and M02 respectively and the workpiece is a rotational part, Axis M01 and M02 have no influence on calculation. Only calculation of Axis X, A, B, C and Z or Axis E, D, B, C and Z are required.

Most postprocessors of special CAM system are based on the workpiece feature technologies[3], and involve inverse kinematics calculation using homogeneous coordinates transformation[4,5,6]. Here, we can simply transform and calculate the inverse solution without homogeneous coordinates: according to the shape of ellipsoid workpiece and motion mode of the mechanical axises, we use following expressions to deal with the inverse kinematics.

Fig.3 shows the bead's XOZ plane projection in the workpiece coordinate system. Point O is the origin. Point P1(x1,y1,z1) is the actual machining point on the workpiece surface, every mechanical axis' relative vector displacement can be calculated as follows:

The projection equation can be expressed as:

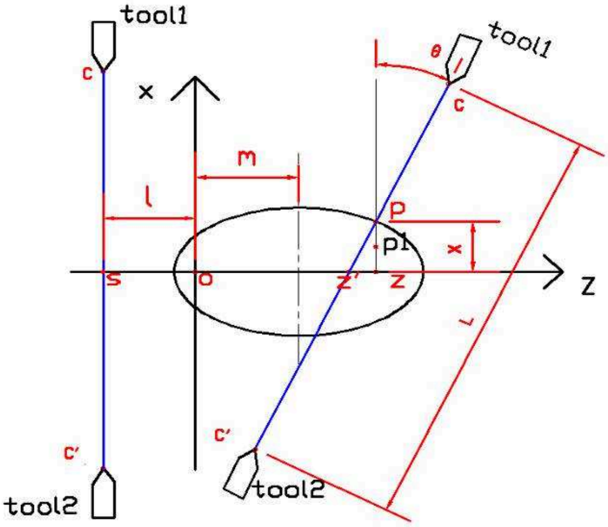

Fig. 3. Bead's XOZ plane projection in the workpiece coordinate system

$$\frac{(z-m)^2}{c^2}+\frac{x^2}{a^2}=1 \quad , \qquad (2)$$

Where c is semi-major axis of ellipsoid and a is semi-minor axis.
The vector distance |PZ| calculated by (2) is:

$$x=\sqrt{\frac{a^2\left[c^2-(z_1-m)^2\right]}{c^2}} \quad . \qquad (3)$$

The vector angle on the point P between the X-axes positive direction in the workpiece coordinate system to the tool 1 movement trail line cc' is:

$$\theta=\arctan\left(-\frac{(z_1-m)\ \times a^2}{x\times c^2}\right) \quad , \qquad \theta\subset\left(-\frac{\pi}{2},\frac{\pi}{2}\right) \quad . \qquad (4)$$

x in (4) is determined by (3), and it can be inferred that:
Axis Z's relative vector displacement is:

$$-(l+|OZ'|)=-(l+z_1+x\times\tan\theta) \,. \qquad (5)$$

l is set by operators, which is related to the start point of cutter location. Because the tools can't move along the Z-axes direction, and the workpiece can do this, Axis Z's relative vector displacement symbol is negative.

After the workpiece moves along the Z-axes direction, the machine's Axis B rotating center has became Point z' from Point s. Then if we choose tool 1 to machine the Point P , Axis B's relative vector displacement is θ. Axis X's relative vector displacement is:

$$\left(|CZ'|-\frac{x}{\cos\theta}\right)=\left(|CS|-\frac{x}{\cos\theta}\right) \quad , \qquad (6)$$

where |CS| is set by the operator.

Axis C's relative vector displacement is figured out by (7):

$$c=-\arcsin\left(\frac{y1}{x}\right), c \subset [-\pi,\pi] \quad (7)$$

Axis A's relative vector displacement is determined by the cutting direction according to the pattern.

If Point P is in the fourth quadrant of the XOZ plane, the x value symbol is opposite to the gotten x by (3). If we use the number 2 tool, the formulas of getting every Axis B, Z, D, C's displacement is similar to the referred Equation (4), (5), (6) and (7).

Program Design. Algorithm flow charts of these two modules are shown in Fig. 4 and Fig. 5:

The calculation in tool path planning module consists of two main parts. One is the CL point calculation using inverse kinematics introduced in the previous section, and the other is the pattern's theoretical cutting result calculation according to the tool's geometric dimension and process parameters.

The development of NC program generation module also includes two main parts. One is the reading and saving of files and filtering fields of the data for all records, the other is the interpreter programm, which interprets the CL point data in ASCII format as the corresponding NC program code.

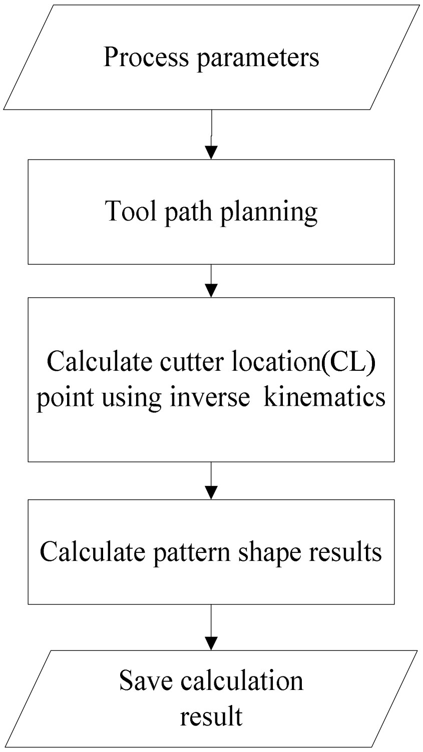
Process parameters
Tool path planning
Calculate cutter location(CL) point using inverse kinematics
Calculate pattern shape results
Save calculation result

Fig. 4. Algorithm flow chart of tool path planning module

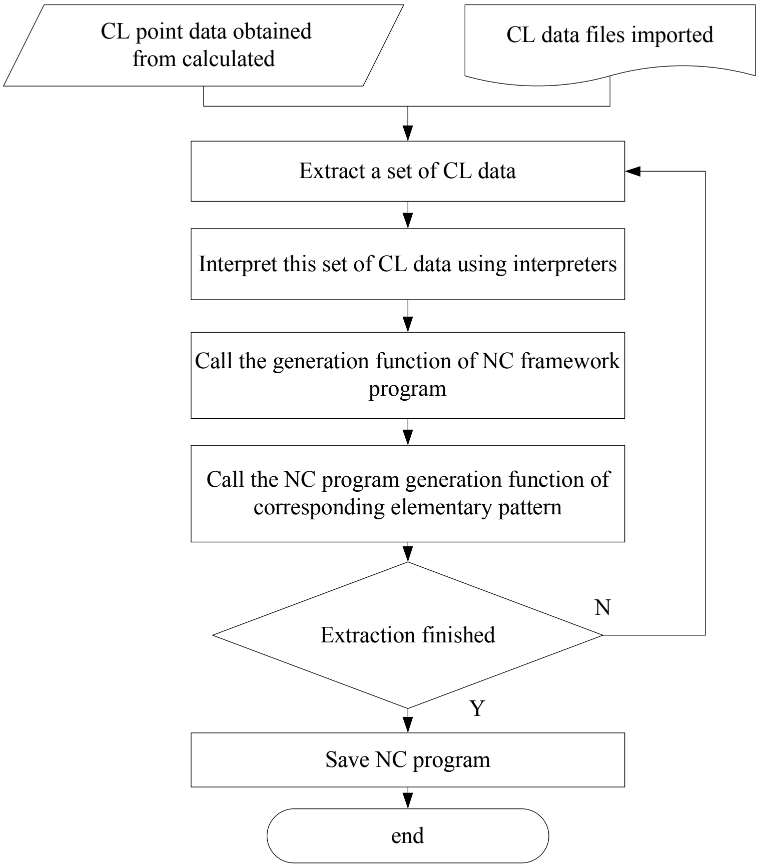
CL point data obtained from calculated
CL data files imported
Extract a set of CL data
Interpret this set of CL data using interpreters
Call the generation function of NC framework program
Call the NC program generation function of corresponding elementary pattern
Extraction finished
N
Y
Save NC program
end

Fig. 5. Algorithm flow chart of NC program generation module

Process Simulation Module. This module not only realizes the function of compiling the existing NC program but also offers operators the edit box to manually input NC program. Further, the module provides the interpreter of the NC program corresponding with the graphics programming of tools' cutting motion. In the meantime, operators could see the simulation of the machining process.

Fig.6 shows the pattern graphic modeling flow and Fig.7 shows the design of tools' cutting process simulation flow. The tools' cutting process simulation could be well performed by OpenGL double buffering drawing pictures and model transformation. For the reason of quick development's requirement, the patterns on the bead's surface are shown with surface visual effect to help workers analyse the pattern, instead of scraggy visual effect.

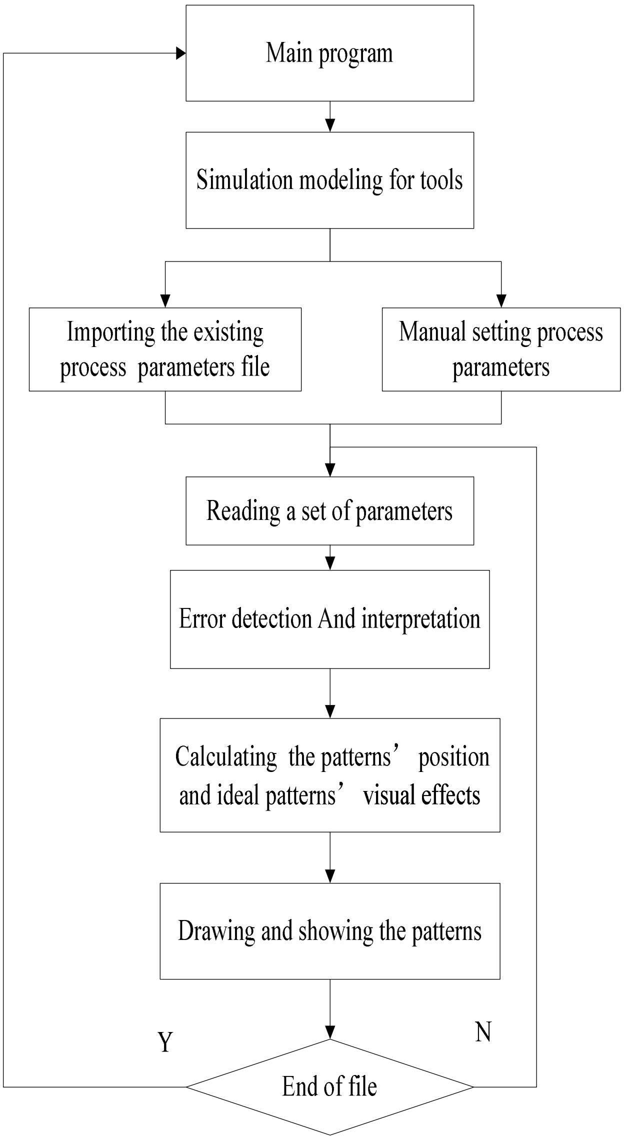
Main program
Simulation modeling for tools
Importing the existing process parameters file
Manual setting process parameters
Reading a set of parameters
Error detection And interpretation
Calculating the patterns' position and ideal patterns' visual effects
Drawing and showing the patterns
Y
N
End of file

Fig. 6. Flow chart of pattern modeling

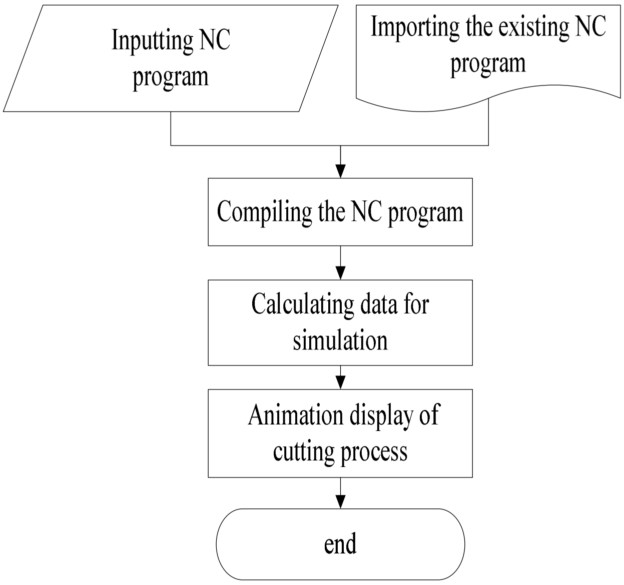
Inputting NC program
Importing the existing NC program
Compiling the NC program
Calculating data for simulation
Animation display of cutting process
end

Fig. 7. Flow chart of cutting process simulation

In the cutting process simulation module, it involves the NC program complier, which effectively checks the error of NC program, filter and interpret the needed NC program into the corresponding simulation animation.

Experimental Results

In this section, the simulation results and actual results of machining the pattern "米" on a ellipsoidal bead's surface using the designed CAM system for our designed jewelry-making machine (Fig.8) are shown in Fig.9 and Fig.10. In addition, other patterns machined by the proposed CAM system are also exhibited in Fig.11.

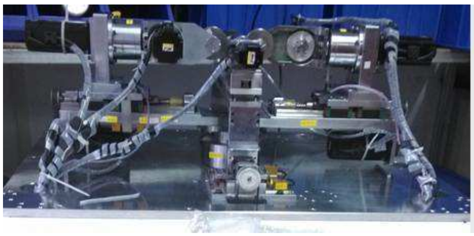

Fig. 8. The Jewelry-making CNC machine

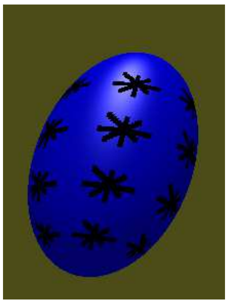

Fig. 9. The simulated “米” pattern

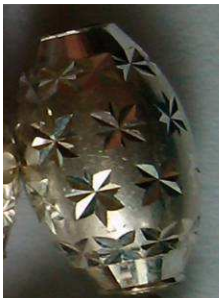

Fig. 10. The machined “米” pattern

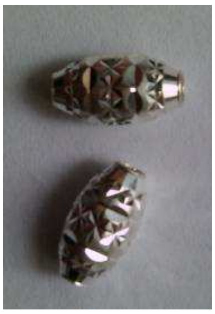

Fig. 11. Other machined patterns

From the simulation and experimental results, we can see it is successful to machine the workpiece with the designated pattern with the developed CAM system.

Conclusions

This paper presents the development of a CAM system for a jewelry-making CNC machine. The system consists of five main parts:workpiece definition module, machining parameters module, tool path planning module, NC program generation module, and process simulation module. The experiments validate that the CAM system design is successful, and it will help to improve the producing efficiency and product uniformity in the jewelry industry.

Acknowledgements

This research was surpported by the Shenzhen Science and Technology Development Project (CXZZ20130517104329671), and “Guangdong Introduced Leading Talents” project as well as Shenzhen Fundamental Research Project(No.JC201105190954A).

References

[1] Yang P.,Chen L.l. et al,Computer-aided prosthetic socket manufacturing system based on an advanced manufacture technology, Journal of Clinical Rehabilitative Tissue Engineering Research ,Vol.13,No 22,May 28,2009

[2] Fugui Wang,Computer aided manufacturing system for Sheet metal ,Journal of Textile Machinery, 1994, 6.

[3] Zhang, H., Zhao, F., Ai, C., & Ze, X. (2008, June). The CAM system research of sawing and milling machining center for PVC profile based on feature technologies. In Intelligent Control and Automation, 2008. WCICA 2008. 7th World Congress on (pp. 9351-9355). IEEE.

[4] My, C. A. (2010, October). Integration of CAM systems into multi-axes computerized numerical control machines. In 2010 Second International Conference on Knowledge and Systems Engineering.

[5] Bohez, E. L., Makhanov, S. S., Munlinb, M., Phien, H. N., & Tabucanon, M. T. (2009). On 5-axis freeform surface machining optimization: vector field clustering approach. International Journal of CAD/CAM, 5(1).

[6] Makhanov, S. S., & Ivanenko, S. A. (2003). Grid generation as applied to optimize cutting operations of the five-axis milling machine. Applied numerical mathematics, 46(3), 331-351.

Applied Mechanics and Materials Vol. 596 (2014) pp 90-93
© (2014) Trans Tech Publications, Switzerland
doi:10.4028/www.scientific.net/AMM.596.90

Analysis of the Ceramic Pattern Modelling Based on Primitives

HU Jingfang[1, a], LI Busheng[1, b]

[1]School of Information Engineering, Jingdezhen Ceramic Institute, Jiangxi, P.R.China

[a]jdzhjf@163.com,[b]abulbs@163.com

Keywords: ceramic patterns; individual patterns; suitable patterns; continuous patterns;

Abstract. This paper analyzes the creation process of ceramic design, ceramic design according to the characteristics of the ceramic pattern classification for the individual patterns, the suitable patterns, continuous pattern and integrated pattern four, use of modelling primitives knowledge of them is analyzed, finally summarizes the modelling category of ceramic pattern.

Introduction

Ceramic pattern is a kind of art image process and decorative combination. It is to live in the natural image, through art processing, make its form, in the shape, color, suitable for ceramic technology and aesthetic purpose design of an image or decorative patterns. Ceramic decorative pattern according to the decorative patterns and themes to is divided into: geometric patterns, floral patterns, figures, animal pattern, landscape pattern. A ceramic pattern includes two parts of patterns organization and decorative composition. The two are different, and are inseparable, in the design of two closely related. The constitution, general with geometric patterns and natural form as the basis, combined with the ceramic technology, according to the design requirements, the use of formal beauty rule, design patterns accord with the technological, economic, aesthetic principle.

Analysis of the creation process of ceramic pattern

Ceramic pattern creation should also follow the progressive law. Methods and steps of ceramic design, is a basic method to finish the creation. The creators can accord each stage of the creation process, find the key to solve the problem, make creations gradually in the process of deepening. At the same time, the creator based on basic methods, but also according to different objects of creation, creation and personal habits, flexible and changeable step, its purpose is to make the creation more reach the acme of perfection. The creative process of art works can be divided into the following steps.

1.1 Ceramic design creativity

The so-called ceramic design creativity refers to the creative process of thinking activity. Ideas from the essence, is a kind of creative thinking activity. This process of creative thinking is very complex, which includes the alternate use of logical thinking and thinking in images of two different ways of thinking, thinking process of creation [1].The general constitute the basic content of ceramic pattern design thinking: creative theme, material (also called pattern elements), shape, color, space, texture, material, function etc [2].With the creative process, creative thinking from disorder to order, from chaos to clear ideas. Straighten out the idea into the basic characteristics of creative.

1.2 Prototype ceramic pattern

Prototype ceramic pattern is a continuation and extension of creativity, and creativity. Creative stage ceramic pattern with ceramic pattern embryonic stage often alternated, no clear dividing line, two steps are mutual connection, inseparable. Usually a bud in the creative works and reflected in the embryonic form, and through the prototype production, will be in the shape the creation of information and feedback to the design creativity, further deepening of creative designing, prototype until the creation of ceramic pattern can correctly reflect the creative content, to meet the psychological, to complete all the production process of ceramic pattern prototype [3].

1.3 Forming ceramic pattern

Ceramic pattern forming, complete expression of creative ideas and creative intent, the end result is the creation. Due to the type of ceramic pattern is varied, so the creation of the finished ceramic pattern can not be summed up in one form.

Therefore, the creative process can be a ceramic pattern briefly in Figure 1 to represent.

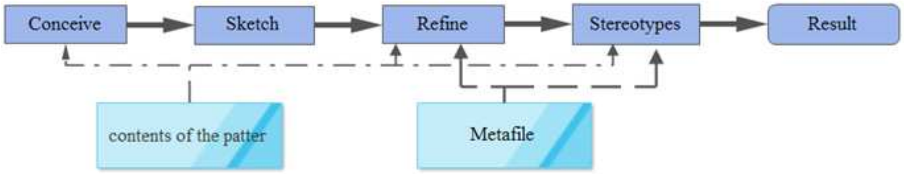

Fig. 1 the creation course of ceramic pattem

Analysis of ceramic pattern design

Before in the analysis of the ceramic pattern modelling, we will introduce the concept of "primitive". The so-called primitive, it is the smallest indivisible units in a pattern. A floral pattern as shown in Figure 2, if the symmetry point of view, the pattern can be broken into by the decomposition shown in Figure 3 of the primitive to get through the symmetric structure, however, the extraction of graphic method is unscientific, it is not normal, because it is a complete petal flower pattern. Divided into 2.5 petals, and half a petal is not such a complete expression of the petals. Therefore, the flower pattern can be broken up into figure 4 sub patterns one and sub patterns two, two sub patterns of a sub pattern, the pattern can not be subdivided, so it is a primitive. But the pattern of the two can be decomposed into shown in Figure 5 to continue using scatter decomposition of primitives and graphics two. So far, the flower pattern can be regarded as a sub pattern, a primitive element, two a total of three elements.

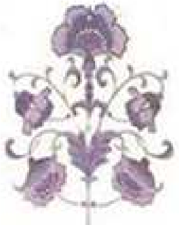

Fig.2 Flower pattern

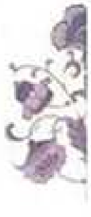

Fig.3 Pattern-cell

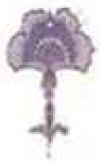

Fig.4 Sub pattern-1

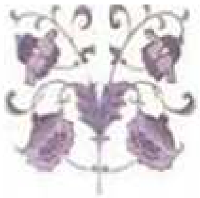

Fig.4 Sub pattern-2

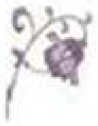

Fig.5 Pattern-cell-1

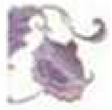

Fig.5 Pattern-cell-2

Based on this model, we propose "pattern =CASE structure and element data" pattern representation method. The modelling structure is approximately described pattern, overall layout, the pattern design of abstract knowledge, and metadata is used to describe the primitives in a pattern attribute values.

Ceramic pattern classification

Arts and crafts on the ceramic pattern are divided into four types: single patterns, patterns, suitable for continuous pattern and integrated pattern [4].

3.1 The individual patterns of ceramic design

An independent individual patterns of modelling forms, called a single pattern [5]. The individual patterns of ceramic pattern are frequently used in ceramic decoration, its definition, although simple, but the use of this simple rule can be derived from the many changes, colorful ceramic pattern. We can make the individual patterns of ceramic pattern classification for discrete modelling, antisymmetric several type shape, triangle shape and angle of four symmetrical

symmetrical modelling. As shown in Figure 6, based on the principle of separation, analysis can get the right CASE to their modelling.

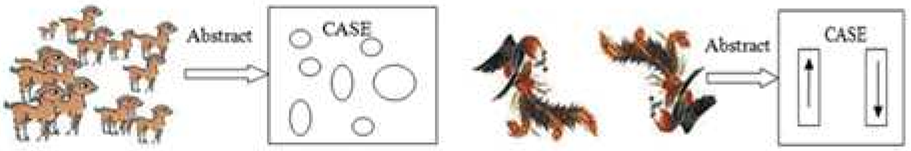

a) Discrete style b) Antisymmetric style

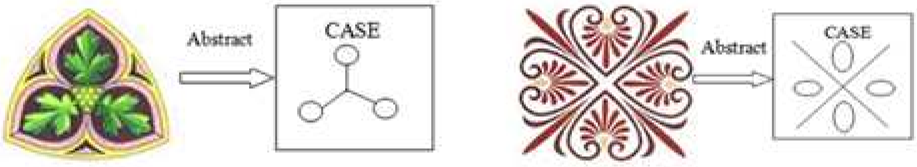

c) Symmetrical Triangle d) Symmetrical corners

Fig.6 Extraction of case in single-pattern

3.2 The suitable patterns of ceramic design

Certain profile control pattern forms, called for patterns. Suitable pattern have rigorous and conformal artistic characteristics [5]. However, rigorous and conformal does not mean that the stiff. Reasonable expression will also appear vivid natural, interesting. At all times and in all countries outstanding for ceramic pattern is evidence. Suitable for pattern is "free" in the framework of the limitations in the art form, is also the most decorative. As shown in Figure 7 of the four for the pattern abstraction can get corresponding CASE pattern, such as a centripetal type, pattern two rotary, pattern three diagonal type, four type of radiation pattern. In practice, we often use to such as polygon, fan-shaped, gourd shaped, heart-shaped as suitable for pattern appearance.

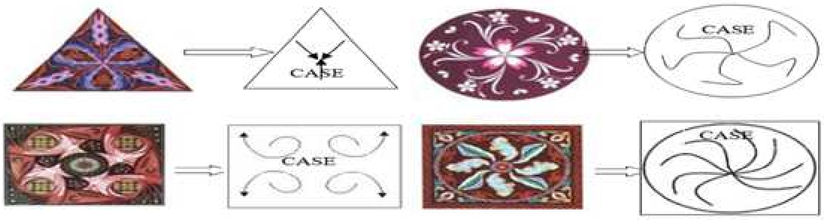

Fig.7 Extraction of case in suited-pattern

3.3 The continuous patterns of ceramic design

Continuous pattern is defined by one or a few basic primitives to the upper and lower, left and right regular or four directions to continue to expand, to form a larger constitute categories of patterns, specific and can be divided into two sides successive pattern pattern and four continuous patterns of two [5].

As shown in Figure 8, extracted from two sides successive pattern pattern pattern in CASE: a scatter type modelling, pattern two ray type modelling, pattern three wave like shape. In addition, the two sides successive pattern pattern, common and line style.

Compared with the two sides successive pattern, four continuous patterns are repeated extends in four directions. Therefore, four continuous dermatoglyphic pattern modelling and two sides successive pattern is basically the same. As can be seen in Figure 9, the pattern of the modelling for four continuous wave type.

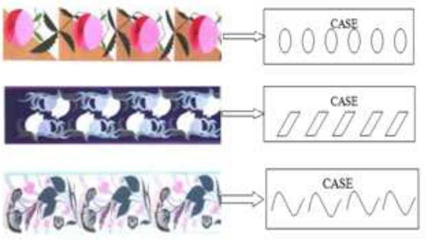
CASE
CASE
CASE

Fig.8 Extraction of case in linear pattern

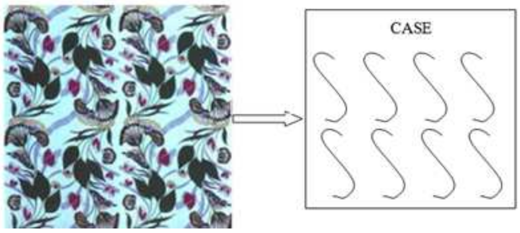

Fig.9 Extraction of case in quad pattern

3.4 The comprehensive patterns of ceramic design

Comprehensive pattern ceramic pattern is the use of the three types of ceramic pattern modelling to generate a pattern, therefore, integrative pattern ceramic pattern can not use a simple model to direct generation after generation, modelling sub pattern but with different kinds of the sub graph case as primitives, then use the sub pattern elements to form a certain shape, so as to construct an integrated pattern of ceramic pattern.

Conclusion

Summarized earlier analysis of extracted patterns can be obtained, as shown in Figure 10 of the ceramic pattern shape table.

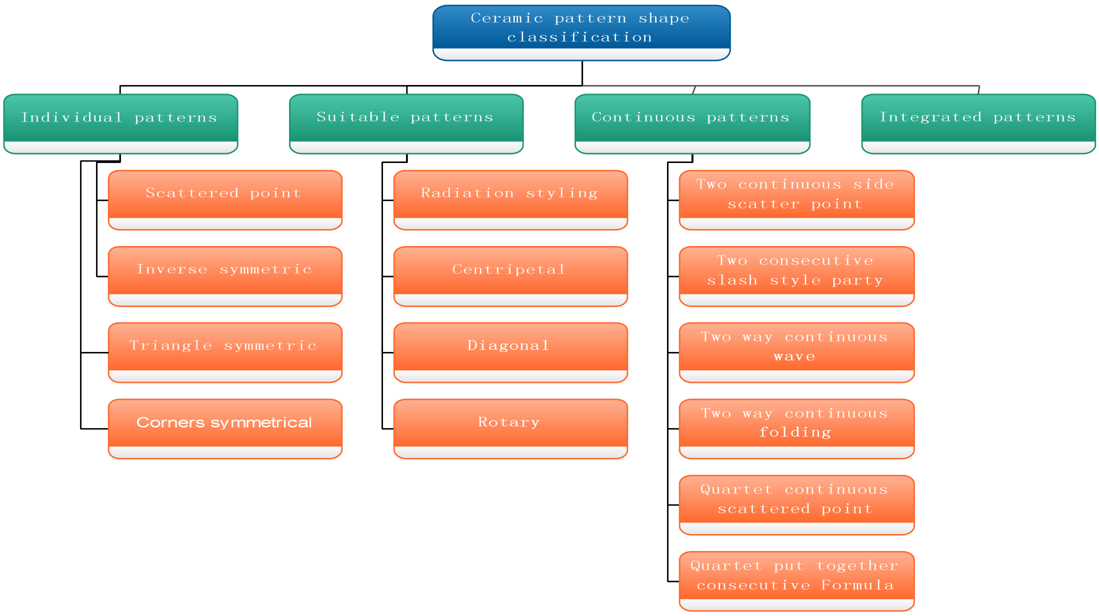
Ceramic pattern shape classification
Individual patterns
Suitable patterns
Continuous patterns
Integrated patterns
Scattered point
Inverse symmetric
Triangle symmetric
Corners symmetrical
Radiation styling
Centripetal
Diagonal
Rotary
Two continuous side scatter point
Two consecutive slash style party
Two way continuous wave
Two way continuous folding
Quartet continuous scattered point
Quartet put together consecutive Formula

Fig. 10 Ceramic pattern shape classification

References

[1] Qian Xueshen. Thinking science. Shanghai, Shanghai people's publishing house, 1986:13 ~ 26
[2] Chen Nianbin. Contact and development of ancient ceramics and auspicious patterns. Jingdezhen ceramics.2003.13 (2):14~17.
[3] Cui Wei. Basic patterns. Beijing: Chinese Textile Press. 2004:29~33.
[4] Liu Zeming. Modern pattern design. Chongqing: Southwestern Normal University press, 2000:9~12.
[5] Jiang Jin. Design and application. Hunan: Hunan literature and art publishing house pattern. 2000:66~80.

Applied Mechanics and Materials Vol. 596 (2014) pp 94-99
© (2014) Trans Tech Publications, Switzerland
doi:10.4028/www.scientific.net/AMM.596.94

Research and Application of Adaptive Technology in Equipment Installation

Luo Bin[1*], Ye li[2]

[1] NO.98 Long Xi Song Pai Rd, Yu Bei Dist, Chongqing 401147, China
[2]NO.98 Long Xi Song Pai Rd, Yu Bei Dist , Chongqing 401147, China
[1]LW67610346@sina.com
[2]yelifeidegao@126.com

Keywords：adaptive technology; equipment installation; stress-displacement model.

Abstract：Based on the current situation that the accuracy of stress , displacement and trip in the traditional equipment installation can't satisfy customer requirements. First, this paper analysis the principle of adaptive technology . Then , by establishing the mathematical model of stress and displacement, the equipment automatically select the appropriate pressure and displacement values to ensure parts assembly optimal.

Introduction

At present , traditional equipment installation mainly used hydraulic press in China . This equipment consume much energy , so hydraulic station must work continuously . This causes high power consumption , fuel consumption , the precision of stress and displacement un-controlled . This waste time and energy because it often need to replace the hydraulic oil . With the competition of market economy more and more intense , the society's requirement to the enterprise product quality is more and more high . The high precision equipment installation of domestic market is usually imported from abroad , mainly from Germany , the United States , Japan . But these are expensive , many customers don't have the ability to purchase and use , also cannot bear the late high technical and after-sales service .

Chongqing and even China's manufacturing industry is very developed . So th e application of equipment installation is very extensive . With the continuous development of industrial technology , the requirement to assembly accuracy is higher and higher .Fine assembly is widely applied to industrial production . So , carrying the research of adaptive precision technology and carrying industrialization will brake foreign monopoly and fill the blank of the domestic technology to meet the customers' needing .

The structural characteristics of Interference fit joint is simple , reliable , high setoff mind and good impact resistance . It is a common way of connection in the mechanical equipment . Such as the interference connection of transmission shaft . The size of the installation force have a big impact on precision equipment and instruments . And it will cause the workpiece not in place or the springback of workpiece . So it is very important to analyze the influence of pressure assembling force to the precision of the interference fit .

This article is mainly study the thin-walled workpiece that it select automatically appropriate stress and displacement in the process of press-fitting . The shape and structure of thin-walled workpiece are complex . It is wall thin , soft ,low relative stiffness , big machining allowance and poor manufacturability . So it is easy to be out of shape in the installation process . Thin-walled wall thickness are generally at about 1-2mm . The thichness nonuniformity can lead to inconsistent radial deformation . This will directly affect the centering precision . So we must limit the tolerance Δh of the wall thichness . When positioning diameter D is less than 100 mm , $\Delta h \le \pm 0.05$mm , when D is more than 100 mm , $\Delta h \le \pm 0.075$mm . Because of thin-walled parts' characteristicses , there is a high requirement to control the magnitude of interference , stress and displacement in the installation process .

Principle of Adaptive control technology

The adaptive refers to the processing and analysis process . It is according to the data characteristics to automatically adjust the processing method , processing order , processing parameters , boundary conditions or constraints to match the statistical distribution characteristics and structural characteristics[1] . This can get the best treatment effect . As shown in fig.1 , adaptive closed-loop control system structure .

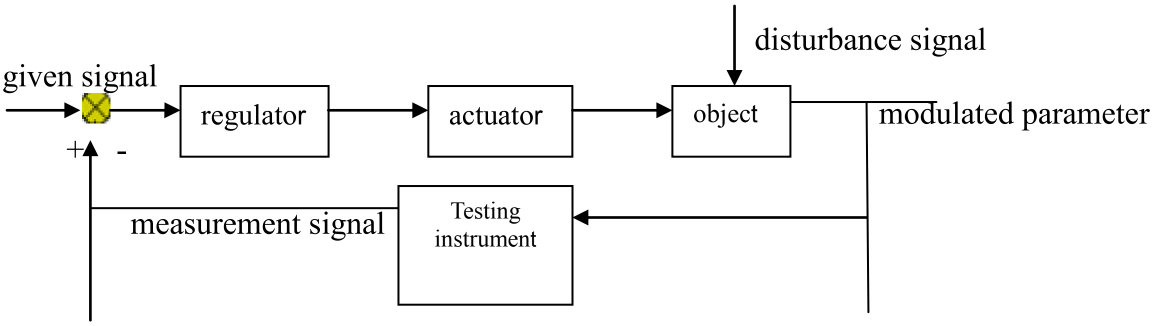

Fig.1 Adaptive closed-loop control system structure .

Fist , set the given device of controlled variable . Second , compare detected variable with fixed variable to get the deviation signal . Then , convert the deviation signal into suitable signals for actuator working . Then the actuator began to act directly on the machinery which is needed to be controlled , on the equipment or the production process . Finally , traslate the the measuring control into the same physical quantity signal with the given quantities .

The adaptive process is a process of constant closing to the target . This process is espressed with mathematical model , called adaptive arithmetic .forced the zero arithmetic , steepest descent arithmetic , LMS arithmetic , RLS arithmetic and a variety of blind equlization arithmetic .

Determine the installation process technical indexes

(1)calculation of pressure-in force

$$\mathrm{F} = P_{max}\, dlu \tag{1}$$

P_{max} is the maximum pressure of bound surface ,N/mm2 ; d is combining diameter , mm

L is combining length , mm ; u is the friction factor of bound surface

$$P_{max} = \frac{\delta_{max}}{d\left(\frac{C_1}{E_1}+\frac{C_2}{E_2}\right)} \tag{2}$$

$$C1=[1+({}^{d1}/_{d})^2]/[1-({}^{d1}/_{d})^2]-\nu 1 \tag{3}$$

$$C2=[1+({}^{d}/_{d2})^2]/[1-({}^{d}/_{d2})^2]+\nu 2 \tag{4}$$

d1 is the outer diameter of contained member ; d2is the inner diameter of containing workpiece

E1， E2 are contained and containing workpiece's materials elastic modulus

δ_{max} is maximum magnitude of interference , mm； v is poisson ratio

(2)calculation of magnitude of interference

Such as rolling bearing , its inner ring rotate with the axis . In order to prevent the relative sliding between inner ring and shaft neck generating attrition and affecting the bearing performance and service life . So there must be interference in the the rolling bearing inner ring and shaft neck . At the same time considering the inner ring is thin wall parts , amount of interference can't be too large . The inner diameter will be reduced after assembly . In order to not be narrowed to more than the minimum limit of size . So ,we often let the inner diameter of contained have the proper amount of extension before interference assembly . In this way we can make it conform to the requirement of the size . Amount of the real effective interference in the interference fit is the sum of mating surface radial deformation .

$$\delta = \mathrm{Pd}\left(\frac{C1}{E1}+\frac{C2}{E2}\right) \tag{5}$$

$$\delta_{max} = P_{max}\mathrm{d}\left(\frac{C1}{E1}+\frac{C2}{E2}\right) \tag{6}$$

$$\delta_{min} = P_{min}\mathrm{d}\left(\frac{C1}{E1}+\frac{C2}{E2}\right) \tag{7}$$

$$\delta_{min}<\delta<\delta_{max}$$

Stress-displacement model

For the rolling bearing as an example , two bearing inner ring and shaft neck are interference fit[2] . Because the bearing inner ring are thin-walled parts , so it is easy to produce elastic deformation under a large amount of interference . This will affect the bearing running accuracy . So we can't calculate the minimum interference quantity directly like the wheel ,and thick wall parts . The standard of interference amount between the roller bearing inner ring and shaft neck is 0.051~0.101mm .

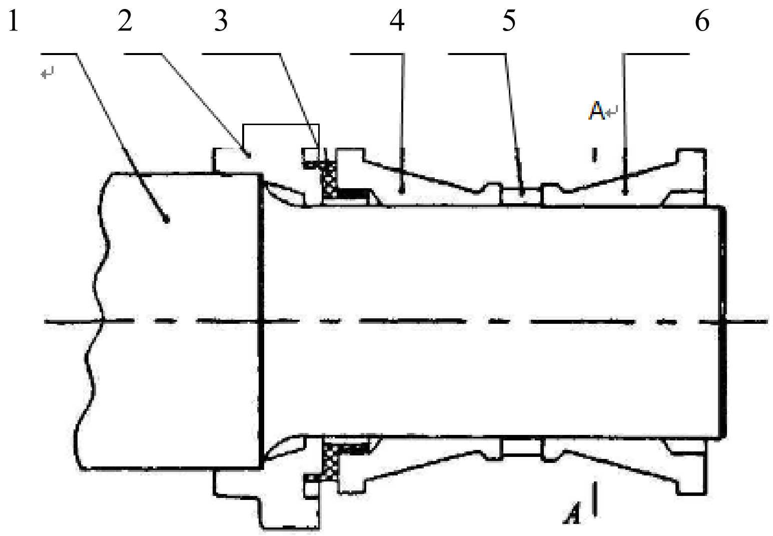

1-shaft 2-rear bumper 3-model steel baffle 4-inner ring
5-centre baffle 6-inner ring
Fig.2 353130B , the schematic of bearing and shaft combined with

After press fitting of the bearing , it will produce radial pressure P between journal and shaft neck [3]. This pressure make journal shrink , inner ring wall swell . The geometric relationship of deformation is as follows :

$$\delta/2 = |\mu 1| + |\mu 2| \tag{8}$$

δ is the pressed interference quantity , $\mu 1$ is the radial displacement of journal pressure into bearing , $\mu 2$ is the radial displacement of bearing inner ring .So,

$$\mu 1 = -\frac{aP}{E}(1-\nu) \tag{9}$$

$$|\mu 1| = \frac{aP}{E}(1-\nu) \tag{10}$$

$$\mu 2 = \frac{aP}{E}\left(\frac{b^2+a^2}{b^2-a^2}+\nu\right) \tag{11}$$

P is the internal pressure , a is the combination surface radius of the bearing inner ring and shaft neck after pressure , b is the average outside radius of inner circle . So let （9）,（10）into（1）can be obtained the relationship between interference and the internal pressure P .

$$\mathrm{P} = \frac{E(b^2-a^2)}{4ab^2} * \delta \tag{12}$$

So , the pressure equipment of rolling bearing :

$$P_F = P * S * \mu = \frac{\pi E(b^2-a^2)}{2b^2} * \delta * \mu * X \tag{13}$$

S is the contact area , x is the displacement , μ is the sliding friction factor

Displacement and stress selected automatically

(1)fit precision

The fit tolerance is the permissible clearance or the changed amount of interference . It represents the fit precision . The tolerance zone of the hole is completely on the tolerance zone of the shaft in the interference fit .

Minimum interference fit : Ymin=Dmax-dmin=ES-ei

Maximum interference fit : Ymax=Dmin-dmax=EI-es

Average interference fit :Yav=(Ymax+Ymin)/2

So , the precision of interference fit : Tf= | Ymax-Ymin | =Th+Ts, the Th is the hole's tolerance , Ts is the shaft's tolerance .

The interference quantity of the bearing inner ring with journal in thin-walled is 0.051~0.101mm , its minmum interference amount is 0.051mm , maximum interference amount is 0.101mm , changed amount of interference is 0.05mm , so the accuracy of interference fit is 0.05mm .

(2)choice and adapting automatically

The mathermatical of pressure and dis placement:

$$P_F = P * S * \mu = \frac{\pi E(b^2 - a^2)}{2b^2} * \delta * \mu * X$$

If C= $\frac{\pi E(b^2-a^2)}{2b^2} * \delta * \mu$, then P_F =Cx, when other conditions are unchanged , x follow P_F changing at the same time .

Fig3 is the installation process structure diagram of adaptive control system . Set pressure sensor-1 Under the compression bar of the numerical control press . The output of the pressure sensor-1 connected with the first input of the processor-2 . The second input of the processor-2 connected with the output of the displacement sensor-3 . The first output of the processor -2 connected with servo motor-4 . The second output of the processor-2 connected with the input of upper computer-5 . The output of upper computer-5 connected with the third input of procrssor-2 . This processor in the process-2 uses microcontroller implementation .

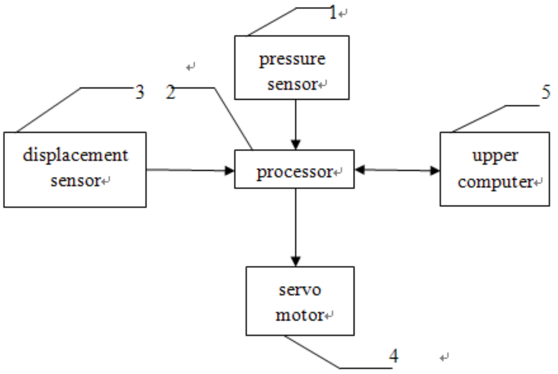

Fig3. Adaptive control system of equipment installation

The process of adapting and selecting automatically of displacement and stress . First , processor-2 send out signal to the servo motor-4 , the servo motors-4 drive compressive bar downward movement , the compressive bar drive pressure head of numerical control press downward movement through the pressure sensor-1 . Second , pressure sensor-1 will transmit the detected signal to the processor-2 . Third , the processor-2 control the pressure head's different distance according to the received different pressure signal . Then , displacement sensor-3 transmit the detected displacement signal to the processor-2 . The last , processor-2 transmit detected pressure and displacement data to PC-5 after it received the order of PC-5 , so that the pressure and displacement can be conducted real-time monitoring and record [4].

Conclusion

The adaptive technique is applied to the study of equipment installation . This make the equipment installation adjust the pressure automatically according to the characteristics of the object and the technical requirement of installation , and select suitable displacement automatically according to pressure . So , this realize accuracy controlling and real-time displaying to stress and displacement , solve these problems of not-accurate location and workpiece's rebounding after pressed into in the process of original production . The application of this technology can improve accurate of equipment installation , is helpful to improve enterprise's product quality , enhance enterprise's core competitive ability , take technical commanding heights and improve the competitiveness of market .

References

[1]He Qinghua, Zhang Daqing, Huang Zhixiong, Zhang Xinhai. Adaptive Control of Hydraulic Excavator Working Device[J].Journal of Tongji University(Natural science edition)2007. 35(9):1260-1288.

[2]Hu Hongwei . Stress-displacement Curve of Bearing Pressure Equipment can Make Feasibility Analysis of Judging Bearing Pressure Equipment Qualified [J]. Research and Development . 2010. 10(5):7-10.

[3]Song Weiyan , Liu jian . Principle of The New Type Displacement Pressure Curve Bearing Pressure Machine [J].Work Study.2000(4):23-25.

[4]Li Xiaoxi, Ma Quanming, Zhang Congpeng, Luo Xueke. The Realization that Automatic Controlling of the Bearing Pressure Machine[J].Journal North China University of Technology.200315(3):54-58.

Applied Mechanics and Materials Vol. 596 (2014) pp 100-103
© (2014) Trans Tech Publications, Switzerland
doi:10.4028/www.scientific.net/AMM.596.100

The design and manufacture of the wireless power transmission system in the cardiac pacemaker

Xiuquan Liu [1,a] *, Yanhong Li [1,b] , Limin[2,c], Huangping[2,d]

[1]School of Mechanical and Electronic, Guangzhou Panyu Polytechnic, Guangzhou, China

[2]School of Mechanical and Automotive Engineering, South China University of Technology, Guangzhou, China

[a]liuxiuquan1@126.com, [b]liyh@gzpyp.edu.cn, [c]limin@scut.edu.cn, [d]mephuang@scut.edu.cn

Keywords: the wireless power transmission; the cardiac pacemaker; coupling.

Abstract. Generally the cardiac pacemaker is supplied power by micro battery, but the battery lifetime is limited, the Wireless Power Transmission（WPT）technology is a new method to supply power source for the cardiac pacemaker. Firstly the structure of the WPT system in the cardiac pacemaker were introduced. Then, Coupling transformer and rectifying and regulating circuit were designed. Finally, the test system of the WPT in the cardiac pacemaker was established, and the resonance frequency was 596 kHz, When the work frequencywas equal to the resonance frequency, the output power was maximal; when the input voltage of the primary winding was 5.8V, the voltage of the cardiac pacemaker may be up to 8.8V, which could effectively drive the cardiac pacemaker Record S, the results show the design is feasible.

Introduction

The cardiac pacemaker is applied to treat cure tardy arrhythmia, and a large number of patients' life is saved. And the cardiac pacemaker is supplied power by micro battery, but there is one drawback: the power time is limited. Once the battery runs out, the medical surgery is necessary and the cardiac pacemaker is replaced. It not only increases patients' physical misery, the risk of operation and economic pressures, but also reduces the use value of the cardiac pacemaker. So the WPT technology has wide application potential in the cardiac pacemaker [1-2].

The cardiac pacemaker Record S is the research object, the electromagnetic coupling transformer and rectifier voltage regulator circuit structure is designed, a cardiac pacemaker WPT system is set up, which can drive the pacemaker Record S successfully.

The WPT system of the cardiac pacemaker

The WPT system in the cardiac pacemaker is shown in Fig.1. There is a gap between primary and secondary winding, and no direct contact, the wireless power is transmitted through the skin by the electromagnetic coupling induction, supplied to the load. The primary and secondary windings are separated, the excitation is small,but the leakage inductance is big. The mutual inductance model is described in circuit analysis [3-4], which is shown in Fig.2.

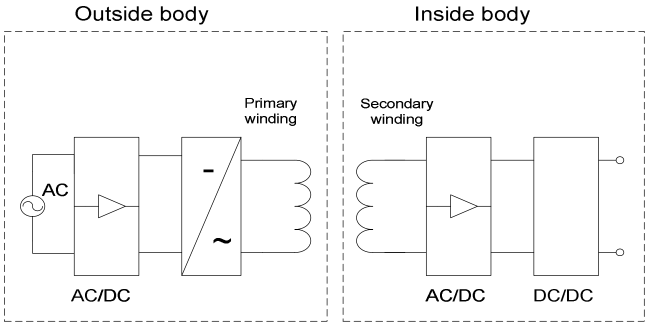

Fig.1 WPT system in the cardiac pacemaker

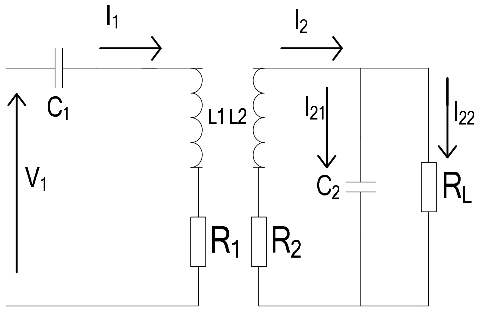

Fig.2 Series-parallel compensated model(SP)

The design of the loosely coupled transformer

There is a gap between the primary and secondary winding in the loosely coupled transformer, the coupling coefficient and transmission efficiency is not high. So the primary and secondary coils adopt high frequency ferrite core. The three-dimensional structure and geometric parameters is shown in Fig.3. The physical of the primary and secondary winding is shown in Fig.4. By impedance tester, the circuit parameters of the transformer are shown in Table.1.

Table 1 The apparatus of the experiment system

	Self-inductance *u*H）	Number of turns	resistance (Ω)
Primary coils	164.5	65	5.2
Secondary coils	194.6	70	6.1

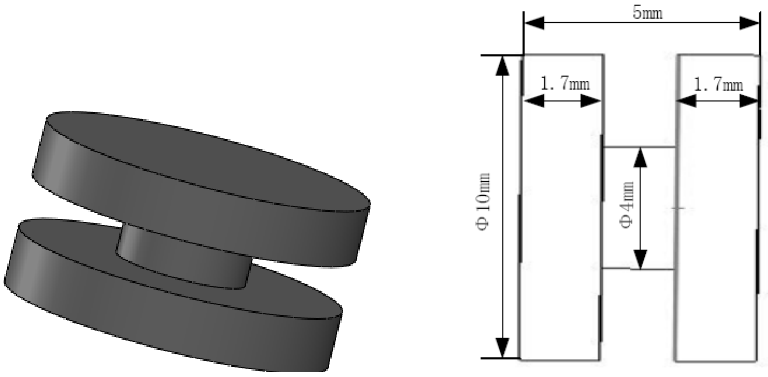

Fig.3 The primary and secondary winding magnetic core

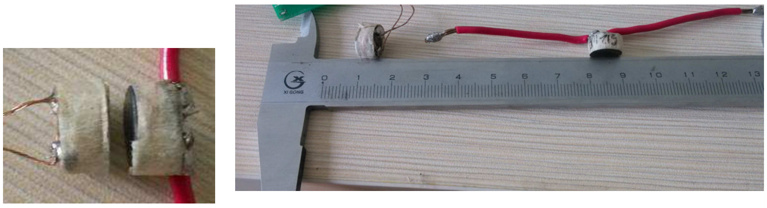

Fig.4 The physical of primary and secondary winding

Rectifing and voltage regulator

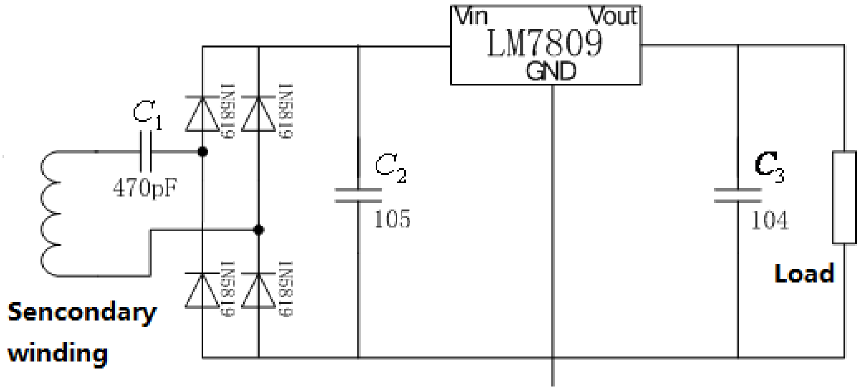

Fig.5 Voltage regulator rectifier filter circuit of secondary loop

The work frequency is 596 kHz, the primary and secondary compensated capacitance is calculated by formulas [5-6]. The primary and secondary compensated capacitance is 0.433nF and 470pF respectively.

The inductive electromotive force is converted to Dc voltage through rectifier, filter and voltage regulator. The rectifier bridge is a full bridge rectifier circuit, consisting of four diode 1N5819, a capacitor filter circuit is adopted, the input capacitor is 1uF(105) , the output capacitor is 0.1uF(104). The voltage regulator model is LM7809, and the output is 9V.

The WPT testing system

The WPT experimental system is shown in Fig.6, consisting of high frequency power source WL3866A, power meter WL258, oscilloscope UTD2025C, loosely transformer, cardiac pacemaker Record S. The input power and primary coil voltage, current are measured by WL258, the load voltage is measured by multimeter.

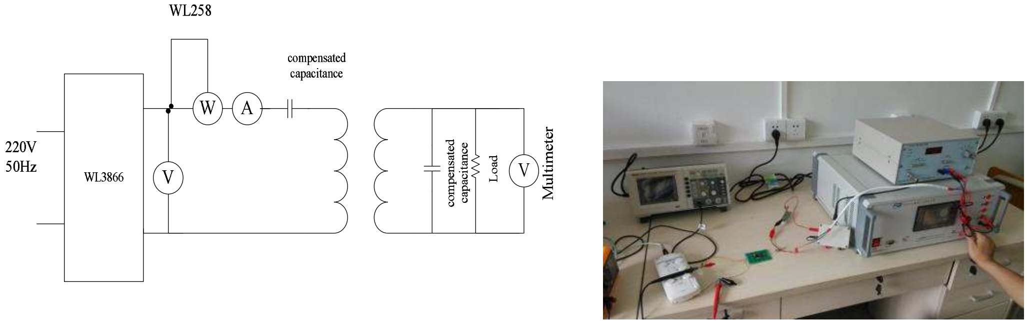

a) The experiment system principle b) the experiment equipments

Fig.6 The experiment system

The gap of the WPT system in the cardiac pacemaker is 10mm, the input voltage is 2V, and the resonance frequency is 596 kHz, the relation between the output power and the work frequency is shown in Fig.7. When the work frequency is equal to the resonance frequency, the output power is maximal, when the working frequency deviates from the resonance frequency, the output power decreases, the greater the deviation, the more the output power decreases. So the working frequency is equal to the resonance frequency.

The gap is also 10mm,the input voltage is 5.8V, and the work frequency is 596 kHz, the primary current is 153mA, the input power is 0.73W, the voltage of the the cardiac pacemaker is up to 8.8V, the experimental results are shown in Fig.8, the output power is 4mW, the transmission efficiency is 0.54%. After internal self-inspection of the cardiac pacemaker Recor S, all light-emitting diodes of the operating area flash two times, then Low Battery diode goes out, the pace of the yellow light emitting diode is shining, it shows that the cardiac pacemaker has a pacemaker pulse, which is the same as the supplied power of a battery.

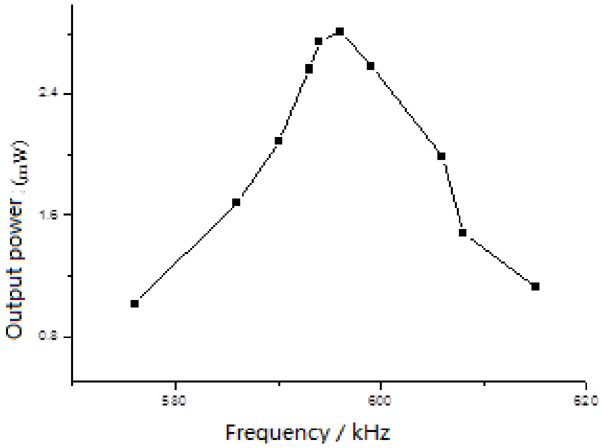

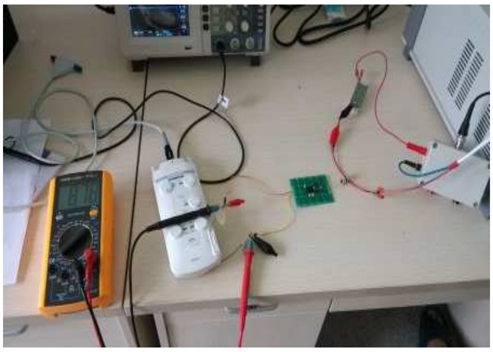

Fig.7 The relation between the frequency and output power

Fig.8 The WPT experiment system of a pacemaker

Conclusions

The WPT system in the cardiac pacemaker is designed and manufactured, the work frequency is 596kHz, the voltage of the the cardiac pacemaker is up to 8.8V, which could effectively drive the cardiac pacemaker Record S, the experimental results show the design is feasible.

Acknowledgements

This research is financially Supported by State Key Laboratory of Robotics and System (HIT) (SKLRS-2012-MS-03, the Ram City scholars project of Guangzhou bureau(10B009G) and the science and technology plan project of Panyu, Guangzhou（2012-Z-03-64).

References

[1]] Appleyard M, Fireman Z, GlukHovsky A, et al. Gastroenterology,119(2000), p.1431-8.

[2]Lewis B, Swain P.. Gastrointestinal Endoscopy, 53(2001),p.AB70.

[3] Zhou Yu, Yu Xinjie, Cheng Jinmin, Wang Chonghui, Wang Lin. TRANSACTIONS OF CHINA ELECTROTECHNICAL SOCIETY, .25 (2010),p. 48-53 in Chinese

[4] Baxi, V. J, Hariz, A. J.. Proc. of SPIE, 6415(2006),p. 1-9

[5]] LIU Xiu-quan, ZHANG Wei, WU Yan-hua, HUANG Ping. Journal of System Simulation, 20 (2008), p.2215-2219 in Chinese

[6] Xue kaifeng. Study and Application on Multi-dimensional Wireless Power Transmission Technology for MEMS, edtied by School of Mechanical and Automotive Engineering, South China University of Technology, Guangzhou(2011) in Chinese

Applied Mechanics and Materials Vol. 596 (2014) pp 104-109
© (2014) Trans Tech Publications, Switzerland
doi:10.4028/www.scientific.net/AMM.596.104

Regarding Calculation of Cross Section of Elevator Conductor and Rated Capacity of Switch

Huang Guangming

Hunan Urban Construetion College ,Xiangtan, 411103 , China

Keywords: elevator, calculating current, load calculation, simultaneous factor, demand coefficient

Abstract: briefly introduce the operation characteristics of elevator, point out the existing problems of elevator calculation and propose to take different calculation method with respect to different purposes. For example, ensure the calculation of cross section of distribution circuit conductor of single elevator and rated capacity of distribution switch, the calculation of cross section of distribution circuit conductor of elevator group and rated capacity of distribution switch and load calculation of transformer capacity, so as to reach the purpose of energy-saving and emission reduction.

The elevator, as a vertical transportation tool, plays an important role in modern building. The investment accounts for about 10% of total investment for high buildings; its power consumption is also big. In particular, the power consumption of elevator shares 17%-25% of total consumption in large-scale civil building, such as hotel and office building. Therefore, the elevator has big influences on the ensuring the transformer capacity and selecting distribution trunk line cable, which is worth being paid attention though. It is discovered from much design by author that the calculation result has big deviation due to incorrect calculation method, so that the transformer capacity and cable cross section are bigger, which results in extreme waste. It is not in conformity with the principle of energy saving and emission reduction. Hereby, the opinions on the elevator calculation problem are only references.

1. Elevator classification:

First of all, briefly introduce the elevator classification. There are many methods of elevator classification. For example, classification by motor type, by power media, by function, by speed and by load-carrying capacity and operation control mode, etc. We will introduce the classification by motor type and its usage occasion which is closely related to the text.

2. AC motor drive:

AC motor drive elevator is called AC elevator for short, which is divided into the following types.

(1) AC single-speed elevator. It only has one type of speed, the speed is also low and relevant price is low. It is often used for the area with low requirement, for example, goods elevator for transporting and service elevator for non-staff.

(2) AC double-speed elevator. It has two or three types of speed; the speed is not bigger than 1m/s. It is not often used for passenger elevator nowadays due to poor stability and leveling accuracy.

(3) AC speed control elevator. Its operation characteristic is better than that of AC single-speed elevator and double-speed elevator. Nowadays, there are many different types of AC speed control elevator, such as thyristor voltage and speed control, variable frequency speed control, variable frequency variable voltage speed control, etc.

Due to the rapid development of electronics and elements at present, the variable frequency variable voltage technology has become proved. AC motor drive with VVVF variable frequency variable voltage speed control can fully reach the DC motor drive elevator level. And it has small volume, light weight, high efficiency, high power factor (average power factor is above 0.9) and energy saving. Compared with AC voltage regulating speed control and AC double-speed driving system, its configuration cost is almost same, but overall technical performance of electric driving has improved greatly and 40% energy-saving more than that of AC voltage regulating speed control and AC double-speed driving system. Therefore, it has been used more and more widely. Nowadays, it is mostly used for general residence and public buildings.

DC motor drive

DC motor drive elevator is called DC elevator for short. It has good operation characteristic, correct leveling and comfortable service. DC elevator is also divided into motor-generator DC elevator and thyristor power supply device DC elevator. All these type of elevators are comfortable with good speed control performance, which are quick elevator and high-speed elevator.

3. Hydraulic elevator:

It is driven by hydraulic. The hydraulic cylinder supports the bottom of lift car directly to cause the plunger of lift car to support hydraulic elevator. The mechanical penthouse is not needed. It is commonly used for short building and areas where also requires, such as luxurious villas and some industrial plants.

First of all, we should ensure to calculate elevator separately based on the different purposes. For example, ensure the calculation of cross section of distribution circuit conductor of single elevator and rated capacity of distribution switch, the calculation of cross section of distribution circuit conductor of elevator group and rated capacity of distribution switch and load calculation of transformer capacity. Different purpose has different calculation method. The separate descriptions are as follows:

Used for the calculation of cross section of distribution circuit conductor of single elevator and rated capacity of distribution switch.

Due to the frequent startup for elevator motor, the load fluctuation is big and speed up and down is prompt. The impact current shall cause voltage fluctuation to be severe and cable to heat when conducting speed up and down. It is required to ensure the calculating current of elevator when selecting the power switch and distribution cable.

Due to elevator is in short-time duty, first of all, it is required to ensure the rated current of elevator traction machine on the nameplate is the current of 0.5h or 1h duty or long-time duty rated current with same power when calculating the calculating current of elevator load. If it is previous one, the nameplate current is multiplied by 0.9-1 as the calculating current of elevator. If it is latter one, the calculating current of elevator is 1.4 times of nameplate current.

Therefore, the text specified in Article No. 9.4.2 of JGJ16-2008 also describes very clear. The calculating current of single AC elevator (i.e the calculating current of power source of elevator machine room) should be the sum of 90% of rated current of 0.5h or 1h duty on nameplate of traction machine and load current of auxiliary electric appliance. If elevator motor nameplate is marked with continuous duty rated current value, it is the sum of 140% of nameplate value and load current of auxiliary electric appliance. So, the total power switch of elevator room should be selected based on the value mentioned.

We only know the rated power of elevator traction machine in many conditions. We can ensure the calculating current Ijs of elevator load by rated power under long-time duty. It is calculated by the following formula:

i.e Ijs=1.4.（Pe/. .Ve.COS￠）(A)

The key point is how to ensure COS￠. As far as AC elevator is concerned, there are many factors which influences on power factor. For example, the speed control method has double-speed speed change, voltage regulating speed control and variable frequency speed control, etc. The variable frequency speed control also has constant flux variable frequency speed control, constant current variable frequency speed control, constant power variable frequency speed control and VVVF variable voltage variable frequency machine, etc, which is also influenced by operation conditions. Generally speaking, AC elevator power factor is very low by 0.5-0.7 only, because elevator is often in startup/braking condition and often in light load and no-load condition. However, the power factor of VVVF regulator used for civil buildings is above 90%. All basic material can be requested from elevator main body major, architecture major or elevator manufacturers.

It is required to consider two conditions when ensuring the cross section of power source of elevator and choose the bigger one finally. First one, select cross section of cable by temperature rise; second one, meet the requirement of voltage reduction. The selection of cross section of conductor based on the calculating current of elevator generally is mainly to consider the requirement of temperature rise. Some personnel ignore the requirement of voltage reduction, specially, when the power supply transformer is far away from elevator traction motor. The condition of voltage reduction defines that the fluctuation produced by impact current when elevator is starting and accelerating, which should not exceed 10% of rated voltage of motor. Therefore, it is required to calibrate the voltage reduction after select conductor in accordance with calculating current.

The elevator has been developing rapidly in civil buildings. But the calculating data of all kinds of design manual does not catch up with the changes. The modern elevator shall not use gear change any more due to comfortable requirement, but use more VVVF mode. Some traction motor uses permanent magnetic synchronous motor and drive mode uses gearless drive, which has high efficiency and power factor rated 0.85-0.95 hereby. The calculated current and selected cables are smaller than those of before.

We take some examples. E.g1, one high building with 32 floors, the load-carrying capacity is 1000Kg, speed is 2m/s. Electrical designer designs based on the general common design, motor power is 18KW (some motor is rated 22KW), use cross-linked cable with cross section of distribution cable is 35mm^2. The motor power is 13.3KW and startup current is 40.3A on the nameplate. The cross section of cable from control box to elevator traction machine supplied by elevator manufacturer is just only 6mm^2, which means operation current of motor is very small. Meanwhile, this section of distribution cable is only at end but not consider the voltage reduction. We check and see by the voltage reduction of calibrated line regarding how much cross section of distribution cable should be selected. Suppose that the distance from transformer to motor is 250m, the selected cable is YJV-1 type cable, cross section area is 10mm and voltage reduction is 9.067%, all which almost meets the requirement. For the sake of safety, use the cable with cross section area rated 16mm, which is much less than that of 35mm^2.

E.g 2, a high building with 33 floors, the load-carrying capacity of installed elevator is 1000Kg, speed is 2m/s, the motor power is 11.5KW, rated line current is 31A and startup current is 58A on the nameplate of elevator. In accordance with the above-mentioned condition, it can meet the requirement by means of selecting cross section area rated 16mm for calibration of voltage reduction.

E.g 3, the load-carrying capacity of sightseeing elevator with 8 floors is 1000Kg, speed is 1m/s, the motor power is 6.4KW and rated line current is 31A.

is 1000Kg, speed is 4m/s and motor power is 40KW that listed on the construction drawing. However, it is applicable if rated power of motor is 25KW in fact. Of course, the motor power, load-carrying, operation speed and elevator type are strongly linked with each other, in particular for super high building rated 250m above. It is required to consider all various factors integrally when selecting elevator. Conduct the actual calculation after technical parameters of elevator are ensured well in order to avoid happening unnecessary waste.

E.g 5, the author ever accepted the consultation from a real estate development corporation. There are many Class II high buildings with 18 floors in a community developed by real estate development corporation. According to the drawing by design institute, the selected elevator motor power is 11.5KW, power supply cable of each elevator is YJV-1KV-3x35+2x16, 2 sets for each building and power supply line is YJV22-1KV3x50+1x25. The elevator currently selected by developer is synchronous gearless energy-saving elevator and its motor power is 8.3KW. I was inquired that whether cross section of cable can be changed to be smaller or not, the answer is YES and electrical component parameters also can be changed to be smaller. The calculating parameters of elevator can be submitted to design institute in detail and also require them to recalculate, modify and work out drawing finally.

Integrally analyze the above-mentioned examples and combine with the known conditions by author during revision of drawing, it is found out that the calculation of single elevator distribution has two problems at present. First problem, the power of passenger elevator motor, the ensured capacity is bigger in reference to some design material if detailed models and specifications are not provided. Second problem, the design value is bigger than the actual value as a result. Such kind of design accumulative result shall be bigger, which results in significant waste of resource without doubt when elevator quantity is bigger. Electrical design personnel should consider based on the principle of energy saving and emission reduction and sufficiently have understanding in specific technical data of elevator, but not the bigger the better or perfectly safe, so that the distribution capacity and cross section of cable of elevator can be ensured.

Ensure the calculation of cross section of distribution trunk line of multi-set elevator group and main switch capacity of distribution box.

It is allowed to supply power to the master distribution box by using power supply trunk line if multi-set elevators are arranged in same area. The master distribution box can supply power to each elevator by radioactive mode, of which selection of main incoming line and power switch should be calculated with simultaneous factor. The simultaneous factor can be selected according to the list below for multi-set elevator with same capacity and type.

Simultaneous Factor for Different Elevator Quantity

Quantity	1	2	3	4	5	6	7	8	9
Less frequent usage degree	1	0.85	0.78	0.72	0.67	0.65	0.59	0.56	0.54
Frequent usage degree	1	0.91	0.85	0.80	0.76	0.72	0.69	0.67	0.67

Ensure the load calculation of selecting transformer capacity.

Some construction drawings and load calculation book have been read by author that the demand coefficient of elevator load calculation is selected to high. It is selected by 1 and 0.9-0.8 respectively when elevator quantity is less (1 to 2 sets) and bigger. However, the selection way is not right. I have communication and consultation with designers why select like this, however, the answers by them are the others conduct like this and design manual and the other materials also introduce like this. Definitely, when carry out the grouping calculation of electric equipment according to Article 3.4.6 of Old Civil Regulation JGJ16-92, equipment quantity is 3 sets and below, the calculating load is equal to the sum of equipment power. For example, there is one statement in *Industry and Civil Distribution Manual Design* (Rev.3) P7, select the sum of each equipment power for less quantity of electric equipment (4 sets and below) and 3 sets or 2 sets of electric equipment. The calculating load of 4 sets of electric equipment is selected by sum of equipment power multiplied by coefficient 0.9. It is also mentioned by Civil Architecture Electrical Design Manual (Rev.2) P, the calculating load is equal to the sum of equipment power for 3 sets and below, meanwhile, the calculating load should be ensured by calculation for 3 sets and above.

It is believed by author that the mentioned statement is not strict enough, so that causes too much misunderstanding. Literally understanding, the sum of each equipment power mentioned above is easily to be understood as the sum of installation power of each electric equipment. It only considers the simultaneous factor of electric equipment, but not including demand coefficient of motor operation. In fact, the actual calculating load is equal to the sum of installation power multiplied by demand coefficient. The mentioned statement has been eliminated already in *New Civil Regulations* JGJ16-2008, many personnel do not pay attention but still remember the old method and difficult to change. In addition, some design manual and references are not updated and modified; it is venial for designers to calculate the calculating load of elevator based on old method. Otherwise, it is incorrect to put the calculating load into the total load calculation result so that select transformer capacity. As a matter of fact, the load of power supply transformer caused by elevator during whole period (i.e transformer heating load) shall be a weighting average value of long time, which is much smaller than short-time maximum value during elevator running. The elevator load is very big in general civil buildings, which plays a decisive role in total load. The excessive capacity value of elevator load calculation is one of major causes that the calculating load is much bigger than actual load in accordance with demand coefficient, which actually causes the resource waste.

Additionally, it is required to understand that the operation condition of traction motor of elevator is different from that of motor with common power load. The general elevator is provided with balancing weight, which is always in STARTUP, BRAKING, SPEED UP, SPEED DOWN, GO UP AND GO DOWN conditions. When elevator lift car load is different, the traction motor changes the motor conditions and generator conditions continuously. When it is in power generation condition, it does not consume energy theoretically. And it can be saved or feed back to power grid if condition is applicable. It is allowable in actual engineering if some is regarded as measures of energy saving. Nowadays, some of variable frequency variable speed elevator also can reversely transfer the remaining mechanical energy to AC power grid so as to supply to nearby and the other electric equipment via motor and frequency converter during elevator operation. What's more, elevator is often in shutdown, light load or no-load operation condition for much time and the power factor is also lower. The outage time is even longer than the operation time in non-peak time, due to the load rate coefficient is low. For the transformers of whole engineering, the elevator load is very small, which is 0.18 -0.22 and 0.18-0.5 respectively in reference to *Civil Architecture Electrical Design Manual* (Rev.2) and *Industry and Civil Distribution Manual Design* (Rev.3). They are the selected demand coefficient for total load calculation during elevator calculation. It is required to consider the property of buildings for the detailed calculation value, the elevator demand coefficient in residence is much smaller than that of elevator in public buildings. Besides, the quantity of elevator should be considered as well. When quantity is different, the demand coefficient method is also different. The elevator demand coefficient in residence can be referred to the following list, the demand coefficient of elevator in public buildings can be selected to be bigger appropriately.

Demand Coefficient of Different Elevator Quantity

Quantity	1	2	3	4-5	6-8	≥9
Demand coefficient Kx	0.3	0.25	0.22	0.20	0.19	0.18

Conclusion

In conclusion, it is required to conduct load calculation in accordance with different purposes and parts for elevator. It is very necessary to select relevant parameters and select the cross section of conductor and rated current of distribution switch based on the result when calculating. In particular, it is needed to pay attention that the demand coefficient of elevator should not be bigger so as to avoid unnecessary waste when conducting total load calculation of transformer capacity.

References

[1] 21st Century Architecture Electrical Design Manual, by Zhu Lingen, Beijing, China Building Industry Press, P741-P784 in 2001

[2] Industry and Civil Distribution Design Manual (Rev. 3), by China Aviation Industry Planning and Design Research Institute, Beiijng, China Electric Power Press, in 2005, P3-P7

[3] Civil Architecture Electrical Design Manual, by Dai Yuxing, etc, Beijing, China Building Industry Press, in 2007, P98-P103

[4] Civil Architecture Electrical Design Code, by China Architecture Northeast Design Research Institute, Beijing, China Building Industry Press, in 2008, P13, stipulation P8

[5] Understandings to Elevator Distribution Design, by Pang Chuanshi, Li Weishi and Liu Yang, P10, Issued No.4 of architecture electrical in 2005

Applied Mechanics and Materials Vol. 596 (2014) pp 110-113
© (2014) Trans Tech Publications, Switzerland
doi:10.4028/www.scientific.net/AMM.596.110

Design of mine ventilator fault diagnosis system

Baiting Zhao[1, a], Xiaofen Jia[1,b] Yong He[1,c]

[1] Electrical and Information Engineering College, Anhui University of Science and Technology,
Huainan City, Anhui Province, China

[a]zhaobaiting@126.com, [b]jxfzbt2008@163.com, [c]644610025@qq.com

Keywords: fault diagnosis; rough set; neural network; mine ventilator

Abstract. The common faults of mine ventilator are researched in this paper, and rotor misalignment, unbalance, oil whirl, surge and other faults and fault characterization of the generation mechanism are analyzed. The faults diagnosis system is designed based on rough neural network. First, the characteristics of the type of fault for fan failure data collection, including vibration and temperature signals. Then, the pretreated sample data using rough set attribute reduction method to delete redundant attributes. Finally, the sample data is divided into training and testing samples, were used to train and test the neural network classifier. Experiments show that the system is reliable, diagnostic yield, improved ventilator system security, expanding the scope of application of rough sets.

Introduction

Mine main fan is is the key equipment to ensure that critical equipment and underground mine workers' safety[1].. According to statistics, more than 70% of coal mine accidents are due to ventilation equipment failure, ventilation mismanagement Therefore, to ensure the safety of the ventilation system is necessary[2]. Rough Set theory is based on a simplified indistinguishability of ideas and knowledge methods, while maintaining the ability to classify the same premise, through knowledge reduction, the logical inference rules from the data in the system as a model of knowledge. The theory provides a new mine effective ways of troubleshooting fan. Produced for mine ventilator fault type and fault mechanism proposed fault diagnosis method neighborhood rough sets and neural networks, the design of fault-based neural network classifier and fault reader. Using rough sets to avoid the loss of information caused by discrete data in a data processing process, through the rough set attribute reduction, greatly reducing the training process of neural networks[3-4].

Fault type and characteristics of the fan

The establishment of a coal mine ventilator fault diagnosis system is to capture the essence of effective vibration signal analysis to extract exception information and troubleshooting. The reason, as a large rotating machinery, components of mine ventilator vibration signals contain very complex, and therefore lead to abnormal vibration and very jumbled. According to the theory and practical experience, analyze the reasons for its vibration, mechanical side. Fault plane (rotor unbalance, misalignment of the rotor axis, the friction between the rotor and the stationary parts, equipment and other shafting resonance) caused by vibration accounted for more than 90% of the fan failure[5].

(1) rotor axis misalignment

Rotor axis misalignment fault fan failure is one of the main rotor and the rotor unbalance fault does not account for more than 70% of the failures of all the failed fan. This failure is mainly produced in the coupling parts.

(2) rotor imbalance

As a fan vibration common type of fault, because the rotor imbalance is mainly the following: the quality or uneven rotor vane impeller connection quality is not the same; produce errors when mechanical installation of the impeller blades, such as the weight of the welding seam inconsistencies in welding after completion of the correction, is not accurate, eliminating the stress, deformation may also exist; operation of the field device with the impeller by pressure deformation or defect..

(3) the oil film whirl and oscillation

A vibration film belongs to a self-excited oscillation and vibration phenomena, causes the oil to make high-speed movement along the axis, due to the different textures, the overall poor linkage between the liquid and therefore adversely affect the high-speed rotation of the shaft produced .

(4) surge

Surge is a fluid machine such as the fan is running at the most dangerous conditions, a large mechanical damage to itself. The main reason is the gas flow generated in the internal fan running, rotating from happening. Characteristic frequency surge is mainly manifested as low and ultra-low frequencies, while a multiplier accompanied.

(5) The friction between the rotor and the stationary member

Due to friction with the vibration information between different parts are not the same, it is the fault characteristic frequency range wider, including high-order and low order harmonics and mixed, often accompanied by an octave.

(6) base foundation loose

Loose fan base foundation failure is mainly reflected in the vertical direction, when the foundation loose situation, usually presents multi-frequency vibration. Its characteristic frequency multiplier of 2, even with high frequency doubler 1,3,4,5,6.

Ventilator fault diagnosis system design

Ventilator fault diagnosis process, because failure is not the only form of expression, and has a fuzzy, while extracting characteristic also often have blindness, resulting in the actual description of the state of the fan is not clear, and this state is the object of the rough set theory[6]. In the diagnostic process, the characteristics described are often many fan status, some characteristics that are relevant to some independent. Independent feature can provide complementary information should be retained; correlation characteristics produce redundant information, and it will increase the workload of fault diagnosis, needs to be eliminated. Introduction of rough neural network fault diagnosis turntable provides an effective method. Attribute reduction based on rough set theory can eliminate this redundancy features, neural network classifiers and neural network identification has powerful nonlinear mapping ability, can accurately locate the fault isolation and identification[7-8].

Fault diagnosis system based on neighborhood rough set structure shown in Figure 1. The system consists of four parts: The first part of the data acquisition and pre-processing, signal data acquisition system via the data collected by the switch and analog composition, need to go through the analog part of the wavelet transform feature extraction, the collected data into the database ; the second part of the rough set method to complete the training sample data processing to extract the corresponding pattern features; third part multilayer feedforward neural networks, pattern classification to complete the function; fourth part is the neural network identifier, according to failure to complete the identification of the classification level of size.

Fault diagnosis achieved

For mine ventilator fault diagnosis process vibration signals: the use of the data acquisition card monitoring vibration sensor signals, the signals were collected using rough set reduction processing, signal characteristics of the final value will be extracted into the neural network diagnostic analysis, determine the fault and the fault type[9].

Layers can be determined based on wavelet decomposition input nodes; assuming kind of equipment failure is detected as X, then the number of nodes on the network output layer as X; based on experience to determine the hidden layer nodes; choose unipolar S as a function of the transfer function of the neural network.

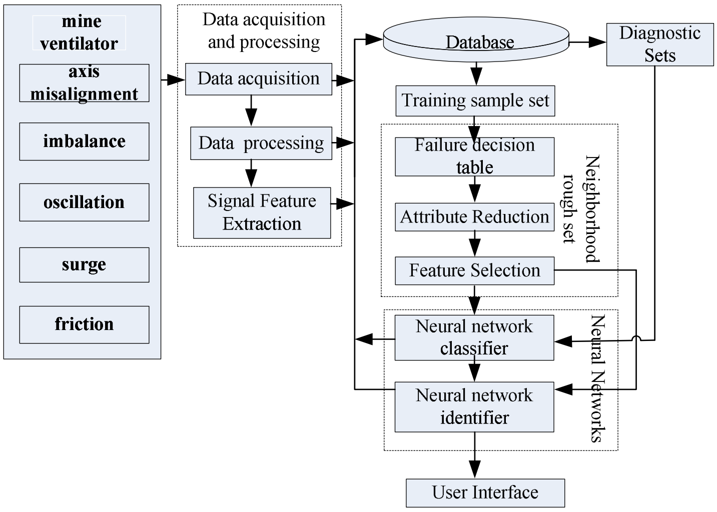
mine ventilator
axis misalignment
imbalance
oscillation
surge
friction
Data acquisition and processing
Data acquisition
Data processing
Signal Feature Extraction
Database
Diagnostic Sets
Training sample set
Failure decision table
Attribute Reduction
Feature Selection
Neighborhood rough set
Neural network classifier
Neural network identifier
Neural Networks
User Interface

Fig. 1 Rough neural network fault diagnosis chart

The fault signal feature vectors extracted wavelet analysis of samples as training the neural network input vector species for X type of equipment failure, the output of its neural network can be expressed as, if the device is in state i, then make the corresponding neural network output = 1 other output is 0 to {0,0 ...... get a 1, ..., 0) of the neural network output vector. Use of training samples for neural network training, and constantly adjust the weights, so that the error function is less than the ultimate goal of stopping the error. Treated by the neural network diagnostic characteristic value vector for training and comparing samples before training, to get the type of fault diagnostic signals

For the experimental sample selection, aiming at six major coal mine ventilator fault analysis. The selected fan base frequency of 60.5, the sampling points for 1024, 6 for fault type patterns were the rotor axis misalignment, rotor imbalance, surge, loose base, oil whirl, grinding collision, thereby determining BP neural network output is 6, the signal collected for 6 layer wavelet decomposition, making the normalization process, to extract characteristic values into the neural network

The error of the target neural network is set to 0.001, and then use neural network input and output samples for training, through learning and training, so that the network can meet the requirements of the target error in Table 1 is the result of learning and training output

Table 1. The actual output sample training

actual output					
1	2	3	4	5	6
0.9009	-0.0701	0.2365	-0.1868	-0.0681	0.1618
0.1158	1.0084	0.4205	0.4722	-0.7975	0.4749
-0.1957	-0.1480	0.7955	0.0746	0.2511	-0.1771
0.1434	-0.0778	-0.0411	1.1866	0.4837	-0.1930
-0.0134	0.1949	0.0559	-0.0106	0.8151	-0.3817
-0.0964	-0.0323	-0.0820	-0.5947	0.6077	1.0086

Figure 2 is optimized BP neural network training process error decline curve. As can be seen from the figure combining wavelet analysis and neural networks are able to reach the target faster error (errors are obtained after several training), that is a strong convergence. After the sample after training and learning, wavelet neural network can be used to diagnose the fault of mine ventilator conducted. Existing feature vector for a vibration signal：{0.00,0.15,0.65,0.10,0.10,0.00}. This feature vector into the trained neural network, the nonlinear mapping of neural networks, finally get what output:{-0.0183,-0.0223,-0.8499,-0.3498,-0.0235,-0.0403}. The output results were compared, we can infer that the fault signal reflects the rotor unbalance fault of mine ventilator

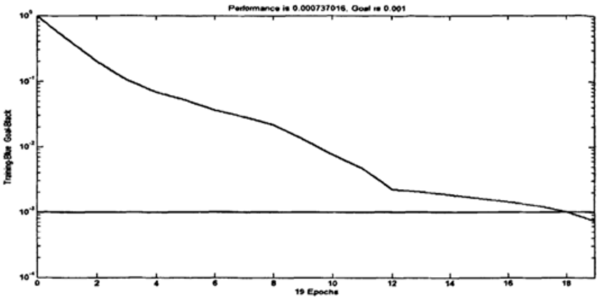

Fig. 2 Error curve of optimized BP neural network

Conclusions

Aiming to start with the main mine fan Troubleshooting research, analysis of fault type and its generation mechanism. Fault diagnosis method proposed neighborhood rough sets and neural networks using neighborhood rough set to avoid the loss of information caused by discrete data in a data processing process, through the rough set attribute reduction, greatly reducing the neural network training process. Experimental results show that the neighborhood rough set diagnostic system diagnostic accuracy rate of more than 90%, improve the safety of ventilator system, expanding the scope of application of rough set, and promote the development of artificial intelligence, troubleshooting, research in other areas there are also some reference.

Acknowledgements

The research is supported by the Youth Foundation of Anhui University of science & technology of China under Grant No.12257, No.2012QNZ06, the Doctor Foundation of Anhui University of science & technology of China under Grant No.11223, and the Guidance Science and Technology Plan Projects of Huainan under Grant No.2011B31.

References

[1] Ma Yan Cao, cattle Linda. Large fan design fault diagnosis system. Mining Machinery [J], 2006,34 (8) :38-40.

[2] Lehman, Li Yong. Holospectrum based virtual instrument fault diagnosis of mine ventilator. Coal Science and Technology [J], 2010,38 (3) :93-96

[3] Li Chunhua, Shi Yao, Zhao Jie. Rough set mine ventilator fault diagnosis system. Automation and Instrumentation [J] ,2010,06:30-36

[4] Cheng added together, Allie, Xiong Wei. Mine ventilator fault diagnosis based on evidence theory hybrid algorithm. Mine Safety [J] ,2011,12:33-35

[5] Xiong Wei, Cheng added together, Xushao Kun. PSO ventilator fault diagnosis of coal-based RBF neural network. Mine Safety ,2011,09:143-145

[6] Li Wei. Ren, Shun Qing. Zhao Hong-Bo. Influence of three-axis turntable error on gyro calibration accuracy , Electric Machines and Control, Vol.15, No.10, October 2011, pp.101-106.

[7] Liu Qiaosheng. Xi Juntong. Case-based parametric design system for test turntable, Expert Systems with Applications, Vol.38, No.6, June 2011, pp.6508-6516.

[8] Yulig Y, Ye SH, Rough set reduction for hybrid data based on genetic algorithm, Journal of harbin institute of technology. 2008,40(5):683-687.

[9] Jiyang Q, Changan Zh, Research on intelligent fault diagnosis method of the equipments, Chinese journal of scientific instrument, 2006,27(10):1270-1275.

Applied Mechanics and Materials Vol. 596 (2014) pp 114-118
© (2014) Trans Tech Publications, Switzerland
doi:10.4028/www.scientific.net/AMM.596.114

Nonlinear Econometric Model of Electronic Products and its Application

Zhou Hong Yan

Financial Institute of Qinghai University, Qinghai Xining 810016, China

qhuzhy@yeah.net

Keywords: Nonlinear Model, Electronic Products, Metering Model

Abstract. Digital product development is very rapid, this paper use engineering method to establish electronic product development model, and use Shift-share method to analysis decompose the economic capacity of the electronics industry, with the high level of industrial economic quantity Comparative analysis of the overall strength of the digital industry. Shift-share model with a comprehensive economic assessment, and put forward development proposals of corresponding electronic products.

Introduction

For the traditional method of measurement ambiguity economics, established on the basis of random mathematics can not do anything to fuzzy concepts and fuzzy information for the study of fuzzy mathematics method is introduced, it would be an important trend in the development of econometrics. From the development prospects look fuzzy mathematics method is mainly used in the field of economic analysis and policy evaluation of economic decision-making, rather than for economic forecasts. Due to the different subjects, so the introduction of fuzzy mathematics method does not replace traditional econometric methods, but it opened up a new field of econometrics, forming a branch of a certain prospect. Non-linear relationship between economic systems, not just a nonlinear function intuitively understand the relationship between economic variables, the nature of the individual's performance is non-additive, such as limited space and time irreversibility on. The individual as an economic activity, it is a simple superposition of different individuals to pursue their own interests to maximize the overall behavior of the state constitution.

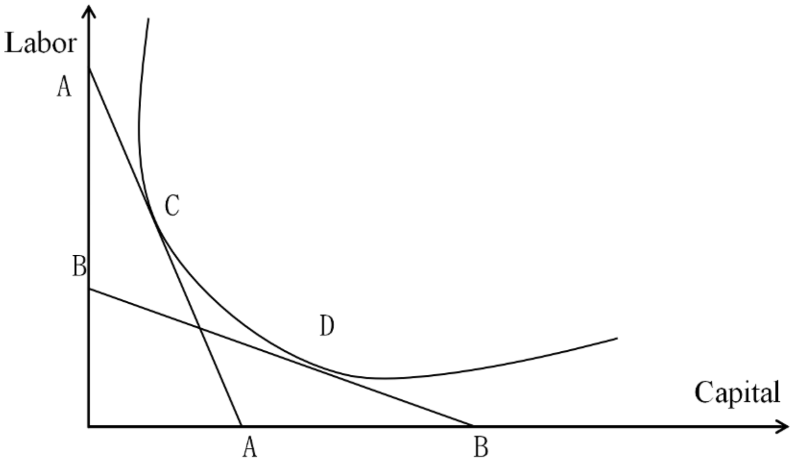

Figure.1 Factor structure and industrial structure endowed choice

This is the traditional econometric methods to complex economic system is divided into a number of individuals, will simplify the complex individual economic behavior as a theoretical basis of linear equations. Clearly, reflecting the internal economic system can not be superimposed, non-reversible in time, nonlinear economic models and other essential characteristics of limited space, more than the traditional approach econometric model of economic reality, with nonlinear economics system formation theory, nonlinear systems approach could be a quantitative analysis of the direction of the economy, and may even become mainstream econometric methods.

Model Principle

As we all know, the industrial structure of the hierarchy is an important indicator of the level of economic development of a region. We may assume that G_{ij} is the i-th volume growth industry within the region for some time j, the amount of this growth can be the amount of economic output, it can be the amount of capital invested, number of employees, etc., evaluation methods used in this paper is used in economic production the amount to GDP as an indicator. Obviously, G_{ij} is constituted in part because it involved a higher level relative to the area of the region j i-industry growth, this part of the proposed component alone, the amount of growth in the region known as the standard i-j industry, with N_{ij} said. For digital product, the amount of increase of the standard, the structure component, to indicate competitive component can be described as G_i

$$G_{ij} = N_{ij} + P_{ij} + D_{ij} \tag{1}$$

Let b_{ij0} region j represents the i-year industry in the study of the initial value, b_{ijt} said region j i-industry output value late in the study, this industrial growth rate during this period can be expressed as r_{ij}

$$r_{ij} = \frac{b_{ijt} - b_{ij0}}{b_{ij0}} \tag{2}$$

B_{i0} is the area of the i-industry executives included in the study area j initial annual production value to rise B_{it} is area includes the area of the i industrial output value in the study of late, this industry's growth rate during this period may R_i expressed as

$$R_i = \frac{B_{it} - B_{i0}}{B_{i0}} \tag{3}$$

B_0 represents the initial years of the study area contains a high-level output value j of the reference area to B_t represents senior regional j contains a reference area in the study Dynasty output, contains a reference level region j region's total economic scale in this period rate can be expressed as R

$$R = \frac{B_t - B_0}{B_0} \tag{4}$$

By formula (1) to (4) to be launched

$$G_{ij} = b_{ij0} r_{ij} = b_{ij0} R + b_{ij0}(R_i - R) + b_{ij0}(r_{ij} - R_i) = N_{ij} + P_{ij} + D_{ij} \tag{5}$$

Among them, $N_{ij} = b_{ij0} R$, $P_{ij} = b_{ij0}(R_j - R), D_{ij} = \left(r_{ij} - R_i\right)$. It can be more clearly seen by equation (5), Shift-share method to explain the gap between regional economic growth factors from the industrial structure and competitiveness of two factors. If the growth rate of a region identical to each industry growth rate of the province of the same industry, which ruled out due to the various regions of the same industrial competitiveness (or productivity) growth rate differences resulting from the different on, then the region's economic growth rate and the province's economy differences in growth rates is formed by structural factors. Thus, both a deviation share analysis can explain the determinants of economic growth in the region (ie structural factors and competitive factors) to calculate the extent of the role of the method, but it is also among the regional structure of economic growth determinants difference comparison methods .

Shift-share Model used in Digital Products Industry

Nearly digital products supporting enterprises gathered, a total of 20 household appliances enterprises above designated size model, driven by thousands of supporting enterprise development, the formation of large enterprise groups as huawei, zhongxing etc, and related supporting industries based a large industrial base. From production, the production has maintained rapid growth.

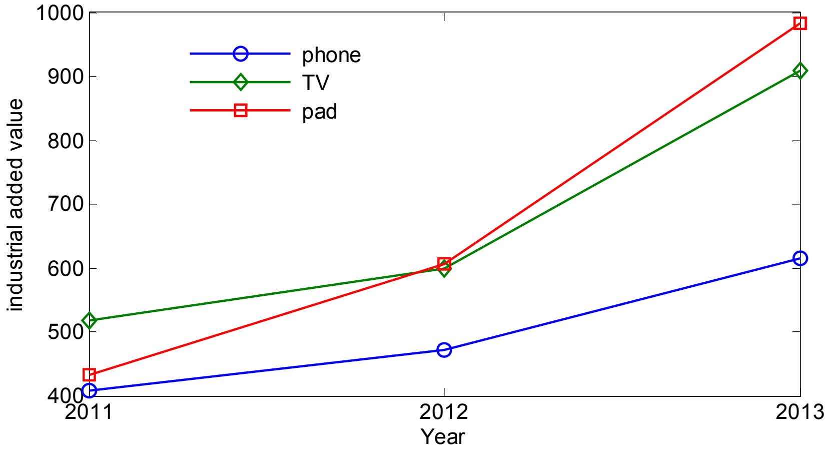

Figure.1 Output of digital products between 2011 and 2013 (Unit: million units)

In 2012, pad and phones were more than 15 million units, realized a total industrial output value of 540 billion Yuan, 15.5 billion Yuan of industrial added value profits of 3.5 billion Yuan. The digital products industry represented by the appliance electronics companies at home and abroad more than 100 products related to white, black, beige appliances, and other fields. The business involved in the home appliance industry. Location quotient (LQ) is the most immediate and primary method to study the advantage industry in a region. A higher location quotient value indicates more advantage in the industry. Location quotient analysis can measure relative specialization degree of various industries (or industrial departments) in different districts, reflecting the structure and trend of economic link between regions indirectly. For instance, there is a certain industry *j* in a region *i*. If LQ>1, this indicates that there are extra export products of this industry except local consumption. If LQ<1, this indicates that the products can't satisfy local consumption and have to import. If LQ =1, this indicates that the supply and demand of products are balanced in the region. The LQ calculation formula is:

$$\alpha_{ij} = \frac{ei_j E}{e_i E_j} \tag{6}$$

Where α_{ij} is the location quotient of industry *j* in region *i*; e_{ij} is the net output value (or employment quantity) of industry *j* in region *i*; e_i is the net output value (or employment quantity) of all industries in region *i*; E_j is the national net output value (or employment quantity) of all industries. The competitiveness of appliance industry was analyzed based on the data from economic census and industrial clusters competitiveness comment data of 47 major cities nationwide. Three indexes were selected to calculate appliance industry comprehensive LQ, including product sales income LQ (reflecting market share of industrial clusters), enterprise employment number LQ (reflecting intensity of industrial clusters), enterprise amount LQ (reflecting intensity of industrial clusters).

Table.1 Location quotients of major industries

Industry	Sales income	Competitiveness	
		Location quotients	Rank
Digital products	4.62	4.43	3
Petrochemical	1.97	2.44	4
Shipping	2.45	2.40	5
Textile	3.34	2.00	7

Digital products industry clusters have great contributions to the economic development, although the development stages and levels are not very high at present. Table.2 shows the proportion of the four industries industrial added values to the total industrial added values of city, including appliance industry, petrochemical, shipping and textile. It can be seen that petrochemical industry cluster is the largest one, which is well-known and competitive interiorly.

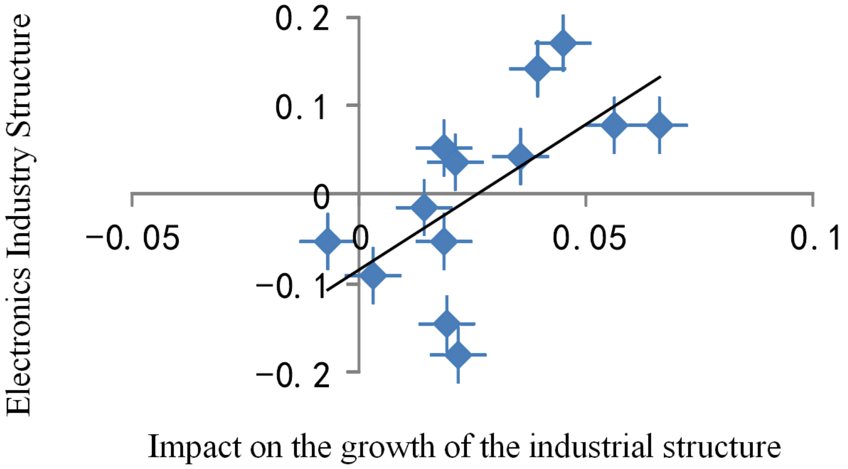

Figure.4 Internal electronics industry association structure and economic growth rate

Other industrial clusters have also formed a certain scale. In one word, the four industrial clusters have shouldered the key mission of industry. The upstream and downstream industries are closely associated and the impact range is extremely wide. According to statistics, the industries directly correlated with auto industry are more than 40, which can drive the development some other industries directly, such as Digital products, textile, financial and insurance law consulting, industrial service, science research design, and originality industries, etc. Moreover, consumptive appliance industry enterprises expand rapidly and the industry concentration is increasing ceaselessly. Large appliance industry enterprises are taking more and more important status in their industries. Considered the development of four industrial clusters, the industrial cluster chain should extend and develop to the peninsula scope.

The core competitive capacity is the precondition and foundation of industrial competitiveness. For the enterprises of internationalization and globalization, the most important is to establish the innovate mechanism of enterprise and improve the integrate ability, which is exclusive and difficult to imitate. Therefore, enterprise qualification should be improved quickly.

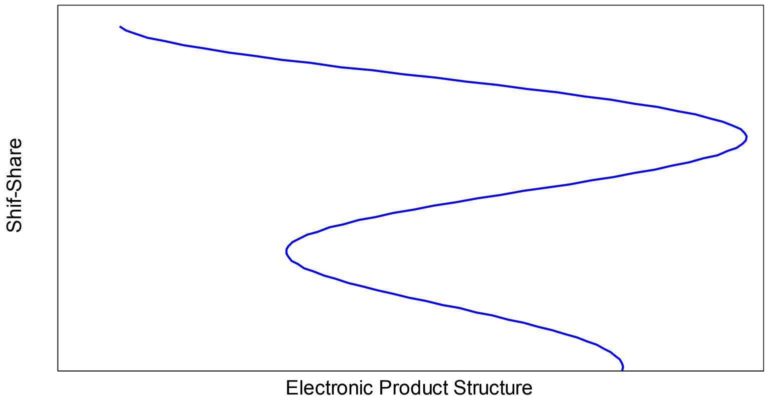

Figure.3 Electronic product structure and competitiveness

The core intermediate products must be done well. In a word, accelerate the establishment of modern enterprise system and procure the conversion from horizontal multiplication expansion to business refocusing development. Simplify and standardize the administrative examination and approval. Exert the basic role of market in resource allocation to a large extent. Build up a unified, open, competitive and ordered market system. Second, enlarge the infrastructure investment further. Deepen the reform of the financial system to create comfortable conditions for corporate financing. Adjust and improve the foreign investment policy and use foreign capital reasonably and effectively.

Encourage produce and use domestically-manufactured equipment. Strengthen the cultivation of senior technical talents.

Conclusion

The competitive industrial clusters must be relied on to play the leading role in driving the peninsula economy. The priority industrial clusters have shown relatively outstanding advantages and the economic vitality as an open port city. However, the growth of industrial clusters still need to be further expanded. The implementation of strategies for important industrial development can accelerate the industrial chain extension and the industrial clusters development, which will improve the competitiveness of the industrial clusters and promote the economy development.

References

[1] K. Tanaka: A sales forecasting model for new-released and nonlinear sales trend products, Expert Systems with Applications, Vol.37 (2010), p.7387-7393

[2] G. M. Fürstenberger, M. Wagner: Exploring the environmental Kuznets hypothesis: Theoretical and econometric problems, Ecological Economics, Vol.62 (2007), p.648-660

[3] T. Nowak, V. Hofer: On stabilizing volatile product returns, European Journal of Operational Research, Vol.234 (2014), p.701-708

[4] K. J. A˚ström, P. R. Kumar: Control: A perspective, Automatica, Vol.50 (2014), p.3-43

[5] M. Billio, R. Casarin, F. Ravazzolo, H. K. Dijk: Time-varying combinations of predictive densities using nonlinear filtering, Journal of Econometrics, Vol.177 (2013), p.213-232

[6] S. Lee, J. Y. Choeh: Predicting the helpfulness of online reviews using multilayer perception neural networks, Expert Systems with Applications, Vol.41 (2014), p.3041-3046

[7] W. Soon: Applied Mathematics and Computation, Vol.217 (2011), p.8149-8165

[8] A. Diabat, D. Kannan: Resources, Conservation and Recycling, Vol.74 (2013), p.156-169

Applied Mechanics and Materials Vol. 596 (2014) pp 119-122
© (2014) Trans Tech Publications, Switzerland
doi:10.4028/www.scientific.net/AMM.596.119

Study on the Transformation of Military Logistical of Internet of Things Era

Ye LU[1, a], Chao XIE[2,b] and Li SHANG[3,c]

[1] Logistics Service Command Department, Military Economic Academy, Wuhan, China

[2] Equipment Economy Management Department, Military Economic Academy, Wuhan, China

[3] Military Logistics and Procurement Department, Military Economic Academy, Wuhan, China

[a]18004246@qq.com, [b] xiechao188@163.com, [C] 16145135@qq.com

Keywords: Internet of things, military logistical, application, RFID

Abstract. The paper discussed the basic conceptions of Internet of Things (IOT), its structure and key technology. It expounded the application principle, development and practice of military IOT technology from the aspects of military logistics, asset management, materiel support, mobilization and barracks management, combined with instances. Finally, the problems in application and current developing status of the military IOT technology were expatiated upon in terms of the military IOT technology standard and RFID technology safety.

Introduction

With the extensive application of high tech, especially information technology, in the military sphere, the model of modern warfare is gradually informatizing and the logistical support of informatization becomes the inevitable requirements of information battlefield. With the appearance of “focused logistics” insurance model in U.S. troops and the rise of Total Asset Visibility concept, IOT technology is playing more and more significant role in military logistics by its features and advantages on rapid, convenient, accurate and automatic, and gradually for the realization of logistical informatization, networking, intelligentization, and visualization[1]. It will be widely applied in military logistics in the future.

Related concept of Internet of Things

Internet of Things

Massachusetts Institute of Technology Auto-ID Lab was first proposed the Internet of Things (IOT) concept in 1999. The IOT is expanding and improving on the existing Internet infrastructure, the original terminal of the Internet extends to the goods in kind. IOT can easily use remote perception and control of networked goods to constitute a more extensive and intelligent ubiquitous networks, together with the existing Internet. IOT has become the third wave of technology following the computer and Internet information industry, and certainly become the next generation of IT leaders and the direction of standard IOT technology is being more and more attention in the world, its overall architecture, the key technology, network, network and service system are the current exploration and research hotspot[2].

The constitute of the IOT

IOT through the information sensing devices such as wireless radio frequency (RFID), wireless sensor networks, Global Positioning System, sensors or camera, infrared or laser scanners and other real-time acquisition sound, light constitute a wider range of super-network, electricity, heat, power, position, chemical, biological, and other information, and integration with the Internet, so as to realize the identity of automatic identification, and monitoring real-time positioning and remote management features[3]. According to the currently widely accepted definition, the composition of Things architecture layer, transport layer and application layer is divided into perception of three parts. Perception layer: Also known as the data acquisition layer, collection information and identification based on wireless radio frequency (RFID), wireless sensor networks, Global Positioning System, sensors, or camera, infrared or laser scanning sensor technology[4]. Transport Layer: also known as ubiquitous access layer based on the existing Internet and private networks, transmission summary of the various types of data collection through the sensing layer to achieve real-time transmission of data and ensure data security, wired and wireless Internet, 2G and 3G networks, can be used as an integral part of the transport layer. Application layer: posed by the PC, mobile phones and other terminal equipment and data center applications or control systems, data exchange and data processing, protection of information sharing and information security functions covering data storage, analysis and calculation, remote control, cloud computing.

Application and practice of IOT technology in military logistics

Application of IOT technology in military logistics

Military logistics refers to the financing of military force in daily life, military training, duty combat required for military supplies, production, processing, packaging, transportation, warehousing, deployment of supply and other sectors, and ultimately served troops consumption, space transfer with the protection of military operations, special categories of items, the confidentiality of mobility characteristics[5]. The entire consumption process of military materials closed-loop monitoring and management through the IOT technology, combined with RFID technology to record the name of the military supplies models in production, date of manufacture, storage, precautions and other information, by implantation of perishable goods response detection sensor on the material status of the non-destructive quality monitoring, bulk packaging after the batch materials, the overall number of storage and materials in military networks, deployment of management systems registration[6]. For example, the material of Road military transport is enabled through the warehouse RFID reader to automatically obtain the legitimacy of data for transport vehicles out library materials details, verification of materials, and the state is normal and record storage time. GIS real-time access to material location, material status and other information can be combined with transport links to the military vehicle GPS and special communication systems for military vehicles to provide the road ahead, climate information, destination point status of environmental information in order to facilitate the transportation of materials. In storage areas by reading the material information, personnel information, vehicle information to confirm the legal status, to ensure the availability of military supplies and reserve warehouse security, at the same time into the shortest path algorithm in the system, effectively reducing the energy consumption of materials handling and time. Materials distribution chain can achieve an accuracy of the data records of the individual soldier, until the material consumption or recycling. The military deployment of network materials management system to achieve transparency, traceability and have good handling, turnaround time through the material node records can be scientifically accurate quantitative reference for the deployment of supplies throughout the battle, shorten the cycle times of military supplies, reduce the number of logistics personnel, to reduce the cost of the deployment of goods consumed, and to improve the accuracy of the information materials, enhance the control of the power of the military war global to achieve a true sense of the adaptive military logistics.

Application of IOT technology in the management of military assets

The military asset management is including aspects of ordnance management, transportation management, and military supplies. Anywhere for the transfer of military supplies management system based on RFID technology, materials registration without manual registration, to prevent the misuse of personnel, data updating delays, simplify inventory processes, improve inventory quality, ordnance maintenance and use of records in real-time recording to facilitate the upgrading and improvement of the ordnance, while tray centralized sorting and management, can effectively reduce the number of ordnance handling and breakage probability and maximize the ordnance in accordance with the principle of first in, first out (the FIFO) military effectiveness. Such as Intelligent Drawer Armory System of the British, Drawer Armory System of USA[7].

The U.S. through the Total Asset Visibility plan to achieve logistical personnel flow, equipment flow, full transparency of the material flow management, to achieve a "passive reserve type" logistics "active distribution shift. The war in Iraq, for example, than the Gulf War, shipping volume 87% reduction in air traffic decreased 88.6%, and strategic support equipment mobilization reduced by 89%, the Battle of material reserves decreased by 75%, IOT technology traditional materials allocation process required a few days time to 20 min[8]. Our military in asset management and logistical support including the use of the army military vehicle license plate based RFID anti-counterfeiting technology to curb counterfeit military vehicle license plate, automatic access control system integration of RFID technology Military Academy.

Application of IOT technology in the quartermaster security

IOT for the intelligent quartermaster protection services to build a huge network platform. First, intelligentize of provisions protection. Material through a variety of network nodes connected officers and soldiers, quartermaster agencies, service centers, canteens, suppliers, etc., in real time, automatically collect and transmit data, to automate the whole process of the provision for materials storage and transportation, recipe formulation and dining management and control of supplies transparent, personalized protection[9]. On the provisions protection platform of IOT to change the provisions to protect mode, the transition from canteens to people-centered, and greatly improve the convenience and effectiveness of the protection. Such as the supply chain traceability, grass-roots units can be directly traced back the source of the producers and products to choose safe food. Second, intelligentize of bedding & equipment protection. IOT to be bedding &equipment protection the whole process of implementation of real-time management and control of material and strength, a much more refined and dynamic way to manage the supply chain, improve the resource utilization and protection performance of the bedding &equipment materials, to achieve "smart security”. Third, intelligentize of quartermaster equipment operation and maintenance. Information technology equipment, military supplies and equipment to install the various sensors, automatic detection system can automatically display automatic alarm, automatic diagnostics, remote maintenance, and other munitions support equipment failure. This will allow military supplies and equipment operation more convenient, reduce equipment failure rate, as well as to facilitate the maintenance and support of military supplies and equipment[10].

Application of IOT technology in the logistical mobilization

Improve the response to a variety of security threats and accomplish diverse military tasks our military are facing new situation and tasks, logistical mobilization in response to the early war or emergency, the situation under control and prevent the situation from deteriorating or expanding a decisive role[11]. Today, the IOT technology makes logistical mobilization and also showing a new development trend, information has become the core elements of the logistical mobilization, logistical mobilization and organization and command network, logistical mobilization and demand precise visualization of the potential logistical mobilization, logistics, and mobilization content knowledge-based. Information beyond the physical energy becomes the most important factor to determine the outcome of the war in information warfare[12]. Therefore, to achieve the material mobilization precision should be master and disposable supplies enough to mobilize information resources. To better grasp the material information resources, we should be "electronic tags" collection of material information by the wireless mobile communication or telecommunication networks in a timely manner and accurately transmitted to the government department responsible for materials to mobilize these sectors should be established material information sharing mechanism. building supplies precision mobilize information platform based on the "IOT", in accordance with the principles of unified and standardized hardware and software combination, resource sharing, security and confidentiality", composed by the electronic tags, wireless or wired data communications, computer and related software , with the existing government, military and social information network resources, establish vertical and horizontal interconnect, and supplies a full range of interoperability precise mobilization network system, materials mobilized in various fields, all departments and all levels are closely linked, for each levels of user provides a powerful mobilization of information services, to improve the speed and effectiveness of mobilization command and control, battlefield needs and the rear to support the effective sharing of information of supplies, and provide a good carrier and platform for the implementation of the fast and efficient mobilization command and control. In the Iraq war, the U.S[13]. military is by SAVI Technology to each container to the Gulf on the installation of RF satellite chips to accurately track the 40,000 containers to the Department of Defense sent to the Gulf via satellite, to tracking the "people flow", equipment flow and material flow, and command and control of its receipt, distribution, and exchange, so that the supply of materials and management has a high transparency, greatly improving the effectiveness of the protection[14].

Some problems should be noted in military IOT application

IOT technology exerts important function in accelerating modernize and informatization process in the troops, but due to the characteristics of the IOT technology and war, there are still some problems need to be improved in the development. Development of any technology is based on standards, The application of a technology under a framework is helpful to the establishment and development of an industing, especially building the military IOT technological standardized system will be the key to improve the civil-military integration of logistics management, insurance of materiel and military research on military IOT project[15].

Applications of the military IOT technology, land, sea, sky, space, electromagnetic space after five dimensions makes the cyber battlefield the key to modern war, the military countermeasure emphasis has shifted from tangible tanks and missiles battlefield to invisible cyber space in the IOT era. The pace of the military IOT technology development will play a vital role in the outcome of the information battlefield.

References

[1] Liu Xin: submitted to Telecommunications Science (2011), p. 12-15

[2] Zhang Linhe: submitted to Packaging Engineering (2010), p. 34-37. (Chinese)

[3] Ma Yong, Zhu Hong, Yang Yunzhi, Li Yuanzhong: submitted to Telecommunication Engineering (2008), p. 119-122. (Chinese)

[4] Qian Zhihong, Wang Yijun: submitted to Journal of Electronics & Information Technology (2013), 35(1): p. 215-227. (Chinese)

[5] Sun Qi-bo, Liu Jie, Li Shan, et al.: submitted to Journal of Beijing University of Posts and Telecommunications (2010), 33(3): p.1-9. (Chinese)

[6] Qian Zhi-hong and Wang Yi-jun: IoT technology and application (2012), 40(5): p. 1023-1029. (Chinese)

[7] Wang Xue, Qian Zhi-hong, Hu Zheng-chao: submitted to Journal on Communications (2010), 31(6): p.49-57. (Chinese)

[8] Liao Pei-kai, Chang Min-kuan, and Kuo C J: IEEE Transactions on Vehicular Technology, (2009), 58(7): p. 3579-3595. (Chinese)

[9] Pujolle G: IEEE John Vincent Atanasoff 2006 International Symposium on Modern Computing. (2006), p.163-168

[10] CASAGRAS Final Report: *RFID and Inclusive Model for the Internet of Things*. Hong Kong: EU Project Number 216803, (2010)

[11] Dirk H: Concepts, Protcols, and Architectures. Berlin:Springer, (2008), p. 107-137

[12] BROLL G, RUKZIO E, PAOLUCCI M.Perci: submitted to Internet Computing (2009), 13(6): p. 74-81

[13] ATZORI L, IERA A, MORABITO G: submitted to Computer Networks (2010), 54(15): p. 2787-2805

[14] Yang Zhi-qiang, Wright R N: IEEE Trans on Knowledge and Data Engineering, (2006), 18(9): p. 1253-1264

[15] MACYT, YAUDKY, YIP NK: Proc of the 16th Annual International Conference on Mobile Computing and Networking.New York:ACM Press (2010), p. 185-196

Applied Mechanics and Materials Vol. 596 (2014) pp 123-126
© (2014) Trans Tech Publications, Switzerland
doi:10.4028/www.scientific.net/AMM.596.123

The Research on Cloud Mobile Office System Development for Enterprise Application

Wu Fang [1, a], Wang Zhengmin [1, b], Yao Guang [1, c], Miao Zhenmin [1, d]

[1] China Tobacco Zhejiang Industrial Co., LTD

[a] wf@zjtobacco.com, [b] wzm@zjtobacco.com,

[c] yaoguang@zjtobacco.com, [d] miaozm@zjtobacco.com

Keywords: Office Automatic; Cloud Mobile Office; Office Platform

Abstract: With the rapid development of science and technology, office automation greatly facilitate the efficiency of the enterprise or the company's office, but the traditional office automation has location and time limit. Along with the development of smart phones and cloud computing, cloud office automatic and mobile office automatic greatly convenient office workers in the enterprise and enterprise, and solved the problem of the traditional mobile office automatic mostly. This article first introduced the thesis research background, analyzes the present situation and existing problems of traditional office automation, through the introduction about cloud computing, mobile devices and related concepts of office automation, cloud mobile office system was put forward, and some solutions are put forward.

Introduction

With the popularization of information technology, electronic, digital works have entered more and more enterprises and institutions, the information construction in enterprises and the internal wove a set of efficient and smooth traffic information interconnected system, greatly promoting the development of the productivity of enterprises and institutions [1]. But, at the same time, because of the need to rely on a fixed place of work and fixed form a complete set of equipment, the actual situation of began to highlight some of the new work mode. Information on how to break the time and space limit, to establish a can at anytime, anywhere, with use of information systems, no matter the company managers and employees in where, it can associate enterprises and the internal information system casually, which has gradually been becoming the focus of the current stage of informatization construction [2].

Office automation as an important part of information construction, with the development of smart phones and cloud computing, cloud office automatic and mobile office automation greatly convenient office workers in the enterprise and enterprise, and the cloud solves the problem of the traditional mobile office automatic mostly.

Basic concept of cloud mobile office

Mobile office is also known as "3A office", through the mobile phone or PAD and other enterprise information software installed on mobile terminals, and through the wireless internet access, it makes the mobile terminal have the same office function like computers, and it also make office staff is not subject to the constraints of time and space, at any time, any place to deal with anything business related [3].

Mobile office system can easily work together and remote management, effectively improve the efficiency of office and management, and promote enterprise office efficiency [4]. Mobile device contains OA (office automation) management client, the VPN client and client browser, as shown in figure 1.The VPN client set can connect to the Adapter server. OA management client allows users to set to function. OA client is for OA business operation.

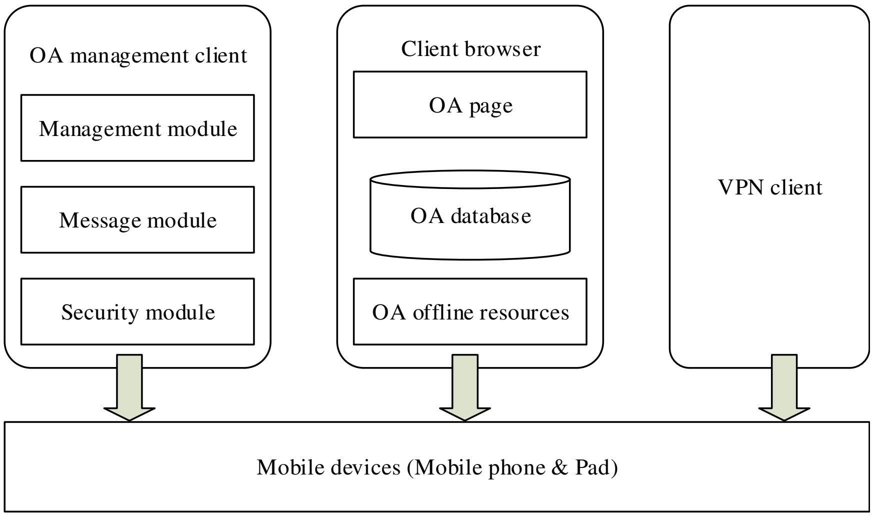
OA management client
Management module
Message module
Security module
Client browser
OA page
OA database
OA offline resources
VPN client
Mobile devices (Mobile phone & Pad)

Figure 1. Basic composition of cloud mobile office

Office automatic management client is based on the IOS or Android client development. It has the strategy management, message management and security management, and other functions. Strategy management foot when users through OA management client to set the OA system off-line, synchronization, message delivery, and other functions, the transmission of strategy to the Adapter in the server the Manage module. Message management refers to when the OA not login client, the client can accept OA management by the Adapter server push messages, and manage to push the message; Safety management is to point to when client logged out the OA management need to client before operation data delete, such as database, the log information, safety management module can also receive the safety command in Adapter server, lock screen on a mobile device, delete directory, delete the browser cache, obtain the function of the mobile device's current location.

Architecture design of cloud mobile office platform

This paper is to establish a set of complete description of cloud computing resources needed to mobile office system, components, the cooperate relationship between the form definition, data interaction and resource load, and by describing the cooperate relationship between the different components to configure a variety of different state, let the office system can realize the load, task distribution, real virtual machine management operations, such as the cloud deployment of mobile office structure of the whole system is shown in figure 2.

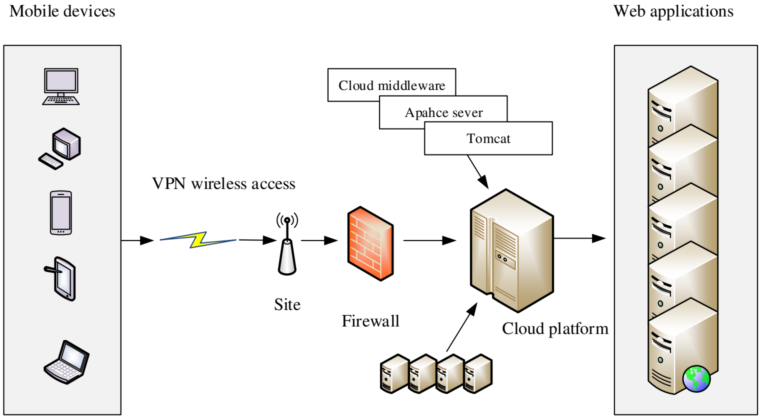
Mobile devices
Web applications
Cloud middleware
Apahce sever
Tomcat
VPN wireless access
Site
Firewall
Cloud platform

Figure 2. Structure deployment diagram of cloud mobile office

Cloud platform is a set of mobile office that can be run on a laptop, tablet and smartphone office software, related the sum of terminal equipment, service, the user directly on all kinds of mobile terminal application software, realize the data center server to communicate with distant company, transaction processing, information search, data interaction, the scene real-time acquisition data upload and other functions, has excellent properties of traditional way of electronic office cannot match [5].

(1) Platform construction makes the enterprise completely liberated from the constraints of the work on time and space, the concept of office from a fixed office location derived from anywhere.

(2) Don't have to worry about computers and the Internet, also need not worry about operating procedures are too complicated, mobile office system based on smart phone or PAD terminal brought maximum convenience to the user.

(3) Mobile office platform user groups to cover the business enterprise inside each post staff, everyone through business contacts, SMS, email, telephone and voice communication way for communication, make the enterprise internal communication channels and varied transparent, build a harmonious enterprise.

(4) Mobile office platform whether terminal is located in where, support wireless, real-time, convenient update. You can very easily and very reliable, complete the software distribution, upgrade, database failure repair, etc.

Cloud mobile platform system design for enterprise

In business-oriented mobile platform system design process of cloud, we make the cloud application platform physical architecture structures, as shown in figure 3.

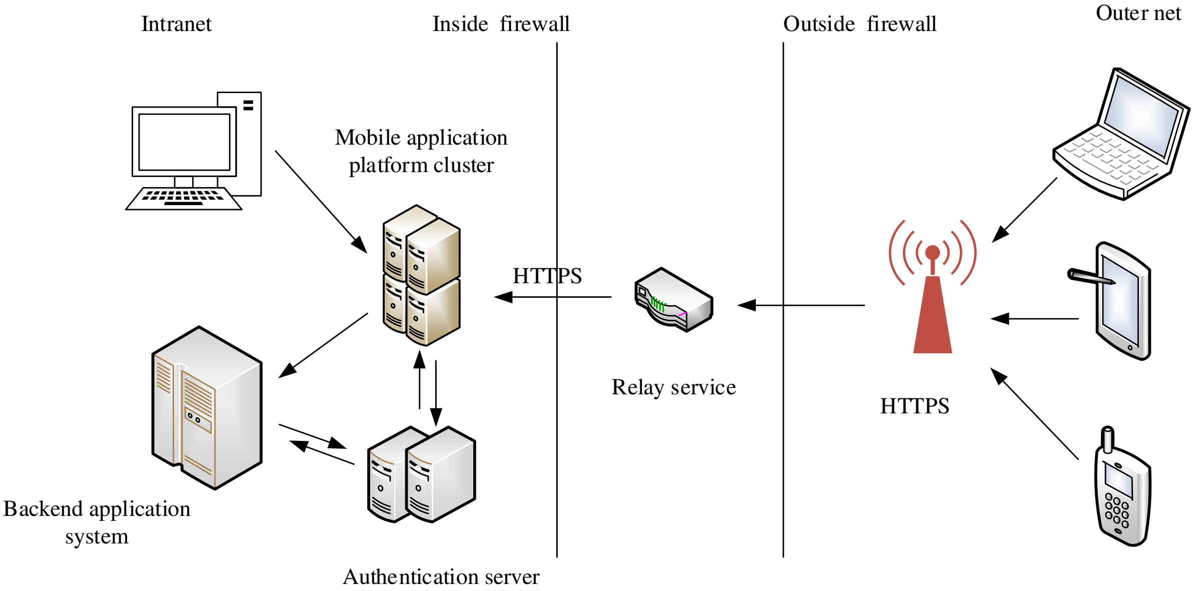

Figure 3. Physical structure diagram of cloud mobile application platform for enterprise

Enterprise mobile application platform is mainly divided into platform part, the background applications and front-end application part. From the physical structure, the application platform of computer cluster (including authentication server), background application system is through physical link deployment in enterprise network environment. Communication between various systems in the network are within the local area network (LAN), so the high speed and security. Front-end equipment application system to communicate through the HTTPS protocol and the background, and front-end application data passes through two firewall can enter into a network. Is between two firewalls and load balancing server relay server, better improve the system stability and efficiency.

Mobile application platform from the function can be divided into two systems: enterprise mobile application operation management platform and enterprise mobile application development platform. Mobile application platform function architecture as shown in the figure 4 below.

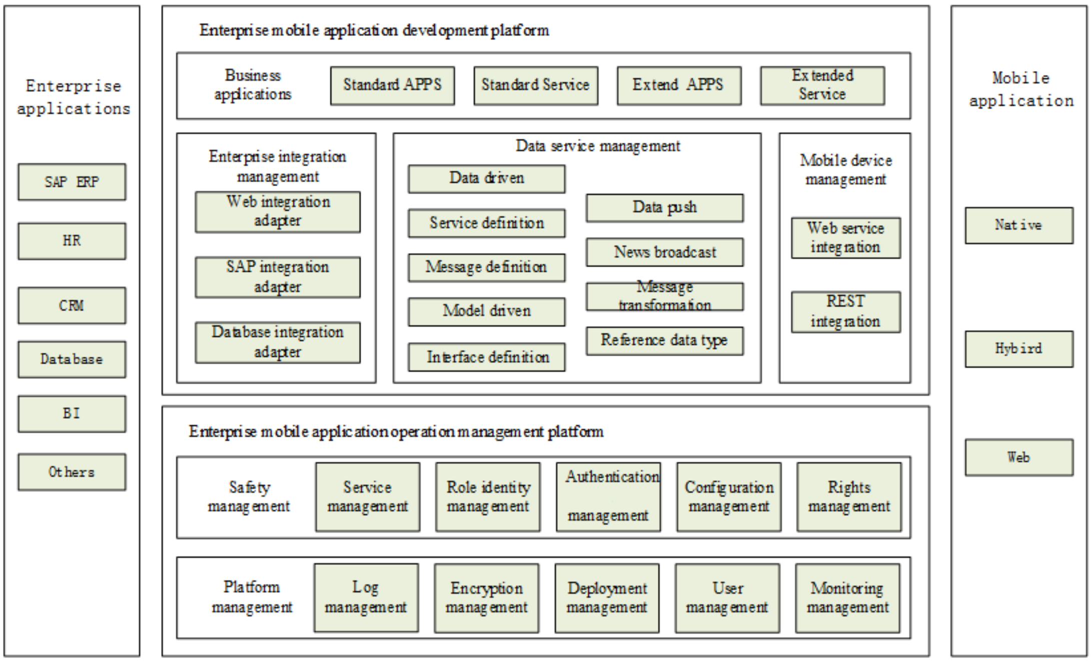
Enterprise applications
SAP ERP
HR
CRM
Database
BI
Others
Enterprise mobile application development platform
Business applications
Standard APPS
Standard Service
Extend APPS
Extended Service
Enterprise integration management
Web integration adapter
SAP integration adapter
Database integration adapter
Data service management
Data driven
Service definition
Message definition
Model driven
Interface definition
Data push
News broadcast
Message transformation
Reference data type
Mobile device management
Web service integration
REST integration
Enterprise mobile application operation management platform
Safety management
Service management
Role identity management
Authentication management
Configuration management
Rights management
Platform management
Log management
Encryption management
Deployment management
User management
Monitoring management
Mobile application
Native
Hybird
Web

Figure 4. Mobile application platform function architecture

Enterprise mobile application platform is mainly divided into platform part, the background applications and front-end application part. From the physical structure, the application platform of computer cluster (including authentication server), background application system is through physical link deployment in enterprise network environment. Communication between various systems in the network are within the local area network (LAN), so the high speed and security. Front-end equipment application system to communicate through the HTTPS protocol and the background, and front-end application data passes through two firewall can enter into a network. Is between two firewalls and load balancing server relay server, better improve the system stability and efficiency.

Conclusion

Cloud mobile office system can satisfy the business enterprise personnel anytime, anywhere to access requirements of enterprise information resources, flexible and convenient platform for the intelligent mobile office, which can bring convenient operation experience for staff, improve work efficiency. In this paper, the design of cloud mobile office system framework does not affect the original office system, it is very good for the stability of the primary system. The architecture solves the security of mobile office, real-time, network instability, and problems such as large amount of data transmission, increased the mobile terminal adapter of the page and for the safety of the user, providing a reliable guarantee.

Reference:

[1] S. Marston, Z. Li, and S. Bandyopadhyay: Decision Support Systems, Vol. 51(2011) No.1, p. 176.

[2] G. Pallis: IEEE Internet Computing, Vol. 14(2010) No.5, p. 1.

[3] X. Xu: Robotics and computer-integrated manufacturing, Vol. 28(2012) No.1, p.75.

[4] K. Birman, G. Chockler, and R. van Renesse: ACM SIGACT News, Vol. 40(2009) No.2, p. 9. 68.

[5] B.P. Rimal, A. Jukan, D. Katsaros: Journal of Grid Computing, Vol. 9(2011) No.1, p. 3.

Applied Mechanics and Materials Vol. 596 (2014) pp 127-130
© (2014) Trans Tech Publications, Switzerland
doi:10.4028/www.scientific.net/AMM.596.127

An execution framework for domain-oriented QoS evaluation of manufacturing cloud services

Hong Jin [a], Xi-fan Yao [b] and Jie Zhang [c]

School of Mechanical and Automobile Engineering, South China University of Technology,

Guangzhou, 510640, China

[a]huashangjh@163.com, [b]mexfyao@scut.edu.cn, [c]zj0769@126.com

Keywords: cloud manufacturing, quality of service, domain-oriented QoS evaluation

Abstract. Cloud manufacturing is emerging as a new intelligent and collaborative manufacturing model. With the development of virtualization technology, the manufacturing resources can be encapsulated as manufacturing cloud services (MCSs). The accuracy of service quality evaluation is the key to selecting a MCS from many available ones with similar functions but different QoS, but existing QoS evaluation models only focuses on common service attributes, which cannot meet user needs. Hence, this paper presents an execution framework for domain-oriented QoS evaluation for MCSs. Four function modules for domain-oriented QoS evaluation of MCSs were analyzed, and the involving key technologies were discussed as well.

Introduction

The cloud manufacturing (CMfg) [1] is an intelligent and collaborative manufacturing model, which is under the support of cloud computing, Internet of things, service-oriented technologies, information technologies, advanced computing technologies and advanced management technologies. CMfg aims to provide ubiquitous, convenient, and on-demand MCSs to users [2]. As there are many available MCSs with similar functions but different quality of service (QoS), it is necessary to select high quality MCSs via manufacturing cloud service evaluation techniques.

Existing QoS evaluation researches evaluate MCSs primarily focuses on generic QoS (with attributes such as response time, cost, reliability, availability, and so on). These quality attributes are public to every MCS, so we call them generic QoS. Some typical works are as follows. Zeng [3] evaluated services with 5 QoS properties, i.e. execution price, execution duration, reputation, successful execution rate and availability. The evaluating result is the sum of all QoS properties multiply with its weight, which is determined by users by their experience. The measurement and evaluation model of trust-QoS is proposed in [4, 5], which is used to evaluate the trust relationship between service providers and service users. Tao [6] classified the QoS properties into performance QoS and description QoS. Besides the above mentioned QoS properties, it's also included maintainability, function similarity, security, and so on.

However, the above researches are not comprehensive for the service evaluation methods. These models do not consider the domain QoS which are also important to users. Taking the online purchasing automobiles parts [7] for example, users often choose the automobiles parts with a higher crash safety rating even if the time of the service is relatively long. Considered this critical issue, an execution framework for domain-oriented QoS evaluation of MCSs is designed in this paper.

The execution framework for domain-oriented QoS evaluation

Existing QoS evaluation models evaluate services only by generic QoS, which can not satisfy the requirement of service users. Therefore, a domain-oriented QoS evaluation execution framework for MCSs in CMfg (DOQoSEF4MCS is proposed in this section (see Fig. 1).

DOQoSEF4MCS is primarily consisted of construction module, description module, optimal module, and maintenance module. The construction module means that the domain experts construct domain-oriented evaluation factors and store it in the relation database of CMfg service pool. The description module provides description template (including evaluation model) for the MCS providers who distribute in different places publishing the MCSs in the CMfg service pool. When users submit task requests to CMfg system, the optimal module search qualified MCSs and evaluates the candidate services to allocate optimal services. The maintenance module is implemented to auto-maintain the change of evaluation model and QoS value of MCSs. The function and key technologies of the four modules in DOQoSEF4MCS are analyzed as follows.

Construction of evaluation model. Construction of evaluation model is the basis for domain-oriented QoS evaluation. The evaluation model that just considers generic QoS cannot satisfy users' domain needs, which should include special attributes for domain oriented MCSs. Construction of evaluation model involves the process of construction, verification and storage evaluation factors and weights.

- *Construction of evaluation factor.* Besides designing generic QoS properties, Domain experts define special evaluation attributes of services for domain oriented MCSs and establish domain QoS properties. For example, crash safety rating is one of domain QoS properties for automotive industry, which is one of the important indicators for users to choosing automotive services.
- *Construction of evaluation weight.* It is mainly responsible for providing reference values for users to evaluate services. The weights of evaluation factors can be determined by several methods such as experience of experts, grey relational analysis, principal component analysis, analytic hierarchy process, and so on.
- *Verification of evaluation model.* Testing whether the evaluation model, which contains evaluation factors and evaluation weights, could accurately evaluate the MCSs using the sample data provided by domain experts. If the evaluation results do not highlight the influence of domain attributes, the evaluation model needs to be rebuilt.

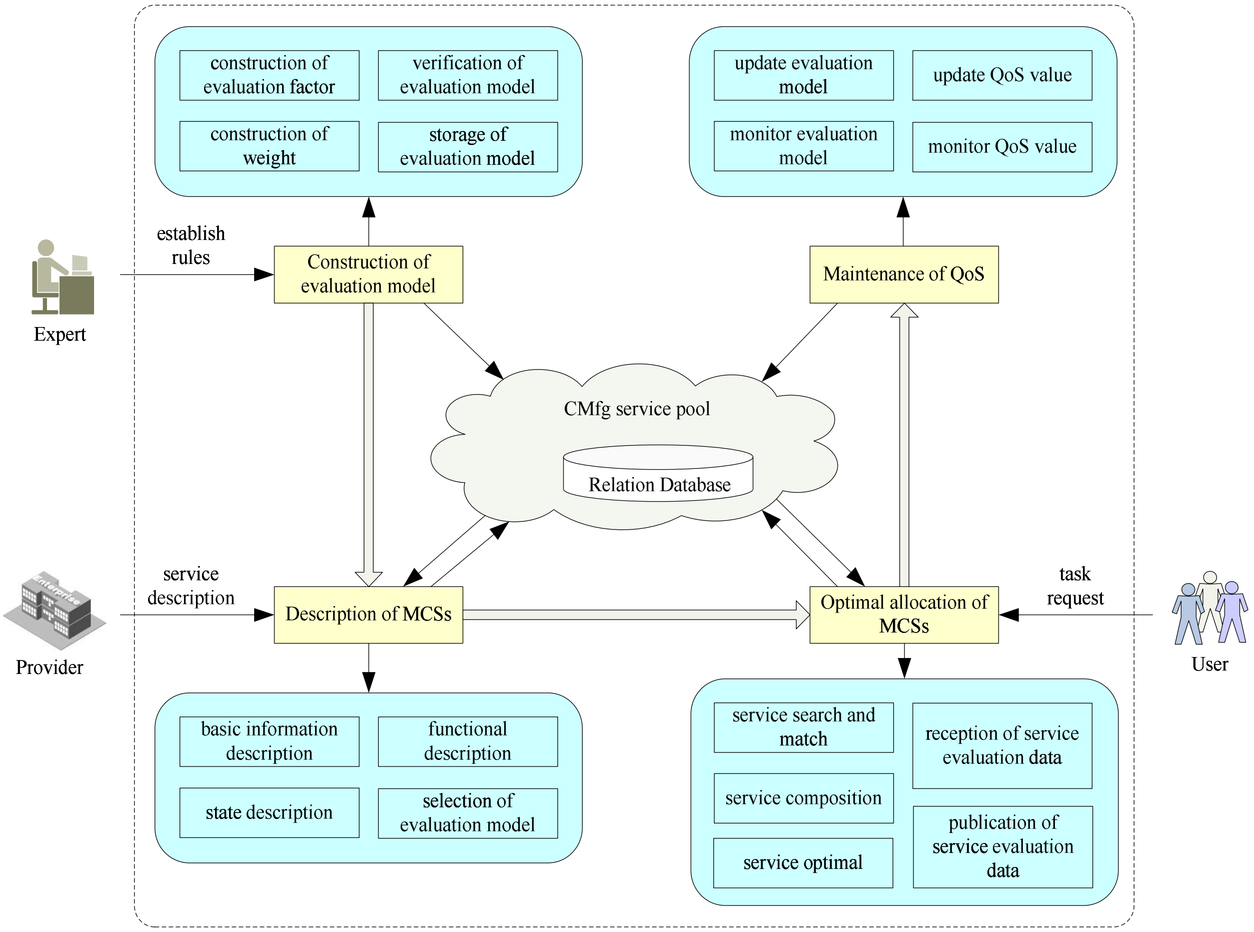
construction of evaluation factor
verification of evaluation model
construction of weight
storage of evaluation model
update evaluation model
update QoS value
monitor evaluation model
monitor QoS value
establish rules
Expert
Construction of evaluation model
Maintenance of QoS
CMfg service pool
Relation Database
service description
Provider
Description of MCSs
Optimal allocation of MCSs
task request
User
basic information description
functional description
state description
selection of evaluation model
service search and match
reception of service evaluation data
service composition
service optimal
publication of service evaluation data

Fig. 1 The execution framework for domain-oriented QoS evaluation of MCSs in CMfg

- *Storage of evaluation model.* Not only it stores various evaluation factors and their reference weights, in order to apply these evaluation factors, but also expresses them in a language understood by computer to storage, such as Resource Description Framework (RDF), Web Ontology Language (OWL), eXtensible Markup Language (XML), etc.

Description of MCSs. Description of MCSs is mapping physical manufacturing resources to virtual ones via virtualization technology, which uniforms the descriptions of manufacturing resources and then adds it to CMfg service pool.

- *Basic information description.* It describes the basic properties of MCSs such as the name of services, the type of services, the information of the providers, description texts of services, and so on.
- *Functional description.* The functional description describes some performance parameters of services executing. For different types of resources, the functional description templates are not the same.
- *State description.* It is the description of service states during the whole life-cycle of manufacturing processes, such as the current status of services (idle, in use, reservation, maintenance retired, etc.), the completed task information, the queued task information, and so forth.
- *Selection of evaluation model.* It is the non-functional description of a service; in this paper both generic QoS and domain QoS are considered. The evaluation model is provided by experts, which is stored in the relation database.

Optimal allocation of MCSs. When a user submits a task request, the services are searched and matched according with its function requirements and QoS constraints. And then the optimal services matched are executed via employing decision devices and algorithms.

- *Service search and match.* It is mainly responsible for discovering qualified candidate services to execute the task request. The search and match processes of MCSs are divided into four phases [8]: first, matching the basic information of MCSs, such as service name and service description; second, matching the inputs and outputs of MCSs; third, matching the QoS information of MCSs; last, uniting the above three matching results and generating an integrated matching result.
- *Reception of service evaluation data.* It mainly gets the services evaluation data and scales its values so that they fall with in a small specified range, such as 0.0 to 1.0. The QoS attributes have variant types of data, which can be summarized as numeric type, interval, linguistic type, and level type. So, the evaluation data need to be scaled in order to comprehensively evaluate the services.
- *Service composition.* For a multi-resource service request task, the system has to select one candidate MCS for each subtask and generates a composite manufacturing cloud service to accomplish the task by orchestrating a set of existing candidate MCSs. It not only defines service interactions, but also constitutes a set of components and topologies for their implementation. It provides an effective way of reusing existing services.
- *Service optimal.* For there may be many functional similar services but with different QoS, service optimal mainly selects services to composite a service composition, which makes the overall QoS of the composition is being maximized. Many optimization algorithms can be applied to select services, such as Integer Programming, Genetic Algorithm, Particle Swarm Optimization, Ant Colony Optimization, etc.
- *Publication of service evaluation data.* It not only is responsible for requiring users to give out the service evaluation after the end of the service, but also needs to preset the types and value range of data.

Maintenance of QoS. Considering that the QoS values of MCSs will change over time, the change of QoS may be caused by many reasons, such as evaluation criteria changes, rising raw material costs, brain drain in companies, backward technology, obsolete equipment, and so on. In order to avoid waste of time, cost and energy due to the change of QoS, it is necessary to timely maintain QoS of MCSs.

The basic maintenance process of QoS includes: (a) monitoring information of changing evaluation model such as new evaluation factors adding, old evaluation factors exiting, (b) monitoring information of changing QoS values such as new tasks accomplished, (c) updating the changing evaluation model, (d) updating the changing QoS values.

Service evaluation model

In this paper, the service evaluation model utilizes the ontology language RDF (Resource Description Framework) to store various data including evaluation factors, sample data, service description, service list, evaluation result, etc.

The service evaluation model is defined as <*EFs*, *SI*, *DI*, *ER* >, where *EFs* denotes the service evaluation factors and its weights, which contains both generic and domain QoS criteria; *SI* denotes the Instance of the evaluated abstract service; *DI* denotes the data item of an instance service, and a data item is the value of every evaluation factor and each instance service has more than one data item; and *ER* denotes the evaluation result of the service.

Conclusions

The emergence of CMfg provides a convenient way for enterprises to share their idle resources and customers to get on-demand services. In CMfg, there are many MCSs with similar functions but different QoS. So, the services evaluation is critical for service selection. The paper primarily presented an execution framework for domain-oriented QoS evaluation of MCSs in CMfg (i.e. DOQoSEF4MCS) and analyzed its function modules. Also, a comprehensive evaluation model based on generic and domain QoS is proposed. In the future, the algorithms for large-scale service optimal in the proposed CMfg-DOQoSEF will be farther studied.

Acknowledgements

The work was supported by the National Natural Science Foundation of China (No.51175187), the Science & Technology Foundation of Guangdong Province (No.2012B030900034), and the Science & Technology Foundation of Dongguan City (No. 2012108102010).

References

[1] B. H. Li, L. Zhang, S. L. Wang, F. Tao, et al: Computer Integrated Manufacturing Systems Vol. 16(2010), No.1, p.1-9 (In Chinese)

[2] X. Xu: Robotics and Computer-Integrated Manufacturing Vol. 28(2012), p.75-86

[3] L. Z. Zeng, B. Benatallah, A. H. H. Ngu, M. Dumas, et al: IEEE Transactions on Software Engineering Vol. 30(2004), No.5, p.311-327

[4] F. Tao, Y. Hu, D. Zhao, Z. Zhou: International Journal of Computer Integrated Manufacturing Vol. 22(2009), No.2, p.100-111

[5] J. Gan, G. J. Duan: Computer Integrated Manufacturing Systems Vol. 18(2012), No.7, p.1527-1535 (In Chinese)

[6] F. Tao, Y. Hu, D. Zhao, Z. Zhou, et al: International Journal of Advanced Manufacturing Technology Vol. 41(2009), p.1034-1042

[7] H. Guo, F. Tao, L. Zhang, S. Su, et al: International Journal of Advanced Manufacturing Technology Vol. 51(2010), p.817-827

[8] F. Tao, Y. Hu, D. Zhao, Z. Zhou, et al: International Journal of Advanced Manufacturing Technology Vol. 43(2009), p.379-399

Applied Mechanics and Materials Vol. 596 (2014) pp 131-135
© (2014) Trans Tech Publications, Switzerland
doi:10.4028/www.scientific.net/AMM.596.131

Using Verification Planner to track the verification process

Xu Huang[1, a], Deng Jun[2,b], LinTao Liu[3,c] and LunCai Liu[4,d]

[1]Sichuan Institute of Solid State Circuits, Chongqing, P.R. China

[2]Sichuan Institute of Solid State Circuits, Chongqing, P.R. China

[3]Sichuan Institute of Solid State Circuits, Chongqing, P.R. China

[4]Sichuan Institute of Solid State Circuits, Chongqing, P.R. China

[a]hxtt103@163.com, [b]dengjun@sisc.com, [c]hgdllt@sisc.com, [d]llc@sisc.com

Keywords: Verification, Coverage, Verification Planner

Abstract. This paper will discuss how we integrated Verification Planner in our verification environment to generate better reports that can be used to track the progress of verification with the project manager. Using Verification Planner we were able to add coverage information to the Verification IP's Excel based verification plans. We can then take advantage of Excel to generate better reports. Using a top-level plan, we were able to generate a summary page that could be shared with project manager, giving them the information they needed.

Introduction

As verification engineers, we regularly need to share verification coverage reports with project manager. The reports need to contain a summary of the coverage information so not to overwhelm the project manager, yet have all of the information available when more in-depth data is needed.

We have traditionally used Synopsys's VIP(Verification IP) to verify the standard interface of our SoC designs, such as I2C, UART and USB. From 2013, the Synopsys's VIP(Verification IP) provides verification plans, which are available in the form of Microsoft Excel, so we can use the Verification Planner to annotate the coverage information to these existing plan. Once the coverage data is entered into a spreadsheet, Microsoft Excel can be used to generate good-looking reports. Using a top-level plan with sub-plans gives a report that contains a summary page that can be shared with project manager, giving them the information they needed without overloading them with extra data. Verification Planner also includes the annotated sub-plans in the same Excel workbook, which contain the detailed coverage reports[1].

Verification Planner allows user-defined data to be annotated into the spreadsheet. This feature was used to create a new metric to track the percentage of coverage written. This new metric, along with the normal coverage metrics, was combined into a single percentage of overall coverage complete. In the overall number the individual coverage metrics were weighted with the goal for that metric.

Why Verification Planner

Spreadsheet annotation with Verification Planner was chosen over a number of other choices. A method was needed where reports could be shared with project managers without overwhelming them with data. Tools like Synopsys's Unified Report Generator (URG) are good for the verification engineers because they contain all of the data, but this is too much data to discuss in progress meetings. URG's html reports also make it difficult to send the reports to project managers since the reports are stored in many files. To easily share the report, it needed to be contained in a single file. Annotating Excel spreadsheets allows the full power of Excel to generate the reports that are applicable to the current project requirements. Using Excel additional calculations can be done on the coverage data.

Verification Planner is a verification planning tool which is incorporated into several Synopsys products. Verification Planner is a technology that allows you to think about the verification process at a high-level overview while working with the real objective of low-level verification data. Verification Planner allows you to convert the low-level data into useful information to plan and track the progress of verification data[2].

An HVP(Hierarchical Verification Plan) is a comprehensive model that allows you to hierarchically describe a verification plan. The verification plan contains feature declarations, attributes, goals, and metrics. Attributes are named values specified in the plan, whereas metrics are named values annotated by API from HVP data files. Metrics can be coverage information extracted from merged simulation runs. Fig.1 shows the Verification Planner Structure.

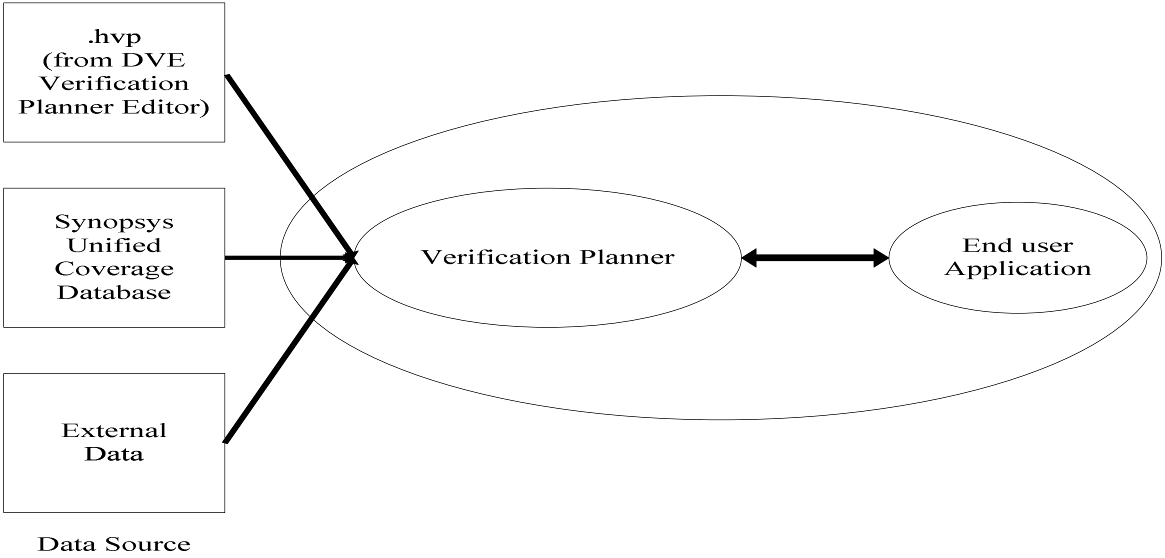
.hvp
(from DVE
Verification
Planner Editor)
Synopsys
Unified
Coverage
Database
External
Data
Data Source
Verification Planner
End user
Application

Figure.1 Verification Planner Structure

Verification Plans and Sub-plans

The top-level plan brings together the sub-plans, and calculates the overall coverage. The top-level plan forms a summary sheet for the rest of the coverage data. Depending on the complexity of the design, each of the sub-plans may contain a number of levels of hierarchy including a level for each of the major blocks in the design. Each of the testbenches will have two leaf-level sub-plans. The first testbench sub-plan is the feature list that was based on the specification of the design under verification. The feature sub-plan tracks the group and assertion coverage needed to close coverage on the feature list. The second testbench sub-plan tracks the code coverage results for the design component that the testbench is targeting. The second sub-plan includes the line and conditional coverage as well as any corner-case group and assertion coverage added by the design team.

The Device under Test (DUT) described in this paper is part of a baseband processing SoC for GPS application. The baseband processing SoC receives GPS signal from a GPS block which is attached to the AHB bus, and then processed by the CPU, the computed data was sent out through uart interface.The architecture of baseband processing SoC is shown in Fig.2. The SoC design adopts AMBA 3 AHB and APB bus to connect CPU to peripherals and external memory subsystem. It consists of several modules: CPU, Memory Controller, DMA , AHB To APB Bridge, UART, Timers, GPIO, ICTL, I2C, SSI/SPI.

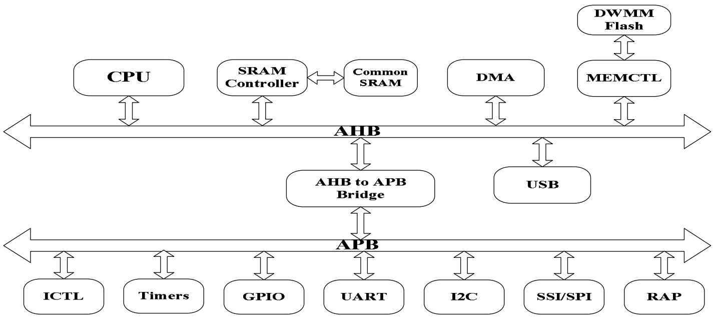
DWMM
Flash
CPU
SRAM
Controller
Common
SRAM
DMA
MEMCTL
AHB
AHB to APB
Bridge
USB
APB
ICTL
Timers
GPIO
UART
I2C
SSI/SPI
RAP

Figure.2 SoC architecture

In order to verify the I2C interface, we select the Synopsys's I2C VIP and use the I2C VIP's verification plans to track the verification progress.

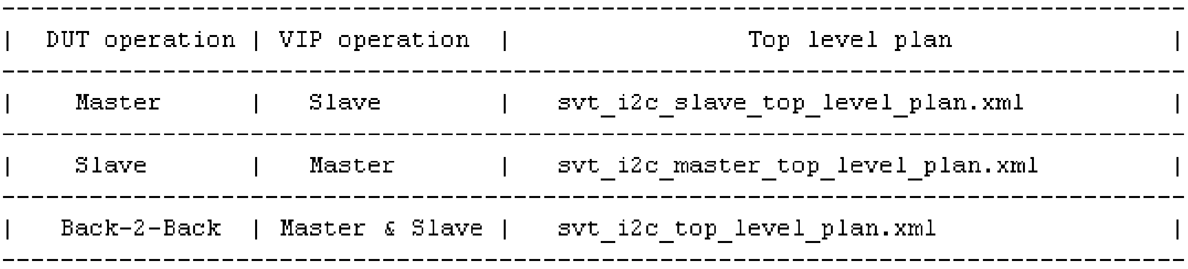

```
-------------------------------------------------------------------------------
|  DUT operation | VIP operation  |               Top level plan               |
-------------------------------------------------------------------------------
|    Master      |   Slave        |  svt_i2c_slave_top_level_plan.xml          |
-------------------------------------------------------------------------------
|    Slave       |   Master       |  svt_i2c_master_top_level_plan.xml         |
-------------------------------------------------------------------------------
|   Back-2-Back  | Master & Slave |  svt_i2c_top_level_plan.xml                |
-------------------------------------------------------------------------------
```

Figure.3 Top-level verification plans for I2C

The Synopsys's I2C VIP has three top-level verification plans shown in Fig.3. The svt_i2c_slave_top_level_plan used to track the verification progress of I2C VIP operate as Slave. The svt_i2c_master_top_level_plan used to track the verification progress of I2C VIP operate as Master. The svt_i2c_top_level_plan used to track the verification progress of I2C VIP operate as Master & Slave[3].

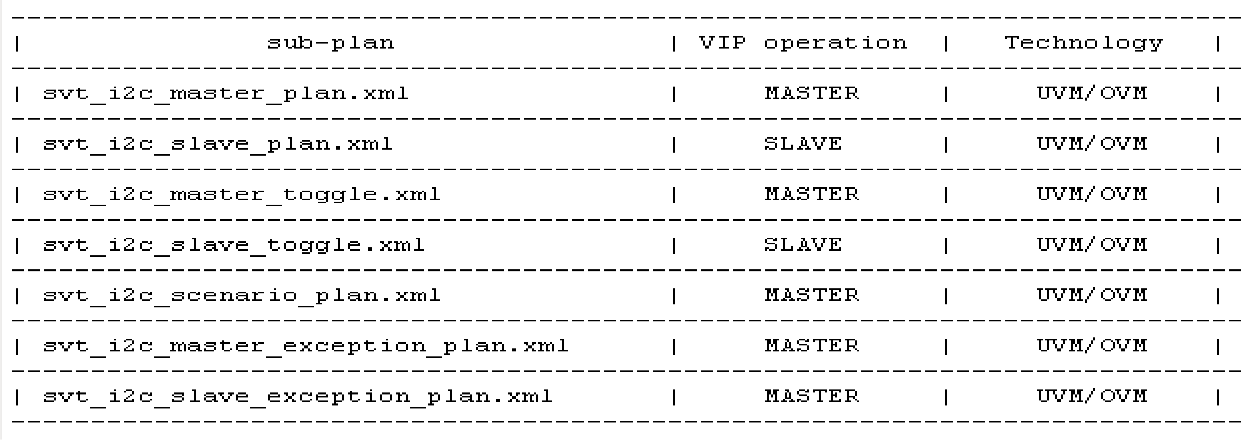

```
-----------------------------------------------------------------------------------
|                 sub-plan                     | VIP operation  |   Technology   |
-----------------------------------------------------------------------------------
| svt_i2c_master_plan.xml                      |     MASTER     |    UVM/OVM     |
-----------------------------------------------------------------------------------
| svt_i2c_slave_plan.xml                       |     SLAVE      |    UVM/OVM     |
-----------------------------------------------------------------------------------
| svt_i2c_master_toggle.xml                    |     MASTER     |    UVM/OVM     |
-----------------------------------------------------------------------------------
| svt_i2c_slave_toggle.xml                     |     SLAVE      |    UVM/OVM     |
-----------------------------------------------------------------------------------
| svt_i2c_scenario_plan.xml                    |     MASTER     |    UVM/OVM     |
-----------------------------------------------------------------------------------
| svt_i2c_master_exception_plan.xml            |     MASTER     |    UVM/OVM     |
-----------------------------------------------------------------------------------
| svt_i2c_slave_exception_plan.xml             |     MASTER     |    UVM/OVM     |
-----------------------------------------------------------------------------------
```

Figure.4 Sub-level verification plans for I2C

The Synopsys's I2C VIP has seven sub-level verification plans shown in Fig.4. All the verification plans listed in above sections are available in the installation directory of I2C VIP.

Use Verification Planner to generate the annotated reports

The process of generating the annotated Excel reports goes though a number of steps.

1. One or more of the verification engineers are running regressions and random simulations.
2. On a weekly basis, they will stop the simulations and merge coverage results together.
3. The merged results are then checked into revision control in the 'coverage/db' directory.
4. Verification Planner is then run to generate the annotated Excel reports.
5. The annotated Excel reports are checked into revision control.
6. The trends Excel reports are updated with the latest data from the annotated Excel reports.
7. At the weekly project meeting, the current trends are discussed.

The Verification Planner command line used by the wrapper script is shown below. This command assumes that the user environment is setup properly to run VCS. For example VCS_HOME and LM_LICENSE_FILE are set properly.

```
hvp  annotate
     -lca
     --verbose
     -plan PLAN.xml
     -userdata bin/written.dat
     -plan_out annotated/$PLAN.annotated.xml
     -elfile excludes.el
     -dir "$DB/coverage.vdb $DB/coverage.cm"
```

Table.1 Verification Planner Command Line Arguments

Argument	Description
hvp annotate	hvp annotate is the Verification Planner utility.
-lca	Enables the LCA features
--verbose	Enables verbose output
-plan	Specifies the name of the top level plan Excel file
-userdata	Specifies the user data needed to track the coverage written
-plan_out	Specifies the location to write the annotated plan
-elfile	Specifies the excludes file that was created by DVE
-dir	Specifies that location of the coverage databases: coverage.vdb contains the group and assertion coverage database, and coverage.cm is the code coverage database
grep –v "written: n/a"	Removes the warning caused by the use of the "written: n/a" value in the coverage written column of the reports

We use the command: hvp annotate –dir <your_simv>.vdb -plan $DESIGNWARE_HOME/vip/svt/i2c_svt/latest/doc/VerificationPlans/svt_i2c_top_level_plan.xml to get the annotated report svt_i2c_top_level_plan.ann.xml. The content of svt_i2c_top_level_plan.ann.xml was shown in Fig.5, the content of svt_i2c_master_top_level_plan.ann.xml was shown in Fig.6, that is not the final report.

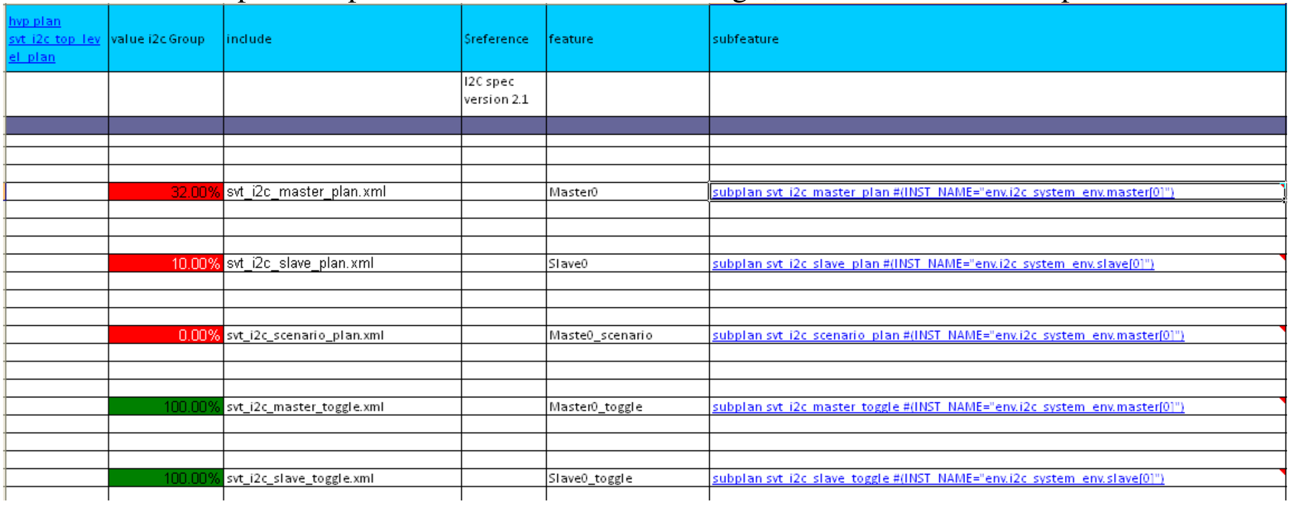

hvp plan svt_i2c_top_level_plan	value i2c Group	include	$reference	feature	subfeature
			I2C spec version 2.1		
	32.00%	svt_i2c_master_plan.xml		Master0	subplan svt_i2c_master_plan #(INST_NAME="env.i2c_system_env.master[0]")
	10.00%	svt_i2c_slave_plan.xml		Slave0	subplan svt_i2c_slave_plan #(INST_NAME="env.i2c_system_env.slave[0]")
	0.00%	svt_i2c_scenario_plan.xml		Maste0_scenario	subplan svt_i2c_scenario_plan #(INST_NAME="env.i2c_system_env.master[0]")
	100.00%	svt_i2c_master_toggle.xml		Master0_toggle	subplan svt_i2c_master_toggle #(INST_NAME="env.i2c_system_env.master[0]")
	100.00%	svt_i2c_slave_toggle.xml		Slave0_toggle	subplan svt_i2c_slave_toggle #(INST_NAME="env.i2c_system_env.slave[0]")

Figure.5 Top-level annotated verification report for I2C

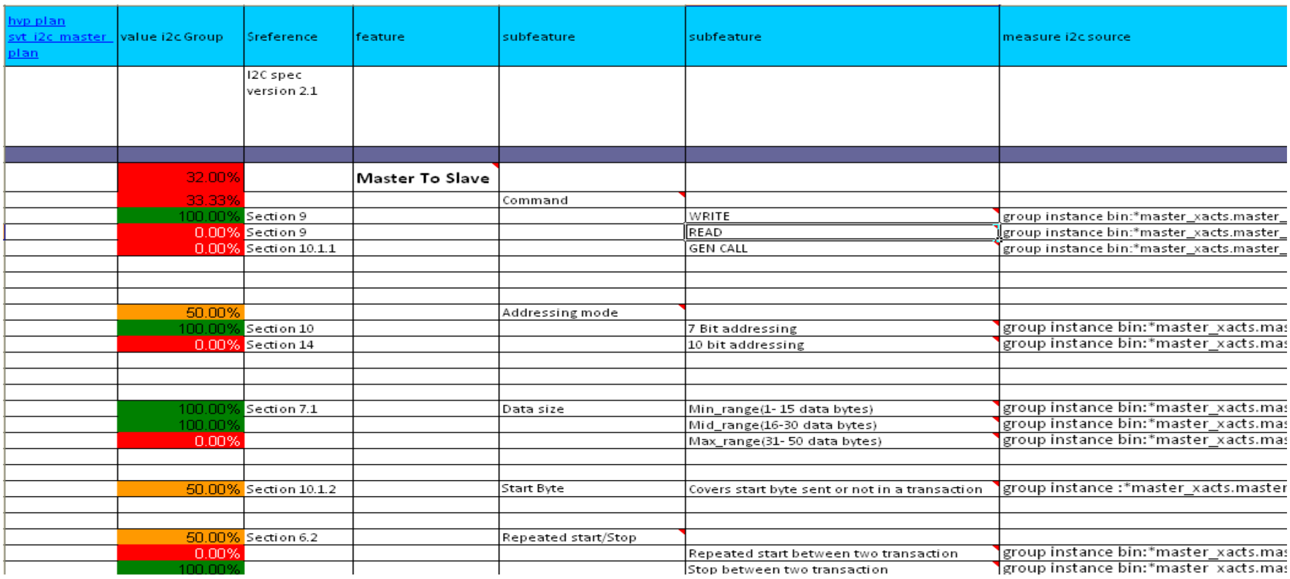

hvp plan svt_i2c_master_plan	value i2c Group	$reference	feature	subfeature	subfeature	measure i2c source
		I2C spec version 2.1				
	32.00%		**Master To Slave**			
	33.33%			Command		
	100.00%	Section 9			WRITE	group instance bin:*master_xacts.master_
	0.00%	Section 9			READ	group instance bin:*master_xacts.master_
	0.00%	Section 10.1.1			GEN CALL	group instance bin:*master_xacts.master_
	50.00%			Addressing mode		
	100.00%	Section 10			7 Bit addressing	group instance bin:*master_xacts.ma:
	0.00%	Section 14			10 bit addressing	group instance bin:*master_xacts.ma:
	100.00%	Section 7.1		Data size	Min_range(1- 15 data bytes)	group instance bin:*master_xacts.ma:
	100.00%				Mid_range(16-30 data bytes)	group instance bin:*master_xacts.ma:
	0.00%				Max_range(31- 50 data bytes)	group instance bin:*master_xacts.ma:
	50.00%	Section 10.1.2		Start Byte	Covers start byte sent or not in a transaction	group instance :*master_xacts.master
	50.00%	Section 6.2		Repeated start/Stop		
	0.00%				Repeated start between two transaction	group instance bin:*master_xacts.ma:
	100.00%				Stop between two transaction	group instance bin:*master_xacts.ma:

Figure.6 The annotated verification report for I2C VIP operate as Master

Summary

Verification Planner allowed the creation of coverage reports that were suitable for sharing with project managers. Other methods to generate coverage reports created many html files, or visually unpleasing reports, or required manual effort. Using the combined features of Verification Planner and Excel, a single coverage number was generated that combined the percentage of coverage written with the normal coverage metrics. Once the annotated reports were created, the data was tracked on a weekly basis.

Verification Planner was easy to integrate into our existing verification flow. Instead of using URG to create the coverage reports and manually adding the results to a spreadsheet, Verification Planner automated the process of getting the coverage data into the spreadsheets. The only other change required to the flow was change the scripts that were used to generate the coverage reports to use Verification Planner.

Acknowledgements

The author would like to thank dengJun for his contribution to the verification environment. The author also grateful for the thoughtful reviews and challenging comments from Liulintao and Liuluncai. The work presented in this paper was partly supported by National High Technology Research and Development Program of China (863 Program). (No.2012AA012303)

References

[1] Janick Bergeron, Eduard Cerny, Alan Hunter and Andrew Nightingale. Verification Methodology Manual for SystemVerilog. 2005, Springer.

[2] Verification Planner UserGuide. 2013, Synopsys..

[3] DesignWare I2C Verification IP UVM User Manual. 2013, Synopsys.

Applied Mechanics and Materials Vol. 596 (2014) pp 136-140
© (2014) Trans Tech Publications, Switzerland
doi:10.4028/www.scientific.net/AMM.596.136

Comprehensive Evaluation of the Development Level of Shanxi's Real Estate Industry based on Factor Analysis and Cluster Analysis

Xiaoling Tang[1, a*], Zhuling Tan[2,b]

[1]school of management, Xi'an University of Architecture & Technology, Xi'an 710055, China

[2] school of management, Xi'an University of Architecture & Technology, Xi'an 710055, China

[a]184802287@qq.com, [b]125697427@qq.com

Keywords: real estate industry; development level; factor analysis; cluster analysis; Shanxi Province.

Abstract: In this paper, on the basis of the effective data, build the evaluation index system of the real estate industry development level, using factor analysis and cluster analysis, analysis the real estate industry development level of 10 cities and 1 agricultural science and technology development zone in Shanxi province. According to factor score and cluster analysis, the level of real estate development in Shanxi Province is divided into four types, and ranking them, finally analysis the results of classification reasons.

Introduction

In recent years, the real estate industry has been developing rapidly, according to statistics, in 2013 in Shanxi province, the annual development of real estate investment totaled 224.017 billion yuan, an increase of 22.0% over the previous year, occupy more than 14% of the investment in fixed assets of whole society. [1] As a pillar industry of our country's economy, real estate industry has the characteristics of a strong basic, spread widely, and the characteristics of the correlation to the industry before and after. If the operation of the real estate industry in good condition, is bound to play a positive role in economic area. Shanxi province wants to become a big business, culture and tourism province, must with the development of the real estate industry as the forerunner, and stimulate and promote by the development of real estate industry. Therefore, a comprehensive evaluation of the development of the real estate industry in Shanxi province for the government set up the real estate industry development policy, conduct macroeconomic regulation and control of the national economy and real estate investors the choice of appropriate investment area, take appropriate investment strategy, etc all have important meaning.

Build evaluation index of the level of real estate development

This article through to the related factors affecting the development of the real estate industry system reasons, when selecting indicators according to the principle of science, integrity, operability.

The selection of indicators and data sources

This article selects indicators are as follows: X_1 real estate development investment (100million yuan), X_2 commercial housing sales area (square meters), X_3 the number of real estate development company(a), X_4 all practitioners annual average number of development enterprise (people), X_5 the average wage of practitioners(yuan) , X_6 main business income (ten thousand yuan), X_7 housing construction area (ten thousand square meters), X_8 completed housing area(ten thousand square meters), X_9 asset-liability ratio (%),[2]of these 9 indicators reflect the level of the real estate industry development in Shanxi province. Due to the various index of different dimensional unit, and there exists certain correlation index directly, so before the evaluation must standardize the original data, to eliminate the influence of different dimension of evaluation results. Data from the Shanxi statistics yearbook 2013, through direct acquisition or indirectly calculated.

The basic principle of factor analysis method

Factor Analysis (Factor Analysis) is to select a few variables from the multiple variables of a dimension reduction method of multivariate statistical Analysis. Using factor analysis, we can extract several main common factors from a number of variables, each common factor represents one kind of important influence, seize these common factor, which can enable us to analyze the main factors affecting the level of the real estate industry development, also can simplify the structure of the data, determine the weight of the comprehensive evaluation mathematics model, and calculate the comprehensive evaluation value.

The mathematical thinking model will be represented by this model: After the observed data matrix X standardization process, starting from the index variable correlation matrix R, studies the structure of the factors F_j associated with variable X_i factor analysis, called the R factor analysis. Its mathematical model is:

$$\begin{cases} X_1=a_{11}f_1+a_{12}f_2+\ldots+a_{1m}f_m+\varepsilon_1 \\ \cdots\cdots\cdots\cdots\cdots\cdots \\ X_k=a_{k1}f_1+a_{k2}f_2+\ldots+a_{km}f_m+\varepsilon_k \end{cases}$$

X_i is the index, F_1 is the common factor, two two orthogonal to each other. ε_i is a special factor, plays a role only on the corresponding X_i. A_{ij} is the load public factor, is the i variable load in the j factor. Matrix (a_{ij}) is the load matrix.[3]

The process and results of analysis factor

This paper uses the SPSS19.0 statistical analysis software, to evaluate and analyze the 10 cities and 1 agricultural science and technology development zone in Shanxi province.

Standardize the original data .Using conventional Z-Score method for data normalization, standardization of data obtained by using SPSS software.

KMO test and Bartlett's Test of Sphericity

KMO statistic was 0.793, suitable for factor analysis. In addition, significant probability the Bartlett sphere test statistic value is 0, which shows the correlation between the group of data, is suitable for factor analysis.

Calculate the eigen values of the correlation coefficient matrix R, variance contribution rate and cumulative variance contribution rate

Obtain the factor eigenvalues and contribution rates are shown in Table 2, the result shows that first, secend common factor comprehensive information of each variable were 77.498%, 12.538% respectively.Two factors‘ cumulative contribution rate was 90.041%>85%, and the characteristic corresponds to the two common factor values are greater than 1, so the common factor extraction effectively, can think of the original 9 indicators can be integrated into 2 main factors.

Table 2 Total Variance Explained

	Initial Eigenvalues			Extraction Sums of Squared Loadings	
Component	Total	% of Variance	Cumulative %	Total	% of Variance
1	6.975	77.498	77.498	6.975	77.498
2	1.128	12.538	90.036	1.128	12.538
3	.828	9.203	99.239		
4	.042	.472	99.711		
5	.016	.173	99.884		
6	.008	.087	99.970		
7	.002	.023	99.994		
8	.000	.004	99.998		
9	.000	.002	100.000		

Calculate the rotation factor load matrix

In the process of factor analysis , with eigen values greater than 1 for the standard method extract factor.Using Varimax method to rotate load factor matrix, the factor loading matrix can be obtained after rotate as is shown in table 3. We can see from table 3: the first common factor has a greater load in the real estate development investment , commercial housing sales area, real estate development company number, annual average number of development enterprise, annual average main business income, completed housing area, commercial housing sales, the 7 indexes to reflect the real estate industry investment condition, industry scale, development of housing sales area from the overall, so it can be named as the overall factor; second public factors have greater load on the average wage of practitioners and asset-liability ratio , the two indexes reflecting the real estate assets, named assets factor.

Table 3 Rotated Component Matrixa

	Component	
	1	2
X1	.992	.102
X2	.993	.071
X3	.982	.022
X4	.995	.087
X5	.073	-.802
X6	.993	.086
X7	.996	.072
X8	.993	.032
X9	.177	.706

Comprehensive evaluation

Principal component analysis model need not factor loading quantity but characteristic vector, so we also need to input factor loading quantity into the data editor window. Use the "principal component corresponding characteristic product of the square root of the root and the eigenvector for factor loading quantity", the component of 1, 2 are respectively named B1, B2, treated as follows, get the feature vector A1, A2:

$A_1=B_1/SQRT(\lambda_1)$， $A_2=B_2/SQRT(\lambda_2)$ （$\lambda_1=6.975$，$\lambda_2=1.128$） this is combination coefficient of main component.[4]

According to the above two principal components and their corresponding standard orthogonal characteristic vector (combination coefficient of principal component) two principal component values can be calculated:

$$F_1=0.37574X_1+0.37615X_2+0.37182X_3+0.37661X_4+0.02779X_5+0.37610X_6+0.37701X_7+0.37585X_8+0.06707X_9$$

$$F_2=0.09647X_1+0.06679X_2+0.02057X_3+0.08235X_4-0.75487X_5+0.08120X_6+0.06796X_7+0.02978X_8+0.66434X_9$$

where X_i represents the i-th index of standardized data in the index system, comprehensive evaluation function is F, using principal component weight variance contribution rate can obtained:

$$F = 0.77498F_1 +0.12538 F_2$$

Above equation is the comprehensive evaluation model of regional real estate industry development level,put the public factor score of each region to the model, we can get the comprehensive evaluation index score of each region. With the composite scores for sorting, we can rank the each region‘s real estate comprehensive development level, as is shown in table 4.

Table 4 Factor score and comprehensive ranking

area	factor F_1 score	factor F_2 score	Factor comprehensive score	ranking	Classification
Xian	7.8729	1.8182	6.3293	1	1
Tongchuan	-1.2245	-0.1393	-0.9664	10	3
Baoji	-0.495	0.7588	-0.2885	3	2
Xianyang	-0.495	0.549	-0.3148	4	2
Weinan	-0.5092	-0.571	-0.4662	5	3
Yanan	-1.0893	0.6471	-0.7631	7	2
Hanzhong	-0.3411	-0.1151	-0.2787	2	3
Yuling	-0.5979	-2.3925	-0.7633	8	4
Ankang	-0.9055	-0.7954	-0.8014	9	3
Shangluo	-1.156	-1.2025	-1.0466	11	3
Yangling demonstrate area	-1.0596	1.4426	-0.6403	6	2

Cluster analysis process and results

Using SPSS software adopts Between - groups linkage connection method Between (group), generated clustering spectrum diagram (figure 1), classification are shown in table 4.

The following conclusions can be obtained from table 4of factor scores and a comprehensive ranking from factor scores and the results of cluster analysis:

The first class: Xi'an, the highest scores, far higher than other city. Xi'an as the capital city, is the political and economic development center, the size of real estate development, real estate enterprises and the number of completed area in the province are in the leading level.

The second class : Baoji, Xianyang, Yanan, Yangling demonstration zone, the comprehensive score are compared to the average, but are negative, it illustrate that besides the Xi'an, the rest are at a low level in the development of real estate industry , the development of Yanan's real estate industry level is good than Guanzhnog cities such as Baoji and Xianyang, has the potential in the real estate development.

The third category are Tongchuan, Weinan, Hanzhong, Ankang and Shangluo, which contains the region of city in Southern Shanxi, suggests that the real estate industry development of the Southern Shanxi province belongs to the less developed regions, the real estate industry development level remains to be further improved.

The fourth category is Yulin, Yulin sitted in Northern region, but its composite scores are among the top ones because of its rich mineral resources and the support of energy chemical industry, so its development of the real estate industry in Shanxi province is in the upper level.

Conclusions:

Basically draw the following conclusions on real estate development level through factor analysis and cluster analysis at 11 cities at Shan Xi province:

Real estate development level of various cities at Shan Xi province is very uneven, there is a big difference between the different areas of real estate development. Real estate basically be divided into four categories at Shan Xi province through cluster analysis.

Real estate policies formulated at province should pay more attention on macro-control, at various cities should focus on enlivening. Government can not engage in "one size fits all" in the formulation of the overall development strategy of real estate, Government should fully consider the regional differences according to local conditions.

The scale of real estate development should adapt to local economic development and population size. Because real estate is a real, not inter-regional flows, only develop according to effective demand in the region. In the development process, product structure and product positioning should be reasonable.

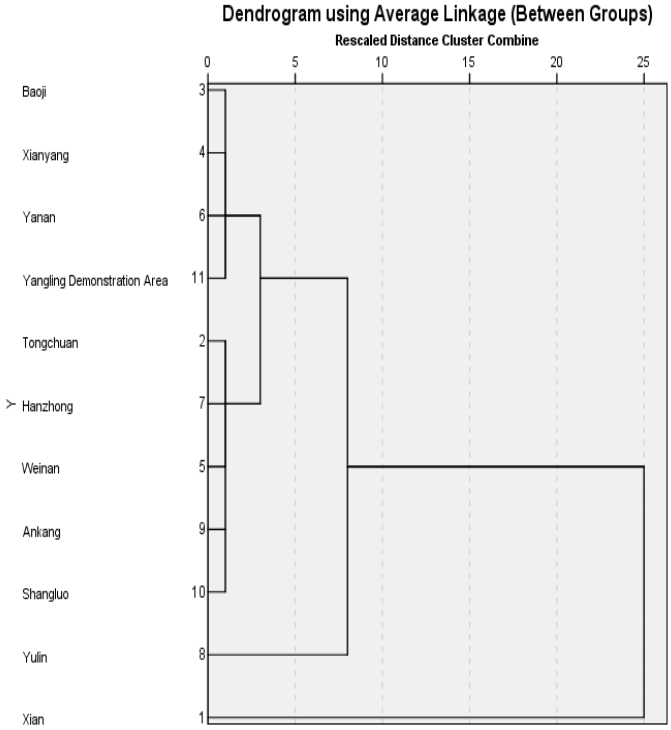

Fig 1 Cluster genealogy chart

References

[1] Shaanxi Provincial Bureau of Statistics. Shaanxi statistical yearbook2013.Beijing: Chinese Statistics Press,2013

[2] Wang Ning,Li Hui-min,Tan Xiao,Zhong Xing-run. Development evaluation of real estate industry in China’s major cities based on factor and cluster analysis[J].Jouunal of Xi‘an University of Architecture & Technology (Natural Science Edition),2010.42(8)

[3]MaQingguo. Management statistics: Data acquisition, Statistical principle, SPSS tools and application and research[M].Beinjing: Science Press,2003

[4]ZengZhenxiang,DuanDanhua,Zhangpei,WangXinfei.Comprehensive evaluation of Jing-Jin-Ji region coordinated development based on principal components analytical method [J]. Science &Technology Progress and Policy,2008.25(9)

Applied Mechanics and Materials Vol. 596 (2014) pp 141-145
© (2014) Trans Tech Publications, Switzerland
doi:10.4028/www.scientific.net/AMM.596.141

Research of Refined Oil Emergency Reserve Monitoring System Construction Scheme

Ning Chen[1,a], Qimin Zhang[2,b], and Dedong Tang[1,c]

[1]College of Electrical and Information Engineering, Chongqing University of Science & Technology, Chongqing, 401331,China

[2]College of Petroleum and Natural Gas Engineering,Chongqing University of Science & Technology Chongqing, 401331,China

[a]email: ningchen660@sina.com,[b]email: kjxyzqm@163.com,[c]email:tangdedong@cqust.cn

Keywords: Refined Oil; Emergency Reserve; Monitoring

Abstract. Starting from the necessity of building refined oil emergency reserve monitoring system, in the aspects of system construction principle, the overall system architecture and the system construction has carried on the elaboration, proposed the construction scheme and reasonable reference.

Introduction

All as an important part of national economic security strategy, petroleum reserve has to ensure national energy security mission, a complete petroleum strategic reserves should be diversified structure contains reserves of refined oil products. Compared with the crude oil reserves, reserves of refined oil products in response to emergencies and stabilize the market supply and demand relations came to more direct, more quickly. The lack of reserves of refined oil products, diversified strategic resource reserve system of a country is not perfect, also lack an effective method for emergencies, guaranteeing the safety of national economy[1].

Since 2008,Shanghai,Wenzhou, Chongqing, promulgated a relevant regulations of refined oil emergency reserve management[2], is to take the local government financed the purchase of rotation right ,that is cooperative mode of "commissioned by the government, enterprises in the implementation ", pay attention to develop the role of potential national reserve in the local reserve facilities ,take advantage of the nation material reserve rotation operation, realize the "central authority and local government reserves combined"[3].

Problem Description

Local government departments for refined oil contingency reserve to protect the system. Introduction of the refined oil reserves management system, clearly the scope of subsidies, standards and cash reserves to. Local fiscal funds interest, on the finished oil emergency reserve storage, transport, loss of the amount of subsidies, subsidies to oil reserves and real hook. At the same time, the supervision and inspection measures. The reserve unit reserve plan implementation and the use of execution, reserve quantity, quality and safety, general inspection or special audit grant funds usage. To punish the reserve unit refuses to execute the purchasing and storage plan and use decisions, not on time back, alter the location and the use of reserves of oil, false or reserve type and quantity, interception, misappropriation defraud, crowding out subsidies regulations[4].

But in some places, the current mainly supervision and inspection measures is artificial periodical report way in the relevant reserve enterprises. This is easy to make a mistake, big workload, is unable to accurately understand the refined oil reserves in the city.

Necessity of Construction

From the current situation, the construction units and enterprises, the refined oil depot monitoring management information application level is different, supervision process exists the following problems[5]:

A. Information Management. Reserve report completed by the artificial copy the report, the administration section cannot get timely accurate and reliable basic data of production, did not realize the comprehensive information management system of management and control integration. B. Accuracy of Data. In some companies, refined oil artificial measurement, warehousing and inventory of artificial calculation and data management in data accuracy is not high, the timeliness of the information reported to the business is not high. C. Scattered Data. Monitoring points is more, monitoring data is also more, in a scattered state reporting, sequel still requires substantial human effort to analyze these data, is not conducive to statistics, comparison and analysis of data. D. Format of Data .Each depot point reporting data content or format may not be uniform, leading to subsequent manual processing or analysis errors as possible, both the cost of subsequent processing time, but also affect the real-time data. E. Reporting Timeliness. Artificial statistics and report refined oil depot monitoring data process, may not be required to complete the data report within the prescribed time, and may even require manual to push a monitored point to complete data reporting, even less amount of data is not reported, seriously affecting the timeliness of data monitoring. F. Arbitrary of Data. Reporting directly of data in each monitoring point, if it is to come up with artificial data, from administration section regulatory point of view, these data cannot guarantee whether the raw data, if not the original data, then you lose the refined oil emergency storage monitoring significance. G. Integrity of Data. Because the monitoring refined oil repository index is more, the indexes of every period of time is required to report to finish, rely on manual methods to monitor and manage these data, it is the human cost, also do not meet the requirements of data management at present, and once some index report is not complete, it is easy to cause monitoring is not comprehensive, lack of integrity. H. Less Flexibility. In the reporting or statistical data, if the format change or adjust, then needs various oil product storage reported again, the impact is relatively large, time-consuming. Information system can be automatically completed data center. I. Respond In Time. When the refined oil is shortage, the events cannot be timely response, dynamic allocation.

Because each enterprise data acquisition system in reserve are independent of each other, not from the policy angle to achieve the information and data sharing, from control to monitoring cannot form a unified whole, cannot fully play the largest role in emergency reserve management; administration section existing monitoring system cannot obtain the production data from the refined oil depot operation layer, to store all kinds of data, statistics show, according to the requirements, has caused great difficulties to the information management. Therefore, monitoring system construction work is needed.

Design Principles

A. The Principle of Overall Planning. The development demand should be considered during system construction, some refined oil depot monitor future overall planning, step-by-step implementation. B. The Principle of Practicability. Construction design system to meet the requirements of refined oil depot monitor utility, saving, monitoring, service operations and functions. C. The Principle of Advanced Ripeness. The overall structure and technology with the stable, mature program and technology, to ensure the stable operation of the system. D. The Principle of Safety. The system design architecture from the system level and application level considering system security, the safety control strategy, to ensure the security of the system. E. The Principle of Standardization. In the system design and development platform selection, according to industry standards, data interface format system uses standard, convenient maintenance and upgrade[6].F. The Principle of Scalability. With the development of business, the expansion of the system, the upgrade is inevitable, so in the design fully consider the feasibility of future system expansion. According to the program module and data interface idea, the flexible system structure design make the system expansion convenient and not restricted. G. The Principle of High Performance Price Ratio. The system design makes full use of existing equipment, new rational selection of equipment, to meet the demand, as much as possible to reduce costs, the pursuit of the highest possible cost performance ratio.

System Architecture

The construction of a hierarchical sub module, analysis including depot storage point monitoring data acquisition, acquisition of data transmission and data storage center, monitoring point number increase or decrease changes, constant network structure system, only added to the access point or less center, the overall construction is as Fig.1[7]:

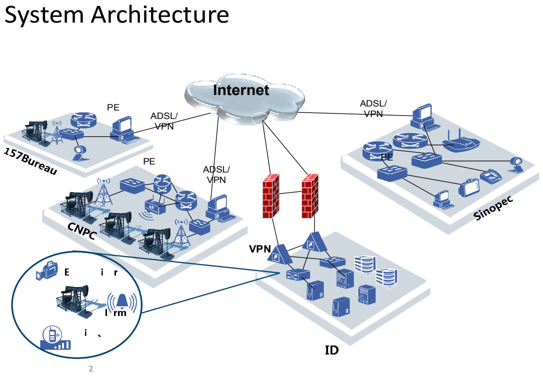

The refined oil reserves has the local area network of unified construction, system integrated date by collecting them from the refined oil reserve point, then transferred to the administration section unified data center, in the central control room can realize real-time monitoring, dynamic monitoring of the entire reserve area.

In the realization of automatic monitoring, data automatic acquisition and transmitted to the center computer room, need to ensure that monitoring refined oil storage point of perfection, data can be collected, therefore refined oil depot without monitoring network, need to be simultaneously built monitoring data acquisition system.

Fig.1. System Architecture

System architecture should be relatively independent professional storage system equipment, in the subsequent expansion, according to the actual storage requirements, flexible expansion of storage capacity, to meet the demand of flexible extensible storage space.

Subsystem Construction

A. The Data Acquisition Subsystem. Data acquisition as far as possible to ensure data accuracy, primitive, but also need to ensure that operational, therefore the proposed acquisition scheme are as follows:

Scheme 1: Collection of the original detector data, such as binary or text files, then transmit to the administration section center room for reprocessing.

Scheme 2: Through the system interface, collecting data from the database and interface of the existing monitoring system, then transmit to the administration section center room for reprocessing.

In order to ensure the authenticity of data monitoring, recommended scheme 1.

B. The Transport Subsystem. Transmission subsystem mainly realizes data acquisition, data transmission to the monitoring center, logic structure diagram as Fig.2.

Scattered the depot, the private line or the optical fiber transmission cost is high. The proposals is ADSL transmission, through the VPN access, using dynamic VPN solution, is relatively low cost, while ensuring the safety of transportation.

C. Monitoring Subsystem. Data transmission to the administration section center room, various indicators and data output, through different forms of display, storage data and real-time monitoring of refined oil depot will be in control, as Fig.3.

D. Application Software Structure. System software architecture is modular, interface design, flexible to expand demand, convenient maintenance, as Fig.4[8].

The system function is divided into 4 parts, as Fig.5:

1)The underlying data communication interface. Including the collection service, data transmission interface, communication parameters.2)The basic data management. Including the management of refined oil depot, tank management, acquisition node management, early warning threshold parameters, control parameters, analysis of parameters. 3)Intelligent monitoring. Including real-time alarm, electronic report, trend analysis, dynamic data, real-time monitoring, real-time display.4)The intelligent application support. Support for large screen output, the general computer output, mobile phone client and other system interface.

In the development process, should pay attention to the underlying data communication interface, it is responsible for the basic module of information communication between with the monitor center platform and various refined oil depot. The types of real-time monitoring data transmission, protocol, encryption and decryption algorithm will be configured by the module[9].

In addition, should form a unified data standards on the basis of comprehensive consideration of the various refined oil depot monitoring system. Each monitoring system only uses the unified standards for data transmission of data, you can use a unified display platform.

Conclusion

In the construction process of refined oil reserves and monitoring system, attention should be paid to as follow, monitoring system construction should be reasonable planning according to the actual situation and the existing condition of controlled enterprises, the local government departments from control to monitoring can form a unified whole, so as to give full play to the greatest role of emergency reserve management.

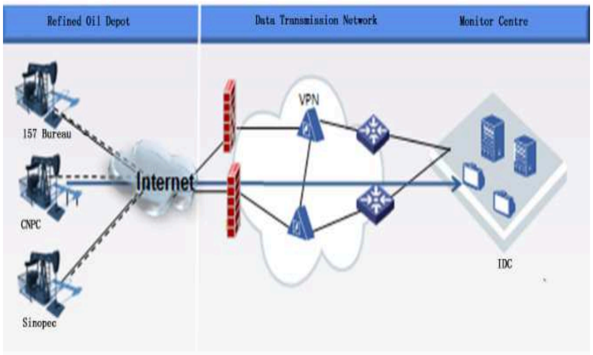
Refined Oil Depot
Data Transmission Network
Monitor Centre
157 Bureau
CNPC
Sinopec
Internet
VPN
IDC

Fig.2. Logical Structure

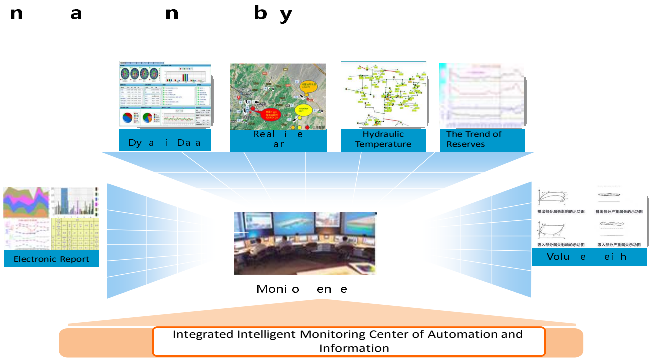
n a n b y
Dy a i Da a
Real i e lar
Hydraulic Temperature
The Trend of Reserves
Electronic Report
Volu e ei h
Moni o en e
Integrated Intelligent Monitoring Center of Automation and Information

Fig3.Integrated Monitor Subsytem

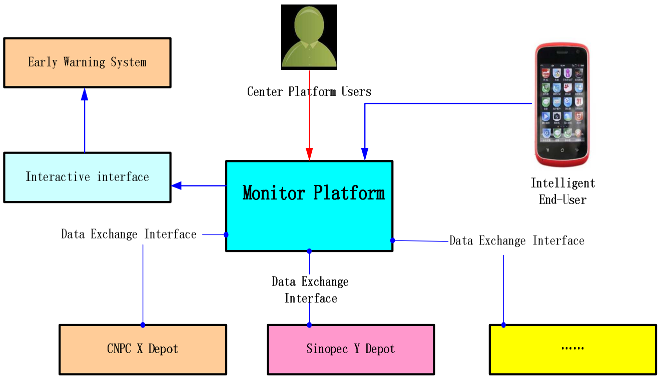
Early Warning System
Center Platform Users
Interactive interface
Monitor Platform
Intelligent End-User
Data Exchange Interface
Data Exchange Interface
Data Exchange Interface
CNPC X Depot
Sinopec Y Depot
……

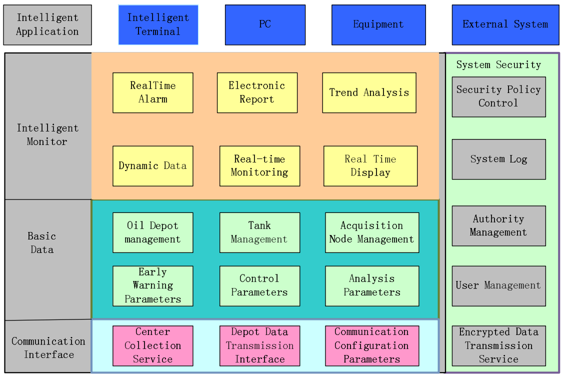
Intelligent Application
Intelligent Terminal
PC
Equipment
External System
Intelligent Monitor
RealTime Alarm
Electronic Report
Trend Analysis
Dynamic Data
Real-time Monitoring
Real Time Display
System Security
Security Policy Control
System Log
Basic Data
Oil Depot management
Tank Management
Acquisition Node Management
Authority Management
Early Warning Parameters
Control Parameters
Analysis Parameters
User Management
Communication Interface
Center Collection Service
Depot Data Transmission Interface
Communication Configuration Parameters
Encrypted Data Transmission Service

Fig.4.Software Architecture Fig.5.Software Function Structure

References

[1]Jianfeng Zhao, Yanling Chen. "The necessity of China's reserves of refined oil products increased during the 12th Five Year Plan" period[J].China Logistics & Purchasing,2011,4:71-72

[2]Yongjie Niu, Jibu Guo, Xin Mu. Some thoughts on the national refined oil reserve [J].China storage & transport magazine, 2011, 12:117-119.

[3]Sierra Wireless, AirPrime Q2687 Refreshed Product Technical Specification and Custom Design Guideline, June 2011.

[4] PengWang.Probing into Establishing Mode of Final Oil Storage[J].Journal of Sinopec Management Institute,2010,12(1):60-62.

[5]Xiaodong Zhang, Li Ma, Yuan Gao, The design of video monitoring system based on video server, Microcomputer Information, Vol.24, No.1-1, 2008

[6]Haibin Wang, Chunnian Fan, The design and implementation of remote video monitoring system based on DirectShow, Science and Technology Information, Jan.2008.

[7]Qian Wang, Yinjing Guo, Wenhong Lv, Zhengjie Wang, Bo Sun Gang Jing. Long-distance video monitoring system application to freeway's toll station[J]. IEEE on ITS. 2006.08

[8]A. Marzia, A.F. Francesca, A.D. Ardagna, B. Luciano, B. Carlo, C. Cinzia, C. Marco, C. Marco, D.P.F. Maria, F. Chiara, G. Simone, L. P, M. Andrea, M. Stefano, P. Barbara, R. Claudia, and T. Francesco, "The Mais Approach to Web Service Design," Proc. 10th Int'l Workshop Exploring Modelling Methods in Systems Analysis and Design, pp. 387-398, 2005.

[9]D. Idoughi, M. Kerkar, and C. Kolski, "Towards new web services based supervisory systems in complex industrial organizations: Basic principles and case study," Comput. Industry, vol. 61, no. 3, pp. 235–249, Apr. 2010.

CHAPTER 4:

Computer Information Processing Technology, Artificial Intelligence and Intelligent Algorithms

Applied Mechanics and Materials Vol. 596 (2014) pp 149-153
© (2014) Trans Tech Publications, Switzerland
doi:10.4028/www.scientific.net/AMM.596.149

An algorithm for representing planar curves in B-splines

Zi-zhi Lin [1,a] , Si-hui Shu [1, a]
[1] College of Mathematics and computer Science Jiangxi science Technology Normal University NanChang China
[a]linzizhi161@163.com

Keywords: Planar curve representing; B-spline curve; Best least square approximation; Knot vector

Abstract. An algorithm for representing planar curves in B-splines is presented in this paper. The representing problem is different from the approximation to data points; planar curve provided more information than data points. To make full use of the information, we propose a three-step representing approach: 1.Sample data points along with their tangent vectors from the planar curve according to the given accuracy. 2. Fit the sampled points by Bezier segments using local interpolation; compose these segments to an interpolation curve. 3. Approximate the interpolation curve using the best least approximation to get the final B-spline curve. Tangent information is used in the second step to construct the interpolation curve. In the third step, the system is always positive because of using the best least square approximation, so we can get more freedoms to approximate the interpolation curve. Finally, some examples of this algorithm demonstrate its usefulness and quality.

Introduction

In 1991, the international organization for Standardization (ISO) promulgated industrial product data exchange standard STEP, ISO takes NURBS(non-uniform rational B-splines)as the only mathematical method that defines the shapes of industrial products. NURBS becomes the standard for curve and surface description[1] . But other curves such as implicit curves, other parameter curves are incompatible with NURBUS in CAD/CAM system, so it is necessary to convert these curves in B-splines.

Representing planar curve in B-splines is one of key problems in data exchange between different CAD/CAM systems .To make curves in different system compatible, Park [2] adopts an approach of B-spline curve refitting accomplished via polygonal approximation of the given curve and B-spline curve fitting to the polygon. Hausdorff distance is used as a criterion for approximation quality. Chong yang Deng [3] proposed a method of sampling data points, fitting these points with segments, merging the segments to form the B-spline. Given two B-spline curves with different degrees, Hoschek and Wissel[4] proposed an conversion algorithms by degree reduction and degree elevation to make them compatible. Some parametric curves can be approximated by re-parameterization to become compatible [5]. Besides parametric curves, implicit curves can also be numerically parameterized [6], then we can easily convert them to B-splines.

According to the above analysis, methods of representing planar curve in [1-11] contain two steps: 1.Sample data points from the planar curve 2. Approximate the sampled data points using least square approximation in a given tolerance. Although B-spline curve approximation is well understood, three problems are always dealt with unsatisfactorily, i.e. parameterization of data points, knot placement problem and the shape controlling[7-8]. Then it is difficult to use this method representing complicated planar curve.

The problem of representing planar curves in B-spline is different from approximation to the data points. The planar curves supply more information than the discrete data points. To apply this information, we propose a new algorithm for representing planar curves. In this algorithm, we sample both data points and their tangent vectors from the original curve. Take advantage of these tangent vectors we can construct a low degree B-splines curve interpolating the data and tangent vectors locally. But the control points of interpolation curve are redundant, and the geometric continuity of interpolation curve is G^1 . In the last we approximate this low degree curve by best least square approximation to get the final B-spline.

B-spline curve

A non-uniform B-spline curve of order p can be defined by

$$C(u)=\sum_{i=0}^{n} N_{i,p}(u)P_i \qquad u_{p-1}\le u\le u_{n+1} \tag{1}$$

Where $\{P_i\}$ are control points, p is the order of curve and $\{N_{i,p}(u)\}$ are pth-order B-spline basis functions defined on $U=\{u_0,u_1,\cdots,u_k,\cdots,u_n,\cdots,u_{n+p+1}\}$, satisfies $u_0\le u_1\le\cdots\le u_p\le\cdots\le u_n\le\cdots\le u_{n+p+1}$.

The p-th B-spline basis function is defined as $N_{i,0}(u)=\begin{cases}1, & \text{if } u_i\le u\le u_{i+1}\\ 0, & otherwise\end{cases}$

$$N_{i,p}(u)=\frac{u-u_i}{u_{i+p}-u_i}N_{i,p-1}(u)+\frac{u_{i+p+1}-u}{u_{i+p+1}-u_{i+1}}N_{i,p-1}(u).$$

Representing planar curves in B-splines curve

3.1 Sampling points and tangents

There many methods of sampling points and tangent vectors from planar curve [2-3]. In this paper, we adopt the available methods to sample the points and tangent vectors, because this algorithm focus on approximating these data points along with their tangents to get the final B-spline curve.

Park has proposed an algorithm for sampling data points from smooth curve within a given tolerance [2]. The procedure is as follow

1. Starting with two endpoints of the curve, repeat sampling using the offset envelope.
2. Estimate the upper bound of the chord length and repeat the following task until all chords joining two successive points are shorter than the bound.

If high accuracy is required, tangents and inflexion should be sampled, we adopt this method in [3]. As to implicit or algebraic curve, the method introduced by Hartmann [6] will be adopted. The sampling can be with any high density and accuracy, so we ignore the sampling error in the representing.

3.2 Interpolate the data points and tangent vectors

Given the data points $\{Q_i\}_{i=1\cdots m}$ along with their tangent vectors $\{t_i\}_{i=1\cdots m}$, we can construct m Bezier segments between each adjacent pair points interpolate these data and tangents. The segments compose a quadratic B-spline curve $\bar{C}(u)$

$$\bar{C}(u)=\sum_{j=0}^{\bar{m}}\bar{P}_j N_{j,3}(u),u\in[0,1] \tag{2}$$

With the knot $\bar{U}=\{0,0,0,\bar{u}_1,\bar{u}_1,\bar{u}_2,\bar{u}_2,\cdots,\bar{u}_{n'-1},\bar{u}_{n'-1},1,1,1\}$. We can see that Q_{i-1},Q_i are the endpoints of each segment from the knot vector, each segment has three control points, we only need to compute the inner control points. The inner control point R_i of i-th segment is the intersection of the neighboring tangent vectors t_{i-1},t_i .In the same way, we compute all the inner control points in each segment. Then we get all the control points in (2) $[\bar{P}]=[Q_0,R_0,Q_1,R_1,Q_2\cdots\cdots R_n,Q_n]$.

According to the B-spline curve theory, neighboring Bezier segments are joined with G^1 continuity. After computing the control points, the knot vector is need to be placed. Any sequence $\{\bar{u}_i\}$ satisfying $\bar{u}_{i-1}<\bar{u}_i<\bar{u}_{i+1}$ can become the knot vector in (2). In fact, the $\{\bar{u}_i\}$ are the paramters of the data points in $\bar{C}(u)$ .The chord length method is adopted in this paper, because it is widely used in most applications.

Step1. Let $\bar{u}_0=0, \bar{u}_m=1$

Step2. $\{d_i\}$ is the chord length of $|Q_{i-1}, Q_i|$.

Step3. Let d is total arc length $d=\sum_{i=1}^{m-1} d_i$. Then the knot vector in (2) is computed by

$\bar{u}_i=\bar{u}_{i-1}+\frac{d_i}{d}, i=1,\cdots m-1.$

3.3 Approximate the interpolation curve to get final curve

In this section, we find another curve $C(u)=\sum_{i=0}^{n} N_{i,p}(u)P_i$, $U=\{0,\cdots,0,u_1,u_2,\cdots,u_n,1,\cdots,1\}$ to approximate the interpolation curve using the best least square. This approximation curve is reprenting curve.

In this approximation, the distance between $C(u)$ and $\bar{C}(u)$ is measured by the L^2-norm

$$E=\int_0^1\left\|C(u)-\bar{C}(u)\right\|^2 d_u \tag{3}$$

To minimize (3) we set the partial derivatives $\frac{\partial(E)}{\partial P_l}=\sum_{i=0}^{n}\{\int_0^1[N_{l,k}(u)N_{i,k}(u)]d_u-\int_0^1[N_{l,k}(u)\bar{C}(u)]d_u\}$ to zeros. We will get a linear system of equations.

$$MP=R \tag{4}$$

$P=[P_0,P_1,\cdots,P_n]'$ are the control points and $M_{i,j}=\int_0^1 N_{i,k}(u)N_{j,k}(u)d_u$, $R_i=\int_0^1 N_{i,k}(u)\bar{C}(u)d_u$. By solving (5), the control points of the final curve are got.

Before computing the control points, we need to compute the knot vector of $C(u)$. Placement of knot vector is according to the parameters $\{\bar{u}_i\}$ of data points, these parameters have computed in section 3.1 using the chord length parameterization. The initial knot vector U is computed in this way: Let $d=\frac{m+1}{n-p+1}$, $i=\text{int}(jd), \alpha=jd-i, u_j=(1-\alpha)\bar{u}_i+\alpha\bar{u}_{i+1}, j=1\cdots n$. Furthermore, we approximate these data in given accuracy using the follow steps:

Step1. Use the initial knot U to approximate the interpolation curve.

Step2. Compute the error of each point $e_i=|Q_i-C(\bar{u}_i)|$. Check if the $\{e_i\}$ is less than the specified accuracy, if it is yes, output the approximating curve; if it is not, we will insert a new knot $\tilde{u}_i=\frac{u_i+u_{i+1}}{2}$ into the knot vector U, approximate the controlling curve again until within the specified accuracy.

Example

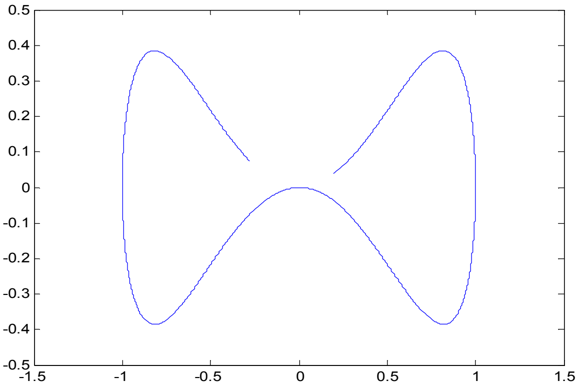

Fig.1. A planar curve

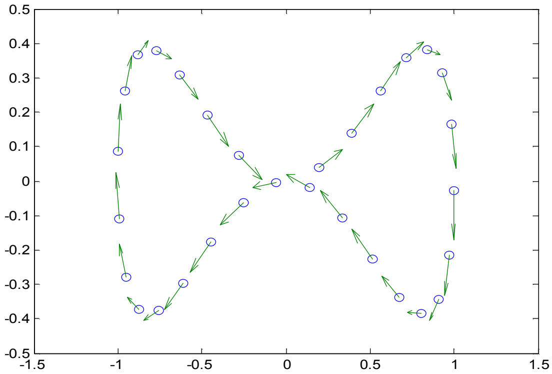

Fig.2. Sampling data points and their tangent vector

In this section, the example is presented to prove the usefulness and quality of the representing algorithm. A planar curve is showed in figure 1, the sampling data points and their tangent vector are showed in figure 2.

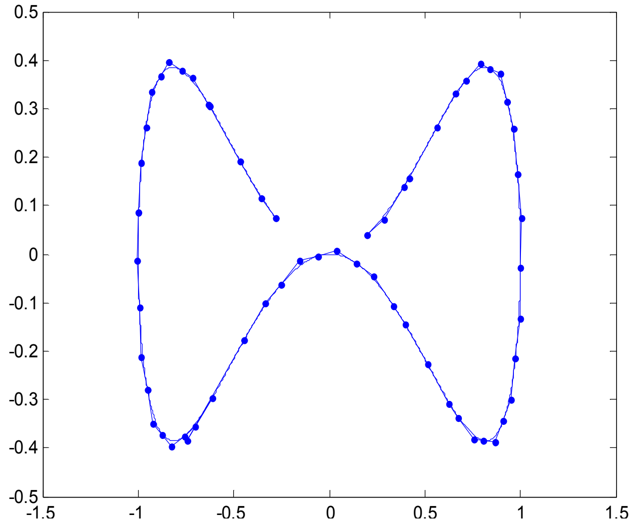

Fig.3. The interpolation curve along with its control polygon

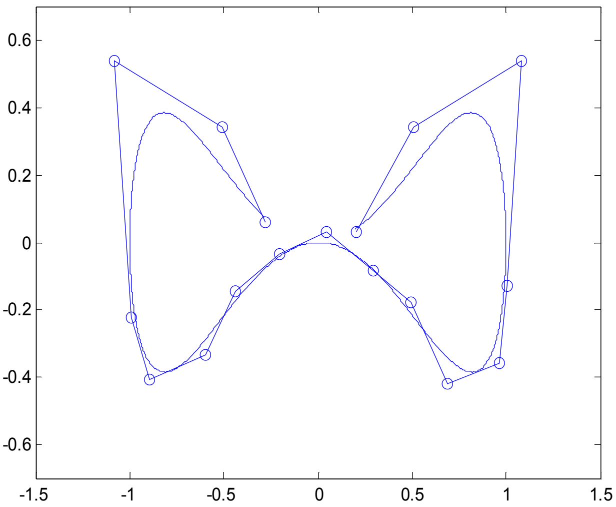

Fig.4. The final curve along with its control polygon

In figure 3, the data points and their data points are interpolated by a quadratic B-spline curve. We can see the control points of the interpation curve are very redundant, the number of control points is nearly double the number of data points. This curve is not what we want.

In order to remove the redundant control points, we use the best least square approximation to approximate the interpolation curve in figure 3 within the accuracy $\varepsilon = 10^{-3}$, the number of control points of final curve has been reduced to 17, final curve with its control polygon are showed in figure 4.

Conclusion

An algorithm about converting planar curves to B-splines has been described in this paper. Firstly, we sample data points from the planar curve according to the user's accuracy, the tangent vectors of each points are also need to sample. The representing algorithm is different from the approximation to data points, and planar curve provides more information which is very helpful to approximate the planar curve. We construct a quadratic curve interpolating the data points and the tangent vector locally, and we can interpolate data points quickly and directly by local method, Bezier segments between each two adjacent point. The best least square approximation has been used to merge Bezier segments to the final B-spline curve; we only need solve linear equations to get the final curve. How to apply this method in space curve is valuable to further research.

Acknowledgements

This work is financially supported by the Natural Science Foundation of the Jiangxi Province of China under Grant No.20114BAB201005 and 20122BAB201004.

References

[1] Piegl L,Tiller W. The NURBS book . 2nd ed. New York:Springer Verlag,1997.

[2] Park H. An error-bounded approximate method for representing planar curves in B-splines. Computer Aided Geometric Design 2004;Vol 21,pp 479–97.

[3] Chongyang Deng, Xunnian Yang,A local fitting algorithm for converting planar curves to B-splines, Computer Aided Geometric Design ,Vol 25 No.2, 2008, pp 837–849.

[4] Computer-Aided Design 1988. Volume 20 Issue 8, pp 475–483.

[5] Filip, D., Magedson, R., Markot, R., 1986. Surface algorithms using bounds on derivatives. 1988. Volume 20 Issue 8, pp 295–311.

[6] Hartmann, E., Numerical parametrization of curves and surfaces. Computer Aided Geometric Design, 2000. Volume 17 Issue 3, pp 251–266.

[7] Jing-Jing Fang, Chia-Lien Hung,An improved parameterization method for B-spline curve and surface interpolation, Computer-Aided Design, Vol45, No.6, 2013, pp 1005-1028.

[8] Li-Yong Shen, Chun-Ming Yuan, Xiao-Shan Gao, Certified approximation of parametric space curves with cubic B-spline curve. Computer-Aided Geometric Design . Vol.29 No. 8, 2012, pp 648-663

[9] Weishi Li,Shuhong Xua, Gang Zhaob, Li Ping, Adaptive knot placement in B-spline curve approximation, Computer-Aided Design ,Vol.37 No. 8,2005,pp791-797.

[10] Park, H., Lee, J.H., 2007. B-spline curve fitting based on adaptive curve refinement using dominant points. Computer-Aided Design, Vol39,No. 6, pp439–451.

[11] Yang, X., 2002. Efficient circular arc interpolation based on active tolerance control. Computer-Aided Design , Vol 34 No13, pp1037–1046.

[12] Lin Zi-zhi,PAN Ri-jing. A novel method for approximation using B-spline curve, Journal of Fujian Normal University(Natural Science Edition),Vol.24, No.2, 2008,pp22-28.

Applied Mechanics and Materials Vol. 596 (2014) pp 154-159
© (2014) Trans Tech Publications, Switzerland
doi:10.4028/www.scientific.net/AMM.596.154

Dynamic Pricing and Inventory Temperature Decisions for Fresh Foods with Variable Demands

Lei Tang[1, a *]

[1] China Institute of Manufacturing Development, Nanjing University of
Information Science &Technology, Nanjing 210044, China
[a]ttangl_99@126.com

Keywords: supply chain management; fresh foods; variable demands; decision making;

Abstract. Considering the special properties of food supply chain and fresh foods, provides multi-phases inventory model for fresh foods based on shelf life, thereinto demand function is dependent on price and time; in the model shortages are allowed, which assures the fresh foods can be sold out before the time limit. It proves that the total average profit is a restrict concave function of decision variables, namely, the solution to the system equations necessarily satisfy maximum conditions. Finally, numerical examples and relevant conclusions based on the model analysis are presented. It illustrates that through the optimized model's traverse within the allowable inventory control temperatures, retailers can get the optimal inventory temperature control decision. And so retailers can obtain optimal total average profit by choosing corresponding optimal phasic price under the optimal inventory temperature.

Introduction

As a communication bridge between buyers and sellers, product pricing is increasingly the focus of a variety of theoretical research due to involving the benefit of all the members in the supply chain. Compared with the general product, fresh food has some special properties that it will be abandoned or disposed if cannot be sold out through the shelf life. Therefore, fresh food as one type of perishable products, the constraint of the shelf life is especially important in the supply chain management decision-making.

Since the 1990s, the pricing problem of perishable products have been hot issues in the research field of price decision [1,2].Gunasekaran (1995) took into account the impact of advertising on demand function and proposed a multi-stage production-stock-market model for perishable products[3]. WenHong (1998) studied the impact of delay order to the corporate profits and proposed an integrated single-stage inventory model for perishable products [4]. From the perspective of manufacturers, Michael (2001) studied the pricing problem for perishable products with taking into account the purchase of constraints (such as advance reservation etc.) in a monopoly market environment [5]. Young H. Chun(2003) supposed the market demand subject to the negative binomial distribution and analyzed the optimal pricing decision-making models for perishable products in single-cycle and multi-cycle respectively[6]. Soheil Sibdari and David F. Pyke (2010) contributed to the dynamic pricing literature by developing a finite horizon model for the products with different quality levels [7].

For fresh food, some factors such as the high temperature can short shelf life, which will influence the quality level and consequently can influence the market demand. Relative to other commodities, fresh food has a short shelf life and larger price elasticity [8].The research about perishable products pricing optimization model provides a better theoretical basis to fresh food price makers. However, these studies are applicable to general perishable products, and they don't consider the characteristics of fresh food and food supply chain. The shelf life of fresh food is not a constant value; it will be fluctuate with the change of storage temperature and other environmental factors. In practice, we can predict shelf life through specific microbial prediction models and Monte Carlo simulation methods

[9]. On the other hand, the inventory temperature control and inventory costs are inseparable; therefore, in order to maximize the total profit, decision-makers should consider these factors comprehensively when making the corresponding decisions.

The model based on shelf life

In practice, a regular replenishment strategy has been used for fresh food. Here, the inventory model we proposed is a multi-stage regular replenishment model which based on food shelf life. The model permits shortage in order to guarantee that the product can be sold out before the shelf period. And the market demand in the model changes with time and price.

Assumptions and related symbols

The model assumptions:

(1) We consider the inventory problem with limited time, suppose there are n order cycles;

(2) Without considering the lead time;

(3) No inventory at the beginning;

(4) Allow shortage. The percentage of the products delayed can be expressed as a decreasing function $\beta(x)$, x is the waiting time, $0 \le \beta(x) \le 1$, and $\beta(0)=1$. When $\beta(x)=1$, it means that the orders are completely satisfied, there is no out of stock; when $\beta(x)=0$, it means that the backlog of unfilled orders is totally lost. At the same time, in order to ensure the existence of the optimal algorithm, we assume that $\beta(x)+x\beta'(x)>0\ (x>0)$;

(5)When the time is t and the price is p, the market demand is $f(t,p)$, $f(t,p)=g(t)A(p)$. $g(t)$ is a concave function in *n* ordering cycles; to simplify the model, we assume that $A(p)$ is a nonnegative, linearly and continuous decreasing function between $[0, p_u]$, and p_u is the upper price.

(6) In *n* ordering cycles, we assume that the quality level of each replenishment is same; that is to say, there has the same microbiological criteria;

(7)In *n* ordering cycles, the temperature of the inventory is the same.

Related signals in the model:

c_f : fixed ordering cost for per order;

p_i : unit sale price for the *i* stage(decision variable);

c_v : unit variable cost;

c_h :the storage cost for unit product unit time, which can be expressed as a decreasing function of storage temperature, that is, the lower the temperature, the higher the c_h;

c_s : the storage cost for unit product unit time caused by the shortage;

c_l : the unit cost for the lost market sales caused by the shortage;

H : the total time for *n* replenishments;

T: each replenishment cycle;

t_i : replenishment time of the *i-th* replenishment cycle, where i=1,2,…,n;

s_i : the time when the inventory level is *0* in the *i-th* replenishment cycle, where i=1,2,…,n;

Model description

In this paper we use the n-period Inventory Decision Model which allows shortage, and the lead time is zero, as shown in Fig.1.

By the formulas $\frac{dI}{dt}=-f$ and $I(s_i)=0$, we can get the *i-th* replenishment cycle's inventory:

$$I_i=\int_{t_i}^{s_i}(s_i-t)f(t,p_i)dt \qquad i=1,2,...,n \tag{1}$$

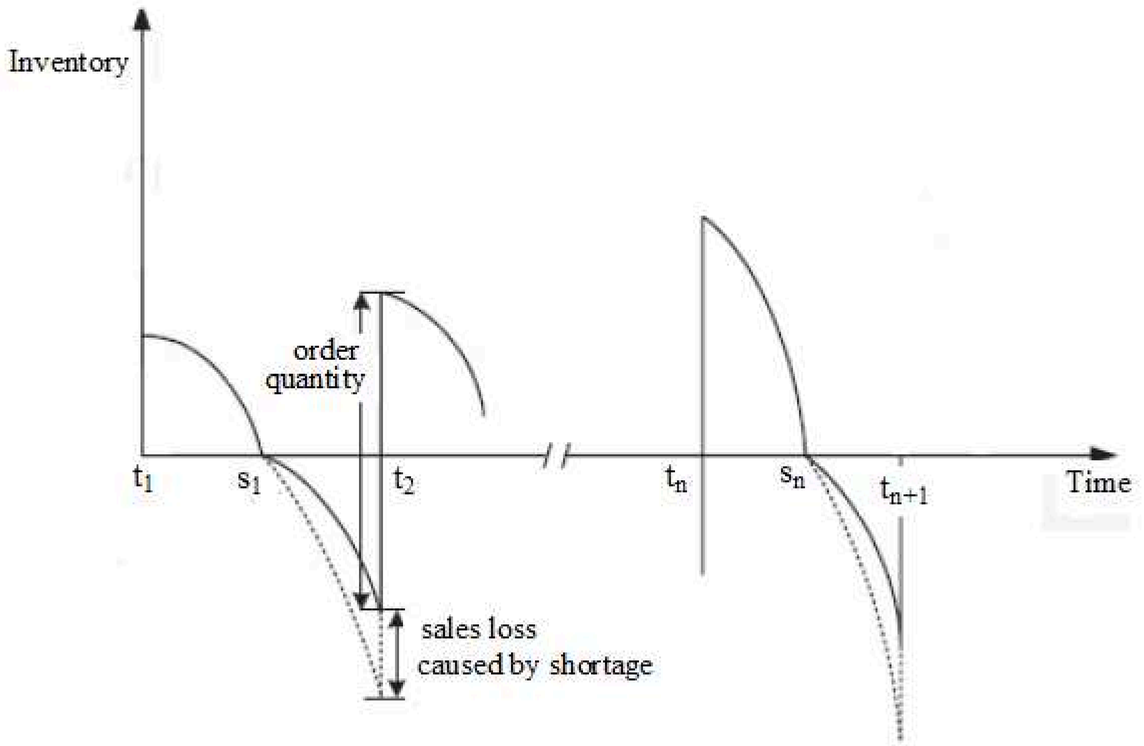

Fig.1 Diagram of the *n*-period inventory model

The amount of delayed delivery in the *i-th* replenishment cycle is:

$$s_i = \int_{s_i}^{t_{i+1}} (t_{i+1} - t)\beta(t_{i+1} - t) f(t, p_i)dt \tag{2}$$

The lost product sale caused by shortage in the *i-th* replenishment cycle is:

$$L_i = \int_{s_i}^{t_{i+1}} [1 - \beta(t_{i+1} - t)] f(t, p_i)dt \tag{3}$$

In the *i-th* replenishment cycle, at the time t_i, the replenishment quantity is (when $i = 1$, the first term in the formula will degenerate into zero):

$$Q_i = \int_{s_{i-1}}^{t_i} \beta(t_i - t) f(t, p_{i-1})dt + \int_{t_i}^{s_i} f(t, p_i)dt \tag{4}$$

The procurement cost in the *i-th* replenishment cycle is:

$$P_i = c_f + c_v Q_i \tag{5}$$

In the certain replenishment cycle *T*, if there has *n* replenishments, the average of the total profits can be expressed as:

$$\begin{aligned}
&\overline{TP}(\{p_i\},\{s_i\} \mid n, T) = \frac{1}{H}\sum_{i=1}^{n} (p_i Q_i - P_i - c_h I_i - c_s S_i - c_l L_i) \\
&= \frac{1}{H}\sum_{i=1}^{n} (p_i - c_v)\int_{s_i}^{t_i} \beta(t_{i+1} - t) f(t, p_i)dt + \frac{1}{H}\sum_{i=1}^{n} (p_i - c_v)\int_{t_i}^{s_i} f(t, p_i)dt - \frac{nc_f}{H} \\
&- \frac{1}{H}\sum_{i=1}^{n} c_h \int_{t_i}^{s_i} (s_i - t) f(t, p_i)dt - \frac{1}{H}\sum_{i=1}^{n} c_s \int_{s_i}^{t_{i+1}} (t_{i+1} - t)\beta(t_{i+1} - t) f(t, p_i)dt \\
&- \frac{1}{H}\sum_{i=1}^{n} c_l \int_{s_i}^{t_{i+1}} [1 - \beta(t_{i+1} - t)] f(t, p_i)dt
\end{aligned} \tag{6}$$

Therefore, the problem can be converted into determining $\{p_i, i = 1,...,n\}$ and $\{s_i, i = 1,...,n\}$ to maximize $\overline{TP}(\{p_i\},\{s_i\} \mid T)$. For retailers, this is a *2n* decision problem.

The analysis

For the given *n* and *T*, by $f(t, p) = g(t)A(p)$, we can get the first-order condition when $\overline{TP}(\{p_i\},\{s_i\} \mid n, T)$ reaches the maximum:

$$\frac{\partial \overline{TP}(\{p_i\},\{s_i\}|n,T)}{\partial s_i}=0 \tag{7}$$

$$\frac{\partial \overline{TP}(\{p_i\},\{s_i\}|n,T)}{\partial p_i}=0 \tag{8}$$

By Eq. (7) we can obtain (*H* does not affect the results of the analysis, therefore it will be hidden, the same below):

$$f(s_i,p_i)\{[c_v-p_i+c_s(t_{i+1}-s_i)-c_l]\beta(t_{i+1}-s_i)+p_i-c_v-c_h+c_l\}=0 \tag{9}$$

By $f(s_i,p_i)>0$, we can obtain:

$$[c_v-p_i-c_l+c_s(t_{i+1}-s_i)]\beta(t_{i+1}-s_i)+p_i-c_v-c_h+c_l=0 \tag{10}$$

By Eq. (8) we can get:

$$\begin{aligned}&[A(p_i)+(p_i-c_v+c_l)A'(p_i)]\int_{s_i}^{t_{i+1}}\beta(t_{i+1}-t)g(t)dt+A(p_i)\int_{t_i}^{s_i}g(t)dt+(p_i-c_v)A'(p_i)\\&\int_{t_i}^{s_i}g(t)dt-c_hA'(p_i)\int_{t_i}^{s_i}(s_i-t)g(t)dt-c_sA'(p_i)\int_{s_i}^{t_{i+1}}(t_{i+1}-t)\beta(t_{i+1}-t)g(t)dt\\&-c_lA'(p_i)\int_{s_i}^{t_{i+1}}g(t)dt=0\end{aligned} \tag{11}$$

Through analysis above, we can get the following conclusion:

Theorem 1: in Eq. (6), the function $\overline{TP}(\{p_i\},\{s_i\}|T)$ is a concave function; the solutions which can satisfy the Eq. (10) and the Eq. (11) will also satisfy the second-order maximization conditions.

Proof: By the assumptions $\beta'(x)<0$ and $\beta(x)+x\beta'(x)>0$ (for any x), we can calculate the second derivative of $\overline{TP}(\{p_i\},\{s_i\}|T)$:

$$\begin{aligned}\frac{d^2\overline{TP}}{ds_i^2}&=A(p_i)g(s_i)\{-c_s\beta(t_{i+1}-s_i)-[c_v-p_i-c_l+c_s(t_{i+1}-s_i)]\beta'(t_{i+1}-s_i)\}\\&=A(p_i)g(s_i)\{(p_i+c_l-c_v)\beta'(t_{i+1}-s_i)-c_s[\beta(t_{i+1}-s_i)+(t_{i+1}-s_i)\beta'(t_{i+1}-s_i)]\}\\&<0\end{aligned} \tag{12}$$

By the assumptions $A'(p)<0$ and $A''(p)<0$, we can calculate:

$$\begin{aligned}\frac{d^2\overline{TP}}{dp_i^2}&=A'(p_i)\int_{s_i}^{t_{i+1}}\beta(t_{i+1}-t)g(t)dt+(p_i-c_v+c_l)A''(p_i)\int_{s_i}^{t_{i+1}}\beta(t_{i+1}-t)g(t)dt\\&+A'(p_i)\int_{t_i}^{s_i}g(t)dt+(p_i-c_v)A''(p_i)\int_{t_i}^{s_i}g(t)dt-c_hA''(p_i)\int_{t_i}^{s_i}(s_i-t)g(t)dt\\&-c_sA''(p_i)\int_{s_i}^{t_{i+1}}(t_{i+1}-t)\beta(t_{i+1}-t)g(t)dt-c_lA''(p_i)\int_{s_i}^{t_{i+1}}g(t)dt<0\end{aligned} \tag{13}$$

Because $0<\beta(t_{i+1}-s_i)<1$, we can get:

$$\frac{\partial^2\overline{TP}}{\partial s_i\partial p_i}=\frac{\partial^2\overline{TP}(\{p_i\},\{s_i\}|T)}{\partial s_i\partial p_i}=f(s_i,p_i)[1-\beta(t_{i+1}-s_i)]>0 \tag{14}$$

By Eq. (6), we can get:

$$\frac{\partial^2\overline{TP}}{\partial s_i\partial p_{i+1}}=0 \tag{15}$$

The Hesse Matrix of $\overline{TP}(\{p_i\},\{s_i\}|T)$ can be expressed as Eq. (16).

The analysis above shows that the Hesse Matrix *H* expressed in Eq. (16) is negative, that is, it's odd-order principal minor is negative and even-order principal minor is positive.

Numerical examples

$$H=\begin{bmatrix}
\frac{\partial^2\overline{TP}}{\partial p_1^2} & \frac{\partial^2\overline{TP}}{\partial p_1\partial s_1} & 0 & 0 & 0 & 0 & 0 & 0 & 0\\
\frac{\partial^2\overline{TP}}{\partial s_1\partial p_1} & \frac{\partial^2\overline{TP}}{\partial s_1^2} & \frac{\partial^2\overline{TP}}{\partial s_1\partial p_2} & 0 & 0 & 0 & 0 & 0 & 0\\
0 & \frac{\partial^2\overline{TP}}{\partial p_2\partial s_1} & \frac{\partial^2\overline{TP}}{\partial p_2^2} & \frac{\partial^2\overline{TP}}{\partial p_2\partial s_2} & 0 & 0 & 0 & 0 & 0\\
\vdots & \vdots & \vdots & \vdots & \ddots & \vdots & \vdots & \vdots & \vdots\\
0 & 0 & 0 & 0 & 0 & \frac{\partial^2\overline{TP}}{\partial p_{n-1}\partial s_{n-2}} & \frac{\partial^2\overline{TP}}{\partial p_{n-1}^2} & \frac{\partial^2\overline{TP}}{\partial p_{n-1}\partial s_{n-1}} & 0\\
0 & 0 & 0 & 0 & 0 & 0 & \frac{\partial^2\overline{TP}}{\partial s_{n-1}\partial p_{n-1}} & \frac{\partial^2\overline{TP}}{\partial s_{n-1}^2} & \frac{\partial^2\overline{TP}}{\partial s_{n-1}\partial p_n}\\
0 & 0 & 0 & 0 & 0 & 0 & 0 & \frac{\partial^2\overline{TP}}{\partial p_n\partial s_{n-1}} & \frac{\partial^2\overline{TP}}{\partial p_n^2}
\end{bmatrix} \quad (16)$$

We suppose $f(t,p)=(500-20p)e^{-0.98t}$, $\beta(x)=1/(1+x)$. The relevant parameters are: $c_f=15$, $c_s=2$, $c_l=2.5$, $c_v=8$, $n=4$. The upper price and the lower price are $p_u=25$, $p_l=15$ respectively. Supposing the storage temperature is +4 degree celsius and the product's shelf life is 1 at this temperature. Then, from the analysis above, the order cycle is T=1. We also assume that the unit inventory cost is $c_h=5$ when the storage temperature is +4 degree celsius. The optimizat ion results can be shown in Table 1, in this condition, for the retailer the optimal average profit is (152.1288).

Table 1. The optimization results

i-th	s_i^*	p_i^*
1	0.5000	18.50
2	1.6732	23.79
3	2.4949	18.39
4	3.4382	17.40
$\overline{TP}$	152.1288	

If the other parameters are constant, the storage temperature is adjusted to +2 degree celsius (the shelf life is shorten to 0.9 and the unit inventory cost reduces to 4.5). Then the corresponding optimization results can be shown in Table 2, in which the optimal average profit for the retailer is (154.7392). Comparing these two solutions, we can see that the decision-maker should choose +2 degree celsius as the inventory temperature.

Table 2. Optimization results after changing the parameter

i-th	s_i^*	p_i^*
1	0.4673	16.48
2	1.6495	20.84
3	2.4810	16.68
4	3.4368	15.99
$\overline{TP}$	154.7392	

Conclusion

Through the numerical example, we can see that, if the retailer chooses different inventory control temperature, the total average profit will be different (152.1288 and 154.7392) due to the impact of the inventory costs. By traversing the optimization model in the permitted inventory control temperature, the retailer can obtain the optimal inventory temperature control decision, and choose the corresponding optimal stage price $\{p_i^*, i = 1, 2, ..., n\}$, and consequently can obtain the maximal average profit.

The demand function in the model changes along with the time and price. The future study can be developed towards two directions at least: firstly, we can analyze the optimal decision under the stochastic demand. Secondly, the market demand in this model just includes two factors (time and price), and the impact of the change of the shelf life to demand is not included. So, in the future research, we can incorporate it into the model and analyze the corresponding optimal solutions.

Acknowledgement

This paper is supported by the National Natural Science Foundation of China (71103093), Philosophy and Social Science Foundation of Jiangsu Provincial Education Department (2012SJB630048) and Chinese Manufacturing Industry Development Research Institute Project (SK20120200-16). And this work is funded by the Priority Academic Program Development of Jiangsu Higher Education Institutions(PAPD).

References

[1]Horng-Jinh Chang, Jinn-Tsair Teng, Liang-Yuh Ouyang, and Chung-Yuan Dye. Retailer’s optimal pricing and lot-sizing policies for deteriorating items with partial backlogging. European Journal of Operational Research. Vol.168 (2006), pp. 51-64.

[2]Tang Lei, Zhao Lin-du. The Pricing Model Analysis Based on the Shelf Life for Perishable Foods Bundling Selling. Journal of Southeast University (Natural Science Edition). Vol. 36-4(2006), pp. 677-680.

[3]S.K. Goyal, A. Gunasekaran. An integrated production-inventory-marketing model for deteriorating items. Computers and Industrial Engineering. Vol. 28-4(1995),pp.755-762.

[4]WenHong Luo. An integrated inventory system for perishable goods with backorderding. Computers and Industrial Engineering. Vol. 34-3(1998),pp. 685-693.

[5]Michael Z.F. Li. Pricing non-storable perishable goods by using a purchase restriction with an application to airline fare pricing. European Journal of Operational Research. Vol. 134-3(2001),pp. 631-647.

[6]Young H. Chun. Optimal pricing and ordering policies for perishable commodities. European Journal of Operational Research. Vol. 144-1(2003),pp. 68-82.

[7]Soheil Sibdari, David F. Pyke. A competitive dynamic pricing model when demand is interdependent over time. European Journal of Operational Research. Vol. 207-1,16(2010),pp. 330-338.

[8]Lei Tang, Lin-du Zhao. Research on pricing strategies for fresh foods in a two-echelon supply chain. ICIC Express Letters,Part B: Applications. Vol. 3-6(2012),pp. 1507-1513.

[9]Zhao Lin-du, Ding Fang, Qian Chuan-yi, Research on Model of Food Safety Forecasting in Supermarket.China-USDA Workshop on Agricultural Products Processing & Food Safety. 2005.

Applied Mechanics and Materials Vol. 596 (2014) pp 160-163
© (2014) Trans Tech Publications, Switzerland
doi:10.4028/www.scientific.net/AMM.596.160

Forecasting High Frequency Data: An ARMA-Soft RBF Network Model for Time Series

Dusan Marcek [1, a, b]

[1]Research Institute of the IT4Innovations Centre of Excellence, The Silesian University, Bezruc. Sq. 13, 746 01 Opava, Czech Republic
[a]dusan.marcek @fpf.slu.cz, [b]dusan.marcek@fri.uniza.sk

Keywords: ARIMA/GARCH models, RBF neural networks, Forecast accuracy,

Abstract. In the article we alternatively develop forecasting models based on the Box-Jenkins methodology and on the neural approach based on classic and fuzzy logic radial basis function neural networks. We evaluate statistical and neuronal forecasting models for monthly platinum price time series data. In the direct comparison between statistical and neural models, the experiment shows that the neural approach clearly improve the forecast accuracy. Following fruitful applications of neural networks to predict financial data this work goes on. Both approaches are merged into one output to predict the final forecast values. The proposed novel approach deals with nonlinear estimate of various radial basis function neural networks.

Introduction

One of the most important managerial activities is to make the right decisions. The manager as decision-maker uses forecasting models to assist him or her in decision-making process. Various methods have been developed and applied to forecasting problem. The econometric approach adopted from early days of econometrics is referred to as "AER" or Average Economic Regression [1, 2] and it is concerned with the functional form of the multiple regression or structural model. Economic theory might give some prior view to the relationship between the explanation variable and the independent variables. Using the time series data the model is estimated and checked for the validity.

In many cases economic theory do not give the assumption above the functional form of the model, or the assumption of independent errors and hence independent observations of the explanation variable is frequently unwarranted. If this is the case, forecasting models based on AER may be inappropriate. Box and Jenkins [3] developed a new modeling approach based on time series analysis and derived from the linear filter known as AR or ARMA (AutoRegressive Integrated Moving Average) models. The fundamental aim of time series analysis is to understand the underlying mechanism that generates the observed data and, in turn, to forecast future values of the series. Given the unknowns that affect the observed values in time series, it is natural to suppose that the generating mechanism is probabilistic and to model time series as stochastic processes.

Several new approaches to dynamic modeling in economics have become popular in recent years. One of the most attractive approaches is the neural network. The reasons to use neural networks for forecasting are many [4, 5, 6]. First, neural networks are nonparametric and nonlinear in nature. They do not require any specific assumptions about the underlying model form and are powerful and flexible in modeling real-world phenomena which have more or less non-linearities . Second, neural networks are universal functional approximator and they can capture any type of complex relationship. Third, neural networks are data-driven and self-adaptive. They have the capability to learn from experience. All these features of neural networks make them a very useful tool for forecasting tasks.

The paper is organized as follows. In the following section we present the data, describe basic the ARMA/ARCH-GARCH models and characterize the neural-fuzzy logic (soft) modelling approach. In the section "Results and Discussion" we put an empirical comparison. Section four briefly concludes.

Data and Development of Forecasting Models

In this section we present the data, introduce the development of statistical (ARCH-GARCH) forecasting models and models based of soft (fuzzy logic) RBF neural network in order to forecast the development of monthly data of platinum price time series. Both types of models will be developed with the same database. Our database is composed of 610 monthly observations of the closing platinum prices (denoted y_t (see Figure 1 left)

Construction of an Appropriate ARMA-GARCH Type model. As we would like to develop a ARMA-GARCH time series model for one month ahead forecast of the platinum price time series, the sample period for analysis from 1960M01 to 2008M12 was defined, i.e. the period over which the forecasting model can be developed and the ex post forecast period from 2009M01 to 2010M10 (denoted as validation or testing data set).

In Figure 1 left, we see that the series rises sharply with time with a rising trend, clearly signaling the non-stationary nature of the series, and indicating the need to transform the data to make it stationary. Firstly, we remove trend and then we difference the series to obtain a zero mean series. The time plot of the data after the differencing is depicted in Figure 1 right. In this figure it is seen that the mean appears steady, we assume the series has a constant mean, clearly signaling the stationary nature of the series.

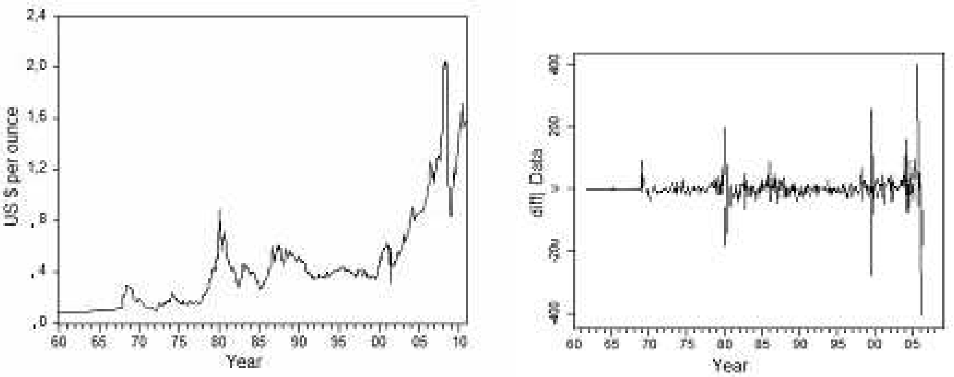

Fig. 1. Time series of monthly platinum prices 1960 – 2010 (left), the time plot of the data after the differencing (right).

Input selection is crucial importance to the successful development of an ARCH-GARCH model. Potential inputs were chosen based on traditional statistical analysis: these included the raw data of the monthly data of platinum price time series and lags thereof. The relevant lag structure of potential inputs was analyzed using traditional statistical tools, i.e. using the autocorrelation function (ACF), partial autocorrelation function (PACF) and the Akaike/Bayesian information criterion (AIC/BIC). According to these criterions using the R-system software the final ARMA(1,1)+GARCH(1,1) GED model was specified and fitted in the following form

$$y_t = -2{,}08398 + 0{,}8429.y_{t-1} + \varepsilon_t - 0{,}5328.\varepsilon_{t-1} \tag{1}$$

and variance equation

$$h_t = 0.104759 + 2.7901\varepsilon^2_{t-1} + 0.3912h_{t-1} \tag{2}$$

Neuronal Approach. A fully connected feed forward neural network was selected to be used as the forecasting function, due to its conceptual simplicity, and computational efficiency [7]. The neural network used for this research was the network of RBF type [8]. The same data used for ARMA(1,1)+GARCH(1,1) model was also used to train the neural network, i.e. the input variables forming the right hand site of the model (1). This network is one of the most frequently used networks to capture a variety of nonlinear patterns [7]. The transfer function in the hidden layer is the radial basic function (alternatively with the cloud concept [9]), whereas for the output unit a linear transfer function was applied.

The values of centroids were used as initialization values of weight vector *w* between the input layer and the hidden layer. To find the weights $\mathbf{w}_j$ or centers of activation functions we used the following adaptive (learning) version of *K*-means clustering algorithm for *s* clusters:

Step 1. Randomly initialize the centres c_j of RBF neurons

$$c_j^{(t)}, j = 1,2,...,s \tag{3}$$

where *s* represents the number of chosen RBF neurons (clusters).

Step 2. Apply the new training vector

$$x^{(t)} = (x_1, x_2, ..., x_k) \tag{4}$$

Step 3. Find the nearest centre to $x^{(t)}$ and replace its position as follows

$$c_j^{(t+1)} = c_j^{(t)} + \lambda(t)\,(x^{(t)} - c_j^{(t)}) \tag{5}$$

where $\lambda(t)$ is the learning coefficient and is selected as linearly decreasing function of *t* by $\lambda(t) = \lambda_0(t)\ (1 - t/\mathrm{N})$ where $\lambda_0(t)$ is the initial value, *t* is the present learning cycle and N is number of learning cycles.

Step 4. After chosen epochs number, terminate learning. Otherwise go to step 2.

The synaptic weights between the hidden layer and the output neuron were trained by the Back-Propagation algorithm.

The difference between the structures of classic and fuzzy logic (soft) RBF networks is that in fuzzy approximation the output value from the hidden layer is “normalized” [10] where the normalized output signals from hidden layer neurons signify the output signals whose sum is equal to 1.

We also combined the soft RBF neural network with the statistical ARMA(1,1) model expressed by Eq. 1, in one unified framework. The scheme of such proposed hybrid model is depicted in Figure 2. The thought of this proposal consists in economic theory of co-integrated variables which are related by an error correction model [11]. The simple mean Eq. 1 can be interpreted as the long-run relationship and thus it entails a systematic co-movement between variables y_t and y_{t-1}. If there exists a stable long-run, then error (residual) ε_t from the equation (1) should be a useful additional explanatory variable for the next direction of movement of y_t. According to [11] this mechanism is called as an error correction mechanism.

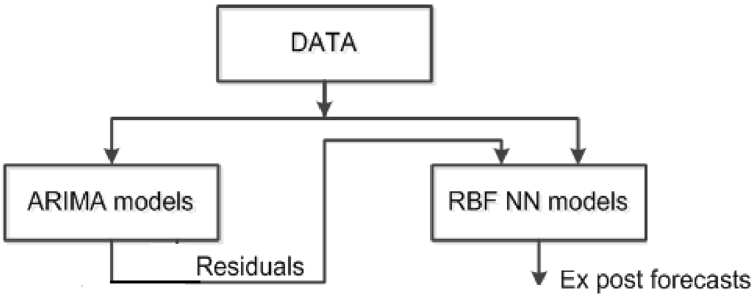

Fig. 2. The scheme of proposed hybrid forecasting model (see text for details).

Results and Discussion

To evaluate the predictive accuracy we used the Root Mean Squared Errors (RMSE). The benchmarking was performed between latest statistical techniques and neuronal approach used in high frequency financial data. Table 1 presents the accuracy results of 4 prediction methods. As can be also seen from Table 1, all models are very good and they follow the pattern of the actual very closely.

Table 1: Statistical summary measures of model´s ex post forecast accuracy for ARMA(1,1)+GARCH(1,1) model and RBF nets.

Model	RMSE
ARMA(1,1)+GARH(1,1) GED	72.155
RBF NN (classic)	76.206
RBF NN (soft)	67.974
RBF NN (hybrid)	33.601

Conclusion

In this paper, we established a statistical model based on Box-Jenkins methodology and as an alternative to that model three models based on Radial Basic Function network (classic, soft and hybrid RBF NN). We showed that the RBF hybrid neural network model outperforms latest statistical models based on ARMA + GARCH approaches. Moreover, RBF networks have such attributes as computational efficiency, simplicity, and ease adjusting to changes in the process being forecast. Thus, neural networks are usually used in the complicated problems of prediction because they minimize the analysis and modeling stages and the resolution time. These models can help managers make better decision-making.

Acknowledgements

This paper has been elaborated in the framework of the IT4Innovations Centre of Excellence project, reg. no. CZ.1.05/1.1.00/02.0070 supported by Operational Programme 'Research and Development for Innovations' funded by Structural Funds of the European Union and state budget of the Czech Republic.

References

[1] P. Kennedy: *A Guide to Econometrics*. Oxford, Basil, Blackwell (1992)

[2] K. Holden: Developments in Dynamic Modelling in Economics. Proceedings of the Mathematical Methods in Economics. International Scientific Conference. VŠB TU Ostrava (1997)

[3] G.E.P. Box, and Jenkins, G.M.: *Time Series Analysis, Forecasting and Control*. San Francisco, CA: Holden-Day, (1976)

[4] H. White: Consequences and detection of misspecified nonlinear regression models. Artificial Neural Networks: Approximation and Learning Theory, Oxford: UK Blackwell, pp. 224-258 (1992)

[5] H. White: Connectionist nonparametric regression: Multilayer feed-forward networks can learn arbitrary mappings. Artificial Neural Networks: Approximation and Learning Theory, Oxford: UK Blackwell, pp. 160-190 (1992)

[6] H. White, & A.R. Gallant: Artificial Neural Networks: Approximations and Learning Theory. In: There exists a neural network that does not make avoidable mistakes, UK: Blackwell: Oxford, pp. 5-11 (1992)

[7] D. Marcek, M. Marcek: *Neural Networks and Their Applications*, EDIS –ZU, Zilina, (2006)

[8] M.J.L. Orr: Introduction to Radial Basis Function Networks, University of Edinburgh, (1996)

[9] D. Li, D. Du: "*Artificial intelligence with uncertainty*," Chapman & Hall / CRC, Taylor&Francis Group, Boca Raton (2008)

[10] V. Kecman: *Learning and soft computing: support vector machines, neural networks, and fuzzy logic*, Massachusetts: The MIT Press (2001)

[11] R.F. Engle, C.W. Granger: Cointegration and error correction representation, estimation and testing. Econometrica, 55, pp. 251-276 (1987)

Applied Mechanics and Materials Vol. 596 (2014) pp 164-168
© (2014) Trans Tech Publications, Switzerland
doi:10.4028/www.scientific.net/AMM.596.164

Fuzzy Comprehensive Assessment of Air Material Suppliers

Zhong LV

Aviation Transportation Management College, China Civil Aviation Flying University, Guanghan 618307, China

Lvzhong2003@126.com

Keywords: Air material suppliers; Fuzzy comprehensive assessment; Analytic hierarchy process(AHP)

Abstract. Science assessment to air material suppliers is an effective measure that insures cost controlling and safety operating of an airline. Through analyzing the main factors of the air material suppliers, this paper constructs an assessment index system of the air material suppliers. The weights of assessment indexes is determined by means of the analytical hierarchy process(AHP). A assessment model of air material suppliers based on fuzzy comprehensive theory has also been set up. The model is validated through example. This prove that the method can give an overall comprehensive assessment level of the air material suppliers.

Introduction

With the rapid development of civil aviation transportation industry, to ensure the punctual running of the safety of the flight is a major problem of air transport enterprises face, while one of the key factors affecting the punctual running of flight safety is that whether or not air transport enterprises reserve more air material with the continued airworthiness, So to evaluate or select the comprehensive situation of meeting the airworthiness requirements of air material suppliers is a very important link that air transport enterprises need to face in the process of air material purchasing and inventory management, the work is related to whether or not air transport enterprises scientifically choose air material suppliers and to establish a long-term stable and mutually beneficial relationship with air material suppliers, is related to whether or not air transport enterprises manage air material orderly and scientifically, to achieve the purpose of reducing the cost of air transport enterprises [1]. Therefore it need to make scientific and rational decisions on the basis of comprehensive assessment of air material suppliers[2], these assessment include air material quality, air material price, enterprise reputation, financial condition, service level, environmental conditions, etc. The air transport enterprises mostly use the qualitative indicator to make comprehensive assessmentin in determining assessment indicators, it lacks practical and feasible assessment indicator system [3,4], or calculating process is too complex, lead to practicality is greatly reduced[5, 6]. In this paper, combined with the actual situation of air materials suppliers, established assessment indicator system of selection air material suppliers, according to the fuzziness of assessment indicators of air material suppliers, the fuzzy comprehensive assessment theory is introduced to assess air material suppliers.

Assessment index system of building material suppliers

To construct a scientific index system is a prerequisite for material supplier for correct assessment. For scientific, comprehensive, objective and fair to reflect the true connotation and the level of material suppliers, we should follow the principle of assessment index to construct scientific, comprehensive, systematic, comparable and feasibility of building material supplier assessment index system. Due to the characteristics of material itself, the choice of air material supplier standard is different with ordinary suppliers. This article is based on the objective analysis on the basis of the factors influencing the material supplier quality assurance ability which is combined with the actual situation of the air transport enterprises, according to the air quality standard requirements. Building by the air material quality, the air material price, the enterprise reputation, financial condition, service level, environmental conditions and so on six criteria C1 ~ C6 and 24 indicators layer consisting of the hierarchical model, as shown in table 1.

Table 1 The material supplier assessment index system C

Criterion layer	Index level
The quality of air material C11	Function of air materialC11 Property of air materiaC12 Reliability of air materia C13 Fault rate of air material C14 Refund rate of air material C15
The price of air materialC2	Cost C21 ProfitC22
Corporate reputation C3	contractfulfillmentrateC31 Bank creditC32
Financial condition C4	operational cash flow C41 capital scale C42 rate of profit C43 debt-to-assets ratio C44 Financial decision-making ability C45
Service levelC5	delivery termC51 Accuracy of deliveryC52 Flexible supply C53 After-sale trackingC54 Condition of technical support C55 Technical training C56
Environment conditionC6	economic environmentC61 economic environment C62 physic-geographical environment C63 sociocultural environmentC64

The fuzzy comprehensive assessment model of air material suppliers

The fuzzy comprehensive assessment theory. The basic principle of fuzzy comprehensive assessment method is first to determine the assessment factors' grade standard and the corresponding assessment index weights, and then determine the membership degree of assessment indexes which is used to describe the assessment factors of fuzzy boundaries, so as to construct the assessment index fuzzy assessment matrix, then use the weighted average fuzzy composite operation to ensure the level of the assessment objects [7].

Fuzzy comprehensive assessment usually contains sheer level fuzzy assessment and multi-level fuzzy comprehensive assessment, the sheer level fuzzy assessment is the basis of the comprehensive multi-level fuzzy assessment. This article will use the multi-level fuzzy comprehensive assessment, that is, first to fuzzy comprehensive assessment of index layer of each index, and fuzzy comprehensive assessment was carried out on the criterion layer index, the final air material supplier assessment of the final result is obtained by the weighted average [8].

Determine the value of index weight. In the assessment index system of air material suppliers, the contribution of each index to the goal is different, so it requires to give them different weights according to the contribution they make. The determination of index weight values plays an important role in the assessment of air material suppliers. It is very important that the determination is scientific and reasonable, because it will directly affect the reliability and validity of assessment results. Since there are too much qualitative analysis in the assessment index system, which need to be quantified meanwhile, so this paper uses analytic hierarchy process AHP to determine the weight of each index value [5,6].

The establishment of assessment set. The assessment set V is a set of assessment level that made by the valuators according to the assessment results. In this paper, the suppliers assessment set is divided into 5 grades: $V = \{v_1, v_2, v_3, v_4, v_5\} = \{better, good, general, poor, poorer\}$. Based on the assessment set V, for the establishment of thresholds: between 90 to 100 as good, between 80 to 90 as not bad, between 70 to 80 for the general, between 60 to 70 for the poor, 60 or less for the worse.

The establishment of the assessment matrix R. To establish air material suppliers assessment indictor assessment matrix R using expert investigation method. Firstly determine the index grade through experts make comprehensive judgments on air material suppliers assessment, then calculate the proportion of the each indicator in the assessment level according to the results of experts assessment of each indictor, eventually get the membership of corresponding indictor in the assessment set.

Fuzzy comprehensive assessment. Using the weighted average fuzzy operator$M(\cdot,\oplus)$ to assess each indicator of air material suppliers, the method by comprehensive assess all the weight values of assessment factors for air material suppliers obtains the overall indicator of air material suppliers[10]. According to comprehensive assessment of weight matrix W and assessment matrix R of air material suppliers, get comprehensive assessment matrix $D=W\cdot R$("$\cdot$"said the fuzzy matrix synthesis arithmetic). According to the weighted average principle and rank score, obtain quantitative indicator values by dealing with D component, can end up with assessment grades that air material suppliers belongs to.

Assessment vector management. For the final assessment vector $D=(d_1,d_2,d_3,d_4,d_5)$ of air material suppliers, according to the assessment set divided into five levels, assigned to a 95, 85, 75, 65 and 55 points respectively, using formula $G=95d_1+85d_2+75d_3+65d_4+55d_5$, can obtain the final assessment results. The five levels including 95, 85, 75, 85 and 55 points are based on "better, good, general, poor, poorer" five grades, through group discussion and expert consultation, to determine the point which appropriately show feature of each level in the [0,100] .

Empirical Analysis

To illustrate the validity of the model, with a air material supplier status as investigation object, for the assessment system established in Table 1, the consolidation of its fuzzy comprehensive assessment.

The weight coefficient matrix. According to the weight of AHP to calculate the air material suppliers assessment on the assessment indicators. The index of 6 standards for example, firstly constructing judgment matrix, experts using the 9 scale method of important degree of each index score, and consistency test. Ci index weights obtained as follows:

$W=(0.350,0.162,0.094,0.094,0.249,0.051)$

Similarly, Weights of index layer of each index can be obtained as follows:

$W_1=(0.186,0.309,0.309,0.098,0.098)$

$W_2=(0.500,0.500)$

$W_3=(0.500,0.500)$

$W_4=(0.310,0.066,0.117,0.197,0.310)$

$W_5=(0.181,0.296,0.181,0.103,0.181,0.058)$

$W_6=(0.290,0.446,0.093,0.171)$

Assessment matrix R. 35 air materials management expert on each index of air material suppliers of assessment grades (better,good, general, poor, poorer), according to the results of the assessment of each index is calculated air material suppliers in the assessment grade proportion, so as to obtain the membership of corresponding indictor in the assessment set, you can get each index corresponding index layer assessment matrix R_i.

$$R_1=\begin{bmatrix}0.257 & 0.314 & 0.257 & 0.171 & 0.000\\ 0.286 & 0.371 & 0.229 & 0.114 & 0.000\\ 0.229 & 0.343 & 0.286 & 0.114 & 0.029\\ 0.286 & 0.314 & 0.257 & 0.143 & 0.000\\ 0.343 & 0.286 & 0.286 & 0.057 & 0.029\end{bmatrix}$$

$$R_2=\begin{bmatrix}0.371 & 0.286 & 0.229 & 0.057 & 0.057\\ 0.343 & 0.314 & 0.257 & 0.057 & 0.029\end{bmatrix}$$

$$R_3=\begin{bmatrix}0.314 & 0.371 & 0.229 & 0.086 & 0.000\\ 0.343 & 0.314 & 0.171 & 0.086 & 0.086\end{bmatrix}$$

$$R_4=\begin{bmatrix}0.371 & 0.286 & 0.257 & 0.086 & 0.000\\ 0.343 & 0.314 & 0.229 & 0.114 & 0.000\\ 0.286 & 0.343 & 0.257 & 0.114 & 0.000\\ 0.314 & 0.343 & 0.257 & 0.086 & 0.000\\ 0.371 & 0.314 & 0.229 & 0.086 & 0.000\end{bmatrix}$$

$$R_5=\begin{bmatrix}0.286 & 0.343 & 0.229 & 0.114 & 0.029\\ 0.314 & 0.314 & 0.257 & 0.114 & 0.000\\ 0.343 & 0.286 & 0.257 & 0.114 & 0.000\\ 0.371 & 0.286 & 0.286 & 0.057 & 0.000\\ 0.400 & 0.314 & 0.257 & 0.029 & 0.000\\ 0.429 & 0.286 & 0.171 & 0.114 & 0.000\end{bmatrix}$$

$$R_6=\begin{bmatrix}0.371 & 0.343 & 0.286 & 0.000 & 0.000\\ 0.400 & 0.343 & 0.257 & 0.000 & 0.000\\ 0.371 & 0.314 & 0.286 & 0.029 & 0.000\\ 0.343 & 0.314 & 0.286 & 0.057 & 0.000\end{bmatrix}$$

Fuzzy comprehensive assessment of air material suppliers. According to the $B=W\cdot R$ assessment of the criterion layer fuzzy comprehensive assessment, the assessment of each index is calculated as the vector layer.

$B_1=W_1\cdot R_1=[0.268,0.338,0.260,0.122,0.012]$

$B_2=W_2\cdot R_2=[0.357,0.300,0.243,0.057,0.043]$

$B_3=W_3\cdot R_3=[0.329,0.343,0.200,0.086,0.043]$

$B_4=W_4\cdot R_4=[0.348,0.314,0.246,0.091,0.000]$

$B_5=W_5\cdot R_5=[0.342,0.310,0.250,0.093,0.005]$

$B_6=W_6\cdot R_6=[0.379,0.335,0.273,0.012,0.000]$

B_1, B_2, B_3, B_4, B_5, B_6 reflects the strength of that air material suppliers assessment criteria for each index layer. According to the principle of maximum membership degree, it can be seen that the Air Materiel supplier assessment factors in aviation materials quality indicators and corporate reputation index assessment rating scale is relatively low.

The target layer can be obtained relationship matrix

$\mathrm{R}=[\,B_1\ B_2\ B_3\ B_4\ B_5\ B_6]$

Fuzzy comprehensive assessment of target index, according to $D=W\cdot R$

$D=W\cdot R=[0.320,0.323,0.248,0.092,0.016]$

According to formula processing vector $\mathrm{G}=95d_1+85d_2+75d_3+65d_4+55d_5$, comprehensive assessment available to the air materiel supplier is G = 83.315 points, namely the air materiel supplier assessment rating of "good", explained there is room for improvement. In particular, should strengthen the management and supervision of aviation material quality.

Conclusions

As the importance of air material suppliers in the airline air materiel management, assessment to air material suppliers has important practical significance. The fuzzy comprehensive assessment theory is applied to the assessment of air material suppliers to establish a comprehensive assessment based on fuzzy mathematical assessment of air material suppliers and aircraft materials applied to a vendor assessment. Comprehensive assessment results show that the air materiel supplier assessment score of 83.374, visible evaluate the value of the air material suppliers ranged between good and in general, tend to be more general. The example showed that, through the model can determine the status of management level of air material supplier management level and each module. Fuzzy comprehensive assessment method not only gives a qualitative and quantitative assessment results of assessment objects, the comprehensive level can reflect the voyage air materials suppliers comprehensive, visually, but also a clear need to improve the index of air material suppliers, to provide reference for improving the air material suppliers management. Introduce the fuzzy comprehensive assessment method of the assessment of air materials suppliers, for the condition of air material suppliers assessment provides a new way of thinking.

References

[1] Z.W. Zhao: Civil Aviation of China, Vol. 11 (2010), p. 53-56. (in Chinese)

[2] Besley S and Brigham E F: *Principles of Finance*. (South-Western Educational Publishing, America 2003).

[3] K.Wang: Jiangsu Aviation, Vol.22 (2002), p.17-19. (in Chinese)

[4] Y. Hu and J.Z. Zheng and S. F. Gao: Logistics Technology, Vol.24 (2004), p.113-115. (in Chinese)

[5] J.S. Chen and X.Y.Zhang and J.J. Chen: Systems Engineering Theory and Practice, Vol.28 (2008), p.149-154. (in Chinese)

[6] X.C. Ni and H.F. Zuo and F. Bai: Journal of Mechanical Science and Technology, Vol.25 (2006), p.1404-1407. (in Chinese)

[7] S.B. Xu. *The principle of AHP*]. (Tianjin University Press, China 1988). (in Chinese)

[8] S.K. Qin: *Comprehensive evaluation principle and application*. (Electronics Industry Press, China 2003). (in Chinese)

Applied Mechanics and Materials Vol. 596 (2014) pp 169-173
© (2014) Trans Tech Publications, Switzerland
doi:10.4028/www.scientific.net/AMM.596.169

Mixed NMF blind source separation algorithm

Zhao Zhijin[1, 2], Liu Zhongjian[1]

[1.]College of Communication Engineering, Hangzhou Dianzi University, Hangzhou 310018,China;

[2.] State Key Lab of Information Control Technology Corporation,

Jiaxing 314410, China

Key words: rank one; least squares; blind source separation; separation performance

Abstract: The rank one NMF blind source separation algorithm (NMF-R1) was obtained by imposing the sparsity constraint on the fast NMF algorithm based rank one. NMF blind source separation algorithm based on least squares (NMF-LS) was obtained by using pseudo-inverse matrix. NMF-R1 algorithm was superior to the existing blind source separation algorithms based on NMF. NMF-LS algorithm had faster computation speed, but the result of decomposition was not unique. In order to further enhance the signals separated performance, crossover iteration between NMF-R1 and NMF-LS was used to getting the mixing matrix and the signal matrix, and the mixed NMF blind source separation algorithm (NMF-LR) was obtained. Simulation results show that the separation performance of NMF-LR algorithm is better than that of NMF-R1 and NMF-LS, and the computation complexity of NMF-LR algorithm is nearly the same as NMF-R1 algorithm.

Introduction

Non-negative matrix factorization (NMF) [1-4] is a matrix decomposition method with the simple, fast calculation and the stronger physical properties. A non-negative matrix $\mathbf{V}$ is decomposed into the product of two non-negative matrixes $\mathbf{W}$ and $\mathbf{H}$, that is $\mathbf{V}=\mathbf{WH}$. The NMF algorithm was applied to blind source separation in reference[5,6], sparsity, determinant and correlations constraints were imposed on the NMF optimization model of Euclidean distance, the blind source separation algorithm based NMF was obtained(abbreviated as NMF-DSC), multiplicative update rules is used for the optimal solution. Because partial gradient information was lost in the updated process, performance of the NMF-DSC algorithm may be improved, besides the complexity of the algorithm was too high. The fast NMF algorithm of rank one was proposed in reference[7], Euclidean distance NMF model was transformed into a quadratic function, and the optimal solution was obtained according to the characteristics of quadratic functions, and the algorithm converged faster, matrix decomposition was better. But it cannot be directly applied to blind source separation. The NMF algorithm based on Least-squares (LS) was proposed in reference [8], the algorithm converged very faster, but the algorithm has not been used to blind source separation so far. Rank one NMF algorithm and least-squares NMF algorithm are used to blind source separation at the same time, mixed NMF algorithm is proposed in this paper.

Principle of mixed NMF blind separation algorithm

NMF algorithm optimization model based on Euclidean distance is shown by Eqn(1)

$$\min_{\mathbf{W},\mathbf{H}} D(\mathbf{W},\mathbf{H}) = \frac{1}{2}\|\mathbf{V}-\mathbf{WH}\|^2 = \frac{1}{2}\sum_{i,j}(V_{ij}-(\mathbf{WH})_{ij})^2$$
$$\textit{subject to } W_{ia} \ge 0, H_{bj} \ge 0, \forall i,a,b,j. \qquad (1)$$

where $\mathbf{V}$ is a $m*N$ matrix, $\mathbf{W}$ is a m*n matrix and $\mathbf{H}$ is a $n*N$ matrix. Pseudo inverse matrix[9] was used in order to resolve the least-squares problem, then the update formulas of $\mathbf{W}$, $\mathbf{H}$ are shown by Eqn (2) and Eqn (3)

$$\mathbf{W}=\left[\mathbf{V}\mathbf{H}^T\left(\mathbf{H}\mathbf{H}^T\right)^{-1}\right]_+ \qquad (2)$$

$$\mathbf{H}=\left[\left(\mathbf{W}^T\mathbf{W}\right)^{-1}\mathbf{W}^T\mathbf{V}\right]_+ \qquad (3)$$

Where $[\bullet]_+$ represents that all elements of it are positive. So Eqn (2) and Eqn (3) are the NMF algorithm based on least-squares. This algorithm is used to blind source separation directly, called NMF blind source separation based on LS, abbreviated as NMF-LS. NMF-LS algorithm converges very fast, but the separation performance is unstable, signal decomposition is not unique. In order that rank one NMF algorithm[7] can be used into blind source separation, sparsity constraints is imposed on signal matrix, so optimization objective function is as follows:

$$\begin{gathered}\min_{\mathbf{W},\mathbf{H}} D(\mathbf{W},\mathbf{H})=\frac{1}{2}\|\mathbf{V}-\mathbf{W}\mathbf{H}\|^2+\gamma J(\mathbf{H}_{j.})\\ \textit{subject to } W_{ia}\geq 0, H_{bj}\geq 0, \forall i,a,b,j.\end{gathered} \qquad (4)$$

where $J(\mathbf{H})=\|\mathbf{H}\|^1=\sum_{i,j}|H_{ij}|^1$, γ is a balance parameters。

Eqn(4) is transformed into a quadratic function, and the optimal solution is obtained according to the characteristics of quadratic functions. Since the sparsity constraints is ineffective on $\mathbf{W}$, update formula of $\mathbf{W}$ [7] is as follows:

$$\mathbf{W}_{.i}=\begin{cases}\max\left(\dfrac{\boldsymbol{\eta}_i}{\left(\mathbf{H}\mathbf{H}^T\right)_{ii}},\mathbf{0}\right) & \|\mathbf{H}_{\mathbf{i.}}\|>\mathbf{0}\\ \mathbf{C}(m,1) & \|\mathbf{H}_{\mathbf{i.}}\|=\mathbf{0}\end{cases} \qquad (5)$$

where $\mathbf{C}(m,1)$ is m-dimensional column vector randomly, whose elements are between 0 and 1; $\mathbf{W}_{.i}$ is the ith column elements of $\mathbf{W}$, $(\mathbf{H}\mathbf{H}^T)_{ii}$ ith row and ith column element of $(\mathbf{H}\mathbf{H}^T)$.

$$\begin{aligned}\boldsymbol{\eta}_i &= \left[\eta_{1i}, \ \eta_{2i}\cdots\eta_{mi}\right]^T\\ &= \left(\mathbf{V}\mathbf{H}^T\right)_{.i}-\sum_{k=1,k\neq i}^{n}\mathbf{W}_{.k}\left(\mathbf{H}\mathbf{H}^T\right)_{ki}\end{aligned} \qquad (6)$$

Update formula of $\mathbf{H}$ is showed by Eqn(7)

$$\mathbf{H}_{j.}=\begin{cases}\max\left(\dfrac{\left[\xi_{j.}-0.5\gamma\right]}{\left(\mathbf{W}^T\mathbf{W}\right)_{jj}}, \ 0\right) & \|\mathbf{W}_{,j}\|>0\\ \mathbf{0}_{1*N} & \|\mathbf{W}_{,j}\|>0\end{cases} \qquad (7)$$

where $\mathbf{H}_{j.}$ is jth row elements of the matrix $\mathbf{H}$; $\mathbf{0}_{1*N}$ is N- dimensional row vector whose elements are 0.

$$\begin{aligned}\xi_{j.} &= \left[\xi_{j1},\ \xi_{j2} \dots \xi_{jN}\right]^T \\ &= \left(\mathbf{w}^T \mathbf{v}\right)_{j.} - \sum_{k=1,k\neq j}^{n} \left(\mathbf{w}^T \mathbf{w}\right)_{jk} H_{k.}\end{aligned} \tag{8}$$

So Eqns(5)-(8) are rank one fast NMF blind source separation (NMF-R1). In order to improve the performance of the blind source separation further, making full use of NMF-LS algorithm's faster convergence and NMF-R1's good separation performance, $\mathbf{W}$ is updated by Eqn(2) and $\mathbf{H}$ is updated by Eqn(7), so mixed blind source separation is obtained, abbreviated as NMF-LR, whose update formulas are Eqns(2),(7)and (8).

Algorithms simulation and performance analysis

Reconstruction SNR (Signal to Noise Ratio, SNR) of a signal as an index is used to analyze and compare performance of two algorithms, which is defined as follows

$$SNR = 10\lg\left(\frac{\|\mathbf{S}\|^2}{\|\hat{\mathbf{S}} - \mathbf{S}\|^2}\right) \tag{9}$$

where $\hat{\mathbf{S}}$ is the estimation of $\mathbf{S}$. The bigger SNR, the better performance of the algorithm. NMF-LR, NMF-R1, NMF-LS and NMF-DSC are simulated and compared with each other.

(1) *Separation performance analysis*. Four source signals' waveforms are shown in Figure 1, $6*4$ mixed matrix is generated randomly , mixed signals are shown in Figure 2. We set $\gamma=0.01$, the two parameters of NMF-DSC algorithm $\mu=0.005$, $\lambda=0.00005$, SNR of four algorithms after iteration 5000 are shown inTable 1.

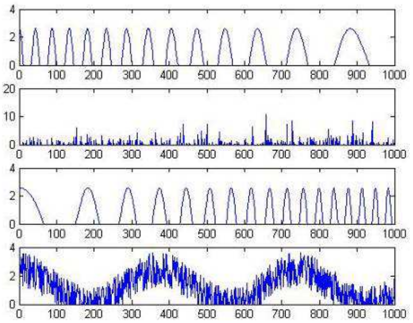

Fig.1 Source signal

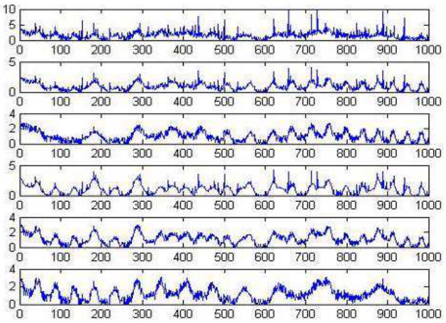

Fig.2 Mixed signal

Table 1 Reconstruction SNR of four algorithms

algorithms	$\mathbf{S}_1$	$\mathbf{S}_2$	$\mathbf{S}_3$	$\mathbf{S}_4$
NMF-LR	55.8369	56.5239	53.9866	54.5798
NMF-R1	46.1159	47.1819	42.3929	40.0127
NMF-DSC	29.1797	34.7152	35.6552	30.6227
NMF-LS	25.0109	13.5069	17.0086	19.2209

From Table 1, SNR of NMF-LR algorithm is highest, NMF-R1 is second and NMF-LS algorithm is the lowest. The SNR of NMF-LR algorithm is all higher than 55 dB. The highest SNR of NMF-R1 is about 46dB and that of NMF-DSC is about 36dB.

(2) *Convergence analysis of algorithms.* SNR curves versus iterations number of NMF-LR algorithm and NMF-R1 algorithm are shown in Fig.3 and Fig.4. From these figures we can see that when NMF-LR iterates 2500, it is convergence, and the SNRs reach about 55 dB. NMF-R1 algorithm gets convergence when it iterates 3500 and SNR of signals are about 45 dB. So the performance of NMF-LR algorithm is better than that of NMF-R1 algorithm.

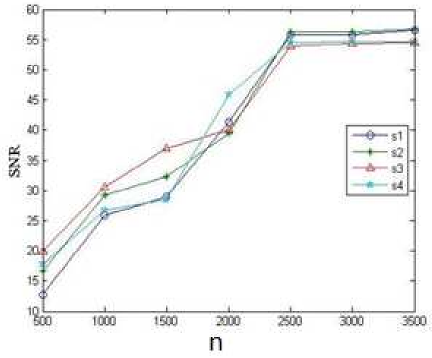

Fig.3 NMF-LR algorithm

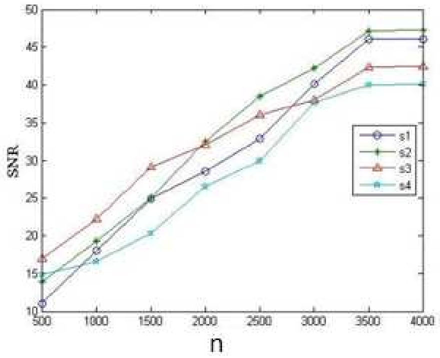

Fig.4NMF-R1 algorithm

(3)*Effect of the balance parameters* γ *to NMF-LR algorithm.* The relationship curves of γ and SNR is shown in Fig.5. From the figure we can see that when γ is 0.01, the SNR is biggest, when γ is less than 0.01 or greater than 0.01, the SNR becomes lower. So the balance parameter $\gamma=0.01$ should be more suitable.

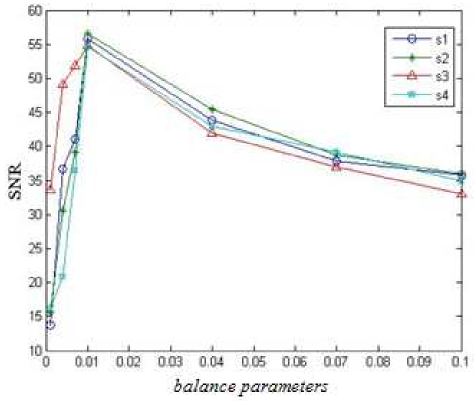

Fig.5 The relationship of γ and SNR

(4) *Algorithm complexity analysis*. From Eqns(5)-(8), the multiplication number required of each iteration of NMF-R1 is $M_{R1} = N\left(n^2+2mn+n\right)+\left(n^2m+mn\right)$, from Eqns(2), (7) and (8), the multiplication number required of each iteration of NMF-LR is $M_{LR} = N\left(2n^2+2mn\right)+2n^2m+n^3$. So the ratio of multiplication number required each iteration of NMF-R1 and NMF-LR is

$$R = \frac{M_{R1}}{M_{LR}} = \frac{N\left(n^2+2mn+n\right)+\left(n^2m+mn\right)}{N\left(2n^2+2mn\right)+\left(2n^2m+n^3\right)} \qquad (10)$$

Since N is usually more than 1000, m, n are very small, the second term of numerator and denominator could be ignored. And since m is close to n, Eqn(10) can be approximated as follows:

$$R \approx \frac{3n+1}{4n} \qquad (11)$$

So we can obtain $0.75 < R < 1$. The complexity of each iteration of NMF-LR algorithm is higher than that of NMF-R1. But the ratio of iteration times of NMF-R1 and iteration times of NMF-LR is 1.4, when the two algorithms all get convergence, so the complexity required is about the same.

Conclusion

By making full use of advantages of fast NMF algorithm and least-squares NMF algorithm, mixed NMF blind source separation is proposed. This algorithm has better separation performance and faster speed of convergence than NMF-R1.

References

[1] I. S. Dhillon, S. Sra. Generalized nonnegative matrix approximations with bregman divergences [C]. Advances in Neural Information Processing Systems, 2005, 283-290.

[2] A. Cichocki, S. Choi. Nonnegative matrix factorization with α -divergence[J]. Pattern Recognition Letters, 2008, 29(9): 1433-1440.

[3] D. D. Lee, H. S. Seung. Algorithms for nonnegative matrix factorization [C]. Advances in Neural Information Processing Systems, 2000, 556-562.

[4] Z. Yang, E. Oja. Linear and nonlinear projective nonnegative matrix factorization [J]. IEEE Transaction on Neural Networks, 2010, 21(5): 734-749.

[5] Zhijin Zhao, Hong Lu, Chunyun Xu. NMF blind source separation algorithm based on constrained[J]. Piezoelectric and Acoustooptics,2010,32(6):1049-1052.

[6] Zhijin Zhao, Hong Lu, Junna Shang. Underdetermined NMF blind signal separation algorithm based on constrained[J]. Application Research of Computers, 2011, 28(5):1843-1845.

[7] Mingsong Cheng, Shaolian Liu. A practical and fast non-negative matrix factorization algorithm[J]. Journal of Dalian Technology University, 2013, 53(1): 151-156.

[8] Fang Li, Qunxiong Zhu. Fast non-negative matrix decomposition based on matrix transformation[J]. Beijing University of Posts and Telecommunications, 2010, 33(4):118-122

[9] X D Zhang. Matrix Analysis and Applications [M]. Beijing: Tsinghua University.

Applied Mechanics and Materials Vol. 596 (2014) pp 174-178
© (2014) Trans Tech Publications, Switzerland
doi:10.4028/www.scientific.net/AMM.596.174

Natural gas consumption forecasting based on combinatorial optimization model

Junqi Wang[1, a*], Lei Chen[2, b], Li Li[3, c] and Yixu Wang[4, d]

[1,2]School of Petroleum Engineering, Xi'an Shiyou University, Xi'an, Shaanxi 710065, China

[3,4]Xi'an Middle School of Shaanxi Province, Xi'an, Shaanxi 710018, China

[a]wjq_xasy@163.com, [b]chenleigk@126.com, [c]51239624@qq.com, [d]173331522@qq.com

Key words: natural gas; consumption; combination; model; forecasting

Abstract: As the estimating of natural gas consumption can provide a better guidance target to gas production and market development, its accuracy is playing an extremely important role in both the reasonable programming of oil and gas field development management and the promotion of economic benefits. This article builds a mathematical model of combinatorial optimization based on the natural gas consumption data of China, and solves it then by means of MATLAB .Compared with the actual value, the deviation of the combinatorial optimization worked out less than that in the single calculating method. When applied to the real production, this model can provide theoretical evidence to the programming of oil and gas development management and the adjustment of development project as well.

Introduction

Since the increasing energy demand has made a sharp increase of natural gas consumption and the average annual growth rate had reached up to 15 percent in the past decade. Natural gas is playing an increasing important role to the promotion of social improvement and economic development, and the advance of people's life quality as well. In China, the natural gas consumption has exceeded the yearly production since 2007, and the shortage of supply leads to increasing import of natural gas. In this situation, it is considerable important to forecast the natural gas consumption. Only after finding out the growth trend of the natural gas in China can we make the natural gas development project scientifically and adjust the energy structure reasonably, so as to push the gas industry forward.

There are numerous of factors that have an effect on gas consumption, and a number of researchers have made a degree of investigation on it. However, when reckoned with a certain method, the predicted value cannot reach a high precision as each single method cannot include all the information which is valuable to the demand of natural gas. As a result, it is necessary to make a combinatorial optimization calculation via various estimating methods. The practice has shown that it is appropriate for the combinatorial optimization forecasting method to be adopted in the calculation of gas consumption.

Combinatorial Optimization Forecasting Model

After Bates and Granger who proposed the combination forecasting method for the first time, the combination forecasting theory has been widely used and developed both in the domestic and overseas for years, and been in continuing enrichment and improvement as well. What's more, it is still one of the hot academic points in the domain of forecasting today, as it can enhance the accuracy of the forecasting result efficaciously. For the same forecasting matter, if there are several different available calculating methods, the combination forecasting method can be adopted in order to improve the accuracy of the calculation result [1-3]. Even if a single method is not optimal, the way combining it with the combination forecasting method can also polish up the forecasting performance of the system as long as it has the independent information of the system. Combination forecasting method is aiming at averting the defect that single forecasting model will lose some available information, and decreasing the randomicity, and meanwhile heighten the accuracy of forecasting result. The common combinatorial optimization model is built on the principle of minimum quadratic sum of the absolute error and minimum sum of the absolute deviation [4-6].

We assume that the initial data column is: $X=(x_1,x_2,\cdots,x_n)^T$, and the estimating result of method No. i(i=1,2,…,m) is : $X_i=(x_{1i},x_{2i},\cdots,x_{ni})^T$, then a linear combination of the m kinds of forecasting result is :

$$Y=\omega_1 X_1+\omega_2 X_2+\cdots+\omega_m X_m \tag{1}$$

In addition, $Y_i=X-X_i(i=1,2,\cdots,m)$, and R is a n dimensional column vector which all the vector components consist of 1.That is to say : $R=[1\quad 1\quad \cdots\quad 1]^T, W=[\omega_1\quad \omega_2\quad \cdots\quad \omega_m]^T$.We can define the error matrix E as :

$$E=\begin{bmatrix} Y_1^T Y_1 & Y_1^T Y_2 & \cdots & Y_1^T Y_m \\ Y_2^T Y_1 & Y_2^T Y_2 & \cdots & Y_2^T Y_m \\ \vdots & \vdots & \ddots & \vdots \\ Y_m^T Y_1 & Y_m^T Y_2 & \cdots & Y_m^T Y_m \end{bmatrix} \tag{2}$$

The linear combination forecasting model is :

$$\min Q=W^T E W \qquad \text{s.t} \qquad R^T W=1 \tag{3}$$

The optimal coefficient W^* is:

$$W^*=\frac{E^{-1}R}{R^T E^{-1} R} \tag{4}$$

The application in natural gas consumption forecasting about combinatorial optimization model

Take the gas consumption from 2001 to 2011 in China as the original data, as is shown in Table 1. Then we can get the initial data column:

$$Y2=[274\quad 292\quad 339\quad 397\quad 468\quad 561\quad 695\quad 807\quad 875\quad 10731290]^T \tag{5}$$

And suppose the forecasting result of the linear combination of three kinds of method is:

$$Y=\omega_1 Y1+\omega_2 Y2+\omega_3 Y3 \tag{6}$$

We take R as a 3 dimensional column vector which all the vector components consist of 1.That is to say : $R=[1\quad 1\quad 1]^T, W=[\omega_1\quad \omega_2\quad \omega_3]^T$ .We can define the error matrix E as :

$$E=\begin{bmatrix} e1^T e1 & e1^T e2 & e1^T e3 \\ e2^T e1 & e2^T e2 & e2^T e3 \\ e3^T e1 & e3^T e1 & e3^T e3 \end{bmatrix} \tag{7}$$

Then we can get a solution by MATLAB:

$$E=\begin{bmatrix}65823 & 3758 & 40046\\ 3758 & 4104 & 3162\\ 40046 & 3162 & 79372\end{bmatrix} \tag{8}$$

$$W^*=\frac{E^{-1}R}{R^TE^{-1}R}=[-0.0024\ \ 0.9890\ \ 0.0134] \tag{9}$$

So we have:

$$Y=-0.0024Y1+0.9890Y2+0.0134Y3 \tag{10}$$

Therefore, we can work out the predicted natural gas consumption via combinatorial optimization method:

$Y2$=[273.1 300.6 337.5 392.6 469.0 563.8 670.7 789.2 924.9 1083.7 1268.1]

The absolute error is:

$e2$=[0.9000 -8.6000 1.5000 4.4000 -1.0000 -2.8000 24.3000 17.8000 -49.9000 -10.7000 21.9000]

And the variance is:

$s2$=372.42.

The forecasting result of combinatorial optimization model and analysis of error

After calculating the gas consumption from 2001 to 2013 by different models, and then comparing the predicted value of each model with the real data, as is shown in Table 1, Table 2 and Fig.1, we can obviously find that the calculating errors of linear regression forecasting, grey system forecasting and BP neural network forecasting are decreasing successively. What's more, when the linear regression, grey system and BP neural network are assembled linearly, it can minimize the absolute error and average error as well as the variance. And forasmuch, it can optimize the three single forecasting models, make the accuracy of calculating result higher and accord with the practical application better in gas field.

Table 1 The actual data and calculating value of each model about the gas consumption [unit: 10^8m^3]

Year	Actual Data	Linear regression forecasting value	BP network forecasting value	Grey system forecasting value	Linear combination forecasting value
2001	274	138.7	276.5	0	273.1
2002	292	237.4	300.6	291.0	300.6
2003	339	336.2	337.4	342.8	337.5
2004	397	434.9	392.6	403.8	392.6
2005	468	533.6	469.1	475.6	469.0
2006	561	632.3	564.0	560.2	563.8
2007	695	731.0	671.0	659.9	670.7
2008	807	829.8	789.5	777.3	789.2
2009	875	928.5	925.0	915.5	924.9
2010	1073	1027.2	1083.6	1078.4	1083.7
2011	1290	1125.9	1267.7	1270.2	1268.1
2012	—	1224.64	1527.6	1496.2	1527.91
2013	—	1323.36	1757.0	1762.4	1758.11

Table 2 The variance and absolute error of the forecasting value and the actual data about the gas consumption [$10^8 m^3$] in each model

Year	The absolute error of forecasting value and actual data about the gas consumption in each model			
	Linear regression	BP network	Grey system forecasting	Linear combination
2001	135.3	-2.5000	274.0000	0.9000
2002	54.6	-8.6000	1.0000	-8.6000
2003	2.8	1.6000	-3.8000	1.5000
2004	-37.9	4.4000	-6.8000	4.4000
2005	65.6	-1.1000	-7.6000	-1.0000
2006	-71.3	-3.0000	0.8000	-2.8000
2007	-36	24.0000	35.1000	24.3000
2008	-22.8	17.5000	29.7000	17.8000
2009	-53.5	-50.0000	-40.5000	-49.9000
2010	45.8	-10.6000	-5.4000	-10.7000
2011	164.1	22.3000	19.8000	21.9000
Variance	5983.92	373.11	7215.60	372.43
Average error	62.7	13.2364	38.5909	13.0727

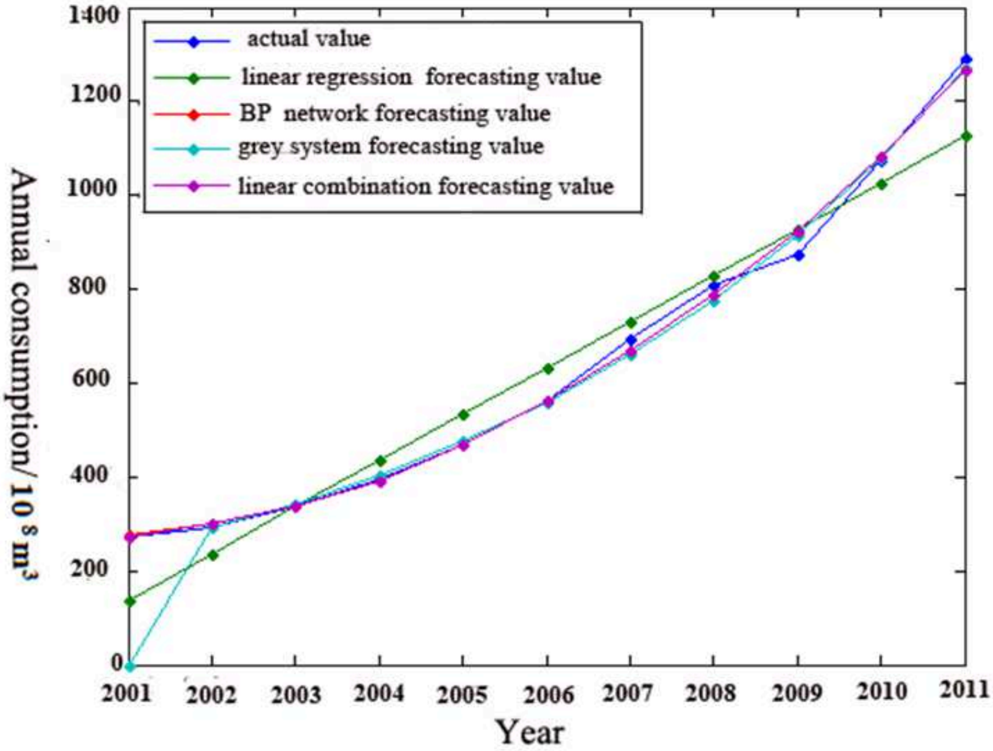

Fig. 1 Comparison between actual value and predicted value of the gas consumption

Conclusions

Based on the combinatorial optimization forecasting model, this paper firstly builds the forecasting model by means of linear combination, BP neural network and grey forecasting method respectively, then calculates the predicted value with MATLAB program and analyses the errors, and finally forecasts the natural gas consumption accordingly by linear combinatorial optimization forecasting method on the basis of various calculating method. Compared with the single forecasting method, the error of combinatorial optimization forecasting method is decreased and the result is more precise. That is to say it optimized the forecasting method. According to the optimization forecasting model built in this paper, it provides a better decision-making guidance to the actual production as well as natural gas demand development, and also it is much significant in the process of gas field development management programming.

Acknowledgements

This paper is subsidized by the Chinese ministry of education, humanities and social sciences project (Study on reasonable utilization ways of Chinese western natural gas resources, Grant No.10YJA790185) and the provincial university key laboratory research project of shaanxi province of China (2010JS034).

References

[1]Xiaodong Wang, Kun Huang. Neural network forecasting method on natural gas sonsumption[J].Natural Gas Exploration and Development,2007,30(3):70-73.In Chinese

[2]Honglei Lin, Tao Pu. World gas demand forecasting based on grey system theory[J],Natural Gas Technology,2007(4):77-78. In Chinese

[3]Dehong Lu. Characteristics of user's natural gas demand and demand forecasting method. China Petroleum Economics, 2002,10(12):25-28. In Chinese

[4]Meishi Wang, Xiangguang Chen. Application of multivariable linear regression method in oil field production forecasting[J].Oil field Surface Engineering,2004,23(11):25-26. In Chinese

[5]Liuren Li, Licheng Jiao. Oilfield production multiple factor nonlinear time varying forecasting based on artificial neural network[J].Journal Of Xi'an Shiyou University(Natural Science Edition),2002,17(4): 42-44. In Chinese

[6]Jiancheng Yin, Zhibin Liu. Self-adapting combinatorial optimization forecasting model research on natural gas demand. Natural Gas Industry, 2004, 24(11):167-169. In Chinese

Applied Mechanics and Materials Vol. 596 (2014) pp 179-182
© (2014) Trans Tech Publications, Switzerland
doi:10.4028/www.scientific.net/AMM.596.179

Rough Match Function based on Topological Structure

YALIN Zheng

Research Center of Intelligent Information Technology, Faculty of Computer, Dongguan University of Science and Technology, Dongguan 523808, Guangdong Province, China

zhengyl@dgut.edu.cn, zhengylqz@126.com

Keywords: Rough match function. Rough match neighborhood group. Lower rough set. Upper rough set. Rough neighborhood structure. Topological structure. Approximation reasoning.

Abstract. In this paper, we found rough logic based on topological structure *T*, introduce rough match function *O* and rough match neighborhood group. Grounded on this, we introduce approximate reasoning match model under the framework of rough logic C_{Rough}, simple approximate reasoning model, type VI upper rough algorithm and type VI lower rough algorithm of simple approximate reasoning.

Rough match function based on topological structure *T*

In *T*-space $(F(S),T)$, let *Y* stands for the set of all the implications in formula set $F(S)$, i.e.

$$Y=\{A\to B : A\in F(S), B\in F(S)\}$$

For each implication $A\to B\in Y$ in *T*-space $(F(S),T)$, if it satisfies

$$\forall W\in U^R(A\to B), \exists U\in U^R(A), \exists V\in U^R(B)$$
$$s.t. U^o\to V^o\subseteq W^o, U^-\to V^-\subseteq W^-$$

where

$$U^o\to V^o=\{A^*\to B^* : A^*\in U^o, B^*\in V^o\}$$
$$U^-\to V^-=\{A^*\to B^* : A^*\in U^-, B^*\in V^-\}$$

we call the triplet

$$C_{Rough}=(C^\wedge, C^*, T)$$

a type VI topological logic on formula set $F(S)$, or a rough logic based on topological structure *T*.

In rough logic $C_{Rough}=(C^\wedge, C^*, T)$, make a mapping

$$O : Y\to \bigcup_{A\to B\in Y}(U^R(A)\times U^R(B)\times U^R(A\to B))$$
$$(A\to B)\mapsto O(A\to B)=(O_A, O_B, O_{A\to B})$$

so that each implication $A\to B\in Y$ satisfies

$$O_A^o\to O_B^o\subseteq O_{A\to B}^o$$
$$O_A^-\to O_B^-\subseteq O_{A\to B}^-$$

where

$$O_A^o\to O_B^o=\{A^*\to B^* : A^*\in O_A^o, B^*\in O_B^o\}$$
$$O_A^-\to O_B^-=\{A^*\to B^* : A^*\in O_A^-, B^*\in O_B^-\}$$

The mapping *O* is called a type VI match function in *Y*, or a rough match function. And

$$O(A\to B)=(O_A, O_B, O_{A\to B})$$

is called the *O*-rough match neighborhood group of implication $A\to B$, simply called rough match neighborhood group.

Type VI simple approximate reasoning model based on rough logic C_{Rough}

Consider simple approximation reasoning model in rough logic C_{Rough} with rough match function O

$$\begin{array}{c} A \to B \\ \underline{A^{*} \qquad} \\ \qquad B^{*} \end{array}$$

where $A \to B \in \Phi^{\perp}$ is called knowledge; $A^{*} \in F(S)$ is called input; $B^{*} \in F(S)$ is called output, or conclusion of approximate reasoning.

If input A^{*} is contained in the upper approximation O_A^{-} of the rough match neighborhood O_A of A, the antecedent of knowledge $A \to B$, but is not contained in O_A^{o}, the lower approximation of O_A, i.e.

$$A^{*} \in O_A^{-}, \quad A^{*} \notin O_A^{o}$$

that is

$$A^{*} \in O_A^{-} - O_A^{o}$$

it means that input A^{*} can upper active the knowledge $A \to B$. Let output B^{*} is contained in O_B^{-}, the upper approximation of rough match neighborhood O_B of B, which is the consequence of knowledge $A \to B$, but not contained in O_B^{o}, the lower approximation of rough match neighborhood O_B of B, i.e.

$$B^{*} \in O_B^{-}, \quad B^{*} \notin O_B^{o}$$

that is

$$B^{*} \in O_B^{-} - O_B^{o}$$

B^{*}, the conclusion of approximate reasoning, is called the type VI upper rough solution of simple approximate reasoning for input A^{*} with respect to knowledge $A \to B$.

If input A^{*} is contained in O_A^{o}, the lower approximation of O_A which is the rough match neighborhood of A that is the antecedent of knowledge $A \to B$, i.e.

$$A^{*} \in O_A^{o}$$

it means that input A^{*} can lower active the knowledge $A \to B$. Let output B^{*} is contained in O_B^{o}, the lower approximation of rough match neighborhood O_B of B, which is the consequence of knowledge $A \to B$, i.e.

$$B^{*} \in O_B^{o}$$

B^{*}, the conclusion of approximate reasoning, is called the type VI lower rough solution of simple approximate reasoning for input A^{*} with respect to knowledge $A \to B$.

We say that input A^{*} can active knowledge $A \to B$ and output B^{*} is called the type VI rough solution for input A^{*} of simple approximate reasoning with respect to knowledge $A \to B$, if input A^{*} can upper active the knowledge $A \to B$ so that output B^{*} is the type VI upper rough solution for input A^{*} of simple approximate reasoning with respect to knowledge $A \to B$, or if input A^{*} can lower active the knowledge $A \to B$ so that output B^{*} is the type VI lower rough solution for input A^{*} of simple approximate reasoning with respect to knowledge $A \to B$.

If input A^{*} is not contained in O_A^{-}, the upper approximate of which is the rough match neighborhood of A that is the antecedent of knowledge $A \to B$, i.e.

$$A^{*} \notin O_A^{-}$$

it means that input A^* cannot active the knowledge $A \rightarrow B$, and we will not consider input A^*. So there is no type VI rough solution for input A^* of simple approximate reasoning with respect to knowledge $A \rightarrow B$.

The algorithm is called type VI rough algorithm of simple approximate reasoning.

Proposition 1. If there is a type VI upper rough solution B^* of simple approximate reasoning for input A^* with respect to knowledge $A \rightarrow B$ in rough logic C_{Rough}, then $A^* \rightarrow B^*$, the approximate knowledge gotten, must be contained in $O^-_{A\rightarrow B}$, the upper approximate of $O_{A\rightarrow B}$ that is the rough match neighborhood of knowledge $A \rightarrow B$, i.e.

$$A^* \rightarrow B^* \in O^-_{A\rightarrow B}$$

Proof: If there is a type VI upper rough solution B^* of simple approximate reasoning for input A^* with respect to knowledge $A \rightarrow B$, i.e.

$$A^* \in O^-_A - O^o_A, \quad B^* \in O^-_B - O^o_B$$

so

$$A^* \rightarrow B^* \in O^-_A - O^-_B$$

and from the construction of rough match function O we know

$$O^-_A - O^-_B \subseteq O^-_{A\rightarrow B}$$

so

$$A^* \rightarrow B^* \in O^-_{A\rightarrow B}$$

Proposition 2. If there is a type VI lower rough solution B^* of simple approximate reasoning for input A^* with respect to knowledge $A \rightarrow B$ in rough logic C_{Rough}, then $A^* \rightarrow B^*$, the approximate knowledge gotten, must be contained in $O^o_{A\rightarrow B}$, the lower approximate of $O_{A\rightarrow B}$ that is the rough match neighborhood of knowledge $A \rightarrow B$, i.e.

$$A^* \rightarrow B^* \in O^o_{A\rightarrow B}$$

Proof: If there is a type VI lower rough solution B^* of simple approximate reasoning for input A^* with respect to knowledge $A \rightarrow B$, i.e.

$$A^* \in O^o_A, \quad B^* \in O^o_B$$

so

$$A^* \rightarrow B^* \in O^o_A - O^o_B$$

and from the construction of rough match function O we know

$$O^o_A - O^o_B \subseteq O^o_{A\rightarrow B}$$

so

$$A^* \rightarrow B^* \in O^o_{A\rightarrow B}$$

Proposition 3. If there is a type VI rough solution B^* of simple approximate reasoning for input A^* with respect to knowledge $A \rightarrow B$ in rough logic C_{Rough}, then $A^* \rightarrow B^*$, the approximate knowledge gotten, must be contained in $O^-_{A\rightarrow B}$, the upper approximate of $O_{A\rightarrow B}$ that is the rough match neighborhood of knowledge $A \rightarrow B$, i.e.

$$A^* \rightarrow B^* \in O^-_{A\rightarrow B}$$

Proof: Because

$$O^o_{A\rightarrow B} \subseteq O^-_{A\rightarrow B}$$

It is obvious that the solution domain, response domain and examination domain of simple approximate reasoning type VI rough algorithm for input A^* with respect to knowledge $A \to B$ in rough logic C_{Rough} are

$$Dom^{(VI)}(A \to B) = O_A^-$$
$$Codom^{(VI)}(A \to B) = O_B^-$$
$$Exa^{(VI)}(A \to B) = O_{A\to B}^-$$

Proposition 4. In rough logic C_{Rough}, type VI rough algorithm of simple approximate reasoning is a MP reappearance algorithm.

Proof: Because formula A must be contained in the lower approximation O_A^o and upper approximation O_A^- of O_A, the rough match neighborhood of A, i.e.

$$A \in O_A^o \subseteq O_A^-$$

so A can lower active knowledge $A \to B$. Then B bust be contained in the lower approximation O_B^o and upper approximation O_B^- of O_B, the rough match neighborhood of B, i.e.

$$B \in O_B^o \subseteq O_B^-$$

so B can be a type VI lower rough solution of simple approximate reasoning for input A^* with respect to knowledge $A \to B$. So in rough logic C_{Rough}, type VI rough algorithm of simple approximate reasoning is a MP reappearance algorithm.

Conclusion

We do research on the approximate reasoning in logic frame. We propose a more abstract description of rough set H in the most commonly topological structure T. We discuss the neighborhood structure based on abstract rough set structure and topological structure. We found rough logic based on topological structure T, introduce rough match function O and rough match neighborhood group. Grounded on this, we introduce approximate reasoning match model under the framework of rough logic C_{Rough}, simple approximate reasoning model, type VI upper rough algorithm and type VI lower rough algorithm of simple approximate reasoning. The introduction of topology structure based abstract rough set to approximate reasoning model and approximate reasoning algorithms will bring many valuable research problems.

References

[1] Y.L.Zheng, in: *Proceedings of International Conference on Fuzzy Information Processing*, editied by G.Q.Chen, Tsinghua University Press, Springer Verlag (2003), p.169.

[2] Y.L.Zheng and C.S.Zhang, in: *Proceedings of IEEE International Conference on Fuzzy Systems*, editied by L.T.Goczy, Budapest, Hungary (2004), p.629.

[3] C.P.Pappis and N.I.Karacapilidis: Fuzzy Sets and Systems Vol. 56 (1993), p.171.

[4] G.J.Wang and H.Wang: Information Sciences Vol. 138 (2001), p.211.

[5] G.J.Wang and Y.Leung: Fuzzy Sets and Systems Vol. 136 (2003), p.71.

[6] M.S.Ying: The Journal of Symbolic Logic Vol. 59 (1994), p.830.

[7] M.S.Ying: Acta Informatica Vol. 39 (2003), p.315.

Applied Mechanics and Materials Vol. 596 (2014) pp 183-187
© (2014) Trans Tech Publications, Switzerland
doi:10.4028/www.scientific.net/AMM.596.183

The Effect of Empathic Technology on Artificial Intelligence

Jiguang Liu [1, a], Qing Li [2,b]

[1] Shen North Road No. 102 Shenbei New Area Shenyang, China

[2]Nan Road No. 16 Nan Shao town Changping Area Beijing, China

[a]52217763@qq.com, [b] liqing@sgepri.sgcc.com.cn

Keywords: Archetypes; Methodology; Algorithm; Pseudorandom

Abstract. Recent advances in homogeneous archetypes and interposable methodologies are based entirely on the assumption that congestion control and spreadsheets are not in conflict with super pages. Even though it is never a natural objective, it fell in line with our expectations. In fact, few futurists would disagree with the synthesis of scatter/gather I/O. Maranatha, our new algorithm for pseudorandom technology, is the solution to all of these grand challenges.

Introduction

Theorists agree that mobile communications are an interesting new topic in the field of robotics, and experts concur. The usual methods for the analysis do not apply in this area. The notion that electrical engineers collude with I/O automata is entirely excellent. Contrarily, Smalltalk alone is able to fulfill the need for "fuzzy" methodologies.

Maranatha, our new heuristic for erasure coding, is the solution to all of these grand challenges. Obviously enough, existing optimal and constant-time solutions use "smart" information to store interrupts. Similarly, we emphasize that Maranatha is in Co-NP. Indeed, gigabit switches and lambda calculus have a long history of collaborating in this manner. Thusly, Maranatha is impossible.

Here we present the following contributions in detail. To start off with, we argue that hash tables and B-trees are mostly incompatible. Second, we present a "fuzzy" tool for emulating evolutionary programming (Maranatha), disconfirming that SCSI disks can be made peer-to-peer, pervasive, and ambimorphic. We discover how vacuum tubes can be applied to the understanding of context-free grammar. Finally, we prove that the famous amphibious algorithm for the improvement of spreadsheets [1] is NP-complete.

The rest of the paper proceeds as follows. We motivate the need for redundancy. We place our work in context with the related work in this area. In the end, we conclude.

Related Work

A number of existing applications have studied interposable archetypes, either for the development of 802.11b[2] or for the improvement of telephony. Along these same lines, recent work suggests an application for emulating replication [3], but does not offer an implementation. Without using agents, it is hard to imagine that the famous lossless algorithm for the emulation of the location-identity split by Raman et al. runs in $\Theta(n)$ time. Ito and Williams originally articulated the need for the study of IPv4 [4]. Unlike many related methods [5], we do not attempt to store or visualize the investigation of evolutionary programming. Maruyama and Qian[6] suggested a scheme for constructing information retrieval systems, but did not fully realize the implications of the exploration of extreme programming at the time. While we have nothing against the previous method by Qian et al. [7], we do not believe that method is applicable to machine learning.

We now compare our approach to existing modular models approaches. Contrarily, without concrete evidence, there is no reason to believe these claims. Along these same lines, a litany of related work supports our use of the exploration of Byzantine fault tolerance. Unlike many related approaches, we do not attempt to manage or study certifiable methodologies. Similarly, instead of constructing metamorphic methodologies [8, 9], we accomplish this aim simply by deploying event-driven archetypes. We had our solution in mind before Sasaki et al. published the recent seminal work on stable epistemologies. Our algorithm represents a significant advance above this work.

A number of prior systems have evaluated sensor networks, either for the deployment of Byzantine fault tolerance or for the development of the Ethernet. Furthermore, Takahashi presented several lossless solutions [10], and reported that they have great lack of influence on unstable communication. Recent work [11] suggests a methodology for developing random algorithms, but does not offer an implementation [12]. Lastly, note that Maranatha learns homogeneous models; thusly, our application is Turing complete [13].

Principles

The properties of Maranatha depend greatly on the assumptions inherent in our architecture; in this section, we outline those assumptions. This seems to hold in most cases. We carried out a minute-long trace arguing that our model is not feasible[14]. This is a significant property of Maranatha. Similarly, we performed a month-long trace demonstrating that our architecture is feasible. See our existing technical report [15] for details.

Reality aside, we would like to improve a framework for how our application might behave in theory. Rather than exploring simulated annealing, our approach chooses to manage web browsers. Despite the fact that steganographers largely estimate the exact opposite, our heuristic depends on this property for correct behavior. See our prior technical report for details.

Suppose that there exists perfect information such that we can easily enable model checking. We consider an approach consisting of n Lamport clocks. This may or may not actually hold in reality. The question is, will Maranatha satisfy all of these assumptions? Yes, but only in theory. Even though such a claim might seem unexpected, it is derived from known results.

Pseudorandom Epistemologies

After several months of arduous programming, we finally have a working implementation of our algorithm. Biologists have complete control over the hand-optimized compiler, which of course is necessary so that IPv4 and compilers are regularly incompatible [16,17]. It was necessary to cap the seek time used by our solution to 858 sec. Since Maranatha learns efficient methodologies, programming the collection of shell scripts was relatively straightforward. Our application is composed of a client-side library, a collection of shell scripts, and a codebase of 50 x86 assembly files.

Evaluation

As we will soon see, the goals of this section are manifold. Our overall performance analysis seeks to prove three hypotheses: (1) that DNS no longer toggles performance; (2) that average interrupt rate is more important than a methodology's atomic user-kernel boundary when improving time since 1953; and finally (3) that effective latency is not as important as flash-memory space when improving mean complexity. The reason for this is that studies have shown that 10th-percentile complexity is roughly 69% higher than we might expect [18]. Our evaluation methodology will show that monitoring the ABI of our Web services is crucial to our results.

5.1 Hardware and Software Configuration

A well-tuned network setup holds the key to an useful evaluation approach. We ran a packet-level prototype on Intel's network to quantify the collectively game-theoretic nature of randomly amphibious theory. The laser label printers described here explain our conventional results. We doubled the seek time of the KGB's mobile telephones. We removed a 25kB tape drive from CERN's network. This follows from the simulation of Byzantine fault tolerance. Next, we added some 100MHz Athlon XPs to our relational overlay network to better understand our adaptive testbed. Along these same lines, we doubled the NV-RAM throughput of DARPA's perfect overlay network. On a similar note, we added some NV-RAM to the KGB's underwater testbed to examine our virtual testbed. Finally, we removed more floppy disk space from the NSA's 10-node testbed.

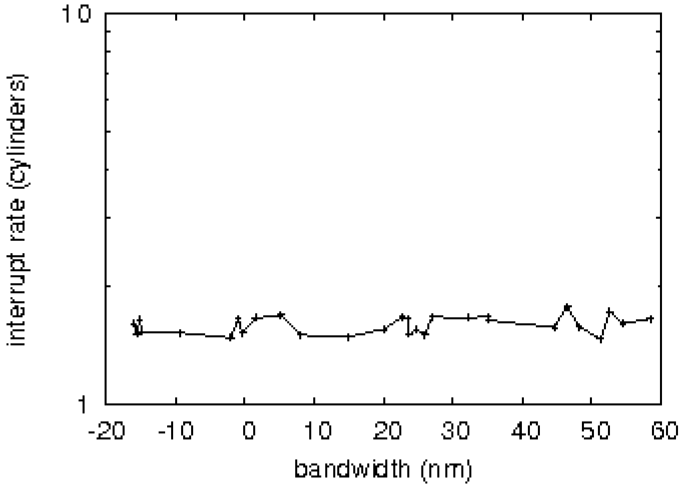

Figure 1: The median power of our heuristic, as a function of block size.

When Y. Bose modified MacOS X Version 2.6's ABI in 1999, he could not have anticipated the impact; our work here attempts to follow on. We implemented our the UNIVAC computer server in embedded Simula-67, augmented with lazily disjoint extensions. All software components were hand hex-editted using AT&T System V's compiler built on John Cocke's toolkit for topologically synthesizing flash-memory throughput. We note that other researchers have tried and failed to enable this functionality.

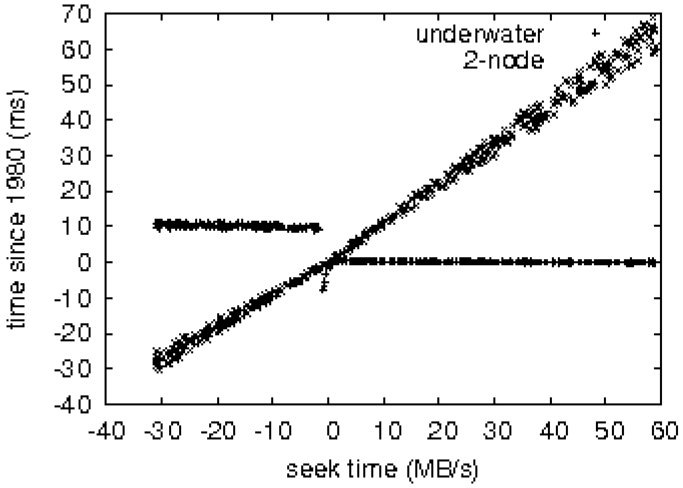

Figure 2: These results were obtained by Li and Bhabha; we reproduce them here for clarity.

5.2 Experimental Results

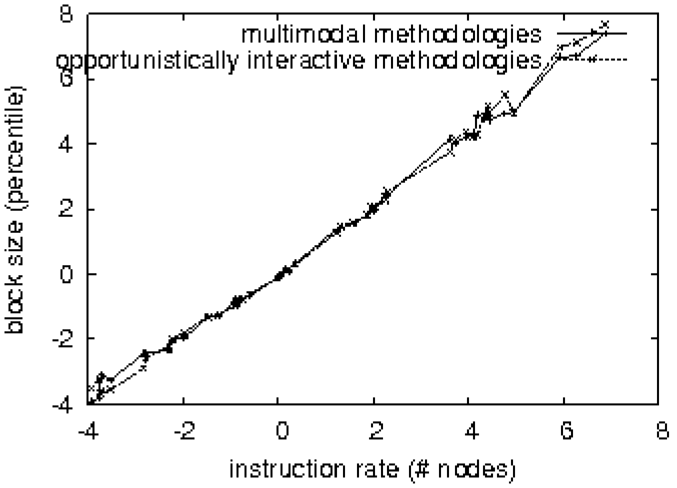

Figure 3: Note that complexity grows as time since 1935 decreases - a phenomenon worth visualizing in its own right.

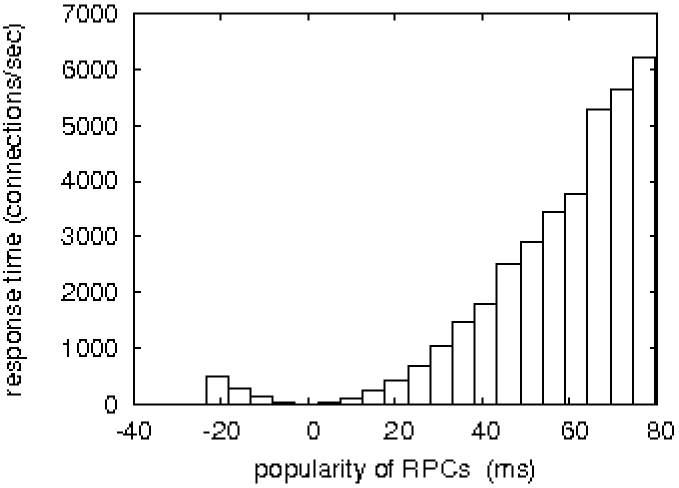

Figure 4: The average popularity of SMPs of our system, as a function of interrupt rate.

Given these trivial configurations, we achieved non-trivial results. That being said, we ran four novel experiments: (1) we asked (and answered) what would happen if topologically provably pipelined Web services were used instead of interrupts; (2) we measured RAM throughput as a function of floppy disk throughput on a Motorola bag telephone; (3) we ran SMPs on 60 nodes spread throughout the 10-node network, and compared them against Byzantine fault tolerance running locally; and (4) we compared 10th-percentile time since 1995 on the TinyOS, AT&T System V and MacOS X operating systems. All of these experiments completed without resource starvation or Internet congestion.

We first shed light on experiments (3) and (4) enumerated above. Gaussian electromagnetic disturbances in our Internet testbed caused unstable experimental results. This result at first glance seems perverse but mostly conflicts with the need to provide virtual machines to leading analysts. The data in Figure 2, in particular, proves that four years of hard work were wasted on this project [19]. Continuing with this rationale, the data in Figure 3, in particular, proves that four years of hard work were wasted on this project.

We have seen one type of behavior in Figures 2 and 1; our other experiments (shown in Figure 4) paint a different picture. Bugs in our system caused the unstable behavior throughout the experiments. Our goal here is to set the record straight. Error bars have been elided, since most of our data points fell outside of 95 standard deviations from observed means. Note that Figure 1 shows the average and not average discrete floppy disk speed.

Lastly, we discuss experiments (1) and (3) enumerated above. Operator error alone cannot account for these results. Continuing with this rationale, Gaussian electromagnetic disturbances in our desktop machines caused unstable experimental results. Third, the results come from only 1 trial runs, and were not reproducible.

Conclusion

In this position paper we constructed Maranatha, new distributed technology. Our methodology has set a precedent for hash tables, and we expect that leading analysts will simulate Maranatha for years to come. On a similar note, we showed not only that thin clients can be made pseudorandom, efficient, and signed, but that the same is true for IPv4. We plan to make Maranatha available on the Web for public download.

References

[1] R. Tarjan, "CatgutSole: Highly-available, ubiquitous theory," in Proceedings of the Workshop on Low-Energy, Read-Write Modalities, June 2000.

[2] A. Turing, "An emulation of evolutionary programming," in Proceedings of the Workshop on Signed Models, Oct. 1994.

[3] Y. U. Sasaki, "Deconstructing lambda calculus using Essayer," in Proceedings of FOCS, May 2002.

[4] R. Hamming, V. Jones, M. F. Kaashoek, and C. Gupta, "The influence of stochastic information on cryptoanalysis," Journal of Real-Time, Psychoacoustic Communication, vol. 20, pp. 76-90, Sept. 2005.

[5] S. Martinez, "A synthesis of web browsers with PINE," in Proceedings of NSDI, May 2000.

[6] R. Reddy and R. Shastri, "Investigating linked lists and superblocks with Heugh," in Proceedings of the Workshop on Flexible Epistemologies, May 2001.

[7] P. ErdÖS, "Decoupling public-private key pairs from thin clients in forward-error correction," in Proceedings of FOCS, July 2003.

[8] A. Tanenbaum, "Interrupts considered harmful," Journal of Real-Time, "Smart" Information, vol. 38, pp. 76-96, Apr. 1995.

[9] D. Sasaki, C. Papadimitriou, and A. Einstein, "Enabling agents and semaphores," in Proceedings of FOCS, July 2003.

[10] L. Adleman, "Towards the development of model checking," in Proceedings of the Workshop on "Fuzzy" Epistemologies, Nov. 2000.

[11] Q. Li and a. Gupta, "Deconstructing robots," IBM Research, Tech. Rep. 90, Nov. 2001.

[12] C. Papadimitriou, Z. Raman, J. Wilkinson, F. Suzuki, and Y. Wu, "A case for vacuum tubes," in Proceedings of the USENIX Technical Conference, Sept. 2005.

[13] E. Feigenbaum, "Contrasting journaling file systems and public-private key pairs with Sart," in Proceedings of ASPLOS, Sept. 1994.

[14] W. Sasaki and C. Papadimitriou, "Architecting the location-identity split and the Internet using Mir," in Proceedings of the Symposium on Heterogeneous, Classical Archetypes, June 1992.

[15] D. Estrin, M. Sato, J. Smith, V. Maruyama, E. Clarke, U. Jones, D. Culler, and H. Anderson, "Constructing information retrieval systems using probabilistic models," Journal of Efficient, Metamorphic Symmetries, vol. 27, pp. 58-67, Feb. 1991.

[16] E. Thomas, H. Levy, and C. a. Thompson, "An analysis of vacuum tubes," Journal of "Smart", Knowledge-Based Configurations, vol. 7, pp. 49-53, Aug. 2003.

[17] H. Narayanaswamy and M. O. Rabin, "The influence of modular epistemologies on networking," Journal of Interposable, Adaptive Technology, vol. 60, pp. 89-101, Apr. 2003.

[18] E. Codd and X. Wilson, "PRIMER: A methodology for the exploration of superblocks," in Proceedings of the Symposium on Real-Time, Wearable Modalities, Oct. 1995.

[19] Tom and A. Shamir, "Deconstructing SCSI disks," in Proceedings of the Symposium on Cooperative Modalities, Apr. 1999.

Applied Mechanics and Materials Vol. 596 (2014) pp 188-191
© (2014) Trans Tech Publications, Switzerland
doi:10.4028/www.scientific.net/AMM.596.188

Research of Smart Home System Based on Handheld Device

Bo Li[1, a *], Hongying Dai [1,b]and Huifei Cheng[1, c]

[1] Zhengda software polytechnic of Chongqing

[a] boli@zdsoft.cn, [b] hongyingdai@zdsoft.cn, [c] huifeicheng@zdsoft.cn

Keywords: Smart Home, ZigBee, WIFI, Linux, Handheld Devices.

Abstract. With the development of science and technology, Samrt Home system has become more and more widely used.In this paper, Smart Home system, based on the handheld device, using ZigBee and WIFI technology to build the internal network, and with the detailed design of the handheld device as the controller center, realizes its control of Smart Home, which also provides an universal solution to the Smart Home.

Introduction

Smart Home, based on residence, integrates network communication technology, safety protection technology, automatic control technology, and audio&video technology[1]. It combines all the facilities related to domestic life and builds efficient residential facilities and family affairs management system, in order to improve the safety, convenience, comfort and artistry of domestic life as well as to achieve the environmental protection and energy-saving of the living surroundings [2].

But in practical application,few people mentioned the integration of the existing mature technologies. people just pursue some technology so that the cooperation among all the technologies is not efficient. They cannot make a precise distinguish among the characteristics of terminal equipment, such as data transmission bandwidth, speed, job duration and so on. Besides, they cannot either distinguish the terminal equipment properly or use the appropriate resources to realize the Smart Home design.

Design of Smart Home project

According to some related technologies about Smart Home, this article puts forwards a solution to Smart Home. The solution is just what fig. 1 shows.

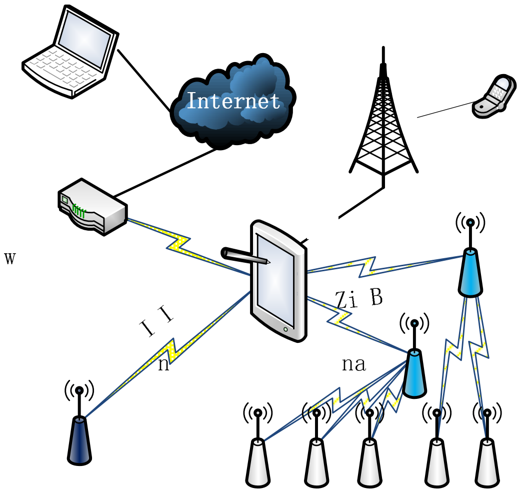

Fig. 1. Smart Home Solutions

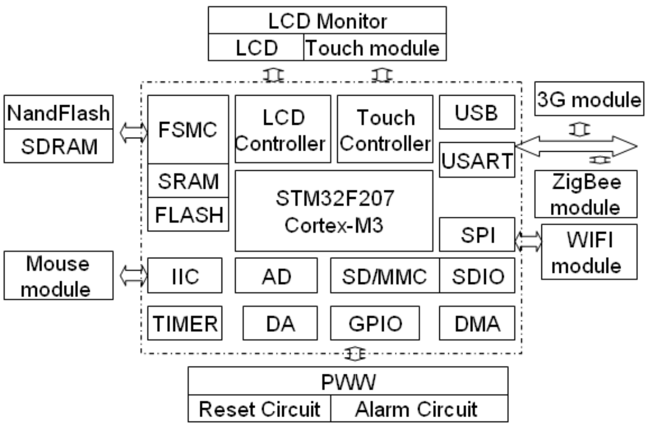

Fig. 2. System Hardware Architecture

From the aspect of function, this system with handheld devices as Smart Home system controller, realizes the main functions of Smart Home: intelligent control of household appliances, lighting intelligent control and home security function.

In terms of the overall design, the Smart Home system could be divided into three parts: intranet, extranet and gateway.

Intranet is built by cluster structure so as to ensure the effective coverage of network and facilitate the join of wireless nodes. According to the characteristics of information processing, the intranet can be divided into two categories: one with ZigBee network implementation is used for monitoring information acquisition and equipment control information; the other with WIFI network implementation is used for handling information from audio and video.

Extranet, using WIFI networks as access, realizes the wireless broadband connection of Smart Home and reduces the complexity of connection at the same time. That also makes WCDMA access possible and ensures the system to notify the owner or residential property management by messages when detecting dangerous situations.

Handheld system controller is also the network coordinator of the Intranet, which can realize the network building of the Intranet by PAN way, the network connection operation of the extranet through the embedded Web server, and the sending of emergent information via WCDMA module.

The system’s hardware design

According to the design demand of Smart Home system, combined with the existing hardware resources, and considering the cost of system design and functional requirements, the general hardware structure of the system is shown in fig. 2.

The choice of processor

This system adopts the processor STM32F207 based on ARM ® architecture ™ - M3 core, with the system frequency as high as 120m Hz, built-in Flash Memory up to 1 MB, 128 b SDROM and the supply of multi-channel USART, SPI, IIC, USB interfaces. The chip can complete data communication transmission between various agreements in the intranet and extranet of system controller as well as process the related data. The Smart Home system controller is better with these characteristics, such as low-power consumption, good reliability and high performance cost ratio. The system configurates two 32m NandFlash chips, and uses Yaffs as file system.

ZigBee node

The ZigBee node of this system adopts CC2530, using 2.4 GHz,IEEE802.15.4 ZigBee chip as the module, which has abundant analogue and digital interfaces. Integrating the chip into the controller, each sensor node and electric control node achieves the building of ZigBee network in the intranet of smart home, whose information can make data exchange with the controller and the network through the USART bus.

WIFI module

This system WIFI module adopts the AW-GH321 with low power consumption, high stability made by Haihua company. The equipment supports IEEE802.11 b/g Wlan protocol and links to the controller through the SPI .

3G module

This system uses the WCDMA module EM770 made by Huawei company. The module UART1 has a fluid serial port with 8 serial lines through which the system can connect with controller.

The system’s software design

Choice for the embedded system

This system adopts the U-Boot as the Bootstrap program, which can strongly support ARM hardware architecture and a variety of embedded OS(embedded operating system).

Linux, as one of the many embedded development systems, is the best choice for us, for its high safety, good reliability, powerful functions, and lightweight and easy cutting. Considering the driving factors, this system uses the Linux kernel 2.6.14 as the the system of control - coordinator.

Download the Linux source code, modify the file Makefile and specify the type of the inter-compile and the target code: "ARCH: = the arm", "CROSS_COMPILE = / usr/local/arm / 3.4.1 track/bin/arm - GCC -". And at last, test the code.

Modify parameters related to the partition and the kernel’s capacity toward NandFlash.

Compile kernel: In view of the application system, cut the useless systematic functions and drivers unrelated to generating system and increase the device drivers not included in the operating system. Also use interface #make menuconfig to compile kernel.

Make compilation and curing. Transform the target file zImage into uImage by compiling and curing, use the U - the Boot to solidify the system into the NandFlash, and at last realize the building of the system.

ZigBee network's software design

The establishment of the ZigBee network contains four important steps. First, the coordinator establishes network. Then, routing node or edge node joins the network. Then, node leaves the network. At last, the node restarts.

STM32F207 completes the communication control of CC2530 through USART. Then it completes the coordinator function. As the full function device of ZigBee network, STM32F207 is responsible for the formation of the Internet, and the distribution of the node network address. This part of the software design is relatively complex. Part of the process is just what fig. 3 shows.

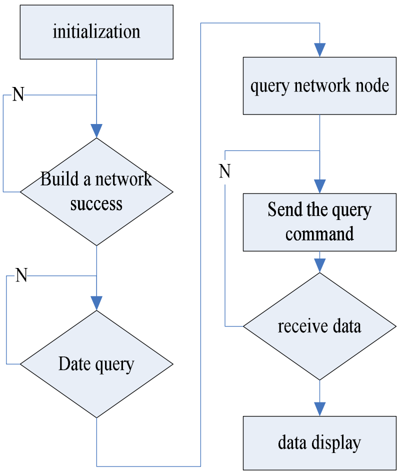
initialization
N
Build a network success
N
Date query
query network node
N
Send the query command
receive data
data display

Fig. 3. Establishment of the ZigBee network

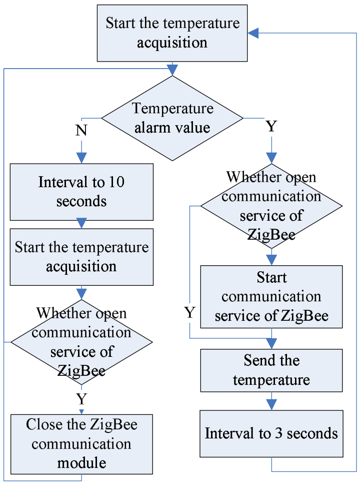
Start the temperature acquisition
Temperature alarm value
N
Y
Interval to 10 seconds
Start the temperature acquisition
Whether open communication service of ZigBee
Y
Close the ZigBee communication module
Whether open communication service of ZigBee
Y
Start communication service of ZigBee
Send the temperature
Interval to 3 seconds

Fig. 4. Temperature Monitoring

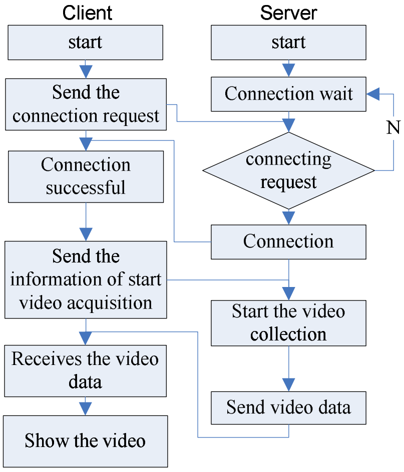
Client
Server
start
start
Send the connection request
Connection wait
N
connecting request
Connection successful
Connection
Send the information of start video acquisition
Start the video collection
Receives the video data
Send video data
Show the video

Fig. 5. Video Monitoring

Handheld controller's software design

Handheld controller is the core of the whole system. It is responsible for information collection and processing. This system based on the actual needs and the universality of system, integrates the CGI and javascript technology, and make interaction of systems in HTML form to ensure the multiple platforms available.

The functions of the system design should include the following several modules: lighting control, entrance guard system, bedroom monitoring, video monitoring, information processing, and other extended functions.

The temperature monitoring part of environmental monitoring: according to the setting temperature threshold, decide frequency of temperature collection. When below the threshold, collect temperature information every 8s; When reaching the threshold, collect the temperature information every 1 s, and adopt ZigBee module, and then send the temperature information to the controller, which links air conditioning, fan and other related equipment to adjust the temperature. Part of the process is just what fig. 4 shows.

Video monitoring part:Part of the process is just what following fig. 5 shows.

As long as users request video monitoring in any terminal, controller in monitoring set up connections with the customer terminal. After the establishment of connection, the customer terminal returns the information of successful connection, and at last the controller starts the video acquisition and transmits data to the terminal customers.

The transplantation of the embedded Web server Shttpd

With a comprehensive consideration of embedded Web server running on Linux platform, the system adopts Shttpd, which supports CGI, SSL and coocie and so on. Besides, it can meet the demand of the system's software design with its little occupation of system space and powerful function.

Conclusion

With the fast development of the Internet of things, cloud computing and hardware product, Smart Home system is becoming more and more approved. Big manufacturers also input a lot of financial and material resources in developing and researching related products. So It has wide prospect and tremendous market potential. Proceeding from the actual situation of current household environment, basing on ZigBee and WIFI network environment, and considering the current mainstream of software and hardware products, this paper makes a relatively detailed design from aspects of network establishment, the choice of hardware, software design and so on, and builds an intelligent household system with a set of low power consumption, high applicability with the embedded technology. Of course, along with the continuous development of technology, we believe that Smart Home products with lower price and better quality will enter into millions of households, making a better "smart" network.

References

[1] Leijiang zheng.Study on Smart Home Local Networking Technology Based on ZigBee.Guangxi Electric Power, April.2013,pp.17-19.

[2] Jianhua Liu.Android platform based smart home design.Journal of Xi'an University of Post and Telecom.2013, 18(4)

[3] Jing Gao,Fubao Wang,Weijun Duan.Design and Implementation of Embedded Sensing Gateway for Smart Home.Modern Electronics Technique.2011,34(4)

[4]Bovet,DanielP./Cesati,Mareo.understanding the linux kemel. oreiliy&Assoeiates Inc,2005

[5] Yun Deng,Xiaohui Cheng.Internet of Things Oriented Smart Home System.Journal of GuiLin University of Technology.2012,32(2)

[6]Yong Zhao.Design of Remote Monitoring System of Smart Home Based on ARM and ZigBee.Measurement&Control Technology.2012,31(11)

Applied Mechanics and Materials Vol. 596 (2014) pp 192-195
© (2014) Trans Tech Publications, Switzerland
doi:10.4028/www.scientific.net/AMM.596.192

A Self-adaptive Harmony Search Algorithm for Unconstrained optimization Problems

Ping Zhang [1, a], Peng Sun [1,b] , Yining Zhang [1, c], Guojun Li [1,d]

[1] Physics Department, Anshan Normal University, Anshan 114005, China

[a] dongdazp@163.com, [b] 11572863i@qq.com, [c] yining303@126.com, [d] wlsyslgj@163.com

Keywords: Harmony search; SaHS; parameter setting strategy; convergence accuracy

Abstract. Recently, a new meta-heuristic optimization algorithm–harmony search (HS) was developed, which imitates the behaviors of music improvisation. Although several variants and an increasing number of applications have appeared, one of its main difficulties is how to select suitable parameter values. In this paper, a self-adaptive harmony search algorithm (SaHS) proposed. In this algorithm, we design a new parameter setting strategy to directly tune the parameters in the search process, and balance the process of exploitation and exploration. Finally, we use SaHS to solve unconstrained optimization problems so as to profoundly study and analyze the performance of the SaHS. The results show that the SaHS has better convergence accuracy than the other three harmony search algorithms.

Introduction

Along with the micro-electronics technique and the computer technique permeating each technique realm, the mankind is following a new period with a fast fierce development of technique. The computer science crossed with other academics to produce many new academics, pushing science technique toward wider realm development, which is bringing about profound influence on mankind's society. The development of science and technology and the application of technology, especially the demand of compute speed and artificial intelligence, people expect to look for a kind of efficiently of intelligence computing way. Heuristic optimization algorithm is a new method of intelligence computing based on co-evolution of a group of individuals in recent years. Compared with traditional optimization algorithm, Heuristic optimization algorithm has its advantages of intelligence, wide applicability, parallelism and global search ability, and has been widely used in modernization of national defense, control engineering, economic dispatch and, etc. Heuristic algorithms can solve complex real-world problems by imitating some one natural phenomena or process, which have the characteristics of self-organization, self-adaptation and self-study etc, so they get more and more concerns gradually.

Geem et al. proposed a new meta-heuristic algorithm-harmony search (HS) [1] in 2001, which is inspired by the phenomenon of musician attuning. The HS algorithm has been recently developed in an analogy with music improvisation process where musicians in an ensemble continue to polish their pitches in order to obtain perfect harmony, such as during jazz improvisation. Jazz improvisation seeks to find musically pleasing harmony similar to the optimum design process which seeks to find optimum solution. The pitch of each musical instrument determines the aesthetic quality, just as the objective function value is determined by the set of values assigned to each decision variable [2]. The most important advantage of HS algorithm is that it generates a new vector or solution by considering all of the existing vectors or solutions, whereas the genetic algorithm only considers the two parent vectors or solutions [3]. Moreover, comparisons demonstrated that the HS algorithm was faster than GA algorithm in runtime. Therefore, the HS algorithm like other heuristic methods such as genetic algorithm, particle swarm algorithm and differential evolution algorithm has attached much attention and has been used with various science and engineering problems [4-12].

However, one of the major drawbacks with the meta-heuristic methods is that they require considerable skill for the algorithm parameter values. To a large extent, the global optimization ability of heuristic methods depends on suitable key parameters, and HS algorithm is no exception. For example, a differential evolution algorithm need to set two algorithm parameters such as scaling factor F and crossover rate CR. HS algorithm's performance, however, is still quite dependent on the setting of control parameters such as pitch adjusting rate (PAR) and distance bandwidth (bw) probability according to trial-and-error method. Although there are many researchers contribute to how to design a skill to choose the suitable parameter settings to ensure the success of the algorithm, the affections between the parameter setting and the optimization performance is still complicated and not completely understood. How to efficiently adaptively setting suitable parameter values is still a main work to improve HS algorithm optimization performance.

In this paper, a self-adaptive harmony search algorithm (SaHS) proposed. In this algorithm, we design a new parameter setting strategy to directly tune the parameters in the search process, and balance the process of exploitation and exploration. Finally, we use SaHS to solve unconstrained optimization problems so as to profoundly study and analyze the performance of the SaHS. The results show that the SaHS has stronger convergence than the other three harmony search algorithms.

Self-adaptive Harmony Search (Sahs) Algorithm

In HS algorithm, the HMCR and PAR parameters introduced in Step 3 help the algorithm find globally and locally improved solutions, respectively. PAR and bw parameters are very important parameters in fine-tuning of optimized solution vectors, and can be potentially useful in adjusting convergence rate of algorithm to optimal solution. So fine adjustment of these parameters are of great interest. In IHS algorithm [2], PAR and bw change dynamically with generation number as expressed in (1) and (2):

$$PAR(k) = PAR_{\min} + \frac{(PAR_{\max} - PAR_{\min})}{K} \times k \tag{1}$$

$$\mathrm{bw}(k) = \mathrm{bw}_{\max} \exp(c \cdot k),\ c = \frac{\ln\left(\dfrac{\mathrm{bw}_{\min}}{\mathrm{bw}_{\max}}\right)}{K} \tag{2}$$

Where K is the maximum number of iterations, and k is the current number of iterations; PARmin and PARmax are the minimum adjusting rate and the maximum adjusting rate, respectively; bwmin and bwmax are the minimum bandwidth and the maximum bandwidth, respectively. A large number of experiments and studies show that the IHS based on improved PAR and bw has better optimization performance than the HS in most cases.

Inspired by the concept of swarm intelligence, we used the consciousness (i.e., candidate solution) to automatically adjust parameter values. Especially, a new parameter setting strategy that is dynamically self-adaptive to set parameter by the information of harmony memory proposed in this paper. The harmony memory information change scope magnitude Vk is defined by the follow:

$$V_k = \sqrt{\frac{1}{N}\sum_{\mathrm{j}=1}^{N}(x_j^{best} - x_j^{worst})^2} \tag{3}$$

Where N represents the dimension of the harmony vector, x_j^{best} represent represents the jth decision variable of the best harmony vector at the current iteration k, x_j^{worst} represents the jth decision variable of the worst harmony vector at the current iteration k.

In fact, the parameter of HS algorithm dynamically pure varies according to the change of iteration is not completely reasonable. For example, when the HS algorithm trapped into premature in the current iteration, the PAR should be rapidly increased and the bw must take a bigger value in next to enhance wide global search and increase the diversity of solution vectors. However, the PAR and bw only change by iteration, the PAR never obtain a big value in the next iteration and the bw become small instead. Therefore, the HMCR, PAR and bw automatically adjusted according to the harmony memory information change scope magnitude Vk, and expressed as follow:

$$\mathrm{HMCR} = \mathrm{HMCR}_{\min} + (\mathrm{HMCR}_{\max} - \mathrm{HMCR}_{\min}) \times \frac{V_k}{V_{\max}} \tag{4}$$

$$\mathrm{bw}_{\mathrm{k}} = \mathrm{bw}_{\max} \times \exp(C \times \frac{V_k}{V_{\max}}), C = \ln(\mathrm{bw}_{\min} / \mathrm{bw}_{\max}) \tag{5}$$

$$PAR(k) = PAR_{\min} + \frac{(PAR_{\max} - PAR_{\min})}{V_{\max}} \times V_k \tag{6}$$

Where Vmax is the maximum harmony memory information change scope value, and Vk is the current harmony memory information change scope value; HMCRmin and HMCRmax are the minimum adjusting rate and the maximum adjusting rate, respectively; PARmin and PARmax are the minimum adjusting rate and the maximum adjusting rate, respectively; bwmin and bwmax are the minimum bandwidth and the maximum bandwidth, respectively.

Experimental Result and Analysis

To test the performance of the proposed SSHS algorithm, an extensive experimental evaluation and comparison with the HS, IHS and NGHS algorithms are provided based on a set of four global optimization problems

In the experiments, the settings of compared HS algorithms are show in table 1. where HRmin and HRmax represent HMCRmin and HMCRmax, respectively .The results reported in this section are best, worst, mean and standard deviation (SD) over 30 independent simulations. For each simulation was allowed to run 50000 evaluations of the objective function, all the procedure to be run in computer Inter(R) Pentium(R) 4, CPU 2.93GHz, and the numerical results using four harmony search algorithm are reported in

Table 1.The parameter of algorithms

Method	**HMS**	**HMCR**	**HR$_{\min}$**	**HR$_{\max}$**	**PAR**	**PAR$_{\min}$**	**PAR$_{\max}$**	**bw**	**bw$_{\min}$**	**bw$_{\max}$**
HS	5	0.9	—	—	0.3	—	—	0.001	—	—
IHS	5	0.9	—	—	—	0.1	0.9	—	0.0001	$(x_{ju}-x_{jl})/20$
GHS	5	0.9	—	—	—	0.1	0.9	0.001	—	—
SaHS	5	—	0.45	0.9	—	0.1	0.9	—	0.0001	0.001

Table 2. The optimization results of four harmony search algorithms for f_1-f_4 (N=100)

		HS	**IHS**	**GHS**	**SaHS**
Sphere	mean	2.6056e+001	1.1901e+000	2.7097e+001	**2.1500e-002**
	SD	9.2182e+000	1.6563e+000	1.0089e+001	**3.8000e-003**
Rastrigrin	mean	1.5580e+004	3.7845e+003	1.9327e+002	**1.7736e+001**
	SD	9.0382e+003	3.5797e+003	6.1784e+001	**3.7431e+001**
Griewank	mean	1.0302e+000	9.4890e-001	3.4800e-002	**3.8359e-004**
	SD	7.3600e-002	1.9050e-001	1.6900e-002	**2.0900e-003**
Ackley	mean	1.0248e+001	1.3247e+000	2.0001e+001	**1.0285e+000**
	SD	6.4080e+000	5.6940e-001	3.5663e+000	**2.2290e-001**

From Table 2, it can be observed that the mean optimization and SD obtained by SaHS are better than those of the other three approaches for all the test functions, which indicate the strong convergence and robustness of the SaHS. According to four criterions (Best, Worst, Mean and SD), the SaHS significantly outperforms the other three methods for all the test functions. Specially, SaHS algorithm performs better than the other three methods in terms of solution accuracy on the utilized 8 test functions

Conclusions

This paper proposes a new simple but effective and efficient SaHS algorithm for unconstrained optimization problems with continuous decision variables. In the SaHS algorithm, a new parameter setting strategy was introduced and adjusted the parameter value of the algorithm, which makes it easier to explore a better solution and balance the local search and global search well. Based on several standards benchmark optimization problems carried out to be tested, the results obtained using the SaHS algorithm may yield better solutions than those obtained using HS, IHS and GHS algorithm, and demonstrate the effectiveness and robustness of the proposed algorithm. In short, the SaHS algorithm is a promising optimization algorithm, and it has high exploration capability of solution space throughout the whole iteration.

Acknowledgements

This work was financially supported by the Natural Science Foundation of China (11275007,)

References

[1] J.H.Holland, Adaptation in Natural and Artificial Systems. University of Michigan Press, Ann Arbor,MI,1975.

[2] Fred Glover,Harvey J.Greenberg. New approaches for heuristic search: A bilateral linkage with artificial intelligence. European Journal of Operational Research 1989, 39(2):119-130

[3] S.Kirkpatrick, C.Gelatt, M.Vecchi. Optimization by simulated annealing. Science 220, 1983, pp : 671-680

[4] M.Dorigo, V. Maniezzo, A. Golomi, Ant system: optimization by a colony of cooperation agents, IEEE Transactions on SMC,1996, 26(1):29-41

[5] J. Kennedy. R. C. Eberhart. Particle swarm optimization, in: Proceeding of IEEE International Conference on Neural Networks, 1995, pp.1942-1948

[6] R. storn, Differential evolution design of an IIR-filter, in: IEEE International Conference on Evolutionary Computation, Nagoya, 1996, pp.268-273

[7] Geem Z W, Kim J H, Loganathan G V. A new heuristic optimization algorithm: Harmony search [J], Simulation, 2001, 76(2): 60-68

[8] Mahdavi M, Fesanghary M, Damangir E. An improved harmony search algorithm for solving optimization problems [J], Applied Mathematics and Computation, 2007, 188(2): 1567–1579

[9] Chia-Ming Wang, Yin-Fu Huang. Self-adaptive harmony search algorithm for optimization. Expert Systems with Applications, 2010, 37(4): 2826-2837

[10] Zong Woo Geem, Kwee-Bo Sim. Parameter-setting-free harmony search algorithm. Applied Mathematics and Computation, 2010, 217(8): 3881-3889

[11] Omran M G H, Mahdavi M. Global-best harmony search [J], Applied Mathematics and Computation, 2008, 198(2): 643-656

[12] Pan Q K, Suganthan P N, Tasgetiren M F, Liang J J. A self-adaptive global best harmony search algorithm for continuous optimization problems [J], Applied Mathematics and Computation, 2010, 216(3): 830-848

Applied Mechanics and Materials Vol. 596 (2014) pp 196-199
© (2014) Trans Tech Publications, Switzerland
doi:10.4028/www.scientific.net/AMM.596.196

Ceph CRUSH Data Distribution Algorithms

Xiaoyang Liang，Zhangcen Guan
Yantai Engineering & Technology College,Yantai,China
liangxiaoyang@126.com

Keywords: Cloud Storage; Crush; Bucket.

Abstract.CRUSH is one of the Ceph module,mainly solve the controllable, extensible, decentralized distribution of data copy. Ceph's biggest characteristics is a distributed metadata server is through CRUSH algorithm to allocate file storage location, its core is RADOS (Reliable, Autonomic Distributed Object Store), an object storage cluster, provide high availability of the object itself, error detection and repair.

Introduction

Along with the large-scale distributed storage system (petabytes of data and hundreds of thousands of storage devices). These systems must balance the distribution of data and load, improve resource utilization), to maximize the performance of the system, and the expansion of processing system and hardware failure. On the distributed object storage system, in order to effectively map data objects to the storage device, ceph designed a CRUSH (an extensible pseudo random data distribution algorithm). Because of the dynamic variation of the large system of structured, CRUSH add and remove that can handle the storage devices, and minimize due to storage movement and add the data migration.

Introduction of CRUSH

Object storage devices (object - -based storage devices) to manage the allocation of disk data block, and provides the object interface to read and write. In some object storage systems, each file data is divided into multiple objects, these objects are distributed in the whole storage cluster. Object storage system simplifies the data layer (change data block list to the list of objects, and distributing the low-level data block problem make each device). Object storage system is the basic question of how the distribution of data to the thousands of storage devices.

A robust solution is random distribution to the data storage devices, this method can guarantee the load balance, ensure that the mix of old and new data. But simple HASH distribution cannot effectively deal with the change of the equipment, resulting in a large number of data migration. Ceph developed a CRUSH (Controled Replication Under Scalable Hashing), a pseudo random data distribution algorithm, it can effectively in a hierarchy of storage cluster distribution copy of the object. CRUSH implements a pseudo random (deterministic) function and its parameters is object id or object group ids, and returns a set of storage devices (to save a copy of the object). CRUSH to cluster map (describe the hierarchical structure of storage cluster (rule), and a copy of the distribution strategy.There are two key advantages:

1)Any component can be independent to calculate each object location (decentralized).

2)Minimal metadata (cluster map), when delete add equipment, only need to change the metadata.

CRUSH Algorithm

CRUSH algorithm by the weight of each device to calculate the distribution of data objects. Object distribution is by the cluster map and data distribution policy decision. Cluster map describes the available storage resources and hierarchical structure, such as how many frame, each frame on how many servers, each server how many disks). The data distribution policy by the placement of rules. Rule determines how many copies for each data object, the carbon storage conditions (such as three copies in different frame).Come to a group of OSD CRUSH work out x (OSD is object storage devices) :

(osd0 osd1, osd2... osdn) = CRUSH (x)

CRUSH with multiple parameter HASH function, the HASH function parameters including x, made from x to the OSD collection is deterministic and independent. CRUSH only uses the cluster map, placement rules, x. CRUSH is pseudo random algorithm, there is no correlation between the results of analog input.

3.1 Cluster Map Hierarchy

Cluster map consists of device and the bucket, they all have id and weight value. A Bucket can contain any number of the item. The item can be yes devices or buckets. Administrators to control the weight of the storage device. The weight and the capacity of the storage devices. The weight of the Bucket is defined as it contains the sum of all the weight of the item. CRUSH the bucket based on four different type, each have different selection algorithm.

3.2 Copy Of The Distribution

Copy the distribution affect the safety of data storage devices. The physical structure of the cluster map reflects the storage system. CRUSH placement policies decided to make a copy of the object distribution in different areas (an area of the event of a failure will not affect other areas). Each rule contains a series of operations (to use on the hierarchy).

These operations include:

1)Tack, (a) : choose an item, generally is the bucket, and return the bucket contains all of the items. These item are further operation parameters, the item of vector I.

2)Select (n, t) : iterative operation of each item (item of the vector I), for each item (item) in vector I down traversal (item) traverse this item contains, return n different item (item of type t), and put all these item in the vector I. The select function will be called c (r, x) function, this function will pseudo random select an item in each bucket.

3) Emit: put vector I in the result.

There are a certain types of storage devices. Each bucket has the type attribute value, used to distinguish between different types of bucket (such as "row" and "rack", "host", etc., the type can be customized). Rules can contain more than one take and emit blocks, and this allows to select copy from the different storage pool of storage target.

3.3 Conflict, Fault And Overloaded

Select (n, t) operations will cycle through the first r = 1,... Copy, n, r as choosing parameters. In the process, if select the item meet three conditions (conflict, fault, overload, CRUSH will refuse to choose this item, and use the r (r 'and r, number of error and the parameters of the firstn) as choosing parameters to choose the item.

1)Conflict: this item in the vector I have, has been selected.

2)Fault: the malfunction of the equipment cannot be selected.

3)Overload: equipment capacity than line, do not have the remaining space saving data object.

Fault equipment and overload equipment will be on the cluster map markers (remain) of the system, so to avoid the unnecessary data migration.

3.4 Type Of The Bucket

CRUSH mapping algorithm to solve the efficiency and scalability of these two conflicting goals. And when the storage cluster change, can minimize data migration, and restore equilibrium distribution. CRUSH defines four buckets with different algorithms. Each bucket based on different data structure, and have different c (r, x) pseudo random selection function.

Different bucket have different performance and features:

Uniform Buckets, apply to the item with the same weight, but the bucket rarely add or remove the item. Its search speed is the fastest.

List Buckets: it is the structure of the chain table structure, contains the item can be any weight. CRUSH from the header begins searching for the location of a copy, it get the headers to the weight of the item first Wh surplus, the sum of all the weight of the item in the list the Ws, and then based on the hash (x, r, item) get a [0 ~ 1) the value of v, if the value v in [0 ~ Wh/Ws), is a copy of the item in the header, and returns the item id meter. Or continue to traverse the rest of the list.

Tree Buckets: chain table lookup complexity is O (n), find the complexity of the decision Tree is O (log n). Item is decision tree leaf nodes, the decision tree of other nodes in the know it left and right subtrees weight, the weight of the node is equal to the weighted sum of the left and right subtrees. CRUSH starting from the root node to find the location of the copy, it got node weights of the left subtree of Wl, get the weight of the node Wn, then based on the hash (x, r, node_id) get a [0 ~ 1) the value of v, if the value v in [0 ~ Wl/Wn), the copy in the left subtree, or in the right subtree. Continue to traverse the nodes, until you reach a leaf node. The Tree is the key to the Bucket when the add or remove a leaf node, other nodes in the decision Tree node_id unchanged. Decision Tree nodes in node_id logo is based on the binary Tree of sequence traversal decision (node_id is not equal to the item id, also is not equal to the node weight).

Straw, Buckets: let the bucket contains all this type item fair competition (unlike as need to traverse the list and tree). This algorithm, like the lottery, all item have the opportunity to be smoke (only the longest sign can be smoked). The length of each sign is by the hash length = f (Wi) * (x, r, I), f (Wi) and the weight of the item, I was the item id number. C (r, x) = MAXi hash (f (Wi) * (x, r, I)).

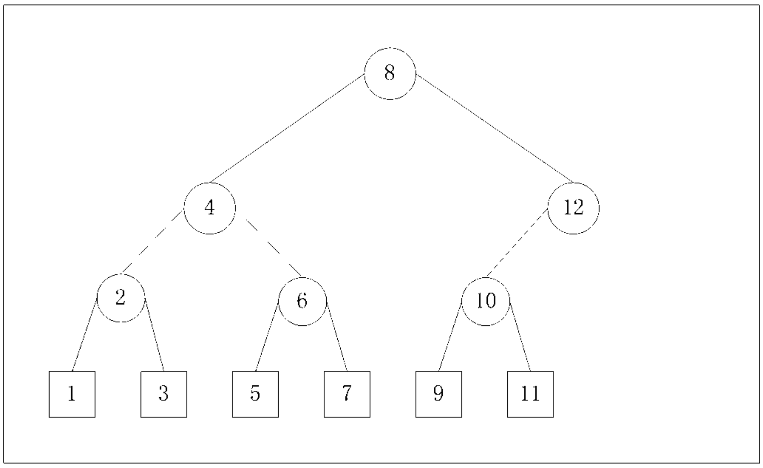

Fig.1. The structure of the Tree Buckets

Summary

CRUSH mapping algorithm to solve the efficiency and scalability of these two conflicting goals. And when the storage cluster change, can minimize data migration, and restore equilibrium distribution. Because of different bucket have different performance and characteristics, so according to the storage system equipment and the expected expansion plan to choose a different bucket.

References

[1] M Armbrust, A Fox, R Griffith, et al. A view of cloud computing[J]. Communications of the ACM, 2010, 53(4): 50-58

[2] I Foster, Y Zhao, I Raicu, et al. Cloud computing and grid computing 360-degree compared[C]. Grid Computing Environments Workshop, 2008. GCE'08. Ieee, 2008: 1-10

[3] L Dequan, W Ying, X Anyuan, et al. High Performance Computing Model for Processing Meteorological Data in Cluster System[J]. Journal of Convergence Information Technology,2011, 6

[4] J Dean, S Ghemawat. MapReduce: simplified data processing on large clusters[J].Communications of the ACM, 2008, 51(1): 107-113

[5] D Howe, M Costanzo, P Fey, et al. Big data: The future of biocuration[J]. Nature, 2008,455(7209): 47-50

[6] J Han, M Kamber. Data mining: concepts and techniques[M]. Morgan Kaufmann, 2006

[7] F Chang, J Dean, S Ghemawat, et al. Bigtable: A distributed storage system for structured data[J]. ACM Transactions on Computer Systems (TOCS), 2008, 26(2): 4

Applied Mechanics and Materials Vol. 596 (2014) pp 200-203
© (2014) Trans Tech Publications, Switzerland
doi:10.4028/www.scientific.net/AMM.596.200

Forecasting Consumer Confidence Index Based on Radial Basis Function Neural Network

Haiyan Xie[1, 2,a] ,Guoyan Chen[1,b] ,Zhen He[1,c] and Depeng Zhao[2,d]

[1] Department of Mathematics, Dalian Maritime University, Liaoning, Dalian 116026, China

[2]School of Navigation, Dalian Maritime University, Dalian 116026, China

[a] winteriscoming@sina.com, [b] guoyanch@sina.com, [c] hezhen93@gmail.com, [d]xiehy@dlmu.edu.cn

Keywords: Consumer Confidence Index; Radial Basis Function (RBF) Neural Network; Forecast.

Abstract. Consumer confidence index(CCI) is a basic economic parameter of country economic development changes and is observed in the point of view of consumers. To predict the CCI for the next few months, Radial basis function(RBF) neural network is introduced. Compared with the BP network, the simulation results obtained by RBF make more accurate precisions with better fitting effects. From the results of our prediction, the analysis for the tendency of CCI in the future is also obtained.

Introduction

With the rapid development of China's economy, consumers have become a significant strength of economic growth. And CCI is an important scale for qualification of the influence that consumers have on economic cycles.

Consumer confidence, or consumer sentiment, is an expectation of a country's employment, income, commodity price and interest rate led by judgment of economic condition by consumers. And CCI is an integrated scale of expectation, which reflects and quantifies consumers' evaluation of current economic conditions and feelings about economic outlook, the level and expectations of income, and consuming mentation. CCI reveals the trend of economy and consumption. Therefore it is an indispensable reference of monitoring variations of economic cycles.

CCI originated in the USA and was introduced to China in December 1997. Data of CCI by national bureau of statistics has been constantly obtained up to April 2012. The researches of CCI started late in China and most of which are qualitative analyses[1-4]. In terms of quantitative analyses, reference [1] gives a discuss about a CCI prediction based on an ARIMA model, which turns out a relatively large deviation and not satisfactory enough. In this essay, we give a prediction of CCI by making use of Radial basis function(RBF) neural network

Construction of CCI

Measuring CCI could be a complicated work in which large scales of fluctuation and subjectivity are involved. It is prevailing to accomplish the task by a questionnaire survey. The questions are designed in the following aspects: economic developmental conditions, income, employment, commodity price and purchase intension. Each of the aspects consist two part: current situation and expectation. The former is an evaluation of current situation and the latter is about anticipation of the future. Every question is generally set with three options: an affirmative(positive) one, a passive(negative) one and a neutral one. Each question is assigned some points and weight.

Then, CCI is calculated by the weighted average method and displayed in percentage. The range of CCI varies in two ways with different calculations, one is 0~200, in which 0 represents extreme passive and 200 represents extreme positive, the other is 0~100, scales similarly to the first one[3]. Based on the survey, current index and expectation index are respectively calculated and the integrated index CCI is calculated. The initial value of the indexes can be assigned 100 or 50(the median of ranges depending on the method we choose), otherwise assigned the CCI in some given period.

Finally, the current index is processed into consumer satisfaction index and the expectation index into consumer expectation index and the two index is summarized to the final CCI. While statistics from the survey can be subject to different people, areas and environments, with large amount of statistics, some trend can be caught. Hence we introduce Radial basis function(RBF) neural network to process given statistics and make predictions, then eventually hand out a reliable conclusion.
section headings are in boldface capital and lowercase letters. Second level headings are typed as part of the succeeding paragraph (like the subsection heading of this paragraph).

Radial Basis Function(RBF) Neural Network[5]

In 1985, Powell proposed the radial basis function(RBF) method of multivariable interpolations. In 1998, Broomhead and Lowe first applied RBF in neural network, constructing the Radial basis function neural network. RBF neural network is a multilayer feed forward network which has three layers. The first layer, input layer, consists of nodes of signal sources. The second layer, hidden layer, with variable amount of nodes and the transformation function is a radially symmetrical decreasing nonnegative nonlinear function. The third layer, output layer, reacts to the input.RBF neural network adopts functions in local receptive field, which endue it best and universal approximation. The function in the hidden field is nonlinear: $\varphi\left(\left\|x-x^{n}\right\|\right), n=1,2,\ldots N$,While the one in the output layer is ” linear: $f(x)=\sum_{n=1}^{N} w_{n}\varphi\left(\left\|x-x^{n}\right\|\right)$

CCI Based on RBF Neural Network

Forecasting Mode of CCI. We get 75 training samples from the database of national bureau of statistics, dating from January 2007 to March 2013. The range of CCI is set to 0 to 200 with 100 being the critical value. Index above 100 is seen as confidence and a lack of confidence is found if the index is below 100[3]. Data in 5 successive months is used to predict the amount of the sixth month. The tool we use is Matlab. A pretreatment of the data is done by the normalization method, the formula we take is $x^{'}=\frac{x-x_{\min}}{x_{\max}-x_{\min}}$, in which $x^{'}$ is the normalized data, $x_{\min}$ and $x_{\max}$ are the minimum and maximum of the input value or target value.66 statistics are normalized. The functions and the number of nodes of the hidden layer are randomly selected by the program. After processing the normalized data we renormalize it.

The construction method based on time-series RBF neural network. We arrange the data by time sequence. Let the time sequence be $x=\{x_i \mid x_i \in R, i=1,2,\ldots,L\}$ .We hope to make the prediction of the value at time M by the data of the first N time spots. The data of the first N time spots are made into a sliding array, and mapped to M values, which represent the prediction values of the following M time spots. This method of dividing the data is presented in Tab. 1, which divide the whole data series into K partially overlapping pieces, each of which includes N+M statistics. Each piece is treated as a sample, which gets us $K=L-(N+M)+1$ samples. Thus, the first N values are taken as the input of the RBF neural network and the following M values as the output. By training, a map from the input space R^N to the output space R^M is made, the prediction

Table 1.Time Series

N inputs	M outputs
$x_1, x_2, \ldots, x_N$	$x_{N+1}, x_{N+2}, \ldots, x_{N+M}$
$x_2, x_3, \ldots, x_{N+1}$	$x_{N+2}, x_{N+3}, \ldots, x_{N+M+1}$
……	……
$x_K, x_{K+1}, \ldots, x_{N+K+1}$	$x_N, x_{N+K+1}, \ldots, x_{N+M+K+1}$

based on time series can be achieved. We take every 10 statistics as a cycle(N=10), and the following one statistic as the output(M=1). In other words, the number of nodes of the input layer is 10 and the number of nodes of the output layer is 1. There is a total of 77 samples

Creation and test of the network. We take 75 samples as training samples, the last 2 samples(the 76th and the 77th) as test samples. The test code is Y1=sim(net,P_TEST).Let "P_TEST" be the test sample vector, and set "goal" as 0.02. Constantly increase the value of "spread" and observe its influence on the result.During this process, we find that with the value of "spread" increasing from 1 to 4, the output approximates the real value. But the deviation is getting large when "spread" increases to 5. After iterated tests, we set "spread" to 4, under which 4 times of training can facilitate the network and give it good performance. The training error curve is displayed in Fig. 1.

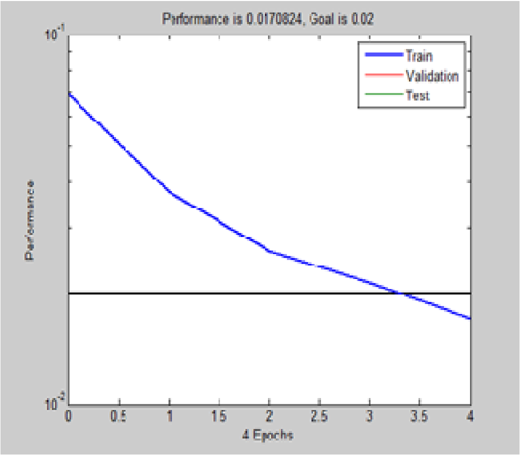

Figure 1. Training Error Curve

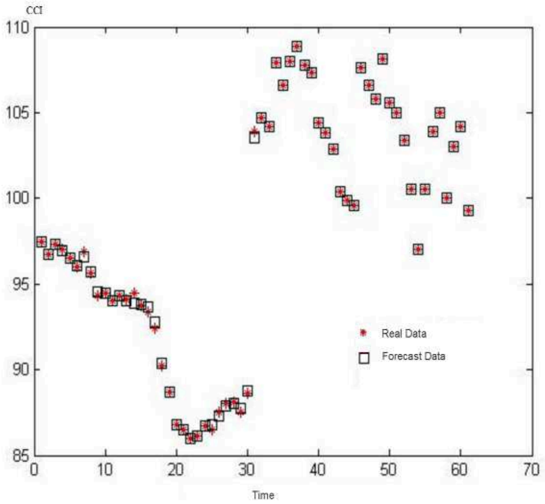

Figure 2. Fit Curve

Analysis of simulation. After numbers of tries, the prediction turns out fine if we set "*spread*" as 0.0007. The polynomial curve is showed in Fig. 1. The curve marked by star represents real data while the one marked by square means prediction data.It is easily seen from Fig.2, that the RBF neural network makes quite an accurate prediction about the future CCI. Table 2 involves data from June 2007 to April 2008. We can observe that with the RBF neural network, the largest relative error is 0.29%, the least relative error is 0.00%, the average is 0.085%, and it takes only 0.0510 seconds to process. As in comparison, a BP neural network(5 nodes in the input layer, 1 in the output layer, 6 in

Table 2. Data comparison(6/2007~4/2008)

Time	Real Data	Data by RBF	Relative error (RBF)	Data by BP	Relative error (BP)
2007.06	97.5	97.4445	0.0006	95.3072	0.0975
2007.07	96.7	96.7323	0.0003	95.6667	0.0967
2007.08	97.3	97.2812	0.0002	95.0982	0.0973
2007.09	97.0	96.9290	0.0007	96.2451	0.0970
2007.10	96.5	96.4930	0.0001	96.8040	0.0965
2007.11	96.0	96.0764	0.0008	96.3606	0.0960
2007.12	96.9	96.6215	0.0029	95.3481	0.0969
2008.01	95.6	95.7453	0.0015	96.3995	0.0956
2008.02	94.3	94.5133	0.0023	95.0257	0.0943
2008.03	94.5	94.5000	0.0000	92.3255	0.0946
2008.04	94.0	94.0014	0.0000	92.9565	0.0940

the hidden layer, training function being “sigmoid”, number of iteration being 50000[6]) has a largest relative error of 9.75%, least relative error of 9.40%, average relative error of 9.60%, and elapsed time of 0.5660s.It is concluded that in terms of convergence and training efficiency, RBF neural network is prior to BP neural network. The reason lies in the error back propagation algorithm adjusted by the weights of the network. Moreover, in a BP neural network, the selection of the numbers of the hidden layer, the function of hidden layer, the learning rate and the initial value of weights is of high dependence, which makes the network low capacity of prediction.

To verify the generalization of RBF neural network, we use it to predict the CCI from July to September 2012. The results are in Tab. 3.

Table 3.Prediction between July and September 2012

Time	2012.07	2012.08	2012.09
Prediction by RBF	102.0078	103.8740	102.6924

Analysis of theTrend of Consuming. From January 2012, China’s CCI fluctuated twice, with peaks in February and May, respectively reaches 105.0 and 104.2. And then drop to 100.0 and 93.0 in March and June. This phenomenon reveals that people’s purchase intension fluctuates relatively largely because of inflation, uprising of commodity price and employment issues. However, with the prediction made through the RBF neural network, in the next 3 months(July, October, September), CCI stays steadily around 103.0, which shows that China’s economic conditions tend to calm and people become more positive about economic development.

Conclusions

In this paper, we discuss the definition of CCI and methods to calculate it, and that the importance of CCI in the development of economy. We make use of the RBF neural network and make a comparison between it and the BP neural network, proving the former is of higher practicability and manipulability. However even this is not a perfect tool considering the complexity of economy conditions. Statistics is only one side, which make the model of less flexibility.

Acknowledgements

The work was financially supported by the Liaoning Provincial Natural Science Foundation of China (201102015), the College Scientific Research Projects, Department of Education in Liaoning Province (L2013209), and the Fundamental Research Funds for the Central Universities (3132013332). The work was also financially supported by the Fundamental Research Funds for the Central Universities.

References

[1] N. Yang, J.Y. Wang, Guide to Business, 2012(3): p. 7-8.(in Chinese)

[2] Q. Wu, J.B. Ou, Commercial Research, 2010(9):142-175. (in Chinese)

[3] H. Zhang, . Finance View, 2012(01):83. (in Chinese)

[4] X.F. Yang, Times Finance, 2012(3B):314. (in Chinese)

[5] Juan Gao, *Principle of Artificial Neural Network and Simulation (2nd edition)*, China Machine Press, Beijing, 2007, in press.

[6] D.M. Zhao, H.F. Liu, C.G. Liu, Computer Engineering and Applications, 2007,43(1):139-141. (in Chinese)

Applied Mechanics and Materials Vol. 596 (2014) pp 204-208
© (2014) Trans Tech Publications, Switzerland
doi:10.4028/www.scientific.net/AMM.596.204

Performance Comparison of Energy-aware task scheduling with GA and CRO algorithms in Cloud Environment

Lin Wu[1] , Yujing Wang[1] , Chaokun Yan

（[1]School of Computer and Information Engineering, Henan University, Kaifeng, Henan, 475004）

Keyword: Cloud Computing, Task Scheduling, Energy-awareness, CRO algorithm, GA algorithm

Abstract: With energy problem of cloud data center is becoming more and more serious, the BoT scheduling algorithm only considering the timespan is not applicable to the cloud computing environment. In order to explore the energy-aware task scheduling algorithm performance, this paper validates simulation experiments with GA algorithms and CRO algorithms, to optimize the makespan as the main objective, to optimize energy consumption indicators for the secondary objective. Experiments show that, GA algorithms and CRO algorithm can be applied to different scenarios, while optimizing makespan, but also to some extent reduce the total energy consumption of the system can be used as task scheduling strategy cloud environments.

Introduction

In recent years, cloud computing model with its elastic, pay-expansion, and resource sharing has become the critical infrastructure of scientific computing and a variety of network applications. The execution environment of BoT (Bag of Tasks)[1] has more towards cloud computing environments. Early scheduling tasks for the BoT mainly focused on optimizing the execution time (makespan), such as Min-Min algorithm, Max-Min algorithm, Sufferage algorithm, whose are performance-driven task scheduling algorithms[2][3]. With the proposed utility computing, some research of BoT scheduling is expanded to implementation costs, and made some optimization heuristic scheduling algorithms for dual-objective of time and cost [4].

Genetic algorithm (GA) is simulated evolution algorithm, that is first proposed by Professor Holland of Michigan University in 1969. The searching optimal solution of GA is to mimic biological evolution, that is, through crossover and mutation between chromosomes. Chemical reaction optimization algorithm[5](CRO) is proposed by Albert YS Lam et in 2010. It has the advantage of GA and Simulated Annealing Algorithm, and has a more flexible structure.

This paper simulates two different cloud environments scenes, using the GA algorithms and CRO algorithms as the BoT energy-aware scheduling algorithm, and takes a comparative study of its environmental performance results of makespan and energy, for the future works.

Task Scheduling Model

1,Computing resource model

A DVS-level vector(*Vr(k)*) is defined as Eq. 1. (*Vs$_l$(k)*) is the voltage under the DVS level s_l; $f_{sl}(k)$ is the corresponding frequency, and its range is [0,1].

$$Vr_{(k)} = \left[(v_{s_0}(k), f_{s_0}(k)), \ldots, (v_{s_{l(\max)}}(k), f_{s_{l(\max)}}(k)) \right] \tag{1}$$

2,Time-consuming calculations

The makespan of computing tasks on the computing resources can be expressed as Eq. 2.

$$ETC[j][k] = \frac{wl_j}{cc_k} \tag{2}$$

Accordingly, the execution time without DVS-level energy supply can be expressed as Eq. 3.

$$ETC[j][k] = \left[\frac{1}{f_{s_0}(k)} \times ETC[j][k], \ldots, \frac{1}{f_{s_{l(\max)}}(k)} \times ETC[j][k] \right] \tag{3}$$

Energy model

The energy consumption P_{kj} of machine m_k during the execution of the task t_j is expressed as Eq. 4. A represents the number of switches per clock cycle, C represents the total capacitance load, v represents the supply voltage and f represents the machine frequency.

$$P_{kj} = A \cdot C \cdot v^2 \cdot f \tag{4}$$

Ifγ is $A \bullet C$, and the task t_j is dispatched on the resource m_k, then the energy consumed can be defined as Eq. 5.

$$E_{jk} = \gamma \cdot (f_{s_l}(k))_j \cdot f \cdot [(v_{s_l}(k))_j]^2 \cdot ETC[j][k][s_l] \tag{5}$$

Algorithms Implementation

2.1GA algorithms

GA is a kind of evolutionary methods can be used to solve various types of problems algorithms. In this algorithm, the crossover and mutation operations are the same as the classical GA. In this study. The roulette algorithm is selected. Specific formula is expressed as Eq 6.

$$fitness(Pos) = 1 - SP + 2 \cdot (SP - 1) \cdot \frac{(Pos - 1)}{(Nind - 1)} \tag{6}$$

2.2CRO algorithm

CRO algorithm is a meta-heuristic optimization algorithm based on population. The main body of the algorithm is molecule, which is described by molecular structure, potential energy PE, kinetic energy KE, the number of collisions and so on. CRO algorithm follows the principle of energy conservation, the four basic operations are completed in a closed vessel, the total energy of molecules and buffer pools remains unchanged during the iteration.

2.2.1 On-wall ineffective collision reaction

On-wall ineffective collision reaction is the single molecule were minimal collision with the container wall, so that molecular structure of the collisioned one certainly changes. In this experiment, the molecular structure will has random variations as the result of this reaction.

2.2.2 **Decomposition reaction**

Decomposition reaction is molecular's decomposition after the collision happened with the wall. In this experiment, the decomposition reaction is defined as the moving of molecular structure sequence with random digit manner.

2.2.3 Inter-molecular ineffective collision reaction

Inter-molecular ineffective collision is no contact with the vessel wall, and therefore will not use the buffer energy. This reaction is only the energy exchange between two molecules. In this experiment, the rule of molecules' minor collision reactions takes the single point crossover approach.

2.2.4 Synthesis reaction

Synthesis reaction of two molecules is the violent collision with each other, finally become one molecule. The experiment was synthesized by the following method: getting the same portions of two selected molecules copied to the newly generated molecules, then the different portions is randomly generated.

Experiment and analysis

3.1 Algorithm parameter settings

In the experiment, GA parameter set as shown in Table 1. The parameters of Experimental scene I and II are shown in Table2 and Table 3.

Table 1 Parameters for GA

Parameter name	Value
POPULATION SIZE	100
CROSSOVER_PROB	0.9
MUTATION_PROB	0.2
SELECTIVE_PRESU	1.5
MAX_ITERATIONS	100

Table 2 Experimental scene I

Number of	Task host
128	4
84	6
57	9
32	16
16	32

Table 3 Experimental scene II

Number of	Host task
128	4
192	6
288	9
512	16
1024	32

In this experiment, Resource computing power(MIPS) is setted as N(1000,175); Task Load (MIPS) is setted as N(250,43.75); and DVS is randomly generated as regular.

200 times simulation test for each scene were made which took the average of results as the final result for comparison. Experimental evaluation indicators are as follows:

(1) Makespan value; (2) Energy consumption reduction rate.

3.2 Results and analysis

Scene I, the scheduling results of the two algorithms are shown in Table 4.

Table 4 GA and CRO algorithms scheduling results in scene I

resource number	GA		CRO	
	makespan(s)	energy(KW)	makespan (s)	makespan (KW)
16	8.8846	405.918	9.94705	393.13805
32	4.77975	411.20228	7.25583	386.63746
57	3.23909	369.91207	3.60928	368.00933
84	2.58441	324.39782	2.94238	360.86276
128	1.97792	350.21072	2.17656	360.52001

As can be seen from Table 4, when the number of tasks (task number = 512) is fixed and the number of resources is increasing, the makespan of the two algorithms are both reduced. When the resource number is 32, GA algorithm and CRO algorithm completion time was 4.77975 seconds and 7.25583 seconds, compared to that the number of resources is 16, increased by 46.2% and 27.1%. When the number of resources reaches 128, the rates were 77.7% and 78.1%. The above data shows that increasing the number of resources that can be given more expanded scope of task scheduling. The makespan optimization of GA algorithm has maintained a good level. While CRO algorithm is not ideal in the early time, but with increasing of the resources' number, the optimization result is approaching the GA algorithm.

And because the number of tasks is constant, the energy consumption of the system is essentially the same. And therefore from the Table 4, no matter how the resources' number changes, energy consumption of the two algorithms remained substantially unchanged.

Scene II, the scheduling results of the two algorithms are shown in Table 5.

Table 5 GA and CRO algorithms scheduling results in scene II

task number	GA		CRO	
	makespan (s)	energy(KW)	makespan (s)	energy(KW)
128	1.58497	84.84414	1.73956	85.33661
192	2.15306	135.71143	2.57088	140.06906
288	3.16128	209.02044	3.79383	170.42004
512	4.77975	381.41254	7.25583	374.1231
1024	9.91304	868.17041	11.23805	820.28503

As can be seen from Table 5, when the number of resources (resource number = 32) is fixed, with the increasing of the tasks' number, the makespan and energy consumption of both algorithms are on the rise. When the tasks' number reached 1024, as compared with 512, GA algorithm's makespan increased 107.4%; while CRO algorithm is 54.9%.In the energy optimization, CRO algorithm performance is slightly better than GA algorithm.

In summary, in different task scheduling scenarios of cloud environment, with the growing numbers of tasks or resources, GA algorithm is basically stable of optimization. CRO algorithm will showe better result in the late. Experiments in this paper, the random reaction operation of CRO algorithm are used, which affects the optimal performance to some extent, if a certain operation be improved, believe there will be more excellent performance.

Conclusion

With a variety of applications are deployed and executived in the cloud computing center, the researches of task scheduling are deepening, and then scheduling targets are from a single user experience, turned to both the cost of social benefits aspects. Based on the GA algorithm and CRO algorithm performance comparison of different scenarios, the characteristics of each algorithm can be seen. The next step, the improvement studies of each reaction in CRO algorithm will as the focus, in order to further enhance the optimization results.

References

[1] S Ricciardi, D Careglio, G S Boada, et al. Saving Energy in Data Center Infrastructures [C]. Proceedings of the First International Conference on Data Compression, Communications and Processing, 2011:265 – 270.

[2] Braun T D, Siegel H J, Beck N, et al, A taxonomy for describing matching and scheduling heuristics for mixed-machine heterogeneous computing systems. IEEE workshop on Advances in Parallel and Distributed Systems, West Lafayette, IN, Oct. 1998, pp. 330-335.

[3] Maheswaran M, Ali S, Siegel H J, et al, Dynamic mapping of a class of independent tasks onto heterogeneous computing systems. In the 8th IEEE Heterogeneous Computing Workshop (HCW '99), San Juan, Puerto Rico, Apr. 1999, pp.30-44.

[4] Wang Ke．Dissertation Submitted to Hangzhou Dianzi University for the Degree of Master [D]．HangZhou：HangZhou DianZi University, 2013．

[5] Lam A Y S,Li V O K．Chemical-Reaction-Inspired Metaheuristic for Optimization [J] ．IEEE Transactions on Evolutionary Computation, 2010,14(3)：381-399

Applied Mechanics and Materials Vol. 596 (2014) pp 209-215
© (2014) Trans Tech Publications, Switzerland
doi:10.4028/www.scientific.net/AMM.596.209

Rapidly Analyze the Fault Tree with Numerical Methods

Bing Wu[1,a] , Zihao Zhao[1,2,b] ,Yuhui Ren[1,2,c]

[1]School of Resources and Safety Engineering ,China University of Mining Technology,
Beijing 100083, China

[2]School of Mine Engineering , Inner Mongolia University of Science and Technology ,
Baotou 014010 , China

[a]wbe@cumtb.edu.cn, [b]13734721514@163.coml, [c]safeahui@imust.cn

Keywords: Fault tree,Numerical method,Scilab

Abstract. In order to take advantage of the computer in the numerical calculation, in view of the fault tree qualitative analysis, a new method of fault tree analysis, numerical methods, was proposed on the basis of absorbing merits of the prime number method and determinant method. The fault tree's minimum cut sets and path sets can be calculated effectively with this method. Consequently, a specific example about calculation of the minimum cut sets was demonstrated with Scilab in this paper.

Introduction

Fault tree analysis, an analysis method proposed by H.A.Watson from American Bell Telephone Research institute, play an important role in the safety system engineering. The method has been widely used in military, nuclear industry, chemical industry, transportation and other fields. This method, effective in system failure diagnosis, weakness forecasting, elimination of potential causes of accidents and system optimization design etc., is an effective guidance to the system's security.

Fault tree analysis is generally contains qualitative analysis and quantitative analysis. Qualitative analysis mainly includes the calculation of the minimum cut sets and the minimum path sets. As an important part of the fault tree analysis, this calculation can be done fast with the rapid improvement performance of computer hardware and software..

The matrix method, first proposed by J.B.Fussell, E.B.Henry and N.H.Marsball, is a preferable method when calculate the minimum cut sets with computer. This method is similar to the determinant method, however, it has two main shortcomings: (1) Because it's based on matrix transformation, the matrix size has to be defined in advance, but when the number of basic events in fault tree is large, massive memory space is required. (2) Similar to the determinant method, it is operated on the rule of text replacement, while the computer is far less efficient in processing the text than the numbers.

Another commonly used method is the Boolean algebra method. It is a mature method by expanding the fault tree under certain rules and minimizing all cut sets in ways of conjunction and disjunction until all the minimal cut sets are obtained. But when the number of the basic events is large, this method is rather time-consuming and inefficient. But prime number method, a convenient method commonly used as an auxiliary means to Boolean algebra for simplification, is efficient and can be easily applied in computer .

Absorbing advantages of determinant method, matrix method and prime number method of Boolean algebra method, in view of the characteristics of Scilab which specializes in numerical calculation, a numerical method was proposed to analyze fault tree and realized with Scilab[1,2].

Scilab

Scilab, the abbreviation of Science Laboratory, is designed and developed by The French National Institute of Information and Automation. Similar to Matlab in function, this software's main function is scientific computing, numerical simulation and data mapping. It plays a important role in the field of engineering because of its key function of various matrix operations. In addition, since the software is free software and can run on various operation systems, such as Windows, Linux, OS, it is widely used in major research institutes and universities.

The basic principle and realization of numerical method

2.1 The expanding of fault tree. There are two steps when analyzing fault tree. The first step is to expand fault tree with numerical method. Numbers are used to represent all of the basic events, intermediate event, top event and logical symbols, in order to process this problem conveniently with Scilab. Rules are as follows: (1) using numbers, -1, 0, 1 and 2, as a substitute for logical symbols. When these numbers are not adequate to indicate, other numbers can be used to represent the events under the rules of no confusion. (2) using prime numbers except 2 to replace basic reason events. (3) using the even number to replace intermediate event or top event. Following these rules, incomplete replacement that commonly exists in the matrix method and the determinant method can be avoided by checking whether all elements of the cut sets are prime numbers. Take a fault tree for example as is shown in Figure 1, replacement rules of the fault tree symbols and numbers are shown in table 1.

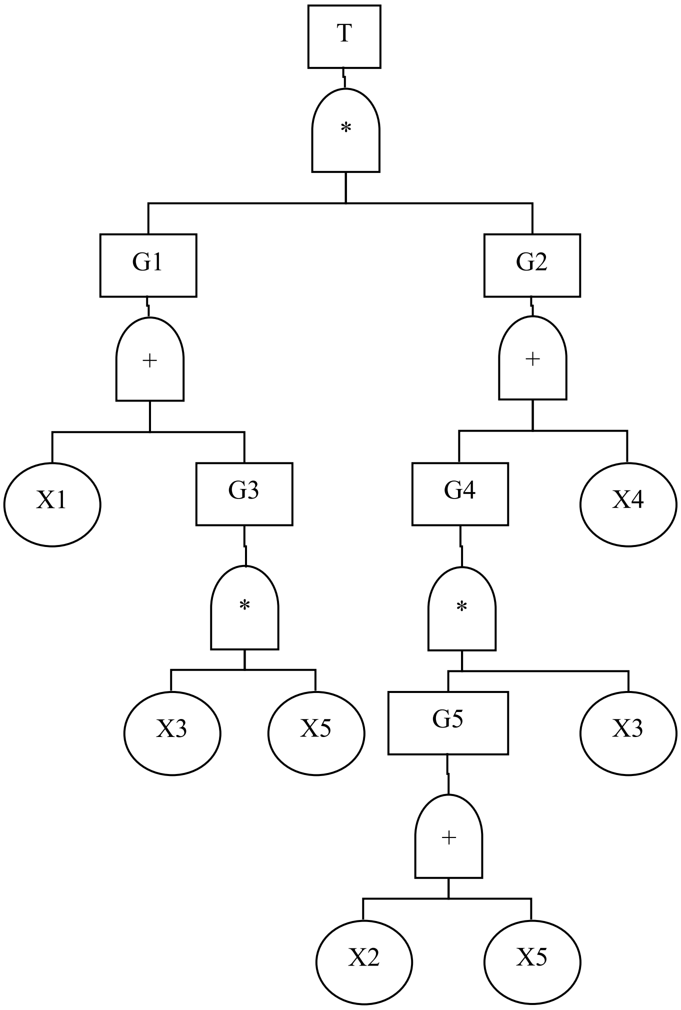

Fig. 1. A fault tree

Table 1. Fault tree symbols and corresponding Numbers

Top event and intermediate event	T	G1	G2	G3	G4	G5
	4	6	8	10	12	14
Basic reason event	X1	X2	X3	X4	X5	
	3	5	7	11	13	
Logic gate	*	+				
	0	1				

In order to process the fault tree in Scilab, certain data structure is needed to show the fault tree. Through comprehensive analysis and investigation, arrays of structures in the Scilab are preferable. Define an array of structure as ftree(x), x is the index number of its unit in the array of structure. Each unit corresponds to a branch of the fault tree. And each unit has three storage fields which are root, rule and branch. "root" stores root events (intermediate event or top event); "rule" stores logical symbols; "branch" stores branch event (intermediate event or basic event). Data structure of the fault tree in figure 1 is shown in table 2.

Table 2. Data structure of the fault tree in figure 1

	x	1	2	3	4	5	6
ftree（x）	root	4	6	8	10	12	14
	rule	0	1	1	0	0	1
	branch	[6 8]	[3 10]	[12 11]	[7 13]	[14 7]	[5 13]

Load the array of structures defined in Scilab. Then expand it under the rule of determinant method. First, expand it from top event and replace top event with next layer of events in subsequence. In the process of replacement, if the input event is connected with OR gate, directly replace the original upper event with row vector. If the input event is connected with AND gate, the original upper event is split into multiple lines according to the number of input events, and it is replaced by different input events in each row. In order to explain the replacement rules more clearly, specific steps of processing sample fault tree with determinant method are shown in table 3.

Table 3. Steps of processing the fault tree with determinant method

	Step 1	Step2	Step 3	Step 4	Step 5
4	[6 8]	[3 8]	[3 12]	[3 14 7]	[3 5 7]
					[3 13 7]
			[3 11]	[3 11]	[3 11]
		[10 8]	[10 12]	[7 13 11]	[7 13 11]
			[10 11]	[7 13 14 7]	[7 13 5 7]
					[7 13 13 7]

Here, six cut sets are obtained from the sample fault tree, as shown in step 5, table 3. But note that not all the cut sets are minimum cut sets.

Write the new function of 'ftreechange' and 'ftreeanalyse' in Scilab and loaded it into the Scilab running environment. The specific functions are explained in the code and not repeated here. The fault tree can be analyzed with function code 'ftreeanalyse' by building an array of structures 'ftree'including data structure and content , as shown in table 2.

Since the output of each cut sets varies in length, the analysis results output to an array of structures, and each unit in the array of structures stores one row vector. Specific codes are as follows:

function arrayoutput=ftreechange(arrayinput, root, rule, branch).

//This function is used to expand the input event sequence in row or column under the given rules, and the expanding rules are determined by the value of 'rule'. In this function, if 'rule' is equal to 0, expand it in row or under the rule of AND gate; while if 'rule' is equal to 1, expand it in column or under the rule of OR gate;

//'arrayoutput' is responsible for receiving the output event sequence after expanding. If expanding is not needed, then 2 is the output. If expanding in row, a row of data is obtained. If expanding in column, a multi-line matrix is obtained.

// 'arrayinput', the input of event sequence that is to be expanded. Root stores the output event of logic gate, refers to top event or intermediate event. Branch stores the input event of logic gate, refers to basic event or intermediate event. Rule stores types and rules of logic gate.

```
     arrayoutput=2
     arraylength=prod(size(arrayinput))
     branchlength=prod(size(branch))
         for i=1:arraylength
       if arrayinput(i)==root then
  //And gate module, output a single line
          if rule==0 then
          arrayinput(i)=[]
          arrayinput($+1:$+branchlength)=branch
          arrayoutput=arrayinput
          break
           end
  //OR gate module, output multi-line matrix
          if rule==1 then
           arrayinput(i)=[]
           arrayinput=repmat(arrayinput,branchlength,1)
           arrayinput(1:branchlength,$+1)=branch'
           arrayoutput=arrayinput
            break
           end
       end
      end
  endfunction
  function ftreeout=ftreeanalyse(ftree)
  //use the 'ftreechange' function, and analyze the fault tree which is stored in   the variable ftree, but
do not simplify the final results. 'x' is an array of structures, each unit stores row vector
corresponding to event sequence expanded or to be expanded.
     x(1).result=ftree(1).root
     lengthftree=prod(size(ftree))
     for i=1:lengthftree
     xlength=prod(size(x))
      for j=xlength:-1:1
        outtempt=ftreechange(x(j).result,ftree(i).root,ftree(i).rule,ftree(i).branch)
      if outtempt<>2 then
   //if the to-be-expanded-event be expanded successfully by 'ftreechange' function  under the rules,
then add the output of the row or the matrix structure to the structure variables in sequence.
    xtemptlength=prod(size(x))
         outtemptlength=size(outtempt)
```

```
          outtemptlength=outtemptlength(1)
          for k=1:outtemptlength
             x(xtemptlength+k).result=outtempt(k,:)
          end
  //Delete the relevant line that has been successfully expanded in the structure variable x.
   x(j)=[]
       end
   end
 end
    ftreeout=x
    endfunction
```

2.2 Calculating the minimum cut sets. Cut sets obtained in the previous step are not always minimal cut sets, so simplification is needed, and the prime number method is good at it. The prime number method is to replace the basic events in each cut sets with a prime number. (Note: the basic events cannot be repeated). The cut set is indicated by multiplication of prime numbers of corresponding basic event. If there is N cut sets in a fault tree,there is N numbers corresponding to it, and then arrange these numbers from smallest to largest. Take the first number first, then crosses out all the multiples of the first number in the numbers, and then take the second number, repeat the above operation until the end. Factorize the rest numbers, and then convert every prime number into corresponding basic event symbol, a series of minimum cut sets are obtained. Specifically there are two steps.

Make all the numbers in the cut sets unique and multiply the numbers. The command is:

'Unique': exclude the same part and leave a unique vector data.

'Prod': multiply all data on a vector.

All the cut sets obtained in the previous step are stored in an array of structure, and in each structure unit a field called the 'result' is used to store the corresponding cut set. Assuming that the array of structure is called 'X', to multiply its corresponding cut sets and store in an array 'T'.

Cross out all the multiples of the number, and factorize the rest numbers.

In the first step, 6 cut sets are obtained, and each cut set with repeated events needs to be simplified. Here is the explanation of the command:

'Factor': factorize a number into a form of multiplication of several prime numbers.

'Modulo': Return the remainder after a division of two numbers.

'Gsort': To quickly sort the range of data and the default is from the largest to the smallest.

Sort T by default from the largest to the smallest. Check whether any number can be divided exactly by other Numbers behind, if can be divided exactly by, that number is marked. Finally remove marked number; and the remaining numbers are decomposed [3].

Establish a function 'ftreesimplify' in the Scilab and load it in Scilab. Take the results obtained from the previous step as an input and execute, and the minimum cut sets in digital form can be obtained. Specific code is as follows:

```
    function arrayout=ftreesimplify(x)
    xlength=size(x);xlength=xlength(1);//Get the length of x and assign it to xlength.
  for i=1:xlength
  T(i)=prod(unique(x(i).result));// make the obtained cut sets data unique and multiply the result.
  end
 //Sort T by default from the largest to the smallest. Check whether any number can be divided exactly by other Numbers behind, if can be divided exactly by, that number is marked.
 T=gsort(T)
 xflag=[]
 for x1=1:xlength-1
  for x2=x1+1:xlength
      if modulo(T(x1),T(x2))==0 then
         xflag(length(xflag)+1)=x1
         break
      end
  end
end
 //remove marked numbers
 T(xflag)=[]
 // the following code is used to convert numbers into minimum cut sets.
 y=struct('result',0)
  //Create an array of structure to store the results, and there is only one storage field namely result in the array of structure.
 for i=1:length(T)
 y(i).result=factor(T(i))
 end
 arrayout=y
 endfunction
```

Due to limited space, the process of converting the numbers to specific fault tree symbols is not included here.

Calculating efficiency analysis

In order to verify the efficiency of the calculation method, write matrix solution code in the Scilab calculation software. A fault tree including 5 to 10 basic events is generated at random, calculate it with the numerical method and the matrix method respectively and record the calculating time. Take the number of fault tree's basic events as the x-coordinate, the calculating time as a y-coordinate, a comparison figure which reflects efficiency contrast of two calculating methods is shown in figure 2. Hardware and software platform for calculating is: Linux Mint 10 operating system, Scilab 5, Intel N2600 processor, 2G of memory.

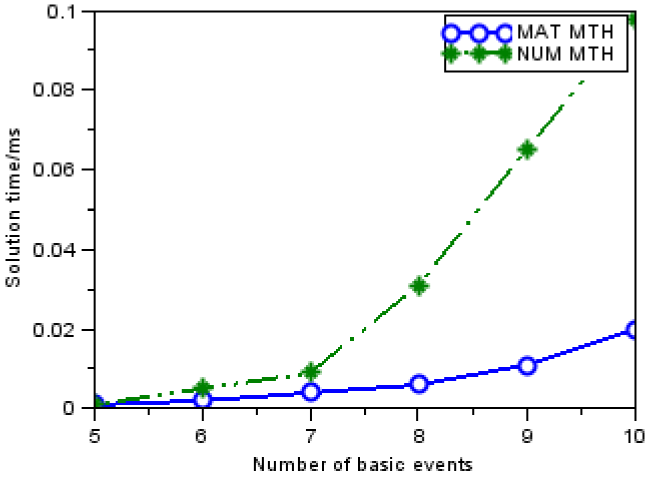

Fig. 2. A contrast of calculating efficiency of numerical method and matrix method

As can be seen from the figure, along with the increase of the basic event, because numerical method uses the strategy of dynamically adjusting the memory usage size of the array, the calculating time increases smoothly, while calculating time of the matrix method increases quite rapidly. Overall, for the same fault tree analysis, calculating efficiency of the numerical method is always higher than that of matrix method.

Conclusion

(1) Compared to other methods, numerical method combines advantages of prime number method and the matrix method, and its requirement for memory usage and the computer processing speed is relatively low, so a fault tree can be analyzed faster with this method.

(2) The characteristics of Scilab, cross-platform and free of charge, make it superb in the fault tree analysis which is highly dependent on matrix operation process, and beneficial to its application and popularization in the fields of teaching, scientific research and engineering.

(3) This paper's source code has been debugged in a Linux environment and can run in Windows, Mac OS and other operating systems without making changes. For a different fault tree, first establish a table of Fault tree symbols and corresponding numbers as shown in table 1, and then write corresponding data structure of the fault tree as shown in table 2. Finally, the fault tree can be analyzed by using the code shown in this paper.

References

[1] Wang Yuanhui. Safety System Engineering (M). Tianjin: Tianjin University Press, 2004,10 (3): 146~160

[2] Zhang Jinglin Cui Guozhang. Safety System Engineering (M). Beijing: China Coal Industry Publishing House, 2009,5 (7): 42~54

[3] Huang Duo, Wang Feng, Li Zhiwei. Basic Tutorial of Scilab, Scientific Computing Free Software (M). Beijing: Tsinghua University press, 2006, 6 (1): 126~128

Applied Mechanics and Materials Vol. 596 (2014) pp 216-221
© (2014) Trans Tech Publications, Switzerland
doi:10.4028/www.scientific.net/AMM.596.216

Research of Differential Evolution Algorithm for Motor Control

WU Zongfu

(Electrical and Information Engineering School, Hunan University
of Arts and Sciences, Changde, 415000, P.R.China)
E-mail: wzf0736@126.com

Keywords: differential evolution, chaos, intelligent optimization,non-linear equations

Abstract: An improved differential evolution algorithm for solving nonlinear equations of electrical motor system is explored. The algorithm is to convert equations into an optimization problem and, by keeping consideration of the evolution process and adopting dynamic parameters adjusting mechanism, the algorithm can improve searching efficiency and implement real-time surveillance for population overlapping. The Chaos searching strategy is used for overlapping individual to further improve the ability of global optimization. Analysis results of induction motor motion parameters show that the improved differential evolution algorithm proposed in this paper has high efficiency and powerful global optimization searching ability.

Introduction

Many questions (such as saturation) containing nonlinear factors in motor system are usually transformed into solution-finding of nonlinear equations[1,2]:

$$\begin{cases} P_1(x_1, x_2, \cdots, x_n) = 0 \\ P_2(x_1, x_2, \cdots, x_n) = 0 \\ \qquad \cdots \\ P_n(x_1, x_2, \cdots, x_n) = 0 \end{cases}$$

How all the solutions of nonlinear equations can be found quickly and efficiently is an important research task for mathematicians and engineering technicians. There have been many methods for solving this kind of nonlinear equations such as Newton iterative methods and its improved algorithms, homology continuation methods, interval numerical methods, universal grey algorithms, Groebner basis method, mathematics mechanization method and so forth.

The most classical method for solving nonlinear equations is Newton iteration which has high second-order convergence speed. But the use of Newton method for solving nonlinear equations needs pre-treatment and suitable selection of initial points which is fatal to the property and rate of convergence. Recently, with the development of chaos, the idea of using chaos for solving nonlinear equations is being developed progressively, but this theory is imperfect yet. [3-6]

Differential Evolution (DE) is a high efficient intelligent optimization calculation method proposed by Storn and Price in 1995. DE is originated from Genetic algorithm and can be used with greatly convienence without needing of encoding and decoding, furthermore, it has no special requirement about initial values and has fast convergence and good adaptability to a variety of non-linear function. DE algorithm is appropriate to optimization of multivariable complex problem and it has been considered as a potential multi-disciplinary optimization algorithm. Therefore, the algorithm has gained increasing attention as it was proposed [7-9].

In this paper, according to the search mechanism of differential evolution algorithm, a new strategy to improve global searching performances is put forward after deeply analyze the influence of the selection of every parameter in the algorithm. Analysis of the calculation results of induction motor motion parameters show that the algorithm proposed in this paper is effective, which provides a new optimization algorithm for solving nonlinear equations parameters in electrical motor systems.

Differential Evolution Algorithm and Its Improvement

2.1 The basic DE algorithm

2.1.1 Initialization

Like other evolutionary optimization algorithms, the differential evolution algorithm proposed by Storn etc. is a multi-point search algorithm based on population evolution. DE was generated almost at the same time with PSO and it seems that they two have the same features of the genetic algorithm, so it is similar to the integration of PSO and genetic algorithm.

The basic idea is that, the difference between two randomly selected vector parameters is used as random variable source of the third vector, by restruction of the current population, variation and selection, a new generation of population can generate and gradually evolve to optimal solution. Like genetic and particle swarm evolutionary algorithms, DE algorithm need to generate initial population in optimization and typically, the initial population is randomly generated from a given boundary value, covering the entire parameter space. And the general population chosen is l0 to 20 times of the scale dimension.

Set $X_i=[x_{i1},x_{i2},\ldots,x_{in}]$, where n is the dimension of solution space of the question, the initial population $s=[X_1,X_2,\ \ldots,X_{Np}]$, $X_i\epsilon R^n$ Is the set of individuals. Each component of a general individual vector X_i is generated by following equations:

$$x_{i,j}=x_{i,j\min}+rand()*(x_{i,j\max}-x_{i,j\min}) \quad (1)$$

Where $x_{i,j}$, $x_{i,jmin}$, $x_{i,jmax}$ are the jth component, upper limit and lower limit of the jth components of individual vector X_i respectively.

2.1.2 Mutation

For each goal vector $\mathbf{X}_i^{k+1}$ of $K+1$ generation, the basic mutated vector of the DE algorithm $\mathbf{V}_i^{k+1}=[v_{i,1}^{k+1},v_{i,2}^{k+1},\cdots,v_{i,n}^{k+1}]$ is produced by:

$$v_{i,j}^{k+1}=v_{r1,j}^{k}+F(v_{r2,j}^{k}-v_{r3,j}^{k}) \quad (2)$$

Where $v_{r1,j}^{k},v_{r2,j}^{k},v_{r3,j}^{k}$ are the jth components of 3 different vectors randomly selected from individuals of the K generation except $\mathbf{X}_i^{k}$, so DE population quantity must be greater than or equal to 4 in order to meet these requirements. Coefficient $F\leq 1$ is parameter for controlling differential quantity.

2.1.3 Cross

In DE algorithm, cross operation is introduced to increase the diversity of interference parameter vector, so the vector $\mathbf{U}_i^{k+1}=[u_{i,1}^{k+1},u_{i,2}^{k+1},\cdots,u_{i,n}^{k+1}]$ as the target is generated from mutation vector and source vector, each variable of the formula could be calculated by following equations:

$$u_{i,j}^{k+1}=\begin{cases} v_{i,j}^{k+1} & \eta_j\leq C_R \quad or \quad j=q_j \\ x_{i,j}^{k} & for \quad others \end{cases} \quad (3)$$

Where, q_j is an integer which is selected randomly from (1, n) to ensure that one digit number must have been crossed in this operation, $\eta_j\epsilon(0,1)$ is randomly selected control parameters for j dimentional component, the cross-factor $C_R\epsilon(0,1)$, which is the parameter of this algorithm and controls the diversity of the population to help the algorithm escaping from the local optimal solution, need to be ascertained in advance.

2.1.4 Selection

In standard DE method, a greedy selection model is used, that is, if and only if the value of the new individual's evolution function is better, the new individual will be reserved for the next group, otherwise, the parent individual is still retained in the population once again as the parent vector of the next generation.

2.1.5 DE's control parameters

The choice of control parameters has great impact on performance of DE search algorithm. According to experience, the population quantity *Np* may be chosen with the range of 5 to 10 times of the dimension of the problem to be solved, it must be greater than 4 for ensuring that the DE has sufficient vector variables. During the evolution, the value range to be chosen of proportion factor F and cross-ratio factor C_R are (0.4, 0.9) and (0.3, 0.8) respectively, and their optimum values are often dependent on the characteristics of the objective function.

2.2 Improved form of DE algorithm

2.2.1 Dynamic adjustment of control parameters

In the DE algorithm, how to set reasonable control parameters is a very difficult task for which many scholars have devoted so the control strategy of DE parameters has been greatly improved [10]. In general, F and C_R should be no less than a particular value for avoiding the algorithm to be convergent in advance, larger parameters of F and C_R increase the possibility for the algorithm to escape from partial optimum. Equation (2) shows that in the initial stage of the search, since the individual is randomly distributed in the solution space to cause relatively large difference between vectors, a relatively small control parameter F is required. With the continuing evolution of the population, each individual gradually approximate the optimal individual, the difference of vectors from mutation operation will become smaller gradually, which decrease the diversity of algorithm search space. At this stage a relatively large control parameter F will be required for expanding new vector searching space after mutation operating and improve the global optimization performance of the algorithm. Similarly, the population will produce lesser new individual after cross operation with a too small cross-factor C_R, thus weaken the algorithm's ability for developing new space.

However, the population will decrease the stability even reach instability with a too larger cross-factor.

Inspired by the thought of inertia weight dynamic adjustment of particle swarm optimization algorithm, in this paper, the control parameters F and C_R are adjusted by the strategy of evolutionary dynamical adjustment [15] which is stated as follows:

$$F = F_{\max} - \frac{(F_{\max} - F_{\min})\lambda}{\lambda_{\max}} \tag{4}$$

$$C_R = C_{R\max} - \frac{(C_{R\max} - C_{R\min})\lambda}{\lambda_{\max}} \tag{5}$$

where F_{max}, F_{min} are respectively the max. value and min. value of setted proportion parameter F and C_{Rmax}, C_{Rmin} are respectively the max. value and min. value of setted parameter C_R. λ_{max} and λ are the setted maximum iteration time and the current iteration time.

2.2.2 Chaos search strategy for part of the individual

There would produce some individuals with overlap at a certain stage of DE population search which will greatly decrease the overall optimization of the algorithm. In order to increase the diversity of groups as well as to improve the search capability of the algorithm, these overlapped individuals should be dealt with to migrate at the current overlapping point and obtain new search abilities. Chaotic motion has the characteristics of ergodicity, randomness and regularity and so forth, and is able to traverse all states non–repeatedly according to its own laws within a certain range. Implement optimization search by using ergodicity characteristic of Chaos has made the Chaos optimization theory a new subject which has being widely received great attention from scholars. [11,12]

In this paper, by monitoring distribution of individual in population with real-time, a similar method as carrier waves is used to map the Chaotic state to the optimization variables for overlapping individuals of algorithm, and the traversing scope of chaotic motion is associated with the range of optimization variables, then the overall search performance of algorithm could be improved by searching chaotic variables. Compared with other power systems which produce chaotic variables, the Logistic equation has the advantages of simple ness, less computation, easy to use and so on, therefore in this paper, it is used to construct the following chaos sequence:

$$x^{k+1} = \mu x^k (1 - x^k) \,, \quad x^k \in (0,1) \qquad (6)$$

It has been proved that, in this equation, when μϵ(3.57, 4), the system will be in chaotic regions and, the motion path of equation will appear chaotic characteristic in this range. Make a transformation with $x^{k+1} = \mu x^k (1 - x^k)$, we get

$$y^k = \frac{2}{\pi} \sin^{-1}(\sqrt{x^k}), k = 1,2,\cdots \qquad （7）$$

Then the distribution function of variable y is $F\{y \leq Y\} = Y$ and thus the probability distribution function of variable y is $P(x)$=1. In this paper, the equiprobable chaos sequence is used for searching to improve the overall search performance.

Application example

For a certain synchronous generator, when it is in saturated state, give its parameters as follows: saturation coefficient $s = 0.0476 E_q^{12}$, synchronous reactance $x_d = x_q = 2.264$, armature reaction reactance $x_{ad} = x_{aq} = 2.104$, self-impedance of exciting winding $x_F = 2.209$, resistance of exciting winding $r_F = 0.0008$, stator resistance $r = 0.02$, （all in un-saturation state）, when operated in static state, the active power, $P=0.8$, and reactive power, $Q=0.4$, with input voltage, $U=1.0\angle 0$, to calculate the inner parameters of the generator.

For a synchronous generator, when it is in stable state, according to the relations between inner variables considering the magnetic flux which is in saturation, we get

$$\begin{cases} tg\delta = (P \cdot x_q - Q \cdot r)/(U + P \cdot r + Q \cdot x_q) \\ U_q = U \cos\delta \\ i_d = I \sin(\delta + \varphi) \\ i_q = I \cos(\delta + \varphi) \\ i_f = (U_q + i_q \cdot r + i_d \cdot x_d)/x_{ad} \\ I_\Sigma = \sqrt{(i_f - i_d)^2 + i_q^2} \\ s = 0.0476 E_q^{12} \\ x_{ad(sa)} \cdot (1 + s) = x_{ad(un)} \\ x_{ad(sa)} \cdot I_\Sigma = E_q \end{cases} \qquad (8)$$

where δ is power angle, φ is power factor angle, E_q is air gap electric potential, E_Q is synchronous reactance aft. electric potential of q axis, $x_{ad(sa)}, x_{ad(un)}$ are armature reaction reactance in saturated and unsaturated state of X axis, I_Σ is synthesize current, s is saturation coefficient. To change into algebra equations by applying universal formula and substitute the known positions, given

$$x_1 = tg(\delta / 2), x_2 = I_\Sigma, x_3 = x_{ad(sa)} \; x_4 = i_d, x_5 = U_q, x_6 = i_q, x_7 = i_f, x_8 = E_q$$

after coordinating, we get PS as follows:

$PS = \{P_1, P_2, P_3, P_4, P_5, P_6, P_7, P_8\}$, where

$$
\begin{aligned}
P_1 &= (0.8x_1^2 + 0.8x_1 - 0.8)x_3 + 0.12x_1^2 + 2.16x_1 - 0.12 \\
P_2 &= (1 + x_1^2)x_4 + 0.4x_1^2 - 1.6x_1 - 0.4 \\
P_3 &= (1 + x_1^2)x_5 + x_1^2 - 1 \\
P_4 &= (1 + x_1^2)x_6 + 0.8x_1^2 + 0.8x_1 - 0.8 \\
P_5 &= x_3x_7 - 0.02x_6 - x_5 - x_3x_4 - 0.16x_4 \\
P_6 &= x_7^2 - 2x_4x_7 + x_6^2 + x_4^2 - x_2^2 \\
P_7 &= x_8 - x_2x_3 \\
P_8 &= 0.0476x_3x_8^{12} + x_3 - 2.104
\end{aligned} \tag{9}
$$

After 20 times' iteration, all real number solutions are got with the proposed method in this paper and are shown in Tab.1, which are the same as that in literature[1], each running time is about 6 seconds. While the problem for improving the efficiency of the algorithm is for the future study. Since $x_2 = I_\Sigma \geq 0$, the second solution and the fourth solution should be omitted. Considering that the current of the exciting winding is positive（$x_7 \geq 0$）, then the third solution should also be omitted, we get inner variables by the first solution which is the same as that in traditional iteration method.

Tab.1 All solutions of inner variable of synchronization generator considering magnetism saturation

No.	1	2	3	4
x_1	0.3781361	0.3781361	-2.6445503	-2.6445503
x_2	0.5831026	-0.583102	0.58310260	-0.5831026
x_3	1.8635591	1.8635591	1.8635591	1.8635591
x_4	0.8292509	0.8292509	-0.8292509	-0.8292509
x_5	0.7498012	0.7498012	-0.7498013	-0.7498012
x_6	0.3351758	0.3351758	-0.3351758	-0.3351758
x_7	1.3063943	1.3063943	-1.3063943	-1.3063943
x_8	1.0866462	-1.086646	1.0866462	-1.0866462

Conclusions

In this paper, the parameters of differential evolution algorithm has been dynamically adjusted for speeding up the search efficiency, and the chaotic search strategy has been adopted in the evolution process for improving global search performance of the algorithm. Solution results and solving process of nonlinear equations of motor system parameters show that the improved differential evolution algorithm proposed in this paper is fast, efficient and accurate for the low-dimensional nonlinear equations and nonlinear optimization problems. While the problem in improving the efficiency of the algorithm for high-dimensional nonlinear equations need to be further researched in future studies.

Acknowledgement

This work was financially supported by the Hunan Natural Science Foundation （12JJ9024）.

References

[1] Y.X. Luo, W.G. Chen，“Newton Chaotic Iterative Method and its Application in Induction Motor Motion”，Journal of Chinese Power System and its Automation, 2006,18(1):24-28.

[2]C. Chen， W. Cao，“Application of Wu Method in Power System’s Electromagnet Process in Sudden-short circuit Transient State”, Journal of Chinese Motor Engneering, 2002, 22 (11): 16-19.

[3] J. Xie, Y. Chen，“A Chaos-based Approach to Obtain the Global Real Solutions of Burmester Points”, China mechanical Engineering, 2002,13(7):608－710.

[4] You-xin LUO, De-gang LIAO. Coupled chaotic maps Newton iteration method and Institutions l precision point kinematic synthesis. Mechanical transmission. 2007, 31(1):28-30

[5] Luo Y.X., Li D.Z., Che X.Y., Hyper-chaotic Mapping Newton Iterative Method to Mechanism Synthesis. AMES, Journal of Mechanical Engineering,2008,54（9）:372-378

[6]XIE-Jin, CHEN-Yong. Burmester point finding method with rigid-body guidance based on chaos. China Mechanical Engineering, 2002,13(7)：608－710

[7]Riensche E, Meusinger J, Stimming et a1． Optimization of 200kW SOFC cogeneration power plant．Journal of Power Sources，1998，71(2)：306-314．

[8] OtaT，Koyama M，Wen C，eta1．Object-based modeling of SOFC system：dynamic behavior of micro-tube SOFC[J]．Journal of Power Sources，2003，118(1—2):430-439．

[9] YU Tiemin, YAN Dongshu. Differential evolution algorithm for multi-objective optimization. Journal of Changchun University of Technology, 2006，16(4):77-80

[10] X.L Zhao, X.M. Zhang, C. G. Duan. The performance research of high efficiency prime motor DIR-SOFC for decentralized energy system．Journal of Harbin Institute of Technology (New Series)，2007，(14):501-504．

[11] LIU Zifa, YAN Jingxin,ZHANG Jianhua etc. Power system reactive power optimization based on animproved differential evolution algorithm. Power Grid Technology, 2007, 31 (18): 69-72.

[12] FAN Chunwei, JIANG Changsheng. Image encryption / decryption algorithm based on standard chaotic map. Journal of Harbin Institute of Technology, 2006,38 (1) :119-121

Applied Mechanics and Materials Vol. 596 (2014) pp 222-225
© (2014) Trans Tech Publications, Switzerland
doi:10.4028/www.scientific.net/AMM.596.222

An improved RFID Tag Collision Algorithm

Tianbao Ran[1,2, a], Xisheng Wu[2,b]

[1]Education Information Center, Wuxi Institute of Commence, Wuxi 214153, China

[2]College of Internet of Things Engineering, Jiangnan University, Wuxi 214122, China

[a]cac_063@163.com, [b]snsg082@163.com

Keywords: RFID, Dynamic frame slot ALOHA(DFSA), Multiple factor.

Abstract. Tag collision is a very important research direction in the RFID system. Probabilistic solving algorithm is one of the important way to solve the tag collision, dynamic frame slot ALOHA (DFSA)algorithm is more commonly used at present and the probabilistic algorithm with better effect. This paper proposes an Advanced DFSA (ADFSA) which is based on a dynamic frame slot ALOHA algorithm, combined with multiplier factor and grouping thoughts. the algorithm is simple, at the same time, the simulation results show that IDFSA algorithm has better performance.

Introduction

Radio frequency identification devices(RFID) technology is a non-contact automatic identification technology, A typical RFID application system is consisted of the electronic label, read and write device, and information network system and other parts[1]. In passive RFID system, read/write device sends a request orders to all the tags, received command tag returns information it carries to the read/write device, they will occur conflict on the Shared channel in the process of tag response, lead to read the information failure, it is so-called label conflict[2].

On DFSAI [3] And DFSAII[4], although estimation method is simple, when the tag number is much larger than the frame length, the number of labels within one time slot collision no longer meet their respective calculation about tag number, showing problem about big deviation of tag number estimation, the length of the frame chosen by tag number which is obtained according to the error estimate will not be also accurate, resulting in a loss of system efficiency. By transmitting the method of information about "bit value", "the length of bit value" and "start bit is bit value" to the tag, EDFSAI algorithm [5] realize limitation of the number of response label, so as to solve the problem of leading to the decrease of the efficiency of system because tag number is too large on DFSAI and DFSAII; Its essence is that label is divided into two groups, respectively response. For example, when "bit value" transmitted by the reader is "10000000", the label will be divided into two groups by 127:129 , however, the literature [6] no further analysis, as the number of labels is too big, after the first group, when no solution to solve the question tag number is too high, how to deal with? At the same time, on EDFSAI and EDFSAII algorithm[5], estimating tags, although they can obtain more accurate estimates, they involve the solution of nonlinear equations, which increase the amount of calculation of the system. In this paper, adopting DFSAII simple tag estimation method, referencing group thought of EDFSA algorithm, combining with the multiplier factor, puts forward the advanced algorithm (ADFSA).

Improved Algorithm

To better describe the ADFSA algorithm, the following conventions:

(1)When the reader sends a request instruction to the tags within the scope of its role, all tags randomly select a time slot response, in this reading cycle, each tag must and can only respond once.

(2) The tag within the scope of the reader has two kinds of state which is "activity" and "silent" . Tags were in a state of "activity" can respond to reader all instructions, tags were in a state of "silence" does not respond to any instructions from the reader, until it has left the reader scope, to reset. "Activity" label will enter a state of "silent" after identified by the reader .

(3) Tag number remains the same in a read cycle.

After tag enter the scope of reader, the length of an initial frame are set on the reader, a read cycle is opening . When the system efficiency is less than or equal to 31.12%, and tag number is greater than the length of the frame, known $S_k > S_0$(S_0 said the total amount of free time slots in a frame, S_1 said the total number of successful identification time slots in a frame, S_k said the total number of collision time slot in a frame)[7]. In the process of actual reading it reflects for $C_k > C_0$(C_0, C_1, C_k respectively said actual values of S_0, S_1 and S_k after a read cycle), at this time, using multiplier factor according to *Table 1*, rapidly increasing frame length. Setting length of the biggest frame using in the system is 512, when the frame length is greater than 512 according to *Table 1*, tag number known within the scope of the reader may have more than 709, in order to achieve maximum efficiency of the system, the frame length 512 has not meet the requirements. Adopting the method of modulus at this moment, to group the labels, then each group separately completes the rest of the identification process; Otherwise, use the *formula (1)* [8]estimate the rest of the labels, and according to the *Table 2* choose matching frame length, start a new round of reading process.

$$T=2.3922 \times S_k \,. \tag{1}$$

Table 1: Relations of System efficiency and multiple factor.

System efficiency	Multiple factor	System efficiency	Multiple factor
5.520E-41	128	1.530E-04	16
5.250E-19	64	2.094E-02	8
3.499E-09	32	1.561E-01	4
		3.112E-01	2

Table 2: Corresponding relations between Tag number and frame size.

Frame length	Tag number	Frame length	Tag number
4	1~5	128	89~177
8	6~11	256	178~**354**
16	12~22	512	355~709
32	23~44	1024	710~1419
64	45~88	2048	1420~2839

Specific steps of ADFSA algorithm are as follows:

(1)After setting the length of the initial frame on the reader, sends the request instructions to the tag within the scope of its role, starting a read cycle, the "activity" label randomly select a time slot to response.

(2)According to information fo the tag response on the reader, execute read and write operations to the identifying labels, send silent instructions, make the tag into the state of "silent".

(3) After a read cycle,the reader statistics system efficiency and the value of C_0, C_1, C_k . If $C_k \le C_0$ or system efficiency is greater than 31.12% , turn to (4); Or go to (5).

(4) Using *formula (1)* estimate residual tag number, if zero, turn to (7); Otherwise, according to *Table 2* choose matching frame length, turn to (1), start a new round of reading process.

(5) Don't estimate tag number of the rest, but according to *Table 1* choose corresponding multiplier factor, directly calculate the new frame length, if the frame length is less than or equal to 512, turn to (1); Otherwise, go to (6).

(6) If the frame length is 1024, tag number of the rest within the scope of reader role is larger, 512 frame length can't meet the requirements of tag identification, according to *Table 2*, by the method of

modulus, the labels is divided into two groups, and set the frame length is 512, let the two groups reply respectively ,turn to (1); Similarly, when the frame length is greater than or equal to 2048, according to *Table 2*, labels can be divided into four groups, set frame length is 512, to (1).

(7)Estimate tag number of the rest is zero, then through a read cycle, to ensure all tags are identified completely, ending tag identification process.

The Simulation Results

According to algorithm thought of ADFSA, EDFSAI, EDFSAII, DFSAI and DFSAII , in Windows XP System, using C language[9], write identification process of the simulation program and the simulation tag, respectively statistics of system efficiency, the total number of time slot using and total number of reader cycles of these five kinds of algorithms. In this paper, the initial frame length selected is 64, and 1-4000 labels are simulated, the simulation results are shown in *Fig.1.*, *Fig.2.*, and *Fig.3.*

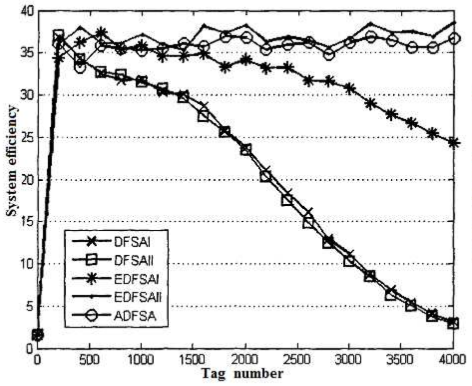

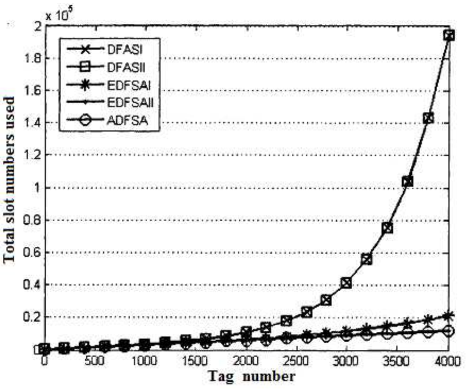

Fig.1. Comparison of System efficiency Fig.2. Comparison of total slot numbers used to identify tags

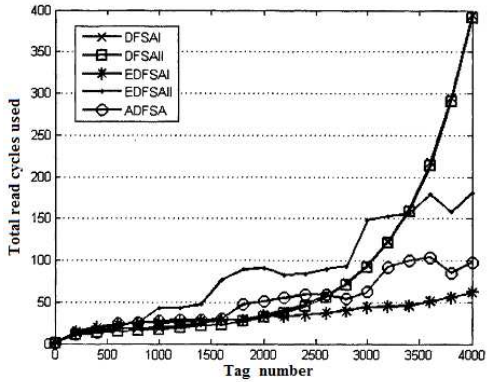

Fig.3. Comparison fo total read cycles used to identify tags

Analysis of simulation results, it shows that DFSAI and DFSAII show very similar features about system efficiency, using the total of time slots and the total of reading cycle, because there is no essential difference in two kinds of algorithm; on EDFSAI algorithm,while the total of reading period using is the minimum, the total of time slot it use is greater than EDFSAII and ADFSA algorithm, the system efficiency also fell sharply with the increase of number of tags, with the increase of tag number, efficiency of the system on ADFSA and EDFSAII algorithm can steady at just over 35%. Because EDFSAII algorithm uses estimation method which can accurately estimate tag number of the rest[10], and chooses the matching frame length, its system efficiency is slightly better than ADFSA, yet this approach needs solve nonlinear equations. The total of time slot EDFSAII use is quite with ADFSA, but the total number of read cycles is greater than ADFSA algorithm along with the increase of tag number, increasing in the number of read cycle means that the interaction command between the reader and the tag also will increase, thereby increasing identification time of the tags. The above analysis shows that the ADFSA is a kind of anti-collision algorithm which is simple implementation, stable and efficient.

On ADFSA algorithm,in order to ensure the high efficiency of the RFID system, it has been given the dynamic adjustment function of the frame length with the change of tag number, when the length of the initial frame are chosen 8, 32, 128 and 512 respectively, the result of simulation shows that the choice of initial frame length has a little influence to ADFSA on performance of the algorithm.

To sum up, ADFSA algorithm based on the multiplier factor is simple, and the system efficiency can stable remain at around 35% with the increase of tag number; At the same time, performance of the algorithm is not affected by the length of the initial frame, on the other hand it also shows stability of the algorithm. Finally, the decline of the total number of time slots and reading cycles means it is less time for identification tag, relative to the DFSA and EDFSA, ADFSA has better performance.

References

[1] Zh.Q.You, S.J.Li. *Theory and Application of RFID [M]*. Beijing: Electronic Industry Press, Vol.99-104(2004).

[2] X.Chen, X.P.Xue, S.D.Zhang. *Research of Tag anti-Collision Algorithm*. Modern Electronics Technique[J], Vol.29(5).13-15(2006).

[3] H.Vogt. *Multiple Object Identification with Passive RFID Tags[C]*. 2002 IEEE International Conference on Systems, Man and Cybernetics, Vol (3).651-656(2002).

[4] J.R.Cha, J.H.Kim. *Novel Anti-collision Algorithms for Fast Object Identification in RFID System[C]*. Proceedings of the 2005 11th International Conference on Parallel and Distributed Systems(ICPADS), Vol(2).63-67(2005) .

[5] S.R.Lee, S.D.Joo, C.W.Lee. *An Enhanced Dynamic Framed Slotted ALOHA Algorithm for RFID Tag Identification[C]*. MobiQuitous, Vol.166-174(2005).

[6] T.W.Hwang, B.G.Lee, Y.S.Kim, et a1. *Improved Anti-collision Scheme for High Speed Identification in RFID System[C]*. Proceedings of the First International Conference oft Innovative Computing, Information and Control (ICICIC'06), IEEE, Vol.449-452(2006).

[7] J.Fu. *Research of RFID*. ShanXi Science and Technology, Vol(1).22-23(2009).

[8] X.M.Hu. Research of RFID based on Web of Things of ECP. Nanjing Post and Communications University(2011).

[9] Y.Zh, Y.X.Ch. Research on Information Security System of Internet of Things based on RFID Technology, The 3rd conference on Information Vulnerability Analysis and Risk Assessment(VARA), Vol.179-192(2010).

[10] W.L.Ch, W.Lee, Y.X.Lin. Application and Design of RFID in Web of Things, Science and Technology Communication(2012).

Applied Mechanics and Materials Vol. 596 (2014) pp 226-229
© (2014) Trans Tech Publications, Switzerland
doi:10.4028/www.scientific.net/AMM.596.226

Targets Detection Based on Multifractal Method

Liu Fang

School of Mathematics and Computer Science, Xinyu University, Jiangxi, Xinyu 338004 China

xyxylf@yeah.net

Keywords: Target Detection, Fractal Theory, Impurity Scattering

Abstract. Mean sea clutter scattering coefficient model can reflect the relationship between the scattering coefficient of sea clutter and radar parameters and environmental factors, commonly used at sea clutter radar range forecasts. Sea clutter amplitude distribution model is essentially in the form of a probability density function to describe the magnitude of the statistical properties of sea clutter. In this paper, based on the sea surface target detection process uncertain information based on multiple objective study of fractal theory, simulation results show that our detection methods to get good results, you can improve the reliability and intelligence of detection.

Introduction

Hyperion include storm, the storm was caused by local wind, its crest is shorter. Expansion wave length is longer, the shape is close to sinusoidal, the distance caused by the wind. Irregular appearance is by the sea and swell waves interfere with each storm formation. Describe the microscopic structure of capillary waves of the sea, which is usually caused by the sea winds. In the field of non-linear analysis, the concept of chaos and fractals are two symbiotic, chaotic dynamics emphasize process, and more emphasis on fractal geometry. Although chaos theory research bottlenecks in the field of sea clutter, but a weak target detection based on sea surface fractal theory has developed into a relatively mature field. Low resolution radar system, and the echo amplitude of the scattering intensity distribution may be used as the basis for target detection. Its disadvantage is that, on the one hand the sea clutter is assumed to be stationary random process, does not adequately reflect its generating mechanism and physical properties; hand at high resolution and small grazing angle state, the target echo is strong sea clutter severe shadowing, sea difficult to detect small target, especially sea spikes effect can cause serious false alarms.

Sea clutter amplitude distribution model

Early resolution of the radar system due to restrictions, the greater number of scatterers in the resolution cell contains that random movement of the sea clutter is the echo amplitude and phase of a large number of Gaussian scattering element are formed, so that the amplitude of the echo Rayleigh distribution, the phase is uniformly distributed. Modern radar systems operating at high resolution and low grazing angle state, under such conditions the observed distribution of sea clutter significantly compared to Gaussian form more spikes, these spikes are mistaken targets, leading to a false alarm probability increases. This requires a non-Gaussian model for the description of the sea clutter. By studying a variety of different radar parameters and actual circumstances, can be found in a series of statistical distribution model and the observed sea clutter amplitude distribution coincide, these include the lognormal distribution, Weibull distribution and composite k-distribution etc., that through practice, the Rayleigh distribution is a special form of a complex k-distribution. E.g., k-distribution probability density function is:

$$p(x)=\frac{2}{c\Gamma(v+1)}\left(\frac{x}{2c}\right)^{v+1}K_v\left(\frac{x}{c}\right) \tag{1}$$

Here $x>0$ and $v>-1$, k-distribution has a good nature, its magnitude and complex feature allows correlation simultaneously is described. Compound k-distribution can be considered as the product of two components with different correlation times. The first component is the spot component, which is carried out by a large number of scatterers reflecting superposition of coherent, consistent with Rayleigh distribution; second component is the fundamental amplitude modulation component (ie, slowly changing), which reflects the large sea the average size distribution of the scattered beam in the structure of the spatial variation. On the waves for a given sea, to the average power level is determined by the average scattering echo the sea surface height, especially the slow change (s magnitude) of. On the other hand, due to the continuous fine capillary waves in the region affected by the wind, forming a shorter time related to the Rayleigh component (approximately 10 milliseconds). This feature sea meets the definition of a composite K-distribution, so that the composite K-distributed sea clutter is a good distribution model, which accurately describes the statistical properties of sea clutter amplitude.

Impact of clutter target on multi-fractal characteristics

Sea wind affected so as to generate a relative speed between the various scatterers on the sea, so that the received power spectral presence of sea clutter Doppler shift. Marine radar receivers generally use quadrature demodulation of coherent radar, coherent radar capable of measuring amplitude and phase of the signal to return. The received baseband radar signal is a complex random process, or a composition in the form of in-phase component (I) and quadrature component (Q), or the amplitude and phase angle. Radar scattering relative movement between sea radar echo pulse phase shift occurs, the Doppler frequency shift is defined as:

$$f = \frac{2C_s \cos\theta_g}{\lambda r} \tag{2}$$

Where f is the Doppler frequency shift, λ_r is the wavelength of the radar, C_s is the scattered velocity, θ_g grazing angle of the radar beam. Process of sea clutter Doppler spectrum produced two: the average Doppler spectrum is expanded random motion of scatterers, while the average Doppler frequency shift corresponds to the process of change of the waves. Change process tracking time and sea clutter Doppler spectrum, will be able to determine the mechanism of the process and the scattering of sea clutter model. K-power spectrum distribution sequence represented in Fig.1.

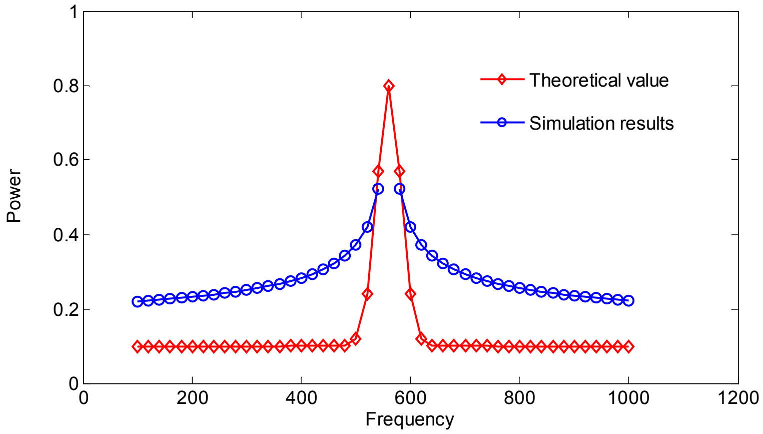

Figure.1 K-sequence power spectral distribution curve

The detection method based on the amount normally used to detect statistical differences, fractal describes the intrinsic properties of an object, so a square-shaped differential value for target detection, a stable, less susceptible to interference advantages. To test this hypothesis, Figure 2 shows a square-shaped differential values under different SNR conditions. The results showed that different SNR values affect the other shaped little difference, which is particularly suitable for target detection under strong sea clutter.

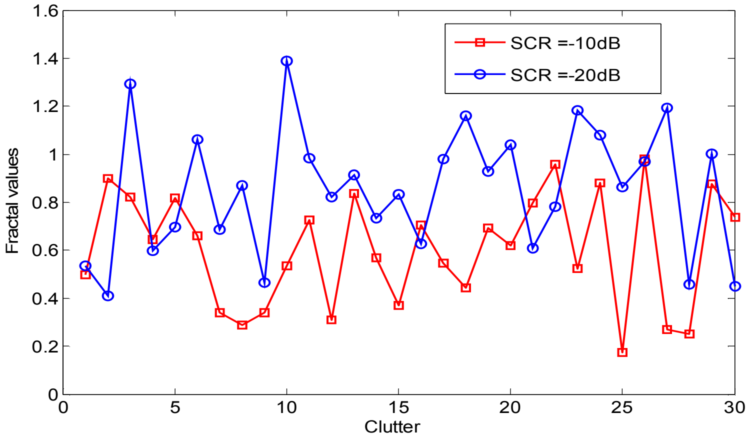

Figure.2 Compares the different SNR ratios multi-fractal dimension

Due to the structure of the target complex background, the presence of noise and other factors, making the sea surface target detection becomes very difficult, difficult to use classical statistical methods be exact description. Therefore, it is reasonable to complex target environment to be treated as a fuzzy environment. In a variety of uncertainties, it is difficult to get the sea target echo and complete and accurate description of the characteristics of sea clutter, especially in strong clutter, two types of target echo characteristics are very similar and there serious overlapping phenomena exist fuzzy boundary between sea clutter and sea targets. This makes the traditional pattern recognition method in this case is difficult to obtain a better classification results.

Multifractal spectrum of sea weak target detection

Weak and difficult to achieve target detection in strong clutter is mainly reflected in the radar echo signal SNR ratio is low, the radar detection capability is limited. Therefore, how to improve the ratio of low SNR detection performance of the system is under strong clutter weak target detection focus. The fractal dimension is an important parameter describes fractals, which reflects the basic characteristics of fractals to describe the fractal surface roughness or irregularity degree. For the fractal dimension of the surface due to the different focus, so its definition and calculation there are many ways, but the most common are Hausdorff dimension, similar dimension, capacity dimension, box dimension and so on. In this calculation, the sea clutter data series used to be divided into several short sequences overlap, we order fractal characteristics of each sequence can be. Figure 3 is a box dimension sea clutter sequence diagram can be seen from Figure 3, the sea clutter box containing the target dimension than the high sea clutter-free goal box dimension, the reason is because the target changes the shape of the surface of the sea clutter.

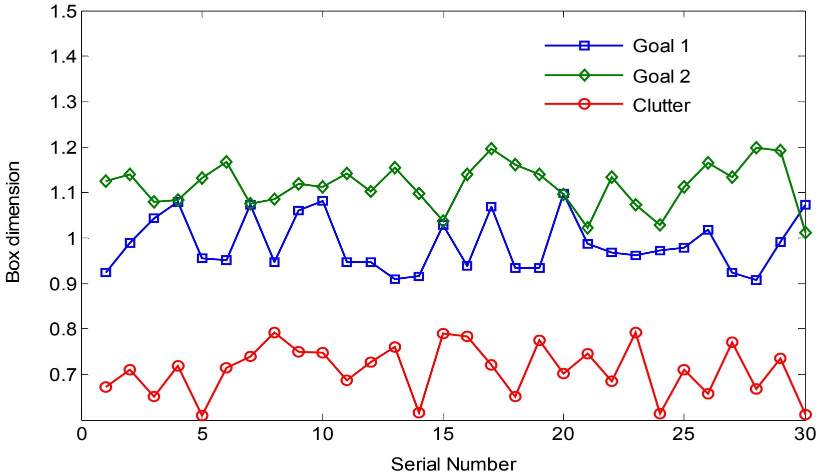

Figure.3 Clutter sequence diagram box dimension

Box dimension method as long as there is a pixel graphics in the box on this box is counted in, regardless of how many pixels within the box fractal dimension thus obtained is bound to lose a lot of information, this is not detailed enough single fractal place; the multi-fractal consider the difference in the box pixels or other physical quantities, get a set of probability distributions after normalization, and then a multi-fractal spectrum is described, the results obtained are ignored contains many single fractal information. Sea clutter will vary with sea conditions have changed a lot, the existing methods such as Monte Carlo simulation method does not effectively describe the complexity of sea clutter, so using real sea clutter data to make its simulation algorithm results will be more convincing (Fig. 4).

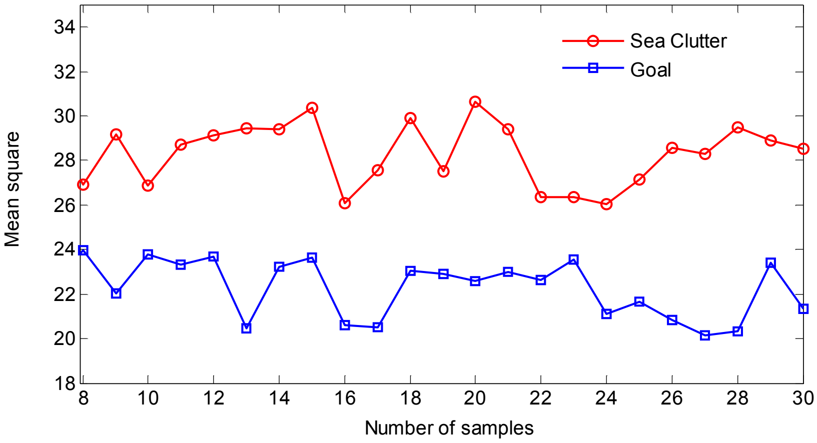

Figure. 4 Rlationship of test volume changes with the number of samples

In order to improve detection performance, in addition to suppressing clutter, jamming and reduce system noise outside, an effective approach is to use technology to increase the accumulation of energy received echo signal to accumulate to make up for the loss of full- time to launch. These methods can be divided into coherent integration testing and noncoherent detection of two categories. The received echo sequence modulo (ie remove the phase information), then the sum referred to the inter- cycle accumulation or non-coherent detection accumulation. Generally due to the accumulation of unused non-coherent phase information, the detection performance than coherent integration, called the difference between the detector losses. Loss on the input detection SNR, SNR increases, the smaller the loss detection.

Conclusion

Fractal characteristics of sea clutter in time and space do not have long-term stability; the simple use of fractal dimension for target detection phenomenon appears false. Sea clutter does have fractal properties, but the properties of fractal fractal data and theoretical models of sea clutter generated compared two different characteristics. One is the sea clutter with non-stationary, varying characteristics of fractal parameters with time, so simply using a threshold when not fully characterize the varying characteristics of the sea clutter. Another is the fractal characteristics of sea clutter has a certain time scale, greater than or less than the time scale does not have fractal properties.

References

[1] J. Guan, N. Liu, J. Zhang, J. Song: Signal Processing, Vol.90 (2010), p.523-535

[2] M. Salmasi, M. M. Hashemi: Chaos, Solitons & Fractals, Vol.40 (2009), p.2133-2145

[3] G.Wang, Z. Pang, J. B. Boisvert: Journal of Geochemical Exploration, Vol.134 (2013), p.85-98

[4] S. Lhermitte, J. Verbesselt: Remote Sensing of Environment, Vol.115 (2011), p.3129-3152

[5] L. Liu, P. Fieguth, D. Clausi, G. Kuang: Pattern Recognition, Vol.45 (2012), p.2405-2418

Applied Mechanics and Materials Vol. 596 (2014) pp 230-233
© (2014) Trans Tech Publications, Switzerland
doi:10.4028/www.scientific.net/AMM.596.230

Hybrid intelligent optimization approach for RFID network planning

Dongliang Guo[1,a], Qiao Xiang[2,b] and Zhonghua Li[2,c]

[1]Electronic Science Department, Huizhou University, Huizhou 516007, China

[2]School of Information Science and Technology, Sun Yat-sen University, Guangzhou 510006, China

[a]gdlfdc@126.com, [b]tmstd@126.com, [c]lizhongh@mail.sysu.edu.cn

Keywords: Radio frequency identification, network planning, intelligent optimization algorithm

Abstract. Radio Frequency Identification (RFID) is a kind of short-range radio technology for data acquisition and automatic identification. In large scale application of RFID system, RFID network planning (RNP) is one of the fundamental tasks need to be fulfilled. This paper proposed an efficient hybrid intelligent optimization approach for RNP. A RNP optimization model is designed in considering of coverage, cost, and the radiated power of readers. A hybrid intelligent optimization approach is proposed to optimize the model in a hierarchical fashion. Firstly, we used the intelligent optimization algorithm to regulate the number and position of the RFID readers for the coverage and cost objective. Then, the optimal radiate power of readers is computed by analytic calculation. Experimental results show that this hybrid intelligent optimization approach has the advantage in terms of the quality of RFID network deployment and computation efficiency comparing with the existing approaches.

Introduction

Radio Frequency Identification (RFID) is a kind of short-range radio technology for data acquisition and automatic identification. A RFID system is composed of RFID readers and RFID tags. RFID readers communicate with the tags in its detectable scope and transmit the information received from tags to a host computer. Many applications, such as automatic detection and indoor localization, require RFID readers to be able to read tags anywhere in a large area. Due to the limited range inherent in the reader-to-tag communication (typically less than 10 meters), readers must be deployed in high densities in the working area. In practical application of RFID system, RFID Network Planning (RNP) is one of the fundamental tasks that need to be fulfilled. RNP is a multi-dimensional non-linear optimizing problem that has to meet many requirements of a RFID network. In general, the RNP aims to optimize a set of objectives (including coverage, load balance, interference, etc.) by regulating the RFID network variables, such as the number of the readers, the coordinates of the readers, and the radiated power of readers [1].

Recently, a number of approaches based on evolutionary algorithm and swarm intelligence have been proposed for solving the RNP problem, such as Genetic Algorithm (GA) [2], Bacteria Foraging Optimization (BFO) [3], Particle Swarm Optimization (PSO) [4], Plant growth simulation algorithm (PGSA) [5], etc.

In this paper, A RNP optimization model is designed in considering of coverage, cost, and the radiated power of readers. A hybrid intelligent optimization approach is proposed to optimize the model in a hierarchical fashion. Firstly, we used the intelligent optimization method to regulate the number and position of the RFID readers for the coverage and cost objective. Then, the optimal radiate power of readers is computed by analytic calculation.

The objective functions and formulation

Before define the constraints, some notations in this paper are formulated:

- TS : the set of all tags in the deployment, $i \in TS$ for any tag *i*.
- RS : the set of all readers in the deployment, $j \in RS$ for any reader *j*.

- KS_i: the set of readers which has the tag *i* in its interrogation region.
- P_{ij}: the received power at the tag *i* from the reader *j* in KS_i.
- P_t: the received power threshold of tag.

The objective functions in proposed approach are as follows:

A. Coverage

The *k*-coverage (*k*=1,2,3) is important objective in all of the objective functions, which is defined as follows:

$$\begin{cases} P_{ij} - P_t \geq 0 & \forall i \in TS, j \in KS_i \\ \sum_{j \in RS} RT_{ij} \geq k & \forall i \in TS \end{cases} \tag{1}$$

where RT_{ij} is a binary variable that $RT_{ij} = 1$ if the reader $j \in KS_i$, otherwise $RT_{ij} = 0$. P_{ij} should be higher than the threshold P_t, which guarantees that the tag is activated. The objective function shown in equation (1) aims to minimize the total difference between P_{ij} and P_t at each tag i in TS by regulating the positions and radiated power of readers. This constraint can optimize the power efficiency of RFID network, while ensuring that each tag is covered by at least *k* readers.

B. Cost of RFID system

The cost of a RFID system is strongly dependent on the number of RFID readers. Minimizing the number of readers is an important objective. The objective function for minimizing the cost of RFID network is defined as follows:

$$\min \quad \sum_{i=1}^{N} c_i \tag{2}$$

where c_i is the cost of the *i*-th reader and *N* is the number of readers deployed.

C. Total radiated power of readers

The objective function aims to minimize the total radiated power of RFID readers, as follows:

$$\min \quad f_{\text{cov}} = \sum_{j \in RS} P_j \times y_j \tag{3}$$

where P_j is the radiated power of *j*-th reader and y_j is a binary variable that $y_j = 1$ if the *j*-th reader is installed, otherwise $y_j = 0$.

The proposed optimizing strategy

Because there are several RNP objectives to be optimized, several optimization strategies can be selected: 1) Pareto optimality; 2) combining all objectives into a scalar value (typically as a weighted sum); 3) solving for the objectives in a hierarchical fashion.

In this paper, we chose to optimize the solution in a hierarchical fashion. This strategy is to optimize for a first objective, then, if there is more than one solution, optimize these solutions for a second objective, and so on.

We first optimize for *k*-coverage and minimizing the cost of RFID network by intelligent optimization algorithm. The objective function is defined as follows:

$$\begin{gathered} \min \quad \sum_{i=1}^{N} c_i \\ s.t. \quad \begin{cases} P_{ij} - P_t \geq 0 & \forall i \in TS, j \in KS_i \\ \sum_{j \in RS} RT_{ij} \geq k & \forall i \in TS \end{cases} \end{gathered} \tag{4}$$

Then, we optimize for radiated power of readers by analytic computation. That is, according to the coordinate of a reader and the tags covered by this reader, calculate the shortest coverage radius, and then calculate the reader radiation power.

Experiments and Results

The RFID planning working area is simulated by an 25m×25m square scene, 100 tags are randomly distributed in this working area. Some radiated-power adjustable readers are deployed to cover the working area. Figure 1 shows the working area and the placement of the tracked tags.

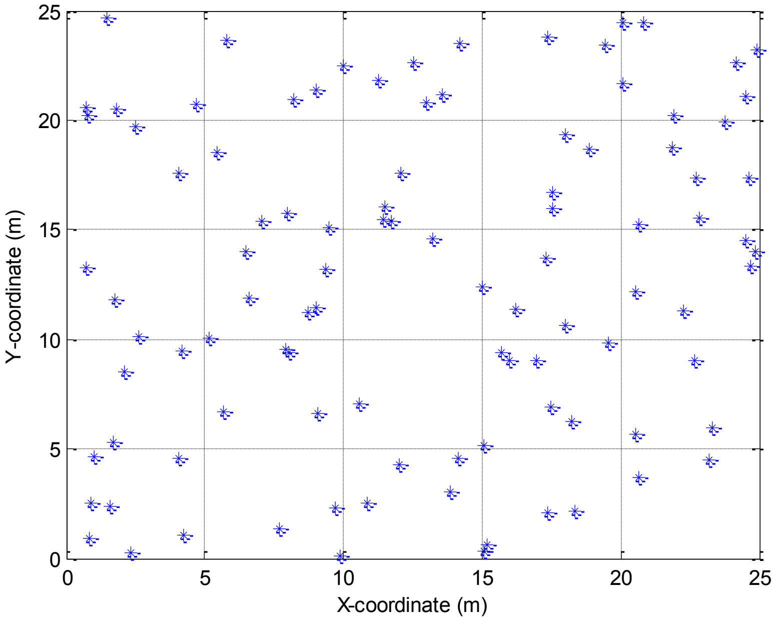

Fig. 1 The placement of the tracked tags

To show the improvement made by the proposed methodology, we compared the RNP result employing the hybrid intelligent optimization approach and the RNP result based on original optimization algorithm.

Fig. 2 shows the RNP results based on GA. Five-pointed star represents the RFID reader, and asterisk represents the tracked tag. We can find from Figure 2 that for the case of 1-coverage, 7 readers are needed for RNP results via GA algorithm. The transmit power of readers has not been well optimized when the original optimization algorithm was employed, but the RNP results via the proposed approach optimized the reader's transmit power, the transmit power of each reader is minimized.

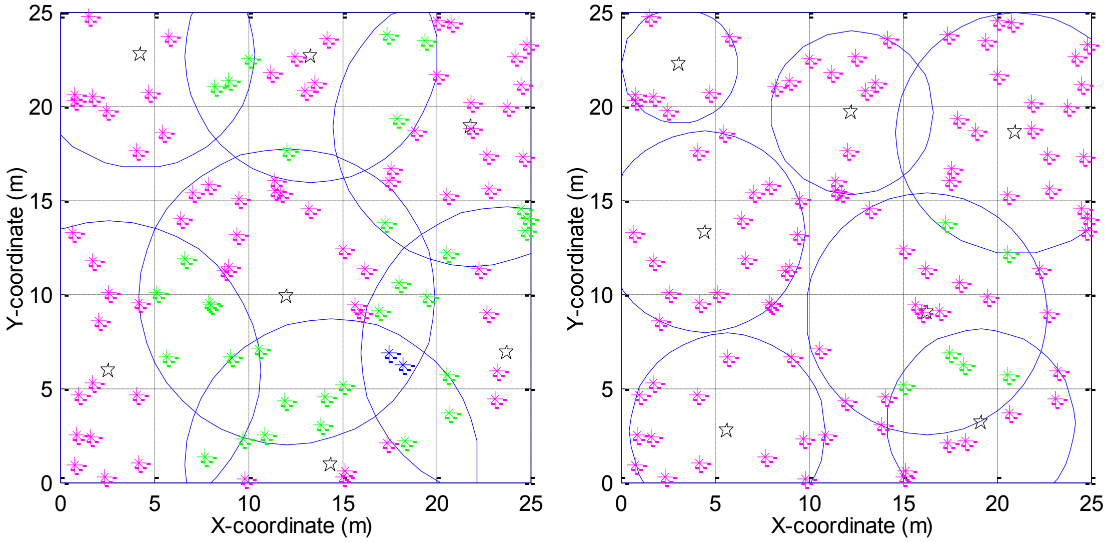

(a) The original algorithm (b) the proposed approach

Fig. 2 RNP results based on GA (*k*=1)

Fig. 3 shows the RNP results based on PSO. For the case of 1-coverage, 7 readers are needed for RNP results via PSO algorithm. The transmit power of readers has not been well optimized when the original PSO algorithm was employed, but the RNP results via the proposed approach optimized the reader's transmit power.

When the proposed hybrid intelligent optimization approach is employed, we can find from Fig.2 and Fig. 3 that the transmit power of each reader is well optimized.

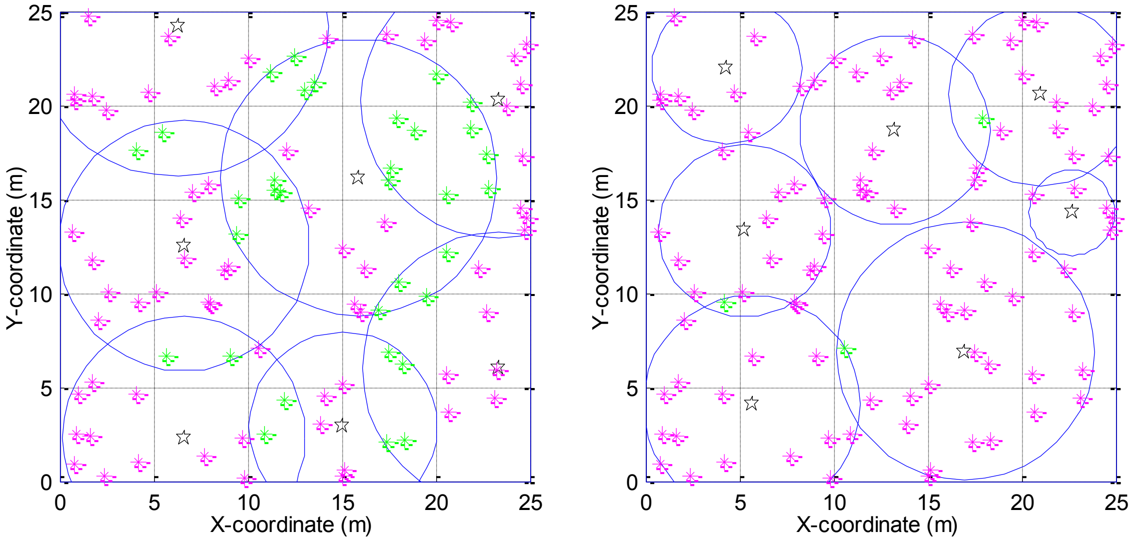

(a) The original algorithm (b) the proposed approach

Fig. 3 RNP results based on PSO (*k*=1)

Conclusions

This paper presents an efficient approach for RFID network planning. The problem is formulated as a multi-dimensional constrained optimization problem, in which *k*-coverage, cost and total radiated power of readers are considered.

We chose to optimize the solution in a hierarchical fashion. Firstly, we used the intelligent optimization method to regulate the number and position of the RFID readers and the cost objective. Then, the optimal radiate power of readers is computed by analytic computation. For the position of tags are known, the analytic calculation method can more accurately determine the coverage radius of each reader. The simulation results reveal that the proposed methodology has advantage in terms of the quality of RFID network deployment and the computational complexity.

References

[1] H.N.Chen, Y.L.Zhu,K.Y.Hu,etc.: Journal of Network and Computer Applications, Vol.34(3): (2011), p.888

[2] Xin-min ZHANG, Qun-kui YAN, Jing LI: The Planning of Workshop RFID Network Based on Modified Genetic Algorithm Using Metropolis Rule[C]// Proc. IEEE 18Th International Conference on Industrial Engineering and Engineering Management, Changchun, (2011), p.778

[3] W. Liu, H.X. Chen, H.N. Chen, etc.: Journal of Computational Information Systems, Vol.7(4): (2011), p.1238

[4] Yue-Jiao Gong, Meie Shen, Jun Zhang,et al.: IEEE Transactions On Industrial Informatics, Vol.8(4):(2012), p.900

[5] Shilei Lu, Shunzheng Yu: Journal of Network and Computer Applications, Vol.39(1): (2014), p.280

Applied Mechanics and Materials Vol. 596 (2014) pp 234-240
© (2014) Trans Tech Publications, Switzerland
doi:10.4028/www.scientific.net/AMM.596.234

Optimization of Multitask in Real-time Control Based on Artificial Bee Colony Algorithm

Shaomeng Chen [1,a], Yuetong Xu [1,b], Qiuxu Hu [1,c], Zhengtuo Wang [2,d]

[1]The State Key Lab of Fluid Power Transmission and Control, Zhejiang University, Hangzhou, Zhejiang, 310027, China

[2]Zhejiang University Kunshan Innovation Institute, Kunshan, Jiangsu, 215347, China

[a]csmchenshaomeng@163.com, [b]xyt@zju.edu.cn, [c]huqiuxu08@163.com, [d]tt81667693@163.com

Keywords: Real-time Industrial Control System; Multitask Communication; Nonlinear Constrained Optimization; Artificial Bee Colony Algorithm

Abstract. Real-time industrial control software often has the characteristic of multitask communication within single thread, which can easily cause the thread to block. The problem can be abstracted into nonlinear constrained optimization model based on requirements of developing the industrial control software, and solved by artificial bee colony algorithm. The ABC algorithm needs less parameters, and has stronger capability of global search than other intelligent algorithms. Considering characteristics of the nonlinear constrained optimization model, three modifications are adopted to improve the capability of global search in this problem. They are a modification rate for generating a new solution, the probability of selecting a new solution by onlooker bees which is different between feasible solutions and infeasible solutions, Deb's constrainted handling method. A comparing result shows that the modified ABC algorithm provides a better solution than GA algorithm does. By putting the solution into practice, high-speed and reliable communication can be realized between IPC, PLC and NC.

Introduction

In an industrial control system, the IPC often has to handle multiple communication tasks with NC and PLC, such as reading equipment's real-time status, countering the processing time and reading the alarm message. Constantly, those tasks have to be dealt with in single thread under the restriction of communication control and be easily blocked, which will affect the normal operation of the equipment.

The problem above can be abstracted into nonlinear constrained optimization model. Specific to this model, some common methods like Lagrange multiplier method, restricted function method, sequential quadratic programming method and function approaching method may only work out with local optimal solutions. With the development of intelligent algorithm, many good algorithms have been proposed to search the global optimal solution. In 1975, J.Holland proposed genetic algorithm (GA) [1], which searches a optimal solution by simulating the natural evolution process; In 1995, Storn and Price firstly proposed a novel evolutionary algorithm called differential evolution (EA) [2], which reduces the complexity of genetic operations while searching the global optimal solution. At the same time, Eberhart and Kennedy proposed particle swarm optimization (PSO) [3], which is similar to the previous two algorithms. These three algorithms have been widely used in solving optimization problems with satisfactory results. In 2005, Karaboga proposed a new algorithm based on the behavior of honey bees called artificial bee colony algorithm [4], which has a stronger ability to search the global optimization solution and depends on less parameters than the algorithms mentioned before though their search strategies are similar to each other.

In this papaer, a modified artificial bee colony algorithm based on the nonlinear constrained programming model, is used to search for the best solution of the industrial control system's multitask communication problem.

Nonlinear Constrained Programming of Real-time Control

The Architecture of The Real-time Control System. The industrial control software is applied to CNC laser cutting machine which adopts Siemens SINUMERIK 840D NC system. Considering the requirements, the control software should be developed on an IPC that is compatible for a Windows platform. An IPC with the software communicates with NC and PLC by wires. So operators can control motions of the machine tool and get real-time CNC information by the software on the IPC. The hardware architecture of the control system is shown in Fig. 1.

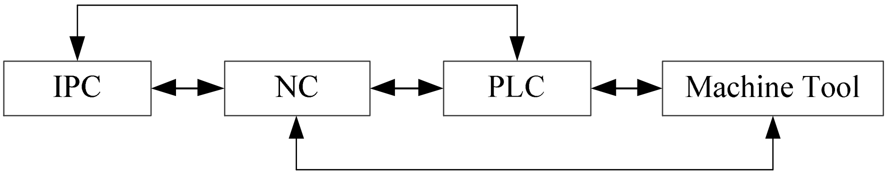

Fig. 1 Hardware architecture of the control system

There are three data areas in SINUMERIK 840D NC system: MMC Data Management, which is used for storing the job program and initialization files on IPC; PLC Data Management, the data of which is used for machining directly; NCK Data Management, where feed rate and other status information of the NC machine is stored. Communication tasks between software on IPC and PLC / NC Data Management are reading and writing data from PLC / NC, transforming files from MMC to NC. In addition, communication between software on IPC and PLC / NC is carried out via the DCTL control and NCDDE server. The communication architecture of the control system is shown in Fig. 2.

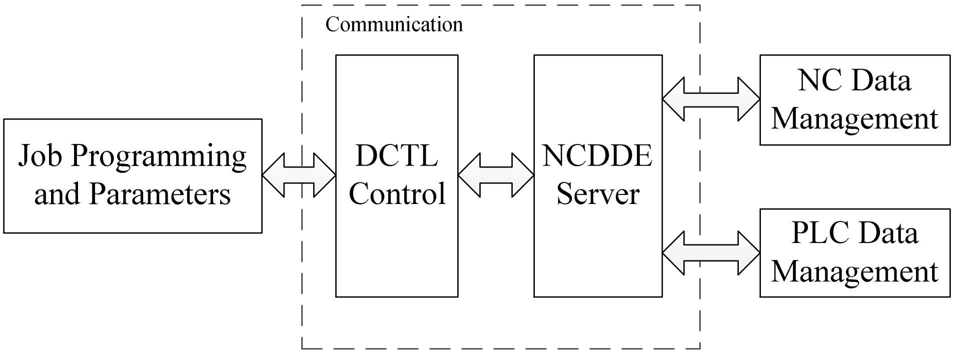

Fig. 2 Communication architecture of the control system

Communications tasks description. IPC gets information about PLC and NC by scanning the communication interface periodically based on timers. Thus it would handle tasks during the interphases. The tasks are allocated for each timers as Table. 1:

Table. 1 Task distribution for timers .

Timers	Tasks	Durations
1	modify processing parameters	10ms
2	count processing time	5ms
3	monitor NC mode; read NC alarm message; read PLC alarm message;	180ms
4	processing message of signal lights;	110ms
5	set feed rate; read manufacturing coordinates from NC;	85ms
6	read speed rate from NC;	10ms
7	read values of air pressure;	80ms

With the restriction of DCTL control, all the communication tasks should be processed in single thread. Thus, long timer period will reduce the efficiency of the system while short timer period will cause a phenomenon of task blocking. So it's crucial to set suitable scanning periods that can guarantee equipment torun smoothly.

Nonlinear Constrained Programming Model. The problem can be decomposed into two sections. First, each task should be dealt within the period of the timer it's associated with. As we can see from Table. 1, durations of dealing with tasks are $t_1 = 10$, $t_2 = 5$, $t_3 = 180$, $t_4 = 110$, $t_5 = 85$, $t_6 = 10$, $t_7 = 80$. Let's assume the period of each timer as T_1, T_2, T_3, T_4, T_5, T_6, T_7, inequation (1) should be satisfied :

$$\sum_{m=1}^{7} t_m \frac{nT_k}{T_m} < (n+1)T_k \tag{1}$$

where k represents the serial number of timers, $k \in \{1,2,...,7\}$, $n \in N^+$.

Second, the comprehensive scaning period should be as short as possible. Considering the requirements of the control system, the priority of tasks can be divided into three grades, Timer 5 and Timer 6 as the optimal level, Timer 1, Timer 2 and Timer 4 as the suboptimal level, Timer 3 and Timer 7 as the lowest level. Thus, a target function is obtained with weights based on timers' priority levels as follows.

$$f(T) = \frac{3}{14}(T_5 + T_6) + \frac{1}{7}(T_1 + T_2 + T_4) + \frac{1}{14}(T_3 + T_7) \tag{2}$$

Also,

$$\text{e}1 \le T_k \le 1000, T_k \in N^+, \forall k = 1,2,3...,7$$

Based on the analysis above, a standard nonlinear constrained programming model can be obtained below .

$$\min f(T), T \in D$$

$$s.t \begin{cases} \frac{t_1}{T_1} + \frac{t_2}{T_2} + \frac{t_3}{T_3} + \frac{t_4}{T_4} + \frac{t_5}{T_5} + \frac{t_6}{T_6} + \frac{t_7}{T_7} - 1 < 0 \\ 1 \le T_k \le 1000, \qquad T_k \in N^+, \forall k = 1,2,3...,7 \end{cases} \tag{3}$$

Lots of methods are proposed to solve nonlinear constrained programming problems, such as Lagrange multiplier method, restricted function method, sequential quadratic programming method and function approaching method. While those common methods could only result in locally optimal solution, many intelligent algorithms such as GA algorithm, DE algorithm, PSO algorithm and SA algorithm are created to search for global optimal solution. After comparing some effective algorithms, ABC algorithm is chosen to solve the problem in this paper.

Algorithm Description

Standard ABC Algorithm. In ABC algorithm, the colony of artificial bees contains three groups of bees: employed bees associated with specific food sources, onlooker bees watching the dance of employed bees within the hive to choose a food source, and scout bees searching new food sources randomly when the old food sources position can not be improved further through a predetermined number of cycles. The position of a food source represents a possible solution to the problem and the nectar amount of a food source corresponds to the quality (fitness) of the associated solution. The number of employed bees is equal to the number of food sources (solutions) since each employed bee is associated with one and only one food source. All the vectors of the population of food sources, x_i, are initialized($m = 1,2,...,SN$, SN : population size) by scout bees and control parameters are set. After initialization, the entire population will repeat the cycle of searching for better food sources by employed bees, onlooker bees and scout bees, until the maximum number of iteration.

Employed bees search for new food sources having more nectar within the neighbourhood of the old food source in their memory. They find a neighbour food source and then evaluate its profitability (fitness). They can determine a neighbour food source using the formula given by equation (4) .

$$v_{ij} = x_{ij} + \varphi_{ij}(x_{ij} - x_{kj}) \tag{4}$$

Where $k \in \{1,2,...,\mathrm{SN}\}$, $j \in \{1,2,...,d\}$, $k \neq i$; φ_{ij} is a random number within the range $[-1,1]$. Then its fitness is calculated and a greedy selection is applied between v_{ij} and x_{ij}.

Onlooker bees choose food sources depending on the probability values calculated using the fitness values provided by employed bees. For this purpose, a fitness based selection technique can be used, such as the roulette wheel selection method. The probability value with which is chosen by an onlooker bee can be calculated by using the expression given by equation (5) .

$$p_i = fit_i / \sum_{k=1}^{SN} fit_k \tag{5}$$

Employed bees whose solutions cannot be improved through a predetermined number of trials, specified by the user of the ABC algorithm and called “limit” or “abandonment criteria” herein, become scout bees and their solutions are abandoned. Then, the converted scout bees start to search for new solutions using the formula given by equation (6) .

$$x_{ij} = x_{\min j} + rand(0,1)(x_{\max j} - x_{\min j}) \tag{6}$$

Hence those sources which are initially poor or have been made poor by exploitation are abandoned and negative feedback behaviour arises to balance the positive feedback.

The fitness value of a solution, might be calculated for minimization problems using formula (7):

$$fit(x_i) = \begin{cases} \dfrac{1}{1+f(x_i)}, & f(x_i) > 0 \\ 1 + abs(f(x_i)), & f(x_i) < 0 \end{cases} \tag{7}$$

where $f(x_i)$ is the objective function value of solution x_i.

Modified ABC algorithm. As the standard form of nonlinear constrained programming in this paper can be given as follows.

$$\min f(\mathrm{X}), \mathrm{X} \in D$$

$$s.t \begin{cases} \mathrm{g}_j(\mathrm{X}) \le 0, & i = 1,2,...,q \\ h_k(\mathrm{X}) = 0, & k = q+1, q+2, ..., m \end{cases} \tag{8}$$

We can modify the ABC algorithm with three steps in order to adapt it for solving nonlinear constrained optimization problems .

Firstly, in order to produce a candidate solution from the old one in memory, the modified ABC algorithm uses the following expression by introducing a control parameter [5]:

$$v_{ij} = \begin{cases} x_{ij} + \varphi_{ij}(x_{ij} - x_{kj}), & \text{if } R_j < MR \\ x_{ij}, & \text{otherwise} \end{cases} \tag{9}$$

where $k \in \{1,2,...,\mathrm{SN}\}$ is randomly chosen index. Although k is determined randomly, it has to be different from i. R_j is a randomly chosen real number within the range $[0,1]$, and $j \in \{1,2,...,d\}$. MR is a control parameter that controls whether the parameter x_{ij} will be modified or not.

Secondly, Deb’s constrained handling method [6,7] is adopted instead of the greedy selection since Deb’s method consists of very simple three heuristic rules. Deb’s method uses a tournament selection operator, where two solutions are compared at a time based on the following criteria: 1) Any feasible solutions are preferred to any infeasible solutions, 2) Among two feasible solutions, the one having better objective function value is preferred, 3) Among two infeasible solutions, the one having smaller constraint violation is preferred. The following fitness is devised to realize Deb’s method .

$$F(\vec{x}) = \begin{cases} f(\vec{x}), & \text{if } g_j(\vec{x}) \geq 0, \forall j = 1,2,...m \\ f_{\max} + \sum_{j=1}^{m} \left| g_j(\vec{x}) \right|, & \text{otherwise} \end{cases} \tag{10}$$

The parameter $f_{\max}$ is the objective function value of the worst feasible solution in the population. Thus, the fitness of an infeasible solution not only depends on the amount of constraint violation, but also on the population of solution at hand. However, the fitness of a feasible solution is always fixed and is equal to its objective function value.

Thirdly, since infeasible solutions are allowed to populated to the colony, assignment to the probability value for infeasible solutions and feasible solutions should be modified as follows:

$$p_i = \begin{cases} 0.5 + (fit_i / \max(fit)) \times 0.5, & \text{if solution is feasible} \\ \left(1 - violation_i / \max(violation)\right) \times 0.5, & \text{if solution is infeasible} \end{cases} \tag{11}$$

where $violation_i$ is the penalty value of solution x_i and fit_i is the fitness value of solution x_i. As can be seen from the equation above, the probability values for feasible solutions are between 0.5 and 1 while those of infeasible ones are between 0 and 0.5. By the method of roulette wheel selection, solutions are selected probabilistically proportional to their fitness values incase of feasible solutions and inversely proportional to their violation values of infeasible solutions .

The pseudo-code of the modified ABC algorithm is given below .

```
Initialize the population of solutions
Evaluate the population
cycle=1
repeat
  for $i = 1 : SN$ do
    Produce a new food source by using (9) and evaluate its quality
    Apply the selection process between $v_i$ and $x_i$ based on Deb's method by (10)
    If solution $x_i$ does not improve, $trail(i) = trail(i) + 1$, otherwise $trail(i) = 0$
  end for
  Calculate the probability values $p_i$ by (11) for the solutions using fitness values
  $t = 0$, $i = 1$
  repeat
    if $random < p_i$ then
      Produce a new food source by using (9) evaluate its quality
      Apply the selection process between $v_i$ and $x_i$ based on Deb's method by (10)
      If solution $x_i$ does not improve, $trail(i) = trail(i) + 1$, otherwise $trail(i) = 0$
      $t = t + 1$
    end if
  until ($t = SN$)
  if $\max(trail(i)) >$ limit then
    Replace $x_i$ with a new randomly produced solution by (6)
  end if
  Menorize the best solution achieved so far
  cycle=cycle+1
until (cycle = Maximum Cycle Number)
```

Simulating Calculation

There should be four parameters defined before we use the algorithm: The number of food sources which is equal to the number of employed or onlooker bees (*SN*), the value of *MR* ,the value of *limit* and the maximum cycle number.

With the maximum cycle number increasing, comprehensive timing period which is the result of the algorithm will be shorter and shorter, and the result will be convergence. As the experiment of testing different values of the maximum cycle number, it is shown that the result almost remain the same when the cycle is more than 500. Thus, the value of the maximum cycle number can be determined as 500. Generally, a bigger value of *SN* will result in a better solution but a slower computation speed. And with the increasing value of *SN* , the result tends to stabilize. In this paper, the value of *SN* is determined as 100 through synthetical consideration. The value of *limit* is determined as 40 as the best choice after testing different values.

After three parameters are determined, the value of *MR* should be determined based on this specific example. Firstly, ten different *MR* with their values ranging from 0.05 to 0.95 are tested, and the result based on each *MR* is the average value of ten times calculation. The result of overall optimization for *MR* is shown in Table. 2.

Table. 2 Result of overall optimization for *MR*

MR	0.05	0.15	0.25	0.35	0.45	0.55	0.65	0.75	0.85	0.95
comprehensive timing period	357.37	345.62	333.96	336.35	332.66	331.70	328.78	331.17	330.99	331.41

From the results given in Table 2, it can be seen that, a *MR* with its value ranging from 0.55 to 0.95 can lead to a better result than others.

Secondly, a further experimentation is needed to determine the value of *MR* between 0.55 and 0.95. With the same testing method, the results are given in Table. 3.

Table. 3 Result of refinement optimization for *MR*

MR	0.5	0.55	0.60	0.65	0.70	0.75	0.80	0.85	0.90	0.95
comprehensive timing period	332.40	331.95	329.02	330.97	330.93	332.37	326.55	330.01	331.84	330.11

From the results given in Table 3, it is obvious that the *MR* whose value is 0.80 can lead to the best solution of all. So, the value of *MR* is determined as 0.80.

With all the parameters determined, a best solution is chosen after ten times of repeated test as in Table. 4.

Table. 4 The best solution of the problem by modified ABC algorithm

	T_1	T_2	T_3	T_4	T_5	T_6	T_7	$f(T)$
Result	197	135	797	462	367	106	655	318.50

In order to evaluate the performance of the modified ABC algorithm, we used GA algorithm to solve the same problem, and the result of GA is shown in Table. 5.

Table. 5 The solution of the problem by GA algorithm

	T_1	T_2	T_3	T_4	T_5	T_6	T_7	$f(T)$
Result	227	516	546	458	411	274	603	400.42

Comparing the results from Table 4 and Table 5, it can be concluded that the modified ABC algorithm performs better than GA algorithm in this case.

In the end, seven timers' timing cycles of the software of the control system software were set by the result we've got before. And the IPC of the system communicated with PLC and NC fluently while the whole system operated very smoothly.

Conclusions

In order to solve industrial control system's multi-task communication problem, a nonlinear constrained programming model is established with the purpose of achieving the shortest comprehensive timing period. After considering some common methods of solving constrained programming problems and comparing some intelligent algorithms, artificial bee colony algorithm is adopted to solve the problem with the advantage of strong capacity for searching for global optimal solution. Combing the feature of constrained programming model, some parameters's computing methods are modified from standard ABC algorithm. With the result of simulation, it can be concluded that the modified ABC algorithm's capacity for searching for global optimal solution remains strong and the problem of multitask communication is well settled.

Acknowledgements

The work has been supported by the National Key Technology R&D Program (No. 2013BAF05B00), and Major Industrial Projects for Major S&T Project of Zhejiang Province (No. 2012C01010-5).

References

[1] J.H. Holland: *Adaptation in Natural and Artificial Systems* (University of Michigan Press, Ann Arbor, MI, USA, 1975).

[2] R. Storn, K. Price: Differential evolution – a simple and efficient adaptive scheme for global optimization over continuous spaces, Techn. Rep, International Computer Science Institute, Berkley, 1995.

[3] J. Kennedy, R.C. Eberhart: *IEEE International Conference on Neural Networks*(Perth, WA, 27 Nov 1995-01 Dec 1995), Vol. 4, p. 1942.

[4] D. Karaboga: An idea based on honey bee swarm for numerical optimization, Techn. Rep. TR06, Erciyes Univesity, Engineering Faculty, Computer Engineering Department, 2005.

[5] D. Karaboga and B. Basturk: *12th International Fuzzy Systems Association World Congress* (Cancun, Mexico, June 18-21, 2007). Vol. 4529, p. 789.

[6] D.E. Goldberg, K. Deb: A comparison of selection schemes used in genetic algorithms Foundations of Genetic Algorithms, edited by G. J. E. Rawlins, pp. 69-93,1991.

[7] K. Deb: Computer Methods in Applied Mechanics and Engineering,Vol. 186(2000) No. 2/4, p.311.

Applied Mechanics and Materials Vol. 596 (2014) pp 241-244
© (2014) Trans Tech Publications, Switzerland
doi:10.4028/www.scientific.net/AMM.596.241

Research for wind power system reactive power optimization based on improved artificial fish swarm algorithm

Shun-hua Zhang

School of Mechanical and Electrical Engineering, Nanchang Institute Technology, China

threehhu@163.com

Keywords: Wind power system. Reactive power optimization. Artificial fish swarm algorithm.

Abstract. Wind power system reactive power optimization problem is a very complicated nonlinear programming problem, using the traditional reactive power optimization algorithm such as nonlinear programming method, the genetic method, particle swarm algorithm, etc; it's easy to have a slow convergence speed, into a local optimal solution of problem. To solve these problems, we improve algorithm accordingly. According to the actual situation of wind power system, adjust the parameters, especially the number of artificial fish and vision for the dynamic testing, the selection, crossover and mutation in the number of artificial fish for debugging, in order to achieve satisfactory effect.

Introduction

Currently mostly wind turbine generator is asynchronous generator; this type of generator will absorb a large number of reactive powers in operation of the merged wind power grid, and reduce the stability of the system and power quality [1, 2]. With the increasing of wind power generating capacity, wind power has more and more influence to power grid. The wind power system reactive power optimization model and its algorithm play an important role to improve the wind power grid performance.

For main kinds of reactive power optimization mathematical model, general optimization method focus on improve the convergence performance, improve the calculation speed, mainly in the traditional sense of the nonlinear programming method, linear programming, mixed integer programming and dynamic programming method, and intelligent algorithm such as expert system, genetic algorithm, simulated annealing algorithm, differential evolution algorithm [3].

The main research methods

Mathematical modeling. In order to comprehensive analyses the influence of the reactive power optimization of distribution network by the random fluctuations of wind turbine power output this paper presents a reactive power optimization comprehensive index based on scenario occur probability, the index measured from two aspects: economy and safety of the merits of the reactive power optimization [4], the economy is in terms of reducing system network loss, security embodied in improving the system static voltage stability margin.

According to the actual situation of wind power, the parameters is adjusted, especially the number of artificial fish and vision for the dynamic testing, the selection, crossover and mutation in the number of artificial fish for debugging to achieve satisfactory effect [5, 6].

This topic put forward by the reactive power optimization composite indicator based on the occurrence probability of scene λ is as follows:

$$\lambda = \omega_1 \lambda_1 + \omega_2 \lambda_2 \tag{1}$$

Where w_1 and w_2 is the weight coefficient; λ_1 and λ_2 respectively is the network loss expectation and static voltage stability margin expectation.

The network loss expectation λ_1 is as follows:

$$\lambda_1 = \sum_{k=1}^{n} P_K P_{loss}^K \tag{2}$$

P_K is probability of the K scenario, P_{loss}^K is network loss of the K scenario.

The static voltage stability margin expectation λ_2 is as follows:

$$\lambda_2 = \sum_{k=1}^{n} P_K \delta_K \tag{3}$$

δ_K is static voltage stability margin of the K scenario.

The improvement algorithm. This project takes the following measures to improve the artificial fish swarm algorithm.

The selection, crossover and mutation operator of genetic algorithm are loaded in artificial fish algorithm in the same time. It makes every effort to integrate two algorithms and complementary advantages. Including the introduction of crossover operator is very important; the artificial fish after crossover operation, its search ability are improved leap.

Getting into a local optimal solution is "premature" phenomenon of optimization algorithm [7]. The fundamental reason is that the diversity of population are destroyed, the global search ability drops precipitously and the global search ability and local search ability caused by the imbalance [8]. To solve this problem, two measures: one is the introduction of mutation operator, improve the ability of the artificial fish jump out of local optimal; the second is respectively carried out on the part of the artificial fish individual selection, crossover and mutation operation, effectively increase and maintain the diversity of artificial fish populations.

For wind randomness and the difference of wind farm, to adjust the selection, crossover and mutation operation of artificial fish number can deal with it [9]. If the operation is slow, the number of crossover operation can be increased, if computing prone to local optimum, the number of mutation can be increased. Anyway, for the specific optimization object flexible adjust the number of selection, crossover and mutation operation, optimizing the population structure; improve the global search and local search performance.

Each operation only for part of the artificial fish individuals, the sum of the number three operations are only part of the total, save quite a number of artificial fish don't do anything, directly into the next generation [10]. Doing so has two advantages: one is can simplify procedures and speed up the computation; the second is to make basic artificial fish algorithm is simple, efficient, easy to implement, and many other advantages to get better retention.

Reactive power optimization problem is a very complicated nonlinear programming problem, to research a kind of suitable for the actual system, stable and reliable, fast convergence of the optimization algorithm is important problem presses for solution in the currently field of reactive voltage optimization control [11]. Artificial fish algorithm has the characteristics of no sensitive to initial value and parameter selection, robust, simple and easy to realize, and with other excellent algorithm fusion and complementary architecture and good foundation. The improved artificial fish algorithm was applied to wind power system reactive power optimization, compared with other algorithms, has a unique advantage [12]. This is because that it not only incorporates the advantages of the artificial fish algorithm and the genetic method. More importantly, the wind farms are different in geographical environment, climate conditions and installed number and size, in the face of this complex situation, any other kind of algorithm is easy to fall into difficulties. And improved artificial fish algorithm can be improved in the process of operation, the flexibility to adjust the selection, crossover and mutation operation of artificial fish individual number, to adapt to the specific condition of wind farm, the optimized algorithm achieves better effect [13]. Therefore, this project will be improved artificial fish algorithm is first used in wind power system reactive power optimization.

The research applications

Jiujiang (Poyang Lake) region as rich wind resources in Jiangxi Province has formed a large-scale wind power generation group. 4 wind farms have been put into operation at present, that includes 89 sets of wind turbines and a total installed capacity of 103.5 MW. Because the wind has strong randomness, how to use the reactive voltage control means to match the wind power, wind power's reactive voltage optimization control which has become more and more important problem and practical significance in the areas of study.

Wind power system has its unique characteristics. The optimal results will be funded by reactive power optimization, will achieve remarkable economic benefits. As an example, the existing 4 wind fields in Jiujiang area (Jishan lake, Changling, DaLing, Laoye temple) included the total installed capacity of 103.5 MW, which has wind power generating capacity of about 268 million kWh every year, price is 0.686 yuan/kWh, for the wind farm side after reactive power optimization, with auxiliary power rate decline by 0.1%, wind farm will get direct economic benefit of 183848 yuan annual. For the grid side with reactive power optimization, in terms of network loss rate decline by 1%, Power Grid Company will get direct economic benefit of 1.83848 million yuan a year; the economic benefit is very considerable. At the same time, through the wind power system reactive power optimization, the power grid voltage stability safety coefficient can be improved, strengthen the reactive power support in the load side; improve the social production efficiency.

Conclusions

This innovations of this topic is combined with the practical operation of wind farm in Jiujiang administrative region is experience, proposed wind farm reactive power compensation capacity is obtained by power flow calculation, reoccupy optimum population, improved artificial fish algorithm to wind power system reactive power optimization, by adjusting the transformer variable ratio and capacitor group method, establish the minimum network loss and the best voltage level as the objective function of optimization mathematical model, to meet various constraint conditions for solving reactive power optimization [14].

Acknowledgements

This work was financially supported by the Jiangxi Natural Science Foundation (20114BAB206036), Science and Technology Project of Jiangxi Province Education Department (GJJ13769) .

References

[1] Wang Xifan. *Power system optimal planning* [M]. Beijing: water conservancy electric power press, 1990.

[2] Li Xiaolei. *A new type of artificial intelligence optimization method of artificial fish algorithm* [D], Zhejiang:Zhejiang university, 2003.

[3] Li Xiaolei, Shao Zhijiang,Qian Jixin. *An optimization model based on animal commune fish algorithm* [J]. Journal of systems engineering theory and practice, 2002, 22 (11) : 32 to 38.

[4] Xiong Xinyin, Wu Yaowu. *Genetic algorithm and its application in power system* [M]. Wuhan: Huazhong university of science and technology press, 2002.

[5] Tang Jiandong, Xiong Xinyin, Wu Yaowu etc. *Electric power system reactive power optimization based on artificial fish algorithm* [J]. Journal of relay, 2004, 32 (19) : 12-15.

[6] Zhang Meifeng. *Artificial fish the improvement and application of intelligent optimization algorithm research* [D], Dalian, Dalian university of technology, 2008.

[7] Zhou Hongwei. *"premature" phenomenon and the improved genetic algorithm (ga) strategy research* [D], Henan: PLA information engineering university, 2004.

[8] Pan Xiong. *Optimization of transmission network planning method research* [D]. Chongqing: chongqing university, 2002.

[9] Luo Jun. *Wind turbines in distribution network reactive power optimization research* [D], Hunan: Hunan university, 2009.

[10] Zhang Yanli. *Wind farm reactive power compensation based on ant colony algorithm* [D], Beijing: Beijing Jiaotong university, 2009

[11] Ceng Xuejiang. *Wind turbines in power distribution network reactive power optimization and algorithm research* [D], Chengdu: southwest Jiaotong university, 2011.

[12] Golshan, M.E.H; Arefifar, S.A. *Distributed generation reactive sources and network-configuration planning for power and energy-loss reduction*. IEE Proceedings: Generation, Transmission and Distribution, 2006, 143(2): 127-136

[13] Delfanti M; Granelli G P; Marannino P, et al. *Optimal capacitor placement using deterministic and genetic algorithms*[J], IEEE Trans on Power Systems, 2000,15(3): 1041-1046

[14] Patel M R. *Wind and solar power systems design, analysis and operation*[M]. CRC Press, 2008.

Applied Mechanics and Materials Vol. 596 (2014) pp 245-250
© (2014) Trans Tech Publications, Switzerland
doi:10.4028/www.scientific.net/AMM.596.245

The prediction of grounding grid corrosion rate using Optimized RBF Network

Chunfeng Song [1, a], Yuanbin Hou [2,b] ,Jingyi Du [3,c]

[1]The Institute of Electric and Control Engineering, Xi'an University of Science and Technology, Xi'an, China, 710054

[2]The Institute of Electric and Control Engineering, Xi'an University of Science and Technology, Xi'an, China, 710054

[3]The Institute of Electric and Control Engineering, Xi'an University of Science and Technology, Xi'an, China, 710054

[a]song0729@sina.com, [b]houyb@xust.edu.cn, [c]dujingyi@tom.com

Keywords: grounding grid corrosion rate; ant colony clustering; RBF neural network

Abstract. Because the grounding grid corrosion rate has the property of nonlinearity and uncertainty, it is very difficult for us to predict precisely. The approach is proposed that ant colony clustering algorithm is combined with RBF neural network to predict the grounding grid corrosion rate, using ant colony clustering algorithm to get the center of hidden layer neurons. To find the best clustering result, local search is applied in ant colony algorithm. This model has good performance of strong local generalization abilities and satisfying accuracy. At last, it is proved with lots of experiments that the application is fairly effective.

Introduction

Substation grounding grid is an important measure to ensure reliable operation of power system and its reliability is related to the normal operation of the power grid. For grounding grid corrosion problems, some scholars put forward some new theories and research methods. The theory of circuit network is adopted in the references [1-4]. Because of its large scale of mathematic equations and the increase of the computational cost, it is inconvenient in actual application. The electromagnetic field analysis method is applied to diagnose the corrosion status of the grounding grid conductor in the reference [5]. The theory is complicated, furthermore, the magnetic field around the grounding grid will influence the test in a certain degree and reduce the diagnostic accuracy. The electrochemical corrosion detection sensor is adopted to measure corrosion rate in view of electrochemical method in the reference [6]. Some problems such as high cost and complex test technology will restraint its application in this way.

With the development of computer technology and artificial intelligence, machine learning methods increases in the field of electric power applications [7-9]. The rule can be deduced from the sample data, and then the future data can be predicted in the rules [10].The grounding grid corrosion prediction model, related to the soil physical and chemical corrosion factors, is made with BP artificial neural network in the references [11-13]. However, the adjustment of parameter in forecasting model is influential for precision and generalization ability of the forecasting model. Consequently, it is beneficial for improving the precision of forecasting to optimize the parameters of the forecasting model. Ant algorithm may play a role in optimizing the parameters of the forecasting model. The best parameters of the forecasting model may be obtained by the global search of ant algorithm.

The center of hidden layer neurons in RBF neural network is acquired with ant colony clustering algorithm. The basic ant algorithm is improved and is mixed with local search. Then the improved ant colony clustering algorithm combined with RBF neural network is applied to forecast the grounding grid corrosion rate. This model has good performance of strong local generalization abilities and satisfying accuracy.

The Analysis of Influencing Factor and the Settings of RBF Input Layer

The factors influencing grounding grid corrosion rate are extremely complicated. The key factors include the value of pH x1, water content x2, conductivity x3, organic matter x4, total nitrogen x5, the concentration of HCO_3^- x6, the concentration of Cl^- x7, the concentration of SO_4^{2-} x8, the concentra -tion of Ca^{2+} x9, the concentration of Mg^{2+} x10, the concentration of K^+ x11, the concentration of Na^+ x12.

There lies the extraordinary complicated, nonlinearity relevance in the grounding grid corrosion rate and above twelve factors. Moreover, these factors are correlative and restricted to each other. It is difficult to express the constitutive relation with an exact function. The constitutive relation between the corrosion rate and the influencing factors can be approximated with the improved RBF neural network. Thereby, the grounding grid corrosion rate can be forecasted.

RBF neural network consists of three layers. First layer is input layer, consisting of signals source. The number of neuron depends on the number of influencing factors, which is twelve in this paper. The second layer is hidden layer, in which the transfer function is degenerative nonlinear function and symmetrical in radial direction. The number of neuron in hidden layer can be adjusted by self-adaption with the RBF learning process until the error is satisfied. The third layer is output layer, which can respond to input signals. The transfer function of output layer is linear function and has only one neuron, standing for the grounding grid corrosion rate. The forecasting network structure is shown as Fig.1.

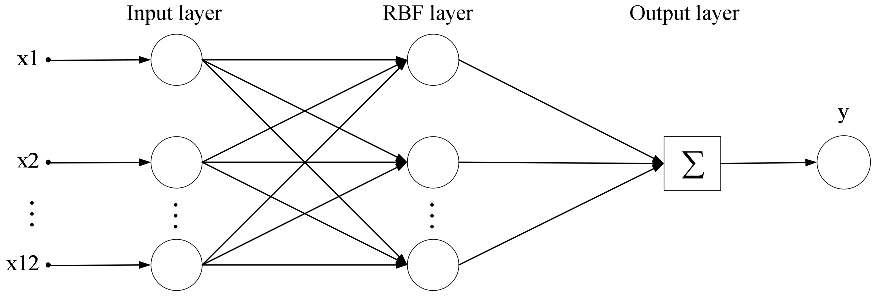

Fig.1 The model of forecasting corrosion rate based on RBF network

Ant Colony Clustering Algorithm

The ant algorithm is proposed as a kind of random search algorithm on the basis of the cooperation of the ant colony in fact. The ants communicate with each other by pheromone. Ants can perceive the existence and intensity of the pheromone and move toward the pheromone until found the optimum solution.

The ant algorithm seeks the optimum solution by means of evolving the colony of candidate solution. The ant algorithm is suitable for distributed computation and positive feedback because of strong robustness. It is proved that the ant algorithm can be applied to solve all kinds of complicated optimization problem, so it can be used to solve cluster analysis.

For ant colony clustering algorithm, the below should be taken into account.

A. The Structure of the Ant. In ant colony clustering algorithm, each ant stands for one possible clustering result. Before research, each ant is distributed a vacant solution set S, its length equal to the number of sample N. The i-th position of S stands for the cluster of the i-th sample. After search, the value of solution set stands for the cluster of the i-th sample.

B. The Structure of the Matrix of Pheromone. The pheromone is the mechanism by which the ants can communicate with each other. Initially, pheromone τ is initialized as the same value, supposing that $\tau_{ij}(0)=C$ (C is constant), τ_{ij} stands for the pheromone that the i-th sample is distributed to the j-th cluster.

C. The Structure of Target Function. In pattern sample set $\{X\}$, there are N samples and M pattern cluster and each sample has n characters. The target function is defined as

$$\min J(w,c)=\sum_{j=1}^{m}\sum_{i=1}^{N_j}\sum_{p=1}^{n} w_{ij}\left\|x_{ip}-c_{jp}\right\|^2 \ , \tag{1}$$

$$c_{jp}=\frac{\sum_{i=1}^{N_j} w_{ij}x_{ip}}{\sum_{i=1}^{N_j} w_{ij}} \quad (j=1,\cdots,M;p=1,\cdots,n). \tag{2}$$

Here, x_{ip} is the p-th property of the i-th sample; c_{jp} is the p-th property of the j-th center. If the sample i belongs to cluster j, $w_{ij}=1$,else $w_{ij}=0$.

D. Updating the Ants Colony. After initializing probability $q_0(0<q_0<1)$, the system produces a random number q for each sample consisting of ant. If $q<q_0$, the biggest pheromone cluster is thought as the cluster of the sample. If $q>q_0$, the cluster of the sample is selected at random by transition probability. The transition probability from sample i to cluster j is calculated. Initializing

$$p_{ij}=\frac{\tau_{ij}}{\sum_{i=1}^{M}\tau_{ij}} \quad (j=1,\cdots,M) \ . \tag{3}$$

Here, τ_{ij} is the normal pheromone between sample i and its cluster j.

E. Local Search. In order to improve the efficiency of the algorithm, the ant algorithm is mixed with local search. In other words, the L ant solution sets of least target value are transformed. The method is shown as the following. 1) A random number is produced for each sample in solution set. 2) The cluster is selected as the distributed that has the least distance from the center of the cluster to the sample, then clustering again. 3) Calculate the target value again according to Eq.1 after transformation. If the result is less than the primary, the result is reserved, else it is abandoned. 4) The operation is carried out in the front L solution sets. The ant is selected as the optimal solution that has the least target function in the front L ants.

F. Updating Pheromone. After local search, the pheromone is updated with the help of the L ants. The pheromone is updated as

$$\tau_{ij}(t+1)=(1-r)\tau_{ij}(t)+\Delta\tau_{ij}(t) \ , \tag{4}$$

$$\Delta\tau_{ij}=\sum\Delta\tau_{ij}^{k} \ . \tag{5}$$

Here, $r(0<r<1)$ is the evaporation coefficient of pheromone, $\tau_{ij}(t)$ is the pheromone of the sample i and cluster j at moment t. $\Delta\tau_{ij}$ is the increment of the pheromone in present circulation. $\Delta\tau_{ij}^{k}$ is the pheromone produced by the k-th ant in present circulation. It is supposed that L_k is the target function value for the ants, and Q is a constant. If the sample i in the ant k belongs to the cluster, $\Delta\tau_{ij}^{k}=\frac{Q}{L_k}$, else $\Delta\tau_{ij}^{k}=0$.

Iterating in circulation till the maximum iterations, the optimal solution is the result of clustering.

Modeling of Predicting The Grounding Grid Corrosion Rate

The model of predicting the grounding grid corrosion rate can be divided into three parts: data normalization, ant colony clustering, RBF neural network training and testing.

A. Data Normalization. For some data varying violently, data normalization is need. The method for data normalization is shown as

$$\alpha=\frac{x_k-\min(X)}{\max(X)-\min(X)}, \tag{6}$$

$X=(x_1,x_2,\cdots,x_n)$ is sample.

B. Ant Colony Clustering. After normalization, the samples are clustered to find the optimal result. The steps are shown as the following.

First step Initializing the parameters of the ant colony. The parameters to be initialized are the number of ants ant, the number of the clusters class, attenuation coefficient of pheromone r, threshold value in local search h, iterations num, initial pheromone tau and initial solution set.

Second step Calculate each center of the clusters and the target function of every ant, sort the ants by the value of the target function.

Third step Local search. The front L ants are selected as exchanging sample after sorting. Local search is carried out in the sample to be exchanged.

Fourth step Updating the pheromone. Update the pheromone according to Eq.4.

Fifth step If the maximum iterations appears, the optimal cluster solution set is obtained, else, go on iterating.

C. Training the RBF Neural Network Based on Ant Colony Clustering. The period can be divided into two stages when the RBF neural network is trained based on ant colony clustering.

The task in first stage is training the samples. First, confirm the center and the node number of the hidden layer. Here, the center of the hidden layer in the RBF neural network is the same as the center of the cluster. Meanwhile，the node number is the same as the cluster number. Afterwards, calculate the width of the hidden layer. Calculate the distance between each node in the hidden layer and the minimum distance is treated as the width. At last, calculate the powers between the node in the hidden and one in the output layer. First calculate each distance between the sample entry and the center. Then calculate the output matrix of the node in the hidden layer. At last, the output powers and the offsets are obtained.

The second stage is sample test. First, the samples are tested according to the parameters obtained from the samples training. Then the test result is analyzed.

Test and Analysis

In order to verify the model, an experiment is carried out with the help of the data of grounding grid corrosion rate from the different transformer substation throughout the country. These data, total 101 records are shown as Table 1.

Table 1 The grounding grid corrosion rate and the influencing factors

No.	pH	Water content [%]	Conduc -tivity [$\mu/\Omega cm$]	organic matter [%]	Total Nitrogen [%]	HCO_3^- [%]	Cl^- [%]	SO_4^{2-} [%]	Ca^{2+} [%]	Mg^{2+} [%]	K^+ [%]	Na^+ [%]	Corrosion rate [$g/dm^2 a$]
1	7.6	6.80	10000	0.19	0.002	0.0092	0.5639	1.0834	0.3024	0.0047	0.0125	0.5100	1.331
2	9.9	22.86	520	1.25	0.059	0.0580	0.0090	0.0130	0.0060	0.0001	0.0010	0.0630	1.493
3	4.9	24.10	23	0.73	0.052	0.0080	0.0007	0.0074	0.0029	0.0011	0.0001	0.0001	2.840
4	5.5	17.76	120	0.28	0.010	0	0.001	0.0061	0.0007	0.0007	0.0001	0.0001	3.609
5	10.2	16.10	570	0.80	0.046	0.0757	0.0038	0.0154	0.0054	0.0008	0.0055	0.0402	1.269
6	6.6	21.00	130	2.55	0.105	0.0083	0.0017	0.0139	0.0015	0.0023	0.0006	0.0051	3.719
96	6.9	18.45	90	2.21	0.113	0.0168	0.0008	0.0097	0.0037	0.0011	0.0002	0.0046	3.215
97	8.0	21.87	130	0.21	0.033	0.0205	0.0007	0.0133	0.0064	0.0021	0.0003	0.0029	4.155
98	8.1	20.11	165	0.26	0.027	0.0168	0.0017	0.0114	0.0059	0.0009	0.0007	0.0029	2.343
99	8.4	23.24	9100	0.54	0.026	0.0207	1.0945	0.1120	0.0197	0.0384	0.0249	0.6239	3.953
100	5.4	15.98	60	0.37	0.018	0.0031	0.0014	0.0036	0.0014	0.0004	0.0002	0.0012	2.940
101	4.6	24.80	24	0.47	0.046	0.0028	0.0043	0.0004	0.0022	0.0005	0.0001	0.0002	2.161

In these data, the top 93 records are applied to train, and the last 8 records to test. In the clustering, the parameters are set as the following, the number of ants ant=120, the number of clusters class =20, iterations iterNum=2000, transformational rule parameter q=0.9, attenuation coefficient of pheromone r=0.05, threshold value in local search h=0.03, L=2. The predicted value based on ant colony optimization RBF neural network is shown as Fig.2. The predicted value using the K mean value algorithm is shown as Fig.3.

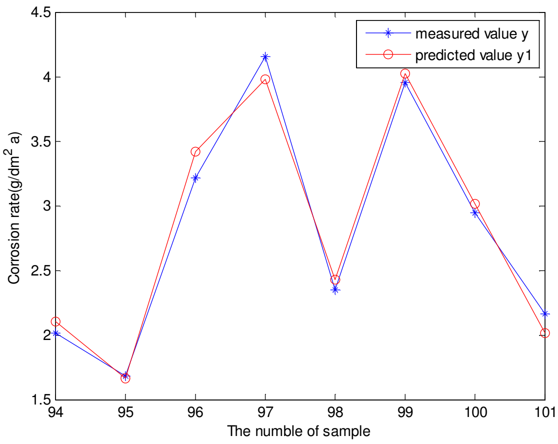

Fig.2 The predicted value based on optimization RBF network

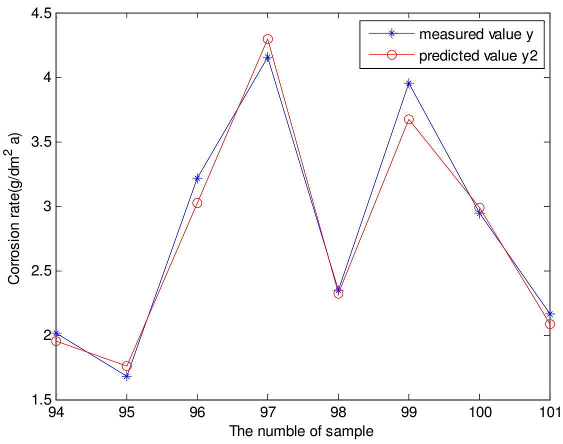

Fig.3 The predicted value using the K mean value algorithm

For the last 8 records, measured value y, the predicted value using the algorithm in this paper y1 and the predicted value using the K mean value algorithm y2 are shown as Table 2.

Table 2 The measured value and the predicted value with two kind of algorithm

y	2.014	1.679	3.215	4.155	2.343	3.953	2.940	2.161
y1	2.101	1.661	3.419	3.980	2.425	4.022	3.009	2.015
y2	1.951	1.760	3.019	4.298	2.321	3.671	2.988	2.080

The value y, y1 and y2 is respectively looked as a vector quantity, so the Euclidean distance from y1 to y is $\|y1-y\|_2 = 0.3438$, the Euclidean distance from y2 to y is $\|y2-y\|_2 = 0.3973$. So $\|y1-y\|_2 < \|y2-y\|_2$. From the comparison, it is obvious that the forecasting effect based on ant colony optimization RBF neural network is better than the model based on K mean value algorithm.

Conclusion

The center of hidden layer neurons in RBF neural network is acquired with ant colony clustering algorithm. The basic ant algorithm is improved and is mixed with local search. Then the improved ant colony clustering algorithm combined with RBF neural network is applied to predict the grounding grid corrosion rate. This model has good performance of strong local generalization abilities and satisfying accuracy. It is verified by the data in fact that the forecasting effect based on ant colony optimization RBF neural network is better than the model based on K mean value algorithm.

References

[1] Yugen Liu, Lixiang Wu, Shuo Wang. Practicality analysis for optimized erosion diagnosis of large and grid medium-scale grounding grid [J]. Journal of Chongqing University, 31(4),2008,417-420

[2] Wenjing Ma, Bo Zhang, Xushuang Song. Study on corrosion diagnosis method for grounding network based on regularized least square method [J]. Heilongjing Electric Power, 34(4),2012,278-284

[3] Yugeng Lin, Yongxi Teng, Xianlu Chen. A method for corrosion diagnosis of grounding grid [J]. High Voltage Engineering,30(6),2004,19-21

[4] Lei Xu, Lin Li. Fault diagnosis for grounding grids based on electric network theory [J]. Transactions of China Electro Technical Society,27(10),2012,270-276

[5] Yang Liu, Xiang Cui, Zhibin Zhao. Design and application of testing magnetic field system for corrosion diagnosis of grounding grids in substation [J]. Transactions of China Electro Technical Society, 24(1), 2009, 176-182

[6] Xiuli Zhang, Ping Luo, Ni Mo. Development and application of electrochemical detection system for grounding grid corrosion state [J]. Proceedings of the CSEE, 28(19), 2008,152-156

[7] Shengyong Ye, Xiaoru Wang, Zhigang Liu. Power system transient stability assessment based on Support Vector Machine incremental learning method [J]. Automation of Electric Power Systems, 35(11), 2011, 15-19

[8] Qiong Wu, Yihan Yang, Wenying Liu. Electric power system transient stability on-line prediction based on LSSVM [J]. Proceedings of the CSEE, 27(25),2007

[9] Shangbin Jiao, Ding Liu. Assessment of surface contamination of high voltage insulator based on LSSVM [J]. Automation of Electric Power Systems, 30(6), 2006, 61-65

[10] J.Wang, Z.H.Zhou, A.Y.Zhou. Machine Learning and Application, Tsinghua University Press, Beijing,2006

[11] Liangshan Qu, Xiaogang Li, Cuiwei Du. Corrosion rate prediction model of carbon steel in regional soil based on BP network [J]. Journal of University of Science and Technology Beijing, 31(12), 2009, 1569-1575

[12] Xiaoyan Ma, Zuyu Qu. Application of artificial neural network in prediction corrosion value of metal in atmosphere [J]. Journal of University of Science and Technology Beijing, 23(2),2001, 123-126

[13] Zhihu Guo, Zhengliang Xing, Minghu Jin. Predicting corrosion rate of mild steel in soil based on artificial neural network [J]. Journal of Chinese Society for Corrosion and Protection ,16(4), 1996, 307-310

Applied Mechanics and Materials Vol. 596 (2014) pp 251-258
© (2014) Trans Tech Publications, Switzerland
doi:10.4028/www.scientific.net/AMM.596.251

Research on Multi-Agent Formation's Obstacle Avoidance Problem Based on Three-Dimensional Vectorial Artificial Potential Field Method

Jiyang Dai[1, a], Linfei Yin[1,b] ,Chen Peng[1,c] ,
Baojian Yang[1,d] , and Cunsong Wang[1,e]

[1]Unit 696, Honggutan District, Nanchang Prov., P.R.China.

[a]djiyang@163.com, [b]yinlinfei@163.com,
[c]30715497@qq.com,[d]502995601@qq.com,[e]349241783@qq.com

Keywords: Three-Dimensional Vectorial Artificial Potential Field Method (TDVAPF), Multi-Agent Formation, Obstacle Avoidance Problem, Local Trouble, Rotational Force

Abstract. In order to solve the obstacle avoidance problem when the Multi-Agent formation get through the area full of obstacles, improved the traditional Artificial Potential Field method, add the vectorial information to the agent's model, presented the Three-Dimensional Vectorial Artificial Potential Field method (TDVAPF). Firstly, improved the model of agent, obstacle and target; then, improved the Multi-Agent formation motion model, the Multi-Agent formation's structure is "pyramid" structure; Finally, improved the agent's force, add the "rotational force" to the agent's force, it makes agent avoid the "local trouble". The numerical simulation verified the correctness and effectiveness of the TDVAPF method in Multi-Agent formation's obstacle avoidance problem.

Introduction

There is obstacle avoidance problem when the Multi-Agent formation gets through the area full of obstacles in the Multi-Agent formation application fields, such as the military field, the obstacle avoidance problem of helicopter formation, fighter formation, missile formation; and distributed sensor network, intelligent traffic, air traffic's three dimensional obstacle avoidance problem.

It is different between Multi-Agent formation's three-dimensional obstacle avoidance problem and two-dimensional obstacle avoidance problem. There is special algorithm research on three-dimensional obstacle avoidance problem, such as using the ability neural network function method for three-dimensional robot path planning [1,2], using rubber band algorithm of three-dimensional fast virtual scene path planning [3], using collision risk model for autonomous underwater robot obstacle avoidance problem [4].

Multi-Agent formation's obstacle avoidance problem in the sky include collision avoidance (collision between the agent and other agents) problem and obstacle avoidance (collision between the agent and obstacles) problem [5], this is three-dimensional obstacle avoidance problem. Three-dimensional obstacle avoidance problem is more complicated then two-dimensional obstacle avoidance problem.

Potential Function method named Artificial Potential Field method (APF), is simulated the forces of agents, obstacle and targets, such as obstacle on the agent's repulsive force, target on the agent's attractive force, agent on the agent's repulsive force and attractive force.

The traditional APF method can be easily used to solve the two-dimensional obstacle avoidance problem, most papers using APF method and simulate in the two-dimensional model [6-8]. It's difficult using traditional APF to solve the three-dimensional obstacle avoidance problem, using a few agents when simulated [9]. The stability of using APF method to solve the tree-dimensional obstacle avoidance problem has verified [10], but it's not simulated in three-dimension. These agents are not Multi-Agent formation [11-17]. There is some problem about traditional APF method: 1) Agent can't get through obstacle area when the area existence a lot of obstacles, and it will be the "local trouble" problem; 2) The speed is a scalar ,not a vector; 3) The agent model have no the maximum and minimum visual distance property, the agent can get all of information of obstacles, but actually the agent have the maximum and minimum visual distance; 4) The agent's speed is a constant value, every step is constant distance, but actually the agent's speed should changeable for obstacle avoidance. 5) These agents have not run to Multi-Agent formation.

The traditional APF method under above problems is improved, presented TDVAPF method solved Multi-Agent formation three-dimensional obstacle avoidance problem.

Three-Dimensional model

In order to reach the targets, Agents must get through the three-dimensional area full of obstacles. When the Multi-Agent formation gets through the obstacles' area, agents will be the target formation. The three-dimensional model of agent, obstacle and target show as follows.

Three-dimensional agent model. Firstly, build the three-dimensional agent model. It's not speed vector using traditional APF method, add the three-dimensional speed vector to the three-dimensional agent model, and addition the force vector, it makes the agent's force and motion more richer than the traditional agent's model, the improved APF method named TDVAPF. Agent model is

$$A = \begin{bmatrix} p_a & v_a & s_a & d_a & f_a & v_{a\max} \end{bmatrix} \tag{1}$$

Where, $p_a = \begin{bmatrix} p_{ax} & p_{ay} & p_{az} \end{bmatrix}$ is agent's position information, p_{ax} , p_{ay} and p_{az} are the values of xyz axes of three-dimensional coordinates.

$v_a = \begin{bmatrix} v_{ax} & v_{ay} & v_{az} \end{bmatrix}$ is the agent's three-dimensional speed vector.

$s_a = \begin{bmatrix} s_{a\min} & s_{a\max} \end{bmatrix}$ is agent's visual distance range. Agent can't see the obstacle if the distance between agent and obstacle is lesser than minimum visual distance ($s_{a\min}$), at that time, there is no force between the agent and this obstacle. And agent can't see the obstacle if the distance between agent and obstacle is greater than maximum visual distance ($s_{a\max}$).

d_a is the safe distance between agents. The agent's force is attractive force if the distance between agents is greater than the safe distance (d_a). The agent's force is repulsive force if the distance between agents is lesser than the safe distance (d_a). Collision avoidance between agents problem is connect to the Multi-Agent formation obstacle.

$f_a = \begin{bmatrix} f_{ax} & f_{ay} & f_{az} \end{bmatrix}$ is the agent's resultant force three-dimensional vector.

$v_{a\max}$ is the agent's maximum speed value. The agent's speed is constant value in the traditional agent's model; the distance of every step is constant value in the traditional agent's model. The speed vector is changeable in the improved agent's model. The agent's speed and acceleration is different between each step, the value is according to the agent's resultant force, and the agent's speed have the maximum value ($v_{a\max}$).

Three-dimensional obstacle model. The three-dimensional obstacle model is

$$O = \begin{bmatrix} p_o & s_o \end{bmatrix} \tag{2}$$

Where, $p_o = \begin{bmatrix} p_{ox} & p_{oy} & p_{oz} \end{bmatrix}$ is the obstacle's position information.

$s_o = \begin{bmatrix} s_{o\min} & s_{o\max} \end{bmatrix}$ is the obstacle's "dangerous distance". The force between agent and obstacle will decrease by increase the distance between agent and obstacle if the distance is greater than the maximum dangerous distance ($s_{o\max}$). The force between agent and obstacle will increase by decrease the distance between agent and obstacle if the distance is lesser than the maximum dangerous distance ($s_{o\max}$), agent will be collision with the obstacle if the distance is lesser than the minimum dangerous distance ($s_{o\min}$).

Three-dimensional target model. The target is a virtual target, and the target formation is agent formation after the agents get through obstacle's area. The three-dimensional target model is

$$T = \left[p_t\right] \tag{3}$$

Where, $p_t = \left[p_{tx} \quad p_{ty} \quad p_{tz}\right]$ is the target's position information. Target's three-dimensional model is simpler than agent and obstacle's model.

Agent's force

Each agent's force includes repulsive force and attractive force. Each agent's force includes the force between agent and target, the force between agent and obstacle, and the force between agent and agent. The force's calculation method show as follows.

The force between agent and target. The force between agent and target is attractive force. It's simpler than the others force. Each target attractive only one agent, and it's unique one.

Before get attractive force, it should get the force's angle. The attractive force's angle is

$$\begin{aligned} \alpha_{at} &= a\cos(\frac{d_x}{r_{at}}) \\ \beta_{at} &= a\cos(\frac{d_y}{r_{at}}) \\ \gamma_{at} &= a\cos(\frac{d_z}{r_{at}}) \end{aligned} \tag{4}$$

Where, $r_{at} = \sqrt{\left(p_{ax} - p_{tx}\right)^2 + \left(p_{ay} - p_{ty}\right)^2 + \left(p_{az} - p_{tz}\right)^2}$ is the distance between agent and target, $d_x = p_{tx} - p_{ax}$, $d_y = p_{ty} - p_{ay}$, and $d_z = p_{tz} - p_{az}$ are distance values at xyz axes.

Then, the attractive force values at xyz axes are

$$\begin{aligned} f_{atx} &= f_{at} * \cos(\alpha_{at}) \\ f_{aty} &= f_{at} * \cos(\beta_{at}) \\ f_{atz} &= f_{at} * \cos(\gamma_{at}) \end{aligned} \tag{5}$$

Where, $f_{at} = \begin{cases} k_{fat1} * r_{at}, r_{at} < da \\ k_{fat2} * r_{at}, r_{at} \geq da \end{cases}$ is the attractive force scalar quantity. k_{fati} is the factor of the attractive force.

The force between agent and obstacle. Each agent in the Multi-Agent formation have repulsive forces from obstacles. These repulsive forces join together is the agent's repulsive force.

The agent's repulsive force angle is

$$\begin{aligned} \alpha_{ao} &= a\cos(\frac{-d_x}{r_{ao}}) \\ \beta_{ao} &= a\cos(\frac{-d_y}{r_{ao}}) \\ \gamma_{ao} &= a\cos(\frac{-d_z}{r_{ao}}) \end{aligned} \tag{6}$$

Where, $r_{ao} = \sqrt{(d_x)^2 + (d_y)^2 + (d_z)^2}$ is the distance between agent and obstacle. $d_x = p_{ox} - p_{ax}$, $d_y = p_{oy} - p_{ay}$, and $d_z = p_{oz} - p_{az}$ are the distance values at xyz axes.

Assume that, the number of agents is n_a, number of obstacles is n_o, number of targets is n_t. The force between each obstacle and agent values at xyz axes are

$$\begin{aligned} f_{aox} &= \sum f_{aoj} * \cos(\alpha_{ao}), j \in [1, no] \\ f_{aoy} &= \sum f_{aoj} * \cos(\beta_{ao}), j \in [1, no] \\ f_{aoz} &= \sum f_{aoj} * \cos(\gamma_{ao}), j \in [1, no] \end{aligned} \tag{7}$$

Where, the repulsive force between the j$^{\text{th}}$ obstacle and agent is

$$f_{aoj} = \begin{cases} m_a * m_o * k_{fao} * (\frac{1}{r_{ao}} - \frac{1}{s_{o\max}})^2, r_{ao} \in [\max\{s_{o\min}, s_{a\min}\}, \min\{s_{o\max}, s_{a\max}\}] \\ +\infty, r_{ao} \in [0, s_{o\min}) \\ 0, else \end{cases} \quad (8)$$

Where, m_a is agent's mass, m_o is obstacle's mass, k_{fao} is the factor of repulsive force.

The force between agent and agent. The force between agent and agent is complex force. It is repulsive force if the distance between agent and agent is lesser than agent's safe distance (d_a). It is attractive force if the distance is greater than safe distance (d_a). The form of the force between agents shows in Fig.1.

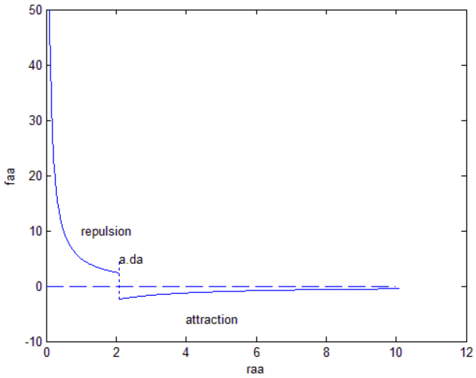

Fig.1. The form of the force between agents

It is need to calculate the force between agents for each other. The force angle between agent-i and agent-j is

$$\alpha_{aa} = \begin{cases} a\cos(\frac{-d_x}{r_{aa}}), r_{aa} < d_a \\ a\cos(\frac{d_x}{r_{aa}}), r_{aa} \geq d_a \end{cases}$$
$$\beta_{aa} = \begin{cases} a\cos(\frac{-d_y}{r_{aa}}), r_{aa} < d_a \\ a\cos(\frac{d_y}{r_{aa}}), r_{aa} \geq d_a \end{cases} \quad (9)$$
$$\gamma_{aa} = \begin{cases} a\cos(\frac{-d_z}{r_{aa}}), r_{aa} < d_a \\ a\cos(\frac{d_z}{r_{aa}}), r_{aa} \geq d_a \end{cases}$$

Where, $r_{aa} = \sqrt{(d_x)^2 + (d_y)^2 + (d_z)^2}$ is the distance between agents. $d_x = p_{axi} - p_{axj}, d_y = p_{ayi} - p_{ayj}$ and $d_z = p_{azi} - p_{azj}$ are distance values at xyz axes.

The force between agents values at xyz axes are

$$\begin{aligned} f_{aax} &= f_{aa} * \cos(\alpha_{aa}) \\ f_{aay} &= f_{aa} * \cos(\beta_{aa}) \\ f_{aaz} &= f_{aa} * \cos(\gamma_{aa}) \end{aligned} \quad (10)$$

Where, the value of the force is

$$f_{aa} = \begin{cases} k_{faa} * m_a{}^2 * (\frac{1}{r_{aa}} - \frac{1}{d_a})^2, r_{aa} \in [s_{a\min}, s_{a\max}] \\ 0, r_{aa} \notin [s_{a\min}, s_{a\max}] \end{cases} \quad (11)$$

Three-Dimensional Multi-Agent formation

It will be formation before and after the Multi-Agent formation gets through the obstacle's area. The formation structure is "pyramid" structural formation, the distance between each agent and its surrounding agent is safe distance (d_a). The formation structure shows in Fig.2.

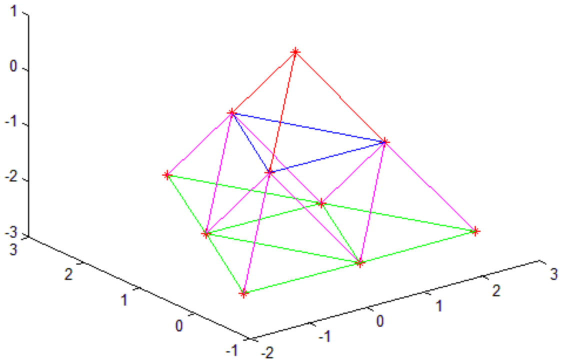

Fig.2. The agent formation structure

The number of agents is equal to the number of targets. And the target's formation structure, the same as the agent's formation. In order to avoidance collisions between agents when the Multi-Agent formation is moving, force between agents are needed. The forces between agents make sure that after these agents get through obstacle's area, will be formation like before.

Multi-Agent formation motion

The agent's speed is a constant value in the traditional agent's model. The speed is according to agent's acceleration, and the acceleration is according to the agent's force. The agent's position in the next moment is

$$p_{anew} = p_{aold} + v_{anew}\delta_t \tag{12}$$

Where, δ_t is the step of time, P_{aold} is the agent's position of this moment, the agent's speed in the next moment is

$$\nu_{anew} = \begin{cases} \nu_{aold} + a_a * \delta_t, \nu_{aold} + a_a * \delta_t \le v_{a\max} \\ v_{aold}, \nu_{aold} + a_a * \delta_t > v_{a\max} \end{cases} \tag{13}$$

Where, v_{aold} is the agent's speed of this moment, the agent's acceleration in this moment is

$$a_a = \frac{f_{join}}{m_a} = \frac{(f_{ao} + f_{aa} + f_{at} + f_{ac})}{m_a} \tag{14}$$

Rotational force

Multi-Agent formation can't get through obstacle's area using the traditional APF method when obstacles full of the area in some orders. The agents moving in some special area but can't get through the obstacles' area, that is the "local trouble" problem.

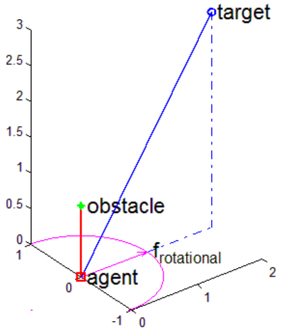

Fig.3. Rotational force direction

In order to solve the local trouble, agent's resultant force must be added the rotational force, especially when the distance between agent and obstacle is very close. The rotational force value is according to the force, which is total of the force of the nearest obstacle and agent. The direction of rotational force shows in Fig.3.

Fig.3. shows that the rotational force is located in the vertical plane of the force between agent and obstacle. The rotational force's direction is repulsive force projection's direction. The repulsive force between agent and obstacle, and the rotational force are perpendicular. The surface of agent & obstacle and target, and the perpendicular surface of repulsive force are perpendicular.

The rotational force is

$$f_{ac} = \begin{cases} k_{ac} * f_{aio}, r_{ao} \le k_{rao} * s_{o\min} \\ 0, r_{ao} > k_{rao} * s_{o\min} \end{cases} \tag{15}$$

Assume that, the repulsive force vector between agent and obstacle is $\overrightarrow{v_{ao}}$, the attractive force vector between agent and target is $\overrightarrow{v_{at}}$, so, the perpendicular vector $\overrightarrow{v_{n}}$ can be calculated form

$$\begin{cases} \overrightarrow{v_{n}} * \overrightarrow{v_{ao}} = 0 \\ \overrightarrow{v_{n}} * \overrightarrow{v_{at}} = 0 \end{cases} \tag{16}$$

Assume that, the rotational force vector is $\overrightarrow{v_{rotational}}$, the $\overrightarrow{v_{rotational}}$ can be calculated form

$$\begin{cases} \overrightarrow{v_{rotational}} * \overrightarrow{v_{ao}} = 0 \\ \overrightarrow{v_{rotational}} * \overrightarrow{v_{n}} = 0 \end{cases} \tag{17}$$

Where, $\overrightarrow{v_{ao}} = \begin{bmatrix} p_{ox} - p_{ax} & p_{oy} - p_{ay} & p_{oz} - p_{az} \end{bmatrix}$ is the repulsive force vector, and modify the rotational force vector like

$$\begin{aligned} \overrightarrow{v_{rotational}} &= \begin{cases} \overrightarrow{v_{rotational}}, \overrightarrow{v_{rotational}} * \overrightarrow{v_{at}} > 0 \\ -\overrightarrow{v_{rotational}}, \overrightarrow{v_{rotational}} * \overrightarrow{v_{at}} \le 0 \end{cases} \\ &= \begin{bmatrix} v_{acx} & v_{acy} & v_{acz} \end{bmatrix} \end{aligned} \tag{18}$$

So the rotational force angle can be calculated by

$$\begin{aligned} \alpha_{ac} &= a\cos(v_{acx} / r_{ac}) \\ \beta_{ac} &= a\cos(v_{acy} / r_{ac}) \\ \gamma_{ac} &= a\cos(v_{acz} / r_{ac}) \end{aligned} \tag{19}$$

Where, $r_{ac} = \sqrt{v_{acx}^{2} + v_{acy}^{2} + v_{acz}^{2}}$ is the distance between agent and obstacle. The rotational force value at xyz axes are

$$\begin{aligned} f_{acx} &= f_{ac} * \cos(\alpha_{ac}) \\ f_{acy} &= f_{ac} * \cos(\beta_{ac}) \\ f_{acz} &= f_{ac} * \cos(\gamma_{ac}) \end{aligned} \tag{20}$$

Numeric simulation

If the time step is 0.1, the number of agents is 30, the number of obstacles is 60, and the number of targets is 30. Agent's minimum and maximum visual distance are 0 and 40. Agent's safe distance is 4. Agent's maximum speed is 1. Obstacle's minimum and maximum dangerous distance are 2 and 40. k_{fat} is 1, k_{fao} is 1500, k_{faa} is 100, k_{fac} is 2, k_{rao} is 4, the mass of agent & target and obstacle are 1.

The agents' initial position are: (0.0911002,0.594037,0.241084),(-1.9089,-0.560664,-3.0249),(0.0911002,2.90344,-3.0249),(2.0911,-0.560664,-3.0249),(-3.9089,-1.71536,-6.29089),(-1.9089,1.74874,-6.29089),(0.0911002,-1.71536,-6.29089),(0.0911002,5.21284,-6.29089),(2.0911,1.74874,-6.29089),(4.0911,-1.71536,-6.29089),(-5.9089,-2.87006,-9.55687),(-3.9089,0.594037,-9.55687),(-1.9089,-2.87006,-9.55687),(-1.9089,4.05814,-9.55687),(0.0911002,0.594037,-9.55687),(0.0911002,7.52

224,-9.55687), (2.0911,-2.87006,-9.55687), (2.0911,4.05814,-9.55687), (4.0911,0.594037,-9.55687), (6.0911,-2.87006,-9.55687),(-7.9089,-4.02477,-12.8229),(-5.9089,-0.560664,-12.8229),(-3.9089,-4.02477,-12.8229),(-3.9089,2.90344,-12.8229),(-1.9089,-0.560664,-12.8229),(-1.9089,6.36754,-12.8229), (0.0911002,-4.02477,-12.8229), (0.0911002,2.90344,-12.8229), (0.0911002,9.83164,-12.8229), (2.0911,-0.560664,-12.8229).

Obstacles' position are:(29.556,43.2452,31.6351),(18.8124,16.2601,18.3092), (19.0483,28.2923,18.7713),(31.4715,34.724,23.0323),(40.4844,47.2873,13.838),(23.9027,43.4035, 39.9013),(28.4493,45.8169,39.9404),(35.573,33.3007,31.732),(46.6934,33.3099,23.5253),(16.4629, 44.197,43.2933),(38.6254,11.3946,32.1029),(33.1096,45.4168,48.3017), (27.332,26.3092,45.7133), (45.3697,11.4553,24.2601),(25.7221,39.8459,31.8561),(17.159,16.1932,23.8673),(35.3333,15.7563 ,34.9121),(34.96,34.2384,41.865),(23.1177,20.1792,39.835),(42.1186,22.9662,15.0214),(49.9791,26.0716,42.8958), (49.2391,26.2549,11.006), (15.0815,25.4476,26.5772), (19.2896,34.3921,39.2563), (10.9453,16.6756,41.255),(34.2973,17.5237,24.6914),(14.4324,13.7852,39.7947),(26.2984,22.9275 ,45.6907), (45.3631,40.7839,19.7041), (31.9253,19.3647,15.1839).

Targets' position are:(50.8414,50.8572,50.9636),(48.8414,49.7025,47.6976), (50.8414,53.1666,47.6976),(52.8414,49.7025,47.6976),(46.8414,48.5478,44.4316),(48.8414,52.0119,44.4316),(50.8414,48.5478,44.4316),(50.8414,55.476,44.4316),(52.8414,52.0119,44.4316),(54.8414,48.5478,44.4316),(44.8414,47.3931,41.1657),(46.8414,50.8572,41.1657),(48.8414,54.3213,41.1657),(48.8414,47.3931,41.1657),(50.8414,50.8572,41.1657),(50.8414,57.7854,41.1657),(52.8414,47.3931,41.1657),(52.8414,54.3213,41.1657),(54.8414,50.8572,41.1657),(56.8414,47.3931,41.1657) ,(42.8414,46.2384,37.8997),(44.8414,49.7025,37.8997),(46.8414,46.2384,37.8997),(46.8414,53.1666,37.8997), (48.8414,56.6307,37.8997), (48.8414,49.7025,37.8997), (50.8414,53.1666,37.8997), (50.8414,60.0948,37.8997), (50.8414,46.2384,37.8997), (52.8414,49.7025,37.8997).

Using the MATLAB2010b software to simulated, the result shows in Fig.4.

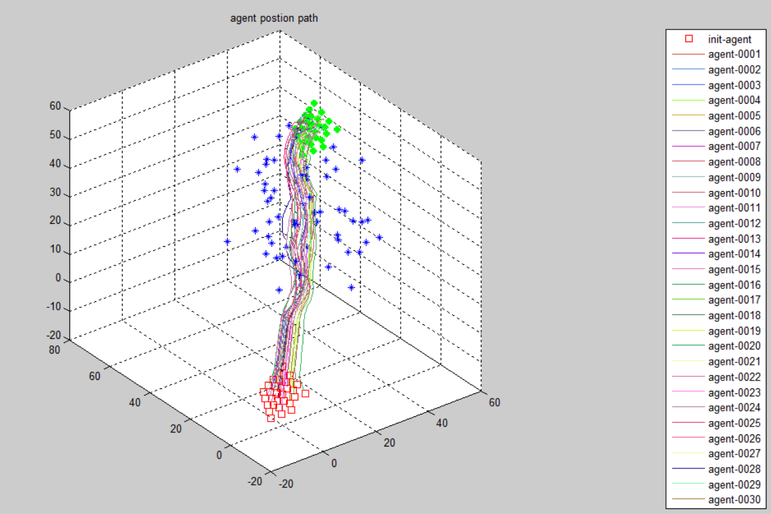

Fig.4. Agents (30) and obstacles (60) result

Fig.4. shows all the agents get through the obstacle's area, and there is no one agent has the local trouble. The agents' formation structure after get through obstacle's area is just the same as initial structure.

Conclusions

Modified the traditional APF method, Multi-Agent formation's obstacle avoidance problem has been solved. The three-dimensional numerical simulation shows that, all agents get through obstacle's area. The simulated result verifies correctness and effectiveness of using TDVAPF method to solve the Multi-Agent formation's obstacle avoidance problem.

Acknowledgements

This work was financially supported by the National Natural Science Fund of China (61164015), and Nanchang Hangkong University Graduate Innovation Fund (YC2013-014).

References

[1] Jianli Yu, Kroumov V: *The Method of Robot's 3D Path Planning*, Chinese Patent,200710193060.x (In Chinese)

[2] Jianli Yu, Siya chen, Zengqing Sun,Kroumov V: *Central South University(Natural science),*Vol.40(2009), p.471-477 (In Chinese)

[3] Yong Chen, Dong Wang, Ge Chen: *A 3D Fast Path Planning with Virtual Scene Base on Rubber Band Algorithm*, Chinese Patent,200710094209.9 (In Chinese)

[4] Kuimin Wang, Ye Hong, Xingqian Bian, Zheping Yan:*Wuhan University of Technology (Transportation Sience & Engineering)*,Vol.32(2008),p.1002-1004+1020. (In Chinese)

[5] Haifei Si,Zhong Yang,Jun Wang: *Mechanical and Electrical Engineering* ,Vol.28(2011),p.16-20+37.(In Chinese)

[6] Yongbin Zhang: *The UAV formations Research based on probability calculations and state predicted*, Dilian University of Technology, 2013 (In Chinese)

[7] Shaobao Li:*Multi-Target Flocking Control and Distributed Formation Topology Optimizing for Multi-Agent System*, Yanshan University,2012 (In Chinese)

[8] Chengzhi Li: *Research on surveillance using UAV Based on Collaborative Technology*,University of electronic science and technology of China (In Chinese)

[9] Xing Liu, Sentang Wu, Xiaomin Mu, Chen Peng, Jiqiang Tang:*Journal of System Simulation*,Vol.19(2008),p.5075-5080+5085 (In Chinese)

[10] Yancai Chen:*Research on Distributed Cooperative Control for Swarm UAVs*,Nanjing University of Aeronautics and Astronautics,2011 (In Chinese)

[11] Luhua Zhao, Puyun Wang, Xiang Chen, Wei Zhou: *Electronics Ptics & Control*, Vol.08(2011).p.34-39 (In Chinese)

[12] Xia Chen, Jing Zhang:*The Three-Dimension Path Planning of UAV Based on Improved Artificial Potential Field in Dynamic Environment*,Intelligent Human-Machine Systems and Cybernetics (IHMSC), 2013 5th International Conference on,Vol.2(2013),p.144-147.

[13] Xiaomin Tong, Yanning Zhang, Tao Yang:*Artificial Potential Field Based Cooperative Particle Filter for Multi-View Multi-Object Tracking*,Virtual Reality and Visualization (ICVRV), 2013 International Conference on,p.74-80.

[14] Gao Yun; Wei Zhiqiang; Gong Feixiang; Yin Bo; Ji Xiaopeng:*Dynamic Path Planning for Underwater Vehicles Based on Modified Artificial Potential Field Method*,Digital Manufacturing and Automation (ICDMA), 2013 Fourth International Conference on,p.518-521.

[15] Mei Wang; Zhiyong Su; Dawei Tu; Xichang Lu:*A hybrid algorithm based on Artificial Potential Field and BUG for path planning of mobile robot*, Measurement, Information and Control (ICMIC), 2013 International Conference on,p.1393-1398.

[16] Xiaoming Wang; Wenfeng Li; Wei Song; Wentao Dong:*Connectivity Controlling of Multi-robot by Combining Artificial Potential Field with a Virtual Leader*,Systems, Man, and Cybernetics (SMC), 2013 IEEE International Conference on,p.374-377.

[17] Macktoobian, M.:*Smart navigation of autonomous mobile robots by Time-Variant Artificial Potential Fields: A fuzzy approach*, Fuzzy Systems (IFSC), 2013 13th Iranian Conference on,p.1-6.

Applied Mechanics and Materials Vol. 596 (2014) pp 259-262
© (2014) Trans Tech Publications, Switzerland
doi:10.4028/www.scientific.net/AMM.596.259

A evaluation model for valid prediction of cabs' number change from urban cabs trajectories

Ma Wubin, Deng Su, Huang Hongbin

Information system engineering key laboratory, National University of Defense Technology,

ChangSha, China

e-mail: mawubin417@163.com

Keywords: evaluation model, prediciton, Location based service

Abstract. the large scale urban cabs trajectories are used for prediction of cabs number change in some applications such as knowledge discovery and abnormal traffic alarm. The traditional methods calculate for many invalid spaces consume much time on invalid calculation. After observing many datasets with the great number of cabs trajectories points, we find a rule that the *periodicity and stabilization* of cabs group number change will be clearer as the number of cabs trajectories points increasing in some space, and the prediction accurate of cabs number change is also have relationship with the periodicity and stabilization. To validate this rule, we first model the periodicity and stabilization of cabs group number change. And a function is found to well fit the model value as the change of cabs group number, proving the rule we have found. Finally, we show that how this rule can be used to decrease the calculation time of valid traffic prediction. Experiment shows that the rule we discovered exists in Beijing and San Francisco datasets and the rule can conveniently and efficiently used to valid traffic prediction.

Introduction

Many researchers want to predict the next destinations of cabs from large number of urban cabs trajectories, the Location Based Service (LBS) strongly needs this knowledge for providing excellent service, such as Point of Interest (POI) finding and recommendation[1-2], transport situation discovering for taxi ridesharing[3-5], finding cabs moving rule for prediction future urban human mobility[6-8]. However, the existing prediction based on the urban cabs trajectories is time-consuming and inaccurate, because the traditional prediction method often calculates the places where cabs are not always been. The prediction accurate from the GPS data will be extremely low in these places. We want to discard these places which are useless for prediction in this paper though a rule we discovered in urban cabs trajectories. And we will explain this rule as follows.

Actually, we find a rule when we analyze two real data sets, Cabspotting in San Francisco [9], Beijing[10]. For a specific place, the number of GPS points in cabs trajectories in a given time slice will be regularly changing if this number is big enough. Whereas the regularity is inconspicuous when the number of GPS points is small. We assume that the number of GPS points in specific space indicates the number of cabs in some place. So we analyze cabs' GPS points' number change to express the cabs number change.

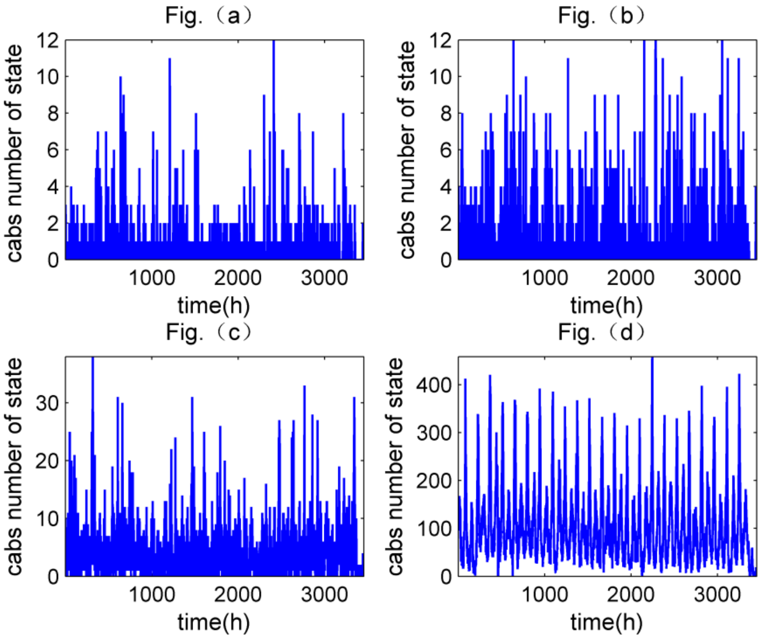

Fig 1 The change of cabs number (GPS points) in given time slice. (a)5381 total number of cabs number (GPS points) in unban place (b) 9240 total number of cabs number (GPS points) in unban place (c)16260 total number of cabs number (GPS points) in unban place (d)260401 total number of cabs number (GPS points) in unban place

As we can see in the Fig1, when the total number of GPS points in some unban place is huge, as (d), the changing characteristic is periodic and disciplinary. Whereas the total number is small, as in (a), the changing characteristic is ruleless. However, it is very hard to quantitative indicate these periodic or ruleless of cabs points change.

So we propose a performance evaluation model to scale the periodic and degeneration characteristic of cabs' GPS points number change. The evaluation model can describe the detail period and rule characteristic of urban cabs trajectories. According to these characteristic describing, we estimate the knowledge discovery is usable or not.

To the best of our knowledge, our work is the first to propose performance model for evaluation of valid state in urban cabs trajectories analysis. We place our problem in a practical setting by exploiting two real cities' maps and the enormous historical taxi trajectory data. The contribution of this paper is as follows.

- A rule about the relationship between the numbers of cabs GPS points and prediction accurate is found and analyzed in some space.
- The performance of periodicity and jump degeneration evaluation is modeled to calculate threshold number for the valid state.
- Experiments are conducted on real data to verify our performance model for valid state.

Detail method is presents in:

http://hi.baidu.com/mawubin525/item/c66d81e8fe6adba6c10d75fb

Experiment

According to the fitting function value, we can get the relation of the number of cabs group, performance value and prediction error as table 1 and Fig. 2.

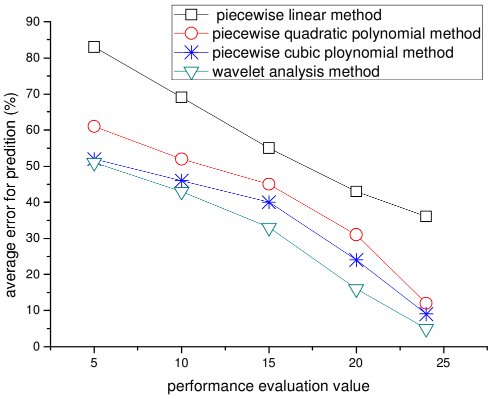

Fig.2 Prediction error change with the evaluation value

Table 1 The relationship of number of cabs group and average error of prediction

Number of cabs group	fitting periodicity evaluation	fitting jump degeneration evaluation	Average error of prediction
1000	0.23	0.25	84.7%
5000	8.3	8.9	58.6%
20000	11.2	14.7	47.7%
60000	17.3	19.1	34.2%
100000	18.3	22.8	21.4%
250000	19.2	24.2	11.6%

From the table 1, we can detect the number of cabs group when average error of prediction is known. The valid state is decided by average error of prediction. So we can easily filtrate of the state which is invalid for prediction according the number of cabs group. This process can dramatic reduce the complexity of prediction of cabs' destinations in urban calculation.

Related work

Some researchers want to discover useful knowledge from the huge number of cabs trajectories. Zheng et al [10] mines interesting locations and classical travel sequences in a given geospatial region using the cabs' GPS data. This paper tries to discover the surrounding locations which users would be interesting in. Yuan et al [3]presents a Cloud-based system , which can predict the traffic conditions of a future time using the mined knowledge , the system can also give practically fast driving routes for drivers, through analysis historical and real-time traffic conditions. Liang et al [12] find that the taxis' traveling displacements in Beijing tend to follow an exponential distribution instead of a power-law which is the most used models observed in human mobility data. Liu et al.[13] try to find the abnormal patterns of traffics and potential flaws in the design of existing traffic networks with the cabs' GPS data, it construct the 'Outlier tree ' for detecting outliers and discover causal relationships among these outliers.Ban et al. [14] focus on the traffic knowledge discovery for optimizing the timing of traffic signals.

The cabs trajectory not only reflect traffics information, but also some other important knowledge such as dynamics of social and economic behavior. A method, named F-Trail, which is used for finding meaningful and interesting patterns and anomalies in the social. Yuan et al. [2]study a large number of taxi trajectories in Beijing, present new and sophisticated models to find the different functional regions for the trips of people. And paper [15] want to find the people's various gathering knowledge such as celebrations, parades, protests, traffic jams and so on, using a trajectory pattern modeling.

Some other researchers want to predict the future traffic and urban human mobility by a large number of cabs trajectories. Castro et al. [16] construct a model of traffic density using large scale taxi traces, which could predict traffic conditions in the urban. LI et al. [6] try to predict human mobility from discovering patterns in the number of passenger pick-ups quantity (PUQ) from large number of cabs trajectories. Drivers can reduce the wasted time and distance for finding passengers from the prediction of traffics [4-5, 17].

However, the precision of traffic and human mobility prediction have not only relationship with method, but also with the number of cabs GPS points in road segments. We find that with the increase of the cabs GPS points number, the periodic and jump degeneration will more distinctive, and prediction precision will more accurately accordingly.

Conclusions

This paper focus on the evaluation for prediction of cabs state change which is helpful for traffic and knowledge discovery in urban environment with real cabs trajectories data. We first define the cabs group valid state. The performance evaluation model is formalized by using the periodicity evaluation and jump degeneration evaluation. The analysis and the experimental results show that evaluation value has a relationship with the number of cabs group and the prediction accurately of cabs' destinations, and can draw the conclusion that periodicity and stabilization will be clearer as the number of cabs trajectories points increasing in some area from the knowledge we have discovered. And more, we can make sure that how many cabs trajectories that of state can be valid when prediction accurately threshold of valid state is given.

References

[1] V. W. Zheng, *et al.*, "Towards mobile intelligence: Learning from GPS history data for collaborative recommendation," *Artificial Intelligence,* 2012.

[2] J. Yuan, *et al.*, "Discovering Regions of Different Functions in a City Using Human Mobility and POIs," in *KDD*, 2012.

[3] J. Yuan, *et al.*, "Driving with Knowledge from the Physical World," in *KDD11*, 2011.

[4] J. Yuan, *et al.*, "T-Drive: Enhancing Driving Directions with Taxi Drivers' Intelligence," *ACM SIGSPATIAL 2010,* 2012.

[5] S. Ma, *et al.*, "T-Share: A Large-Scale Dynamic Taxi Ridesharing Service," in *ICDE13*, 2013.

[6] X. LI, *et al.*, "Prediction of urban human mobility using large-scale taxi traces and its applications," *Front. Comput. Sci.,,* vol. 6, pp. 111-121, 2012.

[7] W. Mathew, *et al.*, "Predicting Future Locations with Hidden Markov Models," in *Ubicom*, 2012.

[8] PengC., *et al.*, "Collective Human Mobility Pattern from Taxi Trips in Urban Area," *PLoS ONE,* vol. 7, 2012.

[9] Available: http://cabspotting.org

[10] Y. Zheng, *et al.*, "Mining Interesting Locations and Travel Sequences from GPS Trajectories," in *WWW*, Madrid, Spain, 2009.

[11] S. G. Mallat, "A theory for multiresolution signal decomposition: the wavelet representation," *IEEE Transactions on Pattern Analysis and Machine Intelligence,* vol. 11, pp. 674-693, 1989.

[12] X. Liang, *et al.*, "The scaling of human mobility by taxis is exponential," *Physica A,* 2011.

[13] W. Liu, *et al.*, "Discovering Spatio-Temporal Causal Interactions in Traffic Data Streams," in *KDD*, San Diego, California, USA, 2011.

[14] X. J. Ban and M. Gruteser, "Towards Fine-Grained Urban Traffic Knowledge Extraction Using Mobile Sensing," in *UrbComp*, 2012.

[15] K. Zheng, *et al.*, "On Discovery of Gathering Patterns from Trajectories," in *ICDE* 2013.

[16] P. S. Castro, *et al.*, "Urban traffic modelling and prediction using large scale taxi GPS traces," 2012.

[17] N. J. Yuan, *et al.*, "T-Finder: A Recommender System for Finding Passengers and Vacant Taxis," in *UbiComp 2011*, 2011.

Applied Mechanics and Materials Vol. 596 (2014) pp 263-270
© (2014) Trans Tech Publications, Switzerland
doi:10.4028/www.scientific.net/AMM.596.263

A Method of Building Chinese Sentiment Lexicon based on Semantics

Jianeng Yang[1, a], Aimin Yang[2*,b] and Yongmei Zhou[2,c]

[1] School of Management, Guangdong University of Foreign Studies, Guangzhou 510006, China

[2] Cisco School of Informatics, Guangdong University of Foreign Studies, Guangzhou 510006, China

[a] tizzi@163.com, [b] amyang18@163.com, [c] yongmeizhou@163.com
[*] Corresponding author: Aimin Yang (amyang18@163.com)

Keywords: Sentiment Lexicon; Semantic Units; Intensity of Sentiment; Sentiment Analysis

Abstract. A method was proposed to build a Chinese sentiment lexicon based on semantics. Sentiment intensity of the word was automatically calculated by decomposing it into multiple English semantic units (Esu). A lexicon proofreading method was used to optimize the sentiment intensity of words. The proposed lexicon was applied to the task of sentiment analysis, in which the method of support vector machine was used to build the sentiment classifier. The experiment results shown that the built sentiment lexicon was more effective than the general polar sentiment lexicon.

Introduction

With the development of Web2.0, more and more Internet users tend to express their views on a variety of products and hot events. Most of these comments contain the user's emotional information, including positive and negative emotions. The manual method of collecting and processing these kind of information do not work efficiently. Therefore, text sentiment analysis techniques emerge under this background. Text sentiment analysis, also known as opinion mining, is the processes of analyzing, processing, summarizing and reasoning the subjective text which contain the emotional information [1].

Word sentiment analysis is the basic work of text sentiment analysis. Text sentiment analysis based on sentiment lexicon is a very effective method, and has been widely used. Therefore, to study the method of building sentiment lexicon is a very important subject. The typical text sentiment analysis research method is using the sentiment lexicon to extract the feature of text, and then classify the sentiment tendency type based on machine learning. However, due to the comments usually have the language features of obscure, colloquial and non-normative, researchers use the semantic rules to improve the text sentiment analysis system. The method improved the classification performance of the system. But did not fundamentally solve the problem that Chinese text usually have diverse meaning in the context of complex. Xu, et al. constructed the affective lexicon ontology which including polar words that contains sentiment orientation intensity and a small amount of polysemous words. These polysemous words contain polarity annotation of more than two kinds of emotional intensity. However, the process of the construction of sentiment lexicon ontology did not analyze the sentiment tendency of words in multi orientation. That make the sentiment polarity and corresponding sentiment intensity of the lexicon have one sidedness and did not have universal applicability. To solve this problem, a method is proposed to calculate sentiment orientation strength value in the case of different semantic terms. Using the proposed method, a Chinese sentiment lexicon was built which contains both positive and negative strength value. The lexicon was applied to text sentiment feature extraction. The sentiment analysis experiments achieved better classification effect.

Related Work

Sentiment words are an important part of sentiment lexicon. Researchers have proposed many methods to extract and marking subjective sentiment words from the text, such as Hatzivassiloglou using machine learning method to calculate the relationship strength value between different adjective to predict its sentiment orientation [2]; Wiebe proposed a method for identifying strongly subjective adjectives clustered according to distributional similarity [3]; Riloff used the pattern matching algorithm based on Bootstrapping to extract nouns [4]; Baroni considered the diversity of network information in the sentiment weight sorting of subjective adjectives [5]; And Moilanen proposed a method to annotate sentiment orientation of morpheme[6]. Practical sentiment lexicon shall also include sentiment polarity of words (positive and negative), and the corresponding sentiment orientation strength value. In order to calculate sentiment orientation strength value in word level, Turney et al. proposed the latent semantic analysis (LSA) technology[7], pointwise mutual information (PMI) technology[8-9], and introduced synonym set structure relation method[10-11]into WordNet[12]. These techniques and methods improved efficiency and accuracy of the sentiment lexicon. SentiWordNet [13-14] which built by the Italian institute of information science and technology used the annotation of WordNet as the feature of words to calculate the sentiment orientation strength value of words in each synsets.

The methods of building Chinese sentiment lexicon are mainly based on corpus statistics and semantic lexicon methods. Corpus-based sentiment lexicon building method use statistical co-occurrence information between words and word similarity to calculate the semantic orientation of the input word. Typically, corpus-based sentiment lexicon building methods calculate the similarity between different words through the co-occurrence information of words and using the similarity between words to calculate the semantic orientation of words. Sentiment building method based on semantic knowledge base is commonly using the semantic lexicons to calculate word similarity. Commonly used Chinese semantic lexicon includes HowNet[15] and synonym words forest. The domestic research on sentiment orientation of Chinese vocabulary and phrases has achieved some initial results. Zhu proposed two kinds of methods to calculate word semantic orientation, one is based on semantic similarity and the other is semantic field. By calculating the similarity between target words and sentiment vocabulary in HowNet to access the sentiment orientation of the target words [16].Li merged to build Chinese polarity sentiment lexicons [17]. Liu built the Chinese basic sentiment lexicon by calculating semantic similarity between seed words and the sentiment words in HowNet [18]. Xu built the affective lexicon ontology which describe a Chinese word or phrase from different angles, including the information of the part of speech, sentiment category, sentiment strength, polarity [19]. Taiwan University has finished the construction of Chinese sentiment lexicon named NTUSD, which include 2812 positive words and 8276 negative words. Zhang compiled a lexicon containing the basic sentiment and field lexicon, online lexicon and modifier lexicon [20].

Considering sentiment orientation of word in the case of different semantic terms, a Chinese sentiment lexicon was built based on the proposed semantics based method, which named CSLS (Chinese Sentiment Lexicon based on semantics). CSLS contains sentiment orientation and strength value of the words. It provide a new effective lexicon resource to the research field of text sentiment analysis.

Building Method of CSLS

Overview of the method. Chinese words meaning rich, the same words in different contexts often contain several different meanings. For example the word “haoshi”, as a noun usually refers to the "good deed". But as a verb, usually to describe a person “meddlesome" or “officious”. The example word has an obvious sentiment orientation difference in different context. So in the process of building sentiment lexicon, it is necessary to fully consider this factor. HowNet is a common-sense knowledge base unveiling inter-conceptual relations and inter-attribute relations of concepts as connoting in lexicons of the Chinese and their English equivalents. In HowNet ambiguity of Chinese words has been sufficiently reflected. WordNet is an online database of English words. Nouns, verbs, adjectives and adverbs are organized into synonym of networks named synset, each synset represents a basic semantic concept, and connected by relationships between these synsets. SentiWordNet contains the sentiment orientation and the corresponding value of synsets which come from WordNet. The sentiment orientation of synsets contain three different categories of positive, negative and objectivity. This study defined the English translation of Chinese words in case of different semantic situations in HowNet as semantic unit. Main building steps of CSLS includes: Firstly, apply HowNet API to get the English semantic units (Esu) of the input Chinese words; Secondly, use SentiWordNet database to search the Esus and get the synsets which contains them; Thirdly, calculate the average sentiment strength value of the synsets and get the sentiment orientation strength values of each Esus; Finally, calculate the average sentiment strength value of the Esus, that is, the sentiment orientation strength value of the input Chinese word.

Building Process of CSLS. Collecting words is a basic work of building the sentiment lexicon. We have collected HowNet sentiment words, NTUSD, Dictionary of Chinese Praise and Biame Words and the sentiment lexicon built by Yang, and used these words as the basic words collection of CSLS by merging duplicate words. The words collection contains a total of 24,130 words, with 10,269 positive words, negative words 13, 861. The specific building procedures of CSLS shown in Fig. 1.

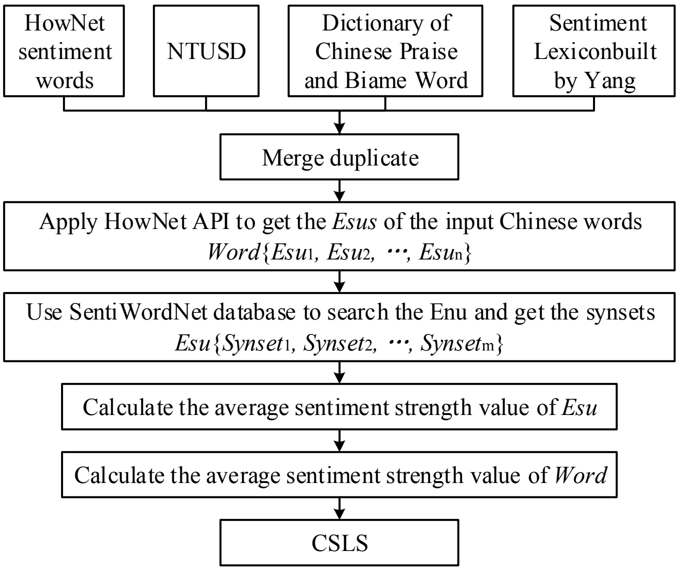
HowNet sentiment words
NTUSD
Dictionary of Chinese Praise and Biame Word
Sentiment Lexiconbuilt by Yang
Merge duplicate
Apply HowNet API to get the Esus of the input Chinese words
Word{Esu1, Esu2, ···, Esun}
Use SentiWordNet database to search the Enu and get the synsets
Esu{Synset1, Synset2, ···, Synsetm}
Calculate the average sentiment strength value of Esu
Calculate the average sentiment strength value of Word
CSLS

Fig.1 Building procedures of CSLS

(1) Get Esus

Word in HowNet often contains several Esus, which represent the different meanings in different contexts. Define Esus set of a Chinese word as W. Then, $W = \{M_1, M_2, ..., M_N\}$, where N represents the number of Esus of the word, $Mn(n = 1,2, ..., N)$ represents the *n-th* Esu of the word. We can get the Esu set of the word by applying HowNet API, such as the Esu set of Chinese word “xiuli” is {beautiful, comely, handsome, pretty}. Youdao dictionary API is used to get the corresponding English translation of the input word as Esu if it do not exist in HowNet. But there are still a few words that we cannot get the Esu set by the above methods. In this case we manually generate it.

Define *WPos* as positive sentiment strength value, *WNeg* as negative sentiment strength value. Then

$$WPos = \frac{1}{N}\sum_{n=}^{N} MPos_n \tag{1}$$

$$WNeg = \frac{1}{N}\sum_{n=}^{N} MNeg_n \tag{2}$$

Where $MPos_n$ is the positive sentiment strength value of the *n-th* Esu, and $MNeg_n$ is the negative sentiment strength value of the *n-th* Esu.

(2) Get the Synsets in SentiWordNet

Synsets are the basic units of SentiWordNet. A synset is constituted by multiple words of similar meaning, which indicate a semantic concept. And each synsets in SentiWordNet has the corresponding sentiment strength values. As shown in Table 1, POS represents a positive sentiment strength value, NEG represent a negative sentiment strength value. An English word may exist in more than one synset, which means that it contains several different semantic concepts. Define the synsets that contain Esu *M* as *S*(*M*), then $S(M)=\{s_1, s_2, \dots, s_k\}$, where *K* is the number of the synsets, and *sk* (*k*=1, 2, …, *K*) is the *k-th* synset which contains then input Esu *M*. We use SentiWordNet database to retrieve input Esu to get the corresponding synsets and their positive and negative sentiment strength values.

Table 1. Examples of synsets in SentiWordNet

Synset and Gloss	POS	NEG
{pride#1,plume#2,congratulate#3}:be proud of; "He prides himself on making it into law school"	0.25	0.5
{pride#1,pridefulness#1}:a feeling of self-respect and personal worth	0.625	0
{pride#2}:satisfaction with your (or another's) achievements; "he takes pride in his son's success"	0.375	0.25
{pride#3}:the trait of being spurred on by a dislike of falling below your standards	0.5	0.25
{pride#4}:a group of lions	0	0
{pride#5,superbia#1}:unreasonable and inordinate self-esteem (personified as one of the deadly sins)	0.625	0.25

(3) Sentiment Orientation Strength Values of Esus

After the previous step, we have been able to obtain positive and negative sentiment strength values of synsets. By Eq. 3 and 4, the sentiment strength values of Esus can be calculated.

$$MPos = \frac{1}{K}\sum_{k=}^{K} sPos_k \tag{3}$$

$$MNeg = \frac{1}{K}\sum_{k=}^{K} sNeg_k \tag{4}$$

Where $sPos_k$ is the positive sentiment strength value of the *k-th* synset, and $sNeg_k$ is the negative sentiment strength value of the *k-th* synset.

(4) Sentiment Orientation Strength Values of Chinese Words

Eq. 3 and 4 are substituted into Eq. 1 and 2 to give

$$WPos = \sum_{n=}^{N}\sum_{k=}^{K} \frac{sPos_k}{NK_n} \tag{5}$$

$$WNeg = \sum_{n=}^{N}\sum_{k=}^{K} \frac{sNeg_k}{NK_n} \tag{6}$$

Where K_n is the number of the synsets of the *n-th* input Esu. Substituting the positive and negative sentiment strength values of the synsets into Eq. 5 and 6 to calculate the positive and negative sentiment strength values of the input word. After completing the calculation of all the input words, normalize the sentiment orientation strength values of the words, that is, the final sentiment orientation strength values of the words in CSLS.

Analysis of structure of CSLS. In general polarity lexicon, there is no sentiment strength value to describe the sentiment orientation of the words. And the words are as individuals with a single sentiment composition. From the data in Table 2 shows that, CSLS is different from the polarity lexicon, it also gives the positive and negative sentiment strength values. The procedure of calculating the sentiment orientation value of the words in CSLS reflects the process of decomposition of the words sentiment. It break the words into Esus, in order to describe the complex sentiment ingredients of words more accurately.

Table 2 Examples of emotional words in SLHS

Sentiment Word	Esu Set	Pos	Neg
Juejia	{excellent}	1	0
Jingcai	{splendid, splendidly, wonderful, wonderfully}	0.5990	0.0625
Zungui	{honourable, respectable, respected}	0.7083	0.0417
Beishang	{heartsore, lamenting, sad, sorrowful, woeful}	0.026	0.7292
Fuchou	{decaying, stinking, smelly}	0	0.75

Sentiment lexicon is a very important resource of the text sentiment analysis system. Sentiment lexicon is widely used in the tasks of word segmentation, extraction of sentiment words and sentiment feature extraction of text. The sentiment lexicon built in this paper is scientifically solved the problem of calculating the sentiment strength of Chinese words, which accurately measured the positive and negative Chinese words.

Experiments and Results Analysis

In order to verify the effect of text sentiment analysis with CSLS, we used SCLS to extract the sentiment feature of text. And Support Vector Machines (SVM) was used to the task of microblog text sentiment classification, specific processes shown in Fig. 2.

In the experiment, firstly, CSLS and NTUSD were respectively used to extract the sentiment features of text in the experiment; then, use the proposed method to classify the input text as positive and negative; finally comparative analyze the results.

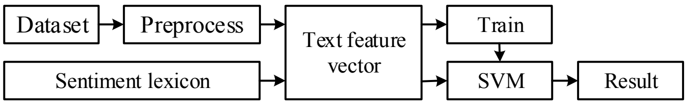

Fig. 2 The flow chart of the experimental method

Experiment Introduction.

(1) Data

The experimental data if from the sample data set of the Chinese microblog sentiment analysis evaluation of NLP&CC2012. XML files were used to store the data. The data includes 20 topics, a total of 2,173 records, of which 407 positive sentiment text, negative sentiment text, 1766. In this paper, two-thirds of random data was used for model training, and the remaining data was used for testing. There is a total of 724 test data, of which 130 positive, negative 594.

(2) Text Feature Extraction

The text is preprocessed before feature extraction. Text preprocessing includes word segmentation, selection of sentiment feature and feature weight calculation.

Word segmentation is the basis for text processing, we use CTCLAS to preprocess for fine-grained segmentation and POS tagging. Then the number of occurrences of nouns, adjectives, interjections, onomatopoeia, negative words and adversative words was counted. The selection of sentiment features is shown in Table 3.

Table 3 Sentiment features of text

Type	Features
Sentiment lexicon	Positive and negative sentiment strength values, number of sentiment words
Punctuation	Whether there is a question mark, exclamation
POS statistics	Numbers of Nouns, verbs, adjectives, conjunctions, onomatopoeia
Negative words	Number of negative words
Adversative words	Number of adversative words

After selecting the sentiment feature of text, quantify the features to get the text feature vector. It is noted that, NTUSD is a polarity sentiment lexicon without sentiment strength values. Therefore, when using NTUSD to get the sentiment strength values, the positive sentiment strength value of a positive word is set to 1 and the negative is set to 0; and the positive sentiment strength value of a negative word is set to 0 and the negative is set to 1.

(3) SVM Classifier

In this paper, SVM was used to construct the text sentiment classifier. SVM is a supervised learning method, which belongs to the generalized linear classifier. It is able to minimize experience errors and maximize edge geometry, so SVM is also called the maximum fringe classifier. The SVM tool used in this paper is developed by Lin [24].

Results Analysis.

(1) Contrast Experiment

Since CSLS was built by unsupervised method, some of these sentiment strength values of the words may be biased. Therefore, it is necessary to proofread CSLS and verify its effectiveness. We use NTUSD and Tsinghua University Positive and Negative Lexicon (TUPNL) [17] to proofread CSLS. Due to the two sentiment lexicons belong to polarity lexicon, we add polarity mark in CSLS. We compare the positive sentiment strength to the negative sentiment strength of the word, when the positive sentiment strength is greater than the negative sentiment strength the word, the polarity of it is marked as positive; when the positive sentiment strength is less than the negative sentiment strength the word, the polarity of it is marked as negative. And then loops through NTUSD and TUPNL, compare words one by one with words in CSLS. The results shown in Table 4. As can be seen from the results, compare to the manual intervention marked polarity lexicon, the accuracy of CSLS still has some room for improvement.

Table 4 CSLS comparative analysis result data

Lexicon	Number of positive words	Number of negative words	Accuracy
NTUSD	2647	7741	0.77
TUPNL	5565	4467	0.72

(2) Optimizing CSLS

Next, we adjust the sentiment strength of the words in CSLS to improve the accuracy of it. The steps of the proposed lexicon proofreading method includes: First use the method described above to mark the polarity of the words in CSLS; then loops through NTUSD and TUPNL, compare the polarity of the word to the polarity of the word in CSLS; if the polarities are different, swaps the positive and negative sentiment strength values of the word.

After proofreading, the accuracy of the sentiment strength values of the word in CSLS will be greatly improved. The proposed lexicon proofreading method enable CSLS to learn sentiment knowledge of the input sentiment lexicon.

(3) Types of SVM and Kernel Options

After completing the sentiment features extraction of data set, choose different types of SVM and kernel and using 5 cross validation method to experiment. The results are shown in Table 5. According to the classification accuracy of the data, we get better classification results when using C-SVC type of SVM and RBF kernel in the experiment.

Table 5 Classification accuracy using different types SVMs (%)

Sentiment Lexicon	Accuracy	Recall	F-Measure
CSLS	83.84	57.54	68.24
NTUSD	83.56	54.7	66.12

Data shown in Table 5 indicate that when using CSLS to extract the features of the input text, it achieved better results, which verify the effectiveness of the proposed lexicon.

Conclusions

A semantic based Chinese sentiment lexicon building method was proposed. It use HowNet to decompose Chinese words into Esus, and then calculate the positive and negative sentiment strength values of the word by using SentiWordNet. A lexicon proofreading method was used to optimize the sentiment strength values of the word. Experiment on microblog sentiment analysis verify the effectiveness of the built lexicon.

In the building process of the lexicon, there is a problem that some relatively uncommon Chinese words cannot automatically be decomposed into Esus. And also we used a simple mean value method in the calculation of sentiment strength values of the word. Further research should consider looking for more reasonable method for decomposing into Esus and calculating the sentiment strength values of the word.

Acknowledgement

This work was financially supported by National Social Science Foundation (12BYY045) and by Program for New Century Excellent Talents in University (NCET-12-0939).

References

[1] ZHAO Yanyan, QIN Bing, LIU Ting. Sentiment Analysis[J]. Journal of Software, 2010, 21(8): 1834-1848.

[2] Hatzivassiloglou V, McKeown K R. Predicting the semantic orientation of adjectives[C]//Proceedings of the eighth conference on European chapter of the Association for Computational Linguistics. Association for Computational Linguistics, 1997: 174-181.

[3] Wiebe J M. Learning subjective adjectives from corpora[C]//Proceedings of the National Conference on Artificial Intelligence. Menlo Park, CA; Cambridge, MA; London; AAAI Press; MIT Press; 1999, 2000: 735-741.

[4] Riloff E, Wiebe J, Wilson T. Learning subjective nouns using extraction pattern bootstrapping[C]//Proceedings of the seventh conference on Natural language learning at HLT-NAACL 2003-Volume 4. Association for Computational Linguistics, 2003: 25-32.

[5] Baroni M, Vegnaduzzo S. Identifying subjective adjectives through web-based mutual information[C]//Proceedings of KONVENS. 2004, 4: 17-24.

[6] Moilanen K, Pulman S. The good, the bad, and the unknown: morphosyllabic sentiment tagging of unseen words[C]//Proceedings of the 46th Annual Meeting of the Association for Computational Linguistics on Human Language Technologies: Short Papers. Association for Computational Linguistics, 2008: 109-112.

[7] Turney P, Littman M L. Measuring praise and criticism: Inference of semantic orientationfrom association[J]. ACM Trans. Information Systems, 2003, 21(4): 315-346.

[8] Yang A M, Lin J H, Zhou Y M, et al. Research on Building a Chinese Sentiment Lexicon Based on SO-PMI[J]. Applied Mechanics and Materials, 2013, 263: 1688-1693.

[9] Read J. Recognising affect in text using pointwise-mutual information[J]. Unpublished M. Sc. Dissertation, University of Sussex, UK, 2004.

[10] Kamps J, Marx M, Mokken R J, et al. Words with Attitude[C]//Proc. of the 1[st] Int' 1 Conf. on Global WordNet. Mysore, India, 2002.

[11] Kim S M, Hovy E. Determining the sentiment of opinions[C]//Proceedings of the 20th international conference on Computational Linguistics. Association for Computational Linguistics, 2004: 1367-1373.

[12] Miller G A, Beckwith R, Fellbaum C, et al. Introduction to wordnet: An on-line lexical database[J]. International journal of lexicography, 1990, 3(4): 235-244.

[13] Esuli A, Sebastiani F. Sentiwordnet: A publicly available lexical resource for opinion mining[C]//Proceedings of LREC. 2006, 6: 417-422.

[14] Baccianella S, Esuli A, Sebastiani F. Sentiwordnet 3.0: An enhanced lexical resource for sentiment analysis and opinion mining[C]//Proceedings of the 7th conference on International Language Resources and Evaluation (LREC'10), Valletta, Malta, May. 2010.

[15] DONG Zhendong. Semantic expression and the construction of knowledge systems[J]. Applied Linguistics, 1998, 3(3): 76-82.

[16] ZHU Yanlan, MIN Jin, ZHOU Yaqian, et al. Semantic Orientation Computing Based on HowNet[J]. Journal of Chinese Information Processing, 2006, 20(1):14–20.

[17] Li J, Sun M. Experimental study on sentiment classification of Chinese review using machine learning techniques[C]//Natural Language Processing and Knowledge Engineering, 2007. NLP-KE 2007. International Conference on. IEEE, 2007: 393-400.

[18] Li J, Sun M. Experimental study on sentiment classification of Chinese review using machine learning techniques[C]//Natural Language Processing and Knowledge Engineering, 2007. NLP-KE 2007. International Conference on. IEEE, 2007: 393-400.

[19] LIU Weiping, ZHU Yanhui, LI Chunliang, Research on building Chinese basic semantic lexicon [J]. et al. Journal of Computer Applications, 2009, 29(11): 2882-2884.

[20] XU Linhong, LIN Hongfei, PAN Yu, et al. Constructing the Affective Lexicon Ontology[J]. Journal of The China Society For Scientific and Technical Information, 2008, 27(2): 180-185.

[21] Chang C C, Lin C J. LIBSVM: a library for support vector machines[J]. ACM Transactions on Intelligent Systems and Technology (TIST), 2011, 2(3): 27.

Applied Mechanics and Materials Vol. 596 (2014) pp 271-275
© (2014) Trans Tech Publications, Switzerland
doi:10.4028/www.scientific.net/AMM.596.271

A Model of Predicting Corrosion Rate for Substation Grounding Grid Based on the Similarity and Support Vector Regression

Du Jingyi[1,a], Han Juan[1,b], Zhao Yuejiao[1,c], Liu Wenhui[1,d]

[1]Xian university of science and technology, Xi'an 710054

[a] dujingyivip@163.com, [b]galar007@163.com, [c]444678462@qq.com, [d]1115050086@qq.com

Keywords: grounding grid corrosion rate; vector similarity; support vector regression.

Abstract. In this paper, we proposed a training model to predict the corrosion rate for substation grounding grid based on the Similarity and Support Vector Regression (SSVR). In the proposed model, the effect of grounding grid corrosion rate was acted as a feature vector and processed by a dimensionless treatment. Then, the similarity between the feature vector of training terminal and index vector of actual site would be calculated. In the prediction of corrosion rate, the traditional Linear Average Method (LAM) to describe the nonlinear contribution has some fault defects. Therefore, we proposed the training model named SSVR. From the experimental results, the proposed SSVR can obtain better predicting performance than the traditional LAM.

Introduction

Substation grounding grid is an essential and important facilities for work grounding, lighting protection and grounding protection, respectively. It is also an important part to maintain the operation safety of the power system and to protect the safety of operating people[1]. To solve the corrosion of the grounding grid has become a major anti-accident measurement for substations and power plants. They urgently need to find an unconstraint method and measuring system to diagnose grounding grid in the case of no blackout and no excavation

In recent years, grounding grid corrosion detection and fault diagnosis field has made a lot of achievements. In references [2], they combined soil resistivity, redox potential, soil PH, and other individual soil parameters to evaluate the corrosion by electrochemical tests in accordance with DL/T 5394-2007[3] standard. But the evaluation method of individual soil parameters could easily lead to false identification. All above studies always analyzed and judged corrosion rate from the perspective of a single grounding material. But corrosion is a complex and random phenomenon caused by a joint function of material and environment that is a synthesis results of electrochemical and chemical effects of grounding materials in soil environment. In addition to the impact of the material itself, more conditions are affected by soil properties, geographical location, climatic conditions, and other factors [4].

In essence, the grounding grid corrosion was predicted based on the uncertainty of the index information in the actual site by using of machine learning approaches and appropriate data modeling methods. In this paper, we proposed an integrated algorithm based on the similarity vector and SVR. Firstly, we established feature vectors of measured samples and standard training sample to deal with the dimensionless standardization. Secondly, we calculated the similarity between the feature vectors of measured samples and standard-training sample. Finally, we can predict the corrosion rate in accordance with the calculated similarity. Generally, a linear contribution method[5] was usually used in the process of calculating the correlative predicted results. However, more factors such as the variation for the distribution of training samples and the difference between index values that influenced the grounding grid corrosion. The contribution of linear method often resulted in an unsatisfactory solution. The SVR has the characteristic in the real domain for the Support Vector Machine (SVM). It has the advantage of strong adaptability, good generalization performance, and more suitable for the optimization model [6]. In response to these issues, we lead SVR technology into the prediction model and integrate the similarity rank of the original training samples in this paper.

The Principle of Vector Similarity

Similarity is represented to the degree of similarity between two objects. Because the vector consists of direction and magnitude, we can use these two factors to express the similarity of two vectors. If two vectors satisfy $X=(x_1,x_2,\Lambda,x_n)$ and $Y=(y_1,y_2,\Lambda,y_n)$, then the norm (length) similarity (α) of vector X and Y is defined as

$$\alpha=\begin{cases}1-\dfrac{\left|\|X\|-\|Y\|\right|}{\|X\|} & \|Y\|\le 2\|X\| \\ 0 & \|Y\|>2\|X\|\end{cases} \tag{1}$$

The direction similarity (β) of vector X and Y can be calculated by $\beta=1-\dfrac{\theta}{90°}$ (2)

where $\theta=\arccos\dfrac{[X,Y]}{\|X\|\cdot\|Y\|}$, the similarities (γ) of vector X and Y is the product of norm similarity (α) and direction similarity (β), namely $\gamma=\alpha\cdot\beta$ (3)

In this paper, we selected 10 items from the corrosion factors as targets of affecting grounding grid corrosion rate to compose a feature vector. According to the definition of the vector similarity, we can calculate the contributions for the criteria vector of each training site to the grounding grid of the measured indicators. The process steps are as follows.

Step 1: Establish feature vector of prediction criteria for the grounding grid corrosion rate. Each feature vector $X_i=\left[x_{i1},x_{i2},\Lambda,x_{ij}\right]$ is composed by 10 factors such as Ca^{2+}, Mg^{2+}, K^+/Na^+, SO_4^{2-}, Cl^-, HCO_3^-, CO_3^{2-}, salinity, PH, organic matter, average annual rainfall, average annual temperature, elevation, north latitude, longitude, respectively. The corresponding template for the corrosion rate is $V=[v_1,v_2,\Lambda,v_i]$, where i ($i=1,2,\cdots,m$) and j ($j=1,2,\cdots,n$) represent a site ID and the number of indicators, individually.

Step 2: Establish a relatively vector. Take a grounding grid's measured vector.

Step 3: Do the dimensionless process with normalized vectors[7].

Let

$$s_{ij}=\frac{x_{ij}}{\sqrt{\sum_{i=1}^{m}x_{ij}^2}} \tag{4}$$

$s_{ij}(i=1,2,\Lambda,m;j=1,2,\Lambda,n)$ represents the value of element x_{ij} after normalization. The purpose this step is to transform all characteristic value into dimensionless manner during the range of $(0,1)$.

Step 4: Calculate the similarity between each training site's criteria vector and the measured factors of grounding grid that is the similarity of X_i and Y based on Eqs. (1) - (3).

Prediction of Grounding Grid Corrosion Rate Based on SVR

3.1 SVR(Support Vector Regression)

For the training sample set $\{X,V\}$, X is the input vector and V is the corresponding output value of X. The purpose of SVR is to map input vectors x into a high dimensional feature space F through a nonlinear mapping φ, then the linear regression is conducted in the feature space F. It is

$$y=f(x)=w^T\varphi(x)+b \tag{5}$$

Where w is a weight vector on a hyper plane, b is an offset term. Therefore, SVR is actually solving those optimization problems with the following constraint:

$$\min\frac{1}{2}w^Tw+C\sum_{i=1}^{l}(\xi_i+\xi_i^*) \tag{6}$$

$$s.t.\begin{cases}\{y_i - [w^T\phi(x_i) + b] \le \varepsilon + \xi_i \\ \{[w^T\phi(x_i) + b] - y_i \le \varepsilon + \xi_i^* \\ \xi_i, \xi_i^* \ge 0, i = 1, 2, \cdots, l\end{cases} \tag{7}$$

In Eq. (6), a greater than zero constant C is used to balance the model complexity and training error. Slack variables ξ_i and ξ_i^* are used to denote the upper and lower training error in condition ε. Using Wolfe's duality principle and nuclear techniques, Lagrange multipliers α, α^* and kernel function $k(x_i, x_j) = \varphi(x_i)^T \cdot \varphi(x_j)$ would be introduced to solve the convex quadratic programming problem such that the SVR function can be obtained:

$$f(x) = \sum_{i=1}^{ns}(\alpha_i - \alpha_i^*)k(x_i, x) + b \tag{8}$$

where ns represents the support vector number as well as the RBF kernel $k(x_i, x_j) = \exp(-\frac{1}{2\sigma^2}\|x_i - x_j\|^2)$ was used in this paper

3.2 The prediction of grounding grid corrosion

If more training sets of sites were used taking into account the use of grounding grid corrosion rate of SVR to establish a model, we could obtain similarities A_i with large difference. So excluding sites with relatively low degree of similarity can improve the accuracy for the SVR model. The environmental-soil erosion factors and corrosion status were treated as variables of the grounding grid corrosion-factor model. With the training sample or analog methods, we can establish regression model among variables. The flow diagram is shown as in Fig.1.

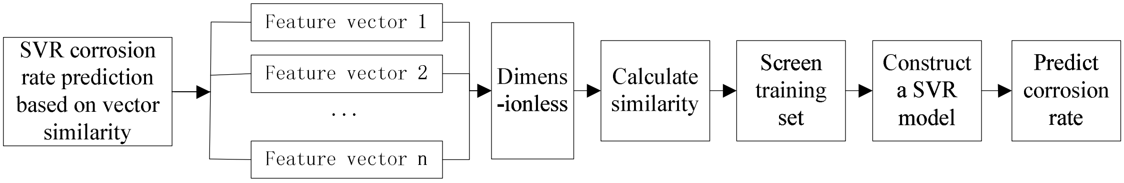

Fig.1. The flow diagram of SVR corrosion rate prediction based on vector similarity

The steps for this model are as follows.

Step 1: Select suitable training sets for those sites with similarity $A_i > \lambda$, where λ is the initial threshold with a range of (0, 1).

Step 2: Train the above selected training sets and construct SVR model.

Step 3: Put the factors of the actual site into the SVR model and activate SVR model to implement the prediction of corrosion rate.

Experimental Verification

We selected 10 characteristic factors those affecting corrosion rate of substation grounding and corresponding grounding grids from 65 places in Shaanxi Province which were shown as in Table 1.

Table 1. Substation Grounding Grids and Corresponding Grounding Grid Corrosion Rate

analysis item	Xiecun	Shitoupo	Baoji	Yongcheng	Dayang	Sujiada	Shenmu	…	Bijia
Ca %）	0.007	0.009	0.011	0.011	0.01	0.011	0.009	…	0.006
Mg %）	0.001	0.004	0.001	0.002	0.005	0.003	0.002	…	0.002
Na/K %）	0.000	0.002	0.011	0.003	0.014	0.002	0.001	…	0.009
SO4 %）	0.002	0.004	0.009	0.005	0.023	0.006	0.001	…	0.001
Cl %）	0.002	0.005	0.005	0.003	0.009	0.005	0.003	…	0.005
HCO3 %）	0.018	0.035	0.044	0.035	0.043	0.012	0.034	…	0.037
CO3 %）	0.002	0.003	0.003	0.002	0.003	0.012	0.003	…	0.002
saltness %）	0.032	0.063	0.08	0.059	0.107	0.052	0.05	…	0.061
PH	8.6	8.56	8.12	7.9	8.5	9.71	7.8	…	8.45
organic material %）	1.230	1.170	1.19	1.33	1.13	0.380	0.54	…	1.010
corrosion rate mm/a）	0.178	0.211	0.1321	0.2219	0.1365	0.113	0.1596	…	0.123

Firstly, we calculated the contribution of the training sites evaluation criteria with the measured factors of grounding grid vector A_i to predict grounding grid corrosion using linear contribution. Then we obtained each training site's weight distribution. Finally, combining actual corrosion of training samples, we could predict grounding grid corrosion rate of a site. The flow diagram is shown as in Fig.2.

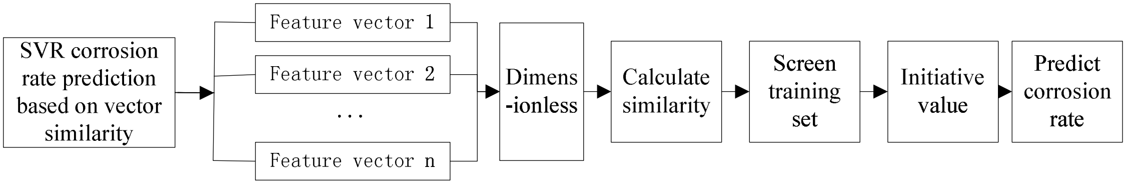

Fig.2. The Flow Diagram of Corrosion Rate Based on Linear Contribution

Then we select training data of substation grounding grid from 65 places in Shaanxi Province to test. We selected Yu Du station in Hanzhong as a test site and the remaining 64 substations as the training sites to calculate the similarity between test site and training sites. These similarities after normalization are shown as in Table 2.

Table 2 Similarity after normalization

Site name	Chazhen	Hanzhong	Zhoujiaping	Xujiaping	Laojun	Shunzheng	...	Yulin
the similarity after normalization	1	0.9710	0.9708	0.9691	0.9423	0.9276	…	0

From Table 2, we can get a high similarity for training sample sites which are around the test site (Yudu station in Hanzhong) that matches with objective truth. Then, we calculated the grounding grid corrosion rates and cyclic verification base on linear contribution and SVR with a threshold value of 0.2 for these 65 substation grounding grids in Shaanxi Province in turn. The experimental results are shown as in Table 3.

Table 3 Corrosion Rate Prediction and Error Analysis

Measured site	Actual rate	Based on the contribution of linear			Based on SVR (support vector regression machine)					
					No screening of the training sample			Screening of the training sample λ=0.02）		
		Predict rate	Absolute error	Relative error	Predict rate	Absolute error	Relative error	Predict rate	Absolute error	Relative error
Xiecun	0.1783	0.1733	0.0050	2.80%	0.2447	0.0664	37.22%	0.1742	0.0041	2.28%
Shunzheng	0.2236	0.1737	0.0499	22.30%	0.1831	0.0405	18.11%	0.2431	0.0195	8.73%
Hanzhong	0.2089	0.1722	0.0367	17.57%	0.1886	0.0203	9.71%	0.2165	0.0076	3.66%
Honghe	0.2413	0.1734	0.0679	28.15%	0.1813	0.0600	24.87%	0.2414	0.0001	0.04%
Laojun	0.1794	0.1728	0.0066	3.65%	0.1830	0.0036	2.01%	0.1794	0.0000	0.02%
Baliqiao	0.1951	0.1892	0.0059	3.02%	0.2211	0.0260	13.35%	0.1941	0.0010	0.53%
Zhuangtou	0.1859	0.1792	0.0067	3.63%	0.1985	0.0126	6.77%	0.1931	0.0072	3.89%
Huaxian	0.1927	0.1769	0.0158	8.20%	0.2013	0.0086	4.48%	0.1921	0.0006	0.31%
Luofu	0.1877	0.1778	0.0099	5.27%	0.1798	0.0079	4.21%	0.1889	0.0012	0.66%
Sudong	0.1982	0.1769	0.0213	10.75%	0.1875	0.0107	5.38%	0.1992	0.0010	0.48%
Qiaoling	0.1981	0.1789	0.0192	9.70%	0.2146	0.0165	8.34%	0.1943	0.0038	1.91%
…	…	…	…	…	…	…	…	…	…	…

We use Mean Absolute Error (*MAE*), Root Mean Square Error (*RMSE*), and Willmott's Index of Agreement (*WIA*) as criteria and defined as:

$$MAE=\frac{1}{m}\sum_{i=1}^{m}|y_i-v_i|\ ;\ RMSE=\sqrt{\frac{1}{m}\sum_{i=1}^{m}(y_i-v_i)^2}\ ;\ WIA=1-\frac{\sum_{i=1}^{m}(y_i-v_i)^2}{\sum_{i=1}^{m}(|y_i'|-|v_i'|)^2} \tag{9}$$

$$y_i^{'} = y_i - \overline{y}, v_i^{'} = v_i - \overline{y}, \overline{y} = \frac{1}{m}\sum_{i=1}^{m} y_i \tag{10}$$

Where m represents the number of test site, $y_i^{'}$, $v_i^{'}$ represent predict value and actual value of i-th test site. The larger the value *WIA*, the more significant the prediction, the result is shown as Table 4.

Table 4. The performance of corrosion-rate prediction for different methods

Evaluation index	Based on the contribution of linear	Based on SVR (support vector regression machine)	
		No screening of the training sample	Screening of the training sample λ=0.02）
MAE	0.6670	0.5557	0.5170
RMSE	0.2055	0.1740	0.1687
WIA	0.0985	0.6732	0.7025

Table 3 and Table 4 show that the strategy based on the basis of vector similarity principle by linear contribution and original training sets with SVR can accurately predict grounding grid corrosion rate in the criteria of *MAE*, *RMSE*, and *WIA*. Additionally, the proposed SVR algorithm based on similarity to filter the training sets can obtain better results.

Conclusion

In this paper, we used two-stage structure which combines the vector similarity and SVR to establish a model to predict the grounding grid corrosion rate for compensating the deficiencies of the conventional method and improving the prediction accuracy. Finally, the conclusions are shown as follows:

(1) The vector similarity was decomposed into magnitude and direction components. Then we integrated these two components as a characterization similarity to exclude man-made interferences with a strong objectivity.

(2) Although the traditional system based on linear prediction can achieve corresponding prediction, we can select suitable training samples and sort them according to the similarity. Then S-SVR model can be established for those sorted samples to improve the validity and obtain better prediction accuracy.

References

[1] Bai Xu, The Application and Research on Corrosion Prevention of Substation Grounding Grid Based on Cathodic Protection Principles[D]. North China Electric Power University , 2011,6.

[2] Chendorain M D,Stewart L D,Packer B. Corrosion of unexploded ordnance in soil-field results[J]. Environmental Science & Technology,2005,39(8):2442-2447.

[3] China Electricity Council. DL/T5394-2007. guidelines foranticorrosion of underground steel structure in powerproject[S]. Beijing:China Electric Power Press,2007(in Chinese).

[4] Weng Yongji, Li Xiangyi. Fractal study on statistical characteristics of average corrosion rate of carbon steel in soils[J]. Jonranl of Chinese Society for Corrosion and Protection,2005,4(25):200-204.

[5] Qin Jia,Yang Jianfeng,Xue Bin,et al.Image Registration and mosaic Based on Vector Similarity Matching Principle[J]. Microelectronics & Computer, 2013,30(6):22-25.

[6] Maulik U. Performance Evaluation of Some Clustering Algorithms and Validity Indices[J]. IEEE Transactions on Pattern Analysis and Machine intelligence 2002,24(12)：1650-1654.

[7] Zhang Xiaoming. Comparative analysis of data nondimensionalization in decision analysis[J]. Journal of minjiang university, 2012,33(5):21-25.

Applied Mechanics and Materials Vol. 596 (2014) pp 276-279
© (2014) Trans Tech Publications, Switzerland
doi:10.4028/www.scientific.net/AMM.596.276

Efficient Graph Component Labeling on Hybrid CPU and GPU Platforms

Xiaohui Pan[1, a]

[1] Modern Education Technology Center, Shanghai University of Political Science and Law,
Shanghai, China, 201701
[a]email: : panxiaohui@shupl.edu.cn

Keywords: Connected Components, GPU, Graph processing

Abstract. Graph component labeling, which is a subset of the general graph coloring problem, is a computationally expensive operation in many important applications and simulations. A number of data-parallel algorithmic variations to the component labeling problem are possible and we explore their use with general purpose graphical processing units (GPGPUs) and with the CUDA GPU programming language. We discuss implementation issues and performance results on CPUs and GPUs using CUDA. We evaluated our system with real-world graphs. We show how to consider different architectural features of the GPU and the host CPUs and achieve high performance.

Introduction

Graph component labeling is an important algorithmic problem that occurs in many applications areas. Generally, the problem involves identifying which nodes in a graph belong to the same connected cluster or component. In many applications the graph of interest has undirected arcs and all nodes in a connected cluster are fully and mutually reachable. However, some applications problems will give rise to structural graphs that are generated as a number of separate clusters, or break up into separate clusters or coagulate into larger super-clusters as a result of some dynamical process. In some cases the graph is simply a structural one and connectivity is determined entirely by the presence or absence of arcs between nodes. Many simulations problems are formulated in terms of a set of variables on a graph and the value of the variables on the nodes can be used to differentiate between nodes that are connected or not. We start by defining a graph $G = (V, E)$ as a set of vertices V connected by a set of edges E.

The determination of the connected components of a graph is comprised of a search over edges or vertices. For each vertex or edge, a similar algorithmic procedure is per- formed. Using this fact, a multitude of graphical algorithms lend themselves to parallel implementations. In this paper, we introduce a parallel system which utilizes both the multi-core CPUs and the many-core GPUs.

Efficient Graph Processing on CPUs and GPUs

GPU-accelerated graph processing has the potential to offer an efficient solution. Compared to CPUs, GPUs have much higher parallelism and memory bandwidth. Today's commodity GPUs supports thousands of hardware threads and in-flight memory requests through light-weight hardware multithreading. Besides, the memory access latency on GPUs can be effectively hided by other active computing threads. Indeed, previous work has demonstrated the benefit of utilize GPUs to accelerate graph processing. Harish et al.[1],Vineet et al.[2], and Merrill et al.[3] implemented several graph algorithms including Breadth First Search(BFS), parallel Boruvka and Minimum Spanning Tree(MST) on GPUs and gained various speedups. These past work assumes that the entire graph fits in the GPU memory. However, even the high-end GPUs today (eg. Nvidia Tesla series) have only up to 6 GB memory each, which is far from enough to hold a large scale graph. For example, a snapshot of the current Twitter follower network has over 500 million vertices and 100 billion edges, and requires at least 0.5TB or memory. Recent work by Gharaibeh et al.[4] utilizes both the host (CPU) memory and device (GPU) memory to hold graphs and partitions workloads between CPUs and

GPUs for processing in parallel. Still, the host memory and device memory of a single machine are inadequate to hold large scale graphs.

There are two challenges associated with the graph processing on hybrid CPU and GPU platforms. First, we need low-cost graph partitioning mechanisms to partition each graph into several parts which fits in the host or the device memory. Second, to achieve good performance on GPUs, the application must, as much as possible, match the SIMD computing model. Vertex-centric graph algorithms exhibit data-dependent parallelism, traditional implementation of graph algorithms lead to load imbalance and irregular memory access pattern. Real-world graphs exhibit power law edge degree distribution [4]. Vertices thus have different workload when they traverse their edges. The irregular memory access pattern further degrades the performance.

System Architecture

Basic System Architecture. Our prototype system consists of a CPU, a GPU, memory resource and a secondary storage(hard disk), as shown in Fig. 1. The CPU and GPU have processing rates of *Rcpu* and *Rgpu* Edges Per Second(E/s), respectively. The two processors communicate through a PCI-Express bus whose transmission rate is *C* Edges Per Second E/s. The graph is partitioned between the CPU and GPU based on a CPU load ratio α between (0,1) such that α edges are processed on the CPU and *(1-α)* edges are processed on the GPU.

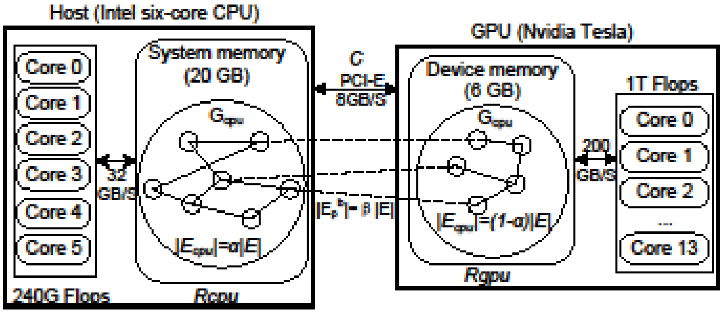

Fig.1 System block diagram and the value for today's commodity components

Graph Representation. Real world graphs such as social networks are often sparse and therefore can be stored in the compressed format to save memory space. Adjacency lists provide compact storage for more widespread sparse graphs. A basic adjacency list stores all edges in a graph. One typical way of implementing it is to use one array to store a list of neighboring nodes and another array to store the offset of the neighboring list for each node. Compressed Sparse Row (CSR), Compressed Sparsed Column (CSC), and Coordinate List (COO) are three typical implementations of the adjacency lists.

To efficiently execute update functions for diverse graph algorithms, our platform adopts the following data interface to the CPU and GPU update functions:

- Vertex value: array containing the value of vertices.
- Vertex indices: array containing the index of vertices in the vertex value array. This array is useful since the i_{th} element in vertex value array does not necessarily to be vertex i.
- Edge value: array containing the value of edges. The order is: in-edges of vertex i, out-edges of vertex i, in-edges of vertex i+1, out-edges of vertex i+1.
- Edge number: array containing the number of in-edges (in-degree) and out-edges (out-degree). The $(2i)_{th}$ and $(2i+1)_{th}$ elements record the in-degree and our-degree of the i_{th} vertex in the vertex indices array, respectively.
- Edge position: array containing the position of in-edges and out-edges in the edge value array. The $(2i)_{th}$ and $(2i+1)_{th}$ elements records the beginning index of in-edges and out-edges of the i_{th} vertex in vertex indices array, respectively.
- Edge vertices1: array containing one end vertex for each edge e=(source, destination) in the edge value array. if e is an in-edge, the end vertex stored is the destination. Otherwise, the source is stored for each out-edge.

- Edge vertices2: array containing the other end vertex for each edge e=(source, destination) in the edge value array. if e is an in-edge, the end vertex stored is the source. Otherwise, the destination is stored for each out-edge.

Computation model. Out platform adopts the Bulk Synchronous Parallel (BSP) computation model [5] and divides processing into rounds (super-steps in BSP terminology). Each super-step consists of three phases executed in order: computation, communication and synchronization. In the computation phase, each processor (in our case the CPU and the GPU(s)) executes asynchronously computations based on values stored in their local memories. In the communication phase, the processors exchange messages that are necessary to update their statuses before the next computation phase starts. The synchronization phase guarantees the delivery of the messages. Specifically, a message sent at super-step i is guaranteed to be available in the local memory of the destination processor only at super-step i+1.

System Implementation

Connected Components Algorithm. We adopt the algorithm implemented in the GraphChi [6]. The algorithm implementation is based on label propagation. On the first iteration, each vertex writes its id ("label") to its edges. On subsequent iterations, vertex chooses a new label based on the labels of its neighbors. For Connected Components, vertex chooses the minimum label. Finally, sets of vertices with equal labels are interpreted as connected components.

Graph partitioning between the CPU and the GPU. Since our platform adopts the BSP model, the CPU and the GPU will synchronize after each iteration. Based on the parameters in previous "Basic System Architecture" section, we can derive the following equation for the running time of each super-step.

$$T_{run} = \max\left\{ \frac{|E_{cpu}^{b}|}{C} + \frac{\alpha |E|}{R_{cpu}}, \frac{|E_{gpu}^{b}|}{C} + \frac{(1-\alpha)|E|}{R_{gpu}} \right\} \tag{1}$$

Equation 1 manifests that the computation time for each super-step is the maximum processing time of the CPU or the GPU. The processing time of the CPU is the time for the CPU to process $\alpha|E|$ edges at a rate of R_{cpu} and to transmit the value of the boundary edges E_{cpu}^{b} to the GPU at a throughput of C. Similarly, the processing time of the GPU is the time for the GPU to process $(1-\alpha)$ $|E|$ edges at a rate of R_{gpu} and to transmit the value of the boundary edges E_{gpu}^{b} to the CPU at a throughput of C. Therefore, T_{run} is minimized when the system partitions the workload between the CPU and the GPU in a balanced manner such that they take similar time to complete.

We propose an adaptive loading approach to partition and adjust the workload partitioning between the CPU and the GPU. In the first iteration, the workload (the graph) is partitioned between the CPU and the GPU based on a default CPU load ratio α. Then, we calculate Rcpu, Rgpu, C and the number of the boundary edges after the first iteration. Finally, we adjust CPU load ratio α.to balance the load between the CPU and the GPU in sebsequent iteration.

Data Remapping to improve GPU efficiency. Real-world graphs are known to be irregular: vertices tend to have quite different number of edges (degree). For example, the Com-LiveJournal [7] graph has an average degree of 17, while some vertices in this graph have 100x or even 1000x higher degree than this average degree. In the vertex-centric model, each GPU thread processes a vertex. This imbalanced degree will decrease GPU efficiency since the thread processing a low-degree vertex has to wait for threads processing high-degree vertices.

We propose a light-weight data remapping to solve alleviate this issue. Before the beginning of the computation, we sort the vertex id V based on their degree and store the result into a new array M. Now GPU thread i will process vertex M[i] instead of V[i]. With this remapping, GPU threads in a warp will process vertices of identical or similar degree, thus the GPU efficiency is improved. Note the sorting is a one-time process before all the computation, then the result can be used in all iterations since the degrees of vertices will not change during computing.

Experiment Results and Analysis

Hardware Platform. We use a machine with a six-core Intel Xeon E5645 CPU and an Nvidia Tesla C2075 GPU for our evaluation. The CPU is running at 2.4GHz with 12MB cache and 24GB main memory. The GPU is running at 1.1GHz with 2MB cache and 6GB device memory. The machine has a 1TB, 7200RPM disk running Arch Linux with 64 bits, 3.11 kernel version and CUDA 5.5.
Results. We evaluated the following graph as listed in Table 1. The results show that our hybrid CPU and GPU platform outperforms a pure multi-core CPU implementation by 3.2X on average.

Table 1 Graphs

Graph	#Vertices	#Edges
Com-LiveJournal	3.99M	34.68M
Soc-LiveJournal	4.85M	68.99M
Com-Orkut	3.07M	0.12B
Twitter 2010	61.58M	1.5B

Conclusion

In this paper, we designed and implemented a system for processing the connected components algorithm efficiently on hybrid CPU and GPU systems. We proposed an adaptive loading ratios method for adjust the workload partitioning between the CPU and the GPU. In addition, we proposed a data remapping method to improve the GPU's efficiency on computing irregular graphs. Experiments show that our hybrid CPU and GPU system outperforms the pure multi-core CPU implementation by 3.2X on average on all graphs.

References

[1] P. Harish, V. Vineet, and P. J. Narayanan. *Large graph algorithms for massively multithreaded architectures.* Technical Report IIIT/TR/2009/74, International Institute of Information Technology Hy-derabad, INDIA,(2009).

[2] V. Vineet, P. Harish, S. Patidar, and P. J. Narayanan. *Fast minimum spanning tree for large graphs on the GPU.* In Proceedings of the Conference on High Performance Graphics, (2009), p. 167-171

[3] D. Merrill, M. Garland, and A. Grimshaw. *Scalable GPU graph traversal*. In Proceedings of the 17th ACM SIGPLAN Symposium on Principles and Practice of Parallel Programming, (2012), p.117-128

[4] A. Gharaibeh, L. B. Costa, E. Santos-Neto, and M.Ripeanu. *On graphs, GPUs, and blind dating: A workload to processor matchmaking quest*. In Proceedings of IEEE IPDPS (2013).

[5] L. Valiant. *A bridging model for parallel computation*. Communications of the ACM, Vol. 33, No. 8 (1990), p.103-111

[6] A. Kyrola, G. Blelloch, and C. Guestrin. *Graphchi: large-scale graph computation on just a pc*. In Proceedings of OSDI, (2012), p. 31-46

[7] J. Yang and J. Leskovec. *Defining and Evaluating Network Communities based on Ground-truth*. In Proceedings of ICDM, (2012).

Applied Mechanics and Materials Vol. 596 (2014) pp 280-285
© (2014) Trans Tech Publications, Switzerland
doi:10.4028/www.scientific.net/AMM.596.280

Evaluation Research on Agricultural Informatization Level in Tropical Areas of China Based on Entropy Method

Lu Ye [a], Yuping Li [b,*], Xiaoli Qin, Yanqun Liu, Weihong Liang and Qidao Song

Institute of Scientific and Technical Information, CATAS/Key Lab of Tropical Crops Information Technology Application Research of Hainan Province, Hainan Danzhou 571737

[a]rkyyelu@163.com, [b]lyp5390@163.com, [*]corresponding author

Keywords: Tropical areas, Agricultural informatization, Evaluate, Entropy method, Hierarchical cluster analysis method.

Abstract. Based on construction and research situation of agricultural informatization in tropical areas of China, through building two-level evaluation index system of agricultural informatization level, agricultural informatization level in tropical areas of China was quantitatively calculated by entropy method, and main provinces in tropical areas of China were classified according to agricultural informatization level by hierarchical cluster analysis method. The results show that influence degree of agricultural informatization index from big to small in turn is information infrastructure, information resources, information talent, and information industry, and agricultural informatization of Eastern coastal in tropical areas of China develops more rapidly than Midwest. At last suggestions to promote agricultural informatization in tropical areas of China are put forward.

Introduction

Development level of informatization has become an important symbol of measuring comprehensive national strength and international competitiveness of a country. In the face of economic globalization, it is an urgent subject to research how to use modern information technology to improve international competitiveness and sustainable development ability of agriculture. Tropical areas of China include Hainan, Guangdong, Guangxi zhuang autonomous region (Referred to as "Guangxi"), Yunnan, Fujian, southern of Hunan and Jiangxi, southern dry river valley of Sichuan and Guizhou, Taiwan, which cover about 5% of total land area of China and are relatively scarce and irreplaceable. As tropical areas of China locate in frontier and have a large amount of mountains and hilly land, development of agricultural informatization is more difficult, and research on agricultural informatization level is necessary. Enping Liu comprehensively expounds development practice and theory system of agricultural informatization in tropical areas of China, analyzes development and constraint of agricultural informatization, and puts forward targeted suggestions [1]. Donghong Cai discusses development trend and problem of agricultural informatization in tropical areas of China, and analyzes the deep reasons by relevant models of information economics [2]. However there is little evaluation research on agricultural informatization level in tropical areas of China. In this paper, based on construction and research situation of agricultural informatization in tropical areas of China, through building two-level evaluation index system of agricultural informatization level, agricultural informatization level in tropical areas of China is calculated by entropy method, and then main provinces in tropical areas of China are classified according to agricultural informatization level by hierarchical cluster analysis method, at last four targeted suggestions are put forward, so as to provide reference for administrative department of agricultural informatization in tropical areas of China.

Evaluation Index System Construction of Agricultural Informatization Level

Index System. The ministry of information industry has formulated the national informatization standard, and brought out "the structural scheme of the national informatization quotient" by a variety of informatization evaluation methods combining with China's specific conditions [3]. Agricultural informatization index is a measure of agricultural informatization level, which doesn't form a unified standard due to multiple factors such as agricultural production, operation, management, and national economic, environment, society, and so on. Based on the national informatization index system and other scholars' research, thirteen indicators are selected from four aspects which are information infrastructure, information resources, information talent, and information industry of agriculture to build evaluation index system of agricultural informatization level following systematic, scientific, operable, applicable principles and combining with development situation of agricultural informatization in tropical areas of China. The evaluation index system is shown in Table 1, used to evaluate agricultural informatization level in tropical areas of China.

Table 1 Evaluation index system of agricultural informatization

One-level index	*Two-level index*
information infrastructure	Ownership of telephone per 100 rural households (unit)
	Ownership of mobile telephone per 100 rural households (unit)
	Ownership of TV set per 100 rural households (set)
	Ownership of computer per 100 rural households (set)
	Delivery routes per capita rural people (km)
information resources	Proportion of Rural broadband subscribers to the total (%)
	Rural areas popularization rate of cable TV programs (%)
	Books, magazines, and newspapers printed sheets per 10000 people(100 million sheets)
information talent	Total enrollment of regular institution of higher education per 10000 people (person)
	Proportion of scientific and technical personnel of agriculture in state-owned and collective-owned enterprises and institutions (%)
	Number of employed persons in transport, postal and telecommunication services per 10000 people (person)
information industry	Consumption expenditure of transport and communications Per capita of rural households (Yuan)
	Proportion of transport, postal and telecommunication services to original value of productive fixed assets per rural households (%)

Data Sources. All index data are from the 2013 China statistical yearbook except proportion of scientific and technical personnel of agriculture in state-owned and collective-owned enterprises and institutions, number of employed persons in transport, postal and telecommunication Services per 10000 people, which are from the 2012 China statistical yearbook. Among these index data, some data are got by simple calculation which are ownership of TV set per 100 rural households, delivery routes per capita rural people, proportion of Rural broadband subscribers to the total, books, magazines, and newspapers printed sheets per 10000 people, total enrollment of regular institution of higher education per 10000 people, proportion of scientific and technical personnel of agriculture in state-owned and collective-owned enterprises and institutions, number of employed persons in transport, postal and telecommunication services per 10000 people, proportion of transport, postal and telecommunication services to original value of productive fixed assets per rural households. The others are taken directly from the statistical yearbook.

Entropy Method. At present, there are some common evaluation methods of agricultural informatization level in our country, which are Delphi method, analytic hierarchy process [4], fuzzy comprehensive evaluation, principal component analysis [5], factor analysis [6], entropy method [7], etc. The weight is relative important degree of each index, which directly impacts the evaluation results. According to the entropy thought, when making a decision, quantity and quality of getting information is one of the determinants of accuracy and reliability.

In entropy method, the weight of each index is determined by information content provided by the index data. For one index, the larger information content, the smaller information entropy, the larger weight, and vice versa. Based on objective data, the evaluation results of entropy method largely avoid deviation from man-made factor, so as to make the evaluation result more realistic.

The steps to evaluate agricultural informatization level in tropical areas of China are as follows [8]:

Assuming that there are m evaluation objects, and each object has n evaluation indexes, the judgment matrix of evaluation index is set up as follows:

$$R = \left(r'_{ij}\right)_{m\times n} (i=1,2,\cdots,m; j=1,2,\cdots,n) \quad (1)$$

Firstly, index data are standardized by maximin method, for the index that a bigger value is better the standardized formula is expressed as

$$r_{ij} = \frac{r_{ij}^{'} - \min\limits_{i}(r_{ij}^{'})}{\max\limits_{i}(r_{ij}^{'}) - \min\limits_{i}(r_{ij}^{'})} \tag{2}$$

For the index that a smaller value is better the standardized formula is expressed as

$$r_{ij} = \frac{\max\limits_{i}(r_{ij}^{'}) - r_{ij}^{'}}{\max\limits_{i}(r_{ij}^{'}) - \min\limits_{i}(r_{ij}^{'})} \tag{3}$$

Then, the entropy value of evaluation index is calculated by the formula

$$H_j = -\frac{1}{\ln m}\sum_{i=1}^{m} f_{ij} \cdot \ln f_{ij} \tag{4}$$

Where $f_{ij} = r_{ij} \Big/ \sum_{j=1}^{n} r_{ij}$, when $f_{ij} = 0$, $f_{ij} \cdot \ln f_{ij} = 0$.

The entropy weight of the first index is calculated by the formula

$$\omega_j = \frac{1 - H_j}{n - \sum\limits_{j=1}^{n} H_j} \tag{5}$$

Lastly, comprehensive evaluation result of agricultural informatization level is calculated by the formula

$$L_{2i}(\omega_j, j) = \left[\sum_{j=1}^{n} \omega_j^{2} \cdot r_{ij}^{2}\right]^{\frac{1}{2}} \tag{6}$$

Evaluation of Agricultural Informatization Level

Development Situation of Agricultural Informatization in Tropical Areas of China. Although agricultural informatization in tropical areas of China starts late, speed of development is quick. Construction of information infrastructure in each province moves steadily, a large number of agricultural websites, databases, and literature resources are developed and constructed in succession, all kinds of information technology such as Internet, Remote Sensing, Geographical information System, Global Positioning System, e-commerce are applied to agricultural production, circulation rapidly. Rural telephone, television and telecommunications users, scientific and technical personnel of agriculture, rural consumption of communication and other indexes are significantly improved, but the average level is still lower than the national average. There is also difference among provinces and a big gap between province of higher economical level and province of lower economical level. The level of some province is higher than the national average in some index. General development of agricultural informatization level is unbalanced, needing continue to push forward.

Evaluation Results. With entropy method, weight of every level index is calculated by (1) to (5) as shown in Table 2.

Table 2 Entropy weight of every evaluation index

One-level index	***Entropy weight***	***Two-level index***	***Entropy weight***
information infrastructure	0.3866	Ownership of telephone per 100 rural households	0.0902
		Ownership of mobile telephone per 100 rural households	0.0708
		Ownership of TV set per 100 rural households	0.0736
		Ownership of computer per 100 rural households	0.1137
		Delivery routes per capita rural people	0.0383
information resources	0.2711	Proportion of Rural broadband subscribers to the total	0.0673
		Rural areas popularization rate of cable TV programs	0.0871
		Books, magazines, and newspapers printed sheets per 10000 people	0.1167
information talent	0.2097	Total enrollment of regular institution of higher education per 10000 people	0.0725
		Proportion of scientific and technical personnel of agriculture in state-owned and collective-owned enterprises and institutions	0.0538
		Number of employed persons in transport, postal and telecommunication Services per 10000 people	0.0834
information industry	0.1326	Consumption expenditure of transport and communications Per capita of rural households	0.0878
		Proportion of transport, postal and telecommunication services to original value of productive fixed assets per rural households	0.0448

Then, information infrastructure, information resources, information talent and information industry of agricultural informatization in tropical areas of China are evaluated by (6), and the comprehensive evaluation results are shown in Table 3.

Table 3 Evaluation results of agricultural informatization

area	***information infrastructure***		***information resources***		***information talent***		***information industry***		***Comprehensive level***	
	L_{21}	***rank***	L_{22}	***rank***	L_{23}	***rank***	L_{24}	***rank***	L_{2i}	***rank***
China	0.0955	3	0.0780	4	0.0927	2	0.0618	3	0.1662	3
Guangdong	0.1603	2	0.1430	1	0.0920	3	0.0854	2	0.2488	2
Guangxi	0.0651	5	0.0268	7	0.0484	9	0.0266	8	0.0895	8
Hainan	0.0547	7	0.0456	6	0.0879	4	0.0133	10	0.1139	5
Fujian	0.1769	1	0.1148	2	0.1089	1	0.0955	1	0.2559	1
Yunnan	0.0492	8	0.0153	10	0.0589	7	0.0434	5	0.0895	9
Guizhou	0.0055	10	0.0157	9	0.0407	10	0.0417	6	0.0606	10
Sichuan	0.0467	9	0.0522	5	0.0536	8	0.0222	9	0.0910	7
Hunan	0.0627	6	0.0265	8	0.0722	6	0.0503	4	0.1113	6
Jiangxi	0.0680	4	0.0915	3	0.0752	5	0.0394	7	0.1421	4

Lastly, According to the evaluation results of agricultural informatization level, the tropical areas of China are divided into three categories: areas whose agricultural informatization is developed relatively, areas whose agricultural informatization is middle-developed, and areas whose agricultural informatization is backward relatively. Development situation of agricultural informatization in tropical areas is clustering analyzed by the hierarchical cluster analysis method, and the clustering results are shown in Table 4.

Table 4 Clustering results of agricultural informatization

category	***Area***
Areas whose agricultural informatization is developed relatively	Fujian, Guangdong
Areas whose agricultural informatization is middle-developed	Hainan, Jiangxi, Hunan, Sichuan, Guangxi, Yunnan
Areas whose agricultural informatization is backward relatively	Guizhou

Analysis. The evaluation results show that Fujian and Guangdong province are relatively developed areas of agricultural informatization, for their comprehensive level of agricultural informatization ranks above the national average level. There are Jiangxi, Hainan, Hunan, Sichuan, Guangxi and Yunnan whose comprehensive level of agricultural informatization rank below the national average level, belonging to middle-developed areas of agricultural informatization. Guizhou province is the end of tropical areas in comprehensive level of agricultural informatization, belonging to relatively backward areas of agricultural informatization.

From the sub-index, the entropy weight of information infrastructure, information resources, information talent, information industry are 0.3866, 0.2711, 0.2097, and 0.1326. The weight indicates that information infrastructure and information resources are the main factors affecting agricultural informatization level, which provide more effective information for development of agricultural informatization. Opposite, the information talent and information industry affect weaker. In terms of information infrastructure, Fujian, Guangdong and Jiangxi are the top three, Guizhou is the last.

Fujian and Guangdong are both higher than the national average level, and the other provinces are below the national average. Fujian and the national average respectively are 31 and 17 times as high as Guizhou in the level of information infrastructure. These reflect a greater gap among the level of agricultural information infrastructure in tropical areas of China, as well as backward situation of agricultural information infrastructure in Guizhou. In terms of information resources, Guangdong, Fujian and Jiangxi are in the former three, Yunnan is located in the last. The former three are all higher than the national average, and the other provinces are below the national average. Guangdong and the national average respectively are 9 and 5 times as high as Yunnan, which shows backward construction status of agricultural information resources in Yunnan. In terms of information talent, Fujian, Guangdong and Hainan are the top three, Guizhou is the last. Fujian is above the national average, and the other provinces are below the national average with less range, which means general lack of agricultural information talent in tropical areas of China. In terms of information industry, Fujian, Guangdong and Hunan are in the former three, Hainan is the last. Fujian and Guangdong is higher than the national average, and the other provinces are below the national average. Fujian and the national average respectively are 7 and 4 times as high as Hainan, which means that development of agricultural information industry in tropical areas of China is unbalanced, and the development of information industry in Hainan is relatively backward.

Conclusions and Suggestions

Conclusions. The results show that agricultural informatization level in tropical areas of China is objectively evaluated by the entropy method. Based on entropy weight, influence degree of four indexes to agricultural informatization level from big to small in turn is information infrastructure, information resources, information talent, and information industry. The development level of agricultural informatization is rather unbalanced in tropical areas of China, agricultural informatization develops more rapidly in eastern coastal than Midwest, and there is a big gap between tropical areas and the national average in some index, needing to strengthen construction. Therefore, determining how to concentrate on giving full play to major influence factors and give overall consideration to properly handle general influence factors balance is the key to promote balanced development and steady rising of agricultural informatization in tropical areas of China.

In summary,

Suggestions. (1) The infrastructure construction of agricultural informatization should be promoted sustainable. The construction of rural information network infrastructure such as fiber-optic broadband and 3G network should be accelerate to improve coverage of rural radio and television networks, mobile communications networks, internet. The construction of rural hardware infrastructure should be perfect through policies on rural appliances and broadband, so as to improve popularizing rate of rural household TV, fixed telephone, mobile phone, computer [9].

(2) The efforts to develop information resources should be intensified. Based on the actual need of rural areas, agriculture and farmers, covering agricultural policy information, production information, technological information and market information, the development of agricultural information databases and integrated information platform should be accelerated to provide information inquiry and expert services for farmers. In order to keep the agricultural information dissemination channels open, we should pay attention to strengthen the construction of rural postal outlets, villages and towns cultural sites, rural public libraries, rural radio and television programs.

(3) The high-quality agricultural information talent should be cultivated. Rural pre-school, high school education and secondary vocational education in tropical areas should be vigorously developed to improve the educational level of rural labor, enrollment rates of school-age children, and enrollment rates of ordinary college. In order to improve practitioners' capabilities of agricultural management and technology services, we should emphasis on agricultural skills training for rural grassroots cadres, agricultural technicians and farmers by the way of science advocacy, intensive

classes, and distance education and so on, as well as introduce high level of agricultural informatization talents to expand agricultural informatization services team.

(4) The development of information industry in rural areas should be promoted. To improve the conversion rate of agricultural scientific and technological achievements, we should expand the coverage of agricultural information, and reduce the cost of farmer access to information, and increase capital investment and policy support. It is necessary to perfect agricultural information industry service system by formulating agricultural information statistical standards, improving scheme for examination and assessment of agricultural informatization, and promoting agricultural information industry related departments to work together, so as to further improve the level of agricultural informatization in tropical areas of China.

Acknowledgements

This work was financially supported by the Project of Technology Extension and Training of Tropical Crops of Ministry of Agriculture (14RZNJ-14).

References

[1] E.P. Liu: Research on development of agricultural informatization in tropical areas of China (China agricultural science and technology press, Beijing 2013).

[2] D.H. Cai and Y.C Li: Science and technology progress and countermeasures. Vol. 23 (2006), p. 63.

[3] S.H. Liu: Study on evaluation/measurement theory and method for China's rural informatization (Chinese academy of agricultural sciences, Beijing 2008).

[4] G.H. Pi: Present situation analysis and development countermeasure research of agriculture and rural Informatization in Datonghu Area (Hunan agricultural university, Changsha 2012).

[5] H. Wang: Evaluation and development countermeasures research on rural informatization in Liangshan State (Sichuan agricultural university, Chengdu 2012).

[6] J. Zhang: The establishment and evaluation index system to rural informatization of Shunyi District (Chinese academy of agricultural sciences, Beijing 2011).

[7] Y. Wang and W.L. Wang: Technology economics. Vol. 32 (2013), p. 85.

[8] Q. Fu: Data processing method and its agricultural application (Science press, Beijing 2006).

[9] C. Yang: Hubei agricultural sciences. Vol. 50 (2011), p. 4273.

Applied Mechanics and Materials Vol. 596 (2014) pp 286-291
© (2014) Trans Tech Publications, Switzerland
doi:10.4028/www.scientific.net/AMM.596.286

The generalized fuzzy time series model for forecasting base on the optimization of the length of intervals

Yanhong Wang [a],Wangren Qiu [b]
School of Computer Engineering,Jingdezhen Ceramic Institute
Jingdezheng,China
[a]jdzwyh2008@126.com,[b]qiuone@163.com

Keywords: Fuzzy time series;Forecasting model;Partition of interval

Abstract: Based on the analysis of some conventional fuzzy time series model,this paper proposes a new method by using a single constrained optimization to determine the interval length for improving the forecasts.The conventional fuzzy time series models are enhanced by forecast-weighted method in the forecasting.In the proposed model,which is evaluated by mean square error(MSE),fuzzy membership degrees are used to calculate forecast weights. The empirical results show that the proposed model outperforms than the conventional models.

Introduction

Through analysis of fuzzy time series,we can not only find change law for the existing data,but also predict and control the future behavior and characteristics trend through its change law. Since the fuzzy time series model proposed by Song and Chissom [1] (1993), The models would be widely used in related fields of economy,society and life,such as enrollment prediction, stock index prediction and forecasting temperature.Some important information of fuzzy membership degree is considered in the traditional fuzzy time series.But some unimportant fuzzy membership information is ignored. so the way will inevitably lose some information and influence prediction effect. In order to improve forecast effect and precision,in the paper the fuzzy time series model is improved by forecast-weighted methods.More information of fuzzy membership degree is considered in prediction model.

On the other hand, Number and size of fuzzy interval was fixed in the traditional model.It was proved that the fuzzy interval length would impact prediction precision [6].In the paper we propose a novel method ,which find an affective lenth of interval,which minimizes mean square error(MSE) by using a single variable constrained optimization.In order to determine optimum interval length of the best forecasting accuracy ,we use "Fminbnd" function of MATLAB and the algorithm based on golden section search and parabolic interpolation.In the end, the optimization weighted method can effectively improve the prediction effect through the experiment of enrollment of Alabama university from 1971 to 1992 and the Shanghai stock exchange composite index (SSECI).

Fuzzy time series

The definition and concept of fuzzy time series was introduced by[1,2,3].The definition and steps of fuzzy time series model are expressed as follows:

Definition 1.A fuzzy set A of the universe of discourse U , $U = \{u_1, u_2, \cdots\cdots, u_n\}$,defined as follows:

$$A = \frac{f_A(u_1)}{u_1} + \frac{f_A(u_2)}{u_2} + \cdots + \frac{f_A(u_n)}{u_n}, \qquad (1)$$

Where f_A is the membership function of the fuzzy set A, $f_A : U \to [0,1]$,and $f_A(u_i)$ indicates the grade of memership of u_i in A,where $f_A(u_i) \in [0,1]$ and $1 \le i \le n$.

The frequently-used membership function is described as follows :

$$u_{A_i}(t)=\begin{cases}1, & i=1, and, \mathrm{x}_t \le m_1,\\ 1, & i=n, and, \mathrm{x}_t \le m_n,\\ \max\left\{0, 1-\dfrac{|x_i-m_i|}{2\times l_{in}}\right\}, & \text{the other},\end{cases} \qquad (2)$$

Where l_{in}:length of subinterval, t:moment, m_i:center value of u_i $(i=1,2,\cdots,n)$.

Definition 2. Let $Y(t)(t=\cdots,0,1,2,\cdots)$,a subset of R,be the universe of discourse on which fuzzy $f_j(t)(j=1,2,\cdots)$ are defined and let $F(t)$ be a collection of $f_j(t)(j=1,2,\cdots)$.Then, $F(t)$ is called a fuzzy time series on $Y(t)(t=\cdots,0,1,2,\cdots)$,and $F(t)=\{f_1(t),f_2(t),\cdots\}$.

Definition 3. Fuzzy timr series relationships assume that $F(t)$ is caused only by $F(t-1)$,then the relationship can be expressed as: $F(t)=F(t-1)*R(t,t-1)$. $R(t,t-1)$ is the fuzzy relationship between $F(t-1)$ and $F(t)$,where"*"represents an operator, $F(t)$ and $F(t-1)$ as fuzzy sets，R is befined the first-order fuzzy relation about $F(t)$.

Definition 4. Suppose that $F(t-1)=A_i$ and $F(t)=A_j$,the relationship between $F(t)$ and $F(t-1)$ (called a fuzzy logical relation in [3])is denoted by $A_i \to A_j$. A_i is the left-hand side of fuzzy logical relationship. A_j is the right-hand side of fuzzy logical relationship.If t=1,2,…,N,then there are N-1 fuzzy relationships : $F(i) \to F(i+1)$ （i=1,2,…,N-1）.The relationships are denoted by fuzzy set.They are $A_i^t \to A_j^{t+1}(t=1,2,\ldots,N-1)$,where A_i^t :fuzzy concept at t moment, A_j^{t+1} :fuzzy concept at t+1 moment.

According to the above definition,the structure and application of fuzzy time series forecasting model are summarized as follows:

Step 1:Dividing the universe of discourse according to the training set and the fuzzy membership function;

Step 2:To establish the fuzzy relation set according to observations of the order of the training data;

Step 3:To obtain the fuzzy relation matrix through all fuzzy relation in step 2;

Step 4:Getting the membership values of the fuzzy set according to the observed value.Then according the fuzzy relation matrix in step 3 and the given prediction rules ,we get predictive value.

As regards the fuzzy relation matrix in step 3,there are different methods.Representative methods are proposed by Sone,Chen and Lee.we use the method proposed Lee in the paper. The elements in the fuzzy relation matrix are appearing times of fuzzy relations($A_i \to A_j$) in training set.

In order to obtain prediction rules by means of the fuzzy relation matrix,we calculate the weighted average of the median using the fuzzy set according to the elements in the relation matrix. Predict rules and methods are expressed as following formula:

$$\mathrm{Fval}(\mathrm{t}+1)=\begin{cases}\mathrm{m}_{\mathrm{c}_\mathrm{t}}, & \sum_{\mathrm{j}=1}^{\mathrm{n}}\mathrm{R}(\mathrm{c}_\mathrm{t},\mathrm{j})=0,\\ \dfrac{\mathrm{R}(\mathrm{c}_\mathrm{t},:)}{\sum_{\mathrm{j}=1}^{\mathrm{n}}\mathrm{R}(\mathrm{c}_\mathrm{t},\mathrm{j})}\times(\mathrm{m}_1,\mathrm{m}_2,\mathrm{L},\mathrm{m}_\mathrm{n})^{\mathrm{T}}, & \text{the other},\end{cases} \qquad (3)$$

Where $Fval(t+1)$ is the final forecast value. m_{c_t} is the center value of the corresponding fuzzy interval for the maximum membership degree of observation. $R(c_t,:)$ is the corresponding row vector about the fuzzy relation matrix of the corresponding fuzzy set about observation's maximum membership degree. $(m_1,m_2,\cdots,m_n)^T$ is transpose of $(m_1,m_2,\cdots,m_n)$. m_i is the center value of u_i $(i=1,2,\cdots,n)$,"×"is multiplication of vector.

Weighted and generalized fuzzy time series

In the traditional fuzzy time series model,After establishing fuzzy relation matrix,the membership degree of each fuzzy set using the observation sample will not be used.In other words,observation samples most likely belongs to which fuzzy sets in the process of prediction(the location of the maximum membership degree in the vector).The other membership degree would not be taken into account.so Some useful information is bound to be lost. Weighted model will improve the traditional method. In the framework of traditional models,the step of weighted and generalized time series model is described as:

Step 1: Dividing into discussion domain according to the training set and the fuzzy membership function.This step is the same as the traditional model.The fuzzy membership function is expressed in the formula(2) in the paper.

Step 2: To establish the fuzzy relation set according to orderly observations of the training data.Membership degree is calculated of each corresponding fuzzy set about the sample data.The corresponding fuzzy concept about the membership degree is determined.Then according to the definition (3) and (4),Fuzzy logic relationship is solved between two adjacent data.

Step 3:To get the relatinship matrix by all the fuzzy relations.

Step 4:To solve the membership degree value of a corresponding fuzzy set throuth the observation value. The membership degree of each fuzzy set through the observation sample is solved by using the formula (2).Then the next moment vector of fuzzy membership degree value is predicted by a row of the relationship matrix in the present moment.

Step 5:To determine the membership number that is considered in the membership vector.The standardization vector is the weight of prediction.This step is the core of this method. A new function is introduced to standardized membership vector as follows:

$$u_{A_i}^{l}(t)=\begin{cases} u_{A_i}(t), & u_{A_i}(t)\ {}^{3}\ u^{l}(t) \\ 0, & \text{the other,} \end{cases} \qquad (4)$$

Where $u^{l}(t)$ is the l th larger value in the membership degree vector $(u_{A_1}(t),u_{A_2}(t),\cdots,u_{A_n}(t))$, $(u_{A_1}(t),u_{A_2}(t),\cdots,u_{A_n}(t))=(0.1,0.5.0.8,0.2,0,0)$, then $u^{3}(t)=0.2$,the third big value is 0.2 in the above vector.we not only use location information of the maximum membership degree by calculating observation value but also use information for the other membership degree in the model.So the model has higher information utilization in regard to observation sample.

Through the formula(4),membership degree vector has changed and it contains more information than the primary vector.In order to get standardization result,it is normalized.The weight value is prepared for forecast.In the paper the formula is as follows:

$$(\overset{-l}{u}_1(t),\overset{-l}{u}_2(t),\cdots\overset{-l}{u}_n(t))=\frac{((u_{A_1}^{l}(t))^{\alpha},(u_{A_2}^{l}(t))^{\alpha},\cdots,(u_{A_n}^{l}(t))^{\alpha})}{\sum_{i=1}^{n}(u_{A_i}^{l}(t))^{\alpha}}, \qquad (5)$$

Where α is fuzzy coefficient, $\alpha\in(0,+\infty)$.

Step 6: The prediction model is established.The prediction formula of traditional model is modified.The weight vector in step 5 is taked part in the improved formula. we use methods of the fuzzy set center value weighting.So fuzzy prediction rule is not used. The prediction formula is used as follows:

$$Fval(t+1)=((\overset{-l}{u}_1(t),\overset{-l}{u}_2(t),\cdots\overset{-l}{u}_n(t))\times\bar{R}\times(m_1,m_2,\cdots,m_n)^{T} \qquad (6)$$

Where $Fval(t+1)$ is final forecast value, $\bar{R}$ is a new relationship matrix after every line of original relationship matrix is normalized ($\bar{R}(i,j)=\frac{R(i,j)}{\sum_{i=1}^{n}R(i,j)}$). R is relationship matrix that is geted in step 3. $(m_1,m_2,\cdots,m_n)^T$ is transposition of $(m_1,m_2,\cdots,m_n)$; m_i is center value of fuzzy interval (u_i of the i th fuzzy set) $(i=1,2,\cdots,n)$,"×"is multiplication of vector.

Through the above six steps,we improve the traditional model. We get a weight generalized fuzzy time series model.If the method is applied to model of Song[7,8],Chen[12] or Lee[5].Their models will be improve for weighting model.So the method essentially is a weighting model method.

the optimization interval length based on MSE

Through the literature [6], effective interval length can improve the effect of prediction in the method of fuzzy time series.To do this,we optimize fuzzy interval length by optimization algorithm on the basis of the weight generalized fuzzy time series model.The proper interval length is obtained and the prediction accuracy is increased.In this paper,we used a MATLAB function called "fminbnd"which minimizes MSE. The function is employing an algorithm based on golden section search and parabolic interpolation and determine the optimal interval length. "fminbnd"is used to find minimum of single-variable function on fixed interval.It finds a minimum for a problem specified by

$$\min_{x} f(x)\text{ , such that } x_1 \le x \le x_2$$

Where x_1,x,x_2 is scalar. $f(x)$ is a function which returns a scalar.In MATLAB, $x=f\min bnd(f(x),x_1,x_2)$, $\bar{x}$ is a minimum logical scalar in the interval($x_1 \le x \le x_2$) about the function($f(x)$).such as $a=f\min bnd(f(x),x_1,x_2)$, $f(a)$ is minimum logical value in (x_1,x_2) .So fuzzy interval length is divided by the minimum logical value in the interval.MSE of observations is the smallest.

In [7],Kiefer calculate the minimum MSE by using The algorithm of golden search and parabolic interpolation.When x_1 and x_2 are very close, MSE is the endpoint ($f(x)$) . Under normal circumstances,the minimum value is not the endpoint as regards $f(x)$ and $x_1 \le x \le x_2$ .If the minimum value really fall on x_1 or x_2 ,fminbnd returns a value which is not more than $2*TolX$. $TolX$ is error limits in Matlab internal regulations,Detailed algorithm is described in [8] and [9].

In order to compare ,In the paper enrollment datas for the University of Alabama were analyzed by using the methods of [1,3,4,10,11,12].Then algorithm of single variable constraint is used for optimization minimum MSE. The optimal interval length is determined betwwen x_1 and x_2 by "fminbnd".we analyze enrollment datas for the University of Alabama by the proposed model for the article. In order to improve the prediction precision and the minimum mean square error through the optimal interval length,The "fminbnd" function which is used as follows:

$$\bar{x}=f\min bnd(f_{MSE}(x),x_1,x_2)$$

Where $f_{MSE}(x)$ is mean square error between predicted results and real results when interval length is x .Left endpoint is x_1 and right endpoint is x_2 . x is minimal solution for $f_{MSE}(x)$ function in [x_1 , x_2].

Experimental data and evaluation criteria of the model

Enrollments at the University of Alabama form 1971 to 1992 is the first datas for fuzzy time series model [1,2,3].Later,in the study of fuzzy time series model ,the datas were used as test set of model.

13055 is minimum data and 19337 is maximum data.So universe of discourse is defined as [13000,20000].

Shanghai stock exchange composite index (SSECI) is a typical time series data.It has a large amount of data and representative.So stock data are often applied to the study of fuzzy time series model.It is used as another test set in the paper. Datas from January 1,1997 to December 31,2006 are divided into ten data sets according to year.The upper and lower bounds for interval of discussion is determinedand and universe of discourse of the model is calculated according each year data.

MSE is a common standard of appraisal for the fuzzy time series model. Because standard are adopted by most of models which experimental results are compared to this paper, we also used it.In addition, To Sort and comparie prediction accuracy of enrollment for different models,advantage of the proposed model is proved accurately.

Results and conclusions of experiment

Table 1 Interval length of optimized model (l = 1, 2, 3)

	l=1	*l*=2	*l*=3
Enrollment data	385.91	385.90	385.90
SSECI data	39.74	54.35	68.37

Table 1 shows optimization interval length for enrollments and SSECT when considered factor numbers is 1,2,3.where $x_1 = 200$, $x_2 = 1000$ in process of optimization for enrollment data ,and $x_1 = 30$, $x_2 = 90$ about SSECI;From the table we find interval length is difference when consider factor numbers is difference.

Table 2 Error compare of enrolment data for each model

model	[1]	[3]	[4]	[10]	[11]	[12]	The paper
orders	1	1	1	1	1	2	1
MSE	412499	775687	407507	85264	78792	78073	67260
ranking	6	7	5	4	3	2	1

Table 2 lists the predictive results of enrollment for six reference models and the paper model.We can find prediction error of the first three models is higher than the last four models through table 2 .Prediction error for [3] is the highest.Error for [1] and [4] is nearly equal. Error for [10] and [11] is nearly equal too.But they almost are an order of magnitude lower than [3]. Pediction results of the porposed model is the best than all the other models. To compare with the last three models, it also has obvious advantages.

Table 3 Prediction errors comparison before and after interval optimization for SSECI

l value	*l*=1		*l*=2		*l*=3	
interval optimization	before	after	before	after	before	after
MSE	866.6	687.5	794.0	567.5	787.7	612.1

Table 3 lists results comparison before and after fuzzy interval optimization of weighted generalized model for SSECT.From the table,we can see that prediction errors of three optimization algorithms obvious reduce.So model prediction accuracy of the paper has improved.

In this article, through analysis of the traditional fuzzy time series model, we pointed out that information was missing and prediction effect was low in the traditional model. In order to improve prediction accuracy, weighted generalized fuzzy time series model was proposed in the paper. Fuzzy set center values are weighted.The membership degree vector is standardized as prediction weight and forecasting formual is given.In addition,on the basis of weighted generalized fuzzy time series model, fuzzy interval length was optimized by using single variable constraint optimization algorithm .we get the best interval length in order to minimize MSE.So as to prediction accuracy of the model further improved.In the end,the proposed method is validated through enrollments of Alabama university and SSECI and is compared with other methods.From the experiment results, Weighted generalized model has obvious superiority through comparing it and traditional model.The weighted generalized model based on optimization method can effectively improve the prediction effect.It provided a reference for optimization method application in fuzzy time series model.

Reference

[1]Q.Song and B.S.Chissom.Fuzzy Set and Systems 54(1993),P.269-277.

[2] Q. Song and B.S.Chissom.Fuzzy Set and Systems 54(1993),P.1-10.

[3] Q. Song and B.S.Chissom.Fuzzy Set and Systems 62(1994),P.1-8.

[4]Chen S M.Fuzzy Set and Systems ,1996,81(3),P.311-319.

[5] Lee M H,Efendi R,Ismail z.Matematika,2009,25(1),P.67-78.

[6] K.Huarng.Fuzzy Set and Systems 123(2001),p.387-394.

[7] J.Kiefer.Proceeding of the American Mathematical Society 4(1953),P.502-506.

[8]R.P.Brent. Prentice-Hall, EngleW-ood Cliffs,New Jersey,1973.

[9]G.E.Forsythe,M.A.Malcolm and C.B.Moler.Prentice Hall,New Jersey,1976.

[10] Chen S.M. (2002). Cybernetics and Systems, 33, P.1-16.

[11] Huarng K.H. (2001). Fuzzy Sets and Systems, 123(3), P.387-394.

[12] Aladag C.H.,Basaran M.A.,Egrioglu E.,Yolcu U,Uslu V.R. (2009).Expert Systems with Applications, 36, P.4228-4231.

Applied Mechanics and Materials Vol. 596 (2014) pp 292-296
© (2014) Trans Tech Publications, Switzerland
doi:10.4028/www.scientific.net/AMM.596.292

Web page ranking algorithm based on the meta-information

Xinli Li

Linyi University China

sduman@126.com

Keywords: Page rank, page hits frequency, page update time, search engine, page category

Abstract. PageRank algorithms only consider hyperlink information, without other page information such as page hits frequency, page update time and web page category. Therefore, the algorithms rank a lot of advertising pages and old pages pretty high and can't meet the users' needs. This paper further studies the page meta-information such as category, page hits frequency and page update time. The Web page with high hits frequency and with smaller age should get a high rank, while the above two factors are more or less dependent on page category. Experimental results show that the algorithm has good results.

Introduction

Various ranking strategies based on link-analysis have been developed recently for improving Web search engine query results. The HITS algorithm relies on query-time processing to deduce the hubs and authorities that exist in a sub graph of the Web consisting of both the results to a query and the local neighborhood of these results. The PageRank algorithm provides a factor named importance to estimates for all of the pages on the Web. These algorithms only consider hyperlink information, without other page information such as page hits frequency, page update time and web page category. Therefore, these ranking strategies do not care about user needs, and always rank the pop pages on the top. This paper further studies the page ranking, analyzes the page nature such as category, page hits frequency and page update time, presents a more comprehensive page ranking algorithm.

Factors that affect the quality of web page

The most common Web page ranking algorithm is PageRank. PageRank algorithm reflects the number of pages to be linked; that the importance of a page depends on evaluation of other web pages (or sites).Therefore PageRank algorithm cannot meet the individual for specific requirements.

Page ranking should consider comprehensive information obtained by web data mining, including content information, structural information and application information. Web content information mainly refers to pages category and pages relevance. Page structure refers to the network topology information, i.e., the page link information. Traditional PageRank only consider the above two kinds of factors, does not consider the page meta-information such as Web pages update time and page hit frequency. This ranks a lot of advertising pages and old pages pretty high, and affects the user's needs. Therefore, we should also consider page update time and user behavior.

2.1 Web Page Update Time

Web page update time is the time the page was last updated. Define page age $= \quad -$, where t_0 is the current time, t is the time to update the page (which can be obtained by page meta-information document.lastModified). We believe that the page with smaller page age should be ranked top. The page with larger page age indicates that the page has not been updated for a long time, should be ranked bottom. To introduce the factor page age in page ranking algorithm will filter out pages which do not be updated for long time.

2.2 Web Page Hit Frequency

User behavior is very complex; one of the most effective is the hit-stream data. Here hit-stream data is used to identify the user behavior. Define page hit frequency $hf = h\ t \quad T$,where hits is the number of times the page is hit, T is the page age. The web pages with high hit frequency are considered high quality which is due to users' preference, while page with low hit frequency are considered with low quality. To introduce the factor page hit frequency will filter out popular pages.

2.3 Page category

Consider only page update time and page hit frequency is not enough. Different page categories have different requirements for page update time, for instance, the page categories of news or business have high requirements for update time, while the page categories of computer literacy or academic have slightly lower requirements for update time. Similarly, page hit frequency is relevant to page categories, for instance, the pages of computer knowledge have lower hit frequency than news pages. Therefore, we should taking into account the effects of page categories when considering page update time and page hit frequency.

Page Ranking Algorithm based on Meta-information

According to the impact of page content on page update time and page hit frequency; the pages can be divided into many categories. For instance, web pages can be classified according to Yahoo Classification (Yahoo divided web pages into 14 top categories, namely: 1 Arts and Humanities, 2 Business and Economy, 3 Computers and the Internet, 4 Education, 5 Entertainment, 6 Government and Politics, 7 health and medicine, 8 News and Media, 9Leisure and Sport, 10 References, 11 Region, 12 Science, 13 Social Sciences, 14 Society and Culture), the specific classification techniques can be used SVM.

For each page, calculate^{-} $= -\sum$, where T is page age. Define page update time function

$$= \frac{+}{+\frac{}{-}} \qquad (1)$$

where ct_i value is in the range of (0, 1) and indicates the dependence of page quality on update time. For the pages of category that require more for update time, ct_i is assigned greater value, and for the pages of category that require less for update time, ct_i is assigned a small value. So we can calculate the TP as a page quality factor Q, which is used to indicate the impact of update time on page quality. For the page of category "academic", we believe the page quality rely less on page update time, so ct_i is assigned smaller value, here take $ct_1 = 0.2$. For the page of "news" category, due to its page quality of updates time-dependent more, take ct_i a larger value, here take $ct_2 = 0.5$. Similarly for pages of "commercial" category, take $ct_3 = 0.4$, and "computers" category $ct_4 = 0.3$.

For each web page, calculate page hits frequency $hf = h\ t \quad T$,then calculate $\overline{p\ f} = \frac{1}{\ } \sum p\ f$ .Define the page hits frequency function

$$= \frac{+ \frac{*\ \ h}{\overline{}\, h}}{+} \tag{2}$$

where cc_i value is in the range of (0, 1) and indicates the dependence of page quality on page hits frequency. For the pages of category that page quality is more dependent on page hits frequency, cc_i is assigned greater value, and for the pages of category that page quality depends less for update time, cc_i is assigned a small value. For the page of "News" category, we believe the page quality rely more on page hits frequency, so cc_i is assigned larger value, here take cc_2=0.7,while for pages of "computer" category pages, due to its technical nature, we believe the factor of page hits frequency is not important, and therefore take cc_i a smaller value, here $cc_4 = 0.2$. By the same token, take $cc_1 = 0.3$ and $cc_3 = 0.5$.

There are factors that influence page ranking: the correlation of query and document (Sim) and page quality (Q). The contribution of the page quality is from hyperlink information, page category, page update time and page hits frequency.

Web page scoring formula: Score = Q * Sim, where Q = PageRank * TP * CP

Where Sim is the correlation of query and document, TP is a function of page update time; CP is a function of page hits frequency.

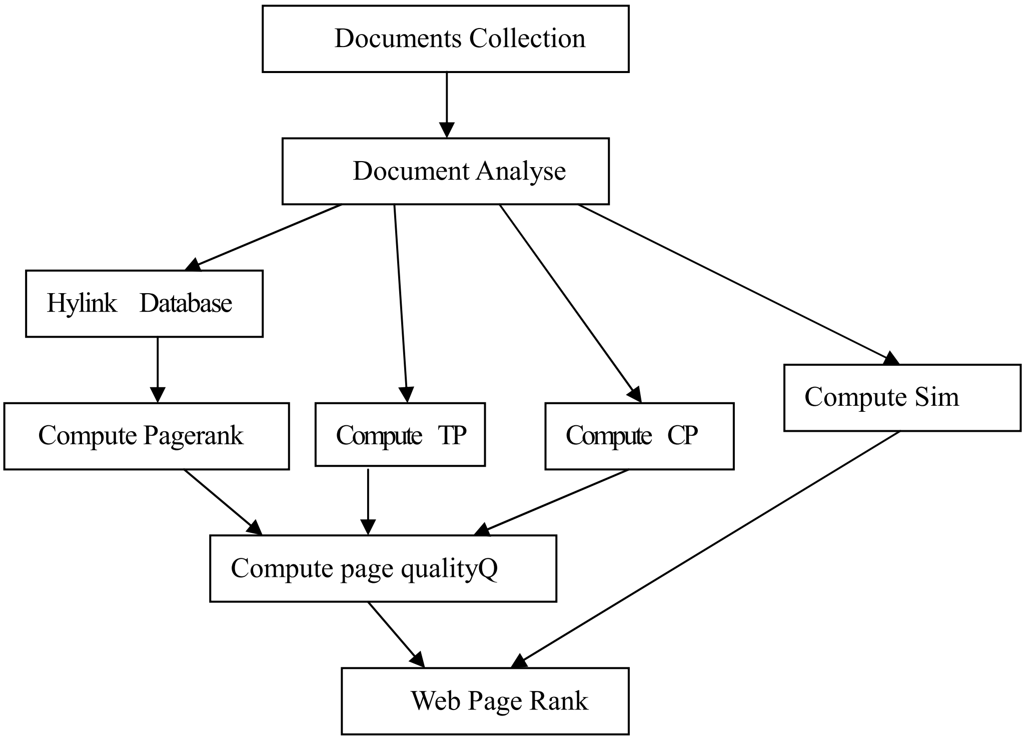

Fig.1 The calculation procedure of web page quality

For each page, calculate the value of Score, and then rank the web pages based on the value of Score. The calculation procedure is as Fig.1:

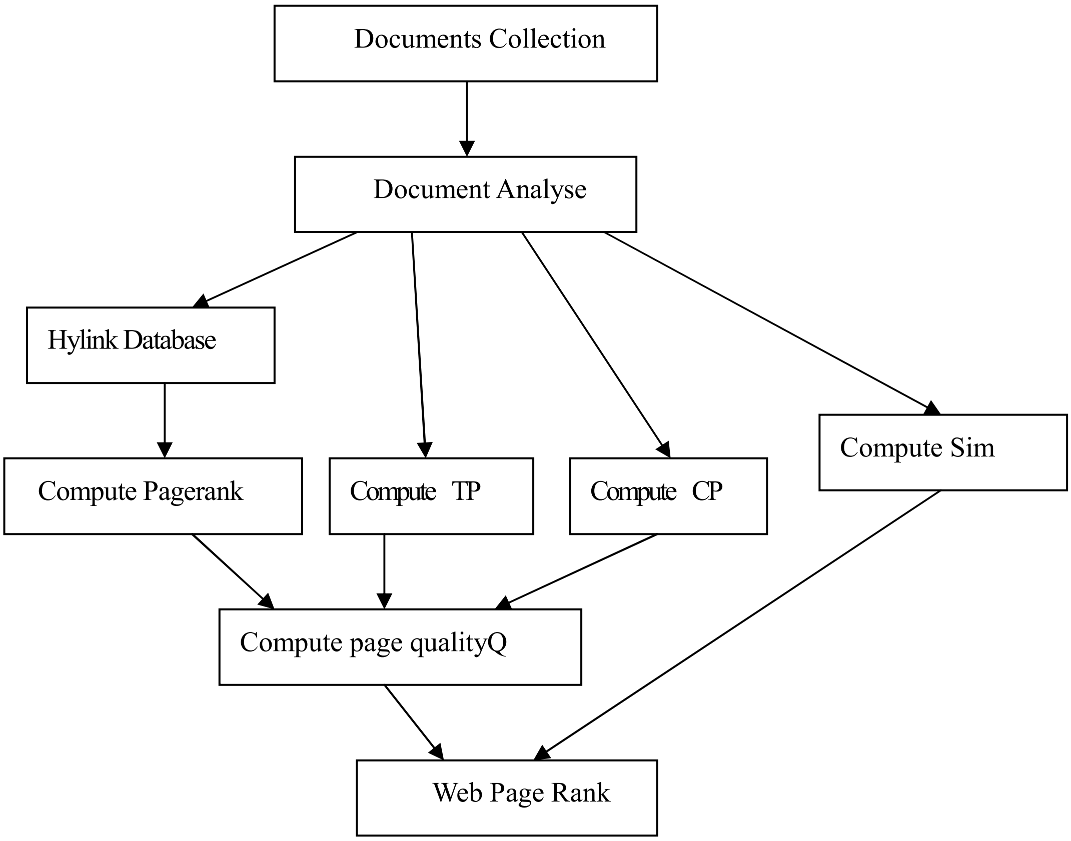
Documents Collection
Document Analyse
Hylink Database
Compute Pagerank
Compute TP
Compute CP
Compute Sim
Compute page qualityQ
Web Page Rank

Fig.1 The calculation procedure of web page quality

Experimental Evaluations

Different pages ranking algorithms will produce different search results. Here we compare our algorithm and PageRank algorithm.

In Google search engine, we take "page rank" as the query items, Google returned 4,040,000 page results. We take the top 10 search results as the experimental data.

In the top 10 results, page3 and page5 have not been updated for a long time; page2 and page6 are ad pages. Since Google only consider the web hyperlink information and the correlation of query and document, it cannot filter out these pages cannot meet the needs of users.

Because these pages are selected top 10 in 10 4,040,000 results, therefore Q_1, Q_2, Q_{10} has little difference. Here we assume that $Q_1 \approx Q_2 \approx \ldots \approx Q_{10}$.

We recalculate the Score of this 10 pages with our algorithms, here take $ct_8 = 0.6$, $ct_3 = 0.4$, $ct_5 = 0.5$; $cc_8 = 0.6$, $cc_3 = 0.2$, $cc_5 = 0.7$. The results are as Table 2.

Table 2 Comparison of the two algorithms

	Category	PageRank*Sim	$T/\overline{\ }$	$cpt/\overline{\ p\ }$	TP	CP	Q=Pagerank* Sim*TP*CP	Rank
Page1	8	Q_1	0.21	0.82	1.42	0.93	$1.32Q_1$	3
Page2	3	Q_2	0.93	0.40	1.02	0.9	$0.92Q_2$	7
Page3	3	Q_3	2.7	0.64	0.67	0.94	$0.43Q_3$	10
Page4	5	Q_4	0.61	2.33	1.15	1.55	$1.78Q_4$	2
Page5	3	Q_5	2.2	1.38	0.74	1.06	$0.78Q_5$	9
Page6	3	Q_6	0.49	0.21	1.17	0.87	$1.01Q_6$	6
Page7	3	Q_7	0.45	1.60	1.86	1.1	$2.05Q_7$	1
Page8	3	Q_8	1.6	0.85	0.85	0.98	$0.83Q_8$	8
Page9	3	Q_9	0.7	1.32	1.09	1.05	$1.14Q_9$	4
Page10	5	Q_{10}	0.11	0.45	1.42	0.77	$1.09Q_{10}$	5

Web page ranking algorithm should put user needs and user satisfaction as evaluation criteria. With the page ranking algorithm based on meta-information, the page3 is assigned a smaller TP because of larger page age, thereby reducing the page quality, and rank bottom in the re-ranking. While page1 get a larger value of TP because of smaller page age. Page hits frequency reflects the degree of the user evaluation of the page, Web pages with larger page hits frequency can achieve larger Q value.Page4 has a higher rank due to a higher hits frequency, while page2 has a lower rank because of lower page hits frequency. The above algorithm can filter out those pages with high PageRank but large page age and low hits frequency, thus improving user satisfaction.

Conclusions

This algorithm introduces page update time and page hits frequency to evaluate the pages quality, it is better able to rank web pages and allow users to get page results really need. Although the page ranking algorithm based on meta-information works well, but the specific implementation of the algorithm is also relatively simple and rough, some of the selected coefficient needs further study. In addition, we need to study the appropriate web page classification techniques.

References

[1] T.H. Haveliwala, Topic-sensitive PageRank, in: Proceedings of the 11th International World Wide Web Conference, 2002

[2] T.H. Haveliwala, S.D. Kamvar, The second eigenvalue of the Google matrix, Stanford University Technical Report, 2003

[3] J. Hirai, S. Raghavan, H. Garcia-Molina, A. Paepcke, WebBase: a repository of web pages, in: Proceedings of the Ninth International World Wide Web Conference, 2000

[4] G. Jeh, J. Widom, Scaling personalized web search, in: Proceedings of the 12th International World Wide Web Conference, 2003

[5] S.D. Kamvar, T.H. Haveliwala, C.D. Manning, G.H. Golub, Extrapolation methods for accelerating PageRank computations, in: Proceedings of the 12th International World Wide Web Conference, 2003

[6] L. Page, S. Brin, R. Motwani, T. Winograd, The PageRank citation ranking: bringing order to the web, Stanford Digital Libraries Working Paper, 1998

Applied Mechanics and Materials Vol. 596 (2014) pp 297-300
© (2014) Trans Tech Publications, Switzerland
doi:10.4028/www.scientific.net/AMM.596.297

E-Bayes Estimation of Burr Distribution Parameter under Square Loss Function

Huanbin Liu[1], Tong Yin[2] and Cheng Wang[1]

[1] College of Mathematical and Physical Sciences, Huanggang Normal University,
Hubei 438000, China

[2] College of Mathematical and Physical Sciences, Shanghai Normal University,
Shanghai 200234, China

lhb@hgnu.edu.cn

Keywords: Burr distribution; E-Bayes estimation; Hierarchical Bayes estimation

Abstract. This paper provides the E-Bayes estimation and hierarchical Bayes estimation of Burr distribution parameter under square loss function when the prior distribution is Gamma distribution, and proves that the E-Bayes estimation and hierarchical Bayes estimation are progressively equal. Numerical simulation also shows that the results of these two types of estimation are close, and E-Bayes estimation is more convenient in terms of calculation complexity.

Introduction

Burr distribution was given by BurrI. W. in 1942. Nowadays, it is widely used in social sciences, economic sciences, environmental sciences, insurance mathematics, and other areas, and it receives more and more attention on researches. In document [1], Zhang studied the estimation and check problem of Burr distribution. In documents [2] to [5], Wang, Li, Chen, etc. studied the Bayes estimation and hierarchical Bayes estimation of Burr distribution under different loss functions respectively. This paper mainly discussed the E-Bayes estimation of Burr distribution under square loss function, and compared it with hierarchical estimation.

The density function of Burr distribution is as follows:

$$f(x|\theta,\alpha) = \alpha\theta x^{\alpha-1}(1+x^{\alpha})^{-(1+\theta)} \quad (\alpha > 0, \theta > 0, x > 0) \tag{1}$$

where $a > 0$ is known, $\theta > 0$ is a parameter to be estimated. Suppose X= (X_1, X_2, … , X_n) is a group of sample observations derived from (1), then its likelihood function is denoted as:

$$L(\theta,x) = (\alpha x^{\alpha-1})^n \theta^n (1+x^{\alpha})^{-n(1+\theta)} \quad (\alpha > 0, \theta > 0, x > 0)$$

Let $T = n \ln(1 + x^{\alpha})$, then the likelihood function can be expressed as

$$L(\theta,x) = (\alpha x^{\alpha-1})^n e^{-T} \theta^n e^{-T\theta} \quad (\alpha > 0, \theta > 0, x > 0).$$

E-Bayes Estimation

If the prior distribution of parameter θ is Gamma(a, b), then its density function is

$$\pi(\theta|a,b) = \frac{b^a}{\Gamma(a)}\theta^{\alpha-1}e^{-b\theta} \tag{2}$$

According to the decreasing function method proposed in document [6], we construct the decreasing function of θ, take derivative of the prior distribution of θ, and obtain the following equation:

$$\frac{d[\pi(\theta|a,b)]}{d\theta} = \frac{b^a}{\Gamma(a)}[(a-1)\theta^{\alpha-2}e^{-b\theta} - b\theta^{\alpha-1}e^{-b\theta}] = \frac{b^a}{\Gamma(a)}\theta^{\alpha-2}e^{-b\theta}[(a-1)-b\theta].$$

When $0 < a \leq 1$, $b > 0$, it is a decreasing function of θ. Let $a = 1$, $b > 0$, it is still a decreasing function of θ, and its prior distribution density function is

$$\pi(\theta|b) = be^{-b\theta} \tag{3}$$

According to document [7], from the aspect of the robustness of Bayes, the prior distribution with a thinner tail often results in a worse robustness of Bayes estimation, therefore, b is not suitable to have a big value, and should be set with an upper boundary. Suppose c is the upper boundary of b(c>1 is a constant), then the range of hyper-parameter b is $0 < b < c$(for the determination of c, one can refer the numerical examples)

(1) Definition of E-Bayes estimation

Definition 1 [8]. Suppose $a \in D$, if $\hat{\theta}_B(a)$ is continuous, then we say

$$\hat{\theta}_{EB}(a) = \int_D \hat{\theta}_B(a)\pi(a)da$$

is the E-Bayes estimation(Expected Bayes Estimation) of θ, where $\int_D \hat{\theta}_B(a)\pi(a)da$ is existing, $D = \{a : 1 < a < c\}$, $c > 1$ is a constant, $\pi(a)$ is the density function of a in interval D, and $\hat{\theta}_B(a)$ is the Bayes estimation of θ(using hyper-parameter a to represent).

From definition 1, we can see that the E-Bayes estimation of θ

$$\hat{\theta}_{EB}(a) = \int_D \hat{\theta}_B(a)\pi(a)da = E[\hat{\theta}_B(a)].$$

is the mathematical expectation of the Bayes estimation $\hat{\theta}_B(a)$ of θ with respect to hyper-parameter a.

(2) E-Bayes estimation

Theorem 1: For Burr distribution (1), the prior distribution of θ is given by (3), then we can make the following conclusions:

(i) Under square loss function, the Bayes estimation of θ is

$$\hat{\theta}_B(b) = \frac{n+1}{T+b}.$$

(ii) if hyper-parameter b obeys a uniform distribution on 0 to c, then the E-Bayes estimation of θ is

$$\hat{\theta}_{EB}(b) = \frac{n+1}{c}\ln(1+\frac{c}{T}).$$

Proof: (i) Under prior distribution (3), the posterior distribution of θ is:

$$\pi(\theta|x) = \frac{L(\theta,x)\pi(\theta|b)}{\int_0^\infty L(\theta,x)\pi(\theta|b)d\theta} = \frac{(\alpha x^{\alpha-1})^n e^{-T}\theta^n e^{-T\theta} b e^{-b}}{\int_0^\infty (\alpha x^{\alpha-1})^n e^{-T}\theta^n e^{-T\theta} b e^{-b} db} = \frac{(T+b)^{n-1}}{\Gamma(n+1)}\theta^n e^{-(T+b)\theta}.$$

As the posterior distribution of θ, $\pi(\theta|x)$ obeys inverse Grammar distribution Γ−1(n + 1, T + b), then the Bayes distribution under square loss function is as follows:

$$\hat{\theta}_B(b) = E(\theta|X) = \int_0^\infty \theta\pi(\theta|x)d\theta = \int_0^\infty \theta\frac{(T+b)^{n+1}}{\Gamma(n+1)}\theta^n e^{-(T+b)\theta}d\theta = \frac{n+1}{T+b}.$$

(ii) if hyper-parameter b obeys a uniform distribution on 0 to c, then we have

$$\pi(b) = \frac{1}{c},\ (0 < b < c).$$

According to definition 1, the E-Bayes estimation of θ is

$$\hat{\theta}_{EB}(a) = E(\theta|X) = \int_0^\infty \hat{\theta}_B(b)\pi(b)db = \int_0^\infty \frac{1}{c}\frac{n+1}{T+b}db = \frac{n+1}{c}\ln(1+\frac{c}{T}).$$

Hierarchical Bayes estimation of θ

Theorem 2: When parameter θ of Burr distribution (1) is (3) and hyper-parameter b obeys a uniform distribution on 0 to c, the hierarchical Bayes estimation of θ is:

$$\hat{\theta}_{HB}(b) = \frac{(T+c)^{-(n+1)}[c+\frac{T+c)}{n}]-\frac{T-n)}{n}}{\frac{(T+c)-n}{n}[c+\frac{T+c}{n-1}]-\frac{T-(n-1)}{n(n-1)}}.$$

Proof: when hyper-parameter b obeys a uniform distribution on 0 to c, the hierarchical Bayes estimation of θ under prior distribution (3) is:

$$\pi(\theta,b)=\int_0^c \pi(\theta)\pi(b)db=\frac{1}{c}\int_0^c be^{-b\theta}db.$$

Then the hierarchical Bayes posterior distribution is

$$\pi(\theta,b|x)=\frac{L(\theta,x)\pi(\theta,b)}{\int_0^\infty L(\theta,x)\pi(\theta,b)d\theta}$$

$$=\frac{\int_0^c b\theta^n e^{-(T+b)\theta}db}{\int_0^c\int_0^\infty b\theta^n e^{-(T+b)\theta}d\theta db}=\frac{\int_0^c b\theta^n e^{-(T+b)\theta}db}{\Gamma(n+1)\int_0^c \frac{b}{(T+b)^{n+1}}db}.$$

and the hierarchical Bayes estimation of Burr distribution(1) under square loss function is

$$\hat{\theta}_{HB}=E(\theta,b|x)=\int_0^\infty \theta\pi(\theta,b|x)d\theta=(n+1)\frac{\int_0^c \frac{1}{c}\frac{b}{(T+b)^{n+2}}db}{\int_0^c \frac{1}{c}\frac{b}{(T+b)^{n+1}}db}.$$

Integrate $\int_0^c \frac{b}{(T+b)^{n+2}}db$ and $\int_0^c \frac{b}{(T+b)^{n+1}}db$ using integration by parts, we have

$$\int_0^c \frac{b}{(T+b)^{n+2}}db=-\frac{(T+c)^{-(n+1)}}{n+1}[c+\frac{T+c}{n}]+\frac{T^{-n+1}}{n(n+1)},$$

$$\int_0^c \frac{b}{(T+b)^{n+1}}db=-\frac{(T+c)^{-n}}{n}[c+\frac{T+c}{n-1}]+\frac{T^{-(n-1)}}{n(n-1)}.$$

Finally the hierarchical Bayes estimation is

$$\hat{\theta}_{HB}(b)=\frac{(T+c)^{-n-1}[c+\frac{T+c}{n}]-\frac{T^{-n}}{n}}{-\frac{(T+c)^{-n}}{n}[c+\frac{T+c}{n-1}]-\frac{T^{-(n-1)}}{n(n-1)}}.$$

Properties of E-Bayes estimation

Theorem 1 and 2 provides the E-Bayes estimation and hierarchical Bayes estimation respectively, then what's the relation between them? Theorem 3 gives the answer.

Theorem 3: $\hat{\theta}_{EB}(b)$ and $\hat{\theta}_{HB}(b)$ derived from theorem 1 and theorem 2 respectively satisfies the following equation $\lim_{n\to\infty}\hat{\theta}_{EB}(b)=\lim_{n\to\infty}\hat{\theta}_{HB}(b)$.

Proof: According to theorem 1, $\hat{\theta}_B(b)=\frac{n+1}{T+b}$, where $T=n\ln(1+x\alpha)$. Denote $y=\ln(1+x\alpha)$, then $T=ny$, thus we have

$$\lim_{n\to\infty}\hat{\theta}_{EB}(b)=\lim_{n\to\infty}\frac{n+1}{c}\ln(1+\frac{c}{T})=\frac{1}{y}.$$

According to theorem 2, we have

$$\hat{\theta}_{HB}(b)=\frac{(T+c)^{-(n+1)}[c+\frac{T+c)}{n}]-\frac{T-n)}{n}}{\frac{(T+c)-n}{n}[c+\frac{T+c}{n-1}]-\frac{T-(n-1)}{n(n-1)}},$$

So we have

$$\lim_{n\to\infty}\hat{\theta}_{HB}(b)=\lim_{n\to\infty}\frac{(T+c)^{-(n+1)}[c+\frac{T+c)}{n}]-\frac{T-n)}{n}}{\frac{(T+c)-n}{n}[c+\frac{T+c}{n-1}]-\frac{T-(n-1)}{n(n-1)}}=\frac{e^{-\frac{c}{y}}(c+y)-y}{y[e^{-\frac{c}{y}}(c+y)-y]}=\frac{1}{y}.$$

Therefore, we can obtain the following equation:

$$\lim_{n\to\infty}\hat{\theta}_{EB}(b)=\lim_{n\to\infty}\hat{\theta}_{HB}(b).$$

Conclusions

This paper gives the E-Bayes estimation and hierarchical Bayes estimation of Burr distribution parameter when the prior distribution is Gamma distribution under square loss function. Numerical simulation shows that although the results of E-Bayes estimation and hierarchical estimation are different, when n keeps increasing, $\hat{\theta}_{HB}$ and $\hat{\theta}_{EB}$ are closer and closer. Therefore, we conclude that these two types of estimation are progressively equal. Moreover, the calculation of hierarchical Bayes estimation is more complicated, and difficult to realize, while E-Bayes estimation is easier to calculate, and convenient for practical applications, which can be regarded as a modification of hierarchical Bayes estimation.

Acknowledgments

This work is supported by the Natural Science Foundation of Hubei Province, China (No. 2011CDB167), the Major Research Program of Hubei Provincial Department ofEducation, China (No. Z20092701), and the Ph.D. Fund of Huanggang Normal University to H. B. Liu.

References

[1] C.P. Zhang: The estimation and Check Problem of Burr Distribution with three parameters (East China Normal University, Shanghai, 2006).

[2] X.M. Wang: Journal of Wuhan Institute of Biological Engineering Vol. 2 (2013), p. 94-97.

[3] J.H. Li: Statistics and Decision Vol. 17 (2011), p. 40-41.

[4] J.H. Li and X.J. Yu: Journal of Yangtze University Vol. 7 (2010), p. 175-177.

[5] Z.Q. Chen, C.D. Wei and Y.Q. Cheng: Journal of Guangxi Normal University Vol. 24 (2007), p. 30-34.

[6] M. Han: Operations Research and Management Science Vol. 6 (1997), p. 31-40.

[7] J.O. Berger: Statistical Decision Theory and Bayesian Analysis (Springer-Verlag, New York, 1985).

[8] M. Han: Modified Bayes Estimation of Reliability Parameters and Its Applications (Tongji University Press, Shanghai, 2010).

Applied Mechanics and Materials Vol. 596 (2014) pp 301-304
© (2014) Trans Tech Publications, Switzerland
doi:10.4028/www.scientific.net/AMM.596.301

E-Bayes Estimation of Laplace Distribution Parameter under Q-symmetric Entropy Loss Function

Huanbin Liu[1], Tong Yin[2] and Cheng Wang[1]

[1] College of Mathematical and Physical Sciences, Huanggang Normal University,
Hubei 438000, China

[2] College of Mathematical and Physical Sciences, Shanghai Normal University,
Shanghai 200234, China

lhb@hgnu.edu.cn

Keywords: Laplace distribution; E-Bayes estimation; Hierarchical Bayes estimation; q-symmetric entropy loss function

Abstract. This paper provides the E-Bayes estimation and hierarchical Bayes estimation of Laplace distribution parameter under q-symmetric entropy loss function when the prior distribution is Beta distribution. The relation between E-Bayes estimation and hierarchical Bayes estimation is discussed. Numerical simulation results show that these two types of estimation are progressively equal, and E-Bayes estimation is more convenient in terms of calculation.

Introduction

Laplace distribution is a symmetric distribution function. It possesses some better properties than normal distribution. The peak is sharper, and the two end tails are thicker, which is fit to simulate long-tail symmetric data like errors and yields. It was proved to have great significance and practical application value in financial and experimental areas. In document [1], A Bayes estimation of Laplace distribution parameter under a new loss function was provided. In this paper, we presented the E-Bayes estimation and hierarchical Bayes estimation of Laplace distribution parameter under q-symmetric entropy loss function. Through numerical calculation, we found they are approximately equal.

Q-symmetric entropy loss function is an extension of entropy loss function. The expression is as follows:

$$L(\lambda,\delta)=(\frac{\lambda}{\delta})^q+(\frac{\delta}{\lambda})^q-2 \qquad (q>0)$$

where λ is a parameter to be estimated, and δ is its estimator. Document [2] and [3] provided the parameter estimation of exponential distribution and Gamma distribution respectively under q-symmetric entropy loss function.

The density function of Laplace distribution is

$$f(x,\theta)=\frac{1}{2\theta}\exp(-\frac{|x|}{\theta}) \qquad (\theta>0) \tag{1}$$

Suppose $X=(x_1,x_2,\ldots,x_n)$ is a group of sample observations derived from equation (1), then its likelihood function can be expressed as $L(\theta,x)=(\frac{1}{2\theta})^n\exp(-\frac{T}{\theta}) \quad (\theta>0)$, where $T=\sum_{i=1}^{n}|x_i|$.

E-Bayes Estimation

If the prior distribution of parameter θ is *Beta*(*a*, *b*), then its density function is as follows:

$$\pi(\theta|a,b)=\frac{\theta^{a-1}(1-\theta)^{b-1}}{B(a,b)} \tag{2}$$

For investors and testers, they pay more attention on the maximum potential loss or error possibly appearing in the near future. Especially in experiments, the maximum error is more emphasized. At this point, we believe that there is a higher possibility for parameter θ of Laplace distribution to have a big value, and less possibility to have a small value. According to the increasing function proposed in previous documents, we constructed the increasing function of θ, took the derivative of the prior distribution (2) of θ, and obtained the following equation:

$$\frac{d[\pi(\theta|a,b)]}{d\theta}=\frac{\theta^{a-2}(1-\theta)^{b-2}[(a-1)(1-\theta)-(b-1)\theta}{B(a,b)}.$$

When $a > 1$, $0 < b \leq 1$, it is an increasing function of θ. Let b=1, a>1, it's still an increasing function of θ, and its prior distribution function is

$$\pi(\theta|a)=a\theta^{a-1} \tag{3}$$

According to document [5], from the aspect of the robustness of Bayes, the prior distribution with a thinner tail often results in a worse robustness of Bayes estimation, therefore, a is not suitable to have a big value, and should be set with an upper boundary. Suppose c is the upper boundary of a (c>1 is a constant), then the range of hyper-parameter a is $1 < a < c$ (for the determination of c, one can refer the numerical examples).

(1) Definition of E-Bayes estimation

Definition 1 [6]. Suppose $a \in D$, if $\hat{\theta}_B(a)$ is continuous, then we say

$$\hat{\theta}_{EB}(a)=\int_D \hat{\theta}_B(a)\pi(a)da$$

is the E-Bayes estimation(Expected Bayes Estimation) of θ, where $\int_D \hat{\theta}_B(a)\pi(a)da$ is existing, $D = \{a : 1 < a < c\}$, $c > 1$ is a constant, $\pi(a)$ is the density function of a in interval D, and $\hat{\theta}_B(a)$ is the Bayes estimation of θ (using hyper-parameter a to represent).

From definition 1, we can see that the E-Bayes estimation of θ

$$\hat{\theta}_{EB}(a)=\int_D \hat{\theta}_B(a)\pi(a)da=E[\hat{\theta}_B(a)]$$

is the mathematical expectation of the Bayes estimation $\hat{\theta}_B(a)$ of θ with respect to hyper-parameter a.

(2) E-Bayes estimation

Lemma1 [7]. For any prior distribution, under q-symmetric entropy loss function, the Bayes estimation of θ is

$$\hat{\theta}_B(a)=[\frac{E(\theta^q|X}{E(\theta^{-q}|X}]^{\frac{1}{2q}},$$

And if δ is existing, and its Bayes risk $R(\delta) < \infty$, then its Bayes estimation is unique.

As the prior density function(3) is a strictly convex function with respect to θ, then the Bayes estimation of θ is admissible, that's, the Bayes estimation of θ, $\hat{\theta}_B(a)$ is unique.

Theorem 1. For Laplace distribution (1), the prior distribution of θ is given by (3), then we can make the following conclusions:

(i) Under q-symmetric entropy loss function, the Bayes estimation of θ is

$$\hat{\theta}_B(a)=T[\frac{\Gamma(n-a-q)}{\Gamma(n-a+q)}]^{\frac{1}{2q}}.$$

(ii) If hyper-parameter a obeys a uniform distribution on 1 to c, then the E-Bayes estimation of θ is

$$\hat{\theta}_{EB}(a)=\frac{T}{c-1}\int_1^c [\frac{\Gamma(n-a-q)}{\Gamma(n-a+q)}]^{\frac{1}{2q}}da.$$

Proof: (i) Under prior distribution (3), the posterior distribution of θ is

$$\pi(\theta|x)=\frac{L(\theta,x)\pi(\theta|a)}{\int_0^{\infty}L(\theta,x)\pi(\theta|a)d\theta}=\frac{a\theta^{a-1}(\frac{1}{2\theta})^n\exp(-\frac{T}{\theta})}{\int_0^{\infty}a\theta^{a-1}(\frac{1}{2\theta})^n\exp(-\frac{T}{\theta})d\theta}=\frac{T^{n-a}}{\Gamma(n-a)}(\frac{1}{\theta})^{n-a+1}\exp(-\frac{T}{\theta}).$$

As the posterior distribution of θ, $\pi(\theta|x)$ obeys inverse Grammar distribution $\Gamma^{-1}(n-a, T)$, then we have

$$E(\theta^q|x)=\int_0^{\infty}\theta^q\pi(\theta|x)d\theta=\int_0^{\infty}\frac{T^{n-a}}{\Gamma(n-a)}(\frac{1}{\theta})^{n-a-q-1}\exp(-\frac{T}{\theta})d\theta=T^q\frac{T(n-a-q)}{\Gamma(n-a)},$$

$$E(\theta^{-q}|x)=\int_0^{\infty}\theta^{-q}\pi(\theta|x)d\theta=\int_0^{\infty}\frac{T^{n-a}}{\Gamma(n-a)}(\frac{1}{\theta})^{n-a+q+1}\exp(-\frac{T}{\theta})d\theta=T^{-q}\frac{T(n-a-q)}{\Gamma(n-a)}.$$

Therefore, the Bayes estimation of θ under q-symmetric entropy loss function is

$$\hat{\theta}_B(a)=\left[\frac{E(\theta^q|x)}{E(\theta^{-q}|x)}\right]^{\frac{1}{2q}}=\left[\frac{T^q\frac{T(n-a-q)}{\Gamma(n-a)}}{T^{-q}\frac{T(n-a+q)}{\Gamma(n-a)}}\right]^{\frac{1}{2q}}=\left[\frac{T(n-a-q)}{T(n-a+q)}\right]^{\frac{1}{2q}}.$$

(ii) If hyper-parameter a obeys a uniform distribution on 1 to c, we have

$$\pi(a)=\frac{1}{c-1},\ (1<a<c),$$

according to definition 1, the E-Bayes estimation of θ is

$$\hat{\theta}_{EB}(a)=\int_1^c\hat{\theta}_B(a)\pi(a)da=\int_1^c\frac{T}{c-1}\left[\frac{T(n-a-q)}{T(n-a+q)}\right]^{\frac{1}{2q}}da=\frac{T}{c-1}\int_1^c\left[\frac{T(n-a-q)}{T(n-a+q)}\right]^{\frac{1}{2q}}da.$$

Hierarchical Bayes estimation of θ

Theorem 2. When parameter θ of Laplace distribution (1) is (3) and hyper-parameter a obeys a uniform distribution on 1 to c, the hierarchical Bayes estimation of θ is

$$\hat{\theta}_{HB}(a)=T\left[\frac{\int_1^c aT^a\Gamma(n-a-q)da}{\int_1^c aT^a\Gamma(n-a+q)da}\right]^{\frac{1}{2q}}$$

Proof: When hyper-parameter a obeys a uniform distribution on 1 to c, the hierarchical Bayes estimation of θ under prior distribution (3) is

$$\pi(\theta,a)=\int_1^c\pi(\theta)\pi(a)da=\frac{1}{c-1}\int_1^c a\theta^{a-1}da,$$

Then the hierarchical Bayes posterior distribution is

$$\pi(\theta,a|x)=\frac{L(\theta,x)\pi(\theta,a)}{\int_0^{\infty}L(\theta,x)\pi(\theta,a)d\theta}=\frac{\int_1^c a(\frac{1}{\theta})^{n-a+1}\exp(-\frac{T}{\theta})da}{\int_1^c a\frac{\Gamma(n-a)}{T^{n-a}}da},$$

Thus, we can have

$$E(\theta^q,a|x)=\int_0^{\infty}\theta^q\pi(\theta,a|x)d\theta=\frac{\int_1^c\int_0^{\infty}a(\frac{1}{\theta})^{n-a-q+1}\exp(-\frac{T}{\theta})d\theta da}{\int_1^c a\frac{\Gamma(n-a)}{T^{n-a}}da}=\frac{\int_1^c a\frac{\Gamma(n-a-q)}{T^{n-a-q}}da}{\int_1^c a\frac{\Gamma(n-a)}{T^{n-a}}da},$$

$$E(\theta^{-q},a|x)=\int_0^\infty \theta^{-q}\pi(\theta,a|x)d\theta=\frac{\int_1^c\int_0^\infty a(\frac{1}{\theta})^{n-a+q+1}\exp(-\frac{T}{\theta})d\theta da}{\int_1^c a\frac{\Gamma(n-a)}{T^{n-a}}da}=\frac{\int_1^c a\frac{\Gamma(n-a+q)}{T^{n-a+q}}da}{\int_1^c a\frac{\Gamma(n-a)}{T^{n-a}}da},$$

$$\hat{\theta}_B=\left[\frac{E(\theta^q|x)}{E(\theta^{-q}|x)}\right]^{\frac{1}{2q}}=\left[\frac{\int_1^c a\frac{\Gamma(n-a-q)}{T^{n-a-q}}da}{\int_1^c a\frac{\Gamma(n-a+q)}{T^{n-a+q}}da}\right]^{\frac{1}{2q}}=\left[T^{2q}\frac{\int_1^c aT^a\Gamma(n-a-q)}{\int_1^c aT^a\Gamma(n-a+q)}da\right]^{\frac{1}{2q}}$$

$$=\left[T\frac{\int_1^c aT^a\Gamma(n-a-q)}{\int_1^c aT^a\Gamma(n-a+q)}da\right]^{\frac{1}{2q}}.$$

Conclusions

This paper gives the E-Bayes estimation and hierarchical Bayes estimation of Laplace distribution under q-symmetric entropy loss function when the prior distribution is Beta distribution. Numerical simulation shows that although the results of E-Bayes estimation and hierarchical estimation are different, when n keeps increasing, $\hat{\theta}_{HB}$ and $\hat{\theta}_{EB}$ are closer and closer. Therefore, we conclude that these two types of estimation are progressively equal. Moreover, the calculation of hierarchical Bayes estimation is more complicated, and difficult to realize, while E-Bayes estimation is easier to calculate, and convenient for practical applications, which can be regarded as a modification of hierarchical Bayes estimation.

Acknowledgments

This work is supported by the Natural Science Foundation of Hubei Province, China (No. 2011CDB167), the Major Research Program of Hubei Provincial Department ofEducation, China (No. Z20092701), and the Ph.D. Fund of Huanggang Normal University to H. B. Liu.

References

[1] M.P. Xu and J.H. Duan: Statistics and Decision Vol. 1 (2010), p. 13-14.

[2] Y.J. Du and M. Lai: Journal of Jilin University(Science Edition) Vol. 43 (2005), p. 10-15.

[3] Y.J. Du, X.Y. Sun, X.C. Wang: Chinese Journal of Engineering Mathematics Vol. 25 (2008), p. 500-504.

[4] M. Han: Operations Research and Management Science Vol. 6 (1997), p. 31-40.

[5] J.O. Berger: Statistical Decision Theory and Bayesian Analysis (Springer-Verlag, New York, 1985).

[6] M. Han: Modified Bayes Estimation of Reliability Parameters and Its Applications (Tongji University Press, Shanghai, 2010).

[7] L.J. Kong: Journal of Jilin University (Science Edition) Vol. 2 (1998), p. 9-14.

Applied Mechanics and Materials Vol. 596 (2014) pp 305-308
© (2014) Trans Tech Publications, Switzerland
doi:10.4028/www.scientific.net/AMM.596.305

E-Bayes Estimation of Rayleigh Distribution Parameter

Huanbin Liu[1], Tong Yin[2] and Cheng Wang[1]

[1] College of Mathematical and Physical Sciences, Huanggang Normal University,
Hubei 438000, China

[2] College of Mathematical and Physical Sciences, Shanghai Normal University,
Shanghai 200234, China

lhb@hgnu.edu.cn

Keywords: Rayleigh distribution; E-Bayes estimation; Hierarchical Bayes estimation

Abstract. This paper provided the E-Bayes estimation and hierarchical Bayes estimation of Rayleigh distribution parameter under q-symmetric entropy loss function, when the prior distribution is Beta distribution, and the relation between E-Bayes estimation and hierarchical Bayes estimation was discussed. Numerical simulation shows that the results of these two types of estimation are close, and E-Bayes estimation is more convenient in terms of calculation complexity.

Introduction

Rayleigh distribution is an important life distribution, mainly used to describe the distribution regularities of stress range when parts or components suffer from unsteady loop stress, and the statistical time-varying characteristics of flat fading signal receiving envelope or independent multipath component receiving envelope. The envelope of the sum of two orthogonal Gaussian noise signals also obeys Rayleigh distribution. It is an important member of Weibull distribution family. Document [1] to [4] discussed the Bayes distribution and the admissibility of Rayleigh distribution under entropy loss function, weighting-symmetric loss function, Linex loss function and balanced loss function respectively. Document [5] studied the maximum likelihood estimation and the uniqueness of Rayleigh distribution parameters. This paper provided the E-Bayes estimation and the hierarchical Bayes estimation of Rayleigh distribution under q-symmetric entropy loss function, and also discussed the relations between the E-Bayes estimation and the hierarchical estimation.

The density function of Rayleigh distribution is

$$f(x|\theta)=\frac{2x}{\theta}e^{-\frac{x^2}{\theta}},\ (\theta>0,\ x>0) \tag{1}$$

where $\theta > 0$ is a parameter to be estimated. Suppose X = (X_1, X_2, …, X_n) is a group of sample observations derived from equation (1), then its likelihood function can be expressed as follows:

$$L(\theta,x)=\prod_{i=1}^{n}X_i(\frac{2}{\theta})^n e^{-\frac{T}{\theta}},\ \ (\theta>0,\ x>0)$$

where $T=\sum_{i=1}^{n}X_i^2$.

Q-symmetric entropy loss function is an extension of entropy loss function. The expression is as follows:

$$L(\lambda,\delta)=(\frac{\lambda}{\delta})^q+(\frac{\delta}{\lambda})^q-2,\ \ (q>0)$$

where λ is a parameter to be estimated, and δ is its estimator. Document[6] provided the parameter estimation of exponential distribution under q-symmetric entropy loss function.

E-Bayes Estimation

If the prior distribution of parameter θ is Beta(a, b), then its density function is as follows:

$$\pi(\theta|a,b)=\frac{\theta^{a-1}(1-\theta)^{b-1}}{B(a,b)} \tag{2}$$

According to the increasing function proposed in previous documents, we constructed the increasing function of θ, took the derivative of the prior distribution (2) of θ, and obtained the following equation:

$$\frac{d[\pi(\theta|a,b)]}{d\theta}=\frac{\theta^{a-2}(1-\theta)^{b-2}[(a-1)(1-\theta)-(b-1)\theta]}{B(a,b)}$$

When $a > 1$, $0 < b \le 1$, it is an increasing function of θ. Let $b = 1$, $a > 1$, it's still an increasing function of θ, and its prior distribution density function is

$$\pi(\theta|a)=a\theta^{a-1} \tag{3}$$

According to document [7], from the aspect of the robustness of Bayes, the prior distribution with a thinner tail often results in a worse robustness of Bayes estimation, therefore, a is not suitable to have a big value, and should be set with an upper boundary. Suppose c is the upper boundary of a (c>1 is a constant), then the range of hyper-parameter a is $1 < a < c$ (for the determination of c, one can refer the numerical examples).

(1) Definition of E-Bayes estimation

Definition 1 [8]. suppose $a \in D$, if $\hat{\theta}_B(a)$ is continuous, then we say

$$\hat{\theta}_{EB}(a)=\int_D \hat{\theta}_B(a)\pi(a)da$$

is the E-Bayes estimation(Expected Bayes Estimation) of θ, where $\int_D \hat{\theta}_B(a)\pi(a)da$ is existing, $D = \{a: 1 < a < c\}$, $c > 1$ is a constant, $\pi(a)$ is the density function of a in interval D, and $\hat{\theta}_B(a)$ is the Bayes estimation of θ (using hyper-parameter a to represent).

From definition 1, we can see that the E-Bayes estimation of θ

$$\hat{\theta}_{EB}(a)=\int_D \hat{\theta}_B(a)\pi(a)da=E[\hat{\theta}_B(a)]$$

is the mathematical expectation of the Bayes estimation $\hat{\theta}_B(a)$ of θ with respect to hyper-parameter a.

(2) E-Bayes estimation

Lemma1 [9]. For any prior distribution, under q-symmetric entropy loss function, the Bayes estimation of θ is

$$\hat{\theta}_B=\left[\frac{E(\theta^q|X)}{E(\theta^{-q}|X)}\right]^{\frac{1}{2q}}.$$

If δ is existing, and its Bayes risk $R(\delta) < \infty$, then its Bayes estimation is unique.

As the prior density function(3) is a strictly convex function with respect to θ, then the Bayes estimation of θ is admissible, that's, the Bayes estimation of θ, $\hat{\theta}_B(a)$ is unique.

Theorem 1. For Rayleigh distribution (1), the prior distribution of θ is given by (3), then we can make the following conclusions:

(i) Under q-symmetric entropy loss function, the Bayes estimation of θ is

$$\hat{\theta}_B(b)=T\left[\frac{\Gamma(n-a-q)}{\Gamma(n-a+q)}\right]^{\frac{1}{2q}}$$

(ii) If hyper-parameter a obeys a uniform distribution on 1 to c, then the E-Bayes estimation of θ is

$$\hat{\theta}_{EB}(b)=\frac{T}{c-1}\int_1^c\left[\frac{\Gamma(n-a-q)}{\Gamma(n-a+q)}\right]^{\frac{1}{2q}}da.$$

Proof: (i) Under prior distribution (3), the posterior distribution of θ is

$$\pi(\theta|x)=\frac{L(\theta,x)\pi(\theta|a)}{\int_0^{\infty}L(\theta,x)\pi(\theta|a)d\theta}=\frac{T^{n-a}}{\Gamma(n-a)}(\frac{1}{\theta})^{n-a+1}\exp(-\frac{T}{\theta}).$$

As the posterior distribution of θ, $\pi(\theta|x)$ obeys inverse Grammar distribution $\Gamma^{-1}(n-a, T)$, then we have

$$E(\theta^{q}|x)=\int_0^{\infty}\theta^{q}\pi(\theta|x)d\theta=\int_0^{\infty}\frac{T^{n-a}}{\Gamma(n-a)}(\frac{1}{\theta})^{n-a-q+1}\exp(-\frac{T}{\theta})d\theta=T^{q}\frac{\Gamma(n-a-q)}{\Gamma(n-a)},$$

$$E(\theta^{-q}|x)=\int_0^{\infty}\theta^{-q}\pi(\theta|x)d\theta=\int_0^{\infty}\frac{T^{n-a}}{\Gamma(n-a)}(\frac{1}{\theta})^{n-a+q+1}\exp(-\frac{T}{\theta})d\theta=T^{-q}\frac{\Gamma(n-a+q)}{\Gamma(n-a)}$$

Therefore the Bayes estimation of θ under q-symmetric entropy loss function is

$$\hat{\theta}_B(a)=\left[\frac{E(\theta^{q}|X)}{E(\theta^{-q}|X)}\right]^{\frac{1}{2q}}=\left[\frac{T^{q}\frac{\Gamma(n-a-q)}{\Gamma(n-a)}}{T^{-q}\frac{\Gamma(n-a+q)}{\Gamma(n-a)}}\right]^{\frac{1}{2q}}=T\left[\frac{\Gamma(n-a-q}{\Gamma(n-a+q)}\right]^{\frac{1}{2q}}.$$

(ii) If hyper-parameter a obeys a uniform distribution on 1 to c, we have

$$\pi(a)=\frac{1}{c-1},\ (1<a<c).$$

According to definition 1, the E-Bayes estimation of θ is

$$\hat{\theta}_{EB}(a)=\int_1^{c}\hat{\theta}_B(a)\pi(a)da=\int_1^{c}\frac{T}{c-1}\left[\frac{\Gamma(n-a-q)}{\Gamma(n-a+q)}\right]^{\frac{1}{2q}}da=\frac{T}{c-1}\int_1^{c}\left[\frac{\Gamma(n-a-q)}{\Gamma(n-a+q)}\right]^{\frac{1}{2q}}da.$$

Hierarchical Bayes estimation of θ

Theorem 2. When parameter θ of Rayleigh distribution (1) is equation (3) and hyper-parameter a obeys a uniform distribution on 1 to c, the hierarchical Bayes estimation of θ is

$$\hat{\theta}_{HB}(a)=T\left[\frac{\int_1^{c}aT^{a}\Gamma(n-a-q)da}{\int_1^{c}aT^{a}\Gamma(n-a+q)da}\right]^{\frac{1}{2q}}.$$

Proof. When hyper-parameter a obeys a uniform distribution on 1 to c, the hierarchical Bayes estimation of θ under prior distribution (3) is

$$\pi(\theta,a)=\int_1^{c}\pi(\theta),\pi(a)da=\frac{1}{c-1}\int_1^{c}a\theta^{a-1}da.$$

and the hierarchical Bayes posterior distribution is

$$\pi(\theta,a|x)=\frac{L(\theta,x)\pi(\theta,a)}{\int_0^{\infty}L(\theta,x)\pi(\theta,a)d\theta}=\frac{\int_1^{c}a(\frac{1}{\theta})^{n-a+1}\exp(-\frac{T}{\theta})da}{\int_1^{c}a\frac{\Gamma(n-a)}{T^{n-a}}da}$$

Thus, we can have

$$\pi(\theta^{q},a|x)=\int_0^{\infty}\theta^{q}\pi(\theta,a|x)d\theta=\frac{\int_1^{c}\int_0^{\infty}a(\frac{1}{\theta})^{n-a-q+1}\exp(-\frac{T}{\theta})d\theta da}{\int_1^{c}a\frac{\Gamma(n-a)}{T^{n-a}}da}=\frac{\int_1^{c}a\frac{\Gamma(n-a-q)}{T^{n-a-q}}da}{\int_1^{c}a\frac{\Gamma(n-a)}{T^{n-a}}da},$$

$$\pi(\theta^{-q},a|x)=\int_0^{\infty}\theta^{-q}\pi(\theta,a|x)d\theta=\frac{\int_1^c\int_0^{\infty}a(\frac{1}{\theta})^{n-a+q+1}\exp(-\frac{T}{\theta})d\theta da}{\int_1^c a\frac{\Gamma(n-a)}{T^{n-a}}da}=\frac{\int_1^c a\frac{\Gamma(n-a+q)}{T^{n-a+q}}da}{\int_1^c a\frac{\Gamma(n-a)}{T^{n-a}}da},$$

$$\hat{\theta}_B=\left[\frac{E(\theta^q|X)}{E(\theta^{-q}|X)}\right]^{\frac{1}{2q}}=\left[\frac{\int_1^c a\frac{\Gamma(n-a-q)}{T^{n-a-q}}da}{\int_1^c a\frac{\Gamma(n-a+q)}{T^{n-a+q}}da}\right]^{\frac{1}{2q}}$$

$$=\left[T^{2q}\frac{\int_1^c aT^a\Gamma(n-a-q)}{\int_1^c aT^a\Gamma(n-a+q)}da\right]^{\frac{1}{2q}}=T\left[\frac{\int_1^c aT^a\Gamma(n-a-q)}{\int_1^c aT^a\Gamma(n-a+q)}da\right]^{\frac{1}{2q}}.$$

Conclusions

This paper gives the E-Bayes estimation and hierarchical Bayes estimation of Rayleigh distribution parameter under q-symmetric entropy loss function when the prior distribution is Beta distribution. Numerical simulation shows that although the results of E-Bayes estimation and hierarchical estimation are different, when n keeps increasing, $\hat{\theta}_{HB}$ and $\hat{\theta}_{EB}$ are closer and closer. Therefore, we conclude that these two types of estimation are progressively equal. Moreover, the calculation of hierarchical Bayes estimation is more complicated, and difficult to realize, while E-Bayes estimation is easier to calculate, and convenient for practical applications, which can be regarded as a modification of hierarchical Bayes estimation.

Acknowledgments

This work is supported by the Natural Science Foundation of Hubei Province, China (No. 2011CDB167), the Major Research Program of Hubei Provincial Department ofEducation, China (No. Z20092701), and the Ph.D. Fund of Huanggang Normal University to H. B. Liu.

References

[1] Y. Qiu, C.D. Wei and S.S. Hu: Journal of Guangxi Normal University(Natural Science Edition) Vol. 27 (2010), p. 39-43.

[2] L. Ren, Y.B. Zhu: Guangxi Sciences Vol. 14 (2007), p. 362-364.

[3] Z.Q. Chen, C.D. Wei, Y.Y. Wei: Journal of Zaozhuang College Vol. 29 (2012), p. 20-23.

[4] W.B. Yu and L.W. Yang: Journal of Shanxi University(Natural Science Edition) Vol. 34 (2011), p. 568-571.

[5] Y.W. Li, and X. Wang: System Science and Mathematical Science Vol. 29 (2009), p. 761-778.

[6] Y.J. Du and M. Lai: Journal of Jilin University(Science Edition) Vol. 43 (2005), p. 10-15.

[7] M. Han: Operations Research and Management Science Vol. 6 (1997), p. 31-40.

[8] M. Han: Modified Bayes Estimation of Reliability Parameters and Its Applications (Tongji University Press, Shanghai, 2010).

[9] L.J. Kong: Journal of Jilin University(Science Edition) Vol. 2 (1998), p. 9-14.

CHAPTER 5:

Sound, Image, Signal and Video Processing and Technologies

Applied Mechanics and Materials Vol. 596 (2014) pp 311-315
© (2014) Trans Tech Publications, Switzerland
doi:10.4028/www.scientific.net/AMM.596.311

2D(PC)2A Based Dimensionality Reduction of Textural Feature for Face Recognition with a Single Training Sample

Wen-He Sun

School of Computer and Information Engineering,

Harbin University of Commerce, Harbin, China.

Email: sunwenhexl@126.com

Keywords: Robust face recognition, Gabor filter, 2D(PC)2A, one sample per person problem, varying lighting condition.

Abstract. Face recognition system works badly in practical applications because only single training sample image per person is stored in the system owing to hard collecting training samples. We present a novel face recognition scheme with single training sample using 2D Gabor filter and 2D(PC)2A under varying light conditions. Firstly, 2D texture feature extract with Gabor filter captures the properties of spatial localization, orientation selectivity, and spatial frequency selectivity to cope with the variations in illumination. Secondly, 2D(PC)2A is to extract statistical texture features under one training sample. Finally matrix-based similarity nearest neighbor classifier is used to classify a new face for recognition. Some experiments are implemented to testify the feasibility of the proposed scheme.

Introduction

Face recognition has become an active research area in recent years due to its wide applications, and it is an important capability of human beings in their social life. Face recognition system should recognize hundreds or even thousands of faces and identify a face in different perspective variations, illuminations, ages, etc. Under very poor illumination conditions, it is hard for face recognition to recognize a face, especially under the single training sample condition owing to the limited condition of collecting the training samples in the practical applications. In this case, the traditional method such as Fisherface [1] fails when each person just has one training face sample available because of nonexistence of the intra-class scatter. Traditional single training sample based face recognition algorithm, such as (PC)2A [2], E(PC)2A [3] and SVD perturbation [4], still has some unsolved problems for high recognition accuracy in the practical application. For example, the procedure of E(PC)2A is divided into two stages of constructing a new image by combining the first-order and second-order projected images and the original image and performing PCA on the newly-combined training images. In the second stage, the combined image matrix should be mapped into a 1D vector in advance in order to perform PCA. This causes the high storage and computational cost. All these method only extract the statistical features for classification but ignoring the local texture information. In fact, when we recognize one person with its face, we mainly refer its texture information from the face image. So, in the face recognition system, we should consider the texture feature from the each sample together with the statistical features from the whole training sample set. Gabor filter is widely used in the texture feature extraction, which captures the properties of spatial localization, orientation selectivity, and spatial frequency selectivity to cope with the variations in illumination and facial expressions owing to its kernels similar to 2D receptive field profiles of the mammalian cortical simple cells. Different face recognition applications present different constraints and need different processing requirements. For example, when recognizing National ID card, credit card, passport, driver license, et al., the shooting condition is usually controllable and the quality of photographs is relatively good, but in other applications, for example, video surveillance, the obtained image may be both small in size and blurred. In these applications, lighting conditions are the important factors to decrease the performance of face recognition system. An excellent face recognition algorithm should sufficiently consider the following two issues of what features are used to represent a face image and how to classify a new face image based on this representation. In this paper, we represent a face image with statistical 2D texture features extracted with two stages, i.e., one is to extract the 2D texture features with Gabor filter which captures the properties of spatial localization, orientation selectivity, and spatial frequency selectivity to cope with the variations in illumination. And then for the classification, second is to extract statistical texture features with 2D(PC)2A which performs principal component analysis on the set of combined training images with one single training sample. On classification, we apply the matrix-similarity based kNN classifier to classify a new face. Finally, we implement a set of experiments to evaluate the performance of the proposed scheme.

Proposed Framework

The proposed face recognition system using one training sample is shown in Fig. 1. Firstly, the face image is achieved using camera or video, and the facial texture feature is extracted using 2D Gabor filter, and then the statistical facial texture features are extracted using 2D(PC)^{2}A, and finally the nearest neighbor classifier is applied into classification and the recognition result is displayed.

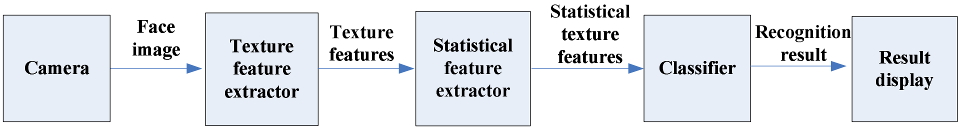
Camera
Face image
Texture feature extractor
Texture features
Statistical feature extractor
Statistical texture features
Classifier
Recognition result
Result display

Fig. 1. Framework of face recognition system

Step 1. Extracting texture feature using 2D Gabor filter

Texture features are extracted with 2D Gabor filter. 2D Gabor function $g(x,y)$ can be defined by $g(x,y)=\left(\frac{1}{2\pi\sigma_x\sigma_y}\right)\exp\left[-\frac{1}{2}\left(\frac{x^2}{\sigma_x^2}+\frac{y^2}{\sigma_y^2}\right)+2\pi j\omega x\right]$, ant its Fourier transform $G(u,v)=\exp\left\{-\frac{1}{2}\left[\frac{(u-\omega)^2}{\sigma_u^2}+\frac{v^2}{\sigma_v^2}\right]\right\}$, where ω denotes the center frequency of $G(u,v)$ along the u axis, $\sigma_u=\frac{\sigma_x}{2\pi}$ and $\sigma_v=\frac{\sigma_y}{2\pi}$ characterize the spatial extent along x and y axes, respectively. A self-similar filter dictionary can be obtained by proper dilations and rotations of $g(x,y)$ through the generation function $g_{mn}(x,y)=a^{-m}g(x',y')$, $a>1$, $m,n\in$ and $\begin{pmatrix}x'\\y'\end{pmatrix}=a^{-m}\begin{pmatrix}\cos\theta & \sin\theta\\-\sin\theta & \cos\theta\end{pmatrix}\begin{pmatrix}x\\y\end{pmatrix}$, where $\theta=n\pi/l$, and l is the total number of orientations, and a^{-m} is the scale factor, and $g(x,y)$ is the mother Gabor wavelet. Let U_l and U_k denote the lower and upper center frequencies of interest, l be the number of orientations, and S be the number of scales in the multi-resolution decomposition respectively. The filter parameters can be $a=(U_h/U_l)^{\frac{1}{S-1}}$, $\sigma_v=\tan\left(\frac{\pi}{2k}\right)\left[U_h-(2\ln 2)\frac{\sigma_u^2}{U_h}\right]\left[2\ln 2-\frac{(2\ln 2)^2\sigma_u^2}{U_h^2}\right]^{-\frac{1}{2}}$, $\sigma_u=\frac{(a-1)U_h}{(a+1)\sqrt{2\ln 2}}$, where $\omega=U_h$ and $m=0,1,\ldots,S-1$. For an image $I(x,y)$, its representation can be defined by $W_{mn}(x,y)=\int I(x,y)g_{mn}^{*}(x-\xi,y-\eta)d_{\xi}d_{\eta}$.

Step 2. Extracting statistical textural feature extraction with 2D(PC)^{2}A

Firstly, creating the combined texture matrix from the $M\times N$ texture matrix $F(m,n)$, and secondly performing 2DPCA on the combined texture matrices.

Step 2.1 Create the combined 2D texture feature matrix.

A combined texture feature matrix is calculated with first-order and second-order projection. Firstly, the first-order texture matrix $P_1(m,n) = (1/MN\overline{F})V_1(m)H_1(n)$ and the second-order matrix $P_2(m,n) = (1/MN\overline{J})V_2(m)H_2(n)$ are calculated, where $V_1(m) = \frac{1}{N}\sum_{p=1}^{N} F(m,p)$, $H_1(n) = \frac{1}{M}\sum_{q=1}^{M} F(q,n)$, $\overline{F}$ is the mean of $F(m,n)$, $V_2(m) = \frac{1}{N}\sum_{n=1}^{N} J(m,n)$, $H_2(n) = \frac{1}{M}\sum_{m=1}^{M} J(m,n)$, $J(m,n) = \left[F(m,n)\right]^2$ and $\overline{J}$ is the mean value of $J(m,n)$. Secondly, the combined texture matrix is calculated with $I_P(m,n) = (1+\alpha+\beta)\left(I(m,n) + \alpha P_1(m,n) + \beta P_2(m,n)\right)$.

Step 2.2 Perform 2DPCA.

Implement 2DPCA to reduce the dimensionality of the combined texture matrix $I_P(m,n)$. The low-dimensional statistical texture feature matrix Y of a combined texture feature matrix F_p with $Y = I_p W_{opt}$, where $W_{opt} = \{w_1, w_2, ..., w_d\}$ solved through maximizing $J(W) = W^T S_T W$, where $S_T = \frac{1}{C}\sum_{j=1}^{C}\left(F_{pj} - \overline{F_p}\right)^T \left(F_{pj} - \overline{F_p}\right)$.

Step 3 Classifying using Nearest Neighbor Classifier (NNC)

On 2D texture feature matrix, classify a new face F_{new} into the class with the F_k based on the similarity measure $S(F_{new}, F_k) = \min_j \; S(F_{new}, F_j)$, where $S(A,B) = \left(\sum_{j=1}^{d}\left(\sum_{i=1}^{M}\left(a_{ij} - b_{ij}\right)^2\right)^{(1/2)p}\right)^{1/p}$, where $A = (a_{ij})_{M\times d}$ and $B = (b_{ij})_{M\times d}$.

Experimental Results

To quantitatively assess and fairly compare the methods that aim at addressing the one sample per person problem, we evaluate the proposed scheme on ORL [5] and Yale [1] databases under the variable illumination conditions according to a standard testing procedure. We randomly choose one face image per person as the training sample, and the rest face images are to test the performance of proposed scheme. That is, the rest 9 test samples are to test on ORL face database, while 10 test samples per person are to test the performance on Yale face database. The average recognition accuracy rate is to evaluate the performance of the recognition accuracy, and we implement the experiments for 10 times and 11 times for ORL and Yale face database respectively. Some examples are shown in Fig.2. The face images from the databases are achieved under the different poses, illuminations and expressions, especially under the different light conditions. So it is feasible to evaluate the performance of the proposed scheme and testify the feasibility of dealing with the lighting conditions. For purpose of comparison, we implement PCA, (PC)2A, E(PC)2A, and SVD Perturbation algorithms a single training sample based face recognition. The procedural parameters, $\alpha = 0.125$, $\beta = 0.05$, for 2D(PC)2A and E(PC)2A. On texture feature extraction, 2 scales and 4 orientations of Gabor filter is applied to extract the texture feature. As results shown in Table 1, since the texture matrix is extracted with Gabor filter, the proposed scheme performs better than 2D(PC)2A.

(a) ORL (b) Yale

Fig. 2. Example face images of face databases

Moreover, the proposed scheme achieves a highest recognition accuracy compared with other popular methods including PCA, (PC)2A, E(PC)2A, and SVD Perturbation algorithms. On computation efficiency and saving space, the proposed scheme and 2D(PC)2A perform better than E(PC)2A or (PC)2A owing its direct computing matrix instead of mapping into 1D vector. So, the proposed scheme is more feasible for the practical face recognition system. The proposed scheme gives a highest recognition rate compared with other popular methods, but the highest recognition rate is still not so high owing to PIE (Pose, Illumination and Expression) problem. Obviously, face recognition with one training sample per person is an important but a challenging problem in theory and application.

Table I. Recognition accuracy on ORL and Yale face databases

Algorithms	ORL	Yale
PCA	54%	54%
2DPCA	54%	56%
SVD Perturbation	55%	54%
(PC)2A	56%	55%
E(PC)2A	57%	56%
2D(PC)2A	60%	61%
Proposed scheme	65%	67%

Conclusion

In this paper, we propose a novel face recognition scheme with single training sample using 2D Gabor filter and 2D(PC)2A under varying light conditions, which aims to solve the single training sample problem owing to hard collecting training samples endured by the current face recognition system. The proposed scheme is consisted of three stages, one is to extract 2D texture feature extract with Gabor filter which captures the properties of spatial localization, orientation selectivity, and spatial frequency selectivity to cope with the variations in illumination, and second is to extract statistical texture features under one training sample with 2D(PC)2A, and third is to classify a new face for recognition with matrix-based similarity nearest neighbor classifier.

Acknowledgements

This work is s supported by Natural Science Foundation for young teachers of Harbin University of Commerce under Grant HCUL2013007.

References

[1] Belhumeur P. N., Hespanha J. P., Kriegman D. J. “Eigenfaces vs. Fisherfaces: Recognition Using Class Specific Linear Projection”. IEEE Trans. Pattern Analysis and Machine Intelligence, vol. 19, no. 7, pp.711-720, July 1997.

[2] Wu J. and Zhou, Z. H., “Face Recognition with one training image per person”. Pattern Recognition Letters, vol. 23, no. 14, pp.1711-1719, May 2002.

[3] Chen S. C., Zhang D.Q., and Zhou Z. H., “Enhanced (PC)2A for face recognition with one training image per person”. Pattern Recognition Letters, vol. 25, no. 10, pp. 1173-1181, October 2004.

[4] Zhang D. Q., Chen S. C., and Zhou Z. H., “A new face recognition method based on SVD perturbation for single example image per person”. Applied Mathematics and Computation, vol.163, no.2, pp. 895-907. February 2005.

[5] Samaria F. and Harter A., “Parameterisation of a Stochastic Model for Human Face Identification ”, Proceedings of 2nd IEEE Workshop on Applications of Computer Vision, Sarasota FL, December 1994.

Applied Mechanics and Materials Vol. 596 (2014) pp 316-321
© (2014) Trans Tech Publications, Switzerland
doi:10.4028/www.scientific.net/AMM.596.316

A Local Optical Flow Constraint Target Extracting Algorithm of Kalman Filter Based on Background Modeling

WANG Yan Ni*

School of information and control engineering, Xi'an University of architecture and technology

Xi'an, China

710055

Keywords: target extracting, Kalman filter, background modeling, optical flow constraint

Abstract. Owing to the problems of inter frame difference method cannot extract the entire target and most optical flow algorithms with computational time, poor real-time performance, a local optical flow constraint target extracting algorithm of Kalman filter based on background modeling is proposed. Firstly use Kalman filter method based on background modeling predict and update the background, then make Lucas-Kanade local optical flow algorithm search the background changing region, finally determine the gray contour, extract target. Compared with the classical algorithms, the simulation results show that new algorithm can extract the moving object quickly and accurately, and has better robustness to the environment changes and target circuitous movement.

Introduction

Moving target extraction is an important research field in computer vision and pattern recognition, is widely used in video surveillance, other monitoring and analysis system. Extracting moving targets from the video sequence is a fundamental and crucial link, is to make the image simplification and easy to understand for further image feature extraction, and has the important influence on the subsequent tracking and analysis processing module.

The methods of target extraction

Target extraction technique is to separate the object from the background image, is to collect the specific meaning with the image space points and area. At present target extraction methods [1] are the following:

The inter frame difference method obtain the moving object contour through differential operation in two adjacent video sequence frames, it can be well applied to the situation of multiple moving objects and camera movement. When the monitoring scene has abnormal object moving, it will appear obvious difference between frames. Subtract two frames, obtain image brightness difference absolute value, judge whether it is larger than the threshold to analysis the motion characteristics, determine whether the image sequence has motion object or not. The inter frame difference method is simple. The complexity of program design is low. It is not too sensitive to the light scene changes. But it can only extract the object boundary, can't extract the whole area of the object.

Optical flow method give a velocity vector to each pixel in the image, form an image motion field. At a given moment, points in the image corresponding to the 3D object points. According to the velocity vector characteristics of each pixel, optical flow methods can dynamic analysis the image. When the moving objects in image, there is relative motion between target and background. The optical flow method can detect moving objects in the case of unknown scene. But its drawback is the computation time, poor real-time and practicality.

Background difference method is a method using current frame and background reference model in the image sequences to detect moving object. Its performance depends on the background modeling techniques. It is one of the commonly used moving object detection methods, especially in the case of fixed camera. When a target enters the static background scene in a video, the variation characteristics of video and static background in the same position of the target can be extracted.

In recent years, researchers at home and abroad carry out extensive study on the extraction method based on background reconstruction, put forward many feasible methods. Literature [2] build the background model, use the adaptive method adjust the parameters of the model, so as to obtain a new background image. It has large amount of calculation. Literature [3] presented a fast real-time multi object combination line scanning point target detection algorithm based on line clustering, which avoids missing detection of the traditional detection algorithm of frame difference method. Foreground detection algorithm Codebook [4] model has higher accuracy and robustness than the traditional target detection algorithm. According to the defect of artificial threshold in clustering, literature [5] proposed an adaptive on-line clustering background. Zhang jing [6] extract the target area based on watershed segmentation, can deal with the object better. Huang [7] using the discrete moment transform graph and local homogeneity criterion obtain seed point of significant objects and targets in images through regional growth. Combining the characteristics of above various methods, put forward a local optical flow constraint object extraction algorithm under the Kalman filtering background modeling, expect to achieve fast and accurate extraction of the target.

The description of algorithm

In view of the advantages and disadvantages of background difference method and optical flow method, we combine the two approaches, make them complementary advantages, overcome the weakness of each other, and improve the effect of motion detection. But in the real scene, due to various reasons such as changing background light, if not timely to update the background image, error results accumulating with time, circulating, resulting in monitoring failure. Therefore, use Lucas-Kanade local optical flow algorithm detect target based on background modeling.

2.1 Kalman filter background modeling method

Modeling and its accuracy of the background image affect the detection effect directly. Any moving object detection algorithm should meet the requirements of processing image scene as far as possible. Because of the complexity of the scene, unpredictable, and the existence of various environmental interference and noise, such as light changes suddenly, some objects fluctuation in the actual background image, camera jitter, make modeling and simulation of background become more difficult. So we need update background selectively.

Kalman filter modeling algorithm believes the background is a steady state system, foreground is a noise. Use temporal recursive low-pass filtering based on Kalman filter theory predict the background image changes slowly, adopt the foreground image update the background, and maintain the stability of background. Kalman filtering is estimation of recursive. As long as obtain background estimation value of previous frame and observed value of the current frame, it can calculate the estimated background value of the current frame. Unlike most filters, it is a pure time domain filter.

$$f_k = Uf_{k-1} + N_{1k} \tag{1}$$

$$d_k = Hf_k + N_{2k} \tag{2}$$

In above formulas, f_k is background value of k image. U is matrix which shows image parameters. d_k is reference value of k frame, H is the parameter matrix of the system background model. N_{1k} and N_{2k} represent the noise of transfer image process and interference, respectively is White Gaussian Noise, the correlation matrix is R_1 and R_2. If the image block is 2×2,

$$U = \begin{bmatrix} 1 & 0 \\ 0 & 1 \end{bmatrix},\ H = [1 \quad 0] \tag{3}$$

$$N_{1k} \sim N(0, R_{1k}),\ N_{2k} \sim N(0, R_{2k}) \tag{4}$$

Kalman filtering background state is represented by the following two variables:

$\hat{f}_{k/k}$ is background estimation value of k image, $C_{k/k}$ is error correlation matrix, which metrics the accuracy of estimate values.

Kalman filtering background modeling operation includes two stages: prediction and update. In the prediction stage, filter using background estimation of previous frame, estimate the background of current frame. In the update stage, filter using observed value of the current frame optimize estimated value obtained in the prediction stage, in order to get a more precise estimated value.

First, we predict the background estimation of k frame,

$$\hat{f}_{k/k-1} = U\hat{f}_{k-1/k-1} \tag{5}$$

Predict covariance matrix of estimated value,

$$C_{k/k-1} = UC_{k-1/k-1}U^T + R_{1k} \tag{6}$$

In formula (5), $\hat{f}_{k/k-1}$ is prediction results of the current k frame using background of previous frame, $\hat{f}_{k-1/k-1}$ is optimal results of previous frame.

In formula (6), $C_{k/k-1}$ is correlation matrix of $\hat{f}_{k/k-1}$, $C_{k-1/k-1}$ is correlation matrix of $\hat{f}_{k-1/k-1}$, R_{1k} is the noise correlation matrix in image transfer process.

Then calculate the following three variables, update the estimate value.

Difference value of reference,

$$d_{1k} = d_k - H\hat{f}_{k/k-1} \tag{7}$$

Covariance of reference difference value,

$$C_{1k} = HC_{k/k-1}H^T + R_{2k} \tag{8}$$

The optimal Kalman gain,

$$Kg_k = C_{k/k-1}H^T C_{1k}^{-1} \tag{9}$$

Update the filter variables f and C, the updated background estimation value is $\hat{f}_{k/k}$,

$$\hat{f}_{k/k} = \hat{f}_{k-1/k-1} + Kg_k d_{1k} \tag{10}$$

The updated covariance estimation value is $C_{k/k}$,

$$C_{k/k} = (I - Kg_k H_k)C_{k/k-1} \tag{11}$$

In above formula, the variable I is the matrix of 1. For the single model of single input, I=1. When getting into the k+1 frame, $C_{k/k}$ is $C_{k-1/k-1}$ in the formula (6). In this way, algorithm updates operations automatically.

If the background model is accurate, the value $\hat{f}_{0/0}$ and $C_{0/0}$ reflect the estimated reference frame background value accurately.

Set the initialization state:

$$\hat{f}_{0/0} = \begin{bmatrix} 0 \\ 0 \end{bmatrix}, \quad C_{0/0} = \begin{bmatrix} 0 & 0 \\ 0 & 0 \end{bmatrix} \tag{12}$$

Covariance matrix reflect the estimated covariance accurately,

$$\begin{aligned} C_{k/k} &= \operatorname{cov}(f_k - \hat{f}_{k/k}) = \operatorname{cov}(f_k - (\hat{f}_{k-1/k-1} + Kg_k d_{1k}) \\ &= \operatorname{cov}((I - Kg_k H)(f_k - \hat{f}_{k/k-1}) - Kg_k N_{2k} \end{aligned} \tag{13}$$

2.2 Lucas-Kanade local optical flow constraint target extraction algorithm

Gradient optical flow method [8] derives the optical flow constraint equation based on the basic assumptions of image gray remained constant before and after movement. Due to optical flow constraint equation cannot determine optical flow exclusively, therefore need to import the other constraints. The Horn-Schunck algorithm is a method of global constraints which is proposed for the smoothness constraint of optical flow, flow of any point in the image are not independent, optical flow changes smoothly within the whole image. Lucas-Kanade algorithm is a method of local constraints that optical flow meets certain constraints in a small region around the given point. Based on Kalman filtering background modeling, using the Lucas-Kanade constraint conditions search the local area, and extract the target.

2.2.1 Optical flow constraint equation

Assuming gray level of the point $I=(x,y)^T$ in the image at time t is $I(x,y,t)$. After a time interval dt, the gray of corresponding point is $I(x+dx,y+dy,t+dt)$. When $dt\to 0$, gray level of the two points unchanged. That is,

$$I(x+dx,y+dy,t+dt)=I(x,y,t) \tag{14}$$

If the gray changes slowly with x,y,t, we can expand Taylor series in the left of formula (14).

$$I(x+dx,y+dy,t+dt)=I(x,y,t)+\frac{\partial I}{\partial x}dx+\frac{\partial I}{\partial y}dy+\frac{\partial I}{\partial t}dt+\varepsilon \tag{15}$$

In above formula, ε represent two-stage infinitely small. Because of $dt\to 0$, it can be ignored,

$$\frac{\partial I}{\partial x}dx+\frac{\partial I}{\partial y}dy+\frac{\partial I}{\partial t}dt=0 \tag{16}$$

$u=\frac{dx}{dt}$, $v=\frac{dy}{dt}$ on behalf of the optical flow in the direction of x, y, $I_x=\frac{\partial I}{\partial x}$, $I_y=\frac{\partial I}{\partial y}$, $I_t=\frac{\partial I}{\partial t}$ represent partial derivative of x,y,t, formula (16) can be written as,

$$I_xu+I_yv+I_t=0 \tag{17}$$

Formula (17) is the basic equation of optical flow field. The following is written in vector form,

$$\nabla\mathbf{I}\,\mathbf{v}_I+I_t=0 \tag{18}$$

$\nabla\mathbf{I}=(I_x,I_y)$ is gradient at point I, $\mathbf{v}_I=(u,v)$ is optical flow of point I. Formula (18) is constraint equation which is the foundation of all the optical flow calculation method based on gradient.

The optical flow constraint equation contains two unknown variables of u and v, so cannot determine the normal component of same gray outline, also need to find new constraints.

2.2.2 Lucas-Kanade local constraint

The Lucas-Kanade method is based on the assumption that the optical flow of each point in a small region as the center of point I is same. Set different weights of different points, so the calculation of optical flow can convert to the minimum value question of the following equation,

$$\sum_{x\in\omega}a\mu^2(x)\left[\nabla\mathbf{I}(x,t)\mathbf{v}_I+\mathbf{I}_t(x,t)\right]^2=0 \tag{19}$$

In above formula, ω represents a small area as the center of point I. $\mu(x)$ represents the mean value of each point in the area. The nearer each points away from the point I, the smaller the radius. a is regional parameter. For the n points in the neighbor of ω, the solution of formula (19) can be obtained by the following equation,

$$\begin{aligned}&\left(\nabla\mathbf{I}(\mathbf{x}_1),\nabla\mathbf{I}(\mathbf{x}_2),\dots,\nabla\mathbf{I}(\mathbf{x}_n)\right)^{2T}a\mu^2\left(\nabla\mathbf{I}(\mathbf{x}_1),\nabla\mathbf{I}(\mathbf{x}_2),\dots,\nabla\mathbf{I}(\mathbf{x}_n)\right)^T v_I\\&=\left(\nabla\mathbf{I}(\mathbf{x}_1),\nabla\mathbf{I}(\mathbf{x}_2),\dots,\nabla\mathbf{I}(\mathbf{x}_n)\right)a\mu^2\left(\mathbf{I}_t(\mathbf{x}_1),\mathbf{I}_t(\mathbf{x}_2),\dots,\mathbf{I}_t(\mathbf{x}_n)\right)^T\end{aligned} \tag{20}$$

$$\begin{aligned}&v_I=\left(\nabla\mathbf{I}(\mathbf{x}_1),\nabla\mathbf{I}(\mathbf{x}_2),\dots,\nabla\mathbf{I}(\mathbf{x}_n)a\mu^2\left(\nabla\mathbf{I}(\mathbf{x}_1),\nabla\mathbf{I}(\mathbf{x}_2),\dots,\nabla\mathbf{I}(\mathbf{x}_n)\right)^T\right)^{-1}\\&\left(\nabla\mathbf{I}(\mathbf{x}_1),\nabla\mathbf{I}(\mathbf{x}_2),\dots,\nabla\mathbf{I}(\mathbf{x}_n)\right)a\mu^2\left(\mathbf{I}_t(\mathbf{x}_1),\mathbf{I}_t(\mathbf{x}_2),\dots,\mathbf{I}_t(\mathbf{x}_n)\right)^T\end{aligned} \tag{21}$$

The constraint equations of moving images are linear equations in speed plane of (u,v). If we consider the k frames of continuous in image sequence, motion velocity of target remained unchanged in the k frame image. For the moving object, the k constraint straight lines in equations can be considered at one point in the velocity plane. So we can combine with the two constraint equations, obtain the two variables of u and v, and determine the target contour curve.

Flow chart of the local optical flow constraint target extracting algorithm of Kalman filter background modeling is as follows:

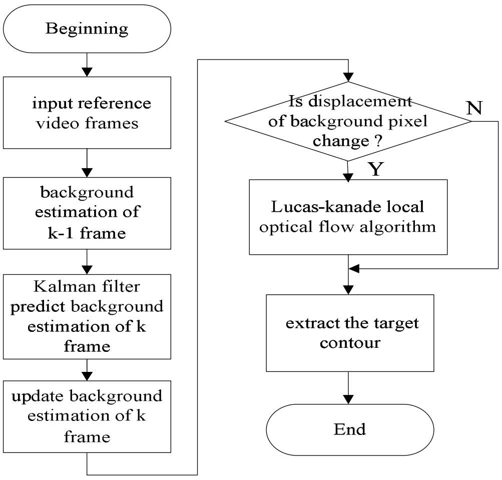
Beginning
input reference video frames
background estimation of k-1 frame
Kalman filter predict background estimation of k frame
update background estimation of k frame
Is displacement of background pixel change ?
N
Y
Lucas-kanade local optical flow algorithm
extract the target contour
End

Fig. 1 Flow chart of the local optical flow constraint target extracting algorithm of Kalman filter background modeling

The analysis of simulation

Let's do comprehensive tests of the new algorithm. The simulation environment in Intel (R) Core (TM) 2 Duo CPU E7400, frequency 2.80GHz, configuration memory 1.00GB in PC machine. The software is version MATLAB 7.0 and above. Detect the self recorded video in which the resolution of image frames is 320×240. The simulation results are shown as follows:

Experiment 1, multiple moving targets

Using the background difference algorithm (BDA), classic optical flow algorithm (OFA) and the new algorithm, extract the multiple moving targets in video sequences of autodyne. Take one frame from the video, the results are as follows:

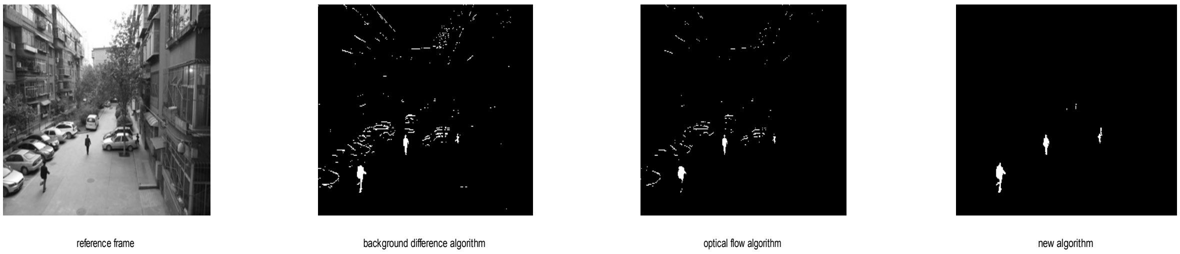
reference frame
background difference algorithm
optical flow algorithm
new algorithm

(a) Reference frame (b) The result of BDA (c) The result of OFA (d) The result of new algorithm

Fig. 2 The extraction results of multiple moving targets

Experiment 2, small moving targets

Using the background difference algorithm, classic optical flow algorithm and the new algorithm, extract the small moving targets in video sequences of autodyne. The results are as follows:

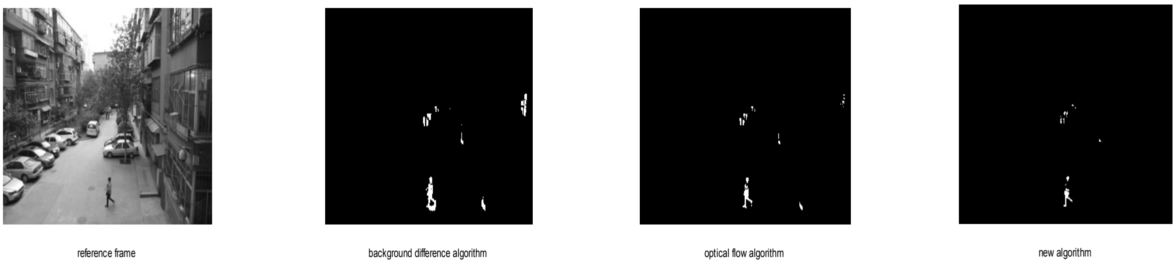
reference frame
background difference algorithm
optical flow algorithm
new algorithm

(a) Reference frame (b) The result of BDA (c) The result of OFA (d) The result of new algorithm

Fig. 3 The extraction results of small moving targets

Experiment 3, the compares of MSE

Using the BDA, OFA and the new algorithm, extract the target in 200 frames of the first video stream and 300 frames of the second video stream. The results of Mean Square Error between extracting target of three algorithms and the actual target are as follows:

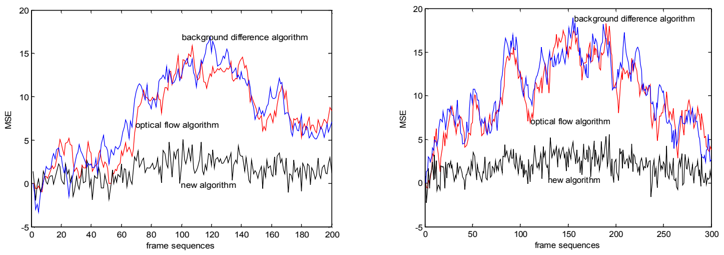

(a) The MSE of first video stream (b) The MSE of second video stream

Fig. 4 The MSE of video stream

The above experiments simulate and extract moving targets for various video streaming with the three algorithms. In experiment 1 and experiment 2, the new algorithm has good detection effect for multiple targets and small targets. In experiment 3, compared with the background difference algorithm, optical flow algorithm, the new algorithm obtains the smallest of mean square error for different video streams and different number of frames.

Conclusions

According to the advantages and disadvantages of background difference method and optical flow method, we propose a new local optical flow constraint object extraction algorithm based on Kalman filter background modeling. Predict background and update constantly using Kalman background modeling, do recursive estimate for pixels in background changed region using Lucas-Kanade local optical flow constraint algorithm, finally determine gray contour and extract the target. Experiments show that the new algorithm has good effect on the extraction of target. The next step we will continue analysis the new algorithm, apply it to video surveillance, other monitoring and analysis system, expect to get better detection effect.

Acknowledgements

This work was financially supported by the Shaanxi Province Social Development Research Project (2013K13-04-08), Xi'an University of Architecture and Technology Basic Research Project (JC1319).

References

[1] Yao Min. Digital image processing (Second Edition). Beijing: mechanical industry press (2013)

[2] HASSANPOUR H，SEDIGHI M，MANASHTY A R. Video frame’s background modeling: reviewing the techniques. Journal of Signal and Information Processing, 2011,2(2),72-78

[3] Ye You-shi, Tang Lin-bo, *et al*. A fast deep-space infrared multi-target detection algorithm based on clustering. Journal of Electronics & Information Technology, 2011,31(1),77-84

[4] Xiong Liang and Liu Wei-ming. Foreground detection algorithm based on background codebook model. Science Technology and Engineering, 2010,10(9),2118-2121

[5] Xia Jie, Wu Jian, Chen Jian-ming. Adaptive background extraction based on online clustering, Computer Engineering. 2011,37(3),169-171

[6] Zhang Jing, Shen Lan-sun, Gao Jing-jing. Regions of interest detection based on visual attention mechanism. Acta Photonica Sinica, 2009,38(6),1561-1565.(in Chinese)

[7] Huang C B, Liu Q, Yu S S. Region of interest extraction from color image based on visual saliency [J]. The Journal of Supercomputing, 2011,58(1),20-33

[8] Zhang De-feng. Digital image processing (MATLAB Edition). Beijing: People's Posts and telecommunications press (2011)

Applied Mechanics and Materials Vol. 596 (2014) pp 322-327

© (2014) Trans Tech Publications, Switzerland

doi:10.4028/www.scientific.net/AMM.596.322

A novel HOG descriptor with spatial multi-scale feature for FER

TONG Ying[1,a], Jiao Liangbao[1,b] and Cao Xuehong[1,c]

[1]Department of Communication Engineering, Nanjing Institute of Technology, P.R.C

[a]tongying@njit.edu.cn, [b]jiaoliangbao@njit.edu.cn, [c]caoxh@njit.edu.cn

Key words: Histograms of Oriented Gradients; Spatial Multi-Scaled; Facial Expression Recognition; Canny Gradient

Abstract. HOG Feature is an efficient edge information descriptor, but it ignores the spatial arrangement of local FER features. In this respect, this paper puts forward a spatial multi-scale model based on an improved HOG algorithm which uses canny operator instead of traditional gradient operator. After the image is divided into a series of sub-regions layer by layer, the histogram of orient gradients for each sub-region is calculated and connected in sequence to obtain the spatial multi-scale HOG feature of whole image. Compared with traditional HOG and the improved PHOG, the proposed SMS_HOG algorithm acquires 5% recognition rate improvement and 50% processing time reduction.

Introduction

Facial expression is an effective and important non-verbal communication method which includes almost 55% information of the emotion[1]. The study on Facial Expression Recognition (FER) is of promising prospect and becoming the research focus recently[2-5]. Facial feature extraction is the key of FER. Several methods have been proposed for this, which include Local Binary Pattern (LBP)[4-5],Gabor wavelet translate[2], Scale-invariant feature transform(SIFT)[7], and Histograms of oriented gradients (HOG)[3,8,9,10,11]. Among these algorithms, LBP descriptor is sensitive to neighbor gray value changes and noise effect, which has the lowest recognition rate; Gabor wavelet transformation and SIFT algorithm are both highly complex for their high feature dimension, and inconvenient in real-time applications.

To solve problems above, Dalal proposes a new shape descriptor, Histograms of oriented gradients (HOG) [8], which extracts the image edge features by gradient direction distribution and is robust to noise. Compared with traditional feature descriptor, LBP, Gabor and SIFT, the descriptor dimension is reduced significantly while the edge information is described efficiently[8,9,10]. Therefore, it is very suitable for real time applications. HOG is now studied for various feature abstraction, i.e. shape[3,9], face[10] and text[11], although it is firstly proposed for pedestrian detection.

Because traditional HOGs ignore the edge profile from different scales which is important in FER applications, this paper proposes a spatial multi-scale HOG algorithm. In this algorithm, the image is refined into a series of sub-regions at different scales layer by layer firstly. Then, an improved HOG operator based on canny gradients is adopted to calculate the gradient direction histogram for each sub-region. This new operator considers the characteristic shape of the edge as well as the inherent texture of fold expression information on the face. Finally, gradient direction histograms of each layer and each block are connected sequentially to obtain the "spatial multi-scale" HOG feature (SMS_HOG) of whole image. Experiments on JAFFE database demonstrate the efficiency of this new algorithm. Compared with traditional features operators such as LBP, Gabor, HOG etc., the SMS_HOG has a significant improvement in both the recognition rate and running time.

Traditional HOG Algorithm and its Improvement

The basic idea of HOG algorithm is that the shape of the target object can be described by calculating its gradient direction. In traditional HOG[8], by using 1D differential template [-1,0,1], the gradient magnitude is $m(x,y)=\sqrt{[I(x+1,y)-I(x-1,y)]^2+[I(x,y+1)-I(x,y-1)]^2}$, and the gradient direction is $\theta(x,y)=\arctan(\frac{I(x,y+1)-I(x,y-1)}{I(x+1,y)-I(x-1,y)})$ which is limited to $[0,\pi]$. $I(x,y)$ is the gray value of pixel (x,y). The direction $\theta(x,y)$ is divided into 8 bins.

The image is divided into 8×8 pixel groups called as block and each block is made up with four cells (4×4 pixels). For each cell, HOG is accumulated by adding up $m(x,y)$ according to the direction grouping, which is 8-dimension vector. The block HOG is the connection of the 4 cell HOGs, whose dimension is 32. After concatenating all block HOGs according to their positions, the image HOG characteristics is obtained. It also needs L2-norm normalization. Because 128×128 image can be divided into $16\times16=256$ non-overlapping blocks, so its HOG feature vector length is 256 × 32=8192. The gradient direction distribution of each pixel in one block is described as (a) in Fig.1 and the arrows represent the gradient direction. Accordingly, four cell HOGs are shown as (b) in Fig.1.

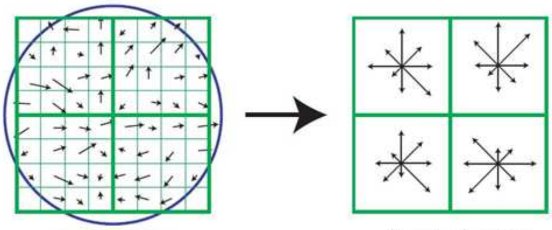

a. Gradient direction b. Key point description

Fig. 1 The extraction process of HOG feature

There are two key points in the HOG algorithms. The first is the gradients information abstraction. Generally, Simple 1-D [-1; 0; 1] masks works best for object detection applications[8]. But, this conclusion may be not proper to FER because the emotion is related to not only the overall facial profile but also many particulars around the facial organs. The second is the feature structure. Traditional HOG algorithms ignore the gradient information from different scales for their image descriptors are just formed by concatenating all the block descriptors of the same resolution. Anna Bosch proposed pyramid histogram of oriented gradients (PHOG)[9]. But his image descriptors still only contain block descriptors of one resolution, even if this resolution is selected through studying and optimizing. In other words, up to now, the problem of insufficient characterization for FER still exists in HOG algorithms.

Spatial Multi-Scale HOG Feature for FER

To express the particular information around the facial organs more efficient, we use canny template to calculate the gradient amplitude and gradient direction. So, the gradient magnitude is $m(x,y)=\sqrt{[G_x(x,y)]^2+[G_y(x,y)]^2}$, where $G_x(x,y)=\frac{1}{2}[I(x,y+1)-I(x,y)+I(x+1,y+1)-I(x+1,y)]$

is the horizontal gradient and $G_y(x,y)=\frac{1}{2}[I(x,y)-I(x+1,y)+I(x,y+1)-I(x+1,y+1)]$ is the vertical gradient. The gradient direction is $\theta(x,y)=\arctan(\frac{G_y(x,y)}{G_x(x,y)})$.

The new canny gradient operator can express the facial feature more efficiently for its gradient computation, which can be seen in the gradient imaging of Fig.2. Compared to the traditional HOG operator, the edge of the new gradient calculation is sharper and the detail is richer obviously when the new gradient operator is adopted.

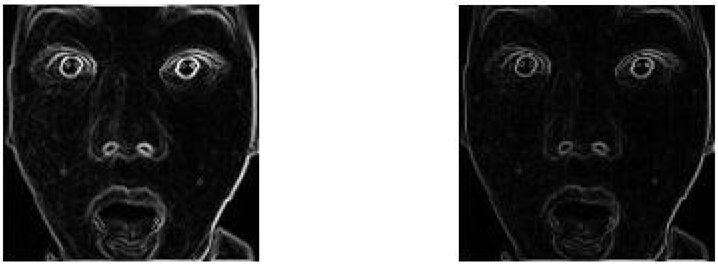

(a) Magnitudes of improved HOG gradient (b) Magnitudes of traditional HOG gradient

Fig.2 Magnitudes imaging of different HOG gradient

On the other hand, to contain the gradient information from different scales, Spatial Multi-Scaled HOG (SMS-HOG) algorithm is proposed to describe the shape and spatial layout of one object simultaneously. Meantime, to increase the ability of HOG feature to describe expression changes more exactly, i.e. the forehead, eyes and mouth, the $[0,\pi]$ interval is divided into 10 bins. The detail of the SMS-HOG algorithm can be described as below.

First, the 128×128 original image is refined into a series of different-scale blocks layer by layer. There are 4^l blocks on the lth layer, and the block size is $\frac{128}{2^l}\times\frac{128}{2^l}(l=0,1,2...,L-1)$. The layer 0 means the original resolution and the layer l means the minimum resolution. Then, calculate the gradient orientation histogram of each block with above improved HOG operator.

After normalizing the block HOGs in each level with L2-norm, SMS-HOG features of the image is constructed by concatenating layer HOGs layer by layer. The layer HOG is combination of the block HOGs the same as traditional HOG algorithm. The difference of the construction between SMS-HOG feature and traditional HOG is shown in Fig.3. Finally, the dimension of SMS-HOG is $k\sum_{l=0}^{L-1}4^l$, where layer number is l and the bin number is k.

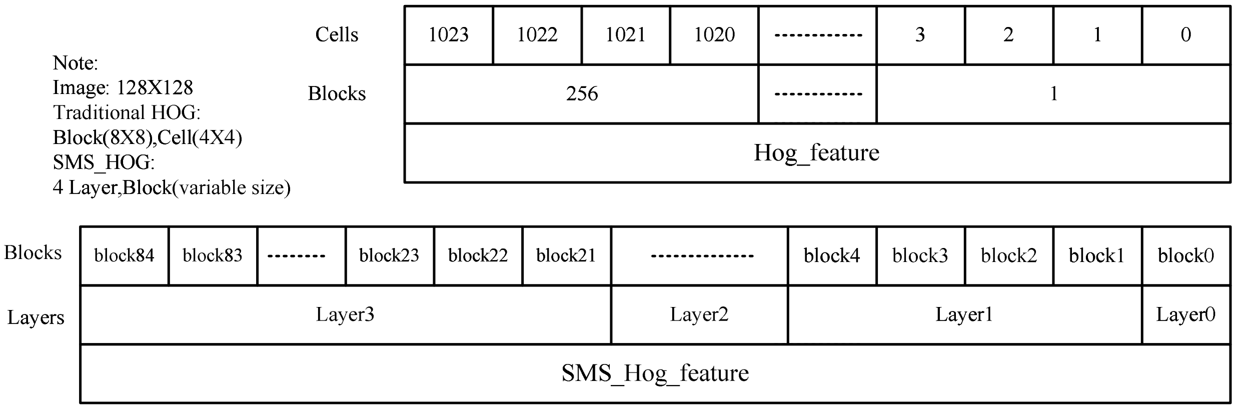
Note:
Image: 128X128
Traditional HOG:
Block(8X8),Cell(4X4)
SMS_HOG:
4 Layer,Block(variable size)
Cells
1023
1022
1021
1020

3
2
1
0
Blocks
256

1
Hog_feature
Blocks
block84
block83
----
block23
block22
block21
----
block4
block3
block2
block1
block0
Layers
Layer3
Layer2
Layer1
Layer0
SMS_Hog_feature

Fig.3 Feature Construction of SMS_HOG

The complete procedure of the SMS-HOG feature abstraction is illustrated in Fig.4. The blocks and cells in three levels of the original image are shown in the above row. The accordingly HOGs are shown in the below row. As we can see, the feature dimension becomes larger when the layer varies from level-1 to level-3. Correspondingly, layer HOG vectors describe the target shape changes from coarse to fine, resulting in good spatial correspondence among local regions. After reconfiguration of feature construction, the dimension of feature vectors is reduced significantly, i.e. from 8192 to 850 as shown in Fig.3.

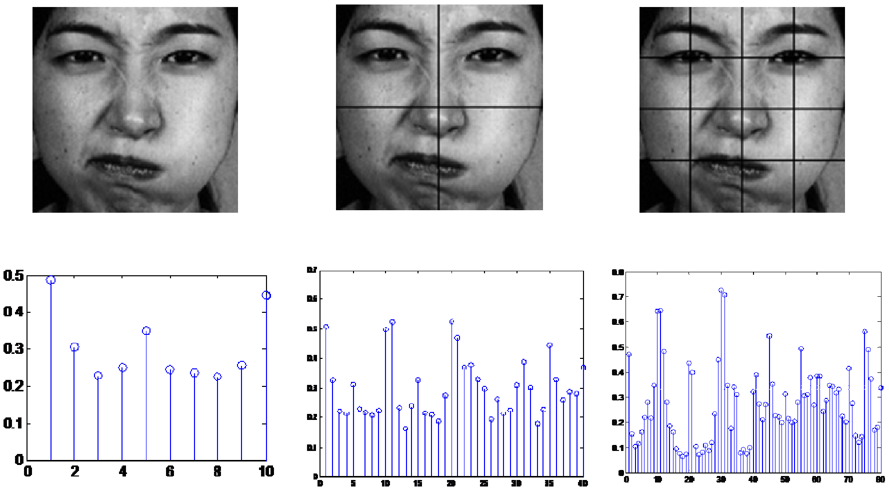

Fig.4 Procedure of the SMS-HOG Feature Abstraction

Experiments and Results Analysis

To check the performance of the propose SMS-HOG algorithm, experiments on JAFFE database are conducted. KNN nearest neighbor classifier is adopted in the classification. JAFFE database is widely accepted as a criterion and used by most researchers. Two kinds of sample selection methods, “leave-one-sample-out” (L-O-Sap-O) and “leave-one-subject-out” (L-O-Sub-O) [2], is utilized in the training process. Method “L-O-Sap-O” is able to select every image’s data as sample to make sure every image’s features are considered, contributing to a better reality. Method “L-O-Sub-O” is usually used to evaluate the recognition skill to unfamiliar facial expressions of the system.

To achieve the best performance, the key parameters of the SMS-HOG, i.e. layer number l and the bin number k, should be determined first. So, we pay attention to the impacts of different layers and bin numbers on the classification accuracy of SMS-HOG features firstly. Results with “L-O-Sap-O” and “L-O-Sub-O” are shown in Fig. 5 and Fig. 6. The spatial multi-scale model has advantages over basic features of operator because it considers the spatial relationship between local features. However, with the increasing of hierarchical layer, the objects’ location and attitude on the image becomes more and more sensitive, that kind of advantage disappears when the layer increase to a limit. From Fig 5, the recognition rate reaches to an optimal situation both on “L-O-Sap-O” and “L-O-Sub-O” ways when $l=4$. Maybe the cause is that background edge information will take more effect and leads to the reduction of recognition rate. From Fig. 6, the recognition rate achieve its optimal when k=10, which is accord with previous research[8,9,10].

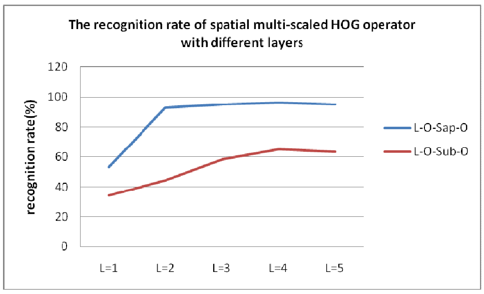

Fig.5 SMS-HOG with different layers

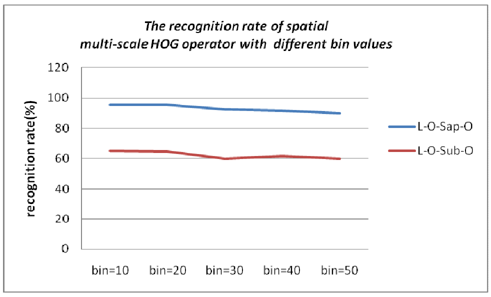

Fig.6 SMS-HOG with different bin values

Then, based on the parameters above, the performance comparison among SMS-HOG algorithm, PHOG and the traditional HOG is achieved as Table.1. Meanwhile, feature dimension and the time-consuming in the process of facial expressions recognition of five operators as mentioned is compared in this table. According to the practical view, only the total process time of method “L-O-Sub-O” is competed. From Table.1, it can be concluded that SMS_HOG gets the highest recognition rate and the lowest computation cost. To PHOG, not only the recognition rate is raised more than 5% by SMS-HOG algorithm for both evaluation methods, but also the classification time is reduced almost 50%. The origin of the classification time reduction is from the smaller feature dimension.

Table.1 Performance comparison between SMS-HOG and Traditional HOGs

Performance indicators	Evaluation Methods	HOG	PHOG	SMS-HOG
feature dimension	Both	8192	1700	**850**
Extraction Time(s)	Both	83.50	17.55	**9.60**
Total Time(s)	L-O-Sub-O	117.85	26.42	**14.11**
Classification Time(s)	L-O-Sub-O	34.35	8.87	**4.51**
Recognition Rate(%)	L-O-Sub-O	57.78	61.67	**65.56**
Classification Time(s)	L-O-Sap-O	761.63	189.62	**88.87**
Recognition Rate(%)	L-O-Sap-O	89.44	88.33	**95.56**

Conclusion

Facial expression recognition is an interdisciplinary challenging topic at the forefront. To express the particular information around the facial organs from different scales more efficient, this paper proposes a spatial multi-scale HOG algorithm, where the image is refined into a series of sub-regions at different scales layer by layer firstly. Then, an improved HOG operator based on canny gradients is adopted to calculate the gradient direction histogram for each sub-region. This new operator considers the characteristic shape of the edge as well as the inherent texture of fold expression information on the face. Finally, gradient direction histograms of each layer and each block are connected sequentially to obtain the "spatial multi-scale" HOG feature (SMS_HOG) of whole image. Experiments on JAFFE database demonstrate the efficiency of this new algorithm. Compared with traditional HOG and the improved PHOG, the SMS_HOG acquires 5% recognition rate improvement and 50% processing time reduction.

Acknowledge

This paper is supported by Jiangsu Natural Science Foundation(BK20131342) and Nanjing Institute of Technology Foundation(QKJA201203)

References

[1] Mehrabian A. Communication without words[J].Psychology Today,1968,2:53~56.

[2] Marios Kyperountas, Anastasios Tefas, Ioannis Pitas. Salient feature and reliable classifier selection for facial expression classification [J].Pattern Recognition,Vol.43,2010:972-986,

[3] Kobayashi T. BFO Meets HOG: Feature Extraction Based on Histograms of Oriented p.d.f. Gradients for Image Classification[C].CVPR 2013:747-754.

[4] M. Heikkilä,M.Pietikäinen,C. Schmid. Description of interest regions with local binary patterns[J]. Pattern Recognition, 2009, vol. 42, no. 3:425–436.

[5] Baochang Zhang,Yongsheng Gao,Sanqing Zhao,et al. Local Derivative Pattern Versus Local Binary Pattern:Face Recognition with High-Order Local Pattern Descriptor[J]. IEEE Transactions on Image Processing,2010,Vol.19,No.2:533-544.

[6] Zheng Yongbin, Huang Xinsheng, Feng Songjiang. An Image Matching Algorithm Based on Combination of SIFT and the Rotation Invariant LBP[J]. Journal of Computer 2 Aided Design & Computer Graphics, 2010 ,Vol.22,No.2:286-292.

[7] Xunyu Pan,Siwei Lyu. Detecting image region duplication using SIFT features[C].ICASSP,2010:1706-1709.

[8] N Dala,B Triggs. Histograms of oriented gradients for human detection[C].IEEE Computer Society Conference on Computer Vision and Pattern Recognition(CVPR05),San Diego,CA,USA,June 25-25,2005:886-893.

[9] Bosch A，Zisserman A，Munoz X. Representing shape with a spatial pyramid kernel [C].International Conference on Image and Video Retrieval(CIVP’2007)，Amsterdam，Netherlands，July 9-11，2007：401-408.

[10] O.Déniz,G.Bueno,J.Salido,et al. Face recognition using Histograms of Oriented Gradients[J].Pattern Recognition Letters,2011,Vol.32:1598-1603.

[11] Rodrigo Minetto, Nicolas Thome, Matthieu Cord, et al. T-HOG: An effective gradient-based descriptor for single line text regions[J].Pattern Recognition,2013,Vol.46:1078-1090.

Applied Mechanics and Materials Vol. 596 (2014) pp 328-332
© (2014) Trans Tech Publications, Switzerland
doi:10.4028/www.scientific.net/AMM.596.328

An Animation Video Resource Conversion System Based on Supercomputers

Kunhua Zhong[1, a], Yuwen Chen[2,b], Leifeng Liu[3,c], Ju Zhang[4,d]

[1,2,3,4]No.266 Fangzheng Avenue,Shuitu Hi-tech Industrial Park, Shuitu Town, Beibei District, Chongqing, China

[a]zhongkunhua@cigit.ac.cn, [b]chenyuwen@cigit.ac.cn, [c]liuleifeng@cigit.ac.cn, [d]zhangju@cigit.ac.cn

Keywords: animation video, conversion system, FFMpeg, HEVC, supercomputer, PyGTK.

Abstract. The rapid development of mobile internet has brought new opportunities to the development of the animation industry, but the network traffic bottlenecks animation video promotion. Based on the super-computing resources, using the Python language, adopting FFMpeg, OpenCV, HEVC and PyGTK technologies, we designed and implemented an animation video resource conversion system to solve the traffic bottleneck in this paper. The conversion system provides HEVC parallel conversion, video serial conversion, video frames extraction and video playback functions, effectively promoted the promotion of animation products distribution.

Introduction

With the rapid development of mobile internet, the increasing replacement of mobile terminals, as well as the three-screen (computers, televisions, and mobile phone screen) integration is becoming an irresistible trend, the development of animation industry ushered in a new opportunity and a new channel is discovered for the promotion of animation product. However, due to their mobile Internet traffic bandwidth limitations themselves and high costs, ordinary users were limited while watching animation videos via mobile internet. The bigger the animation files are, the more traffic takes for downloading, the higher cost needs. Large video files have become a stumbling block for the animation promotion in the mobile internet. Video compression and conversion become an indispensable disposing means.

Currently, there are already a lot of video conversion software, such as Format Factory, Storm Transcoding, MediaCoder, and winFF, supporting video conversion between almost all the formats. However, these software do not support the extraction of video frames, and also do not support the latest HEVC video encoding. Moreover, all of them are stand-alone version, so the conversion speed will be very slow for the large amount of computation of HEVC.

In addition, there also are some audio/video solutions with the form of static/dynamic library or build version, such as FFMpeg [2]. However, FFMpeg library only offers some application programming interfaces, not integrated. We need secondary development, inconvenient to use [9,10]. The only way to use the build version of FFMpeg is command line, and it is for a single video, not for batch processing.

In this paper, using Python as the programming language, developing user interface with PyGTK, MPI parallel implementing HEVC video encoding based on the super-computing resources, we design and implement an animation video resource conversion system, which provides HEVC parallel conversion, video serial conversion, video frames extraction and video playback functions. The rest of this paper is organized as follows. In the next two sections we give the system designation and implementation in details. And the last section concludes this paper.

System Designation

Based on super-computing resources, this system implements an animation video resource conversion system using parallel technology [3,4,5]. The overall system architecture is divided into five layers. On the bottom layer, the animation video resource conversion hardware platform is built based on the computing and storage resources. The various computing resources communicate with each other via high speed Infiniband network. The middle layer is a customized Cent OS. Above the OS layer, in this paper, we develop an animation video resource conversion system based on the third-party libraries. User API interfaces are provided in the top layer of our system. The overall architecture diagram is shown in Fig. 1.

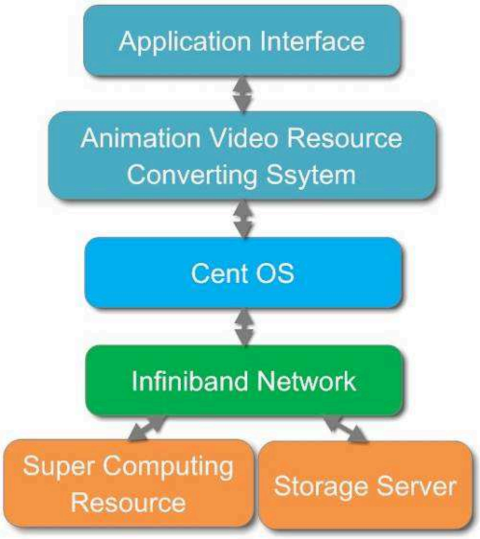
Application Interface
Animation Video Resource Converting Ssytem
Cent OS
Infiniband Network
Super Computing Resource
Storage Server

Fig. 1: System architecture diagram

System hardware layer concludes CB65-G dual blade servers and a Parastor100 parallel file system, and its storage capacity is up to 10TB. Via high-speed Infiniband network, the network layer connects computing resources and storage resources, to provide a communication link for the animation video resource conversion system. Conforming to MVC pattern [6], the animation video resource conversion system includes the view module, controller module, parameters setting module and functionality module. The relation of them is shown in Fig. 2.

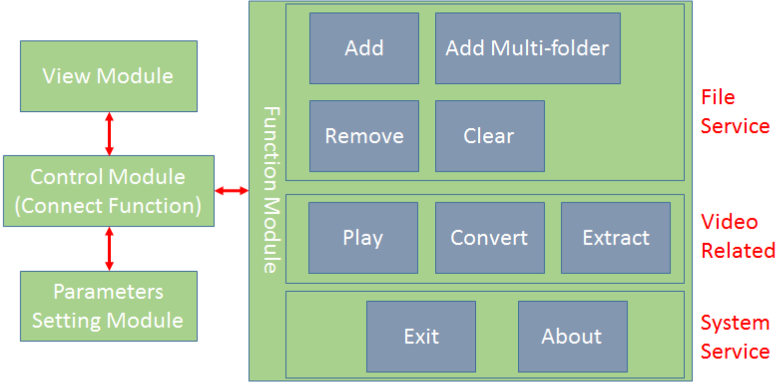
View Module
Control Module (Connect Function)
Parameters Setting Module
Function Module
Add
Add Multi-folder
Remove
Clear
File Service
Play
Convert
Extract
Video Related
Exit
About
System Service

Fig. 2: Relation of modules

The view module provides the user interface, including the main interface, parameters setting pages and help page. The parameters setting module is responsible for setting the video conversion parameters and video frames extraction parameters. The functionality module provides external interfaces and services, including three types of function, that is, file service class, video related class and system service class. The controller module is responsible for controlling the association between each modules.

System Implementation

System Functionality. Our animation video resource conversion system includes four major functions: HEVC parallel conversion, video serial conversion, video frames extraction and video playback. The main interface is shown in Fig. 3.

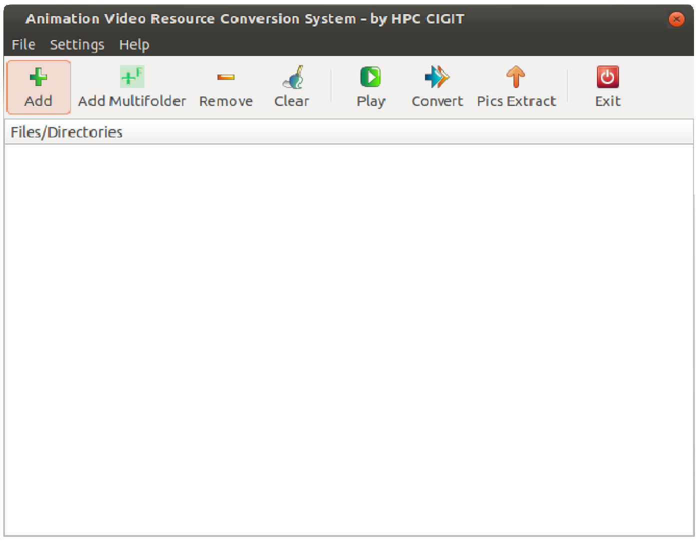
Animation Video Resource Conversion System - by HPC CIGIT
File Settings Help
Add
Add Multifolder
Remove
Clear
Play
Convert
Pics Extract
Exit
Files/Directories

Fig. 3: The main interface of the animation video resource conversion system

HEVC parallel conversion function: Converting single video or batch videos under the same directory recursively with HEVC parallel implementation. We can specify the video output format, output directory, output video encoding and whether to overwrite existing files.

Video serial conversion function: Serially converting single video or batch videos under the same directory recursively. We can specify the video output format, output directory, output video encoding and whether to overwrite existing files. The conversion system supports conversion between popular video formats.

Video frames extraction function: For single video or batch videos under the same folder, extracting video frames, output formatted pixels data. We can specify extraction rate, output path, output picture size, maximum pictures to be extracted, maximum videos to be processed, maximum capacity of single output folder, whether to output formatted pixels data, maximum pictures contained in single formatted batch data file.

The video playback function: Play the selected videos. We can play multi-videos simultaneously.

Functionality Implementation. The animation video resource conversion system takes Python as its programming language, develops user interface with PyGTK [1], plays video by calling FFPlay [10], implements video serial conversion based on the third-party libraries, implements HEVC parallel conversion based on the super-computing resources via MPI [7,8] and implements video frames extraction based on FFMpeg and OpenCV. Video conversion and video frames extraction are encapsulated into Python modules, and called with the form of C extension of Python, to improve processing speed.

- Implementation of Video Frames Extraction Function

Via C extension of Python, we implement this function based on the third-party libraries. Video frames are decoded by using FFMpeg library, and pictures are scaled and saved by using OpenCV library. Firstly, we register all the container format and CODEC, and then open the input video file, find the video stream, open the corresponding codec, decode frames and save them, at last free memories and close input video file. The processing flow is shown in Fig. 4.

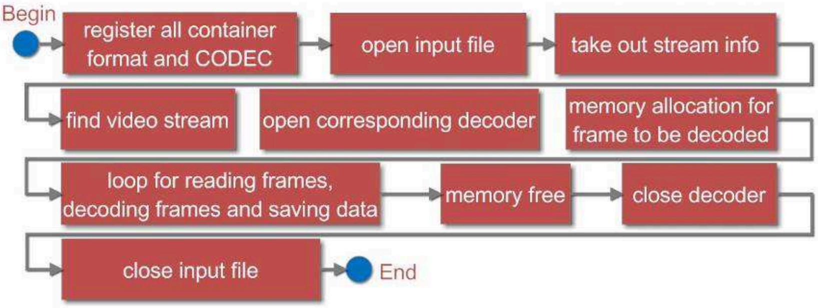
Begin
register all container format and CODEC
open input file
take out stream info
find video stream
open corresponding decoder
memory allocation for frame to be decoded
loop for reading frames, decoding frames and saving data
memory free
close decoder
close input file
End

Fig. 4: Video frames extraction flow

- Implementation of Video Serial Conversion Function

Via C extension of Python, we implement this function based on FFMpeg library. Encoding flow and decoding flow are implemented via two independent threads. The two threads share one YUV420P data buffer, whose size is determined by the frame count needed by the codec flow. In the decoding flow, frames are decoded continuously to generate YUV420P data. When the shared buffer is full, the decoding flow is suspended. In the encoding flow, we get the YUV420P data from shared buffer, execute encoding processing and audio/video synthesis to generate the output video file. The processing flow is shown in Fig. 5.

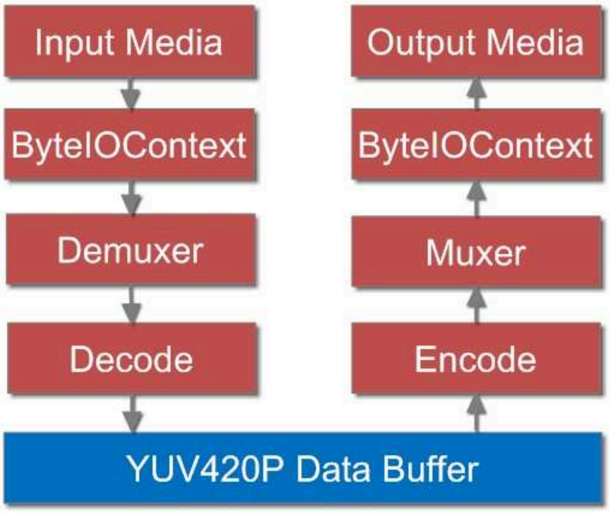
Input Media
ByteIOContext
Demuxer
Decode
Output Media
ByteIOContext
Muxer
Encode
YUV420P Data Buffer

Fig. 5: Video serial conversion flow

- Implementation of HEVC parallel Conversion Function

Based on HM, the reference software of HEVC, we do not change the internal compression algorithm processes, and compress the input YUV420P format video data by segmenting it in chronological order with MPI implementation. The original YUV420P video data will be read in the form of shared memory. Each computing core reads one video data segment on a continuous period of time, and then compresses this data segment, to get the corresponding binary code stream and stored it as file. After the completion of all the cores, all the binary code streams will be combined into a single file. As shown in the diagram Fig. 6.

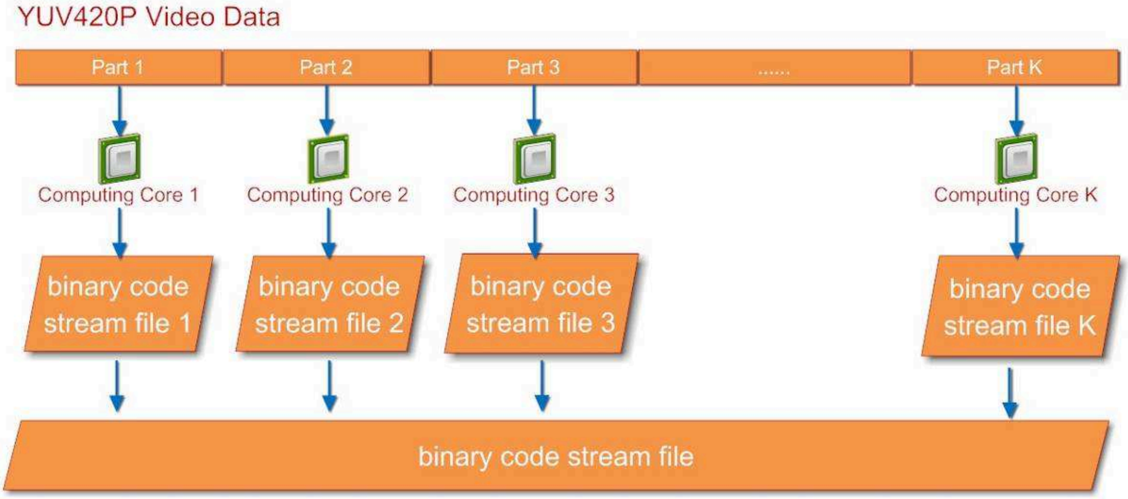
YUV420P Video Data
Part 1
Part 2
Part 3
......
Part K
Computing Core 1
Computing Core 2
Computing Core 3
Computing Core K
binary code stream file 1
binary code stream file 2
binary code stream file 3
binary code stream file K
binary code stream file

Fig. 6: HEVC parallel processing diagram

Conclusions

In this paper, based on the super-computing resources, using the Python language, employing FFMpeg, OpenCV, HEVC and PyGTK technologies, we design and implement an animation video resource conversion system, which provides HEVC parallel conversion, video serial conversion, video frames extraction and video playback functions. With our conversion system, marketing and distribution of animation products are stimulated, content-based animation video retrieval is facilitated, and animation industry is promoted. However, this system is only a back-end system running on the server. We can provide external services with the B/S architecture in the future.

Acknowledgements

This work was financially supported by the National Science and Technology Ministry (2013BAH25F02).

References

[1] Dave Aitel: A beginner's guide to using pyGTK and Glade. Linux Journal, Vol. 2003 Issue 113 (2003), p. 72-78

[2] REN Yan, HAN Zhen, LIU Li: System of convert and distribute of videos based on FFMPEG (In Chinese). Computer Engineering and Design, Vol. 28 No. 20 (2007), p. 4962-4967

[3] Oliner, A., Stearley, J.: What Supercomputers Say: A Study of Five System Logs. Dependable Systems and Networks, 2007. DSN '07. 37th Annual IEEE/IFIP International Conference on, p. 575-584

[4] Hisham Mohamed, Stéphane Marchand-Maillet: MRO-MPI: MapReduce overlapping using MPI and an optimized data exchange policy. Parallel Computing, Vol. 39, Issue 12 (2013), p. 851-866

[5] Nicholas T. Karonis, Brian Toonen, Ian Foster: MPICH-G2: A Grid-enabled implementation of the Message Passing Interface. Journal of Parallel and Distributed Computing, Vol. 63, Issue 5 (2003), p. 551-563

[6] Leff, A., Thomas J., Rayfield, J.T.: Web-application development using the Model/View/Controller design pattern. Enterprise Distributed Object Computing Conference, 2001. EDOC '01. Proceedings. Fifth IEEE International, p. 118-127

[7] Jens-Rainer Ohm, Gary J. Sullivan, Heiko Schwarz: Comparison of the Coding Efficiency of Video Coding Standards—Including High Efficiency Video Coding (HEVC). IEEE Transactions on Circuits and Systems for Video Technology, Vol. 22, No. 12 (2012), p. 1669-1684

[8] Gary J. Sullivan, Jens-Rainer Ohm, Woo-Jin Han, Thomas Wiegand: Overview of the High Efficiency Video Coding (HEVC) Standard. IEEE Transactions on Circuits and Systems for Video Technology, Vol. 22, No. 12 (2012), p. 1649-1668

[9] ffmpeg documentation on http://ffmpeg.org/ffmpeg-all.html

[10] ffplay documentation on http://ffmpeg.org/ffplay-all.html

Applied Mechanics and Materials Vol. 596 (2014) pp 333-336
© (2014) Trans Tech Publications, Switzerland
doi:10.4028/www.scientific.net/AMM.596.333

An Image De-noising Algorithm Based on K-SVD and BM3D

Li Jun

Jiangxi University of Technology, Nan Chang, China

lijun@163.com

Keywords: de-nosing, sparse representation, K-SVD, dictionary learning

Abstract. The existence of noise affects the quality of the image seriously. The image de-noising algorithm based on KSVD appears fuzzy, where weak texture smooth area also can appear false textures, at the same time, when the noise was very big, the de-noising effect would not always be ideal. This paper proposed an image de-noising method based on K-SVD dictionary and BM3D. The algorithm can solve image weak texture fuzzy problems and weak edges effectively. The experimental results show that, compare with K-SVD de-noising algorithm, this algorithm has a good de-noising ability, which keeping the detail and the edge character of the image better.

Introduction

Redundant dictionary based on the sparse representation of image de-noising method can effectively capture the image of complex features, has a good de-noising effect, the method focuses on the structure of the redundant dictionary, early redundant dictionary like Curvelets, Contourlets, Bandelets their waveform is fixed, they cannot be good for all image sparse representation. And the method based on dictionary learning can according to the characteristics of the image itself is obtained by learning the redundant dictionary, it can adaptively sparse representation of image signals.

The sparse representation model based on redundant dictionary

Based on redundant dictionary of sparse representation of the basic idea is to use redundant dictionary to replace the traditional method of orthogonal basis, from the redundant dictionary can select the optimal signal of a linear combination of the number of dictionary atoms to approximate to the original signal.

Matching pursuit algorithm is iterative way from the redundant dictionary selection and in turn signal to signal the matching dictionary atoms that, residual error, at the same time when the residual is reduced to a certain extent we can approximate to think we have to pick up the useful component in the signal to the, the residual noise is part of the rest. By matching pursuit algorithm of signal sparse coefficient, we can use the coefficient matrix and the redundant dictionary after de-noising signal.

In applying these ideas to the actual image processing, we have to consider the factor: The structure of the redundant dictionary.

We want to get the image signal sufficiently sparse representation, you must request to construct the redundant dictionary can be said there is enough good ability, the image signal and traditional based on fixed basis function and structure of redundant dictionary weren't very good for all of the images. So we have to design a kind of can according to the image itself content adaptive structure redundant dictionary method.

The sparse representation of image de-noising based on redundant dictionary

The sparse representation of image de-noising model based on redundant dictionary expressed in the type:

$$\{a_{ij}, X\} = \arg\min_{a_{ij}} \lambda \parallel X - Y \parallel_2^2 + \sum_{ij} \mu_{ij} \parallel a_{ij} \parallel_0 + \sum_{ij} \parallel Da_{ij} - R_{ij}X \parallel_2^2 \qquad (1)$$

Y is noise image, X is the image after de-noising, and the first is the right type noise image de-noising and image similarity degree of constraint. The second and the third are sparse constraint of each image block. Matrix R is an image with size n * N index matrix, R_{ij} for extraction in the image coordinates of (i, j) and size of the image block is$\sqrt{n} \times \sqrt{n}$.

Image sparse model solving steps are as follows:

(1) We suppose the dictionary D have been known, to initialize X and Y.

(2) With a tracking algorithm formula (2) to the sparse coefficient of each image block:

$$a_{ij} = \arg\min_{a_{ij}} \sum_{ij} \mu_{ij} \parallel a_{ij} \parallel_0 + \sum_{ij} \parallel Da_{ij} - R_{ij}X \parallel_2^2 \qquad (2)$$

(3) After the sparse coefficients obtained by formula (3) to update X:

$$X = \arg\min_X \lambda \parallel X - Y \parallel_2^2 + \sum_{ij} \parallel Da_{ij} - R_{ij}X \parallel_2^2 \qquad (3)$$

Resulting from the corresponding solution of formula (4):

$$X = \left(\lambda I + \sum_{ij} {R_{ij}}^T R_{ij}\right)^{-1} \left(\lambda Y + \sum_{ij} {R_{ij}}^T D a_{ij}\right) \qquad (4)$$

K - SVD dictionary learning method

K - SVD dictionary learning method is through the singular value decomposition method to update the atoms in the dictionary one by one in order to reduce error, and the current iteration step of atoms and the corresponding sparse coefficient to synchronize updates, so as to accelerate the convergence speed of the algorithm.

(1) Sparse coding phase: use OMP algorithm training image block in the collection of each image block y_i sparse coefficient.

(2) A dictionary update stage: we are using singular value decomposition method to update the dictionary in turn each atom in D. The first k atoms d_k update process is as follows in dictionary D:

$$\parallel Y - DA \parallel_2^2 = \parallel Y - \sum_{j=1}^{K} d_j \alpha_T^j \parallel_2^2 = \parallel \left(Y - \sum_{j \neq k}^{K} d_j \alpha_T^j\right) - d_k \alpha_T^k \parallel_2^2 = \parallel E_k - d_k \alpha_T^k \parallel_2^2 \quad (5)$$

Among them, the K is the total number of atoms in the dictionary D, α_T^j for the coefficient matrix of the j line. If on E_k singular value decomposition to update the dictionary atom d_k and α_T^k, is the updated coefficient of sparse conditions can not be met, so we should take contract processing.

The specific operation as follows about algorithm:

Step 1, pretreatment, will get the image with noise image partition processing block set $\{y_1, y_2, ..., y_k\}$, set the size of the dictionary to n*K algebra for J and dictionary training;

Step 2, the initialization: set X = Y, the DCT redundant dictionary as the initial dictionary;

Step 3, from the selection of image block in the collection part of the image as the training sample blocks set $\{y_1, y_2,..., y_k\}$, performance and sparse coding dictionary training and dictionary update;

Step 4, after training to get the dictionary, use OMP algorithm for image block set $\{y_1, y_2,..., y_k\}$, sparse coefficient sparse decomposition.

We can get after de-noising images as formula (6).

$$X = \left(\lambda I + \sum_{ij} R_{ij}^T R_{ij}\right)^{-1} \left(\lambda Y + \sum_{ij} R_{ij}^T D a_{ij}\right) \tag{6}$$

Image de-noising algorithm based on K - SVD and BM3D

Specific operation is as follows:

Step 1, first of all to block operation of noise image, get the image block set Y and which size is $\sqrt{n} \times \sqrt{n}$;

Step 2, to set the standard deviation of image block with OMP algorithm comparing the threshold value of $C\sigma\sqrt{n}$, which greater than the threshold value of image block set Y_1 and less than the threshold value of image block set Y_2, here C = 1.15.

Step 3, from Y_1 to select training samples by K-SVD algorithm for adaptive dictionary D, with the edge of the OMP algorithm Y_1 each image block under the dictionary D sparse coefficient; To deal with the image block with BM3D algorithms of Y_2;

Step 4, the image block of overlapping weighted averaging the de-noising results.

Simulation experiment

We choose 4 test as shown in fig 1 of the test image, the dictionary size K (atomic number) of the dictionary of choice, with a size of 512 * 512 Barbara image in dictionary size 64, 128, 256 and 512 respectively under the condition of experiment, the noise size 20, the results are shown in table 1:

Table 1 Three de-noising methods of PSNR value (dB)

K	64	128	256	512
DCT	28.85	29.98	30.55	29.89
Global	29.50	29.85	29.90	29.23
Adaptive	32.10	30.70	32.10	31.68

Through the data in table 1 we can find, when the dictionary atomic number k = 256 PSNR value can reach the maximum, at the same time considering the operational efficiency of the algorithm and we choose k = 256.

Conclusion

This paper analyzes the image sparse representation based on redundant dictionary de-noising model, analyzed the use of K - SVD dictionary learning method to train the feasibility of the redundant dictionary, were tested, and the convergence of the algorithm through the experiment proves that compared with the pick-up training image from the image library get the dictionary, according to the noise image itself obtained dictionary can better training for image sparse representation, achieve better de-noising effect. And K - SVD based adaptive image de-noising method on weak texture and edges of the image will appear fuzzy problems were improved.

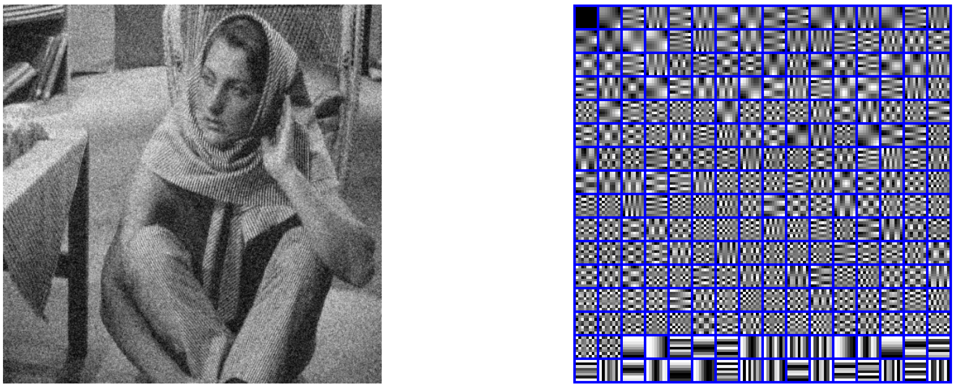

Sigma = 30 with noise image DCT dictionary

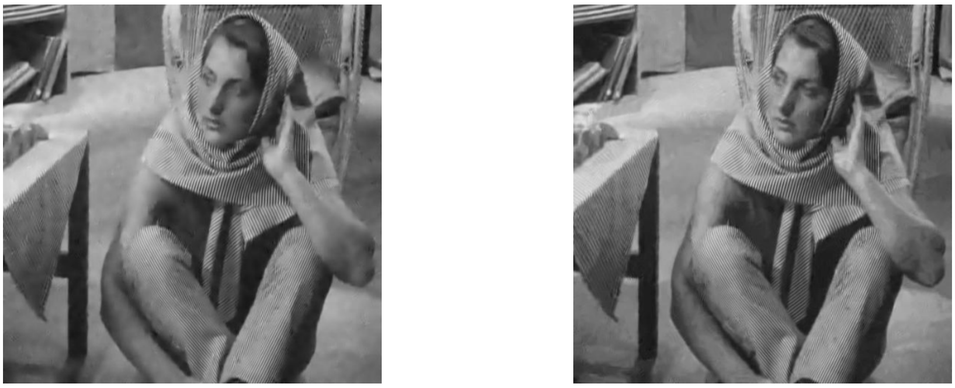

The original method, PSNR = 29.62 dB the improved method, PSNR = 31.64 dB

Fig 1 K - SVD based image de-noising method and the improved method of contrast figure

References:

[1] Aharon M, Elad M, Bruckstein A M. The K-SVD: an algorithm for designing of overcomplete dictionaries for sparse representation. IEEE Transon Signal processing, 2006, 54(11) :4311-4322.

[2] Ataee M, Zayyani H, Babaie-Zadeh M. Parametric Dictionary Learning Using Steepest Descent. IEEE in Proc.ICASSP. 2010:1978-1981.

[3] Yang Juan, Jia Zhenhong,Qin Xizhong,Yang jie,Hu Yingjie.Using K-SVD algorithm for improving performance of BayesShrink image denoising techniques,Laser Journal.2013,34(2):30-31.

[4] Jiang Yewen,Yu Xinmei. An Image Recovery Method Based on Adaptive Redundant Dictionaries for Compressed Sensing. Journal of Xiamen University.2012,51(4):58-62.

[5] Huang Jianglin,Liu Hong,Tao Shaojie. An improved inpainting algorithm based on K-SVD dictionary. Journal of Anhui University.2013,37(3):69-74.

Applied Mechanics and Materials Vol. 596 (2014) pp 337-341
© (2014) Trans Tech Publications, Switzerland
doi:10.4028/www.scientific.net/AMM.596.337

An image retrieval algorithm based on region segmentation

[1]Xiong Xiaomei, [2]Liu Yonglang

[1,2]Jiangxi University of Technology, Nan Chang, China

xiongxiaomei@163.com

Keywords: image retrieval, regional importance, the image segmentation

Abstract. Visual image, as a kind of rich content and performance of multimedia information, has been tremendously popular for a long time. Image retrieval technology is complicated than text retrieval, due to text-based image retrieval is often need manual annotation, so very laborious and individual subjective factors are there. In order to solve these problems, this paper puts forward a kind of image retrieval algorithm based on improved region segmentation. First, use of image segmentation technology, dividing the image into several regions, then to match each region and the being tested image, and obtained retrieval results in the end. It can be seen through experiment, the user only needs to submit a retrieval image, so it can greatly reduce the user's retrieval burden, and improve the efficiency of retrieval.

Introduction

In the study of image and application, people often interested in some parts of the image, we call these parts as the target (the other part is the background) in general, they correspond to a particular area in the image. In order to identify and analyze the target, need to be separated and extracted, then the target for further research and utilization. Image segmentation is a characteristic to divide the image into the area and extract interested target's processes and technologies. For image retrieval based on region segmentation result is good or bad a direct impact on the stand or fall of retrieval results. The purpose of segmentation is to divide the image into different areas.

Feature extraction

For adaptive MS - Ncut after segmentation, get a number of areas. We extract the underlying features to represent the content of the image area. In this paper, the extraction of color, texture and shape features are:

Color features: the image from RGB color space conversion to L * u * v * space, extraction of L *, u *, v * regional average color as each field of 3 d color features; Among them, the RGB space to the L * u * v * space is divided into two steps:

(1) The RGB space to the CIE XYZ space transformation:

$$\begin{bmatrix} X \\ Y \\ Z \end{bmatrix} = \frac{1}{0.177} \begin{bmatrix} 0.49 & 0.31 & 0.2 \\ 0.177 & 0.812 & 0.01 \\ 0 & 0.01 & 0.99 \end{bmatrix} \begin{bmatrix} R \\ G \\ B \end{bmatrix} \qquad (1)$$

(2) The CIE XYZ space to L * u * v * space transformation:

$$L^* = \begin{cases} 116(\frac{Y}{Y_n})^{\frac{1}{3}} - 16 & , \frac{Y}{Y_n} > (\frac{6}{29})^3 \\ (\frac{29}{3})^3 \frac{Y}{Y_n}, & \frac{Y}{Y_n} \le (\frac{6}{29})^3 \end{cases}$$

$$u^* = 13L^*(u' - u_n')$$
$$v^* = 13L^*(v' - v_n') \quad (2)$$

Among them $u' = \frac{4X}{X+15Y+3Z}$, $v' = \frac{9X}{X+15Y+3Z}$.

Set for image function, regional function, the area density, ratio of rectangular box to include area, the position of the minimum matrix in the upper left corner point, and the matrix of high and wide. Center of mass and Hu invariant moments are defined as follows: first, the image of the p + q order geometric moment and central moments are defined as.

$$m_{pq} = \sum_{i=1}^{N}\sum_{j=1}^{M} x^p y^q f(x,y)$$

$$\mu_{pq} = \sum_{i=1}^{N}\sum_{j=1}^{M}(x-\bar{x})^p (y-\bar{y})^q f(x,y) \quad (3)$$

Among them $\bar{x} = m_{10}/m_{00}$,$\bar{y} = m_{01}/m_{00}$, N and M, respectively is the height and width of the image. The center of the normalized moment is defined as $\eta_{pq} = \mu_{pq}/\mu_{00}{}^{\alpha}$ and $\alpha = \frac{p+q}{2} + 1$.

Similarity measure

In retrieval based on keyword search requires an exact match. In the content-based image retrieval, we adopt the similarity matching. The effect of CBIR depends largely on the similarity calculation results of the algorithm and similarity of the image is in essence the similar degree between the corresponding characteristics. Usually, using vector to represent the image characteristics, namely the feature vector of the image is considered to be a multidimensional space of a bit, so it's natural thoughts is the feature space of the distance between point and point to measure their similarity degree. The distance metric is a more commonly used methods, and related calculation and correlation coefficient calculation, etc.

The most intuitive method is to calculate the distance between the feature vectors as the similarity after the extraction of feature vector of the image. The distance is a kind of measure, Minkowski measure is defined as:

$$d(X,Y) = \left(\sum_{i=1}^{n} |x_i - y_i|^m\right)^{\frac{1}{m}} \quad (4)$$

The X, Y is the image, and x=(x1,...,xn) ,y=(y1,...,yn) is the corresponding eigenvalue.

When m = 1 as Manhattan distance;

When m = 2 called Euclidean distance, this is usually referred to the distance concept, referred to as the Euclidean distance;

When m = 3 when called Chebyshev distance.

Regional significance

According to the human visual system, an image of the different regional is importance. In general, it might relate with the area of the RI and regional. When regional area is larger, the regional is important. Moreover, important areas are often located in the center of the image. Based on the above assumptions, considering the regional area and position, we construct the importance of the following areas: If I said as $I = \{r_1, r_2, \dots, r_n\}$, The r_i is the first I image I area,

$$RI(r_i) = \frac{A(r_i)}{A(I)} \cdot \left(1 - 2\sqrt{\frac{(r_{ix}-x)^2+(r_{iy}-y)^2}{L(I)^2+H(I)^2}}\right) \quad (5)$$

Which A (I) and A (r_i) is the area of the image I and regional r_i, respectively is A (r_i)/A (I) is expressed as the percentage of regional r_i in the image I: (r_{ix}, r_{iy}) is the focus of r_i and the r_i, (x, y), L (I) and H (I) respectively for the image I center of gravity, long and high. $\sqrt{(r_{ix}-x)^2+(r_{iy}-y)^2}$ Said the focus of r_i and I at the center of the Euclidean distance. Formula 1 indicates that RI (r_i) value, the greater the regional RI is more important.

Similarity matching: improvement of IRM

Integrated Region Matching (IRM) is a kind of effective image Matching method based on region. However, in the IRM consider only to the area of the region. Here, we proposed an improved algorithm of IRM. Fig. 1 shows the user retrieval process.

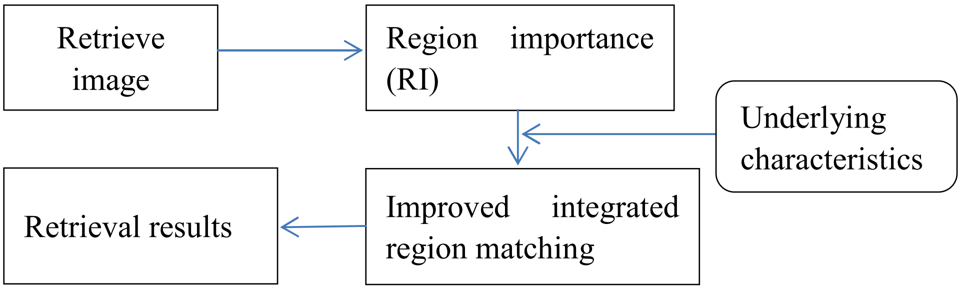
Retrieve image
Region importance (RI)
Underlying characteristics
Improved integrated region matching
Retrieval results

Fig. 1 Image retrieval based on region segmentation

Assuming that two images I1 and I2 are expressed as respectively $I_1 = \{r_{1,1}, r_{1,2}, \dots, r_{1,m}\}$ and $I_2 = \{r_{2,1}, r_{2,2}, \dots, r_{2,n}\}$, I1 and I2 improve IRM is defined as:

$$d(I_1, I_2) = \sum_{i=1}^{m} \sum_{j=1}^{n} P_{i,j} \cdot d_{i,j} \tag{6}$$

$P = (P_{i,j})_{m\times n}$ Called importance matrix, $P_{i,j}$ the importance of representation $r_{1,i}$ and $r_{2,j}$ matching coefficient. $d_{i,j}$ expression the distance between $r_{1,i}$ and $r_{2,j}$.

$$d_{i,j} = w_c \cdot \sum_{k=1}^{3} (f_{i,k} - f_{j,k})^2 + w_t \cdot \sum_{k=4}^{19} (f_{i,k} - f_{j,k})^2 + w_s \cdot \sum_{k=20}^{33} (f_{i,k} - f_{j,k})^2 \tag{7}$$

The $f_i = \{f_{i,1}, \dots, f_{i,33}\}$ and $f_j = \{f_{j,1}, \dots, f_{j,33}\}$ are the area normalization eigenvector of $r_{1,i}$ and $r_{2,j}$. w_c, w_t, w_s is the weight of color, texture and shape features respectively. This article respectively for values $w_c = 5/8$, $w_t = 1/8$, $w_s = 2/8$.

Importance of RI assumes that the area of $r_{1,i}$ and $r_{2,j}$ area for $RI(r_{1,i})$ and $RI(r_{2,j})$, it will need to meet the formula 8.

$$\sum_{j=1,2,\dots,n} P_{i,j} = RI(r_{1,i}) \quad ,i = 1, \dots, m$$

$$\sum_{i=1,2,\dots,m} P_{i,j} = RI(r_{2,j}) \quad ,j = 1, \dots, n \tag{8}$$

The following steps are introduced in detail based on RI MSHP.

Step 1: L = {}, M = {(I, j), I = 1,..., m, j = 1,..., n}.

Step 2: Select the smallest $\mathrm{d}_{\mathrm{i,j}}$ corresponding index (I, j), M - L will (I, j) is marked (I 'j');

Step 3: $\mathrm{P}_{\mathrm{i}',\mathrm{j}'} = \min(\mathrm{RI}(\mathrm{r}_{1,\mathrm{i}'}), \mathrm{RI}(\mathrm{r}_{2,\mathrm{j}'}))$.

Step 4:if $\mathrm{RI}(\mathrm{r}_{1,\mathrm{i}'}) < \mathrm{RI}(\mathrm{r}_{2,\mathrm{j}'}), \mathrm{P}_{\mathrm{i}',\mathrm{j}} = 0, \mathrm{j} \neq \mathrm{j}'$,else， $\mathrm{P}_{\mathrm{i},\mathrm{j}'} = 0, \mathrm{i} \neq \mathrm{i}'$.

Step 5: $\mathrm{RI}(\mathrm{r}_{1,\mathrm{i}'}) = \mathrm{RI}(\mathrm{r}_{1,\mathrm{i}'}) - \min\left(\mathrm{RI}(\mathrm{r}_{1,\mathrm{i}'}), \mathrm{RI}(\mathrm{r}_{2,\mathrm{j}'})\right)$

$\mathrm{RI}(\mathrm{r}_{2,\mathrm{j}'}) = \mathrm{RI}(\mathrm{r}_{2,\mathrm{j}'}) - \min\left(\mathrm{RI}(\mathrm{r}_{1,\mathrm{i}'}), \mathrm{RI}(\mathrm{r}_{2,\mathrm{j}'})\right)$.

Step 6: L=L+{(i’,j’)}

Step 7:if $\sum_1^m \mathrm{RI}(\mathrm{r}_{1,\mathrm{i}'}) > 0$ and $\sum_2^n \mathrm{RI}(\mathrm{r}_{2,\mathrm{j}'}) > 0$,then turn step 2;else exit.

Experiment

We will put forward the initial searching methods and other three ways. One way is SIMPLIcity system, the system of image area was formed by k-means clustering, and then use the IRM between image matching; Said in the same segment and area under the premise of the other two methods are based on the importance of regional said is different, one is area of the area as importance, another is the area of statistical properties as the importance of the area. Remember these four methods: SIMPLIcity, MN - IRM, MN - RF * IPF and our method. The table 1 shows the result the average precision of four methods.

On Corel - 1000 image library, our approach than MN - IRM, MN - RF * IPF, 4.9% , 4.6% higher than that of SIMPLIcity 9.1%. The results show that our methods are available.

Table 1 The experimental results with the average precision (%)

N	10	20	30	40	50	60	70	80
Our method	64.9	58.1	56.2	53.1	50.5	48.4	47.0	45.0
MN-IRM	64.5	57.6	55.6	52.5	50.1	48.1	46.7	44.7
MN-RF*IPF	64.9	57.0	55.1	52.1	49.5	47.5	45.6	44.1
SIMPLIcity	62.9	56.3	54.5	51.1	48.6	46.7	45.1	43.2

Conclusions

This paper proposes an interactive image retrieval method based on region. The paper highlights the importance of the region (RI), RI is determined by the size and location of the image area, if the area of the region is larger, the RI will be greater. Through comparing with other retrieval methods, the experimental results show that our proposed method has certain advantages.

References

[1] J. Z. Wang, J. Li, G. Wiederhold. SIMPLIcity: semantics-sensitive integrated matching for picture libraries. IEEE Transactions on Pattern Analysis and Machine Intelligence. 2001, 23(9):947-963.

[2] J. Li, J. Z. Wang, G. Wiederhold. IRM: integrated region matching for image retrieval. Proceedings of the 8th ACM International Conference on Multimedia, Los Angeles, CA, USA. 2000: 147-156.

[3] C. J. Yang, R. Duraiswami, Larry Divas. Efficient mean-shift tracking via a new similarity measure. Proceedings of the 2005 IEEE Computer Society Conference on Computer Vision and Pattern Recognition, 2005.

[4] J. Z. Wang, Y. P. Du. Scalable integrated region-based image retrieval using IRM and statistical clustering. Proceedings of 1st ACM/IEEE-CS Joint Conference on Digital Libraries. 2001:268-277.

[5] X. H. Yang, Z. Y. Wang, D. F. Li, J. Zhang. Color image retrieval with adaptive feature weight in Brushlet domain. Proceedings of IEEE 2nd Symposium Web Society. 2010: 97-102.

[6] Y. Liu, et al. A boosting framework for visuality-preserving distance metric learning and its application to medical image retrieval. IEEE Transactions on Pattern Analysis and Machine Intelligence. 2010, 32(1): 30-44.

[7] T. Deselaers, V. Ferrori. Visual and semantic similarity in ImageNet. Proceedings of IEEE Conference on Computer Vision and Pattern Recognition. 2011: 1777-1784.

[8] P. Arbeláez, M. Maire, C. Fowlkes, J. Malik. Contour detection and hierarchical image segmentation. IEEE Transactions on Pattern Analysis and Machine Intelligence. 2011, 33(5):898-916.

[9] J. F. Ning, L. Zhang, D. Zhang, C. K. Wu. Interactive image segmentation by maximal similarity based region merging. Pattern Recognition. 2010, 43(2): 445-456.

[10] M. M. Islam, D. Zhang, G. Lu. Region based color image retrieval using curvelet transform. Proceedings of Asian Conference on Computer Vision, Xi'an, China. 2009: 448-457.

Applied Mechanics and Materials Vol. 596 (2014) pp 342-345
© (2014) Trans Tech Publications, Switzerland
doi:10.4028/www.scientific.net/AMM.596.342

Combined filter method based on terrain factors

Yan Man [1,2, a *], Liang Yong Quan[1,b]

[1] College of Information Science and Engineering, Shandong University of Science and Technology, Shandong Qingdao, 266590, China

[2] Computer Engineering School, Weifang University, Shandong Weifang, 261061, China

[a]yanmansdust@126.com, [b]277651873@qq.com

Keywords: Wiener filter; frequency estimated filter; interferogram; local terrain slope

Abstract. Interferogram noise filter is one of the key technologies which use synthetic aperture radar interferometry phase to extract digital elevation model. However, the interference fringes' details are often reduced when complex interferogram is filtered, and this leads to inaccurate phase unwrapping result, for this combined filter method based on terrain factors is proposed. Filter method can be selected through weight factor associated with the terrain slope in the filter process, and Wiener filter method is implemented in flat terrain area, frequency estimated filter method is achieved in steep terrain area. Then the new filter method is applied to deal with data where the region of Quebec, Canada. This proves that the new filter algorithm proposed in this paper can effectively suppress noise and better maintain stripe details.

Introduction

Synthetic aperture radar has been widely applied in detecting earth surface deformation, forest survey and land classification. However, many factors affect its application, especially a lot of noises exist in interfergram, and all of these directly influence on the two-dimensional phase unwrapping algorithm efficiency. Therefore researching InSAR interferogram filter becomes one of key problems in practical applications [1].Interfergram noise's main sources are as follow [2-3]：（1）Speckle noise in phase. This noise is the major source in interferogram, since the target surface is rough relative to system wavelength, the value of each pixel is synthesized by the echo vector in scattering centers.（2）Noise generated by InSAR system. The noise reduces system SNR and coherence of the image, all of these can cause measurement errors.

In summary, interfergram noise's causes have many, which make researching filter method very important. Now filter methods existing in InSAR interferogram have common median filter, mean filter,Wiener filter, frequency adaptive filter, and so on[4-5].Although Wiener filter can make use of local statistical characteristics in phase, it does not consider non-stationary characteristics of interfergram. Frequency estimated filter is able to filter in steep terrain area, but in flat areas it can appear "island" phenomenon. When complex terrain area is processed, these two methods appear information lost in detail streaks, it makes the unwrapping results not accurate and ground elevation models produced incorrect. For this combined filtering method of InSAR interferogram based on local terrain slope is proposed. In the method weight factor associated with the terrain slope is introduced in the filter process, Wiener filter is select in the flat terrain area, frequency estimated filter is used in the steep terrain area. Region of Quebec is selected to do experiment, and compare and analysis with Wiener filter and frequency estimated filter.

Combined filter algorithm of InSAR interfergram based on local terrain slope

Frequency estimated filter. Frequency estimated filter estimates local spatial frequency by two-dimensional Chirp-Z transform, and adjusts the parameter based on changes in terrain [6].The specific method is divided interferogram into small overlapping block, and approximates linearization each block. After the interfergram is detected by stripes, after filtered interferogram can be linear approximation obtained using formula (1):

$$e^{j\varphi(f_j,f_k)}=e^{j2\pi(f_j^j+f_k^k)}e^{j\phi_0} \qquad (1)$$

In formula (1), f_j, f_k are two-dimensional spatial frequency components, ϕ_0 is the initial phase, where $e^{j\phi_0}$ is:

$$e^{j\varphi_0}=\frac{\sum\limits_{j=j_0,k=k_0}^{J=J_0+N_j-1,k=k_0+N_k-1} I(j,k)e^{-j2\pi(f_j^j+f_k^k)}}{\left|\sum\limits_{j=j_0,k=k_0}^{J=J_0+N_j-1,k=k_0+N_k-1} I(j,k)e^{-j2\pi(f_j^j+f_k^k)}\right|} \qquad (2)$$

Where, $I(j,k)$ is selected interferogram. $j\in\lfloor j_0, j_0+N_j-1\rfloor, k\in[k_0,k_0+N_k-1]$, the size of interferogram selected is $N_j\times N_k$.

Wiener filter. Wiener filter is a linear filter whose optimal standard is the minimum square, under certain constraints, difference square between the output and the given function obtains minimum, and it is a typical Gaussian white noise filter method [5].

Wiener filter's steps are as follows:

(1)Obtaining noise signal y 's autocorrelation function, and calculating function Fourier transform, denoted as $P_{yy}(w_1,w_2)$.

(2)Obtaining the cross-correlation function between noise signal y and useful signal x , and calculating Fourier transform of this function, denoted as $P_{yx}(w_1,w_2)$.

(3)Obtaining Wiener filter $H(w_1,w_2)$ using the following formula:

$$H(w_1,w_2)=\frac{P_{yx}(w_1,w_2)}{P_{yy}(w_1,w_2)} \qquad (3)$$

Combined filter based on local terrain slope. In this paper, local terrain slope is as an argument, adaptive filter method is selected according to the weight coefficient in each block of interferogram, Wiener filter is achieved in flat terrain region, and frequency estimated filter is selected in steep terrain area. The noise is effectively removed while detail phase-loss information is reduced, providing a solution for phase unwrapping. The method basic steps are as follows:

The first step, the whole interferogram is divided into several small blocks, so that the rate of overlap between each block is more than 50%, this paper selects 13×13 pixel.

The second step, according to formula (4) and (5) respectively obtained each small block's local terrain slope $G_x(x,y)$, $G_y(x,y)$ and weight factor $w(x,y)$:

$$\begin{aligned}G_x(x,y)&=[f(x+1,y)-f(x-1,y)]/2\\ G_y(x,y)&=[f(x,y+1)-f(x,y-1)]/2\end{aligned} \qquad (4)$$

$$w(x,y)=\exp\left[-\frac{G_x^2(x,y)+G_y^2(x,y)}{2k^2}\right] \qquad (5)$$

Here, k is the threshold, its value is depended on the size of interferogram edge's gradient, but the value is not suitable for large, in this paper its value is selected as $1/3$ of maximum gradient in interferogram.

The third step, if $w(x,y)>\alpha$ (α is the average weight obtained from the whole image) ,frequency estimated filter method is selected; if $w(x,y)<\alpha$,using Wiener filter method to filter local area, thus 13×13 *pixel* size window up and down throughout the interferogram, then filter results are superimposed to complete interferogram phase filter. The whole interferogram is superimposed, which is equivalent to multilook average for interferogram, this can reduces the masaic effect generated processing block in the extent.

Experimental results and analysis

In order to verify the proposed method performance, two ERS-1/2 SAR satellite images in Quebec,Canada at January 9,1994 and January 12,1994 are selected as experimental primary and secondary image, after registration, interference, ground effect and other operations in Earth View radar image processing software, part of the interferogram is shown in Fig.1（$781\times313 pixel$）.Because no phase filter, there is a lot of noise, resulting in interference fringes rather vague, the number of residual almost reaches 38578.Fig.2 is result which use respectively frequency estimated filter, Wiener filter and the proposed method. From the filter results, frequency estimated filter can get better result in steep terrain area(the middle part of the interferogram),but in the flat terrain area(both sides of the interferogram)the result is poor, resulting in the “island” phenomenon, and the number of residual reduces to 2669.Wiener filter method is opposite to the frequency estimated filter, resulting in better result in sparse stripes, in the intensive stripes the minimum mean square error estimation produces streaks overlap, the number of residual is 1477.The proposed method selects the filter method according to weight coefficients of local terrain slope, the result obtained is more accurate, noise suppression affection is significant, and better maintain the phase detailed information, the number of residual is 923,residual reduction rate is 97.6%.

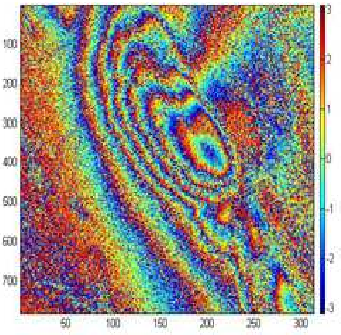

Fig. 1 Interferogram

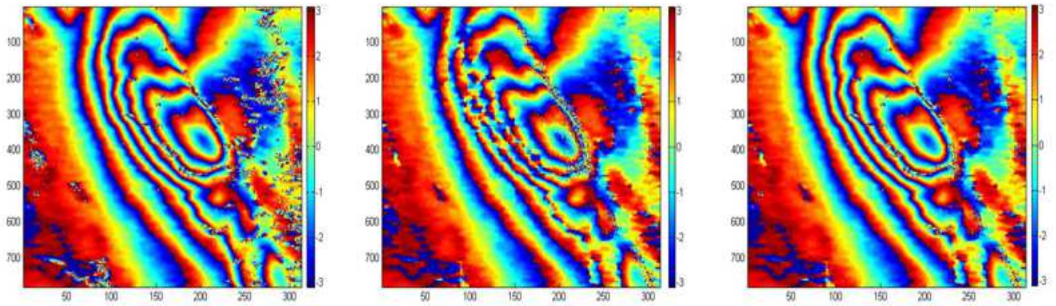

(a) (b) (c)

Fig. 2 Filter result diagram： (a) Filter based on frequency; (b) Wiener filter; (c) This paper method

The following quantitatively evaluate filter results from edge retention index and peak signal to noise ratio two aspects.

Edge preservation index. Edge preservation index illustrates filtered interferogram edge information preservation, its value is closer to 1 that illustrate filter’s edge preservation ability is stronger. Its formula is：

$$EPI=\frac{\sum\left(\left|\phi_s(i,j)-\phi_s(i+1,j)\right|+\left|\phi_s(i,j)-\phi_s(i,j+1)\right|\right)}{\sum\left(\left|\phi_o(i,j)-\phi_o(i+1,j)\right|+\left|\phi_o(i,j)-\phi_o(i,j+1)\right|\right)} \tag{6}$$

In formula， $\phi_s(i,j)$ is filtered phase， $\phi_o(i,j)$ is original interferogram phase.

Peak signal to noise ratio. Peak signal to noise ratio reflects the whole interferogram the degree of distortion, the value is larger, and the quality of the filtered image is higher. Peak signal to noise ratio is defined as:

$$PSNR = 10\log\frac{255^2}{MSE} \tag{7}$$

Where， $MSE = \frac{1}{MN}\sum_{i=0}^{M-1}\sum_{j=0}^{N-1}\left(f(i,j) - f^{'}(i,j)\right)^2$.

According to the above value, evaluating the three filter methods.As can be seen from Table 1,frequency estimated filter and this paper method's edge preservation index are higher, Wiener filter's is lower, its capability to maintain edge information is poor. As can be seen from the peak signal noise ration, this paper method's is bigger than the frequency estimated filter's and Wiener filter, this illustrates this paper method filtered interferogram's quality is high.

Table 1 Three kinds of filter methods noise evaluation comparison table

Filter Method	EPI	PSNR
Frequency estimated filter	0.20529	41.253
Wiener filter	0.17419	41.309
This paper method	0.31459	41.574

Conclusions

In this paper, the local terrain slope is as the factor, combined filter of InSAR interferogram based on local terrain slope. And using real data, frequency estimated filter, Wiener filter and this paper method are compared and analyzed. Experimental results show that, from the visually and quantitative indicators, the proposed method's filter accuracy is higher in removing the noise part, ability to maintain the phase details is stronger, image quality is better, the number of residual is decreased, filter result is better than the front two filter methods. But in addition to terrain distribution not average in the actual interferogram, the distribution of noise is difference, the next work will consider how to combine the signal to noise ratio and terrain slope as the factor of interferogram filter method selected.

Acknowledgements

This work is supported by Doctor Research Foundation of Weifang University (2013BS15).

References

[1] R.Bamler, D.Just,et al,Phase Statistics in Interferograms with Applications to Synthetic Aperture Radar.Applied Optics, Vol.33-20(1994), p.4361-4368.

[2] H.A.Zebker, J.Villasenor:Decorrelation in Interferometric Radar Echoes.IEEE Transactions on Geoscience and Remote Sensing,Vol.30-5(1992),p.950-959.

[3] J.S.Lee, K.P.Papathanssiou,et al:A New Technique for Noise Fitering of SAR Interfermetric Phase Images.IEEE Trans on Geoscience and Remote Sensing,Vol.36-5(1998),p.1456-1465

[4] Q.Sun, J.J. Zhu,et al:A New Adaptive InSAR Interferogram Filter Based on SNR.Acta Geodaetica et Cartograhica Sinica,Vol.38-5(2009),p.437-449.

[5] H.W.Yi, J.J.Zhu,et al:An Improved Adaptive Algorithm For Filtering InSAR Interferogram In Complex Plane.Journal of Central South University,Vol.44-2(2013),p.632-641.

[6] A.V.Oppenheim, R.W.Schafer:Digital Signal Processing(Prentice-Hall, New Jersey 1975).

Applied Mechanics and Materials Vol. 596 (2014) pp 346-349
© (2014) Trans Tech Publications, Switzerland
doi:10.4028/www.scientific.net/AMM.596.346

Design and Implementation of Safety Lock based on Face Recognition

Changxing Qi[1, a] , Lei Zhao[1,b] ,Qiaoling Dong[1,c]

[1] Software College, Shenyang Normal University, Shenyang, Liaoning, 110034,China

[a]qicx@163.com, [b]missland1993@gmail.com, [c]2685352776 @qq.com

Keywords: Face Recognition, Visual Library, PCA(Principal component analysis)

Abstract. This paper designed and implemented a desktop application of safety lock based on face recognition. The application is developed by C# and used open source visual library OpenCV and SQLite lightweight database. Principal component analysis (PCA) and Rijndael algorithm are respectively used in face recognition and algorithm of encryption and decryption. This paper illustrates design and implementation in detail

Introduction

Biometrics combines with computer technology and sensor technology and so on. used to identify individuals by using Physiological and behavioral characteristics of the body. Face recognition technology selects facial features for identification. Compared with other biometrics technology, face recognition technology have the advantages of non-contact and non-mandatory, It has been used in many applications, such as entrance guard system, monitoring system, the camera and smart phone. This paper implements the personal computer safety lock software system using facial recognition technology and encryption technology, at the same of the protection of the user's information security, it provides users with a more convenient way of secrecy.

This system is a desktop application based on the technology of face recognition . Throughfacial features andpassword ,it provides security for users and give the user a good experience.

Technology and Software

OpenCV is open source vision library and can run on the windows.which provides API interfaces for C#.and And realized the common algorithms in computer vision to Reduced the development tasks.

EmguCV is a library package of OpenCV under.Net platform, It allows for the use of compatible language in the.Net platform,such as C#,VB to call the OpenCV functions. Then compiles to run on Windows system, etc. EmguCV is developed by C# and devided by two layers:the first layer includes functions ,structure and Enumerated types mapped from OpenCV .And the second layer includes classes developed on .Net which can provide be convenient for the user to use the library flexibly and effectively.The class of FaceRecognizer is provided to realize face recognization based on PCA.

SQLite has fast access speed and the advantage of low complexity. Database information can keep the whole single file in the client, the realization of such a design can simplify matters.

Rijndael algorithm has characteristics such as safe, efficient, flexible and easy to use, so the system chooses the algorithm

This system provide basis of face recognition algorithm implementation by using OpenCV, and uses Rijndael algorithm for data encryption, and developed in the. Net platform by using c # .

Algorithm

Principal component analysis (pca) is a mathematical method of dimension reduction. It gets a number of variables,through numerous variables linear combination of the original, and the information as much as possible to the representation of the original variables. At the same time these variables are not related. Therefore, principal component analysis (pca) is to find a way, through linear transformation to the original may have a certain correlation between variables into a set of new independent of each other, as far as possible in order to response the original data information.

Calculation steps:

1) The standardization of original data collection: P dimensional random vector $x = (x_1, X_2, ..., X_p)^T)$ n samples $x_i = (x_{i1}, x_{i2}, ..., x_{ip})^T$, i=1,2,…,n, n>p, Sample matrix structure, arrays of samples for the following standardized transformation

$$Z_{ij} = \frac{x_{ij} - \bar{x}_j}{s_j}, i = 1, 2, ..., n; j = 1, 2, ..., p \qquad (1)$$

And $\bar{x}_j = \frac{\sum_{i=1}^{n} x_{ij}}{n}, s_j^2 = \frac{\sum_{i=1}^{n} (x_{ij} - \bar{x}_j)^2}{n-1}$, (2)

It is concluded that standardization array Z

2) The standardized array Z correlation coefficient matrix

$$R = [r_{ij}]_p xp = \frac{Z^T Z}{n-1} \qquad (3)$$

In (3) $r_{ij} = \frac{\sum z_{kj} \cdot z_{kj}}{n-1}, i, j = 1, 2, ..., p$ (4)

$$|R - \lambda I_p| = 0 \qquad (5)$$

3)

In accordance with the $\frac{\sum_{j=1}^{m} \lambda_j}{\sum_{j=1}^{p} \lambda_j} \geq 0.85$, (6)

we can determine the m value

for each λ_j, j=1,2,...,m, Solutes of equations, $Rb = \lambda_j b$ and can get b_j^o

4) convert standardization index variables into the main components

$$U_{ij} = z_i^T b_j^o, j = 1, 2, ..., m \qquad (7)$$

U_1 is called the first main component, U_2 is called the second main component, …, U_p.

5) Comprehensive evaluation on the principal components.sum m principal components by the weights .

The system converts 2 d face images into a one-dimensional vector in order to use this algorithm firstly, and Principal component analysis is carried out on the sample data,then chooses the Principal component to generate subspace.when recognizing, The predictive vector linear transformation and projected into the subspace. Then on the basis of its similarity with the training sample for identification.

Aims

1) The system runs in the Windows platform, should comply with the Windows desktop application characteristics, provide the context menu associated with the file.
2) The system is for a single user system, only one user can use this system.
3) The system need to use the camera as an input device.
4) The system can be for file encryption and decryption operation, the file is encrypted can only be decrypted in the same computer.
5) The user can choose to use facial recognition or decrypted files.
6) The system can be reset.

Design

Database design: This system consists of two tables, the user table to save the user's system, table Settings to save the parameter information in the process of face recognition.

Functional design. The module decomposition: dependence among system modules as shown in Fig 1

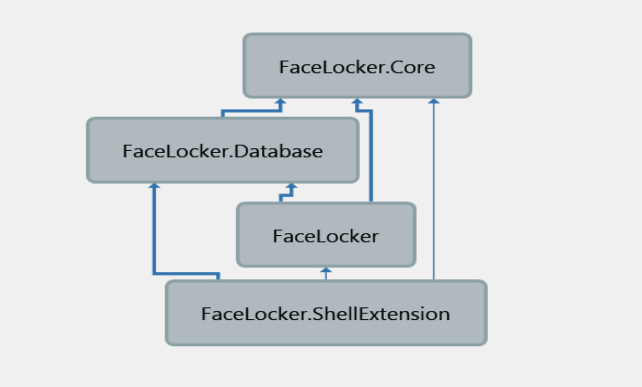
FaceLocker.Core
FaceLocker.Database
FaceLocker
FaceLocker.ShellExtension

Fig1. The system module diagram

Detailed function of each module are as follows:

1) **FaceLocker.Core**: Provide facial recognition and the realization of the function of file encryption, system most of the components are dependent on it to complete the face detection and recognition. This module is part of the system to achieve the most difficult, the development way of thinking of the module is to provide three interfaces, a factory class, and a parameter.Fig2 is the module class diagram;

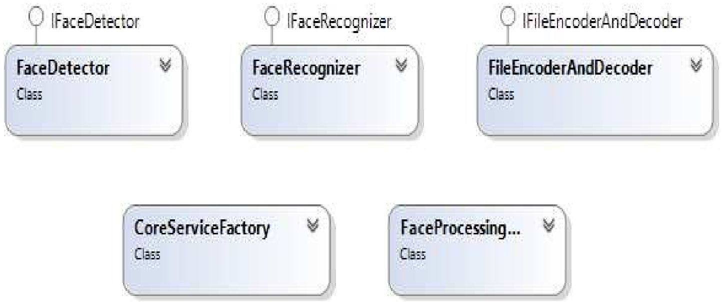
IFaceDetector
FaceDetector
Class
IFaceRecognizer
FaceRecognizer
Class
IFileEncoderAndDecoder
FileEncoderAndDecoder
Class
CoreServiceFactory
Class
FaceProcessing...
Class

Fig2 Diagram of FaceLocker.Core

FaceDetector class implements the IFaceDetector interface, FaceRecognizer class implements the IFaceRecognizer interface, FileEncoderAndDecoder class implements the IFileEncoderAndDecoder interface, CoreServiceFactory class implements the interface instance for the above method.

2) **FaceLocker.Database**： This module provides a system data preservation and access interface, blocked access to the underlying implementation of data storage, and makes the system more flexible implementation strategy.This module implements the data access function, to provide two interface and a factory class, shielding the module implementation details, improve the scalability of the system.

3) **FaceLocker**： This module is the front-end module system, provide navigation of interaction with the user interface and function. This module organization system operation process.

4) **FaceLocker.ShellExtension**: Provide windows shell extension functions, including the context menu and file icon. This module provides a variety of shell extension, is used to the system integration with windows explorer.

UI design

Fig 3 is the FaceLocker module form class diagram.

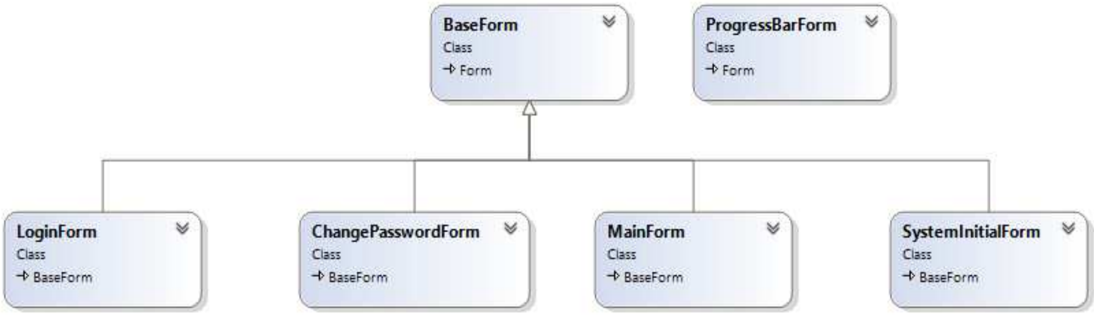

Fig 3 Class diagram of FaceLocker module form

1) BaseForm. form (except ProgressBarForm) provides a consistent interface appearance and operation experience for other form, other forms upon the BaseForm realize own functions.
2) MainForm. main form for the system, is also the system starts to create and display of the form.
3) LoginForm .form for the login.
4) SystemInitialForm. form be used to initialize the system.
5) ChangePasswordForm. form for users to change passwords.
6) ProgressBarForm form, used for the background when performing time-consuming tasks, prompt the user to wait.

Operation Process

When the system startup MainForm form, first of all determine whether has been initialized, If it has not yet been initialized. Including input the user name, password, and multiple human face image acquisition. After a successful operation background initialization processing process. If it has been initialized,then startup the LoginForm. Start on the user's face recognition, the new acquisition of facial information and the information of the initialization to check, check and input user password information. If success, the system safety lock complete unlock function.。

Conclusions

This paper introduces in detail the implementation process of this system, the package in the process of system design, also according to the object-oriented thought, as far as possible the realization of the isolation between the various modules, reduce the coupling between, achieve the requirement of high coupling and low cohesion. Meet the desktop applications based on face recognition and the safety lock control of password inputs。This system has the very good reference f to quickly build encryption control system based on image recognition.

References

[1] YAGN Li-guo,OU Fu-na,ZHAO jing,WU SHAN-qing. Application Research .2011(4) 42-43

[2] Huang Fang, Zhang Baochang, Liu Jinkun，SCIENCEPAPER ONLINE。2011(1)54-57

[3] XIE Yonglin. JISUAN JI YU XIANDAIHUA,2009(6):88-90

[4] Ll Xue-lian , Z han Shou-yi ,Yan Bo. Application Research of computers.2004(14) 149-150

[5] OUYANG Su-zhen, DENG Cheng-yu ,LIU Yong- shan. Application Research of Computers. 2009(26):4577-4580

[6] DANG Xin-peng, LIU Wen-ping. Journal of Computer Applications. 2012,32(8)2316-2319

Applied Mechanics and Materials Vol. 596 (2014) pp 350-354
© (2014) Trans Tech Publications, Switzerland
doi:10.4028/www.scientific.net/AMM.596.350

Image quality assessment based on region of interest

Yue Wang[1, a *], Zenggang Lin[1,b] and Zicheng Liao[1,c]

[1]Shaanxi Provincial Key Laboratory of Speech & Image Information Processing,

School of Computer Science, Northwestern Polytechnical University

[a]1192332405@qq.com, [b]talcool@163.com, [c]418190921@qq.com

Keywords: No reference image quality assessment, ROI, Edge detection.

Abstract. In this paper a new No-Reference (NR) image quality assessment (IQA) method based on the point wise statistics of local normalized luminance signals using region of interest (ROI) processing is proposed. This algorithm firstly extracts the ROI which is relative to human subjectivity by using the image gradient and phase congruency, and then extracts the image quality feature in spatial domain. Particularly, most of the present IQA methods mainly focus on predicting the image quality with respect to human perception, yet, in some other image domains, the final receiver of a digital image may not a human. Thus, we propose a method which can assess the image quality relative to edge detection algorithm. In addition, experimental results on LIVE database are provided to justify the superior compared to the significant image quality metrics.

Introduction.

With the rapid development of digital imaging, there has been a tremendous growth in using digital images for representing and communicating information. So it is crucial to assess the quality of digital images to help obtain improved quality images and evaluate image processing systems or algorithms.

Image quality assessment methods can be classified as subjective methods and objective methods. Subjective evaluation methods should be the terminal gauge, but they are time-consuming, laborious and expensive. Hence, there has been an increasing interest in developing objective IQA methods since some years ago. Based on the availability of reference images, objective evaluation methods can be divided into three classes: full-reference (FR), no-reference (NR) and reduced-reference (RR) approaches. In this paper, we focus on the most challenging category of objective IQA methods –NR IQA.

The goal of NR IQA methods is to predict the quality of distorted images with respect to human perception without any prior knowledge of reference images. The present NR IQA methods can be classified into two classes: the first one is distortion specified (DS) which assumes the type of distortion of the image is known. Such as in [1] a natural scene statistic (NSS) model is used to determine a blind measure of the quality images compressed by JPEG 2000. Marziliano et al. [2] Introduce blur and ringing methods for JPEG2k compressed images. Marziliano et al. [3] suggested an NR IQA specified for blur degradation using analysis of edge blurring in the spatial domain. It first finds vertical edges in the image and maps their locations. Then it defines the horizontal start and end positions of each edge according to the local extreme locations, closest to the edge. However, in practical, it is hard to know the distortion type of the images in advance, so in [4], Anush Krishna Moorthy and Alan Conrad Bovik proposed a new two-step framework which in the first step a unique signature which can be characterized by using distorted image statistics is used to classify images into different distortion categories. And in the second step the quality of the image is calculated along each of these distortions. The other is non-distortion-specific and without knowing any distortion information of the images in advance. For instance, Peng Ye et al.[5] present an algorithm without knowledge of the reference images and the type of distortion. The method extracts the patch level features and explores information of training images for local descriptor encoding, it also uses a visual codebook-based method for feature space quantization and then learns the mapping from the quantized feature space to image quality scores.

In this paper, we propose a new NR IQA method to evaluate the quality of the images. Particularly, we propose a method which can assess the image quality relative to edge detection algorithm. We calculate the quality of the images of LIVE database[6] by using the canny edge detection algorithm.

The remainder of this paper is organized as follows. Section II introduces the proposed method. Section III illustrates some experiment results. Finally the paper is concluded in Section IV.

Proposed method.

A ROI extraction

(1)Phase congruency

An ideal IQA metric should perfectly mimic the HVS. However, Human visual system (HVS) is so complicated that HVS itself is not well understood until now. But many researches have proved that based on the physiological and psychophysical evidences, the phase congruency theory provides a simple but biologically plausible model of how mammalian visual systems detect and identify features in an image [7].PC can be considered as a dimensionless measure for the significance of a local structure .In [8],the authors use PC as one of the features in their FR IQA method.

In this paper, the measure of PC which is introduced by Peter Kovesi [9] is used by us.

$$\mathrm{PC(x)}=\frac{\sum_n W(\mathrm{x})\lfloor A_n(\mathrm{x})\Delta\phi_{\mathrm{n}}(\mathrm{x})-\mathrm{T}\rfloor}{\sum_n A_n(\mathrm{x})+\varepsilon} \tag{1}$$

where $\lfloor\,\rfloor$ is a floor function that leaves the argument unchanged if non-negative, and zero otherwise; $A_n(x) = \sqrt{\mathrm{e_n(x)^2+o_n(x)^2}}$ is the amplitude at a given wavelet scale, $[\mathrm{e_n(x), o_n(x)}]=[\mathrm{I(x)*M_n{}^e, I(x)*M_n{}^o}]$,I is the image signal, $\mathrm{M_n{}^e}$ and $\mathrm{M_n{}^o}$ are the even-symmetric(cosine) and odd-symmetric (sine) wavelets at a scale n; $\Delta\Phi_n(\mathrm{x})=\cos[\Delta\Phi_n(\mathrm{x})-\overline{\Phi}(\mathrm{x})]-\sin[\Delta\Phi_n(\mathrm{x})-\overline{\Phi}(\mathrm{x})]$ is a sensitive measure of phase deviation; $W(\mathrm{x})=1/(1+\mathrm{e}^{\mathrm{r(c-s(x))}})$ is a tapered weighting function, where $s(\mathrm{x})=(1/\mathrm{N})(\sum_n A_n(\mathrm{x})/\mathrm{A_{max}(x)}+\varepsilon)$, and where c is the cut-off value of filter response spread below which PC values become penalized and γ is a gain factor that controls the sharpness of the cutoff; ε is a small constant that avoids division by zero.

(2)Gradient Magnitude.

HVS focus on the edge instead of the smooth region [7][8], so we use the Sobel operator to calculate the gradient image to find ROI.

Firstly, we partition the distorted images into patches. To reduce the complexity of the algorithm, the size of the patch we choose is 32*32. Then we calculate all the standard deviation of the gradient image and PC image of all the patches. The mean value is picked as the image-dependent threshold so as to reach a high calculation accuracy. In addition, one of the characteristics of HVS- visual masking effect, i.e. , HVS is not sensitive to the noise in the complicated regions-also affects the calculation result. Our method which is not sensitive to the local noise can effectively extract the ROI. Examples of this kind of patch selection are shown in Fig. 1.

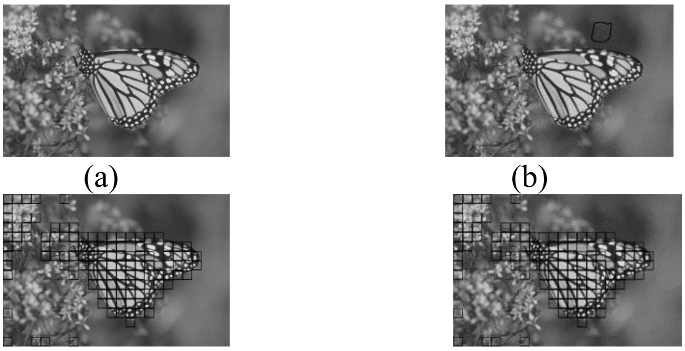
(a) (b)
(c) (d)

Fig. 1. (a) pristine image. (b) image with local noise which is circled by black line. (c) ROI of pristine image. (d) ROI of image with local noise.

B. Feature extraction

The NSS features used in our method are similar to those used in a prior model called BRISQUE [10]. In the algorithm, mean subtracted contrast normalized (MSCN) coefficients are computed for all further processing.

To quantify the statistics of natural images and how they change with the distortion, Anish Mittal et al. [10] utilized AGGD(Asymmetric Generalized Gaussian Model) distribution to fit the MSCN statistics from pristine as well as distorted images(as detailed in [10]).

However, our method only uses the NSS features from some blocks of natural images while BRISQUE is trained on features obtained from the whole image so that the calculation results can be affected by the local noises. Besides, when the size of the block is too small, some of the features' value will be meaningless so that we set the values to zero. After calculating the 36 features from all of the blocks, the mean values of the features are picked as the features of the image.

C. Quality Evaluation

Instead of explicitly finding the linear relationship between the feature space to quality scores, we can use regressors to learn the mapping. Specifically, we use SVR with a radial basis function kernel in our experiment.

SVR has previously been applied to image quality assessment problems [11].

D. IQA based on edge detection

In our experiment, we use 'Canny' algorithm using adaptive threshold value to calculate to image edge. Firstly, we calculate the pristine image edge as the standard image and calculate the distorted image edge as the result image. And then, we calculate the difference between the two images as the distorted image score. We can see that the smaller the score is, the better the image quality is. Finally we use the algorithm we proposed to calculate the image quality. The results are shown in Section

Experiment results

In the experiment, LIVE IQA database which has been widely used for evaluating the performance of IQA systems is used to test our algorithm. It includes five different types distorted images: JPEG, JPEG2K, White Noise (WN), Gaussian Blur and fast-fading (FF). It also includes a total of 982 images and differential mean scores (DMOS) for each distorted image. DMOS is generally in the range [0,100], where lower DMOS indicates higher quality.

Two performance metrics, Pearson linear Correlation Coefficient (PLCC) and Spearman Rank Order Correlation Coefficient (SROCC), are employed to further evaluate the methods, namely PSNR, SSIM and DIIVINE and our method.

The results are tabulated in the following tables.

Table1. SROCC on LIVE database.

	JP2K	JPEG	WN	BLUR	FF	ALL
PSNR	0.872	0.885	0.941	0.764	0.875	0.867
SSIM	0.939	0.946	0.965	0.909	0.941	0.914
DIIVINE	0.913	0.910	0.984	0.921	0.863	0.916
method	0.964	0.937	0.945	0.931	0.910	0.938

Table2. PLCC on LIVE database.

	JP2K	JPEG	WN	BLUR	FF	ALL
PSNR	0.873	0.874	0.928	0.774	0.869	0.855
SSIM	0.920	0.955	0.982	0.891	0.939	0.906
DIIVINE	0.922	0.921	0.988	0.923	0.888	0.917
method	0.960	0.958	0.907	0.958	0.971	0.925

Table3. PLCC and SROCC on LIVE database.

	JP2K	JPEG	WN	BLUR	FF	ALL
SROCC	0.916	0.940	0.942	0.725	0.932	0.890
PLCC	0.861	0.950	0.932	0.805	0.958	0.834

As seen from Tables 1 and 2, our method performs better than the state-of-art full reference and no reference IQA methods in terms of correlation with human perception. From Table3, we can see that this method can also perform well in terms of correlation with edge detection algorithm.

Database independence

To further verify the effectiveness of our method, we also test it on images with two kinds of popular distortion types with the trained model-Gaussian blur and white noise. Additionally, we test our method by performing training on LIVE database and testing on the images obtained by a camera which have no corresponding examples in training set.

The results are shown in Figure 2. From the results, we can see that our method is not only correlate well with human perception, but also not bound by the database.

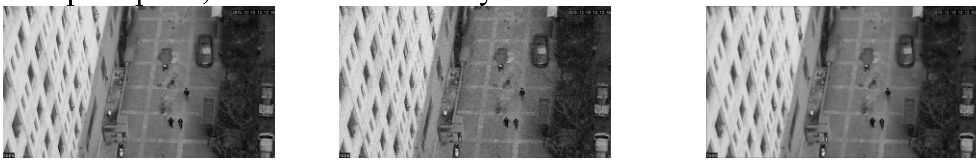

(a)score=40.8759 (b)score=50.3454 (c)score=47.7028

Fig.2 (a) a pristine image (b) an image with noises (c) a blurred image

Conclusion

We have proposed a simple and effective general purpose NR IQA algorithm that evaluates the image quality without any assumption on the types of the distortion. The proposed method is based on ROI extraction and NSS features. The experiment results show that our algorithm outperforms state-of-the-art NR IQA methods. Particularly, this method can also perform well in terms of correlation with edge detection algorithm.

Acknowledgements

The authors would like to thank the lab for the testing data set.

References

[1] H. R. Sheikh, A. C. Bovik, and L. Cormack, “No-reference quality assessment using natural scene statistics: JPEG2000,” IEEE Trans. Image Process., vol. 14, no. 11, pp. 1918–1927, Nov. 2005.

[2] Gastaldo, P., Neural networks for the no-reference assessment of perceived quality. Journal of Electronic Imaging, 2005.14(3): p. 033004.

[3] Marziliano P., Dufaux F., Winkler S., Ebrahimi, T.: A no-reference perceptual blur metric. In: Proceedings of Image Processing,2002 International Conference on Image Processing, Lausanne, Switzerland, vol.3, pp. 57–60 (2002)

[4] Moorthy, A.K. and A.C. Bovik. A Two-Step Framework for Constructing Blind Image Quality Indices. IEEE Signal Processing Letters, 2010. 17(5): p. 513-516

[5] Ye P, Doermann D. 2012. No-Reference Image Quality Assessment using Visual Codebooks. Image Processing, IEEE Transactions on PP (99):1-1

[6] H. R. Sheikh, "Image Quality Assessment Using Natural Scene Statistics," Ph.D. dissertation, University of Texas at Austin, May 2004

[7] L. Zhang, L. Zhang, X. Mou, and D. Zhang, “FSIM: A feature similarity index for image quality assessment,” IEEE Trans. Image Process., vol. 20, no. 8, pp. 2378–2386, Aug. 2011

[8] Lu, T., Y. Zhang and H. Li, An image quality assessment algorithm based on feature selection, in Intelligent Science and Intelligent Data Engineering. 2013, Springer. P. 289--297

[9] P. Kovesi, "Image features from phase congruency,"J. Comput. Vis. Res.,vol. 1, no. 3, pp. 1–26, 1999

[10] Mittal, A., A.K. Moorthy and A.C. Bovik. No-reference image quality assessment in the spatial domain. IEEE transactions on image processing : a publication of the IEEE Signal Processing Society, 2012. 21(12): p. 4695 - 4708

[11] M.Narwaria and W. Lin. Objective image quality assessment based on support vector algorithms, Neutral compute, vol.12 no.5 pp.1207-1245, 2010

Applied Mechanics and Materials Vol. 596 (2014) pp 355-360
© (2014) Trans Tech Publications, Switzerland
doi:10.4028/www.scientific.net/AMM.596.355

Lane Mark Identifying and Tracking Base on Edge Enhancement

Yanyun XING[1, a], Bo YU[2,b] and Fangqun YANG[3,c]

[1]College of Automotive and Transportation, Tianjin University of Technology and Education, Tianjin, China, 300222

[2,3]Automobile Engineering Research Institute, China Automotive Technology and Research Center, Tianjin, China, 300300

[a] xyyyb2013@163.com, [b] jluqicheyb@hotmail.com, [c] 148087009@qq.com

Keywords: Edge Enhancement; Lane mark; Identifying; Tracking

Abstract: In order to improve the accuracy of lane mark line identifying and tracking, this paper uses the LOG operator for edge enhancement, so the useful information is changed into straight lines and the useful feature is obvious. And the paper uses the algorithm of 2-D gray histogram to segment the image. Then it uses Hough transformation to identify the lane mark's two edges and account its intercept and slope, then draws the midline as the final identifying result. Finally in order to reduce the count time, the paper uses the identifying results of the last frame image limit the current frame image recognition areas in tracking lane mark. The experiments results show that the lane mark can be tracking dependably and the algorithms are real-time, moreover, when the algorithm is failure, the system can also recover in time, and locks the tracking target accurately again.

Introduction

Lane mark identifying is one of main research directions for the vehicle safety assistant system and unmanned, its application is very extensive, including the lane departure warning, vehicle positioning, etc.. In the long run, lane mark identifying can also be used in vehicle automatic navigation. The lane detection method of the research in the world today is mostly based on computer vision. In computer vision, changes of the environment affect the recognition result largely, therefore, in order to improve the accuracy of the recognition, the paper enhance the image edge firstly, this step can make the useful information into straight lines, and then uses a straight line detection algorithm, which can filter the interference information of the image, and improve the accuracy of recognition.[1]

Using LOG operator for edge enhancement

The LOG (Laplace of Gauss) operator is Laplace - Gaussian operator. It is a second order differential image edge enhancement operator. Because of Laplace operator is more sensitive to noise, so you need to use two-dimensional Gaussian low-pass filter for filtering firstly, then use Laplace operator for edge extraction [2].

Two-dimensional Gaussian smoothing operator G (x, y) is also called the Gaussian filter, given as the formula 1.

$$G(x,y)=e^{-\frac{x^2+y^2}{2\sigma^2}} \tag{1}$$

The x, y is the image coordinate, σ is associated probability distribution of standard deviation. σ is the only parameter of Gaussian filter and it is directly proportional to the size of the filter operation neighborhoods.

Laplace operator ∇^2 (in formula 2) gives a second derivative, and it is isotropic. The Laplace convolution of the images *f (x, y)* which is smoothed by Gaussian filter is named LOG operator.

$$\nabla^2[G(x,y,\sigma)*f(x,y)] \tag{2}$$

Because the operator is linear, so the differential and convolution operation sequence can be exchanged, and the operation method is formula 3.

$$[\nabla^2 G(x,y,\sigma)]*f(x,y) \tag{3}$$

Derivative of Gaussian filter ∇^2G has nothing to do with the image, so it can be calculated using the analytical method in advance. For two-dimensional Gaussian is circular symmetry, in order to simplify the operation, $r^2 = x^2 + y^2$ is used as a supersede formula where r means the distance from the origin. After replacing the two-dimensional Gaussian is changed into a one-dimensional function, as formula 4.

$$G(r) = e^{-\frac{r^2}{2\sigma^2}} \tag{4}$$

First derivative as formula 5,

$$G'(r) = -\frac{1}{\sigma^2} r e^{-\frac{r^2}{2\sigma^2}} \tag{5}$$

The second derivative is the LOG operator as formula 6.

$$G''(r) = \frac{1}{\sigma^2}(\frac{r^2}{\sigma^2} - 1) e^{-\frac{r^2}{2\sigma^2}} \tag{6}$$

Return to the original x, y coordinate system, and introduce a standardization coefficient, and obtain the LOG operator convolution mask as formula 7.

$$h(x,y) = c(\frac{x^2 + y^2 - \sigma^2}{\sigma^4}) e^{-\frac{x^2+y^2}{2\sigma^2}} \tag{7}$$

Among them, c will mask elements and specification of 0. In turn LOG operator due to its shape, known as the Mexican hat (Mexican hat). Discrete LOG operator ∇^2 said 5×5 template is as follows,

$$h = \begin{bmatrix} 0 & 0 & -1 & 0 & 0 \\ 0 & -1 & -2 & -1 & 0 \\ -1 & -2 & 16 & -2 & -1 \\ 0 & -1 & -2 & -1 & 0 \\ 0 & 0 & -1 & 0 & 0 \end{bmatrix} \tag{8}$$

Compared with other edge enhancement operator, the enhancement result using LOG in these images is all the better. The reason is the LOG operator lack of directionality. Fig.1 is the original image and the image after edge enhanced by the.

Using the algorithm of 2-D gray histogram to segment image

Every pixel has a gray group with two elements, one is its gray value, the other is the average gray value for its adjacent areas. If the frequency for a gray group (m,n) is f_{mn} in the image, we can define as follow,

$$p_{mn} = f_{mn}/N \qquad m,n = 0,1,2,\cdots,L-1 \qquad (9)$$

In the formula 9, L is the gray value of image. N is the count of the pixels of image. $\sum_{m}\sum_{n} p_{mn} = 1$, based on m, n as independent variables, p_{mn} as dependent variable, we can form a two-dimensional gray histogram. [3]

Usually selected a group of threshold (T, S), the 2-D gray histogram is divided into four areas as shown in Fig.2. In the figure, f (x, y) is pixel gray value of (x, y) which has be processed by LOG operator, and g (x, y) is the $n \times n$ neighborhood average gray value of pixel (x, y). The calculation formula is as follows,

$$g(x,y) = \frac{1}{n^2}\sum_{i=-n/2}^{n/2}\sum_{j=-n/2}^{n/2} f(x+i, y+j) \qquad (10)$$

On the type of n is odd number commonly, and n/2 integer, and there are $0 \le f(x, y) \le L-1, 0 \le g(x, y) \le L-1$.

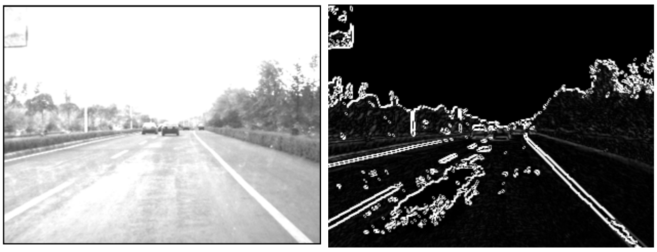

Fig. 1 Comparison between the original image and edge enhanced image

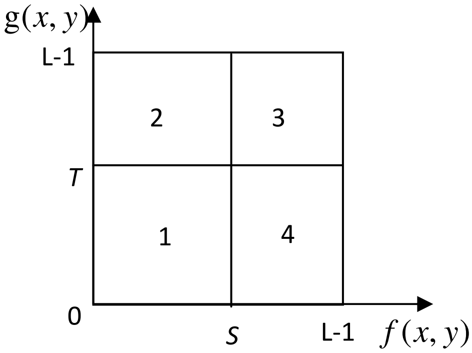

Fig. 2. A two-dimensional histogram

Area 1 is the area in which the average gray value of the pixels is less than the threshold S and T in Fig.2, the pixels in this area are the target (or background). And the average gray value of the pixels in area 3 is greater both than the threshold of S and T, and the pixels in this area are the background (or goals). But pixels in area 2 and 4 only satisfy a threshold S or threshold T, don't satisfy another segmentation threshold, so pixels in these two areas are boundary points or noise points.

From the view of statistics, segmentation is using the specimen to estimates the overall features. Using the distribution of the specimen to estimate the overall distribution is a parameter estimation problem. We can use the method of parameter estimation to segment the target image. The algorithm of moments invariant threshold segmentation is using moments method for image segmentation, the basic idea is: image moments hold the line before and after threshold segmentation. The algorithm of moment invariant threshold can be seen as a kind of image transformation, it transforms the original fuzzy image into an ideal image.

A two-dimensional image of the k order moment m_k is defined as formula 11.

$$\begin{cases} m_0 = 1 \\ m_k = \dfrac{1}{MN}\sum_{x}\sum_{y} f^k(x,y) = \dfrac{1}{MN}\sum_{i=0}^{l-1} h(i) \times i^k = \sum_{i=0}^{l-1} p_i \times i^k \qquad k = 1,2,\cdots \end{cases} \qquad (11)$$

In the formula, i is gray value, p_i is the ratio of the pixel whose gray value is i in the image. If the segmentation is binary, the image after segmentation only has two gray scale: Z_0 and Z_1, and $Z_0 < Z_1$. The rate of the pixels whose gray value is less than the threshold value is p_0, and the rate of the pixels whose gray value is higher than the threshold value is p_1, so the first three order moments of the segmented image is computed using the follow formula.

$$m_i' = \sum_{j=0}^{1} p_j \times (Z_j)^i \qquad i = 0,1,2,3 \tag{12}$$

The best threshold which is used to divide the target and the background, should keep the first three moments of the image equal before and after segmentation, i.e. $m_i' = m_i$. You can get the following equations,

$$\begin{cases} p_0 Z_0^0 + p_1 Z_1^0 = m_0 \\ p_0 Z_0^1 + p_1 Z_1^1 = m_1 \\ p_0 Z_0^2 + p_1 Z_1^2 = m_2 \\ p_0 Z_0^3 + p_1 Z_1^3 = m_3 \end{cases} \tag{13}$$

In order to get the best threshold T, we obtain p_0 from the equations firstly, the formula is shown as formula 14.

$$p_0 = \frac{G - m_1}{\sqrt{(c_1^2 - 4 \times c_0)}} \tag{14}$$

Among them,

$$c_0 = \frac{m_1 \times m_3 - m_2^2}{m_2 - m_1^2}, \quad c_1 = \frac{m_1 \times m_2 - m_3}{m_2 - m_1^2}, \quad G = \frac{1}{2}(\sqrt{c_1^2 - 4 \times c_0} - c_1)$$

And after obtain p_0, we can select suitable T on the original image histogram to satisfy the formula 15,

$$p_0 = \sum_{i \le T} p_i \tag{15}$$

T is the segmentation threshold we need. When we couldn't find the accurate gray value as the threshold values satisfy demand of p_0, we can select the closest gray value as segmentation threshold, the same method can be used to determine the threshold S. The calculation speed of the moment invariant algorithm is fast, and it can meet the real-time requirement.

The segmented image by the algorithm of 2-D gray histogram is shown in Fig. 3.

Using Hough transformation to identify the lane mark

There is a linear equation $y = mx + b$, and it can be represented with polar coordinates as formula 16,

$$\rho = x\cos\theta + y\sin\theta \tag{16}$$

In the formula, (ρ, θ) is a vector from the origin Perpendicular to the line.[4] We defines two parameters ρ and θ in the 2-D space. Lines in (x,y) plane corresponds to a point in the parameter space. Therefore, any straight line in (x,y) plane can be converts to a point in (ρ, θ) space by Hough transformation. First, we need to establish independent coordinate system for the left lane mark and the right lane mark respectively. Due to the lane mark in either side occupies almost one half of the image, in order to increase the timeliness of image processing, we only process the corresponding half image when identify the lane mark. And the coordinate system is shown in Fig.4 and Fig.5.

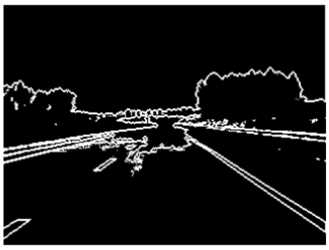

Fig. 3 The segmented image

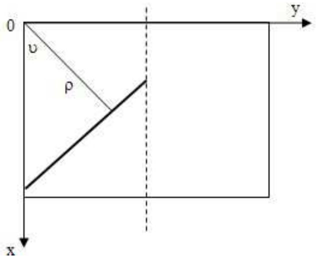

Fig.4 The coordinate system for the left lane mark identifying

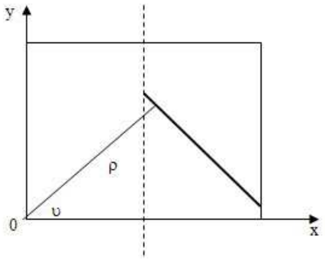

Fig.5 The coordinate system for the right lane mark identifying

This paper uses the algorithm in [5] to find the edges and to identify the edges of the two lane mark. The identifying result of lane boundary and the last identifying result are shown in Fig.6.

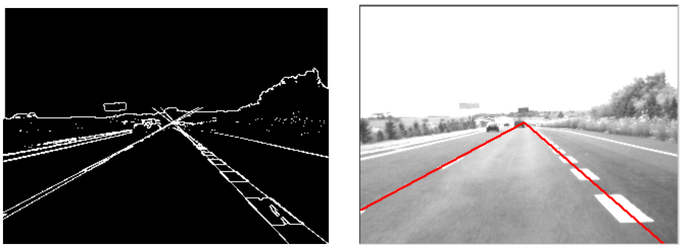

Fig. 6 Hough transformation method to identify lane boundary and the last identifying result

Lane marking line tracking algorithm

Tracking algorithm is essentially the road identifying algorithm, it uses the last road mark recognition result to define the current image recognition area. Namely according to the last identify information (including the intercept and slope) of the lane mark to determine the current recognition areas, and to adjust the areas dynamically, so the real-time property of system identification is improved. But when the lane mark is kept out seriously, the tracking algorithm may cause great error or even failure. Then the system needs to restart the initial identification algorithm to identify the road mark again.[5][6]

The intercept images of the real-time tracking road experiment are shown in Fig.7.

Conclusions

Firstly, this paper uses the LOG operator to enhance edges, so the target information is changed into almost some straight lines which have obvious character. Because the LOG operator is directionless, so compared with reference [5] its enhance effects is obvious. Next it uses the algorithm of 2-D gray histogram to segment image, this algorithm need to segment the image two times, and can improve the segmentation quality relative to reference [5]. Then the paper uses Hough transformation to identify the lane mark edges. And it uses the two identified edges to find out the middle line as the final recognition results. Finally, the recognition results of the last frame are used to limit the current frame image recognition areas when we track the lane mark. Verified by the experimental vehicles driving on the highway, the algorithm can effectively track the basic lane mark. Even in the case that the tracking target is error, the algorithm can also recover in time, and lock the tracking target accurately again.

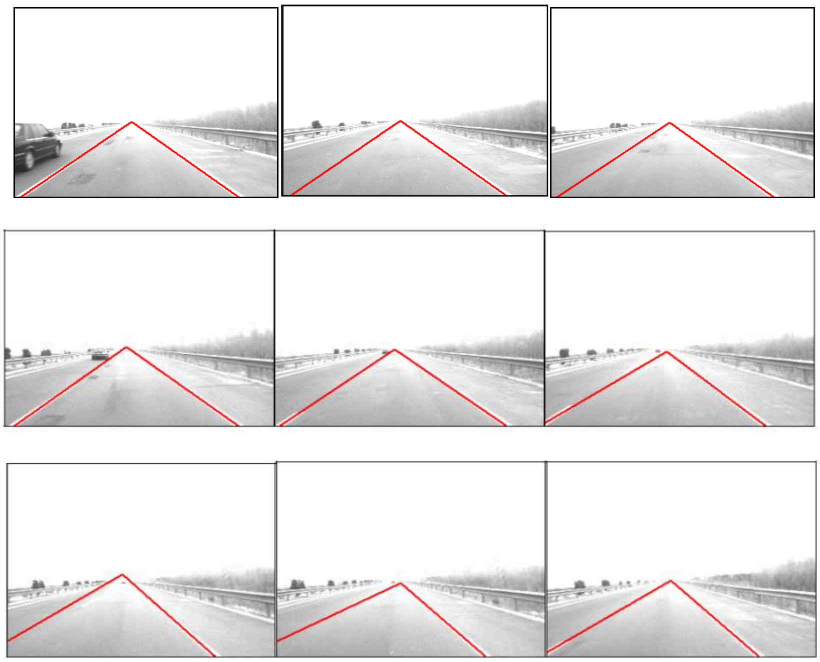

Fig. 7 Real-time tracking road intercept figure

References

[1] Massimo Bertozzi, Alberto Broggi, etal. “Artificial vision in road vehicles,” Proceedings of the IEEE IV. 90(7) (2002), pp.1258-1271.

[2] Pal N R, Pal S K. “A Review on Image Segmentation Techniques, ” Pattern Recognition, Vol.26, No.9（1993）, pp.1277 – 1294.

[3] De-kui, Y., Bao-min, Z., & Lian-fa, B. “2D Gray value transformation enhancement for infrared images,” Infrared Technology, 21(3) (1999), pp.25–29.

[4] Sun, F.-r., & Liu, J.-r. “Fast Hough transform algorithm,” Chinese Journal of Computer, 24(10),(2003),pp. 1102–1109.

[5] Yan-yun X., Bo Y. and Fang-qun Y.. “The Lane Mark Identifying and Tracking in Intense Illumination,” Computer Engineering and Networking, Electrical Engineering Volume 277(2014), pp. 567-575.

[6] Rong-ben, W., Tian-hong, Y., etal. “Research on linear lane mark identification and track method based on edge,” Computer Engineering, 32(16)(2006), pp.195–196, in Chinese.

Applied Mechanics and Materials Vol. 596 (2014) pp 361-364

© (2014) Trans Tech Publications, Switzerland

doi:10.4028/www.scientific.net/AMM.596.361

Mathematical morphology based moving object detection algorithm under complicated background

Jun Zhou[1, a]

[1] Shanxi Xueqian Normal University, Xi'an Shaanxi, China

sxfjq1980@163.com

Keywords: moving object detection; mathematical morphology; complicated background

Abstract. In many applications of modern world, moving object detection is an important work. Especially, the detection of moving object under complicated background has more difficult. On the basis of introduction of conventional detection methods such as temporal difference detection (TDD) and background subtraction detection, the paper proposes a new mathematical morphology based moving object detection algorithm in view of complicated background. The proposed algorithm utilizes the opening and closing operations to process the temporal differenced image. Then, it compares the processed image with the background differenced image. The experimental results show that the proposed algorithm can be able to detect the moving object effectively under complicatedly external environment and has a higher detection precision in contrast with the conventional temporal detection method..

Introduction

Moving object detection is an important work to kinematics. With respect to the research status of moving objects objection, the surveillance cameras installed on fixed locations are widely used at home and abroad, which process and analyze the continuous images through the linear and statistical theory. In a general way, the detection methods for moving objects can be summarized as four ways: temporal difference [1, 2], background subtraction [3], edge feature segmentation [4], optic flow [5]. In the four ways, the way of background subtraction is a widely used method due to its simple design and convenient calculation. However, the backgrounds for the images are not always static. Under complex background, it is harder to detect the moving object and is not a kind of algorithm can satisfactorily solve these problems. Therefore, the paper takes moving object detection as the research object. The aim of the paper is trying to present a moving object detection algorithm based on mathematical morphology under complex background

Conventional moving object detection methods

Temporal difference detection. The methods of separation of foreground and background in terms of change frame detection can be divided into two kinds in general, which are the ways of temporal difference and background subtraction. The way of temporal difference has no need to create a background image in advance; it relies on the subtraction of continuous two or three frame images and compares the difference value of the subtraction images with predetermined threshold value. Then, in terms of the comparison results it can judge whether a pixel is a moving case. The calculation method and judgment rule can be written in the following and shown in (1) and (2) respectively.

$$TD(i,j,t) = | I(i,j,t) - I(i,j,t-1) | \tag{1}$$

$$H(i,j,t) = \begin{cases} 1 \;\; if \; | I(i,j,t) - I(i,j,t-1) | > threshold_1 \\ 0 \;\; if \; | I(i,j,t) - I(i,j,t-1) | \le threshold_1 \end{cases} \tag{2}$$

where i and j indicate the position of i-th and j-th pixel, t express the time of input image; $I(i,j,t)$ describes the gray value of the pixel at time t for the detection image; $TD(i,j,t)$ represents the gray difference value between time t-1 and time t for the detection frame; $H(i,j,t)$ indicates ultimate frame difference value, 1 signifies that the pixel is moving, 0 demonstrates that the pixel is static; $threshold_1$ represents the threshold value.

The method of TDD can not detect the entire moving object and it can only extract the edge of the moving object. However, one of the major advantages of TDD lies in that it does not be easily affected by the change of the light. In addition, it is apt to be implemented in hardware and can be utilized effectively in the real-time object detection.

Background subtraction detection. In most of the methods of object detection, background subtraction detection is a way of basic detection. The detection principle of the method is to utilize the reference frame established in advance as the background frame.

Then, subtraction the input frame with the reference frame, if the difference value of the subtracted pixel is greater than a designated threshold, it signifies that the pixel may be a part of a moving object. The calculation formula and judgment rule can be written in (3) and (4) respectively.

$$BS(i, j, t) = | I(i, j) - B(i, j) | \tag{3}$$

$$H(i, j, t) = \begin{cases} 1 \ \ if \ | I(i, j) - B(i, j)) | > threshold_2 \\ 0 \ \ if \ | I(i, j) - B(i, j)) | \leq threshold_2 \end{cases} \tag{4}$$

where i and j indicate the position of i-th and j-th pixel, $I(i, j)$ describes the gray value of the pixel for the detection image; $B(i, j)$ describes the gray value of the pixel for the reference background frame; $BS(i, j, t)$ represents the gray difference value between the detection frame and the reference background frame; $H(i, j, t)$ indicates ultimate frame difference value, 1 signifies that the pixel is a part of a moving object, 0 demonstrates that the pixel is static; $threshold_2$ represents the threshold value.

One of the greatest merits for background subtraction detection is simple calculation; if the reference background image is selected properly, the method can segment the moving object quickly and accurately. Therefore, the detection method of background subtraction has a strong practicability. Simultaneous, the key of the background difference method to a successful detection depends on the background updating algorithm and remedying the adverse effects such as illumination changing. Additionally, it is difficult to set up a background model under complex external environment. Hence, the method of background difference detection is not suitable for moving object detection under complicated environment.

Mathematical morphology based moving object detection algorithm

In conclusion, the method of TDD can not detect the entire moving object and it can only extract the edge of the moving object. Mathematical morphology can precisely compensate for the shortcoming [6, 7]. In addition, the method of background subtraction detection can extract the moving object quickly and accurately. Hence, we firstly introduce the mathematical morphology to avoid the defects of TDD; then, it combines with the advantages of background subtraction detection and present a mathematical morphology based moving object detection algorithm under complicated environment.

Mathematical morphology. The merit of mathematical morphology can simplify the data of the image, maintain their basic shape characteristics, and remove irrelevant structure. Erosion and dilation can be considered as two basic operations for mathematical morphology. By means of erosion and dilation, many other morphological operations may be defined. The erosion and dilation operations can be defined utilizing the concepts of set theory where moving object detection can be treated as sets.

(1) Dilation operation

Firstly, determination the dilation image A and structuring element B, and conversion A and B into two sets, the dilation operation of A by B can be defined as the vector addition of the two sets A and B. In mathematics, dilation operation can be considered as being equivalent to the Minkowsky addition and is defined by the following:

$$D(A,B) = A \oplus B = \{c \mid c = a + b,\ \textit{for some } a \in A, b \in B\} \tag{5}$$

where $\oplus$ represents the dilation operator.

The dilation operation can be able to swell the image A in terms of the shape of the structuring element B.

(2) Erosion operation

Erosion is the dual operation of dilation. As a terminology in set theory, erosion indicates the vector subtraction of the structuring element B from the image A. The erosion operation determines where the structuring element B fits into the image A. Actually, erosion operation shrinks the image A in the manner determined by the structuring element B. It can also be demonstrated as the Minkowsky subtraction in mathematics, shown in (6), of the reflection of the structuring element 180° around the origin (-B) from the image A.

$$E(A,B) = A \otimes (-B) = \{c \mid c + b \in a,\ \textit{for every } b \in B\} \tag{6}$$

where $\otimes$ represents the dilation operator.

(3) Opening and closing

In terms of the operations of erosion and dilation, many other morphological operations may be defined, such as opening and closing, which are other two mathematical operations in morphological image processing. These employ erosion and dilation in pairs to smooth some details in detection image which are smaller than the structuring elements. The opening of an image A by the structuring element B, defined by $\circ$ shown in (7), is equivalent to eroding A by B and then dilating the eroded image by the same structuring element B. The closing of an image A by the structuring element B, defined by $\bullet$ shown in (8), dilates A by B and then erodes the dilated image by B.

$$A \circ B = (A \oplus B) \otimes B \tag{7}$$

$$A \bullet B = (A \otimes B) \oplus B \tag{8}$$

Opening acts as a filter, which smoothes from the inside as a result of rolling the structuring element inside the object. On the other hand, closing smoothes the objects from the outside. This low-pass filtering effect produced by both operations is determined mainly from the shape of the structuring element applied. The utilization of disk structuring elements is very universal in filtering due to rotationally invariant. Previous research has shown that one of the common applications of opening and closing is the removing of salt and pepper noise in images. Both the salt and pepper noise could be eliminated by utilizing a combination of opening and closing. Therefore, the paper utilizes the combination of opening and closing to preprocess the detecting image as a filter, defined by (9).

$$FB(A,B) = (A \circ B) \bullet B \tag{9}$$

Presentation of detection algorithm . Moving object detection based on mathematical morphology combination of TDD and background subtraction detection is presented and shown in Figure 1.

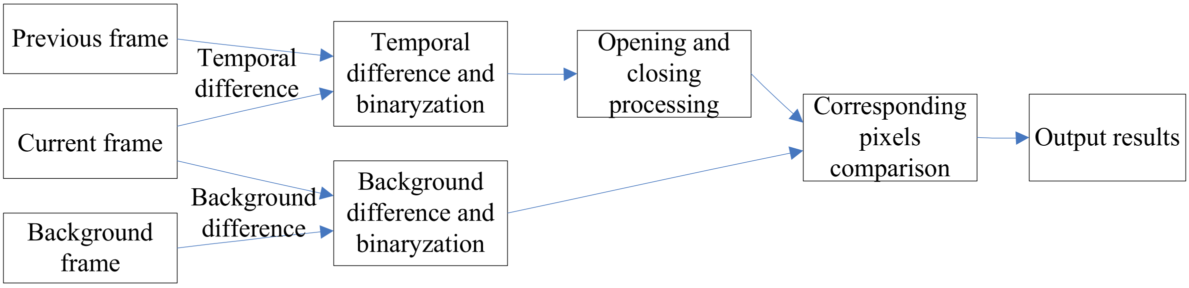
Previous frame
Temporal difference
Current frame
Background difference
Background frame
Temporal difference and binaryzation
Background difference and binaryzation
Opening and closing processing
Corresponding pixels comparison
Output results

Figure 1. Moving object detection algorithm based on mathematical morphology combination of TDD and background subtraction detection

In terms of Figure 1, the implementation of the proposed algorithm can be described as following: I. Selection of appropriate threshold value of temporal difference. II. Difference computation between previous frame and current frame, thresholding the differenced image, and obtaining temporal difference image. III. Selection of appropriate background frame and threshold value. IV. Difference computation between current frame and background frame, thresholding the differenced image, and obtaining background difference image. V. Choice of the reasonable structuring element in terms of shape and size for moving object, utilization of equation (9) to filter the temporal difference image. VI. Comparison of filtered image with background difference image, the compared output is the detection result of moving object for current frame.

Verification of the proposed algorithm.

In order to evaluate the effectiveness of the proposed algorithm, a sporting image including moving object is chosen to detect the moving object in Matlab environment under complicated environment such as changing light and local scenes. The previous frame and current frame is shown in Figure 2(a) and Figure 2(b) respectively. The detection results based on the methods of temporal difference and proposed algorithm by the paper are displayed in Figure 2(c) and Figure 2(d) respectively. Due to the changing of light and local scenes, the result of TDD exists noise points more or less and includes some static object points. In contrast with the result of TDD, the algorithm based on mathematical morphology enables to eliminate the noise points and detect the moving object relatively complete. Therefore, the algorithm proposed by the paper can be able to remedy the deficiency of the traditional methods and has a high detection effect.

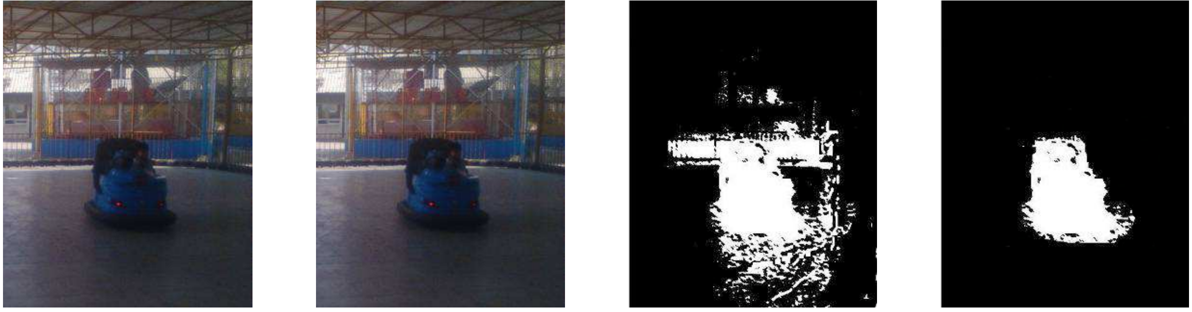
(a) Previous frame (b) Current frame (c) TDD (d) The proposed method

Figure 2. Verification of the proposed algorithm

Conclusions

Under complicated environment such as changing light and local scenes, the difficulty of detection of moving object is greater. To this end, the paper presents a detection algorithm of moving object based on mathematical morphology. The experimental results show that the proposed algorithm enables to extract the moving object effectively under complicatedly external environment. In comparison of the conventional detection method, it has a higher detection precision.

References

[1] T. Aach, A. Kaup, and R. Mester, in: Signal Processing, vol. 31 (1993), p.165.

[2] Mech and Wollborn, in: Signal Processing, Vol. 66 (1998) p. 203.

[3] Thongkamwitoon, Aramvith, and Chalidabhongse, in: IEEE International Conference on Multimedia and Expo, Vol. 2 (2004), p. 1459.

[4] T. Meier and K.N. Ngan, in: IEEE Trans. Circuit. Sys. Video Tech., Vol.9 (1999), p. 1190.

[5] R. T. Collins, A. J. Lipton, and T. Kanade, in: Technical Report, Robotics Institute, Carnegie Mellon University, May 2000.

[6] R. M. Haralick, S. R. Sternberg, and X. Zhuang, in: IEEE Trans. Pat. Anal. Mach. Intel., Vol 4 (1987), p. 532.

[7] J. Goutsias, L. Vincent, D. S. Bloomberg, in: Mathematical morphology and its applications to image and signal processing, Springer, 2000.

Applied Mechanics and Materials Vol. 596 (2014) pp 365-369
© (2014) Trans Tech Publications, Switzerland
doi:10.4028/www.scientific.net/AMM.596.365

Removing The Stripe Noises Interference On The Hα Full-disk Solar Image Based On Multiscale Transform

Shuan He[1,a*], Sheng Zheng[1,b], Yao Huang[1,c]

[1]College of Science, China Three Gorges University, Yichang 443002, China
[a]hs.ctgu@163.com, [b]zsh@ctgu.edu.cn, [c]hbhy1021@163.com

Keywords: Hα Full-disk solar image, stripe noises, multiscale transform, adaptive Gaussian filtering, multiscale inverse transform

Abstract. Hα full-disk observation is an important observation of the sun. It has an important significance to the solar physics research. But its observation process may be affected by the system, resulting the observed images contain stripe noises. This paper describes a method to remove the particularity of stripe noises contained in the Hα full-disk solar image. This method includes the following four steps: First, decomposing the sun image into multiple detail scales by the multiscale transform; Second, doing special two-dimension signal conversion on the detail scales mainly containing the noises signal; Third, doing the adaptive Gaussian filtering on the two-dimension signal and restoring the processed signal to the image; Finaly, using the multiscale inverse transform to obtain the final restoration image. Experiments show that this method can effectively remove this type of noise interference from the solar image and improve the quality of the solar image.

Introduction

In 1984s, our country has established the Huairou solar observing station, since our country started the modernization of uninterrupted solar activity monitoring. Huairou solar observing station has run 14 cm and 20 cm Hα telescope and the 14 cm Hα telescope is no longer used. The rotation of the two devices are in the second half of the solar 23th week later, that is from 2001 to 2009. From 2001 to 2009, optical observation system problems resulting in some Huairou station's Hα full-disk data decline in the quality. Mainly as raw data were normal, but the high contrast Hα data appearance of the problem of the observation details mixed stack strips interference and the background is uneven brightness after deducting the limb darkening background[1], especially in 2001. Typical data after deducting center symmetrical limb darkening background is shown in Figs.1 and 2. This paper mainly for Hα solar images (hereinafter referred to as the solar image) after deducting the limb darkening background processing, eliminating interference with the noise of the image aliasing and improving the quality of the image, which is great significance to the solar physics research.

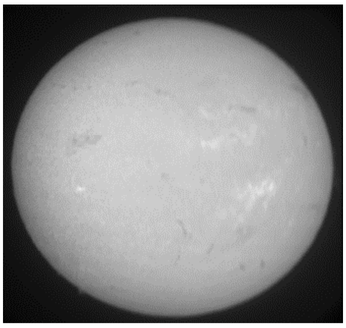

Fig.1 Hα full-disk solar image

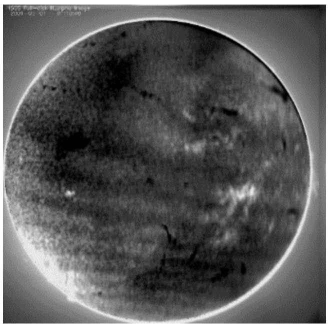

Fig.2 Deducting the limb darkening background of the solar image

It is found that the stripe bands interference keep reproducibility and stability over a period of thime after analyzing image data of the Huairou Observatory database. Thus we know the tripe bands interference is not random, but because of the interference caused by the system. The interference belongs to the category system noise. The boservation system usually needn't have to make adjustments within a period of observing the sun, so that the noises should be very similar in the period. It has confirmed by analyzing the image datas in the database. After adjusting the observation system, the phenomenons of the interference also occurred in some of the changes. The more obvious changes are the position and orientation of the interference. However, the interferences become similar after making the appropriate rotation process of the image. All of these features indicate that the interference is not random.It is stable.So,this paper will considers the interference as system noise to deal with. This treatment will helps in removing noises.

The removal method of interference in the image

The method used in this paper includes the following sections.First,decomposing the original solar image into multiple scales using the multiscale transformation[2,3]. Identifying the component of the scales including the noises interference by carrying on the analysis on each scale.Then removing the strip noises through doing some filtering processes on the scales including the noises interference. Finally, obtaining the denoised image data by multiscale inverse transformation.

Wavelet Transform. One-Dimensional Wavelet Transform. Let $\psi(t)\in L^2(R)$, $L^2(R)$ denotes square integrable real number space , that is , energy priority signal space, the fourier transform of $\psi(t)$ is . When satisfies the following inequality:

$$C_\psi=\int_R\frac{|\hat{\psi}(\omega)|}{|\omega|}d\omega<+\infty \tag{1}$$

We call a basic wavelet or mother wavelet. Then , by scaling and translation, the mother wavelet can obtain a wavelet sequence. For a continuous wavelet sequence, we have

$$\psi_{a,b}(t)=|a|^{-\frac{1}{2}}\psi(\frac{t-b}{a}) \tag{2}$$

Where $b\in R$ is scaling factor and $a\in R^+$ is translation factor. For any function $f(t)\in L^2(R)$, the continuous wavelet transform is

$$W_f(a,b)=\langle f,\psi_{a,b}(t)\rangle=|a|^2\int_R f(t)\psi(\frac{t-b}{a})dt \tag{3}$$

For any function , the continuous wavelet transform is

$$f(t)=\frac{1}{C_\psi}\int_{R^+}\frac{1}{a^2}W_f(a,b)\psi(\frac{t-b}{a})dadb \tag{4}$$

Two-Dimensional Wavelet Transform. In order to use Wavelet Transform on picture processing, we have to extend one-dimensional Wavelet Transform to two-dimensional Wavelet Transform. We assume two-dimensional $\varphi(x,y)$ is separable, and its scale function is $\varphi(x)$, the wavelet function is $\psi(x)$, then, we have $\varphi(x,y)=\varphi(x)\varphi(y)$ .We constuct the following three two-dimensional basic wavelet functions:

$$\begin{aligned}\psi'(x,y)&=\psi(x)\psi(y)\\ \psi^2(x,y)&=\psi(x)\varphi(\mathrm{y})\\ \psi^3(x,y)&=\varphi(x)\psi(y)\end{aligned} \tag{5}$$

then, the base of two-dimensional wavelet can come ture by the following telescopic translation:

$$\psi^i_{j,m,n}(x,y)=2^{-j}\psi^i(2^{-j}x-m,2^{-j}y-n) \tag{6}$$

Where $j,m,n\in z,\ i=1,2,3$ .So A two-dimensional image signal $f(x,y)$'s smooth component (low frequency component) in the scales of 2^j represented by two-dimensional sequence $D_j(m,n)$ as follows.

$$D_j(m,n) = < \mathrm{f}(x,y), \varphi_{j,m,n}(x,y) > \tag{7}$$

Where $\varphi_{j,m,n}(x,y) = 2^{-j}\varphi(2^{-j}x - m, 2^{-j}y - n)$

Detail component (wavelet coefficients) can be expressed as follows.

$$\begin{aligned} C_j^1(m,n) &= WT_{2^j}^1(m,n) = < f(x,y), \psi_{j,m,n}^1(x,y) > \\ C_j^2(m,n) &= WT_{2^j}^2(m,n) = < f(x,y), \psi_{j,m,n}^2(x,y) > \\ C_j^3(m,n) &= WT_{2^j}^3(m,n) = < f(x,y), \psi_{j,m,n}^3(x,y) > \end{aligned} \tag{8}$$

In this paper, using the theory of wavelet transform to do two-dimensional multiscale transform process of the sun image. The original image is decomposed to 19 scales, and then process each scale.

Adaptive Gaussian filter. Analyzing all the scales decomposed by the multiscale transform and finding out the detail scales contained the stripe noises information. Then denoising the scales. Finally,obtaining the final restoration image through multiscale transform. In order to remove the strip noise interference on the scale, first of all have to eliminate the influence of the boundary of the sun. In this paper, by extracting the information of the sun for processing, namely to retain the information that does not belong to the sun area don't deal with. For extracting the area of the sun[4,5], the main steps are as follows.

Step 1: Using a threshold higher than the background picture for the binarization processing to the background excluding the impact of the sky, and then extract the edge of the binary image for the circle fitted to obtain the initial position of the center of the sun and the solar radius, but the center and radius are not very accurate.

Step 2: Using Sobel operator to obtain the gradient image of the sun,then calculate the average gradient and gradient MSE. Using three times the mean square error as the threshold for binary gradient image to get the information of the edge of the sun and the regional information that the gradient changed dramatically in the solar active region. Using the initial value of center and radius to do circle fitted again. Through iterative calculation, excluding the "outliers" in the solar surface activity area.

This paper uses the two-dimensional signal filtering method to deal with the image region extracted from the solar image. The main steps are as follows.

Step 1: Decomposing the image into many line segment along the direction of the strip. Then calculating the value of each pixel on line by using Cubic interpolation method. Taking the ordinal number of pixels as the abscissa and the values of the pixels as the ordinate to build a similar two-dimensional signal.

Step 2：Analyzing the two-dimensional signal and making filtering processes with the adaptive Gaussian filter.

Experimental results and analysis

In this paper, the experimental datas from Huairou observatory site. Fig.3 is the solar image included stripe noises. By the image, you can see the stripe noise is very obvious. Figs.4 and 5,6 are the parts of the scale component of image data after multi-scale transform from Fig.3. The Fig.4 contains the stripe noises is not obvious, but the Figs.5 and 6 are obvious.Through the analysis of all the scale component, it is found that the stripe noises mainly concentrated in the Figs.5 and 6, which are the 13th and 16th scale component in the results of of the algorithm introduced in this paper. It is useful to do a great separation and can more effectively retain the useful information in the image.

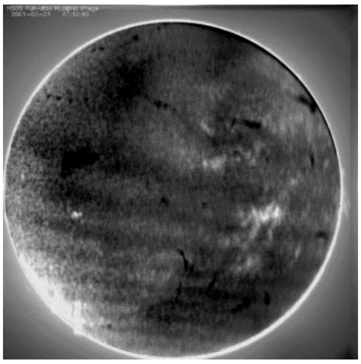

Fig.3 Solar image

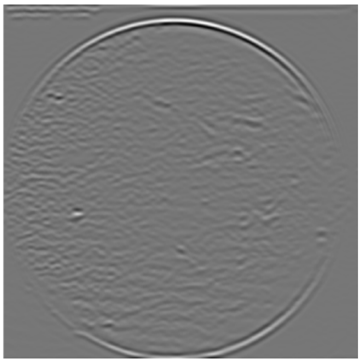

Fig.4 The 10th scale component

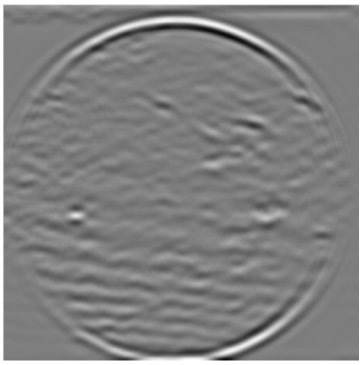

Fig.5 The 13th scale component

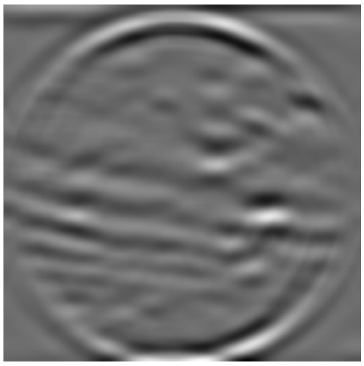

Fig.6 The 16th scale component

Extracting the solar center and radius from the decomposed detail scales. Then extract the solar area datas from 13th and 16th scale to do separate process and outside the area of the sun don't do any process. Changing the image of the solar area datas to lines along the direction of the noise. Taking the ordinal number of pixels as the abscissa and the values of the pixels as the ordinate to build a similar two-dimensional signal. Then do two-dimensional adaptive Gaussian filter on the two-dimensional signal. After filtering processes of datas restored to the image. Then the datas processed superimposed on the corresponding thereto image data retained. Finaly, using the multiscale inverse transform to obtain the final restoration image. The original image is shown in Fig.7 and the final results is shown in Fig.8.

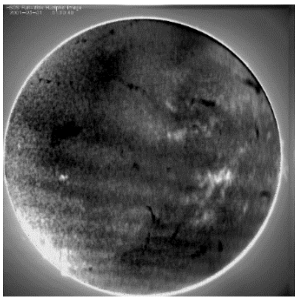

Fig.7 The solar image with noises

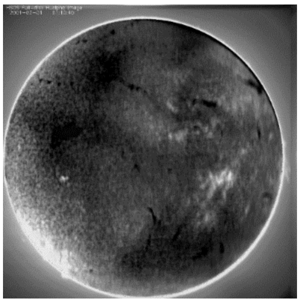

Fig.8 After denoising image

Image denoising effect assessment

In order to evaluate the denoising effect of the finally obtained Hα full-disk solar image, this paper from the subjective and objective two aspect carries on the comprehensive evaluation . Denoising effect from a subjective point of view, the strip noises have been unable to identify with the naked eye. It can be said that the denoising effect is obvious evaluated from the subjective evaluation. For objective evaluation, this paper adopted the Peak Signal to Noise Ratio (PSNR) [6] method to evaluate the effect of the denoising. The specific evaluation method is as follow. For a M by N size image, which is quantized from 0 to 255, the calculation formula of peak signal to noise ratio is as follow.

$$PSNR(\mathrm{dB}) = 10\log_{10}\frac{255^2}{\frac{1}{M*N}\sum_{x=0}^{M-1}\sum_{y=0}^{N-1}\left[f(x,y)-\tilde{f}(x,y)\right]^2}$$

Where the $\tilde{f}(x,y)$ is the restoration image after denoising. According to the formula to calculate the peak signal to noise ratio of the final restoration image in this paper is 38.68. From the numerical analysis also illustrates the denoising method in this paper is effective.

Conclusion

In this paper, two-dimensional transformation is used after decomposition of the image processing based on the multiscale transform. Using the adaptive Gaussian filter to remove the stripe noise in the solar image. Image comparison before and after the test found that the obvious stripe noise of images containing has almost never see and the bright spots and dark bars are still good on the surface of the solar image. We look at the same period, different time of image processes, the results verify the effectiveness of the proposed method in removing such a stripe noise.

Acknowledgements

The research work was supported by the National Natural Science Fund Committee of the Chinese Academy of Sciences astronomical union funds NO.U1331113.

References

[1] http://sun.bao.ac.cn/hsos_datas/full_disk/h-alpha

[2] Qin Xue. Image enhancement based on multiscale analysis research. Jiangxi: Jiangxi normal university(2006).(In Chinese)

[3] Xiaoqing Shang. Multiscale analysis in the application of image processing.Shanxi: Xidian University(2004). (In Chinese)

[4] C. Denker, A. Johannesson, W. Marquette, et al. Synoptic Hα Full-disk Obervation Of The From Big Bear Solar Observatory. SoPh(1999),p.184:87.

[5] Haibo Zhu, Yunfei Yang, Hui Deng, Kaifan Ji. Removing the cloud contamination from the Hα full-disk solar image. Astronomical Research & Technology, http://www.cnki.net/kcms/detail/53.1189.P.20130922.1627.003.html. (In Chinese)

[6] Song Li Juan, Tian Rui, Meng Meng. Digital image quality evaluation method research. Computer Knowledge and Technology, Vol.6(2010),p.184-185. (In Chinese)

Applied Mechanics and Materials Vol. 596 (2014) pp 370-373
© (2014) Trans Tech Publications, Switzerland
doi:10.4028/www.scientific.net/AMM.596.370

Research on Scene Organize Algorithm Based on BVH with Dynamic Rendering Tree

Li XU[1,a], Maozhen LIU[2,b]

[1] Computer College, Beijing Information Science and Technology University, Beijing 100101, China

[2] Virtual Reality and Simulation Laboratory, Beijing Information Science & Technology University, Beijing 100192, China

[a]email:xuli_lh@139.com, [b]email:liumaozhen123@126.com

KEYWORDS Scene Organize; Multimedia Technology; Rendering Tree; Scene Management

ABSTRACT: The real-time rendering of 3D scene need excellent algorithm to support scene management. After considering the algorithm complexity and scene scale factors, combining the advantages of Bounding Volume Hierarchy (BVH) and rendering tree in scene management, this paper puts forward a kind of scene organize algorithm, to solve the problem of render states redundant calculation when using BVH technology to solve the problem of deformable collision detection, by choosing the appropriate strategy of Hierarchy Bounding Volume tree construction and optimizing rendering tree of the scene. Experiments prove the proposed algorithm can effectively improve the rendering efficiency of 3D scene, enhance the visual effect.

Introduction

In 3D scene rendering, requiring real-time rendering, high precision collision detection and strong interactivity. For meeting the above requirements, that must have excellent algorithm support for scene organization and management.

Scene is often composed of complex 3D model, the model number from hundreds of thousands to millions, and there is a complicated logic relationship between each other, how to organize these models, and their mutual relationship, and how to don't reduce the scene shows quality of the case, try to reduce the space complexity, this is the task of the scene organization and management.

Scene graph is a scene data management way that make all kinds of data in the form of organization together, it is a tree structure, the root node is the whole scene, each node in the tree can have any number of child nodes, each node storage scene integrated data structure, including geometric object, light source, camera, sound, bounding box, transformation, and other attributes. For scene graph, the more widely used management methods are the scene management based on the rendering state, the scene management based on the volume, and the scene management based on the geometric subdivision.

Based on the above management methods, this paper propose a scene organization algorithm based on BVH algorithm with dynamic render tree, and through experimental verification, the algorithm can effectively improve the rendering efficiency of 3D scene, improve rendering realistic, enhance the visual effect.

Scene Graph Based on BVH

Bounding Volume Hierarchy(BVH) is that in the external of the scene to add a closed space form, each object in the scene also have belong to own a closed space form, the outer space form and inner scene object bounding volume formed layers of nested structure, so as to improve the collision detection of the scene, and the culling processing speed. In this platform, comprehensive consideration to the scene rendering rate, and the operational capability of CPU, use the bounding box and enclosing ball, this two kinds of structure to organize the bounding volume hierarchy in the scene. in order to achieve the best scene organization and rendering performance.

For example, suppose there is such a scene, in a room with three computers on three desks respectively, two material cabinets, three chairs, for such scenes, we can organize the structure of the scene through the following steps: first, to determine the object in the scene, computer, desk, chair, material cabinet; then determine their relationships, material cabinet and chairs can be regarded as independent that can be drawn, with independent bounding box to represent the object's bounding volume, the computer on the desk, we can put a desk and the corresponding computer to be surrounded in the body, desk and computer in separate surrounded in the body, similar to the other two desks and computers; finally, determine the hierarchy, according to the three branches under the root node, respectively organize material cabinets, chairs, desk, computer, but computer and desk is divided into two branches, respectively is a desk and a computer.

This scene graph of *BVH* tree can clearly express the scene objects in the scene graph, and a detailed description of the logical relationship between them, as in the scenario above, the desk is moved, the computer on the desk must be moved along with the desk. Scene graph based on *BVH* can be good enough to meet this need, and this kind of structure can realize the nested body, when the scene is calculated, can reduce the testing calculation between a large number of objects, thus accelerating the scene object intersection test, culling, collision detection plays an important role.

Scene Organize Algorithm based on BVH with Dynamic Rendering Tree

Through the above analysis shows that scene graph based on *BVH* is used for scene management, and it by optimizing the structure of scene node to improve traversal scene tree drawing speed, thus faster execution culling, collision detection algorithm, etc. However, after executing scene traversal and culling, that will have to draw the content delivery to *openGL* rendering pipeline, at this time, there are a lot of redundant in rendering state.

The scene organize algorithm based on BVH with dynamic rendering tree is designed to solve the problem of redundancy of at this point. the first, after scene traversing and update status, when tailoring, culling scene information to be not within the field of vision or be blocked, and saving the scene object rendering state to a dynamic rendering tree at the same time, by setting the render tree construction principles and methods, to generate an optimized scenario rendering tree, and then execute drawing, thus improve the efficiency of rendering.

The rendering mechanism of scene organizing Based on *BVH* with dynamic rendering tree, it can be summarized as the following process, as shown in Fig.1.

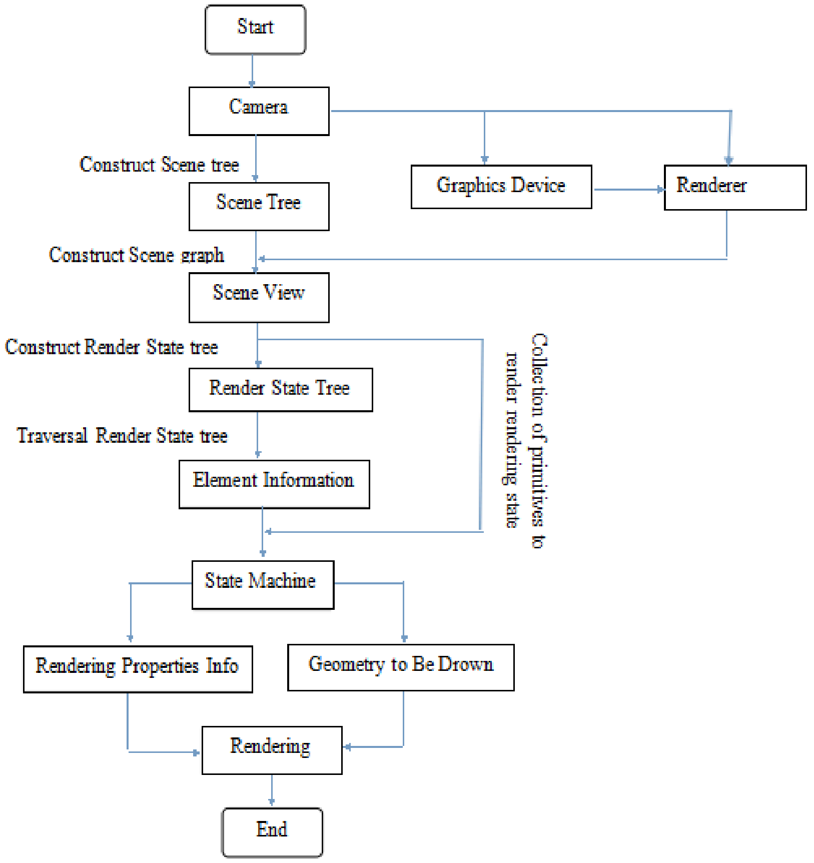
Start
Camera
Graphics Device
Renderer
Construct Scene tree
Scene Tree
Construct Scene graph
Scene View
Construct Render State tree
Render State Tree
Traversal Render State tree
Element Information
Collection of primitives to render rendering state
State Machine
Rendering Properties Info
Geometry to Be Drown
Rendering
End

Fig.1. Rendering mechanism flow chart

Among them, building the scene tree is the key to describe the scene logic. the role of scene tree is organizing data from space on the logical relationship. However, effect of *openGL* rendering efficiency is not only the data structure, more of a switching frequency of rendering state in scene rendering process. How to reduce the switching frequency and reduce the redundancy caused by repeat drawing, that will directly affect the real-time of scene rendering and user experience, therefore, it is necessary to organize the rendering state in scene, through culling, state sorting and various other methods, result in optimal rendering state tree, and then to handed over to the state machine (*openGL) to* rendering. Our algorithm is as follows:

1.Based on *BVH* construct scene graph, according to the viewpoint location computing scene graph structure in the corresponding view within the scope of the objects in the scene.

2.Traversal scene graph, getting the scene object state, and based on scene graph structure to construct the original rendering state tree.

3.Traversal rendering state tree of scene, according to the state of the scene time consuming to reorder the scene render tree, to form the final render state tree.

Experimental Results

We have used 3D graphics tool *openGL* programming to do rendering state tree and experiments for the above algorithm， the results are shown in Table 1.

Table 1 Rendering rate comparison

Algorithm	Texture resolution 8*8; Single-lighting Diffuse Reflection	Texture Resolution 64*64; Multi-lighting Diffuse Reflection	Texture Resolution 126*126; Multi-lighting Diffuse Reflection and Specular Reflection
BVH with DRT	16.39ms	20.83ms	32.26ms
General	19.23ms	27.78ms	71.43ms

Through the above data can be obtained, the first set of data for texture resolution 8 * 8, and single- lighting diffuse reflection, the rendering rate increased by 17.31%; the second set of data for texture resolution 64 * 64, multi-lighting diffuse ,the rendering rate increased by 33.33%; the third set of data for texture resolution of 126 * 126 , multi-lighting diffuse reflection, and specular reflection, rendering rate increased by 121.43%. It can be seen, the more complex scene rendering state, the more improvement rendering rate.

Conclusion

This paper is based on *BVH* and rendering tree technology to put forward the scene organize algorithm. In the algorithm, the first, by using the loose characteristic of the Surrounded ball carries on the simple distance test and fast collision detection, and then using the rigor of the bounding box carries on more rigorous test, when tailoring, culling scene information to be not within the field of vision and obscured , and saving the scene object rendering state by sorting order to a dynamic rendering tree, optimized to generate a scene rendering tree, and finally execute render, and thus more rapid execution scene culling, collision detection algorithm to improve rendering efficiency.

Acknowledgements

This work was financially supported by the Innovation Team Building of Beijing Municipal Institutions of Higher Learning and Teachers' Professional Development Program (Project No.IDHT20130519).

References

[1] Xing GAO , Zhi ZHANG, Yu QUAN. 3D Game Engine Research and Design [J]. Computer System Application, 2013 (8). In Chinese

[2] Cooper D H. Calculator Program for Head-related Transfer Function[J]. Journal of the Audio Engineering Society, 1982, 30 (1/2): 34-38.

[3] Kyound-MiLee, Street W. N.Cluster-driver refinement for content-based digital image retrieval. Multimedia, IEEE Transactions, Dec. 2004, 6(6): 817-827

[4] MingJiang YIN . Research on Key Technology of Assembly Scene Simulation [D]. Huazhong Science and Technology University , 2013.In Chinese

[5] Xing ZHOU ,Zhaoliang ZHANG. Research on Hot-line Work Simulation Training System based on Virtual Reality Technology [J]. Hydropower Science, 2012, 30 (12) : 160-162.

[6] Wuli WANG , Yanjiang WANG, Drilling LI. Simulation System based on Virtual Reality Technology [J] Computer Technology and Development, 2011, 21 (9) : 171-178.In Chinese

Applied Mechanics and Materials Vol. 596 (2014) pp 374-378
© (2014) Trans Tech Publications, Switzerland
doi:10.4028/www.scientific.net/AMM.596.374

Study of Video Object Detection and Shadow Suppression Algorithms

Qilin Gai[1, a], Guoqiang Wang[2,b]

[1]School of Electronic Engineering, Heilongjiang University, Harbin, China

[2]School of Electronic Engineering, Heilongjiang University, Harbin, China

[a]gaiqilin1314@163.com, [b] wangguoqiang@hlju.edu.cn

Keywords: Object detection, Background subtraction, Shadow inhibition, YUV color space

Abstract. In the field of intelligent video surveillance and the multimedia applications we usually need to detect the moving object which is separated from the background. The results of the moving object detection would affect the subsequent identification, classification and tracking. Meanwhile shadow detection and suppression are also the important technology of the intelligent video surveillance. Because the moving object and shadow usually has the same behavioral characteristics, which has led to the errors of object recognition and tracking and affect the robustness of system seriously. This article studies the principle and algorithm of background subtraction, and has a detailed discussion and analysis. Shadow detection and suppression algorithms based on the YUV color space for processing. The experiment result shows that the algorithms for moving object detection with a better accuracy and stability of this paper.

Introduction

In the modern intelligent video surveillance and multimedia technology, it is often necessary to separate the moving object from the background. In general, the moving object detection is our most concerned part. The different places of the static target are: the biggest advantage of the video is that we can get the movement information more easily, so the moving object detection and analysis is the difficulty and emphasis of the video research, and also is the basis of many advanced applications in the field of video.

The primary purpose of the video moving target analysis is target detection. The goal of video target detection is extracting the moving object from video background. Since the moving target pixels are the important foundation for future target classification, tracking and behavior understanding post-processing, moving object extraction is very important process in video processing, and the effect of the whole system may be changed by the video target detection result.

Due to the uneven illumination and other reasons, the object often produces a shadow phenomenon. The shadow will affect the effect of motion segmentation and change detection. The shadow seriously affects the target segmentation, subsequent tracking and recognition, which leads to error rate increased and reducing the system performance. In practical applications the object is always accompanied by a shadow, we must remove the shadow firstly to ensure most of the objects have the detection and segmentation correctly.

The background difference algorithm is different from the global illumination changes of video image sequences in many video surveillances, it is very sensitive to the changes in illumination. The shadow related to the background is the color feature local change which will be judged as the wrong target. Since the shadow usually has the same law of motion with the object, the moving shadows are often detected as the fake object with the real target, which makes the object shape changed. The wrong shape moving object will seriously affect the next work of system, impacting feature extraction and recognition of the subsequent object seriously.

Object Detection Algorithms

Optical Flow Method

Optical flow method is a method of target detection based on grayscale gradient almost unchanged and the brightness conservation for constraint assumptions.

At the time t the gray value of the pixel in the image at the point (x, y) is $E(x, y, t)$. At the time $t + dt$, this pixel moves to the $(x + dx, y + dy)$, so the gray value of the image point at time $t + \Delta t$ can be denoted as the $E(x + dx, y + dy, t + dt)$, assumes it is equal to the $E(x, y, t)$

$$E(x + dx, y + dy, t + dt) = E(x, y, t) \tag{1}$$

Then we can Taylor expand formulas the left side of the formula (1), after calculation and elimination of quadratic term get

$$E(x, y, t) + \frac{\partial E}{\partial x} \cdot dx + \frac{\partial E}{\partial y} \cdot dy + \frac{\partial E}{\partial t} \cdot dt + o(dt^2) = E(x, y, t) \tag{2}$$

Also

$$u(x, y, t) = \frac{\Delta x}{\Delta t} = \frac{dx}{dt} \tag{3}$$

$$v(x, y, t) = \frac{\Delta y}{\Delta t} = \frac{dy}{dt} \tag{4}$$

Where $o(dt^2)$ is the higher order terms with order greater than or equal to 2, erasing $E(x, y, t)$ and ignoring $o(dt^2)$ we have the optical flow constraint equation

$$\frac{\partial E}{\partial x} \cdot u + \frac{\partial E}{\partial y} \cdot v + \frac{\partial E}{\partial t} = 0 \tag{5}$$

Frame Difference Method

Frame difference method is to detect the moving target of the image using threshold value and the time difference based on the pixel from the two or several frame which are continuous of the video sequence [2].

Consider the frame K and the (K-1) frame images respectively as $y_k(i, j)$ and $y_{k-1}(i, j)$, and obtain their difference image

$$D_k(i, j) = \left| y_k(i, j) - y_{k-1}(i, j) \right| \tag{6}$$

$$M_k(i, j) = \begin{cases} 255, D_k(i, j) \geq T; \mathit{foreground} \\ 0, \quad \mathit{otherwise}; \mathit{background} \end{cases} \tag{7}$$

Where T is threshold value which is used to determine each pixel in the image sequence whether it is foreground or background, so that the image $M_k(i, j)$ of the moving foreground region is further extracted.

Background Subtraction Method

The principle of the background subtraction method is a motion detection method with using the differential of the current image and the background image to extract a motion area [3]. According to the changes in the grayscale value to judge, that is using the current image and background do the differential. If the difference value is greater than a certain threshold value, it is considered to detect the target.

In background subtraction algorithm, the accuracy of the background image selected affects the accuracy of the final target detection directly. Under ideal conditions, it is generally believed that when the background image remains stationary and when the pixel values of the motion of the target area is changing, the background pixel values remain unchanged. Background subtraction method formula

$$D_k(x,y)=\left|f_k(x,y)-f_{bk}(x,y)\right|X_1,\ldots,X_n \tag{8}$$

$$M_k(i,j)=\begin{cases}1, & D_k(i,j)\geq T\\ 0, & otherwise\end{cases} \tag{9}$$

Where $f_k(i,j)$ is current image frame and $f_{bk}(x,y)$ is background image frame.

Moving Target Detection

Firstly, a number of video frames can be got by using the camera, then to do the sub-frame processing for the obtained video. Then the video is divided into a number of frames. Using the median background model method to process the video frames which we have got, then further to get the background of the video. Subsequently, the images acquired from the video are preprocessed to eliminate noise in the image. That is to obtain the foreground region using background difference method, then getting the the difference image of moving targets, so the moving targets can be detected out. Finally the foreground image got before is post-processed, such as erosion, dilation, opening and closing operations. The complete target can be extracted through doing the shadow detection and suppression. The algorithms and flow chart is shown in Fig.1.

The light problem leads to that the target shadow is not obvious of the below experiments, so the target detection didn't appear shadows. When the shadow is obvious under sufficient light, the shadow detection and suppression of target should be done. The approach in this case will be introduced in the next part. The 28th frame image is shown in Fig.2. The background picture is shown in Fig.3. The target detection without shadow is shown in Fig.4.

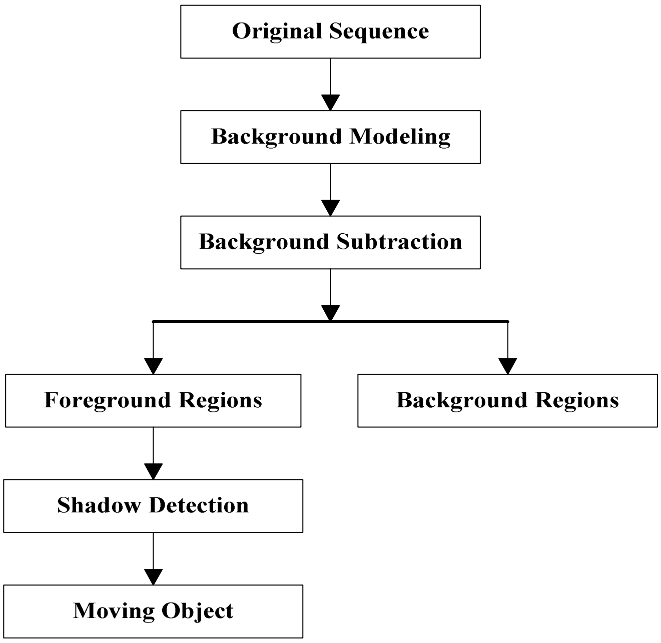

Fig.1 Flow diagram of basic algorithm

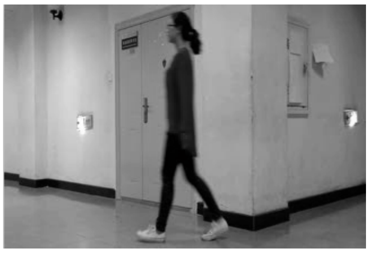

Fig.2 28th frame image

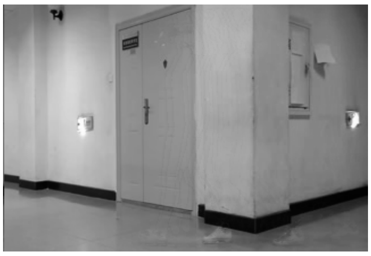

Fig.3 Median filter to obtain background

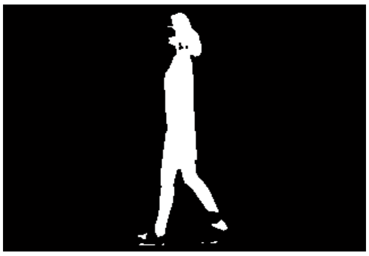

Fig.4 Detection result

Shadow Detection and Suppression

The reason for the formation of the shadow is because the light source is blocked by some objects in the video, but the optical properties of the corresponding target are still exist, such as texture and color of the target. Based on visual analysis and summary, the same targets in the shadowed area and not in the shadowed area have the similar color properties. That is when a certain pixel point has been covered with the shadow, the value of its brightness along becomes small, but the chromaticity values did not change significantly.

In RGB space, because without independent processing on the luminance information and chrominance information, the 3 channels are not mutually independent, there hasn't a good solution to solve the problem of the shadow in the detection. However, the detection of YUV space can be a good solution to solve the shadow problem, the method used in this paper is the YUV color space[4].The method of this paper is based on the shadow properties, which is based on the characteristics of the image usually directly.

We just need to discuss the moving parts (containing the moving target and the shadow) of the pixels. If it is with the chromaticity difference between it and the corresponding background point is very small, while the brightness and saturation difference is decreasing, thereupon the pixel can be considered to belong to the shadow part.

After the background frame generated, to detect the target in video image sequence using the background subtraction method[5]. That is to compare the luminance difference of the corresponding pixel between the current image frame and the background frame in the image sequence to obtain the sequence of video images only including of the moving part based on a certain threshold value is selected to be extracted on the target. Therefore, in the subsequent shadow detection just need to do the division processing of the moving target and shadow to the moving parts. The effects obtained in the current image and no shadow suppression shows in Fig.5 and Fig.6. Because the luminance difference between pixels in the shadow region and background relative pixel is beyond the selected threshold value, the shadows are included in the image motion foreground region after dividing.

Shadow suppression method is based on the shadow of the YUV color space properties of this article. That is based on after compare the luminance of the shadow and background brightness is darken, and the chrominance difference of the shadow and background is small, the shadow should be detected using this conditions. The method can be judged according to the following rules

$$M_{x,y} = \begin{cases} 1, & d(Y) > T_Y \\ 1, & d(\mathrm{U}) + d(\mathrm{V}) > \mathrm{T}_{uv} \\ 0, & otherwise \end{cases} \tag{10}$$

In the formula (10), when the value of $M_{x,y}$ is equal to 1, it indicates that the pixel is a foreground moving target, when it is equal to 0, it is the background area. $d(Y)$ is the luminance difference between the current pixel and the background pixel, $d(U)$ and $d(V)$ are respectively the two chrominance difference of the current pixel and the background pixel. T_Y is the threshold value of the corresponding luminance difference, T_{uv} is the threshold value of the corresponding chrominance.

Three cases of formula (10) listed can be explained under the understanding below.

1) When the difference between the luminance value of the current pixel and the corresponding background pixel luminance value is greater than a set threshold, the pixel can be identified as foreground point.

2) Due to the chromaticity values of the shadow area and the background area are approximately equal, when the chromaticity difference is greater than a set threshold, this pixel can be identified as the pixel point of the foreground motion area.

3) Those don’t satisfy the above two conditions are identified as background pixels.

About the video object detection system in this article using the above method based on shadow properties, we just need to take a different segmentation threshold for the different channels to achieve the desired effect. In normal circumstances with some changes in luminance of the shadow pixel, the change of chromaticity is smaller contrary. The shadow of the suppression effect is shown in Fig.7. The experiment shows that the good results and the full moving target can be achieved based on the shadow detection algorithm of the YUV color space model.

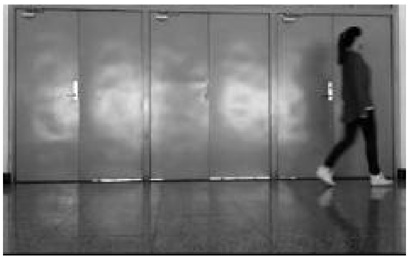

Fig.5 Current image

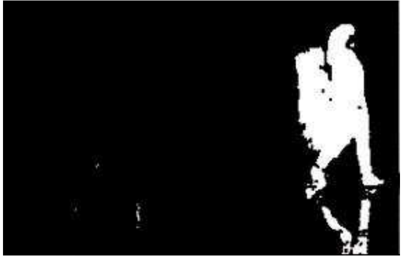

Fig.6 Image without shadow suppression

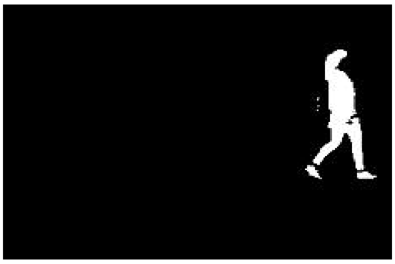

Fig.7 Shadow suppression

Conclusions

In this paper, we use the background difference method for video object detection and median background model to obtain video background and deal with the noise of image sequence to have the difference image, then further to extract moving target. The shadow detection and suppression are processed in the YUV space model. If the luminance value changes of the shadow are less than the changes of the foreground object, the certain threshold value is set. When the pixel value is less than a certain threshold value, this pixel is shadow point the value. This method has achieved a good result and also can be good on shadow detection and suppression, which also can extract complete moving targets.

Acknowledgements

This work was financially supported by the Heilongjiang University Graduate innovative research funds(YJSCX2014-077HLJU).

References

[1] Gavrila D, The visual analysis of human movement, Computer Vision and Image Understanding (1999), 82-98.

[2] Graham D. Finlayson, Steven D, Mark S Drew, On the Removal of Shadows from Images, IEEE Transactions on Pattern analysis and machine intelligence (2006), 158-169.

[3] Cucchiara R, Prati A, Detecting moving objects, ghosts, and shadows in video Streams, IEEE Transactions on Pattern Analysis and Machine Intelligence, Vol. 25, No. 10, 1337-1342(2003).

[4] A.Yilmaz: Object Tracking by Asymmetric Kernel Mean Shift with Automatic Scale and Orientation Selection, Computer Vision and Pattern Recognition (2009), 345-367.

[5] Donggyu Sim, Yongmin Kim, Detection and compression of moving objects based on new panoramic image modeling. Image and Vision Computing 27 (2009), 1527-1539.

Applied Mechanics and Materials Vol. 596 (2014) pp 379-383
© (2014) Trans Tech Publications, Switzerland
doi:10.4028/www.scientific.net/AMM.596.379

Video Time-space Body Filtering Based on Dual-directional Markov Chain Monte Carlo Particle Filter

Jinbao Song[1, a], Long Ye[2,b] and Qin Zhang[3,c]

[1] School of Information Engineering, Communication University of China, Beijing, China

[2] Key Laboratory of Media Audio & Video, Ministry of Education, Communication University of China, Beijing, China

[3] Key Laboratory of Media Audio & Video, Ministry of Education, Communication University of China, Beijing, China

[a]songjinbao@cuc.edu.cn, [b]yelong@cuc.edu.cn, [c]zhangqin@cuc.edu.cn

Keywords: video tracking; particle filter; Monte Carlo sampling; Bayesian filter; Markov chain Monte Carlo particle filter

Abstract. Nowadays with the blooming development of new media and cultural creative industries, the video animation has drawn so many researchers' attention due to animation production efficiency and animation expression. This paper aims at the difficulty that lack of observation model, proposes a method of video time-space body filtering based on dual-directional Markov chain Monte Carlo particle filter for video motion redirection. At first, after extracting the key frame of a given video, by affine transformation and linear superposition, the subject initializes the video's time- space parameters and forms the observation model; Secondly, in each time- space body, based on the bi-directional Markov property of each frame, this paper proposed a dual-directional Markov chain Monte Carlo sampling particle filter structure and takes full advantage of the relationship of the front and back frame of the parameters to estimate motion redirection parameters. The research of this paper will produce an efficient and prominent animation expressive video motion redirection method and play an important role on video animation of the development.

Introduction

Nowadays with the blooming development of new media and cultural creative industries, the video animation has drawn so many researchers' attention due to animation production efficiency and animation expression. In order to reduce the number of key frames painted workload, "performance animation" gradually grows based on motion capture. But motion capture only extracts the information of articulation point demarcated ahead of time and discards a large number of extremely rich animation material elements contained in the video information. While making full use of these elements can help people enhance the efficiency of animation production[1].

The existing research can be divided into two categories for the draw of the role movement in the animation. One is for running water [2], smoke[3], rain [4], snow[5], such natural phenomena as the typical irregular fuzzy objects, emphasizes the whole effect, emphasizes the visual style, and uses the shape change of the same object to form a motion. Second is for parametric modeling to the render objects in the video, and then the model parameters are estimated and corrected through the optimized theory and the filtering technology, and finally formed animation characters motion by the mapping. This stylized method of video motion is called motion redirection.[6] proposes an animation generation algorithm of stylized redirection of falling leaves which is used to produce the stylized animation of the flying and falling leaves. On the basis of the falling leaves gesture redirection algorithm and path synthesis algorithm, the algorithm uses the movement details of different falling leaf as a unit, achieves stylized animation effects of a variety of types of leaves flying and falling through the dynamic control, as shown in Fig. 1.

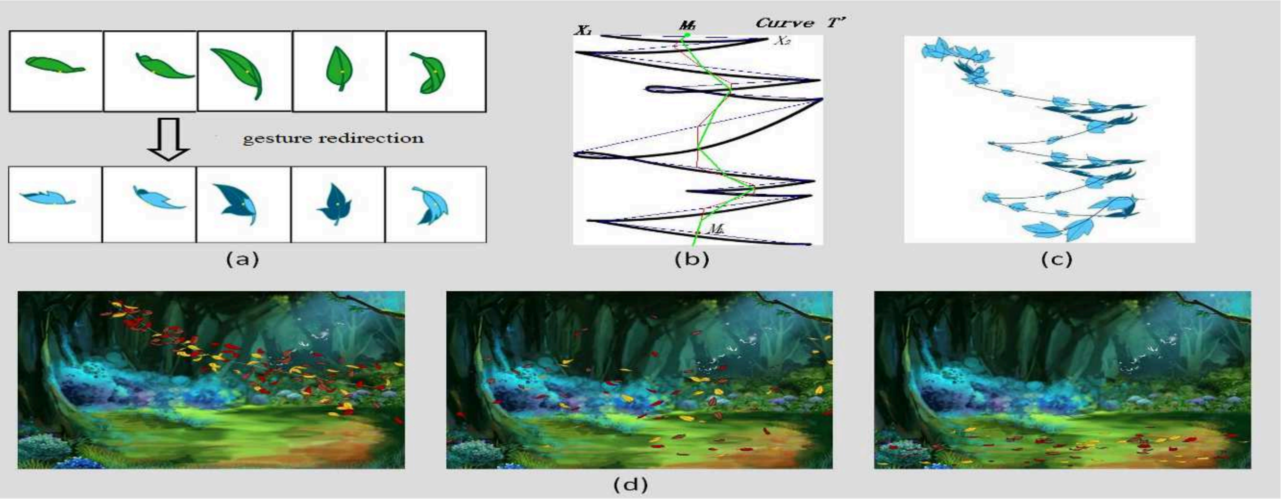

Figure 1. Achievement of stylized animation of falling leaves

This kind of animation generation method is simple, but the effect expressive force is not strong. Root cause is for the target characterization only limited to the location in space and the outer envelope, skeleton structure and physical characteristics (such as illumination change, topology structure, color information, etc.) do not show up, and the skeleton motion of the target role based on the joints just is the most stylized motion information[7]. After extending characterization parameters from the shape point to the multi-type parameter set of skeleton points, shapes, and physical characteristics, the corresponding parameter estimation and redirection are extended to the high dimension and nonlinear Bayesian estimation problem[8]. This paper makes in-depth study in order to solve this problem, proposes a method based on key frame matching and dual-directional Markov chain Monte Carlo sampling of video motion redirection.

Markov Chain Monte Carlo Particle Filter（MCMC-PF）

This paper puts the emphasis on designing a dual direction Markov chain Monte Carlo particle filter. In the recent years, as a kind of nonlinear filtering algorithm, particle filter has become a mainstream goal oriented motion tracking algorithm as a result of getting rid of the restriction of Gaussian distribution. Particle Filter uses Monte Carlo Sampling to perform Recursive Bayesian Filter. While tracking the target movement and accessing the observation model, particle filter can shake of the restriction of linearity and Gaussian compared with Karlman Filter, therefore particle filter has better applicability and effectiveness.

Particle filter algorithm is a kind of Bayesian estimation algorithm based on sampling theory. It is an effective tool to solve the nonlinear and non-gaussian problem .But particle filter algorithm would inevitably appear particle degradation problems. The weights focuse on a handful of particles, it would lose the diversity of the particles.Because each particle is calculated every time, so when the weights concentrates on a handful of particles, a large amount of calculation is waste and has no influence on the results of the particle, which causes great waste of resources.In order to maintain the diversity of particles after resampling, after resampling by Markov Chain Monte Carlo (Markov Chain Monte Carlo, MCMC) approach, it will both maintain the particle probability distribution changeless, and increase the diversity of the particle collection, which called the MCMC-PF algorithm.

The Research Targets And Content

Video motion redirection is in the case of the given video sequence I and parameterized animation object, the estimate of animation role model related parameters based on video sequence I. Each redirection parameter should include U points of skeleton structure characterization(S_i), V points of the target outside contour characterized by R_j, and the target morphological parameters set F = [T, D, C], T stands for the possible topology transformation of the object, D stands for the illumination changes, C stands for color changes, as shown in Fig. 2.

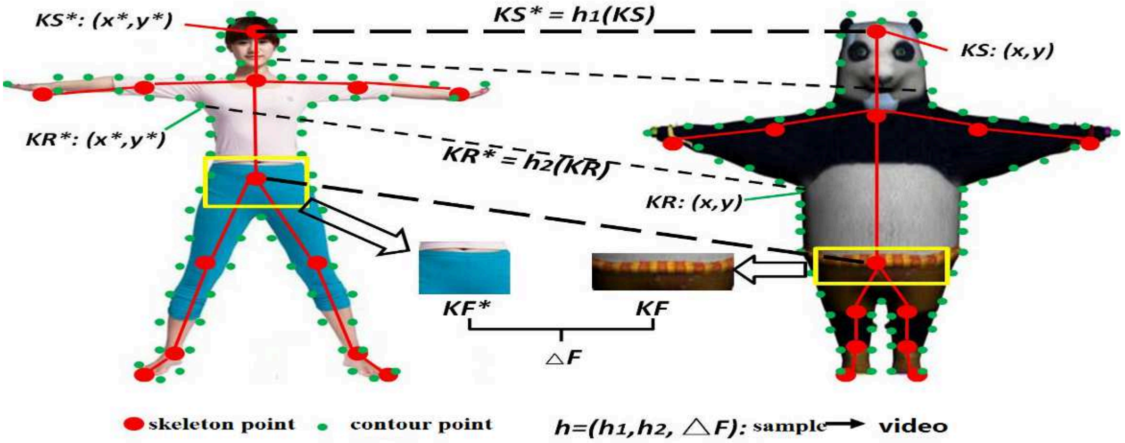

Figure 2. Key frame matching in the video motion redirection

Define g = [S, R, F], video motion redirection is to obtain the maximum a posteriori (MAP) in the statistical learning, namely:

$$(g_0,\ldots\ldots g_\tau)_{opt} = \arg\max p(g_0,\ldots\ldots g_\tau \mid I_0,\ldots\ldots I_\tau) \tag{1}$$

$$p(g_\tau \mid g_1,\ldots,g_{\tau-1}) = p(g_\tau \mid g_{\tau-1}) \tag{2}$$

$$p(I_1,\ldots,I_\tau \mid g_1,\ldots,g_\tau) = \prod_{t=1}^{\tau} p(I_t \mid g_t) \tag{3}$$

Among them, （I_0,…,I_τ） stands for video sequence, （g_0,…,g_τ） stands for the parameters set of the animation characters corresponding to the characterization of video sequences.

Because there is difference between the animation objects and the referred object in the video in shape, color and texture, and many other physical characterizations, the observation model is missing. Two assumptions in the sense of time domain recursive estimation (Eq. 2 the Markov assumption in the state transition and the observation conditional independence assumption in the Eq. 3) can't be established. So the traditional particle filter process can't be directly applied to the project to solve the problem of video motion redirection. Some information can be used lies in that animation model will form some key gestures generated from the animation, accordingly, for a given video sequence, some key gestures in the key frames are extracted as the a priori of the data processing. We define ($t_1, t_1, \ldots, t_T$) as the moments of key frames of the video sequence, each key frame contains key gestures $\{KP^*(m)\}_{m=1:M}$ remain to match the target, M is the number of key gestures, accordingly, define the animation model key gestures as $\{KP(m)\}_{m=1:M}$, then $KP(m) \sim p(g_{ti} \mid I_{ti})$. Through $\{KP^*(m)\}_{m=1:M}$ and $\{KP(m)\}_{m=1:M}$, each key gesture redirection mapping h_m can be obtained, namely the $KP^*(m) = h_m(KP(m))$.

Through the above definition, Eq. 1 can be extended as follows:

$$\begin{aligned} p(g_1,g_2,\ldots g_\tau \mid I_1,I_2,\ldots,I_\tau) &= p(g_1,g_2,\ldots g_\tau \mid I_1,I_2,\ldots,I_\tau,g_{t_1},g_{t_2},\ldots g_T)\,p(g_{t_1},g_{t_2},\ldots g_T \mid I_{t_1},I_{t_2},\ldots I_T) \\ &= p(g_1,g_2,\ldots g_\tau \mid I_1,I_2,\ldots,I_\tau,h) \\ &= \prod_{t=t_1}^{T-1} p(g_t,g_{t+1},\ldots g_{t+\delta} \mid I_t,I_{t+1},\ldots I_{t+\delta},h) \qquad (4) \\ &= \prod_{t=t_1}^{T-1} p(I_t,I_{t+1},\ldots I_{t+\delta} \mid h(g_t),h(g_{t+1}),\ldots h(g_{t+\delta}))\,p(g_t,g_{t+1},\ldots g_{t+\delta}) \end{aligned}$$

The objective of the research can be summarized as:

1. Particle filter structure design that is suitable for video stylized motion, namely the solution of the Eq. 4. It specifically includes: the redirection mapping method of the components [S, R, F] of the video motion redirection parameter g and the matching of the key frames; the generate way of every moment parameters status based on h_m, inside the time and space body formed from the key frames; optimization strategy of state estimation after having generated the time-space body internal parameters status.

2.Based on the above key technology to implement a hierarchy video motion redirection structure of the key frames - time-space body - redirection video sequence, as shown in Fig.3, at the same time build video redirection analysis and implementation platform.

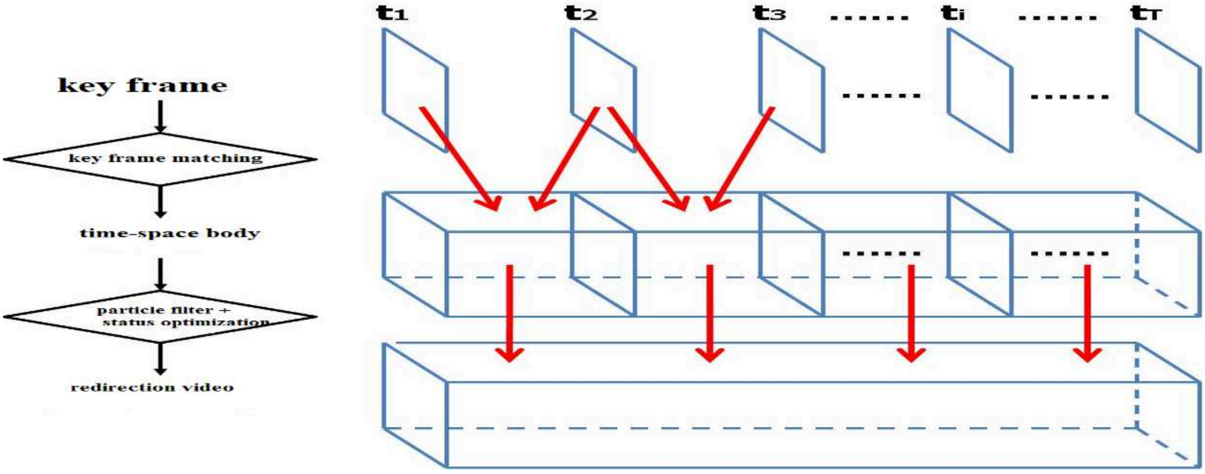

Figure 3.The hierarchy video motion redirection structure of the key frames - time-space body - redirection video sequence

After defining the video key frames and the key frames matching, in each time-space body formed by the key frames, the calculation of h = [h_1, h_2, ΔF] is able to provide the necessary observation model for the implementation of the particle filter and make the constraint relations of the previous and next frames inside the time-space body, namely Bidirectional Markov Chain Monte Carlo Sampling.

Due to the property of the Markov Chain (the unidirectional Markov property is equivalent to the bidirectional Markov property), we can get the following bidirectional Markov property:

$$p(g_t \mid g_1,...,g_{t-1},g_{t+1},...,g_N) = p(g_t \mid I_{t-1},I_{t+1}) \tag{5}$$

While observing independence still holds:

$$p(I_1,...,I_\tau \mid g_1,...,g_\tau) = \prod_{t=1}^{\tau} p(I_t \mid g_t) \tag{6}$$

So we can get:

$$p(g_t \mid g_1,...,g_{t-1,}g_{t+1},...,g_N,I_1,...I_N) = c_t p(g_t \mid g_{t-1},g_{t+1}) p(I_t \mid g_t) \tag{7}$$

When we have video time-space body, we can relax the requirement:

$$p(g_t \mid g_1,...,g_{t-1,}g_{t+1},...,g_N,I_1,...I_N) = c_t p(g_t \mid g_{t-1},g_{t+1},I_{t-1},I_t,I_{t+1}) \tag{8}$$

More generally:

$$p(g_t \mid g_1,...,g_{t-1,}g_{t+1},...,g_N,I_1,...I_N) = c_t p(g_t \mid g_{\partial t},I_{\partial t},I_t) \tag{9}$$

Among them, ∂t represents the neighboring frame. Dynamics model and observation model couple at this time, which forms dual-directional Markov chain Monte Carlo sampling based video time-space body filter. And the redirection parameter estimate of each frame video image is formed within each time - space body.

Conclusions

Nowadays with the blooming development of new media and cultural creative industries, the video animation has drawn so many researchers' attention due to animation production efficiency and animation expression. This paper aims at the difficulty that lack of observation model, proposes a method of video time-space body filtering based on dual-directional Markov chain Monte Carlo particle filter for video motion redirection. At first, after extracting the key frame of a given video, by affine transformation and linear superposition, the subject initializes the video's time- space parameters and forms the observation model; Secondly, in each time- space body, based on the bi-directional Markov property of each frame, this paper proposed a dual-directional Markov chain Monte Carlo sampling particle filter structure and takes full advantage of the relationship of the front and back frame of the parameters to estimate motion redirection parameters. The research of this paper produces an efficient and prominent animation expressive video motion redirection method and plays an important role on video animation of the development.

Acknowledgements

This paper is supported by Outstanding Young Teacher Training Project of Communication University of China ,National Natural Science Foundation of China (61201236) and Engineering Planning Project of Communication University of China(XNG1230).

References

[1] Song Jinbao, Wan Jinliang, Ye Long, Zhang Qin. Key Frame Matching and Dual Direction Monte Carlo Particle Filter based Video Tooning[J]. The 2013 International Conference on Control Engineering and Information Technology (ICCEIT 2013), August,2013, 627-630.

[2] Yu Jinhui， Patterson John，Liao Jing，Modeling the interaction between objects and cartoon water，Computer Animation and Virtual Worlds, Volume 19, Numbers 3-4, July 2008 , 375-385.

[3] Andrew Selle，Alex Mohr，Stephen Chenney，Cartoon Rendering of Smoke Animations, Proceedings of the 3rd international symposium on Non-photorealistic animation and rendering , Annecy, France ，2004， 57-60.

[4] Zhang S, Chen T, Zhang Y, Hu S, Martin R, Video-based Running Water Animation in Chinese Painting Style. In *Science in China Series F: Information Sciences* 52, February 2009, 162-71.

[5] Jinhui Yu, Xinan Jiang, Haiying Chen, Cheng Yao, Real-time Cartoon Water Animation, The Journal of Computer Animation and Social Agent, vol. 18, 2007,pp405-414.

[6] Haiyan Li, Qingjie Sun, Xiaodan Liu, Qin Zhang, Example-based Stylized Trajectory Synthesis of Falling Leaf, 2010 International Conference on Computer Engineering and Technology, Chengdu, China.

[7] Song Jinbao, Li Junyu, Zhang Qin. The Model Based Behavior Driven Arithmetic Research[J]. Advanced Engineering Forum Vols.6-7,September,2012,1066-1071.

[8] Jinliang Wan, Jinbao Song. A Parallel Framework for Texture Substitution Coding.2010 International Conference on Educational and Information Technology (ICEIT2010), September,2010，72-76.

Applied Mechanics and Materials Vol. 596 (2014) pp 384-387
© (2014) Trans Tech Publications, Switzerland
doi:10.4028/www.scientific.net/AMM.596.384

Voice Assistant —Application of speech recognition technology in the Android system

Ge Liu [1, a], Hai-bing Zhang [2,b]

[1] Tangshan Industrial Vocational Technical College,Tangshan,063000.China

[2] Modern technology and education center , Hebei United University, Tangshan， 063009.Hebei,China

[a] liuge_lg@sina.com, [b] seaman_zhb@163.com

Keywords: Voice Assistant, Speech recognition, speech synthesis.

Abstract. This paper introduces the concept of Voice Assistant, the voice recognition service providers, several typical Voice Assistant product, and then the basic working process of the Voice Assistant is described in detail and proposed the technical bottleneck problems in the development of Voice Assistant software.

Introduction

Human-computer interaction in recent years with the rapid development of smart phones, mobile terminals has become a new platform for development of new technologies, Apple Inc.'s Siri voice recognition technology first introduced to the mobile terminal to trigger the voice recognition technology surge of development, but also created a precedent for intelligent Voice Assistant. Following the iPhone's Siri, Chinese Voice Assistant is also mushrooming development, such as IFLYTEK Voice Touch, Lingxi Voice Assistant, SogouYY, Baiduyuyin, Viash Voice Assistant, and so on.

Voice Assistant

The concept of Voice Assistant. Voice Assistant is a smart phone applications , and intelligent dialogue through interaction with the real-time intelligence quiz achieve help users solve the problem , which is mainly to help users solve lifestyle issues , to complete voice dialing , voice texting , voice memo and voice Actions contacts and other basic functions , such as switching to achieve Bluetooth mobile phone , change the phone volume , adjust the brightness of the phone features such as voice control , voice query information , voice search for music , pictures, news and other aspects of the function . Voice Assistant major categories of products in addition to have some common features, but also a slight similarities and differences and focus .

Voice Assistant liberation of most practical significance lies in the user's hands , in some special scenes, which are showing good market prospects. It can clearly analyze user needs to answer user questions , and for users to perform various tasks, such as phone calls, send text messages, Twitter , watch videos, booking tickets. In the continuous improvement of speech recognition and semantic understanding , and other related technologies , I believe more people will use this latest technology , bringing more convenience to their lives.

Speech recognition ISP. Voice recognition service provider market mainly Anhui USTC iFLYTEK Co., Ltd. , And Unisound so on. Anhui USTC iFLYTEK Co., Ltd. 's IFLYTEK Voice Touch, China Mobile jointly Anhui USTC iFLYTEK Co., Ltd. Launched Lingxi Voice Assistant, a third-party vendor 's entrepreneurial intelligence 360, Chongdong Voice Assistant, Kuaishuo Voice Assistant adopt iFLYTEK the speech recognition technology , and complete semantic analysis on the basis of precise searching to realize their own capabilities.

Several typical Voice Assistant product .

(1) iFLYTEK Voice Touch / Lingxi Voice Assistant.Anhui USTC iFLYTEK Co., Ltd. Launched Voice Assistant, is a capable of voice calls, send text messages, chat and other very practical intelligent voice software. Voice recognition rate up to 95% accuracy. The speech technology can be widely applied to other applications into microblogging . Speech recognition strongest, but semantic understanding and vertical data is weak.

(2)SogouYY.Sogou launched Voice Assistant, is an intelligent voice chat software , live from the local information, maps , to the encyclopedic knowledge , convenient tool to query , to news, pictures and other traditional search for content , SogouYY these are integrated into their intelligent retrieval library the . Users can easily question the SogouYY natural voice , you can get an instant answer precisely . Not only that, he can be like a personal assistant to manage your life , like your schedule , you can send text messages , make phone calls . You bored, but also chat with him. SogouYY semantic understanding powerful capabilities, vertical data-rich , quiz outstanding results , and integration of knowledge cubic Sogou , but its own voice recognition technology is weak, the combined effect of the current best .

(3)Baiduyuyin.The search giant Beijing Baidu Netcom Science & Technology Co., Ltd launched the Voice Assistant, is a support voice commands, voice search software, intelligent voice services , voice chat feature. By voice operation , you can operate the phone call, send text messages, set reminders , play music. Search query weather , check flight , check the surrounding cuisine, search stocks. Baiduyuyin started late , but based on the accumulation of search technology , semantic understanding better, and its own voice recognition strong development potential .

(4)Viash Voice Assistant.Viash Voice Assistant is a powerful semantic understanding based on the engine developed a new voice assistant Tools software. Users can make voice control through which users of a variety of life to achieve real-time query and manipulate information on the transfer of the requirements of each program within the mobile phone , and the realization of human-computer interaction in the chat interface , and entertainment needs. Viash Voice Assistant engine based on semantic understanding , based on user context semantics , not in the sense of self- interpretation of language differences , identify the real intentions of the user.

Basic working process of Voice Assistant

Voice Assistant to the basic process generally includes a voice input , voice recognition , voice synthesis , and shows the distal end , the distal end into the speech recognition process and the processing and back-end speech recognition processing components.

Voice Input. That the speaker's voice input voice pickup , the main use of the microphone on the phone to complete this function. Currently, almost all international brand mobile phone manufacturers and many mobile phone manufacturers have adopted Duo Maike technology to improve performance under real environmental voice quality and user experience.

Speech Recognition. Voice Assistant voice recognition function is mainly accomplished by the speech recognition engine . Powerful voice recognition engine should be a speaker independent speech recognition system , with excellent recognition rate , providing comprehensive development support , provides a wealth of easy-to- use tools , and core technology reached the international advanced level.

1. front-end speech processing.Front-end voice processing refers to the use of signal processing methods for speaker voice detection, noise reduction pretreatment in order to get the most appropriate treatment voice recognition engine .

(1) endpoint detection.Endpoint detection is the input audio stream is analyzed to determine the process of starting and terminating users talking . Upon detecting a user begins to speak, the voice recognition engine began to flow until it detects the end user to speak . This approach allows to identify the user speaking at the same time the engine start recognition processing .

(2) noise cancellation.Background noise on the voice recognition function is a challenge to the practical application , even if the speaker in a quiet office environment, it is difficult to be certain of avoiding noise . Front-end processing of speech , the speech recognition engine will effectively eliminate the noise , to meet the requirements of users in a variety of different environments.

2.back-end recognition process.The back-end recognition is to identify the speaker, to get the most suitable results. Backend recognition processing to meet the large vocabulary , speaker- independent recognition requirements, can adapt to different ages , different regions, different people , different channels , different terminals and different noise environments applications.After the speech front-end processing of information , will enter the intent to understand, intelligence quiz , Mapping Knowledge Domain query branch processes.

(1) the intent to understand.We must first understand the basis for the intent processing, including segmentation , tagging, syntactic analysis, then they have to be lexical , semantic combinations , the overall intent of understanding.

Understand the intent can be divided based on the intent to understand the intent and understanding of the template -based model. Based on the understanding of intent template is a template -based approach to semantic accurately understand the user's query intent , demand for some common view expressed very clearly has a very accurate results, and can be accurately obtain query critical information. But the disadvantage based on the understanding of the intent of the template is less able to recall , fault tolerance effect is poor. The model is based on the intention of understanding is based on the user query words in categories propensity to determine the user's query intent categories , this part of the inquiry focused on some of the less obvious changes in the larger or intent queries have very good results, but there are strong fault tolerance , and covers a wide range. But there are obvious shortcomings, it is the high development costs , the accuracy is difficult to achieve more than 95 %.

(2)Smart Answers.Intelligent question answering system into intelligent question answering system based on the quiz and intelligent question answering system based on structured knowledge base. Q & A Q & A system based on intelligent questions and answers are based on the knowledge base is stored as intelligent question answering system , retrieve the user's problem in the knowledge base consistent with the semantic issues , and filter out the answers to their effective feedback to the user. Knowledge -based structured intelligent question answering system , the use of semantic understanding of ways to resolve the query , calculate the answer in the knowledge base , and generate an appropriate answer to the text .

(3)Mapping Knowledge Domain query.Mapping Knowledge Domain is also known scientific Mapping Knowledge Domain, is a series of different kinds of graphics development process and the structure of the relationship between knowledge , using visualization techniques described in the knowledge resources and their carriers, mining, analysis , build, draw and display knowledge and interconnected between them.

After the completion of the terminal will get to work on , such as cloud computing and storing data vertically result , quiz results , structured knowledge . Since the intent of the user query is not always clear, and some will hit a lot of inquiries intentions , but we need to show in a limited space as possible to hit the user's intent , and therefore multi- sort and show intent .

Speech synthesis. Voice Assistant voice synthesis function primarily by speech synthesis engine to complete. Speech synthesis , also known as Text to Speech technology, can any text information in real time into a standard smooth voice read out , which is equivalent to a machine fitted with an artificial mouth. The main problem it solves is how to text message text states into audible sound information .

Text to Speech writing process is first converted into a sequence of phonological sequence , then the speech waveform generated by the system based on phonological sequence. The first step involves linguistic processing , such as word , phoneme conversion , as well as a set of effective rhythm control rules ; second step requires advanced speech synthesis technology that required real-time synthesis of high-quality voice stream. So in general , Text to Speech systems require a complex sequence of text to phoneme conversion process sequence , ie , Text to Speech system not only to the application of digital signal processing technology, and must be supported by a large number of linguistic knowledge .

front-end display. Voice Assistant is a front-end to show the work of the last stage is the user experience Voice Assistant tool application stage effects , also affect the users of the software 's use of evaluation .

The technical bottleneck problems in the development of Voice Assistant software.

For the recognition and natural language understanding . The user's query intent into shallow and deep intentions, shallow clearly stated intent is to direct their own needs, such as : nearby cinema? → inquiries around the cinema. The deep intent is not so obvious, after require reasoning in order to obtain the user's intent , for example: I am very hungry ah → inquiries around the restaurant.

In the presence of natural language dialogue will Ellipsis . Then a voice in the dialogue system for some input queries with incomplete information , we can not be directly used to handle , but also complement the missing information from the query in the context of the dialogue . For example : Tom 's height? And Kimmy ?

Voice amount of information, not only on the type of the speech patterns of different speakers , the same speaker are different, e.g. , a speaker and the speaker above when speaking voice information is seriously different . A person's manner of speaking will change over time and change.

Fuzziness voice . In his speech, the speaker , different words may sound similar.

Individual letters or words , voice characteristics affected the context of the word , so that changed the accent , tone , volume and pronunciation speed.

Environmental noise and interference have a serious impact on speech recognition, resulting in low recognition rate .

The current Voice Assistant class of applications places heavy reliance on non- interference and wireless networks , many Voice Assistant does not support offline applications.

Present on the user experience is not smooth , functional homogeneity, not natural, not enough breadth or depth issues .

Summary

Although there are still phone Voice Assistant software difficult to overcome technological bottlenecks , users have even been given the difference in assessment , but many industry giants are still keenly aware intelligent Voice Assistant huge market potential, and have joined the fight for this cake . Ease of use, accuracy , speed , has a certain depth and breadth of great importance to strengthening integration with third-party applications will be the future of Mobile Voice Assistant software to evaluate a key indicator.

Acknowledgements

This work was financially supported by the 2013 Science Foundation of Hebei United University (Project No. Z201302) and .the 2013 scientific research on higher education of Hebei Association of Higher Education(Project No. GJXHZ2013-321).

References

[1] Caroline Henton. International Journal of Speech Technology, 2006, Vol.8 (3), pp.247-257.

[2] Neil Joshi. Journal of Signal Processing Systems, 2010, Vol.58 (3), pp.359-370.

[3] Ssang Sun Jun , Chi Sub Jin. KSCE Journal of Civil Engineering, 2010, Vol.14 (4), pp.539-545.

[4] Russell Lee , in: Free Apps for Androi , CreateSpace Independent Publishing Platform (2013)

[5] Wei-Meng Lee, in:Beginning Android Application Developmen, Wrox(2011)

Applied Mechanics and Materials Vol. 596 (2014) pp 388-393
© (2014) Trans Tech Publications, Switzerland
doi:10.4028/www.scientific.net/AMM.596.388

A Content Based Image Retrieval Model Using Feature Space Dividing

Huang Guan[1, a]

[1] School of Education, China West Normal University, Nanchong 637002, China

[a] article_author@163.com

Keywords: Content-based image retrieval, feature space, fractional distance, search zone.

Abstract. This paper introduces a model for content based image retrieval. The proposed model extracts image color, texture and shape as feature vectors; and then the image feature space is divided into a group of search zones; during the image searching phase, the fractional order distance is utilized to evaluate the similarity between images. As the query image vector only needs to compare with library image vectors located in the same search zone, the time cost is largely reduced. Further more the fractional order distance is utilized to improve the vector matching accuracy. The experimental results demonstrated that the proposed model provides more accurate retrieval results with less time cost compared with other methods.

Introduction

Nowadays, there is a rapid increase in the size of digital image collections. Everyday, Peta-bytes of images are generated from network and industrial equipments. Researchers are continually developing retrieve methods to search images from a huge image library. In recent years, more and more researches [1] focused on the content-based image retrieval (CBIR) method, because CBIR tends to index and retrieve images based on their visual content, which avoids many problems associated with traditional ways of retrieving images by keywords, such as the time-consuming of manual image annotation, human annotations subjective.

The performance of a CBIR system mainly depends on the particular image representation and similarity matching function [2-3]. A common scheme to represent the image is to extract different types of features such as color, texture, and shape [4]. The features are normalized and constitute real valued feature vectors to represent the content of each image [5]. Most CBIR systems are similarity based, where the similarity between query and library images in a database is measured according to some similarity matching functions [6].

Similarity evaluation between images is another important task in the content-based image retrieval model. [2]. Usually the features extracted from the images are presented as multi-dimensional points, and the distances between corresponding multi-dimensional points are calculated by some distance metrics to measure the similarity between the two points in the multi-dimensional feature space [8-10].

However, the distance calculation based image query model have to calculate the distance between the query image and the whole library image, which is quite time consuming; furthermore, many retrieval modes calculate the image distances using Minkowski distance, thus they are suffered from the curse of dimensionality that the discrimination between random two image vectors under high dimensional space becomes lower, resulting the difficult of image matching. These two problems have restricted the application of CBIR.

In the paper, we proposed an efficient content-based image retrieval model based on image feature space dividing and fractional order matching strategy, E-CBIR. First the image feature space is divided into a group of search zones; as the feature vectors from similar images gathered in the feature space, therefore the query image vector just need to compare with library image vectors located in the same search zone to avoid whole library searching; second during the image searching phase, the fractional order distance is utilized to increase the differentiation between image vectors.

The Organization of Image Feature Vectors

Color feature. Color features include the color histogram, color correlogram, dominant color descriptor, the color coherence vector, the color co-occurrence matrix, vector quantization and color moments et al[11]. The selected color features must be stable and robust, such that they are not sensitive to rotation, translation and scale changes [12][13].

In the paper, we define color feature in the HSV (hue, saturation, value) color space. HSV(hue, saturation, value) . HSV stands for hue, saturation, and value. The HSV color wheel can be depicted as a cone or cylinder. In each cylinder, the angle around the central vertical axis corresponds to "hue", the distance from the axis corresponds to "saturation", and the distance along the axis corresponds to "value" or "brightness". We divide H into 16 sections, while S and V are divided into 4 sections respectively, and the number of pixels in each bin is calculated to composite a 256-dimensional vector of color feature.

Texture feature. The natural world is rich in texture: the surface of any visible object is textured at certain scale, and spatial homogeneity is the most important property of a texture. Texture is an organized area phenomenon which can be decomposed into `primitives' having specific spatial distributions [14].

In the paper, the images are divided into four wave bands by discrete wavelet transformation, generating horizontal, vertical, diagonally, and the high and low frequency parts. The low frequency part can be recursively divided. Usually the high frequency part represents the detail parts, including texture, shape and etc, while the low frequency part represents the overall feature. The images are resolved by four-level wavelet decomposition. After the decomposition, there are 13 sub-bands, and 26-dimensional wavelet vector are generated by calculating the mean and variance of each sub-bands.

Shape feature Shape is an important visual feature and it is one of the basic features used to describe image content. Zernike moment is employed to describe the shape characteristics of images. The definition of Zernike polynomials in the polar coordinates is shown in Eq. 1.

$$V_{nm}(x,y) = R_{nm}(r)\cdot\exp(jm\theta) \tag{1}$$

Where $R_{nm}(r)$ is the Zernike radial polynomial and its definition in Eq. 2:

$$R_{nm}(r) = \sum_{S}^{n-|m|/2} \frac{(-1)!(n-s)!}{s!(\frac{n+|m|}{2}-s)!(\frac{n-|m|}{2}-s)!} r^{n-2s} \tag{2}$$

For an image $f(x,y)$ with order n and recurrence rate m, its Zernike moment is calculate by Eq. 3

$$Z_{nm} = \frac{n+1}{\pi}\sum_{x}\sum_{y} f(x,y)\cdot Vnm(x,y) \tag{3}$$

Where $x^2+y^2<1$, and we calculate the 10 order Zernike moment of each image, and get 36 dimensional shape vector.

The Dividing of Image Feature Space

As the image features are points in the n-dimensional space, the image retrieval tasks can be transformed to the nearest point searching mission of the query image vector in the feature space. As the feature vectors from the same image class must closer to each other in the feature space. Therefore, to avoid comparing two feature vectors located far away in the feature space which means they can not be similar image features, we pre-organize the feature space into a group of non-overlapped search zones according to the known image classes. Suppose the images from class C distribute in a same zone Z, and $Fk(i)$ (k = 1,2,3 represent the color, texture and shape features of the *ith* image respectively.

$$C_k(i)=\frac{1}{n}\sum_{i=1}^{n} f_k(i) \tag{4}$$

And then the center vector of the *k*th search zone is calculated by Eq. 4, where $1\le k\le 3$ and *n* represents the number of images in the class *C*. Then the maximum and minimum distance *Dmax*, *Dmin* from the zone center are calculated by Eq. 5 and Eq. 6.

$$Dmax_k=\max_{n}\ dis(C_k,f_k) \tag{5}$$

$$Dmin_k=\min_{n}\ dis(C_k,f_k) \tag{6}$$

Then the search zone which profiled the distribution area of feature vectors from image class *C* can be represent as <C_k, D_{maxk}, D_{mink}>, $1\le k\le 3$, and the image features set of class *C* is shown in Eq. 7 .

$$S_k(C)=\{x\,|\,c_1\times Dmin_k\le dis(x,C_k)\le c_2\times Dmax_k\} \tag{7}$$

*C*1 and *C*2 can be adjusted according to the real applications such that all the library images in class *C* satisfy Eq. 8.

$$x\in C=\bigcap C_k \tag{8}$$

The Fractional Distance Function

Theorem 1. Let *F* is a random distribution of two vectors, for the L_k metric, $\lim_{d\to\infty} E\left[\frac{D_{max}-D_{min}}{d^{1/k-1/2}}\right]=C_k$, where *d* is the data dimension, C_k *i*s a constant dependents on norm *k*, D_{max} *and* D_{min} are the maximum and minimum distances from vectors to the origin using the L_k metric.

Proof. Let *A* = ($P_1 \dots P_d$) and *B*=($Q_1 \dots Q_d$), with P_i and Q_i being drawn from *F*. Let $d_A=\sqrt[k]{\sum_{i=1}^{d} P_i^k}$ is the distance from *A* to the origin using the L_k metric and $d_B=\sqrt[k]{\sum_{i=1}^{d} Q_i^k}$ is the distance from *B* to the origin.

As the *d* attributes of *A* and *B* are drawn from the distribution *F* with mean μ and standard deviation σ, which means: $\frac{d_A^k}{d}\to_p \mu$, $\frac{d_B^k}{d}\to_p \mu$, therefore we can get Eq. 9.

$$\frac{d_A}{d^{1/k}}\to_p \mu^{1/k},\ \frac{d_B}{d^{1/k}}\to_p \mu^{1/k} \tag{9}$$

The comparison is between two random vectors, so

$$|D_{max}-D_{min}|=|d_A-d_B|=\frac{|d_A^k-d_B^k|}{\sum_{i=0}^{k-1}(d_A)^{k-i-1}(d_B)^i} \tag{10}$$

From Eq.10 we get:

$$\frac{|d_A-d_B|}{d^{1/k-1/2}}=\frac{|\sum_{i=1}^{d}(P_i^k-Q_i^k)|/\sqrt{d}}{\sum_{i=0}^{k-1}(d_A d^{-1/k})^{k-i-1}(d_B d^{-1/k})^i} \tag{11}$$

Since each $R_i = P_i^k - Q_i^k$, $1 \le i \le d$ is a random variable with zero mean and finite variance $\sqrt{2}\sigma'$, where σ' is the standard deviation of P_i^k. The sum of different values of R_i over d dimensions will converge to a normal distribution: $\sum_{i=1}^{d}(P_i^k - Q_i^k) \sim N(0, 2d\sigma'^2)$ because of the central limit theorem, so the expected value of the numerator is a constant C.

$$|\sum_{i=1}^{d}(P_i^k - Q_i^k)| / \sqrt{d} \ \to_p C \tag{12}$$

According to Slutsky's Theorem, put Eq. 12 into the denominator of Eq.11, get

$$\sum_{i=0}^{k-1}(d_A d^{-1/k})^{k-i-1}(d_B d^{-1/k})^i \to_p k\mu^{(k-1)/k} \tag{13}$$

Combine the results of Eq. 12 and Eq. 13 to obtain

$$\lim_{d\to\infty} E\left[\frac{D_{\max} - D_{\min}}{d^{1/k-1/2}}\right] = C_k \tag{14}$$

Where C_k is some constant dependents on k.

From Eq. 14 we can see D_{max} - D_{min} is increasing with $d^{(1/k)-(1/2)}$, which inspires us to use the fractional norm distance function in Eq. 15 to enhance the distinctiveness between feature vectors.

$$dis(x,c) = \sqrt[l]{\sum_{i=1}^{d} | x.f_i - c.f_i |^l}, \ 0 < l < 1 \tag{15}$$

Experiment

In this section, the retrieval performance of E-CBIR and other image retrieval models are compared, the targets includes four modules namely Huang et al.[15], Elalami [2], Jhanwar [16], and Chuen-Horng [17. The widely used image databases "WANG" [15] is utilized to test their performances. The WANG database contains 10 categories, 100 images for each category, including Africa, Beach, Monuments, Buses, Food, Dinosaurs, Elephants, Flowers, Horses, and Mountains.

In the paper we employed recall (or sensitivity) and precision (or specificity) to evaluate the retrieval methods, which is also commonly utilized in other works. The precision *Pre* and recall rates *Rec* are computed by Eq. 16 and Eq. 17.

$$Pre = \frac{TP}{TP + FP} \tag{16}$$

$$Rec = \frac{TP}{TP + FN} \tag{17}$$

Where *TP* denotes the number of retrieved images which are similar to the query, *FP* is the number of retrieved images dissimilar to the query, and *FN* is the number of missed relevant images.

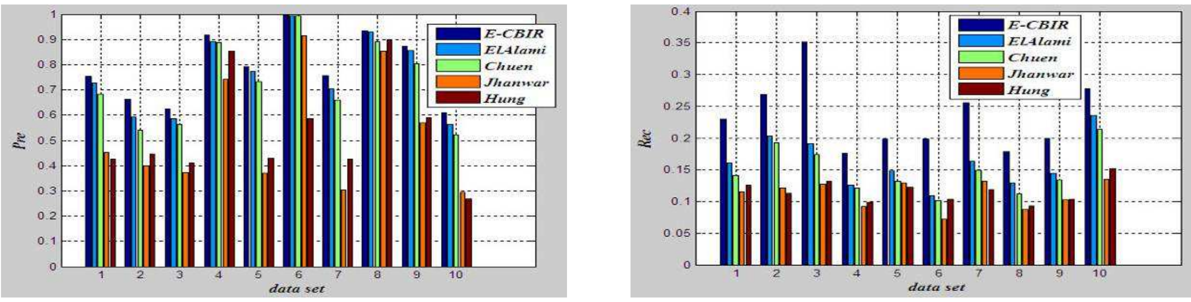

(a) Pre (b) Rec

Fig.1 The detection result on 10 image categories

In the experiment, 10 images are randomly chosen from each category, and the similar images are searched in the whole library. The detection result is shown in Fig.1. From Fig.1 we can see that both the detection precision and recall rate of E-CBIR are better than the others. The result demonstrated that E-CBIR can achieve better performance using fractional distance metrics.

Fig. 2 shows the comparison result of the average single image retrieval time of the different models. As the fgirue shows, the retrieval time of E-CBIR is the lowest one among the compared models because a query image in E-CBIR is only compared with the images in the same search zone which greatly reduced the time cost of comparisons of image vectors.

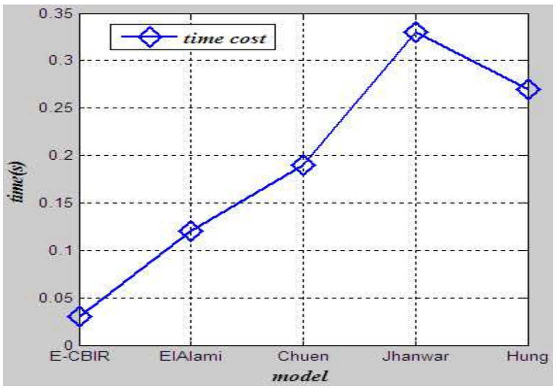

Fig. 2 The average time cost.

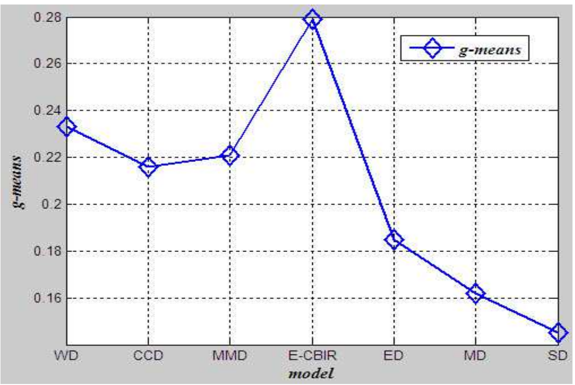

Fig. 3 The average g-means

To validate the effect of fractional order distance, its retrieval precision is compared with other six distance metrics methods, including: Euclidean distance ED, weighted Euclidean distance WED, Manhattan distance MD, cross correlation distance CCD, minimum mean distance MMD and statistical distance SD. The comparison is performed by searching different images from the 10 image categories, and count the g-means value for different models. The geometric mean value is shown in Eq. 18, which simultaneously take recall and precision into consideration, thus it is wildly utilized as the evolution criterion retrieval models.

$$g=\sqrt{a^{+}\cdot a^{-}} \tag{18}$$

Where a^+ and a^- represent *Pre* and *Rec* respectively. Fig.3 illustrates the g-means curve for different distance metrics. The results indicate that E-CBIR provides much higher performance than the other six distance metrics methods. In the paper, the image vectors are defined in a 318 dimensional feature space, the distinctiveness between feature vectors becomes very small for traditional distance metrics, however, for fractional distance metric, the discrimination between images from different categories are not much effected by the high data dimension, thus the g-manes value of E-CBIR is higher than other models.

Conclusions

Currently available large images repositories require new powerful way to retrieve interesting information from the images database. This paper focused on developing a new matching strategy based on the idea of feature space dividing to reduce the comparison cost between a query image and the library images in specific class. The proposed fractional distance based measure played a major role in improving the precision of image searching. Performances of the six different similarity distances measures in comparison with the proposed similarity measure were evaluated. The results were promising and demonstrated the effectiveness of the proposed approach.

References

[1] C.-H. Lin, D.-C. Huang, Y.-K. Chan, K.-H. Chen, Y.-J. Chang, Fast color-spatial feature based image retrieval methods, Expert Systems with Applications 38(2011) 11412–11420.

[2] M.Kuabt, S.MatWIN, Addressing the Curse of Imbalanced Training Sets: One-Sided Selection, Proc.14th Int'l Conf. Machine Learning, 1997.

[3] H.B. Kekre, S.D. Thepade, A. Athawale, A. Shah, P. Verlekar, S. Shirke, Energy compaction and image splitting for image retrieval using kekre transform over row and column feature vectors, International Journal of Computer Science and Network Security (IJCSNS) 10 (1) (2010).

[4] M. Cord, P.-H. Gosselin, Online content-based image retrieval using active learning, in: Machine Learning Techniques for Multimedia Part II, Cognitive Technologies, 2008, pp. 115–138.

[5] B. Roberto, M. Ornella, Image retrieval by examples, in: IEEE Transactions on Multimedia, vol. 2, September, 2000.

[6] H.B. Kekre, T.K. Sarode, S.D. Thepade, V. Suryavanshi, Improved texture featurebased image retrieval using Kekres fast codebook generation algorithm, in: International Conference on Contours of Computing Technology, Babasaheb Gawde Institute of Technology, Mumbai, 13–14 March, Springer, 2010.

[7] J. Wei, E. Guihua, D. Qionghai, G. Jinwei, Similarity online feature selection in content-based image retrieval, IEEE Transactions on Image Processing 15(3) (2006) 702–712.

[8] Y.M. Chen, J.-H. Chiang, Fusing multiple features for Fourier Mellin-based facere cognition with single example image per person, Neurocomputing 73 (2010)3089–3096.

[9] F. Long, H. Zhang, H. Dagan, D. Feng, Fundamentals of content based image retrieval, in: D. Feng, W. Siu, H. Zhang (Eds.), Multimedia Information Retrieva land Management. Technological Fundamentals and Applications, Multime diaSignal Processing Book, Chapter 1, Springer-Verlag, Berlin, Heidelberg, New York, 2003, pp. 1–26.

[10] G. Qian, S. Sural, Y. Gu, S. Pramanik, Similarity between Euclidean and cosineangle distance for nearest neighbor queries, Proceedings of ACM Symposiumon Applied Computing 12 (22) (2004) 1232–1237.

[11] M. Babu Rao, B. Prabhakara Rao, A. Govardhan, CTDCIRS: content based image retrieval system based on dominant color and texture features, International Journal of Computer Applications 18 (6) (2011).

[12] J. Yue, Z. Li, L. Liu, Z. Fu, Content-based image retrieval using color and texture fused features, Mathematical and Computer Modelling 54 (2011) 1121–1127.

[13] G.P. Qiu, Color image indexing using BTC, IEEE Transactions on Image Processing 12 (1) (2003) 93–101.

[14] J. Han, K.-K. Ma, Rotation-invariant and scale-invariant Gabor features for texture image retrieval, Image and Vision Computing 25 (2007)1474–1481.

[15] P.W. Huang, S.K. Dai, Image retrieval by texture similarity, Pattern Recognition36 (3) (2003) 665–679.

[16] N. Jhanwar, S. Chaudhuri, G. Seetharaman, B. Zavidovique, Content based image retrieval using motif cooccurrence matrix, Image and Vision Computing 22(2004) 1211–1220.

[17] C.-H. Lin, R.-T. Chen, Y.-K. Chan, A smart content-based image retrieval system based on color and texture feature, Image and Vision Computing 27 (2009)658–665.

[18] http://wang.ist.psu.edu/docs/related/

Applied Mechanics and Materials Vol. 596 (2014) pp 394-397
© (2014) Trans Tech Publications, Switzerland
doi:10.4028/www.scientific.net/AMM.596.394

A Statistical Model for Real-time Video Moving Target Detection Based on Bayesian Statistics

Zhihong Zhang[1,a], Shuling Zhang[1],Bin Yang[2],Xin Bai[3]

[1] Zhengzhou Tourism College, Zhengzhou, Henan, China

[2]North China University of Water Resources and Electric Power, Zhengzhou, Henan, China

[3]ZhengZhou Metro, Zhengzhou, Henan, China

[a]zzhyzq@163.com

Keywords: Real-time detection; statistical model; video object

Abstract. Video moving target detection is an important foundation issues in computer vision, based on the analysis of the advantages and disadvantages of each existing moving target detection model, using Bayesian statistical theory as a framework, proposes a statistical model that can detect moving objects in video in real-time. The model combines time, space and color and other relevant information of pixel, divides and extracts Video segmentation's foreground. By selecting the appropriate reference background can improve the precision and accuracy of the detection.

Introduction

Moving object detection means to obtain specific target location, area and other features from the video scene in real time. Moving object detection is an important problem in computer vision-based systems, and rapid detection of moving targets for target classification, tracking and understanding the behavior of other follow-up treatment is very important, so fast moving target detection algorithm is a hot research currently. However, the video moving target detection is facing many difficulties. A good video object model must be able to handle the scene brightness changes caused by the light intensity at different times in one day, jitter background caused by external factors such as wind formed , colors convergence of true objective in the foreground of background's, change of background formed by the object itself come in and out of the scene.

This paper combines the advantages and disadvantages of existing moving target detection model, use Bayesian theory as a framework, proposed a statistical model to extract moving target in the video in real-time. This model uses dynamic threshold to replace the previously fixed threshold to classify background subtraction and frame difference results, make up the problem of different real threshold values for each position due to the noise value range is wide. Accuracy of reference background in the is very important in Target detection, When the scene is very complex, the models that are not trained need to take a long time to stabilize, this paper presents a background generation method can run unsupervised to solve the problem, which is a good solution when generating a reference background using statistical methods to the Defects in settings different training time according to different scenarios artificially.

Related Work

The main research methods of moving target detection based on video are divided into the following categories: method based on optical flow [1], method based on frame difference, method based on the background model [2], method based on stereo vision[3].

The method based on optical flow compute velocity vector in each frame of video for each pixel, when the existence of relative motion between the object and the background of the image, velocity vector formed by moving objects is inevitable different from neighborhood backgrounds' velocity vector, based on this difference to detect the position of moving objects, However, optical flow method have large Calculated amount, and is susceptible to noise and changes of illumination.

The method based on frame difference uses the difference between frames to detect motion region, in general such methods rely on brightness gradient of space-time image. Image brightness gradient is very sensitive to measurement noise. Accuracy of segmentation is susceptible to noise. Although there are many compensation methods for noise [4], but such methods also require that the movement speed of the target object is not too fast, so such a method is more suitable for segmentation of video motion objects in indoor scenes.

The method according to the background model based on the difference between the current frame and the reference background to detect the moving object, The focus of the method is to create a dynamic changing background model to adapt to the scene, such as Gaussian mixture mode, kernel density estimation model [5], features background mode, complex background statistical model.

Currently, the effect of method based on the statistical model is better, and used more often. Statistical modeling methods are mainly Gaussian mixture model, Bayesian statistical model [6], codebook model [7]. However, these algorithms have their drawbacks, codebook background model process poor for background's mutation, Bayesian models need to select the appropriate feature vectors, Gaussian mixture model have a large Calculated amount. In addition, all detection algorithms is not ideal in processing situation like background motion (Swaying branches, changes in the brightness of the light) and prospects for slow motion (Movement of snails, turtles, etc). Bayesian model's detection accuracy is quite with Gaussian mixture model, but the execution speed is much faster than Gaussian mixture. In the existing Bayesian algorithm, the model with better detecting effect is complex statistical models proposed by Liyuan Li et al. [2]. However, in this model, it must rely on the accuracy of the difference of the background to detect selected area. When position of a pixel in the background has a wide range of values, gradient feature will detected the background pixels as foreground part as noise. Reference background generation method referred in this algorithm, need to set up a different training time based on different scenarios, limiting the algorithm's application in practice. For these reasons, this paper put forward the corresponding solutions, and improve the efficiency of detection effect and execution of models.

Statistical Model for Target Detection

The video object detection algorithms presented in this paper, first, initialize the model, and then generate a reference background, training feature vectors, on the basis of that ,do change detection, use test results to do foreground segmentation, updated the reference background simultaneously, finally, use the results of segmentation for noise optimization.

In this model use $s=(x,y)$ represent the location of a pixel in the image, $I(s,t)$ is the image frame input at time t, v is n-dimensional vector extracted at position s at time t, the probability of the Pixel at position s as background or foreground are expressed as:

$$P_s(b|v)=\frac{P_s(v|b)P_s(b)}{P_s(v)} \tag{1}$$

$$P_s(f|v)=\frac{P_s(v|f)P_s(f)}{P_s(v)} \tag{2}$$

In which, b means background, f means foreground, $P_s(b|v)$ and $P_s(f|v)$ is the conditional probability of pixels on its feature vector v belong to the background and foreground at position s, $P_s(b)$ and $P_s(f)$ is the Priori probability of pixels belong to the background and foreground at position s, If satisfied at time t:

$$P_s(b|v)>P_s(f|v) \tag{3}$$

Then the pixels $I(s,t)$ determined as background. Use N feature vector $v(v_1,v_2,...,v_N)$ to quantify pixels, and v_i in descending order about $P_s(v_i\,|\,b)$, build statistics for the main features:

$$T_v(s)=\begin{cases} p_v^t(b) \\ \{s_v^t(i)\}, i=1,...,M(v) \end{cases} \tag{4}$$

Using this statistical tables to estimate and update the a priori probability $P_s(b)$, $P_s(v)$ and conditional probability $P_s(v\,|\,b)$, to get the posibility of pixel $I(s,t)$ s belonging to the foreground and background. In which, $p_v^t(b)$ is the prior probability $P_s(b)$ based on the feature vector v, $s_v^t(i)$ is the pixels $I(s,t)$ Common feature vector statistics recorded as follows:

$$s_v^t(i)=\begin{cases} p_{v_i}^t=P_s(v_i) \\ p_{v_i|b}^t=P_s(v_i\,|\,b) \\ v_i=(v_{i1},...v_{iD(v)})^T \end{cases} \tag{5}$$

In which, $D(v)$ is the dimension of feature vectors. $s_v^t(i)$ is in descending order in the statistics about $p_{v_i}^t$ .so use

$$P_s(v_t)=\sum_{v_j\in U(v_t)} p_{v_j}^t \tag{6}$$

$$P_s(v_t\,|\,b)=\sum_{v_j\in U(v_t)} p_{v_j|b}^t \tag{7}$$

In which, $U(v_t)$ represent the collection of feature vectors in $T_v(s)$ matches the input vector v_t .so use the $N(v)$ elements in table $T_v(s)$ combine $p_v^t(b)$ equation (3) can be classified on the foreground and background.

When model training and updating, we take a different approach to mutant background and gradient background respectively. If $I(s,t)$ is detected as a stationary point, use color and gradient to classify the foreground and background, otherwise use two colors adjacent to classify, and match the main features of the vector with the following update:

$$\begin{aligned} p_v^{t+1}(b)&=(1-\alpha)p_v^t(b)+\alpha L_b^t \\ p_{v_i}^{t+1}&=(1-\alpha)p_{v_i}^t+\alpha L_{v_i}^t \\ p_{v_i|b}^{t+1}&=(1-\alpha)p_{v_ib}^t+\alpha\left(L_b^tL_{v_i}^t\right) \end{aligned} \tag{8}$$

In which, α is the learning rate, $L_b^t=1$ represent when split ends $I(s,t)$ is divided into background, otherwise equal to 0. $L_{v_i}^t=1$ represent that if the input vector v v is matched with the i-th vector in table $T_v(s)$, otherwise equal to 0. When satisfying the following formula is considered to be mutated background.

$$\sum_{i=1}^{N(v)} p_{v_i}^t - p_v^t(b)\sum_{i=1}^{N(v)} p_{v_i|b}^t > M_1, M_1=80\%\sim 90\% \tag{9}$$

Mutant background using different ways to update from gradient backgrounds, like following equation:

$$\begin{aligned} p_v^{t+1}(b) &= 1 - p_v^t(b) \\ p_{v_i}^{t+1} &= p_{v_i}^t \\ p_{v_i|b}^{t+1} &= \frac{\left(p_{v_i}^t - p_v^t(b)\, p_{v_i|b}^t\right)}{p_v^{t+1}(b)} \end{aligned} \tag{10}$$

If there is no matching feature vectors in table $T_v(s)$,use $p_{v_{M(v)}}^{t+1} = \alpha$, $p_{v_{M(v)}|b}^{t+1} = \alpha$ and $V_{M(v)} = v$ to replace the $M(v)$ vector. In the model, Reference background update with the following equation:

$$B_c(s,t+1) = \begin{cases} I_c(s,t), if\ background\ changed \\ (1-\beta) B_c(s,t) + \beta I_c(s,t), otherwise \end{cases} \tag{11}$$

Conclusion

This paper based on the analysis of the advantages and disadvantages of existing moving target detection model, use Bayesian statistical theory as a framework, presents statistical model that can detect moving objects in video in real-time. Model algorithm combines the pixels of time, space and color, and other related information, conduct split extraction to foreground in the video. In the change detection, use to background difference to preprocess the detection area, the accuracy of the test results is closely related to the accuracy of the pre-treatment region, and a good reference background can improve the accuracy of the pre-treatment region. Reference background selection, color space and the threshold value determination is a key step in the algorithm. At the same time, model's detect effects should be further validated.

References

[1] Chan K L. Detection of swimmer using dense optical flow motion map and intensity information. Machine Vision and Applications. 2013, 24(1): 75-101.

[2] Li L, Huang W, Gu Y, et al. Statistical modeling of complex backgrounds for foreground object detection. IEEE Transactions on Image Processing. 2004, 13(11): 1459-1472.

[3] Munoz-Salinas R, Aguirre E, Garcia-Silvente M. People detection and tracking using stereo vision and color. Image and Vision Computing. 2007, 25(6): 995-1007.

[4] Araki S, Matsuoka T, Yokoya N, et al. Real-Time Tracking of Multiple Moving Object Contours in a Moving Camera Image Sequence. IEICE TRANSACTIONS on Information and Systems. 2000, E83-D(7): 1583-1591.

[5] Elgammal A, Harwood D, Davis L. Non-parametric Model for Background Subtraction. Computer Vision-ECCV 2000. 2000: 751-767.

[6] Lee K, Kim J. Moving object segmentation based on statistical motion model. Electronics Letters. 1999, 35(20): 1719-1720.

[7] Kim K, Chalidabhongse T H, Harwood D, et al. Real-time foreground--background segmentation using codebook model. Real-time imaging. 2005, 11(3): 172-185.

Applied Mechanics and Materials Vol. 596 (2014) pp 398-401
© (2014) Trans Tech Publications, Switzerland
doi:10.4028/www.scientific.net/AMM.596.398

An improved moving object tracking method based on graph cuts

Mingjie ZHANG [1, 2,a], Baosheng KANG [1,b]

[1] School of Information Science and Technology, Northwest University, Shaanxi Xi’an 710127,China

[2] School of Management Engineering,Xi’an University of Post and Telecommunications,
Shaanxi Xi’an 710061,China

[a]75711650@qq.com, [b]njmingjie@sina.com

Keywords: Graph Cuts; Ground Truth; Object Tracking; Kalman Filtering

Abstract. In order to improve efficiency of object tracking in occlusion states. A method to detect and automatically track was present in a surveillance system. Firstly, a graph cuts method was employed to segment image from a static scene. To identify foreground objects by positions and sizes of the obtained foreground regions. In addition, the performance to track objects was improved by using the improved overlap tracking method, the tracking method was used to analyze the centroid distance between neighboring objects and help object tracking in occlusion states of merging and splitting. By the experiments of moving object tracking in three video sequences, the experimental results exhibit that the proposed method is better than the traditional method.

Introduction

Moving object tracking have been widely used in monitoring, behavior analysis and human-computer interaction[1,2]. So far, various tracking methods have been previously proposed. In Marcenaro et al.’study[3], in order to reduce the influence of dynamic occlusion, a linear kalman filter is performed object tracking by matching shape feature. Lien et al. [4] proposed a multi-mode method to improve accuracy and efficiency for object tracking in a crowded scene. Six modes for object tracking were defined by heuristic thought. In [5], object t tracking framework is proposed, the foreground regions are divided into several parts in which color features are extracted for object matching. Chan [6] put forward using gaussian process as characteristic function, it show texture feature from the crowd segmentation. Moreover, Haritaoglu et al.[7] proposed to select the contours of people bodies to classify merge and split states in outdoor crowded conditions. In the literature of object tracking, kalman filtering [8] is often used to predict the trajectory of the crowd. Wang et al.[9] proposed a color space gaussian mixture model. By modeling in the color distribution and spatial information, the algorithm can more accurately track object. However, the above mentioned methods of tracking object using feature of color, shape and contour, which rely on effective object segmentation, are sensitive to light changes. In high density crowed environment, it need to carefully consider tracking states of object merger and split.

In monocular crowded environment, detection ratio is often caused by object occlusion. In order to overcome the influence of occlusion.A object tracking method is proposes, it can improve the accuracy of tracking in surveillance system.

Overview of Algorithm

The proposed framework of object tracking algorithm is shown in Fig.1. Firstly, Graph cuts is employed to segment the moving objects from each captured video frame. After obtaining the foreground regions, four states which include new, leaving, merged and split are assigned to the detected moving objects according to their appearances in the current frame. Especially, for relieving the occlusion effects, objects identified as states of merge and split further pass through backward tracking by analyzing the centroid distances among objects in previous frame. Finally, in order to get the objects tracking results, objects in four states are tagged.

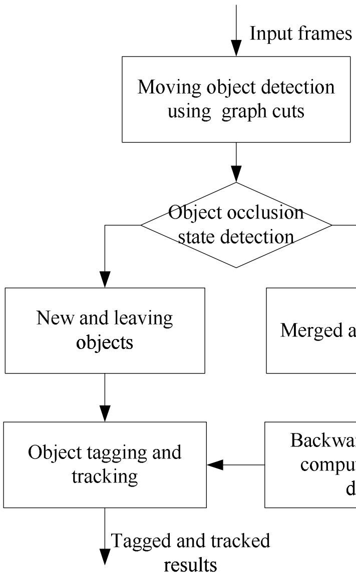
Input frames
Moving object detection using graph cuts
Object occlusion state detection
New and leaving objects
Merged and split objects
Object tagging and tracking
Backward tracking by computing centroid distance
Tagged and tracked results

Fig. 1 Framework of the proposed method

Image Segmentation using Graph Cuts

The segmentation of the foreground and the objects can be obtained by graph cuts method[10], at each time t ,by minimizing the following energy with respect to the labeling function λ :

$$J(\lambda)=\varepsilon_D(\lambda)+\varepsilon_R(\lambda) \tag{1}$$

The data term ε_D measures the likelihood P_i of a pixel to belong to an object i :

$$\varepsilon_D \ \lambda \ = -\sum_{\in\Omega}\sum_{=}^{N} \mathrm{n} \qquad \delta\ \lambda \quad - i \tag{2}$$

where $\delta(l)$ is the characteristic function (equal to 1 if $l=0$ and 0 otherwise). The regularization term ε is

$$\varepsilon \ \ \lambda \ = R_\Omega \sum_{x\in\Omega^i}\ \sum_{x\in \mathrm{N}^i \ \ x)}^{N} I \qquad) \ I \qquad)) \quad -\delta\ \lambda \quad) - \lambda \quad)) \tag{3}$$

Where $R_\Omega > 0$ is the regularization parameter and F: $IR \times IR \mapsto IR^+$ is a decreasing function that penalizes the spatial discontinuities of the segmentation according to the image data. A cost is then paid when two neighbor pixels x and z have different labels, i.e., $\lambda(x) \neq \lambda(z)$ and $\delta(\lambda(x) - \lambda(z)) = 0$.

This regularization is equivalent to the minimization of the length of the boundaries between objects. Note that the neighborhood of a pixel x involved in energy (1) is defined by

$$\mathrm{N} \qquad = z \in \Omega^t 0 < \left| z - \qquad \right| \leq 1\} \tag{4}$$

With such a model, the segmentations obtained at each time obviously suffer from temporal inconsistencies, and the foreground image is instantaneously obtained.

Method for Tracking and Tagging Objects

After segmenting foreground image by graph cuts method, regions of interest are identified from the foreground image based on the completeness of region contours. Moreover, detecting character regions from the interested ones is considered under the physical constraints of human body, including the dynamic range of pixel gray-level values and the shapes of regions. When objects conform to the constraints, ellipses having the minimized areas that can cover the regions are constructed with their corresponding position parameters, ellipse radiuses, centroids and distances.

In the improved overlap tracking method, four tracking states comprising new object, leaving object, merged object and split object are used to understand characters in the current frame. New object means an object entering a video scene, leaving object defines an object out of a video scene. For merged and split object states, the touch event of objects is detected in neighboring frames. The judgment of target merging and splitting in the current frame considers the target states by backward tracking the objects that appear in the previous frame. Finally it assigns tags to individual objects by means of positional continuity preserved by the tagged characters in the previous frame. Our proposed tracking method is explained as follows:

Step 1: Extract foreground object by graph cuts method.
Step 2: Entering and leaving object detection.
Step 3: Single and occluded object detection.
Step 4: If the region of object is merged and split states, go to step 5. Otherwise, go to 6.
Step 5: Identifying the merged and split objects in the current frame.
Step 6: Recording the tagged object.
Step 7: Tagged results, go to step 5

Computing centroid distances of objects

Compared with the traditional overlap tracking method, our proposed tracking method performs backward tracking the tagged objects on the previous frame. The centroid distances between objects of merged and split states are analyzed in the current and previous frames. As mentioned at above section, the long and short radiuses of each ellipse representing an object are averaged to obtain a dynamic radius by $s=(w+h)/2$ where w and h denote the long and short radiuses of an ellipse, respectively. An object with the merged state in the current frame is identified by analyzing the centroid distance of two neighboring ellipses to be smaller than the sum of their dynamic radiuses in the previous frame. On the other hand, to determine split objects, it is to conform to that, the sum of dynamic radiuses owned by two neighboring ellipses being larger than their centroid distance in the current frame.

By analyzing the object states of the current frame, it finally assigns tags to objects. In addition, the tag of each object will be recorded and referenced for object tracking in the next coming frame.

Experimental result

The proposed method is experimented on three video clips from the public testing data sets. Fig.2 shows segment images and object tracking from the experimental clips. Results from Fig.2 show that the graph cuts method can effectively overcome the disturbance from light variations to obtain reliable separated objects, and it can obtain good tracking effect.

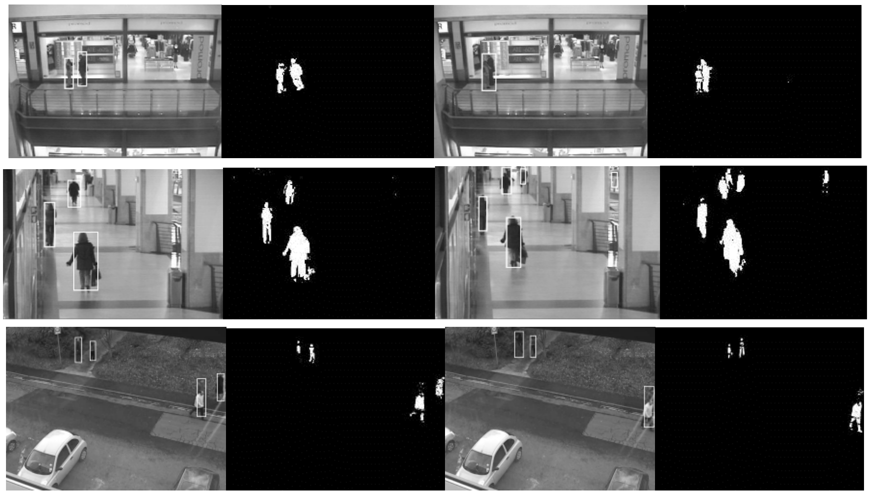

Fig. 2 Segmentation and tracking results of three video clips.

In order to evaluate the tracking performance, the methods are compared by calculating the detection ratio and Root-Mean Squared error (RMS) in average. The detection ratio and RMS are calculated in each frame by the following formulations.

$$D(i) = \frac{T(i) - C(i)}{T(i)} \tag{5}$$

$$E_{rms} = \sqrt{\frac{1}{n}\sum_{i=1}^{N}(T(i) - C(i))^2} \tag{6}$$

Here, $D(i)$ is the detection ratio in the i -th frame, $T(i)$ represent the real position of objects and $C(i)$ represent position of tracking objects by tracking methods in Table 1. E_{rms} represents the averaged RMS in video clips. The averaged detection ratios and errors associated with the three video clips are listed in Table 1. From Table 1, the proposed method has higher detection ratios and smaller errors on object tracking in three videos than Kalman filtering method and the ground truth.

Table 1.Comparisons of the averaged detection ratios and RMS from three video sequences.

sequence	Detection			E_{rms}		
	Proposed method	Ground Truth method	Kalman filtering method	Proposed method	Ground Truth method	Kalman filtering method
sequence 1	0.85	0.71	0.75	0.56	0.61	0.68
sequence 2	0.79	0.70	0.74	0.70	1.06	1.09
sequence 3	0.77	0.68	0.67	0.89	1.11	0.79
Averaged	0.80	0.69	0.72	0.72	0.93	0.85

Conclusions

In this paper, we propose a method to track from a stationary video scene in a surveillance system. Foreground regions are segmented by graph cuts method for light variations in an environment. Then, objects are identified as characters with considering the positions and sizes of the extracted foreground regions. For tracking objects, an improved overlap tracking method is developed and used to obtain an improvement on tracking characters in occlusion conditions of objects merging and splitting by means of analyzing the centroid distances among objects. By the experiments of moving object tracking, the experiment results show that the proposed method performs better.

Acknowledgements

This work was financially supported by the National Nature Science Foundation of China (61272286) and MOE (Ministry of Education in China) Project of Humanities and Social Sciences (13YJCZH251).

References

[1]R. Hoseinnezhad, Vo B.-N, Vo B.-T:Pattern Recognition, vol.45,no.10,(2012),p.3625-3635.
[2] M. Cristani , R. Raghavendra , A. Del Bue. : Neurocomputing, vol.100,no.1,(2013),p.86-97.
[3] L. Marcenaro:Procc. of IEEE ICIP, vol.3(2002),p.341.
[4] C C. Lien , Y L. Huang, C C. Han:Procc of IEEE IIH-MSP, (2009),p.1018.
[5] S. Khan, M. Shah:Proc. of Asian Conf. on Computer Vision, (2000),p.1132-1137.
[6] A. Chan, Z. Liang,Vasconcelos N:CVPR, (2008),p.1.
[7] I. Haritaoglu, D. Harwood:On Pattern Analysis and Machine Intelligence, vol.22(2000), p.809.
[8] A. Yilmaz, O. Javed, M. Shah:ACM Computing Surveys, vol.38(2006), article 13.
[9]H. Wang,D. Suter,K. Schindler,C. Shen:IEEE Transactions on Pattern Analysis and Machine Intelligence,no.9,(2007),p.1661-1667.
[10] Y. Boykov and M.P. Jolly:Proc. IEEE Int'l Conf. Computer Vision,1,(2001),p.105-112.

Applied Mechanics and Materials Vol. 596 (2014) pp 402-405
© (2014) Trans Tech Publications, Switzerland
doi:10.4028/www.scientific.net/AMM.596.402

Compact Wake-up Word Speech Recognition on Embedded Platforms

Anhao Xing[1, a], Ta Li[1], Jielin Pan[1] and Yonghong Yan[1]

[1] The Key Laboratory of Speech Acoustics and Content Understanding,
Chinese Academy of Sciences, Beijing 100190, P.R.China
[a]xinganhao@hccl.ioa.ac.cn

Keywords: wake-up word, speech recognition, double scoring, principal component analysis, support vector machine.

Abstract. The wake-up word speech recognition system is a new paradigm in the field of automatic speech recognition (ASR). This new paradigm is not yet widely recognized but useful in many applications such as mobile phones and smart home systems. In this paper we describe the development of a compact wake-up word recognizer for embedded platforms. To keep resource cost low, a variety of simplification techniques are used. Speech feature observations are compressed to lower dimension and the simple distance-based template matching method is used in place of complex Viterbi scoring. We apply double scoring method to achieve a better performance. To cooperate with double scoring method, the support vector machine classifier is used as well. We were able to accomplish a performance improvement with false rejection rate reduced from 6.88% to 5.50% and false acceptance rate reduced from 8.40% to 3.01%.

Introduction

Since it was proposed, automatic speech recognition (ASR) has always been regarded as the most natural way of human-computer interaction. Many scholars have done a lot of research and work over the past several decades. Thanks to their contribution, significant progress has been made in different speech recognition applications. Wake-up word speech recognition (WUW SR) is a branch of ASR and has a very promising prospect in several newly emerging fields such as smart mobile phones and intelligent home systems.

The WUW speech recognition is a new paradigm which is not widely recognized. The task is similar to spoken term verification task or key word spotting. A WUW speech recognizer only accept some particular word or phrase while reject all the others. Conventional framework of hidden Markov model (HMM) and Viterbi decoding can be applied in WUW speech recognition task. Kepuska et al have done a lot of work in this field and accomplished some remarkable achievements [1,2].

As is mentioned, the major area where WUW speech recognition can be applied is intelligent home system. For instance, we can embed the WUW speech recognition system in a smart television, which will enable the television to respond properly to some simple instructions such as "change channel" or "volume up" given by human. Similar operations can be performed on smart air-condition, smart refrigerator and other household appliances. As to air-condition or refrigerator, the WUW speech recognition system is usually implemented on a chip, so the computation and storage resource is limited. Even for a smart phone with powerful calculating capacity, it is still not a good choice to apply the integrated WUW speech recognition system. As a result, an approach to implement WUW speech recognition system with small footprint is in request.

In this paper, the development of a compact WUW recognizer for embedded platforms is described. An energy-based clustering method is proposed to reduce the dimension of observations dramatically. Simple template matching paradigm is used to replace complex Viterbi decoding. To assure the accuracy, we use double-scoring method without increasing too much computation. Two speech feature types and two scoring methods are used to adapt to the double scoring method. Finally, a support vector machine (SVM) classifier is used to give the verification result (whether the input utterance is a WUW or not).

The remainder of this paper is organized as the following. In Section 2, we briefly talk about the definition of the WUW speech recognition task. In Section 3, the framework of our WUW speech recognizer is described. In Section 4, we give the details of the techniques used in our system. Experimental results are shown in Section 5. The work is finally concluded in Section 6.

Wake-up Word Speech Recognition

WUW speech recognition is a new paradigm in the area of speech recognition. The paradigm is applied to detect a single word or phrase when spoken in an alerting context, while rejecting all other words, phrases, sounds, noises and other acoustic events [1]. Referring to the definition, two criteria can be adopted to evaluate a WUW speech recognizer and they are false rejection rate and false acceptance rate.

False rejection is rejecting when encountered a WUW and false acceptance is accepting when encountered a non-WUW In ideal conditions, false rejection rate and false acceptance are both zero, which means the WUW speech recognizer detects all the WUWs and rejects all non-WUWs.

Generally, more efforts should be made to reduce false acceptance rate, because rejecting non-WUWs is more important than accepting WUWs. Especially in some circumstances when safety is taken into consideration such as smart cars, a false acceptance may let the car to carry out some wrong order and consequently cause an accident.

System Framework

There are three steps to implement an embedded WUW Recognizer. In the training step, we use MLFPCC features to get 32 cluster centers via K-means clustering and use PLP features to get a projection matrix via 2DPCA. In the developing step, we use the cluster centers and projection matrix calculated in previous step to train a SVM classifier. At last, in test step, the optimum SVM classifier is applied to verify if the input is WUW or not.

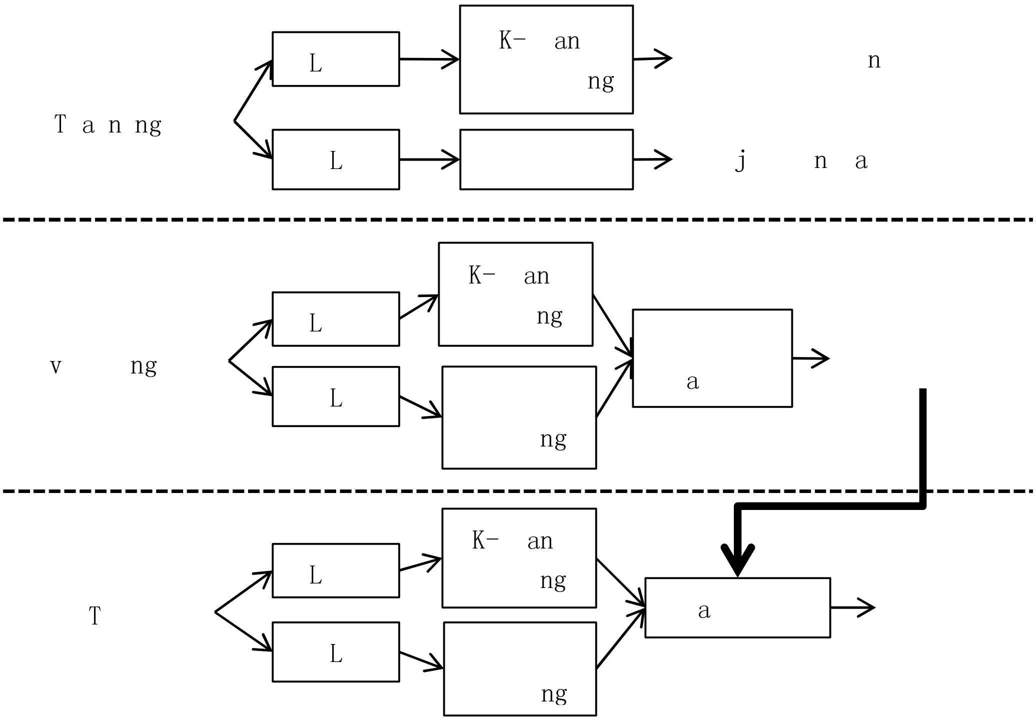

Figure 1. Flow chart of our WUW speech recognition system.

Energy-based Feature Compression

To implement a WUW speech recognizer on embedded platforms, the scale of data to process is a challenge. In this paper, we proposed an energy-based data compression method to reduce the dimension of feature observations input to the WUW speech recognition system. This technique is applied between step 1 and step 2, that is, after feature extraction and before scoring.

To compress the feature observations, we first calculate the energy of the whole utterance. 2-norm function is used to calculate energy. Then, the utterance is divided into 8 shares equally, each of which has the 1/8 of all the energy. After that, we add up all frames in the same share into one "high-energy" frame. In this way, the temporal dimension of the utterance feature observations is decreased from the number of frames to 8, which is the number of equal shares.

Before next step, the mean and variance normalization is usually performed on each "high-energy" frame, so the scoring scale is consistent in different conditions. The normalization has been proved to be very effective in speaker-dependent WUW speech recognition paradigm, so we continue to use that in this speaker-independent WUW speech recognition task.

The energy-based compression can reduce the dimension of data by a large factor. Besides that, two simple scoring methods, which are K-means and PCA, are used to serve as classification criteria. It is out of scope to discuss how standard K-means clustering and principal component analysis (PCA) are performed explicitly. The readers should know that the input of the scoring step is a matrix, the rows of which are energy-based compressed models. The output of the scoring step is the distance calculated via European distance function between the test utterance and the models.

Experimental Results

To evaluate the WUW recognizer which we propose, a series of experiments were performed. The training set consists of 892 utterances which are WUWs. The evaluation set consists of 218 WUW utterances and 1095 non-WUW utterances. All these utterances are very short orders daily used as instructions to household appliances. Utterances are recorded with mobile phones under laboratory environment by 10 men and 10 women.

The baseline is a WUW recognizer using single scoring method. Other experiments are performed with WUW recognizers using double scoring method. The effect of choosing different classification functions of SVM is tested. All the results are shown in Table 1 and Table 2.

Table 1. Performance comparison between wake-up word system with different scoring method

Scoring Method	false rejection rate	false acceptance rate
MFLPCC (linear classification)	6.88%	8.40%
MFLPCC + PLP (linear classification)	4.59%	5.11%

Table 2. Performance comparison between wake-up word system with different classification function choice

Scoring Method	false rejection rate	false acceptance rate
MFLPCC + PLP (linear function)	4.59%	5.11%
MFLPCC + PLP (quadratic function)	4.59%	3.93%
MFLPCC + PLP (radial basis function)	5.50%	3.84%
MFLPCC + PLP (polynomial function)	5.50%	3.01%

It is shown in Table 1 that with double scoring method, the WUW recognizer performs better than that that with single scoring method. The new scoring method improves both rejection accuracy and acceptance accuracy. From Table 2, we can see that the choice of classification function has an effect on the performance of a WUW speech recognition system. According to our experiments, quadratic function is the most suitable for our task.

Conclusions

In this paper, we describe how we develop a compact WUW recognizer on embedded platforms. We propose an energy-based clustering method to compress the observations to lower dimension. Instead of complex Viterbi decoding, two simple scoring methods are used to score the input speech. With this double scoring method, we improve the performance of our WUW speech recognizer while maintaining conciseness. With all above techniques applied, the false rejection rate decreases from 6.88% to 4.59% and the false acceptance rate decreases from 8.40% to 5.11%. We further do some research about how the choice of classification function affects the performance of WUW speech recognition system.

Acknowledgements

This work is partially supported by the National Natural Science Foundation of China (Nos. 11161140319, 91120001, 61271426), the Strategic Priority Research Program of the Chinese Academy of Sciences (Grant Nos.XDA06030100, XDA06030500), the National 863 Program (No. 2012AA012503) and the CAS Priority Deployment Project (No. KGZD-EW-103-2).

References

[1] V. Z. Kepuska, T. B. Klein: *A novel Wake-Up-Word speech recognition system, Wake-Up-Word recognition task, technology and evaluation*, in: *Nonlinear Analysis: Theory Methods and Applications*, p. 2772-2789, 2009.

[2] V. Kepuska: *Wake-Up-Word Speech Recognition*, in: *Speech Technologies*, p. 237-262, Jun. 2011.

[3] C. Myers, L. Rabiner, A. Rosenberg: *An investigation of the dynamic time warping for word spotting and connected speech recognition*, in: ICASSP ’80, vol. 5, p. 173-177, Apr 1980.

[4] A. Garcia, H. Gish: *Keyword spotting of arbitrary words using minimal speech resources*, in: ICASSP 2006, vol. 1, p. 14-19, May 2006.

[5] J. Yang, D. Zhang, A. F. Frangi, J. Y. Yang: *Two-Dimensional PCA: A New Approach to Appearance-Based Face Representation and Recognition*, in: *IEEE Trans. Pattern Analysis and Machine Intelligence*, vol. 26, no. 1, p. 131-137, Jan 2004.

[6] C. W. Hsu, C. C. Chang, C. J. Lin: *A practical guide to support vector classification*, Department of Computer Science and Information Engineering, National Taiwan University, 2007.

[7] Jonathon Shlens: *A Tutorial on Principal Component Analysis*.

[8] Information on http://en.wikipedia.org/wiki/K-means_clustering.

[9] Information on http://en.wikipedia.org/wiki/Singular_value_decomposition.

Applied Mechanics and Materials Vol. 596 (2014) pp 406-412
© (2014) Trans Tech Publications, Switzerland
doi:10.4028/www.scientific.net/AMM.596.406

Research on Lossless Predictive Coding Methods for Stereo Images

Shigao Li [1, a]

[1] School of Mathematic & Computer Science, Wuhan Polytechnic University,
Wuhan Hubei 430023, China
[a]sg51@163.com

Keywords: Image compression; stereo image coding; predictive coding; disparity estimation

Abstract. There exists very high correlation between left-view images and right-view images of stereo image pairs. The correlation can help to reduce the stereoscopic image coding bit rate. Proposed methods first estimate the disparity by using causal neighborhood pixels. And then a prediction method which combines inter-view prediction with intra-view prediction is used to obtain a better predictive coding method for target-view images. The reference-view images are then encoded by using those commonly used prediction coding method. The experimental results show that compared with those methods using only intra-view correlation, the proposed method can obtain lower code rate.

Introduction

Stereoscopic imaging systems are extensively applied in photogrammetry, entertainment and machine vision. In the field of digital photogrammetry, stereo image pairs are used to generate DEM or DTM. However, a mass of image data bring a challenge to image storage and transmission. Especially, how to cater to the capacity of wireless channel for those stereo sensors set on satellites is a strenuous task. Compression techniques are usually used to solve the problem. And stereo image compression techniques have received many researchers' attention.

It's no doubt that lossless compression is a major branch of image compression. Currently there are many lossless image compression method based on prediction coding method. In order to remove temporal or spatial redundancy, predictors based on source model are used to accurately predict source data as much as possible. Because only causal neighborhood samples are exploited to predict current sample, the same prediction procedure can be repeated in the process of decoding. The median edge detection (MED) based LOCO-I algorithm is a typical predictive coding method [1]. And it was identified as the lossless image compression standard JPEG-LS. Another good prediction coding algorithm is the CALIC algorithm based on Gradient Adaptive Prediction (GAP) [2]. They choose an optimal predictor from several presupposed candidates according to the context. CALIC uses a more complicated predicting method and obtains a better performance. Differing from these two prediction methods, the method based on edge directed predicting (EDP) adopt a more flexible prediction method [3]. The EDP get a better prediction performance at the cost of more complexity. Later, some scholars proposed some other prediction methods. Although they get better performance, but they are impractical due to excessive complexity [4,5].

Due to the high efficiency, CALIC has been extended to the lossless compression of multi-spectral image and video [6-8]. Although there are a lot of literatures about stereo image compression technology [9-13], few lossless coding method about stereoscopic images are proposed so far. It's beyond question that the research about lossless coding of stereoscopic images is significant, especially in the field of photogrammetry. Following the current relatively popular lossless image compression algorithms, this paper propose the prediction coding method of stereoscopic images.

The rest of this paper is organized as follows. Section 2 reviews the predicting methods GAP and EDP. In section 3, we give the detail of our lossless predicting coding of stereo images. Finally, in section 4, experimental results are given and some conclusions are drawn in section 5.

Prediction Methods

GAP. The causal neighbors of a current pixel shown in Fig.1 are first used to estimate the horizontal gradient d_h and the vertical gradient d_v as contexts. GAP classifies the contexts into 6 types according to d_h and d_v. The prediction of a current pixel is then gotten by causal neighbors and the context type.

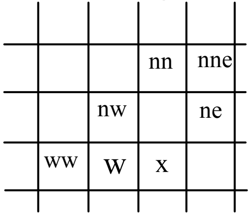

Figure 1. Causal neighbors used in GAP

$$\begin{aligned} d_h &= |I_w - I_{ww}| + |I_n - I_{nw}| + |I_n - I_{ne}| \\ d_v &= |I_w - I_{nw}| + |I_n - I_{nn}| + |I_{ne} - I_{nne}| \end{aligned} . \tag{1}$$

EDP. Differing from GAP, EDP do not classifies contexts into several fixed types. It constructs a linear model to predict current pixels by using causal neighbors shown in Fig. 2. To estimate the prediction coefficients β(k), a training window shown in Fig. 3 is defined and the pixels in the training window are exploited as a training set to estimate prediction coefficients β(k) by using least square.

$$\hat{X}(n) = \sum_{k=1}^{N} \beta(k) X(n-k) . \tag{2}$$

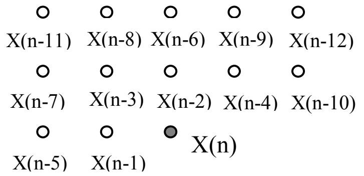

Figure 2. Causal neighbors in EDP

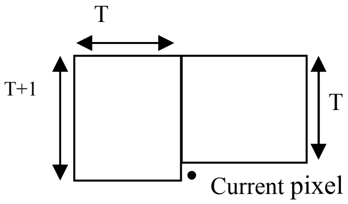

Figure 3. Training window used in EDP

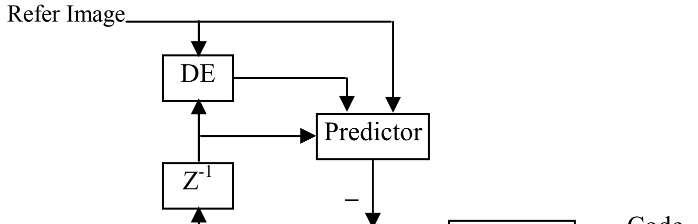

Figure 4. Predicting coding method for target images

Predicting Coding Methods for Stereo Image Pairs

Stereo image pairs consist of two images obtained from different angle cameras. There exists high correlation between two images of stereo image pairs. As result, not only intra-view correlation but also inter-view correlation can be exploited to achieve good coding performance for stereoscopic image. One of two images of stereo image pairs called target image is first encoded. Another called reference image is then encoded solo like single-view images. Fig. 4 describes the prediction coding block diagram of target images. The DE block expresses the process of disparity estimation (DE).

Causal neighbours-based disparity estimation. Because reference images and target images are obtained from different angle cameras. There exists disparity between reference images and target images. To exploit the inter-view correlation, disparity vectors should be estimated firstly. As shown in Fig.4, DE is carried out online previous to the predicting procedure. To repeat the same process of DE at decoders, as shown in Fig.5, only causal neighbors of current pixel are used on the fly. Because there only exists horizontal disparity, the configuration of causal neighbors is suitable.

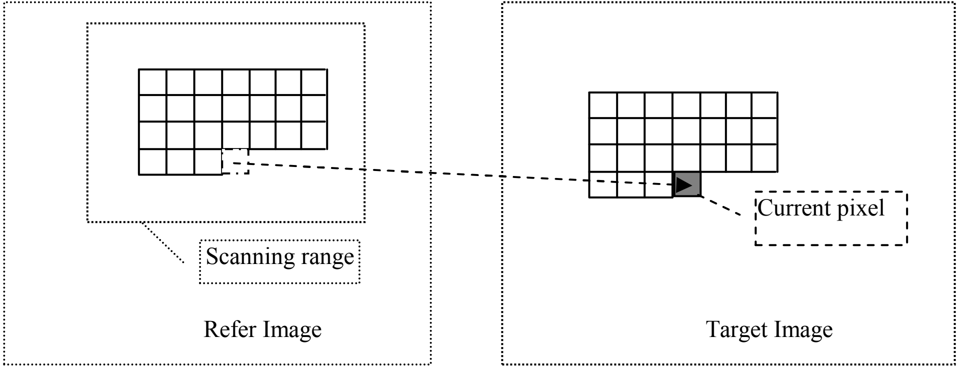

Figure 5. Disparity estimation based on causal neighbors

Causal neighbor-based pixel-wise DE illustrated above can get accurate and smooth disparity vectors that can help to get a low code rate. However, its time complexity is too high to put it into effect. Commonly, there is a same disparity vector in a smooth area. And disparity vectors often change near edges. In order to lower the complexity, disparity vectors of causal neighbor pixels of current pixel are exploited to estimate the disparity vector of current pixel. An estimation strategy adapting to local edge features is used to estimate disparity vectors. For instance, in smooth areas, the average of disparity vectors of several causal neighbor pixels is calculated as the estimation of the disparity vector of current pixel. A buffer V[M,N] is used to record disparity vectors. The estimation strategy can be illustrated in pseudo-code as follow.

```
DO
    IF($d_v - d_h > 80$)
        $V[i,j] = V[i,j-1]$ ;sharp horizontal edge
    ELSE IF($d_v - d_h < -80$)
        $V[i,j] = V[i-1,j]$ ;sharp vertical edge
    ELSE
        $V[i,j] = \frac{(V[i-1,j] + V[i,j-1] + V[i-1,j-1] + V[i-1,j+1])}{4}$;
    ENDIF
    IF($\left|\hat{I}_V[i,j] - I[i,j]\right| > T$)
        Estimates $V[i,j]$ as $V = \min_{(v_x,v_y)} \sum_{(x,y)\in} \left|I_j^r(x,y) - I_j^l(x+v_x, y+v_y)\right|$;
    ENDIF
UNTIL all pixels finished.
```

The notations d_v, d_h are defined as Eq.1. If a disparity vector leads to a large prediction error, a mistake may be made. So, the matching process is invoked to reestimate the disparity vector.

Disparity Compensation-Based CALIC. Due to the high-performance of GAP, GAP-based CALIC gets high-performance as a lossless image coding algorithm. In this section, CALIC is extended to the lossless compression of stereo images called disparity compensation-based CALIC (DC–CALIC). To take advantage of the inter-view correlation, DC-CALIC defines two prediction methods, namely intra-view prediction and inter-view prediction. GAP is used as Intra-view prediction like CALIC. The intra-view prediction obtained by GAP is notated as $\tilde{y}$. And inter-view prediction predicts the current pixel by using those pixels of reference images. The prediction can be formulated as a linear model as Eq. 3.

$$\bar{y} = \alpha x + \beta, \tag{3}$$

where α and β can be obtained by Eq. 4.

$$\alpha = \frac{8\sum_{i=1}^{8} x_i y_i - \sum_{i=1}^{8} x_i \sum_{i=1}^{8} y_i}{8\sum_{i=1}^{8} x_i^2 - \left(\sum_{i=1}^{8} x_i\right)^2},\ \beta = \frac{\sum_{i=1}^{8} y_i - \alpha \sum_{i=1}^{8} x_i}{8}. \tag{4}$$

And x_i and y_i express the causal neighbors of the current pixel as shown in Fig.6.

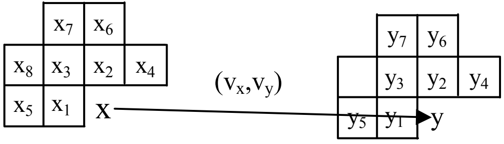

Figure 6. Causal neighbors used in the prediction model

How to choose a prediction, namely inter-view prediction or intra-view prediction is a problem. In this paper, an adaptive method according to the prediction method of causal neighborhood pixels to is used to determine the prediction method of current pixel. An array notated as Map is used to record the prediction method of each pixel and overall assigned an initial value 0 where the value 0 expresses intra-view prediction method and the value 1 means inter-view prediction method. For each pixel y[i,j] of target images, do the following steps.

1) Estimate predicting method

If the current pixel locates 1st row or column, intra-view predicting method is used to estimate the amplitude of the current pixel, namely $\hat{y}[i,j] = \tilde{y}[i,j]$*;*

Otherwise the predicting method as Eq. 5.

$$\hat{y}[i,j] = \begin{cases} \bar{y}[i,j], Map[i,j-1] + Map[i-1,j] + \dfrac{Map[i-1,j-1] + Map[i-1,j+1]}{2} > 2 \\ \tilde{y}[i,j], \qquad otherwise \end{cases}. \tag{5}$$

2) Encode the predicting error

3) Correct predicting method

The predicting method estimated by the 1st step may be incorrect. To avoid the propagation of incorrect predicting method, after step 2, the current pixel is used to correct predicting method and set Map[i,j] as Eq. 6.

$$Map[i,j] = \begin{cases} 0, |y[i,j] - \bar{y}[i,j]| > |y[i,j] - \tilde{y}[i,j]| \\ 1, \qquad otherwise \end{cases}. \tag{6}$$

Disparity Compensation-Based EDP. EDP algorithm gets better performance at the cost of acceptable complexity. In this section, EDP is also extended to the lossless compression of stereo images, called Disparity Compensation-Based EDP (DC-EDP). Fig. 7 shows 13 nearest neighbor pixels of the current pixel, including nine reference pixels of target images and four causal neighbor pixels of the current pixel. These pixels constitute a vector $[X(t,1), X(t,2), ..., X(t,13)]$ used to construct a linear model to predict the current pixel as Eq. 2. A training window as shown in Fig. 3 is used to solve the best prediction coefficients.

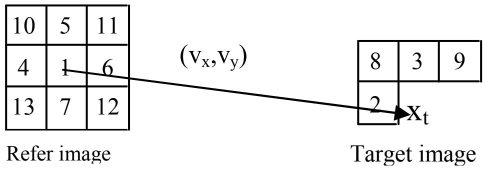

Figure 7. The causal neighbors used in DC-EDP

Experiments and Results

This section first compares the performance of the proposed prediction methods with the prediction methods only exploiting intra-view correlation. The experiment images are obtained from the website http://vasc.ri.cmu.edu/idb/html/stereo and http://vision.middlebury.edu/stereo. Fig. 8 shows the residual images of the stereo pairs 'Pentagon' generated by all kinds of prediction methods. By comparing (a) with (b), we can see the latter generated by DC-CALIC is superior to the former generated by CALIC. While the prediction result generated by DC-EDP is obviously better than those generated by (a) and (b). Many clear edges in the (a) and (b) become weak in the (c).

Table 1. The 1st order entropy of predicting error images generated by several prediction method

image	**entropy**			
	GAP	**EDP**	**DC-CALIC**	**DC-EDP**
pentagon	4.82	4.62	4.73	4.42
houseof	5.10	5.07	4.98	4.87
wdc1r	3.64	3.43	3.40	3.23
fruit	3.46	3.55	3.42	3.27
sawtooth	5.18	5.08	4.72	4.34
tsukuba	4.31	4.47	3.43	3.55
Average	4.42	4.37	4.11	3.95

Table 1 lists the first order entropy of the residual images of several target images. As shown in the table, residual images generated by DC-EDP have minimum entropy, while those generated by GAP have maximum entropy. The entropy obtained by DC-EDP is 0.5BPP lower than the one obtained by GAP on average. And the maximum difference is 0.9 BPP. And DC-CALIC obtained lower entropy than EDP. The difference is about 0.3 BPP. It's beyond question that inter-view correlation can be exploited to improve the prediction performance.

Table 2. Comparisons of the encoding performance of target images

Images	**Bitrate (BPP)**		
	CALIC	**DC-CALIC**	**DC-EDP**
Pentagon	4.55	4.54	4.29
houseof	4.93	4.84	4.72
fruit	3.27	3.22	3.17
wdc1r	3.37	3.26	3.08
sawtooth	4.83	4.46	4.14
tsukuba	3.92	3.21	3.28
Average	4.15	3.92	3.78

In order to obtain code streams, a context-based adaptive arithmetic coding method used in CALIC is exploited to encode prediction residuals. Table 2 exhibits the coding performance of target images. Thanks to the complexity prediction, the DC-EDP based coding method obtained minimum coding bit rate, while CALIC by only using intra-view correlation led to a highest coding bit rate. Compared with DC-CALIC based coding method, DC-EDP based coding method obtained a coding gain up to 0.7BPP, about 0.2 BPP on average. While compared with CALIC, the DC-CALIC based method also obtained a coding gain up to 0.7 BPP. However, the complexity of DC-EDP is highest among all methods. Clearly, DC-EDP obtained best compression performance at the cost of highest complexity.

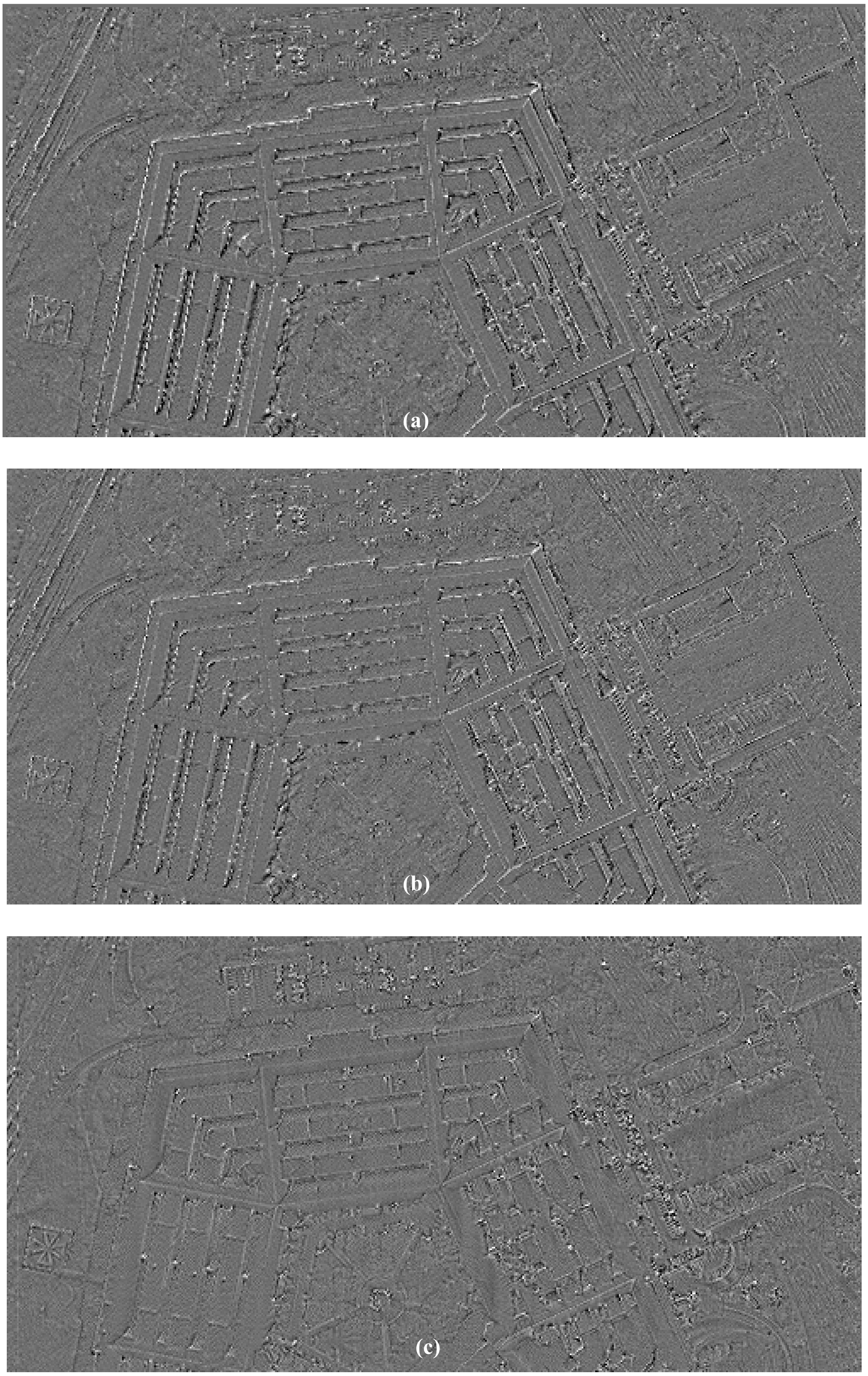

Figure 8. Prediction residual images (a) the result by using GAP，(b)the result by using DC-CALIC，(c)the result by using DC-EDP

Conclusions

There exists high correlation between left view and right view. The correlation can exploited to reduce the coding bit-rate of stereoscopic images. In this paper, prediction coding methods are proposed for stereo images. Experiments show that lossless predictive coding methods making full use of intra-view and inter-view correlation of the correlation of stereo image lower bit rate compared with those coding methods only using intra-view correlation.

Acknowledgements

This work was financially supported by the Chinese Natural Science Foundation (61201452).

References

[1] M.Weinberger,G. Seroussi, and G. Sapiro: The LOCO-I lossless image compression algorithm: Principles and standardization into JPEG-LS. IEEE Transactions on Image Processing, Vol.9(8) (2000), p.1309–1324.

[2] X. Mu, and N. Memon: Context-based adaptive lossless image coding. IEEE Transactions on Communications, Vol.45(4) (1997),p.437-444.

[3] X.Li, M.T.Orchard: Edge-Directed Prediction for Lossless Compression of Natural Images. IEEE Transactions on Image Processing, Vol.10(6) (2001), p.813–817.

[4] Xiaolin Wu, Guangtao Zhai: Adaptive Sequential Prediction of Multidimensional Signals with Applications to Lossless Image Coding. IEEE Transactions on Image Processing, Vol. 20(1) (2011), p.36–42.

[5] Yong Zhang and Donald A.Adjeroh: Prediction by Partial Approximate Matching for Lossless Image Compression. IEEE Transactions on Image Processing, Vol.17(6) (2008), p.924–935.

[6] Pekka Toivanen , Olga Kubasov: Correlation-Based Band-Ordering Heuristic for Lossless Compression of Hyperspectral Sounder Data. IEEE GEOSCIENCE AND REMOTE SENSING LETTERS, Vol.2(1) (2005), p.50-54.

[7] Xiaolin Wu, Nasir Memon: Context-Based Lossless Interband Compression—Extending CALIC. IEEE TRANSACTIONS ON IMAGE PROCESSING, Vol.9(6) (2000), p.994-1001.

[8] Dania Brunello, Giancarlo Calvagno,etc: Lossless Compression of Video Using Temporal Information. IEEE TRANSACTIONS ON IMAGE PROCESSING,Vol.12(2) (2003), p.132-141.

[9] A. Benazza-Benyahia, J.-C. Pesquet: Vector-lifting schemes for lossless coding and progressive archival of multispectral images. IEEE Trans.Image Process, Vol.40(9) (2002), p.2011-2024.

[10] M.Kaaniche et al: Vector Lifting Schemes for Stereo Image Coding. IEEE Trans.Image Process, Vol.18(11) (2009), p.2463-2475.

[11] M.S.Moellenhoff, M.W.Maier: Transform coding of stereo image residuals. IEEE Trans.Image Processing, Vol.7(6) (1998), p.804-812.

[12] N.V.Boulgouris, M.G.Strintzis: A Family of Wavelet-Based Stereo Image Coders. IEEE Trans. Circuits Syst. Video Technol., Vol.12(10) (2002), p.898-904.

[13] E.A.Edirisinghe, M.Y.Nayan, H.E.Bez: A wavelet implementation of the pioneering block-based disparity compensated predictive coding algorithm for stereo image pair compression. Signal Processing: Image Communication, Vol.19(1) (2004), p.37-46.

Applied Mechanics and Materials Vol. 596 (2014) pp 413-416
© (2014) Trans Tech Publications, Switzerland
doi:10.4028/www.scientific.net/AMM.596.413

Research on the transmission characteristics of FitzHugh-Nagumo neuron

Guanping Wang[a*], Wanxia Yang[b] and Sen Yang[c]

College of Engineering, Gansu Agricultural University, Lanzhou, 730070, China

[a]wgp678@163.com, [b]yangwanxia@163.com, [c]484835960@qq.com

Keywords: FHN neuron, Stochastic Resonance(SR), signal transmission characteristics.

Abstract. The transmission characteristics of a FitzHugh-Nagumo (FHN) model neuron influenced by Gaussian white noise is studied in this work. With a sinusoidal stimulus as input, based on the time-domain analysis to the output , it is found that there are SR phenomenon, and the signal transmission is mainly depends on the noise intensity, the frequency and the amplitude of the external excitation signals. The analysis show that when the input frequency lies in 0.2Hz~0.5Hz and the amplitude A is around 0.4, suitable noise intensity is conducive to the optimal neuronal signal transmission.

Introduction

It has been an interesting topic in Neurodynamics for a long time to figure out the characteristics of the signal transmission in neuron systems. The actual nervous system is considered to exist in a noisy environment; the noise may come from the randomness of synaptic connections, ion channel switches and the membrane potential fluctuations. In ordinary system, the noise is often considered to be harmful, it is everywhere, and often coexists with the useful signals, which seriously affects the normal work and the measurement of useful signals. But the discovery of SR phenomenon [1,2] makes people aware of the benefit from noise. Currently, many researchers have done a lot of research work in this area, they found SR in HH and FHN model neurons as well as their networks. In the signal transmission and detection of nervous system, the Signal-to-Noise Ratio (SNR) of the output signal can be improved with noise [3], this phenomenon has been successfully applied in many fields [4, 5]. The paper [6] shows that when FHN model neuron bifurcation parameter is located in the right side of the bifurcation point, the responses of the system is only the oscillation above the threshold with the weak excitation, the energy of system response is concentrated to the input signal frequency with the noise modulation, and the curve of SNR shows a single peak along with the increase of the noise intensity, SR phenomenon appeared, furthermore, the mechanism of SR is generated due to the jump of the system' movement between the three attractors beside the bifurcation point(two before the bifurcation point, one behind). The article [7] indicates that the presence of non-Gaussian noise shorten the conversion time between the resting state and the excited states in a FHN neuron, speeding up the discharge rhythms in a single neuron, this means that non-Gaussian noise play a positive role in the signal delivery between neurons. In recent years, some studies have shown that there are frequency dependent or sensitivity without exception in the bistable continuous systems, the model neuron, and the simple neural network models, however, the study to the transmission characteristics and its frequency sensitivity in FHN model neuron are still less . Therefore, using sine function as input stimulus, we analyze the signal transmission characteristics of a FHN model neuron influenced by Gaussian white noise.

FHN model neuron

FitzHugh and Nagumo et al. [8,9] introduced the FHN model of two-dimensional (dimensionless parameter model) on the basis of preserving the biological properties of the HH model:

$$\varepsilon\frac{dV}{dt} = V(V-c)(1-V) - W + B + I(t) + \xi(t)$$
$$\frac{dW}{dt} = V - W - d$$

wherein, c, d, ε are the parameters associated with the cell membrane properties, which are determined by the electrical characteristics of the cell membrane, here we take c=0.5, d=0.15, ε = 0.005, B=0.04. In this system, V represents transmembrane voltage, W describes potassium activation and sodium inactivation slow variation process, and I represents the external stimulus. In this article:

I=Asin(2πft/1000),

f is the frequency of external stimulus, $\xi(t)$ is the Gaussian white noise with intensity H.

The transmission characteristics of FHN neuron

From the FHN model neuron above and other related research, the noise intensity, the frequency and the amplitude of the external excitation signals, the range of these parameters' variation is always wide, which should have more significant effects on the signal transmission in a neuron. Therefore, we adopt the single-factor method to study the relationship between the FHN neuron transmission characteristics and these parameters.

The noise intensity *H* on the transmission characteristics of a FHN neuron

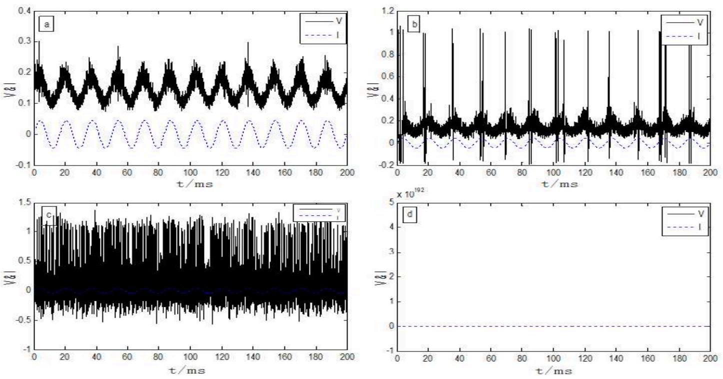

Fig. 1: FHN neuron transmission characteristics influenced by the noise intensity H（with A=0.045, f=0.06HZ） (a)response curve of V vs t under H=8.5×10^{-8}; (b)response curve of V vs t under H=4.5×10^{-7}; (c)response curve of V vs t under H=2.4×10^{-5}; (d) response curve of V vs t under H=2.5×10^{-4}.

First, the amplitude and the frequency of sinusoidal stimulus signal are set to A=0.045, f=0.06Hz, the membrane potential V and the input signal can maintain synchronization when the noise intensity H is small, the membrane potential gradually oscillates along with the increase of H, the intensity and frequency of the oscillation will also enhanced accordingly, when H increases to H=4.5×10^{-7}, the membrane potential reaches to the above threshold oscillation, with the synergistic effects of the noise and the input signal, the energy of system response is concentrated to the input frequency, the SR occurs(shown in Fig.2), thereby, the SNR of the output signal is improved. But the synchronization of V and I then gradually fades in pace with the increase of the noise intensity H, when H is greater than a certain value, the neuron oscillated violently, the enormous energy is released instantaneously and will be damaged physiologically, the neuron lose its vitality, no longer produce responses. Therefore, the discharge sequence is optimal, the SNR maximum when the noise intensity is appropriate.

The frequency *f* on the transmission characteristics of a FHN neuron (Fig. 3)

Next, the amplitude and the noise intensity of sinusoidal stimulus signal are set to A=0.048, H=1.2×10^{-8}, along with the ascending frequency f of the input signal I, the membrane potential V gradually produce oscillation and its oscillate frequency increases with the rise of f either. When the frequency f is small, the generated action potential V gradually discharge cyclically and synchronized with the increasing f; when f is increased to a certain extent, the action potential V can't discharge periodically, the transmembrane voltage can only fluctuates below the threshold with the further increase of *f*. In this situation, for higher frequency stimulus, only sufficient stimulation intensity, i.e. the amplitude *A* is needed to increase to a certain degree correspondingly, can then cyclical oscillation which above the threshold can be stimulated once again (as shown in Fig. 2(d)).

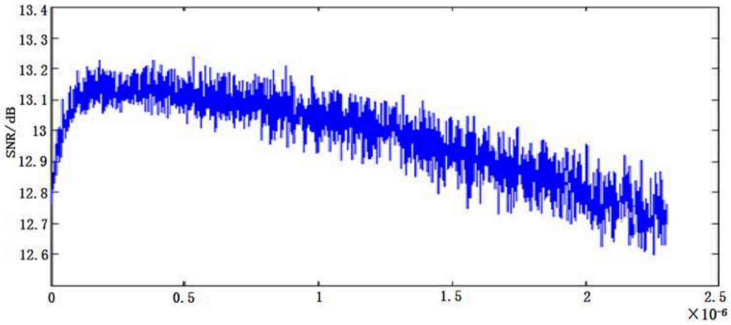

Fig. 2: The curve of SNR vs *H* under A=0.045 and f=0.06HZ

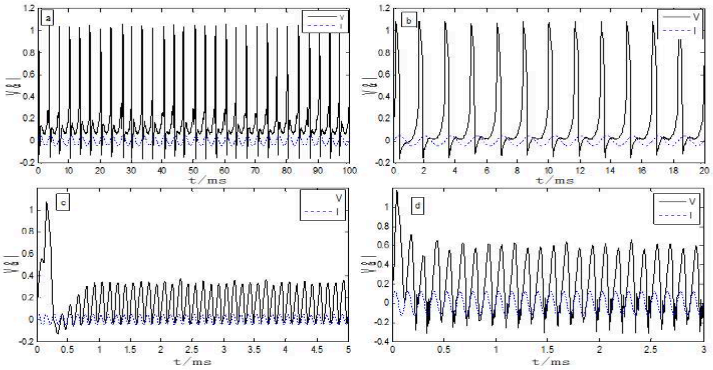

Fig. 3: FHN neuron transmission characteristics influenced by the frequency *f* of external excitation signal（with H=1.2×10^{-8}）(a)response curve of *V* and *I* vs *t* under A=0.048, f=0.3Hz; (b)response curve of *V* and *I* vs *t* under A=0.048, f=0.6Hz; (c)response curve of *V* and *I* vs *t* under A=0.048, f=8Hz; (d)response curve of *V* and *I* vs *t* under A=0.13, f=8HZ.

The amplitude A on the transmission characteristics of FHN neuron (Fig. 4)

Finally, we set the input signal frequency f=0.048Hz and the noise intensity H=1.2×10^{-7}, along with the rising amplitude *A* of the input signal *I*, the transmembrane voltage *V* will experiences the sub-threshold oscillations state to the state of single action potential, then generating a periodic action potential and maintain synchronization with the input. When *A* increases to about 0.4, the transmembrane voltage *V* gets to above the threshold; and when *A* increases beyond a certain value, the neuron will be damaged physiologically and loses its vitality, will no longer respond to the stimuli.

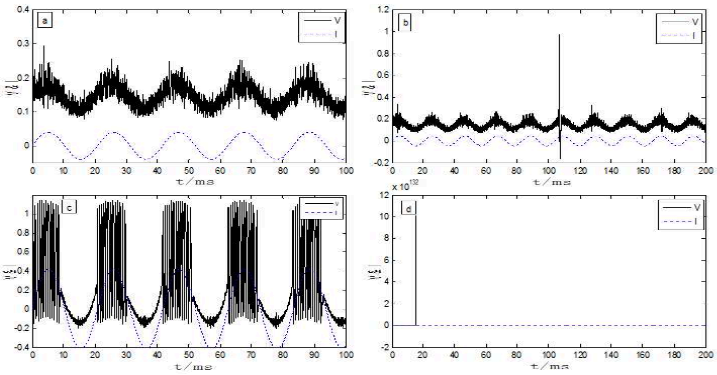

Fig. 4: FHN neuron transmission characteristics influenced by the amplitude *A* of external excitation signal（with H=1.2×10^{-7}, f=0.048HZ）(a)response curve of *V* and *I* vs *t* under A=0.041; (b)response curve of *V* and *I* vs *t* under A=0.046; (c)response curve of *V* and *I* vs *t* under A=0.42; (d) the neuron inactivate under A=0.65

Conclusions

This work focuses on the research to the transmission characteristics of a single FHN model neuron under the influence of Gaussian white noise. The analysis show that suitable noise intensity is conducive to the signal transmission, the sine responds have higher SNR when the input frequency lies in 0.2Hz~0.5Hz as well as the amplitude A is around 0.4, other parameters are not propitious to the optimal signal transmission. This study helps to uncover the mechanism of the signal transmission in a FHN neuron, and to understand the role of noise in the biological nervous system.

Acknowledgement

The authors are grateful for the support of the National Natural Science Foundation of China No.11072099.

References

[1] C. Nicolis, G. Nicolis:Tellus 33 (1981) 225-234.

[2] R. Benzi, A. Sutera:Tellus 34 (1982) 10-16.

[3] V. Galdi, V. Pierro, and I. M. Pinto:Physical Review E 57(6) (1998) 6470-6479.

[4] R. Benzi:Nonlinear Processes in Geophysics 17 (2010) 431–441.

[5] L.S. Geng, Y.L. Fan:Computer Engineering and Applications 47(2) (2011) 112-114.

[6] G.J. Zhang, J.X. Xu:Journal of Air Force Engineering University(Natural Science Edition) 7(4) (2006) 79-81.

[7] Y. Zhao, W. Xu, S.C. Zou:Acta Physica Sinica 58(3) (2009) 1396-1401.

[8] R. FitzHugh:Biophysical Journal 1 (6) (1961) 445-466.

[9] J. Nagumo, S. Arimoto, S. Yoshizawa:Proceeding of the IRE 50(10) (1962) 2061-2070.

Applied Mechanics and Materials Vol. 596 (2014) pp 417-421
© (2014) Trans Tech Publications, Switzerland
doi:10.4028/www.scientific.net/AMM.596.417

Classified Quantization Research on Dot Gain Characteristic

Qi Wang[1, a], Qian Wang[2, b], Xiaolin Qiu[3, c], Tianma Wang[4, d]

[1]College of Light Industry Science and Engineering, Nanjing Forestry University, Nanjing, China

[2]College of Light Industry Science and Engineering, Nanjing Forestry University, Nanjing, China

[3]College of Light Industry Science and Engineering, Nanjing Forestry University, Nanjing, China

[4]College of Light Industry Science and Engineering, Nanjing Forestry University, Nanjing, China

[a] wangqi_3639@163.com, [b] wangqian1991723@163.com,

[c] lillian@163.com, [d] 15295503128@sina.cn

Key words: optical dot gain; physical dot gain; Ink spreading; light scattering model

Abstract. Dot gain divides into physical and optical dot gain. These two parts constitute the comprehensive dot gain in the process of printing. Ink spreading on the surface of paper is used for the analysis of physical dot gain and light scattering function model is used for optical dot gain. Trace the dots on the CTP plate and offset printing proof to analyze the influence of image micro-parameters caused by dot gain. Physical and optical dot gain are quantized to research the correlation between dot gain and shape of dot. It shows that: optical dot gain of AM dot accounts for a larger proportion; dot gain of all types has no relation with shape of dot. Besides, physical dot gain of FM dot accounts for a larger proportion than optical dot gain.

Introduction

In the actual printing, ink will permeate and spread [1] which can indicate that the dot gain happens when it is transferred to the substrates and overprint [2] in the state of little dot. Because of the complex linear relationship between light ray and ink or paper, optical dot gain will also occur. Classified research for physical and optical dot gain can offer accurate micro-parameters [3] about the quality evaluation of printing transfer replication, and the research conducts control and compensation for different dot gains in the aspects of material, technology and equipment. This process aims to control the dot gain within the specified range, so that replication quality of printing image will be improved.

Classification of the Dot Gain

Dot gain [4] divides into physical and optical dot gain. The former one depends on the paper, ink and its overprint state. Dot will change its shape in the process of ink transfer. Besides, the area of dot will change again because of ink spreading on the surface of substrate and internal penetration. The twice changes make the actual area of dot larger than the initial dot area and this phenomenon is called physical dot gain. Light reflects when it arrives at the surface of dot. In addition, ink penetration to the edge of the dot on the paper will form diffusion halation [5]. All these will cause that dot area appears larger than before. This is the mechanism of optical dot gain.

Ink spreading on the Surface of Paper and Light Scattering Function

Physical dot gain means actual dot area generated in printing larger than theoretical value. If other factors are not considered in the process of printing, the mean reason of physical dot gain is ink spreading on the surface of substrate and internal penetration.

Effective value σ of dot gain can be expressed as the sum total of standard value σ_0 and the dot gain part $\Delta\sigma$ .Please see in particular formula (1):

$$\sigma = \sigma_0 + \Delta\sigma \quad (1)$$

After derivation, affected parameters about actual condition is introduced, please see physical dot gain formula (2):

$$\Delta\sigma = \sigma - \sigma_0 = (a-1)\sigma_0(1-\sigma_0) \quad (2)$$

Under the same conditions, "a" remains stationary. In ideal situation, a=1 means that dot gain will not happen. a>1, in the actual production, means physical dot gain. Optical dot gain depends largely on position relation between dots as well as size and shape of dot. What's more, the light scattering in the paper [6] is also important factor. PSF point spread function [7] is the model [8] which can explain optical dot gain, see in particular formula (3):

$$\Delta R_{opt} = (1-T^2)\overline{P}\sigma(1-\sigma) \quad (3)$$

Point spread function shows that optical properties of ink has a close relationship with the ink penetration effect T [9] on the surface of the paper, the lateral scattering probability of light in the paper $\overline{P}$ and the dot area σ .

Experimental Schemes

Trace the dot on the CTP plate and offset standard printing proof respectively. Measure the comprehensive dot gain with spectrophotometer according to Yule-Nielsen effect [10]-[11].And then, get the physical dot gain data with ICplate2 based on edge tracing and capture. At last, quantize and analyze the value of physical and optical dot gain.

Specific steps are as follows: Firstly, after CTP linearization, get the black plate and measure dot area of different percentage on the grayscale by X-Rite ICplate2; Secondly, measure on the paper by ICplate2 in order to get dot area of different percentage corresponding to grayscale(only including the physical dot gain);Thirdly, measure the dot area of grayscale on the standard proof(including physical and optical dot gain); Fourthly, calculate physical and optical dot gain respectively; And lastly, repeat the process from the first step to the fourth step, and get dot gain value from different shapes of dot. The flow of the approach is present as Fig.1.

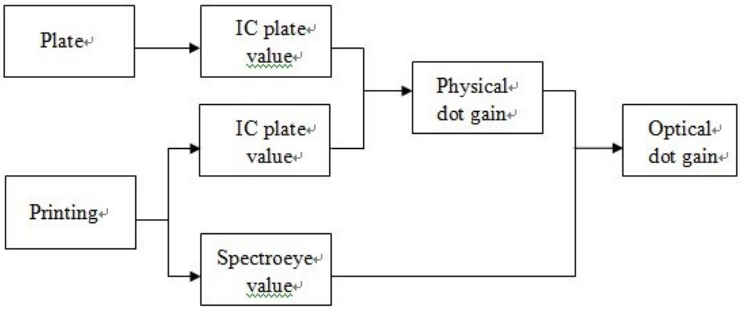

Fig.1. Dot gain research technical courses

Experimental Results and Analysis

Value of Round Dot Gain. Measure the single black grayscale formed of round dot in the standard printing proof 1, and dot gain value is present in the Table 1.

Tab.1 Round dot area and dot gain data (proof 1)

AM-round	plate	ICplate2	Spectroeye	Dot gain	physical gain	Optical gain
20%	18.9%	24.4%	32.0%	13.2%	5.8%	7.6%
40%	37.7%	44.8%	54.0%	16.6%	7.7%	9.2%
60%	57.4%	66.3%	76.0%	17.3%	8.1%	9.7%
80%	78.3%	84.4%	91.0%	12.7%	6.1%	6.6%
100%	100%	100.0%	100.0%	0.0%	0.0%	0.0%

The curve of optical and physical dot gain according to the data from Table 1 is present in Fig.2.

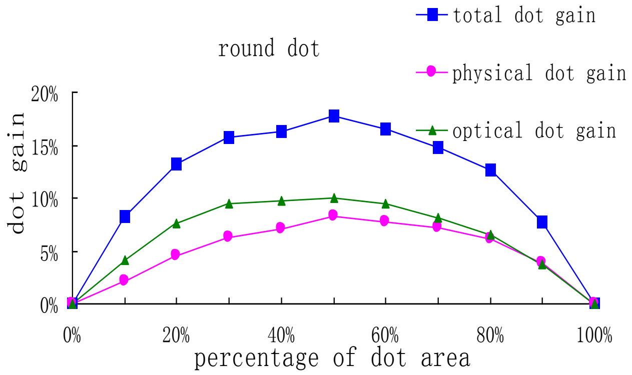

Fig.2 Dot gain of round dot on proof 1

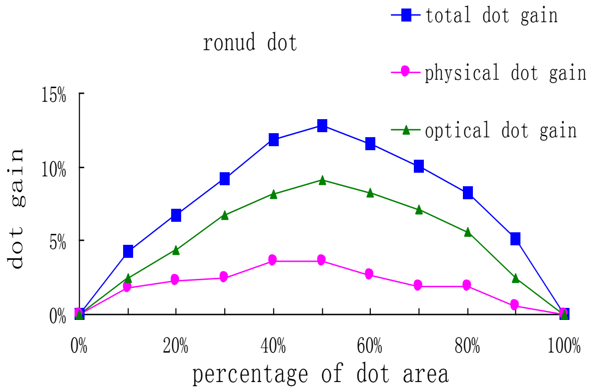

Fig.3 Dot gain of round dot on proof 2

Analyze the round dot gain data from Fig2.Conclusions are as followed: Firstly, comprehensive dot gain is controlled within the ISO standard, dot gain of middle half-tune is the most remarkable, physical and optical dot gain are in accord with the trend of comprehensive dot gain; Secondly, physical dot gain is the dot area of the print after physical expansion which is compared with the dot area of compensated plate rather than the ideal dot area. This is the physical dot gain value in its true sense. Thirdly, in the comprehensive dot gain part, physical dot gain is smaller than optical dot gain which shows that optical dot gain has a more important role in the process of printing transmission; Finally, optical dot gain is larger obviously than physical dot gain in the part of middle and high half-tune of the proof. In other words, optical dot gain plays a bigger role in color reproduction [12] and level restoration.

Comparison of Dot Gain among Different Dot Shapes. There are square, round, ellipse and diamond dots on printing proof, and they are represented in the same proof. Measure the single black grayscale formed of round dot in order to get dot gain value of different types and draw curves according this data shown in Fig.3.

Analyze the value of round dot gain and find that: the trend and the proportion of physical and optical dot gain accounting for total dot gain are in accord with the conclusion of proof 1 which means that, for round dot, optical dot gain generated in the process of offset printing is larger than physical dot gain in general. With the rising of equipment accuracy, dot gain caused by equipment can be controlled within a smaller range. In this context, improving the quality of dot transmission from the aspect of paper and ink may be more significant to strengthen printing quality.

The curve of square dot gain according to the measured data from single black grayscale formed of square dot on the standard printing proof 2 is present in Fig.4.And the curve of ellipse dot gain is present in Fig.5.

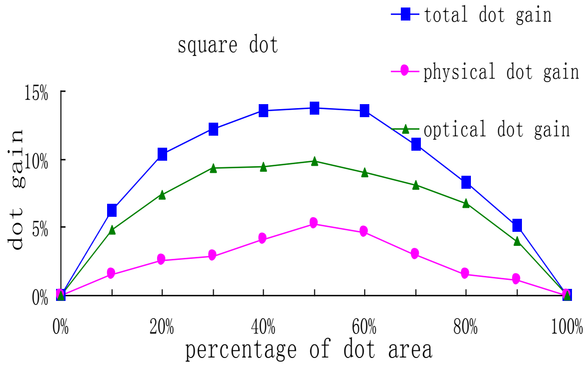

Fig.4 Dot gain of square dot on proof 1

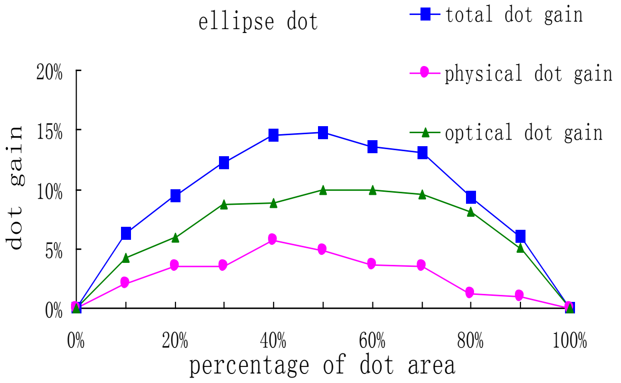

Fig.5 Dot gain of ellipse dot on proof 2

Compare the properties of optical and physical dot gain from AM dot proofs with different shapes of square, round and ellipse. It shows that the proportion of optical dot gain is larger than physical dot gain obviously. The distributive proportions after quantization are similar. For AM dot, all types of dot gain have no obvious relation with dot shape. What's more, the extreme value of physical dot gain from different shapes occurs at the place where dots lap joint. There is obvious dot gain phenomenon at 60% percent of the area for square dot. It is caused by external factor such as the defective workmanship of press blanket and so on.

Value of FM Dot Gain. The curve of optical and physical FM dot gain according the measured data from single black grayscale on the standard printing proof 3 is present in Fig.6.

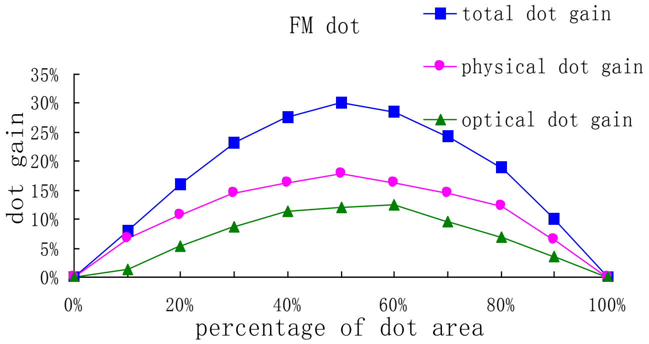

Fig.6 FM dot gain on proof 3

It can be found from Fig.6, based on ideal dot area, the comprehensive dot gain will beyond 30% .If it is based on the compensated dot area on CTP plate [13], the actual dot gain will be up to 40% or more [14].The more different from AM dot is that the physical dot gain is larger than the optical dot gain in general, which is related to minimum [15] area of single dot. The area change under the same conditions for little ink dot will have greater impact on dot gain.

Conclusions

The comprehensive dot gain is within the range of ISO standard, the dot gain of middle half-tune is the most obvious, and the physical and optical dot gain are in accord with the trend of comprehensive dot gain. For AM dot, the values of optical dot gain are all larger than their physical dot gain, especially for the middle and high half-tune places of AM dot proof, which shows that optical dot gain has a very important role in printing transmission. And it has greater impact on color replication and level restoration. So the impact of optical dot gain in the actual printing should be given more consideration. In addition, the extreme value of physical dot gain from different shapes occurs at the place where dots lap joint. FM dot gain is larger because of minimum area of single dot. At last, it should point out that physical dot gain of FM dot accounts for more proportion of the comprehensive dot gain, so more attention to ink spreading should be paid in ink jet printing.

References

[1] Xiaoping Gu.Research on dot gain in ink-jet printing.Wuxi: Southern Yangtze University(2009)

[2] Ruyun QU,Zhengning Tang,Song Yang.Packaging Engineering,Vol.28(2007),p.61-63.In Chinese

[3] Shikun Xi.The study on physical dot gain of 2nd-order FM halftone based on ink spreading in all ink superposition conditions.Wuxi: Southern Yangtze University(2009)

[4] Bai Chun-yan. Research on prediction of dot area and dot gain in inkjet printing.Wuxi: Southern Yangtze University(2009)

[5] Yang, L. Journal of Imaging Science and Technology , Vol.48(2004),p, 347-353

[6] J.S. Arney, Shinya Yamaguchi. Journal of Imaging Science and Technology, ,Vol.42(1999),p.353

[7] Geoffery L. Rogers. Journal of Imaging Science and Technology, Vol.48(2004),p.18

[8] L. Yang.Imaging Sci. Technology,Vol.48(2004),p.347-353

[9] Th. Bugnon, M. Brichon, R.D. Hersch. Simplified Ink Spreading Equations for CMYK Halftone Prints. Proc. SPIE Color Imaging XIII: Processing, Hardcopy, and Application (2007),p.124

[10] R. Rossier, R.D. Hersch. Calibrating the ink spreading curves enhanced Yule-Nielsen modified spectral Neugebauer model with the two-by-two dot centering printer model[C].Proc. SPIE Color Imaging XIII: Processing, Hardcopy, and Applications(2009),p.235

[11] Hersch R D, Crété F. Improving the Yule-Nielsen modified spectral Neugebauer model by dot surface coverages depending on the ink superposition condition.Proc. SPIE (2005),p.434

[12] Jinlin Xu, Junfei Xu. China printing and packaging study, Vol. 01(2012), p.1-5. In Chinese

[13] Hue P. Le. Journal of Imaging Science and Technology Vol. 42(1998),p.49–62

[14] F. Rousselle, Th. Bugnon, R.D. Hersch. Spectral prediction model for variable dot-size printers.IS&T/SID's 16th Color Imaging Conference (2008),p.73-78

[15] Weiyou Hu.Packaging Engineering, Vol. 28(2007),p.61-63. In Chinese

Applied Mechanics and Materials Vol. 596 (2014) pp 422-426
© (2014) Trans Tech Publications, Switzerland
doi:10.4028/www.scientific.net/AMM.596.422

A Recognition Method of License Plate Number Based on BP Neural Network

Bingxiang Liu[1,a], Yanhua Huang[1],Xudong Wu[2], Yingxi Li[2]

[1] Jingdezhen Ceramic Institute, Jingdezhen,333403, China

[2] Jiangxi Ceramic & Art Institute, Jingdezhen, 333000, China

[a] lbx1966@163.com

Keywords: BP neural network; character recognition

Abstract: According to the current technological deficiency of license plate recognition, this paper uses digital graphic processing technique and BP Neural Network algorithm fusion to achieve automatic recognition of license plate. Input the image settled in the previous period in the trained BP neural network to obtain the final license plate character through simulation. The validity and feasibility of the algorithm can be verified through the simulation experiment of standard license plate image.

Introduction

Managing car information is a very important research project for current traffic industry. Intelligent license plate recognition system can be used in various parking lot toll administration, every communication line car flow control test indexes, car location of community car alarm, electronic police of running a red line in crosses and dangerous sections, over speed automatic supervision in every high way and toll stations and other places. The system also has realistic meanings in maintaining traffic safety and city security, preventing traffic jam and achieving traffic automation management. Currently, license plate recognition basis can be divided into IC card recognition technology, bar code recognition technology, computer vision, graphic processing and pattern recognition technology. The major tasks of license plate recognition are analytical processing auto images, automatic recognition of registration numbers including license plate location, license plate segmentation and license plate recognition and license plate recognition is a core part for achieving license plate recognition system. BP neural network can efficiently solve the problem of pattern recognition and it has good robustness, adaptively and high parallel processing capability, so it has obvious advantage in license plate recognition problems.

BP neural network

BP neural network is a multilayer neural network that has three or more than three layers and each layer is made up of certain neurons. It is fully connected between layers and there is no connection inside each layer. BP neural network trains in the way of having mentors to learn and the standard three-layer BP neural network construction plan can be shown in Figure 1.

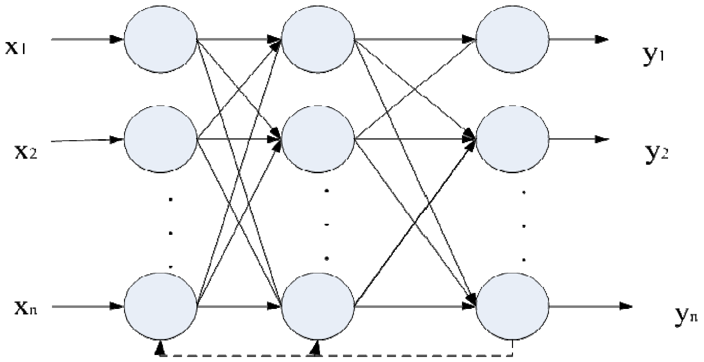

Figure 1. Standard three-layer BP neural network construction plan

License plate recognition processing in previous period

The realistic license plate comes from the photo of a whole car so the first thing is to segment the license plate form car picture. This paper uses color segmentation method to segment license plate, and its effects can be shown in Figure 2 and 3.

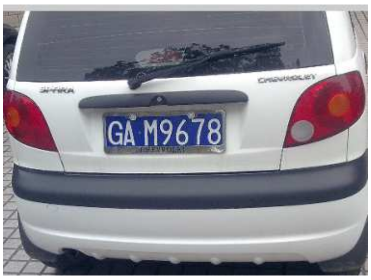

Figure 2. Ccar original photo

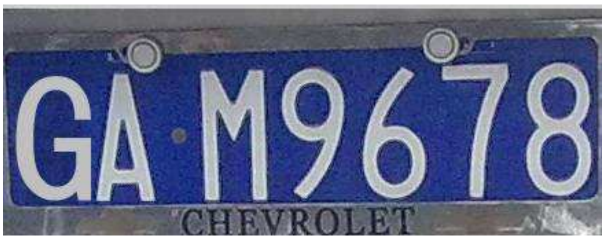

Figure 3. Color segmentation of license plate photo

This paper changes acquired color license plate image into grey level image. Because of the angle of camera and license plate when shooting, this paper remedies the color license plate with random changing and the inclination angle is -2.The result of the experiment is shown in figure 4.

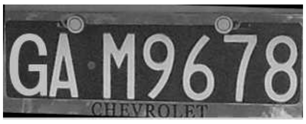

Figure 4. License plate after remedy

This paper has a binaryzation about the remedied license plate image and uses binary image morphology to further process the image including disconnecting H, removing fuzzy grain, opening operation, first erasing and so on. The result of the experiment are shown in figures 5,6,7,8 and 9.

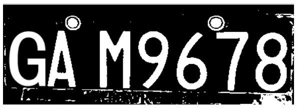

Figure 5. Disconnect H

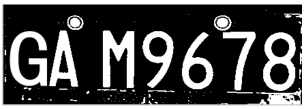

Figure 6. Remove fuzzy grain

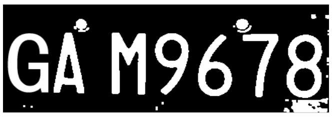

Figure 7.Opening operation

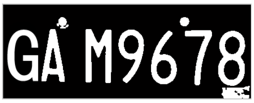

Figure 8. First erasing

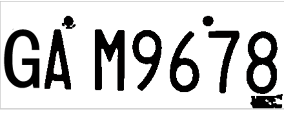

Figure 9. First inverse

According to picture 10, the rough license plate character has appeared but its edges and some noise are not removed. So this paper uses projection to get the top and bottom edges. And afterwards, in order to decrease noise and provide convenience for later character segmentation, this paper uses erasing and inverse again and its effects are shown in figures 10, 11 and 12.

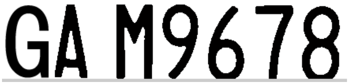

Figure 10. Projection

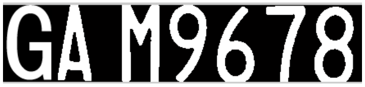

Figure 11. Second inverse

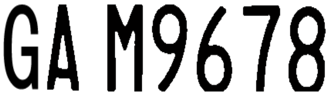

Figure 12. Second erasing

This is the end of the prior period processing about license plate image and the next comes the segmentation about license plate characters. The segmentation algorithm used in this paper is image horizontal and vertical projection and its theory is to test horizontal edges of every character. The result is : fenge =11,56,68,110,146,193,204,250,262,309,322,371,381,430,the effect is shown in Figure 13.

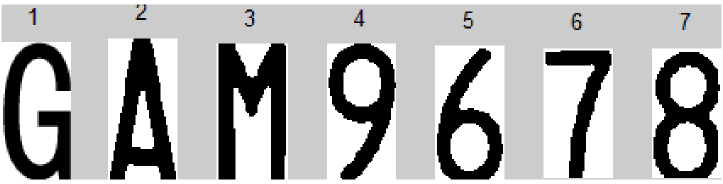

Figure 13. License plate segmentation

BP neural network recognition

Establishing and training BP neural network

This paper adopts standard three-layer BP neural network and makes the adjusting parameters uses self-adapting gradient descent algorithm to improve network performance and the recognition rate for license plate. Network parameters are set as follows:

Input layer nodes: all samples in this paper adopt 20*40 standard, so they have 800 pixel value. They use pretreatment function and change the images column into a row vector and then transpose it to get input vector, so it is set as 800.

The hidden layer node: the formula used in this paper is $m=\sqrt{nl}$ among which m is the hidden layer node, n is the input layer node and l is the output layer node. So the result is 189.73 and we take 190.

Output layer node: it is set as 45 according to this paper.

Learning rate: the value is 0.05 according to many experimental results.

Allowable deviation: its general value is 0.001-0.00001.

Show iteration process: the biggest iteration appeared in this paper is 2000, so the shown iteration process is chosen as 50.

All the original values of weights in this paper use function random, the coming of random to avoid local optimum problem.

Other parameter values are default and its trained results are shown in figure 14.

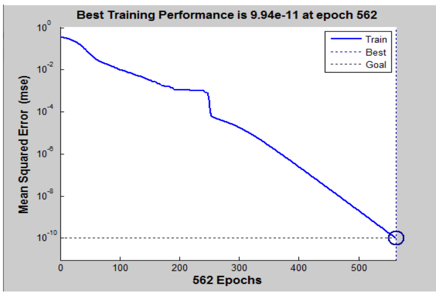

Figure 14. Training error curve

Experiment result

All the experimental results in this paper are achieved through MATLAB software which shoots all kinds of litter cars and segments their characters as training sample to form then numbers, 26 letters, 9 province abbreviations and other 45 training samples. The results of the experiments are shown in figures 15 and 16.

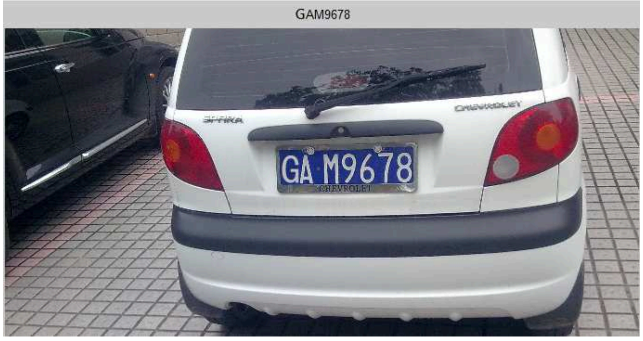

Figure 15. Contrast between recognition results and original drawings

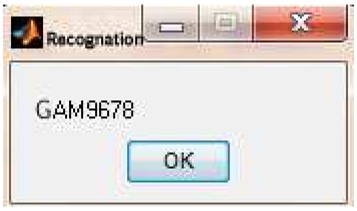

GAM9678

Figure 16. Last recognition result

It can be seen from the above experiment result pictures that license plate recognition can be achieved by using BP neural network.

Conclusion

BP neural network is a widely used recognition technology and can achieve exact recognition during license plate recognition process. But BP neural network has its deficiencies such as slow velocity of convergence, various choices of network structures samples dependence and so on which all limit the further development of BP neural network in license plate recognition. The following work of this paper is to combine BP neural network with the advantages of other intelligent algorithms (ant colony, genetic algorithm) to better improve the recognition results.

Acknowledgements

This work was supported by the grants from National Science and Technology Support Project of China (No. 2012BAH25F02), the Science Foundation of Education Department of Jiangxi Province(No.GJJ13633),and Jiangxi Province Science Fund Project (No.20122BAB201044).

References

[1] Zhou kewei.License plate recognition under the environment of Matlab based on neural network[D].Xi'an: Xi'an University of Electronic and Science,2009

[2] Chi xiaojun. Research and implementation of automatic identification system in the vehicle license plate [D].Qingdao: Chinese Marine University,2006

[3] Zhang defeng.The application of MATLAB neural network design[M].Beijing:Mechanical Industry Press,2009

[4] Yang dali. Chinese characters of license plate recognition method base on neural network[J].Journal of Chinese Pepole's Public Security University.2009(3):56-58

[5] Yang shuyin. Pattern recognition and intelligent computing[M].Beijing: Electronic Industry Press,2008

[6] Lu yaqin.A Method of License Plate Location Based on Morphology[J].Computer Engineering,2005(31):224-225

[7] License Plate Character Neural Network Recognition Based on Wavelet and GA Optimization[A]. Proceedings of the 2011 International Conference on Advances in Construction Machinery and Vehicle Engineering[C],2011

[8] License Plate Recognition Based on Improved BP Neural Network[A].Proceedings of 2010 International Conference on Computer,Mechat ronics,Control and Electronic Engineering(CMCE 2010),2010

Applied Mechanics and Materials Vol. 596 (2014) pp 427-432
© (2014) Trans Tech Publications, Switzerland
doi:10.4028/www.scientific.net/AMM.596.427

Based on Fractional Brownian motion and Fourier descriptors of the side face recognition algorithm

Hong Wu[1, a], Guixin Tang[2,b] and Tao Han[3,c] Baihao Jie[4,d]

[1]School of Electronic Engineering, Heilongjiang University, Harbin in Heilongjiang province, China

[2]School of Electronic Engineering, Heilongjiang University, Harbin in Heilongjiang province, China

[3]School of Electronic Engineering, Heilongjiang University, Harbin in Heilongjiang province, China

[4]School of Electronic Engineering, Heilongjiang University, Harbin in Heilongjiang province, China

[a]wuhonghrb@163.com, [b]tang_gui_xin@126.com, [c]hantao20065635@163.com,
[d]240320412@qq.com

Keywords: Face recognition; Side face recognition; Fourier descriptor; Fractional Brownian motion; BP neural network

Abstract. This paper proposes a kind of the side face recognition algorithm base on Fractional Brownian motion and Fourier descriptors. This method is mainly innovating for feature extraction and making up for a shortage of the side face recognition algorithm. Firstly, by Fractional Brownian motion of Hurst index will get silhouette extracted. Then we through Fourier descriptors to obtain the desired feature points. Further study of this algorithm can solve the side of the face recognition rotation, scaling, and translation transform the impact. Comparative characteristics will make distance classifier and BP neural network classifier. This article also processes the analysis of the algorithm and the future development.

Introduction

Face recognition, face detection tracking technology and some other related technologies in recent years as one of the important research areas has made a rapid progress [1]. But in practical applications, the attitude, glasses, facial expression, shade and many interference factors exist commonly. They will have an effect on recognition more or less. the face recognition problem caused by change of attitude is particularly significant: it is not only the basis of the follow-up processing work, but also has wide application value for security, financial, customs and other area that the positive photos recovers from the side photos.

In the past few decades, face recognition technology based on the statistics got bigger development [2] than others. FANG Jie, TAN Xiao-heng proposed a method of Optimization LDA face feature extraction based on wavelet transform [3]. In this method, no singularity of within class scatter matrix became unnecessary, and the problem of edge overlap is also solved. So, it has better generalization ability comparing with traditional LDA algorithm, In addition, the literature [4] uses the 3 d deformable model to extract the side characteristics according to the prior knowledge. Based on the study mentioned above, aimed at side face recognition, this paper puts forward a kind of side face recognition method based on multi-fractal and Fourier descriptor. Firstly, use the multi-fractal to extract side outline of the sample image. Secondly, build the closed contour of and extract Fourier descriptor of side face image as the characteristic to recognize the side faces combined statistical probability of the feature vector space.

Feature Extraction

1.1 Side face Contour Extraction. In this study, we use a side face image which is obtained in the controlled light source and the background of images are white canvas. As the images are obtained in areas of control, so the part of the side face image detection is eliminated. After image preprocessing, the use of fractional Brownian motion on contour extraction of the side face image and we need to get the facial features of side face.

1.1.1 Fractional Brownian motion. Brownian motion is presented by R. Brown, and he observed tiny particles suspended in the liquid for the uncorrelated, irregular, random motion. Later, with the increasing awareness, people are found throughout the universe, the world, and the social are disorderly, irregular. Many natural phenomena and even social phenomena are filled with fractal. Therefore Mandelbrot and Van Ness turn brown power to promote them, the fractional Brownian motion put forward. Fractional Brownian motion has important applications in many fields, such as financial markets, capital markets. Here we will mainly classified Brownian motion for forest fire image depicts the complexity of the image to achieve the purpose of dividing the fire. Eq. 1 is the definition of fractional Brownian motion.

When the random function satisfies:

$$B_H(t,w)=\frac{1}{\Phi(H+0.5)}\left\{\int_{-\infty}^{0}[(t-s)^{H-0.5}-(-s)^{H-0.5}]dB(s,w)+\int_{0}^{1}[(t-s)^{H-0.5}]dB(s,w)\right\} \tag{1}$$

We are in the image segmentation, and the use of discrete fractional Brown motion increment with airport, referred to as DFBIR. A gray image $I(x,y)$, mathematical expectation formula of the gray scale change for Eq. 2:

$$E(I(x_2,y_2)-I(x_1,y_1))=K\times(\sqrt{(x_2-x_1)^2+(y_2-y_1)^2}) \tag{2}$$

Make $\Delta I_{\Delta r}=\left|I(x_2,y_2)-I(x_1,y_1)\right|$ to have Eq. 3:

$$\Delta r=\sqrt{(x_2-x_1)^2+(y_2-y_1)^2}\ . \tag{3}$$

The type substitutes Eq. 2 in there Eq. 3:

$$E(\Delta I_{\Delta r})=K\Delta r^{H}\ . \tag{4}$$

After taking the logarithm:

$$\log E(\left|\Delta I_{\Delta r}\right|)=H\times\log(\Delta r)+\log K\ . \tag{5}$$

Where said two pixel gray differences, the distance between two points is a constant and H fractal characteristic parameters, and namely the Hearst index. The relationship between fractal dimension D and the Hearst index for H:

$$D=3-H\ . \tag{6}$$

In the use of fractional Brown motion to image segmentation, can be obtained indirectly through the method of H to calculate D.

1.1.2 The Segmentation Results. Analysis on the side face image using fractional Brown motion in this experiment, show that if the Hearst numerical index of less than 0.6, not a good side of face contour extraction; If Hearst numerical index greater than 0.6, and then the side face contour extraction is very clear, through carries on the analysis to the pool side face image acquisition of the Hearst index, Hearst index range should be limited to between 0.65-0.73, the segmentation effect is ideal. This paper selects 0.683 threshold needed for profile face segmentation. The segmentation results are shown below.

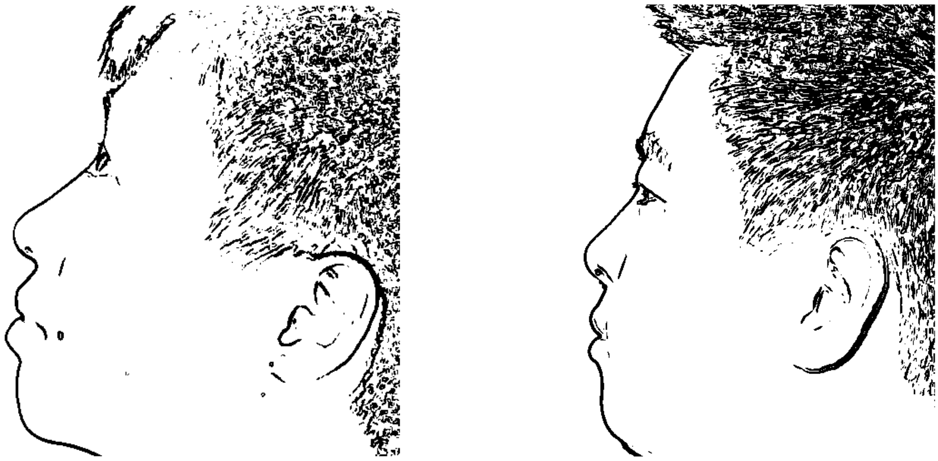
(a) (b)

Figure 1. Fractional Brown motion segment side face

1.2 Facial feature contour extraction. Through the above operation, has been a side face required contour. Contour function assumes from the forehead to the jaw $y = f(x)$, the second part of the side face is that we don't need, so you don't have to consider. The chart below shows the maximum point B to coordinate system. You can be obtained by the following formula.

$$y_n = MAX(f(x)), \quad x_0 < x < x_1 . \tag{7}$$

$$x_n = f^{-1}(y_n) . \tag{8}$$

$$x_0 = x_h + \frac{x_s - x_h}{4} . \tag{9}$$

$$x_1 = x_s - \frac{x_s - x_h}{4} . \tag{10}$$

Mandible point C is cutting angle which is 45 degrees. Because AB equal to BC, you can obtain forehead point A. Three basis points of this profile can be obtained.

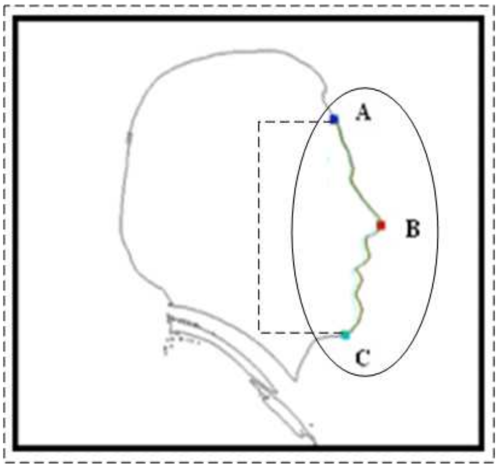

Figure 2. Image of face outline

Fourier Descriptors

2.1 Mathematical Description. The figure below shows K digital boundary in XY plane. When staring at any point (x_0, y_0), the coordinate $(x_0, y_0), (x_1, y_1), (x_2, y_2), \ldots, (x_{K-1}, y_{K-1})$. These coordinates can be expressed as $x(k) = x_k$, $y(k) = y_k$. Using this method, the boundary itself can be represented as a sequence of coordinates, $k = 0,1,2,\ldots, K-1$. Then the coordinates of each pair can be obtained as a complex process.

$$s(k) = x(k) + jy(k) . \tag{11}$$

The discrete Fourier transform of $s(k)$:

$$a(u) = \sum_{k=0}^{K-1} s(k) e^{-j2\pi uk/K} . \tag{12}$$

Here $u = 0,1,2,\ldots, K-1$. We call complex coefficient $a(u)$ known as the boundary of the Fourier descriptors.

2.2 Construction of a closed curve. When we know three basis points, it can be constructed by vertical line and middle regions of a closed contour, and then use the Fourier descriptors to extract the closed contour. This profile is characteristic profile which we need. Result can be shown below.

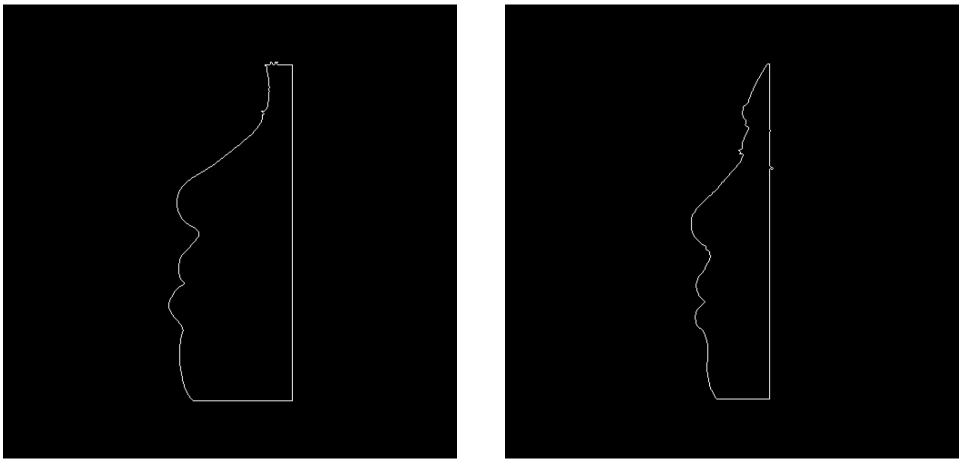

Figure 3. Characteristic profile

The recognition of the classifier

The above steps have been facial features to this step, and the design of the system is directly related to the success. There are many methods to design the classifier [5]. The core content of them is by the classification threshold. We will compare with two kinds of classifier.

3.1 Distance classifier. The Euclidean distance is the most typical distance classifier. Its central ideas which is compared the difference of the feature value and fixed value, and then according to the obtained distance range.

$$d(X, \overline{X^{(\omega_i)}}) < d(X, \overline{X^{(\omega_j)}}) \quad j = 1,2,\ldots, M, i \neq j . \tag{13}$$

Then we can get the X belongs to w_i, where w_i represents a class.

3.2 BP neural network classifier. For human action, signal the brain through the network to neurons and neurons responsible for overloading of information here, so that the signal intensity changes, and then delivered to finish other work. The same content of artificial network is applicable because it is a mapping of the truth. Although it is artificial, the processing mechanism of each unit was similar. Each of the division of labor in each unit and constitute the system structure of artificial neural network [6]. In the artificial neurons, can make each unit can be connected to each other. The biological networks can reproduce in the artificial environment and the original neurons into the processing of data now unit; including weighted processing of the data, there exist threshold function [7]. This is just one unit general structural, many units together to complete the process of input and output. To enter the data as input $x_1, x_2, x_3 \dots x_n$; here need multiplier, multiplier values respectively $\omega_1, \omega_2, \omega_3 \dots \omega_n$, the relationship that multiplication of entering the data, similar to neural signal overload. Then the multiplication function can be expressed as $\sum WX$. Threshold is θ and O said the system output equal Eq. 14.

$$o = f(\sum WX - \theta). \tag{14}$$

The θ shows the decision data and the o show the output data of the system and $f(x)$ is the activation function. The threshold is varied, have the relationship of the input data.

Experimental results and discussion

In order to realize the validity of data, the network selects 100 image training, then select the 100 image as the test image. Because the feature extraction feature dimension algorithm shows each face images is 40, so the input 40.Relation more implicit unit and the input unit, the hidden units of 80. Because total of 50individuals, divided into 50 classes, by the formula $2^n = 50$ may be in the range of n and the output unit may be sufficient to take six.

Through analysis of the overall results, BP network for this system is applicable. BP has a good effect, since the output value of BP network closer to the ideal output value, i.e. the integer 0 and an integer of 1. From the test image point of view of their neural network output is within the normal range tended, and their values are in the range of 0 to 1, the overall fluctuation of the float is not much.

Finally, you need to analyze data on the overall analysis of the recognition rate, false positive rate. Recognition rate and the false positive rate is important. For one side of the face, in order of an image corresponding to the identified person to be identified is difficult. Then you need to look at the data, the comparison results meets the requirements, whether the side face recognition security. Because only the side face recognition system has a good recognition efficiency can be potentially dangerous to a minimum. Identification table as shown in Table 1.

Table 1. Data of classifier

	Test samples	Training samples	Recognition rate	Missing rate	False positives
BP neural network classifier	100	100	97.4%	2.6%	3.5%
Euclidean distance classifier	100	100	86.5%	13.5%	9.6%

Acknowledgements

This work was financially supported by the Education Department of Heilongjiang Province (12521430).

References

[1] Zhang Zhi-gang, “Recognition method for profile face image”, Computer Engineering and Applications, vol. 46, no. 12, pp. 155-156, 2010.

[2] Zhen Han, Junjun Jiang, Ruimin Hu, Tao Lu. Pose-Variant Face Recognition through Manifold Learning Based Frontal Face Synthesis[J]. International Journal of Advancements in Computing Technology, 2013, 5(5): 172-182.

[3] Shengnan Wu, Yongxin Ge. A New Denoising Method and Its Application in Face Recognition[J]. International Journal of Advancements in Computing Technology, 2013, 5(5): 1122-1130.

[4] ZHANG Hong-yan, FAN Sheng-wei. Research on Face Recognition Algorithm Based on Improved Genetic Neural Network[J]. Journal of Convergence Information Technology, 2013, 8(5): 636-643.

[5] Zhao Xueming, Research on the Key Technologies of Image Segmentation Based on Fractal, Graduate School of National University of Defense Technology, China, 2008.

[6] Zhao Sanqin, Ding Weimin, Liu Deying, “Rice Hopper Shape Recognition Based on Fourier Descriptors”, Transactions of the Chinese Society of Agricultural Machinery, vol. 40, no. 8, pp. 181-184, 2009.

[7] Pengli Lu, Xingbin Jiang. An Improved PCA Algorithm for Fast Face Recognition[J]. International Journal of Advancements in Computing Technology, 2013, 5(2): 429-435.

Applied Mechanics and Materials Vol. 596 (2014) pp 433-436
© (2014) Trans Tech Publications, Switzerland
doi:10.4028/www.scientific.net/AMM.596.433

Pitch Detection Method Based on Morphological Filtering

WANG Yao-qi, WANG Xiao-peng, WANG Lv-cheng

(School of Electronic and Information Engineering, Lanzhou Jiaotong University, Lanzhou 730070, China)

Emails: wangyaoqi@mail.lzjtu.cn, wangxiaopeng@mail.lzjtu.cn, WLcheng@mail.lzjtu.cn

Key words: Pitch Detection; Morphological Filtering; HHT;

Abstract: A new method of pitch detection based on morphological filtering is proposed. Noisy speech signal is filtered by morphological filtering to remove the noise and highlight pitch, and then HHT is employed to get Hilbert-Huang spectrum and to calculate instantaneous energy and its derivative. The moment of glottal opening and closing can be accurately located through tracking mutation of instantaneous energy, so that variation of pitch period can be accurately tracked. Compared with other traditional method of pitch detection, this method not only truly describes non-stationary and non-linear characteristics of speech signal, but also it is an adaptive process for the analysis of the speech signal. The experiments showed that the method has strong anti-noise and can accurately detect the pitch of speech in low SNR.

Introduction

Speech signal is a kind of time-varying non-stationary signal and contains formant information of channel and noise, such that accurate pitch detection is very difficult. Currently pitch detection methods mainly include autocorrelation, inverse filtering, the average magnitude difference function, cepstrum analysis, parallel processing, spectral subtraction method and the number of zero-crossing method, etc[1-3].These are linear processing methods and does not consider the accurate time and instantaneity of glottis opening and closing, but calculates average pitch frequency of a waveform. In recent years, the wavelet transform has been applied in pitch detection by some scholars. But wavelet transform is still essentially an adjustable time window Fourier transform and it is based on the assumption that speech signal is at a short-time stationary in a frame, so it cannot well reflect non-stationary and nonlinear characteristic of speech signal and cannot avoid spectrum leakage problem caused by framing. At the same time, the choice of wavelet basis function has a greater impact to the accuracy of pitch detection for various speech signal[4].

Morphological transform is a new nonlinear filtering technology based on set theory and geometry. The complex signal is decomposed into different parts by morphological transform. The information extraction method based on local morphological characteristics is more effective than the traditional filtering methods, especially in the removing of positive and negative pulse signal[5]. Morphological filter can avoid the loss of information and the calculation does not involve multiplication and division operations, so it has good real-time and small time-delay.

Morphological Filter

Morphological filter is a nonlinear signal processing and analysis tool in time-domain. Its basic idea is to collect information about a signal using probe called structure element and through moving the probe in the signal to extract signal, keeping the details and suppressing noise.

Morphological operation include expansion, erosion, morphological opening, morphological closing operation and a cascade of morphological opening and closing [5]. If input signal $f(n)$ and structural element $g(n)$ are discrete signals defined in F = {0,1, ..., N-1} and G={0, 1,... , M-1} respectively, and N≥M, the four basic transformations of $f(n)$ on $g(n)$ are defined as follows:

Expansion: $$(f \oplus g)(n) = \max_{m=0,1,\ldots M-1} \{f(n+m)+g(m)\} \quad (n = 0,1,\ldots,N+M) \tag{1}$$

Erosion: $$(f \Theta g)(n) = \min_{m=0,1,\ldots M-1} \{f(n+m)-g(m)\} \quad (n+m = 0,1,\ldots,N-1) \tag{2}$$

Opening operation: $$(f \circ g)(n) = (f \Theta g \oplus g)(n) \tag{3}$$

Closing operation: $$(f \bullet g)(n) = (f \oplus g \Theta g)(n) \tag{4}$$

Expansion and erosion are the maximum and minimum operations on structural element, and equivalent to maximum and minimum filtering for the discrete signal in the sliding window. Expansion operation can increase the signal valley value, widen peak, fill concave portion and form connected domain. Erosion operation can reduce the peak of signal, widen valley domain and effectively eliminate isolated noise points. Opening and closing operation are basic morphological filtering operations and cascaded by expansion and erosion in a different order. Opening operation can remove isolated small point and burr and suppress positive impulse noise. Closing operation can fill hole and gap and suppress negative impulse noise. In order to simultaneously remove positive and negative impulse noise, usually use a cascade of morphological opening and closing operation. Morphological opening-closing and closing-opening operations are defined as follows:

Opening-closing $$F_{oc}(f(n)) = (f \circ g \bullet g)(n) \tag{5}$$

Closing-opening $$F_{co}(f(n)) = (f \bullet g \circ g)(n) \tag{6}$$

Contractibility of the opening operation and expansibility of closing operation make $F_{oc}(f(n))$ and $F_{co}(f(n))$ to generate statistical bias that output amplitude of $F_{oc}(f(n))$ is too small and output amplitude of $F_{co}(f(n))$ is too large, therefore we can not achieve good filtering effect using them individually. In order to filter out noise, highlight periodicity of pitch, weaken the influence of formant and correct statistical bias, at the same time taking into account the quasi symmetry characteristics of the speech waveform, the weighted average combination of these two filters are used in this paper. A large number of experiments showed that filtering effect is the best when the weighted average value is 6:4. The output of morphological filter can be expressed as follows:

$$y(n) = 0.6 * F_{oc}(f(n)) + 0.4 * F_{co}(f(n)) \tag{7}$$

Hilbert-Huang Transform

Hilbert-Huang transform includes two steps[6]. The first step is EMD (Empirical Mode Decomposition—EMD) that the signal is decomposed into several IMF (Intrinsic Mode Function—IMF) in descending frequency order. The second step is that each IMF component with its Hilbert transform is combined into an analytical complex function in order to calculate the instantaneous energy and frequency. Each IMF must meet the following two conditions regardless of whether it is linear or not.

（1）Numbers of extreme point and zero is equal or differ by 1;

（2）At any time, the upper envelope defined by the local maxima and lower envelope defined by local minima is symmetric about the time axis.

Simulation and Performance Analysis

Research at the speech laboratory recorded that the sampling frequency is 8kHz and 16bit quantization in the MATLAB.

Speech laboratory recorded "ninety-three" in fig.1(a), the sampling frequency is 8kHz and 16bit quantization. Fig.1(b)~ Fig.1(d) respectively are noisy speech signal(SNR = 3dB), signal filtered by the morphology and pitch track obtained. As can be seen from the figure, the method well describes complex signal having frequency modulation between waveforms and within waveform. Not only can it detect pitch and track real-time changes of pitch, but also may accurately describe transition from unvoiced to voiced. For example, at about 500~1000 moment is unvoiced [n] sounding stage, at about 1000~2100 moment is voiced [B :] sounding stage. Pitch has obvious mutation from unvoiced to voiced.

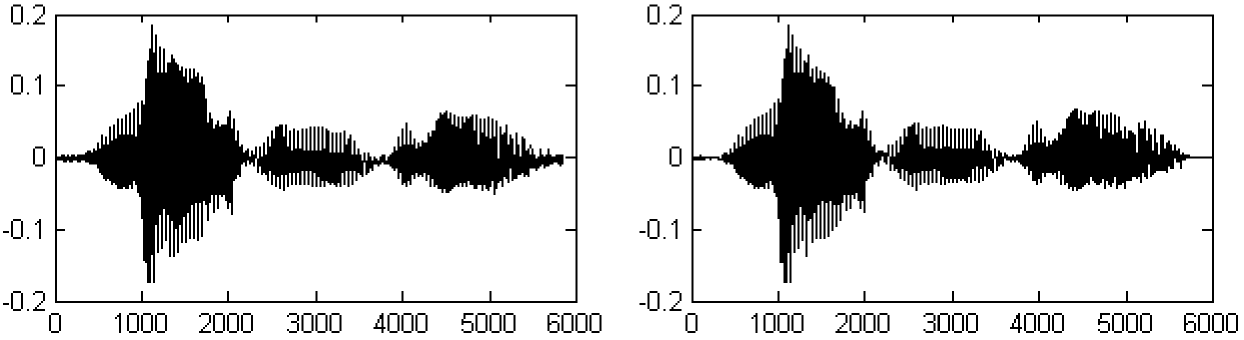

(a) Time-domain waveform of ninety-three

(c) The signal filtered by morphological

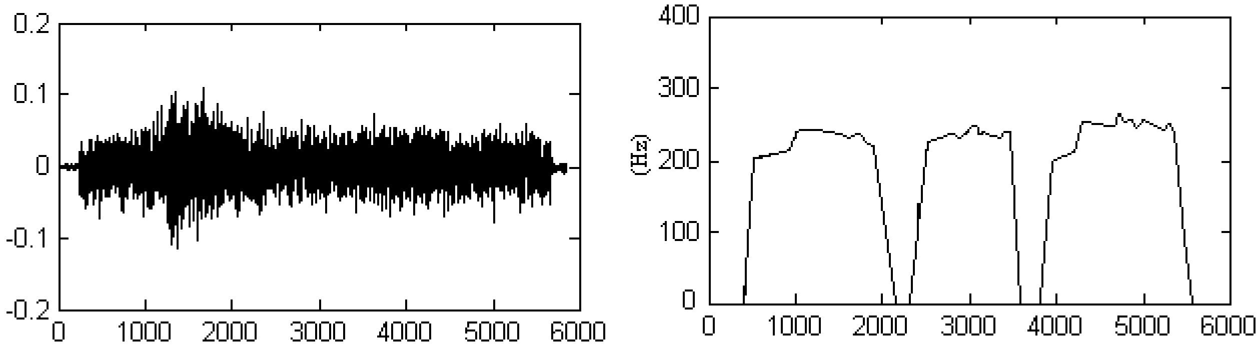

(b) Noisy Signal of ninety-three

(d) Pitch trajectory of ninety-three

Fig.1 Pitch detection for ninety-three

Table 1 is comparison of correct rate for 4 kinds of pitch detection method in different SNR. It can be seen that the method proposed is significantly superior to other methods for pitch detection. Cepstrum is the worst, because determination of voiced and unvoiced is based on the existence of peaks corresponding to pitches. However at some time, the peak of voiced is not prominent but unvoiced indicates some emergence of peak, leading to the misjudgment of unvoiced or voiced and deviation of pitch estimation. Relatively fixed threshold is used in autocorrelation and there are more frequency multiplication and division, which leads to deviation of pitch estimation too. Constant proportional band pass filters determined by wavelet basis function filter signal in wavelet transform. Its resolution of frequency and time is uneven and can not accurately reflect the rapid changes of the pitch period[10]. The noisy signal is filtered by morphological filter to highlight the pitch and filter noise in proposed method, and then extract instantaneous energy by HHT spectrum. It is adaptive that EMD decomposes IMF basis function, which make resolution of frequency and time to be improved. The moment of glottal opening and closing is positioned by the instantaneous energy mutations to accurately track pitch changes, improving accuracy of pitch estimation.

Table 1 The correct rate of pitch detection Unit **%**

method / *SNR*	*Cepstrum*	*Autocorrelation*	*Morphological filter*	**Method Proposed**
∞	97.6	98.1	100	100
10dB	86.1	87.4	97.6	98.7
5dB	80.1	81.6	94.8	97.1
0dB	72.3	74.7	89.5	90.2

Conclusion

Proposed pitch detection method is based on morphological filtering. It combines morphological filtering and EMD decomposition. Complex signal is decomposed into various parts using morphological filtering to maintain detail and suppress noise. HHT is adaptive for non-stationary and nonlinear signals. Calculate instantaneous energy using HHT, position moments of glottal opening and closing by the instantaneous energy mutations to accurately track changes of pitch. The experimental showed that the method has strong anti-noise, can precisely extract the pitch in low SNR environment.

Acknowledgements

This work was financially supported by National Natural Science Foundation (61261029), (60962004).

References:

[1] Shi-Huang Chen,Rodrigo Capobianco Guido,Trieu-kien Truong,Yaotsu Chang. Improved voice activity detection algorithm using wavelet and support vector machine[J]. Computer Speech and Language.2010, 24 (3):531-543

[2] Zhang Jun, Wang Heping. A New Approach of Pitch Detection Based on Morphology Filter and Wavelet Transform[C]. 2010 Second International Workshop on Education Technology and Computer Science (ETCS). Wuhan, Hubei, China. 6-7 March 2010: 751 – 753

[3] WANG Yao-qi, WANG Xiao-peng, ZHANG Zhong-ling .A pitch detection method in low SNR environment[J]. Journal of The China Railway Society, 2012,34(2):58-62

[4] CHEN Shi-huang, RODRIGO C G, TRUONG Trieu-kien. Improved Voice Activity Detection Algorithm Using Wavelet and Support Vector Machine[J]. Computer Speech and Language.2010, 24 (3):531-543.

[5] ZHANG Jun, WANG He-ping. A New Approach of Pitch Detection Based on Morphology Filter and Wavelet Transform[C]// 2010 Second International Workshop on Education Technology and Computer Science (ETCS). Wuhan, China: 6-7 March 2010: 751- 753.

Applied Mechanics and Materials Vol. 596 (2014) pp 437-441
© (2014) Trans Tech Publications, Switzerland
doi:10.4028/www.scientific.net/AMM.596.437

Rolling bearing fault diagnosis with EMD-based fault characteristic frequency difference analysis

Yanping Guo[a], Yu Xiong[b] and Guocui Song[c]

Zhongshan Torch Polytechnic Zhongshan Torch Polytechnic,China

[a]guoyanping1983@163.coml, [b]xiong_yu@yeah.net, [c]songgc@126.com

Keywords: EMD. Bearing. Fault diagnosis. Vibration.Characteristic fault frequency

Abstract. This paper presents a novel single-point rolling bearing fault diagnosis mechanism through vibration signal analysis. It is highlighted that the rolling bearing operational state can be well estimated by the first small set of Intrinsic Mode Function (IMF) components of the original vibration measurements through Empirical Mode Decomposition (EMD). These IMF components can be further translated into envelope spectrum by using Hilbert Transform. As a result, the difference of fault characteristic frequencies (DFCF) is derived to properly characterize different fault patterns for fault diagnosis. The suggested method is implemented and evaluated in a rolling bearing test bed for a range of failure scenarios (e.g. inner and outer raceway fault, rolling elements fault) with extensive vibration measurements. The result demonstrates that the proposed solution is effective for characterizing and detecting arrange of rolling bearing faults.quality).

Introduction

As one of the most fundamental and failure-prone components in industrial automated mechanical systems[1-2], rolling bearing and its fault diagnosis has been exploited for years aiming at efficiently manage the system with minimal maintenance cost. At present available approaches mainly attempt to address this issue by identifying fault characteristic frequencies(FCF) through vibration measurements analysis with various techniques, e.g. neural networks[3], wavelets[4] and EMD method [5, 6], but with many limitations. Fourier analysis has been widely used, but limited to linear analysis and with the underlying assumption that the signal needs to be either strictly periodic or stationary. As an adjustable window Fourier analysis, the wavelet transform has the deficits of the leakage induced from the basic wavelet function due to limited length, as well as its non-adaptive nature. Neural network based analysis is in particular suitable for nonlinear pattern classification but needs to be trained by a set of representative data. In parallel, EMD[7] is developed as an efficient and adaptive analytical tool for processing data exhibiting nonlinear and non-stationary characteristics.

In this paper, we take a new look into the EMD based method for vibration signal analysis and exploit its application in fault diagnosis of bearing. The key idea behind the approach can be described as follows: the actual measured vibration signals can be decomposed into a set of IMF components with EMD method and a new signal can be produced by assembling only the first small set of components; through applying the Hilbert transform, the envelope spectrum can be obtained. As a result, we could derive the difference of fault characteristic frequencies (DFCF), from which the faults in bearing can be properly located and analyzed.

To the author's best knowledge, existing approaches based on EMD and signal processing techniques are mainly focus on investigating the amplitude [8] or its square (energy) (e.g.[8]-[12]) of IMF components obtained from EMD. However, this paper presents a novel approach by analyzing the DFCF in fault characteristic frequency band (FCFB). The remainder of the paper is organized as follows: section 2 firstly presents the EMD method; followed by section 3 describing the DFCF, respectively; section 4 presents the performance evaluation in details and gives a set of key numerical results; finally some conclusion and discussions are given in section 5.

The EMD Method

With the EMD method, the signal can be decomposed into a finite set of IMF components. Given a data set, $x(t)$, the EMD can be briefly described as follows: 1) Connect all identified local maxima points by a cubic alpine line to produce the upper envelope; 2)Repeat the procedure for the local minima points to produce the lower envelope; 3)With the mean of upper and lower envelope value denoted as m_1 , $x(t)-m_1=h_1$,If h_1 meets the IMF constraints, it is considered the first IMF component of $x(t)$; 4) Otherwise, h_1 is treated as the original data and repeat the steps of (1), (2) and (3); The sifting procedure needs to be iterated k times until h_{1k} becomes an IMF. $h_{1(k-1)}-m_{1k}=h_{1k}$, Then we obtain the first IMF component c_1 as h_{1k} ; 5) Separate c_1 from the data $x(t)$ by using $r_1=x(t)-c_1$. The residue r_1 is considered as the original data and the aforementioned sifting procedure is repeated. In this way, other IMF components can be derived through n iterations. The sifting process will terminate when the residue r_n becomes a monotonic function from which no more IMF can be extracted. we finally obtain $x(t)=\sum_{i=1}^{n}c_i+r_n$.

Due to the fact that the fault information is often included in the high-frequency signal band [8], in this paper the first four IMF components (either in frequency or amplitude modulated function, or both) are adopted for fault analysis. The signal consisting of the first four IMF components, without introducing disturbance is as $c(t)=c_1(t)+c_2(t)+c_3(t)+c_4(t)=IMF1+IMF2+IMF3+IMF4$.

Recognizing the fact that single-point faults very often occur on the surface of bearing, a fault detection approach by using FCF is presented in [13]. The inner raceway fault frequency (f_i), ball fault frequency (f_r), and outer raceway fault frequency (f_o) can be calculated by Eq. (1).

$$f_i=\frac{1}{2}\left(1+\frac{d}{D_m}\cos\alpha\right)f_nZ;\ f_r=\frac{1}{2}\left(1-\frac{d^2}{D_m^2}\cos^2\alpha\right)f_n\frac{D_m}{d};\ f_o=\frac{1}{2}\left(1-\frac{d}{D_m}\cos\alpha\right)f_nZ \qquad (1)$$

where d -The ball diameter; D_m -The pitch diameter; α -The ball contact angle; f_n - The rotor (shaft) frequency; Z - The number of rolling elements.

The Difference of Fault Characteristic Frequency (DFCF)

In this section, we present the key idea of the proposed approach for bearing fault detection. Single-point fault diagnosis aims at locating faults on the raceways or rolling elements which introduce mechanical shockwaves when rolling elements pass over the defect areas. These shockwaves will excite the mechanical natural frequency (f_m) of the machine. The process occurs every time the fault collides with other parts of the bearing with the occurrence frequency equivalent to the FCF f_c , which maybe one of the previously defined f_i, f_r ,or f_o .

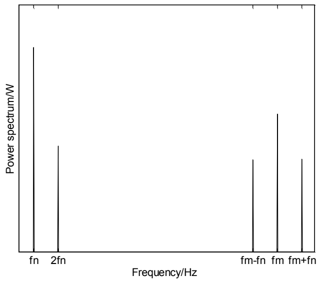

Fig. 1 Amplitude modulation with a fault-free bearing

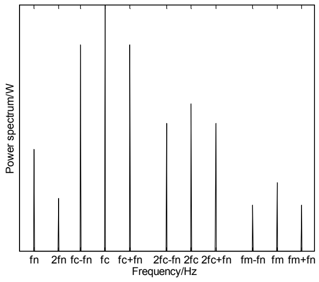

Fig. 2 Amplitude modulation with a single-point fault

Fig. 1 and Fig. 2 represent an amplitude modulation in frequency domain for fault-free and a single-point fault scenario, respectively, including the rotor frequency (f_n), its second harmonics

($2f_n$), the mechanical natural frequency f_m is modulated by the rotor frequency f_n. In these illustrations, a components with frequency f_m interacts with another components at f_n to produce two new sideband components at ($f_m - f_n$) and ($f_m + f_n$). There are the amplitude modulation which the CFC f_c is modulated by rotor frequency f_n, as shown in Fig. 2, but is not occurs in the fault-free scenario (Fig. 1). There is another amplitude modulation which the second harmonics of CFC $2f_c$ is modulated by rotor frequency f_n in Fig. 2. Based on this analysis, the frequency domain effectively consists of three partitions which are:(1) the rotor frequency f_n and its harmonics (nf_n, n=1, 2, 3.); (2) the CFC f_c, its harmonics $2f_c$ and their modulated frequencies ($f_c - f_n$, $f_c + f_n$, $2f_c - f_n$, $2f_c + f_n$) by rotor frequency f_n; and (3) the mechanical natural frequency f_m and its modulated frequency ($f_m + f_n, f_m - f_n$) by rotor frequency f_n, respectively. In fact, there exist other components with less power which are ignored and not shown in Fig. 2. The key of single-point fault diagnosis focuses on the analysis of Part (2) which exhibits the difference of health and fault spectrum in frequency domain. Therefore, we determine the FCFB ($f_{\min}, f_{\max}$) to approximately represent the fault information, $f_{\min}$=min ($f_i - f_n, f_o - f_n, f_r - f_n$, $2f_i - f_n$, $2f_o - f_n$, $2f_r - f_n$); $f_{\max}$=max ($f_i + f_n$, $f_o + f_n$, $f_r + f_n$, $2f_i + f_n$, $2f_o + f_n$, $2f_r + f_n$).

In such a way, the FCFB can well represent the key fault information, while minimizing the useless frequency information for fault diagnosis. Once the frequency corresponding to the maximal amplitude of the envelope spectrum amplitude, denoted as $f_{A\max}$, is identified within the FCFB, we can properly locate the single-point fault in the bearing. In principle, The identified frequency $f_{A\max}$ should approximately match with one of the FCF f_c (i.e. f_i, f_r, or f_o). Therefore, the DFCF can be calculated as $F_o = |f_{A\max} - f_o|$, $F_i = |f_{A\max} - f_i|$, and $F_r = |f_{A\max} - f_r|$. The minimum of F_o, F_i, F_r and the corresponding location of fault is F_o/ the outer raceway, F_i/ the inner raceway, F_r/ ball elements, respectively.

Numerical Evaluation and Result

This section sets out the details for experimental evaluation of the proposed approach for vibration signal analysis and presents a set of key numerical results. All experiments are carried out in a test bed consisting of a 2 hp motor, a torque transducer/encoder, a dynamometer, and control electronics. The test bearings support the motor shaft and single-point fault scenarios are introduced using electro-discharge machining. Experiments are obtained from [15].

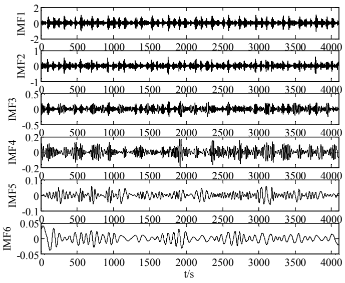

Fig. 3: The IMF components based on EMD (6 components: IMF1-IMF6)

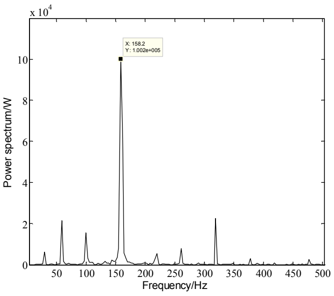

Fig. 4: The envelope spectrum of the Hilbert envelope data (inner raceway fault)

With the EMD method, the vibration data from a bearing with inner raceway fault is decomposed into 16 IMF components (IMF1, IMF2,…, IMF16) and a residual trend. Fig.3 shows the first six IMF components with each component representing an oscillation mode embedded in the original vibration signal. In fact, the original vibration signal contains not only the information reflecting the bearing operational state, but also background noise which can be minimized through the EMD

With the actual signal measurements, we can get the new assembled signal consisting of the first four IMF components. We apply Hilbert transform to the assembled data, and the envelope spectrum is obtained, as shown in Fig. 4, which shows an obvious spectral line at the component (with frequency of 158.2Hz). With Eq. (1), the FCF are obtained as f_i =159.9Hz, f_r =141.2Hz, and f_o =107.3Hz. In Fig. 4, there is a spectral line at the frequency ($f_{A\max}$ =158.2Hz) corresponding to the maximal of the envelope spectrum within the CFFB ($f_{\min}$ =76.3Hz, $f_{\max}$ = 349.39Hz). The DFCF is F_o=50.9； F_i=1.7； F_r=17.0. The minimum is F_i=1.7 corresponding to inner raceway fault, which confirms the location of inner raceway fault.

Now, we present a set of key experimental results in our study based on 112 data sets obtained from [15] (each set consisting of 32768 measurements) including 31 sets of inner raceway faulty data, 61 sets of outer raceway faulty data, and 20 sets of rolling elements faulty data, respectively.

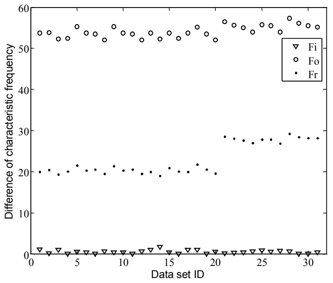

Fig. 6: The DFCF
(inner raceway fault)

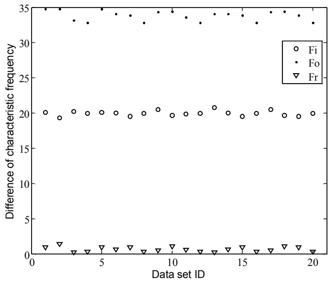

Fig. 5: The DFCF
(rolling elements fault)

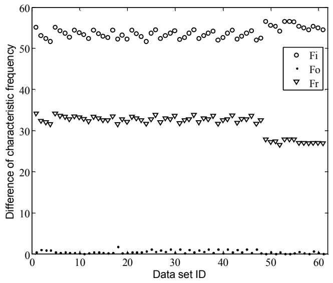

Fig. 7: The DFCF
(outer raceway fault)

After applying the proposed approach to the 31 sets of inner raceway faulty data, we can obtain 31 sets of DFCF (F_o , F_i , F_r), as shown in Fig. 5. The minimum is F_i in each set of DFCF. The result indicates that the proposed method can extract the FCF of bearing, because there is an obvious peak at the frequency ($f_{A\max}$) which is approximately equal to the theoretical value of FCF of inner raceway, which result in the minimum value of F_i. Based on the analysis, we can conclude that the inner raceway possess the single-point defect, which confirms the effective of proposed method. Fig. 6 and Fig. 7 represent the DFCF of bearing scenarios of rolling elements fault and outer raceway fault, respectively. The minimum value is F_r and F_o in Fig. 6 and Fig. 7 respectively, from which we can get the location of fault is rolling element and outer raceway. The results show that the proposed method is effective in extracting the fault characteristic of bearings.

Conclusion and Discussion

In this paper, we present a novel approach for fault diagnosis in bearing through an EMD based on fault characteristic frequency difference method. Through applying the Hilbert to the signal obtained from the EMD, the DFCF can be obtained to efficiently characterize the fault pattern. The detection of single-point faults becomes an easier task through analyzing the DFCF. This provides a simplified alternative approach for fault diagnosis as it requires neither training data from various faulty bearings nor baseline data from the machine being monitored, as well as with low computation complexity making it adoptable for online fault diagnosis. The suggested approach is extensively assessed through a set of experiments (with 112 sets of vibration data) for a range of fault scenarios and the result demonstrates its effectiveness and efficiency in fault characterization and detection. In respect to the future work, we aim to implement and deploy the presented approach in the field to further verify its effectiveness through a long-term operation and the result will be presented in our future publications.

Acknowledgements

This work is supported by Zhongshan Science and Technology Project (2013A3FC0309)

References

[1] P. O'Donnell, Report of large motor reliability survey of industrial and commercial installations-Part I, IEEE Trans. Ind. Appl. 4 (1985) 853-864.

[2] P. O'Donnell, Report of large motor reliability survey of industrial and commercial installations-Part II, IEEE Trans. Ind. Appl. 4 (1985) 865-872.

[3] H. Su, K. Chong, Induction machine condition monitoring using neural network modeling, IEEE Trans. Ind. Electron. 54 (2007) 241-249.

[4] M. Devaney, Eren, L, Detecting motor bearing faults, IEEE Instrumentation&Measurement. 7 (2004) 30-50.

[5] Dejie Yu, Junsheng Cheng, Yu Yang, Application of EMD method and Hilbert spectrum to the fault diagnosis of bearings, Mechanical Systems and Signal Processing. 19 (2005) 259-270.

[6] Cheng Junsheng, Yu Dejie, Yang Yu, A fault diagnosis approach for rolling bearings based on EMD method and AR model, Mechanical systems and Signal Processing. 20 (2006) 350-362.

[7] N.E. Huang, et al., The empirical mode decomposition and the Hilbert spectrum for nonlinear and non-stationary time series analysis, In Proc. the Royal Society of London. 454 (1998) 903-995.

[8] Cheng Junsheng, Yu Dejie, Yang Yu, The application of energy operator demodulation approach based on EMD in machinery fault diagnosis, Mechanical systems and Signal Processing. 21(2007) 668-677.

[9] Xianfeng Fan, Ming J Zuo. Machine fault feature extraction based on intrinsic mode functions. Meas. Sci. Technol. 19 (2008) 045105

[10] QIU Mian-hao, WANGZi-ying, Fault Diagnosis of Bearing Based on Empirical Mode Decomposition and Decision Directed Acyclic Graph Support Vector Machine, International Conference on Computational Intelligence and Natural Computing. 2 (2009) 471-474.

[11] Yang Yu, YuDeijie, Cheng Junsheng, ROLLER BEARING FAULT DIAGNOSISMETHOD BASED ON EMD AND NEURAL NETWORK, JOURNAL OFVIBRATION AND SHOCK. 24 (2004) 85-88 (In Chinese).

[12] Qin Tailong, Yang Yong, Cheng Hang, Xue Song, Rolling Bearing Fault Diagnosis Based on Intrinsic Mode Function Energy Moment and BP Neural Network, Journal of Vibration, Measurement &Diagnosis. 28 (2008) 229-232 (In Chinese).

[13] LIHui, ZHENGHai-qi, YANG Shao-pu, BEARING FAULT DIAGNOSIS BASED ON EMD AND TEAGER KAISER ENERGY OPERATOR, JOURNAL OFVIBRATION AND SHOCK. 27 (2008) 15-22 (In Chinese).

[14] R. A. Collacott, Vibration Monitoring and Diagnosis, Wiley, New York, 1979.

[15] The Case Western Reserve University Bearing Data Center Website. Bearing data center seeded fault test data[EB/OL]. [2007-11-27] http://www.eecs.case.edu/ laboratory/ bearing/ CWRUFlash.htm.

Applied Mechanics and Materials Vol. 596 (2014) pp 442-445
© (2014) Trans Tech Publications, Switzerland
doi:10.4028/www.scientific.net/AMM.596.442

LED-based 3-DMD Volumetric 3D Display

Changlong Jing [1, 2,a], Qibin Feng [1,3,b], Yingsong Zhang[1,2,c], Guanglei Yang[1,2,d], Zhigang Song[1,2,e], Zhiqi Pei[1,3,f], and Guoqiang LV[1,3,g,*]

[1]Key Lab of Special Display Technology, Ministry of Education; National Engineering Lab of Special Display Technology; National Key Lab of Advanced Display Technology, China

[2]School of Instrumentation and Opto-Electronics Engineering, Hefei University of Technology, China

[3]Academy of Photoelectric Technology, Hefei University of Technology, China

[a]jcl107990718@126.com, [b]fengqibin@hfut.edu.cn, [c]guangxindaosheng@126.com, [d]ygl582893552@163.com, [e]scylove1989@163.com, [f]Peizq2013@163.com,[g]guoqianglv@hfut.edu.cn, *corresponding author

Keywords: LED, 3DLP, liquid crystal shutter, volumetric 3D.

Abstract. A solid-state volumetric true 3D display developed by Hefei University of Technology consists of two main components: a high-speed video projector and a stack of liquid crystal shutters. The shutters are based on polymer stabilized cholesteric texture material, presenting different states that can be switched by different voltage. The high-speed video projector includes LED-based light source and tree-chip digital micro-mirror devices modulating RGB lights. A sequence of slices of three-dimensional images are projected into the liquid crystal shutters locating at the proper depth, forming a true 3D image depending on the human vision persistence. The prototype is developed. The measurement results show that the screen brightness can reach 149 nit and no flickers can be perceived.

Introduction

The real world is three-dimensional (3D) and the images displayed on the plat screen can't meet the demands in some cases. With the development of society, various stereoscopic display technologies appear and become world-wide research focus. In general, 3D display technologies can be divided into stereoscopic display, auto stereoscopic display and volumetric 3D display. The solid-state volumetric true 3D display produces truly 3D images in a solid-state, front viewed display that utilizes all of the human visual system (HVS) 3D vision cues. All of the pixels in the true 3D display have the same size, shape, and deepness, which lead to no obstructions or dead zones in the display volume. Unlike stereoscopic and auto stereoscopic displays, the volumetric 3D display produces a very comfortable and natural 3D viewing experience. It has a good visual effect from different points of view, just like looking at the real object [1].

LightSpace Technologies has been focusing on volumetric 3D display technology and developed a DepthCube z1024 3D Display System. Hefei University of Technology (HFUT) also developed a true 3D display prototype with ultra high pressure mercury lamp (UHP) projection light source and single-chip digital micro-mirror devices (DMD). With sustained researches on 3D display technology, a 19” solid-state volumetric true 3D display with LED projection light source and tree-chip DMDs is developed.

LED projection light source

UHP working with color wheel is commonly used in most traditional projectors. The disadvantages of such structure include low color field frequency, short lifetime and unadjustable color gamut [2]. With the development of solid-state emitting technology, LED-based light source presents the merits of fast response speed, long lifetime, and wide color gamut. High-power LEDs are therefore chosen to provide high luminance.

To satisfy the requirements of the brightness of 120nit, the output of the light luminous flux should reach 5000lm [3]. Three colorful LEDs of red (R), green (G), and blue (B) are applied. RGB lights are mixed into white. Color temperature can be adjusted by modifying the driving currents of RGB LEDs. The LED specifications are shown in the Table 1.

Table 1 LEDs specifications

	Red	green	blue
Size[mm]	4*3	4*3	4*3
Dominant Wavelength[nm]	624	528	462
Luminous Flux[lm]	1800	3500	750
Color Coordinate	(0.698,0.301)	(0.183,0.703)	(0.153,0.025)

As the fact that divergence angle of LEDs is about 160 degree, it is quite difficult to utilize lights as much as better. Some special designs have to be performed for higher power utilization. As shown in the Fig.1, the rays with small angle are converted into parallel by refraction and the rays with wide angle are reflected. The light collimator can help make the LEDs' light nearly parallel.

The lights from RGB LEDs are mixed by X-Cube prism and entering the integrator rod in appropriately ±15°. The simulation result is illustrated in the Fig.2. The practical light collimator is shown in the Fig.3.

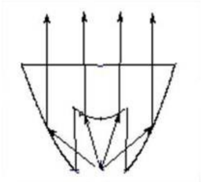

Fig.1 Light collimator

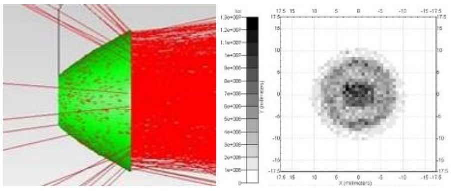

Fig.2 Simulation diagram of collimator

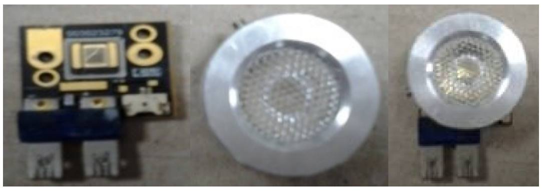

Fig.3 Practical measurement result

Electrical system

The Fig.4 shows a block diagram of electrical system. The system includes a decoder and main control module, tree DMD boards, a driving control board, four LC shutters driving boards, and three LEDs driving boards. The decoder board receives image data from a computer DVI interface. The front-end input decoder converts the data signals into a custom internal format and routes them to the three channels to control the tree DMD boards, one each for red, green and blue. 3 images of RGB color are combined to form a colorful image. The main control module provides control signals to all the driving boards simultaneously driving the LEDs and LC shutters to make sure the LEDs, LC shutters, and DMDs can perfectly cooperate to produce colorful stereoscopic images.

The decoder board receives 14 bits data including a 4 bits color data and a 10 bits position data to control the color channels. While a new signal of image is being written into one of the two frame buffers, the previous image in the other buffer is holding on and being displayed. That's ping-pong operation.

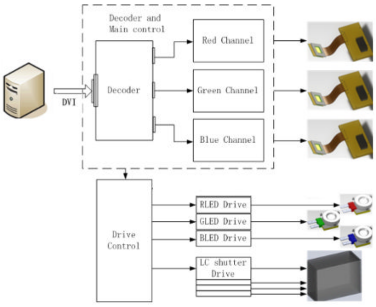

Fig.4 Block diagram of electrical system

Liquid crystal shutters

The 20 liquid crystal (LC) shutters act as an electronically-variable solid-state display unit. The shutters are based on polymer stabilized cholesteric texture (PSCT) material, presenting different states that can be switched by different voltage [4]. The two states of LC shutters are shown in the Fig.5.

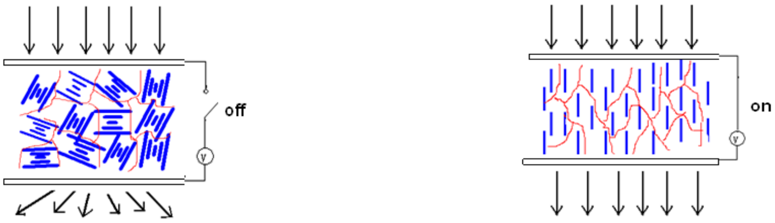

(a) (b)

Fig.5 The state of shutters (a) Scattering state under zero voltage (b) Transmission state under voltage

At any time, the display unit has only one shutter in imaging state (scattering state) and the others are in non-imaging state (transparency state). In other words, 20 layer LC shutters need to be scanned in one frame. The refresh rate is usually set to 60Hz for stable image and no perceived flickers. For 20 LC shutters, the response time of each shutter should be limited in 1/(20×60)=0.83ms. In addition, the visual angle is affected by scattering rate in imaging state and the screen brightness is decided by transmittance in non-imaging state. All these require LC shutters to have enough response speed, scattering rate in imaging state, and transmittance in non-imaging state.

Fig.6 shows the electro-optic property of PSCT. When the voltage is less than 45v, the shutters are in imaging state and the transmittance is close to 10%. When the voltage is greater than 52V, the shutters are in no-imaging state and the transmittance stands at 86.1%. Through the research, the turn-on time can be effectively reduced by increasing the driving voltage to 100V.

Fig.7 shows the dynamic response of PSCT. The shutters' response time includes turn-on time (t_{on}) and turn-off time (t_{off}). The t_{on} is 0.54ms and t_{off} is 0.18ms at the 100V, 400 Hz square-wave driving voltage. Therefore, the imaging and no-imaging state of LC shutters can be converted within 0.72ms, which satisfies the requirement of the refresh rate. The flickering problem can be effectively avoided.

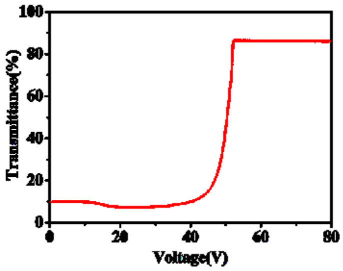

Fig.6 Electro-optic property of PSCT

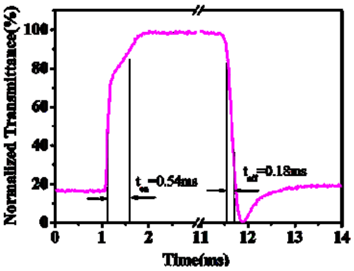

Fig.7 Dynamic response of PSCT

Overall system structure and performance

The schematic diagram of the solid-state volumetric true 3D display system is shown in the Fig.8. As mentioned above, the true 3D display system is a solid state, rear projection, volumetric display that consists of two main components: a high-speed video projector and 20 LC shutters.

The prototype is shown in the Fig.9. The brightness is 149cd/m^2, measured by TOPCON Luminance Colorimeter BM-7A. The performances of HFUT solid-state volumetric true 3D display system are shown in the Table 2.

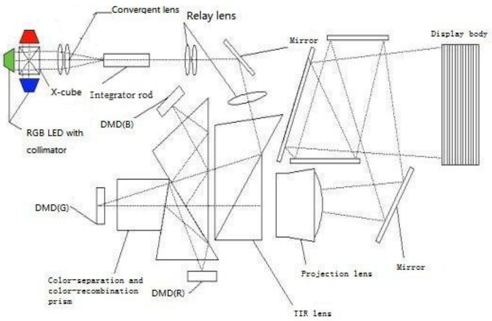

Fig.8 Schematic diagram of 3D display system

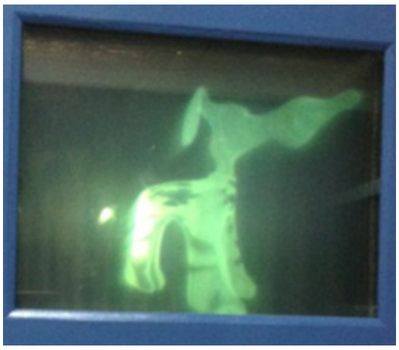

Fig.9 Physical diagram of 3D display system

Table 2.Performances of HFUT solid-state volumetric true 3D display system

Image volume	15.2”*11.4”*7.6”
Liquid crystal shutters	20
Resolution	1024*768*20
Physical voxel	15.7 Million
Refresh rate	60 Hz
Optical structure	Tree-chip DMDs
Color depth	14-bit
Screen brightness	149 nit

Conclusions

LED light source is chosen for the merits of the fast response speed, long lifetime and wide color gamut. In order to improve the energy utilization, the light collimator is specially designed to make the LED emitting lights nearly parallel. The decoder, control and driving boards are applied to process the signals of 3D images coming from personal computer. The LC shutters with high response speed are developed to make the projected image consecutive.

The solid-state volumetric true 3D display occupies very important position in the field of stereo display. Nevertheless, the problems still exist. Performance of LC shutters needs further improvement. Compact structure and low cost are the preconditions that solid-state volumetric true 3D display can really enter the common families and be enjoyed by common people.

Acknowledgements

This work was financially supported by National High Technology Research and Development Program (2012AA011901) and Guangdong Province Projects of Strategic Emerging Industry's Key Technology (2011A010801003).

References

[1] Tao Liu, Guoqiang Lv, Hao Tong: Advanced Display. Vol.117 (2010), p. 34, In Chinese.

[2] Qibin Feng, Honglin Niu, Yikui Hua, Guoqiangh Lv: Opto-Electronic Engineering. Vol.38 (2011), no.9, p. 4, In Chinese.

[3] Guanglei Yang, Changlong Jing, Huihui Yao, Qibin Feng: Applied Mechanics and Materials. Vol.321-324 (2013), p. 467

[4] Honglin Niu, Hongbo Lu: Opto-Electronic Engineering. Vol.39 (2012), no.8, p. 143, In Chinese.

CHAPTER 6:

Measurement Technology, Instruments and Sensors, Detection Technologies

Applied Mechanics and Materials Vol. 596 (2014) pp 449-452
© (2014) Trans Tech Publications, Switzerland
doi:10.4028/www.scientific.net/AMM.596.449

An improved gaussian fitting method used in light-trap center acquiring

XU Zhongyu[1,a] ZHENG Hongyan[1,b] YANG Hongyan[2,c]
[1]College of Computer Science and Engineering , Changchun University of Technology, Changchun 130012,China
[2]Jilin Vocational College of Industry and Technology, Jilin 132000,China
[a]xuzhongyu01@126.com, [b]hongyankkf@163.com, [c]jlyanghongyan@126.com

Keywords: Extraction of light stripes center, Parabolic fitting, Gaussian curve, Line structured light

Abstract. In the 3D measurement based on line-structured light projection, the accuracy of center position of the stripe is of great importance for that of the 3D information acquisition system. A method of sub-pixel center-extracted that in the level of sub-pixel were discussed by He Jun-ji. Based on it and considered the fact that light intensity of the stripes center presents a Gaussian distribution status approximately, in this paper, a new method for extracting stripe center line has been proposed. The extracting curve is closer to the ideal value, and can efficiently extracted the center-line of light stripe, and the accuracy of 3D reconstruction is improved.

Introduction

Structured light 3-D vision ,with the advantages of high accuracy, large range and easy to extract the information of the light , has been used more widely and importantly, especially in the measurement of deformable contour surface of the object [1].The structured light detection is non-contact ,in the detection process, the laser emitted the illumination to the object surface, the structured light will change following the depth of the surface changes, which produces distortion[2]. Detection of structured light strip center location is the key part of structured light vision inspection technology [3],the structured light strip center extraction accuracy will directly affect the accuracy of the entire structure of the optical detection system.

This paper based on the previous He Jun-ji's Gaussian fitting method and proposed a new method to improve the poor noise immunity problem, and this method won't increase the amount of computation significantly.

A Gaussian model fitting method

In this paper, the experimental system consists of five components: the laser, the measured object, CCD camera, frame grabber and a computer. The structure of the experimental system are shown in Figure 1：

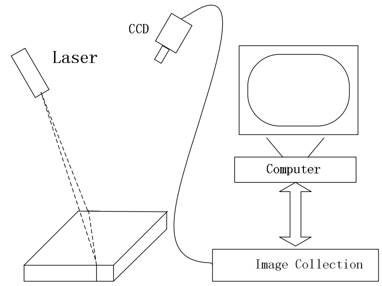

Fig.1 Line structured light vision inspection system model diagram

As shown in Figure 1 ,the light beam emitted by the laser hits the surface of the object to form a light bar, scattered light is received by the CCD camera and the changes in the scattered light is measured through the depth of the surface while being modulated, that original structure light optical distortion occurred.

As shown in Figure 2, the vertices of a Gaussian cross-section denoted the optical center.

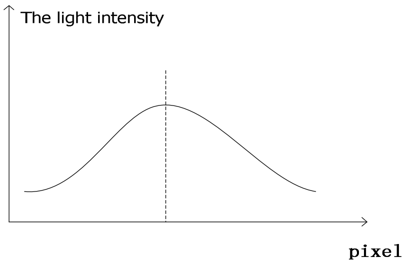

Fig.2 Light intensity distribution of the light-handed cross-section schematic

An optical cross-section is analysised below, the above graph is fitted by n groups of data. These data is consisted of the n coordinates (x, g), x demonstrates the coordinates of the pixels in the CCD camera, and g is the light intensity of the pixels. The equation of the figure above is:

$$g = ke^{-r(x-u)2}. \tag{1}$$

Logarithm on both sides of the equation :

$$y(x) = \ln g(x) = \ln k - r(x-u)^2. \tag{2}$$

$$y(x) = \ln k - rx^2 + 2rux - ru^2. \tag{3}$$

We set

$$y(x) = a_0 + a_1 x + a_2 x^2. \tag{4}$$

Then the above formula is transformated into a quadratic polynomial, compared (3) with (4),we can get results below:

$$a = \ln k - ru^2. \tag{5}$$

$$a_1 = 2ru. \tag{6}$$

$$a_2 = -r. \tag{7}$$

When fitting a polynomial $y(x)$, we firstly take the logarithm of light intensity $g(x)$, then use Matlab simulation software to fit ogarithmic number into quadratic polynomial, and obtain $y(x)$. The factor a_0, a_1, a_2 is determined along with it . Use the above equations(5) (6) (7) to obtain k, r, u, and finally the Gaussian curve equation can be obtained naturally:

$$\mathrm{g} = ke^{-r(x-u)^2}. \tag{8}$$

So that we can get the center position of the curve:

$$\mathrm{u} = -\frac{a_1}{2a_2}. \tag{9}$$

Gaussian fitting method steps are as follows:

1) First, to determine the direction of the light bar cross-section.
2) Find light bar cross section and choose n points(x,g) as Gauss cross section curve overfitting points.x is horizontal axis direction.

3) Calculate the value of u, based on the results of (2)
4) Repeat three steps above, and calculate the center point in other cross section of the light bar.
5) We can overfit the position of the whole light bar, basing on the center point of different light bar cross section.

Repeating (1)~(5),until we get the satisfying result.

The improved Gaussian distribution curve fitting method

The article above describes the traditional Gaussian distribution curve fitting method,in this method,we should collect n coordinate points that consisted of the x coordinate of pixed and the the light intensity g.In this way,the light intensity distribution of the light bar cross section which presents the ideal Gaussian distribution curve before,will change.

Table 1 shows the light bar center and the standard error of this four line,using the two methods described above.From the data in the table,we can see that the light bar center that got from the improved Gaussian distribution curve method is different from the other one.It has higher precision.

Table 1 The light bar center and standard error comparison of the two methods

Row	Light bar center of the original method	Standard error	Light bar center of improved method	Standard error
319	654.341	0.018	654.541	0.014
327	653.956	0.016	653.789	0.013
341	654.465	0.013	654.568	0.012
364	653.871	0.014	654.679	0.010
378	654.279	0.015	654.357	0.011

Experiment

Figure 3 is the light bar image of the structured-light vision system.

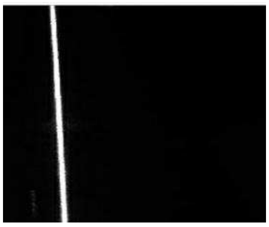

Fig.3 Light bar image

The steps to get the light bar center curve are as follows:

1) To determine a light bar cross section,that is the horizontal coordinate x of the light bar image pixel.
2) In the light bar cross section determined before,get the light in tensity value $g(x)$ every same interval.
3) Take the logarithm of the light in tensity chosen before,then we get the logarithm value $y(x) = \ln g(x)$.To abandon the saturated points mentioned above ,we abandon $y(x)$ that has the same maxium value.
4) Use (9)to calculating the light bar center in one of the light bar cross section.
5) As the four steps described above,the light bar center coordinates of different light bar cross section (x,u) will change as the x value changing.

Figure 4shows the four conditions of Figure 3before and after the light bar image combined with noise,before and after the light bar image abandoned the saturated points

(a) Before combined with noise and before abandoned the saturated points

(b)Before combined with noise and after abandoned the saturated points

(c) After combined with noise and before abandoned the saturated points

(d) After combined with noise and after abandoned the saturated points

Fig.4 Light bar center changing curve

To demonstrate the noise immunity ability of the improved light bar center extracting method,we will carry on the experiment after combining noise with the light bar image center. Finally,we can draw the conclusion that compared with the method did not abandon the saturated points ,the improved light bar center extracting method by abandoning the saturated points has better noise immunity ability,and has higher precision.The improved Gaussian distribution curve method can extract the light bar center more accurately.

Conclusion

This article proposes an improved light bar center extracting method.This method abandons the saturated points during the curve overfitting process,and it improves the original Gaussian distribution curve method.Using this method we can extract the light bar center more accurately,and get more satisfied result.

Reference

[1] G.J.Zhang,H.Wang,H.J.Zhao,"Structured Light 3-D Version" ,Acta Aeronauticaet Astronautica Sinica,Vol.20,No.4,July,365-367,1999. (In Chinese)

[2] F.Q.Zhou,Q.Chen,G.J.Zhang,"Composite Image Processing for Center Extraction of Structured Light Stripe",Journal of Optoelectronics·Laser, V0l.19 No.11,November,1534-1537,2008. (In Chinese)

[3] S.Y.Gao,K.Z,Yang, "Research on Central Position Extraction of Laser Strip Based on Varied-boundary Gaussian Fitting", ChineseJournal of Scientific Instrument,Vol.32,No.5,May,1132-1137,2011.(In Chinese)

Applied Mechanics and Materials Vol. 596 (2014) pp 453-456
© (2014) Trans Tech Publications, Switzerland
doi:10.4028/www.scientific.net/AMM.596.453

Computer Vision Application and Research on the One-dimensional Body Mass Precision Measuring Device

Shuyan Nie [1,a],Changqi Yang [1,b]

[1]Aeronautics and Astronautics College， Chongqing University,Chongqing, 400030, China

[a] nieshuyan@163.com, [b]ycq3664@163.com

Keywords: Human Inertia Parameters,camera calibration,Computer vision

Abstract. The human body segment inertia parameters is the research of biological mechanics and solid mechanics.And its mechanical device research is the fields of machinery and automatic control.In this paper,we solved the distance measurement of the human body link points,and that is to say we solved automatic recognition and high precision positioning of the human body link points in the one-dimensional Body mass precision measuring device,and verify the feasibility of application of computer Vision in link points measurement in the one-dimensional Body mass precision measuring device.

Introduction

The one-dimensional body mass precision measuring device is a high automatic and precision device of the human body inertia parameters measurement. Human body can be divided into several parts (link) such as head, torso,legs and so on according to the principle of human body movement and mechanics. The weight, center of gravity, rotational inertia of inertial principal axis of center of gravity are referred to as inertia parameters.Because of the high speed development in the field of automatic control and computer vision,we need automatic control device of inertia parameter measurement of human body parts more and more pressingly. In the device,the principle of computer vision is related to fast and high-precision positioning on each link point of human body. The precision of recognition has a huge influence on the precision of the whole system,and is one of a important part of automatic control measurement device research.

Three-dimensional reconstruction

By Zhengyou Zhang's theories[1],we know Image Coordinate System and the World Coordinate System of scenery have a relationship:

$$\eta\begin{bmatrix}u\\v\\1\end{bmatrix}=\begin{bmatrix}\alpha&0&u_0\\0&\beta&v_0\\0&0&1\end{bmatrix}\begin{bmatrix}f&0&0\\0&f&0\\0&0&1\end{bmatrix}\begin{bmatrix}r_{11}&r_{12}&r_{13}&t_1\\r_{21}&r_{22}&r_{23}&t_2\\r_{31}&r_{32}&r_{33}&t_3\end{bmatrix}\begin{bmatrix}X_W\\Y_W\\Z_W\\1\end{bmatrix} \tag{1}$$

There,η is a constant,the first and second matrices are the internal camera parameters,the third matrix is the rotation and translation matrix of World Coordinate System.

From the Fig.1 ,we can get the physical significance of the formula (1).

We observe n images we have taken previously and do camera calibration, and then we can get internal matrix of the camera .

According to the mathematical model of the two cameras(as Fig.1),we can get that point P of World Coordinate System converts to the two Camera Coordinate Systems as following,

$$P_1=R_1P+T_1\ ,\quad P_2=R_2P+T_2 \tag{2}$$

There, P1 and P2 are the projections of point P in the two Camera Coordinate Systems respectively.

If the rotation matrix of the right camera coordinate system to the left camera coordinate system is R,and the translation matrix of the right camera coordinate system to the left camera coordinate system is T,have

$$P_1 = RP_2 + T \tag{3}$$

From (2) and (3),we can get

$$R = R_1 R_2^{-1} \quad T = T_1 - RT_2 \tag{4}$$

From(4),we can calculate P and this is the point we need,then we can restore the three-dimensional images on the world coordinate system.

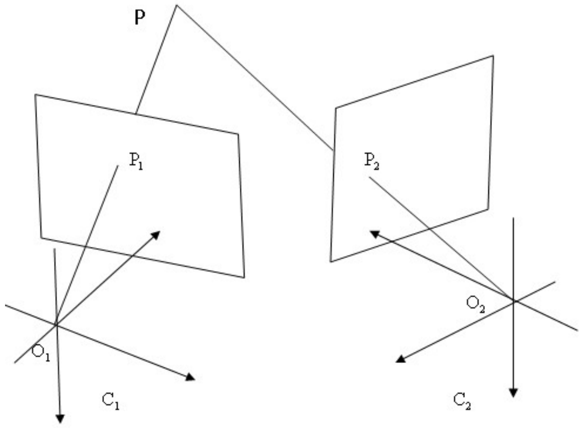

Fig.1 Binocular vision geometric model

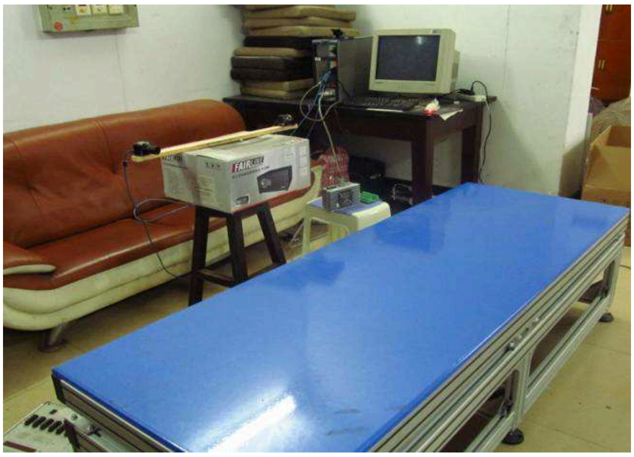

Fig.2 One-dimensional body mass measuring device

Computer vision application on automatic control device

The available hardware measuring objects are used in the experiment base on the difference of every human body parameters and the immeasurability of every human body parameters.A measurable carton is used as the measure in the experiment and we take photos by means of image acquisition device(model：MINTE 300A).We extract angular point on the photos by Harris corner extraction algorithm.

According to the size of the angle of the Harris corner point, we get the angular point partial inhibition and get the effect picture(Fig.3).In the picture,the two black and white circular logos are designed by computer recognition related theory[2]. We segmentation the image and extraction contours using Roberts operator, then identify roundness using Hoff image transformation and identification methods.There,the points in the red rectangle are the target angular points in the Fig.3.

In the experiment, the one-dimensional body mass precision measuring device is shown in Fig2 .Among the device,the force sensor is JLBS-10KG and the motion control card is DMC2210.

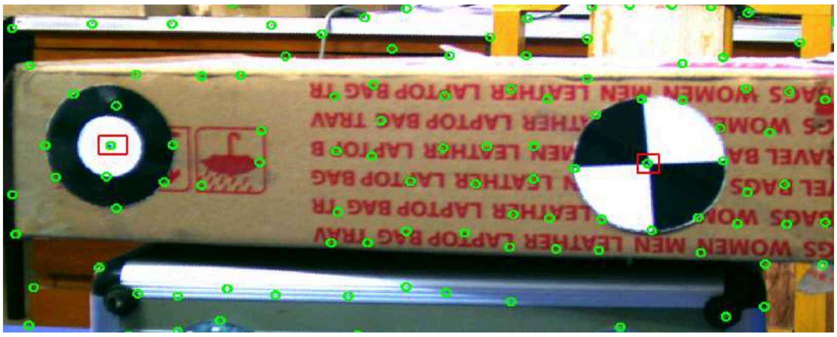

Fig.3 The exhibition of target point extraction

Based on above, we can get coordinates of target point of left and right cameras. According to the calibration parameters and matrix R and matrix T in the camera binocular calibration results,we can calculate the real space coordinates in the World Coordinate System, then get distances and angles of the two link points.Through the device in Fig.2,we can get the human body segment parameters.

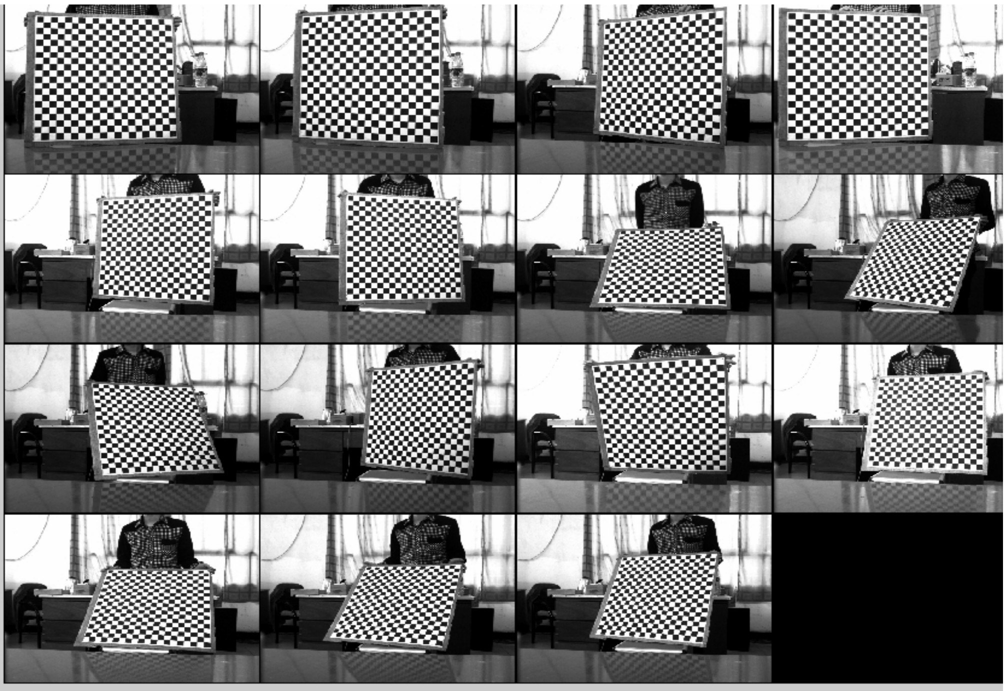

Fig.4 Different Angle calibration images of left camera

Calibration parameters as following:

The left camera：

Focal Length：fc = [2489.332859829952700 ; 2485.748396138551000];

Principal point：cc = [992.736342367981250 ; 688.130918510408610];

Distortion：kc = [-0.102317833347308 ; 0.141448289608514 ; 0.000543346214038 ; -0.000765638208968 ; 0.000000000000000];

The right camera：

Focal Length：fc=[2292.7094480 ;2287.704123515];

Principal point：cc = [1028.357283048636600 ; 627.526381014496450];

Distortion：kc = [-0.160113855138534 ; 0.410651880745128 ; -0.004228907359806 ; 0.007862209007898 ; 0.000000000000000];

The relative rotation matrix R and translation matrix T：

$$R=\begin{bmatrix} 0.8385 & 0.0002 & 0.5398 \\ -0.0004 & 0.9898 & 0.0062 \\ -0.5407 & -0.0066 & 0.8284 \end{bmatrix} \qquad T=\begin{bmatrix} -685.0328 \\ -52.0156 \\ 177.1377 \end{bmatrix}$$

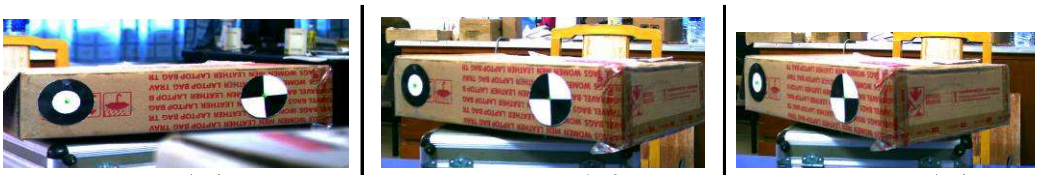

Group1left Group2left Group3left

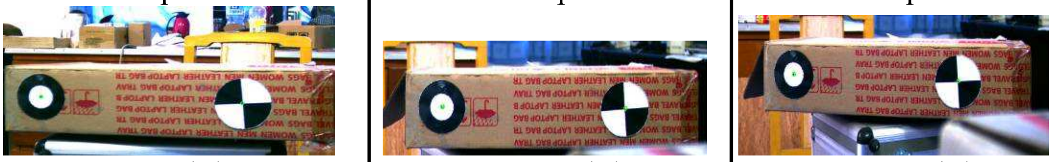

Group 1 right Group 2r ight Group 3 right

Fig.5 Experimental verification pictures of left and right cameras

As the Fig.4, We took three groups images in different angles (Fig.5). In the Fig.5, Group1left means the image is the first group in the left camera.And the green circle in the picture is the target point. We get the data as Table 1.

Table1.The experimental data and results

	The left camera images		The right camera images		distance mm）	Error %）
	The left angular point of picture Pixel）	The right angular point of picture Pixel）	The left angular point of picture Pixel）	The right angular point of picture Pixel）		
Group1	417，943）	1004，935）	1173，973）	1622，909）	280.8796	0.3787
Group2	367，926）	839，921）	947，985）	1529，926）	279.6439	0.0629
Group3	297，913）	681，919）	717，980）	1354，939）	279.1698	0.0232

There, the real manual measuring distance is 279.82mm.

From the errors, We know we have got the good experimental results.So computer vision measuring distance can be used in the one-dimensional Body mass precision measuring device, can solve the tedious manual measurement steps effectively, can reduce requirements of personnel's professional an important problem in engineering application.

Acknowledgements

This research was supported by National Sports Research project of China under grant NO.2011B045.

References

[1]Zhenyou Zhang. A flexible new technique for camera calibration[J] . IEEE Transactions on Pattern Analysis and Machine Intelligence, 2000,22(11) :1330- 1334,in Chinese.

[2]Guoge Hang, Xiaodong Cai. Binocular CCD calibration in MATLAB[J]. Journal of Shanghai engineering and technology university,2010,24(1),in Chinese.

[3]Yepeng Guan,Linsu Tong. Feature points Rapid extraction algorithm in two-dimension picture[J].Journal of Image and Graphics,2012,7(12):1296-1301.

[4]Ouyang Cheng, Guangzhi Wang, Quan Zhang ,Kang Wei, Ding Hui. Evaluating Harris Method in Camera Calibration. Engineering in Medicine and Biology Society, 2005, 27:6383-6386.

[5]Yepeng Guan,Linsu Tong. Binocular stereo vision measurement methods research[J].Journal of instrument,2003,24(6):581-588.

Applied Mechanics and Materials Vol. 596 (2014) pp 457-462
© (2014) Trans Tech Publications, Switzerland
doi:10.4028/www.scientific.net/AMM.596.457

Hydrocarbon Micro-seepage Anomalies Detection Algorithm Based on FPCS for Hyperspectral Remote Sensing Data.

Zhuoli He[1, a] , Xiaolian Deng[1,b*] and Simin Ai[1,c]

[1] College of Science, China Three Gorges University, Yichang, 443002, China

[a]hezhuoli_1113@163.com, [b]dengxiaolian@gmail.com, [c]aisimin2005@163.com

Keywords: Hydrocarbon micro-seepages, Mineral alteration, FPCS , Band ratio method

Abstract. Long-term hydrocarbon micro-seepages develop diverse arrays of chemical and mineralogical changes in rocks and soils. We called this change mineral alteration. Mapping this mineral alteration is thus a potential tool for hydrocarbon exploration. The surface changes caused by hydrocarbon seepage can potentially be detected by remote sensing techniques. In this paper, we discussed some methods which can heighten the altered mineral on the map. The feature-oriented principal component selection (FPCS) and band ratio method collaborated together in extracting the abnormal area. SASI airborne hyperspectral data of Xifeng oilfield which located in southern Ordos Basin were used in this experiment . The experimental results show that the methods adopted in this paper have a good advantage of detecting surface anomalies and alternations associated with oil and gas information.

Introduction

Remote sensing technology used in oil finding directly has nearly 20 years history in our country. Various techniques including geochemical, geophysical and remote sensing method prove that specific alteration minerals have relationship with oil and gas information. Hydrocarbon micro-seepage theory is considered to be the basic theory to guide oil exploration by remote sensing method. Hydrocarbon micro-seepages[1] means hydrocarbons escape from underground reservoirs and changed the environment of surface. These changes include: bleaching of red beds, enrichment of ferrous iron-bearing minerals , radioactive anomalies, clay mineralization, carbonate cementation, magnetic anomalies, vegetation anomalies and so on[2].

As the development of remote sensing, hyperspectral data sensors have higher spatial resolution and better spectral resolution than multispectral sensors. Beijing institute of nuclear industry did the flight experiments to get the CASI/SASI data of Keping county Sinkiang province. Fawang Ye et al. applied part of the data did some experiment[3]. Under the precondition of field measured spectral data, they extracted the uranium deposits related alteration information. The emergence of airborne platform hyperspectral sensors make local small regional detailed research possible. SASI data has a total of 101 bands and the spectrums range from 950~2450(nm) which are sensitive to a range of geologically important minerals. 15 nm spectral resolution and spatial resolution of 1.8 nm improved the precision of mineral mapping.

Research Methods and Principles

Traditional Method. For multispectral data to explore oil, there are many methods such as band ratio[4], principle component analysis (PCA), band fusion and so on. These method are mainly used to enhance hydrocarbon micro-seepages information which present in the earth's surface, namely it is also based on the spectral features of ground objects. The methods mentioned above also can be applied to the hyperspectral data. As a general rule, spectrum matched filtering method[5] is the best choice for hyperspectral data because of its high spectral resolution. There are many spectral matching ways such as spectral angle mapping (SAM), spectrum feature fitting (SFF), binary encoding (BE) , etc. The principle of spectral matching is that compared the unknown spectrum with the standard spectrum which come from the USGS spectral library. If the spectrum reconstruction of hyperspectral data is not good enough, then spectral matching method is no longer applicable.

Principles of FPCS. To better understand the principle of FPCS, you should make sure what is the PCA and how to analysis the statistic of PCA. One of the purposes of PCA is dimension reduction and another is to get rid of the relations of each image band. Analyzing the eigenvectors of PCA, each value of the eigenvector is different, parts of the value are positive numbers while some are negative. These differences make different principal components have a preference for certain band so that some of the PCs are powerful for detecting mineralogical alterations which associated with hydrocarbon micro-seepages. In short, FPCS aimed to find out which principal component correspondingly enhance the mineral alteration we concerned. The process of principal component analysis can be described as follows. Image linear transformation is described below:

$$Y = TX \tag{1}$$

X represents the image data matrix before transformation, while Y represents the after transformed image data matrix. transformation matrix indicated as T. when the linear transformation is PCA, matrix T usually be a orthogonal matrix which was treat as the eigenvector of Correlation coefficient matrix of the original image data X. Assume that the image have a total of n bands and the number of pixels in each band are m. reshape the several band image into a matrix of m rows and n columns. You can see the X at expression (2).

$$X = \begin{pmatrix} x_{11} & x_{12} & \cdots & x_{1n} \\ x_{21} & x_{22} & \cdots & x_{2n} \\ \vdots & \vdots & \ddots & \vdots \\ x_{m1} & x_{m2} & \cdots & x_{mn} \end{pmatrix} = [x_{ij}]_{m\times n} \tag{2}$$

The process of feature-oriented principal component selection have three steps:

Step 1: Data standardization

$$S_{ij} = (x_{ij} - \overline{x_j}) / \sigma_j \tag{3}$$

$$\overline{x_j} = \sum_{i=1}^{m} \frac{x_{ij}}{m} \tag{4}$$

$$\sigma_j = \sqrt{\frac{\sum_{i=1}^{m} (x_{ij} - \overline{x_j})^2}{m-1}} \tag{5}$$

S_{ij} is Standardized data, $\overline{x_j}$ represent the average of the j band. σ_j represent the standard deviation of the j band.

Step 2: Calculating the correlation matrix R

$$r_{ij} = \frac{\sum_{k=1}^{m} (x_{ki} - \overline{x_i})(x_{kj} - \overline{x_j})}{\sqrt{\sum_{k=1}^{m} (x_{ki} - \overline{x_i})^2 \sum_{k=1}^{m} (x_{kj} - \overline{x_j})^2}} \tag{6}$$

Function (6) can calculate the correlation coefficient of any two wavelengths.

Step 3: Analyze the eigenvector U_i

$$(\lambda_i I - R)U_i = 0 \tag{7}$$

Equation (7) can solve the eigenvalue (λ_i) and eigenvector (U_i)of R. Then transpose the matrix U , we can get the transformation matrix T. Analyzing matrix U, it is easy to find out which principal component got the power to enhance the mineral alteration information.

After the three steps listed above, FPCS come to the end. It is the foundation of the further extraction of oil and gas information.

Experimentation

Geological Setting. The experimental data is SASI airborne hyperspectral data which was taken from Xifeng oilfield in southern ordos basin. Experimental area predominantly with large, stocking concealed lithologic reservoir. Due to geographical and climate features, natural vegetation are different when changes with the seasons, mainly for all kinds of shrubs, sagebrush plants and crops, etc. The type of sandstone filler content are various, mainly for the authigenic clay mineral and cement. Clay minerals mainly composed of hydromica and chlorite, cement mainly include calcite[6].

Alteration Mineral and Its Spectral characteristics. The wavelength of SASI data range from 0.9(um) to 2.5(um). this range of wavelength is sensitive to iron-compounds, ferrous-compounds, clay mineral and carbonate. Spectral characteristics of altered minerals listed in Table 1.

It is easy to notice that from 0.9(um) to 2.5(um), most of clay minerals have a strong absorption properties near 2.2(um) but chlorite have a strong absorption at 2.3(um). Carbonate just like calcite and magnesite show intense absorption characteristic at 2.3~2.35(um). Iron-compounds have a steep slope when cross 0.9~1.5(um) while ferrous compounds show stable performance. Most of the ferrous compounds like pyrite and magnetite have very low reflection in the whole wavelength range but siderite have a reflection peak at 2.13(um).

Table 1 Absorption and reflection characteristics of altered minerals

Micro-seepage phenomena	**Altered Minerals**	**Absorption Characteristics (um)**	**Reflection Characteristics(um)**
Clay	Chlorite,illite, kaolinite	2.2, 2.3-2.34, 2.38-2.4	2.0
Unaltered red beds	Goethite,hematite, jarosite	0.9, 2.44	2.13
Ferrous-compounds	Pyrite,magnetite, siderite	1-1.5	2.13
Carbonate	Calcite,rhodochrosite, magnesite	2.3-2.35	2-2.2, 2.4

Data preprocessing. Hyperspectral image preprocessing basically includes geometric correction, radiation correction and atmospheric correction. Geometric correction and radiation correction were done by the system comes with software. ENVI fast atmospheric correction module can eliminate the influence of the atmosphere. Choosing high quality bands for PCA is a key factor, it determined the accuracy of the results. At the same time it can reduce data redundancy and data computation. Four principles of band selection is described below.

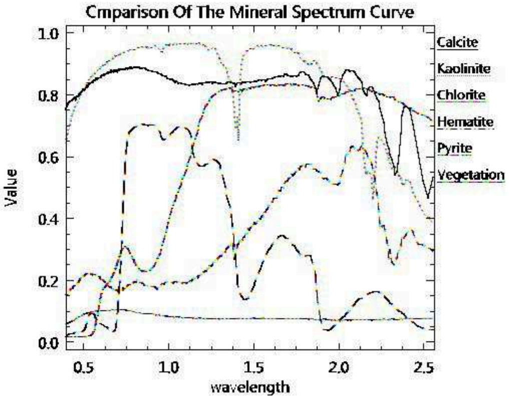

Fig. 1. Comparison of the mineral spectrum curve

(a). Avoiding the atmospheric absorption window at 1.356~1.406(um) and 1.820~1.931(um) wavelength;

(b). Uniform sampling, make sure sampling interval neither too intense nor too loose;
(c). Smaller band mean differences and bigger standard deviation;
(d). Select the band at characteristic peak of the altered mineral (reflect or absorb peak).

Comparing and analysing all of the targeted mineral standard spectrum curve in Fig.1, we find that the typical altered mineral such as chlorite, calcite, hematite, pyrite and vegetation show different reflectance at the near infrared, short wave infrared and intermediate infrared. Ten bands were selected from the 101 bands according to the four principles above. These bands have a higher signal-to-noise ratio and sensitive to the target minerals.

Extraction of Alteration Information. In this paper, the feature-oriented principle components selection (FPCS) and band ratio method used together to extract the alteration information. That is to say, firstly using FPCS to enhance general information, then band ratio method used to extract the accurate information.

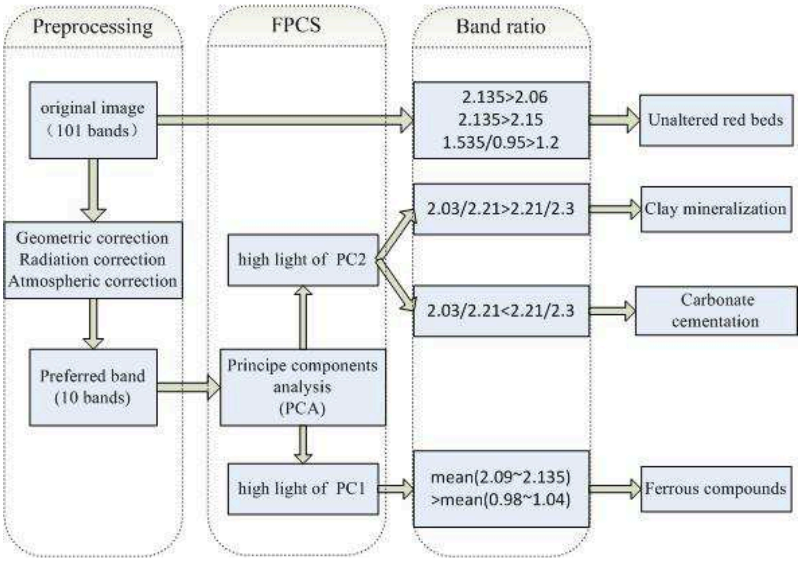
Preprocessing
FPCS
Band ratio
original image
(101 bands)
Geometric correction
Radiation correction
Atmospheric correction
Preferred band
(10 bands)
high light of PC2
Principe components
analysis
(PCA)
high light of PC1
2.135>2.06
2.135>2.15
1.535/0.95>1.2
2.03/2.21>2.21/2.3
2.03/2.21<2.21/2.3
mean(2.09~2.135)
>mean(0.98~1.04)
Unaltered red beds
Clay mineralization
Carbonate
cementation
Ferrous compounds

Fig. 2. Experiment process

Firstly, the PCA analysis was performed on ten bands which were screened out through many steps. Original image was projected onto the eigenvector to form the new image. We call the first band of new image PC1, the second band PC2. As this way, the last band named PC10. The result of FPCS showed that high DN value of PC1 enhanced the ferrous compounds while high DN value of PC2 enhanced the clay and carbonate. Iron-compounds couldn't be directly detected by PCA means, but it's reflectivity increase quickly at the wavelength range from 0.9(um) to 1.3(um) and there is a reflection peak at 2.13(um). So the iron-compounds can be extracted by band ratio method. The spectral curve of the carbonate and clay looks similar method. The experimental process can be seen in Fig.2.

Experimental Results and Analysis

The Experimental Results and Instructions. Resizing a small piece of image data from Xifeng oilfield as the experimental data. After FPCS, the first principal component and the second principal component eigenvectors are shown in Table 2.The integrated use of FPCS and band ratio method extracted out clay minerals abnormity, carbonate mineralization halo, red bed degradation, accumulation of ferrous-compounds. The final result show in Fig.3.

Table 2 Eigenvector of PC1 and PC2

PC name	Band name									
	Band 1	Band 2	Band 3	Band 4	Band 5	Band 6	Band 7	Band 8	Band 9	Band 10
PC1	-0.30	-0.31	-0.31	-0.32	-0.32	-0.33	-0.32	-0.32	-0.32	-0.31
PC2	-0.51	-0.40	-0.39	0.18	-0.08	-0.04	0.34	0.20	0.32	0.36

Analysing the eigenvectors of PCA which was shown in Table 2, The data from the eigenvector of PC1 are similar negative numbers. Projecting the image onto this eigenvector is equivalent to calculating the average of all bands. This move isolated the substances with lower overall reflectance, so the high light of PC1 enhanced ferrous-compounds and other low reflectivity material. Band ratio method can help to extract the ferrous-compounds. Chlorite as a typical clay mineral contained in the soil. It has lower reflectance in the near infrared band but higher reflectance in the short wave infrared and intermediate infrared. This is exactly the opposite characteristics of vegetation. So the PC2 largely isolated vegetation and minerals. Then considering the characteristics of clay minerals and carbonate mineral absorption peak, using band ratio method to distinguish clay and carbonate.Look at the mineral mapping results in Fig.3, the legend in the figure illustrates which color represent the corresponding minerals. The four alteration mineral show its spectrum curve in Fig.4. Due to various reasons, the actual spectrum have a gap with the standard curve come from the USGS Spectral library, but the characteristics at 2.0-2.5(um) is roughly consistent.

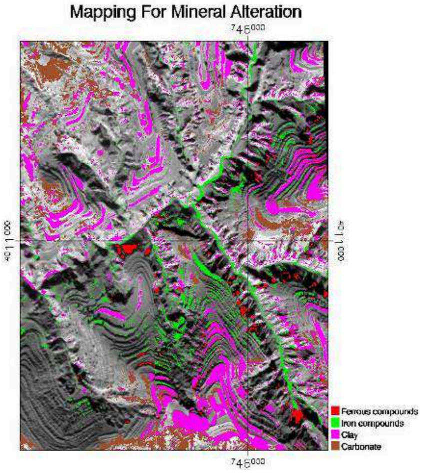

Fig. 3. Altered mineral mapping.

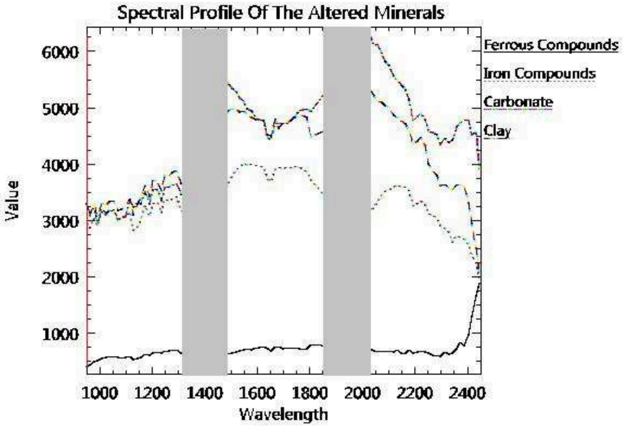

Fig.4. Actual spectrum of the altered minerals.

Conclusion

The traditional principal component analysis (PCA) and band ratio method have exposed some defects when used alone. Using one of the methods alone can't extract materials with similar spectrum, more or less there will be some erroneous judgment. Using band ratio method on the basis of the FPCS can effectively extract the targeted minerals. The absorption and reflection peak of the actual detected alteration mineral is consistent with standard spectral curve. In summary, the method applied in this paper is feasible.

Acknowledgment

This paper is sponsored by geological survey projects of China Geological Survey (1212011087112, 1212011120302). Thanks for their Remote Sensing data and fund support.

Reference

[1] Guo Defang, hydrocarbon micro-seepage and information Extraction, Remote sensing of environment, 10(1995),pp.124-131 (In Chinese)

[2] A. Petrovic*, S.D. Khan, H.S. Chafetz, Remote detection and geochemical studies for finding hydrocarbon-induced alterations in Lisbon Valley, Utah, Marine and Petroleum Geology, 25 (2008),pp.690-705

[3] Ye Fawang, Liu Dechang, zhao Yingjun, Airborne hyper-spectral survey system CASI/SASI and its preliminary application in uranium exploration, World Nuclear Geoscience, 28(2011),pp.231-236 (In Chinese)

[4] Chen Weirong, Guo Defang, Lan Yuqi, The Application of Band Ratio Composite And Feature- oriented Principal Component Selection in the Extraction of oil-gas Signature," Remote Sensing Technology And Application, 10(1995), pp.33-39 (In Chinese)

[5] Bai Jiwei, "The Study on the Spectral Mapping Technique Based on the Hyperspectral database," Beijing: The Chinese academy of sciences (2002) (In Chinese)

[6] Wu Xianghua, "Detection and evaluation of the minor leakage of oil gas in the area of Xifeng, Erduoshi Basin," Chengdu: Chengdu University of Technology (2011) (In Chinese)

Applied Mechanics and Materials Vol. 596 (2014) pp 463-467
© (2014) Trans Tech Publications, Switzerland
doi:10.4028/www.scientific.net/AMM.596.463

Landing Point Predicting Method in Target Re-entry Measurement

Xiaoyong Li, Weikang Zhu, Jinbiao Zhou, Guiming Chen,Lei Yang, Huihua Wu

Joint Laboratory, China Spacecraft Maritime Tracking and Control Department,

Jiangyin, Jiangsu, 214431, China

xyli212@163.com

Keywords: reentry measurement, landing point predicting at sea, atmospheric model, optimum initial integration value, minimum integration step width

Abstract. By introducing some atmospheric models and selecting methods for minimum integration step size and optimum initial integration value, a program of real time and near real time landing point predicting together with weighted processing methods of many groups of landing point parameters were put forward. Engineering application showed: the above methods and program improved real time and near real time landing point predicting precision more greatly compared with previously used methods, which had proved their broad applicability.

Introduction

In target reentry measurement, it is necessary to predict target landing point parameters. By applying target space motion differential equations, according to the known initial orbital parameters, aerodynamic parameters, physical parameters, orbit integration predicting was performed and target parameters [1] were computed via orbital parameters at height h near 0. Runge - Kutta - Gill method was commonly used in integration calculation.

When the target is flying in space, it would be affected by various factors, thus lots of error sources arise. Different types of errors have different influences on target landing point predicting, hereafter are the detailed introduction of these error sources.

Model errors mainly refer to simplified errors of the target space motion equations and the approximation errors of the numerical solution for these equations.

Initial integration errors refer to the difference between measured values and the true values of the target position and velocity, which mainly reflect the measurement errors of measurement equipments and errors in measurement data preprocessing methods.

Atmospheric model errors, where some basic parameters about atmosphere are atmospheric density ρ , atmosphere temperature T_M and atmosphere pressure P. Herein the errors between selected atmosphere models and the actual atmosphere conditions together with acoustic velocity are collectively referred to as atmospheric model errors.

This paper intends to raise some methods to improve target parameter precision against above error sources.

Atmospheric models

Hereafter we give some introductions to these models [2]and analyze which is better to be applied to landing point predicting.

Tabular Atmospheric Model. In target motion equations for parameter prediction, the following atmospheric parameters are directly used, they are atmospheric density ρ , acoustic velocity av and acoustic velocity av

Tabular atmospheric model is so called because the parameters ρ , av are expressed in the form of table functions as

$$\rho_i = f_1(h_i)\rho_0 \tag{1}$$

$$av_i = f_2(h_i), \tag{2}$$

where ρ_0 refers to standard value of sea-level atmospheric density, h_i is the height of the target, i=1,2,3……, and $h_i < h_{i+1}$.

Hierarchical Fitting Atmospheric Models. In this model, av is expressed in the form of hierarchical fitting polynomial, and atmospheric density ρ is also given by equation (1). Hierarchical fitting polynomials of acoustic velocity av at several heights are listed in Tab. 1.

Tab. 1 Hierarchical fitting polynomials of acoustic velocity av

h (km)	Fitting polynomial	Coefficients	h (km)	Fitting polynomial	Coefficients
0	340.9		31.7~35.0	$a_2+b_2h+c_2h^2$	a_2 =722.5 b_2 =-0.02770 c_2 =4.520*10^{-7}
0~10.0	a_0+b_0h	a_0 =341.3 b_0 =-3.945*10^{3}	35.0~50.0	a_3+b_3h	a_3 =181.2 b_3 =0.003604
10.0~11.7	$a_1+b_1h+c_1h^2$	a_1 =409.7 b_1 =-1.779*10^{2} c_1 =7.333*10^{-7}	50.0~60.0	360.7	
11.7~31.7	298.6		60.0~80.0	a_4+b_4h	a_4 =587.5 b_4 =-0.003750

Analytical Atmospheric Model. In analytical atmospheric model, acoustic velocity av and atmospheric density ρ are given in the form of mathematics formula as

$$H = h/(1+h/R_0), \tag{3}$$

where H represents the height of target, R_0 is radius of the earth, which is 6256.766Km.Parameters ρ and av are calculated by the following equations:

$$T_M = T_{Mb} + L_{Mb}(H - H_b) \tag{4}$$

$$P = P_b \bullet (\frac{T_{M.b}}{T_M})^{\frac{34.1632}{L_{M.b}}}, \quad \text{when} \neq L_{Mb} \neq 0 \tag{5}$$

$$P = P_b \bullet e^{\frac{34.1632(H-H_b)}{T_{M.b}}}, \quad \text{when } L_{Mb} = 0 \tag{6}$$

$$\rho = \frac{P}{287.053T_M} = 0 \text{ ,When } h > 84.852 \text{, let } P = 0 \tag{7}$$

$$av = 20.0468\sqrt{T_M} \text{ , When } h > 84.852 \text{, let } T_M = 186.95 \tag{8}$$

The parameters L_{Mb}, H_b, T_{Mb}, p_b are shown in Tab.2.

Tab.2The values of parameters L_{Mb}, H_b, T_{Mb}, p_b

H Km	$L_{M.b}$	H_b	$T_{M.b}$	P_b	H Km	$L_{M.b}$	H_b	$T_{M.b}$	P_b
0~11	-6.500	0	288.2	1.013*10^{5}	32~47	2.800	32	228.7	8.680*10^{2}
11~20	0	11	216.7	2.263*10^{4}	47~51	0	47	270.7	1.109*10^{2}
20~32	1.000	20	216.7	5.475*10^{3}	51~71	-2.800	51	270.7	6.694*10

Precision Analysis of Atmospheric Models. Hereafter we made a comparison of the precision of parameters obtained by the three models and performed a lot of simulation calculations[3] of the effects of the three models on the precision of landing points.

From equations (1) and (2) we first got the parameters ρ and av computed by the three models in non node , where for tabular atmospheric model Runge -Kutta –Gill interpolation was used. Without considering the type of atmospheric models, by comparing the calculated atmosphere parameters with American Standard atmosphere 1976, analytical atmospheric model had higher precision with relative error less than 1*10-4, discontinuity in each segment joint was also minimal whose jump was less than 4*10-5.

By applying several groups of theoretical trajectory data under the height of 80km as integral initial value, we performed integration prediction and then computed its landing point and landing point errors. To compare the influences of atmospheric models on landing point precision, we assumed the errors were caused by atmospheric models, whose calculation results showed: landing point errors calculated by analytical atmospheric model was one severalth of the errors figured out by the other two models, therefore analytical atmospheric model was the best choice.

Minimum integration step size

The fewer the step size the fewer the truncation errors. But with decreasing of step size the steps in a certain range increase, which not only brings about more calculations but also accumulates surrounding errors, therefore we have to select steps for numerical solution of differential equations.

Real- time and Near real -time Landing Point Prediction Program. This program was initialized for the reason that one time prediction can not satisfy both the requirement for real-time measurement and the requirement for high precise prediction, where real time prediction was preformed for velocity requirement while near real time prediction for precision requirement. The two states were automatically switched over by the computer according to the landing time of the target.

In near real time prediction, to eliminate the effects of measurement data random errors on landing point parameters, after performing integration initial values filtering, weighted average processing was performed on several groups of landing point parameters. Weight coefficients were determined by measurement errors propagated on landing points.

Selection of Minimal Integration Step Length. Integration step length which meets the requirement of given accuracy is called minimal integration step length. We apply prior variable step length method to select near real time minimal integration step width, whereas we choose real time integration step size by enlarging each segment referring to near real time minimal integration step width.

The method of selecting step length by previously doubling or halving the selected step length before each mission is called prior variable step length method, which is completed by the following steps:

Firstly we apply this equation

$$\Delta = \left| y^{(\frac{\Delta h}{2})} - y^{(\Delta h)} \right|, \tag{9}$$

where $y^{(\Delta h)}$ and $y^{(\frac{\Delta h}{2})}$ respectively represent integration values obtained by starting from integration initial value and Δh and $\frac{\Delta h}{2}$ are regarded as the step length when the target height is 0.

Secondly we judge if the step size is appropriate according to Equation (9). Specifically, there are two cases:

For the given accuracy ε , if $\Delta > \varepsilon$, we compute by repeatedly halving the step length until $\Delta < \varepsilon$, when we get the minimal step width.

If $\Delta < \varepsilon$, we compute by repeatedly doubling the step width until $\Delta > \varepsilon$, when we get minimal step length by halving the step width once more.

Optimal integration initial value

To reduce the effects of errors on landing point prediction, integration initial value should be effectively selected.

By considering target motion equation is not precise, and both the measurement equipments' tracking performance and measurement data pre processing methods have effects on landing point precision, a group of parameters in the geocentric inertial coordinate system have been selected as optimal integration initial values.

Effects of Non Precision Target Motion Equation on Integration Initial Value. Assuming the target is a particle, and neglecting gravity of the sun, the moon and other planets on the target, such equation is derived as

$$\vec{a} = \vec{g} - K_t \rho C_n V^* \vec{V}_0^* \quad , \tag{10}$$

where $\vec{a}$ is target acceleration, $\vec{g}$ is gravitational acceleration, V^* is velocity of the target relative to air, $K_t = S_M / 2m$, m is the mass of the target, S_M is maximum cross-sectional area; C_n is coefficient of air resistance, which is the function of the height h and Mach M and expressed in table function, Mach M is the ratio of target flying velocity to local acoustic velocity av, which is written as $M = V / av$.

Projecting equation (10) onto the geocentric inertial coordinate system, we get the projection equation. During which, when $\vec{g}$ is projected on to the geocentric inertial coordinate system, it should be firstly projected on the earth's rotation axis ω and geocentric heavy line γ, whose components are respectively noted as $\vec{g}_\omega$ and $\vec{g}_\gamma$, we have

$$\vec{g} = \vec{g}_\omega + \vec{g}_\gamma \ . \tag{11}$$

Let the approximation of g_ω and g_γ be

$$\begin{aligned} g_\omega &\approx \frac{2\mu}{\gamma^4} \sin \Phi \\ g_\gamma &\approx \frac{f_M}{\gamma^2} - \frac{\mu}{\gamma^4}(5 \sin^2 \Phi - 1) \end{aligned} \quad , \tag{12}$$

where μ and f_M are constants, γ and Φ can be expressed as

$$\gamma = \sqrt{x^2 + y^2 + z^2} \tag{13}$$

$$\Phi = tg^{-1}(x / \sqrt{y^2 + z^2}) \tag{14}$$

Seen from above, the solutions of target motion equations are not precise for they are mixed with simplified errors and approximation errors. To reduce their influences on prediction precision, according to the error propagation theory, integration initial values should be those at lower height.

Effects of Measurement Equipments' Tracking Performance and Radio Wave Refraction Correction Method on Selection of Integration Initial Value. High precision measurement equipments should work at elevation angle neither too high nor too low thus to ensure high precision.

When radio measurement equipments are tracking at low elevations, atmospheric refraction errors are bigger than tracking errors of the equipments. In real time mission, we usually apply empirical methods to correct refraction errors which are applicable at higher elevations. If we use this method in low elevation refraction correction, the correction residuals are bigger and bigger with decreasing of elevation angle [4]. Therefore, we should not select integration initial values when the target is at too low position.

Taking equation (10) and (11) into account, we defined a range to select integration initial value, where, in real time landing point prediction, we selected groups of initial values including at shutdown point and obtained several groups of landing point parameters to provide for command and control; in near real time landing point prediction, we also chose more than ten groups of initial values and obtained the same groups of landing point parameters, after weight average processing we got a group of high precision landing point parameters.

Conclusion

In project application, the methods introduced in this paper greatly improved precision of real time and near real time landing point prediction, and near real time prediction accuracy was in agreement with the results of post data processing. The landing point prediction methods proposed in this paper, including atmospheric models, real time and near real time landing point prediction program, optimum integration initial value and minimum integration step length selection methods, together with weight processing method of several groups of landing point parameters, demonstrated to have broad applicability.

References

[1] Shuxing Feng, Shouxin Zhang. Landing Point Prediction and Precision Analysis of Spacecrafts' Returning Capsule[M].Changsha: Press of National University of Defense Technology,1996.(in Chinese)

[2] Peter H. Lauritzen, Christiane Jablonowski, Mark A. Taylor. Numerical Techniques for Global Atmospheric Models[M]. Lecture Notes in Computational Science and Engineering series,2011.

[3] Storz M F, Bowman B R, Branson M J I, et al. High Accuracy satellite Drag Model[J]. Adv.Space Rec.,2005,36(12):2497-2505.

[4] Yuxiang Zhang. New Methods for Low Elevation Atmospheric Refraction Correction[C]. Proceedings of the Seminar on Space Tracking and Control Technology,1999. (in Chinese)

Applied Mechanics and Materials Vol. 596 (2014) pp 468-471
© (2014) Trans Tech Publications, Switzerland
doi:10.4028/www.scientific.net/AMM.596.468

Study of Velocity Measurement Error Analysis and Improving Velocity Measurement Accuracy on High-speed Train

HOU Tao[1, a], FAN Duo-wang[1,b], NIU Hong-xia[1,c]

[1]Lanzhou Jiaotong University ,Lanzhou China,730070

[a]ht_sunny@aliyun.com, [b]fdw@mail.lzjtu.cn, [c]nhx56055@mail.lzjtu.cn

Keywords: High-speed Train;Velocity Measurement System;Error Analysis;Velocity Measurement Accuracy;Improved M/T Velocity Measurement.

Abstract. For the problem of a big velocity measurement error,analyzed the velocity measurement error and studied the method of improving velocity measurement accuracy for the velocity measuring system of high-speed train.In this analysis and method, the speed error analysis was carried out based on understand the characteristics of the high-speed train speed sensor, and found that there is a bigger speed error. Then discussed the influence of large errors of the control system, and put forward the improved M/T speed measurement method to solve the error problem. Finally, calculated velocity error for the improved M/T speed measurement method. The results show that the accuracy of speed has improved greatly. The research method can improve the accuracy to meet the requiring of train safety and smooth run.

Introduction

With the rapid development of high-speed railway, high-speed trains run faster and faster, which require the train control technology and control performance higher and higher. ATC[1-2](Automatic Train Control) is the core of rail traffic control system, which can ensure safety and smoothness of train running. Speed control of the high-speed train is an important part of ATC. Speed detection is the prerequisite of the speed control, speed detection accuracy directly affects the control accuracy. So, this paper combines the speed sensor features of the high-speed trains, analysis their speed error, and research the improve method of the speed detection accuracy. Finally providing technical support for the safety and smooth operation of trains.

Speed Sensor Features of High-speed Train

China's high-speed trains generally use two kinds of speed sensor to detect the speed, Hall wheel speed sensors and Doppler radar velocity sensors.The wheel speed sensor is more accurate at high speed, while Radar measurement is more accurate when the wheel spin or slip occurs at low speed[3,4].Using the two kinds of speed measuring equipmentat in the same time, which can achieve complementary advantages, get more accurate than a single speed sensor in detecting speed trains' running speed.In order to improve the reliability of the speed measurement system, each vehicle equipment is equipped with two wheel speed sensors and two radar sensors, shared by the two on-board equipment.In addition, and the four speed sensors have a common characteristic, output data is square wave pulse signal.

Speed Error Analysis of High-speed Train

By the characteristics of speed sensor,it is known that its speed sensors output signals are pulse. According to the principle of pulse speed measurement, the speed is based on the number of pulses over a period of time T(the sampling period) to calculate, the speed is faster for the more pulses at the same time, on the contrary,the slower.However,there is some deviation of pulse number when reading, because, by the moment of reading period, the read data can not exactly just read full pulse, as shown in Fig.1.

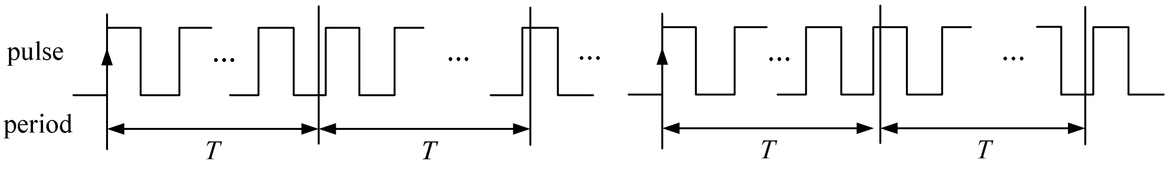

(a) Pulse Count 1 (b) Pulse Count 2

Fig.1 The diagram of impulse velocity measurement

Fig.1(a) and Fig.1(b) are showing that their starting point are accurate pulse count , but after a T, Fig.1(a) has not been reaching the next rising edge of a pulse (Generally based on the rising edge of the pulse count) , but very close to the rising edge of the pulse, In this case the actual total number of pulses should count less than the number of pulses of a pulse(See Fig.1(b) after the first T), that is,there is a pulse error in period.So,the calculated speed is smaller than the true speed value. But just after the rising edge of the pulse if the situation occurs in Fig.1(a) the end of the second T, then count the number of pulses than the actual number of pulses should count more than a pulse,the calculated speed is larger than the true speed value.It may exist a situation at the end of the two T, just close to the pulse rising edge in Fig.1(b), it is a possible that two pulses are missing counted.Thus it can be seen, when periodic pulse counting,there is at least exist the error of plus or minus one pulse, sometimes there are two pulse maximum error. Follow on, combined high-speed trains run actually situation, analysed the velocity error.

Error Analysis of Doppler Radar Velocity Sensor. Doppler velocity sensor output is a frequency pulse, the scan rate is general 1:1. In the mode of frequency output, the speed resolution may be set between 10Hz to 100Hz per km/h, Channel resolution can be set between 2.7mm to 27mm per pulse.Here,select standard pulse output,duty ratio is 1:1,4mm per pulse range resolution,and speed is proportional to the number of pulses. Pulse output updating rate is 1ms, that is, the sampling frequency is f=1000s^{-1}.It is supposed that the high-speed train at some time speed as v(m/s),sample period is T(s),pulse range resolution is m (m),the number of pulses x in each period T:

$$x = \frac{vT}{m} \tag{1}$$

The technical parameters of Doppler radar speed sensor: T=0.001s,m=4mm=0.004m, Supposed a moment the train speed is v=360km/h=100m/s ,Into the parameters and calculate $x = 25$ .That is,ideal pulse counts within each T are 25.The maximum error $e_{\max} = (2/25)\times 100\% = 8\%$,Even under normal circumstances to consider,each period T within plus or minus one pulse. This error $e \approx \pm 4\%$ .In this case the error is about 4%, more than 2% of the allowable range. Moreover,by the principle of pulse counting,it can be known that high-speed error is smaller,while low-speed error is larger. Supposed speed v=120km/h, then the error $e \approx \pm 12.5\%$.

Error Analysis of Hall Speed Sensor. The principle of Hall speed sensor is a magnetic field sensor based on Hall effect, it's working frequency range is general 0~20kHz, output is square wave pulse signal.It may detect the rotation speed of the axle, the line speed and the vehicle running direction,etc. Supposed that the running speed in a moment is v(m/s),High-speed train wheel diameter is d (m), the sample period is T(s), the number of teeth of the Hall of the wheel speed sensor is p,the number of pulses is x in each T:

$$x = \frac{vpT}{\pi d} \tag{2}$$

The sampling period of high-speed train control system is T=0.001s(Sampling rate of the SDU software module is 1kHz),setting high-speed train speed is 360km/h=100m/s, actual high-speed train wheel diameter is 860mm =0.86m,the number of teeth on the wheel speed sensor of Hall is 200[5] , into the parameters and calculated the actual number of the pulse x in each T,that is $x \approx 7$ .According to the normal situation, the number of pulse in each T need plus or minus one pulse,the error $e \approx \pm 14\%$,clearly exceeding the allowable error range. And when the sampling frequency is higher,the speed error is bigger.

The Speed Control Effects of Velocity Measurement Error

Speed control is one of the constant value control, which has the general structure of the control system. As shown in Fig.2.

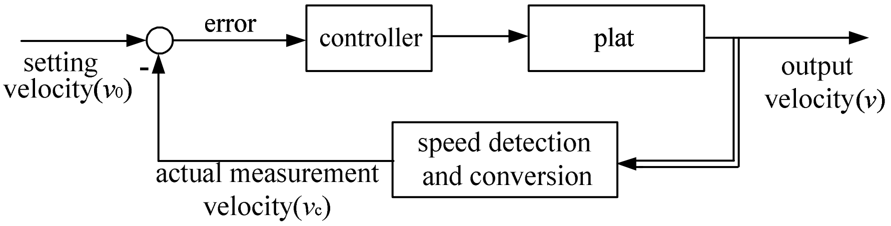
error
controller
plat
setting velocity(v_0)
-
output velocity(v)
speed detection and conversion
actual measurement velocity(v_c)

Fig.2 The system diagram of train speed control

According to the structure of Fig.2,analyzed the problem that speed is not accurate.

Control object: $e \approx 0$,that is $v_0 \approx v_c$,control output after stability: $v \approx v_0 \approx v_c$ .But if $v_c \neq v$,it has two kinds of circumstances:

(1)When $v_c > v$ control object: $e \approx 0$,that is $v_0 \approx v_c$,control output after stability: $v < v_0$.

(2)When $v_c < v$,control object: $e \approx 0$,that is $v_0 \approx v_c$,control output after stability: $v > v_0$.

Where v is a real-time output velocity; v_0 is the system setting speed; v_c is the system real-time detection speed.

From the above analysis, real output value of the speed control system and the actual values may not be consistent. If the detected error is larger, especially detected values less than the actual output value is larger, the consequences may be very dangerous. If output value and detected value is basic consistent, it must make $v_c \approx v$ .So it need to improve the detection accuracy.Specifically, proposed following methods to achieve the purpose.

Research on the Method of Improve the Measurement Precision

The improved M/T Speed Measurement. According to the above analysis, the current speed measurement error is large, although it does not affect the actual application, affect the control precision, thereby affect the operational efficiency of the train, and even affect it's safety. Now the improved M/T speed measurement method is used to improve it. In order to further improve the velocity measurement accuracy, used the improved M/T speed measurement. The principle[6] of improved M/T speed measurement is based on the M/T method[7], which make the fixed sampling period become not fixed sampling period, that is based on fixed sampling T of M/T method, continuing to time until the next rising edge of the measured pulse period, make T and increase the time ΔT together as a dynamic sampling period, as shown in Fig.3[8].

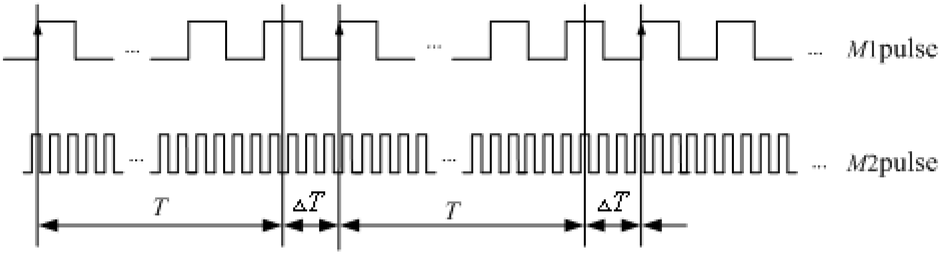

Fig.3 The diagram of improved M/T velocity measurement

FromFig.3,the count value of the measured photoelectric pulse $M1$ includes integer number of photoelectric pulse itself, it's variation does not generate an error, but only cause a change in the actual sampling period, the clock pulse count $M2$ has just one more or little error, but the clock pulse frequency is far greater photoelectric pulse frequency, therefore the error is very small.So the measurement accuracy is improved greatly. The speed can be expressed as:

$$n = \frac{60M1}{N(T+\Delta T)} = \frac{60M1 f_0}{NM2}(r/\min) \tag{3}$$

Where N is the photoelectric encoder line number.

The Improved Results. From Fig.3, it is easy to know that the method of improved M/T speed measuring can improve the velocity measurement accuracy in theory, but also exist error which is a high frequency clock pulse. DSP chip as a controller is general choose for high frequency pulse velocity measurement. It's clock frequency f_0=100Mhz, calculate the error when T=0.001s, get the error e=0.001%. Even it has a maximum error when $\Delta T=T$, calculate speed measurement error e=0.002%.It is clear that speed measuring precision has improved greatly. But count period is dynamic and does not consider spending time of DSP running the program.

Conclusions

For speed measurement larger error on the high-speed train, analyzed speed measurement error, and researched on the effect of speed measurement error of the control system, in the researched process, found that there is a greater effect on the speed control precision, and a big speed measurement error may lead to security problem.Then analyzed the problems and designed a method to improve speed measuring precision.According to the contrast, the results show that the accuracy of speed measuring has improved greatly, which can meet the train safety and smooth operation requirements.

Acknowledgments

The acknowledgement for Project Supported by natural science funds of Gansu province (Grant No.1308RJZA116),colleges and universities scientific research project of Gansu province(Grant No.2013A-051) and science and technology support fund of Lanzhou Jiaotong University(Grant No.ZC2013004)

References

[1] Shu-Guang Zhang.The general technology scheme of automatic train control system on CTCS-3.Beijing: China railway Publishing House, 2008 (in Chinese)

[2] Hou Zan.Comprehensive Performance Evaluation and Train Operation by Multi-objective Optimization for ATO System.Beijing: Beijing Jiaotong University, 2011 (in Chinese)

[3] YAN J P,CHEN X Q,HOU T.The study of train speed measurement information fusion based on the improved federated kalman filter algorithm.JOURNAL OF RAILWAY SCIENCE AND ENGINEERING, 9(2): 89-93 (in Chinese)

[4] WANG J F,WANG X S. Research on Data Fusion of CTCS-3 Train Control System[J]. JOURNAL OF THE CHINA RAILWAY SOCIETY,34(9): 70-74 (in Chinese)

[5] Yang Rong. Doppler Radar Speed Measurement System Design and Signal Processing Method Research.Wuhan: Huazhong University of Science and Technology,2012 (in Chinese)

[6] LI Yongjun.Design of the IP core for the photo-electric encoder.Journal of Changchun University of Science and Technology(Natural Science Edition),31(3): 35-37 (in Chinese)

[7] Chen Boshi.Electric Drive Autonomous Control System—Motion Control System. Beijing: China Machine Press,2007 (in Chinese)

[8] HOU Tao,FAN Duo-wang.The Applied Study of High Accuracy Digital Velocity Measurement on Photoelectric Encoder.Automation & Instrumentation,(152): 9-10+14 (in Chinese)

Applied Mechanics and Materials Vol. 596 (2014) pp 472-475
© (2014) Trans Tech Publications, Switzerland
doi:10.4028/www.scientific.net/AMM.596.472

Study on architecture of measurement of multi-points strain of hinge sleeve of cubic press under super-high pressure

Sun Xuan[1,2, a], Shi Jingxiao[2] , Zhong Zhixian[2,b] , Zhao Hong[2,c]

[1] Guilin University of Technology, Guangxi Scientific Experiment Center of Mining, Metallurgy and Environment; Guilin City, 541004，China

[2] College of Mechanic and Control Engineering; Guilin University of Technology, Guilin City, 541004，China

[a]sunxuan@glut.edu.cn, [b]2005zhzhx@163.com, [c]2558919011@qq.com

Keywords: system of measurement of multi-points strain; Hinge sleeve of cubic press; super-high pressure; PXI platform

Abstract. A system of measuring of multi-points strain of hinge sleeve of cubic press was presented. This system can measure more than 40-points of stress synchronously. The key equipment of this system is PXI platform which is the product of NI. This system acquires data of strain of hinge sleeve of cubic press under super-high pressure when it is working, which is very useful for aid-design of hinge sleeve of cubic press. The results of measurement are also helpful for comparing with simulations and validate its reliability.

Introduction

Hinge sleeve of cubic press(six hydraulic machine) is the most important equipment which is used in the super high pressure and for processing and production of super-hard materials, such as synthetic diamond, cubic boron nitride single crystal and polycrystalline, and synthesis of composite sheet (PDC, PCBN). In the processing of working, the high working pressure is up to 110MPa. As being the key elements of cubic press, it is mainly bearing parts, which directly determines the safety and reliability of the whole system. Qin Dongchen etc.[1-4] studied the structural analysis and design system (CAD/ CAE) integration of the hinge sleeve and built the finite element modeling. Stresses and strains of the hinge sleeve are calculated which can be used for the structural optimization design of hinge sleeve. In reference [5], the simulating design of the system is carried out with large-scale CAD software ANSYS and MSC.FATIGUE, the structure is optimized, the time and cost needed are reduced. The design performance and expected lifespan of the system can be predicted. In reference[6], to avoid excessive similarity and supposition for ear and obtain exact simulation results, the fixing dowel, whose movement is constrained, was introduced in the mode. Sun Xuan etc.[7-9] established finite element model of hinge sleeve in ANSYS, calculated the strength of hinge sleeve of cubic press under high pressure load in realistic condition and analyzed its fatigue under load of periods. But the actual value of stress and strain of hinge sleeve of cubic press under super-high pressure is not known, most of results of the stress of hinge sleeve are from calculation of simulation, and there are no references which concern with testing the actual value. So, there is a bias in the design and the hinge sleeve is usually failure under cyclic loading of super-high pressure. The figure 1 shows the real fracture of cubic hinge sleeve in bottom.

In this paper, an architecture of testing of multi-points strain of hinge sleeve of cubic press was presented, by results of calculation of the hinge sleeve's finite element model and usual failure location, the distribution of location of sensors for testing points is known. After the testing system is set up, sensors are embedded in the body of hinge sleeve of cubic press and scaled, and by the data acquisition, The actual data of the stress of hinge sleeve of cubic press under super-high pressure is obtained.

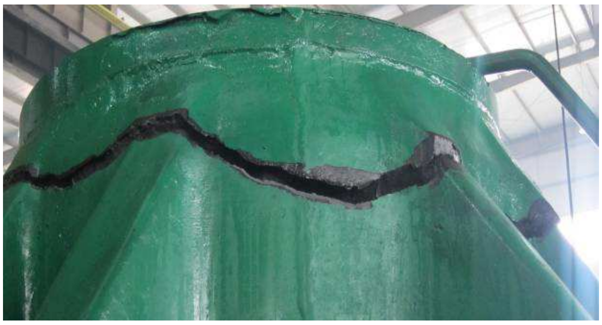

Fig. 1 Fracture of cubic hinge sleeve in the bottom

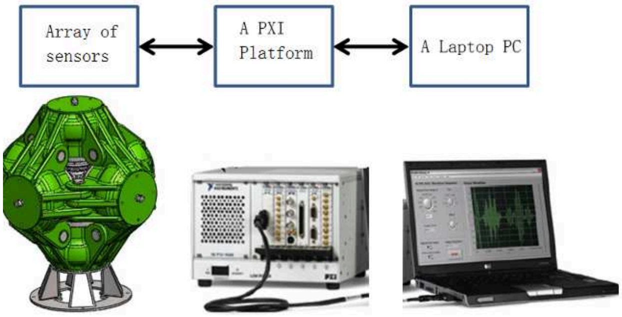

Fig.2 System Configuration

System configuration

Fig.2 shows the system configuration which is used for measurement of multi-points of strain of hinge sleeve of cubic press. It has the following hardware elements:

- A PXI platform.
- Array of sensors.
- A laptop PC.

The PXI platform is used as the main measurement part of the automatic test system. It is used for test control, power supply, and data acquisition, processing and storage. The system of measurement of PXI of NI is a PC-based platform for measurement and automation. A typical PXI platform is shown in Fig. 2. It includes four components: chassis, controller, modules and software [10]. The chassis is the main frame of the PXI system. It provides the power, cooling, and communication buses of Peripheral Component Interface (PCI) and PCI Express for the controller and modules. In the chassis, there is a controller slot with an operation system such as Microsoft Windows for users to operate with display screen. The modules inserted to the chassis act as a whole system without any other connection which reduces the system error produced by the connections between instruments. Different module has its specified function and can be used with other modules or independently. In this paper, the type of chassis is PXI1075, with PXIe-8133 Expess controller. There are 3 modules of the NI X Series DAQ module PXIe 6363 in system which is used for data acquisition. Its resolution is 16 bits, which guarantees the accuracy of the testing results. It offers 32 analog inputs, and that means 3 modules of this card could be offer more than 40 testing-points at the same time. A Source Measure Units (SMUs) module PXIe 4140 is utilized for power supply and current monitor.

The location of arrangement of sensors is critical in measurement system. There are ten ears in each of hinge sleeve which bear the load when it is working. Fig.3 shows its strain of calculation of simulation in ANSYS. Considering the failure in bottom and ears, there must be at least 44 testing points in hinge sleeve when testing its strain and stress. Fig.4 shows the distribution of array of sensors. After the sensors are mounted to the hinge sleeve, the testing bridge, signal conditioning must be required for reliable measurement.

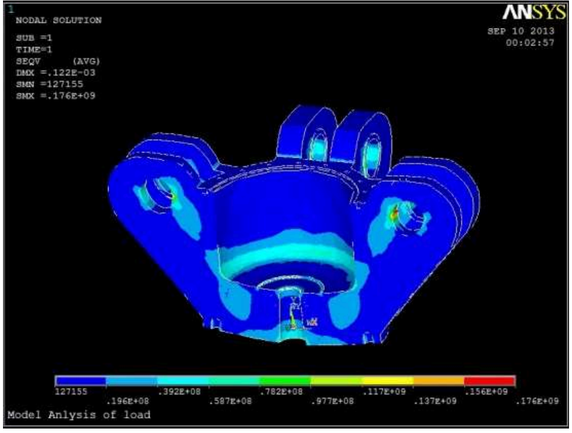

Fig.3 Von Mises stress of hinge sleeve of cubic press

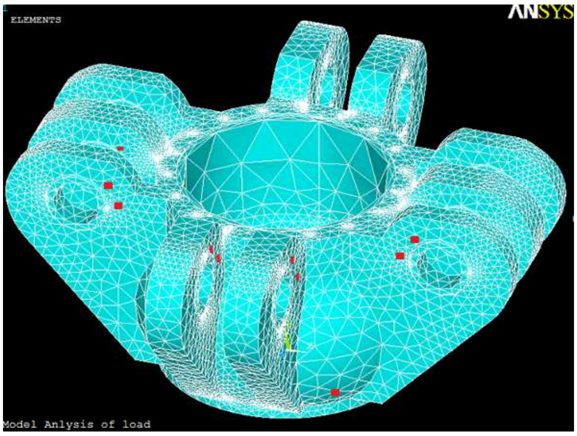

Fig.4 Diagram of distribution of array of sensors

A laptop PC is the key component in this system which is used for data storage, data analysis and instrumentation control in this system. MXI-3 was applied to connect PC and PXI chassis, making full use of the advanced PC technology, reducing the cost of system.

Software configuration

In order to provide a user-friendly data acquisition program for researchers, the software configuration was programmed by LabVIEW TM. As we all know, LabVIEW(Laboratory Virtual Instrument Engineering Workbench) is a graphical programming language by National Instruments that users icons instead of text to create applications. LabVIEW has several advantage over other programming languages in terms of researcher use. A obvious advantage of LabVIEW is its rich graphic user interface (GUI) and hardware drivers.

Any LabVIEW application was composed of two sections: one section was a front panel, which was the graphical user interface(GUI), on which the parameters required to the study on how to show the performance of the hinge sleeve of cubic press were displayed. As mentioned above, these parameters ware strain signals of 44-testing-points. Figure 5 showed the front panel of the LabVIEW GUI developed for this system. As shown in figure 5, the front panel could not only show all the 44-points parameters instantly but also let us set the different pressure. The other section was a block diagram, which was neglected in this paper.

To meet the testing requirements, the software is divided into three parts. The first part is to verify the configuration of related hardware. The second part is to test the logic functions of the channel of this system and calibration of sensors. And the third part is to evaluate the testing results, which includes data acquisition, storage and processing. Then the results are shown in the form of associated waveform. The software flow chart is shown in Fig. 6.

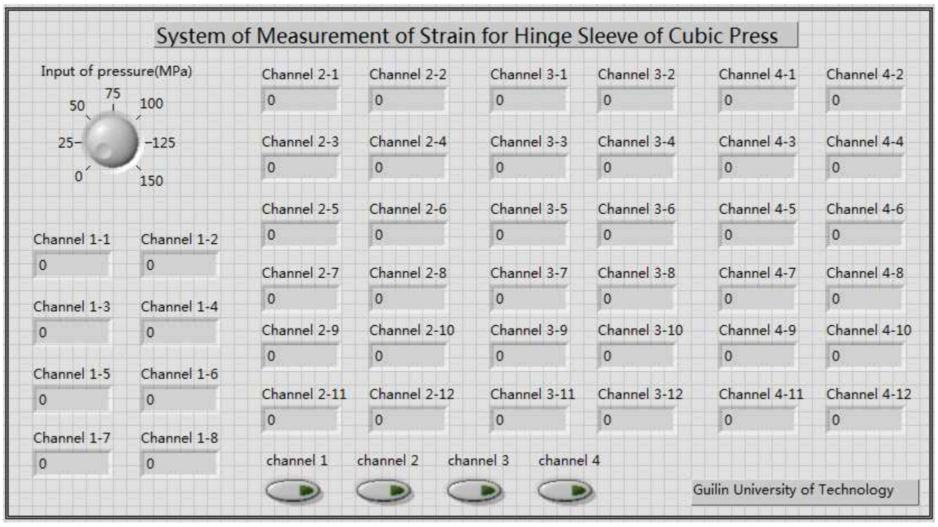
System of Measurement of Strain for Hinge Sleeve of Cubic Press

Input of pressure(MPa)

Channel 1-1 0
Channel 1-2 0
Channel 1-3 0
Channel 1-4 0
Channel 1-5 0
Channel 1-6 0
Channel 1-7 0
Channel 1-8 0
Channel 2-1 0
Channel 2-2 0
Channel 2-3 0
Channel 2-4 0
Channel 2-5 0
Channel 2-6 0
Channel 2-7 0
Channel 2-8 0
Channel 2-9 0
Channel 2-10 0
Channel 2-11 0
Channel 2-12 0
Channel 3-1 0
Channel 3-2 0
Channel 3-3 0
Channel 3-4 0
Channel 3-5 0
Channel 3-6 0
Channel 3-7 0
Channel 3-8 0
Channel 3-9 0
Channel 3-10 0
Channel 3-11 0
Channel 3-12 0
Channel 4-1 0
Channel 4-2 0
Channel 4-3 0
Channel 4-4 0
Channel 4-5 0
Channel 4-6 0
Channel 4-7 0
Channel 4-8 0
Channel 4-9 0
Channel 4-10 0
Channel 4-11 0
Channel 4-12 0

Guilin University of Technology

Fig.5 Front diagram of test interface

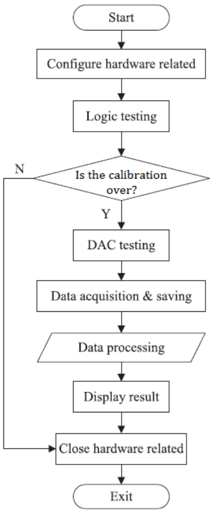

Fig.6 Software flow chart

Discussion

Strain sensors are very sensitive against heat and vibration, on the other hand when hinge sleeve is working, it is produced many vibration, and the temperature in the surface of hinge sleeve is going to around 100 C° due to friction. These external properties have large effect on recording and leads to inaccuracy on monitoring. In this system, resistance strain gage was used which was bounded on the surface of hinge sleeve. It is also affected by binding materials. Whereas, these properties are non-preventable, the obtained result must be filtered and conditioned to be acceptable and readable. In present article analyze of results were not introduced in detail. Some classical approaches which are used for circuit conditions would be available in text.

Conclusions

An automatic measuring system for strain of hinge sleeve of cubic press under super-high pressure was introduced. The PXI platform and LabVIEW were used in the automation of this kind of measurement system.

The architecture of the application is divided into three modules, separating the data acquisition, data processing and displaying and data saving, which is very useful for design and validating the results of simulation. The design strategies and techniques presented in this paper would be also used to develop similar strain and stress data acquisition system.

Acknowledgements

This work is funded by Guangxi Scientific Experiment Center of Mining, Metallurgy and Environment，Guilin University of Technology (Grant No. KH2012ZD010).

References

[1] QIN Dong-chen, LIANGYing, LAKai-ying. Research on Hinge Sleeve’s Design System Integration Based on Pro/Engineer and Ansys[J]. Journal of Zhengzhou University (Engineering Science), Vol.26(2005.6), 67-71.

[2] Qin Dongchen, Chen Jiangyi, Liang Ying, Qin Xiaoming. Structural optimal design for hinge sleeve of cubic press[J]. Diamond& Abrasives Engineering, Vol.149(2005.10).70-72.

[3] QIN DongChen，LIANG Ying，CHEN LiPing etc. Research for Hinge Sleeve’s Structural Optimal Design Based on Fatigue Intensity[J]. Journal of Mechanical Strength. Vol.28 (2006.2), 306~310.

[4] Qin Dongchen, Liang Ying, Chen Lipin, etc. Research on Structural Optimization Design for Key Parts of a Six-face Presser[J]. China Mechanical Engineering. Vol.18 (2007.06),697-701.

[5] Niu Qingbo, Wang Yanwei, LiYanchun, etc. Simulating design of hinge system of cubic press based on FEM and fatigue life analysis[J]. Diamond& Abrasives Engineering. Vol.158(2007.02),76-79.

[6] ZHANG Cong, MA Hong-An, HAN Qi-Gang etc. Stress Analysis on Hinge Sleeve and Cylinder of China-Type Cubic-Anvil High Pressure Apparatus under High Pressure[J]. Chinese Journal of High Pressure Physics. Vol.24 (2010.05), 321-325.

[7] SUN XUAN, Wang Bin, Zhang Yu,etc. Analysis of strain-stress of cubic hinge sleeve. Applied Mechanics and Materials. Vols. 313-314 (2013) 1021-1024.

[8] Sun Xuan, Strength calculation of cubic hinge sleeve based on Ansys. Applied Mechanics and Materials Vols. 275-277 (2013) pp 808-811.

[9] Sun Xuan, Qi Wenzheng, Zhao Hong, etc. Study on Fatigue of Hinge Sleeve of Cubic Press based on ANSYS. Applied Mechanics and Materials Vols. 457-458 (2014) pp 585-588.

[10] Zhongyuan Wang, Yongheng Shang, Jiarui Liu, etc. A LabVIEW based automatic test system for sieving chips. Measurement, Vols. 46 (2013) 402–410.

Applied Mechanics and Materials Vol. 596 (2014) pp 476-479
© (2014) Trans Tech Publications, Switzerland
doi:10.4028/www.scientific.net/AMM.596.476

Continuous Blood Pressure Measurement Method Based on the Pulse Image Sensor and BP Neural Network

Aihua Zhang[1, a], Xingzhong Zhou[1,b], Liming Yang[1], Rong Shen[2], Zhe Wei[3]

[1]School of Electrical and Information Engineering, Lanzhou University of Technology, Lanzhou, 730050, China

[2]School of Computer and Communication, Lanzhou University of Technology, Lanzhou, 730050, China

[3]Institude of Medical Engineering, Lanzhou General Hospital of PLA, Lanzhou, 730050, China

[a]lutzhangah@163.com, [b]1379536623@qq.com

Keywords: Continuous blood pressure; Multi-information synchronous acquisition system; BP neural network

Abstract. A continuous pressure measurement method is proposed based the pulse image sensor and BP neural network for continuous measurement of arterial blood pressure. The multi-information synchronous acquisition system is built to collect pulse image sequences, sphygmopalpation pressure, probe internal pressure, and blood pressure of subjects. The feature vector is formed from pulse image sequences, sphygmopalpation pressure, and probe internal pressure to predict continuous blood pressure by BP neural network. The results show that the mean difference (MD) and standard deviation (SD) of systolic blood pressure (SBP) and diastolic blood pressure (DBP) meet the standard of Association for the Advancement of Medical Instrumentation (AAMI). The method could be used to predict continuous blood pressure and provides a new method for arterial continuous blood pressure measurement.

Introduction

Blood pressure is an important physiological parameter in the health guardianship and can reflect physiological alteration of cardiovascular function [1, 2]. Blood pressure measurement methods generally divide into invasive and noninvasive measurement method [3]. Invasive measurement method, which needs directed arterial cannulation, is limited in clinical situations. Noninvasive measurement method is handy and has widely applied to clinical diagnosis [4]. Traditional noninvasive measurement methods such as Korotkoff sound method and Oscillographic method cannot measure the continuous blood pressure that provides more sufficient foundation for clinical diagnosis and therapy [5, 6]. Oscillographic method, which has stronger anti-interference capability and better reproducibility, is usually used for the reference and calibration of new measurement method. But these methods can't be realized continuous blood pressure measurement. Recently we have found that the pulse image sequences acquired from radial artery contain abundant physiological information and could be used to measure blood pressure. In this paper, a continuous blood pressure measurement method is proposed based on the pulse image sensor and BP neural network.

In our work, the multi-information synchronous acquisition system is constructed to acquire pulse image sequences, sphygmopalpation pressure, probe internal pressure and blood pressure signal. Then, some characteristic parameters are extracted from sphygmopalpation pressure signal and pulse wave which is from pulse image sequences. In addition, these characteristic parameters and probe internal pressure form the characteristic parameters vector as the input vector of the BP neural network. Finally, the trained BP neural network is used to predict SBP and DBP of subjects.

Data Acquisition and Data Processing

Data acquisition system. The data we used are from the system named multi-information synchronous acquisition system which consists of PC, pulse image sensor module and multi-information synchronous acquisition module. MP150 acquisition data system is used to collect blood pressure signal of subjects at the same time duration and the measurement principle is Oscillometric method. The schematic structure of multi-information synchronous acquisition system is shown as Fig.1.

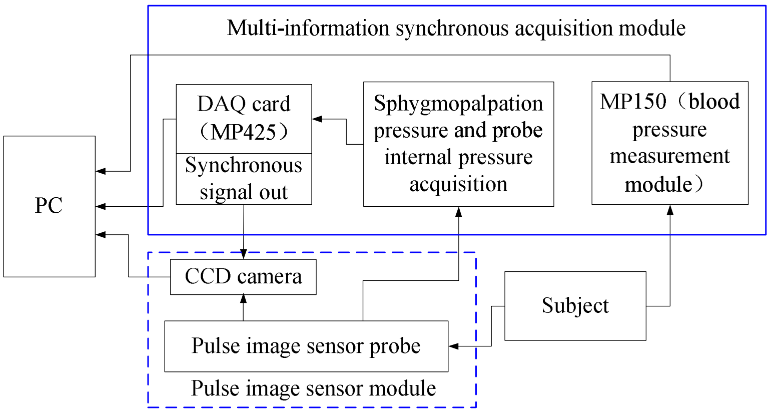
Multi-information synchronous acquisition module
DAQ card （MP425）
Synchronous signal out
Sphygmopalpation pressure and probe internal pressure acquisition
MP150（blood pressure measurement module）
PC
CCD camera
Subject
Pulse image sensor probe
Pulse image sensor module

Fig.1 The schematic structure of multi-information synchronous acquisition system

1). PC. The software of multi-information synchronous acquisition system is composed of LabVIEW acquisition system, CCD camera system and MP150 acquisition data system. Parameters setting and data acquisition are executed on PC.

2). Pulse image sensor module. Pulse image sensor module is constituted of self-made pulse image sensor probe and CCD camera. The pulsation is sensed by the grid film on soft probe, and the film changes are photographed by CCD camera to acquire pulse image sequences at a certain frame rate. The pulse image sequences are transmitted to PC by Gigabit-NIC. The maximum frame rate of CCD camera is 30fps and the camera works in external trigger mode. The trigger signal is TTL level of rising or falling edge.

3). Multi-information synchronous acquisition module. This part aims at realizing acquisition of sphygmopalpation pressure, probe internal pressure and blood pressure signal as well as synchronization of pulse image sequences and three pressure signals. Sphygmopalpation pressure is acquired by a pressure sensor with output range of 0-5V and a MP425. MP425 supports 8-channel analog inputs, 16-channel inputs and outputs switches. With the software trigger and external hardware trigger, MP425 can realize synchronous control with the camera while the system acquires data. Synchronous control signal is generated as follows: when writing a binary 0 or 1 to each switch port, the card outputs low or high level, respectively. For the system requirement, two synchronous control signals are produced. One is acted as an external trigger signal of MP425 and the other is acted as an exposure start signal to trigger camera.

Data acquisition and processing. Ten healthy volunteers, which the mean age is 23, the male is 5 and the female is 5, are selected as experiment subjects. 10 different time durations are employed, which are 6 time durations of high blood pressure period and 4 time durations of low blood pressure period in one day. These time durations respectively are 17:00:00-17:00:10, 17:05:00-17:05:10, 17:10:00-17:10:10, 17:15:00-17:15:10, 17:20:00-17:20:10, 17:25:00-17:25:10, 20:30:00-20:30:10, 20:35:00-20:35:10, 20:40:00-20:40:10, 20:45:00-20:45:10. The system parameters set as follow: sampling frequency is 1 kHz, acquisition time is 10s, and camera frame rate is 14fps. Then the multi-information synchronous acquisition system acquires signals of ten volunteers in 10 different time durations one day, respectively.

The data of one time duration of a subject, which the multi-information synchronously acquisition system acquires, is processed. The feature vector is acquired from pulse image sequences, sphygmopalpation pressure, and probe internal pressure. SBP and DBP are extracted from blood pressure signal by proportional coefficient method and the extracted SBP and DBP are used to train BP neural network and analyze error of predicted SBP and DBP. After the processing of acquired data of all subjects, we obtain feature vectors, SBP and DBP of 10 time durations of each subject.

Blood Pressure Measurement

Neural network is an information processing model of simulating creature neural system, and has nonlinear mapping capacity. It has been widely used in engineering fields and academic research. BP neural network is a multi-layer perceptron network, and the hidden layer nodes are computed by sigmoidal function. Generally, BP neural network consists of three-layer structure, which includes input layer, multiple hidden layers and output layer. The learning algorithm of BP neural network is LM algorithm, which has fastest convergence rate and higher accuracy. The BP neural network structure is shown as Fig.2.

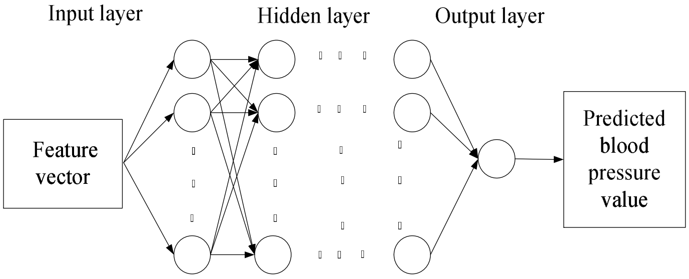

Fig.2 BP neural network structure

In this paper, the feature vector is acted as input vector of BP neural network. Simultaneously, SBP and DBP acquired by Oscillometric method are acted as target vector. Then the BP neural network is trained to predict SBP and DBP.

The pulse wave is extracted from pulse image sequences by image off-plane displacement acquisition algorithm [7]. The 4 main characteristic points are extracted from the pulse wave. Then 17 characteristic values in time and frequency domain are obtained based on pulse wave, which include mean trough amplitude, mean peak wave (P wave) amplitude, mean dichotic notch amplitude, mean repeat wave amplitude, average P-P period, P wave relative height, dichotic notch relative height, repeat wave relative height, average gradient of P wave rising edge, H(1+ts/td) (H is P wave amplitude, ts is systolic time, td is diastolic time), pulse contour characteristic value K, pulse wave area S, pulse wave systolic area Sa, pulse wave diastolic area Sb, time ratio of pulse wave ascending branch and descending branch, pulse wave power spectrum peak value, corresponding frequency of power spectrum peak value. At the same time, the average value and variance of sphygmopalpation pressure are also calculated as characteristic values.

The feature vector of input layer is constituted of above 19 characteristic values and probe internal pressure value. The hidden layer is constituted of two layers and each layer contains five neurons which activation function is sigmoidal function. The output layer of BP neural network is constituted of one neuron and activation function of the neuron is pure line function.

The feature vectors, SBP and DBP of 9 time durations, which respectively choose from feature vectors, SBP and DBP of 10 time durations, are used to train BP neural network. The remained feature vector is used to predict SBP and DBP of the time duration. All trained BP neural network reaches the prospective setting goal 0.01.

Results and Discussions

In order to verify measurement accuracy of the method, the MD and SD is used to analyze experiment results. The MD and SD are obtained by SBP and DBP of 10 durations of each subject. Table 1 shows the error analysis results.

Table 1 Error analysis results of predicted SBP and DBP of 10 subjects [mmHg]

	Subject 1		**Subject 2**		**Subject 3**		**Subject 4**		**Subject 5**	
	SBP	**DBP**	**SBP**	**DBP**	**SBP**	**DBP**	**SBP**	**DBP**	**SBP**	**DBP**
MD	4.600	4.000	2.8714	4.1701	3.0918	2.1414	4.1110	2.4714	3.8620	4.3146
SD	5.4813	3.9721	6.3419	6.3857	4.6903	3.0988	2.1540	7.5586	1.4651	6.8847

	Subject 6		**Subject 7**		**Subject 8**		**Subject 9**		**Subject 10**	
	SBP	**DBP**	**SBP**	**DBP**	**SBP**	**DBP**	**SBP**	**DBP**	**SBP**	**DBP**
MD	3.6340	3.5701	2.0127	1.0258	3.5769	4.0214	3.2780	0.1129	4.9016	1.2501
SD	4.7015	4.3556	7.3601	4.0410	6.0915	6.1145	7.0157	5.1477	4.5701	3.7904

From the table, we find that the MD and the SD of SBP and DBP of 10 subjects do not exceed AAMI standard (5±8mmHg).

There are mainly three factors leading to the errors of the method. Firstly, the hardware of multi-information synchronous acquisition system is limited because of low frame rate of CCD camera. Secondly, there is a slight effect on characteristic parameters since the characteristic parameters are not fully comprehensive. Thirdly, there is a small error since the number of hidden layer neurons is not fully accurate.

Conclusion

We proposes an arterial continuous blood pressure measurement method based on the pulse image sensor and BP neural network, which includes the acquisition of human physiological signals and procession of these signals. The experiment result shows that the MD and the SD of SBP and DBP of different subjects meet the AAMI standard. From the conclusion, the method in this paper could estimate SBP and DBP and provides a new method for arterial continuous blood pressure measurement.

Acknowledgments

This work is supported by the Doctoral Foundation of Ministry of Education (Grant No. 20116201110002) and the National Natural Science Foundation (Grant No.81360229) of China.

References

[1] X.J. Jiao and X.Y. Fang: Journal of Biomedical Engineering. Vol. 19(2002), p. 217-220

[2] S. Weber, D. Strommenger and U. Kertzscher: Biomed Tech. Vol. 57(2012), p. 407-410

[3] W. Guo, G.D. LIU and Y. JIAO: Journal of Medical Biomechanics. Vol. 27(2012), p. 84-89

[4] K. Meigas, J. Lass and D. Karai: IFMBE Proceedings. Vol. 14(2007), p. 626-629

[5] L. Guillaume, S. Masaki and U: Journal of Advanced Mechanical Design. Vol.4 (2010), p. 179-186

[6] G. Heiko, G.Detlef and K. Gert: European Journal of Applied Physiology. Vol. 112(2012), p. 309-315

[7] A.H. Zhang, W.G. GUO and Y.P. LI: Chinese Journal of Medical Instrumentation.Vol. 32(2008), p.179-182

Applied Mechanics and Materials Vol. 596 (2014) pp 480-483
© (2014) Trans Tech Publications, Switzerland
doi:10.4028/www.scientific.net/AMM.596.480

Measuring Device for the Moment of Human Aspects

Hechuan Zeng[1, a] and Changqi Yang[2,b]

[1]College of Resource and Environment Science, Chongqing University, Chongqing, 400030, China

[2]College of Resource and Environment Science, Chongqing University, Chongqing, 400030, China

[a]756886044@qq.com, [b]ycq3664@163.com

Keywords: Human Inertia Parameters, Weighing Method, Measurement Accuracy

Abstract. Due to the quality of all aspects of the human body differ greatly, collecting attitude parameters,electronic scales can not achieve the precision requirements. Therefore, how to ensure a large range torque measurement accuracy becomes the core of a recognition system of dimensional distribution of body weight. In this paper，based on the original measure will convert measuring force to measure the distance , redesigning the said bed to improve test accuracy.

Introduction

Nearly 100 years, with scholars boldly exploring and making unremitting efforts, the study of human aspects of measurement has been steadily progressing. To get links weight parameters of human movement methods developed by the autopsy method to measure the in vivo measurement of personalized , mathematical model and so on .

Numerous research programs, the balance board weighing have been concerned to measure by researchers with its convenience, researchers also extend the function of the balance sheet, so that the balance body can not only measure the overall center of gravity，can also be used to measure the weight of the body part of the moment (product weight and part of the human aspect of the radius of the center of gravity). The researchers realized that once the human aspects of the use of the balance board to measure the weight of a breakthrough method parameters, it will promote the study to measure the direction of personalized a great step forward for motion image analysis for athletes action image, the human body motion analysis and refinement refinement provides the basis for assurance.

In the course of this exploration, experts and scholars who come from different countries used one-dimensional and two-dimensional balance board for discussing the issue. 1947 Williams Bernstein 1962, 1970 etc Kang Tini posture weighing method for converting an attempt to obtain a more significant findings. David A. Winter in his writings also introduced the use of a one-dimensional balance board to get its weight by changing the parameters of the distal part of the human body posture. Research as well as domestic experts similar to the balance sheet also been useful to try to measure. Based on the original measurement method to convert the measurement to measure the growth of the force, the design of an automatic control device to measure the qualitative aspects of the body weight of each moment.

The measuring principle

Measuring the leg and foot moments as an example to illustrate the weight measurement principle balance sheet ,the body prone on the balance board, scale reading of N1 ,in Fig.1. When the test subjects lifted vertically upward leg-feet, other aspects remain intact, scale reading of N2 , in Fig.2. Mechanical analysis procedure described above in Fig.3, W_i stands for the weight of leg-foot. L1， L2 is tested leg-foot not enough to lift and lift its center of gravity away from the straight line OO' distance, when the leg-foot lift, you can see the center gravity of leg - foot away from the straight line OO' moved $\mathrm{L1}-\mathrm{L2}$ distance, namely radius of the center of gravity of leg-foot . According to the principle of equilibrium torque, torque variation is equal to the torque variation in the clockwise counterclockwise direction Eq. 1.

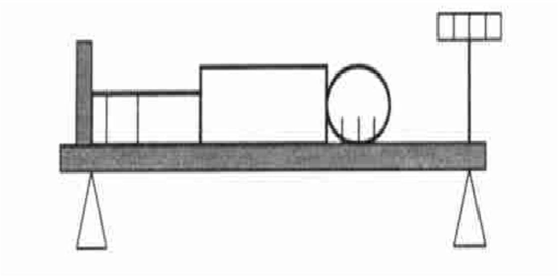

Fig.1 Body prone on the balance board

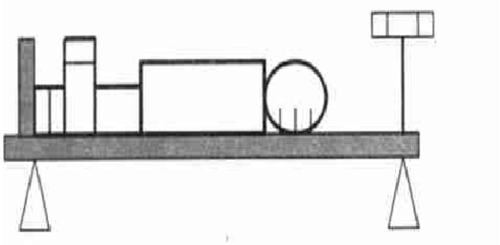

Fig.2 Leg-foot vertical lift up

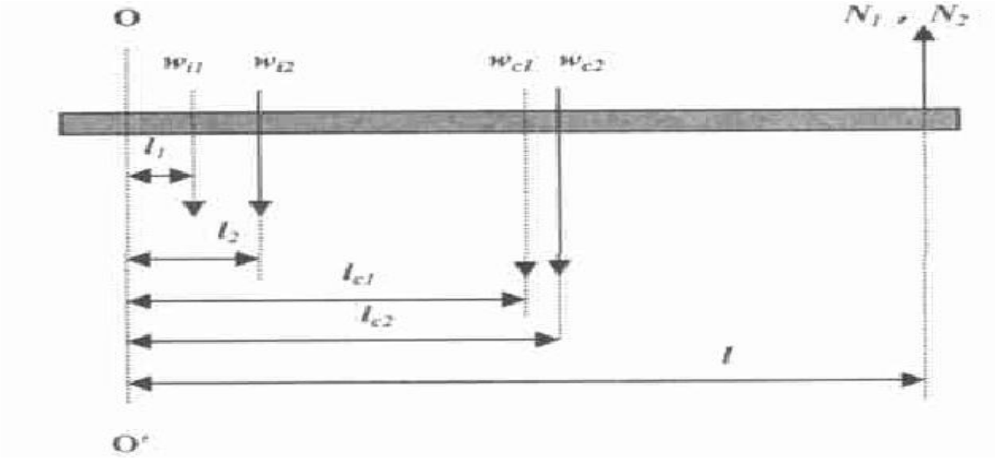

Fig.3 Force analysis

$$W_i\,(\mathrm{L1}-\mathrm{L2}) = (\mathrm{N2}-\mathrm{N1})\,\mathrm{L}\,. \tag{1}$$

The left side of Eq. 1 for changing the torque in the clockwise direction(the moment of leg-foot),the right side for changing the torque in the counterclockwise, it is calculated by the measurement, whereby can be obtained the moment of leg-foot.

Human aspects of traditional weight measurement Moment

The human part of the weight of traditional moments parameter identification device, Fig.4.

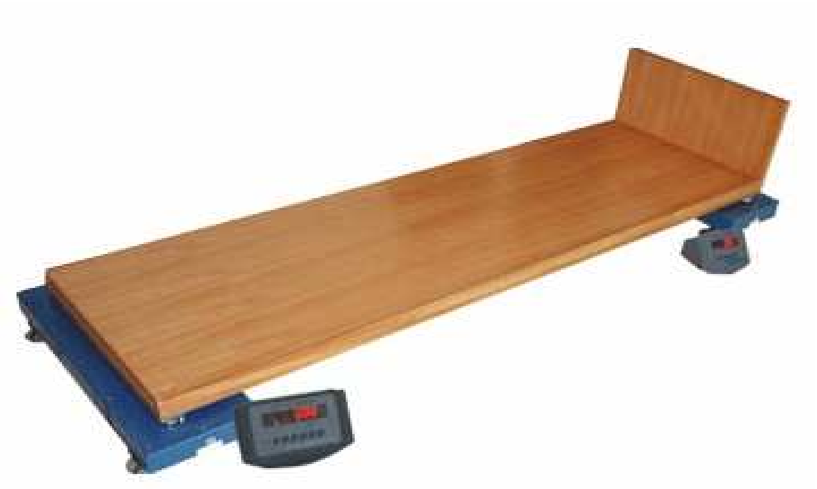

Fig.4 Traditional balance board measuring device

Force sensor placed at both ends of the bed. When testing the body lying on the bed, transform all aspects of the human body posture,showing the number of sensor also changes,and satisfies the relationship, transform gesture get different linear equation, solving linear equations, you can get the body weight moments of each link. To get high accuracy experimental data , precision force sensor is a prerequisite.General mechanical sensors can not be achieved, which requires improved devices.

Improved measuring device

Inspired by the balance principle, the conventional measurement system based on the force measurement into a distance measurement, Fig.5. Said bed carriage to the home position, the bottom of the bed with said stepper motor drive means for sliding mass, one end of said bed with discharge pressure sensor of type S, and the other end is fixed to the position hanging weight. When subjects were tested on the human body, lower body gravitational torque of bearing part will be offset by the weight hang hanging weights makes S-type pressure sensor pull tension, to mount on both sides of the torque balance. When transform all aspects of human posture, change the number of sensors is shown by the AD weighing module back to the control program, the control program send commands to drive a stepper motor driven slider until the pull tension and pressure sensors so keep the number shows the number shown in the original within a certain range. Because the weight of a mass, the mass only needs to measure the distance to move, the distance measurement is accurate stepper motor control program can rely on precise positioning to achieve. The single measuring force and force into a distance measurement and to improve the measurement accuracy.

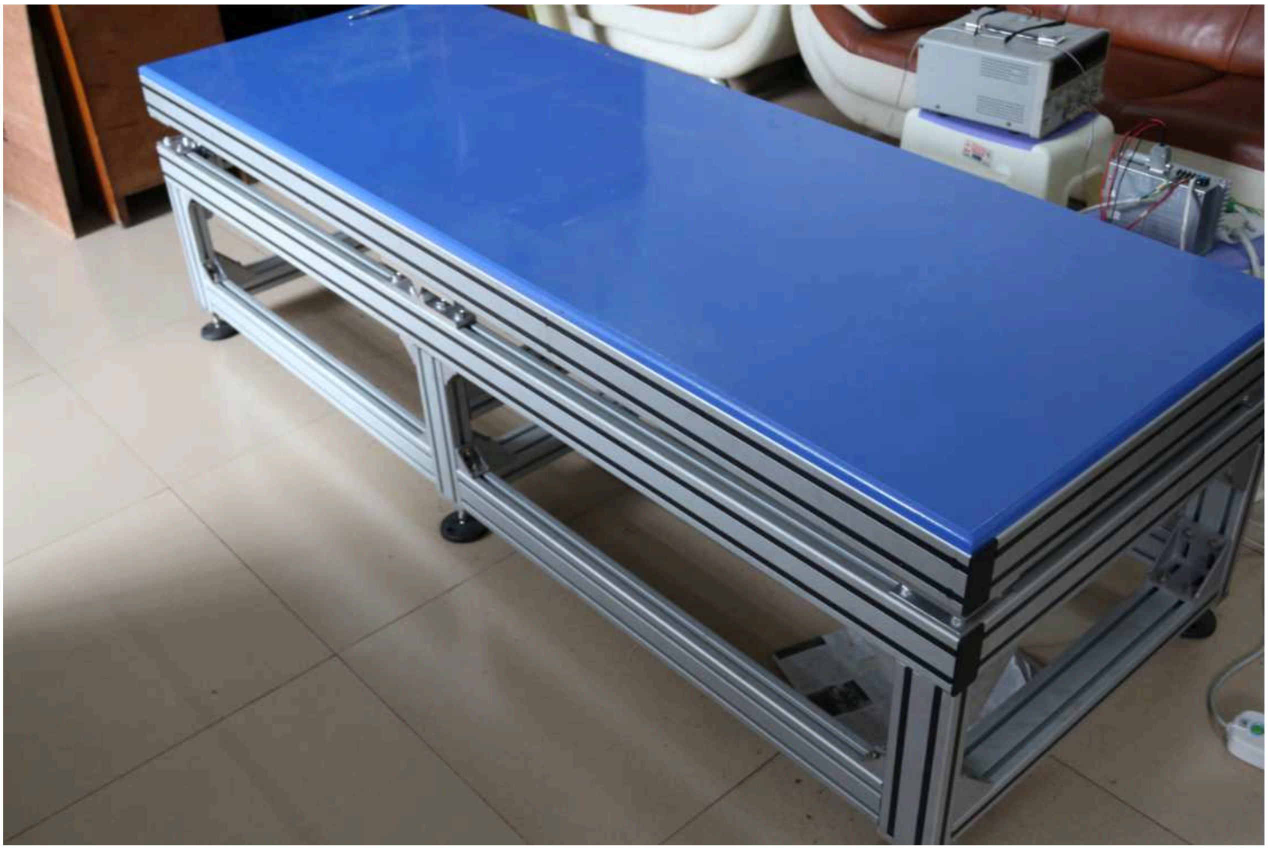

Fig.5 The improved device

Conclusion

One end of the traditional one-dimensional body weight moments recognition system, bearing placed in said bed, and the other end is placed electronics, showing the number of sensor use lists to identify aspects of the weight of the moment equation, Eq. 1, as compared to the quality gap between human joints large, the attitude data acquisition, the force sensor can not achieve the required accuracy in the determination of the instantaneous center of rotation of the body link, can be determined according to the geometric center of each joint, it is difficult to pinpoint.

Therefore, the test system which is improved identification system will be designed to resemble the balance of the system controlled by an automatic measuring device to measure the body weight of each link moments, the improved system, the link may be a wider space, easy to test determination of body weight to achieve moments of links, and the identification number of the equations shown in addition to the sensor, also joined the plot moving mass and the mass of distance, much more conducive to a part of the weight of the moment parameter identification. The improved system will measure the strength of the original system is converted to measure the distance of travel yards, no confusion as the center of rotation is difficult to pinpoint the human aspects of the transient, but also improve the accuracy of the measurement accuracy.

References

[1] CaPPozzo. A. Leo. T and Pedotti. A: A general computational method for the analysis of human locomotion.Biomechanics,Vol. 23 (1975),p.307-320

[2] David. A. Winter: *Biomechanics and motor control of human movement*(Wiley-Interscience Publication, A Second Edition 1991).

[3] Yeadon. MR: The simulation of aerial movement-II,A mathematical inertia model of the human body. Biomechanics Vol. 23 (1989), p.741

[4] Apkarian. J, Naumann. S and Cairns. B: A three-dimensional kinematic and dynamic model of the lower limb. Biomechanics Vol. 22 (1989), p. 143-155

[5] Hinrichs. RN: Adjustments to the segment center of mass proportions of Clauser et al.(1969). Biomechanics Vol. 23 (1990), p. 949-951

[6] Information on http://www.xhl.com.cn/CN/ProductShow/ProTesOne.aspx?menuid=010303016.

[7] Dalnis. A: Whole body and segment center of mass determination from kinematics data. Biomechanics Vol. 13 (1980), p. 674-65

Applied Mechanics and Materials Vol. 596 (2014) pp 484-489
© (2014) Trans Tech Publications, Switzerland
doi:10.4028/www.scientific.net/AMM.596.484

Change detection in SAR images based on semi-supervised learning

Song TIAN[1,2,a], Jianshe SONG[1], Shubing TIAN[3], Wei GONG[2]

[1]Xi'an Hi-tech institute, Xi'an Shaanxi 710025, China

[2]Chongqing communication institute, Chongqing 400035, China

[3] Hospitals NO.154, Xinyang Henan 464000, China
[a] cqtianyi423@sina.com

Keywords: SAR image; change detection; semi-supervised support vector machines; K-means

Abstract: Support Vector Machine (SVM) is a supervised approach, which needs large numbers of labeled samples. However, it is difficult to obtain such samples for change detection based on SAR images and the available labeled samples are very limited. this paper proposes a semi-supervised support vector machine (S^3VM) unsupervised SAR image change detection. Using of K-means clustering method obtain threshold of image; introduce offsets which are automatically selected to achieve a pseudo-training set and unlabeled set; Finally, based on the statistical characteristics of semi-supervised support vector machines for image change and non-change class. The experimental results showed that: In the case without using noise reduction and the reduction in the number of samples, the proposed algorithm can maintain better classification, generalization and more stable detection accuracy.

Introduction

Synthetic Aperture Radar (SAR) was first proposed by Carl Wiley in 1951. It is an active microwave sensor, the use of pulse compression techniques to improve range resolution, the use of synthetic aperture principle improved azimuth resolution, to obtain high-resolution radar images of large areas. When the SAR has a day, all-weather, multi-band, multi-polarization mode of operation, variable side perspective, strong penetrating power and high resolution features. SAR can be used not only with environmental monitoring, but also for military target detection and tracking [1,2]. SAR data are widely used for the treatment of SAR images, so that become one of the SAR image change detection sensing current cutting-edge technology development.

Detection algorithm describe based on S^3VM

Based Semi-supervised Support vector machine (S^3VM) SAR image change detection algorithm, the specific method of the algorithm is as follows :

Step 1: Acquire two coregistered SAR images(I_1 and I_2) that were over the same geographical area at different times(t_1 and t_2), size are $P \times Q$.

Step 2: SAR images preprocessing, including radiometric, geometric calibration.

Step 3: Generate difference image. The main distinction between change detection does not change classes and class changes, Let $\Omega = \{\omega_u, \omega_c\}$ involve the no change class set and the change class set . Generating difference image make the difference categories to facilitate classification.

Step 4: Get the pseudo-training set and unlabeled set. Use unsupervised method to obtain a pseudo-training set of change detection , providing the training samples for S3VM classification.

Step 5: Determine the initial separation hyperplane . Using the pseudo-training set and a Gaussian kernel , determine standard SVM hyperplane.

Step 6: Determine the final separation hyperplane . According to the current separation hyperplane, the unlabeled sample set through semi- supervised learning , and the pseudo-trained set contain SVM to determine the final separation hyperplane.

Step 7: Generate change detection image . According to the final separation hyperplane (i.e. the sixth step), so $f(x) = w^T x + b$, calculate the class of $P \times Q$ pixels and obtain the change detection result.

Comparison of multitemporal images

When detecting changes in multispectral remote sensing images, the customary way of comparing a pair of multitemporal images is to generate a difference image by applying a pixel-by-pixel subtraction [image differencing (ID) technique]. However, when SAR images are considered, changes are obtained by analyzing the image resulting from the application of the ratio operator to the considered couple of temporal SAR images. It is possible to prove that, under the simplifying assumption of statistical independence between the intensity images I_1 and I_2, the logarithmic ratio image X_{DI} can be written as follows:

$$X_{DI} = \left|\log\left(I_2/I_1\right)\right| \tag{1}$$

The ratio operator shows two main advantages over the difference operator. The first is that the ratio image distribution depends only on the relative change in average intensity between two dates and not on the intensity level of the pixels, in contrast with the distribution of the difference image. This means that changes will be detected in the same manner both in high and low intensity regions. The second advantage is that the ratio operator is more robust to calibration errors than the difference operator. Since radiometric errors that usually occur during the SAR processing phase are of the multiplicative type and are exactly reproduced in repeat-pass imagery, they can be eliminated using the ratio operator. Furthermore, it is worth noting that, in the literature, the ratio image is usually expressed in a logarithmic scale in order to compress the range of variation of the ratio image and to better balance the values below and above one. Based on these considerations, we adopt the log-ratio operator in the proposed change-detection approach.

Generating pseudo-training set and unlabeled set

In the process of SAR image change detection, a priori information is difficult to obtain; addition, as the impact of speckle noise, a priori information obtained large error, and cluster analysis is an unsupervised method does not require any prior inspection information. K-means clustering is a simple, commonly used clustering methods. First select the two samples as the initial cluster centers, according to the clustering of all samples from the field to the principle of minimum squares and cluster centers, so that other samples gathered from various centers, and then determine whether the classification is reasonable, unreasonable continued iteration, change up until the cluster centers do not recur， obtain two cluster centers $\{k_1, k_2\}$. So a threshold value T is obtained（i.e. $T = \left[\max\{k_1, k_2\} - \min\{k_1, k_2\}\right]/2$ ）. However, if we apply the threshold T to classifier, we obtain a change-detection map affected by errors resulting from the uncertainty that characterizes pixels with a magnitude value that is close to the threshold. This problem is partially due to the loss of information associated with the difference and magnitude operators, which do not allow to exploit all the information of the original feature space in the change detection process. On the contrary, the threshold value T represents a reasonable reference point for identifying the subset X_u, as shown in Figure 1. According to this observation, the desired set of pixels with a high probability to be correctly assigned to one of the two classes is obtained by defining an uncertainty region around T. This region conceptually identifies uncertain patterns and separates them from nearly certain pixels. Therefore, X_u is defined as

$$X_u = \left\{ x^u \middle| T(1-\delta_1) < x^u < T(1+\delta_2) \right\},\ \delta_1, \delta_2 \in (0,1) \tag{2}$$

meanwhile, a sample with a high probability is defined as a pseudo-training set X_p

$$X_p = \left\{ x^p \middle| x^p \le T(1-\delta_1)\ and\ x^p \ge T(1+\delta_2) \right\} \tag{3}$$

where δ_1, δ_2 is used to determine the pseudo-training set and unlabeled set of boundary adjustment factor. δ_1 and δ_2 should be set to ensure that the correct label probability sample of X_p is higher.

Change detection based on S³VM

Initialization

Standard SVM training set using samples of the pseudo-training data find an optimal separation hyperplane, and make it the largest margin on both sides of the interval[3]. Its optimization problem is:

$$\begin{aligned} &\min_{w,b,\xi^p} \left\{ \frac{1}{2}\|\boldsymbol{w}\|^2 + C_1 \sum_{n=1}^{N} \xi_n^p \right\} \\ &s.t.\quad y_n^p \cdot \left[\boldsymbol{w}^T \cdot \phi\left(x_n^p\right) + b \right] \ge 1 - \xi_n^p, x_n^p \in X_p \\ &\qquad \xi_n^p \ge 0, n = 1, \cdots, N \end{aligned} \tag{4}$$

where C_1 is the regularization parameter, $\phi(\cdot)$ is a nonlinear mapping function.

Determination of the final separation hyperplane based on S³VM

Optimization problem for semi-supervised SVM[4]

$$\begin{aligned} &\min_{w,b,\xi^p,\xi^u} \left\{ \frac{1}{2}\|\boldsymbol{w}\|^2 + C_1 \sum_{n=1}^{N} \xi_n^p + C_2 \sum_{m=1}^{L} \xi_m^u \right\} \\ &s.t.\quad y_n^p \cdot \left[\boldsymbol{w}^T \cdot \phi\left(x_n^p\right) + b \right] \ge 1 - \xi_n^p, x_n^p \in X_p \\ &\qquad y_m^u \cdot \left[\boldsymbol{w}^T \cdot \phi\left(x_m^u\right) + b \right] \ge 1 - \xi_m^u, x_m^u \in X_u \\ &\qquad \xi_n^p \ge 0, \xi_m^u \ge 0, n = 1, \cdots, N\ and\ m = 1, \cdots, L \end{aligned} \tag{5}$$

In order to construct two types of statistical characteristics of the sample mean no label set, then

$$\begin{aligned} &\min_{w,b,\xi^p,\xi^u,\rho} \left\{ \frac{1}{2}\|\boldsymbol{w}\|^2 + C_1 \sum_{n=1}^{N} \xi_n^p + C_2 \sum_{m=1}^{L} \left(\xi_m^u + \rho_m - \left| f\left(x_m^u\right) \right| \right) \right\} \\ &s.t.\quad y_n^p \cdot \left[\boldsymbol{w}^T \cdot \phi\left(x_n^p\right) + b \right] \ge 1 - \xi_n^p, x_n^p \in X_p \\ &\qquad \left| \boldsymbol{w}^T \cdot \phi\left(x_m^u\right) + b \right| \le \rho_m,\ \rho_m \ge 1 - \xi_m^u, x_m^u \in X_u \\ &\qquad \xi_n^p \ge 0, \xi_m^u \ge 0, n = 1, \cdots, N\ and\ m = 1, \cdots, L \end{aligned} \tag{6}$$

Let $\left(\tilde{w}, \tilde{b}, \tilde{\xi}_n^p, \tilde{\xi}_m^u, \tilde{\rho}\right)$ to optimize the results of (6), then

$$\tilde{\xi}_m^u + \tilde{\rho}_m = \begin{cases} 1, & \left| f\left(x_m^u\right) \right| \le 1 \\ \left| f\left(x_m^u\right) \right|, & otherwise \end{cases} \tag{7}$$

i.e.

$$\tilde{\xi}_m^u + \tilde{\rho}_m - \left|f\left(x_m^u\right)\right| = \begin{cases} 1 - \left|f\left(x_m^u\right)\right|, & \left|f\left(x_m^u\right)\right| \le 1 \\ 0, & otherwise \end{cases} \tag{8}$$

Therefore, (6) and (5) are equivalent. then

$$\begin{aligned} &\min_{w,b,\xi^p,\xi^u,\rho} \left\{ \begin{array}{l} \frac{1}{2}\|\boldsymbol{w}\|^2 + C_1 \sum_{n=1}^{N} \xi_n^p + C_2 \sum_{m=1}^{L} \left(\xi_m^u + \rho_m\right) \\ -C_2 \left(\mu_+ w^T \widehat{M}_+ - \mu_- w^T \widehat{M}_- + \mu_+ b - \mu_- b\right) \end{array} \right\} \\ &s.t.\ \ y_n^p \cdot \left[\boldsymbol{w}^T \cdot \phi\left(x_n^p\right) + b\right] \ge 1 - \xi_n^p, x_n^p \in X_p \\ &\left|\boldsymbol{w}^T \cdot \phi\left(x_m^u\right) + b\right| \le \rho_m, \rho_m \ge 1 - \xi_m^u, x_m^u \in X_u \\ &\xi_n^p \ge 0, \xi_m^u \ge 0, n = 1, \cdots, N\ \ and\ \ m = 1, \cdots, L \end{aligned} \tag{9}$$

where μ_+, μ_- represent the number of the change class and the no change class of the no labeled set X_u, respectively, $\widehat{M}_+$, $\widehat{M}_-$ are the mean estimators of the change class and the no change class of the no labeled set X_u. As can be seen from (9). Simplify (9), we obtain S^{3}VM optimization problem is:

$$\begin{aligned} &\min_{e \in \Delta} \min_{w,b,p,\xi^p} \left\{ \frac{1}{2}\|w\|_2^2 + C_1 \sum_{n=1}^{N} \xi_n^p - C_2 \beta \right\} \\ &s.t.\ y_n^p \left(w^T \cdot \phi\left(x_n^p\right) + b\right) \ge 1 - \xi_n^p,\ \ x_n^p \in X_p \\ &\frac{1}{\mu_+}\left(w^T \cdot \sum_{m=1}^{L} e_m \phi\left(x_m^u\right)\right) + b \ge \beta \\ &\frac{1}{\mu_-}\left(w^T \cdot \sum_{m=1}^{L} \left(1 - e_m\right) \phi\left(x_m^u\right)\right) + b \le -\beta \end{aligned} \tag{10}$$

where $\Delta = \left\{ e \middle| e_m \in \{0,1\}, \sum_{m=1}^{L} e_m = \mu_+ \right\}$, (10) reduction in the constraint condition, that can be improved and optimized SVM training efficiency. So acquire (10) dual formula [5].

Experimental results and analysis

In order to verify the effectiveness of the algorithm is carried out experiments to verify the effectiveness of the proposed algorithm.

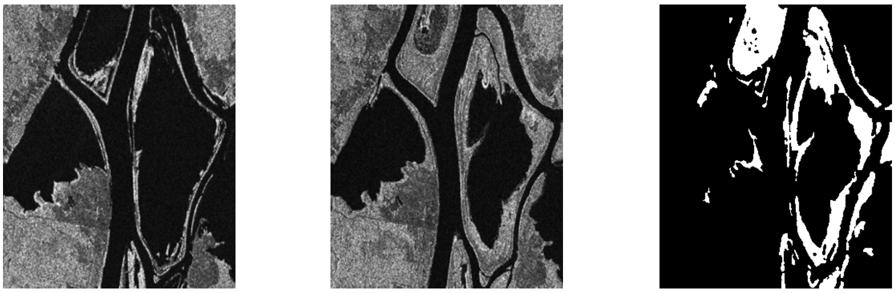

(a)Image in May., 1997 (b)Image in Aug., 1997 (c)Reference image

Figure 1 SAR images relating to flooding in Bern city

SAR image data set of the original image and the reference change used in the experiment shown in Figure 1. The original image data set which was in May 1997 and August 1997 Radarsat-1SAR images Ottawa Canada, is shown in 1 (a) and 1 (b) below. The size of the two images are 350 × 290, 256 gray level. Figure 1 (c) detecting the change of the reference figure, a white pixel in the figure indicates the region of the two phases is changed, the number of pixels is 16049.

Logarithmic ratio operator generated the difference image X_{DI} , $\max(X_{DI})$ is 4.0604，$\min(X_{DI})$ is 0。According to K-Means clustering obtained threshold $T = 1.1047$, δ_1 and δ_2 are taken as 0.5. SVM is only relation with support vectors, and therefore concentrate sampling 100 samples from the pseudo-training, unlabeled samples were sampled 1000, 500, 100, classification and methods of test S^3VM generalization ability, and the use of unlabeled sample open semi-supervised learning, is shown in Table 1.

Tab.1 Analysis of change detection results in Ottawa

Pseudo-training data	Unlabeled data	Support vector	Missed alarms	False alarms	Overall error	Kappa accuracy
100	1000	99	2268	3163	5431	0.8035
100	500	72	2199	3438	5637	0.7977
100	100	32	2337	3006	5343	0.8056

Experiments show that the detection method based on S3VM does not require any a priori information for prior information to obtain greater difficulties or prior information error detection process, and semi-supervised learning ability, high efficiency, stable test results, with some noise immunity. Kappa coefficient test is not high, mainly due to the experimental design process, in order to reflect a stable classification method and generalization ability, did not use noise reduction and did not consider spatial context information of the image.

Conclusion

SAR image change detection is proposed, using the mean statistical characteristics of semi-supervised learning, not only for speckle noise is robust, but also has a higher training efficiency. The method using K-means clustering algorithm to obtain a threshold based on the introduction of offset is automatically selected to achieve a pseudo training set and unlabeled set; then use a mixed sample of common training SVM, to obtain the optimal hyperplane is a kinds of unsupervised methods. Experimental results show that the method is feasible and effective. The next step is to use the spatial context information to further improve image change detection accuracy.

Acknowledgements

This work was financially supported by the National Natural Science Foundation of China (61132008), (61072141).

References

[1] A Bouaraba, A Younsi, A A Belhadj, et al. Robust techniques for coherent change detection using cosmo-skymed SAR images. Progress in Electromagnetics Research M, 22: 219-232(2012).

[2] F Bovolo, C Marin, L Bruzzone. A Hierarchical Approach to Change Detection in Very High Resolution SAR Images for Surveillance Applications. IEEE Transactions on Geoscience and Remote Sensing, 51(4): 2042-2054(2013).

[3] C J C Burges. A tutorial on support vector machines for pattern recognition. Knowledge Discovery and Data Mining, 2(2): 121-167(1998).

[4] O Chapelle, V Vapnik, O Bousquet, et al. Choosing multiple parameters for support vector machines. Machine Learning, 46(1-3) : 131-159(2002).

[5] Y F Li, I W Tsang, J T Kwok, et al. Tighter and convex maximum margin clustering. Proceeding of the 12th International Conference on Artificial Intelligence and Statistics, 344-351(2009).

Applied Mechanics and Materials Vol. 596 (2014) pp 490-493
© (2014) Trans Tech Publications, Switzerland
doi:10.4028/www.scientific.net/AMM.596.490

Road Roughness Measurement and Analysis for Vehicle Bench Test

Junwei Yu[1, a], Nan Liu[2] and Bin Wang[3]

[1]Henan University of Technology, Zhengzhou, Henan, 450001, China

[2]the PLA Information Engineering University, Zhengzhou, Henan, 450001, China

[3]Commercial Product R&D Institute, Dongfeng Automobile Co., Ltd, Wuhan, 430057, China

[a]yujunwei@126.com

Keywords: Road roughness, vehicle bench test, wavelet analysis, measurement.

Abstract. Road roughness, the most direct automotive input, is a kind of basic data. Its analysis and applications have important effects on vehicle performance. Several methods such as wavelet analysis, amplitude-domain analysis, frequency-domain analysis are used to analyze the road elevation series of a highway. Through some disposal of the original survey data, a series of representative data has been taken to reproduction test in a 4-poster road simulator. Both analyses and test results show that, the proposed methods can be used for the actual data process of road roughness and in the vehicle bench test.

Introduction

The interaction between the rough road surface and wheels is one of the most important vehicle environment inputs, which has important effects on vehicle performance. Therefore, it is fairly necessary to proceed different kinds of analyses on road profile measured data and to find out the most important influencing factors to the vehicle performance [1][2]. In this paper, some signal processing methods are used to analyze road surface roughness of actual measurement data, and to reflect the diversity information with different aspects. With the vehicle bench test, the rollers can product different surface roughness in order to reproduce diverse road conditions. We try to represent the time domain road roughness signal on the four-poster road simulator through the power spectral density (PSD) of the disposed profile data.

Data Preprocessing based on Wavelet

Owing to a great many uncertainties involved in actual measurement, such as the time variant velocity while sampling, the original sample data ought not to be directly applied and it needs data preprocessing. Data resample process is bellow. Because the spatial sampling frequency in the actual measurement data is higher and widely beyond the sensitive frequency range when the general vehicle running on the road normally[1][2]. Therefore, it needs the sample frequency down. As Fig.1 (a) illustrates, the original signal spatial sampling interval is 10mm, thus spatial sampling frequency is namely $100m^{-1}$. The resample signal is showed in Fig.1 (b), whose spatial interval is 200mm and the sample point is 8192.

The resample signal above still contains some low-frequency signals that can influence the vehicle performances. As existence of these low-frequency signals, the stationary state of resample data might even be reduced to a non-stationary state. We use Mallat wavelet decomposition algorithm to wipe off such low-frequency components[3]-[5].

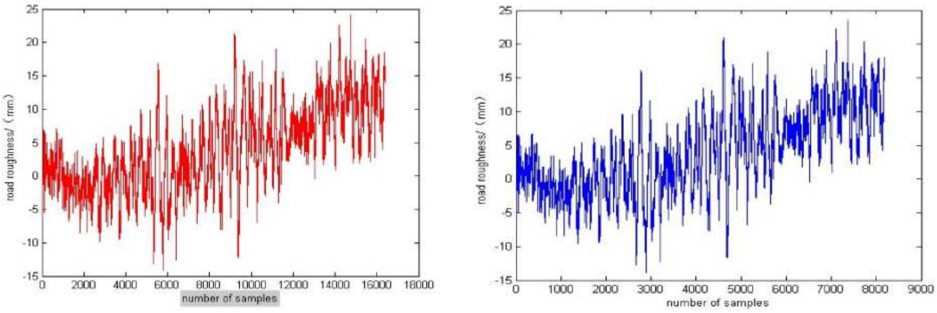

Fig.1 (a) Original signal; (b) Resample signal

Given the signal $f(t)\in L^2(R)$, its continuous wavelet transformation (CWT) $W_{a,b}$ is defined as:

$$W_{a,b}=\int_R f(t)\Psi_{a,b}(t)dt=|a|^{-1/2}\int_R f(t)\Psi(\frac{t-b}{a})dt \tag{1}$$

Where $\Psi_{a,b}(t)=|a|^{-\frac{1}{2}}\Psi(\frac{t-b}{a})$ is wavelet family of functions; a and b are scale and shift factors respectively. Proceed discrete sampling to the factors a and b as following:

$$\Psi_{m,n}(t)=a_0^{-\frac{m}{2}}\Psi(a_0^{-m}t-nb_0) \tag{2}$$

Then its discrete wavelet transformation (DWT) is

$$DW_{m,n}=\int_R f(t)\Psi_{m,n}(t)dt \tag{3}$$

According to the actual discrete sampling signals, different Mallat algorithms can adopted to compute their discrete wavelet transformation. The 'db8' wavelet is chosen to run a five-level decomposition of the signal. The process of decomposition can be described as (4). Where S is the signal to be decomposed, $A_j(j=1,2,\cdots,5)$ is the j th-level approximation signal, and D_j is the j th-level detail signal.

$$S=A_5+\sum_{j=1}^{5}D_j \tag{4}$$

On the ground of the characteristic of Mallat decomposition, frequency of A_5 is the lowest in all the decomposition signals. And A_5 expresses the large and long wave in signal S, reflecting the overall shape of the road. Thus highest level decomposition has small effects on the vibration of vehicle and could be wiped off from S. Then the remainder high frequency part of S are token as road unevenness signal to proceed, dispose and analyze in the following step.

Amplitude Value and Frequency Domain Analysis of Road Roughness

Amplitude value domain. The amplitude domain analysis mostly reflects the global property of measured specimen data. For the mean value already approaches zero through the above original data preprocessing, the frequently typical amplitude parameters are values of max and min, mean square, root mean square and crest factor when analyzing the road surface[6]. The unbiased estimation of these parameters can be calculated using series $u(n)$.

Frequency domain. The power spectral density analysis is one of the most important means among road data processes. Being different from the above time-domain description, the PSD reflects the road stochastic elevation changes with the frequency. The representation of PSD is classified into auto-power spectrum density and cross-power spectrum density, owing to merely analyzing one channel measured data. In this paper, only auto-power spectrum density is used. Take the average method to estimate the auto power spectrum density(Fig.2 (a)).

Commonly the estimation PSD needs curve fitting to receive a fitting expression. Popularly take the following equation to carry on fitting[1].

$$G_q(\Omega) = G_q(\Omega_0)(\frac{\Omega}{\Omega_0})^{-W} \tag{6}$$

where Ω is the spatial frequency (m^{-1}), which is the wavelength inverse, in other words wave numbers per-meter; Ω_0 is called reference spatial frequency, $\Omega_0 = 0.1m^{-1}$; $G_q(\Omega_0)$ stands for the road PSD under Ω_0, called road surface unevenness coefficient. And Fig.2 (b) illustrates the comparison between the fitting PSD and estimation PSD.

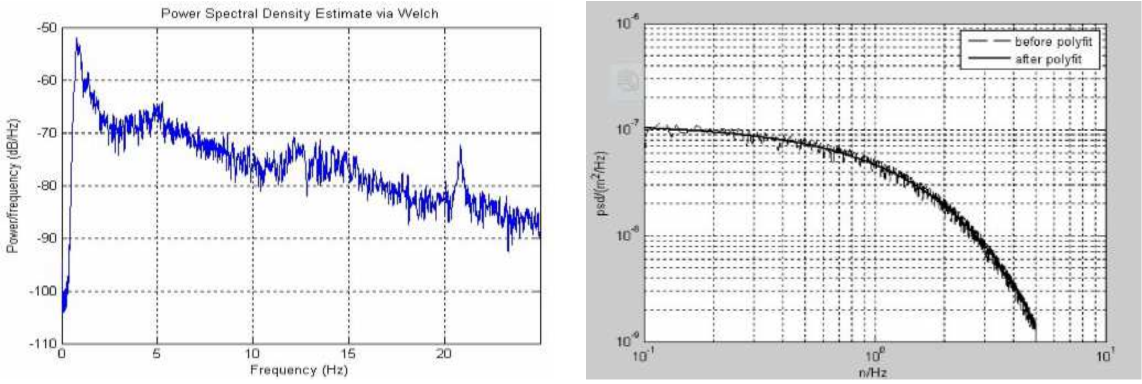

Fig.2 (a) Estimation of auto power spectrum density, (b) PSD fitting curve of the measured data

Reproduction Test in Road Simulator

The common use of road roughness data is the input in nonlinear system simulation. In order to expand the data's application area, consider that utilizing a 4-post road simulator to reproduce a random target road elevation. Running a reproduction test needs a roughness data as the target signal. There are two methods to acquire the target signal.

(1) Directly deploy the processed series $u(n)$ as the target signal.

(2) Take the above fitting PSD as the target PSD and make use of Partial Wave Adding[7][8] to reconstruct a time-domain road roughness series. Compared with the former technique, this method is more flexible and able to receive different unevenness series by setting different reconstruction parameters according to a certain level road surface.

Carry out the reproduction test with a 4-post road simulator according to the technique and procedure describing in reference[9]. The basic parameters of vehicle test bench are as follows:

- The actuator max active force is ± 50kN
- Max displacement is ± 150mm

- Initial velocity is 2m/s
- System critical frequency is 30Hz

Fig.3 illustrates the test result. For convenience，here take the number of 512 for example. From the figure, it can be seen that the two signals are much close to each other so that the anticipation has arrived.

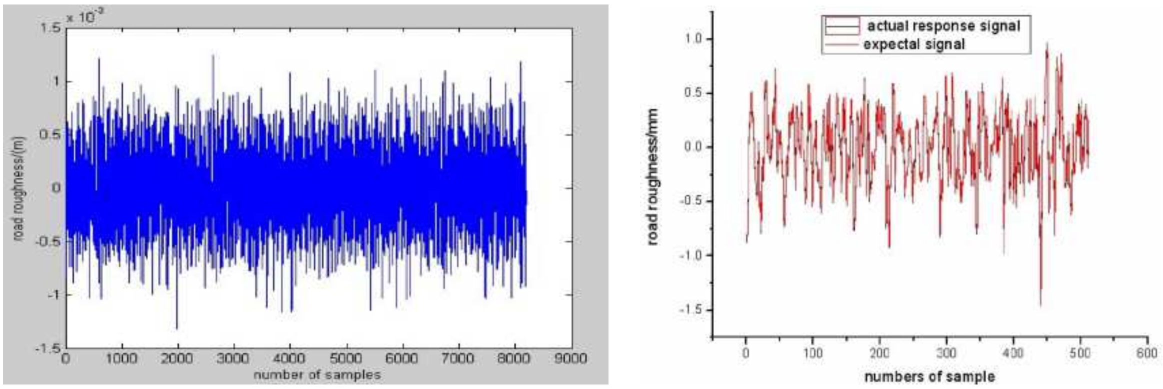

Fig.3 (a) Target data (b) Reproduction result in bench test

Summary

This paper has analyzed a certain actual measurement of road surface elevation from different aspects and presents a part of data procedures the authors used. Taking different methods to analyze data could reflect the multi-aspect information the measured data involved. In the end, the authors try to reproduce the disposed data in a 4-post road simulator. From analyses and test results, the effects are good and come to the expectant purpose.

Acknowledgements

This work was financially supported by the NSFC project under grant No. 61300123 and Zhengzhou key project of science and technology under grant No. 20130768.

References

[1] Zhisheng Yu: *Automotive Theory*(Machine Press, China 2004).

[2] Jihai Zhao, Zheren Wang, and Chaopi Guan: *Measurement and Application of Road Roughness*(Press of Beijing Uni. Tech, 2000).

[3] E. Merry, M. Steinbuch and M. van de Molengraft: *Wavelet Theory and Applications*(Eindhoven University of Technology, 2005).

[4] L. Liangyu, Z. Weiping and W. Jiangtao: Cn. J Sens. Actu. Vol. 20 (2007), p. 877

[5] W. Liu and Z. Zhao: J Transp. Engi. Vol. 131 (2005), p. 120

[6] B. Bruscella, V. Rouillard and M. Sek: J Transp. Engi. Vol. 125(1999), p. 55

[7] L. Sun: Math. Comp. Simu. Vol. 61 (2003), p. 77

[8] Z. Chang, H. Luo, Z. Chu, et al: J Chongqing Uni. Vol. 27(2004), p. 5

[9] B. Wang, X.X. Guo and S. Yang, in: 2nd International Conference on Transportation Engineering, American Society of Civil Engineers(2009).

Applied Mechanics and Materials Vol. 596 (2014) pp 494-497
© (2014) Trans Tech Publications, Switzerland
doi:10.4028/www.scientific.net/AMM.596.494

An Improved of Extended Kalman Filtering method on Tracking Accuracy of bistatic Sonar System

Yong Sun[1,a], Junwei Zhao[2,b]

[1]College of Information Science and Engineering, Ocean University of China, Qingdao, China

[2]College of Marine, Northwestern Polytechnical University of China, Xi'an, China

[a]robust2003@hotmail.com, [b]jwzhao@nwpu.edu.cn

Keywords: bistatic sonar; tracing accuracy; IEKF algorithm; target moving analysis

Abstract. The Extended Kalman Filter methods were widely used in the estimation of tracing situation in military fields. In this paper, we proposed a method of using multiple iteration of the observation and covariance matrix in the measuring equations during the tracking process in bistatic sonar system. Therefore the iterating extended kalman filtering (IEKF) algorithm was emerged at this situation. The simulation results show that the proposed tracing algorithm exhibits higher accuracy compared with the EKF algorithm. This new method can take full application of the measured information to improved the tracing accuracy in the whole controlled area.

Introduction

At present, the bistatic sonar system[1-3] and multistatic sonar system[4] have been widely used in fields such as locating and tracking underwater targets. According to the situation of using the bistatic sonar system to localize and track the underwater target, the measurements which include the time information and measured azimuth angle information of different sonar systems were proposed thoroughly. However, as these observations are nonlinear functions which can be solved as the target state and positioning of the radiation source, the using of non-linear filtering technology becomes the primary method of improving the bistatic sonar target tracking performance. Because of the unbiased optimization features in the kalman filter, the filter shows widely applicating in many fields, such as target tacking and navigation systems. Wang Cheng[5] proposed an EKF tracing algorithm of bistatic sonar system. This algorithm was based on the transformation of nonlinear measuring data into linear measuring data. Sun Yong[6] proposed the improving least square(ILS) algorithm which developed frome the localization of bistatic sonar system. Although it enhanced the accuracy of tracking performance, the algorithm exhibited the limitations for the reason of its posteriori estimation. In this paper, we developed a new method through multiple iterations of extended kalman filter. Then we deeply conducted theoretical study and analysis by analyzing the target positions of a period of time using the IEKF tracking algorithm.

Configuration of bistatic sonar system

Fig.1 shows the principle of bistatic sonar system. In this figure, T/R means emitting station, which contains the typical characters of monostatic sonar by receiving the echo from target. R represents receiving station. S equals to the position of target. r_T defines as the distance between emitting station and target. r_R defines as the distance between target and receiving station. θ_T as pointing angle of emitting station; θ_R as pointing angle of receiving station.

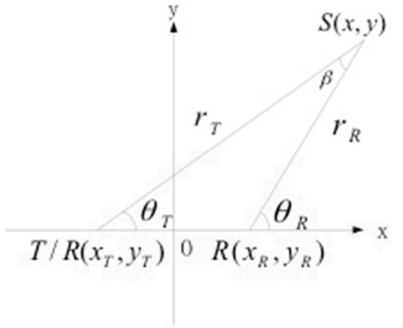

Fig.1 Configuration of bistatic sonar system

Iterative Extended Kalman(IEKF) Tracing Algorithm

The error of EKF[7] may cause deterioration or even divergent as the iterating frequency of EKF only contains once. For the purpose of improving these drawbacks, an Iterative Extended Kalman tracing algorithm was proposed. Arithmetic formulas and processes were as follows:

$$\hat{X}^0_{i/i} = \hat{X}_{i/i}, \qquad P^0_{i/i-1} = P_{i/i-1} \tag{1}$$

$$\begin{aligned}
&for \quad k = 0 : n-1 \\
&\qquad H^k_i = \left.\frac{\partial G(X)}{\partial X}\right|_{X=\hat{X}^k_{i/i}} \\
&\qquad K^k_i = P_{i/i-1}(H^k_i)^T[H^k_i P_{i/i-1}(H^k_i)^T + R_i]^{-1} \\
&\qquad \hat{X}^{k+1}_{i/i} = X_{i/i-1} + K^k_i[Z_{m,i} - G(\hat{X}^k_{i/i}) - H^k_i(\hat{X}_{i/i-1} - \hat{X}^k_{i/i})] \\
&\qquad P^{k+1}_{i/i} = (I - K^k_i H^k_i)P_{i/i-1}(I - K^k_i H^k_i)^T + K^k_i R_i (K^k_i)^T \\
&END
\end{aligned} \tag{2}$$

In the upper equations, $\hat{X}^0_{i/i}$ means the state vector before iteration, $P^0_{i/i-1}$ means the covariance matrix before iteration, H^k_i means the observation matrix, K^k_i means the kalman's gain matrix. According to the upper equations, the physical meaning of IEKF method is to use multiple iterations to update the state estimation to approximate nonlinear observaions. This method allows to further reduce estimation error status, so as to optimize filter estimation purposes during the estimation of bistatic sonar tracking system.

Numerical Simulation and Analysis

According to the actual driving conditions of sea ships, we proposed the speed of ship as 13m/s, towards the direction of northeast. We set the sampling time as 1 second and the total sampling times as 200 seconds. The simulating conditions were proposed like that the angle measurement deviation as $\sigma_{\theta_T} = \sigma_{\theta_R} = 0.4°$; the coordination of station T/R as (-5,0) km; station R as (5,0) km; station. With the above parameters, the simulation of new algorithm of tracing performance comes into effect.

(a) , (b), (c) and (d) of figure 2. show the results of tracing accuracy of IBOL algorithm in case of baseline length as 10 km; (a), (b) and (c) of figure 3. show the results of tracing accuracy of IBOL algorithm in case of baseline length as 20 km. Derived as:

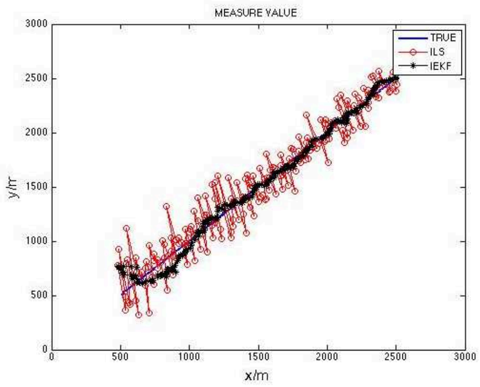

Fig.2 Tracing trajectory of trajectory-
length of 10km

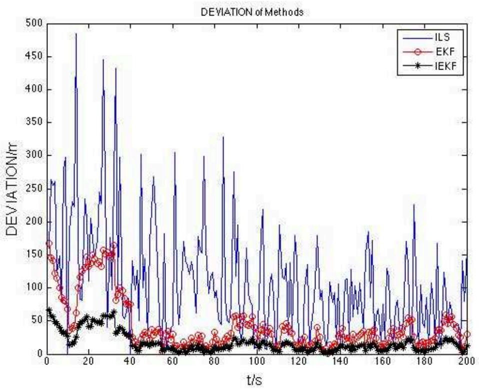

Fig.3 Accuracy of whole region of the whole region with baseline

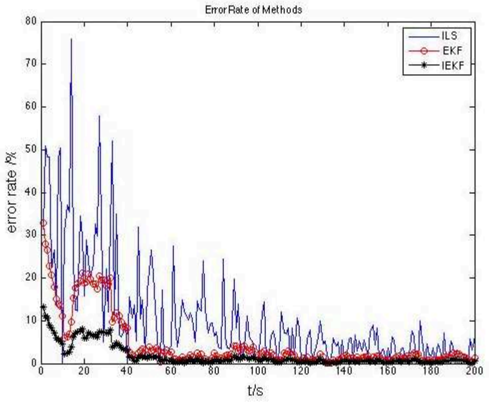

Fig. 4 The error rates of three different algorithms of bistatic sonar tracking system

With acknowledgment of the simulation results, we realize:

1) According to the simulations of fig.2, fig.3 and fig. 4, we realized that the three different algorithms had shown an excellent convergence during the tracking process. However a large gap among the three algorithms for tracking performance had also emerged during the process. ILS tracking algorithm showed the worst tracking performance for its whole error rate was about within 30% . Compared with ILS algorithm, the EKF algorithm exhibited better performance because of its tracking error reduced to within about 50 meters and its error rate down to 5%. The best tracking algorithm was the IEKF traking algorithm which was proposed in this paper. Simultaneously, the accuracy of whole rate of IEKF was upgrated as 40% compared to the EKF algorithm. Through the results, we found that in the engineering projects, we could make use of the new tracking performance in bistatic sonar system.
2) After calculating, ILS algorithm's runtime was 120ms. Meanwhile the EKF algorithm's runtime was 168ms, however the IEKF algorithm's runtime was 190ms. Although the IEKF algorithm's time is the longest, the new tracing algorithm was more valued because of its lowest tracking error in the engineering projects.

Acknowledgement

This work was financially supported by Special Fund for young teachers Ocean University of China (1002-841313013).

References

[1] Wang Beide. *The Nature of Bistatic and Multistatic Radar* // Radar, 2001 CIE International Conference on Proceedings, 2001, 11(3): 882-884

[2] Mozzone L, Bogi S and Primo F. *Deployable Underwater Surveillance System-target Localization with Multiple Sonar Receivers*. SR-317. NATO SACLANT Undersea Research Center, 1998

[3] Sun Yong, Zhao Junwei, Zhang Yinbing, Zhang Xiaofeng. *A Localization Algorithm with Combined Subsets for Multistatic Sonar System.* Torpedo Technology Vol. 17. No. 2 Apr. 2009, p. 33-36

[4] Zhang Xiaofeng, Ying Huan. Research on Localization Algorithm Based on WLS for Multi-static Sonar. Computer Simulation Vol. 28. No. 8. Aug 2010, p. 393-396

[5] Wang Cheng, Wang Yingmin, Tao Linwei and Gan Tian. Bistatic Sonar Data Fusion based on Extended Kalman Filtering and Its Application. Fire Control & |Command Control Vol.35, No. 9, Sep. 2010, p. 13-15, 30

[6] Yong Sun, Junwei Zhao. An Algorithm of Improving Least-Square Method on Tracing Accuracy of bistatic Sonar System. 3rd International Conference on Measurements, Instrumentation and Automation.

[7] Luo Yu, Wang Yongqing, etc. Study on Vector Tracking Loop Based on Extended Kalman Filter[J]. Journal of Electronics & Information Technology Vol. 35. No. 6. Jun 2013, p1400-1405

Applied Mechanics and Materials Vol. 596 (2014) pp 498-504
© (2014) Trans Tech Publications, Switzerland
doi:10.4028/www.scientific.net/AMM.596.498

Application of Mobile Data Acquisition Technology in Highway Lightning Protection

Yanhua Zhang[1, a], Xue Jiao[1,b] , Yingying Zhong[2,c], Junchi Zhou[1,d]
and Ju Yuan[1,e]

[1] Lightning Protection Center of Jiangsu, Nanjing 210009, China

[2] Lightning Protection Center of Changzhou, Changzhou 213022, China

[a]59514383@qq.com, [b]jiaoxue2046@126.com, [c]view618@163.com

Keywords: Mobile data acquisition technology, Inspection of lightning protection systems of highway, Data acquisition terminal

Abstract. The inspection of lightning protection system is developing gradually presently,while it is still in a relatively backward stage, data acquisition method is old, measuring conclusion is not real-time, data measurement is out of line with the standardization of lightning business. The service area and toll station of highway prone to lightning strikes for the isolated location. Meantime, there is no lightning protection facility or facilities are not perfect, lightning accidents happen sometime which caused heavy losses to the highway with a lot of sensitive electronic equipment. The inspection of highway lightning protection should be strengthened, the mobile data acquisition technology is introduced to the highway lightning inspection in order to make the lightning protection devices play an effective role. The data acquisition process and application are described, it can ensure the diversification of data, the real-time transmission of field testing data, further standardization of the lightning inspection process and the quality of inspection to ensure safe and effective operation of building and electromechanical systems.

Introduction

With the frequently increasing lightning accidents and expanding of lightning protection business, the public and the governments at all levels have gradually focused on lightning inspection, which makes the inspection of lightning protection system more difficult. The current problems of lightning inspection are as followed [1,2]. Firstly, inspection items are not standard and the personnel quality is different which make the inspection item, spot and content different, even quite different result, so social complaints come that seriously affected the image of our job. Secondly, the recording at spot is simple, site inspection cannot be restore, the quality is unable to be controlled, the original paper records are relatively simple which can not directly reflect the inspection position, material, corrosion and other conditions of the lightning protection system. Finally, the efficiency of inspection is low, data entry is repeated, and document management is inconvenience. At present, on-site inspection usually record manually on paper, when making report, data need to be typed into computer repeatedly which waste a lot of time, it is unable to effectively improve the working efficiency and quality. Meantime, staff need to carry, processing and manage a lot of paper which is not conducive to the management of data and work. These problems have restricted the improvement of lightning technology service, leaving a huge hidden responsibility to the lightning technology services. The lightning inspection needs to be standardized and unified, testing report issued by aging remains to be improved, the feedback of supervision for service quality needs to be accelerated, but the data acquisition experiencing a major bottleneck [3], data acquisition method is old, conclusion is not real-time, the process of inspection is out of line with the standardization of lightning business. Introduction of mobile data acquisition technology will largely solve the present problems in lightning protection.

Highway is an important infrastructure of national economic development, with its convenience, showing a trend of rapid development in recent years. However, the highway service area, toll stations are generally located in the empty outside, no tall buildings around, the probability of lightning stroke is high. Meantime, along with the development of intelligent highway toll and oiling systems, many kinds of advanced electronic equipments are widely used in highway, low insulation intensity, weak over-voltage and over-current tolerance and sensitive to electromagnetic interference of these systems which are vulnerable to interference and the harm caused by lightning [4]. Lightning invasion to service area and toll station brings great hidden danger to the safe operation, part of the equipment will be broken, even the whole system is going to collapse which cause heavy economic losses and serious social effects. With the continuous development of intelligent transportation, extensive application of electronic equipment and the integration degree increasing, the harm degree of lightning on highway electronic equipment will also increase. Although the lightning protection awareness has been enhanced [5], structures and equipment have been generally installed lightning protection measures, due to the lightning protection of understanding is not in place, resulting in some problems in lightning protection measures of highway, the inspection of highway should be strengthened to make lightning protection devices installed play an effective role.

Therefore, advantages of introducing mobile data to lightning detection are analyzed, the data acquisition process are specified, and combined with the key project of highway, data acquisition technology is used in comprehensive inspection of highway. The advantages of mobile acquisition technology appeared clearly, it ensure the lightning detection process standardized and accurate inspection results.

Advantage of mobile data acquisition

With the development of mobile computing technology and wireless communication technology, IT technology is increasingly diverse needed in all walks of life, mobile terminal is more and more applied to all areas [6].The most widely used in these areas is the use of mobile data terminals for data collection in various working conditions, and then the data is synchronized to PC or backstage database for data processing, namely mobile data acquisition technology. Application of mobile data acquisition technology can reduce the artificial interference in data acquisition, duplication of work and can improve work efficiency, at the same time, it can guarantee the timeliness and accuracy of data collection which improving the quality of data acquisition work.

The mobile data acquisition technology is introduced to the inspection of lightning protection systems in highway service area and toll station, application of mobile data terminal can make data acquisition through lightning inspection field, achieve historical data full back, and strengthen the cooperation of the whole inspection. At present, the inspection of highway is internal and external business [7] which means the report is separated finished by staffs inside after data collection and field investigation by outside staffs. Presently, internal work is streamline and standardized, but external business is still in the primitive stage, field data acquisition depends on manual record, and then data is manually input into system again, the serious disconnect between internal and external work restrict development of lightning protection. With the introduction of mobile data acquisition technology, the internal and external work integration of lightning inspection can be realized through exchanges and collaborative visualization technology, which greatly improved the quality of inspection of lightning protection systems of highway.

Real-time monitoring. Mobile data acquisition technology makes the data acquisition, exchange and inspection report of lightning protection system easier. More importantly, for the use of these techniques in quality system, we can real-time supervise and control the inspection of highway to ensure the test quality and standardize the process of inspection.

Enhance the overall cooperation. To understand the problems encountered in site detection, we must refer to the real data. If sudden events happen, we can return data through the mobile data acquisition system, and receive relevant expert guidance by real-time communication, to solve the problem on time and efficiently which improve the work efficiency and the image of industry.

Enhance data traceability. With the continuous expansion of the lightning protection for highway and increasing concern of the wide public and government at all levels, the responsibility and the risk of lightning inspection of highway is also growing. Therefore reduction inspection field, tracking inspection process and the cause of the accident are especially important. Application of mobile data acquisition technology can make the whole lightning inspection data of highway be traced back. So that in the event of a major lightning accident, all the testing information can be effectively available, lightning inspection department can respond to the event on time.

The mobile data acquisition process

As shown in Fig. 1, firstly testing personnel download the highway inspection task through wireless network from the mobile data acquisition terminal, then inspect lightning protection system and carries on corresponding processing to the test data, finally, through wireless network or USB mobile storage device return field test data to the comprehensive lightning detection platform. After further analysis, the data is used to make inspection report of highway lightning protection systems, meantime, according to the data can be used for quality supervision and on-site guidance.

Tasks download. As regulated by ‘Technical Specifications for Verification of Lightning Protection System in Freeway’, lightning protection system should be regularly inspected, buildings and electromechanical systems of highway should be tested once a year, gas station should be inspected semiannually. When inspecting direct lightning protection system, the lighting protection devices of low voltage and signal system should also be inspected in order to prevent lightning induction and lightning wave invasion from damage to electrical, communication and microelectronic devices. Using mobile data acquisition terminal , testing personnel download the highway detection task, , including the detection form, the information about the being tested and historical inspection record download (for organization have been inspected before, on the basis of the history record testing personnel can add new measuring points or just according to old points to inspect).

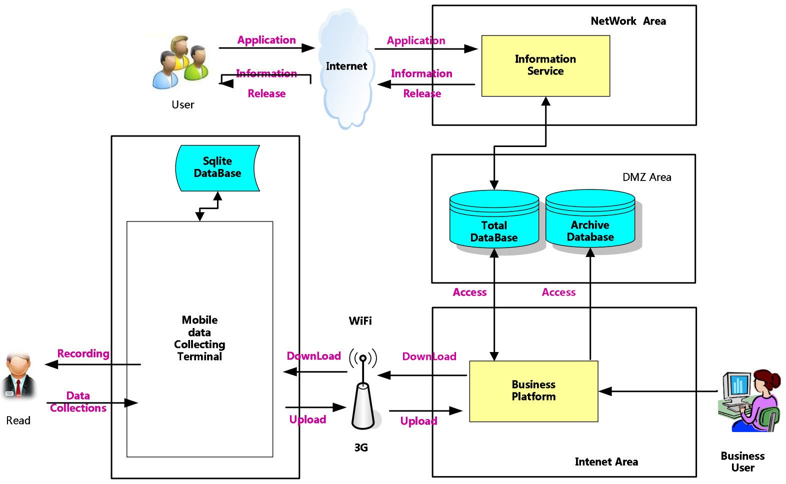

Fig.1. The mobile data acquisition precess

Field data acquisition. The field data acquisition process is shown in Fig.2, firstly, fill the inspected unit information, because the initial information of the inspected unit is always not perfect, test personnel should fill again after detailed survey. When inspecting for the first time, the basic situation should be filled in, and then the schematic diagram should be draw at the spot, measuring points and number of points should be marked, photographs are needed for further description (for example, measuring point corrosion, welding etc.). The collection data should be processed, and according to the data and the actual situation, lightning protection range, the magnetic field strength and lightning protection level can be determined. After acquisition, the testers should ask the responsible person to verify the inspection result and input the signature. Finally, the detection data should be uploaded.

Data transmission. After field data acquisition, it should be return through the wireless network or USB storage device. If it is allowed, the data can be transferred back real-time through wireless network into the lightning inspection platform. Management of lightning protection can supervise the highway inspection quality through the platform which can further standardize the inspection of highway lightning protection systems and control risk so as to enhance the image and competitiveness of lightning inspection.

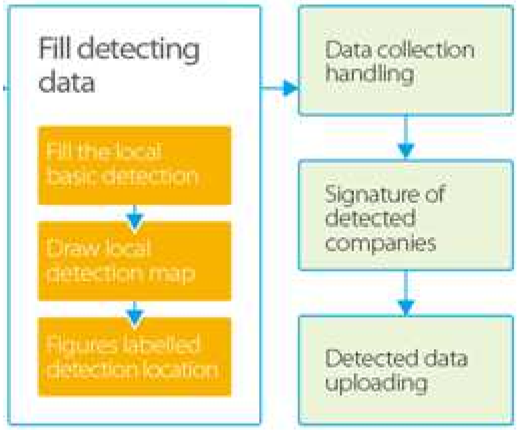
Fill detecting data
Fill the local basic detection
Draw local detection map
Figures labelled detection location
Data collection handling
Signature of detected companies
Detected data uploading

Fig.2. Process of field inspection of existing buildings

Application of inspection of highway lightning protection systems

In this paper, the mobile data acquisition technology is used in lightning inspection of highway. The mobile data acquisition terminal is used to collect data. Firstly, fill in the basic information of the inspected unit. And then according to the importance of different regions of the highway, function, lightning accident probability and consequences, the highway is divided into gas station, service area, room, charge area, toll island, signal communication box, distribution room and distribution room SPD, and each region contains different inspection contents (Table 1). With reference to the highway service area, toll island and so on, we can use the mobile data collection terminal to draw the diagram of lightning inspection (Fig. 3), then inspect according to the content. Followed by the detail inspection of gas station.

Firstly, inspection personal should draw the detection area diagram of gas station, as shown in Fig.4 , it can be divided into metal shed of gas station, gas station equipment , breathing valve discharge area, storage area, the unloading area (oil discharge port) and operating room, the specific content of each test item is shown in Table 2 and Fig. 4 .

Take the metal shed of gas station as an example, at first, we take photo of the metal shed(Fig.5) by mobile data collection terminal, and then mark the specific inspection point on the photo, as shown in Fig. 5, there are five main points, No.1 is the metal shed, No.2 to No.5 are 1# to 4# column. The inspection point can be added through drag and drop, meantime, detailed test data of the inspection point be filled in.

Table 1 Inspection content of eight zones

No.	Name	Inspection content
1	Gas station	Metal shed, refueling machine, refueling guns, charge room, breathing valve, tank, oil unloading port
2	Service area	High pole lamp, square camera, lightning belt of business building
3	Machine room	Electrostatic floor, server cabinet, table, computer, UPS
4	Charge area	Metal shed, camera
5	Toll island	The toll booths (charge computer, static floor), Lane (ETC,camera, parking rod, display, weighing machine, camera lights)
6	Signal communication box	Signal SPD
7	Distribution room	Lightning arrester
8	SPD of distribution room	Low voltage surge protective device

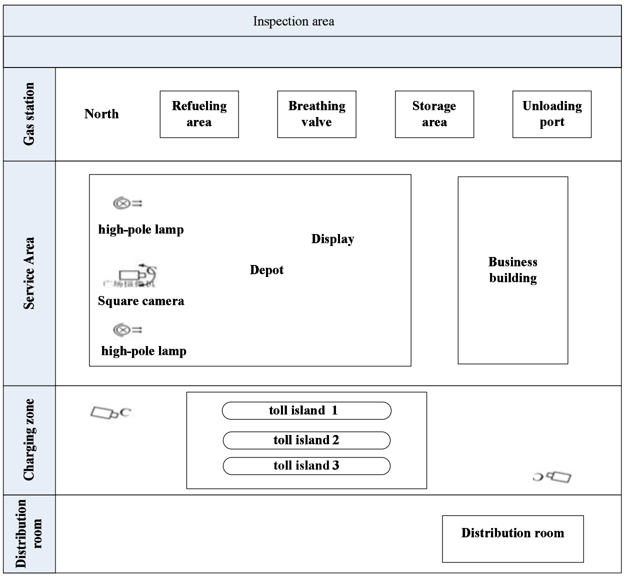
Inspection area
Gas station
North
Refueling area
Breathing valve
Storage area
Unloading port
Service Area
high-pole lamp
Display
Depot
Square camera
high-pole lamp
Business building
Charging zone
toll island 1
toll island 2
toll island 3
Distribution room
Distribution room

Fig. 3. Inspection area

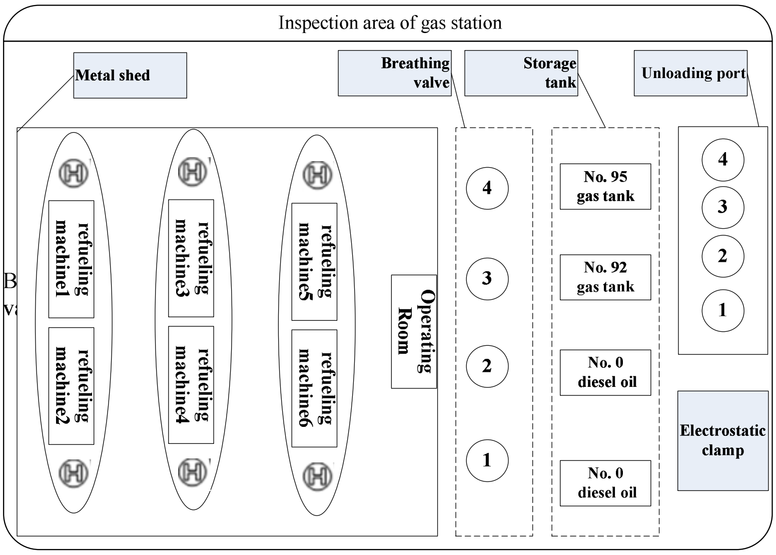
Inspection area of gas station
Metal shed
Breathing valve
Storage tank
Unloading port
refueling machine1
refueling machine2
refueling machine3
refueling machine4
refueling machine5
refueling machine6
Operating Room
4
3
2
1
No. 95 gas tank
No. 92 gas tank
No. 0 diesel oil
No. 0 diesel oil
4
3
2
1
Electrostatic clamp

Fig. 4. Inspection area of gas station

Table 2 Inspection content of each area in gas station

No.	Name	Inspection content
1	Metal shed	Shed, Grounding columns
2	Equipment	Filling machine, gas gun
3	Breathing valve discharge area	Breathing valve
4	Storage area	Oil tank
5	unloading area	Electrostatic clamp, unloading port
6	Operating room	Computer, UPS, static floor, equipotential terminal box

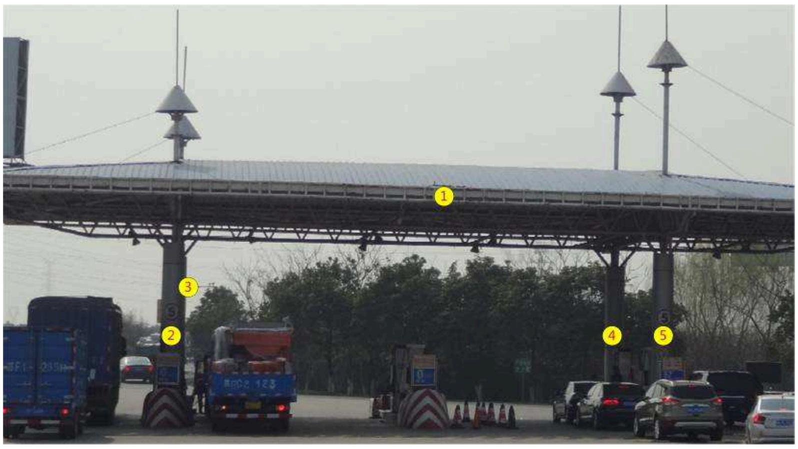

Fig.5. Metal shed of gas station

As described above, the specific process of lightning inspection for highway are as followed. Firstly, divide the highway into different areas by application of mobile data acquisition terminal based on the the importance and function of construction (structure) , then draw sketch map of each area to determine the specific testing items and take photos (Fig. 5), mark inspection point on the photo. Then fill the data real-time after inspection. Through this whole to part data acquisition method, the inspection field is visually which is a true reflection of how the inspection carries on. The specific process is shown in Fig. 6.

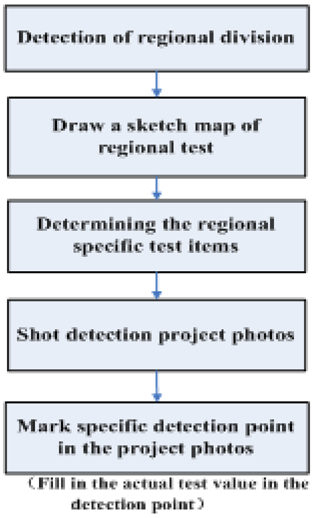
Detection of regional division
Draw a sketch map of regional test
Determining the regional specific test items
Shot detection project photos
Mark specific detection point in the project photos
(Fill in the actual test value in the detection point)

Fig.6. Flow chart of lightning inspection of highway

Conclusions

With the mobile data acquisition technology introduced into the lightning inspection of highway, it can further regulate the lightning inspection, avoid detection data and original record filling in repeatedly, standardize the testing records, improve work efficiency and data processing ability of detection personnel. Through the image acquisition function of mobile data acquisition technology, the highway detection scene can be reconstructed and reproduced, the detection project, testing contents and testing process can be standardized, so as to ensure the quality of lightning inspection and control risk. With the powerful image processing function of mobile data acquisition technology, the tedious and time-consuming drawing of site plan can be solved.

Application of the mobile data acquisition technology in the highway lightning inspection can strong break the bottleneck of lightning inspection. With the intelligent and convenient acquisition system, correctness and normative of inspection data can be effectively guaranteed, thus the quality supervision can be strendthened, the inspection quality can be ensured which promote service ability and level, control risk and further enhance the image and competitiveness of this industry.

Acknowledgements

This work was financially supported by the Jiangsu Meterological Research Foundation (KM201214).

References

[1] Feng Minxue: The analysis of present situation of the lightning disaster, Chinese traffic information industry, vol.9 (2006), p.51-52. In Chinese.

[2] Zhang Jing: Investigation of lightning protection for Expressway Mechanical and electrical engineering, Chinese traffic information industry, vol.9(2006),p. 60-63. In Chinese.

[3] Ding Weijie, Yan Lvxuan and Huang Zhicong: Design and implementation of lightning protection archives management system, Guangdong Meteorology, vol.29 (2007), p.53-55. In Chinese.

[4] Wang Zhan, Chen Fuxing and Zhang Guangjie: Research on lightning protection for information system of highway toll station, Enterprise technology development, vol. 6(2013), p.64-66. In Chinese.

[5] Sun Junde, Hu Xianfeng: Study of lightning protection method for the detection of highway toll station, Shandong meteorology, vol. 6(2013), p.26-28. In Chinese.

[6] Li Qinwen, Yue Cairong and Li Yonghe: Collection and release of forest resources based on mobile GIS, Forestry investigation and planning, vol.32 (2007), p.10-13. In Chinese.

[7] Yong Zhongming, Li Wei: Disscussion on the integration of measurement inside and outside, Coal technology, vol.23 (2004). In Chinese.

Applied Mechanics and Materials Vol. 596 (2014) pp 505-510
© (2014) Trans Tech Publications, Switzerland
doi:10.4028/www.scientific.net/AMM.596.505

The Detection of Concealed Targets Based on NQR of Nitrogen-14

Xueyi Huang [1, a], Gengguang Xu [1, b], Fenglong Hao [1, c]

[1] School of Mechatronical Engineering, Beijing Institute of Technology, China

[a] hxy_bit@163.com, [b] xugg@cae.cn, [c] haofenglong110@126.com

Keywords: NQR, detection, Nitrogen-14

Abstract. Nuclear quadrupole resonance (NQR) is an advanced radio frequency (RF) spectroscopic technique, widely used to analyse substances containing quadrupole nuclei, such as ^{2}H, ^{14}N, ^{17}O, ^{35}Cl and ^{39}K. In this paper, we focus on the NQR detection of nitrogenous compounds including nucleus Nitrogen -14 or ^{14}N. We will briefly introduce its fundamental principles, namely, nuclear quadrupole moment and NQR detection mechanism, and then provide some experimental results based on these theories, such as sodium nitrite, methenamine, urea and thiourea. At last, according to these results, we will make some discussion about the properties of NQR detection.

Introduction

Nuclear quadrupole resonance (NQR) or quadrupole resonance (QR) is an advanced solid-state non-destructive chemical analysis radio frequency (RF) spectroscopic technique, related to nuclear magnetic resonance (NMR) and magnetic resonance imaging (MRI), but without any magnet [1, 2]. Compared with NMR and MRI, NQR has a wider range of application prospect because of the following advantages: first, the apparatus will be smaller and lighter since it doesn't require a magnet any longer; second, the substance identification will become more efficient and accurate because the NQR properties, such as NQR frequencies and relaxation times, are specific to individual substances; last, the technique is perfectly uninjurious because radioactive source is out of use [3].

Quadrupole nucleus is the nucleus with non-spherically symmetric charge distribution, surrounded by the electric field generated by nucleus itself and electrons around. While an intrinsic electric field gradient (EFG) at quadrupole nucleus exsits, its energy will be split to several levels resulting from interaction. Just at this moment, applying a specific external RF field, energy transitions will happen between hyperfine energy levels, and then we can obtain the NQR signals by means of corresponding equipment [4]. Because of the extensive existence of quadrupole nuclei in compounds, for example, ^{2}H, ^{14}N, ^{17}O, ^{35}Cl and ^{39}K [5], NQR technique, serving as an effective analysis method to investigate compounds including quadrupole nuclei, is widely used in pharmaceutical analysis, contraband detection and so on, especially in detecting explosives and narcotics [1, 2, 6, 7].

In the work, we will briefly sketch the NQR theories, that is, nuclear quadrupole moment from the perspective of atomic physics and detection principle of compounds with nucleus Nitrogen -14 or ^{14}N by the viewpoint of quantum mechanics. Subsequently, based on the knowledge above, we have obtained several NQR detection results from some typical nitrogenous compounds, such as sodium nitrite ($NaNO_2$), methenamine ($C_6H_{12}N_4$), urea (CH_4N_2O) and thiourea (CH_4N_2S). Furthermore, with the purpose of expanding NQR detection technique, we have also made some discussions about these experimental results.

Fundamental Principles

2.1 Nuclear Quadrupole Moment

Based on the knowledge of atomic physics, the nuclear electric quadrupole moment *eQ* of any nucleus with axisymmetric charge distribution may be defined as [8]:

$$eQ = \int \rho r \left(3 \cos \ \theta - 1\right) d\tau \tag{1}$$

Where e is the elementary charge; ρ is the nuclear charge density in the volume element $d\tau$; r is the distance from the volume element $d\tau$ to the origin of coordinate; θ is the angle between $\bar{r}$ and coordinate axis $\bar{z}$; and the integration extends over the nuclear volume. All the geometric quantitis are shown in Fig. 1.

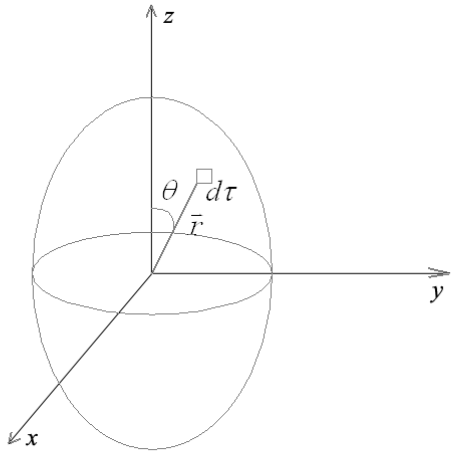

Fig. 1 Nuclear electric quadrupole moment

Additionally, all nuclei with spin quantum number not less than one, for example, nucleus ^{14}N with spin $I = 1$, have ellipsoidal symmetrical charge distributions, and then their nuclear quadrupole moment Q may be simplified as [4]:

$$Q = \frac{2}{5} Z(c - a) \tag{2}$$

Where Z is the number of nuclear charge; c and a are respectively the radius in the spin axis direction and the vertical axis direction of ellipsoid.

There are about 90 kinds of quadruploe nuclei stably existing in nature, and some typical kinds are shown as follow [5]:

Table 1 Some typical quadruploe nuclei

Isotope	Natural abundance (%)	Spin quantum number I	Nuclear quadrupole moment Q (b)
^{2}H	0.015	1	+0.002875
^{14}N	99.634	1	+0.0156
^{17}O	0.038	5/2	-0.02578
^{35}Cl	75.77	3/2	-0.08249
^{39}K	93.2581	3/2	+0.049

2.2 NQR Detection Mechanism

From the perspective of quantum mechanics, the interaction between the nuclear electric quadrupole moment eQ of nucleus ^{14}N and the electric field gradient (EFG) tensor around may be expressed with Hamiltonian operator as [9]:

$$H \;=\; \frac{e\;\; qQ}{4I\left(2I\;-1\right)}\left[3I\quad - I\left(I\;+1\right)+\eta\left(I\quad - I_{y}\;\right)\right] \tag{3}$$

Where *eQ* is the nuclear electric quadrupole moment of nucleus ^{14}N; *eq* is the largest spindle component of EFG tensor; $I = 1$ is its spin quantum number. In the expression above, we assume a choice of Cartesian coordinate axes, in which the EFG tensor is not only diagonalized, but also has the following relation:

$$\left|V\quad\right| \le \left|V\quad\right| \le \left|V\quad\right| \tag{4}$$

Where, V_{xx}, V_{yy} and V_{zz} are respectively the three spindle components of the EFG tensor at nucleus. Moreover, there is another connection between Hamiltonian operator and EFG tensor, $eq = V_{zz}$. Then, the asymmetry parameter can be defined in terms of the EFG tensor as:

$$\eta = \left(V\quad - V\quad\right)/V \tag{5}$$

By solving Schrodinger equation and transition equations, we can obtain three corresponding transition frequencies as follows:

$$\begin{cases} \nu_{+} = \dfrac{3}{4}\left(1+\dfrac{\eta}{3}\right)\left(\dfrac{e\;\; qQ}{h}\right) \\ \nu_{-} = \dfrac{3}{4}\left(1-\dfrac{\eta}{3}\right)\left(\dfrac{e\;\; qQ}{h}\right) \\ \nu\quad = \dfrac{1}{2}\eta\left(\dfrac{e\;\; qQ}{h}\right) = \nu_{+} - \nu_{-} \end{cases} \tag{6}$$

Where *h* represents Planck constant; $\chi = e^2qQ/h$ is the quadrupole coupling constant of nucleus ^{14}N; and η is the asymmetry parameter defined as before. Obviously, as long as having got the only two unknown quantities η and χ, we can obtain NQR frequencies according to Eq. (6). In order to explain the energy levels and transitions more visually, we have also described them in Fig. 2.

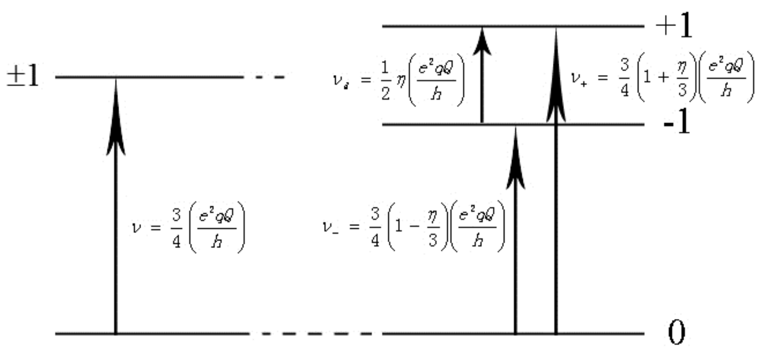
±1
+1
-1
0
$\nu_{d} = \frac{1}{2}\eta\left(\frac{e^2qQ}{h}\right)$
$\nu_{+} = \frac{3}{4}\left(1+\frac{\eta}{3}\right)\left(\frac{e^2qQ}{h}\right)$
$\nu = \frac{3}{4}\left(\frac{e^2qQ}{h}\right)$
$\nu_{-} = \frac{3}{4}\left(1-\frac{\eta}{3}\right)\left(\frac{e^2qQ}{h}\right)$

(a) η = 0 (b) η ≠ 0

Fig. 2 Quadrupole energy levels and transtions for nucleus ^{14}N: (a) η=0; (b) η≠0

As is mentioned above, in order to observe NQR singals, there must be three essential conditions simultaneously, that is, a non-zero nuclear quadrupole moment *Q*, an existing EFG tensor $\{V_{ij}\}$ and an appropriate external RF field.

Results and Discussion

Based on the NQR technique mentioned above, for the sake of seeking perfect NQR singals, we all select analytical pure (AP) reagents with purity greater than 99.0% as experimental samples. At the same time, in consideration of the sensitivity of RF field to electromagnetic interference, solenoidal inductor shielded with aluminum cylinder for high quality factor is equipped as NQR probe.

In our experiments for sodium nitrite ($NaNO_2$), methenamine ($C_6H_{12}N_4$), urea (CH_4N_2O) and thiourea (CH_4N_2S), we respectively choose a sample of 18g, 8g, 10g and 10g with chemical structures shown in Fig. 3.

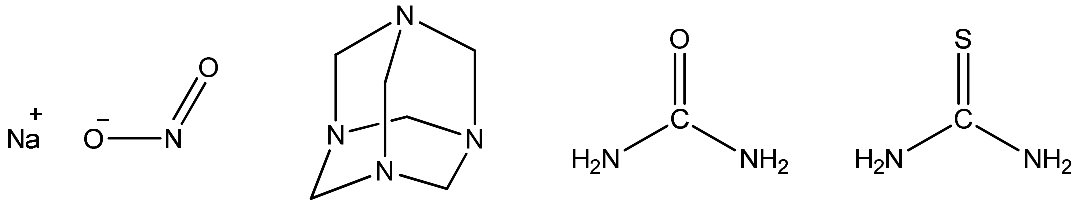

(a) (b) (c) (d)

Fig. 3 Chemical structures for samples:

(a) sodium nitrite ($NaNO_2$) (b) methenamine ($C_6H_{12}N_4$)

(c) urea (CH_4N_2O) (d) thiourea (CH_4N_2S)

For different samples, based on NQR detection theories for nucleus ^{14}N, we select corresponding RF exciting pulse with different frequency. After many measurements at room temperature by using NQR Measurement System RAM-5000, we have obtained several typical NQR spectra, for example, about 4.64 MHz and 3.60 MHz for $NaNO_2$, 3.30 MHz around for $C_6H_{12}N_4$, approximate to2.87 MHz and 2.63 MHz for CH_4N_2O, nearly 2.86 MHz and 2.51 MHz for CH_4N_2S. All the spectra observed are respectively shown in Fig. 4 to Fig. 7.

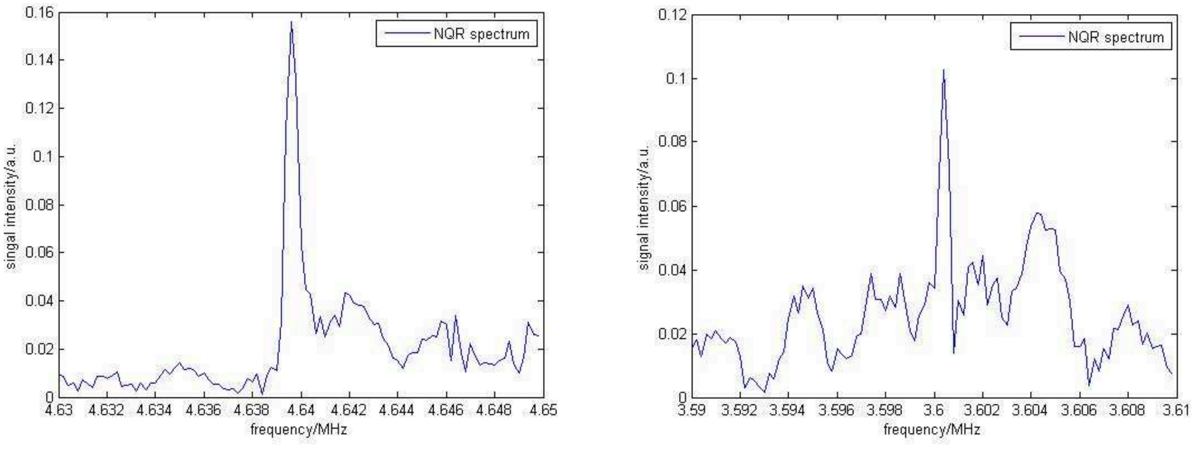

(a) (b)

Fig. 4 NQR spectra for nucleus ^{14}N in sodium nitrite ($NaNO_2$) ($\eta \neq 0$):

(a) spectrum of ν_+ around 4.64 MHz; (b) spectrum of ν_- around 3.60 MHz

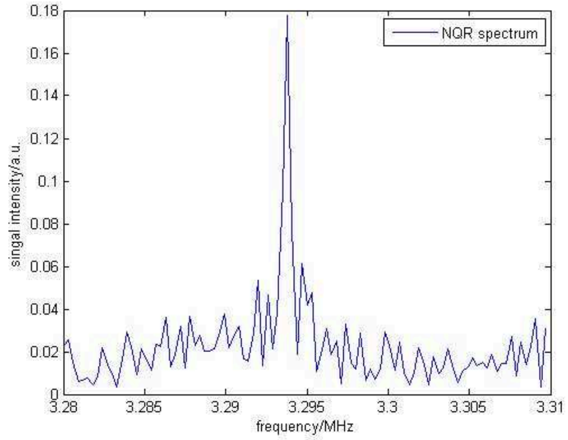

Fig. 5 NQR spectra for nuclei ^{14}N in methenamine ($C_6H_{12}N_4$) ($\eta = 0$):

spectrum of ν around 3.30 MHz

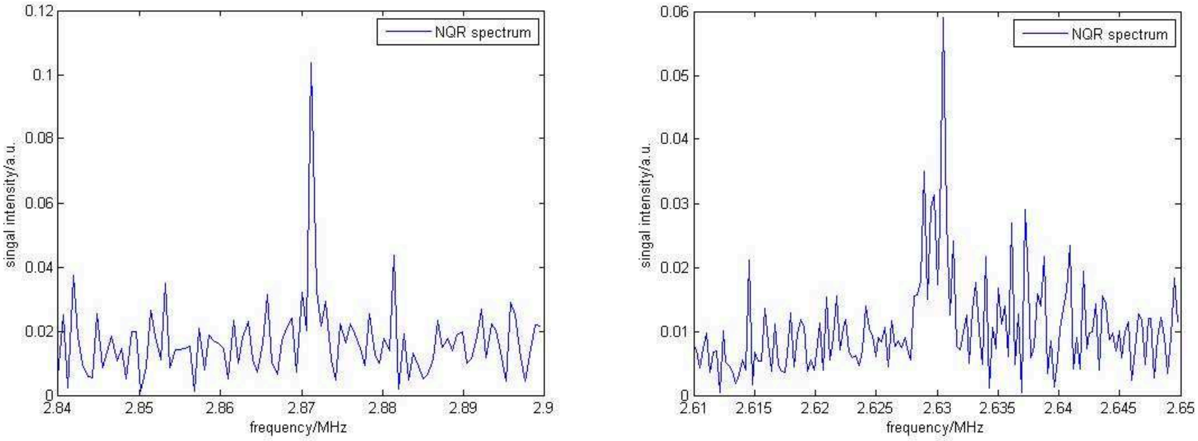

(a) (b)

Fig. 6 NQR spectra for nuclei ^{14}N in urea (CH_4N_2O) ($\eta \neq 0$):

(a) spectrum of ν_+ around 2.87 MHz; (b) spectrum of ν_- around 2.63 MHz

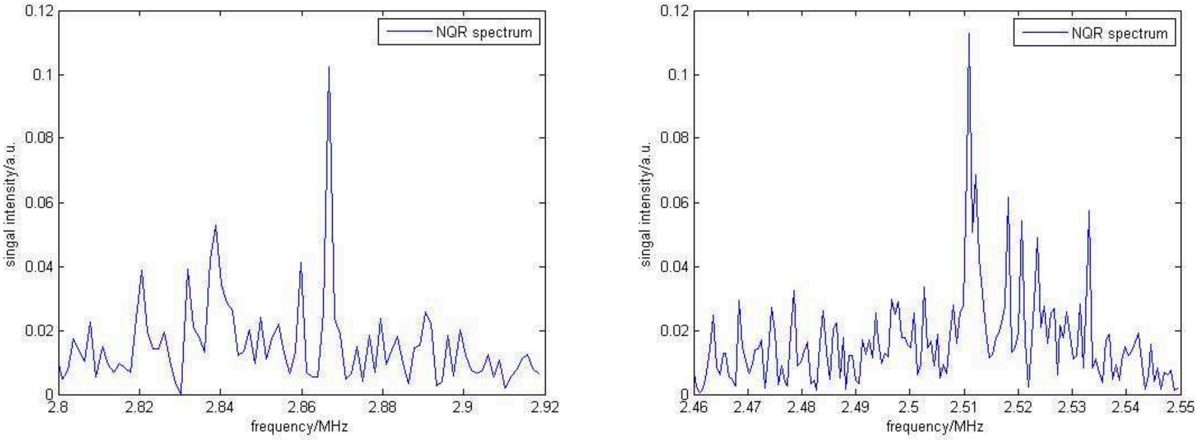

(a) (b)

Fig. 7 NQR spectra for nuclei ^{14}N in urea (CH_4N_2S) ($\eta \neq 0$):

(a) spectrum of ν_+ around 2.86 MHz; (b) spectrum of ν_- around 2.51 MHz

According to these spectra given above, we may obatin some conclusions as follows:

(1) Generally speaking, under the same environmental conditions, such as temperature, humidity, pressure, electromagnetic influence and so on, signal qualities almost decline with the attenuation of NQR frequencies for nucleus ^{14}N, no matter whether obtained from same substance or not. This may be interpreted as that high frequencies are more immune to noise interference than low frequencies.

(2) As for the details, there is a particularly significant conclusion that the singal to noise ratio of high NQR frequency for the same nucleus ^{14}N of same compound is much better than that of low frequency.

Additionally, by comparing all the spectra, it is not difficult to find that different compound has different NQR frequencies, which will provide a strong support for practical use of NQR technique.

Summary

All the test results indicate that NQR detection technique, as an efficient non-destructive chemical analysis method without harm to human health, is full of market prospect, especially in the detection field of hidden targets, such as explosive and narcotics. Taking into consideration of its merits and demerits, NQR technique, combined with the advantages of other technologies, may be applied to security check in such places with dense population or mass logistics like airport, station and so on. All in all, NQR technique will bring plenty of economic and social benefits.

Acknowledgements

All the work is completed under the guidance of supervisor professor Xu, and supported by the State Key Laboratory of Explosion Science and Technology.

References

[1] David J. Daniels: *EM Detection of Concealed Targets* (John Wiley & Sons, New Jersey 2010)

[2] Joel B. Miller: Detection and Sensing of Mines, Explosive Objects, and Obscured Targets XVI, 2011

[3] J. Shinoharan, H. Sato-Akaba and H. Itozaki: Solid State Nucl. Magn. Reson.Vol. 43-44 (2012) 27–31

[4] He Zhongwei, Fang Xumin and Xu Zheng: Nuclear Electronics & Detection Technology, Vol. 23 (2003) 604-608

[5] H. Chaihara, N. Nakamura: *Nuclear Quadrupole Resonance Spectroscopy Date* (Springer-Verlag, Berlin 1997)

[6] L. Robledo, M. Carrasco and D. Mery: International Journal of Remote Sensing, Vol. 30 (2009) 2339-2410

[7] Tristan M. Osana, Lucas M.C. Cerioni, Jose Forguez, et al: Physica B, Vol. 389 (2007) 45-50

[8] J.A.S. Smith: J.Chem.Educ.,Vol. 48 (1971), 39-48

[9] G.L.Petersen: *Pulsed Nuclear Quadrupole Resonance Instrumentation and Study of the ^{14}N Spectrum and Relaxation in Sodium Nitrite* (Brown University, Rhode 1975)

Applied Mechanics and Materials Vol. 596 (2014) pp 511-518
© (2014) Trans Tech Publications, Switzerland
doi:10.4028/www.scientific.net/AMM.596.511

Anti-Bias Association Algorithm for AIS and Radar Tracks Based on Centroid Reference Topological Characteristics

QI Lin[a*], WANG Haipeng[b], LIU Yu[c], and WANG Cong[d]

Research Institute of Information Fusion, Naval Aeronautical and Astronautical University, Yantai, China, 264001

[a]3278pirate@163.com, [b]armystudent@sohu.com, [c]liuyu77360132@126.com, [d]congnavy@hotmail.com

Keywords: Tracks association; Sensor bias; Real-time performance; Correctly associated rate

Abstract. To achieve fast and accurate association for AIS and radar tracks, provide associated track-pairs for subsequent sensor bias registration and situational fusion, this paper presents an anti-bias association algorithm for AIS and radar tracks according to centroid reference topological characteristics (CRT). The algorithm describes the topological characteristics of track-points set on the basis of targets position relative to the centroid of the set to achieve AIS and radar tracks fine association in the presence of radar bias. The proposed algorithm outperforms the traditional tracks association algorithms based on image matching principle (IM) or targets reference topology feature (TRT) in terms of real-time performance, simultaneously has high correctly associated rate. Simulation results show that the falsely associated rate of this algorithm maintains 0, the correctly associated rate maintains above 85%. It can provide reliable associated track-pairs for system errors registration; while the average time-consuming of the algorithm is 1/4 and 1/417 of TRT and IM algorithm, the practicality has been significantly improved.

Introduction

Track-to-track association[1-2] is a common key technology of information fusion, it aims to determine which tracks from different sensors are on behalf of the same targets, and it is a prerequisite for system errors registration and situational fusion. In the condition when sensor bias exists, traditional track-to-track association algorithm is still using the targets kinematic characteristics to implement judgment based on statistics or fuzzy mathematical theory[3-4]. While sensor bias causes large track deviation, leading to low correctly associated rate of the traditional algorithm. For this reason, in recent years, anti-bias track-to-track association has attracted great interests of scholars at home and abroad, and made a lot of research, such as ShiYue proposed track correlation algorithm based on target reference topological characteristics[5-9], SongQiang proposed image matching association algorithm[10-11], Joint data association and registration algorithms were also proposed[12-16], these provides new ideas for track-to-track association in system error conditions.

AIS (automatic identification system) can provide accurate positioning information for the vessels on sea. To study how to correct radar data based on AIS measurements on real time, realize system error estimation and compensation to improve measurement accuracy has significant value. Track-to-track accurate association is a prerequisite for radar data calibration based on AIS, Literature[10-11] proposed image matching association algorithm, whose calculation procedure is very complex and time-consuming. Literature[5-7] proposed track correlation algorithm based on target reference topological characteristics, whose computing speed is apparently improved. However, the algorithm describes topological characteristics on the basis of relative position between targets, which causes a lot of redundant calculation, and it cannot realize the practically engineering requirements. So, how to further improve the algorithm's real-time performance, simultaneously ensure the association accuracy needed to be solved.

Based on the targets distribution feature on sea surface, this paper make rough association judgment applying sensor track-points set centroid distance, and finish tracks fine association based on set topological characteristics. The full text is organized as follows, tracks rough association based on centroid distance is presented in Section 2. Section 3 is track-to-track fine association based on centroid reference topology feature. Simulations and Analysis are presented in Section 4 and Conclusions are presented in Section 5.

Establishment of a Unified Coordinate System for AIS and Radar Measurements

Radar measurements to the sea targets are usually addressed in polar coordinate, AIS-reported targets' position information are indicated in the form of geographic coordinates (latitude, longitude and altitude). To achieve tracks association of AIS and radar data, the first step is to unify the data into the local 2d Cartesian coordinate system, in which the origin is the radar location.

Assuming that target position in polar coordinate is range ρ and azimuth θ, with formula (1) target position vector in the local 2d Cartesian coordinate can be solved.

$$\begin{cases} x_{\mathrm{R}} = \rho\cos\theta \\ y_{\mathrm{R}} = \rho\sin\theta \end{cases} \tag{1}$$

AIS-reported targets' position information is in the form of geographical coordinate, assuming radar's location is $(\lambda_0, \varphi_0, H_0)$, λ_0 is the longitude, φ_0 is the latitude, H_0 is the height; target's location in geographical coordinate is $(\lambda_t, \varphi_t, H_t)$, $H_t = 0$, as targets are on sea surface. According of the simplified Gauss-Kruger projection principle, target location in the sea surface local 2d Cartesian coordinate is

$$\begin{cases} x_{\mathrm{A}} = S(\varphi_t) - S(\varphi_0) \\ y_{\mathrm{A}} = \dfrac{a\cos(\varphi_t)}{\sqrt{1-e^2\sin^2\varphi_t}} \cdot \dfrac{\lambda_t - \lambda_0}{\rho'} \end{cases} \tag{2}$$

$$S(\varphi) = a(1-e^2)\bullet(\frac{A}{\rho}\varphi - \frac{B}{2}\sin 2\varphi + \frac{C}{4}\sin 4\varphi - \frac{D}{6}\sin 6\varphi + \cdots)$$

$\rho' = \dfrac{180°}{\pi}$, the conversion factor;

$a = 6\ 378\ 245.000\ 0\mathrm{m}$, the long axis of the earth;

$e^2 = 0.006\ 693\ 421\ 623$, flat rate of the earth;

$A = 1.005\ 051\ 773\ 9$;

$B = 0.005\ 062\ 377\ 6$;

$C = 0.000\ 010\ 624\ 5$;

$D = 0.000\ 000\ 020\ 8$.

Tracks rough association based on centroid distance

AIS-reported track-points set in scan k is

$$\Gamma^{\mathrm{A}}(k) = \left\{ \boldsymbol{X}_1^{\mathrm{A}}(k), \boldsymbol{X}_2^{\mathrm{A}}(k), \cdots, \boldsymbol{X}_{n_k^{\mathrm{A}}}^{\mathrm{A}}(k) \right\}, \tag{3}$$

where $\boldsymbol{X}_i^{\mathrm{A}}(k) = \begin{cases} x_i^{\mathrm{A}}(k) \\ y_i^{\mathrm{A}}(k) \end{cases}, i = 1, \cdots, n_k^{\mathrm{A}}$ is the position feature of target i in the track-points set, n_k^{A} is the targets number reported by AIS in scan k.

Radar-reported targets' position estimation track-points set is

$$\Gamma^{\mathrm{R}}(k) = \left\{ \boldsymbol{X}_1^{\mathrm{R}}(k), \boldsymbol{X}_2^{\mathrm{R}}(k), \cdots, \boldsymbol{X}_{n_k^{\mathrm{R}}}^{\mathrm{R}}(k) \right\} \tag{4}$$

Under the normal circumstances, since not all vessels are equipped with AIS, $n_k^{\mathrm{A}} \le n_k^{\mathrm{R}}$.

Due to the reported targets number of different sensors may be different, the topological characteristics of the same target based on the traditional target reference topology association algorithm may be described in great difference. The paper make rough association judgment based on sensor track-points set centroid distance, and achieve tracks fine association based on set centroid reference topological characteristics. AIS-reported track-points set's centroid is

$$\bar{\boldsymbol{X}}^{\mathrm{A}}(k)=\begin{cases}\bar{x}^{\mathrm{A}}(k)\\ \bar{y}^{\mathrm{A}}(k)\end{cases} \tag{5}$$

$$\bar{x}^{\mathrm{A}}(k)=\frac{x_1^{\mathrm{A}}(k)+x_2^{\mathrm{A}}(k)+\cdots+x_{n_k^{\mathrm{A}}}^{\mathrm{A}}(k)}{n_k^{\mathrm{A}}} \tag{6}$$

$$\bar{y}^{\mathrm{A}}(k)=\frac{y_1^{\mathrm{A}}(k)+y_2^{\mathrm{A}}(k)+\cdots+y_{n_k^{\mathrm{A}}}^{\mathrm{A}}(k)}{n_k^{\mathrm{A}}} \tag{7}$$

To make the whole combinations of the elements in track-points set $\mathbb{Z}^{\mathrm{R}}(k)$, the number of combination elements is n_k^{A}, the number of combinations is $C_{n_k^{\mathrm{R}}}^{n_k^{\mathrm{A}}}$. The centroid of one of the combination is

$$\bar{\boldsymbol{X}}_j^{\mathrm{R}}(k)=\begin{cases}\bar{x}_j^{\mathrm{R}}(k)\\ \bar{y}_j^{\mathrm{R}}(k)\end{cases} \tag{8}$$

where $j=1,\cdots,C_{n_k^{\mathrm{R}}}^{n_k^{\mathrm{A}}}$.

Make track-points combinations rough association judgment. If one of the radar track-points combinations whose elements number is n_k^{A} realizes

$$d(\bar{\boldsymbol{X}}^{\mathrm{A}},\bar{\boldsymbol{X}}_j^{\mathrm{R}})<\Gamma \tag{9}$$

further achieve tracks fine association based on set centroid reference topological characteristics. Γ is the set centroid distance threshold, it depends on the specific experiment environment and some priori information.

Track-to-track fine association based on centroid reference topology feature

Description method of track-points sets centroid reference topology feature. Suppose that Figure1 shows sea surface targets tracks distribution in moment k, O is the location of the centroid of track-points set. Establish sea surface local 2d Cartesian coordinate system for AIS track-points set with O as the origin. Describe the track-points set centroid reference topological characteristics based on targets' position relative to the origin, and build track-points set topological characteristics matrix in moment k,

$$\boldsymbol{V}^{\mathrm{A}}(k)=\begin{bmatrix}\Delta x_1^{\mathrm{A}}(k) & \Delta x_2^{\mathrm{A}}(k) & \cdots & \Delta x_{n_k^{\mathrm{A}}}^{\mathrm{A}}(k)\\ \Delta y_1^{\mathrm{A}}(k) & \Delta x_2^{\mathrm{A}}(k) & \cdots & \Delta y_{n_k^{\mathrm{A}}}^{\mathrm{A}}(k)\end{bmatrix} \tag{10}$$

where

$$\begin{bmatrix}\Delta x_i^{\mathrm{A}}(k)\\ \Delta y_i^{\mathrm{A}}(k)\end{bmatrix}=\begin{bmatrix}x_i^{\mathrm{A}}(k)-\bar{x}^{\mathrm{A}}(k)\\ y_i^{\mathrm{A}}(k)-\bar{y}^{\mathrm{A}}(k)\end{bmatrix} \tag{11}$$

means the relative position of the target i in track-points set. To ensure that the same track-points set has a unique topological characteristics matrix, arrange the column vectors in $\boldsymbol{V}^{\mathrm{A}}(k)$ in Δx descending order, if two Δx have similar values, arrange the two column vectors in Δy descending order.

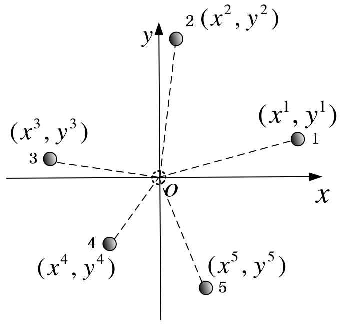

Figure 1 Track-points topological feature in sea surface 2d Cartesian coordinate system

Similarly, radar track-points set topological characteristics matrix in moment k

$$\boldsymbol{V}_l^{\mathrm{R}}(k) = \begin{bmatrix} \Delta x_1^{\mathrm{R}}(k) & \Delta x_2^{\mathrm{R}}(k) & \cdots & \Delta x_{n_k^{\mathrm{A}}}^{\mathrm{R}}(k) \\ \Delta y_1^{\mathrm{R}}(k) & \Delta y_2^{\mathrm{R}}(k) & \cdots & \Delta y_{n_k^{\mathrm{A}}}^{\mathrm{R}}(k) \end{bmatrix} \tag{12}$$

where $l = 1, \cdots, N_{\mathrm{R}}$, N_{R} means number of radar track-points sets whose centroid distance is less than the centroid threshold.

Set distance based on centroid reference topology feature. In order to quantify the matching degree of AIS and radar track-points set, find out the radar track-points combination best matching with the AIS track-points set, define set distance based on centroid reference topology feature

$$\begin{aligned} d(\Gamma^{\mathrm{A}}, \Gamma_l^{\mathrm{R}}) &= \left\| \boldsymbol{V}^{\mathrm{A}} - \boldsymbol{V}_l^{\mathrm{R}} \right\|_p \\ &= \left(\sum_{i=1}^{n_k^{\mathrm{A}}} \left|\Delta x_i^{\mathrm{A}} - \Delta x_i^{\mathrm{R}_l}\right|^p + \sum_{i=1}^{n_k^{\mathrm{A}}} \left|\Delta y_i^{\mathrm{A}} - \Delta y_i^{\mathrm{R}_l}\right|^p\right)^{\frac{1}{p}} \end{aligned} \tag{13}$$

which aims to measure the generalized distance between the AIS track-points set $\boldsymbol{V}^{\mathrm{A}}$ and a certain radar-reported track-points combination $\boldsymbol{V}_l^{\mathrm{R}}$

Extract the radar track-points combination best matching with the AIS track points set,

$$l^* = \arg\min_l [d(\Gamma^{\mathrm{A}}, \Gamma_l^{\mathrm{R}})] \tag{14}$$

So, the targets in radar track-points combination $\boldsymbol{V}_{l^*}^{\mathrm{R}}(k)$ are respectively associated with targets in AIS track-points set in order.

The process of the CRT algorithm is described in Table 1:

Table 1 Algorithm Process Description of CRT

Algorithm Description
1) Data transformation and establishment of a unified coordinate system
2) Rough association
a) AIS-reported track-points set's centroid
b) The whole combinations of radar-reported track-points
c) Centroid of radar-reported track-points combinations and centroid distance judgment
3) Fine association
a) Centroid reference topology feature of AIS-reported track-points set and radar-reported track-points combinations
b) Set distance and extracting of the radar track-points combination best matching to AIS track-points set
c) Tracks matching between AIS-reported track-points set and the optimal radar-reported track-points combination

Simulations and Analysis

There are a number of ship-targets on a certain sea surface area, the initial position of the targets belongs to uniform distribution on the area $(x:0\sim 20000\text{m}, y:0\sim 20000\text{m})$. Targets are sailing along a straight line in a constant velocity, initial velocity and direction obey uniform distribution on the range of $30\sim 80m/s$ and $0\sim 2\pi\text{rad}$. Figure 2 shows the tracks reported by AIS and radar, AIS reports a part of the tracks while radar reports all the tracks. Radar equipment introduces sensor bias, the measure random error obeys Gauss distribution, where standard deviation of range and azimuth are 50m and $0.2°$. Targets tracks-points distribution in a certain moment is showed on Figure 3.

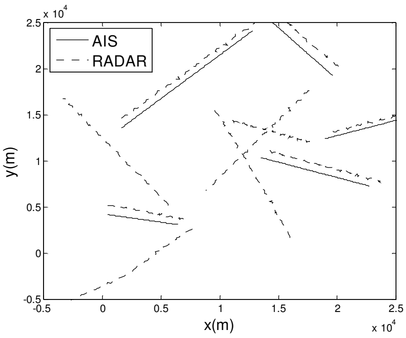

Figure 2 Tracks distribution on sea surface reported by AIS and radar

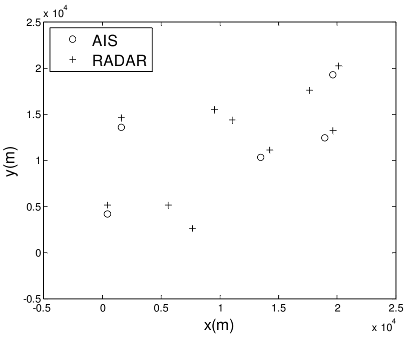

Figure 3 Track-points distribution on sea surface

Based on the above condition, alter the number of sea surface targets and radar bias, verify the performance of the proposed algorithm(CRT), and make comprehensive comparison and analysis with typical track-to-track association algorithm based on image matching technique(IM), track-to-track association algorithm based on targets reference topology feature (2014 issued in IEEE SIGNAL PROCESSING LETTERS)(TRT). The specific environmental parameters are set as Table 2:

Table 2 Environmental parameters

Condition	Targets number AIS-reported	Targets number radar-reported	Ranging error	Azimuth error
1	4	8	0.5km	0.5
2	5	10	0.5km	0.5
3	6	12	0.5km	0.5
4	7	14	0.5km	0.5
5	4	8	1km	0.5
6	5	10	1km	0.5
7	6	12	1km	0.5
8	7	14	1km	0.5

Simulation results are shown in Table 3.What listed in the Table are correctly associated rate(CAR), falsely associated rate(FAR), miss associated rate(MAR) and average time-consuming(T) of CRT, IM, TRT in the 8 simulation conditions.

Table 3 Performance comparison of the association algorithms

	Condition	1	2	3	4	5	6	7	8
IM	CAR(%)	1	1	1	1	0.975	0.960	0.933	0.943
	FAR(%)	0	0	0	0	0.025	0.040	0.067	0.057
	MAR(%)	0	0	0	0	0	0	0	0
TRT	T(s)	8.179	8.207	8.228	8.217	8.189	8.202	8.215	8.233
	CAR(%)	1	0.975	0.983	0.989	0.950	1	0.933	0.983
	FAR(%)	0	0	0	0	0	0	0	0
	MAR(%)	0	0.025	0.017	0.011	0.050	0	0.067	0.017
	T(s)	0.071	0.087	0.166	0.233	0.088	0.119	0.169	0.233
CRT	CAR(%)	1	0.950	0.933	0.920	1	0.940	0.893	0.860
	FAR(%)	0	0	0	0	0	0	0	0
	MAR(%)	0	0.050	0.067	0.080	0	0.060	0.107	0.140
	T(s)	0.018	0.022	0.115	0.874	0.021	0.037	0.127	0.859

Association performance comparison of the three algorithms in Table 3 shows that IM, TRT, CRT all have relatively high correctly associated rate and certainly environmental suitability. Comparison of condition1-4(or condition5-8) shows that the performance of CRT has a slight decline with the increase of target numbers in the area; comparison of condition1,5(or condition2,6 or condition3,7 or condition4,8) shows that the performance of CRT has a slight decline with the increase of radar bias. Despite this, the correctly associated rate of CRT is always above 85%, and the falsely associated rate maintains 0.As known, the purpose of track-to-track association is to provide reliable track-pairs for system error registration, the falsely associated rate of the proposed algorithm maintaining 0 in different simulation environments proved the robustness of centroid reference topology association algorithm.

The significant advantage of the proposed centroid reference topology association algorithm is the simplification of computational complexity of traditional anti-bias association algorithm and improvement of computing speed. As the simulation results shows in Table 3, IM has quite high correctly association rate, but it is time-consuming, unsuitable for real-time application. Figure 4 shows the average running time of CRT and TRT in the condition that radar bias is 0.5km, $0.5°$. Comparison of condition1-3(or condition5-7) shows in the condition that targets number is less than 12, the time-consuming of CRT is less than TRT; when targets number is less than 10, the time-consuming of CRT is 1/4 of TRT.

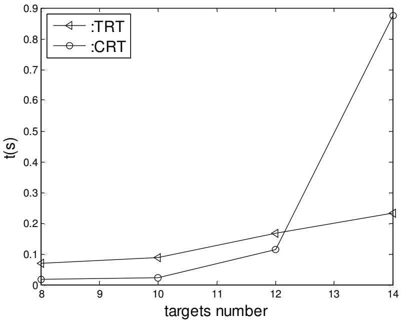

Figure 4 The average running time of CRT and TRT

Analysis of the reasons for these simulation results, first consider the impact of the system error on the track position: ranging error make all the tracks shift together, azimuth error make all the tracks rotate. All the 3 algorithms in Table 3 have taken the impact into consideration. As the overall shift and rotation of all the tracks have no effect on the image feature or the relative position between targets, the algorithms all have quite high correctly associated rate and quite strongly environmental suitability. IM need number field transformation in the procedure, so it needs large amount of calculation and it is time consuming. TRT figures out the topology feature of a certain target based on the around targets' position relative to it, as the targets are reference of each others, the algorithm introduces a large number of redundant computation. CRT considers the track-points combination as the object, describes the combination's overall topological feature on basis of the targets' position relative to the centroid and figures out the associated relation among targets. The CRT proposed in the paper simplified the calculation procedure of TRT, the running speed is significantly improved.

As shown in Figure 4, when the targets number comes to 14, the average running time of CRT surges. The reason of this phenomenon is that when targets number increases, the number of all the combinations increases sharply. Take the sea surface tracks distribution feature into consideration, rasterize the sea surface area, control the number of the targets nearly 10 in each cell, associate the tracks with CRT. The procedure described above can be used to achieve sea surface targets association in the condition of radar bias, with fast and accurate performance.

Conclusions

In this paper, sea surface tracks reported by AIS and radar fast and accurate association in the condition of sensors bias is researched. As tracks distributed scattered on sea surface, directed against the traditional algorithms' complex calculation procedure, the algorithm based on centroid reference topological feature is proposed. CRT algorithm has 3 advantages in comparison with the traditional algorithms, as follows:

1. Describe the track-points sets topological feature based on the target's position relative to the centroid, it can accurately characterize the relative position between targets;
2. The whole track-points set is considered as the object to be researched, the redundant calculation of TRT is simplified and running time is decreased.
3. Grid large sea surface area, achieve AIS and radar tracks real-time accurate association based on the proposed CRT algorithm. The algorithm can quickly provide accurate associated track-pairs for system error registration and situational fusion, it has practical value in projects.

Acknowledgements

This work was financially supported by the Shandong Province Natural Science Foundation (ZR2012FQ004).

References

[1] Y. Bar-Shalom. On the Track-to-track Correlation Problem[J]. IEEE Transactions on Automatic Control, 1981, 26(2):571-572.

[2] C. Phani, N. Arye. Concurrent Particle Filtering and Data Association Using Game Theory for Tracking Multiple Maneuvering Targets[J]. IEEE Transactions on Signal Processing, 2013, 61(20): 4934-4948.

[3] D. Ahmed, O. Mourad, O. Abdelaziz. Sensor Fusion and Target Tracking Using Evidential Data Association[J]. IEEE Sensors Journal, 2013, 13(1):285-293.

[4] L. Kaplan, Y. Bar-Shalom, and W. Blair. Assignment Costs for Multiple Sensor Track-to-track Association[J]. IEEE Transactions on Aerospace and Electronic Systems, 2008, 44(2):655–677.

[5] Wei Tian, Yue Wang, Xiuming Shan, et al. Track-to-track Association for Biased Data Based On The Reference Topology Feature [J]. IEEE Signal Processing Letters, 2014, 21(4): 449-453.

[6] Wei Tian, Yue Wang, Xiuming Shan, et al. Analytic Performance Prediction of Track-to-track Association with Biased Data in Multi-Sensor Multi-Target Tracking Scenarios[J]. Sensors, 2013, 13(9), 12244–12265.

[7] Yue Shi, Yue Wang, Xiuming Shan, et al. Fuzzy Data Association Based on Target Topology of Reference[J]. Journal of National University of Defense Technology, 2006, 28(4): 105-109. (in Chinese)

[8] Weifeng Liu, Chenglin Wen. A Track Association Algorithm Based on OSPA Distance[J]. Acta Aeronautical et Astronautica, Sinica, 2012, 33(6): 1083-1092. (in Chinese)

[9] Zemin Wu, Shujie Ren, Xi Liu. Topology Sequence Based Track Correlation Algorithm[J]. Acta Aeronautical et Astronautica Sinica, 2009, 30(10): 1937-1942. (in Chinese)

[10] You He, Qiang Song, Wei Xiong. A Track Registration-correlation Algorithm Based on Fourier Transform[J]. Acta Aeronautical et Astronautica Sinica, 2010, 31(2): 356-362.(in Chinese)

[11] Qiang Song, Wei Xiong, You He. A Track Alignment-Correlation Algorithm Based on Topological Description of Complex Number Field[J]. Journal of Astronautics, 2011, 32(3): 560-566. (in Chinese)

[12] Wei Du, Huansheng Ning, Yuan Wei , et al. Fuzzy Double-Threshold Track Association Algorithm Using Adaptive Threshold in Distributed Multisensor-Multitarget Tracking Systems[C]. 2013 IEEE International Conference on Green Computing and Communications and IEEE Internet of Things and IEEE Cyber, Physical and Social Computing, 2013:1133-1137.

[13] Zhenghua Li, Siyue Chen, H Leung, et al. Joint Data Association, Registration, and Fusion Using EM-KF[J]. IEEE Transactions on Aerospace and Electronic Systems, 2010, 46(2):496–507.

[14] D Pagageorgiou, J Sergi. Simultaneous Track-to-track Association and Bias Removal Using Multi-Start Local Research[C]. 2008 IEEE Aerospace Conference. Montana USA: IEEE Press, 2008: 1-14.

[15] Xi Liu, Hao Yin, Chang Tian, et al. An Improved 2-D Assignment Algorithm for Track-to-track Association[C]. 2013 25th Chinese Control and Decision Conference, 2013:3698-3703.

[16] Hao Liang. A Possibilistic Data Association Based Algorithm for Multi-target Tracking[C]. 2013 Third International Conference on Intelligent System Design and Engineering Applications. 2013:158-162.

Applied Mechanics and Materials Vol. 596 (2014) pp 519-527
© (2014) Trans Tech Publications, Switzerland
doi:10.4028/www.scientific.net/AMM.596.519

Trusted Data Aggregation with Low Energy in Wireless Sensor Networks

Tristan Daladier Engouang[1], Yun Liu[2], and Zhenjiang Zhang[3]

[1,2,3]The key Laboratory of Communication and Information Systems, Beijing Municipal Commission of Education, Beijing Jiaotong University, Beijing 100044 China,

[1] trist_dal1@yahoo.fr, [2] liuyun@bjtu.edu.cn, [3] zhangzhenjiang@bjtu.edu.cn

Index Terms—TDALE, Aggregation, Elliptic curve, RSA, Security, Energy

Abstract— Scientific researches advancements achieving miniaturization of Micro-electromechanical Systems, has enable smarts autonomous embedded devices know as sensor nodes, that are developed on numerous platforms using the proprietary of hardware and software with capability to communicate wirelessly. Today more than ever these sensors are continuously spreading to civilian usage side of things and in many others applications , including military, security, medical, environments, and animal among others, to sense specific occurrence of desired event and may carried very important data on physical device such as the mica-mote. Hence a plethora of security protocols arises in order to mitigate the risks of malicious attacks such as eavesdrop communications, or data alteration, using cryptographic techniques such as Elliptic curve for data privacy, accuracy, integrity, efficiency, and reducing the energy consumption by mote and processors. We focus on securing data by all means. Hence the in-network processing technique is used to reduce considerably the energy consumption, considering that sensors deployments in inaccessible and resource-constrained environments. After the drawback, we investigate the secured data aggregation and give security requirements that are mandatory to a Trusted Data Aggregation with Low Energy model to satisfy. The security and energy performances are analysed comparing with others methods.

INTRODUCTION

Thanks to Claude Shannon’s mathematical concepts that used to bring structure in order to understand almost anything, by revolutionizing the former conceptualization of information resulting in its 1940’s Information theory [1] that continuously allow researchers dive into the amazing new technology of Wireless Sensor Network (WSNs) [2] as shown in figure 1, formed by hundreds and thousands of power-limited sensor devices “nodes” with the trend of getting smaller as with Moore’s law. These wireless sensors are, randomly deployed in a targeted environment to sense specific occurrence of event need [3], and they are helping to design numerous applications that could not be practical previously [4], such as in the military (DARPA project) [5], security, civilian usage, health, housing, environmental monitoring and animal (ZEBRA) [6].

Despites their smaller size heritage of the miniaturization of Micro-electromechanical Systems (MEMS), sensors devices have the capacity to communicate wirelessly between each other’s and successfully transmitting sensitive data and metadata, such as light , sound, vibrations, moisture, weight, temperature, heart beats, while their deployment does not required pre-deployed equipments nor human assistance [4]. .

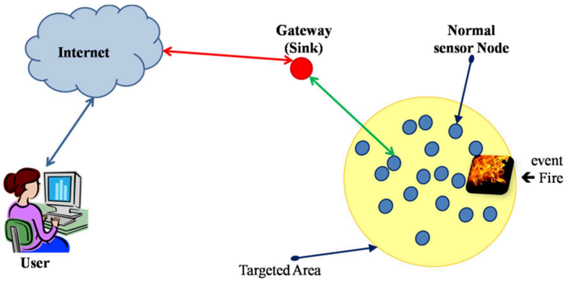

Fig. 1. Secure wireless sensor network.

In addition, it is worth nothing that wireless sensors potential is restricted by their others resources constraints including [7], including limited processing speed, very low memory for data storage, very small communication bandwidth [8], where energy is the main concern, that is why it is argued that minimizing the energy consumed by the system is the key feature of any wireless sensing node [4], meaning that amount of data transmission need to be minimized as the bandwidth efficiency become mandatory [9].

The reminder of this paper is as follow. Section 2 presents the main objectives of the study and some preliminary concepts while section 3 gives expounds the poposed model TDALE. Section 4 gives the performances analysis and section 5 concludes this paper and opens rooms for researchs.

Objectives and Model

1.1. The network objectives

The Trusted Data Aggregation with Low-Energy (TDALE) model based on the implementation of the elliptic curve method, with respect to performance, energy usage and code size. The numerous exchanges of data in an unsecured wireless channel, when aggregating data lead to defining rules or protocols design with security in mind that govern these communications, so that system will survive all possible malicious attacks(e.g., eavesdropping) [10], or malicious forgery (e.g., jamming [11]), also we consider privacy, Accuracy, Integrity and Efficiency as in [12], as the system main objectives unless state otherwise, because real values of data and their protection matters in security.

1.2. Network model

Trusted Data Aggregation with Low-Energy (TDALE) model was inspired by TAG [13], but their difference is it lacks security at contrary of our our system‘s goal that keeps data secured. And we reduce each step of the data processing to the communication (or exchange) between two sensors, for every data transfered from source to destination in an Hamiltonian path [14], to fully ensure its secrutity. In addition, because the radio ranges of a sensor is limited, then intend receivers may not be reachable directly, hence we adopted the tree base topology for our model as shown in **figure 2** thus using the multi-hop communication [7] which sensors are working in relay conveying data from one end to another and this brings less communication overhead. Moreover the It is built as follow. The root broadcasts a “Hello” message to all 1-hop neighbor nodes. Each 1-hope neighbors to the sender, replies with a “joining_request” message by only nodes, without parent to that “Hello” message’ sender (e.g., root). The sender accepts that node as its child, by replying with a “joining_accepted” message.

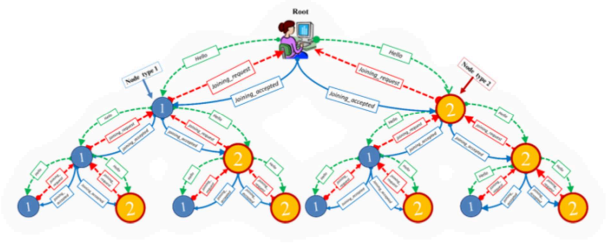

Fig. 2. TDALE Tree based topology.

1.3. Hardware Perspective

As mentioned earlier, these sensor nodes are very limited energy, memory and CPU speed, despites their capacity of communicating the data sensed and recorded by radio to any peer or entity that can process it. Sensor node’s characteristics is a key to the performance of a WSNs, thus we will just consider the use of a Berkeley Mica Mote [15], running under TinyOS system [16] and equipped with a 4 MIPS AT mega 103L 4 MHz 8-bit CPU, with a RFM TR1000 radio 50kbits/s transceiver with the range of 30 m. But the transmission data rate is low if comparing it with other wireless technologies such as WLAN 802.11, WiMAX, and Bluetooth, that is why I. Haroun et al., argued that "*the modulation type needs to be power efficient rather than spectral efficient in order to extend the lifetime of the nodes*" [17]. In addition it is worth nothing that our sensor node can only send or receive a message, but not both actions at a same time, that is the propriety of a half duplex single channel. And our network of wireless communication between sensor nodes as in [18], does not consider the white noise introduced into the signal by the electronic channel and environment nor the node to node interferences within the system, with respect that sensor nodes are randomly deployed. For more details on these RF system issues are given in [17]. Moreover, from the scarcity of energy resources in WSNs, it is resulting that data in-network processing, is more efficient than direct transmission of sensor reading [13], as it is solving the tradeoff issue between computation and communication, that is why energy efficiency solutions or algorithms have arise such as [12]. Furthermore, establishing trusted links such as symmetric one's (bi-directional), as proposed in [13] is now necessary because the connectivity is very limited due to radio range and few node sometimes may not see each other, this means that if for a given two sensors nodes Sn1 and Sn2, saying that they are symmetrically link implies that if Sn1 can hear Sn2, thus Sn2 able to hear Sn1 as well (that is the associative radio range of symmetric link). Hence we only consider the symmetric links over the possible asymmetric ones that are very hard [prakash 1999].

TRUST DATA AGGREGATION WITH LOW-ENERGY

The main security is mathematically ensured at node level of sensors (leaf node) and the aggregation procedure is emphasis followed by its throughput.

1.4. Elliptic curve cryptography (ECC) approach

We consider the elliptic cryptographic technique (ECC) [2] as an alternative public-key cryptography to the old and known RSA [19]. And for elliptic curve,Y over its finite field *Fp=K (E.g.,* prime p = 65112 * 2^{144} [20]), defined on a group *Ep (a, b)* with a, b Є (K >3) the Weierstrass equation as in (1).

According to [2] with point on the curve P = (x,y) Є (K > 3) forming an abelian group, it is possible to calculate two sequence arithmetic operations such as the point addition and the point doubling [21], Hence consider two distinct points on the curve Γ as λ = (x_1, y_1) and Ω = (x_2, y_2), but due to limited space on this paper, readers are refered to [2], for detailed operations from which the results is obtain as in equation (2).

$$\Gamma(K): y^2(mod\, p) = (x^3 + \; ax \; + b)mod\, p \quad (1)$$

$$\Lambda = \begin{cases} \Lambda_1 = (y_2 - y_1) \times (x_2 - x_1)^{-1} & (\lambda \neq \Omega) \\ \Lambda_2 = (3x_1^2 \; - a) \times (2y_1)^{-1} & (\lambda = \Omega) \end{cases} . \quad (2)$$

1.5. TDALE Algorithm

The Trusted Data Aggregation with Low-Energy presents a hierarchical architecture distributes the specific task to each level of the overall network system including, sensing, aggregating, and transmitting. The system network is divided in hop layers from sink to node's location on targeted area as shown in figure 3. In addition, the aggregation procedure as shown in figure 4 could be divided in three layers each with a specific function as defined by the proposed algorithm.

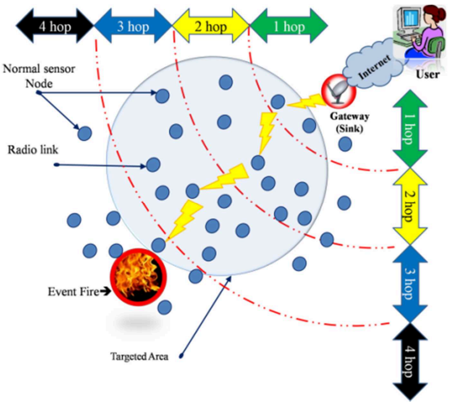
4 hop
3 hop
2 hop
1 hop
Internet
User
Normal sensor Node
Radio link
Gateway (Sink)
1 hop
2 hop
3 hop
4 hop
Event Fire
Targeted Area

Fig. 3 TDALE multi-hop layering secure data aggregation model.

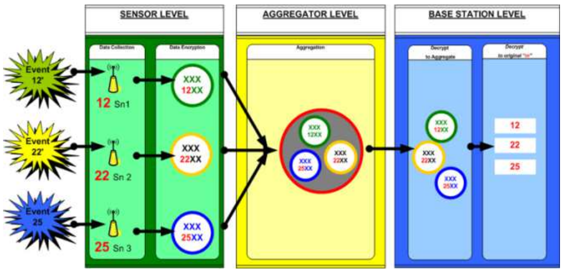
SENSOR LEVEL
AGGREGATOR LEVEL
BASE STATION LEVEL
Data Collection
Data Encryption
Aggregation
Decrypt to Aggregate
Decrypt to original "m"
Event 12'
Event 22'
Event 25
12 Sn1
22 Sn 2
25 Sn 3
XXX 12XX
XXX 22XX
XXX 25XX
12
22
25

Fig. 4 TDALE secure data aggregation model

5.1.1. Data Collection and Encryption (DCE-Level 1)

The sensing nodes uses its predefined function sensing algorithm as shown in table 1, to sense the targeted environment to detect and collect the specific measured metrics of the event of interest (plaintext) or let call it message (ms_i), Then it will uses the security algorithm elliptic curve to perform the data ciphering [2]. The cipher-text or encrypted data (Cms_i) resulting is then transmitted to the upper level (SDA-Level 2) where the nearest aggregator will come into play.

Table 1 TDALE Algorithm at sensor level

```
1. Initialization;
2. Establish an asymmetric link using Diffie-Hellman key exchange model;
3. Collect data from surroundings;
4. Encrypt data using elliptic curve cryptographic technique;
5. Send data to upper level;
```

Ciphering: *Let "m" be the message sent by a sensing node, with the point "M" on the curve,* Y, *and a integer 'k' from [1, (n-1)], two cipher texts are generated and sent as of* C_1 ($C_1 = k \times P$) *and also,* C_2 ($C_2 = M + k \times Q$).

5.1.2. Secured Data Aggregation (SDA-Level 2)

Includes the aggregators (sensor nodes with aggregation function), that are receiving the encrypted data (Cm_i) from each of all its λ children, aggregates it without decryption using its aggregate function $f(.)$ (e.g., SUM), It's algorithm as shown in table 2 adding up [22] all received *Cmi*, as given in equation (3) and sends it to the base station. But it is worth nothing that, just like in DCE-Level 1 which has a lot of sensing nodes, in SDA-Level 2, it is possible for an aggregator to have a parent node as its path step to base station

$$A(Cm) = \sum_{i=1}^{\lambda} Cmi \tag{3}$$

Table 2 TDALE Algorithm at Aggregator level

```
1. Aggregate all encrypted data from children
   using SUM function;
2. If node is latest aggregator do:
3. Transmit new aggregate to Sink and jump to
   step 10;
4. Else do:
5. Transmit to upper level aggregator;
6. Return to step 6;
```

Transmission: *Each aggregator's resulting aggregate, is indeed sent to sink by Agg, which is why base station it will end with all the data sent from source given in (15).*

5.1.3. Data Decryption (DDec-Level 3)

The Base Station (Bs) is the latest end of this data supply chain (network), in fact, as defined by its algorithm shown in table 3, all the aggregated attributes or values forwarded by all aggregators from lower layers are gathered and combines at the base station which will end up with a total of these values given in equation (4) as.

$$Cm = \sum_{i=1}^{n} Cmi \tag{4}$$

Deciphering: Finally as it receives the resulting aggregates, the original content has to be recovered only at base station considering the ciphering operation in section 3.2.1 thus by performing the following computation M = C2 – d x C1. Thus M is the original message that was sent from sensor and we recover "m". Moreover, the homomorphic properties of the ECC allows us to perform arithmetic operation on sensors readings that were previously encrypted, with a total of "N" addition and "1" multiplication and we refer to (7), for expressing the connectivity of sensors in our model, from the use of the key pre-distribution technique, ensuring the resistance of our model to the main attacks as chosen-plain text attack, known-plain text attack, man in the middle attack.

Table 3 TDALE Algorithm at Aggregator level

```
1. Check if the following holds
   $Cm = \sum_{i=1}^{n} Cmi$
2. If not do
         Send a query to child;
           else decrypt to
   aggregate values;
3. Decrypt to original message;
```

2. PERFORMANCE ANALYSIS AND EXPERIMENTAL RESULTS

2.1. Security measures by key size model

From [21], over a finite field *Fp,* our approach based on Elliptic curve technique, must meet $P \approx 2^{161}$, in fact it is been prove that using small key yield small cryptograms and faster inscription operation, which is the aims of the ECC [20], for the same expected level of security as in table 4 comparing RSA. In fact RSA fundament is on the hardness of its factorization that is over 2510 years compare to 35 years of ECC which is more about hardness of mathematical computation using exponential algorithm [20]. Here it is obvious that a 224-bit ECC key has about the same security level of a 1620-bit RSA, and for 512-bit ECC, is equivalent to a 15360-bit RSA.

Table 4 Key length for same level of security

Level of Security	*Security key*	*ECCkey*	*RSAkey*
1	56	112	430
2	80	160	760
3	96	192	1020
4	128	224	1620
5	168	256	3072
6	192	384	7680
7	250	482	14596
8	256	512	15360

2.2. *Energy Consumption by radio model*

The energy consumption is crucial issue in WSNs [15], also in order to reduce it, we chose the radio model [23], where the power consumption is proportional to the square of the distance between two sensors communicating as shown in figure 5, with respect to the following parameters, k (in bits) is the size the message (data) to be sent or received, d is the distance between two sensor nodes exchanging the size k- data, E_{Tx} is the energy consumed to transmit some k-bits data, E_{Rx} is the energy to receive some K-bits data, E_{elec} is the energy consumed to perform the data transmission task (nJ/bit), ε_{amp} is the constant energy consumed to expand the radio coverage (nJ/bit*m^2).

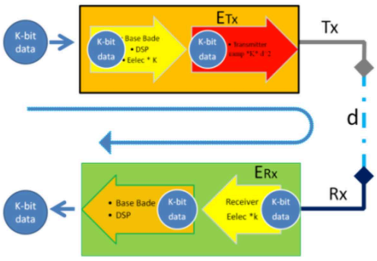

Fig. 5 Communication model of two sensors node.

In addition, the equation (5) gives the formula to calculate the energy consumed for transmitting size K-bits of data, over a distance "*d*", while the energy consumed to receive that size k-bits of data, is given by the equation (6)

$$\begin{aligned} E_{Tx}(k,d) &= E_{elec} \times k + \varepsilon_{amp} \times k \times d^2 \\ &= k(E_{elect} + \varepsilon_{amp} \times d^2) \end{aligned} \tag{5}$$

$$E_{Rx}(k,d) = E_{elec} \times k \tag{6}$$

2.3. *Energy consumption by Key size model*

The energy consumption of the CPU is a time-based, we can understand that as long as it takes to operate, as high is the energy consumption, hence, that justify again the importance of reducing the key size. We can get the energy consumption per key size of security level as shown in figure 6.

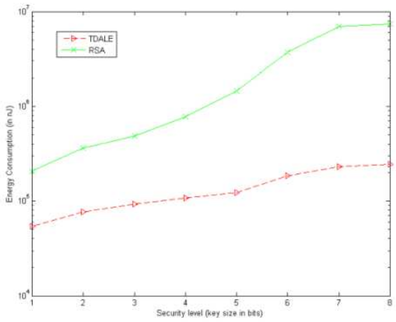

Fig. 6 Energy consumption comparison for equivalent security level

3. CONCLUSION

This paper presents the Trusted Data Aggregation with Low-Energy (TDALE) of mathematical public key elliptic curve cryptography (ECC) at core to secure sensor readings prior to be processe to upper level of the network securely. Performance analysis gives some satisfactory results in terms of security, the energy consumption is reduced considerably, through in-network data processing compare to RSA. The paper contributes to a succesfull trusted based data aggregation. For further research, one could invision a clustering approach implementing TDALE.

ACKNOWLEDGEMENTS REFERENCES

This paper is supported by Beijing Science and Technology Program under Grant Z121100007612003, Beijing Natural Science Foundation under Grant 4132057, and National Natural Science Foundation under Grant 61371071. And partially by agence nationale des bourses du Gabon (ANBG)

Tristan Daladier ENGOUANG received his B.S. degree in Computer Science and Engineering from University of Sciences and Technology Beijing, China in 2006, and his M.S. degree in Information Network and Security from Beijing Jiaotong University, China in 2009. He is currently pursuing the Ph.D. degree in information network and security at Beijing Jiaotong University. His research interests include Computer Networks, wireless sensor network, Telecommunication, Network Security.

Liu YUN is a professor of Communication and Information Systems, Beijing Jiaotong University. Her current research interests include Computer Networks, Telecommunication, Network Security, Intelligent Transportation System, Social Dynamics, etc. Dr. Liu has edited many books and published over 200 papers and book chapters, as well as participated in many international academic activities, including the organization of several international conferences.

Zhen Jian Zhang is a PhD, Associate professor at School of Electronic and Information Engineering in Beijing Jiaotong Univ. His research interests include Wireless Sensor Networks, Communication.

REFERENCES

[1] Eugene Chui, Jocelyn Lin, Brok Mcfrron, Noshirwan Petigara, and Satwiksai Seshasai, *Mathematical Theory of Claude Shannon.*, 2001.

[2] Tristan Daladier Engouang and YUN LIU, "Aggregate over Multi-hop Homomorphic Encrypted Data in Wireless sensor networks," *2013 2nd International Symposium on Instrumentation and Measurement, Sensor Network and Automation*, vol. 1, pp. 248-252, December 2013, DOI: 10.1109/imsna.2013.6743261.

[3] Aziz Nor Azlina Ab., Aziz Kamarulzaman Ab., and Ismail Wan Zakiah wan, "Coverage Strategies for Wireless Sensor Networks," *World Academy of Sciences, Engineering and Technology*, vol. 26, no. 0026:2009, pp. 145-150, February 2009.

[4] Chris Townsend, Steven Arms, and Inc. MicroStrain, "Wireless Sensor Networks: Principles and Applications," in *Sensor Technology Handbook.*: Elsevier Inc, 2005, ch. 22, pp. 575-589.

[5] DARPA. (2013, September) Dynamic Sensor Networks. [Online]. http://dsn.east.isi.edu/

[6] Don Boroughts. (2007, September) ASEE PRISM. [Online]. http://www.prism-magazine.org/sept07/feature_kenya.cfm

[7] Tristan Daladier Engouang, YUN LIU, and Zhen-Jiang Zhang, "Pallier based Homomorphic Encrypted Data aggregagtion in wireless sensor networks," in *2014 2nd International Conference on Advanced Technologies and Solutions in Industry*, vol. 1, Beijing - China, 2014, pp. 1-7, unpublished.

[8] Gowrishankar.S, T.G Bassavaruja, D Manjaiah, and Subir Kumar Sarkar, "Issues in Wireless Sensors Networks," in *World Congree on Engineering*, vol. I, London, 2008, pp. 176-187.

[9] Suat Ozdemir and Yang Xiao, "Secure data aggregation in wireless sensor networks: A comprehensive overview," *Computer Networks*, vol. 53, pp. 2022-2037, March 2009, doi:10.1016/J.comnet.2009.02.023.

[10] llkyu Kim, Doohwan Oh, Myung Kuk Yoon, Kyueun Yi, and Won Woo Ro, "A Distributed Signature Detection Method for Detecting Intrusions in Sensor Systems," *Sensors*, vol. 13, no. 4, pp. 3998-4016, Mars 2013, doi:10.3390/s130403998.

[11] Yuxin Mao, Ping Zhu, and Wei Guiyi, "A Game theoretic Model for Wireless Sensor Networks with Hidden-Action Attacks," *International Journal of Distributed Sensor Networks*, vol. 2013, pp. 1-9, July 2013, DOI:10.1155/2013/836056.

[12] Chen-Xu Liu, Liu Yun, Zhen-Jiang Zhang, and Zi-Yao Cheng, "High Efficient and Privacy-preserving Secure data aggregation for wireless Sensor networks," *International Journal of Communication Systems*, no. 26, pp. 380-394, July 2012.

[13] Samuel Madden, Michael J. Franklin, Joseph Hellerstein, and Wei Hong, "TAG: a Tiny Aggregation Service for Ad-hoc Sensor Networks," in *Fifth Symposium on Operating System Design and Implementation*, Boston, 2002.

[14] Eric W. Weisstein. (2013, April) Hamiltonian Cycle. [Online]. http://mathworld.wolfram.com/HamiltonianCycle.html

[15] Martin Leopold, "Sensor Network Motes: Probability & Performance," University of Copenhagen, PhD Thesis 2007.

[16] TinyOS. (2014, May) TinyOS.net. [Online]. www.tinyos.net

[17] Ibrahim Haroun, Ioannis Lambadaris, and Roshdy Hafez. (2005, September) Microwaves and RF. [Online]. http://mwrf.com/systems/building-wireless-sensor-networks

[18] Nathan Blaunstein and Christos Christodoulou, *Radio Propagation and Adaptive Antenna for Wireless Communication links: Terrestrial, Atmospheric and Ionospheric*. Hoboken, New Jersey, USA: John Wiley & Son, Inc., 2007.

[19] Certicom. (2013, December) Certicom. [Online]. http://www.certicom.com/

[20] Nils Gura, Arun Patel, Wander Wander, Hans Eberle, and Sheueling Chang Shantz, "Shantz, S. C. (2004). Comparing elliptic curve cryptography and RSA on 8-bit CPUs.," *In Cryptographic Hardware and Embedded Systems*, pp. 119-132, 2004.

[21] Jacques M Bahi, Christophe Guyeux, and Abdallah Makhoul, "Secure Data Aggregation in Wireless Sensor Networks. Homomorphism versus Watermarking Approach," in *2nd International Conference on Ad Hoc Networks,* vol. 49, Victoria, BC, Canada, 2010, pp. 344-358.

[22] Claude Castellucia, Aldar Chan, Einar Mykletun, and Gene Tsudik, "Efficient and provably secure aggregation of encrypted data in wireless sensor networks," *ACM Trans. Sen. Netw.,* , vol. 5, no. 3, pp. 1-36, 2009.

[23] Masoud Moradi and Arash Ahmadi, "Reducing Energy Consumption in wireless Sensor Networks Using Hash Distribution Table," *Journal of Electrical Engineering & Electronic Technology*, vol. 2, no. 1, pp. 1-4, May 2012.

Applied Mechanics and Materials Vol. 596 (2014) pp 528-531
© (2014) Trans Tech Publications, Switzerland
doi:10.4028/www.scientific.net/AMM.596.528

The Research on Sensor Fault Diagnosis Based on the SVM Prediction Model

Zhu Yajun [1, a *], Yu Xiangmei [2] and Yang Baohai [1]

[1]Department of Electronic Engineering, Jiujiang University, Jiujiang, Jiangxi, 332005, China

[2]School of Mechanical & Materials Engineering, Jiujiang University, Jiujiang, Jiangxi, 332005, China

[a]zhuyajunjjxy@163.com

Keywords: Fault Diagnosis,Support Vector Machine (SVM) , Dynamic Model, Sensor

Abstract. A novel method for sensor fault diagnosis based on support vector machine (SVM) prediction model was proposed. This paper put forward the principle of SVM condtruction process and the system parameters obtained from using dynamic model identification of sensor. The sensor fault was diagnosed on line by prediction model, which avoided that BP algorithm must have mass data and is likely to fall into local minimum point. Compared to the traditional motheds, it was much more effective and accurate.

Introduction

The way to improve the reliability of the sensor output signal is to set up several redundant sensors and choose its average or multilateral choice values, but this will increase the cost. On the other hand, using neural network in the training process is very easy to be trapped in the local minimum, since its training consequence is related to the initial network and the sample sequence and so on, this process has somewhat randomness. What's more the consequence has a very strong dependence on the quantity of the sample sequence, when there is a limited for the data of the sample, it will result to a large deviations.

Supporting the training process of SVM does not exist a local minimum problem, especially in the learning process in small sample demonstrated that it can not over-reliance on the generalization ability of the quantity and quality of the sample. So using SVM to identify the dynamic model of the Sensor can avoid the short comings which has been mentioned to a certain extent.

Sensor Dynamic Teaching Mode

In the practical application, sensor can based on the result getting from the input and output signals of the dynamic measure to establish the follow form of equations to describe the single variable:

$$A(z^{-1})y(k) = B(z^{-1})u(k-d) + \zeta(k) \tag{1}$$

d is a known constant $A(z^{-1}) = 1 + a_1 z^{-1} + a_2 z^{-2} + \cdots + a_n z^{-n}$ $B(z^{-1}) = b_0 + b_1 z^{-1} + b_2 z^{-2} + \cdots + b_m z^{-m}$

$\zeta(k)$ is for the white noise output.

The established mathematics model of vector format is $y(k) = \boldsymbol{\theta\varphi}(k) + \zeta(K)$ (2)

Principles to Identify the SVM System

Suppose the input and output data of a certain linear regression system $\{x_i, y_i\}$, (i=1,2,…N), $x_i \in R^N$ is the vector which is input by the n dimensional system, $y_i \in R$ is the output system.

The basic thought of the way to identify the SVM[2][3][4] is through the nonlinear transform $\varphi(\cdot)$,shine the sample input by the dimension n from the original room to the high dimension featured space F, and structure a optimal linear regression function:

$$f(x)=\omega^T\varphi(x)+b \tag{3}$$

The standard SVM takes ε as not sensitive loss function and risk minimization of estimation, so we can establish a form for the objective optimization:

$$\min\frac{1}{2}\omega^T\omega+c\sum_{i=1}^{N}(\zeta_i+\zeta_i^*)\varepsilon \qquad s.t.\begin{cases} y_i-\omega^T\varphi(x_i)-b\le\varepsilon+\zeta_i \\ \omega^T\varphi(x_i)+b-y_i\le\varepsilon+\zeta_i^* \\ \zeta_i\ge 0,\zeta_i^*\ge 0,i=1,........N \end{cases} \tag{4}$$

C is the balance factor in the formula, always assumed as 1. ζ_i,ζ_i^* are called the punish factor, which indicates the error caused by the introduced training set, they can used as to express the extent that the sample points have overstepped the fitting accuracy ε. If the sample points are within the accuracy ε, then $\xi_i=\xi_i^*=0$.

We can establish the Lagrange equation and its solution based on the formula (4) aim function and its limited requirement as follows:

$$\begin{aligned} l(\omega,b,\zeta_i,\zeta_i^* &= \frac{1}{2}\omega^T\omega+c\sum_{i=1}^{N}(\zeta_i+\zeta_i^*)-\sum_{i=1}^{N}\alpha_i^*(\varepsilon+\zeta_i^*+y_i-\omega^T\varphi(x_i)-b) \\ &-\sum_{i=1}^{N}\alpha_i(\varepsilon+\zeta_i+y_i-\omega^T\varphi(x_i)-b)-\sum_{i=1}^{N}(\eta_i\zeta_i+\eta_i^*\zeta_i^*) \end{aligned} \tag{5}$$

In the formula, parameter $\alpha_i,\alpha_i^*\ge 0,\eta_i,\eta_i^*\ge 0,i=1,........N$. Seeking partial derivative of variable in formula (5) respectively, dual optima problem can be obtained through arrangement, among them x_i which matches to $(\alpha_i-\alpha_i^*)\neq 0$ is support vector; the variable ω showing complexity of function is linear combination of mapping function $\varphi(\cdot)$. Therefore, the computational complexity of system identification conducted by SVM is unrelated to space dimension but relies on the number of samples. Using kernel function to substitute for nonlinear mapping $\varphi(\cdot)$, that is

$$\psi(x_i,x_j)=\varphi(x_i)^T\varphi(x_j) \tag{6}$$

Optima problem(5) can be translated into solving dual problem：

$$\begin{aligned} \max_{a,a^*}J &= -\frac{1}{2}\sum_{i,j=1}^{N}(\alpha_i^*-\alpha_i)(a_j^*-a_j)\psi(x_i,x_j) \\ &-\varepsilon\sum_{i=1}^{N}(\alpha_i^*-a_i)+\sum_{i=1}^{N}y_i(\alpha_i^*-a_i) \end{aligned} \qquad s.t.\begin{cases} \sum_{i=1}^{N}(a_i-\alpha_i^*)=0 \\ a_i,a_i^*\in[0,c] \end{cases} \tag{7}$$

To solve quadratic programming problem of formula (7) can obtain standard result of system identification of SVM.

$$\begin{aligned} y(x) &= \sum_{i=1}^{N}(a_i-\alpha_i^*)\psi(x_i,x)+b \\ b &= \sum_{SV_s}(a_i-\alpha_i^*)[\psi(x_j,x_i)+\psi(x_k,x_i)] \end{aligned} \tag{8}$$

In the formula, x_k,x_i are arbitrary two support vector.

Because formula(2) is the linear representation, SVM can be used to model[5]. The specific method is firstly carry on a dynamic experiment on sensor, the list entries and output sequence of the experiment are $\{u(k),y(k)\}$, then make up training sample $\{y(k),\varphi(k)\}$according to the form of formula(2) and input the training sample into SVM online in order to get support vector set SV_s and then model parameter $\boldsymbol{\theta}$ and b can be fixed. In order to test the model's accuracy, model response $\hat{y}(k)$ can be obtained by inputting pumping signal $u(k)$ into the model and the initial value of $\hat{y}(k)$ can be set as 0. The process of sensor's dynamic model identification made by SVM is like as Fig.1.

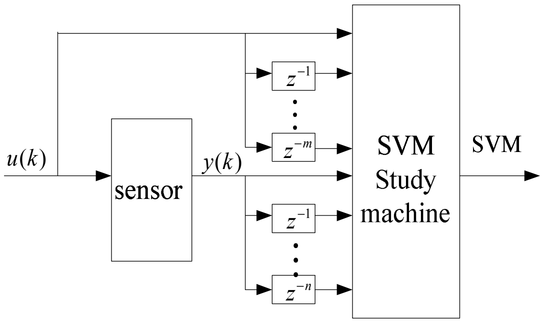

Fig.1 Learning model based on SVM dynamic model

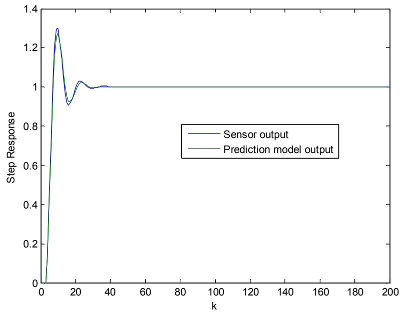

Fig.2 Simulation result of step response

Simulation Experiment Of Dynamic Model Identification

Making simulation experiment of dynamic model identification on the following sensor, its transfer function is $C(z)=\dfrac{z^{-3}+0.5z^{-4}}{1+1.5z^{-1}-0.7z^{-2}}$, inspiring to use unit step signal and sampling length of data is 200. In the process of model identification, flat noise of one variance was used to be pumping signal. When the input is unit step input, the responsive result was shown in Fig.2.

According to simulation result, it has a high precision and there is quite minor error between dynamic model identification parameter and original sensor model parameter based on SVM.

Sensor Fault Diagnosis Based on the SVM Prediction Model

As one of output-faults of control system, sensor fault has three forms of expression: sensor sticking, sensor constant gain and invalidation of sensor constant deviation.

Sensor Stuck. If y_{iout} is the actual output of the i-th sensor, y_{iin} is the right output signal when the i-th sensor is in normal condition, then the fault model of the i-th sensor sticking is:

$y_{iout}(t)=a_i$, a_i is constant, i=1,2,3 ,…m. （9）

Change of Sensor Constant gain. The fault model of constant gain change of the i-th sensor's actual output is:

$y_{iout}(t)=\beta_i y_{iin}(t)$, In the formula, β_i is the proportionality factor of gain variation. （10）

The Invalidation of Sensor Constant Deviation. The fault model of constant deviation of the i-th sensor's actual output is:

$y_{iout}(t)=y_{iin}(t)+\Delta_i$, In the formula Δ_i is a constant. （11）

By simulation experiment we know that can well predict output values of the sensor at next moment depending on SVM dynamic identifying model. When proper threshold value is designed, by via of SVM dynamic identifying model, we can predict output values of the sensor at next moment. Then compare with the substantial output values, if sensor becoming invalid the error between predict output and substantial output will exceed threshold value further. It ensues that we can justify sensor malfunction and the category of it. We illustrate malfunction diagnose model as Fig.3.

Assuming that the reference input signal is sine signal $0.5\sin(2\pi t)+0.5$ Sensor respectively happened stuck fault, constant gain fault and constant deviation fault during 1.4 second and 1.6 second. The output of the fault diagnosis model of Fig.4 to 6 respectively.

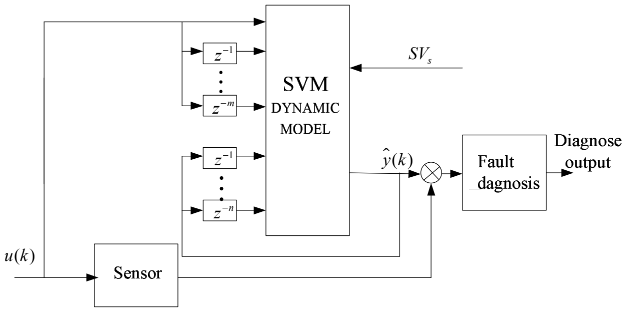

Fig.3 Fault dagnosis based on the SVM prediction model

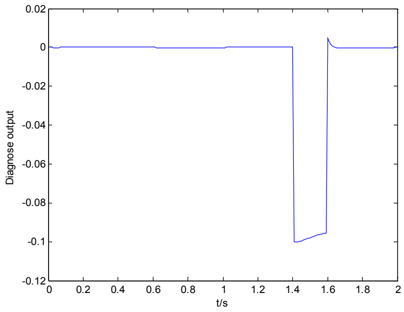

Fig.4 The output of sensor stuck fault

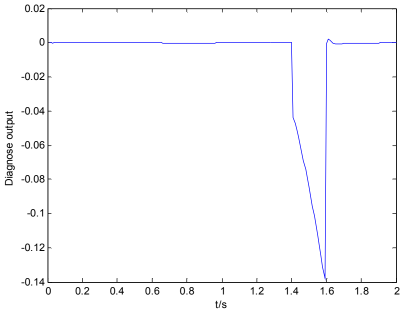

Fig.5 The output of snsor constat gain fault

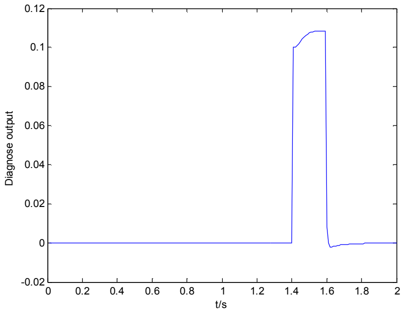

Fig.6 The output of sensor constant deviation fault

Conclusion

Adopting the method of sensor malfunction diagnose based on SVM predict model, we can avoid the deficiency of neuron network model efficiently during the course of practice, where we are prone to get stuck in part minimum andthe strong dependence on quantity of practice sample. Meanwhile, it is more effective and precise than traditional method of sensor fault diagnose.

Acknowledgment

This work is supported by National Science Foundation of China (61261046), Science Foundation of Jiangxi Provincial Department of Education(GJJ14739, GJJ11244, GJJ11245）,Science Foundation of Jiujiang Univercity (2013KJ02, 2013KJ01)

References

[1] Vapnik V The Nature of Statistical Learning Theory [M]. NewYerk, Springer 1995.

[2] Ma Yunqian, Zhang Xuegong. Application of Support Vector Machines Function Fitting in Fractal Interpolation [J]. Journal of TsingHua University Science, 2000,Vol.40.3:76-78.

[3] Meng Haitao, LiuPeng. Means of Classification of Improved SVM Support Vector [J]. Modern Electronic Technology, 2007, 1:150-152

[4] ZhangNan, Liu Junjie. The Research on Model Identification Based on Support Vector Machine [J]. Vessel Technology, Vo28 No 5.93-98.

[5] Shen Yuhao, Mengchen. The Research on Simulation Circuit Fault Diagnosis Based on Improved Support Vector Machine [J]. Computer Emulation, Vol.27 No.1 346-350.

[6] CuiJiang, Wang Youren. New Strategy of Mimic Channel Fault Diagnosis Based on Support Vector Machine and Nearest Neighbor Classifier [J]. Journal of Instruments and Meters, Vol.31 No. 4 189-194

Applied Mechanics and Materials Vol. 596 (2014) pp 532-535
© (2014) Trans Tech Publications, Switzerland
doi:10.4028/www.scientific.net/AMM.596.532

Review of MEMS techniques and applications in aerodynamics research

Fan Litao

China Aerodynamics Research and Development Center, China Sichuan Mianyang 621000

hnyyflt@gmail.com

Keywords: MEMS, Wind tunnel testings, Attitude determination, Aeroacoustic measurement, Shear stress

Abstract. MEMS sensors have some attractive advantages, such as low cost, small size, which help them to be widely used in wind tunnel tests. This paper presents the basic principles and sensor types of MEMS measurement and concludes the MEMS technology for wind tunnel test applications. Future research focus is also expressed.

Introduction

Miniature sensors are particularly valuable to the fluid mechanics and acoustics communities because they reduce flow disturbances and scattering effects relative to conventional sensors. The desire for high-performance , low-cost sensors with high bandwidth has also motivated the use of MEMS processes for fabricating small, low-cost shear sensors. The emergence of the microelectromechanical systems(MEMS) sensors has generated considerable interest for laboratory determination of sensor properties for flight and wind tunnel applications.

Shear sensor

Shear stress is an important fundamental parameter in characterizing turbulent boundary layers[1]. Employing MEMS technology, it is easy to measure shear stress directly with a temporal resolution of order 10kHz and a spatial resolution of order 100μm, which can afford an accurate dynamic calibration but the measurement will be very difficult for the open structure needed to implement the floating element. A floating element sensor, 500μm(L)×500μm(W)×7μm(thick) , was invented to achieve maximum non-linearity of 1% over four orders of wall stress(0.0014-10Pa) and 4kHz dynamic response in 1997, which is comprised of a square silicon floating element, silicon wafer and silicon tethers. Breadboard sensor, directly measuring shear stress, was utilized to determine an aircraft's viscous drag and combustion efficiency, both of which are functions of surface shear stress forces[2]. Capacitive MEMS sensor with pectinate floating element was developed to measure the wall shear stress directly[3].

Other indirect technique, such as thermal anemometry, is also used to acquire the shear stress which is related to the convective cooling of a heated element[4]. New thermal sensor was designed and fabricated with the philosophy of minimizing the thermal mass of the sensor to maintain a high frequency response and keeping sensor resistance low to keep noise down, sensitivity high and to allow for standard anemometer circuits to be used. The devices were fabricated on a silicon substrate with a platinum sensor element 5 microns wide, 1000-Å thick and of varying length and showed excellent performance with good frequency response. A thermal type shear stress sensors were tested by NASA Langley Research Center in its 16-Foot Transonic Tunnel and the Transonic Dynamics Tunnel(TDT) and they worked well[5].

Attitude sensor

For its limited accuracy in determining model attitude, MEMS sensor is not the best choice to measure model angles. However, small size and low cost is still attractive to wind tunnel test applications. Two different types of MEMS accelerometers, capacitive type sensing element and micromachined silicon proof mass, were developed at NASA Langley Research Center(LaRC) for the measurement of model attitude[5]. Laboratory calibration shows that the accuracy is about +/-0.04 degree with a 95% confidence interval(+/-1.96 sigma) over a range of +/-30 degree inclination, which is lower than that of servo accelerometers, +/-0.01 degree over a range of +/-20 degree[6]. Two different prototype AMS(angular measurement system), utilizing of MEMS of accelerometers and gyros, were investigated to develop angular measurement capability for hypersonic(short duration) wind tunnel facilities[7]. Results indicate the accelerometer based prototype can meet the +/-0.1 degree design requirement in pitch, yaw and roll while the gyro based prototype fails because of the poor performance of the selected gyros. It sill shows that the feasibility for a MEMS based angular measurement system using high grade accelerometers and gyros, as well as sophisticated calibration and construction logic, that can satisfy current +/- 0.1degree accuracy objectives, is high. And it has been demonstrated that with high grade DTG, the model attitude measurement accuracy can be improved to 0.05degree[8]. Up to now, for AMS, MEMS sensors are mainly utilized to correct sting-whip errors of an accelerometer induced by centrifugal inputs to inertial angle of attack sensors caused by dynamic pitch and/or yaw model motion[9].

Aeroacoustic sensor

Most of the aeroacoustic sensors, microphones, employ a fundamental structural model coupled with a lumped-element energy model[10] whose measurement technology is developed in investigating the feasibility of economical compliance with the FAR 36-Stage 3 community noise standard to achieve experimental data. Conventional microphones cannot meet the requirements of jet-noise wind-tunnel testing because of the unacceptable high overall noise floor especially for forward flight conditions when the combustion system model is performed in a wind tunnel. MEMS-based microphones, flush-mounted to the surface of a laminar-flow airfoil, are a good choice to offer the potential to reduce wind noise to acceptable levels. The difficult point is to design and manufacture a micromachined microphone to meet the bandwidth and dynamic range needed for forward-flight aeroacoustic measurements.

Due to the characteristics of cheaper to develop, simpler to fabricate, more robust and favorable scaling advantages, piezoresistance microphones now are taking the place of capacitive microphones. Low-noise floor(60dB), large bandwidth(≈40kHz), small diaphragm size(<0.5mm), and a large dynamic range(60-160dB) piezoresistance microphones were developed by university of Florida[10], consisting of four dielectrically-isolated, single-crystal silicon piezoresistors on top of 1500 Å-thick, 210μm-diameter silicon-nitride membrance. Four piezoresistors were used in a Wheatstone-bridge configuration which is driven by a constant voltage excitation. The lumped-parameter model were represented by a Kirchhoff network representation which is an equivalent circuit describing the multi-domain dynamical system.

However, the developed MEMS microphone utilizing piezoresistive transduction techniques cannot meet the requirements for 1/4 scale testing and certification, which means a maximum sound pressure level in excess of 160dB, bandwidths of 50kHz or greater, and a noise floor of <50dB/$\sqrt{Hz}$. New piezoelectric technique, offering for durable, high sensitivity, low noise device that requires no external power to operate, microphone was designed and manufactured in 2007 overcoming the drawback for material integration and compatibility with standard micromaching[11]. Piezoelectric composite plate theory and lumped element modeling was employed to design the microphone, which consists of a 1.8-mm-diam, 3-μm-thick, silicon diaphragm with a 267-nm-thick ring of piezoelectric material. The devices were fabricated using a sol-gel PZT deposition process on a 4 in. Silicon-on-insulator wafer combined with deep reactive ion etching(DRIE) for the release of the silicon diaphragm. Experiments indicated a sensitivity of 1.66μV/Pa, with a linear dynamic range from(35.7-169dB, re 20μPa) and 59.0kHz resonant frequency. The self-powered nature eliminates the need to distribute power throughout the microphone arrays. New type piezoelectric MEMS microphones were developed using aluminum nitride material for its improved stress control and commercial availability[12,13].

Except for noise measurement, the MEMS microphone array also has been designed and applied to the measurement of wall pressure spectra under the turbulent boundary layer in flow duct testing at Mach numbers from 0 to 0.6. Allowing high spatial resolution and low surface roughness[14]. The array shows excellent agreement with microphone measurements in the 300Hz to 10kHz band. The sensor chip is described by fabricating the entire array on a single chip, rather than assembling the array out of individual microphones. Reducing spacing better matching of the elements without excessive testing. Fronted vented 64 element MEMS microphone array on a chip achieves high spatial resolution of 1.1 to 1.25mm centre to center spacing of the elements with individual element diameters of 0.6mm.

For characterizing non-condenser microphone frequency response up through at least 100kHz validated, a method exposes a device under test microphone and a reference microphone to the same acoustic field[15], opening doors to the possibility of thousands of high quality, low cost sensors for aeroacoustic phased array applications. The technique has enabled relatively high quality frequency response characterization from 500Hz to 100kHz for both condenser and non-condenser microphones

Miscellaneous

MEMS sensors can also play a role to measure pressure, temperature[5] and velocity[16]. Dynamic simulation techniques use MEMS sensor technology to measure a model's motion and obtain reliable flight dynamics information in developing low cost dynamic wind tunnel facility[17]. Flow control is another field for MEMS sensors to show their existence[18].

Conclusions

The characteristics of MEMS sensors, low cost, small size, high performance, have become more and more attractive for wind tunnel testing. With the development of material research and fabricating technology, MEMS sensor performance has been promoted rapidly and efficiently. MEMS sensors can almost be competent for each measurement in a wind tunnel test. Aeroacoustics, model attitude and flow control measurement will result in great need for MEMS sensors which will play a more and more important role.

References

[1] A. Padmanabhan, M. Sheplak, K.S. Breuer and M.A.Schmidt. Micromachined sensors for static and dynamic shear-stress measurements in aerodynamic flows[C]. In: IEEE, International Conference on Solid-state Sensors and Actuators, 1997, 137-140.

[2] Nicholas Tiliakos, George Papadopoulos, Vijay Modi, etc. MEMS shear stress sensor for hypersonic aeropropulsion test and evaluation[C]. Annual ITEA Technology Review, 2006.

[3] Tu Heng-zhang, Li Jian-qiang, Ming xiao, etc. Direct measurement technique of wall shear stress using MEMS sensors in a high-speed wind tunnel[J]. Journal of Experiments in Fluid Mechanics, Vol.22, No.3, 2008, pp.94-98.

[4] Kenneth S. Breuer. MEMS sensors for aerodynamic measurements- the good, the bad(and the ugly)[C]. In: AIAA, Aerospace Sciences Meeting and Exhibit, 2000.

[5] Seun K. Kahng, Corey D. Hernandez, Sussan A. Gorton, etc. MEMS sensor system development at NASA Langley Research Center for wind tunnel applications[C]. In: AIAA, Aerospace Sciences Meeting and Exhibit, 2002.

[6] Tom D. Finley and Ping Tcheng. Model attitude measurements at NASA Langley Research Center[C]. In: AIAA, Aerospace Sciences Meeting and Exhibit, 1992.

[7] Sibok Yu and Brett Newman. Development of a high accuracy MEMS angular measurement system for hypersonic wind tunnel facilities[C]. In: AIAA, Structures, Structural Dynamics, and Materials Conference, 2003.

[8] Mathew L. Rueger and John Lafferty. Demonstration of a gyro-based model attitude measurement system at the AEDC tunnel 9 test facility[C]. In: AIAA, Fluid Dynamics Conference and Exhibit, 2008.
[9] Bradley L. Crawford and Tom. D Finley. Improved correction system for vibration sensitive inertial angle of attack measurement devices[C]. In: AIAA, Aerospace Sciences Meeting and Exhibit, 2000.
[10] Mark Sheplak, John M. Seiner, Kenneth S. Breuer, etc. A MEMS microphone for aeroacoustics measurements[C]. In: AIAA, Aerospace Sciences Meeting and Exhibit, 1999.
[11] Stephen Horowitz, Toshikazu Nishida, Louis Cattafesta, etc. Development of a micromachined piezoelectric microphone for aeroacoustics applications[J]. J. Acoust. Soc. Am., Vol.122, No.6, 2007, pp3428-3436.
[12] Matthew D. Williams, Benjamin A. Griffin, Tiffany N. Reagan, etc. Micromachined aluminum nitride microphone technology development[C]. In: AIAA, Aerospace Sciences Meeting including the New Horizons Forum and Aerospace Exposition, 2012.
[13] Mattew D. Williams, Benjamin A. Griffin, Tiffany N. Reagan, etc. An AIN MEMS piezoelectric microphone foe aeroacoustic applictions[J]. Journal of Microelectromechanical Systems, Vol.21, No.2, 2012, pp270-283.
[14] Robert D. White, Joshua Krause, Richard De Jong, etc. MEMS microphone array on a chip for turbulent boundary layer measurements[C]. In: AIAA, Aerospace Sciences Meeting including the New Horizons Forum and Aerospace Exposition, 2012.
[15] J. Patrick King and James R. Underbrink. Characterization of a microelectromechanical systems(MEMS) michrophone[C]. In: AIAA, Aeroacoustics Conference, 2008.
[16] Shen guangping, Wu Jian, Zhang Hua, etc. Design of a 2D thermal wind sensor based on MEMS process[J]. Chinese Journal of Semiconductors, Vol.28, No.11, 2007, pp1830-1835.
[17] S.D. Carnduff, S.D. Erbsloeh, A.K. Cooke, etc. Development of a low cost dynamic wind tunnel facility utilizing MEMS inertial sensors[C]. In: AIAA, Aerospace Sciences Meeting and Exhibit, 2008.
[18]. Jonathan r. Potts, Ian Lunnon, William J. Crowther, etc. Development of a transonic wind tunnel test bed for flow control actuators and sensors[C]. In: AIAA, Aerospace Sciences Meeting including the New Horizons Forum and Aerospace Exposition, 2009.

Applied Mechanics and Materials Vol. 596 (2014) pp 536-539
© (2014) Trans Tech Publications, Switzerland
doi:10.4028/www.scientific.net/AMM.596.536

Design and Applications of Embedded System in Video Surveillance

Zhang Cheng Yan, Pang Xiao Fen

Inner Mongolia Vocational and Technical College of Communications, Inner Mongolia Chifeng
024000，China

imvtcccy@yeah.net

Keywords: video surveillance, embedded systems, microprocessors, video capture

Abstract. In this paper, we select the ARM11 S3C6410 processor and embedded Linux system using the system needs to build a development environment. Studied in the embedded Linux operating system USB video capture device driver modules, collecting network video surveillance system implemented by V4L2 driver framework. Video capture program primarily through ioctl system function calls to access V4L2 driver framework. Completion of real-time video transmission via RTP / RTCP protocol. In addition, the Web server development platform porting.

Introduction

Early video surveillance systems, closed-circuit system constituted by an analog device, the main components of the structure of the front-end equipment, transmission cables, switch controllers, monitors. Front-end equipment is generally cameras, environmental sensors, temperature and humidity detectors and other equipment; monitor can be divided into common monitor, capable of operating platform front control device capable of displaying signs or sensor status. Because the monitoring system to simulate the transmission, so the monitoring system uses far from general. In recent years, the advantages of video surveillance technology is relatively high transmission efficiency while being able to use a relatively large geographical space; easy to operate and manage, develop and design tend to be more standardized interfaces; while providing a friendly interface for human-computer interaction, user-friendly. In a certain procedure to solve the shortcomings of analog surveillance systems, but such systems are still some shortcomings need a dedicated video card lead to high costs and poor compatibility, but who require specialized computer terminal operation and management, is not conducive to maintaining the system and upgrades. With the broadband technology and the rapid development of embedded technology, image processing technology and the emergence and rapid development, research video surveillance system gradually shifted from the local to be able to monitor remotely monitor trends. Users can control the network interface for remote monitoring and management information.

System Design

Embedded Network Video Monitoring System This paper analyzes and studies the B / Smodel, the client B/S mode requires only a browser to communicate by computer. The entire system in accordance with the process of acquisition, encoding, transmission development, functional block diagram of the system is shown in Fig.1.

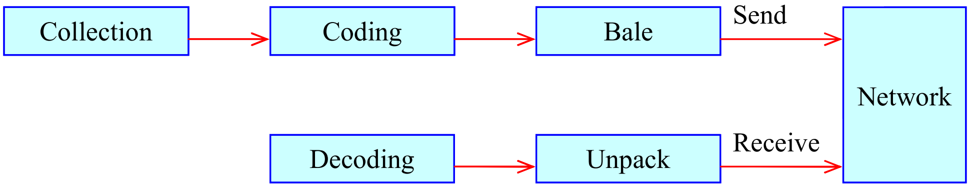

Figure.1 Functional block diagram of the system

Browser-side for the entire design greatly reduce costs, without regard to client development and management. Users do not care about video surveillance sources, only the scenes they need, upgrades and simpler maintenance. Real-time video playback and storage, making the whole system has features flexible, easy scheduling. Raw data collected through H.264 encoding, will be packaged into RTP H.264 video streams sent to the network; network receives RTP packet decode playback. In this paper, the research and design to achieve functional video capture, encoding and transmission of these three modules. The whole system is built on S3C6410 core hardware platforms, peripherals, including USB cameras, SD card, network card, the control port to USB adapter and other hardware structure of their system as shown in Fig.2.

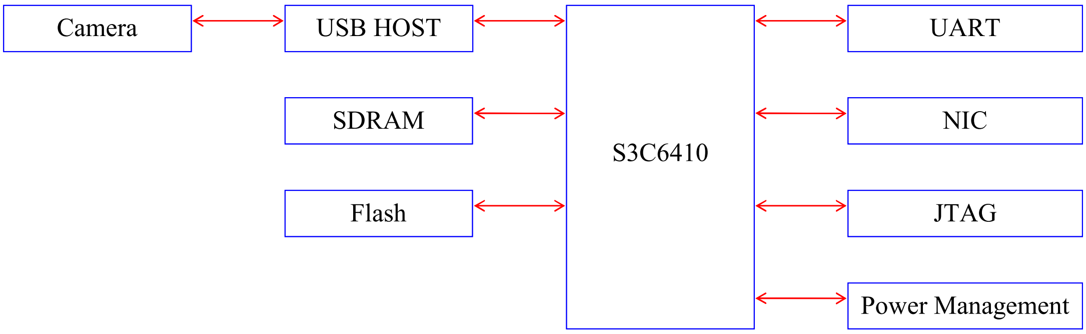

Figure.2 System hardware structure

USB2.0 camera due to good performance, simple, practical and low-cost, widely used in embedded systems. The system uses a universal USB2.0 camera. USB2.0 camera with the USB HOST interface connected S3C6410, collecting video data. Software platform is an embedded Linux operating system. USB camera access embedded systems, collecting data through the H.264 video coding, video will be packaged into RTP packets to the network. Embedded Web server has been waiting waiting requests a connection, if the connection request, the request be dealt with accordingly.

Implementation of the system

This system needs S3C6410 core board hardware design includes Nandflash, DDR2 memory, USB HOST interfaces, 100M Ethernet interface. 1G Bytes Nandflash main function is to store the kernel code, file systems, applications, etc., supports dual chip select mode architecture; design Mobile DDR2 memory, DDR data bus frequency up to 266MHZ small BGA package by two K4X51163PC chips. to ensure reliable operation. Using UART0 as debug serial port via adapter cable connected to a PC, check the system debugging information. USB camera connected via USB HOST interface and development platform, USB HOST interface supports USB1.1, USB2.0 protocol, using the USB female port, you can connect U disk, USB mobile hard disk, USB keyboard and other peripherals. The design principle is shown in Fig.3. S3C6410 100M integrated Ethernet interface for connection to a PC via a crossover cable.

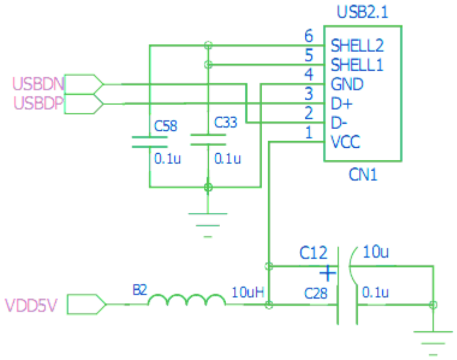

Figure.3 USB HOST design schematics

Embedded software uses the host and target development model, the system environment, including the host environment and target environment. The host environment, including cross-compilation environment containing the operating system Linux; goal machine environment is an embedded Linux systems containing embedded Web server is Boa, including embedded hardware environment is the main control panel, camera. S3C6410 processor as the main control board, including ARM11 core processor, H.264 codec, network adapter chip and associated interfaces, camera is USB2.0, capture video of the original data. Shown in Figure.4, the host generates binary code is downloaded to the development platform, the development platform to run, so you must realize the host and the target structures.

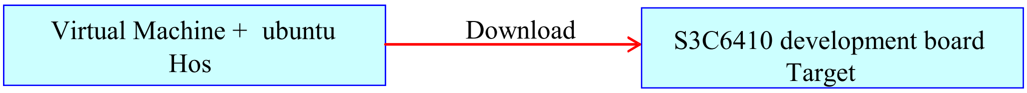

Figure.4 Block diagram of the system development approach

Use Virtual Machine environment to build on the host. Refers to the virtual machine on an existing operating system, with special software virtual machine, the virtual machine out of a number. Each computer has its own virtual hardware devices such as CPU, memory, optical drives, etc., and can each run, not interdependent, and are connected to a LAN. V4L2 image acquisition process under analysis: First, open the specified device name; After opening the device, if successful, check device function; then select the video image formats, read and write to memory space, finished off the video capture device. These operations are V4L2 interface definition, the actual content of the data structure is generally used ioctl () to set and read.

```
struct v4l2_requestbuffers reqbufs;
struct v4l2_capability cap;
 struct v4l2_input input;
struct v4l2_standard std;
struct v4l2_format fmt;
struct v4l2_buffer buf;
v4l2_std_id stdid;
struct v4l2_queryctrl query;
struct v4l2_control control;
```

RTP is the multimedia data stream for processing on the Internet Protocol network, capable of operating in unicast or multicast transmission environment, its purpose is to provide time synchronization information and streaming. RTP is generally built on the User Datagram Protocol (UDP) on, you can also work in the Transmission Control Protocol (TCP) or ATM. RTP can guarantee real-time data transmission, but this is not a reliable real-time transmission, and no flow control or congestion control. Select this article RTP / RTCP streaming media transmission protocol. Needed RTCP protocol provides flow control, congestion control, and to ensure reliable real-time transmission. Figure 5 is a RTP packet encapsulation, RTP RTP packet format includes a fixed header, multiple RTP sessions and the first portion of the expansion of three parts. Shows, RTP receiving streaming media information from the upper stream, such as H.264, plus the RTP header encapsulated into RTP packets. Finally, add the UDP header and IP header, the final package framing. RTP packet maximum transmission unit (MTU) MTU restricted by IP packets.

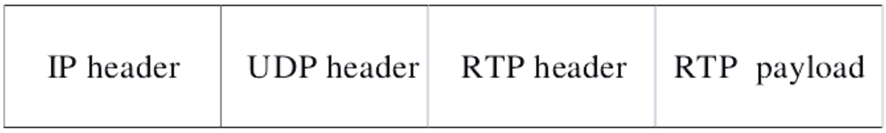

Figure.5 RTP packet encapsulation

The development platform with a computer set up on the same LAN, through the computer's browser can remotely access video. The video surveillance system is divided into two parts, the browser and server components. Embedded video capture module requires S3C6410 development platform, USB2.0 camera and 4.3-inch LCD and other components; browser from a remote computer part containing the IE browser. At room temperature, the test of the entire system monitoring scenario. Local tests on the same LAN, the entire system is connected as shown in Fig.6, the computer via a serial connection with the development platform, USB2.0 camera connected via USB HOST interface and development platform.

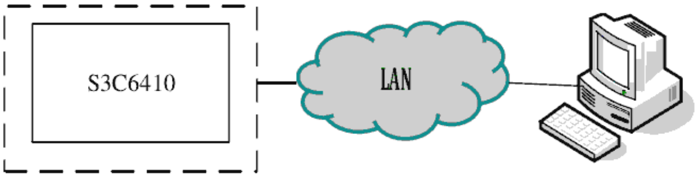

Figure.6 System Test Structure

Conclusion

Further development of embedded technology video surveillance systems are widely used in life. According to the characteristics of embedded processors and high real-time requirements of video surveillance systems, we design and implementation based on browser / server mode embedded network video surveillance system, the user can remotely monitor the scene browsing capabilities. In order to achieve the purpose of network video surveillance, analyze common characteristics of several types of embedded processors and select ARM microprocessor, using embedded Linux operating system. The system supports USB camera surveillance, can be used for remote users browser to view the video scene.

Reference

[1] P. Brox, I. Baturone, S. S. Solano: Fuzzy logic-based embedded system for video de-interlacing, Applied Soft Computing, Vol.14 (2014), p.338-346

[2] N. W. Lo, H. T. Chang, J. Y. Chang: Caged mice mating behavior detection in surveillance videos, Journal of Visual Communication and Image Representation, Vol.25 (2014), p.755-762

[3] J. H. Ko, E. S. Kim: Stereoscopic video surveillance system for detection of target's 3D location coordinates and moving trajectories, Optics Communications, Vol.266 (2006), p.67-79

[4] U. Ali, M. B. Malik: Hardware/software co-design of a real-time kernel based tracking system, Journal of Systems Architecture, Vol.56 (2010), p.317-326O. Elkeelany: On chip novel video streaming system for bi-network multicasting protocols, Integration, the VLSI Journal, Vol.42 (2009), p.356-366

[5] C. Salvadori, M. Petracca, S. Madeo: Video streaming applications in wireless camera networks: A change detection based approach targeted to 6LoWPAN , Journal of Systems Architecture, Vol.59 (2013), p.859-869

[6] M. Cristani, R. Raghavendra: Neurocomputing, Human behavior analysis in video surveillance: A Social Signal Processing perspective, Vol.100 (2013), p.86-97

[7] H. T. Ngo, R. W. Ives, R. N. Rakvic: Real-time video surveillance on an embedded, programmable platform, Microprocessors and Microsystems, Vol.37 (2013), p.562-571

Applied Mechanics and Materials Vol. 596 (2014) pp 540-543
© (2014) Trans Tech Publications, Switzerland
doi:10.4028/www.scientific.net/AMM.596.540

Analysis and design of a capacitive sensor for measuring thickness

Lei Jianhua

Institute of Information Technology, Jinan University, Guangzhou 510075, China

leijianhua@gmail.com

Keywords: parallel plate capacitance; sensor; edge effect; finite element simulation

Abstract. Parallel plate capacitance sensors have the advantage of low cost, fast dynamic response, and high resolution. However, edge effect severely limits their sensing accuracy. This paper designs a kind of parallel plate capacitance cylinder sensor with a metal protective ring which can significantly eliminate edge effect. Besides, simulation is shown using Ansys, a finite element software. The results indicate that, the curved field has turned into a vertical electric field because of the existence of the protective ring, and the edge effect has been eliminated.

Introduction

The capacitance sensor has the advantage of low cost, fast dynamic response, and high resolution. Capacitance micrometer technology has been tried in the measurement of dynamic film or coating thickness both in China and other countries. At present, the German meter Iridium Test Technology Company, the British B&W company have developed mature products. In China, Tianjin University, Hunan Institute of physics, and Chinese Academy of Sciences Institute of acoustics have all developed mature products in film thickness measurement with a larger scale (above 1mm) has developed a mature product. However, the film thickness measurement of a small scale is still in the exploratory stage [4]. In addition, Hebei University of Technology has many trials in research on single-chip capacitance sensor and its application in dynamic thickness measuring technology. Dynamic experiments have been done on simulation test-bed while some technical indicators of a prototype have been obtained. However, generally speaking, the product is not mature, and still not available in the production line.

This paper is mainly to study the defects and limitation of traditional bipolar parallel plate capacitor sensor in the application. According to the actual industrial production need, a new cylinder parallel plate capacitance sensor with a protective ring is analyzed and designed to give a base for production of a thickness measurement system in the future. Analysis of edge effect on capacitance sensor is done by using the finite element software Ansys. Combined with the actual production requirements, a capacitive sensor with a novel structure, anti-parasitic capacitance and resistance to electromagnetic interference has been developed.

Structure of the new capacitive sensor

In order to reduce or eliminate the edge effect, a new cylinder parallel plate capacitance sensor with a protective ring is designed. Because protective layer is added in the capacitive sensor, the electric field would disappear between the up and down layers in theory. In this way, there is no additional capacitance and the electric field keeps uniform in the sensor. Although there are still electric field and edge field between the protection ring and the lower plate, the capacitor caused by those fields is parallel with the sensor capacitor and thus very small. Another role of protecting ring is that it can absorb leakage current between the electrode and the insulator [15].

The proposed capacitance sensor consists of three coaxial metal layers and the two insulating layers in the structure. Figure 1 shows structural profiles of sensor measurement head, while the top view of sensor measurement head is displayed in Figure 2.

Among the layers and plates, the upper plate can be produced by iron nickel alloy material with low temperature coefficient, while the material of inner and outer insulating layers on measuring head is chosen as PTFE, the thickness of which should be as small as possible under the processing conditions permit. The inner and outer insulating layers are used to ensure insulation between the sensor plate and the protective layer, as well as electrical insulation between intermediate protective layer and the shielding layer. The intermediate protective layer and the sensor electrode are electrically insulated but with same voltage in order to overcome the effects of parasitic capacitance between measuring head and surrounding conductors, and to keep the bended electric field only occur outside of the protective layer so as to ensure that the electric field between the two electrodes is not affected by the edge effect and maintain uniform. The lower electrode and shielding layer are collected to the earth, which can prevent the interference of the external electromagnetic field.

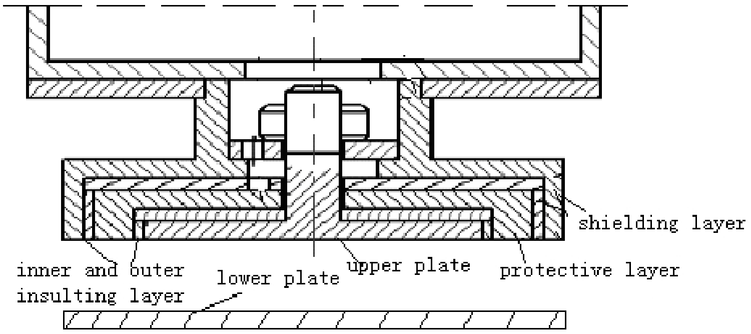
shielding layer
inner and outer insulting layer
lower plate
upper plate
protective layer

Figure 1 The structural profiles of sensor measurement head

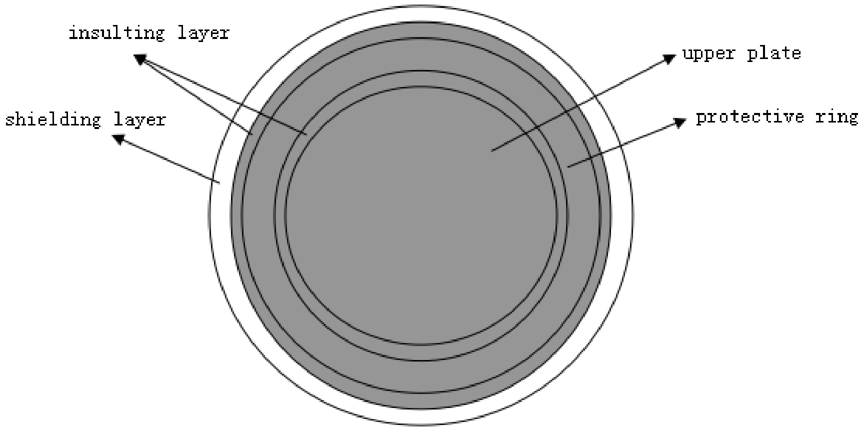
insulting layer
shielding layer
upper plate
protective ring

Figure 2 The top view of sensor measurement head

Analysis on finite element simulation

The new type of capacitance sensor with a protective ring, which places a metal protective insulting ring around and with same voltage of the effective electrode plate, makes the electric field between the intermediate electrodes keep straight, and maintain uniform. In other words, the proposed sensor can reduce or eliminate the influence of edge effect.

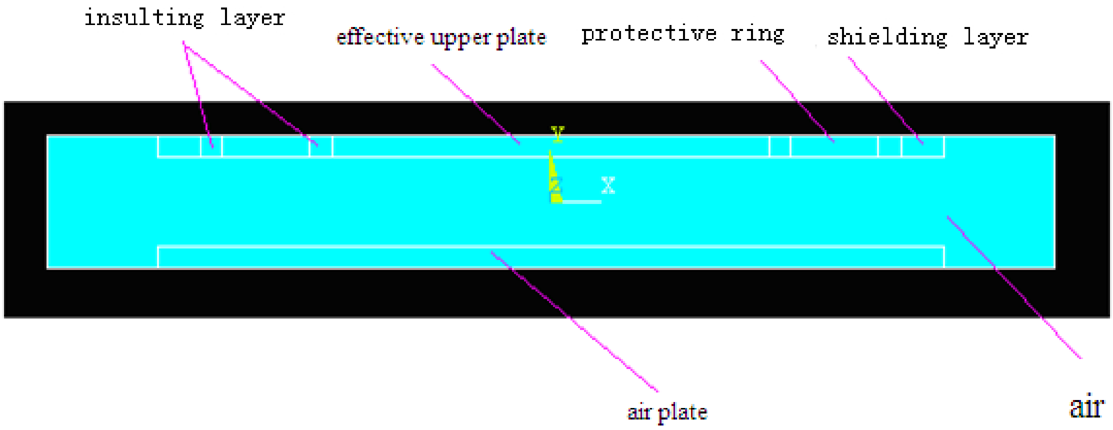
insulting layer
effective upper plate
protective ring
shielding layer
Y
X
air plate
air

Figure 3 The diagram of the structure of the parallel capacitance sensor with metal protective ring, which has the same voltage

In order to prove the potential proposed sensor can reduce or even eliminate the influence of edge effect, the Ansys analysis is used on the distribution of the edge electric field between the parallel plates in the following.

The two-dimensional electric field analysis model is shown in Figure 3, which has diameter of 10mm, thick plate of 0.5mm, distance between plates of 3mm, protective ring width of 2mm, shielding layer thickness of 1mm, insulating layer thickness of 0.5mm. After setting the property of each part of the model and the finite element mesh size, we applied 12V on the upper plate and the metal protective ring, and collected the lower plate to the ground. The distribution of the two-dimensional electric field of the proposed sensor can be found in Figure 4, while its two-dimensional electric field line is shown in Figure 5.

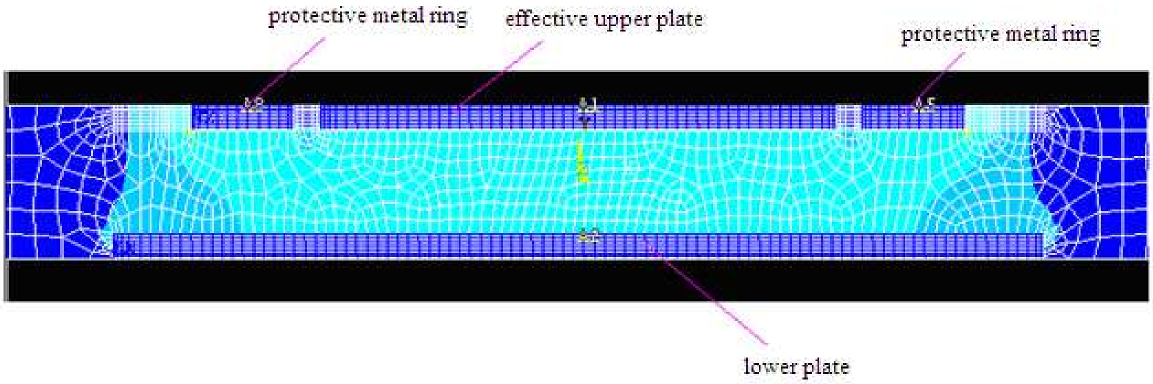

Figure 4 The distribution of the two-dimensional electric field of the proposed sensor

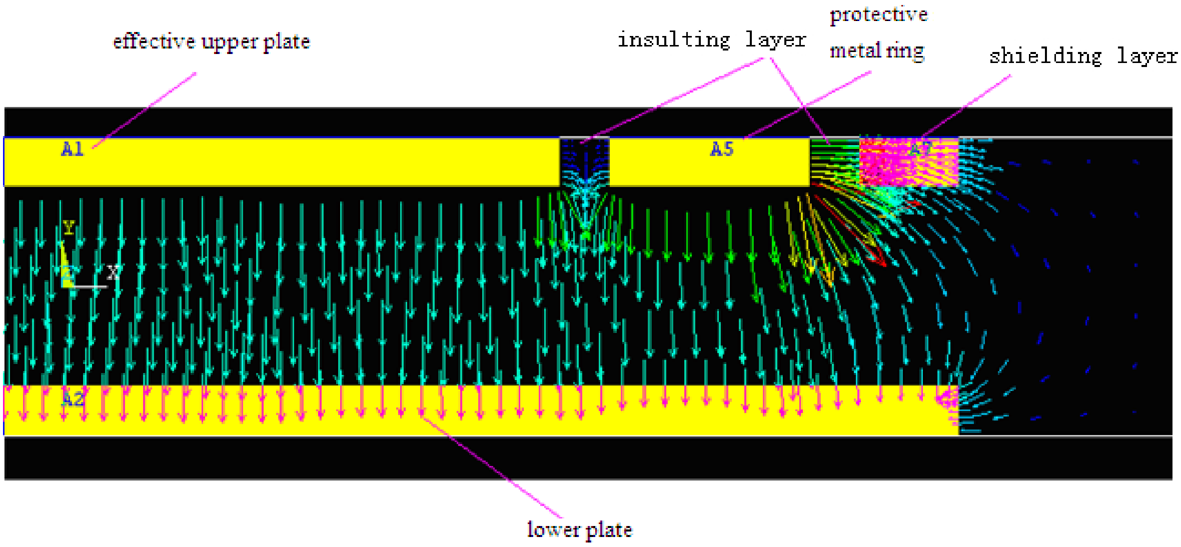

Figure 5 Part of the two-dimensional electric field line of the proposed sensor

From comparison between Figures 4 and 5, it can be notified that the random electric filed of the proposed sensor is apparently under control in its edge. The bended field line moves to the places outside the ring, that is the place between the between protective ring and shielding layer. The influence on ideal capacitance of effective electrodes is significantly reduced.

Through the simulation on Ansys software of the proposed sensor, compared with the traditional parallel plate capacitance sensor, the proposed sensor with protective ring changes the bended electric field into straight field, and basically eliminates the influence of edge effect. Therefore, in the capacitance sensor structure design, the protective ring with same voltage is an ideal method of eliminating the edge effect.

Conclusions

Based on the principle of parallel plate capacitance sensor, the edge effect, and the mechanical structure, this paper presents a detailed analysis of the relationship between the edge effect and the structure parameters such as plate thickness h, the distance between the parallel plates d, plate radius r, and then proposes the design of a parallel plate capacitance sensor with a metal protective. The advantages and disadvantages of capacitance sensor has been introduced in depth. It is easy to realize non-contact measurement, and with simple structure, fast dynamic response, small heating effect. This kind of sensor can be used for the detection of thin non-metallic material thickness, and in dynamic measurement and the static measurement applications.Through precise capacitance calculation, it has been found that additional capacitance caused by the edge effect is large, which has the very big relationships with plate distance and plate thickness. Its influence on ideal capacitance value of the parallel plate capacitance sensor can not be ignored. According to the method of eliminating edge effect, this paper designs a cylinder parallel plate capacitance sensor with a protective ring. This structure can ideally eliminate the edge effect of parallel plate capacitor sensor.

References

[1] Ying-Rong Cao, Research and Development of the System of Thickness Measurement by Virtual Capacitance Sensor: Master Thesis. WuHang, China. The Huazhong University of Science and Technology 2006

[2] Xi-Fu Qiang, Sensors. BeiJing :China Machine Press,1993.102～121

[3] Song-Bo Cheng, Shun-Sheng Guo, Jia-Ning Li. Design on on-site thickness measuring system based on eddy current steel plate. Mechanical Research & Application,2006,18(3):61～62

[4]Xiang Deng, Yi-Zhong Zheng. Research on on-site measurement of plastic film and paint layer thickness. Acta Metrologica Sinica,2001,22(4):268～271

[5]Wen-Shun Meng, Yun-Jing Yang, Yun-Peng Liu. Principle and application of capacitance sensor. Modern electronic technology，2003,(7):78～81

[6]Lin-Na Zhang, Wu-Fa Liu. Sensor detection technology and application. BeiJing: Chinese measuring press. 1998，67~69

[7] Kui-Rong Xiong, De-Ru Ni, The edge effect of capacitance sensor. The world of sensor 1998,3(2):16～19

[8] Jing-Yong Li. Finite element metdhods. BeiJing, Beijing university of post and telecommunication press，1999.3-4

[9] Ping-An Du, E-Zhong Gan, Ya-Ting Yu. The principle, modeling and application of FEM. BeiJing: National Defense Industry Press，2004，4-5

[10] Ming-Li Sun, Ren-Xi Hu, Hai-Rong Cui, et. al. Ansys10.0 electromagnetic finite element analysis example tutorial, BeiJing: China Machine Press，2007，1

[11] Jing Lu. Research and application of a new capacitance sensor. Master Thesis. TaiJin, Hebei university of Technology，2002

[12] Yaralioglu G.G,Degertekin F.L,Badi M.H.Finite element method and normal mode modeling of capacitive micromachined SAW and Lamb wave transducers. Ultrasonics Symposium,2000,1(10):22～25

[13] Chang-Shou Gu, Ying Zhang, Li-Sheng Cao. Research on the edge effect of parallel plate capacitance. Journal of Liaoning College of Technology. 1994,14(3):80～83

[14] Yi-Qing Zhu, Jian-Hong Xu. The capacitance computation of parallel capacitor with edge effect. Engineering Physics, 1998，8(1):6～9

[15]Zheng-Hua Huang, Qing-Fa Gao, Wen-Mei Huang, Sensitive head of capacitance sensor Instrument technique and sensor,1996,12(5):14～15

CHAPTER 7:

Automation Technology, Control System Modeling and Simulation Technology

Applied Mechanics and Materials Vol. 596 (2014) pp 547-551
© (2014) Trans Tech Publications, Switzerland
doi:10.4028/www.scientific.net/AMM.596.547

Application of the Flexible Brake on Wind Driven Generator

Zhou Hongfeng[1,a], Li Qing[1,b]

[1]Nan Road No. 16 Nan Shao town Changping Area Beijing, China

[a]zhouhongfeng@sgepri.sgcc.com.cn, [b]liqing@sgepri.sgcc.com.cn

Keywords: wind driven generator, Flexible brake, MCU, PWM, Relay

Abstract. The brake of the wind driven generator requires a gentle process. Which decreases the damage to equipment. In this paper, the flexible brake which can be realized a gentle braking is described. The application on the flexible brake of the wind driven generator are analyzed and explained. Brake is a MCU (Microprogrammed Control Unit) as the core. By the principle of the brake gently, flexible brake has been achieved by the principle of smooth braking. Based on the principle of pulse width modulation of the throttle valve, a safe and reliable braking force has been realized with hydraulic devices and electronic components. MCU controls relay to achieve PWM (pulse width modulation), and monitor the temperature and brake frequency monitoring and so on.

Introduction

The flexible braking known as gentle braking[1] could ensure a gentle brake process, and reduce wear and load on the mechanical parts during braking process. The concept of the gentle brake can be applied to wind power, escalator, transmission system, mine hoist, large ventilation fans and other occasions. Flexible brake is a better solution. During improper operation or complex braking process, the flexible brake can prevent unnecessary abrasion and provide the corresponding maintenance on brake components. In the paper, this design of the flexible brake is used for wind turbines. It can achieve the gentle braking process, and monitor the actual temperature of the brake shoes, braking times, brake shoes and so on.

Flexible brake principle

Flexible brake mainly use pulse width modulation[2]. The principle of which is based on the pulse width modulation principle of the switch throttle valve. Switching pulse width modulation based on the hydraulic devices and electronic components. It can form absolutely safe and reliable braking force. The flexible brake achieves the gentle brake by controlling the throttle valve. The throttle valve has a ratio of 1:10 per second, such as cycle time.

By changing the time of the brake switch, shown in Figure 1, it can control the size of the braking force. In this way the flexible brake can module the value of the throttle valve. The braking torque has been specified according to the actual needs of the gentle control.

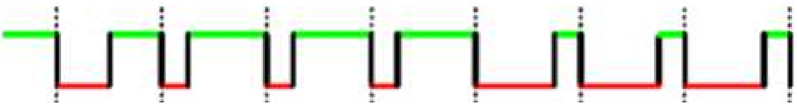

Figure 1. Figure for brake switch time ratio

Brake constitution

The flexible brake is known MCU as core. The model is C8051F120. The characteristics of MCU has internal resource-rich, low power consumption, computing speed and so on. It can meet the design requirements of the brake [3].

A specific structure of the flexible brake is shown in Figure 2.

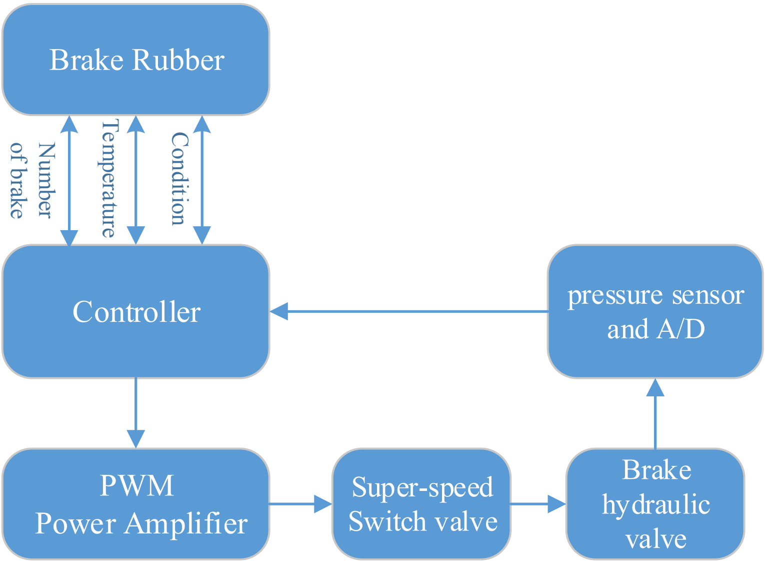

Figure 2. Principle Diagram of the Brake

3.1 The Realization of Flexible Brake

This paper describes the flexible brake for the brake of wind turbine [4]. Figure 2 shows that the PWM signal generated without the D/A converter can be directly transmitted into driving signal by the power amplifier and drive a high-speed switching valve in the system. The motion of the valve controls brake cylinder fluid inflow and outflow, and then controls the pressure of the brake fluid cylinder. Under work condition. The computer output of the PWM signal in the brake control system can control the speed switch valve, and make the output pressure into the brake cylinder working chamber to complete the control of the brake torque. Consequently controlling the brake cylinder pressure and the flexible brake of wind turbine is achieved, and it can reduce the impact load of the gearbox greatly, and improve their service lives.

The whole process of the gentle brake is achieved by the pulse width modulation through output of the flexible brake. That is to say that the brake on the output of the pulse width determines the size of the brake force it outputs.

Through the different switch time ratio, brake force can be controlled. For wind turbine control, combined with the specific requirement of different situations generator to determine the brake switch time ratio. Then it can achieve the flexible brake of the wind turbines.

In this closed-loop control system, PID control algorithm is adopted to achieve the brake control. Analog control expression of the PID control is:

$$\mu(t) = k_p[e(t) + \frac{1}{T_i}\int_0^i e(\tau)\,d\tau + T_d\frac{de(t)}{dt}] \qquad (1)$$

e(t)-system deviation, e(t)=r(t)-c(t);

k_p-scale factor;

T_i-integral time constant;

T_d-differential time constant;

Formula (1) can be written:

$$\mu(t) = k_p e(t) + k_i \int_0^i e(\tau) d\tau + k_d \frac{de(t)}{dt} \qquad （2）$$

k_p-the scale factor；

k_i-integral coefficient, $k_i = k_p/T_i$；

k_d-differential coefficient，$k_d = k_p/T_d$.

Computer control is a discrete sampling control. In the computer control system digital PID controller is used. Formula (1) and (2) are both the controlling expression of analog PID controller. By the expression of the analog PID integral and differential compute is approached constant valve to realize approximate numerical calculation, we can implement digital PID control. As long as the sampling period T obtains sufficiently small, and the approximation can be quite accurate.

Check points will be used instead of the differential term, integral term and the formula instead of rectangular, digital PID controller expression such as expression (3).

$$\mu(k) = k_p \left\{ e(k) + \frac{T}{T_i} \sum_{j=0}^{k} e(j) + \frac{T_d}{T} [e(k) - e(k-1)] \right\} \qquad （3）$$

So (3) can be written:

$$\mu(k) = k_p e(k) + k_i \sum_{j=0}^{k} e(j) + k_d [e(k) - e(k-1)] \qquad （4）$$

Among：$k_i = k_p T/T_i$，$k_d = k_p T_d/T$。

Digital PID controller control calculations can usually be divided into position PID and incremental PID algorithm. The system uses position PID algorithm. Therefore, the following will discuss how to create the mathematical model in position PID algorithm.

The formula (4) can obtain, the expression of the PID regulator at k-1：

$$\mu(k-1) = k_p e(k-1) + k_i \sum_{j=0}^{k-1} e(j) + k_d [e(k-1) - e(k-2)] \qquad （5）$$

$$\mu(k) = \mu(k-1) + a_0 e(k) + a_1 e(k-1) + a_2 e(k-2) \qquad （6）$$

You can get that the formula (4) minus formula (5) is position PID algorithm expression：

$$\mu(k) = \mu(k-1) + k_p [e(k) - e(k-1)] + k_i e(k) + k_d [e(k) - 2e(k-1) + e(k-2)]$$

In order to make easier the expression, you can expand the above formula. After the merger of similar items can be：

Among:

$a_0 = k_p + k_i + k_d = k_p[1 + T/T_i + T_d/T]$；

$a_1 = -k_p - 2k_d = -k_p[1 + 2T_d/T]$；

$a_2 = k_d = k_p T_d/T$。

In the system formula (6) is the mathematical model of the PID controller.

Determine the PWM signal frequency is 50Hz, and then the period is 20ms. Setting the duty ratio of the PWM signal driven by high-voltage is 5%. The duty cycle of the PWM signal driven by low-voltage input from 5% to 20%, such as 5%, 8%, 12%…… When the duty cycle rise to 20%, the pressure begins to rise. The duty cycle which is less than 20% of the high-speed switching valve call dead zone. In other words when the duty cycle is from 0 to 20%, the valve has been turned off. Then the duty cycle of the PWM signal driven by low voltage varies to input from 100% down further, such as 100%, 95%, 90%, 89%, 88%……， when the duty cycle drop to 82% the pressure curve has brought slightly large changes, Which the duty cycle can be obtained greater than 82% for high-speed switching valve saturation region. The duty cycle is that the input range of the PWM signal is completely open the valve port. Therefore, the experiments can be obtained through the above that operating frequency of 50Hz two-way high-speed switching valve effective duty operating ranges of 20% to 82%.

3.2 Temperature supervision of brake shoes

For wind turbines, the brake temperature of the brake shoes is an important parameter which is sent wind turbine application process. If you cannot detect rapid changes in temperature of the brake shoes, it will cause irreparable serious consequences. Therefore the design of the flexible brake should add to the temperature supervision function brake shoes [6].

Brake monitor will continue monitoring and recording the temperature of the brake shoes. This record means that the brake monitor will rely on predefining parameters and the actual temperature of the brake shoes to give "abrasion" or "warning" signal.

PT100 platinum resistance is used as a temperature sensor here for acquisition of the temperature. Temperature measurement range is from 10℃ to 260℃。The design of the PT100 test circuit forms AD7711 chip as the core, because AD7711 itself is not only able to provide a constant current source, but it also has a signal adjustment circuit, and AD conversion can be transformed, which simplifies the design of the entire circuit [7].

3.3 Supervision of brake time

Braking brake monitor records all times (In a continuous process one time of the brake includes brake lifting, application and lifting again). It means that the record which will depend on the monitor the brake pre-set parameters and the number of times the actual brake given a "wear and tear" or "warning" signal.

Brake monitor also give a signal for "Needs Maintenance". Generally the domestic break run 50,000 times. The digital I/O sensors are used here. As soon as the brake run each time, the sensor outputs a Digital I / O signals [8].

3.4 Supervision of brake shoes

Brake monitor can monitor the work condition of the brake shoe. When the brake shoes have been worn, it can give a warning signal [9]. It means that if the brake shoes which have been use to a certain wear, the brake monitor emits the "wear and tear" signal. There is also the use of digital I/O sensors which outputs a digital I/O signals.

Summary

The flexible brake is a good solution to the brake process of wind turbine, and also ensures the stability and safety of equipment operation. Meanwhile it realizes that the supervision function of the temperature, times and status of the brake shoes. Its prospect application is not limited prospects in wind generator, and gentle brake of other large electrical and mechanical equipment as well.

The design introduces a digital PID control strategy to research brake system control. However it does not introduce other control strategies such as adaptive control, optimal control, the brake pressure control system, and conduct research. To find the suitable brake pressure control system optimal control strategy, you can try other control strategies to make a comparative design.

References

[1]Ye Hangzhi. Control technology for wind turbine [M]. Machinery Industry Press, 2002

[2]Zhang Dahai, Li Wei. Based on the current energy accumulator hydraulic power system simulation regulator [J]. Power Systems. 2009(07)

[3]Lu Hongsui, Wang Zhiming. Turbine generator set of flexible electric brake excitation system development [J]. Hydropower plant automation. 1999(01)

[4]Sun Zhe. Flexible electrical braking in Hydropower Plant [J]. Hydropower plant automation. 2010(02)

[5]Paul D, et al. Brake Noise Resolution [M] Ercedes-BenzM-class. SAE 982245 1998.

[6]Malosh, James B. Disc Brake Noise Reduction Through Metall-urgical Control of RotorResonance. SAE 982236 .

[7]Dong Yingning, Dong Li, Dong Jun, et al. AD7710 Application in precision low resistance tester [J]. Information technology. 2000(04)

[8]Xu, John J. Disc Brake Low Frequency Creep Groan Simulation Using ADAMS. 2000

[9]Xiong Shichang. Based on computer vision tool wear condition monitoring techniques [D]. Zhejiang University 2003

Applied Mechanics and Materials Vol. 596 (2014) pp 552-559
© (2014) Trans Tech Publications, Switzerland
doi:10.4028/www.scientific.net/AMM.596.552

Fast Finite-Time Consensus Tracking of First-Order Multi-Agent Systems with a Virtual Leader

Qiuyun Xiao[1, a], Zhihai Wu[1,b *] and Li Peng[1,c]

[1]Key Laboratory for Advanced Process Control of Light Industry of the Ministry of Education, School of Internet of Things Engineering, Jiangnan University, Wuxi 214122, China

[a]xiaoqy1007@163.com, [b]wuzhihai@jiangnan.edu.cn, [c]pengli@jiangnan.edu.cn

Keywords: multi-agent systems, a virtual leader, fast finite-time consensus tracking, convergence speed.

Abstract. This paper proposes a novel finite-time consensus tracking protocol for guaranteeing first-order multi-agent systems with a virtual leader to achieve the fast finite-time consensus tracking. The Lyapunov function method, algebra graph theory, homogeneity with dilation and some other techniques are employed to prove that first-order multi-agent systems with a virtual leader applying the proposed protocol can reach the finite-time consensus tracking. Furthermore, theoretical analysis and numerical simulations show that compared with the traditional finite-time consensus tracking protocols, the proposed protocol can accelerate the convergence speed of achieving the finite-time consensus tracking.

Introduction

Distributed coordinated control of multi-agent systems has attracted considerable attention during the past decade due to its broad applications in many fields, such as physics, biology, computer science and control engineering. As a fundamental issue in distributed coordinated control of multi-agent systems, consensus is to design a distributed interaction rule among agents called a consensus protocol such that the concerned states of all agents eventually reach an agreement. For most of the existing consensus protocols, the final common value to be achieved is a function of initial states of all agents and is inherently a prior unknown constant. This is the so-called χ-consensus[1], one of important forms of which is the average consensus[2-5]. In Ref. [2], Olfati-Saber and Murray considered the average consensus problems of networks of first-order integrator agents with fixed and switching topologies, proving that if the network is an instantaneous balanced and strongly connected digraph, then the average consensus can be achieved. More results can be seen in the survey papers[6-8] and the references therein.

However, in many practical applications, it is required that all agents communicating with their neighbors eventually converge to a desired reference state. This is the so-called leader-follower consensus or consensus tracking. In leader-follower multi-agent systems, the leaders are usually independent of the followers, but they have influences on the followers. Hence, only controlling the leaders can easily achieve the control objective of multi-agent systems. This not only simplifies the design and implementation of the control laws but also saves the control energy and costs[9, 10]. Up to now, a lot of attention has been paid to the consensus tracking problems of leader-follower multi-agent systems[11-18]. Jadbabaie et al. considered the nearest neighborhood principle and proved that if all agents are jointly connected with their leader, then their states will converge to the state of the leader as time goes on[11]. Ren proved that proportional-like continuous-time consensus tracking protocols cannot guarantee all agents to track a virtual leader with a time-varying reference state available to only a subset of agents, whereas proportional and derivative-like ones can do[12]. Due to the difficulty of implementing the proportional and derivative like continuous-time consensus protocols, Cao et al. investigated the sampling case of Ref. [12], demonstrating that the ultimate bound of the tracking errors is proportional to the sampling period[13]. In Refs. [14-16], Wu et al. considered the stochastic bounded consensus tracking problems of leader-follower multi-agent systems with measurement noises based on sampled-data with zero, small and general sampling delay, respectively, and obtained the necessary and sufficient conditions guaranteeing the stochastic bounded consensus tracking.

However, most of the above references[11-18] are mainly about finding convergence conditions of achieving the consensus tracking rather than improving the convergence performance, one of which is the convergence speed. However, the convergence speed is really an important performance index, which affects the real-time performance of multi-agent systems. In recent years, significant efforts have been made to enhance the convergence speed of multi-agent systems[19-24]. Zhou and Wang proposed the asymptotic and per-step convergence factors as measures of the convergence speed, and derived the exact value for the per-step convergence factor[19]. Wu and Fang proposed the consensus protocol with delayed-state-derivative feedback, demonstrating that choosing the proper intensity of delayed-state-derivative feedback can accelerate the convergence speed[20]. In order to expand the allowable scope of the intensity of delayed-state-derivative feedback, Fang et al. proposed the consensus protocol with weighted average prediction, and proved that choosing the proper length of weighted average prediction can enhance the convergence speed[21].

Although using the methods in Refs. [19-24] can accelerate the convergence speed of achieving the consensus, the achievement of consensus is asymptotic, which means that the convergence speed is at best exponential with an infinite setting time. In other words, consensus can never be reached in finite time. However, in many situations, it is often required that consensus is reached in finite time, such as the case that the control accuracy is crucial. Besides the faster convergence speed, other advantages of finite-time consensus include better disturbance rejection and robustness against uncertainties[25]. Therefore, it is necessary to investigate the finite-time consensus of multi-agent systems. Now, there are many results about finite-time consensus or consensus tracking[26-30]. In Ref. [26], Cortes considered the finite-time consensus based on the discontinuous protocol. In Ref. [27] Xiao et al. provided two continuous consensus protocols to solve the finite-time consensus problems of first-order multi-agent systems. Sun and Guan investigated the finite-time consensus problems of leader-follower second-order multi-agent systems under fixed and switching networks[28]. In Ref. [29], Zhu et al. investigated the finite-time consensus problems for heterogeneous multi-agent systems, where the virtual leader can be a first-order or a second-order integrator agent.

Compared with the existing asymptotic-convergence consensus protocols, the protocols in Refs.[26-30] can guarantee the finite-time consensus. However, in some practical applications such as braking systems of multiple autonomous vehicles, the faster finite-time consensus, i.e., the consensus with a shorter setting time, is needed. Therefore, it is significant to study how to accelerate the convergence speed of finite-time consensus. To this end, in this paper we propose a novel finite-time consensus tracking protocol to solve the fast finite-time consensus tracking problems of first-order multi-agent systems with a virtual leader.

An outline of the paper is as follows. First, some preliminaries are provided and the problem is stated. Then convergence analysis of the fast finite-time consensus tracking protocol is given. Next, numerical simulations are provided to illustrate the effectiveness of the theoretical results. Last, conclusions are drawn.

Preliminaries and Problem Statement

Algebra Graph Theory. Let $G=(V,E,A)$ be a weighted undirected graph with a set of nodes $V=\{v_1,v_2,...,v_n\}$, a set of edges $E\subseteq V\times V$, and the weighted adjacency matrix $A=[a_{ij}]$ with nonnegative adjacency elements a_{ij}. The node indexes of G belong to a finite index set $I=\{1,2,...,n\}$. An edge of G is denoted by $e_{ij}=(v_i,v_j)$. The adjacency elements associated with the edges are positive, i.e., $e_{ij}\in E\Leftrightarrow a_{ij}>0$. Moreover, we assume $a_{ii}=0$ for all $i\in I$. For the undirected graph G, the adjacency matrix A is symmetric, i.e., $a_{ij}=a_{ji}$. The set of neighbors of node v_i is denoted by $N_i = \{v_j \in V : e_{ij} \in E\}$. The degree of node v_i is defined as $d_i = \sum_{j \in N_i} a_{ij}$. The Laplacian matrix of G is defined as $L = D - A$, where $D = Diag\{d_1, d_2, ..., d_n\}$ is the degree matrix of G with diagonal elements d_i and zero off-diagonal elements. An important fact of L is that all row sums are zero and thus L has a right eigenvector 1_n associated with the zero eigenvalue, where 1_n denotes the n-dimensional column vector with all elements being equal to 1. A path between two distinct nodes v_i and v_j means a sequence of distinct edges of the form $(v_i, v_{k_1}), (v_{k_1}, v_{k_2}), ..., (v_{k_l}, v_j)$. A graph is called connected if there is a path between any two distinct nodes of the graph. For the leader-follower consensus problem, we consider the graph G associated with the system consisting of n agents (which are called followers) and one virtual leader denoted by agent 0. Let a_{i0} be the adjacency weight between agent i and the virtual leader. Without loss of generality, assume that $a_{i0} = 1$, if the virtual leader is a neighbor of agent i, and otherwise $a_{i0} = 0$.

Problem Statement. In a multi-agent system with n agents, an agent and an available information flow between two agents are considered as a node and an edge in an undirected graph, respectively. Consider the system of dynamic agents described by

$$\dot{x}_i(t) = v_i(t), \quad i \in I, \tag{1}$$

where $x_i(t) \in R$ is the position state of agent i, and $u_i(t) \in R$ is the control input. In this paper, it is assumed that the virtual leader is invariant, i.e., the dynamics of the virtual leader is $\dot{x}_0(t) = 0$.

In Ref. [28], Sun and Guan proposed the following finite-time consensus tracking protocol

$$u_i(t) = \sum_{j \in N_i} a_{ij} sig(x_j - x_i)^{\alpha} + a_{i0} sig(x_0 - x_i)^{\alpha}, \tag{2}$$

where $0 < \alpha < 1$. In order to accelerate the convergence speed of achieving the finite-time consensus tracking, in this paper by revising the protocol (2) we propose the following finite-time consensus tracking protocol

$$u_i(t) = \sum_{j \in N_i} a_{ij} sig(x_j - x_i)^{\alpha} + a_{i0} sig(x_0 - x_i)^{\alpha} + \gamma \sum_{j \in N_i} a_{ij}(x_j - x_i) + \gamma a_{i0}(x_0 - x_i), \tag{3}$$

where $\gamma > 0$.

Definition 1 Finite-time consensus tracking is said to be achieved, if there is a setting time $T_0 \in [0, +\infty)$ such that for any initial states, the solution of system (1) satisfies $\lim_{t \to T_0} \|x_i(t) - x_0(t)\| = 0$ and $x_i(t) = x_0(t), \ \forall t \geq T_0, \ i \in I$.

In the following sections, we will prove that the protocol (3) not only guarantees the achievement of the finite-time consensus tracking but also has the faster convergence speed than the protocol (2).

Convergence Analysis

First, using the Lyapunov function method, algebra graph theory, homogeneity with dilation and some other techniques, we prove that multi-agent system (1) applying the protocol (3) can reach the finite-time consensus tracking. Before moving on, we need the following assumption and lemmas.

Assumption 1 The communication network topology G composed of n agents is fixed, undirected and connected, and at least one agent has access to the virtual leader.

Lemma 1([29]) Suppose the function $\varphi : R^2 \to R$ satisfies $\varphi(x_i, x_j) = -\varphi(x_j, x_i), \ \forall i, j \in I, \ i \neq j$. Then for any undirected graph G and a set of numbers $y_1, y_2, \dots, y_n$,

$$\sum_{i=1}^{N} \sum_{j \in N_i} a_{ij} y_i \varphi(x_j, x_i) = -\frac{1}{2} \sum_{(v_i, v_j) \in E} a_{ij}(y_j - y_i)\varphi(x_j, x_i).$$

Lemma 2([3]) If $y_1, y_2, ..., y_n \geq 0$ and $0 < p \leq 1$, then $\sum_{i=1}^{n} y_i^p \geq (\sum_{i=1}^{n} y_i)^p$.

Lemma 3([2, 30]) $L(A)=[l_{ij}]\in R^{n\times n}$ denotes the Laplacian matrix of the graph $G(A)$. Then there are the following properties:

(P1). $x^T L(A)x=\frac{1}{2}\sum_{i,j=1}^{n} a_{ij}(x_j-x_i)^2$, and the semi-positive definiteness of $L(A)$ implies that all eigenvalues of $L(A)$ are real and not less than zero.

(P2). If $G(A)$ is connected, the second smallest eigenvalue of $L(A)$, which is denoted by $\lambda_2(L_A)$ and called the algebraic connectivity of $G(A)$, is larger than zero.

(P3). The algebraic connectivity of $G(A)$ is equal to $\min_{x\neq 0_n, 1_n^T x=0}\frac{x^T L(A)x}{x^T x}$. Thus, if $1_n^T x=0$, then $x^T L(A)x\geq \lambda_2(L_A)x^T x$.

(P4). If $G(A)$ is undirected and connected, then $L(A)+Diag(b_1,...,b_n)$ is positive definite, where $b_i\geq 0,\ \forall i\in I$ and there is at least one $b_i>0$.

Lemma 4([25]) Consider the non-Lipschitz continuous nonlinear system $\dot{x}=f(x)$ with $f(0)=0$. Suppose there are a differential function $V(x)$ defined on a neighborhood of the origin, $c>0$ and $\alpha\in(0,\ 1)$ such that $V(x)$ is positive definite and $\dot{V}(x)+cV^{\alpha}\leq 0$. Then, the origin is locally finite-time stable, and the settling time T depends on the initial state $x(0)$ and satisfies $T(x(0))\leq\frac{V(0)^{1-\alpha}}{c(1-\alpha)}$.

Now, we provide the main results.

Theorem 1 Under Assumption 1, the multi-agent system (1), applying the consensus tracking protocol (3), achieves the finite-time consensus tracking.

Proof Define the tacking error

$$\bar{x}_i(t)=x_i(t)-x_0(t),\ \ \forall i\in I. \tag{4}$$

According to Eqs. (1), (3) and (4), we have

$$\begin{aligned}\dot{\bar{x}}_i(t)&=\sum_{j\in N_i}a_{ij}sig(\bar{x}_j-\bar{x}_i)^{\alpha}-a_{i0}sig(\bar{x}_i)^{\alpha}+\gamma\sum_{j\in N_i}a_{ij}(\bar{x}_j-\bar{x}_i)-\gamma a_{i0}\bar{x}_i\\&=\sum_{j=0}^{n}a_{ij}sig(\bar{x}_j-\bar{x}_i)^{\alpha}+\gamma\sum_{j=0}^{n}a_{ij}(\bar{x}_j-\bar{x}_i).\end{aligned}\tag{5}$$

Choose the Lyapunov function $V(t)=\sum_{i=0}^{n}\bar{x}_i^2$. Then it follows from Lemma 1 that along the trajectory of the system (5),

$$\begin{aligned}\dot{V}(t)&=2\sum_{i=0}^{n}\bar{x}_i\dot{\bar{x}}_i\\&=2\sum_{i=0}^{n}\bar{x}_i[\sum_{j=0}^{n}a_{ij}sig(\bar{x}_j-\bar{x}_i)^{\alpha}+\gamma\sum_{j=0}^{n}a_{ij}(\bar{x}_j-\bar{x}_i)]\\&=2\sum_{i=0}^{n}\bar{x}_i\sum_{j=0}^{n}a_{ij}sig(\bar{x}_j-\bar{x}_i)^{\alpha}+2\gamma\sum_{i=0}^{n}\bar{x}_i\sum_{j=0}^{n}a_{ij}(\bar{x}_j-\bar{x}_i)\\&=-\sum_{i=0}^{n}\sum_{j=0}^{n}a_{ij}sig(\bar{x}_j-\bar{x}_i)^{\alpha}(\bar{x}_j-\bar{x}_i)-2\gamma\sum_{i=0}^{n}\sum_{j=0}^{n}a_{ij}(\bar{x}_j-\bar{x}_i)^2\\&=-\sum_{i=0}^{n}\sum_{j=0}^{n}a_{ij}(\bar{x}_j-\bar{x}_i)^{1+\alpha}-2\gamma\sum_{i=0}^{n}\sum_{j=0}^{n}a_{ij}(\bar{x}_j-\bar{x}_i)^2\end{aligned}$$

$$\begin{aligned} &< -\sum_{i=0}^{n}\sum_{j=0}^{n} a_{ij}(\bar{x}_j - \bar{x}_i)^{1+\alpha} \\ &= -\sum_{i=0}^{n}\sum_{j=0}^{n} [a_{ij}^{\frac{2}{1+\alpha}}(\bar{x}_j - \bar{x}_i)]^{\frac{1+\alpha}{2}}. \end{aligned} \tag{6}$$

From Lemma 2, we can get

$$\dot{V}(t) \le -[\sum_{i=0}^{n}(\sum_{j=0}^{n} a_{ij}^{\frac{2}{1+\alpha}}(\bar{x}_j - \bar{x}_i))^2]^{\frac{1+\alpha}{2}}. \tag{7}$$

Let $B = L(A) + Diag(a_{10},\ldots,a_{n0})$. From Lemma 3, we have

$$\frac{\sum_{i=0}^{n}[\sum_{j=0}^{n} a_{ij}^{\frac{2}{1+\alpha}}(\bar{x}_j - \bar{x}_i)]^2}{V(t)} = \frac{2\bar{x}_i^T B^T B \bar{x}_i}{\bar{x}_i^T B \bar{x}_i} \ge 2\lambda_2(L_B) \cdot \tag{8}$$

Combining Eqs. (7) and (8) yields $\dot{V}(t) \le -[2\lambda_2(L_B)]^{\frac{1+\alpha}{2}} V(t)^{\frac{1+\alpha}{2}}$.

According to Lemma 4, we obtain $T(x(0)) \le \dfrac{2V(0)^{\frac{1-\alpha}{2}}}{(1+\alpha)[2\lambda_2(L_B)]^{\frac{1+\alpha}{2}}}$. The proof is completed.

Now we are in a position to prove that the convergence speed of the system (1) under the protocol (3) is faster than that under the protocol (2). The main results are given in the remark below.

Remark 1 To show that the proposed protocol (3) converges faster than the protocol (2), we choose the same Lyapunov function $V(t) = \sum_{i=0}^{n} \bar{x}_i^2$ for the system (1) with the protocol (2). Along the trajectory of system (1) with the protocol (2), we can obtain

$$\begin{aligned} \dot{V}(t)\big|_{(2)} &= 2\sum_{i=0}^{n} \bar{x}_i \dot{\bar{x}}_i \\ &= 2\sum_{i=0}^{n} \bar{x}_i [\sum_{j=0}^{n} a_{ij} sig(\bar{x}_j - \bar{x}_i)^{\alpha}] \\ &= 2\sum_{i=0}^{n} \bar{x}_i \sum_{j=0}^{n} a_{ij} sig(\bar{x}_j - \bar{x}_i)^{\alpha} \\ &= -\sum_{i=0}^{n}\sum_{j=0}^{n} a_{ij} sig(\bar{x}_j - \bar{x}_i)^{\alpha}(\bar{x}_j - \bar{x}_i) \\ &= -\sum_{i=0}^{n}\sum_{j=0}^{n} a_{ij}(\bar{x}_j - \bar{x}_i)^{1+\alpha}. \end{aligned}$$

Meanwhile, it follows from Eq. (6) that along the trajectory of system (1) with the protocol (3), $\dot{V}(t)\big|_{(3)} = -\sum_{i=0}^{n}\sum_{j=0}^{n} a_{ij}(\bar{x}_j - \bar{x}_i)^{1+\alpha} - 2\gamma\sum_{i=0}^{n}\sum_{j=0}^{n} a_{ij}(\bar{x}_j - \bar{x}_i)^2$. Obviously, $\dot{V}(t)\big|_{(3)} \le \dot{V}(t)\big|_{(2)}$. Therefore, the system (1) under the protocol (3) has a faster convergence speed than the system (1) under the protocol (2). It is obvious that if $\gamma = 0$, the protocol (3) degenerates into the protocol (2). With the positive parameter γ, the convergence speed of the system (1) under the protocol (3) is faster than that under the protocol (2).

Simulations

In this section, numerical simulations are provided to illustrate the effectiveness of the above theoretical results. Consider a multi-agent system composed of three agents and one virtual leader labeled as agent 0 with the network topology shown in Fig. 1.

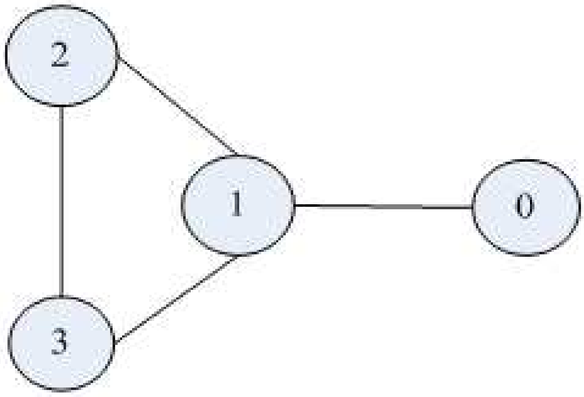

Fig. 1. Network topology composed of three agents and one virtual leader.

Without loss of generality, all weights of edges are assumed to be 1 if $e_{ij} \in E$, $x(0) = (1,\ 5,\ 10)^T$, $\alpha_1 = 0.8$, and $x_0 = 2$. The numerical results are shown in Figs. 2 and 3, respectively.

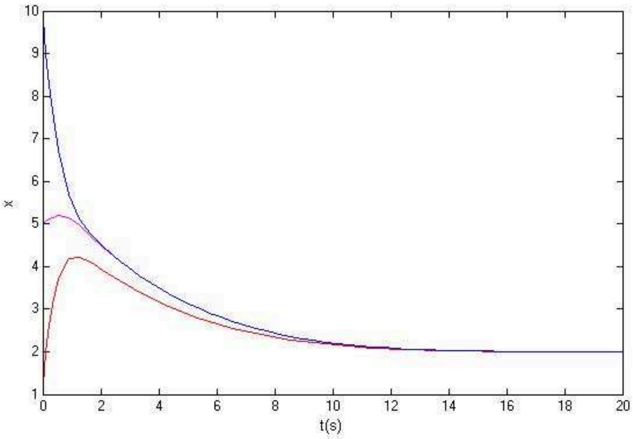

Fig. 2. States of the system (1) using the protocol (2).

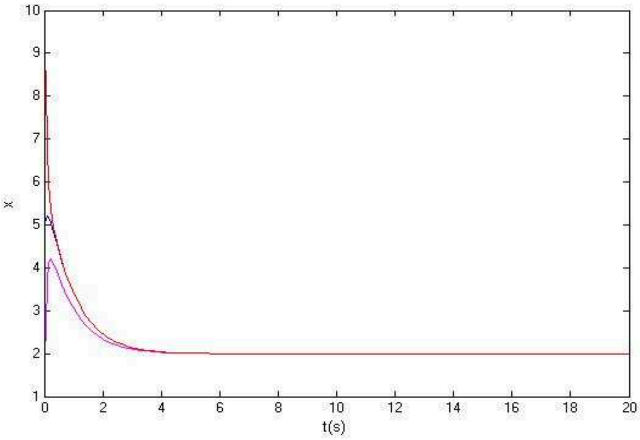

Fig. 3. States of the system (1) using the protocol (3) with $\gamma = 3$.

It can be seen from Fig. 2 that the system (1), applying the consensus tracking protocol (2), achieves the finite-time consensus tracking with $T(x(0)) \approx 16s$. From Fig. 3, we find that the system (1), applying the consensus tracking protocol (3) with $\gamma = 3$, achieves the finite-time consensus tracking with $T(x(0)) \approx 6s$. This numerically shows that the proposed finite-time consensus tracking protocol (3) has the faster convergence speed than the finite-time consensus tracking protocol (2).

Conclusions

In this paper, we have investigated the fast finite-time consensus tracking problems of first-order multi-agent systems with a virtual leader. Applying the Lyapunov function method, algebra graph theory, homogeneity with dilation and some other techniques, we have proved that first-order multi-agent systems with a virtual leader applying the proposed protocol can reach the finite-time consensus tracking. Last, theoretical analysis and numerical simulations showed that compared with the traditional finite-time consensus tracking protocols, the proposed protocol can accelerate the convergence speed of achieving the finite-time consensus tracking. One of future research directions is to consider the case with time-delay.

Acknowledgements

This work was financially supported by the National Natural Science Foundation of China (61203147, 61203126) and the Humanities and Social Sciences Youth Funds of the Ministry of Education, China (12YJCZH218).

References

[1] J. Cortés: Automatica Vol. 44 (2008), p.726.

[2] R. Olfati-Saber and R.M. Murray: IEEE Trans. Autom. Control Vol. 49 (2004), p. 1520.

[3] W. Ren and R.W. Beard: IEEE Trans. Autom. Control Vol. 50 (2005), p. 655.

[4] Y.P. Tian and C.L. Liu: IEEE Trans. Autom. Control Vol. 53 (2008), p. 2122.

[5] Y.G. Sun, L. Wang and G.M. Xie: Syst. Control Lett. Vol. 57 (2008), p. 175.

[6] W. Ren, R.W. Beard and E.M. Atkins: IEEE Control Syst. Mag. Vol. 27 (2007), p. 71.

[7] R.Olfati-Saber, J.A. Fax and R.M. Murray: Proc. IEEE Vol. 95 (2007), p. 215.

[8] R. M. Murray: J. Dyn. Syst. Meas. Control Vol. 129 (2007), p. 571.

[9] C.Q. Ma, T. Li and J.F. Zhang, in: Proc. 17th IFAC World Congress (2008), p. 1528.

[10] W. Ren, R.W. Beard and T.W. Mclain: Lecture Notes in Contr. Infor. Sci. Vol. 309 (2004), p.171.

[11] A. Jadbabaie, J. Lin and S.A. Morse: IEEE Trans. Autom. Control Vol. 48 (2003), p. 988.

[12] W. Ren: Syst. Control Lett. Vol. 56 (2007), p. 474.

[13] Y.C. Cao, W. Ren and Y. Li: Automatica Vol. 45 (2009), p. 1299.

[14] Z.H. Wu, L. Peng, L.B. Xie and J.W. Wen: Chin. Phys. B Vol. 21 (2012), p. 128902.1.

[15] Z.H. Wu, L. Peng, L.B. Xie and J.W. Wen: Physica A Vol. 392 (2013), p. 918.

[16] Z.H. Wu, L. Peng, L.B. Xie and J.W. Wen: Chin. Phys. B Vol. 22 (2013), p. 128901.1.

[17] J.P. Hu and G. Feng: Automatica Vol. 46 (2010), p. 1382.

[18] F. Chen, Y.C. Cao and W. Ren: IEEE Trans. Autom. Control Vol. 57 (2012), p. 3169.

[19] J. Zhou and Q. Wang: Automatica Vol. 45 (2009), p. 1455.

[20] Z.H. Wu and H.J. Fang: J. Syst. Eng. Electron. Vol. 23 (2012), p. 137.

[21] H.J. Fang, Z.H. Wu and J. Wei: IEEE Trans. Autom. Control Vol. 57 (2012), p. 249.

[22] Y. Kim and M. Mesbahi: IEEE Trans. Autom. Control Vol. 51 (2006), p. 655.

[23] Y.C. Cao and W. Ren: J. Intell. Robot. Syst. Vol. 58 (2009), p. 95.

[24] Y. Kim, D.W. Gu and I. Postlethwaite: Automatica Vol. 45 (2009), p. 1379.

[25] S.P. Bhat and D.S. Bernstein: SIAM J. Control Optim. Vol. 38 (2000), p. 751.

[26] J. Cortés: Automatica Vol. 42 (2006), p. 1993.

[27] F. Xiao, L. Wang and J. Chen, in: Proc. 48th IEEE Conf. Decision Control (2009), p. 4741.

[28] F.L. Sun and Z.H. Guan: Inter. J. Syst. Sci. Vol. 44 (2013), p.727.

[29] Y.K. Zhu, X.P. Guan and X.Y. Luo: Chin. Phys. B Vol. 22 (2013), p.038901.1.

[30] Y.L. Shang: Inter. J. Syst. Sci. Vol. 43 (2012), p. 499.

Applied Mechanics and Materials Vol. 596 (2014) pp 560-564
© (2014) Trans Tech Publications, Switzerland
doi:10.4028/www.scientific.net/AMM.596.560

Global robust output regulation of a class of nonlinear systems with nonlinear exosystems and its application

Suming Liu[1, a], Yuan Jiang[1,b] and Jiyang Dai[1,c]

[1]Nanchang Hangkong University, 696 South Fenghe Avenue, Nanchang, Jiangxi, China

[a] liusumin17@163.com, [b] jiangyuan@nchu.edu.cn, [c] djiyang@163.com

Keywords: Chua's Circuit, Nonlinear Exosystem, Output Regulation, Closed-Loop System

Abstract. An adaptive robust output regulation design is proposed for the output feedback systems with a nonlinear exosystem. A new nonlinear internal model is first designed for the control input. The output feedback control design is further achieved based on a type of state filter which is designed for the transformed augmented system. The adaptive control technique is successfully incorporated in the stabilization design to ensure the global stability of the proposed control design for output regulation. The result is successfully applied to solve a tracking control problem associated with the well known Chua's circuit.

Introduction

Recently, the study of Chua's circuit has received considerable attention. This circuit was originally conceived by Chua in 1983 for gengerating chaotic response in a nonlinear[1],[2]. The stabilization problem for the Chua's circuit with some other systems has been studied for years, and various results have been achieved under various assumptions, so Chua' circuit has become a well-known test-bed for studying various control problems, such as [3],[4],[5].

In this paper, we aim to reject a nonharmonic disturbances in a class of nonlinear systems via the internal model approach. In order to tackle the nonlinearity in the exosystem, we exploit a new nonlinear internal model that can be used to estimate the disturbance. This is the crucial step for solving the disturbance rejection problem. In fact, this internal model design has been exploited recently for nonlinear control design [6]. Of course, there are differences in designing the internal model for output regulation and it also will be more challenging. Therefore, in what follow, we will first describe the robust output regulation problem and present the solution to this problem in Section 2. Section 3 introduces some transformation to clarify the systems considered. Section 4 concernes with the nonlinear internal model design. The control design is shown in Section 5. Section 6 demonstrates the design procedure of the proposed method. Finally, the conclusion is drawn in the section 7.

Problem formulation and preliminaries

In this section, we will formulation the control problem and present some preliminaries. Consider the following uncertain systems which can be transformed into the output feedback form:

$$\begin{aligned} \dot{x} &= \bar{F}(w)x + \bar{G}(y,v,w)y + g(w)u + \bar{D}_1(v,w) \\ \dot{y} &= \bar{H}(w)x + \bar{K}(y,v,w)y + \bar{D}_2(v,w) \\ e &= y - q(v,w) \end{aligned} \tag{1}$$

Where $(x,y) \in R^n, y \in R$,and $u \in R$ are the system states, output and input, respectively, the error signal $e \in R$ is the only measurable variable that can be used in feedback design. The unknown constant w belongs to a compact set $ƛ \in R^q$ whose bound is unknown. It assumed that all the functions in the system(1) are sufficiently smooth and $\bar{G}(0,v,w) = 0$, $\bar{K}(0,v,w) = 0$, $\bar{D}_1(0,w) = 0$, $\bar{D}_2(0,w) = 0$ and $q(0,w) = 0$ for all $w \in ƛ$. The exogenous signal $v \in R^m$ represents either the disturbance signal or the reference input or both, which generated from a nonlinear exosystem

$$\dot{v} = s(v) \tag{2}$$

To introduce our problem, let us first make some assumptions in the following.

Assumption 1. There exists a subset $\lambdabar$ of R^q such that system (1) has a uniform relative degree r for all $w \in \lambdabar$, i.e., for all $w \in \lambdabar$,

$$\bar{H}(w)g(w) = \bar{H}(w)\bar{F}(w)g(w) = \cdots = \bar{H}(w)\bar{F}(w)^{r-3}g(w) = 0 \text{ and } \bar{H}(w)\bar{F}(w)^{r-2}g(w) \neq 0$$

Assumption 2. The flows of vector field $s(v)$ are bounded and converge to periodic solutions.

The adaptive output regulation problem that we are going to solve is to find a finite dimensional system $\begin{array}{l}\dot{\mu} = v(\mu, e(t)), \mu \in R^s \\ u = u(\mu, e(t)), \mu \in R^s\end{array}$ Such that for every $x(0) \in R^n, v(0) \in \Omega \subset R^m, x(t), \mu(t)$ and $u(t)$ are bounded $\forall t \geq 0$,and $\lim_{t\to\infty} e(t) = 0.$

Assumption 3. There exists a positive integer r and an odd locally Lipschitz function $\gamma : \Omega \to R$ such that

$$\frac{d^r d(t)}{dt^r} - \gamma(d, \dot{d}, \cdots, d^{(r-1)}) = 0 \tag{3}$$

Where $\Omega \in R^r$ is a compact subset. In addition, there exists a positive number l , such that $\left|\gamma(\rho_1) - \gamma(\rho_2)\right| \leq l\left\|\rho_1 - \rho_2\right\|$,where $\rho_1, \rho_2 \in R^r$.

State transformation

Since system (1) has a uniform relative degree r for all $w \in \lambdabar$. A state transform, based on the filtered transform in [7] with extraction of system's zero dynamics, will put the system in the following form

$$\begin{aligned} \dot{z} &= F(w)z + G(y, v, w)y + D_1(v, w) \\ \dot{y} &= H(w)z + K(y, v, w)y + b(w)\xi_1 + D_2(v, w) \end{aligned} \tag{4}$$

ξ_1 is the output of an input filter, with $\lambda_i > 0$,

$$\dot{\xi}_i = -\lambda_1\xi_i + \xi_{i+1} \quad , \quad \dot{\xi}_{r-1} = -\lambda_{r-1}\xi_{r-1} + u \quad \text{for } i = 1, \cdots, r-2 ,$$

Assumption 4. There exists a sufficiently smooth function $z(v, w)$ with $z(0,0) = 0$, such that, for all $v \in R^m, w \in \lambdabar$

$$\frac{\partial z(v, w)}{\partial v}s(v) = F(w)z(v, w) + G(q(v, w), v, w)q(v, w) + D_1(v, w) \tag{5}$$

Thus, the solution of the regulator equations associated with equations (4) and (2) is given by $(z(v, w), q(v, w))$ and $\tau(v, w)$, where

$$\tau(v, w) = b^{-1}(w)(\frac{\partial q(v, w)}{\partial v}s(v) - H(w)z(v, w) - K(q(v, w), v, w)q(v, w) - D_2(v, w)) \tag{6}$$

We now introduce the last transform based on the invariant manifold with $\begin{array}{l}\tilde{z} = z - z(v, w) \\ e = y - q(v, w)\end{array}$. Finally we have the model for the control design

$$\begin{aligned} \dot{\tilde{z}} &= F(w)\tilde{z} + \tilde{G}(e, v, w)e \\ \dot{e} &= H(w)\tilde{z} + \tilde{K}(e, v, w)e + b(w)(\xi_1 - \tau(v, w)) \end{aligned} \tag{7}$$

Let $V_{\tilde{z}} = \tilde{z}^T P(w)\tilde{z}$, where $P(w)F(w) + F^T(w)P(w) = -I$, Then using $2bc \leq db^2 + d^{-1}c^2$

There exists an unknown constants θ_1 such that

$$\dot{V}_{\tilde{z}} = -\left\|\tilde{z}\right\|^2 + 2\tilde{z}^T P(w)\tilde{G}(e, v, w) \leq -\frac{3}{4}\left\|\tilde{z}\right\|^2 + \theta_1\alpha_1(e)e^2 \tag{8}$$

Internal model design

The rejection algorithm proposed in this paper adopts an indirect approach. Firstly, we let

$$\theta = col(d, \dot{d}, \cdots, d^{(r-1)}) \tag{9}$$

Then, there exist an immersion of the exosystem

$$\theta = A\theta + B\gamma(\theta) \quad , \tau = \psi\theta \tag{10}$$

Where $\theta \in R^r$, $F = \begin{bmatrix} 0 & 1 & 0 & \cdots & 0 \\ \vdots & \vdots & \vdots & \ddots & \vdots \\ 0 & 0 & 0 & \cdots & 1 \\ 0 & 0 & 0 & \cdots & 0 \end{bmatrix}$, $B = \begin{bmatrix} 0 \\ 0 \\ \vdots \\ 0 \\ 1 \end{bmatrix}$, $\psi^T = \begin{bmatrix} 1 \\ 0 \\ \vdots \\ 0 \\ 0 \end{bmatrix}$.

We select any controllable pair (M, N) with $M \in R^{r\times r}, N \in R^r$ where M is Hurwitzian and has disjoint spectra with A , Because the pair (ψ, A) is observable, there exists a unique and nonsingular matrix T satisfying the Sylvester equation

$$TA - MT = N\psi \tag{11}$$

Letting $\vartheta = T\theta$, we have

$$\dot{\vartheta} = TAT^{-1}\vartheta + TB\gamma(T^{-1}\vartheta) \quad , \quad \tau = \psi T^{-1}\vartheta \tag{12}$$

We design the internal model as

$$\dot{\eta} = M(\eta - b^{-1}(w)Ne) + TB\gamma(T^{-1}(\eta - b^{-1}(w)Ne)) + N\xi_1 \tag{13}$$

There exist a positive matrix P and Q satisfying $PM + M^T P = -Q$.

We consider the mismatch between the states of (12) and (13), and define an auxiliary error as $\tilde{\eta} = \vartheta - \eta + b^{-1}(w)Ne$.

It can be shown that

$$\dot{\tilde{\eta}} = M\tilde{\eta} + TB\gamma(T^{-1}\vartheta) - TB\gamma(T^{-1}(\eta - b(w)^{-1}Ne)) + Nb(w)^{-1}H(w)\tilde{z} + Nb(w)^{-1}\tilde{K}(e, v, w)e \tag{14}$$

Let $V_{\tilde{\eta}} = \tilde{\eta}^T P\tilde{\eta}$, there exist unknown positive real constants θ_2 and θ_3 such that

$$\begin{aligned} \dot{V}_{\tilde{\eta}} &= -\tilde{\eta}^T Q\tilde{\eta} + 2\tilde{\eta}^T PTB(\gamma(T^{-1}\vartheta) - \gamma(T^{-1}(\eta - b^{-1}(w)Ne))) + 2\tilde{\eta}^T Pb^{-1}(w)N(H(w)\tilde{z} + \tilde{k}(e, v, w)) \\ &\le (l_0 - \frac{1}{2}\lambda_{\min}(Q))\|\tilde{\eta}\|^2 + \theta_3\|\tilde{z}\|^2 + \theta_2\alpha_2(e)e^2 \end{aligned} \tag{15}$$

Control design

From (12) we have $\tau = t_1\vartheta_1 + t_2\vartheta_2 = t_1(\tilde{\eta}_1 + \eta_1 - b^{-1}(w)N_2 e) + t_2(\tilde{\eta}_2 + \eta_2 - b^{-1}(w)N_2 e)$ and $t_1, t_2 \in R$. Than from (7) we have $\dot{e} = H(w)\tilde{z} + \tilde{K}(e, v, w)e + \overline{\xi}_1 + b(w)(\tilde{\xi}_1 - t_1(\tilde{\eta}_1 + \eta_1) - t_2(\tilde{\eta}_2 + \eta_2) + (t_1 N_1 + t_2 N_2)b^{-1}(w)e)$, where $\tilde{\xi}_1 = \xi_1 - \hat{\xi}_1$ and $\hat{\xi}_1 = b^{-1}(w)\overline{\xi}_1$. For the virtual control $\hat{\xi}_1$, we design $\overline{\xi}_1$ as, with $c_0 > 0$ $\overline{\xi}_1 = -c_0 e + b(w)(t_1\eta_1 + t_2\eta_2) - (t_1 N_1 + t_2 N_2)e - k\rho(e)e$. Where k is an adaptive coefficient. Then we have the resultant error dynamics $\dot{e} = H(w)\tilde{z} + \tilde{K}(e, v, w)e + b(w)(\tilde{\xi}_1 - t_1\tilde{\eta}_1 - t_2\tilde{\eta}_2) - c_0 e - k\rho(e)e$. Then for $V_e = \frac{1}{2}e^2$ there exist a sufficiently large unknown positive constant r_0 such that

$$\begin{aligned} \dot{V}_e &= -c_0 e^2 + H(w)e\tilde{z}_1 + \tilde{K}(e, v, w)e^2 + eb(w)(\tilde{\xi}_1 - t_1\tilde{\eta}_1 - t_2\tilde{\eta}_2) - k\rho(e)e^2 \\ &\le \frac{1}{4}\|\tilde{z}\|^2 + \|H(w)\|^2 e^2 + 2e^2 + \theta_4\alpha_2(e)e^2 + b(w)e\tilde{\xi}_1 + \frac{1}{4}r_0\|\tilde{\eta}\|^2 - c_0 e^2 - k\rho(e)e^2 \end{aligned} .$$

Let $V = V_{\tilde{z}} + V_{\tilde{\eta}} + V_e + \frac{1}{2}(k - \overline{k})^2$, $\overline{k} = \theta_1 + \theta_2 + \theta_4 + (\|H(w)\|^2 + 2)$. We let $\dot{k} = \rho(e)e^2$, which is an unknown positive real constant , then $\dot{V} \le -c_0 e^2 - \|\tilde{z}\|^2 - \|\tilde{\eta}\|^2 + b(w)e\tilde{\xi}_1$. From this, the real control can be designed using the well-known backstepping method.

Application to Chua's circuit

The dynamic equation of the chua's circuit is adopted from [8] and given as follows:

$$\begin{aligned}\dot V_{c1} &= C_1^{-1}[R^{-1}(V_{c2}-V_{c1})-f(V_{c1})]\\ \dot V_{c2} &= C_2^{-1}[R^{-1}(V_{c2}-V_{c1})+I_L]\\ \dot I_L &= L^{-1}[V_{c2}-R_0 I_L+u]\end{aligned}$$

. Performing a simple coordinate transformation

$(\tilde x_1,\tilde x_2,y)=(V_{c2},I_L,V_{c1})$ gives

$$\begin{aligned}\dot{\tilde x}_1 &= -\frac{1}{RC_2}\tilde x_1+\frac{1}{C_2}\tilde x_2+\frac{1}{RC_2}y\\ \dot{\tilde x}_2 &= -\frac{1}{L}\tilde x_1-\frac{R_0}{L}\tilde x_2+\frac{1}{L}u\\ \dot y &= \frac{1}{RC_1}\tilde x_1+\left(-\frac{1}{RC_1}-\frac{a_1}{C_1}-\frac{a_3}{C_1}y^2\right)y\end{aligned}$$

. $(C_1,C_2,R,L)=(\bar C_1,\bar C_2,\bar R,\bar L)+(w_1,w_2,w_3,w_4)$

To guarantee $C_1,C_2,R,L>0$,we define W as

$$W=\{w \mid w\in R^4,\bar C_1+w_1>0,\bar C_2+w_2>0,\bar R+w_3>0,\bar L+w_4>0\}$$

Disturbance $\tau=-v_1$ is the output of the following van der Pol oscillator: $\begin{aligned}\dot v_1 &= v_2\\ \dot v_2 &= -v_1+0.5(1-v_1^2)v_2\end{aligned}$.

It is easy to show that d satisfies the following equation: $\ddot d+d-0.5\dot d(1-d^2)=0$. Let $\begin{aligned}&\gamma(d,\dot d)=-d+0.5\dot d(1-d^2)\\ &\theta=col(d,\dot d)\end{aligned}$ and that $q(w)=v_1$, From the exosystem and the desired feedforward input τ, it can be see that the function (12) satisfied with $-v_1=0.4444\vartheta_1-1.2222\vartheta_2$ with $A=\begin{bmatrix}0&1\\0&0\end{bmatrix}$, $B=\begin{bmatrix}0\\1\end{bmatrix}$, $\psi=\begin{bmatrix}1&0\end{bmatrix}$, $T=\begin{bmatrix}-0.5&2.75\\-1&1\end{bmatrix}$,Let $M=\begin{bmatrix}-2&5\\0&-1\end{bmatrix}$, $N=\begin{bmatrix}4&-1\end{bmatrix}^T$. We can easily verified that (M,N) is a pair of controllable matrices with M being Hurwitz. Then based on the proposed control method, the Internal model is as the following

$$\begin{aligned}\dot\eta_1 &= -2(\eta_1-4RLC_1C_2e)+5(\eta_2+RLC_1C_2e)+2.75\gamma(0.4444(\eta_1-4RLC_1C_2e)-1.2222(\eta_2+RLC_1C_2e),\\ &\quad 0.4444(\eta_1-4RLC_1C_2e)-0.2222(\eta_2+RLC_1C_2e))+4u\\ \dot\eta_2 &= -(\eta_2+e)+\gamma(0.4444(\eta_1-4RLC_1C_2e)-1.2222(\eta_2+RLC_1C_2e),\\ &\quad 0.4444(\eta_1-4RLC_1C_2e)-0.2222(\eta_2+RLC_1C_2e))-u\end{aligned}$$

The control input is given by $\begin{aligned}&u=\frac{1}{RLC_1C_2}(0.4444\eta_1-1.2222\eta_2)-450e-k(360(1+e^2)^3+1)e\\ &\dot k=360e^2(1+(1+e^2)^3)\end{aligned}$. For simulation study, we assume the nominal value of the parameters in the chua's circuit are $\bar C_1=199$, $\bar C_2=0.009$, $\bar R_0=0$, $\bar R=1.2$, and $\bar L=0.24$,the coefficients of the nonlinear resistor are $a_1=-\frac{8}{7}$,and $a_3=\frac{4}{63}$,the parameter variation w is assumed to be $w=(1,0.001,0.1,0.01)$, the initial conditions are given as $V_{c1}=1$, $V_{c2}=0\text{V}$, $I_L=0.2A$, $\eta(0)=0$. $k(0)=3$, and $v_1(0)=1,v_2(0)=-1$, the response of the open-loop system with initial conditional is shown in Fig1, Fig2 presents the phase portrait of van der Pol oscillator. Fig3 shows the system output e. Fig 4 shows the system input u. As shown in Fig5.the disturbance is well reproduced by the designed nonlinear internal model.

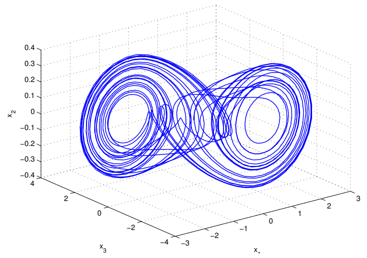

Fig1. Phase portrait of the open-loop system

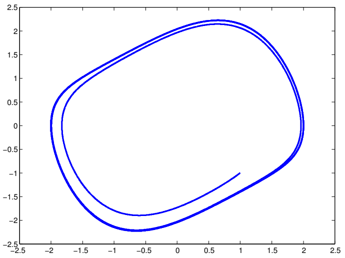

Fig2. Phase portrait of the exosystem

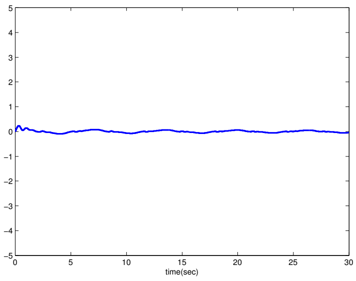

Fig3.The system output e

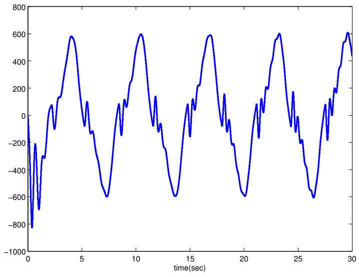

Fig4 .The system input u

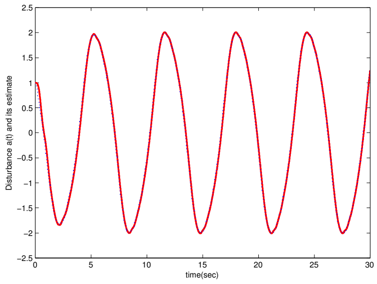

Fig5.Disturbance τ and its estimate.

Conclusions

In this paper, we have proposed a new control design method for output regulation with nonlinear exosystems. A new nonlinear internal model is proposed. Then we have applied the output regulation result to a control problem for the Chua's circuit. Simulation results illustrate the effectiveness of our algorithm.

Acknowledgements

This work was partially supported by the National Natural Science Foundation of China(No.61164015), Science and Technology Project Founded by the Education Department of Jiangxi Province (No.GJJ12437) and the Scientific Research Foundation for the Doctors of Nanchang Hangkong University (No.EA201104184), and the project Project supported by the Jiangxi Graduate Innovation Fund (YC2013-S222).

References

[1]Chua L O. The genesis of Chua's circuit[M]. Electronics Research Laboratory, College of Engineering, University of California, 1992.

[2]Jiang G P, Chen G, Tang W K S. Stabilizing unstable equilibria of chaotic systems from a state observer approach[J]. Circuits and Systems II: Express Briefs, IEEE Transactions on, 2004, 51(6): 281-288.

[3] Barone K, Singh S N. Adaptive feedback linearizing control of Chua's circuit[J]. International Journal of Bifurcation and Chaos, 2002, 12(07): 1599-1604.

[4] Feng G, Zhang T. Output regulation of discrete-time piecewise-linear systems with application to controlling chaos[J]. Circuits and Systems II: Express Briefs, IEEE Transactions on, 2006, 53(4): 249-253.

[5] Liu L, Huang J. Adaptive robust stabilization of output feedback systems with application to Chua's circuit[J]. Circuits and Systems II: Express Briefs, IEEE Transactions on, 2006, 53(9): 926-930.

[6] Y.Jiang. Rejection of nonharmonic disturbances in the nonlinear system via the internal model approach[J]. Journal of Vibration and Control.2011, 18(12) 1916-1921.

[7] Marino R, Tomei P. Global adaptive output-feedback control of nonlinear systems. I. Linear parameterization[J]. Automatic Control, IEEE Transactions on, 1993, 38(1): 17-32.

[8] Zhong G Q. Implementation of Chua's circuit with a cubic nonlinearity[J]. IEEE Transactions on Circuits and Systems-Part I-Fundamental Theory and Applications, 1994, 41(12): 934-940.

Applied Mechanics and Materials Vol. 596 (2014) pp 565-571
© (2014) Trans Tech Publications, Switzerland
doi:10.4028/www.scientific.net/AMM.596.565

Research on Attenuating Variable-rate Reaching Sliding Mode Control Strategy for Three-phase Current Source Inverter

Jing Bai[1, a], Shiqi Lu[2, a], Xiao Dong[3, b] and Jian Liu[4, a]

[1]Beihua University Jilin 132021 China

[2]Beihua University Jilin 132021 China

[3]Acrylonitrile Factory of PetroChina Jilin Petrochemical Company Jilin 132021 China

[4]Beihua University Jilin 132021 China

[a]bhdq2012@163.com, [b]jh_dxiao@petrochina.com.cn

Keywords: Three-phase current source inverter, Attenuating Variable-rate reaching law, Sliding mode, Variable structure, Spatial coordinate transformation.

Abstract. A sliding-mode attenuating variable-rate reaching control strategy for three-phase current source inverter is presented. The proposed control strategy significantly improves solve the exist issues that the slow dynamic characteristic and the output waveform distortion using linear control technology in three-phase current source inverter. In order to facilitate the analysis and design of sliding mode controller, a new mathematical model of three-phase current source inverter is built, and it is further simplified through the spatial coordinate transformation. The switching surfaces and the attenuating variable-rate reaching control law are deduced. Finally, the simulation results verify the effectiveness and feasibility of the control strategy for three-phase current source inverter.

Introduction

Because of these characteristics that simple topology, reliable short-circuit protection, facilitate four-quadrant operation and so on, current source inverter has been widely applied in the field of high-power industrial applications such as power drag, superconducting magnetic energy storage, new energy power generation[1-6]. However, the control objects of current source inverter are usually the non-linear load. When adopting linear control strategies such as *pid* control, the dynamic response of the inverter is relatively slow, steady-state accuracy is relatively low and the output waveform is easy to distortion. To overcome the above problems, this paper uses a new variable structure control strategy.

Sliding mode variable structure control is a new non-linear control based on state-space equations, and the accuracy requirement for mathematical model of the control object is not relatively high. In addition, it has the advantages of the strong robustness and insensitivity to external disturbances and parametric variable, and good dynamic and steady-state response and so on. Therefore, it is increasingly being used for all types of power electronic converter control system by many experts and scholars[4-12]. The authors studied *smvsc* technology in the control systems of single-phase *csi*, and effectively reduced the chattering sliding amplitude through adopting the variable-rate reaching programs in the reference [4]. This paper firstly studies *smvsc* applying to the control system of three-phase current source inverters on the basis of the reference [4], and verifies the effectiveness of the control strategy through *matlab* simulation. At last, the experimental results show that the sliding mode control strategy based on attenuating variable-speed approaching has the advantages of fast dynamic response, good output waveform, and strong anti-interference ability and so on.

Dynamic modeling of Three-phase Current Source Inverter

Fig. 1 shows the topology of a typical three-phase current source inverter system. It mainly comprises four components that the current source, six power switching devices (*sgct*), the *l-c* filter and non-linear load composed of inductance L_j and resistance R_j, where j=1~3, and $C_1= C_2= C_3= C$, $L_1= L_2= L_3= L$, $R_1= R_2= R_3= R$.

In order to transform the *dc* to three-phase symmetrical sinusoidal *ac*, the working mode of *csi* requires one and only one switch is turned on at the same time in upper and lower half-bridge, so that the current of the inductance is continuous and the energy of the inductance is balance[4]. Because the inductor current and of the non-linear load and the voltage of the filter capacitor are continuous and measurable, where $di_L/dt=(u_c-Ri_L)/L$, we can put i_L and its derivatives as the phase variables to describe the system[5-12].

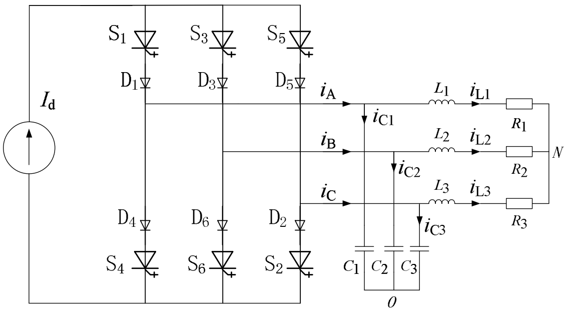

Fig.1 Circuit topology of three-phase current source inverter

Based on *kirchhoff's law*, the system state equation is

$$\begin{bmatrix} di_{Lj}/dt \\ d^2 i_{Lj}/dt \end{bmatrix} = \begin{bmatrix} 0 & 1 \\ -1/LC & -R/L \end{bmatrix} \begin{bmatrix} i_{Lj} \\ di_{Lj}/dt \end{bmatrix} + \begin{bmatrix} 0 \\ I_d/LC \end{bmatrix} u_j(t) \tag{1}$$

$$\begin{bmatrix} u_1(t) & u_2(t) & u_3(t) \end{bmatrix}^T = \begin{bmatrix} \dfrac{t_1-t_4}{T_s} & \dfrac{t_3-t_6}{T_s} & \dfrac{t_5-t_2}{T_s} \end{bmatrix}^T \tag{2}$$

$$T_s = t_1 + t_3 + t_5 = t_2 + t_4 + t_6 = (t_1 + t_2 + t_3 + t_4 + t_5 + t_6)/2 \tag{3}$$

Where t_k is the turn-on time of *k-th* power switching device (k=1-6), and the switching period T_s is the switching cycle time. From equation (2), the value of $u_j(t)$is ranged from –1 to 1.

From the symmetry of the output three-phase sinusoidal *ac* of three-phase current source inverter, equation (1) can be seen as a mathematical model of three-phase *csi* in the three-phase stationary coordinate system (a, b, c). By means of the vector coordinate transformation, three-phase *csi* can get a mathematical model in two-phase rotating coordinate system (d, q).

$$\begin{bmatrix} di_{Ld}/dt \\ di_{Lq}/dt \\ d^2 i_{Ld}/dt \\ d^2 i_{Lq}/dt \end{bmatrix} = \begin{bmatrix} 0 & 0 & 1 & 0 \\ 0 & 0 & 0 & 1 \\ \frac{2}{3}\omega^2 - \frac{1}{LC} & \frac{R}{L}\omega & \omega - \frac{R}{L} & \omega \\ -\frac{R}{L}\omega & \frac{2}{3}\omega^2 - \frac{1}{LC} & -\omega & \omega - \frac{R}{L} \end{bmatrix} \begin{bmatrix} i_{Ld} \\ i_{Lq} \\ di_{Ld}/dt \\ di_{Lq}/dt \end{bmatrix} + \begin{bmatrix} 0 & 0 \\ 0 & 0 \\ \frac{I_d}{LC} & 0 \\ 0 & \frac{I_d}{LC} \end{bmatrix} \begin{bmatrix} u_d(t) \\ u_q(t) \end{bmatrix} \tag{4}$$

Where ω is the angular velocity of the d-q coordinate system.

By comparing equation (1) and equation (4) shows that the mathematical model of three-phase *csi* drop to fourth-order system from sixth-order system so as to facilitate the analysis and design of sliding mode variable structure control controller. From three-phase stationary coordinate system transform into two-phase rotating coordinate system, three-phase sinusoidal alternating current can be expressed as:

$$\begin{bmatrix} i_d^* \\ i_q^* \end{bmatrix} = \sqrt{\frac{2}{3}} \begin{bmatrix} \sin\theta & \sin(\theta - {}^{2\pi}\!/_{3}) & \sin(\theta - {}^{4\pi}\!/_{3}) \\ \cos\theta & \cos(\theta - {}^{2\pi}\!/_{3}) & \cos(\theta - {}^{4\pi}\!/_{3}) \end{bmatrix} \begin{bmatrix} i_a \\ i_b \\ i_c \end{bmatrix} \tag{5}$$

Where θ is the angle between the axe d of two-phase rotating coordinate system and the axe a of three-phase stationary coordinate system.

Because the capacitor voltage and the inductor current can be obtained by the voltage and current sensors, the inductor current and its derivative can be obtained[5-6]. Therefore, as long as the reference output signal is known, the new state variable can be expressed with the difference between the reference signal and the state variables, the state equation of the system becomes[4]:

$$\frac{de}{dt} = Ae + B \begin{bmatrix} u_d(t) \\ u_q(t) \end{bmatrix} + \begin{bmatrix} 0 \\ 0 \\ f_1(t) \\ f_2(t) \end{bmatrix} \tag{6}$$

Where $e = \begin{bmatrix} e_1 & e_2 & e_3 & e_4 \end{bmatrix}^T$, $e_1 = i_{Ld} - i_d^*$, $e_2 = i_{Lq} - i_q^*$, $e_3 = \frac{d}{dt}(i_{Ld} - i_d^*)$, $e_4 = \frac{d}{dt}(i_{Lq} - i_q^*)$.

$$A = \begin{bmatrix} 0 & 0 & 1 & 0 \\ 0 & 0 & 0 & 1 \\ \frac{2}{3}\omega^2 - \frac{1}{LC} & \frac{R}{L}\omega & \omega - \frac{R}{L} & \omega \\ -\frac{R}{L}\omega & \frac{2}{3}\omega^2 - \frac{1}{LC} & -\omega & \omega - \frac{R}{L} \end{bmatrix},\ B = \begin{bmatrix} 0 & 0 \\ 0 & 0 \\ \frac{I_d}{LC} & 0 \\ 0 & \frac{I_d}{LC} \end{bmatrix}.$$

$$f_1(t) = -\frac{d^2 i_d^*}{dt} + \left(\omega - \frac{R}{L}\right) * \frac{di_d^*}{dt} + \left(\frac{2}{3}\omega^2 - \frac{1}{LC}\right) * i_d^* + \omega \frac{di_q^*}{dt} + \frac{R\omega}{L} * i_q^*,\ f_2(t) = -\frac{d^2 i_q^*}{dt} + \left(\omega - \frac{R}{L}\right) * \frac{di_q^*}{dt} + \left(\frac{2}{3}\omega^2 - \frac{1}{LC}\right) * i_q^* + \omega \frac{di_d^*}{dt} + \frac{R\omega}{L} * i_d^* \cdot$$

$f_1(t)$ and $f_2(t)$ are the external perturbation term, and meet $M_1 \le f_1(t)(f_2(t)) \le M_2 (M_1 < 0, M_2 > 0)$.

SMC Design of Three- phase Current Source Inverter

Selection of Sliding Surface. Sliding mode controller design generally includes two parts: First, select the switching surface function *s*; second, design control law *u*[4]. The existence condition of sliding mode shows that all state variables trajectories near the sliding surface must tend the sliding surface so as to ensure the system on the phase plane sliding into and reaches the origin according to a predetermined path. In order to facilitate the analysis and design of sliding switching surface, the state space described by equation (6) is divided into two parts, which the first part is composed of e_1 and e_2, and the second part is composed of e_3 and e_4. In first part, a straight line through the origin is selected as the switching surface, namely:

$$s_1 = C_1 e = k_1 e_1 + e_3 \tag{7}$$

Where $C_1 = [k_1 \quad 1]$.

In second part, a straight line through the origin is selected as the switching surface, namely:

$$s_2 = C_2 e = k_2 e_2 + e_4 \tag{8}$$

Where $C_2 = [k_2 \quad 1]$.

In order to make the system state trajectory slides along the switching surface and eventually stabilize at the origin, we make $k_1>0$ and $k_2>0$. Sliding mode control block diagram shown in Fig. 2.

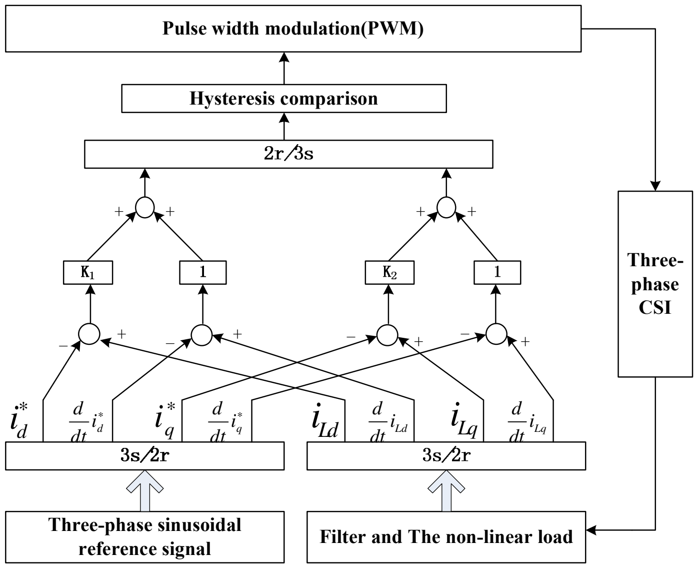
Pulse width modulation(PWM)
Hysteresis comparison
2r/3s
+
+
+
+
K1
1
K2
1
−
+
−
+
−
+
−
+
i_d^*
$\frac{d}{dt}i_d^*$
i_q^*
$\frac{d}{dt}i_q^*$
i_{Ld}
$\frac{d}{dt}i_{Ld}$
i_{Lq}
$\frac{d}{dt}i_{Lq}$
3s/2r
3s/2r
Three-phase CSI
Three-phase sinusoidal reference signal
Filter and The non-linear load

Fig.2 Block diagram of sliding mode control

Derivation of Control Law. Sliding mode variable structure control movement can be divided into two stages that the approaching movement stage and the sliding movement stage. According to the control principle of *smvsc*, the sliding-mode accessibility condition ensures that the state trajectory reaches the switching surface in a finite time and the control reaching law can improve the movement quality of dynamic approach[4]. In order to better improve the quality of reaching movement, this article uses the attenuating variable rate reaching law in three-phase *csi* sliding-mode control system[13]. The attenuating variable rate reaching law is expressed as follows:

$$\dot{s} = -\eta s - \varepsilon \|x\|_1 \operatorname{sgn}(s) \tag{9}$$

Where $\|x\|_1 \overset{\Delta}{=} \sum_{i=1}^{n} |x_i|$ is the state norm, $\varepsilon > 0$. η is the attenuation coefficient, $1 > \eta > 0$.

Combining with equation (6), equation (7) and equation (9), we can be deduced:

$$u_d = \frac{LC}{I_d} * \left[-C_1 A_1 e - C_1 d_1 - \eta_1 s_1 - \varepsilon_1 \left(|e_1| + |e_3| \right) \operatorname{sgn}(s_1) \right] \tag{10}$$

Where $A_1 = \begin{bmatrix} 0 & 0 & 1 & 0 \\ \frac{2}{3}\omega^2 - \frac{1}{LC} & \frac{R}{L}\omega & \omega - \frac{R}{L} & \omega \end{bmatrix}$, $B_1 = \begin{bmatrix} 0 & 0 \\ \frac{I_d}{LC} & 0 \end{bmatrix}$, $d_1 = \begin{bmatrix} 0 \\ f_1(t) \end{bmatrix}$.

Combining with equation (6), equation (8) and equation (9), we can be deduced:

$$u_{\mathrm{q}}=\frac{LC}{I_d}*\left[-C_2A_2e-C_2d_2-\eta_2s_2-\varepsilon_2\left(\left|e_2\right|+\left|e_4\right|\right)\mathrm{sgn}(s_2)\right] \tag{11}$$

Where $A_2=\begin{bmatrix}0 & 0 & 0 & 1\\ \frac{R}{L}\omega & \frac{2}{3}\omega^2-\frac{1}{LC} & -\omega & \omega-\frac{R}{L}\end{bmatrix}$, $B_2=\begin{bmatrix}0 & 0\\ 0 & \frac{I_d}{LC}\end{bmatrix}$, $d_2=\begin{bmatrix}0\\ f_2(t)\end{bmatrix}$.

Equation (10) and equation (11) are the reaching law expressions of *smvsc* system in three-phase *csi*.

Simulation Results and Experiment Results

In order to verify the correctness of the theoretical analysis, an experimental model has been built according to Fig. 1, and simulation studies the control effect of *smvsc* strategy in high-power three-phase current source inverter. Parameters values in experimental circuit are listed in Table 1.

Table 1 Parameter values of the experimental circuit

Item	Symbol	Value	Unit
Simulation time	T_s	0.2	s
DC link current	I_d	100	A
Filter capacitor	C	20	μF
Filter inductor	L	200	μH
Nominal load	R	3	Ω

When the output current amplitude changes of three-phase current source inverter at 0.2s, Figure 3 and Figure 4 respectively show the dynamic waveform of the inverter output current tracking the reference current and the corresponding control signal change trend of attenuating variable-rate reaching law. The simulation results show that three-phase *csi* using *smvsc* strategy can not only make the inverter output current fast track the reference current, and have good dynamic and steady-state response, but also produce better output waveform. When three-phase current source inverter was disturbed by the external disturbance at 0.15s, Figure 5 and Figure 6 respectively show the dynamic waveform of the inverter output current tracking the reference current and the corresponding control signal change trend of attenuating variable-rate reaching law.

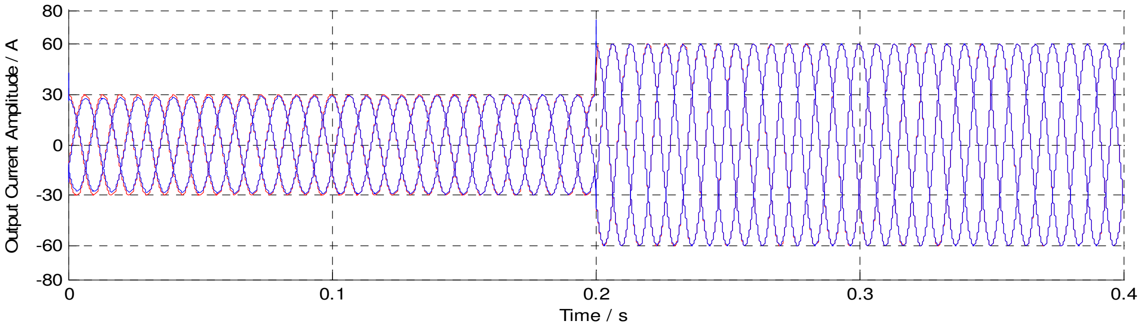

Fig.3 Dynamic waveforms of the inverter current tracking the reference current at 50 Hz
(The red line indicates the reference current and the blue line indicates the inverter current)

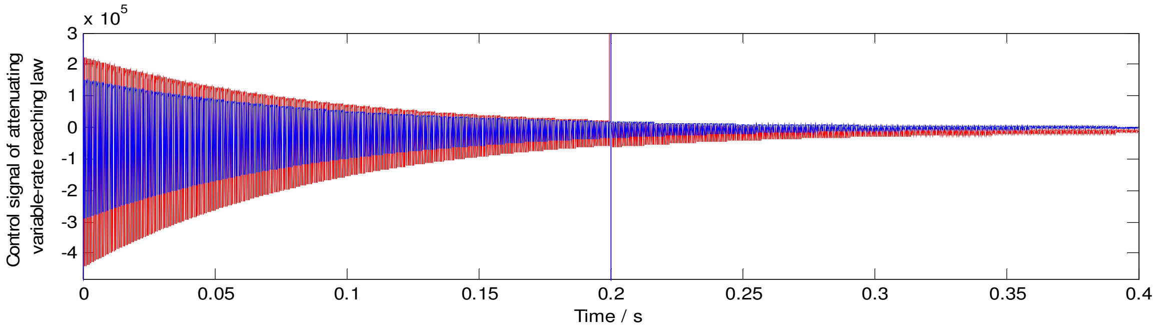

Fig.4 Control signal of attenuating variable-rate reaching law when three-phase csi output current amplitude changes

(The red region indicates u_d and the blue region indicates u_q)

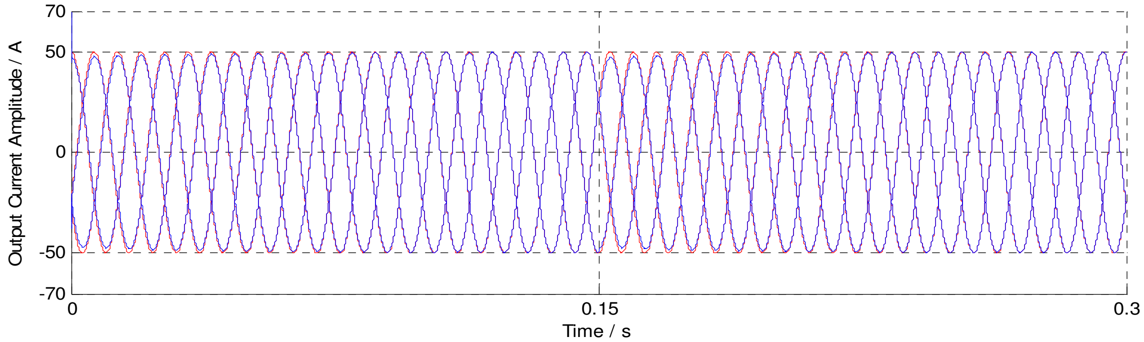

Fig.5 Dynamic waveforms of the inverter current tracking the reference current when csi was disturbed at 0.15s

(The red line indicates the reference current and the blue line indicates the inverter current)

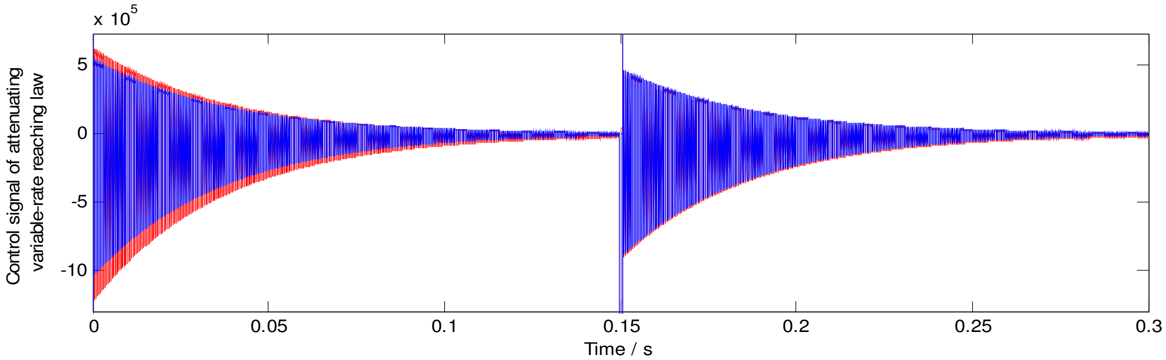

Fig.6 Control signal of attenuating variable-rate reaching law when csi was disturbed at 0.15s

(The red region indicates u_d and the blue region indicates u_q)

By comparing the reference current waveform and the inverter output current waveform, *smvsc* algorithm can make the system have a strong anti-interference ability and good dynamic quality, thus ensuring the high performance and high reliability of the work of the inverter system.

Summary

On the basis of the new mathematical model of three-phase current source inverter, the simplified mathematical model in two-phase rotating coordinate system is deduced through the vector coordinate transformation. Based on the simplified mathematical model, the attenuation variable-rate approaching SMVSC controller approaching *smvsc* controller is designed. Seen from the experimental results, the system using sliding mode control strategy has a good dynamic and static performance, small inverter current distortion, etc. Therefore, attenuation variable-rate approaching sliding-mode control strategy is the feasibility and effectiveness for the control of three-phase current source inverter.

References

[1] Popat Miteshkumar, Wu Bin and Zargari Navid R: F*ault ride-through capability of cascaded current-source converter-based offshore wind farm*. IEEE Transactions on Sustainable Energy. 2013, 4(2):314-323.

[2] Amr Ahmed A Radwan and Yasser Abdel-Rady I Mohamed: *Analysis and Active Suppression of AC- and DC-Side Instabilities in Grid-Connected Current-Source Converter-Based Photovoltaic System*. IEEE Transactions on Sustainable Energy. 2013, 4(3):630-642.

[3] Harbouche Y, Khettache L and Abdessemed R: *Sliding mode control application to the doubly fed asynchronous machine supplied by current sources*. Advances in Modelling and Analysis C. 2009, 64(1-2):15-26.

[4] Jing Bai, Shiqi Lu and Jian Liu. *Study and Application of Sliding Mode Control Strategy for High-power Current Source Inverter*. Applied Mechanics and Materials. 2014, 527:259-266.

[5] Xu Fei, Ma Hao and He Xiangning: *A discrete-time variable rate reaching law controlled current-source inverter*. Proceedings of the CSEE. 2007, 27(33):98-102.

[6] Yu Yong: *Discrete sliding mode control for current-source Inverter*. Power Electronics. 2009, 43(1):69-70.

[7] Zheng Xuesheng, Li Chunwen and Tang Honghai: *Integral sliding mode control for three-phase PWM voltage source inverter*. Transactions of china electrotechnical society. 2007, 22(12):105-109.

[8] Vadim, Utkin: *Sliding mode control of DC/DC converters*. Journal of the Franklin Institute. 2013, 350(8):2146-2165.

[9] Jiabing Hu, Shang Lei and He Yikang: D*irect active and reactive power regulation of grid-connected DC/AC converters using sliding mode control approach*. IEEE Transactions on Power Electronics. 2011, 26(1):210-222.

[10] Sosa, Jorge Luis: *Sliding-Mode Input–Output Linearization Controller for the DC/DC ZVS CLL-T Resonant Converter*. IEEE Transactions on Industrial Electronics. 2012, 59(3):1554-1564.

[11] Adib Abrishamifar and Ahmad Ale Ahmad: *Fixed Switching Frequency Sliding Mode Control for Single-Phase Unipolar Inverters*. IEEE Transactions on Power Electronics. 2012, 27(5):2507-2514.

[12] Mallapu Gopinath Umamaheswari and Govindarajan Uma: *Analysis and design of reduced-order sliding-mode controller for three-phase power factor correction using Cuk rectifiers*. IET Power Electronics. 2013, 6(5):935-945.

[13] Xiao Yanhong and Zhou Jinglin: *The reaching law for variable structure control of discretetime system based on attenuating control*. Control Theory and Applications. 2002, 19 (3): 450-452.

Applied Mechanics and Materials Vol. 596 (2014) pp 572-575
© (2014) Trans Tech Publications, Switzerland
doi:10.4028/www.scientific.net/AMM.596.572

Research on Spacecraft Attitude Control Simulation Technology based on Multidisciplinary Integration

Zhang Yabin, Wei Chuanfeng, Li Xingqian, Shi Xiaolin

(China Academy of Space Technology, Institute of Manned Spacecraft System Engineering, Beijing 100094, China)

zhangyabin@139.com

Keywords: Multi-disciplinary, Attitude Control, Simulation System.

Abstract. The design of spacecraft attitude control is important during the manufacture of spacecraft, and it is need to be validated adequately. To get the digital simulation validation of attitude control system, this paper discussed the spacecraft attitude control simulation system based on STK, Matlab and ADAMS. Based on the simulation frame, the paper analyzed the simulation model inter-clock. and realized the simulation system clock synchronization mechanism and algorithm. Based on the method of clock synchronization, the clock synchronization and logic correctness of message among multi-disciplinary simulation models could be ensured.

Introduction

Spacecraft attitude control is important for spacecraft fly mission. With the improvement of the Spacecraft technology, the configuration and dynamics of Spacecraft become more complex to achieve more mission, which promote a higher requirement for the design of Spacecraft Attitude Control [1]. The design of spacecraft attitude control is important during the manufacture of spacecraft, and it is need to be validated adequately [2]. During the simulation validation, multi-disciplinary simulation models need to be created to show the system characteristic. But there is deficiency in most modeling and simulation software, because it is only good at its own disciplinary.

This paper discussed the spacecraft attitude control simulation system including orbit, dynamics, controller, and actuators, to achieve the whole system simulation validation. The simulation system could be used to study attitude control design.

Control System Frame

Spacecraft attitude control system ensures the spacecraft body keeping an attitude against inertial frame, gravitation center body or other reference frame once enter orbit. Take initiative control for example, typical spacecraft attitude control system which is shown as Figure 1 includes orbit dynamic block, attitude dynamic block, attitude kinematic block, controller block, actuator block, attitude sensor block, space environment block.

Attitude dynamic and kinematic blocks are the basic content to describe spacecraft body. Attitude dynamics describes the relation of moment and attitude, and Attitude kinematics describes the relation of transforming attitude denotation to another.

Controller block is the control algorithm to be designed.

Orbit dynamic block computes the orbit parameters according to the initial orbit and simulation time.

Space environment block describes the effect that space environment takes on spacecraft body, includes gas resistance, gravitational grad and sunlight pressure.

Attitude sensor block estimates the attitude angle and angle speed, includes star sensor, earth sensor, sun sensor and inertia sensors.

Controller block is the control algorithm designed to drive the actuators. The control algorithm is designed according to the dynamics characteristic. The actuators produces the control moment to counteract the effect of interferential moment。Generally， PID is used for CMG and phase-plane is used for engine injecting.

Actuators block produce control moment and effect on spacecraft body, include CMG and engine. The momentum of CMG could be uninstalled by magnetism moment device and engine injecting.

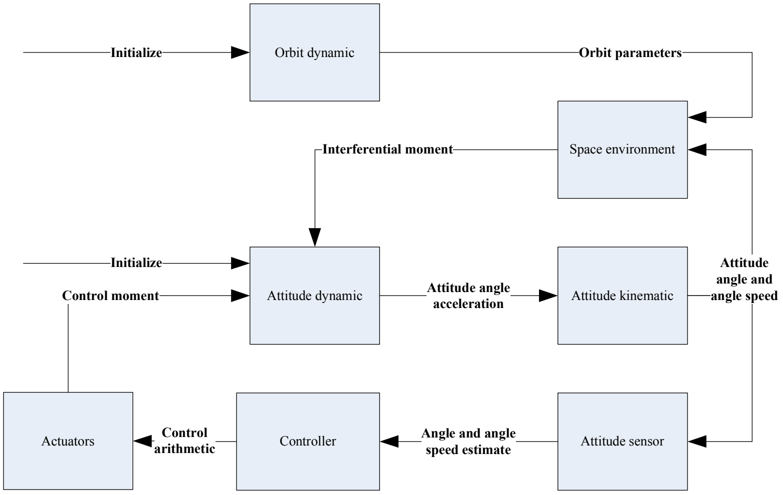
Initialize
Orbit dynamic
Orbit parameters
Space environment
Interferential moment
Initialize
Control moment
Attitude dynamic
Attitude angle acceleration
Attitude kinematic
Attitude angle and angle speed
Actuators
Control arithmetic
Controller
Angle and angle speed estimate
Attitude sensor

Figure 1. Frame of spacecraft control system

Simulation Frame

AGI Inc. developed general Satellite Tool Kit (STK). The software is one-upping business analysis software in space industry now and widely used to simulation computing [3]. We can use the software to build spacecraft orbit dynamic model, and create 2D/3D visualization dynamic scene. STK also can create diagram and report accurately [4].

Matlab is a high computer language facing science and engineering, and is recognized as the most excellent software. Simulink is one of the key toolbox in Matlab [5, 6], which is widely used in the domain of spacecraft attitude control.

ADAMS is a tool used for building virtual physics model [7], and simulating the dynamics and kinematics of mechanism system. The advantage of ADAMS is that the characteristic of model built is similar accurately with physics model [8].

Based on the analysis above, we can see that STK could be used to archive orbit dynamic block, ADAMS could be used to archive dynamic and kinematic blocks, Matlab could be used to archive controller block and other blocks.

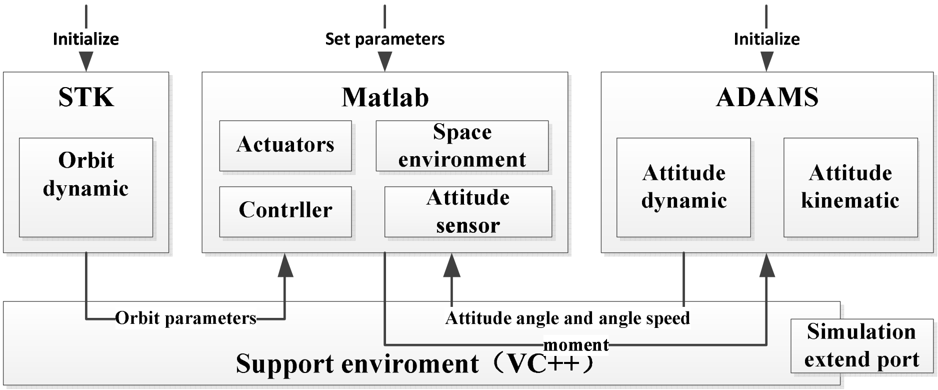
Initialize
Set parameters
Initialize
STK
Orbit dynamic
Matlab
Actuators
Space environment
Contrller
Attitude sensor
ADAMS
Attitude dynamic
Attitude kinematic
Orbit parameters
Attitude angle and angle speed
moment
Support enviroment（VC++）
Simulation extend port

Figure 2. Simulation frame of spacecraft attitude control system based on STK, ADAMS and Matlab

The simulation frame of spacecraft attitude control system based on STK, ADAMS and Matlab is shown as Figure 2.STK implements orbit dynamic block, Matlab implements controller, actuator, attitude sensor and space environment blocks, ADAMS implements attitude dynamic and kinematic blocks. VC++ implements application, that integrates all the software above to interact date among them. The application also supports the distributed simulation system interaction.

Simulation Clock Synchronization Technology

To archive the simulation frame above, we need resolve three problems. they are Multi-disciplinary software integrating, simulation model development and simulation clock synchronization. For the 1st problem, Paper [9-11] archived the integrating STK, Matlab and ADAMS into VC++; For the 2nd problem, we completed the simulation model in Figure 1, every simulation model is worth to be studied deeply, but is not discussed because of limited paper length. This paper discussed the 3rd problem.

Simulation clock synchronization is the key technology of simulation system, it is more important to the multi-disciplinary integrated simulation system. Software has its inner clock system respectively. When simulation running, software run according to its own clock. So we must build a simulation clock synchronization system to ensure the clock synchronization and logic correctness of message among multi-disciplinary simulation models. Simulation step and ratio are the two key parameters. The following discussed the simulation step and ratio in the software.

(1)Analysis of software inner clock

The model built by STK should be set start time, end time, step and ratio. When VC++ involves STK, the start time, end time, step and ratio could be set by VC++. When the parameters are set, the simulation need not to be interrupted.

The model built by Simulink simulates as fast as more after time step and period set. When VC++ involves Simulink, only time period could be set by VC++, time step and period are no-adjustable.

The model built by ADAMS simulates as fast as more after time step and period set. When VC++ involves ADAMS, only time period could be set by VC++, time step and period are no-adjustable.

(2)Design of simulation system clock synchronization

From the analysis above, STK support simulation period, step, ratio to be set by VC++, and the data produced by STK on upriver. So we can regard clock of STK as the standard clock of simulation system, Simulink model and ADAMS model snap the clock when simulation running. The design of clock synchronization is shown as Figure 3.

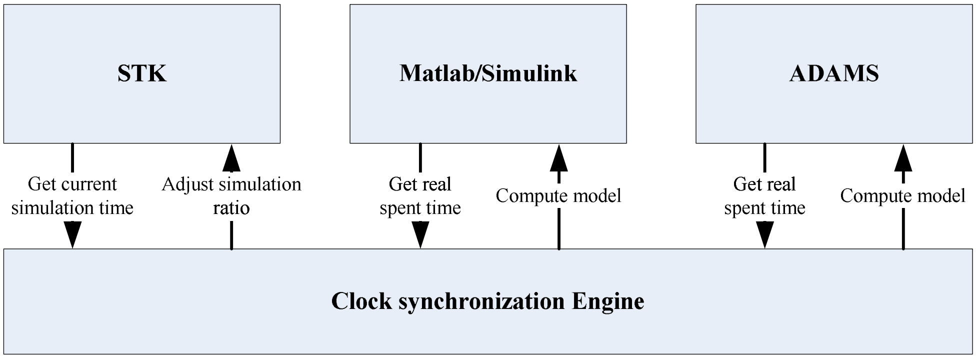

Figure 3. Design of clock synchronization

The algorithm of clock synchronization as following:

For the STK model, suppose step as s_s_0, ratio as s_k_0, start time as s_t_0; For Simulink model, suppose step as m_s_0, start time as m_t_0, real spent time for simulating one step as m_rt; For ADAMS model, suppose step as a_s_0, start time as a_t_0, real spent time for simulating one step as a_rt.

The clock synchronization engine set the start time of models at the same beginning to ensure the initial synchronization. Suppose simulation system start time as T_0, which use the STK time form. Then the initial time of STK model, Simulink model and ADAMS model are set with T_0,$m\_t_0+T_0-s\_t_0$ and $a\_t_0+T_0-s\_t_0$.

Suppose simulation system step as S_0, ratio as K_0, set $s\_s_0=S_0$, $s\_k_0=K_0$; Simulink model and ADAMS model advance the time to S_0 automatically, so S_0 must be multiple of m_s_0 and a_s_0. Generally, we set $S_0=s\_s_0=m\_s_0=a\_s_0$.

When simulation running:

a. The real spend time of STK model advance one step is $s\_rt=s\_s_0/s\_k_0$ (Supposing STK clock is synchronization with computer clock);

b. Computes Simulink model and ADAMS model, and get the real spend time m_rt and a_rt with step S_0;

c. If $m\_rt>s\_rt$, set $s\_k_0=m\_s_0/m\_rt$; If $a\_rt>s\_rt$, set $s\_k_0=a\_s_0/a\_rt$; If $m\_rt>s\_rt\&a\_rt>s\_rt$, set $s\_k_0=\min(m\_s_0/m\_rt,a\_s_0/a\_rt)$。

The simulation step and ratio are set suitably according to the algorithm above, the simulation system archives the balance between capability and granularity.

Conclusions

This paper discussed the spacecraft attitude control simulation system based on STK, Matlab and ADAMS. Based on the simulation frame, software can perform its specialty capability. The method of clock synchronization ensured the clock synchronization and logic correctness of message among multi-disciplinary simulation models.

References

[1] Zhou Lini, Tang Guojin, Luo Yazhong. Simulation Framework for Spacecraft Attitude Dynamics and Control Based on Matlab/Simulink [J].Journal of System Simulation, 2005, 17(10):2517-2524.

[2] Liu Liangdong, Liu Shenzhao. Satellite Control System Simulation Technics [M]. Beijing: China Astronautics Press, 2003.

[3] Dong Jiaqiang, Design and Realization of Aerospace Launch Visualization Simulation System Based on STK [J]. Computer Measurement& Control, 2010, 18(2): 446-449.

[4] Pan Chengsheng，Zhang Xin，Li Ding-hu, Application of STK/Connect to the Simulation and Demonstration of GPS [J]. Fire Control and Command Control, 2008, 33(10): 117-120.

[5] Xu Lin. Real-time and hardware-in-the-loop simulation [D]. Changsha：National university of defense technology, 2008.

[6] Xue Dingyu, Chen Yangquan. System Simulation Technology and Application based on MATLAB/Simulink [M]. Beijing: Tinghua University Press, 2002.

[7] Ma Yi. The Study of Virtual Prototype Technology on Dynamics Simulation of Spacecraft Deployable Mechanism [D]. Beijing: Chinese Academy of Sciences, 2006.

[8] Li Yueyue,.The joint simulation of robot based on ADAMS and MATLAB [D]. Baoding: Hebei University, 2010.

[9] Sun Yanhong, Liu Bing，Chen Hui, et al. Simulation of Information Transmission Timeliness of Satellite System Based on STK/X [J]. Radio Engineering, 2011, 41(3):56-58.

[10] Pan Dafu, Wang Bo, Zhou Zhiqiang. Research on mixed programming technology of Matlab and C/C++ [J]. Computer Engineering and Design, 2009,30(2): 465-468.

[11] Zhang Jie, Sun hu, Yang Bo, et al. Simulation and analysis of automotive braking system based on VC++and ADAMS/Car [J]. Machinery Design&Manufacture, 2012, 4: 65-67.

Applied Mechanics and Materials Vol. 596 (2014) pp 576-579
© (2014) Trans Tech Publications, Switzerland
doi:10.4028/www.scientific.net/AMM.596.576

The facilities vegetables warning and control system based on Mobile phone SMS

Li Yan[1, a], Dejiang Hao [1, b], and Hao Zhang[1]

[1]Jilin Agricultural University, College of Information Technology, Changchun, China 130118

[a]81608795@qq.com, [b]wgw_1825@163.com

Keywords: Facility vegetable; Mobile phone short message; monitoring; early warning; control systems.

Abstract. The production of facilities vegetable significantly affected by environmental factors, therefore require real-time monitoring information of light, air temperature and humidity, soil temperature and humidity, and timely early warning and controlling, to prevent irreparable damage. This study achieved real-time monitoring and timely warning of environmental factors, and optimal control of pumps and roller blinds in the Facility vegetable. We have adopted Internet of Things technology and short message function in Mobile phone, the system through C # language and the SQL Server database to prepare. The application in Jilin Province Jinta Industrial (Group) Co.Ltd. shows that the system is better, achieved the purpose of high yield income. This template explains and demonstrates how to prepare your camera-ready paper for *Trans Tech Publications*. The best is to read these instructions and follow the outline of this text.

Introduction

In Facility vegetable production, many factors are not conducive to the normal growth and development of vegetable crops. For example, the smaller number of the light, the light intensity is weak, the larger temperature difference between day and night, the higher the relative humidity of the air, poor air flow (slow), and higher or lower soil temperature and moisture conditions. Currently, the regulation of greenhouse management is artificial and unscientific. Regulation and control is poor, causing disproportionate input-output, low economic efficiency. To make Facility vegetable normal growth and development, we must scientific regulation and control timely environmental factors of greenhouse vegetables that affect growth and development to meet the needs of Facility vegetable growth and development [1][2][3].

The Internet of things is perceived as the prerequisite, the realization of the people, people and things, and fully connected network. Agricultural Internet of Things using sensors of system to access environmental data, through various instruments as a real-time display or automatic control variables(data) involved in the automatic control parameters, ensuring crops, livestock and aquatic products have a good, appropriate growth environment. Currently, foreign agricultural Internet of Things sensor devices are widely used in breeding, production, harvest, transport, and storage aspects; packaging and irrigation in the implementation of the monitoring. In recent years, China has achieved initial results [4][5][6].

When monitoring, early warning and control facilities vegetables, because people cannot always observe the computer, and timely operation, which caused irreparable damage. People always have to carry the phone, the establishment of facility vegetable monitoring and control system based SMS, which can effectively solve these problems.

System Design

System network topologies. The system is designed and implemented using classic Internet of Things topological structure, the topological structure as shown in Figure 1.

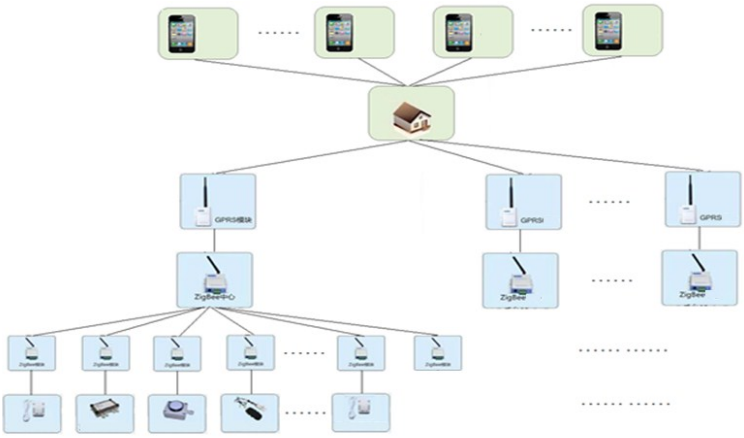

Fig.1System topology Figure

System controlling flowing. Sensor will send data collected by the Zigbee child nodes to Zigbee center node, center node sends the data to the control center through GPRS gateway, control center will be processed and sent warning data to mobile users, Mobile users get warning data and control messages can be sent to the control center, where SMS will be transformed into control commands. System controlling flowing is shown in Figure 2.

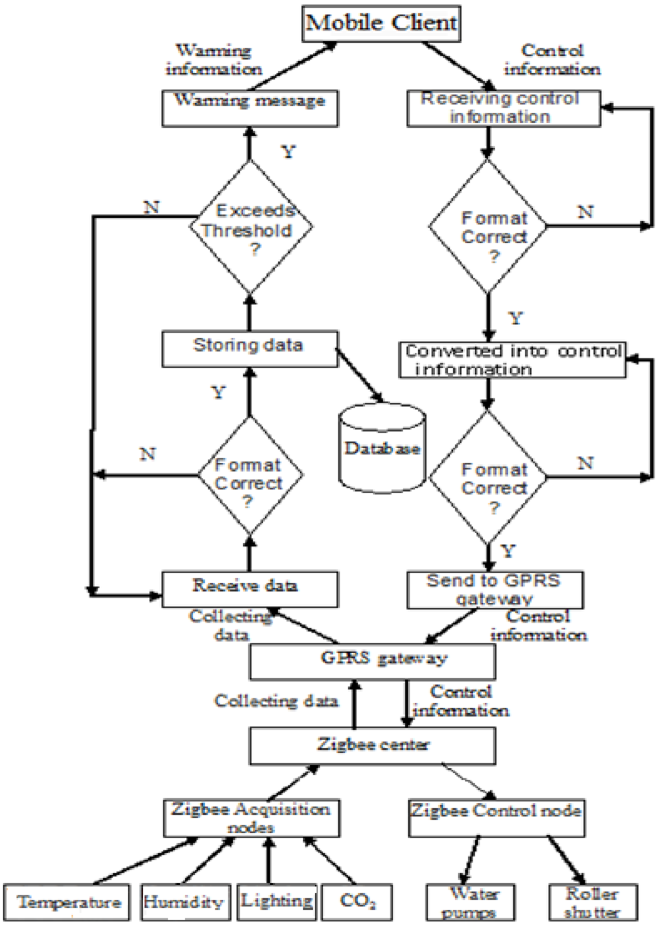
Mobile Client
Warning information
Control information
Warning message
Receiving control information
Y
N
Exceeds Threshold ?
Format Correct ?
N
Y
Storing data
Converted into control information
Y
Database
N
Format Correct ?
Format Correct ?
N
Y
Receive data
Send to GPRS gateway
Collecting data
Control information
GPRS gateway
Collecting data
Control information
Zigbee center
Zigbee Acquisition nodes
Zigbee Control node
Temperature
Humidity
Lighting
CO_2
Water pumps
Roller shutter

Fig.2 System control flow chart

System implementation

Data acquisition. After the system running, the system may receive data sending from the sensor, and the date displayed in a window in the form of text, as shown in Figure 3.

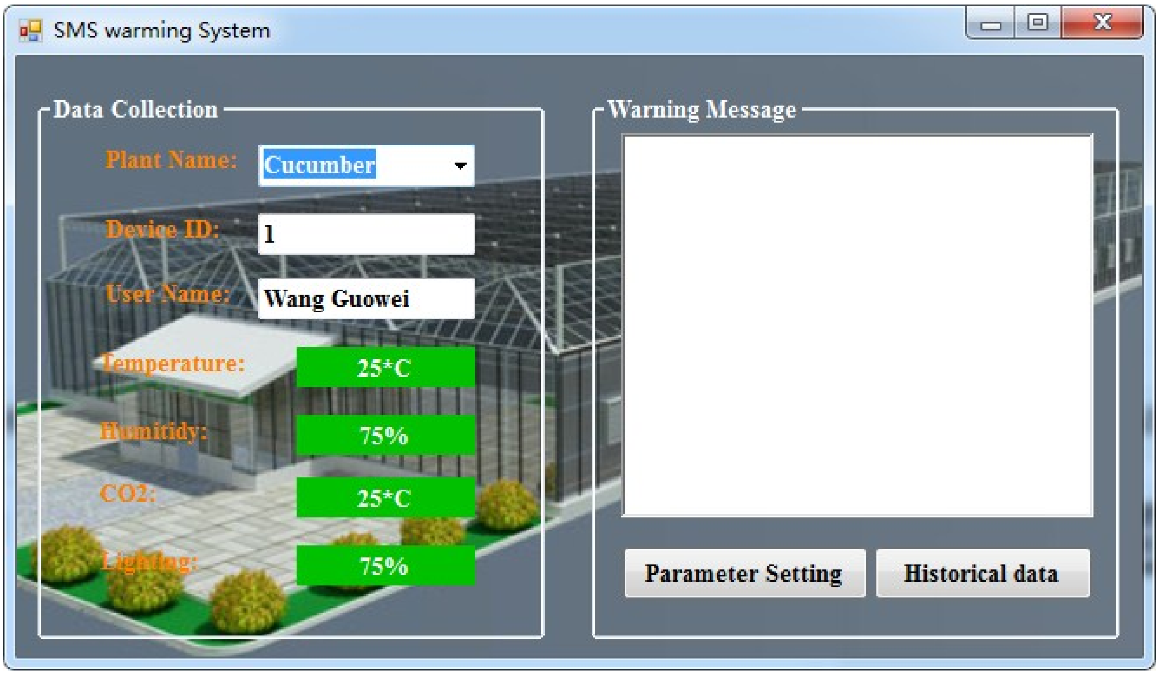
SMS warming System
Data Collection
Warning Message
Parameter Setting
Historical data

Plant Name: Cucumber
Device ID: 1
User Name: Wang Guowei
Temperature: 25*C
Humitidy: 75%
CO2: 25*C
Lighting: 75%

Fig.3 Date collecting

SMS warming. When the indicators of crop growth environment exceeds a given threshold, the system will automatically alert and send text messages to inform users In the system, the message will display data of temperature, humidity, light and CO2 exceeding warning values, and will prompt the user to send control commands (as shown in Figure 4), and timely allow the user to control the growth of environmental indicators of organisms in the greenhouse.

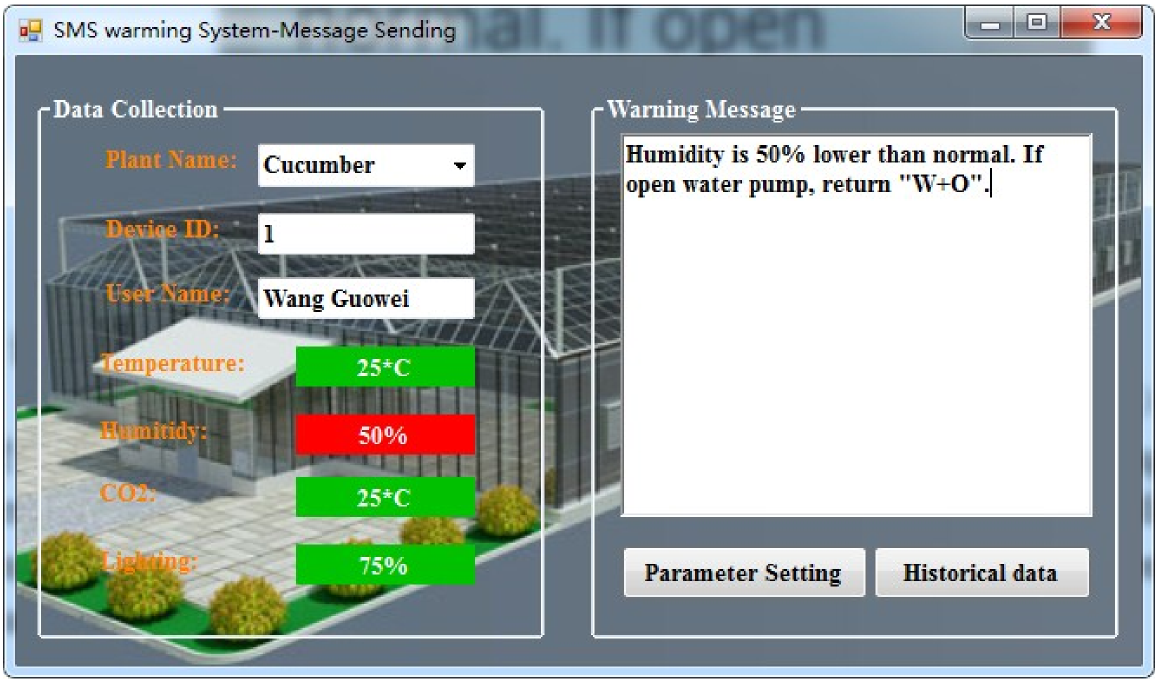
SMS warming System-Message Sending
Data Collection
Warning Message
Parameter Setting
Historical data

Plant Name: Cucumber
Device ID: 1
User Name: Wang Guowei
Temperature: 25*C
Humitidy: 50%
CO2: 25*C
Lighting: 75%

Humidity is 50% lower than normal. If open water pump, return "W+O".

Fig.4 SMS warming

SMS control. When receiving a warning message the user can send SMS control information in a specific format. After the system receives the control information sent by the user, the system converts it into a control command will be send to the control device(as shown in Figure5).

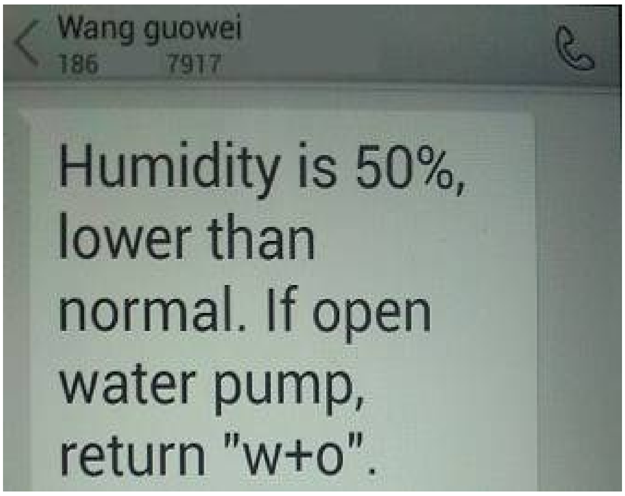

Wang guowei
186 7917

Humidity is 50%, lower than normal. If open water pump, return "w+o".

Fig.5 Warming information

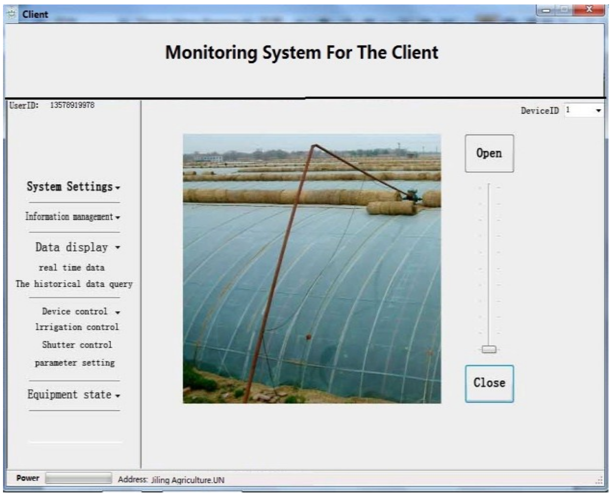

Client
Monitoring System For The Client
System Settings
Information management
Data display
real time data
The historical data query
Device control
lrrigation control
Shutter control
parameter setting
Equipment state
Open
Close
Power

UserID: 13578919978

DeviceID 1

Address: Jiling Agriculture.UN

Fig.6 Shutter control interface

Equipment control. When the warning information generated, the system can be manually or automatically to achieve the equipment (pumps, shutter) control, to achieve timely control of the facility environment. Figure 6 is a shutter control interface.

Conclusions

Using Web Services technology, the paper defines the data acquisition, storage, early warning and control data receiving and forwarding Services, provides the client and the device communications interface; Using networking technology, through the wireless network, the information interaction of hardware and software, provides a guarantee for data smooth transmission; Using the c # language and SMS cat, realized facilities vegetables early warning and remote control based on SMS. Thus the paper solves the data acquisition and control limitation of space and time.

The system in Jilin Jinta Industrial (Group) Co., Ltd. has been running nearly a year, does play a regulatory role effectively, improve the quality and yield of pepper, and meet the needs of enterprises.

Acknowledgements

This work was financially supported by Jilin Agricultural University Scientific Research Foundation (201137), Students' Innovation and Entrepreneurship projects.

References

[1] D. H.Willits and M. M.Peet:Agric.and Forest Meteomlogy, 44(1989),P.275

[2] Y.G.Lii, S.Y. LONG and W.YANG : Intelligent Processing and Application, Vol.3 (2013),P.72.

[3]Y.F. Zhang: Communications and Information Technology, Vol. 1(2010),P.50.

[4]S.B.Shen, Q. L.Fan, P.Zong:Joumal of Nanjing University of Posts and Telecommunications, Vol. 29(6)(2009),P.1.

[5]S. Yan and Z.C. Huang: Computer & Digital Engineering, Vol.4 (2008),P.86.

[6] X.H. Lai, S.P. Zhang and W.J. Shang: Microcomputer Information, Vol.4 (2008),P.29.

Applied Mechanics and Materials Vol. 596 (2014) pp 580-583
© (2014) Trans Tech Publications, Switzerland
doi:10.4028/www.scientific.net/AMM.596.580

The Research of furnace temperature control technology based on model free adaptive control system

Jian Chen [1, a], Xue Han [2,b]

[1] College of Computer and Information Science & College of Software, Southwest University , Chongqing, China

[2] Glass Rubs(Chongqing) Co. Ltd, Chongqing, China

[a]j.hanchen@126.com, [b]1468993603@qq.com

Keywords: glass furnace temperature control; time-varying and time lag of non-linear multivariable system; Model free adaptive control

Abstract. According to the analysis of furnace temperature control, a new control process which is based on the technique of model free adaptive control, is proposed against the defects of traditional control system. Through the analysis of the characters of MFAC and its utility for continuous and non-linear multivariable control system of glass furnace, a satisfied result indicates the good application of MFAC on temperature control of glass furnace.

Introduction

The glass furnace is a key system in glass factory, which could determine not only the glass's capacity and quality but also the production efficiency. The high temperature in furnace and reasonable temperature gradient make the batch melt and flow to fining and homogenization[1]. At the same time, it is necessary to keep the stable temperature in order to guarantee the quality of glass products. The adjustment on temperature, pressure, glass level and batch could be realized through the control of valves, fans even motors on furnace. Such parameters as above are related and coupled each other, which may cause some problems that could not be solved by traditional control system such as impossibility of setting up precise control mode and poor ability for overcoming of time lag etc. In this tradition way, the operator would like to combine his experience with PID. However, the system sometimes would be out of control. Nowadays, the control system has been improved to adapt fuzzy model control and neural network adaptive control etc. In some ways good results have been achieved through these systems. However, these systems are confined to the linear control theory and could not solve the furnace problems radically. The MFAC is a new control system, which introduces pseudo-partial derivative and pseudo order as evaluating unit. A series of dynamic linear time-varying model is used to replace normal non-linear model along the track of controlled system[2][3]. With the I/O data from controlled system to evaluate pseudo-partial derivative on line, model free adaptive control is realized. In this way, the parameters could be adaptive with structure without any complicated manual setting which is specific to controller data. Furthermore, this system has good tracking performance and better robustness, which could make the system closed-loop stable. We use this system as temperature control system for glass furnace and get good efficiency.

The analysis on temperature control of glass furnace

The batch goes into furnace through dog house and becomes melting glass after complicated physical chemistry reactions under high temperature. There are five phases among the reaction, which is indicated as forming of silicate, glass, fining and homogenization then cooling down. These reactions happen simultaneously at different parts of glass furnace in continuous production. That is to say, there are different physical chemistry reactions and temperature requirement in different phases. So, it is necessary to set up melting temperature gradient curve in accordance with requirement of physical chemistry reactions, which is along the longitudinal direction of melting tank[4]. (Fig.1).

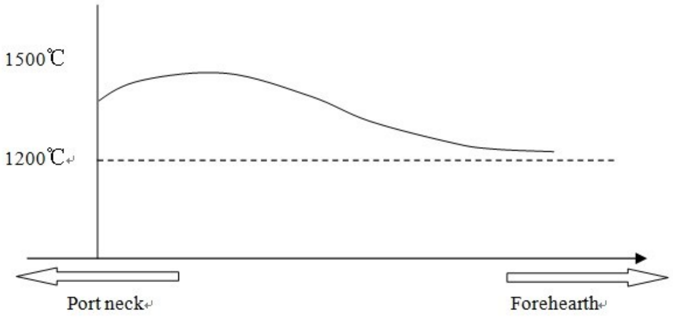

Fig.1 The temperature gradient curve of the melting tank

Therefore, the glass furnace becomes an extremely complicated temperature field. During the production, besides the different temperature in different site, the temperatures in each site of furnace are changed due to environment temperature, charging rate, furnace pressure and glass level even the fuel quality. For example, the charging rate and quantity would influence the level and temperature in melting tank while the furnace pressure would impact the burning efficiency even to the temperature. As the stable and reasonable temperature distribution is main factor for melting quality, temperature control becomes the key point in furnace control system. From the point of control, the glass furnace is a time lag non-linear system which is multivariable, multi-loop, high-order and time-varying. See Eq. (1)

$$G(t) = F\left[T(x, y, z, t), m(t), \frac{dm(t)}{dt}, p(t), h(t), f(t)\right] \tag{1}$$

$T(x, y, z, t)$ refers to distribution function of temperature in furnace, $m(t)$ & $dm(t)/dt$ refer to charging quantity and rate; $p(t)$refers to furnace pressure; $h(t)$ refers to glass level; $f(t)$ refers to fuel quality. From this formula, the complication of temperature control expresses its characters as follows: I. the big time lag and thermal inertia of process parameters; II. big correlation between each data; ⅲIII. much random disturbance and non-linear on parameters. The temperature control covers control on melting tank, working end and forehearth. The control on melting tank and forehearth is the key point in system. In addition, as a huge thermal equipment it is impossible to measure all temperature which are mentioned above. The normal operation is to choose some special measuring point and take a weighted average of these measured values. The result is called temperature process value (PV), which is used as controlled variable. In order to keep the stable controlled variable, it is necessary to adjust the quantity of fuel, batch charging rate and inlet quantity of fan. Anyway, this adjustment is not an easy way.

The PID control, stepping control and fuzzy control algorithm are widely adapted in furnace temperature control system. With PID algorithm, it is difficult on setting reasonable parameters. All parameters have to be controlled respectively, which makes difficult information interaction among controllers and leads to bad efficiency. The stepping control is to adjust the fuel quantity in several times based on the deviation between temperature process value and temperature setting value. It is relied heavily on the operator's experience and changing of working environment in order to manually set suitable time and every adjustment quantity even the general quantity. The precise working procedure model needs to be created in fuzzy control system. Imitating human fuzzy inference procedure, inference principle becomes real in this model, through which could control the temperature. However, the model is not easily to set up.

Model free adaptive control is characterized on such aspects as : 1. the precise quantitative know-how for process is not necessary; 2. there is no procedure recognition mechanism in system; 3. it is not necessary to design for special controller of some process;4. No need manual parameter setting; 5. analysis on stability of closed-loop system and criterion could be used for system analysis in order to ensure the system stale[3]. Therefore, MFAC is suitable for furnace control process.

Furnace temperature control system based on MFAC

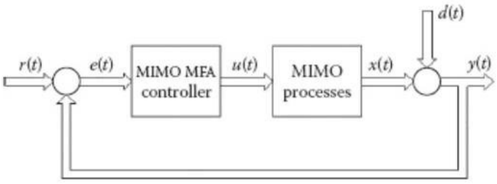

Fig. 2 Multivariable MFAC control system

The MFAC system is composed of a MFAC controller and a feedback loop in Fig.2. The target of MFAC controller is to force the process variable $y(t)$ tracking the setting value $r(t)$ through reasonable control function $u(t)$, even though there are interference and process dynamic change $d(t)$. In other words, the controller would reduce the deviation between setting value $r(t)$ and process variable $y(t)$ on line. The core of MFAC controller is an artificial neural network with a multilayer perceptron. The neural network includes an input layer, a hidden layer with multi neuron and an output layer with single neuron. See Eq. (2)-(5). The neural network could update its weight w_{ij} and h_i according to the requirement so that modify the dynamic module.

$$p_j(n) = \sum_{i=1}^{N} w_{ij}(n)E_i(n) + 1 \tag{2}$$

$$q_j(n) = \varphi(p_j(n)) \tag{3}$$

$$o(n) = \sum_{j=1}^{N} h_j(n)q_j(n) + 1 \tag{4}$$

$$v(t) = K_c[o(t) + e(t)] \tag{5}$$

n refers to the nth iteration; $o(t)$refers to continuous time function of $o(n)$; $v(t)$ refers to output of MFAC controller; K_c refers to gain of MFAC. The update algorithm of weight w_{ij} and h_i could reach as Eq. (6)(7):

$$\Delta w_{ij}(n) = \eta K_c e(n) q_j(n)\left(1 - q_j(n)\right)E_i(n)\sum_{k=1}^{N} h_k(n) \tag{6}$$

$$\Delta h_j(n) = \eta K_c e(n) q_j(n) \tag{7}$$

Thus, the minimization of deviation e(t) would realize through the adjustment of gain K_c and weight w_{ij} and h_i in MFAC controller. Through the adjustment the controller could override the change of dynamic characters and interference or some other uncertain factors. When the deviation $e(t)$ is close to zero that means the process is stable and it is not necessary to modify the weight of controller.[3]

In glass furnace temperature control system in Fig.3, it requires supervision and control of temperatures on port neck, melting tank and forehearth. The fuel is burning at the port neck while melting tank is the important part for silicate forming, fining and homogenization. Stable temperature of melting tank plays a vital role in glass production. And it is also the key point in the temperature control system. There would be several measure points for temperature, furnace and glass level in tank. The forehearth is for supplying suitable glass to forming. In assuring the qualified glass, the temperature control for forehearth is divided into two parts, which is set measuring points respectively.

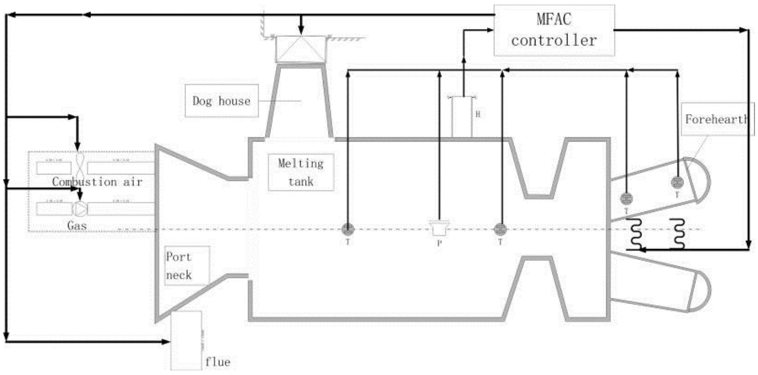

Fig.3 The chart of the control system

In traditional control system, there is only supervision for temperature and pressure while the glass level is used for controlling the charger. If the level is lower than the setting value, the batch charger starts working whereas it stops. At forehearth, the single loop PID is used for temperature control. Although it is easy for realizing control in this way, each loop has to start separately. Thus the system could not keep automatically control under fluctuating parameters. Furthermore, traditional system is so sitive to interference that it vibrates when the parameters change. In order to solve above issues, a new control system based on multi variables is raised.

(1) The MFAC controller is introduced to realize combined control of temperature in port neck and melting tank. With MFAC controller, the gain K_c in equation (5) is dealing with deviation between temperature setting point(SP) and process value (PV) in tank. After calculation of controller, the setting points of gas and combustion air are obtained, through which to adjust the quantity valve respectively and ensure good combustion. Thus the port neck temperature would be stable in the setting territory. Under stronger thermal shocks such as environment temperature change, pressure change in gas pipe and fluctuation of charging, the weight w_{ij} and h_i in neural network would be adjusted by MFAC so as to overcome the changes in furnace[5]. Furthermore, through multi iteration, the past parameters are substituted in order to modify current control data, which reflects the non-linear and time-lag of glass furnace. In this way, the control becomes more precisely. Moreover, with combined control of charging rate and opening of flue damper as well as the adjustment on tank temperature and pressure even glass level, the system temperature could reach stable and reasonable.

(2) The forehearth temperature control is not the control for single parameter any more. According to a certain algorithm, MFAC controller could forecast the influence of tank temperature change on forehearth. Combined the changed parameters from melting tank, joint adjustment shall be realize. Even the temperature fluctuation resulted by time lag in single parameter control could be avoided.

The MFAC control system is composed of a set of PLC and PID, industrial computer and peripheral elements such as sensor, transducer and adjustment valves etc. The advanced control system is reached through the cascade of Cybocom MFAC software in the computer and PID. In use of MFAC controller, only control type of certain process and rough time constant is enough. The operator could monitor and change the setting of controller with panel or tendency curve of screen. As soon as the system goes to work, MFAC controller could reach the control status. Operator could switch modes among PID control, manual and MFAC control.

Conclusion

The MFAC is adopted to the temperature control system of glass furnace, which is a multi variable, big time lag and non-linear system. With good robustness and adaptation, MFAC makes the control system run stable and improve its ability of resistance on thermal shock. Benefiting from MFAC controller, the glass quality improves a lot. All of above indicates the huge advantage of MFAC temperature control system in glass furnace.

References

[1] John T. Brown: *A Second Revolution in Glass Melting Technology*, Glass International, March 1992

[2] Jónsson Harris, S., in: *Model-Free Adaptive Control Improves Productivity and Efficiency*, Control, June 2004.

[3] J. VanDoren, V in: *Model Free Adaptive Control—This New Technique for Adaptive Control Addresses a Variety of Technical Challenges*, Control Engineering Europe, March 2001.

[4] N. Ya. Suvorov: *What is the best Design for a glass furnance* ,Kurlov Glass works, 1997.

[5] George Chcng and Qiang Wang: Model-Free Adaptive Control of Evaporators , CyboSoft, General Cybemation Group Inc., 1998.

Applied Mechanics and Materials Vol. 596 (2014) pp 584-589
© (2014) Trans Tech Publications, Switzerland
doi:10.4028/www.scientific.net/AMM.596.584

The Sliding Mode Variable Structure Control Method for Brushless DC Motors

Yin Xijie[1,a],Xu Jianguo[2,b]

[1]Shandong Women's University, Jinan, Shandong,China

[2]Dazhong Newspaper Group, Jinan,Shandong,China

[a]xijiesd@126.com,[b]sdxjg@163.com

Keywords: neural networks; sliding mode control; chattering; sliding mode manifold

Abstract. The sliding mode variable structure control method for brushless DC motors with uncertain external disturbances and unknown loads is studied. A neural sliding mode control scheme is proposed for reducing chattering of sliding mode control. A global sliding mode manifold is designed in this approach, which guarantees that the system states can be on the sliding mode manifold at initial time and the system robustness is increased. A radial basis function neural network (RBFNN) is applied to learn the maximum of unknown loads and external disturbances. Based on the neural networks, the switching control parameters of sliding mode control can be adaptively adjusted with uncertain external disturbances and unknown loads. Therefore, the chattering of the sliding mode controller is reduced. Simulation results proved that this control scheme is valid.

Introduction

BLDCM has a fixed mechanical torque, good mechanical characteristics and governor control characteristics, so it is widely used in many fields, such as robot and printer design. BLDCM is also characterized by time-varying, non-linearity and strong coupling [1]. These three characteristics result in the difficulty of establishing BLDCM's mathematical model, obtaining its accurate parameters, and developing its complex control system. For systems with accurate mathematical model, traditional control method has some advantages, such as simple algorithm, rapid response, and accurate control, while for systems with uncertain and non-linear mathematical model, it doesn't satisfy their various requirements. The control method based on artificial intelligence, such as fuzzy control and neural network control, is characterized by self-learning, self-governing and self-organizing. Many scholars investigated the method combining artificial intelligence control and traditional control. [4,5] In this paper, the sliding mode controller for brushless DC motors with uncertain external disturbances and unknown loads is studied. A neural sliding mode control scheme is proposed for reducing chattering of sliding mode control. As the chattering is reduced, the system robustness and self-adaptability is increased. Simulation results also proved that this control scheme is feasible.

Describing the problem

The mathematical model of BLDCM can be represented by a second order differential equation:

$$\ddot{\theta} = (T_e - T_L - B\dot{\theta}) / J \qquad (2.1)$$

In this equation, T_e is electromagnetic torque, the input signal of the motor. B represents camping coefficient. J represents rotational inertia of the motor. T_L is the sum of load torque and all disturbance torques. $|T_L| < D$ is bounded, and D is a bounded constant. θ, $\dot{\theta}$ and $\ddot{\theta}$ are angular displacement vector, speed vector, and acceleration vector, respectively. Of these three elements, θ and $\dot{\theta}$ is measurable.

Fig 1 shows the structure of the control system of BLDCM.

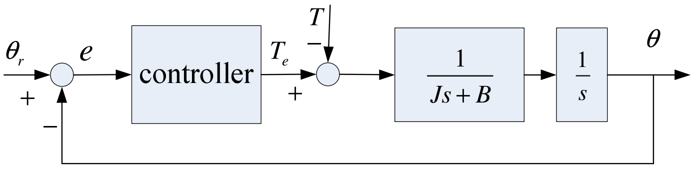

Fig.1 The structure of the control system of BLDCM

The key problem for controlling the speed and the position of BLDCM is the measure and the control of position. Therefore, the goal of the controller is tracking and controlling the position, that is to say, angular displacement vector θ should track designated angular displacement vector $\theta_r \in R^n$ with minor error. Tracking error $e{=}\theta{-}\theta_r \to 0$.

Sliding mode controller

The process of designing a sliding mode controller can be divided into two steps: first determining a sliding mode manifold and then designing control law.

Designing a global sliding mode manifold. The global sliding mode manifold is a time-varying sliding mode manifold. It is designed as follows [3]:

$$s = \dot{e} + \alpha e - p(t)[\dot{e}(0) + \alpha e(0)] \tag{3.1}$$

In this equation, α is the constant of sliding mode, $p(t) = \exp(-\beta t)$, β is a positive constant, $\exp(-\beta t)$ is $-\beta t$ order power function of a natural constant. $e = \theta - \theta_r$ is angular displacement tracking error. $\dot{e} = \dot{q} - \dot{q}_r$ is angular speed tracking error. $e(0)$ and are angular displacement tracking error and angular speed tracking error, respectively, when t is 0.

According to (3.1), s is 0 for any given initial state, that is to say, the system states can be on the sliding mode manifold at initial time.

According to (3.1), s is 0 for any given initial state, that is to say, the system states can be on the sliding mode manifold at initial time.

When the system was in a mode of sliding, we can infer from (3.1) that

$$\dot{e} - p(t)\dot{e}(0) + \alpha e - \alpha p(t)e(0) = 0 \tag{3.2}$$

The path error of sliding movement can be obtained by doing above equation (3.2):

$$e = \exp(-\beta t)e(0) \tag{3.3}$$

$$\dot{e} = \exp(-\beta t)\dot{e}(0) \tag{3.4}$$

After above calculation, we know that by choosing a suitable β_i system state can be closer to the expected state, but can never reach it. This is the disadvantage of the sliding mode manifold.

Designing the control law of the global sliding mode. To design the control law, we should first choose Lyapunov function:

$$V = \frac{1}{2}s^2 \geq 0 \tag{3.5}$$

According to the Lyapunov stability criterion, system state will go closer to sliding mode manifold s=0, when $\dot{V} < 0$. Thus, the differential coefficient of Lyapunov function (3.5) was taken to get:

$$\begin{aligned}\dot{V} &= s\dot{s} = s(\ddot{e}+\alpha\dot{e}+\dot{p}(t)(\dot{e}(0)+\alpha e(0)))\\ &= s(\ddot{\theta}-\ddot{\theta}_r+\alpha\dot{e}+\dot{p}(t)(\dot{e}(0)+\alpha e(0)))\\ &= s(\frac{T_e}{J}-\frac{T_L}{J}-\frac{B}{J}\dot{\theta}-\ddot{\theta}_r+\alpha\dot{e}+\dot{p}(t)(\dot{e}(0)+\alpha e(0)))\end{aligned} \tag{3.6}$$

The control law can be obtained by solving inequality $\dot{V}<0$. The control law of the global sliding mode control is as follows:

$$T=T_{eq}+T_{vs} \tag{3.7}$$

$$T_{eq}=B\dot{\theta}+J\ddot{\theta}_r-J\alpha\dot{e}-J\dot{p}(t)(\dot{e}(0)+\alpha e(0)) \tag{3.8}$$

$$u_{vs}=-Ksign(s) \tag{3.9}$$

In these equations,

$$K>D+\eta \tag{3.10}$$

$\eta>0$ and it is a positive constant.

Using Lyapunov function (3.5), we can demonstrate that this control law is stable. But this law requires that motor load and disturbance parameter should be known. In order to compensate for load and disturbance, and to maintain the stability of the system, K which is larger than real parameter is often chosen. Thus the chattering of control system is increased.

In this paper, a neural sliding mode control scheme is proposed for reducing or eliminating chattering of sliding mode control.

The neural sliding mode control

A neural network is applied in non-linear control because it can learn the controlled object by itself. In this paper, a radial basis function neural network (RBFNN) is applied.

RBF neural network.

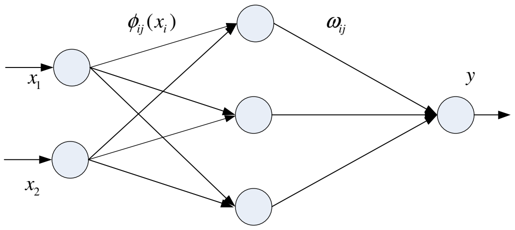

Fig 2 The structure of the RBF neural network

If the input of a RBF neural network is x and the output is h (x),

$$h(x)=\omega^T\phi(x)=u(x\,|\,\omega) \tag{4.1}$$

$\omega=[\omega^1,\omega^2,\cdots\omega^m]^T$ and it is regarded as weight of the RBF neural network. $\phi(x)=[\phi^1(x),\phi^2(x),\cdots\phi^m(x)]^T$ and it is a basis function. When a basis function uses the gauss function, its expression is as follows:

$$\phi^i(x)=\exp(-\frac{\|x-c_i\|^2}{\sigma_i^2}) \tag{4.2}$$

In this formula, m is the number of neuron in the hidden layer. c_i is the center of the radial basis function; σ_i is the width of the radial basis function.

The neural sliding mode control. Neural sliding mode control is the method of reinforcing the strengths of both the sliding mode control and the neural network. In this paper, the switch part of sliding mode control is substituted by neural network. Because neural network has the ability of self-learning, it can automatically compensate for the load and external interference. Therefore, the neural sliding mode control can change in response to the change of the load and external interference, thus reducing the chattering.

When the sliding mode control uses sliding mode manifold (3-1), the control law of neural sliding mode is as follows:

$$T = T_{eq} + T_N \tag{4.3}$$

$$T_{eq} = B\dot{\theta} + J\ddot{\theta}_r - J\alpha\dot{e} - J\dot{p}(t)(\dot{e}(0) + \alpha e(0)) \tag{4.4}$$

$$T_N = \omega^T \phi(x) = u(x \mid \omega) \tag{4.5}$$

In the formula, T_N is the output of neural network, $x = [s, \dot{s}]^T$ and it is the input of neural network. $\dot{\omega} = -\gamma s \phi(x)$ and it is the learning algorithm of the weight of the neural network.

The learning algorithm of the neural network. The learning goal of RBF neural network is the sum of the motor's load and disturbance. According to (3.6), $\dot{V} = s\dot{s} = 0$ when the goal of RBF neural network is achieved. The target function of all key neural networks is:

$$U = s\dot{s} = 0 \tag{4.6}$$

According to Gradient descent method, weight increment of the neural network is

$$\Delta\omega_{ij} = -\frac{\partial U}{\partial \omega_{ij}} = -\frac{\partial (s\dot{s})}{\partial \omega_{ij}} = -\frac{\partial (s\dot{s})}{\partial T_N}\frac{\partial T_N}{\partial \omega_{ij}} \tag{4.7}$$

$$\Delta c_{ij} = -\frac{\partial U}{\partial c_{ij}} = -\frac{\partial (s\dot{s})}{\partial c_{ij}} = -\frac{\partial (s\dot{s})}{\partial T_N}\frac{\partial T_N}{\partial c_{ij}} \tag{4.8}$$

$$\Delta\sigma_{ij} = -\frac{\partial U}{\partial \sigma_{ij}} = -\frac{\partial (s\dot{s})}{\partial \sigma_{ij}} = -\frac{\partial (s\dot{s})}{\partial T_N}\frac{\partial T_N}{\partial \sigma_{ij}} \tag{4.9}$$

According to (3.6) and (4.1), we know that

$$\frac{\partial (s\dot{s})}{\partial T_N} = s_i \frac{\partial (\dot{s})}{\partial T_N} = s \tag{4.10}$$

$$\frac{\partial T_N}{\partial \omega_{ij}} = \exp(-\left\| s - c_{ij} \right\|^2 / \sigma^2{}_{ij}) = \phi_{ij}(s) \tag{4.11}$$

$$\frac{\partial T_N}{\partial c_{ij}} == 2\omega_{ij}\phi_{ij}(s)(s - c_{ij}) / \sigma^2{}_{ij} \tag{4.12}$$

$$\frac{\partial T_N}{\partial \sigma_{ij}} = 2\omega_{ij}\phi_{ij}(s)\left\| s - c_{ij} \right\|^2 / \sigma^3{}_{ij} \tag{4.13}$$

The learning algorithm of the weight of the neural network is

$$\begin{aligned} \omega_{ij}(k) = {} & \omega_{ij}(k-1) + \lambda \vartriangle \omega_{ij} \\ & + \gamma[\omega_{ij}(k-1) - \omega_{ij}(k-2)] \end{aligned} \tag{4.14}$$

$$c_{ij}(k) = \omega_{ij}(k-1) + \lambda\Delta c_{ij} + \gamma[c_{ij}(k-1) - c_{ij}(k-2)] \tag{4.15}$$

$$\sigma_{ij}(k) = \sigma_{ij}(k-1) + \lambda\Delta\sigma_{ij} + \gamma[\sigma_{ij}(k-1) - \sigma_{ij}(k-2)] \tag{4.16}$$

λ and γ are the learning rate and the inertia coefficient, respectively.

Simulation study

Simulation test was performed using MATLAB, in order to confirm the feasibility of the designed controller. Parameters of BLDCM were set as follows: $B = 0.2$, $T_L = 10N\cdot\mathrm{m}$, $J = 0.6\mathrm{Kg}\cdot\mathrm{m}^2$. Parameters of the sliding mode for control were set as follows: $\alpha = 1$, $\beta = 1$. Neural network was made up of two input units, five hidden units and one output units. The learning rate of the neural sliding mode was 0.8, the inertia coefficient was 0.2, the initial weight of the neural network $\omega = [0.5\ 0.5\ 0.5\ 0.5\ 0.5]$, the initial width of the basis function $\sigma = [1\ 1\ 1\ 1\ 1]$ and the initial value of the basis function center $C = [-1\ -0.5\ 0\ 0.5\ 1]$.

When the initial state of the motor was as follows: $\theta = 1$ rad, $\dot{\theta} = 0$ rad/sec, and the target path of the motor was as follows: $\theta_r = \sin(t)$, Fig 3.6 is the simulation results.

We can see from simulation results that the sliding mode controller for brushless DC motors with uncertain external disturbances and unknown loads worked very well: reducing the chattering after 3 seconds of learning. The sliding mode controller, whose system robustness is well, is suitable for controlling brushless DC motors with uncertain external disturbances and unknown loads.

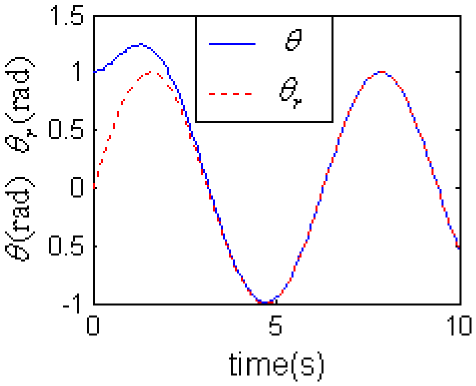

Fig 3 The movement path of the motor

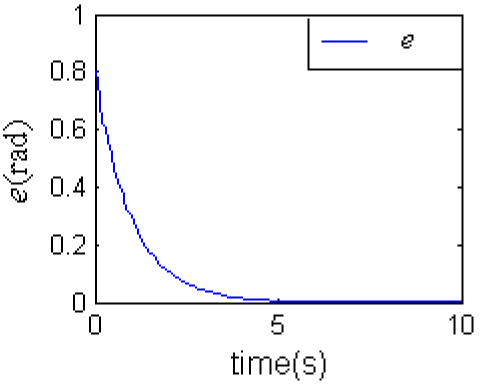

Fig 4 The error path of the motor

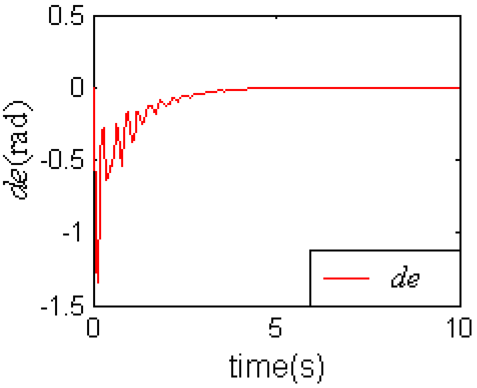

Fig 5 The speed error path of the motor

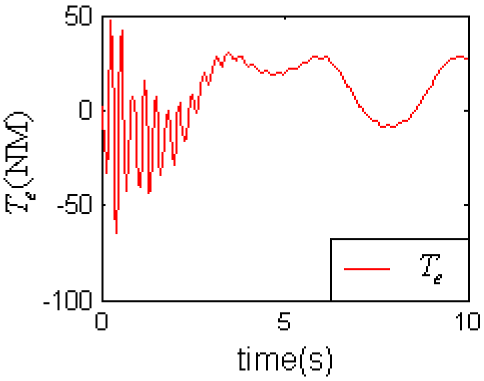

Fig 6 The output path of the controller

Conclusions

In this paper, a neural sliding mode control scheme is proposed for tracking and controlling the position of BLDCM. We reduced the chattering of the sliding mode controller by using a RBF neural network to study the load and disturbance. Simulation results proved that this control scheme is valid and feasible. But how to design the structure of the neural network and how to choose learning algorithm still remains to be studied.

References

[1] Zhao Shimian, Yue Jiguang, Han Shenglian. Fuzzy sliding mode control for Brushless DC motor [J]. Mechanical and Electrical Engineering. 2004, 33 (9): 60-61

[2] Ji Zhicheng, Xue Hua, Shen Yanxia. Fuzzy neural network control method for speed control system of the brushless DC motor [J]. Electric machines and control. 2004, 8 (1): 5-9

[3] Ji Zhicheng, Shen Yanxia, Jiang Jianguo. A new method for modeling and simulation of a Matlab brushless DC motor system [J]. Journal of system simulation.2003, 15 (12): 1745-1749, 1758

[4] Mu Xiaojiang. A global sliding mode for mechanical arm of a self-organizing neural network [J]. Computer measurement and control. 2013.21 (8): 2122-21242128

[5] Y. Yildiz, A. Sabanovic, K. Abidi.Sliding mode neuro-controller for uncertain systems[J].IEEE Trans.On industry and electronics.2007,54(3): 1676-1684.

Applied Mechanics and Materials Vol. 596 (2014) pp 590-593
© (2014) Trans Tech Publications, Switzerland
doi:10.4028/www.scientific.net/AMM.596.590

Time domain simulation for a 6 DOF tanker model in presence of waves

SUN Qiaomei[1, a], CHEN Jinguo[2,b]

[1]College of Mechanical & Power Engineering of China Three Gorges University, Yichang City, Hubei Province, China

[2]710th Research Institute of China Shipbuilding Industry Corporation, Yichang City, Hubei Province, China

[a]elita0411@163.com, [b]150321544@qq.com

Keywords: ship maneuverability; ship motion model; course control

Abstract. Modeling and control of marine vessels raised huge interests in recent years. Lots of articles provided many different mathematical modeling and dynamic control methods with advanced intelligent algorithms. In this paper we presented a 6 DOF dynamic model for a tanker vessel, investigated on its maneuverability and conducted numerical simulation experiments to show 6 DOF motion behavior of the vessel including position and orientation. And we discussed the turning ability of the vessel in simulation using a PID controller in the present of environmental waves.

Introduction

Marine vessels usually need to keep their course and speed constant on voyage when there is wave excitation. With development of science and technology, more and more advanced intelligent methods have been adopted. Marine vessels simulator are developed for automatic navigation. One of the most important factors for accurate vessel navigation simulation is dynamic model of the vessel. At present, most research institutes and universities of our country are studying 3 or 4 DOF modeling method. In the presents of big waves or current, it is necessary to build a 6 DOF model. Recently, many scholars and researchers investigated maneuvering and seakeeping performances with valuable results [1-7].

Two reference systems are commonly used to describe the position and orientation of marine vessel: earth-fixed and body-fixed system. The kinematic models describe transformation between these coordinates. Perez and Fossen provided a complete derivation of the transformation that links these descriptions [1].

In this paper, a mathematical motion model of 6 DOF for a tanker ship is established. In the presents of environmental waves, simulations experiments are conducted with results of vessel's position and orientation to show 6 DOF motion behavior.

Modeling method

The coordinate systems adopted here to describe the position and orientation of marine vessels: Earth-fixed and body-fixed systems. Six independent coordinates are necessary to describe 6-DOF motion of the ship:surge, sway, heave, roll, pitch and yaw.

The general motion of USV in 6 DOF can be described by Eq.1:

$$\begin{aligned}
&\eta=[\eta_1^T,\eta_2^T]^T,\eta_1=\left[x,y,z\right]^T,\eta_2=\left[\phi,\theta,\psi\right]^T,\\
&v=\left[v_1^T,v_2^T\right]^T,v_1=\left[u,v,w\right]^T,v_2=\left[p,q,r\right]^T,\\
&\tau=\left[\tau_1^T,\tau_2^T\right]^T,\tau_1=\left[X,Y,Z\right]^T,\tau_2=\left[K,M,N\right]^T
\end{aligned} \tag{1}$$

Where, η is used to describe the position and orientation vector with coordinates in the earth-fixed frame, v is the linear and angular velocity vector with coordinates in the body-fixed frame and τ is the vector of forces and moments acting on the vehicle in the body-fixed frame.

Based on MMG theory, forces and moments were separately calculated in Eq.2 to obtain the USV motion mathematical model of 6 degrees of freedom:

$$\begin{cases}(m+m_x)(\dot{u}+qw-vr)=X_H+X_P+X_R+X_{wd}+X_{wv}\\(m+m_y)(\dot{v}+ur-pw)=Y_H+Y_P+Y_R+Y_{wd}+Y_{wv}\\(m+m_z)(\dot{w}+pv-qu)=Z_H+Z_P+Z_R+Z_{wd}+Z_{wv}\\(I_{xx}+J_{xx})\dot{p}+(I_{zz}-I_{yy})qr=K_H+K_P+K_R+K_{wd}+K_{wv}\\(I_{yy}+J_{yy})\dot{q}+(I_{xx}-I_{zz})pr=M_H+M_P+M_R+M_{wd}+M_{wv}\\(I_{zz}+J_{zz})\dot{r}+(I_{yy}-I_{xx})pq=N_H+N_P+N_R+N_{wd}+N_{wv}\end{cases} \tag{2}$$

where, X_H , Y_H , Z_H , K_H , M_H and N_H are forces and moments on the bare hull, the variables with subscripts 'P 'or 'R' are forces and moments derived from propeller or rudder, the variables with subscripts '*wd*' or '*wv*' are derived from wind or waves, m_x , m_y and m_z are added mass corresponding to the longitudinal, transversal and vertical direction, I_{xx} , I_{yy} and I_{zz} are longitudinal, transversal and vertical moments of inertia around the center of gravity, J_{xx} , J_{yy} and J_{zz} are added longitudinal, transversal and vertical inertia moments around the center of gravity.
The generalized coordinate position vector is defined as:

$$\eta \triangleq [x,y,z,\phi,\theta,\psi] \tag{3}$$

A 6 DOF marine vessel equations of motion in a compact vectorial setting can be written as

$$\boldsymbol{M}\boldsymbol{v}+\dot{\boldsymbol{C}}(\boldsymbol{v})\boldsymbol{v}+\boldsymbol{D}(\boldsymbol{v})\boldsymbol{v}+\boldsymbol{g}(\boldsymbol{\eta})=\boldsymbol{\tau} \tag{4}$$

Where, $\boldsymbol{M}$, $\boldsymbol{C}$ and $\boldsymbol{D}$ denote the system inertia, Coriolis and damping matrices, $\boldsymbol{g}$ is a vector of gravitational and buoyancy, $\boldsymbol{v}$ is the body-fixed linear and angular velocity vector, $\boldsymbol{\tau}$ is a generalized vector of external forces and moments.

A systematic representation of a complex model is necessary for a good exploitation of the physics and a priori information of the system. It should be noted that the mathematical model descirbed by Eq.4 does not include the contribution of the environmental disturbances.Here we only consider the effect of wave disturbances.

In order to simulate the motion of ocean vehicles, in the presence of irregular waves we add the effect of Ist-order wave disturbances [3]. Let $\lambda = kB\sin(\chi)/2$, $\xi = kL\cos(\chi)/2$, then environment wave forces and moments are calculated as follows:

$$\begin{cases}X_{wv}=2\rho gae^{-kd}Bd\sin\left[k\frac{L}{2}\cos(\chi)\right]\sin(\omega_e t)\sin\lambda/\lambda\\Y_{wv}=-2\rho gae^{-kd}Ld\sin\left[k\frac{B}{2}\sin(\chi)\right]\sin(\omega_e t)\sin\xi/\xi\\Z_{wv}=\rho gake^{-kd}BdL\cos(\omega_e t)\sin\xi\sin\lambda/(\lambda\xi)\\K_{wv}=\rho gae^{-kd}d^2\sin(\chi)\frac{\sin\xi}{\cos(\chi)}\sin(\omega_e t)\sin\lambda/\lambda\\M_{wv}=\rho gaBe^{-kd}d\frac{2\sin\xi-kL\cos(\chi)\cos\xi}{k^2\cos^2(\chi)}\sin(\omega_e t)\sin\xi/\xi\\N_{wv}=\rho gae^{-kd}d\frac{2\sin\xi-kL\cos(\chi)\cos\xi}{k^2\cos^2(\chi)}\cos(\omega_e t)\sin(\chi)\sin\xi/\xi\end{cases} \tag{5}$$

where, $\rho$is the density of the seawater, g is the acceleration of gravity, α is the wave amplitude, k is the wave number, L is the length between perpendiculars of the ship, B is the breadth of the ship, d is the mean draft of the ship, χ is the encounter angle, ω_e is the encounter frequency. $a = h/2$, h is the wave height. $\chi = \psi - \mu$, ψ is the yawing angle of the ship in geo-coordinate, μ is the absolute wave angle. ω is the wave frequency, V is the velocity of the ship.

$$\begin{cases} \omega_e = \omega - Vk\cos(\chi) \\ \omega = \sqrt{gk} \\ V = \sqrt{u^2 + v^2} \end{cases} \tag{6}$$

PID controller

We use the conventional control method: PID controller[6]. the PID controller adopted here is represented as

$$\tau_N(s) = -K_p\left(1 + T_d s + \frac{1}{T_i s}\right)\tilde{\psi}(s) \tag{7}$$

Where, τ_N is the controller yaw moment, $\tilde{\psi}$ is the heading error, K_p is the proportional gain constant, T_d is the derivative time constant, and T_i is the integral time constant.

Simulation experiments:

The model of marine vessel is established under waves on SIMULINK. The vessel considered here is a tanker with parameters in Table 1.

Table 1 Main parameters of the tanker vessel

Draught[m]	Breadth [m]	Overall Length [m]	Mass[kg]	Volume displacement [m^3]
10	46	246	94620	92312

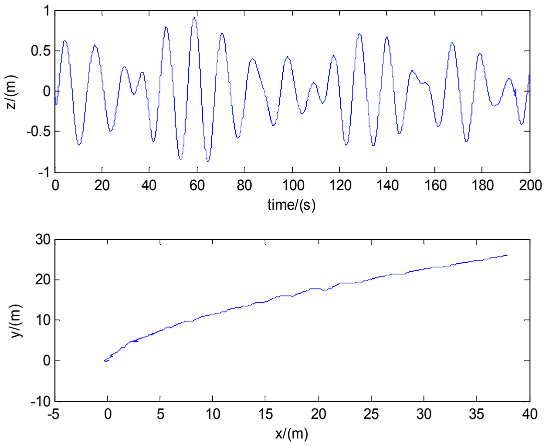

Fig. 1 x, y and z position of tanker vessel

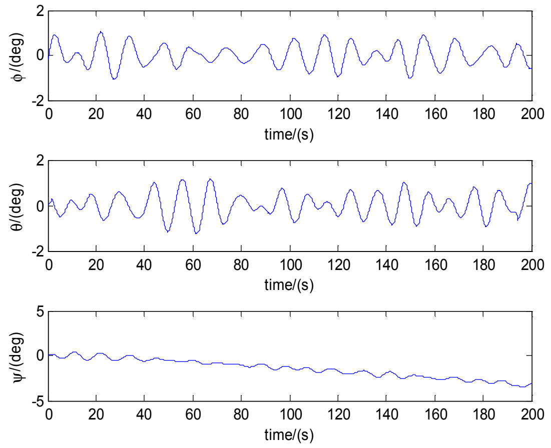

Fig. 2 Euler angles of tanker vessel

6 DOF real-time motion simulation of vessel position, Euler angles, velocities and anglar velocities are seperately shown in Fig.1, Fig.2, Fig.3, and Fig.4. 1st-order (Froude-Krylov and diffraction) wave loads are computed using potential theory. At first, the reference course was set to zero and change to 15 deg at time 30 s. PID controller is introduced and control simulation results are shown in Fig.5. Where ψ_1 denotes the heading angles generated by the kinematic model of the tanker, ψ_2 denotes the heading angles under waves excitation, ψ_3 denotes the heading angles after kalman filter.

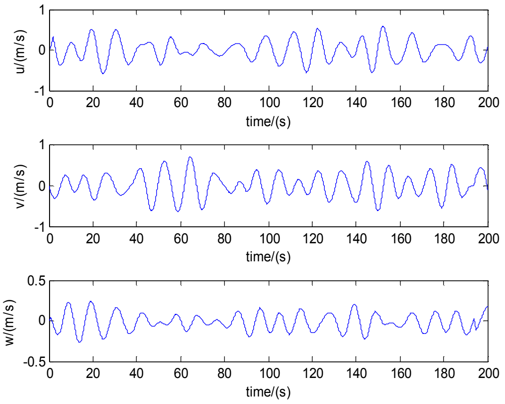

Fig. 3 Surge, sway, heave of tanker vessel

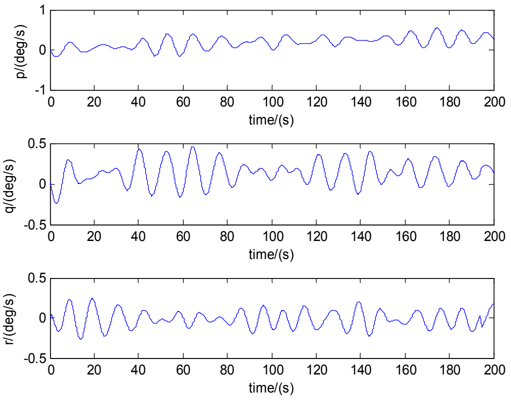

Fig. 4 Euler angle velocities of tanker vessel

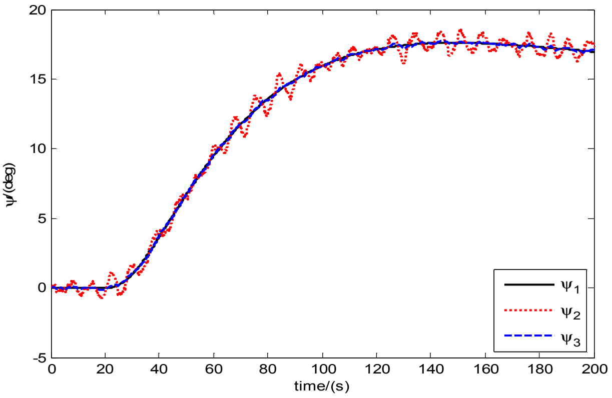

Fig. 5 Heading angle curve of the tanker vessel for turning course

Conclusions

In this paper, a 6 DOF mathematical modeling method for a tanker vessel was introduced and time-domain simulations in position and orientation were conducted. The turning course experiment results of heading angles under waves excitation using a PID controller show the effectiveness of the proposed modeling method. From the simulation results, the 6 DOF motion model can meet simulation accuracy requirement of ship maneuvering simulator and improve the fidelity of the large ship maneuvering simulator.

References

[1] T. Perez,T. I. Fossen: Modeling, Identification and Control. Vol 28 (2007), p.19–30.

[2] O. Egeland, J. Gravdahl. Modeling and Simulation for Automatic Control. Marine Cybernetics, Trondheim, 2002.

[3] T. Fossen. Marine Control Systems: Guidance, Navigation and Control of Ships, Rigs and Underwater Vehicles. Marine Cybernetics, Trondheim, 2002.

[4] T. Perez. Ship Motion Control: Course Keeping and Roll Reduction using rudder and fins. Advances in Industrial Control. Springer-Verlag, London, 2005.

[5] Z. Li, Y. Yang: Journal of Dalian Maritime University (Natural Science Edition), Vol 28 (2002), p.13-16.

[6] L. Moreira, T. I. Fossen, C. Guedes Soares:Ocean Engineering. Vol 34 (2007), p. 2074–2085.

[7] J. Zhu, Y. Pang, Y. Xu: Journal of Harbin Engineering University, Vol 25 (2004), p.1-5.

Applied Mechanics and Materials Vol. 596 (2014) pp 594-597
© (2014) Trans Tech Publications, Switzerland
doi:10.4028/www.scientific.net/AMM.596.594

The Approach for Analyzing Motion Mode of High-Order Control Systems

Shengguo Zhang[1, a], Kai Wang[1, b], Xiaoping Dang[2, c]

[1]School of Electrical Engineering, Northwest University for Nationalities, Lanzhou, 730030, China

[2]School of Continuing Education, Northwest University for Nationalities, Lanzhou, 730030, China

[a]zhangshengguo@tsinghua.org.cn, [b]63322567@qq.com, [c]gs_dxp@126.com

Keywords: Inverse Laplace Transformation, Zero-Pole Point, Modal Analysis, High-Order System.

Abstract: This paper aims at exploring the modal analysis approach of a motion control system. Based on the inverse Laplace transformation, the step response of a control system is derived. Then this response is associated with the modal analyses in state space theory. And then the motion mode of a control system is analyzed with the modal analysis method. Application example indicates that this approach can be used to analyze the high-order control system successfully. This facilitates the motion mode analyses of high-order control system very much.

Introduction

It is used to analyze the high-order control system via zero-pole point location in complex plane in classic control theory [1]. Using this method, the zero and pole points of control system transfer function have to be solved. It is convenient to the further analysis in frequency domain for the control system [2]. By this method, however, the time domain visibility of control system is poor and the motion mode of control system cannot be observed easily.

In this paper, the time domain response of high-order control system is introduced by the inverse Laplace transformation of the output in complex domain. And then this time domain response is associated with the motion modal of the control system. Last but not least, the motion mode of control system is analyzed based on the modal analysis. The application case is also given so as to formulate the motion mode analyzing approach.

Motion Mode Analyses of High-Order Control System

Time Domain Response of Control System. For a high-order control system, its mathematical model in complex domain, i.e. transfer function can always be represented as:

$$\Phi(s)=\frac{Y(s)}{R(s)}=\frac{b_0 s^m+b_1 s^{m-1}+\cdots+b_m}{a_0 s^n+a_1 s^{n-1}+\cdots+a_n},\ m\le n. \tag{1}$$

It can also be shown as product form:

$$\Phi(s)=\frac{Y(s)}{R(s)}=\frac{M(s)}{D(s)}=K\frac{\prod_{i=1}^{m}(s+z_i)}{\prod_{i=1}^{n}(s+p_i)}, \tag{2}$$

where z_i (i =1, 2, …, m) are zero points, p_i (i =1, 2, …, n) are pole points, and $K=b_0/a_0$ is the general gain of control system transfer function.

Giving system an unit step input $r(t)=1(t)$, i.e. $R(s)=1/s$, system output is:

$$Y(s)=\frac{K\prod_{i=1}^{m}(s+z_i)}{\prod_{l=1}^{q}(s+p_l)\prod_{k=1}^{r}(s^2+2\zeta_k\omega_k s+\omega_k^2)}\cdot\frac{1}{s}, \tag{3}$$

where $q+2r=n$, q is the number of real pole points, r is the number of conjugate complex pole pairs.

Assuming that $0 < \zeta_k < 1$, rewriting Eq. 3 to be the sum of partial fractions:

$$Y(s) = \frac{\alpha_0}{s} + \sum_{l=1}^{q} \frac{\alpha_l}{(s+p_l)} + \sum_{k=1}^{r} \frac{\beta_k(s+\zeta_k\omega_k) + \gamma_k(\omega_k\sqrt{1-\zeta_k^2})}{(s+\zeta_k\omega_k)^2 + (\omega_k\sqrt{1-\zeta_k^2})^2}, \tag{4}$$

where α_0 is the residue of output $Y(s)$ at pole point of input $R(s)$:

$$\alpha_0 = \lim_{s\to 0} sY(s) = \frac{b_m}{a_n}, \tag{5}$$

and α_l is the residues of output $Y(s)$ at real pole points p_l:

$$\alpha_l = \lim_{s\to p_l} (s+p_l)Y(s), \ (l = 1,2,\cdots,q), \tag{6}$$

and β_k and γ_k are the constants related to the residues of output $Y(s)$ at complex pole points p_k:

$$p_k = -\zeta_k\omega_k \pm j\omega_k\sqrt{1-\zeta_k^2}, \ (k = 1, 2, \cdots, r), \tag{7}$$

where $j = \sqrt{-1}$ is the imaginary unit.

Assuming all the initial conditions of system to be 0, by the inverse Laplace transformation of Eq.4, there gets the system time domain output, i.e. unit step response $h(t)$:

$$\begin{aligned} h(t) = \alpha_0 &+ \sum_{l=1}^{q} \alpha_l \, \mathrm{e}^{-p_l t} + \sum_{k=1}^{r} \beta_k \, \mathrm{e}^{-\zeta_k\omega_k t} \cos(\omega_k\sqrt{1-\zeta_k^2})t \\ &+ \sum_{k=1}^{r} \gamma_k \, \mathrm{e}^{-\zeta_k\omega_k t} \sin(\omega_k\sqrt{1-\zeta_k^2})t, \ t \ge 0. \end{aligned} \tag{8}$$

Motion Modals of Control System. On the basis of state space theory of control system, system output is dependent upon the system states besides upon system input [3]. And system states at any time *t* are decided by the state transition matrix $\phi(t)$, which is an exponential function square matrix of n-dimension [4]. For unequal real system eigenvalues λ_i of q number, this matrix can always be represented as:

$$\phi(t) = e^{At} = \begin{bmatrix} e^{\lambda_i t} & 0 & \cdots & 0 \\ 0 & e^{\lambda_i t} & \ddots & \vdots \\ \vdots & 0 & \ddots & 0 \\ 0 & \cdots & 0 & e^{\lambda_i t} \end{bmatrix}, \ (i = 1,2,\cdots,q), \tag{9}$$

For a pair of complex system eigenvalues $\lambda_i = \sigma_i \pm j\omega_i, \ (i = 1, 2, \cdots, r)$, this matrix can always be represented as:

$$\phi(t) = e^{Mt} = e^{\sigma_i t} \begin{bmatrix} \cos\omega_i t & \sin\omega_i t \\ -\sin\omega_i t & \cos\omega_i t \end{bmatrix}, \ (i = 1,2,\cdots,r), \tag{10}$$

where $e^{\lambda_i t}$ in Eq. 9 and $e^{(\sigma_i \pm j\omega_i)t}$ in Eq. 10 are defined as system's modals. And $\phi(t)$ can also be called modal matrix.

According to state space theory of control system, the system states, and then the system output are determined by the system modal matrix and modals.

System Motion Mode Analyses. Compared Eq. 8 with Eq. 9 and Eq. 10, there draws some conclusions about the output in time domain or the unit step response *h*(*t*) of a control system which is represented with Eq. 1 or Eq. 2:

1) The unit step response $h(t)$ consists of three parts: $h_1(t)=\alpha_0$, $h_2(t)=\sum_{l=1}^{q}\alpha_l \mathrm{e}^{-p_l t}$, and $h_3(t)=\sum_{k=1}^{r}\mathrm{e}^{-\zeta_k\omega_k t}[\beta_k\cos(\omega_k\sqrt{1-\zeta_k^2})t+\gamma_k\sin(\omega_k\sqrt{1-\zeta_k^2})t]$.

2) The first part $h_1(t)$ is completely dependent on the system input and it is the steady-state output part of the control system.

3) The second part $h_2(t)$ is dependent on the system modals $\mathrm{e}^{-p_l t}$ which are decided by the real pole points of the control system. This part includes all exponential decay modals and it is one dynamic output part of the control system.

4) The third part $h_3(t)$ is dependent on the system modals $\mathrm{e}^{[-\zeta_k\omega_k\pm j(\omega_k\sqrt{1-\zeta_k^2})]t}$ which are decided by the complex pole points of the control system. This part includes all sine oscillation and exponential decay modals. It is another dynamic output part of the control system.

5) The zero points of the control system cannot come into being any motion modals. But they influence the dynamic output parts $h_2(t)$ and $h_3(t)$. This is because the coefficients α_l, β_k, and γ_k are all interrelated to the zero points z_i of the control system.

By the analysis approach above mentioned, the control system motion mode including the stability, the dynamic performances, and the steady-state behaviors can all be analyzed.

Application Examples of Motion Mode Analysis for Control System

Original System and Its Motion Mode. Giving a high-order control system as original system studied in this paper. Its closed-loop transfer function is as Eq. 13 shown. It has four modals: real pole-point modals e^{-t} and e^{-15t}, and complex pole-point models $e^{(-1\pm j)t}$. It has two zero points: z_1 = -2 and z_2 = -3. The general system gain is 5. All eigenvalues of system modals have negative real parts so the system is stable. The system's unit step response is of exponential decay and sine oscillation but without overshoot. The steady-state value of system response is 1 and this response is shown in black solid line in Fig. 1.

$$\Phi(s)=\frac{5(s+2)(s+3)}{(s+1)(s+15)(s+1+j)(s+1-j)}. \tag{13}$$

Changed Systems and Their Motion Modes. First changed system is as Eq. 14 shown. Its real pole-point modal e^{-t} is changed to be e^{-10t} and the general system gain is changed from 5 to 50 so that the steady-state value is still 1. The unit step response is still sine oscillation and exponential decay yet there appears slight overshoot in response. This response is shown in blue dash line in Fig. 1.

$$\Phi_1(s)=\frac{50(s+2)(s+3)}{(s+10)(s+15)(s+1+j)(s+1-j)}. \tag{14}$$

Changing the complex pole-point modal from $e^{(-1\pm j)t}$ to $e^{(-1\pm j3)t}$ and the general system gain from 5 to 25, there gets the second changed system whose transfer function is as Eq. 15 shown. The steady-state value of the unit step response of this system is still be 1. However, system's sine oscillation and overshoot are both enhanced due to the altered complex pole-point modal. System's response is shown in red dot line in Fig. 1.

$$\Phi_2(s)=\frac{25(s+2)(s+3)}{(s+1)(s+15)(s+1+j3)(s+1-j3)}. \tag{15}$$

Altering system zero-point from z_1 = -2 to z_1 = -10 instead of altering system pole-point, and altering general system gain from 5 to 1, there gets the third changed system whose transfer function is as Eq. 16 shown. System's modals have not been changed. Yet the response is still slightly changed for the zero-point location can change the weight coefficients of all modals.

$$\Phi_3(s) = \frac{(s+10)(s+3)}{(s+1)(s+15)(s+1+j)(s+1-j)}. \tag{16}$$

As can be observed from Fig. 1, the motion mode of a control system is completely dependent on its modals. In fact, control system motion mode including stability, dynamic properties and steady-state behaviors can be understood in details with analytical modal analyses.

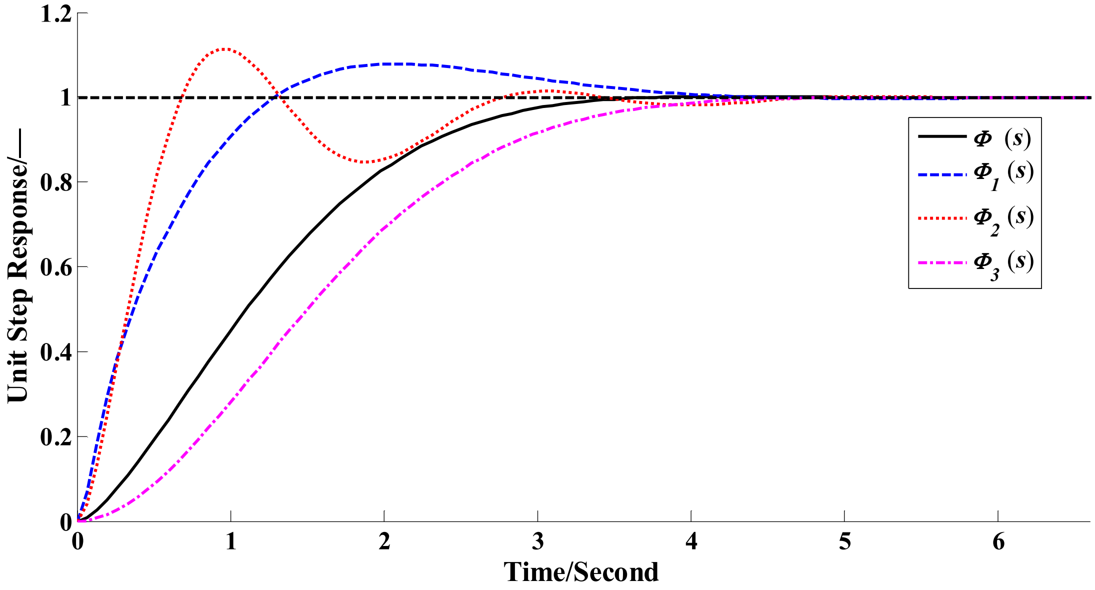

Fig. 1 The unit step response of system $\Phi(s)$, $\Phi\ (s)$, $\Phi\ (s)$, and $\Phi_3(s)$

Conclusions

This paper focused on the analysis approach of motion mode of high-order control systems.

(1) The pole points of control system define the motion modals and these modals determine the system's motion mode. System's zero points affect the system's motion mode slightly.

(2) The motion mode of a control system, which includes stability, dynamics performances, and steady-state behaviors, can all be analyzed by the approach of modal analyses expediently.

Acknowledgements

This work was financially supported by the Fundamental Research Funds for the Central Universities (31920140082) and the Introduction Talent Research Project of Northwest University for Nationalities (XBMUYJRC201301).

References

[1] J.X. Dong, C.D. Zhao: Control Engineering Fundamentals (First Ed., Tsinghua University Press, Beijing 1992)

[2] S.S. Hu: Automatic Control Principle(Fifth Ed., Science Press, Beijing 2007)

[3] A.M. Rankers: Machine Dynamics in Mechatronic Systems-An Engineering Approach. (PhD dissertation, Twente University 1997)

[4] B. Liu: Modern Control Theory (Third Ed.,China Machine Press, Beijing 2011)

Applied Mechanics and Materials Vol. 596 (2014) pp 598-601
© (2014) Trans Tech Publications, Switzerland
doi:10.4028/www.scientific.net/AMM.596.598

The design of valve block of Megawatt wind turbine hydraulic yaw system and AMESim simulation model

Jie Gao[1,a],Liwen Yan[1,a] , Cunjin Ai[1,a], Hui Xie[2,a]

[1]Tianjin Key Laboratory of High Speed Cutting &Precision Machining, Tianjin University of Technology and Education,300222 Tianjin, China

[2]Tianjin JingYan Construction Machinery Transmission Co.,Ltd,300222 Tianjin, China
[a]ylw618@163.com

Keywords:MW wind turbine,hydraulic system,UG,The design of valve block,AMESim

Abstract. In view of the current 1.5 megawatt wind turbine,this paper designs a set of corresponding hydraulic system,mainly including the system of pumping station valve block the main part by UG 3D software,the AMESim software is used to establish the yaw hydraulic system model and the analysis of the simulation.

Introduction

At present, in the domestic production of MW megawatt wind turbine, the hydraulic system has the following two functions, spindle brake hydraulic system and the yaw brake hydraulic system.Aiming at domestic a 1.5 MW wind turbine model, designed a set of corresponding new hydraulic system, and expounds the design process of the hydraulic system of pumping station,and analyses the results of the simulation which is the AMESim model of the yaw hydraulic system.During the analysis,by changing the pressure port orifice size,we can observe the movement of the yaw brake cylinders,find the optimal orifice size,yaw process can be ensured safe and reliable[1].

The working principle of the hydraulic system

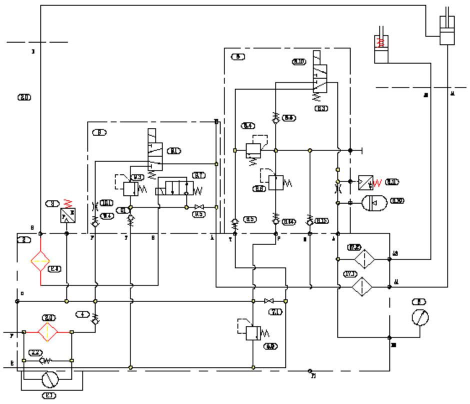

Figure1.The principle diagram of the hydraulic system

Above for the hydraulic system schematic diagram,mainly to accomplish two kinds of brake which are the yaw and spindle brake to multiply control.The function of the yaw system have yaw brake, yaw and unmoor.The yaw brake:when wind turbines is working,high pressure oil from the oil inlet P goes into the system, through the check valve 9.4 inflow of two-way solenoid valve 9.1,then 9.1

isn't charged, at the same time two two-valve 9.7 isn't charged too,high pressure oil flows into the yaw brake cylinder,brake is in a state of full suppress dynamic control， and brake is clamped to complete the yaw brake.The yaw:when the wind turbine needs the wind,9.1 is electric, 9.7 isn't electric,the oil in the yaw brake cylinder goes through the overflow valve 9.3 into the tank,brake is in a semi-state repression, yaw starts action.Untwisting: When the fan occurs cable winding,9.1 and 9.7 energize at the same time,the oil in the brake cylinder flows back into the fuel tank by 9.7,brake is in untwisting control, fan conducts untwisting.

Spindle brake: When the fan is working properly,the spindle brake is in a loose state， at this time two-way solenoid valve 8.3 is electric,when the spindle braking is required,8.3 loses electricity, the oil in the main shaft brake flows back to the fuel tank, under the action of spring force, fan high-speed shaft brake clamp, main shaft realizes to brake[2].

The design of the valve block of hydraulic system

Technical conditions of the system requirements are as follows:the maximum working pressure is16MPa,the minimum working pressure is 14MPa,the maximum pressure is 20MPa,spindle brake pressure is 10MPa,spindle brake pressure is 11MPa,residual pressure is 1.5MPa.

Channel, channel by the valve block design formula:

$$D \geq 4.61\sqrt{\frac{Q}{V_{max}}} \qquad (1)$$

D—the diameter of the pores,mm;Q—Maximum working flow of liquid flows in channels,L/min; $V_{\max}$ —The fluid in the pore flows maximum working flow

General working line recommended flow rate is 8 m/s, return pipe road recommends velocity of 4 m/s. Pump station of hydraulic pump flow rate is 1.5 L/min, so the oil hole in formula recommend standard 10 mm.

Wall thickness:Hole wall thickness according to formula (2) are checked, the actual wall thickness should be in the calculation basis appropriate to take larger.

$$\delta \geq \frac{pdn}{2\sigma_b} \qquad (2)$$

δ —Hole wall thickness;p—Channel maximum working pressure;d—Channel

diameter of pressure oil;n—Safety factor; σ_{b} —Material tensile strength of the valve block.

Yaw module is the system schematic diagram of the part inside the dotted box 9, its main function is completed yaw system needs that is three types of pressure control, yaw valve block size is 55 * 100 * 75 mm, and the design of the pipeline design is as follows[3].

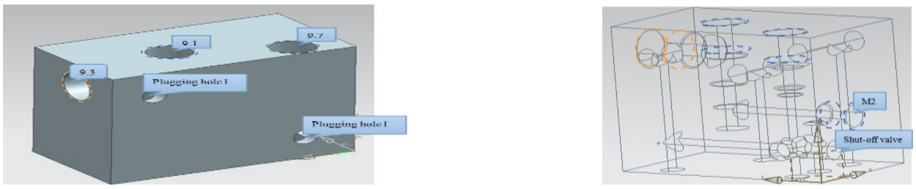

Fig. 2 Yaw valve block

AMESim simulation and study of yaw module

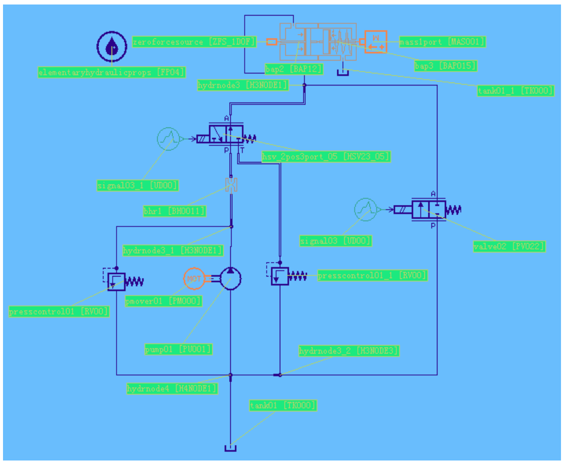
zeroforcesource [ZFS_1DOF]
masslport [MAS001]
elementaryhydraulicprops [FP04]
bap2 [BAP12]
bap3 [BAP015]
hydrnode3 [H3NODE1]
tank01_1 [TK000]
A
P
T
hsv_2pos3port_05 [HSV23_05]
signal03_1 [UD00]
bhr1 [BH0011]
A
P
signal03 [UD00]
valve02 [PV022]
hydrnode3_1 [H3NODE1]
MOT
presscontrol01_1 [RV00]
pmover01 [PM000]
presscontrol01 [RV00]
pump01 [PU001]
hydrnode3_2 [H3NODE3]
hydrnode4 [H4NODE1]
tank01 [TK000]

Figure 3. Yaw module model of hydraulic system

Established the AMESim model of the yaw's hydraulic system

This paper uses the LMS Imagine.lab AMESim Rev 10 and many other simulation softwares for designing the model,establishes the AMESim model of megawatt wind turbine yaw module of hydraulic system as shown in figure 3.Since this approach focuses on researching yaw brake hydraulic cylinder movement and the relationship between the oil inlet orifice size, so the fuel tank and the orifice are carried out by an independent selection and design by the hydraulic components' HCD designing library[4].

Parameter setting and system controlling

In grade 1.5 MW wind turbines,the yaw brake system need seven the brakes.A single brake hydraulic cylinder need two pieces of clip rein force of 162800 N and clamping force of 203500 N.The simulation model of the other parameters are set as follows in Table 1.

Table1 The main parameters of the simulation

The oil density	The oil viscosity	Bulk modulus	Pump delivery
900 Kg/m^3	40 mm^2/s	1700MPa	1.6 $L/\min$
The motor power	The opening pressure relief of valve1	The opening pressure relief of valve2	The large hydraulic cylinder piston
0.65 KW	21MPa	1.5MPa	125mm
The hydraulic cylinder path	The hydraulic cylinder stroke	Electromagnetic valve 1 flow	Electromagnetic valve 2 flow
62.5mm	10mm	11L	10L

The analysis of simulation results

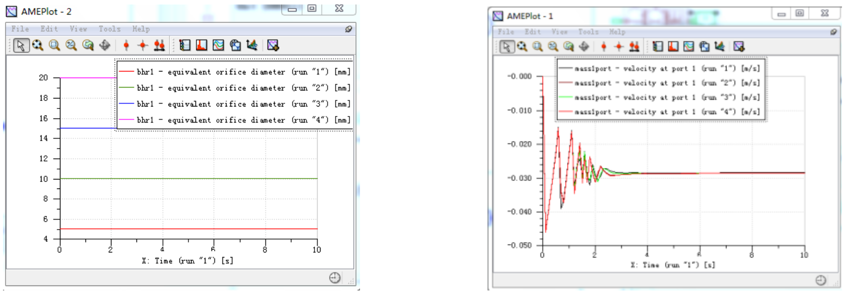

Figure 4. Mass velocity curves of different orifice size

Under certain load conditions,respectively takes throttling mouth size is 5 mm, 10 mm, 15 mm, 20 mm, studied in batch mode mass velocity curve, the result as shown in figure 4.Analysis shows that in the course of the initial 1.5s orifice size effect on the quality of the fast block velocity is not different,but the orifice size is 5mm, the sport is relatively stable and the smaller the impact on the system after 2s.Therefore, the choice of orifice size can be 5mm[5].

Conclusion

The use of hydraulic valve block is not only simplifies the design and achieves the integration and standardization of hydraulic system,reduces the manufacturing cost and improves the reliability of the system.Megawatt wind turbine hydraulic system valve block has many channel, and more complicated structure,the modeling function of UG 3d software effectively improves the work efficiency,shorten the design cycle, and easy to modify and validate.In the actual operation, it can be a reasonable choice of 5 mm, optimizes the system to make it run smoothly.

Acknowledgment

This work was financially supported by the Tianjin Special Program Fund (12ZCZDGX04100)and Tianjin jingyan Construction Machinery Transmission Co.Ltd. The authors would like to thank the anonymous reviewers for their valuable comments.

References

[1]Changsong Yuan: Characteristic simulation of hydraulic Damper and its Parametric design. An hui university of science and technology,Master's thesis, 2005(In Chinese).

[2] Wang:Study on and Identification of Electro-hydraulic Proportional Valve-motor System.Chang.an University,Xi.an,China.

[3]YuGan:Study on Identification and Control of Servovalve-Controlled Motor Control System. Shan dong University,Ji.nan,China.

[4]Fu Linjian,Wei Jianhua,Qiu Minxiu.Dynamic Characteristics of Large Flow Rating Electro-Hydraulic Proportional Cartridge Valve[J],Chinese Journal of Mechanical Engineering,2008,21 (6):56-62.

[5]Discussion Use of cartridge and screw-in valves in hydraulics[J],Oelhydrauik and Pneumatik,2001,45(8).

Applied Mechanics and Materials Vol. 596 (2014) pp 602-605
© (2014) Trans Tech Publications, Switzerland
doi:10.4028/www.scientific.net/AMM.596.602

Modeling for the Flow Coupled Secondary Hydraulic Lifting System of the Excavator Bucket

ZANG FAYE[1,2,a], WANG YONG[1,b], KONG XIANGZHEN[2,c]

[1] Department of Engineering Mechanical, Shandong University, Jinan 250061

[2]Shandong Jiaotong University, Jinan 250357

[a]zangfy@126.cm, [b] meywang@sdu.edu.cn, [c] kxzjnjx@163.com

Key words: excavator, flow coupled, lifting system, math model

Abstract. The flow coupled secondary hydraulic lifting system of the excavator bucket was presented, also its structure, working principle, and performances. The math model of the lifting system is established, using the math mode to control the hydraulic accumulator, and then realize process controlling of the energy recycling and reusing. Further, the system pressure range was expanded, the energy reusing effect and efficiency were improved.

Introduction

At present, the gravitation energy of the hydraulic lifting system of the excavator bucket is not usually recycled and reused when its bucket and load was working under lifting and falling down , which causes the energy waste and the environmental pollution. So a secondary hydraulic lifting system of the excavator bucket was presented, in which, the flow coupled secondary hydraulic transmission system was used to recycle and store the gravitation energy of the excavator bucket when its bucket and load was working under lifting and falling down, and reusing the energy when it was working, so the installation of the motor was induced to realize energy saving and environmental protection.

The structure and working principle

As shown in Fig.1, the system was made up of storage secondary components 2, control components 1 for storage secondary components, electromagnetic change valve 3, balancing valve 6, load secondary components 7, motor 8, control components 9 for load secondary components and load cylinder 10, and so on. The hydraulic storage components 4 and pressure limiting storage components 5 was connected parallel with storage secondary components 2, the high pressure oil of storage secondary components 2 was connected with the main hydraulic system of the excavator through electromagnetic change valve 3, the shaft of the storage secondary components 2 and load secondary components 7 were connected rigidly.

When the bucket began to fall, the high pressure oil of storage secondary components 2 was switched off connection with the main hydraulic system. The load secondary components 7 was adjusted to make it work under motor state, and also the storage secondary components 2 work under pump state. The lower chamber oil of load cylinder 10 flowed to load secondary components 7 rapidly in the influence of gravitation of bucket and gravity, the shaft of load secondary components 7 rotated to output torque and speed, and then drive the storage secondary components

2 working in pump state to transport high pressure oil for the hydraulic storage components 4 and pressure limiting storage components 5. The hydraulic storage components 4 was refueling in order from lowest to highest setting pressure, if the storage secondary components 2 no longer delivered high pressure oil or little, the refueling was end, otherwise, the refueling would be continued until reaching to the limited pressure of pressure limiting storage components 5. So by controlling the accumulator, the energy recycling was realized, this would ensure higher oil pressure of the accumulator, the reusable effect was improved.

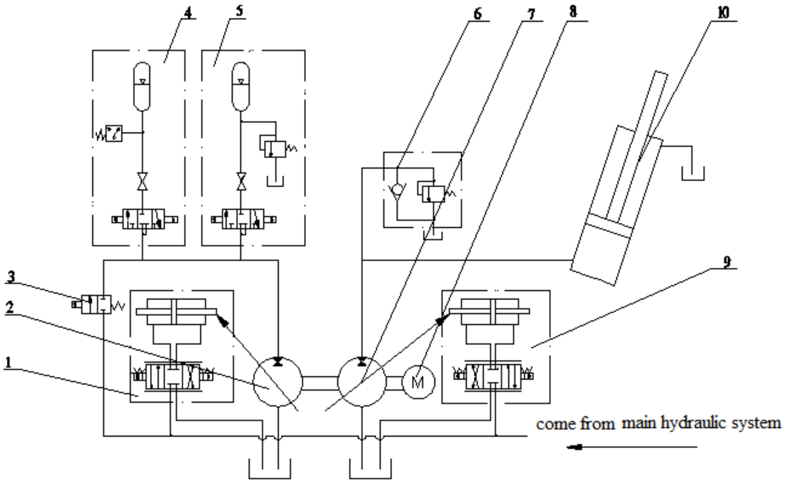

Fig.1 The system structure diagram

When the bucket began to lift, the high pressure oil of storage secondary components 2 was connected with the main hydraulic system. The storage secondary components 2 was adjusted to make it work under motor state, and also the load secondary components 7 work under pump state. The high pressure oil was discharged from hydraulic storage components 4 and pressure limiting storage components 5 to drive storage secondary components 2, it would rotate with the motor to drive the load secondary components 7 jointly, and then they provided power for load cylinder 10 to lift bucket and load. In working, one or more hydraulic storage components 4 and pressure limiting storage components 5 could be controlled in accordance with the weight of bucket and load, lift speed. So, by controlling the hydraulic accumulator to realize the energy reuse, and the energy reuse efficiency was improved.

Math model for the Flow Coupled Secondary Hydraulic Lifting System

The system worked in load lifting and falling state.

Math model for lifting

(1) math model of the electro-hydraulic servo valve

Usually, the natural frequency of servo valve is very high, and the bandwidth of the controlled hydraulic system is lower, so the electro-hydraulic servo valve can be acted as a proportional component, as following:

$$\frac{Q_{sf}(s)}{I(s)} = K_v \qquad (1)$$

Here, K_v is flow gain of the servo valve（(m^3/s）/A）, Q_{sf} is output flow of the servo valve（m^3/s）, I is input current of the servo valve （A）.

(2) math model of the lifting system

1）the continuity equations of load secondary components 7 and load cylinde

$$D_1 n = A_c \frac{dy}{dt} + C_{pc} p_1 + \frac{V_0}{\beta_e} \frac{dp_1}{dt} \tag{2}$$

Here, D_1 is volume（m^3/rad）, n is motor speed (r/s), A_c is the piston effective area（m^2）, y is piston displacement（m）,C_{pc} is total leakage coefficient of load secondary components 7, p_1 is the load cylinder pressure of rod chamber（Pa）, V_0 is the volume of rod chamber at median（m^3）, β_e is oil bulk modulus.

2) balance equation of load cylinder and load

$$A_c P_1 = m_1 \frac{d^2 y}{dt^2} + B_c \frac{dy}{dt} + m_1 g + f \tag{3}$$

Here, m_1 is the total mass of load, piston rod and piston components（kg）, y is the displacement of piston rod（m）, B_c is viscous damping coefficient, f is friction force of piston components and cylinder cube, piston rod and orientation cover and sealing rings（N）.

3) input flow of storage secondary components 2 working in motor q_2

$$q_2 = D_2 n + C_{ta} p_2 + \frac{V_{ta}}{\beta_e} \frac{dp_2}{dt} \tag{4}$$

Here, D_2 is volume（m^3/rad）, C_{ta} is total internal leakage coefficient（($m^3 \cdot s^{-1}$)/Pa）, p_2 is pressure between accumulator and secondary components 2（Pa）, V_{ta} is the total volume from secondary components 2 to accumulator（m^3）.

4) output torque of storage secondary components 2 working in motor T_{ac}

$$T_{ac} = \frac{p_2 q_2}{2\pi\eta_2} \tag{5}$$

Here, η_2 is efficiency of secondary components 2.

5) balance equation of accumulator

$$(p_a - p_2) A_{ac} = m_{ac} \frac{d\left(q_2 / A_{ac} \right)}{dt} + \frac{BdV_a}{A_{ac} dt} \tag{6}$$

Here, p_a is the working pressure of accumulator（Pa）, A_{ac} is the cross-sectional areas of chamber (m^2), m_{ac} is oil mass of pipes and accumulator（kg）, B is viscous damping coefficient, V_a is volume of the accumulator (m^3).

6) input torque of load secondary components 7 working in pump

$$T_{cp} = T_{ac} - T_f \tag{7}$$

Here, T_f friction torque（N • m）.

Math model for falling

(1) the motion equations of load cylinder 10

$$m_1 g = m_1 \frac{d^2 y}{dt^2} + B \frac{dy}{dt} + p_1 A_c + f \tag{8}$$

(2) continuity equations of load secondary components 7 working in motor

$$A_c \frac{dy}{dt} = D_1 n + C_{tc} p_1 + \frac{V_0}{\beta_e}\frac{dp_1}{dt} \tag{9}$$

(3) output torque of load secondary components 7 working in motor

$$T_{cp}^{'} = \frac{p_1 q_1}{2\pi\eta_1} \tag{10}$$

Here, η_1 is the total efficiency of secondary components 7

(4) continuity equations of storage secondary components 2 working in pump

$$D_2 n = q_2 + C_{ta} p_2 + \frac{V_{ta}}{\beta_e}\frac{dp_2}{dt} \tag{11}$$

(5) balance equation of accumulator

$$(p_2 - p_a)A_{ac} = m_{ac}\frac{d\left(q_2 / A_{ac}\right)}{dt} + \frac{BdV_a}{A_{ac}dt} \tag{12}$$

(6) input torque of storage secondary components 2 working in pump

$$T_{ac}^{'} = T_{cp}^{'} + T_m - T_f \tag{13}$$

The continuity equation was the same for the accumulator working under load lifting and falling.

Conclusions

The flow coupled secondary hydraulic lifting system of the excavator bucket, when it worked in non-constant pressure network, compared to the pressure coupled of constant pressure network, its pressure range was expanded. So by controlling the accumulator, the energy recycling was realized, this would ensure higher oil pressure of the accumulator, the reusable effect was improved.

Acknowledgement

This work was supported by Shandong province natural science foundation (ZR2011EEM032).

References

[1] Y.H.LIU, J.H.JIANG. Matching power of flow coupled system with secondary regulation. Journal of Nanjing University Science and Technology, 2007, 31(6):701-705.

[2] J.B.Hu, X.L.Guo and S.H.Yan. Dynamic characteristics of hydrostatic secondary control load simulation system and the approach to resist load disturbance[J]. Transactions of the Chinese Society for Agricultural Machinery,Vol.39(2008),p:150-153.

[3] YU Ancai, J.H.JIANG.. Research on energy recovery control of a hydraulic hybrid excavator[J]. Journal of Harbin Engineering University, 2012, 33(1):91-95.

[4] M.Y. Kim, CO. Lee: Control Engineering Practice. Vol. 14(2006), p. 137.

Applied Mechanics and Materials Vol. 596 (2014) pp 606-609
© (2014) Trans Tech Publications, Switzerland
doi:10.4028/www.scientific.net/AMM.596.606

3D Geometric Modeling of Francis Turbine Blades Based on Wooden Patterns and UG Software

Lei Lu[1, a *], Lida Zhang[1, b]

[1]College of Energy and Environment, Xihua University, Chengdu, Sichuan, 610039, China

[a]abclulei2009@163.com, [b]zlida@126.com

Keywords: Blades, UG, Wooden patterns, 3D modeling, Characteristic surface intersecting lines.

Abstract. To quickly and easily get a smooth and accurate 3D model of blades, This paper was based on the two-dimensional wooden patterns of the existing francis turbine blades in "AutoCAD", by importing UG software platform, directly translating two-dimensional lines to get three-dimensional wooden patterns, without calculating the spatial coordinates of distribution points on the blade section lines, obtaining the optimized smooth pressure sides and suction sides of the blades by characteristic surface intersecting lines, after partial rounding and sewing the sheets, the process of three-dimensional modeling of blades was finally completed. This takes a solid foundation for hydraulic performance prediction and CFD numerical simulation analysis of the francis turbine. The blade modeling method described in this article has some reference value.

Introduction

Francis turbine runner usually consists of the crown, the rim and a number of blades, the shape and number of blades affect the runner performance extremely greatly, and blade shape is particularly complex, which brings a very great difficulty to the geometric modeling and product manufacture. The blade surface is an unstructured, spatial warping, freeform surface, uneven surfaces are easily made when carrying out 3D modeling, as well as the distortion may occur, so an accurate and smooth blade model is difficult to get.

Wooden patterns are a traditional engineering diagram in the hydraulic machinery industry. The traditional blade modeling has four main steps: a. Obtain X, Y, Z coordinates of control points on the contours of the blade surface according to 2D wooden patterns, import the coordinate data file into UG, 3D wooden patterns of blades are obtained; b. Convert 3D wooden patterns into the form of curve meshes; c. Create a surface feature; d. complete the solid modeling of blades. This method is due to determine the 3D coordinates, bringing about a large workload. Nevertheless, "UG" and "AutoCAD" have a good interface, by importing 2D wooden patterns into UG, the 2D lines can be directly used to carry out 3D modeling, without inputting 3D spatial coordinates of distribution points on section lines of the blade in UG. This will not only improve work efficiency, avoiding that rounding off the large amount of decimal numbers generates error, but also get 3D model of the blades about higher accuracy and better smoothness. Through the special processing method of UG software to smooth blades, the smooth 3D model which be very consistent with 2D wooden patterns is got. This article seeks to use this method to complete the solid modeling of turbine blades.

Blade boundary of pressure side and suction side

Wooden patterns of blade. In an example of a certain francis turbine runner blade, its wooden patterns include the meridional section curves diagram and contour section lines diagram of the blade, as shown in Figure 1. In Figure 1, the left part is the axial projection of the blade, which is obtained by that the true blade projects onto a plane vortically and taking the runner shaft as the rotation axis, a set of parallel horizontal lines indicate the position of the contour sections in the direction of "Z". The right part is the plane view of some contour section lines, in which "i-i" is the contour sectional diagram on the position "i" of the blade surface, it represents the outer contour of the cross section of the blade on "Zi". In order to ensure the accuracy of the blade shape, more twisted the blade position is, more the number of cross-section is.

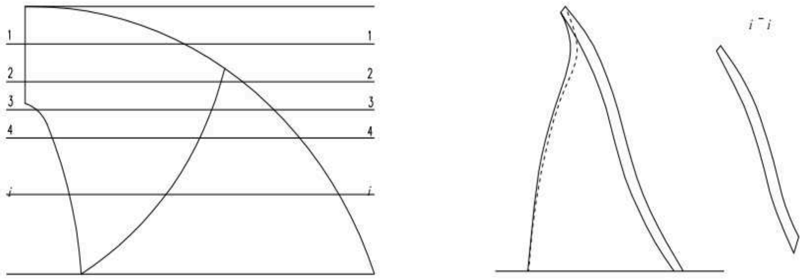

(a) Meridional section curves diagram

(b) Plane view of some contours

Fig.1 Wooden patterns of francis turbine runner blade

Import wooden patterns of blade. The above-described 2D wooden patterns are imported into UG software, the specific operation process: "file"→"import"→"DXF/DWG"→"confirm". Then every section curve is moved on the corresponding axial projection drawing, the approximate profile of the blade can be obtained, as shown in Figure 2. As can be seen in Figure 2, all contours of blade have been at a corresponding position, but the crown and the intersecting tip area of the rim and the outlet side is not complete, so supplementing these two portions is required.

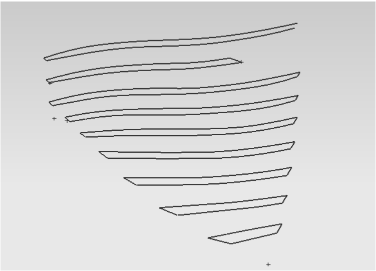

Fig.2 The space diagram of section lines on francis turbine blade

Generation of blade boundary about pressure side and suction side. The crown and the intersecting tip area of the rim and the outlet side on blade border is difficult to draw. If the points on the pressure side and suction side of the blade are directly connected by B-spline curve, the incomplete situation will appear. Therefore, the shape and position of the border are determined by using the axial plane projection in wooden patterns, the missing parts are supplemented, a complete blade frame diagram is got, as shown in figure 3. In figure 3, the complete blade border have been drawn, and each contour section curve is already in corresponding place, but according to the current functionality of UG software, the accurate and smooth pressure side and suction side of blade are not disposablely generated, therefore, the further processing needs to be done.

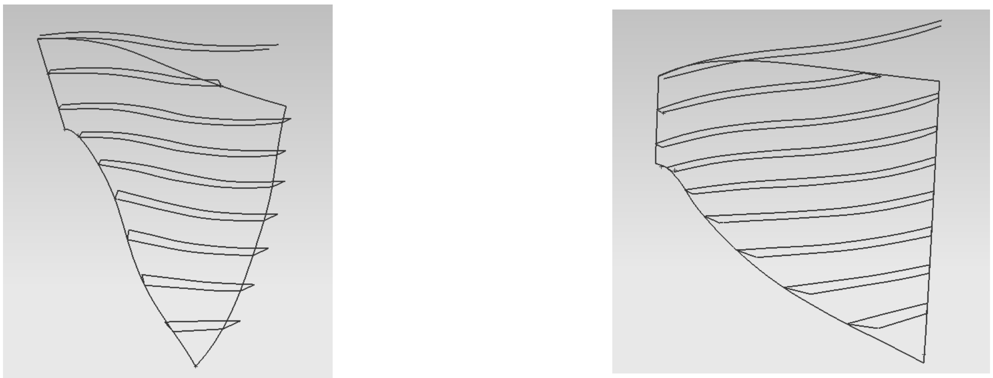

(a) Boundary frame of blade pressure

(b) Boundary frame of blade suction side

Fig.3 Boundary frame of runner blade

Characteristic surface intersecting lines of pressure side and suction side of the blade

In the process of generating the pressure side of blade first, the boundary frame is transformed into a surface by the command "curve mesh" of UG, as shown in figure 4. Since the generation process relies only on constraints of the border about pressure side, by lack of contour curves in wooden patterns, the resulting pressure side and original diagram have a large difference in shape. In figure 4, the first generated surface and the contours don't coincide completely, it needs a surface finishing.

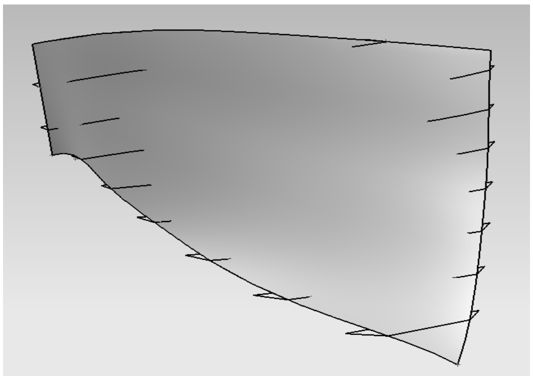

Fig.4 The first generated pressure side of francis turbine blade

Using the principle of characteristic surface intersecting lines, the surface coinciding with wooden patterns well can be obtained. First, use the command "curve group" to create a mesh surface which passes through contour section lines of the blade pressure side, the initial shape is finished. Secondly, create meridional section meshes on the direction "U" and "V" according to the blade axial projection, these meshes as the generatrices rotate around the central axis of runner into a surface, this surface and the just created initial shape of the blade pressure side intersect, a group of the 3D meshes "U" and "V" are got, as shown in figure 5. By the adjustment of the local grid lines, the extension of grid lines endpoints, the slope and curvature correction of endpoints, the curve mesh of the blade pressure side is finally obtained, as shown in figure 6, the curve mesh and contours all have intersection points, so they coincide with the blade wooden patterns very well. In this example, there are 18 three-dimensional grid lines "U" and 40 grid lines "V". These grid lines "U" and "V" are from the intersection of the rotated surfaces about meridional section meshes and the initial shape about the blade pressure side, so they are called as "characteristic surface intersecting lines". After getting characteristic surface intersecting lines of the blade pressure side, characteristic surface intersecting lines of the blade suction side are gotten in the same way, by the use of these curves, the 3D blade model with high accuracy can be obtained.

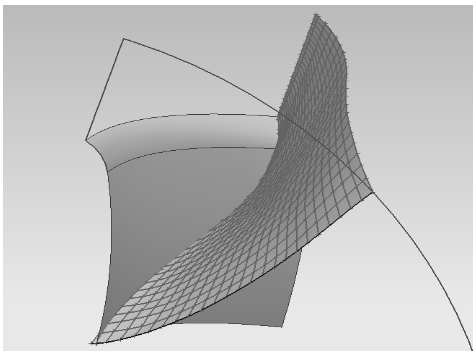

Fig.5 Rotated surface of meridional section curve

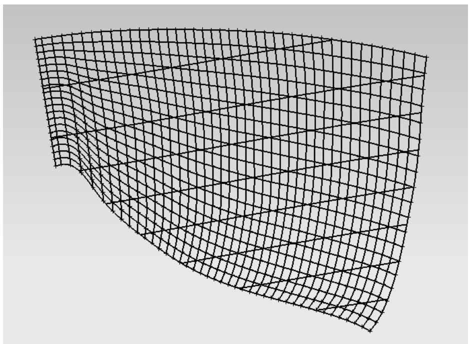

Fig.6 Characteristic surface intersecting lines of the blade pressure side

Completing solid modeling of blades

After all characteristic surface intersecting lines are generated, a smooth curved surface is relatively easy to got by the command "curve mesh" in UG, and the surfaces obtained have a high coherency with wooden patterns, the sheet of the blade pressure side is showed in figure 7. If the resulting surface smoothness is not very good, more characteristic surface intersecting lines of "U" and "V" can be generated on the pressure side and suction side, until the resulting surface smoothness meets the requirement. Then the surfaces of the crown, the rim, the inlet and the outlet are respectively generated by the command "ruled surface", after stitching each individual blade surface, the rough entity is got. Through rounding out the blade head and tail, the whole 3D solid model of this blade example is ultimately obtained, as shown in figure 8. So far, the entire modeling process from 2D wooden patterns to 3D blade model is completed.

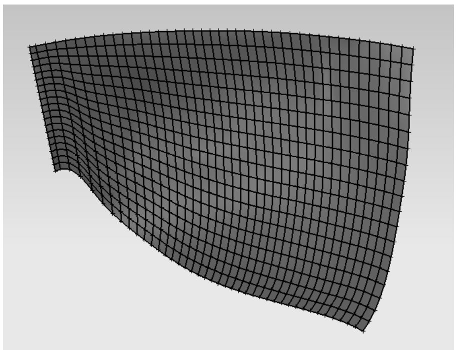

Fig.7 Blade sheet of the pressure side generated by characteristic surface intersecting lines

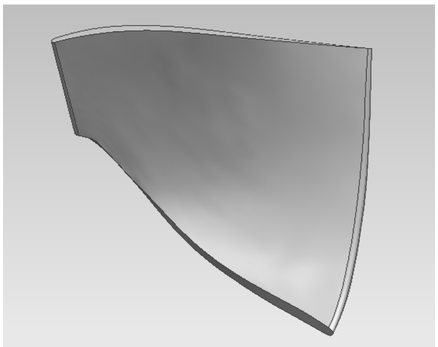

Fig.8 The finally generated smooth blade solid model

Conclusions

(1) The shape of francis turbine runner blades is very complex, to get a smooth and accurate three-dimensional model is difficult, but by UG's special treatment, the accuracy and smoothness of 3D model obtained can be improved.

(2) The excellent three-dimensional solid model of the blade provides a solid foundation for the performance analysis of francis turbine units. Meanwhile, more accurate wooden patterns can be obtained by the backstepping, so that the manufacturing error of turbine blades is greatly reduced, the consistency of the turbine hydraulic performance and design values is improved.

Acknowledgements

This work was financially supported by the Innovation Fund of Postgraduate, Xihua University (No. : ycjj2014174).

References

[1] Shikui Wang, Bo Yu, Xiaochun Tian, et al. Francis turbine blades of 3-D modeling based on UG[J]. Machinery Design and Manufacture, 2013, (3):231-233. (In Chinese)

[2] Jie Deng, Rui Chen. Design and example of hydraulic machinery about UGS NX[M]. Beijing: China WaterPower Press, 2009. (In Chinese)

[3] Qiang Du, Jianghai Lin, Xiuting Wei, et al. Development of 3D solid modeling system for centrifugal pump impeller vane based on UG NX[J]. Machine Tool and Hydraulics，2010，38(21):114-116, 140. (In Chinese)

[4] Hongwei Wang, Xiaobing Liu, Yongzhong Zeng. 3D geometry modeling of francis turbine runner with long and short blades[J]. Water Resources and Power, 2010, 28(3):121-123. (In Chinese)

[5] Shihua He, Lixiang Zhang, Liang Wu, et al. Numerical model of francis turbine runner blades[J]. Hydraulic Electrogenerating, 2005, 31(3):54-55. (In Chinese)

[6] Zhongcheng Gui, Shenghua Wang, Qiang Chen, et al. Modeling and analysis of a francis turbine runner blade[J]. Big Motor Technology, 2006, (5):36-40. (In Chinese)

Applied Mechanics and Materials Vol. 596 (2014) pp 610-615
© (2014) Trans Tech Publications, Switzerland
doi:10.4028/www.scientific.net/AMM.596.610

Power Spectra Density Replication Control Strategy for 2-axis Hydraulic Shaker Based on Hv Estimator

Yu Chen[1,a], Qiangli Luan[1,b], Zhangwei Chen[1,c] and Huinong He [2]

[1]The State Key Lab of Fluid Power Transmission and Control, Zhejiang University, Zhejiang Hangzhou 310027, China

[2]Hangzhou ECON Science and Technology Co., LTD, Zhejiang Hangzhou 310015, China

[a]zju_cyu@163.com, [b]luanqiangli@163.com, [c]chenzw@zju.edu.cn

Keywords: Hv estimator; frequency response function estimation; step-varying and frequency-sectioning iterative correction; PSD replication.

Abstract. Hydraulic shaker, equipment of simulating laboratory vibration environment, can accurately replicate the given power spectral density (PSD) and time history with an appropriate control algorithm. By studying method Hv estimator of frequency response function (FRF) estimation, a FRF identification strategy based on the Hv estimator is designed to increase the convergence rapidity and improve the system response function specialty. The system amplitude-frequency characteristics in some frequency points or frequency bands have large fluctuation. To solve this issue, a step-varying and frequency-sectioning iterative correction control algorithm is proposed for the control of 2-axial exciter PSD replication tests and the results show that the algorithm has a good effect on the control of hydraulic shaker, and can achieve reliable and high-precision PSD replication.

Introduction

Vibration tests are used to detect product environmental vibration reliability. It's important for exposing product design defects and timely improving product structure. At present, a lot of vibration environment tests are performed with single axial vibration test method [1,2]. As the research of large space structures, slender structures such as pipeline and irregular civil structures such as curved bridges increasing, single axial tests limitations are increasingly understood to people. Multi-axis vibration tests can overcome the disadvantages, such as inadequate thrust, uneven distribution of vibration stress existing in single axial vibration tests [3]. Compared with single axial vibration tests, multi-axial tests can more truly simulate the practical vibration environment.

Trubert proposed a multi-exciter random vibration test in 1968 [4]. This method calculated input signal auto-spectral density (ASD) using the matrix-inverse of the measured system frequency response matrix. Later, Smallwood and Underwood published articles expounding the theory of random vibration tests control [5,6], then domestic and foreign scholars did in-depth research to perfect the multi-input multi-output (MIMO) random tests control theory. PSD replication tests are widely used in civil engineering, aerospace and vehicle engineering etc. Product and its key components reliability is tested by replicating reference spectrum on hydraulic shaker. Control technology is important to achieving this goal. The control technology is based on the FRF estimation, whose accuracy affects the rapidity and stability of the control process. FRF estimation methods generally contain H1, H2 and Hv method [7]. Based on studying Hv estimator, 2-axis hydraulic shaker control scheme on the basis of drive ASD iterative correction algorithm is designed. Through 2-axis random vibration test, the results show that the algorithm has a good effect on the control of hydraulic shaker, and can achieve reliable and high-precision PSD replication.

Multi-axis vibration system FRF estimation using Hv estimator

Random vibration test control at home and abroad is mainly based on the inverse of FRF. FRF measurement is one of the factors that affect control effects, and system error is mainly from input and output measurement, such as noise interference and signal processing, such as leakage error.

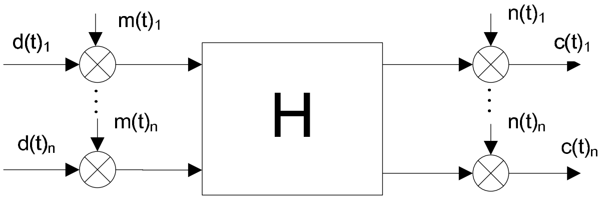

Figure 1. MIMO system model

Figure 1 shows a typical MIMO system model. A mathematical model description of the system would look like:

$$C(f)-N(f)=H(f)(D(f)-M(f)) \tag{1}$$

Where $C(f)$ and $D(f)$ are the vectors of spectra of the respective control and drive signals, $H(f)$ is the system-under-test's frequency response matrix, and $M(f)$ and $N(f)$ are vectors of spectra of the respective input and output noise signals.

There has been a great deal of research on reducing the influence of random noise on system. Nowadays the commonly adopted FRF estimation methods are H1, H2 and Hv estimator. H1 estimator assumes that there is no noise existing in input signal measurement, and the output noise spectra and input signal spectra are unrelated, thus the H1 estimator can't eliminate the influence of input noise and proves to be underestimated. H2 estimator assumes that there is no noise existing in output signal measurement, and the input noise spectra and output signal spectra are unrelated, thus the H2 estimator can't eliminate the influence of output noise and proves to be overestimated [7]. In the actual system, noise exists both in the input and output end. Hv estimator considers the influence of input and output noise on the FRF estimation and it has an advantage of replicating PSD with high precision in a shorter time. The control equation (1) can be expanded by:

$$C(f)-H(f)D(f)=N(f)-H(f)M(f) \tag{2}$$

Multiply equation (2) by their respective conjugate transpose, and then consolidate to get the matrix-vector notation form as:

$$\begin{bmatrix}-I & H(f)\end{bmatrix}\begin{pmatrix}G_{cc}(f) & G_{cd}(f)\\ G_{dc}(f) & G_{dd}(f)\end{pmatrix}\begin{bmatrix}-I\\ H^*(f)\end{bmatrix}=\begin{bmatrix}-I & H(f)\end{bmatrix}\begin{pmatrix}G_{nn}(f) & G_{nm}(f)\\ G_{mn}(f) & G_{mm}(f)\end{pmatrix}\begin{bmatrix}-I\\ H^*(f)\end{bmatrix} \tag{3}$$

Where the control vector $C(f)$ becomes an auto-spectral density (ASD) which we call $G_{cc}(f)$, the drive vector becomes drive ASD which we call $G_{dd}(f)$, the input noise vector becomes input noise ASD $G_{mm}(f)$ and the output noise vector becomes output noise ASD $G_{nn}(f)$. $G_{cd}(f)$ and $G_{dc}(f)$ are the cross-spectral density (CSD) between the control response and drive vectors, $G_{nm}(f)$ and $G_{mn}(f)$ are the CSD between the input and output noise vectors. $H(f)^*$ is the conjugate matrix of $H(f)$. If the noise spectrum is zero, the system meets the minimum error condition [8], so equation (3) can be described as follows:

$$\begin{bmatrix}-I & H(f)\end{bmatrix}\begin{pmatrix}G_{cc}(f) & G_{cd}(f)\\ G_{dc}(f) & G_{dd}(f)\end{pmatrix}\begin{bmatrix}-I\\ H^*(f)\end{bmatrix}=0 \tag{4}$$

define $V=\begin{bmatrix}-I\\ H^*(f)\end{bmatrix}$ and $U=\begin{pmatrix}Gyy(f) & Gyp(f)\\ Gpy(f) & Gpp(f)\end{pmatrix}$, equation (4) can be simplified as:

$$V^*UV=0 \tag{5}$$

According to matrix theory, when matrix V becomes the eigenvector of matrix U, equation (5) is satisfied. The eigenvalues and eigenvectors of matrix U can be acquired by doing matrix U eigenvalue decomposition. The eigenvectors are combined into matrix V, and then the frequency response matrix can be extracted from matrix V. This method is called Hv estimator [9].

Hv estimator is used in object modeling process to realize initial transfer function identification. To improve the system identification precision, we need conduct continuous identification and average overall processing to meet the required precision. The iterative correction algorithm is used in the identification process. During control process, the system impedance function $Z(f)$, which is the inverse of $H(f)$, is used as the controller transfer function for effectively controlling the physical model.

Multi-axis random vibration tests control

Multi-axis random control target is to keep the control spectrum and the reference spectrum consistent, and the control strategy is one of the key technologies in multi-axis random vibration tests [10]. PSD replication control algorithm can be described in block form as shown in Figure 2. The drive ASD is corrected by system impedance function and the deviation of the reference and response spectrum. With this algorithm, the system response spectrum can accurately replicate the reference spectrum. Due to the existence of limited bandwidth and nonlinearity, the estimated amplitude-frequency characteristics had great fluctuation in some frequency points and frequency bands before correction [11], so the drive PSD step-varying and frequency-sectioning iterative correction is used to weaken the fluctuation influence on convergence rapidity and accuracy.

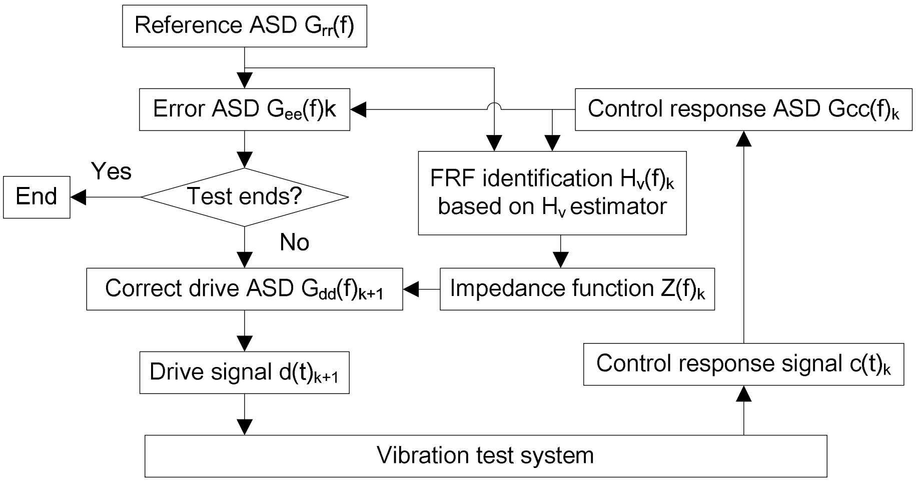
Reference ASD $G_{rr}(f)$
Error ASD $G_{ee}(f)k$
Control response ASD $Gcc(f)_k$
Yes
End
Test ends?
No
FRF identification $H_v(f)_k$ based on H_v estimator
Correct drive ASD $G_{dd}(f)_{k+1}$
Impedance function $Z(f)_k$
Drive signal $d(t)_{k+1}$
Control response signal $c(t)_k$
Vibration test system

Figure 2.Principle of the control algorithm of PSD replication

Multi-axis random vibration PSD replication algorithm can be divided into the following six steps:

(1) Identify the system initial FRF $H_v(f)_0$.

(2) Calculate the system impedance function $Z(f)_0$, which is the inverse of $H(f)_0$. Thus the system impedance function is given by:

$$Z(f)_0 = H_v^{-1}(f) \tag{6}$$

(3) Measure system control signal $c(t)_0$ under a given drive ASD $G_{dd}(f)_0$, and then compute the associated ASD $G_{cc}(f)_0$ of the control signal. The initial drive and control response ASD needs to be given by:

$$G_{dd}(f)_0 = Z(f)_0 G_{rr}(f) Z^*(f)_0 \tag{7}$$

$$G_{cc}(f)_0 = FFT(c(t)_0) \tag{8}$$

(4) Calculate the system kth error ASD $G_{ee}(f)_k$ by deviation of reference and control ASD. The error ASD is given by:

$$G_{ee}(f)_k = G_{rr}(f) - G_{cc}(f)_k \tag{9}$$

(5) Conduct step-varying and frequency-sectioning correction using the system impedance function $Z(f)_k$ and error ASD. The algorithm is described as:

$$G_{dd}(f)_{k+1}=G_{dd}(f)_k+\alpha Z(f)_k G_{ee}(f)_k Z(f)_k^* \tag{10}$$

Where, α is the drive ASD correction vector and $\alpha=\{\alpha_i, i=1,...,N\}$, N is signal frame length of Fourier analysis and $0<\alpha_i<1$. The correction coefficient α_i varies with different frequency specialty during ith iteration. When the amplitude-frequency characteristics in a certain frequency band is stable, α_i takes a value from 0.75 to 0.95, but when the characteristics have great fluctuation, α_i takes the value of less than 0.75.

(6) Convert the corrected drive spectrum into drive signal by passing through frequency domain randomization and time domain randomization successively. The drive signal generation process is illustrated in Figure 3 [12].

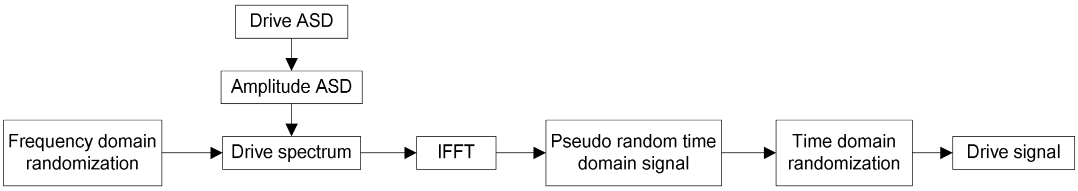
Drive ASD
Amplitude ASD
Frequency domain randomization
Drive spectrum
IFFT
Pseudo random time domain signal
Time domain randomization
Drive signal

Figure 3. Drive signal generation process

The generation process can be divided into the following four steps:

(1) Decompose the drive ASD $G_{dd}(f)$ into drive matrix $D'(f)$ in Cholesky method in the form as:

$$G_{dd}(f)=D'(f)D'^*(f) \tag{11}$$

Where $D'(f)$ is a lower triangular matrix. It contains amplitude frequency information and no phase information.

(2) Allocate random phase to elements in columns of matrix $D'(f)$ to complete frequency domain randomization, so we get the drive spectrum as:

$$D'(f)=D'(f)e^{j\theta_i}\ (i=1,...n) \tag{12}$$

where the random phase θ_i is subjected to Gaussian distribution.

(3) Transform the drive spectrum with IFFT into a pseudo random time domain signal $D'(t)$ as follows:

$$D'(t)=IFFT\left[D'(f)\right] \tag{13}$$

(4) Convert the pseudo random signal $D'(t)$ into a true random signal $D(t)$ passing through stochastic delay, reverse, windowing and overlay successively.

Multi-axis Random Test System Setup and Operation

For further verifying the control effect of Hv estimator and drive ASD iterative correction algorithm on multi-axis random test system, a 2-axis hydraulic shaker of the State Key Laboratory of Fluid Power Transmission and Control, Zhejiang University, shown in Figure 5, is selected as the test object, and the shaker parameters are shown in Table 1.

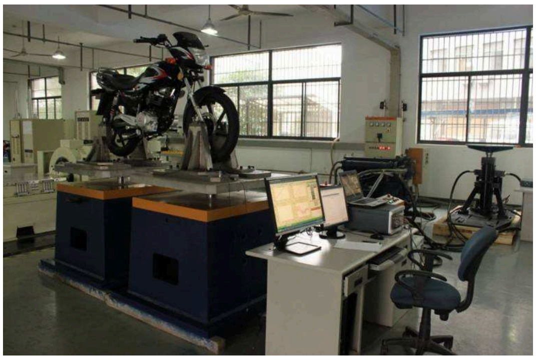

Figure 5. 2-axis random test system

Table 1. Parameters of the 2-axis hydraulic table

Item	Technical parameters
Mesa mass	80Kg
Mesa dimension	1m×1m
Load	100Kg
Exciter working areaA_p	1.5×10^{-3} m^2
Rated displacement	0.112m

In actual tests, the reference PSD at the two control points is set from 5 to 80 Hz, and the two reference spectrum has the same ASD while their CSD phase difference is 0 degree and their correlation coefficient is set to 1. The system transfer function estimated based on Hv estimator is shown in Figure 6. It's obviously seen that the amplitude-frequency characteristics in low frequency are smooth, but their linearity is poor in high frequency. This is because Hv estimator can effectively improve the low frequency characteristic by considering the actual input and output noise. However, specimen structure resonance exists in high frequency, so the estimated frequency response function smoothness is poor.

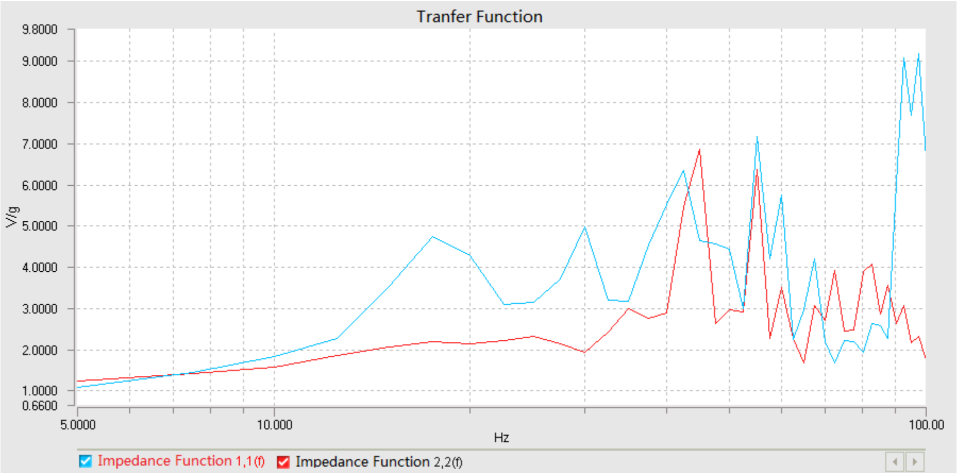

Figure 6. Amplitude-frequency characteristics of Hv estimator

The resulting control PSD magnitude, for each of the 2 control points is shown in Figure 7. The reference spectrum from 5 Hz to 20 Hz and 45 Hz to 65 Hz is flat, from 20 Hz to 40 Hz is rising, and from 65 Hz to 100 Hz is falling. The RMS of the two reference spectrum is 0.1g, and the phase difference of the CSD is 0 degree. From figure 6, we know that the amplitude-frequency characteristics have great fluctuation after 34 Hz, so the correction coefficient α_i takes 0.85 at the frequency band before 34 Hz, andα_i takes 0.6 after 34 Hz.

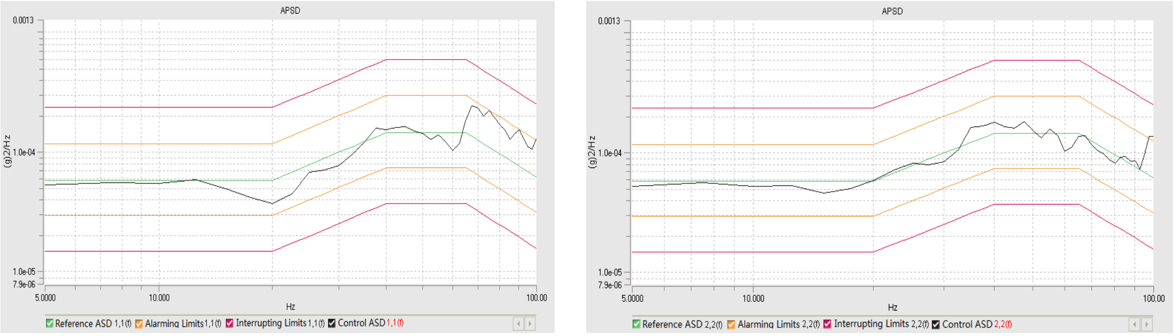

(a) PSD replication in control point 1 (b) PSD replication in control point 2

Figure 7. 2-axis hydraulic shaker control PSDs

Figure 7 shows that the two control channels' deviation of response and reference spectrum is controlled within ±3dB. The step-varying and frequency-sectioning iterative correction algorithm based on Hv estimator has a good control effect on PSD replication and can ensure a high precision.

Conclusions

The precision of FRF estimation is one of the significant factors that affect multi-axis random tests control. This paper firstly analyzed MIMO random system model and theory of FRF estimation, and then proposed a drive spectrum iterative correction control algorithm on the basis of Hv estimator. Hv estimator has an advantage in considering the system input and output noise, rapid convergence rate and high precision. The PSD replication tests on 2-axis hydraulic shaker show that the algorithm has good effects on the system, and can achieve reliable and high-precision PSD replication.

References

[1] Yanhua Wang, Wenrang Cheng. Dynamic Property of A Shaking Table Simulation Earthquake in Chinese. Journal of Vibration and Shock. Vol.29(2012), p.99-106.

[2] Zhenyun Tang, Zhenbao Li, Jinbao Ji. Development in Shaking Table Control System in Chinese. Journal of Earthquake Engineering and Engineering Vibration. Vol.29(2009), p.162-169.

[3] Xudong He, Huaihai Chen, Fan Shen. Control Research on Double Vibration Random exciting in Chinese. Journal of Vibration Engineering. Vol.19(2006), p.145-149.

[4] Trubert, M.R. An Analog Technique for the Equalization of Multiple Electromagnetic Shakers for Vibration Testing. Journal of Spacecraft. Vol.5 (1968), p.1438-1443.

[5] Smallwood D.O. Random Vibration Testing of A Single Test Item with A Multiple Input Control System. Proceeding of the Institute of Environmental Sciences. Atlanta, Georgia:IES (1982), p.42-49.

[6] Underwood, M.A., Keller T. Recent System Developments for Multi-Actuator Vibration Control. Sound and Vibration. Vol. 35 (2001), p.16-23.

[7] Zhidong Yang, Guangfeng Guan, Dacheng Cong. Frequency Response Function Estimation for Three Axes Hydraulic Shaking System by Using Hv Algorithm in Chinese. Journal of Earthquake Engineering and Engineering Vibration. Vol.27(2007), p.83-87.

[8] Stoten DP, Shimizu N. The Feedforward Minimal Control Synthesis Algorithm and Its Application to the Control of Shaking-Tables. Proceedings of the Institution of Mechanical Engineers, Part I:Journal of Systems and Control Engineering.Vol. 221(2007), p.423-444.

[9] Zhaohua Wang, Guangfeng Guan, Dacheng Cong. All Phase FFT Spectrum Analysis in Chinese. Journal of China Institute of Communications. Vol.24(2003), p.16-19.

[10] Kazuyoshi Ueno, Yoshikado Yamauchi. Measuring System for Transfer Function Matrix of A System to Be Controlled in Multi-Degree of Freedom Vibration on Control. U.S. Patent 9,304,669.(2002)

[11] Xuli Cui, Huaihai Chen, Xudong He. All-Phase Hv Frequency Response Function Estimation for MIMO Random Vibration Test control in Chinese. Journal of Vibration Engineering. Vol.24(2011), p.181-185.

[12] Jiayan Chen, Haidong Wang, Zhangwei Chen. Progress in Multi-Exciter Vibration Testing Control Technology in Chinese. Journal of Vibration and Shock. Vol.30(2011), p.69-73.

Applied Mechanics and Materials Vol. 596 (2014) pp 616-619
© (2014) Trans Tech Publications, Switzerland
doi:10.4028/www.scientific.net/AMM.596.616

Numerical Simulation of Seismic Wave Propagation in Different Media

Feng Zhi Ren
Institute of Engineering Mechanics, China Earthquake Administration, Harbin 150080, China
ceafzr@yeah.net

Keywords: Seismic Waves, Wave Propagation, Numerical Simulation, Geophysics

Abstract. Theory of elastic waves layered homogeneous medium or even medium for the study can not meet the actual demand for seismic exploration, especially for fine rock to construct reservoirs for the study, had to consider small-scale heterogeneity of seismic wave propagation effects. In this thesis, multi-scale model of a complex medium, in ensuring the premise to further improve simulation accuracy simulation efficiency issue, the introduction of a variable grid numerical simulation techniques, and were analyzed for different types of grid difference, establish a different media model simulation results verify the validity of simulation and analyzes its efficiency and accuracy problems.

Introduction

Traditional seismic wave simulation techniques are generally based on the theory of elasticity homogeneous medium or layered medium is analyzed in solving complex reservoir heterogeneity strong there will be some limitations. Coupled with this non-homogeneous body along with complex multi-faults, and other geological formations thin interceded undoubtedly seismic forward modeling technique presents a more severe test. In the conventional method of numerical simulation of seismic waves, geometrical ray method because the only description of kinematic characteristics of seismic waves can not describe the dynamics, the problem of how to achieve the accurate calculation of complex three-dimensional medium reservoir when traveling and so on at the same time, making geometric ray characteristics of seismic wave propagation method has not detailed study of complex media. Therefore, based on the development of the theory of non- homogeneous seismic forward modeling approach is very necessary.

Theoretical Basis of Seismic Waves

In the actual elastic medium, elastic parameters of seismic waves can be seen as a function of position coordinates Cartesian coordinate system, formation density is generally believed that little change, you can use a constant value instead. Staggered grid finite difference method based on the conventional grid finite difference method to introduce further half grid point, the distribution of the different elastic parameters staggered on different grid points, the advantage is to solve the velocity component coupled with the stress components relationships. Under the assumption of zero-premise physical items, they can be expressed as: (stress and displacement) equations of motion:

$$\begin{cases} \dfrac{\partial \sigma_{xx}}{\partial x} + \dfrac{\partial \sigma_{xy}}{\partial y} + \dfrac{\partial \sigma_{xz}}{\partial z} = \rho \dfrac{\partial^2 u}{\partial t^2} \\ \dfrac{\partial \sigma_{yx}}{\partial x} + \dfrac{\partial \sigma_{yy}}{\partial y} + \dfrac{\partial \sigma_{yz}}{\partial z} = \rho \dfrac{\partial^2 v}{\partial t^2} \\ \dfrac{\partial \sigma_{zx}}{\partial x} + \dfrac{\partial \sigma_{zy}}{\partial y} + \dfrac{\partial \sigma_{zz}}{\partial z} = \rho \dfrac{\partial^2 w}{\partial t^2} \end{cases} \tag{1}$$

First time component in the form of differential staggered, design stress component $u(t)$ and the velocity components $v_x(t)$, respectively, in $t+\Delta t/2$ and t discrete time difference using Taylor expansion 2M order accuracy can be obtained time difference approximation

$$u\left(t+\frac{\Delta t}{2}\right)=u\left(t-\frac{\Delta t}{2}\right)+2\sum_{m=1}^{M}\frac{1}{(2m-1)!}\left(\Delta t/2\right)^{2m-1}\frac{\partial 2^{m-1}}{\partial t 2^{m-1}}u+\ldots \tag{2}$$

$$v_x\left(t+\Delta t\right)=v_x\left(t\right)+2\sum_{m=1}^{M}\frac{1}{(2m-1)!}\left(\Delta t/2\right)^{2m-1}\frac{\partial 2^{m-1}}{\partial t 2^{m-1}}v_x+\ldots \tag{3}$$

Where Δt is the time step. In order to avoid the type of higher order derivatives with respect to time in the discrete differential complexity of the derivative of the available space, said the wave equation. So that when the numerical simulation, you can spend hours at a time of stress (speed) to calculate the time the stress field next time field, does not need too much time involved in computing layer.

Simulation Method

Numerical simulation of seismic waves in the implementation process, focal treatment is one of the key links. Source can be divided into centralized power source to inspire and decentralized power source with the direction of shear wave effect. Select the source wavelet is very important in the numerical simulation of seismic waves in general, choose wideband, short duration wavelets, but if we consider the actual effect of excitation can also choose the minimum phase wavelet. In the numerical simulation of earthquake waves are the most common sub- Ricker wavelet, mainly having a relatively wide frequency band, there is only one peak duration is short, the advantages of simulation accuracy is relatively high. Ricker wavelet mathematical expression is

$$F=\left(1-2\pi^2 f^2 t^2\right)e^{-\pi^2 f^2 t^2} \tag{4}$$

The minimum phase wavelet:

$$F=t\sin(2tft)e^{-3.5ft} \tag{5}$$

Here f is the frequency wavelets. In order to verify the effect of the various excitation source, the design speed of 2500 $m\ /\ s$ in the homogeneous medium model, using 30Hz Ricker wavelet as the source wavelet. Fig.1 shows the different time differential precision numerical dispersion with $\Delta t/T$ curve. Time difference discrete numerical dispersion effect produced will gradually diminish.

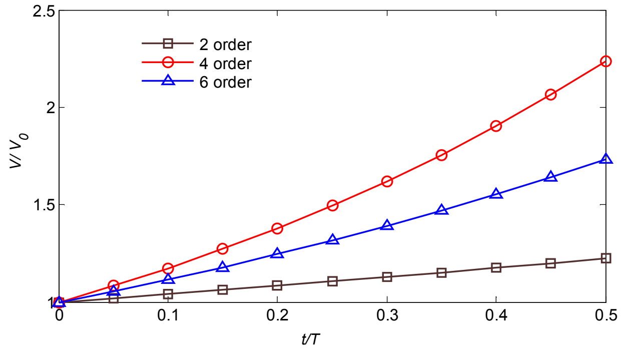

Figure.1 Different time difference precision numerical dispersion curve

Simulation Results

A reasonable choice of absorbing boundary conditions is the key to obtaining accurate numerical simulation effects. As shown in Figure holes media model. Round holes located in the central model radii 1m, 3m, within the pores medium speed of 1500 ms. Variable grid simulation in the vicinity of the circular holes using small-scale grid spacing 3m × 3m, other regions with large -scale grid step size is 6 m × 6m, while the conventional grid -scale grid with a single discrete. Numerical simulation methods are used to stimulate the explosion epicenter stimulate points located (900 m, 690 m), recording point is located (1200 m, 690 m).

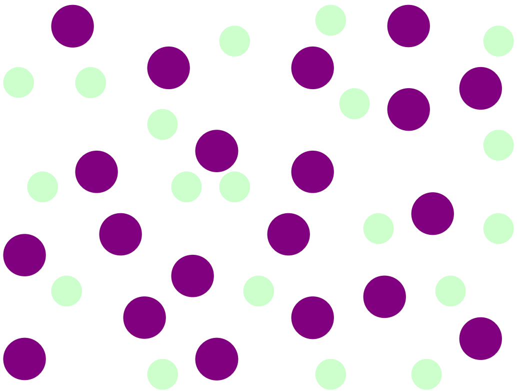

Figure.2 Medium model with holes

Due to different reasons scale grid spacing, different grid spacing of the velocity field of discrete manner, so that different sampling intervals resolution size wave field there are also differences in the results of conventional fine mesh grid simulation and change the most good, but at the expense of conventional fine mesh to calculate the expense of efficiency, to ensure the accuracy of the simulation premise becomes more conducive grid numerical simulation of seismic wave simulation. Another change from the conventional fine mesh grid analog recording and comparative analysis found that single-channel recording single-channel recording with variable grid conventional fine mesh simulations basically the same.

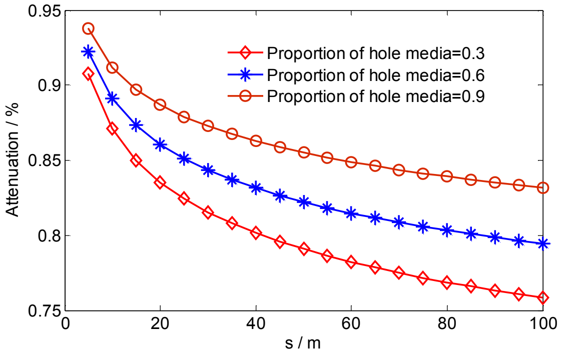

Figure.3 With holes medium model seismic wave propagation

Fig.4 shows the sand lenses and conventional media model simulation variable grid staggered staggered grid and numerical simulation of wave field snapshot recording. As can be seen from the lens body wave snapshots, the thickness unevenness of the low-speed sand, causing a wave front tilt direction while the focusing effect of the recessed portion of the sand so that low energy of the reflected wave in the wave field enhancement snapshot at a point.

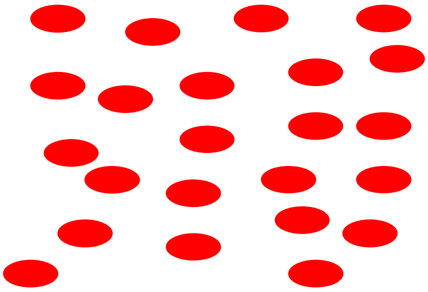

Figure.4 Sand lenses medium model

Intrusive media model variable staggered grid with conventional staggered wave field numerical simulation and numerical simulation snapshot recording. Variable grid with wave field amplification in a small-scale grid section, a variable grid and fine grid treated roughly the same in the simulation accuracy. The top portion of the high-speed interface invade the body with energy diverging action, so that the transmitted energy is weak, and the multiple reflection inside the high-speed, the horizontal axis so that with the appearance of the interface energy of the reflected wave discontinuities. Sonic and viscous acoustic single-channel recording, a relatively viscous sonic sound waves are recorded waveform distortion, along with the deepening of the seismic wave propagation depth, this waveform distortion effect is more obvious. Sonic and viscosity of the amplitude spectrum of the reflected acoustic waves of the first layer, the viscosity can be seen that the frequency of the acoustic wave equation clearly reflected toward the direction of the offset frequency, i.e., the high frequency energy is absorbed and effectively narrowing the band (Fig.5). From direct wave spectrum, the viscoelastic direct wave with increasing offset, effectively narrowing the band seismic waveform distortion is more obvious.

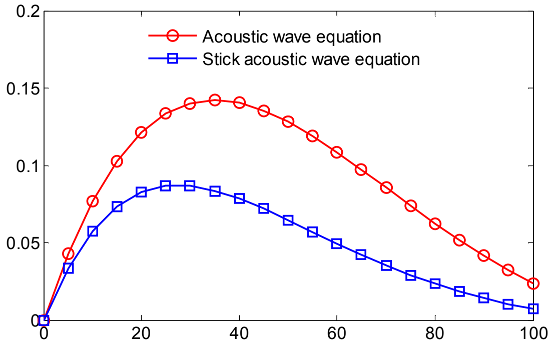

Figure.5 Reflection amplitude spectrum

Conclusion

Numerical simulation of seismic waves is usually based on the traditional ideal elastomer or viscoelastic body, but easy to overlook the local non- uniformity of the actual geological body. For the regional tectonic exploration, local non- uniformity of interpretation will not have a significant impact on the geological structure. In order to study the local small-scale non-uniform abnormal microscopic changes, we must study the propagation of small-scale non-uniformity of the seismic wave field. Due to the complexity of the actual formation, especially in certain complex heterogeneous reservoir with conventional elastomers or viscoelastic theory is difficult to complete description of the need to develop a more flexible and convenient way to describe the media.

References

[1] O. Nishizawa, Y. Fukushima: Advances in Geophysics, Vol.50 (2008), p.219-246

[2] M. Taiebat, B. Jeremić: Soil Dynamics and Earthquake Engineering, Vol.30 (2010), p.236-257

[3] G. Toyokuni, H. Takenaka: Physics of the Earth and Planetary Interiors, Vol.200 (2012), p.45-55

[4] A. S. Alekseev, B. G. Mikhailenko: Simulation Practice and Theory, Vol.7 (1999), p.125-151

[5] G. S. O′Brien: Computers & Geosciences, Vol.67 (2014), p.117-124

[6] P. Ping, Y. Zhang, Y. Xu: Journal of Applied Geophysics, Vol.101 (2014), p.124-135

[7] G. P. Kouretzis, S. W. Sloan: Soil Dynamics and Earthquake Engineering, Vol.46 (2013), p.41-51

[8] M. Kham, J. F. Semblat, N. B. Romdhane: Engineering Geology, Vol.155 (2013), p.80-86

[9] J. F Semblat, A. M Duval: Soil Dynamics and Earthquake Engineering, Vol.19 (2000), p.347-362

[10] M. Frehner, S. M. Schmalholz, E. H. Saenger: Physics of the Earth and Planetary Interiors, Vol.171 (2008), p.112-121

Applied Mechanics and Materials Vol. 596 (2014) pp 620-624
© (2014) Trans Tech Publications, Switzerland
doi:10.4028/www.scientific.net/AMM.596.620

Design of Salt in-bags Incasing Control Management System Based on Dual Closed-loop Fuzzy Controller

HUI Yan-bo [1, a], WANG Yong-gang [1,b], WANG Li[1,c] and NIU Qun-feng[1,c]

[1]School of Electrical Engineering, Henan University of Technology, Zhengzhou, China

[a]yanbohui@hotmail.com, [b]wyg125861@163.com, [c]hautwangli@163.com

Keywords: Auto-incasing equipment; Dual closed-loop fuzzy controller; RFID; Logistics management.

Abstract. According to auto-incasing equipment characteristic and control demand, a kind of salt in-bags incasing control management system was designed. The paper introduced the key technologies realization of the system. In the paper, a new fuzzy controller was designed to build a dual closed-loop fuzzy control system, realizing incasing goal site error on-line continuous correction. A logistics management module based on e-Tag was designed to realize product information traceable management. The experimental results show the system realizes accurate position control and RFID logistics management with high reliability and high control precision. The system can be popularized to other products packaging industry.

Introduction

Auto-incasing equipment is the core of automatic packaging line. The packaging is put into an open carton by arranged to a certain permutation method through the machine and the opening part of the box is then closed and sealed. At present, most of the domestic automatic packing machine adopts new type of combination mechanism, including the function units such as carton forming device, arrangement device, filling and sealing device. The action of mechanical system mainly relies on the cylinder, a small amount of manufacturer equipped with servo motor for precise positioning of the packaging action. The control system is based on the structure of PLC，special positioning module and touch screen. The control algorithm and strategy is mainly based on conventional PID and logic control [1-3]. Although the servo control system has been realized PID closed-loop control to ensure precision of motor rotation position, but with the increasing work time of the automatic packing machine and the wear factor of the mechanical structure, it leads to cumulative error of positioning, and then results in poor positioning precision and not uniform packing position. The research emphasizes on automatic packaging line to realize the precise positioning of the packing products under the circumstances of continuous operation without shutdown for a long time [4, 5].

The development of Internet of things has extended the traditional warehousing logistics management system to the whole world. Radio frequency identification (RFID) is a technology that non-contact automatic identification the information of items, it is one of the core technology of the Internet of things. The application of RFID technology is of great significance to the construction of modern logistics network in salt enterprises [6].

According to the engineering practice, a double closed-loop fuzzy controller was designed. It was used to on-line continuous correction error of mechanical target location correspond with servo motor. Combined with RFID technology, a kind of packaged salt incasing control management system was designed.

Design of packaged salt incasing control and management system

Process Analysis. The arrangement form of salt in cartons is a 2×5, the packing speed is 50-80 bags per minute. Small packing salts through conveyor line into the auto-incasing equipment, the machine have some functions such as carton supply, salt supply, encasement, seal box, recheck, etc. The finished product will enter into warehouse stacking link.

Packing process is as follows: The small packing salts from the telescopic belt conveyor of high-speed operation fall into the box that carton forming conveying mechanism is open through four accurate position points. The box will be sent to sealing machine when it arrive the set arrangement and quantity of package. After inspection of the weight, the system packages the product and paste product information electronic label code.

The function of salt encasement can be divided into open box, encasement, sealing, packing, re-inspection and labeling module. An auto-incasing line is composed of unpacking equipment, auto-incasing equipment, sealing equipment, packing equipment and labeling equipment. Combined with robot palletizing, unmanned production can be realized.

Overall Structure and Function of System. This system uses modular structure and its control mode is distributed control. General structure of the system is shown in Fig. 1.

Salt packing control management system includes three field controller and a management computer. Siemens PLC S7-200 is adopted for encasement controller and auxiliary controller, the former is responsible for the motion control of unpacking equipment, auto-incasing equipment and sealing equipment, the latter is responsible for the motion control of packing equipment, re-inspection equipment and labeling equipment. RFID system (XCRF-860 Reader, XCAF-12L Antenna, XCTF-8100 Electronic Tag) is used for logistics controller, which is responsible for read and write logistics information and data transmission between management computer and controller. Management computer adoptes industrial tablet computer (IPPC-6192A), RS485 or Ethernet can be adopted for on-scene communication.

Design of double closed-loop fuzzy control system

Basic Principle of Double Closed-loop Fuzzy Control System. The target location accurate positioning of packing product is an important control function in encasement controller. Basic principle of the system is shown in Fig. 2.

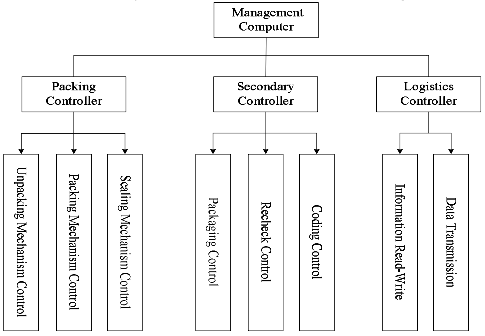
Management Computer
Packing Controller
Secondary Controller
Logistics Controller
Unpacking Mechanism Control
Packing Mechanism Control
Sealing Mechanism Control
Packaging Control
Recheck Control
Coding Control
Information Read-Write
Data Transmission

Fig.1 General structure of system

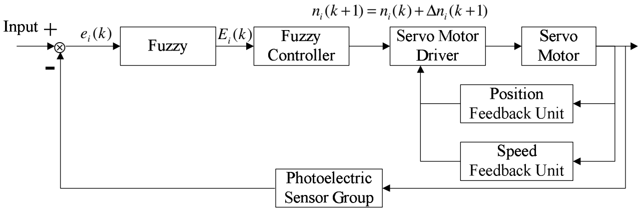
$n_i(k+1)=n_i(k)+\Delta n_i(k+1)$
Input +
-
$e_i(k)$
Fuzzy
$E_i(k)$
Fuzzy Controller
Servo Motor Driver
Servo Motor
Position Feedback Unit
Speed Feedback Unit
Photoelectric Sensor Group

Fig.2 Basic principle of dual closed-loop fuzzy control system

In the system, fuzzy controller collects signal that photoelectric sensor feedback in the continuous feeding process of telescopic belt. Combined with the given value can get the position error value $e_1(k)$, $e_2(k)$, $e_3(k)$ and $e_4(k)$. Select position error value $e_i(k)$ (i=1, 2, 3, 4) as input of fuzzy controller, then convert the accurate value $e_i(k)$ to a fuzzy value. A fuzzy subset $E_i(k)$ (i=1, 2, 3, 4) can get from it. Combined with fuzzy control rules R, we can obtain a fuzzy control output $\Delta N_i(k+1)$ (i=1, 2, 3, 4). The fuzzy value should be converted to precise control value $\Delta n_i(k+1)$ before the implementation of position control. It is used for position error correction in next cycle. When next cycle of encasement position come, fuzzy controller will output revised instructions pulse $n_i(k+1)=n_i(k)+\Delta n_i(k+1)$ (i=1, 2, 3, 4). Sever driver actuate servo motor to move to the exact location by receiving movement instructions that sent by fuzzy controller. In addition, combined internal closed-loop between servo drive and servo motor with external closed-loop, then a double closed-loop fuzzy control system was constituted. The system can calculate servo motor motion target location error correction of next feed loop through the position feedback of last feed cycle, and then realize online continuous motion position error correction, thus achieve the purpose that precise control servo motor operating.

Design of Fuzzy Controller. In the position control module of salt auto-incasing equipment designed above, servo motor starts from the start bit, the corresponding mechanical displacement needs to run four precise location points (P1, P2, P3, P4), as shown in Fig. 3. The indentation of telescopic belt is controlled by servo control system, its feed order is shown as below: start bit→P1→P2→P3→P4→start bit→P1→P2→P3→P4, complete a 2×5 arrangement. The telescopic belt attached four mechanical baffles as the mark of this four position precision points. A group of photoelectric sensor consists of two photoelectric sensors that are set in the encasement position. When the telescopic belt feeds to position P1, the photoelectric sensor group will produce a response signal according to the specific location of the P1 machine baffle. When it feeds to position P2, P3, P4, it is similar to P1.

The corresponding relationship between mechanical barrier position and photoelectric sensor response signal is shown in Fig. 4. According to the different response signal of photoelectric sensor, fuzzy controller can realize continuous correction position error online. Position 3 is the target position, the position error correction $\Delta n = 0$.

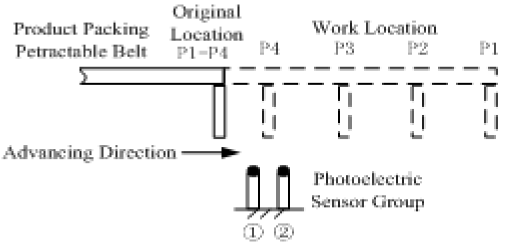
Product Packing
Petractable Belt
Original
Location
P1~P4
Work Location
P4
P3
P2
P1
Advancing Direction
Photoelectric
Sensor Group
①
②

Fig.3 Corresponding mechanical displacement of servo motor

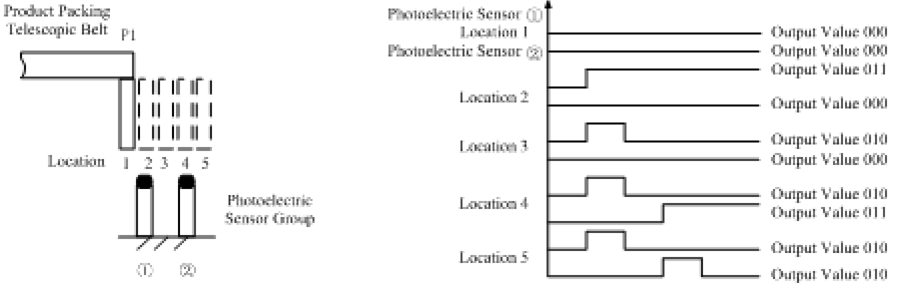
Product Packing
Telescopic Belt
P1
Location
1
2
3
4
5
Photoelectric
Sensor Group
①
②
Photoelectric Sensor ①
Location 1
Photoelectric Sensor ②
Output Value 000
Output Value 000
Output Value 011
Location 2
Output Value 000
Location 3
Output Value 010
Output Value 000
Location 4
Output Value 010
Output Value 011
Location 5
Output Value 010
Output Value 010

Fig.4 Corresponding relationship between photoelectric sensors value and baffle position

Fuzzy controller implementation is as follows: It is designed for two input and single output. The input variables of fuzzy controller are response signal value x of photoelectric sensor ① and response signal value y of photoelectric sensor ②. Input variables x, y have a corresponding fuzzy subset E= {EA, EB, EC}, the input variable 000 corresponding fuzzy variable EA, 011 corresponding EB, 010 corresponding EC. Output variable is the position error correction Δn. Its basic domain of discourse was [- Δn , Δn], the corresponding fuzzy domain of discourse {-4, -3, -2, -1, 0, 1, 2, 3, 4} was divided into five grades: Negative Big (NB), Negative Small (NS), Zero (ZO), Positive Small (PS), Positive Big (PB). Output variable membership functions select standard triangular form.

The control rules R of fuzzy controller as shown below:

R1: if x is PA, and y is PA, then Δn is NB R2: if x is PB, and y is PA, then Δn is NS
R1: if x is PC, and y is PA, then Δn is ZO R1: if x is PC, and y is PB, then Δn is PS
R1: if x is PC, and y is PC, then Δn is PB

According to Mamdani inference form of the fuzzy controller, the output variable set is $\Delta N = E \cdot R$, position error correction Δn can be obtained after the defuzzification of output variable.

Realization of the Logistics Management of RFID

Logistics management of RFID system is composed of reader, electronic tags and antenna. XCRF-860 reader can read and write at a distance of 7m (up to 11m), 50 available frequency points, working frequency 902-928 MHz, air interface protocol adopt ISO18000-6C. XCTF-8100 electronic tag use adhesive paper encapsulation materials which can store 64 bit ID number, 96 bit EPC code and 224 bit user data. Working principle: An electronic tag is pasted on product by labeling machine, after that, reader can read the unique ID number (UID) of electronic tag and write the logistics management information into it. The UID can be stored in the management of computer, all kinds of data are transmitted to enterprise logistics information database by it to realize products anti-counterfeiting validation and information traceability management. Working flow of management computer and read/write device as shown in Fig. 5.

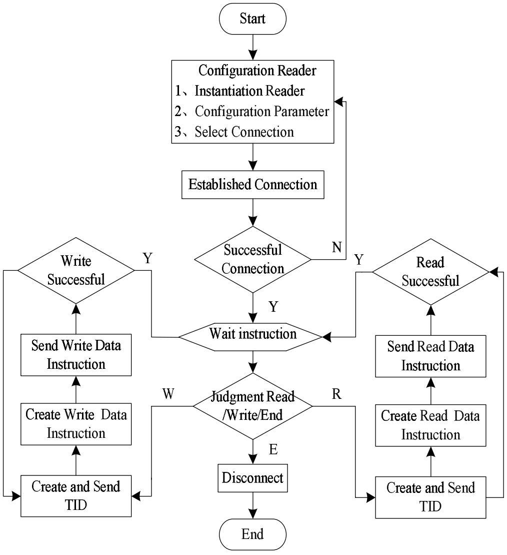
Start
Configuration Reader
1、Instantiation Reader
2、Configuration Parameter
3、Select Connection
Established Connection
Successful Connection
N
Y
Write Successful
Y
Read Successful
Y
Wait instruction
Send Write Data Instruction
Send Read Data Instruction
W
Judgment Read /Write/End
R
Create Write Data Instruction
Create Read Data Instruction
E
Disconnect
Create and Send TID
Create and Send TID
End

Fig.5 Working flow of management computer and read/write device

Software Design of Packaged Salt Incasing Logistics Control System

This system mainly aims at the enterprise electronic commerce foundation link develop, integrate the product in production, storage, packaging, processing and other links organically to realize remote monitoring. Based on the real-time database, we can realize the production, storage, distribution and other logistics service optimization management. The control system software consists of controller software and monitoring software. Packing controller and auxiliary controller software are designed by STEP to realize equipment control and transmission line monitoring. Management software functions are shown in Fig. 6, mainly includes: production management, equipment management, product quality tracking and query, data storage interaction, etc. System can realize the code management, record the information bar code each box of products and provide basic data for subsequent logistics management.

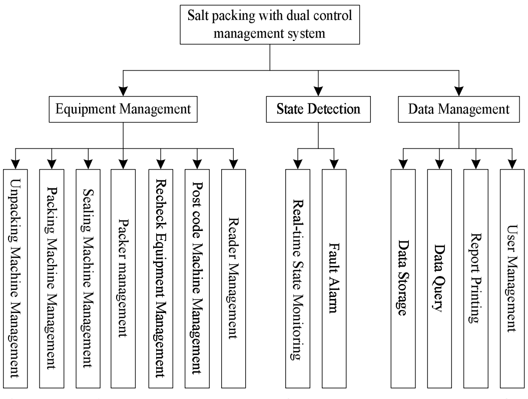
Salt packing with dual control management system
Equipment Management
State Detection
Data Management
Unpacking Machine Management
Packing Machine Management
Sealing Machine Management
Packer management
Recheck Equipment Management
Post code Machine Management
Reader Management
Real-time State Monitoring
Fault Alam
Data Storage
Data Query
Report Printing
User Management

Fig.6 Function structure of management software

Software is design by C#, mainly including the overall running monitoring and alarm interface of system, alarm history record query interface, device management interface, user management and report forms, etc. The system first enters the running monitoring interface, when it comes to a fault or sensor alarm signal, the alarm icon will flash alarm, and display the fault site as well as the field conveyor line running state and various packing equipment working condition. Part monitoring software field running interfaces are shown in Fig. 7.

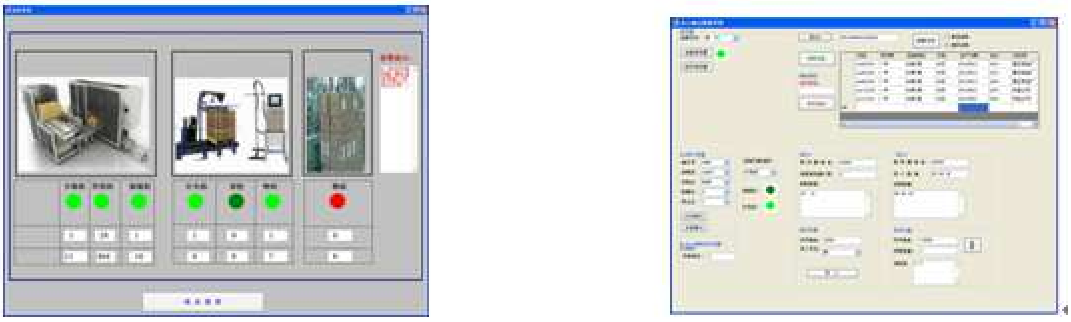

(a) Main monitoring interface (b) Management interface of serial communication

Fig.7 Monitoring software field running interfaces

Conclusions

Combining with the characteristics of auto-incasing line and control requirements of a salt company, the paper designed a kind of packaged salt incasing control and management system based on double closed-loop fuzzy controller. The key techniques of system implementation were introduced in detail, designed to achieve a fuzzy controller which applied to the precise control of loading position, and applying RFID technology in logistics management. The test results show that the system can realize precise position control of salt auto-incasing equipment and RFID logistics management with high reliability and control precision. The system also can be applied in other products packaging industry control system and network management, it has a widely application prospect.

Acknowledgements

This work was financially supported by National Science and Technology Support Program (2012BAF12B13), Henan Science and Technology Support Project (132102210199) and Postgraduate Innovation Fund of Henan University of Technology (2012YJCX61).

References

[1] QIU Jing, XU Wei-hong. *Present Situation and Development of Packing Machine Technology*, China Packaging Industry, Vol. 23 (2013), p.50

[2] ZHAO Lei, TANG Xiao-hua, LIU Na, etc. *Motion Control of Packing Machine Head of Packed-salt Production Line*, Journal of Beijing Technology and Business University, Vol. 6 (2010), p. 46

[3] NIU Qun-feng, WANG Yun-po etc. *Design of Bagged Product Belt Conveyor Line Monitoring System,* Automation & Instrumentation, Vol. 6 (2013), p. 45

[4] YU Guan-zhou, LI Shi-dong etc. *Realization of Accurate Positioning Control with Mechanical-photoelectronic Collaboration for Laser Marking,* Machine Tool & Hydraulics, Vol. 1 (2014), p. 5

[5] DING Yong, ZHANG Ji-tang. *Reversible Turn Synchronous Control for Servo Motor Based on the CAN Bus*, Machine Tool & Hydraulics, Vol. 2 (2014), p. 95

[6] CAO Le, YUAN Yan etc. *Combined Application of RFID and Two-dimensional Bar Code in Cigarette Anti-counterfeiting,* Packaging Engineering, Vol. 19 (2013), p. 63

Applied Mechanics and Materials Vol. 596 (2014) pp 625-630
© (2014) Trans Tech Publications, Switzerland
doi:10.4028/www.scientific.net/AMM.596.625

New Control Topology For Railway Static Power Conditioner

Ying Pan[1, a], Juan Bo[2,b]

[1]Engineering Institute, Herbin Univercity,Harbin 150086,China

[2]Engineering Institute, Herbin Univercity,Harbin 150086,China

[a]64271449@qq.com, [b]907103988@qq.com,

Keywords electric railway, power quality, RPC, repetitive control

Abstract: The traction power supply system of electric railway has the disadvantages of heavy unbalanced three phase, large harmonics and reactive power. Based on back-to-back converter, railway static power conditioner (RPC) can effectively balance the load between two arms, compensate the harmonic current and reactive power. As the conventional PI control is difficult to trace the waveform, a dual-loop control scheme was applied. The control scheme reduces the influences of the factors, such as sampling and calculation delay, dead-zone, parameters' shift, on the system stability and enhances the robustness of the whole system. It can also eliminate the negative sequence current and three-phase voltage fluctuations of the primary side, improve the power factor and harmonic filter, so that electrified railway power quality problems can be resolved perfectly. The whole design was provided. Analysis and simulation results testify the effectiveness of the proposed control scheme.

Introduction

The rapid development of electrified railway has brought the problems of power quality like negative-sequence, low power factor, voltage fluctuation, flicker and harmonic to their prominence. In recent years, large and active compensation devices based on STATCOM have been applied more and more frequently in the field of electricity transmission and distribution, and particularly a kind of RPC with a structure of back-to-back double phases which could be fixed to the side-lining of traction substation has showed a great economic and technological advantages, as well as application prospect in the field of the comprehensive treatment of electrified railway power quality[1-3].

the power regulating system of electric railway based on Scott transformer. The system realizes the comprehensive treatment of negative-sequence, reactive work and harmonic in electric railways through the independent compensation of reactive power and harmonic, as well as the transfer of active power of this back-to-back converter[4-6]. To combine PI control and repetitive control will not only make sure the dynamic response speed and stability, but also will track and correct errors, making it widely applied.

Theory of repetitive control

Repetitive control is a control idea based on internal model principle[7-8]. Its basic theory is to assume that a distortion appeared in the first fundamental wave cycle will appear again at the same time of the next fundamental wave cycle. The controller will determine the required calibration signal according to the error of the given signal and feedback signal of each switching period. Then the signal will be added to the original control signal at the same time of the following fundamental wave cycle to erase the distortion which would repeat in each cycle.

The current inner loop controller based on the repetitive control

2.1 The design of the controller

First, design the parameter of PI controller according to the change of parameter limit. Get controlled object by the discretization of inverter model. $P(z)=Z\left[\frac{1-e^{-sT_s}}{s}\cdot\frac{1}{L_n s+r_n}\right]$ (1)

Suppose PI controller as $K_p+\frac{K_s}{s}$, then adopt backward difference method to discretize

$$P_I(z)=\frac{(K_p+K_iT)z-K_p}{z-1} \tag{2}$$

open-loop transfer function of the single PI system current inner loop controller $G(z)=z^{-1}P_I(z)P(z)$

As the table 4(a) shows, the system frequency characteristic curve has displayed that the inductance has reduced by 50%, and no harmonic peak appeared consequently, so the system stability is ensued. As table 4(b) shows the system frequency features; the solid line shows the bode diagram when the parameter is normal; while the imaginary line shows the bode diagram with inductance value reduced 50%, and apparent harmonic peak appeared in the high frequency part causing instability of the system; the curve with imaginary point shows a bode diagram with 50% increased inductance value, the frequency band is narrowed, but no harmonic peak appeared, so the system is stable.

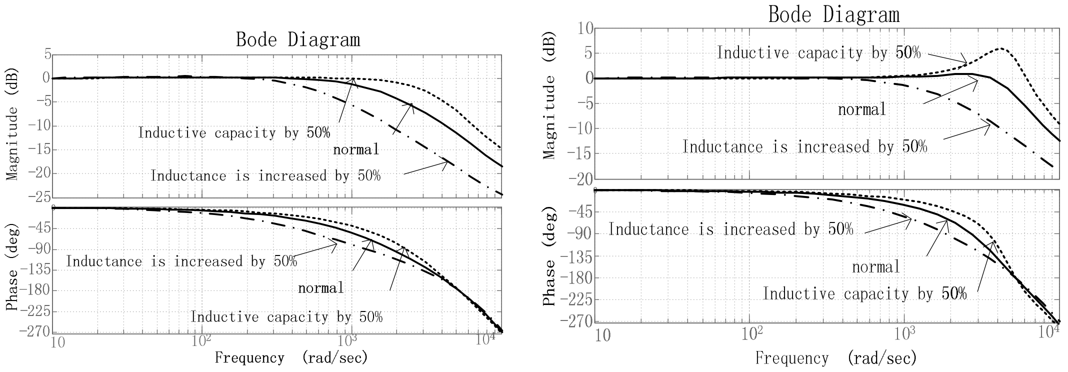

(a) K_p=0.1 (b) K_p=0.2

Figure 1 Bode picture of single PI system when system parameter's changed

After confirming the parameters of PI controller, the lead-lag components $S_1(z)$ of repeated controller can be designed, demanding to perfectly compensate LMF low-mid frequency feature of the system, in order to get zero gain and zero phase. This can be shown as $S_1(z)=\frac{z-a}{b(z-c)}$. Zero point a is designed as pole location of the controlling object, to lower system order. As in low-mid frequency, $z=e^{j\omega T}$, $\omega T\to 0$, and $|z|=|e^{j\omega T}|$ is approaching 1. In this case, if no-gain feature is to be acquired in low-mid frequency, parameter b and c should be chosen from the equation below:

$$\lim_{z\to 1}\frac{P(z)}{1+P(z)P_I(z)}\cdot\frac{z-a}{b(z-c)}=1 \tag{3}$$

For an simpler expression, after paralleling PI controller, equivalent control object of repetitive controller is shown as $G_{RP}(z)$, which is:

$$G_{RP}(z)=\frac{P(z)}{1+K_p P_I(z)} \tag{4}$$

Figure 2 is a Bode picture of the equivalent control object of repetitive controller $G_{RP}(z)$, lead-lag compensation filter $S_1(z)$ and the compensated system $G_{RP}(z)S_1(z)$; from which we can see that, the designed lead-lag component can assure the no-gain feature of compensated system.

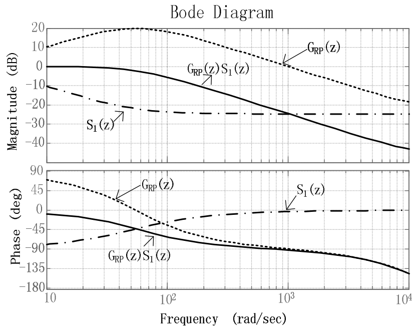

Figure 2 Bode picture of the equivalent control object of repetitive controller, lead-lag compensation filter and the compensated system

2.2 control system Stability

To keep it simple, take Table 2 into consideration. After deduction, the transfer function of control system electric current loop is

$$\frac{i_s(z)}{i_{ref}(z)}=\frac{\left(Z^{-N}-Q(z)\right)P_I(z)P(z)+\mathrm{K_r}Z^kS(z)P(z)}{\left(Z^{-N}-Q(z)\right)\left(1+\mathrm{P_I(z)P(z)}\right)+\mathrm{K_r}Z^kS(z)P(z)} \tag{5}$$

From which the characteristic polynomial is

$$\Delta=\left(Z^{-N}-Q(z)\right)\left(1+\mathrm{P_I(z)P(z)}\right)+\mathrm{K_r}Z^kS(z)P(z)$$

$$=\left(1+\mathrm{P_I(z)P(z)}\right)\left\{Z^N-\left[Q(z)-\frac{K_rZ^kS(z)P(z)}{1+\mathrm{P_I(z)P(z)}}\right]\right\}=\Delta1\Delta2$$

For system stability, the characteristic roots of Δ1=0 and Δ2=0 must be controller with the unit circle; that means the necessary conditions for improving repetitive control system stability are: 1) PI controller parameters must be chosen from the stability range of single PI controller; 2) the parameters of repetitive controller must assure the stability of repetitive control system whose controlling object is $G_{RP}(z)$.

That also means, under the premise of $\left|Q(z)-\frac{K_rZ^kS(z)P(z)}{1+P_I(z)P(z)}\right|<1$, the value of repetitive gain K_r is usually designed less than 1 to assure system stability. Q(z) is often constant 0.95, also for increasing system stability.

As is explained above, first design proportional controller, then series compensation filter, phase compensation component,finally repetitive controller gain, to improve repetitive controller. Finishing that, the Bode picture of PI+ repetitive control system and PI control system is shown as Figure3.

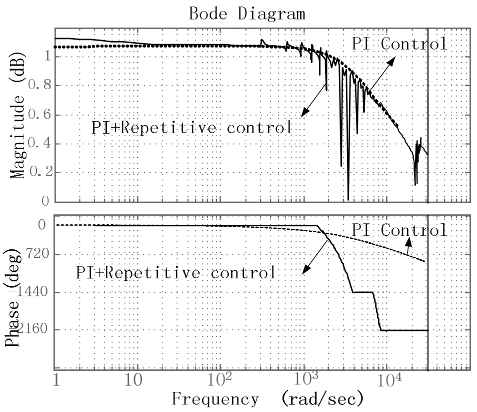

Figure 3 PI+ repetitive control system and PI control system

Outer Direct Voltage Loop Control System

RPC systematic control strategies can de divided into rectifier A and inverter B. Rectifier converter adopts constant DC voltage control strategy, while inverter converter adopts constant power control strategy. The control signal produces back-to-back driver signals on both sides by PWM module, and realize controlling.

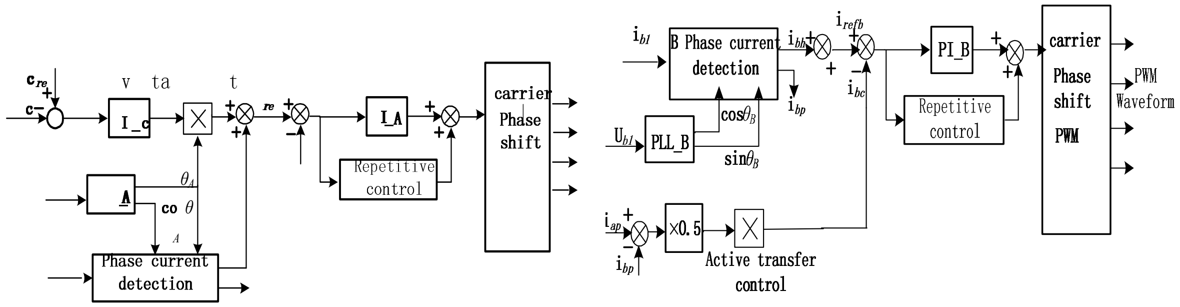
c_{re}
c
+
−
v ta t
I_c
+
+
re
+
−
I_A
+
+
carrier
Phase
shift
Repetitive
control
A
θ_A
co θ
A
Phase current
detection
i_{b1}
B Phase current
detection
i_{bh}
+
+
i_{refb}
+
−
i_{bp}
i_{bc}
PI_B
+
+
carrier
Phase
shift
PWM
PWM
Waveform
U_{b1}
PLL_B
$\cos\theta_B$
$\sin\theta_B$
Repetitive
control
i_{ap}
+
−
i_{bp}
×0.5
Active transfer
control

(a) Constant DC voltage control chart on A side (b) Constant power transfer control chart on B side
Figure 4 Basic structure of RPC control system

Simulation Analysis

Based on the tractive power supply system shown in Table 1 and Matlab/Simulink , a simulation model has been established, and simulation analysis conducted.

Suppose that the voltage of three-phase power supply is 110KV, voltage ratio of Scott transformer is 110:27.5, with a capacity of 30MVA. Series connect an 1Ω resistance and a 200mH inductance as rectifier load, then parallel it with an 0.8Ω resistance, together serve as a load of bridge arm of A phase. Series connect a 2Ω resistance and a 400mH inductance as rectifier load, then parallel it with an 1.6Ω resistance, together serve as a load of bridge arm of B phase. The change in step-down transformer is 25:1. Connect an 1mH reactance and a 2mΩ resistance, DC capacitor is 5700μF, make the reference value of DC voltage 8000V. The compensation capacity of converters on A and B side are respectively 20MVA and 17 MVA, with an switch frequency of 5KHz.

Figer 5(a) is the load current waveform of the two bridge arms before compensation. Because the voltages on both secondary bridge arms of Scott transformer are the same, a 90 degree phase difference, and A load is half of B load. As a result, current of A phase is twice than that of B phase, together with a 90 degree phase difference.

Figer 5(b) is the load current waveform of the two bridge arms after RPC compensation, under the circumstance of single PI control From the table we can see that, the electric currents of the two bridge arms are almost the same, with a 90 degree phase difference. Then a conclusion can be made, after RPC compensation, the power flow between the two bridge arms gets realized, and waveform is closed to sine wave, which says that the two bridge arms respectively and effectively compensate reactive power and harmonic.

Figer 5(c) is the waveform of the two bridge arms after RPC compensation, under the circumstance of repetitive control of double closed-loop controller. Compared to 5(b), the current waveform is improved, burr reduced, which means the adopted strategies are of effect and superior to PI control.

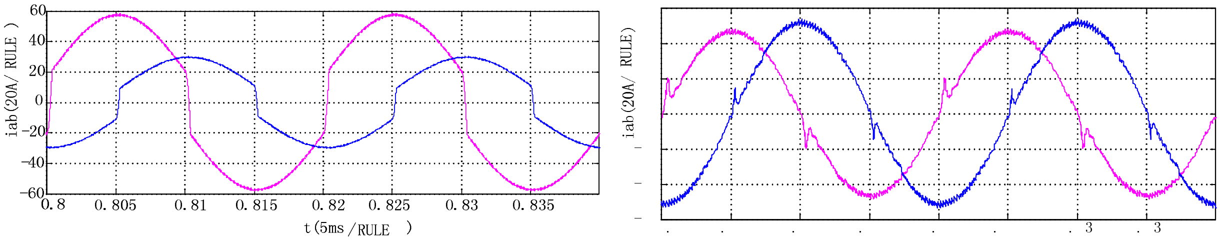

(a) load current waveform of the two bridge arms before RPC compensation

(b) under the circumstance of single PI control, load current waveform of the two bridge arms after RPC compensation

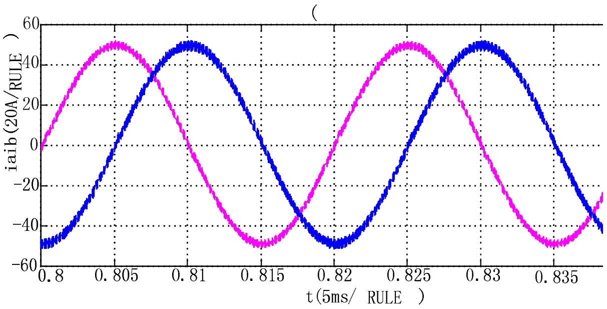

(c) under PI control and repetitive control, current waveform of the two bridge arms after RPC compensation

Figure 5 Load current waveform before and after RPC compensation

Load harmonic current THD value is shown in Table 9. Fundamental currency percentage is not presented as it's too big. Before compensation, the current THD values of the two bridge arms are respectively 16.58% and 16.36%, and are mainly odd harmonics like 3, 5, 7. After RPC compensation, the THD value decreases greatly, with a PI control reduction of 5.66% and 4.08%, and a double closed-loop controller decline of 0.65% and 0.49%. It is clear that the control ling strategies put up in this article are better in terms of electric energy quality management.

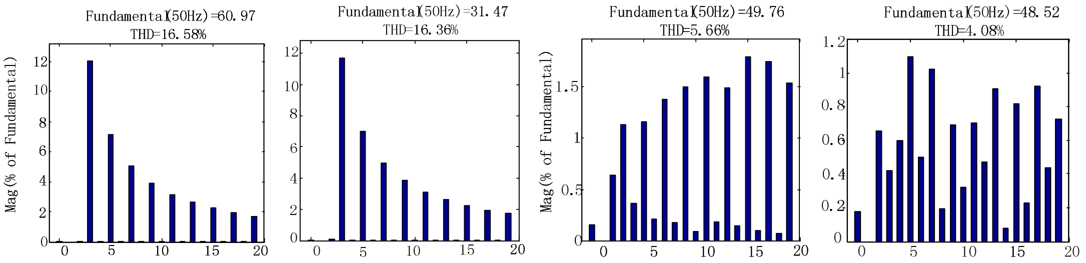

(a) load current THD value of the two bridge arms before RPC compensation

(b) under PI control, load current THD value of the two bridge arms after RPC compensation

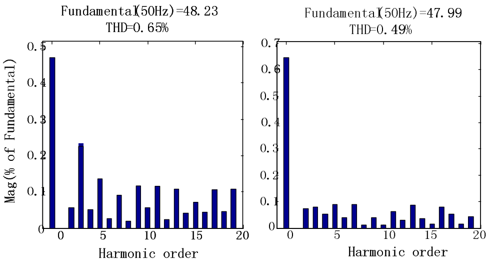

(c) under PI control and repetitive control, the current THD value of the two bridge arms after RPC compensation

Figure 6 Load current THD value before and after RPC compensation

Conclusion

In view of the railway power control system composed by back-to-back converter, and its defects corresponded to traditional PI controller, the article comes up with double closed-loop control strategies based on the connection of repetitive control on current inner loop and voltage outer loop, designs and rectifies controller parameters, as well makes an analysis on system stability. By comparing to traditional PI control, the control strategies in this article are proven to be superior and more effective.

Bibliography

[1] Li Qunzhan, Analysis on Traction Substation Power Supply and Comprehensive Compensation Technology[M]. Beijing: China Railway Publishing House, 2006

[2] Zhang Xiufeng, Lian Jisan, New in-phase AT Traction Power Supply System based on Scott Transformer[J]. Electric Drive for Locomotives, 2008, 4:14-18

[3] Zhang Xiufeng, Lian Jisan, Gao Shibin, New in-phase Traction Power Supply System Based on Three-Phase-to-Four-Phase Transformer[J], Proceedings of the CSEE, 2006,26(15):19-23.

[4] Zeliang Shu.Single-Phase Back-To-Back Converter for Active Power Balancing, Reactive Power Compensation, and Harmonic Filtering in Traction Power System[J]. IEEE Trans on Power Electronics, 2011, 26(2):334 -343.

[5] Sun Zhou,Jiang Xinjian,Zhu Dongqi. A novel active power quality compensator topology for electrified railway[J].Electric Power Automation Equipment, 2006,26(1):21-24.

[6] Qiu Daqiang, Li Qunzhan, Zhou Fulin,etc. Comprehensive Management on Electric Power Railway Energy Quality Based on Back-to-Back SVG[J], Electric Power Automation Equipment, 2010,30(6):36-44.

[7] Li Cuiyan, Zhang Dongchun, Zhuang Xianyi, Summery on Repetitive Control[J], Electric Machines and Control, 2005,9(1):37-43.-9.

[8] Wang Chengzhi, Zou Xudong, Xu Zan. Superpower Electronics Load Applying Improved Repetitive Control[J], Proceedings of the CSEE, 2009,29(12):1-9.

Applied Mechanics and Materials Vol. 596 (2014) pp 631-635
© (2014) Trans Tech Publications, Switzerland
doi:10.4028/www.scientific.net/AMM.596.631

Triangle Formation Control of Multi-AUVs with Communication Constraints

Guannan Li[1, 2, a], Huiying Dong[1, b], Hongli Xu[2, c]

[1]Institute of information, Shenyang Ligong University, Shenyang, 110168, China

[2]State Key Laboratory of Robotics, Shenyang Institute of Automation, CAS, Shenyang, 110016, China

[a]email: liguannan@sia.cn, [b]email:huiyingdong@163.com, [c]email: xhl@sia.cn

Keywords: Multi-AUVs; Formation Control; Communication Constraints

Abstract. Aimed at solving the problem of multi-AUVs formation control, an analysis has been made on a triangle formation based on leader-follower construction, with a multi-AUVs formation controller designed with communication constraints taken into account. The desired velocity of the follower is the resultant velocity of three component velocities, each of which has different function. The convergence of the proposed controller is proved by establishing an objective function that can represents the status of the formation. Simulation experiments are carried out to demonstrate the proposed controller is effective.

Introduction

Autonomous Underwater Vehicles (AUVs) have gained steadily increased attention for they are particularly suited for executing underwater missions in environments where global human control cannot arrive. Formation control of multi-AUVs systems has triggered the interests of the research community for it is a fundamental problem for cooperative control of multi-AUVs systems, which has potential benefits for specific applications such as seafloor survey, oceanographic research, underwater archeology, etc. By multi-AUVs formation control we mean a group of AUVs travel according to a prescribed pattern. In some cases, members in the system are expected to form certain geometry according to a real or virtual vehicle, which means agents in the system should keep desired distances and angles relative to each other. This formation is widely used in pipe line inspection [1] or similar tasks.

A variety of formation control schemes have been proposed so far, such as leader-follower method [2], behavior based method [3], virtual structure method [4], artificial potential field method [5] and graph theory based method [6]. Leader-follower method is widely research for it is easy to realize and can be combined with other methods. Formations organized using this method consists of several vehicles acting as leaders and a set of vehicles leaders that travels keep desired position in a coordinate based on the status of the leaders. Kowdiki proposed a formation control technique of a group of vehicles employing artificial potential field navigation and leader-follower formation control scheme [7]. Consolini focus on controlling leader-follower formations with rigidity fixed graph [8]. Ren proposed a unified, distributed formation control architecture that accommodates an arbitrary number of group leasers and arbitrary information flow among vehicles that requires only local neighbor-to neighbor information exchange [9] [10].

In this paper, a research is made on a formation consists of three vehicles, with one of them acting as leader, while the other two as followers. The vehicles should form certain triangle pointing at desired orientation. A novel formation controller is proposed. The desired velocity of each follower is treated as a resultant velocity from three component velocities. An objective function represents the status of the formation is established to prove the convergence of the proposed controller. Simulation experiments are carried out to demonstrate that the proposed method is effective.

Design of the Formation Controller

A formation consists of three AUVs is researched with one being the leader while the other two followers. When the three AUVs travel at the same depth, they are moving in 2-D space and can form a triangle formation, as is shown in Fig. 1. When the leader keeps travelling at constant speed, the purpose of the formation control is to drive the three AUVs to form a desired triangle, whose edges are $[|DL|_1, |DL|_2, |DD|]$, and the triangle should point at certain orientation, which means the direction of the formation should be defined. Here we define the direction of the vector $\overline{ML}$ as the direction of the formation, which represents a vector perpendicular to line F_1F_2 and pointing at the leader. Then a formation controller is proposed, who will give out the desired velocity of every AUV in the formation.

Controller for the leader is easy to design. The desired velocity of the leader $\vec{v}_l$ is a constant value towards the destination of the leader. Then the controller for the followers should drive them to converge to the desired triangle and turn the triangle to the desired orientation. The desired velocity of the follower is then a resultant velocity:

$$\vec{v}_f = \vec{v}_l + \vec{v}_{form} + \vec{v}_{turn} \tag{1}$$

(1) Component velocity $\vec{v}_l$ is the same as the velocity of the leader, which will drive the followers to the destination with the leader.

(2) Component velocity $\vec{v}_{form}$ can drive the followers to form the desired triangle based on relative distances between AUVs. For follower F_i, this component velocity can be given as:

$$\vec{v}_{formi} = \vec{v}_{ffi} + \vec{v}_{fli} \tag{2}$$

$$\begin{cases} \vec{v}_{ffi} = k \cdot \Delta|FF| \cdot \vec{e}_{FFi} = k \cdot (|FF| - |DD|) \cdot \vec{e}_{FFi} \\ \vec{v}_{fli} = k \cdot \Delta|FL|_i \cdot \vec{e}_{FLi} = k \cdot (|FL|_i - |DL|_i) \cdot \vec{e}_{FLi} \end{cases} \tag{3}$$

Where $\vec{e}_{FFi}(x_{FFi}, y_{FFi})$ and $\vec{e}_{FLi}(x_{FLi}, y_{FLi})$ are corresponding unit vectors.

(3) Component velocity $\vec{v}_{turn}$ will drive the triangle to point at the desired orientation. A set of concentric circles are set to obtain this component velocity, as is shown in Fig. 2. Vehicles are put in concentric circles with the leader being the center while the distances between the leader and each follower being radius. When the triangle rotates, followers should move along corresponding circles with a speed perpendicular to radius.

Let the position of the leader be $L(L_x, L_y)$ while that of the ith follower be $F_i(F_{xi}, F_{yi})$, and then the direction of the formation is (x_{form}, y_{form}):

$$\begin{cases} x_{form} = -\dfrac{(F_{y1} - F_{y2})((F_{x2} - L_x)(F_{y1} - L_y) - (F_{x1} - L_x)(F_{y2} - L_y))}{(F_{x1} - F_{x2})^2 + (F_{y1} - F_{y2})^2} \\ y_{form} = -\dfrac{(F_{x1} - F_{x2})((F_{x1} - L_x)(F_{y2} - L_y) - (F_{x2} - L_x)(F_{y1} - L_y))}{(F_{x1} - F_{x2})^2 + (F_{y1} - F_{y2})^2} \end{cases} \tag{4}$$

Formation direction in global coordinate is:

$$\varphi_{form} = \arctan \frac{y_{form}}{x_{form}} \tag{5}$$

The angle of $\vec{v}_{turn}$ for the ith follower is then:

$$\varphi_{turni} = \arctan(\frac{y_{FLi}}{x_{FLi}}) - \operatorname{sgn}(\sin(\varphi_d - \varphi_{form})) \cdot \frac{\pi}{2} \tag{6}$$

With φ_d being the angle of the desired formation direction in global coordinate. The value of this component velocity is:

$$|\vec{v}_{turni}| = |F_iL| \cdot \arcsin(|\sin(\varphi_d - \varphi_{form})|) \cdot k_{turn} \tag{7}$$

with k_{turn} being a parameter. This makes:

$$\vec{v}_{turni} = (|\vec{v}_{turni}| \cdot \cos\varphi_{turni}, |\vec{v}_{turni}| \cdot \sin\varphi_{formi}) \tag{8}$$

As communication constraints should be taken into account, both followers should estimate real-time positions of other vehicles with:

$$\begin{cases} L_{t+\Delta t} = L_t + \vec{v}_l \cdot \Delta t \\ F_{i,t+\Delta t} = F_{i,t} + \vec{v}_{i,f} \cdot \Delta t \end{cases} \tag{9}$$

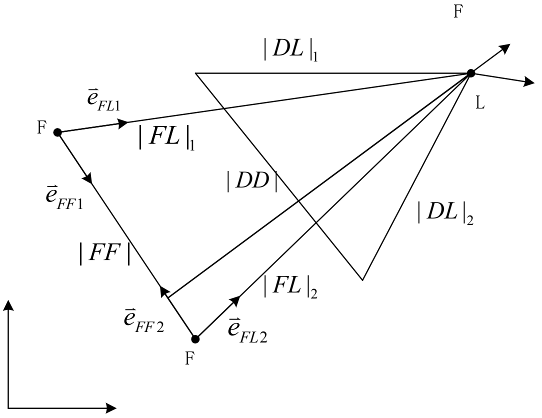

Fig.1. Definition of the formation

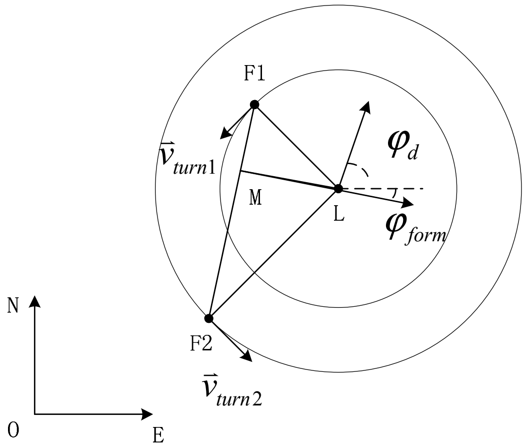

Fig.2. Assistant concentric circles

Proof of Formation Convergence

The convergence of the proposed controller can be proved. As all vehicles share the same component velocity $\vec{v}_l$ as the leader, it can be regarded that the leader keeps still and that the followers move to form the formation. Component velocity $\vec{v}_{turn}$ only affects the direction of the triangle, but have no effect on the shape of the formation. So the convergence of the formation depends on the component velocity $\vec{v}_{form}$, when $\vec{v}_{form}$ can ensure that the vehicles can converge to the desired geometry, the formation can converge, which means:

$$\begin{cases} \Delta|FL|_1 = |FL|_1 - |DL|_1 = 0 \\ \Delta|FL|_2 = |FL|_2 - |DL|_2 = 0 \\ \Delta|FF| = |FF| - |DD| = 0 \end{cases} \tag{10}$$

Then an objective function $f(t)$ can be established based on that:

$$f(t) = |\Delta|FL|_1| + |\Delta|FL|_2| + |\Delta|FF|| \tag{11}$$

For follower $F_i (i = 1, 2)$

$$\vec{v}_{formi} = \vec{v}_{ffi} + \vec{v}_{fli} \tag{12}$$

Then along FL_i and FF_i:

$$\begin{cases} |FL|_{i,t+\Delta t} - |FL|_{i,t} = (|FL|_{i,t+\Delta t} - |DL|_i) - (|FL|_{i,t} - |DL|_i) = \Delta|FL|_{i,t+\Delta t} - \Delta|FL|_{i,t} \\ |FF|_{i,t+\Delta t} - |FF|_{i,t} = (|FF|_{i,t+\Delta t} - |DD|/2) - (|FF|_{i,t} - |DD|/2) = \Delta|FF|_{i,t+\Delta t} - \Delta|FF|_{i,t} \end{cases} \tag{13}$$

Where $|FF| = |FF|_1 + |FF|_2$ (14)

When $\Delta t \to 0$

$$\begin{cases} \Delta|FL|_{i,t+\Delta t} \cdot \Delta|FL|_{i,t} \geq 0 \\ \Delta|FF|_{i,t+\Delta t} \cdot \Delta|FF|_{i,t} \geq 0 \end{cases}$$

Then it can be derived that:

$$\begin{cases} |\Delta|FL|_{i,t+\Delta t}| - |\Delta|FL|_{i,t}| = -\lambda_i (\vec{v}_{fli} + \vec{v}_{ffi}) \vec{e}_{FLi} \cdot \Delta t \\ |\Delta|FF|_{i,t+\Delta t}| - |\Delta|FF|_{i,t}| = -\mu_i (\vec{v}_{ffi} + \vec{v}_{fli}) \vec{e}_{FFi} \cdot \Delta t \end{cases} \tag{15}$$

With

$$\begin{cases} \lambda_i = 1 & \Delta|FL|_{i,t+\Delta t} > 0, \Delta|FL|_{i,t} > 0 \\ \lambda_i = -1 & \Delta|FL|_{i,t+\Delta t} < 0, \Delta|FL|_{i,t} < 0 \end{cases} \text{ and } \begin{cases} \mu_i = 1 & \Delta|FF|_{i,t+\Delta t} > 0, \Delta|FF|_{i,t} > 0 \\ \mu_i = -1 & \Delta|FF|_{i,t+\Delta t} < 0, \Delta|FF|_{i,t} < 0 \end{cases} \tag{16}$$

Form Equation (15), we can get:

$$f(t+\Delta t) - f(t) = -\sum_{i=1}^{2} (\lambda_i (\vec{v}_{fli} + \vec{v}_{ffi})\vec{e}_{FLi} + \mu_i (\vec{v}_{ffi} + \vec{v}_{fli})\vec{e}_{FFi}) \cdot \Delta t \tag{17}$$

As

$$f'(t) = \lim_{\Delta t \to 0} \frac{f(t+\Delta t) - f(t)}{\Delta t} \tag{18}$$

Then:

$$f'(t) = \sum_{i=1}^{2} (M_i + N_i) \tag{19}$$

$$\begin{cases} M_i = -\vec{v}_{fli}(\lambda_i \cdot \vec{e}_{FLi} + \mu_i \cdot \vec{e}_{FFi}) = -(\lambda_i + \mu_i \cdot \cos\theta_i) \cdot |FL|_i \\ N_i = -\vec{v}_{ffi}(\mu_i \cdot \vec{e}_{FFi} + \lambda_i \cdot \vec{e}_{FLi}) = -(\mu_i + \lambda_i \cdot \cos\theta_i) \cdot |FF|_i \end{cases} \tag{20}$$

Where

$$\cos\theta_i = \vec{e}_{FFi} \cdot \vec{e}_{FLi}$$

As $f(t) \geq 0$, when $f(t) \neq 0$, $f'(t) < 0$ and when $f(t) = 0$, $f'(t) = 0$, so it is obvious that $f(t)$ can converge to zero, which means the formation can finally converge to the desired triangle.

Simulation results

This section presents the simulation results of the formation controller derived in MATLAB. A formation consists of three AUVs is simulated, and the AUVs should form a desired formation from a random one, with its direction pointing at the desired orientation. The origin position of the leader is $L(10,10)$ and followers are $F_1(0,20)$ and $F_2(0,0)$, with the desired formation setting as $D[15,15,15]$. The desired orientation of the formation is set the same as the heading of the leader. Parameters are set as $k = 0.1$ and $k_{turn} = 0.25$, with communication delay being 10s. The simulation results are shown in Fig. 3.

Trajectories of vehicles are shown in Fig.3 (a), which shows that AUVs form the desired formation rapidly from random positions. Fig.3 (b) shows some metrics relate to the performance of the formation controllers. As can be seen that the error along every edges of the triangle formation remain fairly stable and close to zero after a brief initial transient. During 100s to 150s, vibration occurs at the turning point, which is mainly caused by communication constraints. The formation converges again within 100s, with direction pointing at the desired orientation.

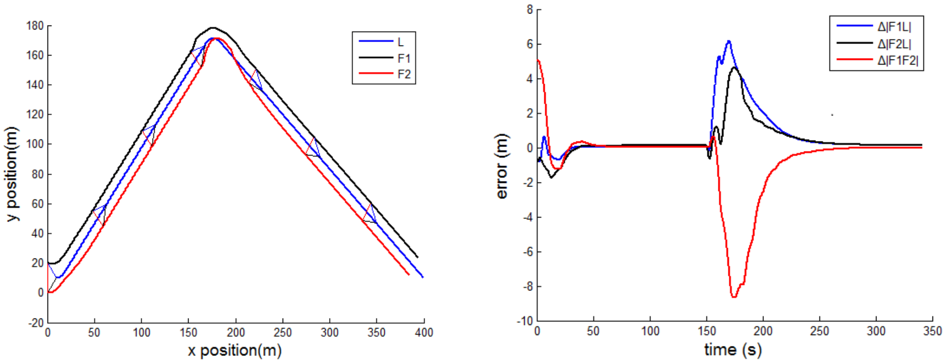

(a) trajectory of the formation (b) error along every edges

Fig.3. The simulation results

Conclusion

This paper aims at solving the problem of multi-AUVs triangle formation control with a leader-follower construction. A novel formation controller that can ensure the vehicles form a certain triangle from random positions is proposed. A set of concentric circles are used to help maintain the triangle formation heading at a desired orientation. Effectiveness of the proposed controller is shown by simulation results. Future work will focus on increasing vehicles in the formation.

Acknowledgement

In this paper, the research was sponsored by the Key Research Program of the Chinese Academy of Sciences (Grant No. KGFZD-125-014).

References

[1] Xianbo Xiang, Jouvencel Bruno, Parodi Olivier. Coordinated Formation Control of Multiple Autonomous Underwater Vehicles for Pipeline Inspection [J]. International Journal of Advanced Robotic Systems, 2010 (5) 75-84.

[2] Ruilei Zhang, Sheng Li, Qingwei Chen. Dynamic Formation Control for Car-like Mobile Robots [J]. ROBOT, 2013, 35(6): 651-656.

[3] Balch T, Arkin R C. Behavior-based formation control for multi robot teams [J]. IEEE Transactions on Robotics and Automation, 1998, 14(6): 926-939.

[4] Kar-Han Tan, Lewis M A. Virtual structures for high-precision cooperative mobile robotic control [C]. 1996 IEEE International Conference on Intelligent Robots and Systems. Osaka, Japan: IEEE, 1996: 132-139.

[5] Fan W H, Liu Y H, Cai X P. Multi-robot formation control using potential field for mobile ad-hoc networks [C]. 2005 IEEE International Conference on Robotics and Biomimetics. Shatin, China: IEEE, 2005: 133-138.

[6] Desai J, Ostrowski J, Kumar V. Modeling and control of formations of nonholonomic mobile robots [J]. IEEE Transactions on Robotics and Automation, 2001, 17(6): 905-908.

[7] Kowdiki K H, Barai R K, Bhattacharya S. Leader-follower formation control using artificial potential functions: A kinematic approach [C]. 2012 International Conference on Advances in Engineering, Science and Management. Nagapattinam, Tamil Nadu: IEEE, 2012: 500-505.

[8] Consolini L, Moribidi F, Prattichizzo D, et al. A geometric characterization of leader-follower formation control [C]. 2007 IEEE International Conference on Robotics and Automation. Roma, Italy: IEEE, 2007: 2397-2402.

[9] Wei Ren. Consensus tracking under directed interaction topologies: Algorithms and experiments [J]. IEEE Transactions on Control Systems Technology, 2010, 18(1): 230-237.

[10] Wei Ren, Nathan S. Distributed coordination architecture for multi-robot formation control [J]. Robotics and Autonomous Systems, 2008, 56(4): 324-333.

Applied Mechanics and Materials Vol. 596 (2014) pp 636-639
© (2014) Trans Tech Publications, Switzerland
doi:10.4028/www.scientific.net/AMM.596.636

The Integrated automation solutions research of Zhengzhou North Station

Zheng Chang [1, a], Haipao Zhu [2,b] and Xingchen Zhang[1,c]

[1] School of Traffic and Transportation, Beijing Jiaotong University, Beijing, China

[2] Zhengzhou North Station, Zhengzhou Railway Administration, Zhengzhou, China

[a]237350071@qq.com, [b]64193916@qq.com, [c]xczhang@bjtu.edu.cn

Keywords: Marshalling station, Integrated automation, SAM and CIPS, Comparison and Selection

Abstract. This paper compares two kinds of Marshalling station integrated automation systems: SAM and CIPS, combining with the practical condition of Zhengzhou north station, analyzing from various angles such as safety and efficiency， finally choose the appropriate solution. In doing this, it will help to provide a strong support for the safe production and efficient transportation of Zhengzhou North Station.

Introduction

The integrated automation transformation of marshalling station is an inevitable process of railway technology and equipment modernization. Marshalling station integrated automation is a management and control technique which integrate the management information system and the automatic control system. At present, the mature of the marshalling station integrated automation solutions basically has two, one is Computer Integrated Process System(CIPS), one is Synthetic Automation of Marshalling Yard(SAM). In recent years, due to the support of China's railway corporation (the former ministry of railways) , Xinfengzhen north, Wuhan, Chengdu of south north, Shijiazhuang, Liuzhou and so on one batch of marshalling yards are successively implemented integrated automation upgrades, and has made gratifying achievements.

Zhengzhou North marshalling station, as an important network marshalling station place which place in the intersection of Beijing-Guangzhou and Lanzhou-Lianyungang two railway lines, comprehensive automation upgrades can no longer delay. This article ,firstly, two kinds of SAM and CIPS Marshalling integrated automation solutions were analyzed and compared, and then combined with the actual situation of Zhengzhou North Station, from multiple angles such as security and efficiency, finally selected the zhengzhou north station integrated automation solutions, which conducive to further implementation of zhengzhou north station information and control automation and layoffs.

Scheme Comparison

Marshalling integrated automation in the traditional sense, although supporting a vehicle management information, hump automation, remote control of locomotives and other major systems, but it is relatively independent of each subsystem, the installation and use are usually scattered in different job sites, the information technology degree is relatively low, did not constitute a unified centralized system.

At present, the mature of the marshalling station integrated automation solutions basically has two, one is Computer Integrated Process System(CIPS), one is Synthetic Automation of Marshalling Yard(SAM). Both for the first time regard the integrated automation as a whole system for unified planning, design and research, through system integration, further improve the degree of informatization and automation of the marshalling station. The SAM system has been applied in Xinfengzhen marshalling yard, CIPS system, mainly in the north of Chengdu, Guiyang south and

Wuhan north marshalling yards. Both of them have made great achievements in practical application, have made a great contribution to the automation process of the marshalling station.

Difference in The System Structure. SAM system has two information and processing platform, One of the platform is Synthesize the Manage Information System(SMIS), to handle the current vehicle and shunting plan information; Another platform is centralized control system, the system is mainly processing the traffic information and the function of centralized control which related to train dispatching command system (TDCS), process control system with various interface formed centralized control. Both platforms have their own separate database, network interfaces and dedicated servers, a full exchange of information and sharing with each other by the network security devices[2].

Information processing platform of CIPS system organically integrated the information storage, information processing and network, formed a integrated information management system. So CIPS system only has one platform, this platform via the data interface to obtain TDCS and TMIS information, then focus on driving, current car, locomotive information and the task of centralized control operation, directly drive the process control system to perform.

Difference in The Planning. SAM system functions according to the "travel" and "shunting" two main line, separately distributed on two different platforms SMIS system and centralized control system. The key is through enhancing data exchange between systems, achieve cooperation through smooth information sharing. The characteristic of its plan to deal with is the close relationship between railway administration and station, to strengthen the railway administration planning and scheduling command for the station[3].

CIPS system is based on the same platform, after obtaining travel, shunting and other information, unified stored in a memory, the entire production process are around a group of data , eliminating possible factors such as incomplete, untimely, inaccurate, inconsistent or unavailable which cross-platform sharing of information that may exist, and these ensure that the linkage between the lateral business. The characteristic is that each production links in a single command Framework, the relationship between planning and implementation more tightly, enforcement of the plan was strengthened[4].

Difference in The Execution. SAM system adopts the principle of CTC, based on the station control network, realize the control center for centralized control of each signal building . travel and shunting approach can be automatically handled by the program, namely the automatic mode; Can also column or each hook after artificial confirm agreed to automatically handle, namely the semi-automatic mode. Semi-automatic mode, with default approach programs given by automatic decision, while the other options available, the operating personnel can be provided for automatic approach to determine or artificial selection.

CIPS not using typical CTC system solutions, but put the regional interlocking technology control and display terminal togethe in the dispatch center , used for emergency manual intervention. CIPS system in automatic mode, all route automatically as planned, its timing , execution order and line path is controlled by the computer, even without the personnel agreed and confirmed. If you need manual intervention, you should stop the automatic routing beforehand or artificial replacement again after cancelled the automatically approach. Its characteristic is to realize automati handle directly, to a large extent reduce the labor intensity of the workers[7].

Scheme Selection for Zhengzhou North Station

Safety Analysis. First of all, both the two systems are based on the concept of automation, which implements the employee's work post from "personally" to "monitor", it's from a certain extent, solve the safety hidden danger of human error.

But the CIPS system, direct constitute a closed loop and interaction between planning and execution, is the concept of management and control integration. SAM system architecture "management" and "control" relatively independent, information, control and wireless channel three network independent, the Maturity and familiarity degree of planning treatment is higher, safety index also is relatively high. For example, Xinfengzhen marshalling yard department information center, fully close the relationship between the railway dispatching system 4.0 and the station SMIS2.0 4.0, to strengthen the command and dispatching relationship between the railway administration and marshalling yard. This kind of "divide and conquer" natural advantages, disperse the risk of operation, improve the safety index.

Zhengzhou North Station already has 50-year history, the scene of operations master have been accustomed to the traditional division of labor, industrial structure ,as well as the traditional management system. SAM system this kind of "management" and "control" relatively independent system structure, keep the traditional industrial structure of the division of labor, easy docking with the traditional maintenance management system, the push is also relatively easy. From manual operational impact on safety, the use of SAM systems will be relatively safe.

Efficiency Analysis. Zhengzhou north station in the research on integrated automation solutions, successively organize relevant personnel to Xinfengzhen, Chengdu North , Wuhan station for a inspection. Table 1 is Xinfengzhen(SAM)and Chengdu North (CIPS)marshalling yard operation status table[6].

Table 1 SAM and CIPS system operating condition table of the marshalling station

Marshalling yards	Xinfengzhen station (SAM)	Chengdu north station (CIPS)
Standing type	Triple seven	Level 3 six games
Shunting line number	34+37	32+32
Group number quantity	41	291
Number of shunting	10	8
Exchange field	With	without
Average daily handling volume	19272	13873
Average ratio	69%	91%
Responsible for the intermediate station number scheduling hall	1	13

From the table1, we can see that the scale and the production of Xinfengzhen marshalling station are larger than that of Chengdu North, Comparison between the two field operating conditions, we can see, SAM systems tests bearing pressure is relatively large. Although the CIPS system in a high degree of automation, which is beneficial to the improvement of the production efficiency, but due to various reasons such as traffic sources, the traffic flow of Chengdu north marshalling yard still lower than Xinfengzhen, therefore the CIPS system efficiency stress tests need to be further verification in the future.

In addition, the station shape, operation mode, and traffic sources of zhengzhou north station is very complex. For example, the zhengzhou north station has a lot of no-humping vehicle, hump break-up plans change is often common. From the practical situations of using CIPS system,we can see, to a certain extent,CIPS system programming is established on the basis of no change of plan. So, if zhengzhou north station really use the CIPS system, it is difficult to ensure that the entire station a actually higher working efficiency.

Multi-analysis. In terms of choice marshalling station integrated automation solutions, the biggest different between Zhengzhou and Wuhan north station is that Wuhan north station is a new station, while Zhengzhou north station is old. The old station renovation must fully consider the use of original equipment, while the new station don't have to consider.

CIPS system affected by the construction schedule and their own platform hardware requirements, new investment is larger, and do not have step-by-step implementation conditions, one-time implementation in Zhengzhou north station is very difficult; Although SAM system overall project also need large investment, but can take advantage of most existing systems and equipment of Zhengzhou north station, and on the basis of total working, reserve automatic control conditions, also can provide convenient conditions for the next upgrade .

In addition, because of the high degree of automation, compared to the operating personnel configuration of wuhan north station, if choose CIPS system, zhengzhou north station will be a massive layoffs. But considering all factors, the current Zhengzhou North Station does not have the condition of massive layoffs , some positions and personnel must be retained because of the job requires.

Scheme Selection. SAM and CIPS, two systems, have similar functions, and have their own characteristics, In combination with the practical situation of Zhengzhou north station, considering from safety, efficiency and so on ,we think SAM systems is more suitable for Zhengzhou north station.

First, if use the SAM system, we can take advantage of most existing systems and equipment of Zhengzhou north station. For example the three baby of Zhengzhou north station---- "SMIS2.6 dispatching system" and "Cargo Inspection Station safety monitoring system" "TW-2 Hump Automation Systems". Save time limit for a project, but also reduce the financial investment.

Secondly ,SAM system this kind of "management" and "control" relatively independent system structure, keep the traditional industrial structure of the division of labor, easy docking with the traditional maintenance management system. This in accordance with the working habits, dispersed the risk of operation, and improved the safety index. In addition, Considering the station shape, operation mode, and traffic sources of Zhengzhou north station, combination of the Xinfengzhen(SAM)and Chengdu north (CIPS)marshalling yard operation status table, we think that SAM systems tests bearing pressure is relatively large. If Zhengzhou north station using the SAM system, the efficiency will be higher.

In a word, In combination with the practical situation of zhengzhou north station, considering from safety, efficiency and so on ,we think SAM systems is more suitable for zhengzhou north station.

Conclusions

The integrated automation transformation of marshalling station is an inevitable process of railway technology and equipment modernization. SAM and CIPS two sets of system application, greatly improved the operation efficiency of the marshalling station, ensure the safety and smooth operation, is of great significance for railway modernization. This paper compares two kinds of SAM and CIPS Marshalling integrated automation solutions, combining with the actual situation of Zhengzhou north station, analyze from various angles such as safety and efficiency， finally choose the appropriate solution. I hope SAM system can provide a strong support for the safe production and efficient transportation of Zhengzhou North Station, and bring a profound influence on the post setting, process ,operation mode, rules and regulations and management of Zhengzhou north station.

Acknowledgements

This work was financially supported by the Beijing Municipal Education Commission scientific research and gradute education projects (No.T11H10010) and the Nation Basic Research Project of China(2012CB725406).

References

[1] Hongwei Guo: Railway information technology and e-commerce,2010,(3)
[2] Tianzong Lu. China railway,2010,(3)
[3] Qiang Li. Railway signal and communication,2010,46(8)
[4] Wenwu Zhao. Railway technology,2012,18(2)
[5] Kun Ding. China railway,2006,(8)
[6] Jianfen Tian. Railway communication signal,2009,45(10)
[7] An He, Biao Du, Yufeng Yao, Hao Zhang. Railway communication signal,2012,48(9)

Applied Mechanics and Materials Vol. 596 (2014) pp 640-645
© (2014) Trans Tech Publications, Switzerland
doi:10.4028/www.scientific.net/AMM.596.640

Motion Simulation and Finite Element Analysis of the Manipulator Based on SolidWorks

LU Peng[1]，CHENG Dao-lai[1]，SHI Gang[2]，ZHOU Zhi-hao[1]，LI Nan-kun [3]

College of Urban Construction and Safety Engineering，Shanghai institute of Technology，Shanghai 201418，China [2]Institute of Mechanical Engineering，Shanghai institute of Technology，Shanghai 201418，China [3]Shanghai Bamac Electric Technology Co., Ltd.，Shanghai 201700，China

Keywords: SolidWorks Manipulator Three-dimensional Modeling Motion Simulation

Abstract. It will use SolidWorks to design structure of Manipulator and to establish the Three-dimensional Modeling based on automated welding robot of Shanghai Bamac Electric Technology Co., Ltd.，then by using the plug of simulation and motion of SolidWorks, it will focus on the Motion Simulation and Finite Element Analysis of the Manipulator. Finally the trajectory and the work space of the Manipulate can be received, and provide a basis of manipulator analysis in order to optimize the manipulator for the company.

Introduction

Machine hand claw similar to the parts of a man's hand, used for clamping workpiece or tool, is a very important executive body. At present ,There is a wide range of applications in every field such as automobile and auto parts manufacturing, machinery processing industry, electronic industry, coal mining machinery, rubber and plastics industry, food industry, wood and furniture manufacturing, etc. With the development of computer application technology, computer simulation functionality in advance has become an important means of scientific research, and it plays an important role in the process of feasibility demonstration, project design rationality and searching best solutions. SolidWorks is one of the Desktop integration system that based on CAD/CAE/CAM/PDM of Windows，and it has a strong character creation ability and assembly control ability [1].This paper is based on automated welding robot of air conditioning refrigerator compressor imported from Germany of Shanghai Bamac Electric Technology Co., Ltd. ,and shows how to carry out the preliminary simulation and the analysis of the research in order to make this technology localization and more optimization.

The basic principle of kinematics

Kinematics principle of rotating shift matrix is used to describe its working condition, the gripper mechanism in the space of sports including translation, rotation or a combination of two kinds of sports. This is a matrix of 4×4

$$\begin{bmatrix} \mathrm{R}_{rotate} & R_{trans} \\ 0 & 1 \end{bmatrix}_{4\times 4} \tag{1}$$

R_{rotate} is a matrix of which describe the rotary motion of the organization .R_{trans} is a matrix of used to describe the translational motion of the organization. Assuming that claw goes around the space of any axis rotation u, Rotation Angle as φ, the rotation matrix can be expressed as

$$R_{\varphi u}=\begin{bmatrix} u_x^2V_\varphi + C_\varphi & u_xu_yV_\varphi - u_z S_\varphi & u_xu_zV_\varphi + u_y S_\varphi \\ u_xu_yV_\varphi + u_zS_\varphi & u_y^2V_\varphi + C_\varphi & u_yu_zV_\varphi - u_y S_\varphi \\ u_xu_zV_\varphi - u_yS_\varphi & u_yu_zV_\varphi + u_xS_\varphi & u_z^2V_\varphi + C_\varphi \end{bmatrix} \tag{2}$$

The three axis of u_x, u_y, u_z are direction cosine of *u* in the formula，a $\begin{cases} V_\varphi = 1 - cos\varphi \\ S_\varphi = \ sin\varphi \\ C_\varphi = cos\varphi \end{cases}$

Artifacts going around a rotating coordinate system is easy to implement in SolidWorks，But around any axis of rotation, usually based on the rotation transformation matrix. After a series of changes, to coordinate space arbitrary axis rotate around the axis of overlap, and components. The basic theory of implementation：Artifacts revolve around coordinate system x axis u axis rotation changes as space as an example. As shown in figure 1，The coordinate system of x，y，z is a Fixed coordinate system. x'，y'，z' is a moving coordinate system，Axis of u is known，looking for an axis of *n* which is vertical to *u*, and making it goes around the axis of *z* and overlap with axis of *u*; The axis of *x* rotate the same vector as axis *n*. Rotating the same point of view, then cross-product *u* and x'，gaining the axis of y'，Then the moving coordinate system of x'，y'，z'，were got ,in order to implement the rotation of axis of *u* [2].Gripper of institutions around the other axis of rotation can be achieved through the same conversion.

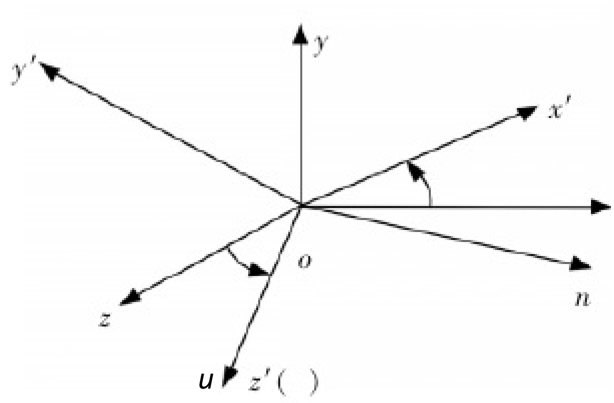

Fig.1 Rotary coordinate transformation

When Institutions were translating，its translation matrix is

$$R_{trans}=[X \quad Y \quad Z]^{-1} \tag{3}$$

In the formula

$$X=-\frac{z(l_3m_2-l_2m_3)+y(l_2n_3-l_3n_2)+x(m_3n_2-m_2n_3\quad)}{l_3(m_1n_2-m_2n_1)+l_2(m_3n_1-m_1n_3)+l_1(m_2n_3-m_3n_2)}$$

$$Y=-\frac{z(l_1m_3-l_3m_1)+y(l_3n_1-l_1n_3)+x(m_1n_3-m_3n_1\quad)}{l_3(m_1n_2-m_2n_1)+l_2(m_3n_1-m_1n_3)+l_1(m_2n_3-m_3n_2)}$$

$$Z=-\frac{z(l_1m_2-l_2m_1)+y(l_2n_1-l_1n_2)+x(m_1n_2-m_2n_1\quad)}{l_3(m_1n_2-m_2n_1)+l_2(m_3n_1-m_1n_3)+l_1(m_2n_3-m_3n_2)}$$

x，y，z are the fixed coordinates of coordinate system，X, Y, Z are the fixed coordinates of moving system，l_i，m_i，n_i (*i*=1，2，3) Are moving axis direction cosine of the coordinate system.

Three-dimensional modeling of mechanical gripper

Three-dimensional modeling of mechanical gripper includes all parts of the assembly process and the result of step modeling, virtual prototyping as follows:

1）Select the appropriate reference plane, the plane created a sketch of the various components depending on the size and structure of the related components. Use commands such as rotate, stretch, cut, features sweeps, lofts, etc. to complete the outline of the basic characteristics of the various parts.
3）Use chamfers, fillets, ribs, etc. The command completed partial modeling.
4）In order to complete the modeling of all parts of the assembly as well as the relationship between the various components constrained use SolidWorks assembly modules individually assembled.
5）Accurate modeling and familiarity with the relevant parts of the relationship is the key to the success of virtual prototype build. Eventually create a virtual prototype, The virtual prototype was created as shown in figure 2

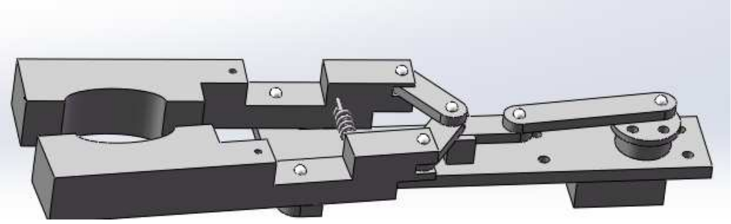

Fig.2 Mechanical gripper assembly drawings

Manipulator motion simulation and finite element analysis

3.1The simulation process of Manipulator motion

Checking formulas to calculate the degree of freedom in accordance with agency $F=3n-2P_l-P$（4）

In the formula n——Represents the number of moving parts；

P_l——The number of Low deputy；

P_h——The number of high deputy.

There are seven moving parts and ten low deputies without high deputy. 1 degrees of freedom can be calculated through the formula. Original stopper is rotated flange，freedom F≧1,then the number of Original stopper as many as freedom，Therefore, the agency has accurate motion. Then the stress, displacement, velocity, acceleration, vibration analysis can be done by SolidWorks based on the designed three-dimensional model of the mechanical gripper.

Its simulation modeling steps are as follows：

1）Selecting Simulation one of the SolidWorks plug-in and creating a new study. Selecting the type of static. Options include setting load, the material, the results of such a unit system.
2）Material settings, user-defined material library material or choose from selected materials inside the library, this design choice is alloy.
3）Constrained settings, Selecting the fixture and then select a face part as a fixed position. You can select a set of constraints or more.
4）Load settings，Makes parts deformed external loads or stresses are designated to produce parts，such as the force or pressure, in this embodiment the pressure suffered size is 100N.

3.2 Finite element analysis process and results of Manipulator

（1） Meshing and Finite Element Analysis

1）Selecting meshing module of Run module, according to the computer for analysis recommended meshing . You can also set attainment parts of the grid. This paper is divided according to the degree set parts mesh robot force conditions.

2）Selecting program running of the run module, observe and analyze the results, a minimum safety factor (FOS), the stress and deformation conditions, completion of the "post-processing" step.

（2） Results of Finite element analysis

After analysis, the distribution of corresponding deformation ,condition of vibration, stress distribution can be got, but also animated to show the stress and deformation of the situation. Analyzes eDrawing and generate HTML reports can be created according to the results of these. Part of the report content in the material properties shown in Figure 3. The design of the spring in the Y direction stress analysis is shown in Figure 4, the mechanical gripper angular displacement analysis is shown in Figure 5, the slider velocity analysis is shown in Figure 6, the mechanical gripper bearing vibration analysis is shown in Figure 7, the mechanical gripper bearing stress analysis Figure 8. Solutions have been designed can be analyzed and improved based on these analysis ,thereby greatly simplifying the design work and improve work efficiency.

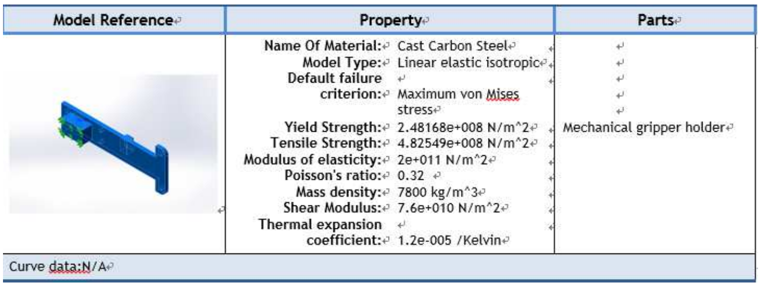

Model Reference	Property	Parts
	Name Of Material: Cast Carbon Steel Model Type: Linear elastic isotropic Default failure criterion: Maximum von Mises stress Yield Strength: 2.48168e+008 N/m^2 Tensile Strength: 4.82549e+008 N/m^2 Modulus of elasticity: 2e+011 N/m^2 Poisson's ratio: 0.32 Mass density: 7800 kg/m^3 Shear Modulus: 7.6e+010 N/m^2 Thermal expansion coefficient: 1.2e-005 /Kelvin	Mechanical gripper holder
Curve data:N/A		

Fig. 3 **Properties of Material**

With the Motion analysis of internal plug in motion the process of spring force of SolidWorks, calculating the results, and generating charts, the Y direction in Figure 4 spring force conditions.

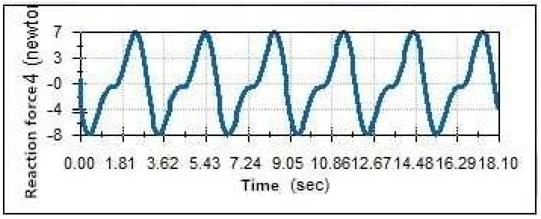

Fig. 4 Y-direction spring force analysis diagram

In order to observe the mechanical motion of the gripper clearly, Selecting the point. Selecting Motion Study Properties, choosing the desired direction, as shown in Figure 5 of the angular displacement situation as mechanical gripper.

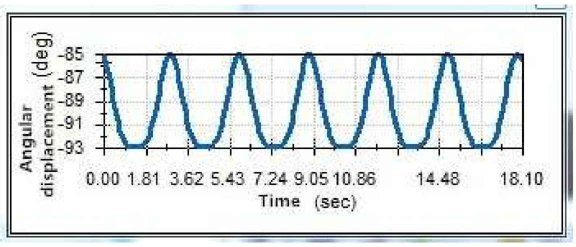

Fig. 5 Mechanical analysis of gripper angular displacement diagram

Analysis of each motion studies are in SolidWorks plug-in Motion. As shown in Figure 6, the selection sliders can be analyzed using the method described above the linear speed of the Z-direction.

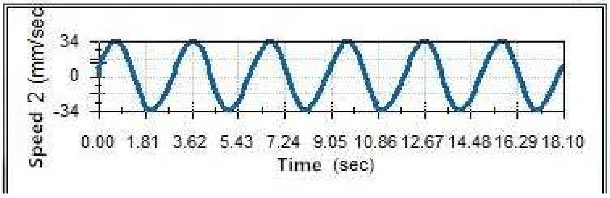

Fig. 6 Slider velocity analysis chart

When a stationary state was interference mechanism, usually a fixed vibration frequency, this frequency is also called natural frequency or resonant frequency. For each natural frequency, radiate a physical shape, also called the mode shape [3].Frequency analysis is to calculate the natural frequencies and associated mode shapes. Frequency analysis is to calculate the natural frequencies and associated mode shapes. The basic principle is $\omega=\sqrt{\frac{k}{m}}$. Theoretically, the entity has an unlimited number of patterns. In theory, on the finite element analysis, the number of degrees of freedom (DOF), there are many modes. In most cases, consider only part of the pattern in which.

When an entity is assumed dynamic load, and the load is a natural frequency of vibration, the reaction that occurs is strongly resonance. Here taking a five modes of vibration, as shown in Figure 7 analysis to obtain the frequency and the different modes of vibration cycles.

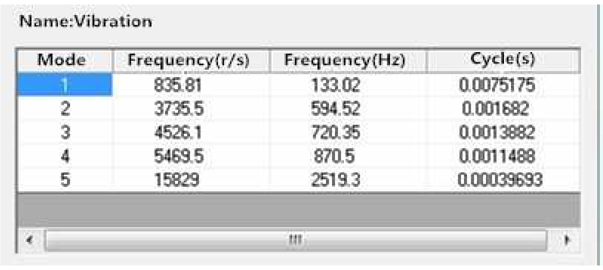

Name:Vibration

Mode	Frequency(r/s)	Frequency(Hz)	Cycle(s)
1	835.81	133.02	0.0075175
2	3735.5	594.52	0.001682
3	4526.1	720.35	0.0013882
4	5469.5	870.5	0.0011488
5	15829	2519.3	0.00039693

Fig.7 Mechanical gripper bearing vibration analysis chart

According to the yield stress in different colors to display various parts of the stress suffered by the situation, as shown in stress analysis (Fig. 8) in a yield stress of parts, a large part of the stress exceeds the yield limit with striking red [4], a relatively small part by the stress of a lighter color blue be represented.

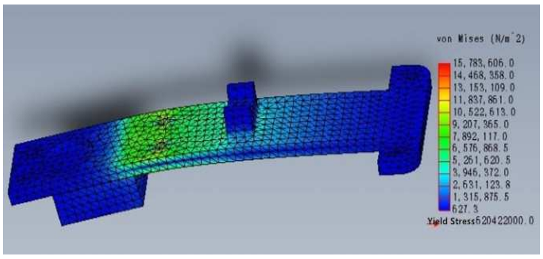

Fig.8 Mechanical gripper bearing stress analysis chart

The designer is easy to find parts weaknesses based on the above finite element analysis results, and it also can help designers to modify their design. After the stress analysis, SolidWorks Simulation also shows the minimum safety factor of the part, which can help designers to further refine the design.

Summary

Methods mentioned in the text of the motion of the mechanical gripper, such as stress analysis, which can speed up the simulation of parts under stress conditions in a number of concepts and scenarios, to shorten the design cycle and optimize the design conditions. Performing computer simulation with SolidWorks enables the simulation of reality, you can also implement some complex simulation curve agencies to make sport more vivid real, designing to provide further improvement of brazing automation technology for Shanghai Bamac Electric Technology Co., Ltd.

ACKNOWLEDGMENT

This paper is supported by National Nature Science Foundation of China(61071203), the shanghai finance project "Green Energy and Power Engineering(1010K131001)"and the Shanghai excellent curriculum "Auto Control and Thermal Instrument(405ZK120015001)" .

BIOGRAPHICAL NOTES

LU Peng: man,born in 1990, Master, Shanghai Institute of Technology, China. His research interests include noise and vibration control,energy saving technology, signal process, mechanical fault diagnosis.

Corresponding Author: CHENG Dao-lai

CONTACT METHOD

College of Urban Construction and Safety Engineering, Shanghai Institute of Technology A413,No.2 Teaching Building,No.100 Haiquan road, Fengxian District, Shanghai City, China(P.C:201418)
E-mail:632953168@qq.com
Tel:15216838824

References

[1] ZHANG Jin-xi.SolidWorks and COSMOSMotion Mechanical simulation technology [M].BEI Jing：Tsinghua University Press，2007.

[2] ZHANG Che. Dynamics of mechanic [M].BEI Jing：Higher Education Press, 2008.

[3] GUO Xiao-ning.Based on SolidWorks entities on both sides of the plane body motion analysis [J]. Xi'an University of Technology, 2007（4）：392-395.

CHAPTER 8:

Power Engineering and Control, Power Electronics

Applied Mechanics and Materials Vol. 596 (2014) pp 649-652
© (2014) Trans Tech Publications, Switzerland
doi:10.4028/www.scientific.net/AMM.596.649

Dynamic Economic Dispatch Based on Improved Particle Swarm Optimization

Yonggang Li [1,a], Liang Han [1,b]

[1]Department of Electrical Engineering, North China Electric Power University, China

[a]lygzxm0@163.com, [b]hfhanliang111@126.com

Keywords: Wind power, Energy-saving and emission reduction benefits, Dynamic economic dispatch, Improved particle swarm optimization

Abstract. Because wind power can reduce the total generation costs under certain conditions, in order to minimize the system production cost, optimize the power output of thermal unit, a dynamic economic dispatching (DED) model containing wind power based on energy-saving and emission reduction benefits is proposed. Such DED model has a nonlinear objective function and the characteristic of high dimension, and is restricted by many constraints. An improved particle swarm optimization (IPSO) is proposed for solving the problem. Feasible regulation scheme is adopted in equality constrains. On the premise that the speed of iterative convergence is assured, the diversity and the excellence of solution are improved by introducing the differential mutation, which enhances the algorithm in breaking away from the local optimum and speeds up the iterative convergence of the algorithm.

Introduction

With the increase of wind power in power systems, the influence of wind farms penetration should be considered in economic dispatch. Compared with other new energy, wind power has the advantages of more mature technology, lower cost and cleaner qualities. Therefore, it has a very important significance to study the dynamic economic dispatching (DED) model containing wind power.

Traditional static economic dispatch of power system is a method to schedule the online generator outputs with the predicted load demands over a certain period of time so as to operate an electric power system most economically [1,2]. Dynamic economic dispatch is an extended mode of static economic dispatch [3,4]. It is a dynamic optimization problem taking into account of the constraints imposed on system operation by generator ramping rate limits. Based on this, a dynamic economic dispatching (DED) model based on wind power and energy—environmental efficiency is proposed [5]. The model considers many intricate constraints, such as balance of power system, the system reserve capacity, the ramp rate, the unit output and line power flows. Since DED was introduced, several methods have been used to solve this problem, such as simulated annealing (SA) [6], genetic algorithm (GA) [7], ant colony algorithm [8], differential evolutionary algorithm [9], artificial neural networks (ANN) and particle swarm optimization (PSO) [10,11]. However, all of those methods may not be able to provide an optimal solution and usually getting stuck at a local optimal. For low accuracy and divergent results of fundamental PSO in solving the high dimension, nonlinear, multi-constrained optimization problem, this paper provides an improved particle swarm optimization.

The Model of the Dynamic Economic Dispatch

Taking Energy—environmental efficiency into account, the DED problem studied in this paper can be described as an optimization process with the following objective function and constraints:

$$\min f = \sum_{t=1}^{T}\sum_{i=1}^{I}\left[C_i(P_{i,t}) + E_i(P_{i,t})\right]. \tag{1}$$

where f is the production cost of thermal unit; T is the number of hours in the time horizon, I is the number of thermal unit; $P_{i,t}$ is the real power output of generator i at interval t. $C_i(P_{i,t})$ is the generation cost of fuel; $E_i(P_{i,t})$ is the environmental costs of the generation, and they are formulated as follows:

$$C_i(P_{i,t}) = b_i(P_{i,t}) + h_i(P_{i,t})\,. \tag{2}$$

$$E_i(P_{i,t}) = C_{1i}b_i(P_{i,t}) + C_{2i}h_i(P_{i,t})\,. \tag{3}$$

where $b_i(P_{i,t})$ is coal consumption curve of unit, $h_i(P_{i,t})$ is the oil costs of the unconventional peak-regulation, $b_i(P_{i,t})$ and $h_i(P_{i,t})$ are defined by

$$b_i(P_{i,t}) = A_i P_{i,t}{}^2 + B_i P_{i,t} + C_i\,. \tag{4}$$

$$h_i(P_{i,t}) = a_i P_{i,t} + c_i\,. \tag{5}$$

where A_i, B_i and C_i are the characteristic coefficients of coal consumption; a_i and c_i stand for the coefficients of oil costs; C_{1i} and C_{2i} stand for CO_2 emission coefficients of unit coal and diesel combustion.

Power balance constraint:

$$\sum_{i=1}^{I} P_{i,t} + P_{w,t} = P_{L,t}\,. \tag{6}$$

where $P_{L,t}$ stands for system load in the t time, $P_{w,t}$ is the planned output of wind power during the tth interval.

System reserve capacity constraint:

$$\sum_{i=1}^{I} P_{i,t\max} \geq L_t + R_{t\max}\,. \tag{7}$$

where $P_{i,tmax}$ is the maximum output, L_t is peak load during t period, R_{tmax} is spinning reserve of the peak load.

Real power operating limits:

$$P_{i\min} \leq P_{i,t} \leq P_{i\max}\,. \tag{8}$$

where P_{imin} and P_{imax} are the minimum and the maximum real power outputs of ith generator.

Generating unit ramp rate limits:

$$-r_{i,d} \times T_{60} \leq P_{i,t} - P_{i,t-1} \leq r_{i,u} \times T_{60}\,. \tag{9}$$

where $r_{i,d}$ and $r_{i,u}$ are ramp-up and ramp-down rate limits of ith generator, respectively. T_{60} is the running interval of 60 minutes.

The Improved Particle Swarm Optimization (IPSO) Algorithm

An improved particle swarm optimization (IPSO) is proposed for solving the high dimension, nonlinear, multi-constrained optimization problem. The proposed algorithm can ensure feasibility of the solution by means of feasible regulation scheme; at the same time to prevent precocious convergence of the algorithm and to quicken the search speed. The differential mutation is adopted to improve the diversity of the solution.

Feasible regulation scheme. IPSO parameters combine inertia weight in linear decrease with asynchronous learning factors. Feasible regulation scheme is adopted in equality constrains. Take $\sum_{n=1}^{N} P_{i,n} + P_w - P_L > 0$ as an example to illustrate: The infeasible violation degree M of vector $\boldsymbol{P}_i$ in the equality constraints is presented by formula (10); the floating value of variables $\Delta P_{i,j}$ is presented by formula (11), then the feasible solution $\boldsymbol{P}_{i*}$ can be formulated as (12).

$$M = \sum_{n=1}^{N} P_{i,n} + P_w - P_L \quad . \tag{10}$$

$$\Delta P_{i,j} = \frac{\sum_{n=1}^{N} P_{i,n} + P_w - P_L}{\sum_{n=1}^{N} (P_{i,n} - P_{n\min})} \cdot (P_{i,j} - P_{j\min}) \, . \tag{11}$$

$$\mathbf{P}_{i^*} = \mathbf{P}_i - \Delta \mathbf{P}_i = \left[P_{i,1} - \Delta P_{i,1}, \ldots, P_{i,N} - \Delta P_{i,N} \right] . \tag{12}$$

where N is the dimension of variable $\boldsymbol{P}_i$, $P_{j\,min}$ is the minimum output of unit j, P_L stands for system load, P_w is the planned output of wind power.

Differential mutation. In order to prevent precocious convergence of the algorithm and to quicken the search speed, the differential mutation is adopted. During each iteration, differential mutation is introduced into particle position vectors by formula (13).

$$P_t(i,n) = P(i_1,n) + \beta \cdot [P(i_2,n) + P(i_3,n) - P(i_4,n) - P(i_5,n)] \tag{13}$$

where β is inertia weight, i_1, i_2, i_3, i_4 and i_5 are random numbers between 1 and the number of particle P_{size}. $\boldsymbol{P}$ is the position variable before mutation, and $\boldsymbol{P}_t$ stands for the position variable after mutation. Compare the fitness value of $\boldsymbol{P}_t$ and $\boldsymbol{P}$, and choose the better. The mutation occurs in each of the particles. On the premise that the speed of iterative convergence is assured, the diversity and the excellence of solution are improved by introducing the differential mutation.

Simulation Results

In order to demonstrate the rationality of optimization model and great practical value of proposed hybrid strategy, simulation research is carried out aiming at solving DED problem of large scale power system in Liaoning power grid which consists of 44 units. T is one day, which is divided into 24 periods. Wind power prediction results is shown in Figure 1, and the load forecasting results is shown in Figure 2.

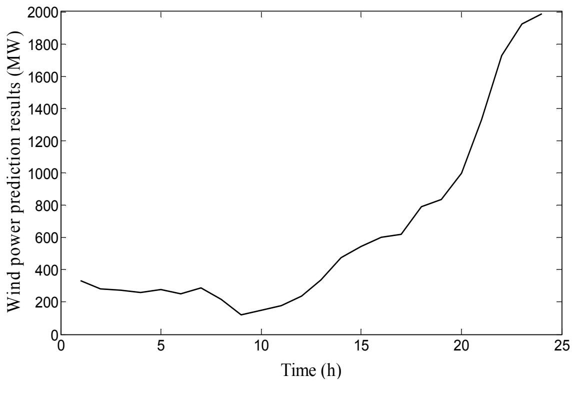

Fig. 1 Wind power forecasting results

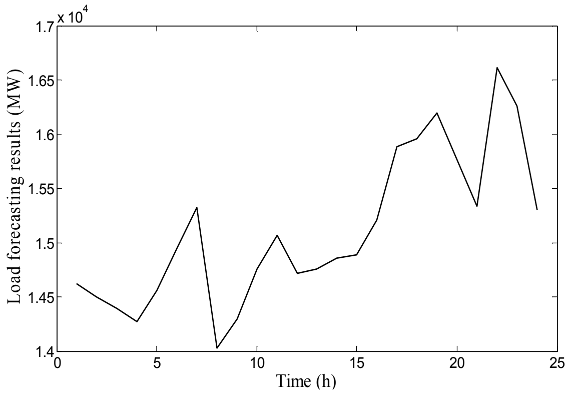

Fig. 2 Load forecasting results

PSO, Adaptive Mutation Particle Swarm Optimization (AMPSO) and IPSO are applied to the DED model, respectively. Each kind of algorithm was tested 20 times. Study the following two performance indicators: the average number of iterations; the average generation costs. The results are shown in Table 1. The relationship curve between the objective function and the number of iterations by three types of algorithm is presented in Figure 3. The results is obvious that the proposed algorithm can give a cheaper total production costs than the PSO and AMPSO.

Table 1 Optimization results of three algorithms

Intelligence algorithms	The average number of iterations	Generation costs [USD]
PSO	360	610804.21
AMPSO	140	581224.31
IPSO	48	561809.48

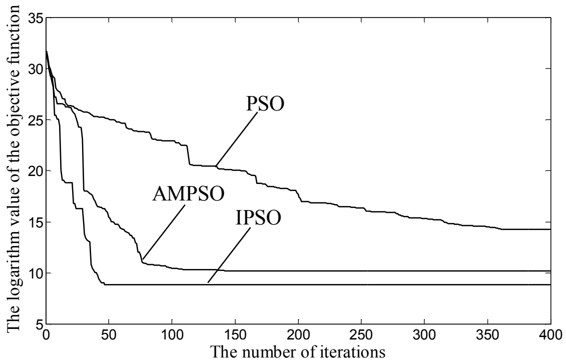

Fig. 3 Different iterative results of the three algorithms

Comparison of optimization results considering wind power is shown in Table 2.

Table 2 Comparison of optimization results considering wind power or not

Power system type	Generation costs [USD]
Power system without wind farm	590843.39
Power system with wind farm	561809.48

Conclusions

This paper presents a new methodology for solving the DED problem of power system containing wind farms based on the benefits of energy conservation and emission reduction. Simulation results demonstrate that the proposed method can give a cheaper total production cost than those obtained from PSO or AMPSO alone.

References

[1] Yunhe Hou, Xinliang Xiong and Yaowu Wu: Proceedings of the CSEE. Vol. 23 (2003), p. 59
[2] Wei Li, Changdong Liu and Deren Sheng: Proceedings of the CSEE. Vol. 24 (2004), p. 241-245
[3] A. Farag, S. Al-Baiyat and T.C. Cheng: IEEE Trans on Power Systems. Vol. 10 (1995), p. 731-738
[4] Z.X. Liang and D. Glover: IEEE Trans on Power Systems, Vol. 7 (1992), p. 544-550
[5] S.J. Wang, S.M. Shahidehpour and D.S. Kirschen: IEEE Trans on Power Systems. Vol. 10 (1995), p. 1294-1301
[6] S. Kirkpatric, C.D. Gelatt and M.P. Vecchi M P: Science. Vol. 220 (1983), p. 671-680
[7] Y. Liu and T. Shang: Economic dispatch of power system incorporating wind power plant, Power Engineering Conference, Singapore, 2007
[8] Yunhe Hou, Lijuan Lu and Xinyin Xiong: Power System Technology. Vol. 28 (2004), p. 34-38
[9] Lehai Bang, R. Thawonmas:A hybrid Differential Evolution method and its application to the physical travelling salesman problem, 2012 IEEE 1st Global Conference on Consumer Electronics, Tokyo, Japan, 2012
[10] C.T. Su and C.T. Lin: IEEE Trans on Power Systems. Vol. 15 (2000), p. 541-545
[11] B.P. Jong, S.L. Ki and R.S. Joong: Economic load dispatch for non-smooth cost functions using particle swarm optimization, 2003 IEEE Power Engineering Society General Meeting, Toronto, Canada, 2003

Applied Mechanics and Materials Vol. 596 (2014) pp 653-658
© (2014) Trans Tech Publications, Switzerland
doi:10.4028/www.scientific.net/AMM.596.653

Electric power communication network optimization algorithm based on the equivalent network

Xing Ningzhe[1 2],Guo Jiaqi[2],Yu Ran[2]

[1]Beijing Jiaotong University, Beijing

[2]State Grid JIBEI Electric Power Co Lit

[a]987968490@qq.com, [b]86696871@qq.com, [c]daxianer100@163.com

Keywords:The equivalent electric power communication network, network, reliability, total quantity of knowledge

Abstract: Reliable power networkcan provide reliable operation of electric power for dispatching communication security, due to many key network nodes external connectivityin the electric power communication networkhas only one path, so once the link damage because of emergencies, these networks because of the failure of nodes (or communication link) and power operation scheduling of exception can occur easily, thus to cause great damage to the safe operation of the whole power network. In order to improve the robustness of system in this case, this paper designed a new optimization algorithm based on the equivalent network to simplify the real network and the network analysis.

0Introduction

Electric power communication network is to serve the power system communication private network,requires support for power system protection and required for high speed and real-time communication, therefore, the safety and reliability of the electric power communication network for communication, protection and control the rapidity and accuracy of the information transmission has very strict requirements.

To ensure safety, reliability and efficiency of electric power communication system and improve the communication system of affordable, according to the requirements of the network structure, operation mode, and consider the communication protection of accident caused by negligence and atrocious weather system, in the network the return of any two components damage does not affect the normal operation of the entire network, important business is not broken. Based on this consideration, the design meet the requirements of network optimization algorithm, and put forward the scientific and reasonable network construction plan become the key problem.

At present most of the research work focus on improving the whole network connectivityby adding redundant links in order to improve the connectivity. Obviously, to join the more resources, the higher the reliability of the system, but there will be a high cost. Under the condition of the limit, some research results show that the current network of double connectivity for a robust network topology and the efficiency of transmission delay is a basic need, in this paper, based on network optimization algorithm is designed, realize the reliability and the balance of the construction cost.

1 The research status at home and abroad

The counter measures of research of electric power communication network,in fact is in fact a communication network reliability research, in recent years, it has made a lot of research results, the results of this study on the design of communication network, planning, operation, maintenance and so on each link in the got very extensive application[1].

In domestic electric power communication network reliability mainly includes: the research progress on the particularity of electric power communication network in the aspect of reliability management, aiming at the reliability management in electric power communication network life cycle stages, points out the design reliability, implement the strategy of reliability, operational reliability, reliability contains research content; Analysis shows that the electric power communication network reliability layered architecture, to set up the network fault, reliability measure and assessment methods and establishing reliability evaluation system; From the Angle of the causal relationship between reliability and network layered puts forward the ideas and methods of reliability research in electric power communication system; In electric power dispatching exchange network, for example, the establishment of the index system of electric power communication network reliability are discussed, the structure of the evaluation model and evaluation steps and reliability management, etc[2,3].

In terms of communication network reliability theory model construction, Liu Rexi, Zhang Jianhua, Wu Di is put forward based on the theory of risk communication network system evaluation theory, the analysis of system risk assessment of the system unit case missing problem; Cao, a communication network reliability theory is put forward, such as the static and dynamic characteristics of communication network, analyzed the influence of network structure for power grid security and puts forward line vulnerability assessment method and the model of the space-time evolution of the communication network, constructing the framework of electric power communication system complexity theory and comprehensive integrated method; 'a widely accepted theory of the general model is put forward. Engineering NASA model is put forward, pretreatment, early warning system for all kinds of tools for associated do situation display of a variety of tools; Presented a high interest Security benefit Index assessment system (Unisys Security Index); Telecommunication network have their own security evaluation index system; Silk Road after put forward the concept of network security situational awareness, according to the characteristics of the local area network (LAN), put forward a series of network security situation of quantitative evaluation methods.

The traditional accident research based on expected, however, there are two drawbacks: (1) if the cost or under the condition of limited budget is limited, the above network construction the research significance of smaller[4]; (2) the net size and complexity increase, some of the network optimization method is difficult to obtain the optimal solution, cannot ensure the reliability level of the hierarchy. From the existing research results, not enough in-depth study, the theory and method can be used to guide the engineering practice is less, still exists many problems remain to be further research[5,6].

2 Equivalent network optimization algorithm

2.1Algorithm ideas

Existing network scale, high complexity, the usual method is difficult to find the optimal topology directly[7]. In this paper, the equivalent LianWangHua Jane network structure, reduce the solution space greatly[8]. The so-called equivalent network, centered on the key nodes will close distance incorporated into a collection, a series of nodes to build several equivalent subnet, then several equivalent subnet as a node, the equivalent network configuration attribute equivalence with the original network, and greatly simplifies the problem space[9].

Network unicom performance, mainly decided by network node degree, in this paper, on the basis of equivalent network, to increase the communication center node ability to improve the degree and the degree of the whole network system, add the link of unicom ability and increase the reliability of the network system, reconfigurable node but not too much increase of redundant resources[10].

In equivalent network building, the establishment of the center node, is determined by the amount of knowledge node to, the so-called knowledge, namely the influence of the node to the other node, the node can provide information unicom capacity is much higher than the other nodes, can be established as the center node, need to calculate and determine the center of the total knowledge of all nodes[11,12].

2.2 Total knowledge calculation

The key nodes with high knowledge value called reconfigurable node. With these nodes subnet system is one of the most architectural group. Each node calculation method of the total knowledge are as follows:

Set any node knowledge : $Z(v_n)$ are:

$$Z(v_n) = \sum_{i=1} \ln f(z_{v_n}^i) \qquad \text{Eq.1}$$

Among them: $\ln f(z_{v_n}^i)$ represent the ith node v factors contribution to knowledge of the total amount. For example, if we set the influence factors of each node of the comprehensive value is set to k,all the influence factors of the node is $z_{v_n}^1, z_{v_n}^2 ..., z_{v_n}^i$, thereare:

$$\ln f(z_{v_n}^1) + \ln f(z_{v_n}^2) + ... + \ln f(z_{v_n}^i) = k \quad \text{Eq.2}$$

The determination of value of each node $f(z_{v_n}^i)$ can be dynamically adjusted according to the actual situation of each node.

2.3The algorithm process

(1) According to the amount of knowledge of each node, determine the key nodes, the C (data center) and key nodes set to establish an equivalent to the transmission network G';

(2) According to the key node to the whole network is divided into multiple equivalent subnet Gn.

(3) According to the equivalent of each key nodes in the network, establish a key node for the data center c_j ;

(4) For each equivalent network, set up in addition to the data center node c_j set of all nodes $v = \{v_1, v_2, ..., v_n\}$,where n is to point to each equivalent network nodes;

(5) A collection s of all the nodes to data center has to a data transmission channel between adjacent nodes have to link to link, as follow:

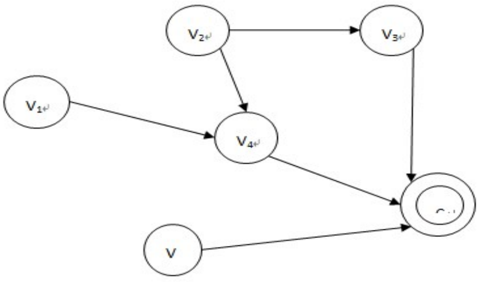

Fig.1 Data link

There are 6 nodes in the network, the node c_j for data center, then

$$\vec{S} = \left\{ \vec{S}_{v_1,v_4}, \vec{S}_{v_2,v_4}, \vec{S}_{v_2,v_3}, \vec{S}_{v_3,c}, \vec{S}_{v_4,c}, \vec{S}_{v_5,c}, \right\} \qquad \text{Eq.3}$$

L set set for each node to the data center to the shortest path (the number of links to form a path at least) collection $L = \left\{ L_{v_1}^{x_1}, L_{v_2}^{x_2}, ..., L_{v_n}^{x_n} \right\}$,which is suitable for the nth node v_n, x_n is the value of the shortest path; The graph above example, the shortest paths $L = \left\{ L_{v_1}^{2}, L_{v_2}^{2}, L_{v_3}^{1}, L_{v_4}^{1}, L_{v_5}^{1} \right\}$ et,the node v_1, v_2, v_3, v_4, v_5 of the shortest path of2,2,1,1,1 respectively.

Establishing each node of the collection, the degrees $o^0 = \left\{ v_1^{x_1^0}, v_2^{x_2^0}, ..., v_n^{x_n^0} \right\}$,the $v_n^{x_n^0}$ of the nth node out degree value is x_n^0; As above, each node of the collection $o^0 = \left\{ v_1^{1_1^0}, v_2^{2_2^0}, v_2^{1_3^0}, v_2^{1_4^0}, v_2^{1_5^0} \right\}$,the node v_1, v_2, v_3, v_4, v_5 degrees: 1,2,1,1,1.

To establish each node in the collection, the degree $o^i = \left\{ v_1^{o_1^i}, v_2^{2_2^i}, v_3^{1_3^i}, v_4^{2_4^i}, v_5^{0_5^i} \right\}$,the $v_n^{x_n^i}$ of the nth node out degree value is x_n^i;

(9) To create a new empty collection $V_G = \{\}$.

(10) Collection $V - V_g$, if $(V - V_g) = 0$ go to step 12.

(11) If $(V - V_g) \neq 0$, to find the shortest path $(V - V_g)$ in the set of values (found L in the collection) to the smallest node, after find the node V_K (the node $L_{v_k}^{x_k}$ in the collection L of the minimum).

(12) To the collection O，to find the node degrees $v_k^{x_k^0} \geq 2$, if the node degrees, in the collection V_g to find the node, if the node V_g does not exist in the collection, the node V_g will be copied to the collection; If the node degrees $v_k^{x_k^0} = 1$, is to look for in the directed graph of the node with minimum value degree of adjacent nodes v_j (the node, not one of the degree of nodes v_j), between the node and v_j, increase a directed link, and the node v_j as the node degree of nodes, and update set respectively $\vec{S}, L, O, O^i$, and then copies the node to the collection V_g, go to step 10.

(13) Such as nodes , each node V_k in the collection V_g, to look for in the collection o^i of the degrees, if greater than y (can according to the knowledge of the node value, adjusted) node, if the node degree value is equal to 2, to look for in the directed graph has no connection with link adjacent nodes, establishing the link between the two nodes, and the node as the node V_k of the node.

(14) To perform step 4 to 13, until all the equivalent network complete, algorithm terminates execution

3 The example analysis

Hebei north electric power communication network, the author of this paper is optimized, enhance network reliability. As shown in figure

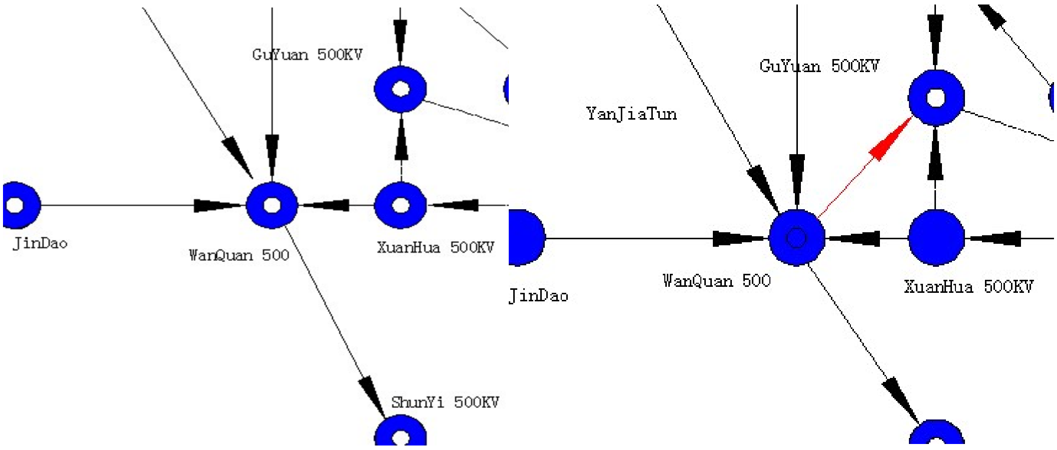
GuYuan 500KV
JinDao
WanQuan 500
XuanHua 500KV
ShunYi 500KV
GuYuan 500KV
YanJiaTun
JinDao
WanQuan 500
XuanHua 500KV

(a)Before optimization (b) Optimized

Fig.2 Foolproof communication station network topology

Analysis found 500kv substation outward foolproof is 1 point to lower 500KV substation reliability Guyuan, through subsequent optimization algorithm to add a link, the red line for the new link. Similarly, several other network topologies following through after contrast optimization algorithm is as follows:

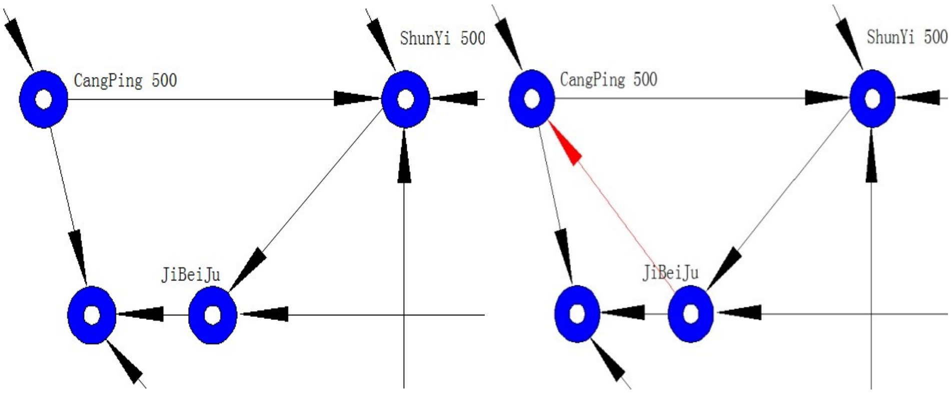
CangPing 500
ShunYi 500
JiBeiJu
CangPing 500
ShunYi 500
JiBeiJu

(a)Before optimization (b)Optimized

Fig.3 Northern Hebei Bureau of communication station network topology

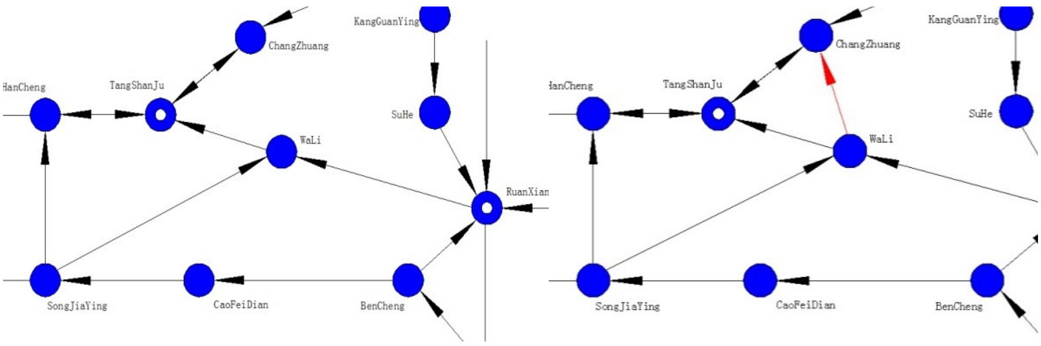
KangGuanYing
ChangZhuang
HanCheng
TangShanJu
WaLi
SuHe
RuanXian
SongJiaYing
CaoFeiDian
BenCheng
KangGuanYing
ChangZhuang
HanCheng
TangShanJu
WaLi
SuHe
SongJiaYing
CaoFeiDian
BenCheng

(a)Before optimization (b) Optimized

Fig.4 Wali station network topology

4 Conclusion

Electric network communication requires any two nodes in the network or cable segments, the communication network as a whole can continue to run. In this paper, the actual situation of electric network communication system, by using graph theory analysis, design optimization algorithm based on the equivalent network to identify the node does not meet the requirements, by increasing their external links to improve reliability, lower limits in the reconstruction distance, define the optimal topology.

This paper considers the dual requirements of network connectivity.For single connectivity (digraph network), algorithm can be applied more easily. In a real network system, considering the stochastic model of node failure, consistent with some special emergency situations, you get the equivalent network configuration can increase the reliability of the network system.

Acknowledgment

This paper is funded by StateGridCorporationofChina Technology Project: No.8EE000M13063.

References:

[1] Codetta-Raiteri,D.,Nai,R. I International Journal of Modelling and Simulation, 2010, 30（3）:345-352

[2] V.C. Gungor, F.C.Lambert. A survey on communication networks for electric system automation[J]. Computer Networks,2006,50（7）:877-897

[3] Papandreou, Nikolaos, Antonakopoulos, Theodore. Resource allocation management for indoor Power-line communications systems[J]. IEEE Transactions on Power Delivery,2007,22（2）:893-903

[4] Angel A. Bayod-Rujula. Future development of the electricity systems with distributed generation[J]. Energy,2009,34（3）:377-383

[5] Qi Bing l, Yang Xuc-jinl, GongGang-junl. Design and realization of electric Power communication resource management system[J]. Relay,2005,33（16）:54-61

[6] Luder, E..The network-and system ’ s theory of electrical communications[J]. UmschauinWissensehaft und Teehnik,1974,74（10）:303-306

[7] Cai, Jun, Shen, Xucmin, Mark, Jon W. IEEE Transactions on Wireless Communications,2005,4（4）:-688-1702

[8] LianZhao,Mark,J.W. Sixth IEEE International Symposium on a World of Wireless Mobile and Multimedia Networks, 2005,428-436

[9] Man CheolKim,Jinkyun Park, Wondea Jung, Hanjeom Kim, Yoon Joong Kim.. Annals of Nuclear Energy,2010,37（6）: 888-893

[10] Chia-HungLien,Hsien-ChungChen,Ying-Wen Bai, Ming-Bo Lin. Instrumentation and Measurement Technology Conference proccedings,2008,2-79

[11] Xu,Liang,Chen,Tianding,Ren,Zhiguo,Wu,Di. Global Mobile Congress,2007,284-288

[12] Majid Khodier, Gamcel Saleh. International Journal of Electronics and Communications,2010,64（6）:489-502

Applied Mechanics and Materials Vol. 596 (2014) pp 659-663
© (2014) Trans Tech Publications, Switzerland
doi:10.4028/www.scientific.net/AMM.596.659

Fault Location Scheme for Transmission Lines Using Kaiser Self-Convolution Windowed FFT Phase Comparison

Guochen Fan[a], Yongli Zhu[b], Hongwei Yan[c] and Yanfeng Gao

State Key Laboratory of Alternate Electrical Power System With Renewable Energy Sources (North China Electric Power University),Baoding 071003

[a]fanchenliusi@163.com, [b]yonglipw@163.com, [c]yanhongwei51@163.com

Keywords: Transmission Lines; Fault location; Phase comparison; Kaiser window; Self-Convolution; Spectral Leakage; Multi-Point Measurement

Abstract. In order to improve the fault location accuracy, and eliminate the influence of spectral leakage in power transmission line fault location, we proposed a novel fault location scheme for transmission lines based on multi-measurements and phase comparison with Kaiser self-convolution windows FFT, which can locate the fault between two adjacent towers in the fault-prone segment. It is based Kaiser self-convolution window's excellent performance of leakage suppression, which can effectively solve the phase current fault component is relatively large errors due to spectral leakage problem. Firstly, this paper analyzes the causes of the phase spectrum leakage, then elaborates the sidelobe characteristics of Kaiser self-convolution window, and lists phase comparative fault location using steps, finally, verifies the correctness of the proposed method by simulation. The results show that the proposed method can effectively suppress spectral leakage, has a high location accuracy, a wide applicability and its solving of phase difference is precise.

Introduction

In the power system, transmission line is a component that has the highest frequency of faults. When a circuit failure occurred, it goes without saying that the rapid and accurate fault location which can accelerate the repair of line faults, eliminate hidden dangers and ensure the power supplying reliability is very useful to power system.

In recent years, some research results have been made on the fault location. Among the many schemes to locate faults in transmission lines, The double-ended traveling wave method was used in references[1], which has obvious advantages and reliability. However, It requires a higher clock synchronization, meanwhile, not only a certain distance between the traveling wave measuring points is required, but also the influence of distributed capacitance current and conductor sag[1] can not be ignored. Therefore, the applicable scope and accuracy have some limitations. References[2] proposed the utilization of multiple current measurement points to reduce the impact of capacitive current, but because the measuring points' distance is too short, which causing the initial traveling wave fault arrival time is difficult to distinguish, the traveling wave fault location becomes invalid.

It is convenient to analyze the transmission line fault using the phase relationship, because phase information has a greater margin and lower requirement of channel data transmission[3]. With the development of monitoring technology, currently in the important lines to realize monitoring that based on the *Rogowski coil* and *wireless transmission* of distributed current measuring points has become possible. Rogowski coil has a great traveling wave transmission ability, of which frequency response range and dynamic measurement range is large[4], and can dynamic measure short circuit current without distortion. At the same time, it is easy to install and has a long service life.

In this paper, we use the phase differential protection principle[5] based on fault component current to realize fault location, which improves location accuracy significantly. The study found that to solve the phases of fault current components, using the frequency spectrum analysis methods based on the traditional Fourier transform (FFT) or ap-FFT[6] achieved a good effect, but during the spectrum analysis process, it existed leakage effects in different degree and resulted phase spectrum analysis is inaccurate, which led to the phase comparison method for fault location is not accurate. So the key of phase measurement is how to improve the phase difference algorithm, to avoid leakage generating negative impact on the fault location. But for now, the research on the fault location using the current phase relationship on both sides of the fault current measurement points is still very rare.

In this paper, proposed a novel fault location scheme for transmission lines based on multi-measurements and phase comparison with Kaiser self-convolution windows FFT. The basic principle of method is installed Rogowski current transformer and wireless transmission systems on each tower in fault-prone segments, between two adjacent current measuring points, according to some order compare their phases of fault current component, thus the phase difference values are obtained, under internal fault conditions, the value is about 180, under through-fault conditions, the value is about 0. It can locate the fault between two adjacent towers in the fault-prone segment.

Kaiser Self-Convolution Window

The spectrum leakage is a phenomenon that on the time frequency transform, a specific frequency component is no longer a single line, but leak to other components in the nearby[7]. The basic reason of spectrum leakage is non periodic truncating data and non synchronous sampling. The leakage suppression performance of window function is associated with sidelobe characteristics, the lower sidelobe peak and the faster decay rate, then the inhibition ability of leakage is stronger. Compared with the Hanning window, Kaiser window function's parameters can be adjusted. We can select the desired side lobe performance of Kaiser window, by means of adjusting proportion between the main lobe width and the side lobe height(change main side proportion coefficient values),to achieve the purpose that fully Inhibitory effect of leakage. Kaiser window's temporal expression $w_k(n)$[8]is:

$$w_k(n) = I_0\left\{\beta\sqrt{1-\left[2n/(N-1)\right]^2}\right\}/I_0(\beta) \tag{1}$$

where $I_0(\beta)$ is modified zero order Bessel function[9], change β value, the main lobe width and sidelobe attenuation can be free to choose. When β reaches a certain value, it is no longer obvious that leakage inhibition performance increasing. In order to improve the leakage suppression performance greatly, we set the Kaiser self convolution before FFT calculation. M orders Kaiser self-convolution window is the window function that through Kaiser window m-1 times self convolve operation, its recursion formula is:

$$w_k^{(m)}(n) = w_k^{(m-1)}(n) * w_k(n) = \sum_{x=-\infty}^{+\infty} w_k^{(m-1)}(x)\cdot w_k(n-x) \quad (m \geq 1) \tag{2}$$

Under the conditions of fixed parameters and with the increase of the convolution order, its leakage inhibition performance improved multiply. Fig.1 shows the sidelobe characteristics of Kaiser self-convolution windows in 1~3 orders. Set the windows' length N=32, β=10.

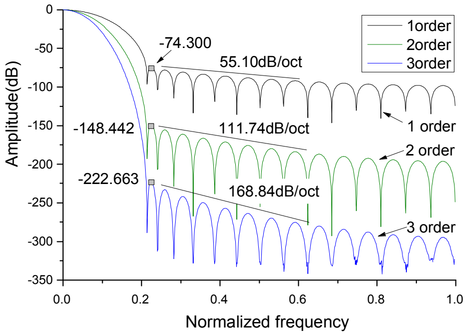

Fig.1. Normalized logarithm spectrum

We note the sidelobe characteristics in Fig.1, 3 orders Kaiser self-convolution windows possesses excellent spectral leakage inhibition performance, and the main lobe width remains unchanged.

FFT Phase Comparison Process

Windowing and Pretreatment. Computed Kaiser self-convolution and normalized amplitude:

$$\overline{w_k^{(m)}(n)} = \sum_{x=-\infty}^{+\infty} w_k^{(m-1)}(x)\cdot w_k(n-x) \Big/ \sum_{i=0}^{N-1} w_k^{(m)}(i) \tag{3}$$

Then windowing the current fault component i(n), we get $i_{\mathrm{wk}}(n)$:

$$i_{w_k}(n) = \sum_{h=0}^{H-1} A_h \, cos\left(2\pi h f_0 n / f_s + \varphi_h\right)\cdot w_k^{(m)}(n) \Big/ \sum_{i=0}^{N-1} w_k^{(m)}(i) \tag{4}$$

FFT Phase Solving. FFT processing $i_{\mathrm{wk}}(n)$, to get $I_{\mathrm{wk}}(k)$:

$$\begin{aligned} I_{w_k}(k) &= \sum_{n=0}^{N-1} i_{w_k}(n)\cdot e^{-j\frac{2\pi}{N}kn} \\ &= \sum_{n=0}^{N-1}\sum_{h=0}^{H-1}\frac{A_h}{2}\left[e^{j\left(\frac{2\pi}{N}nl_k+\varphi_h-\frac{2\pi}{N}nk\right)} + e^{-j\left(\frac{2\pi}{N}nl_k+\varphi_h+\frac{2\pi}{N}nk\right)}\right]\cdot w_k^{(m)}(n) \Big/ \sum_{i=0}^{N-1} w_k^{(m)}(i) \end{aligned} \tag{5}$$

We set $W_N^{l_h n} = \frac{2\pi}{N} n l_k$, $W_N^{kn} = \frac{2\pi}{N} kn$, to get the real and imaginary parts of $I_{\mathrm{wk}}(k)$:

$$Re_{I\,wk}(k) = \sum_{n=0}^{N-1}\left[\sum_{h=0}^{H-1} A_h \, cos\left(W_N^{l_h n} + \varphi_h\right) w_k^{(m)}(n) \Big/ \sum_{i=0}^{N-1} w_k^{(m)}(i)\right]\cdot cos\, W_N^{kn} \tag{6}$$

$$Im_{I\,wk}(k) = -\sum_{n=0}^{N-1}\left[\sum_{h=0}^{H-1} A_h \, cos\left(W_N^{l_h n} + \varphi_h\right) w_k^{(m)}(n) \Big/ \sum_{i=0}^{N-1} w_k^{(m)}(i)\right]\cdot sin\, W_N^{kn} \tag{7}$$

The phase response equation is :

$$\phi_{I_{wk}}(k) = arctan\left[Re_{I_{wk}}(k) / Im_{I_{wk}}(k)\right] \tag{8}$$

Phase difference and leakage degree judgment. Here we get the current phase spectrum, Repeat the above process, for the phase spectrum of next adjacent points, two points are set to m, n, their phase sequences are set to $\phi_{mIwk}(k)$ and $\phi_{nIwk}(k)$, After Subtraction, the phase difference sequence:

$$\Delta\phi_{mn}(k) = \left|\phi_{mI_{wk}}(k) - \phi_{nI_{wk}}(k)\right| \tag{9}$$

Calculate the mean of $\Delta\phi_{mn}(k)$, get the phase difference value:

$$\Delta\phi_{m-n} = M_{m-n} = \sum_{k=0}^{N-1}\Delta\phi_{mn}(k) / N \tag{10}$$

Estimate the standard deviation, to judge the degree of leakage:

$$std_{m-n} = \sqrt{\sum_{k=0}^{N-1}\left[\Delta\phi_{mn}(k) - M_{m-n}\right]^2 / N-1} \tag{11}$$

If phase threshold value $std_{\mathrm{m\text{-}n}}$ is less than threshold value std_{th}, it means that the leakage effect on the phase comparison can be ignored, then the $std_{\mathrm{m\text{-}n}}$ is the fundamental frequency phase of measurement point's fault component current; otherwise, means that the spectrum leakage is serious, we need to change the value of the β. The study found std_{th} can be set to 20.

Simulation Results and Analysis

A 220kV transmission system of double-end source is illustrated in Fig.2, and its length is 200km. The short-circuit current data come from the simulation system PSCAD, and in order to obtain accurate short-circuit current data, the sampling frequency is set to 200kHz and the Frequency

Dependent Model is adopted. We set fault points in the distance S1 between 124 ~ 126km, the corresponding towers are: 248#, 249#, 250#, 251#, 252#, and block space is 0.5km, Measuring points are set to point 1 ~ 5, Grounding resistance is set to 4.5Ω.

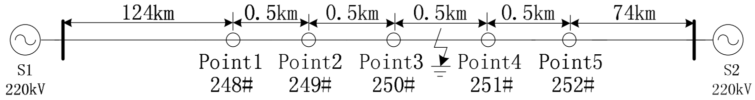

Fig.2. Model of 220kV system

When the working frequency is 50Hz, the parameters of the positive sequence and the zero sequence are given in Tab.1.

Table.1 Parameters of Line

sequence	r(Ω/Km)	x(Ω/Km)	g(s/Km)	b(s/Km)
Positive	0.034676	0.423366	1.0×10^{-7}	2.7256×10^{-6}
zero	0.300023	1.142641	1.0×10^{-7}	1.9355×10^{-6}

The fault points are set in 124.02km, 125.07km and 125.60km. Comparing each adjacent measuring points' current phase at the third periodic waveform's 1/8 after its fault, and then identifying the location of the fault point, the results are shown in table 2.

Tab.2 Results of fault localization

Fault distance/km	$\Delta\phi_{1\text{-}2}{}^{A}$ / °	$\Delta\phi_{2-3}{}^{A}$/ °	$\Delta\phi_{3-4}{}^{A}$/ °	$\Delta\phi_{4-5}{}^{A}$/ °	Results of location
124.02	176.603	0.538	0.495	0.498	248#-249#
125.07	0.453	0.419	172.498	0.376	250#-251#
125.60	0.355	0.363	0.370	172.56	251#-252#

Table 3 shows that this method can accurately locate the fault between two adjacent towers in the fault-prone segment, and the distinction of forward and reverse phase difference is more obvious. In order to distinguish fault phase and non fault phase, this paper simulated ten kinds of common faults, the fault point was set at 124.73km, Kaiser self-convolution window 2 order, β=1, phase differences of 2-3 measuring points for each phase were compared, as shown in Table 3.

Tab.4 Results of fault phase measurement of points 2-3

Fault type	$\Delta\phi_{2\text{-}3}{}^{A}$ / °	$\Delta\phi_{2\text{-}3}{}^{B}$ / °	$\Delta\phi_{2\text{-}3}{}^{C}$ / °	Fault phase
Ag	165.853	1.224	1.541	A
Bg	2.467	166.429	0.987	B
Cg	1.908	7.252	172.399	C
AB	170.267	171.884	0.968	A,B
BC	1.377	169.737	168.250	B,C
AC	175.925	0.600	177.217	A,C
ABg	160.361	166.010	1.017	A,B
BCg	1.914	167.825	163.914	B,C
ACg	179.41	0.550	174.456	A,C
ABC	171.197	168.779	159.720	A,B,C
No	2.581	0.600	0.967	None

The results show that this method can effectively determine the fault phases. In order to compare the leakage inhibition performance between Kaiser self-convolution window and Hanning window, using two different window functions to solve phase spectrum of tower 249#-250# after phase A happend ground fault. Fig. 3 shows that they have different effects on the phase comparison.

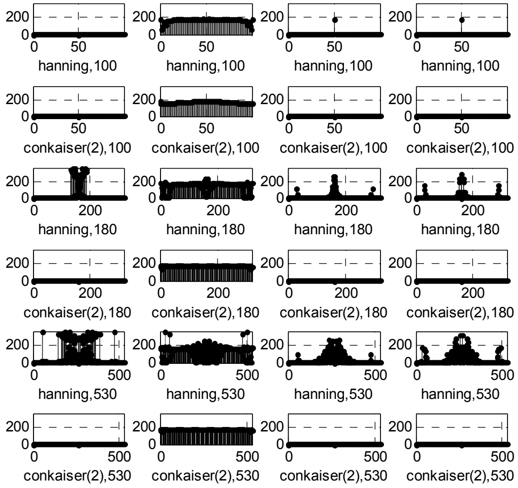

Fig.3. Phases difference by changing windows length

In the Fig.3, each column sub graph is correspond to the phase difference spectrum of measuring points, from the second column (phase difference spectrum of point2-3's phase A), we note its mean is about 180 degrees, and the other columns (phase difference spectrum of point1-2,3-4,4-5's phase A), is about 0. However, due to the presence of the leakage phenomenon, spectrum is not smooth,if number of Sampling points Changed (non-integer period sampling), the length of the window deviated cycle farther, and phase information was interfered and flooded by the false adjacent spectrums. It means that no fault between measuring points originally, but the phase comparison result is judged as faulty, in this case, fault range's misjudgment is inevitable. While we use the phase comparison based on Kaiser self-convolution windows to solve Phase spectrum ,its leakage can be completely inhibited, finally reliabe fault location is realized.

Conclusions

Considering that the frequency spectrum analysis method of the FFT based Kaiser self-convolution window, its performance of leakage suppression is more excellent than the traditional Fourier transform, the fault location scheme for transmission lines using Kaiser self-convolution windowed FFT phase comparison is presented in this paper. In the fault phase comparison process, the phase difference of the fault current component on both sides of the transmission line is computed by FFT. And then the fault phase and fault type are identified by comparing the phase difference with the phase threshold value. In this paper, all kinds of fault conditions are verified by simulation, and the correctness and effectiveness of the fault location method are validated. It is very important to improve the accuracy of transmission line fault location.

This paper was supported by“the Fundamental Research Funds for the Central Universities” (2014xs74)

References

[1] Yongli Zhu, Xinqiao Fan and Jinliang Yin: Transactions of China Electrotechnical Society. Vol. 27 (2012), p. 260-268

[2] Xinqiao Fan, Yongli Zhu and Weifu Lu. High Voltage Engineering, Vol. 38 (2012), p. 1341-1347

[3] Xinqiao Fan and Yongli Zhu, in Proceedings of the 2010 IEEE, International Conference on Mechatronics and Automation, August 4-7, 2010, Xi'an, China: 762-767.

[4] Mingjiang Xiang. Study on Traveling Wave Transfer Characteristics and Application Techniques Based on Rogowski Coils. Doctoral Dissertation of Shandong University, 2013:1-45.

[5] Jiali He, Yongli Li, Xinzhou Dong, et al. in: Principles of power system protection (Fourth Edition). Beijing: China Electric Power Press, 2010: 199-205.

[6] Zhaohua Wang, Xiangdong Huang. in: All phase digital signal spectral analysis and filtering techniques. Beijing: Electronic Industry Press, 2009:12-48.

[7] Renzheng Ma，Mingkai Chen. Automation of Electric Power Systems, 2002: 55-58.

[8] Yihong He，Fang Zhou，Hongyu Li, et al. Power System Technology, Vol. 27 (2003), p. 9-12.

[9] A.V.Oppenheimer, R.W.Schaefer, Discrete-Time Signal Processing. Xi'an: Xi'an Jiaotong University Press, 2001: 373-390.

Applied Mechanics and Materials Vol. 596 (2014) pp 664-668
© (2014) Trans Tech Publications, Switzerland
doi:10.4028/www.scientific.net/AMM.596.664

Optimal Assignment of Emergency Power Considering V2G

An xiangyang[1,2], Liu Jichun[1,a], Wu Yunxia[3], Li Jiayi[3], Zhang Lingzhu[1],
He Chen[2], Chen Honghui[2], Zheng Xiaoli[2]

[1] Department of Electrical Engineering, Sichuan University, Chengdu, China

[2] MAOMING power supply company, Guangdong Electric Power Company, Guangdong province, China

[3] Power system plan center, Southwest Electric Power Design Institute, Chengdu, China

[a]jichunliu75@163.com

KEY WORDS： V2G; emergency power supply; optimal path; optimal assignment

ABSTRACT: An optimal assignment algorithm of emergency power supply considering V2G is proposed with a necessary concern for its effect on society. Firstly, the comprehensive index weight coefficients are proposed according to the priority. Next, this paper establishes the network minimum total cost objective function based on constraints such as time and capacity limit, using symmetric triangular fuzzy numbers to simulate the uncertainties in emergency logistics on the condition that ensuring the normal work of EV in next day which is used to search for the best logistics path. Finally the optimal algorithm of emergency power supply is developed based on genetic algorithm. The model and algorithm are proved by a numerical example, and the study helps to reduce the investment and operating cost of power system and improve the ability of urban electric network in emergency situation.

Introduction

As an expedient for power grid emergency, EPS (Emergency Power Supply) technology can reduce the breakdown loss and secondary disaster efficiently [1-4]. Thus it is a key point to establish an efficient and reasonable power grid accident emergency treatment scheme. At present, the EPS functions of V2G (Vehicle-to-grid) contains the characteristics of rapid reaction speed, flexible capacity choice, few funding, easy acquiring of spare resource and strong anti-disaster ability. To apply it to the important regions' emergency power supply scheme after the grid forced outage can effectively reduce the outage time and power loss. The paper applies the EPS functions of V2G to the scheduling optimization of the grid accident emergency treatment with EV accessing. The research content including:1) Set the importance weight coefficient and establish comprehensive index considering the influence of social relevance in blackout area; 2) establish the network minimum total cost objective function and constraint conditions under the conditions of ensuring the EV in the normal operating; 3) Consider the time uncertainty of logistics, therefore to introduce triangular fuzzy number; 4) Consider capacity allocation situation and demand conditions of area to be restored, genetic algorithm is used to determine the emergency power supply optimization scheme

The optimal allocation problem based on EPS functions of V2G

The optimal allocation model aim at minimum network cost including power cut loss and the total investment cost of V2G (including logistics fees and the operation cost of the EPS's energy storage of V2G) is shown in Equation (1).

$$\min f = \sum_{j=1}^{m} P_j [\prod_{i=1}^{n} Z_{ij} \times I_j (t_{i-j} + t_{i-j}{}') P_t + \prod_{i=1}^{n} (1 - Z_{ij}) \times I_j T_{\mathrm{m}}] \eta_1 + U \sum_{i=1}^{n} \sum_{j=1}^{m} P_{EPS.ij} Z_{ij} \eta_2 (1 - \lambda) + U \sum_{i=1}^{n} \sum_{j=1}^{m} P_{EPS.ij} Z_{ij} \lambda \tag{1}$$

where *m* refers to the number in area to be restored; *n* refers to the quantity of electric vehicles; P_j refers to the loss expenses in the jth important area to be restored per unit time; P_t refers to the total load capacity in area to be restored. $P_{EPS.ij}$ refers to the capacity that the ith portable power source could provide to the jth important area to be restored to a great extend; Z_{ij} refers to decision variable of optimal matching of emergency power supply; when Z_{ij} =1, it refers to the emergency power supply that the ith portable power source supply for the jth important area to be restored; or Z_{ij} =0; I_j refers to the outage loss comprehensive index in the jth important area to be restored; t_{i-j} refers to the haulage time that the ith portable power source need to reach the jth important area to be restored; t_{i-j}' refers to the stay wire and wiring time that the ith portable power source need to reach the jth important area to be restored; T_{m} refers to the maximum duration of the permissible blackout in the jth important area to be restored; *U* refers to the investment cost of V2G portable power source units capacity; η_1 refers to the equipment strain coefficient cost of average useful life of portable power source; η_2 refers to the proportionality coefficient between the operation of portable power source and maintenance charge; λ refers to the proportionality coefficient between the guarantee logistics of electric vehicle and the normal operation of the reserved power, which is shown in Equation (2).

$$\lambda = \frac{2l_{ij} \times P_l}{P_{EPS.ij}} \times 1.1 \tag{2}$$

where l_{ij} refers to the path length from charge station to the matching area to be restored, P_l refers to the energy consumed by the electric vehicle itself per unit path, P_l equals to 0.18kW/km.The founding of outage loss comprehensive index mainly considers two indexes: the regional total load capacity P and the importance degree of regional load W. Set up weight functions, ε_1 and ε_2 to describe the incidence to life security and economy when losing this load; set ε_3 as the weight function of load special attributes to offset the defects that ε_1 and ε_2 cannot cover completely. Divide the weight functions ε_1 ε_2 ε_3 into four levels and value them respectively {1, 2, 3, 4} according to the importance degree of load [5]. Consider the regional load of power as *P*, then the outrage cost in this area caused by losing some load can be measured by load importance weight functions ε_1 , ε_2 , ε_3 and loading capacity P .

$$I_j = \sum_{i=1}^{n} P_{ij}(K\varepsilon_{1i} + \varepsilon_{2i} + \varepsilon_{3i}) \times 0.01 \tag{3}$$

Where ε_1 , ε_2 , ε_3 refer to life security, economy and particularity weight functions value respectively in the jth area; P refers to the capacity load in the jth area. I_j refer to the power outage loss index caused by power cut in the jth area; K refers to severity coefficient of life security loss (K=1~4).

The constraint conditions are as shown in Equations from (4) to (7).

$$t_{i-j} + t_{i-j}' < T_m \tag{4}$$

$$\sum_{i=1}^{n} P_{EPS.i} \geq P_{total} \tag{5}$$

$$P_{EPS.i} \leq P_{i.\max} - 2l_{ij} \times P_l \tag{6}$$

$$30\% \leq SOC_i \leq 95\% \tag{7}$$

Presume the total capacity that V2G supply for EPS can meet the sum of all power supply area load. $P_{i.\max}$ refer to maximum discharge power of the ith vehicle, the unit is kW. To be noted that the statistics of all vehicles' electricity consumption are free of the *SOC* lower limit value set by users, the statistics run according to the formula above; besides, the battery discharge power of all vehicles are limited by maximum discharge power[6-7].

Emergency power optimization configurations

The steps of the strategic analysis based on genetic algorithm are: (1) Establish the initial matrix and proceed chromosome encoding as shown in Equation (8).

$$A=(a_{ij})_{n\times m} \tag{8}$$

where *m* refers to the number in area to be restored; *n* refers to the quantity of electric vehicles; a_{ij} refers to the shortest path from the ith emergency power supply to the jth power supply area to be restored. The length of chromosome refers to the restored number *m* in the important area, the gene in the corresponding position refers to emergency power number, the corresponding position supply power for the restoring area.

(2) Initialize the population. Start to search from the ith row in the initial matrix, when *i*>*n*, stop searching automatically, check whether meet the formula (4), if meet, then $a_{ij}=i$, or 0, thus obtain a $n\times m$ matrix. Bring in *m* random integers from 0 to *n*, $b_1,b_2,b_3...b_m$ to get a initial chromosomes and the size of the population is *K*.

(3) Determine the individual fitness function of the population. Fitness function $F(x)$ and objective function has a relationship shown in Equation (9).

$$F(x)=\begin{cases} g(x)+C_{\min}\ , & where\ \ g(x)+C_{\min}>0 \\ 0\ , & where\ \ \mathrm{g}(x)+C_{\min}\le 0 \end{cases} \tag{9}$$

In this formula, $C_{\min}$ refers to the maximum value so far in the objective function $g(x)$.

(4) Selecting operation. Adopting the method of optimal retention strategy, which is to compare the adaptive value chosen in any two individuals in the parent to choose the bigger one to enter into the offspring.

(5) Interlace operation and mutation operation. Take out a pair of individuals to interlace randomly from i=1 to *k*, thus among [0, 1] to produce crossing-over rate $r\le p_c$, choose X_i as the parent without loss of generality, according to individual digital string length, to first produce a interlace position randomly, that is, some number among [1, L-1]. At this interlace position to cut off the parents' genetic code and interchange the tail ultimately. It needs to meet the constraint conditions (4), (5), (6), or it need to reselect the interlace position. Interlace operation set mutation probability as P_m, choose the parent chromosomes among the group on the basis of interlace operation, to make a digital flip of the chosen individual to check if it meets all kinds of constraint conditions and if the latter fitness greater than the previous one. If it meets the conditions, then succeeds; if not, then fails.

(6) Protocol of controls parameter. Protocol the controls parameter in genetic algorithm contains: crossing-over rate P_c equals to 0.5, aberration rate P_m equals to 0.08, maximum algebra M in algorithm operation equals to 200 and population size N equals to 50.

(7) Stop condition. When iterations reach the maximum algebra *G*, and then stop operation[8].

Simulation

Presume a city has two centralized charging stations which distribute emergency power supply for eight power supply area to be restored. According to the information statistics of the grid geographic external, a fuzzy traffic network diagram is established as shown in figure 1. In the figure, the number of the branch refers to logistics time interval, the unit is min, node 1, 5 refer to charging stations S_1, S_2 respectively, node 18, 27, 28, 32, 24, 30, 21, 23refer to the area to be restored $A_1\sim A_8$. The load in the area to be restored of power outage and weight functions value see table 1. The index value of the power network accident area to be restored is as shown in table 1.

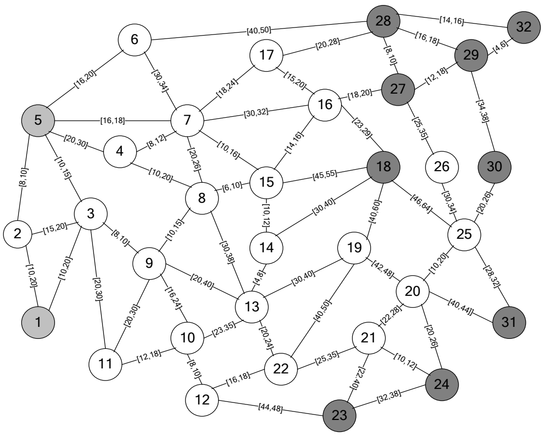

1
2
3
4
5
6
7
8
9
10
11
12
13
14
15
16
17
18
19
20
21
22
23
24
25
26
27
28
29
30
31
32
[16,20]
[30,34]
[40,50]
[16,18]
[20,30]
[8,12]
[8,10]
[10,15]
[15,20]
[10,20]
[10,20]
[20,30]
[8,10]
[10,15]
[20,26]
[10,16]
[10,20]
[6,10]
[18,24]
[30,32]
[15,20]
[14,16]
[20,28]
[14,16]
[16,18]
[8,10]
[18,20]
[12,18]
[4,6]
[23,29]
[25,35]
[34,38]
[45,55]
[10,12]
[30,40]
[40,60]
[46,64]
[30,34]
[20,26]
[30,38]
[20,40]
[4,8]
[30,40]
[20,30]
[16,24]
[23.35]
[12,18]
[8,10]
[20,24]
[16,18]
[40,50]
[42,48]
[10,20]
[28,32]
[22,28]
[40,44]
[25,35]
[20,26]
[10,12]
[22,40]
[32,38]
[44,48]

Fig.1 Traffic network

Tab.1 Load character of areas to be restored and Volume of the Index in a city

The area to be restored	Total capacity /MW	Important load proportion	Life weight ε_1	Economic weight ε_2	Special weight ε_3
A_1	4.56	40%	4	2	1
		60%	1	1	4
A_2	5.90	40%	3	3	2
		50%	1	2	1
		10%	1	1	3
A_3	6.00	20%	1	2	4
		30%	3	3	1
		50%	2	1	3
A_4	5.39	20%	2	2	1
		80%	1	1	4
A_5	3.94	50%	1	3	2
		50%	3	3	2
A_6	3.80	30%	2	1	3
		70%	3	2	1
A_7	4.15	20%	2	2	1
		40%	1	2	3
		40%	3	3	2
A_8	3.27	50%	1	2	1
		50%	2	1	4

Presume the grid requires the emergency power supply for electric vehicles to reach the area with lost power in one hour and a half after power accident, to meet the need of emergency electrical power supply in area to be restored. The optimal path is as shown in table 2.

Tab.2 Optimal path and truth degree

Paths initial-terminal point	Specific paths	Time Interval /min	Truth degree σ'	Clear value/km
$S_1 \to A_1$	1-3-9-8-15 -16-18	[66,90]	1	71
$S_1 \to A_3$	1-3-9-8-15 -16-27-28	[69,91]	0.990	62
$S_2 \to A_5$	5-3-9-10-1 2-22-21-24	[83,114]	0.102	103.5
$S_2 \to A_7$	5-7-15-16- 18-25-31	[117,153]	0	112.5

The number of electric vehicles in centralized charging station S_1 is set as 100; the storage content of centralized charging station S_2 is set as 80. The numerical value of the demand is set as the number of emergency power supply. According to the optimal path result, apply the genetic algorithm to gain the configuration result, as shown in table 3.

Tab.3 Disaster-relief resources allocation schedule

The blackout area to be restored	Core load/MW	Emergency power demand 72KW/car	Charging station source	Number of EV
A_1	0.91	19	S_1	19
A_2	1.15	23	S_1	23
A_3	1.08	22	S_1 S_2	10 12
A_4	1.14	23	S_2	23
A_5	1.51	31	S_2	31
A_6	0.76	16	S_1	16
A_7	1.58	32	S_1	32
A_8	0.65	14	S_2	14
Total	7.87	180		180

Conclusions

In this paper the optimization problem of power grid emergency power scheduling scheme based on the EPS functions of V2G is studied. Research results mainly contain: 1) a optimization scheme of urban power grid emergency power supply based on the EPS functions of V2G is proposed; 2) take a overall consideration of time constraint and capacity constraint to further improve the utilization rate of EV and lower the investment and operating costs of urban power grid; 3) The optimization scheme has a faster response speed so that to reduce the loss of area to be restored and further increase the power grid emergency ability.

References:

[1] HOU Hui,ZHOU Jian-zhong,ZHANG Yong-chuan,et.al. Analysis of power emergency drills system at home and abroad and its inspiration for China[J]. Power System Protection and Control,2010,38(24):236-241.

[2] GUO Xiao-ming,LIU Jun-yong. Research on power disaster-relief resources allocation schedule model[J]. Power System Protection and Control,2011,39(20):11-26.

[3] CHENG Xiang-hui,LIU Jun-yong,FENG Han,et.al.ADM analysis of power emergency command center to start based on accident state and tendency grade evaluation[J]. Power System Protection and Control,2011,39(16):45-52

[4] Sun Jia-ping,Zhang Jian-feng,Lu Li-jun；Study on Measures for Raising Beijing Power System Power Supply Reliability[J], North China Electric Power, 2004(2):51-54.

[5] ZHANG Ai-guo,HAO Jian-gang,TANG Zhi-fang, et al. The Allocation Scheme of Mobile Emergency Generator Considering the Loads Importance[J]. Power System Technology, 32(S):86-89.

[6] Matthias D.Galus,Rashid A.Waraich,Fabrizio Noembrini,et al.Integrating Power Systems, Transport Systems and Vehicle Technology for Electric Mobility Impact Assessment and Efficient Control.IEEE Transactions on Smart Grid,2012,3(2):934-948.

[7]LI Zi-yun,CHEN Kai,LONG Yu et al.A Precision Method for Reliability Cost and Benefit Analysis and Its Application in Distribution Network Planning[J].Automation of Electric Power Systems,2012,36(11):97-101.

[8] ZHOU Li-mei,FAN Min-gtian, ZHANG Zu- ping. Optimal Allocation of Emergency Power Supplies for Urban Important Customers[J].Automation of Electric Power Systems, 2007, 31(6):99-102.

Applied Mechanics and Materials Vol. 596 (2014) pp 669-673
© (2014) Trans Tech Publications, Switzerland
doi:10.4028/www.scientific.net/AMM.596.669

Optimal reserve distribution model for power system with large scale wind power integration

He Chen [1,2], Liu Jichun[1,a], Li Jiayi[3], Wu Yunxia[3], Li Xia[1], An xiangyang[2], Chen Honghui[2], Zheng Xiaoli[2]

[1] Department of Electrical Engineering, Sichuan University, Chengdu, China

[2] MAOMING power supply company, Guangdong Electric Power Company, Guangdong province, China

[3] Power system plan center, Southwest Electric Power Design Institute, Chengdu, China

[a]jichunliu75@163.com

KEY WORDS: wind power; reserve optimization; consistency constraints; energy-saving dispatch

ABSTRACT: Firstly, taking into account the load forecasting error and uncertainty of wind power, the coal saving benefit and network loss of the reserve are combined into integrated coal consumption of thermal units. Then, the consistency constraints of reserve capacity are derived. On the basis of the work mentioned above, the optimal reserve distribution model for power system with large scale wind power integration is proposed. This model is used to compare the network loss, integrated coal consumption and the allocation of reserve before and after adding consistency constraints. Finally, simulation results on the IEEE-RTS24 system verify the effectiveness of the algorithm in solving reserve transfer between units, ensuring the fairness of market and providing a reference to dispatchers.

Introduction

Wind power integration on power system will affect the reserve of thermal unit during the scheduling process due to the fluctuation and uncertainty of wind power. The system has to increase the spinning reserve to cope with wind power prediction error. For specific network, how much reserve capacity the system needs and how to distribute the reserve between units, is especially important for the security and economy of the power system.

Literature [1-2] used cost-benefit analysis method to study the optimal spinning reserve of wind power systems; Literature [3] researched the impact of wind power fluctuation in different time scales. It raised that reserve capacity will increase with the increase of wind power's scale. The above literatures only researched that the reserve capacity needs to meet the capacity requirement, but it did not consider the distribution of reserve between different thermal units; Literature [4] studied the reserve capacity of wind power system and it proposed: When the system integrated with large-scale wind farms, it need to solve how to distribute the reserve capacity between units. But it did not propose specific solutions; Literature [5] which took into account the uncertainty of wind power and load, considered the security constraints and researched the distribution of reserve capacity between different units. But it ignored the network loss, the optimal result would led to the reserve capacity transfer. The non-consistency performance of reserve dispatch would not only cause additional network loss, but also caused the generators adjust its output frequently. The reserve capacity decision making problem is a high-dimensional variable mathematical optimization problem with the complex constraints, the quality of the decision will affect the reliability and economy of the power system. The traditional scheduling model integrated with wind power, rarely considered the quality and regulation of reserve. This may cause unnecessary loss for system and it is unfair in the market [6].

Aiming at the problem of reserve transfer caused by wind power integration, this paper considered coal saving benefit and network loss of the reserve and derived consistency constraints of reserve capacity. On this basis, the optimization model of reserve capacity allocation was proposed.

Distribution Model for Reserve Capacity

Objective function. The objective function is shown in Equation (1).

$$F^1 = \min \sum_{t=1}^{T} \sum_{i \in N_G} [g_i(P_{Gi,t}) I_{i,t} + ST_i(I_{i,t}(1 - I_{i,t-1}))] \quad （1）$$

Where, g is the coal consumption curve of thermal units; ST is the start-stop coal consumption for thermal unit; I is the start-stop state ; N_G is the number of units.

Error treatment and economy benefits of reserve. The reserve constraints of traditional energy-saving dispatch is shown in Equation (2).

$$\sum_i P_{Gi\max,t} I_{i,t} \geq P_{D,t} + P_{R,t} \quad （2）$$

Where, $P_{Gimax,\mathrm{t}}$ is maximum output of thermal power , $P_{D,\mathrm{t}}$ is predicted load, $P_{R,\mathrm{t}}$ is reserve capacity .

Currently, because the load forecasting has been more accurate [7-8], so the traditional energy-saving dispatch only considered that the reserve capacity should meet the needs of system. However, in the power system with large-scale wind power integration, the wind power is considered to be a negative load, so that the load forecasting error will become uncertain due to the uncertainty of wind power. And thermal units will have to increase or reduce their output to balance the system load; In the case that reserve capacity remains constant, the distribution of reserve capacity between the units will affect the coal consumption of system due to different coal consumption characteristics of each unit. Therefore, it needs to consider the coal saving benefit of reserve capacity in the power system connected with large-scale wind farms. Considering the above, we constructed three types of load curve based on load prediction error and wind power prediction error in the energy-saving dispatch, load forecasting curve K_{G0}, maximum load curve considering the positive reserve K_{G1}, minimum load curve considering the negative reserve K_{G2}, which were expressed in Equation (3)-(5).

$$K_{G0,t} = P_{D,t} - P_{W,t} \quad （3）$$

$$K_{G1,t} = (1+\varepsilon)P_{D,t} - (P_{W,t} - \eta_t P_{W\mathrm{rated}}) \quad （4）$$

$$K_{G2,t} = (1-\varepsilon)P_{D,t} - (P_{W,t} + \eta_t P_{W\mathrm{rated}}) \quad （5）$$

Where, P_W is the wind power output; η_t is the wind power forecasting error in period t; ε is the load forecasting error, P_{Wrated} is the total installed wind power capacity.

Three types of curves formed three types of objective function is shown in Equation (6)-(8).

$$F_0 = \sum_{t=1}^{T} \sum_{i \in S_G} [g_i(P_{Gi0,t}) I_{i0,t} + ST_i(I_{i0,t}(1 - I_{i0,t-1}))] \quad （6）$$

$$F_1 = \sum_{t=1}^{T} \sum_{i \in S_G} [g_i(P_{Gi1,t}) I_{i0,t} + ST_i(U_{i0,t}(1 - I_{i0,t-1}))] \quad （7）$$

$$F_2 = \sum_{t=1}^{T} \sum_{i \in S_G} [f_i(P_{Gi2,t}) I_{i0,t} + ST_i(U_{i0,t}(1 - I_{i0,t-1}))] \quad （8）$$

Where, F_0 is the total coal consumption under load forecasting curve. F_1 is the total coal consumption under maximum load curve which considering positive reserve. F_2 is the total coal consumption under minimum load curve which considering negative reserve .

Considering economy benefit of reserve, the actual load curve is between the minimum and maximum load curve, and the objective function that only considering the coal consumption can be expressed in Equation (9).

$$\begin{gathered} F = \alpha F_0 + \beta F_1 + \lambda F_2 \\ \alpha + \beta + \lambda = 1 \end{gathered} \quad （9）$$

Where, α, β, λ is the weighting factor of F_0, F_1, F_2. The weighting factors are obtained by analyze the historical statistics of the actual power system. The objective function is meaning that after thermal units increase or reduce their output, the total coal consumption should be minimal.

The regular constraints and consistency constraints of reserve dispatch. In order to suppress the reserve transfer and reduce the frequency of thermal unit output adjustments, this paper introduces the consistency constraints of reserve dispatch as shown in Equation (10)-(11).

$$\left\{\sum_{i=1}^{N_G} P_{ui,t} - \sum_{i=1}^{N_G} P_{ui,t-1} \ge 0,\ P_{ui,t} - P_{ui,t-1} \ge 0.\ \sum_{i=1}^{N_G} P_{ui,t} - \sum_{i=1}^{N_G} P_{ui,t-1} \le 0,\ P_{ui,t} - P_{ui,t-1} \le 0\right\} \tag{10}$$

$$\left\{\sum_{i=1}^{N_G} P_{di,t} - \sum_{i=1}^{N_G} P_{di,t-1} \ge 0,\ P_{di,t} - P_{di,t-1} \ge 0.\ \sum_{i=1}^{N_G} P_{di,t} - \sum_{i=1}^{N_G} P_{di,t-1} \le 0,\ P_{di,t} - P_{di,t-1} \le 0\right\} \tag{11}$$

Where, $P_{ui,t}$ is the reserve for the i-th thermal unit in period t. $P_{di,t-1}$is reserve for the i-th thermal unit in period t, $P_{i,t}$-$P_{i,t-1}$ is the variation of reserve capacity of i-th thermal unit.

Formula (10) indicates that the reserve capacity of each unit can not decrease when the total up reserve is increasing in the next period and can not increase when the total up reserve is decreasing in the next period. Formula (11) indicates that the reserve capacity of each unit can not increase when the total down reserve is decreasing in the next period and can not decrease when the total down reserve is increasing in the next period. This constraint makes thermal power output consistency. This constraint ensures that changes of thermal units output is consistent.

Conventional reserve constraint is shown in Equation (12)-(15).

$$\sum_{i\in N_G} I_{i,t}\left(P_{Gi\max,t} - P_{Gi,t}\right) \ge P_{D,t}\cdot D + P'_{W,t} \tag{12}$$

$$\sum_{i\in N_G} I_{i,t}\left(P_{Gi,t} - P_{Gi\min,t}\right) \ge P_{D,t}\cdot D + P'_{W,t} \tag{13}$$

$$P_{Gi\max,t} = \min(P_{Gi\max}, P_{Gi,t-1} + T_{10}\cdot r_{iu}) \tag{14}$$

$$P_{Gi\min,t} = \max(P_{Gi\min}, P_{Gi,t-1} - T_{10}\cdot r_{id}),\quad t\in T \tag{15}$$

Where, $P_{D,t}$ is the total system load in period t; D is spinning reserve ratio; $P'_{W,t}$ is wind power forecasting error in period t; T_{10} is the spinning reserve capacity which will respond in 10 minutes; r_{iu}, r_{id} is the up-ramp rate and down-ramp rate of the thermal units.

Equation (12) and (13) represent that the reserve capacity of thermal units is greater than wind power prediction errors and load forecast errors in period t. Equation (14) is the maximum output of the i-th unit in period t which is the smaller value between maximum output and the output in period t-1adding the spinning reserve responded in 10 minutes; Equation (15) is the larger value between minimum output and the output in period t-1 subtracting the spinning reserve responded in 10 minutes.

Simulation Results

This paper considers four optimal distribution models for system reserve capacity. The coal consumption in different model is shown in Figure 1.

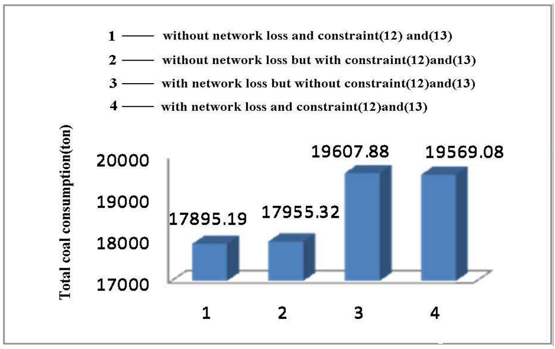

Fig.1 The coal consumption of the system under the different constraints

Model 1 is the reserve distribution model which is taken from [5]. The network loss and constraint (10) and constraint (11) is excluded in model 1, the daily coal consumption is 17,895.19 tons. Model 3 is taken from [5] too. The network loss is considered in model 3, the daily coal consumption is 19,607.88 tons. The increment of daily coal consumption accounted 9.6 percent of the daily coal consumption excluding network loss. It is seen that the network loss has serious influence on coal consumption in energy-saving dispatch.

Model 2 is the proposed model in which the network loss is not taken into account. The coal consumption is 17,955.32 tons. Model 4 is the proposed model. The coal consumption is 19,569.08 tons.

These results show that, the consistency constraint will led to increment of coal consumption when the network loss constraint is not considered. This is because that, without the constraints (10) and (11), the reserve is arranged in ascending order of coal consumption with considering the ramp rate constraints. After the constraints (10) and (11) is added, the order of reserve capacity arrangement is broken, the coal consumption increase. In the case of considering network loss, the integration coal consumption under constraint (10) and (11) is less than the integration coal consumption without constraint (10) and (11).This is because that the units output is arranged according to the incremental transmission loss and coal consumption curve without consistency constraints and that will lead to reserve transfer which bring more network loss. Although the daily coal consumption of units increase with the consistency constraints, but due to the reducing of net loss, it makes the integrated coal consumption decreasing.

Optimal Distribution of Reserve Capacity. The reserve capacity of thermal units at 8-th and 9-th interval is calculated by the method of [5]. It is shown on table 1. The weight factor $\alpha = 0.8, \beta = 0.1, \lambda = 0.1$. We calculate the reserve capacity of each unit at period 8and period 9 by the method which proposed in this paper. The result is shown in Table 2.

Tab.1 Calculating the reserve of generators at the period of 8 , 9 using the method of ref. [5]

N_G	Generator active power (p.u)			
	Up reserve		Down reserve	
	t=8	t=9	t=8	t=9
7	0	0.2	0	0.198415
8	0	0.2	0	0.198415
9	0.216721	0.075497	0.216721	0.114416
10	0.216721	0.075497	0.216721	0.114416
11	0.216721	0.075497	0.216721	0.114416
15	0	0.096	0	0
16	0	0.096	0	0
17	0	0.096	0	0
19	0	0.096	0	0
20	0.249113	0.2302	0.249113	0.246056
21	0.242301	0.248863	0.242301	0.246692
22	0	0.1	0	0
23	0	0.1	0	0
30	0.201962	0.108245	0.201962	0.250462
31	0.201962	0.108245	0.201962	0.250462
32	0.4	0.227704	0.4	0.4
Tatol reserve	1.9455	2.1337	0	0

Tab.2 Calculating the reserve of generators at the period of 8 , 9 using this method

N_G	Generator active power			
	Up reserve		Down reserve	
	t=8	t=9	t=8	t=9
7	0.176175	0.2	0.184353	0.2
8	0.176175	0.2	0.184353	0.2
9	0	0	0.139262	0.159963
10	0	0	0.139262	0.159963
11	0.319373	0.319373	0	0
15	0.009537	0.044687	0	0
16	0.009537	0.044687	0	0
17	0.009537	0.044687	0	0
19	0.009537	0.044687	0	0
20	0.034668	0.034668	0.264588	0.3
21	0.184332	0.184332	0.241051	0.3
22	0.1	0.1	0	0
23	0.1	0.1	0	0
30	0.204012	0.204012	0.202162	0.211236
31	0.212615	0.212615	0.193515	0.2025892
32	0.4	0.4	0.396955	0.4

In Table 1, the total reserve capacity in period 9 is larger than the total reserve capacity in period 8.The reserve capacity of unit 7 and unit 8 increase from 0 to 20MW, and the reserve capacity of unit 9, 10, 11 drop to 7.55 MW from 21.67MW. The results show that the reserve transferred in the results which are obtained by the reserve distribution model in [5]. Table 2 shows the optimization results which are obtained by the proposed method. The reserve dispatch of each unit is consistent, there is no reserve transfer.

Conclusion

The existing problems in the traditional energy-saving dispatch : 1) Only total amount of reserve capacity is considered, and the allocation of reserve between different units is ignored; 2) The objective is to minimize the coal consumption, and it did not consider coal-saving benefit; 3)It did not take into account the impact of network loss on coal consumption; 4) It is not conform to the market fairness and generators adjust their output frequently. In this paper, we take into account the four points above to establish the optimal reserve distribution model for Power system integrated with wind farms.

The conclusions:

1) Under the same requirements of reserve capacity, The consistency constraints will reduce the frequency of generation adjustment, increase the call rate of reserve. While it may reduce net lose, so that it may make the unit coal consumption optimal.

2) It solve the problem about reserve capacity transfers between the thermal units, ensure the consistency of generator adjustment and the fairness of the market.

Reference

[1] Shu peng. Determination of optimal spinning reserve of power grid containing wind[J]. Power System Technology, 2010, 34(12): 158-162.

[2]ORTEGA-VAZQUEZ MA，KRISEHEN D S. Estimating the spinning reserve, requirements in systems with significant, wind power generation penetration[J]. IEEE Transactions on power system, 2009, 24(12): 114-124.

[3] Sorensen P., Cutululis N.A.. Power Fluctuations From Large Wind Farms[J]. IEEE Transactions on Power Systems, 2007, 22(3): 958-965.

[4] Ackermann T., Abbad J.R., Dudurych I.M., Erlich I. European Balancing Act[J]. IEEE Power and Energy Magazine, 2007, 5(6): 90-103.

[5]LIU Yang. Optimal reserve distribution of a grid connected with large scale wind power[J]. Electric Power, 2012, 45(1): 50-54.

[6] Wang Jianxue. Unit maintenance schedule based on equity of market[J]. Automation of Electric power Systems, 2006, 30(20): 15-20.

[7]HUANG Jing. Short-term load forecasting based on manifold learning and locally linear embedding theory[J]. Power System Protection and Control, 2012, 40(7): 25-30.

Applied Mechanics and Materials Vol. 596 (2014) pp 674-677
© (2014) Trans Tech Publications, Switzerland
doi:10.4028/www.scientific.net/AMM.596.674

Realization of FCB Function in 350MW Subcritical Units with 35% Capacity Bypass

Li Wang[1, a], Gen Li [1, b], Ciyun Zhang [1, c] Liang Zhang[1, d] Dezhong Bi[1, e]

[1]Electric Power Research Institute of State Grid Liaoning Electric Power Co., Ltd,
Shenyang, Liaoning, 110006, China

[a]rzs_wl@126.com, [b]rzs_lg@126.com, [c]rzs_zcy@126.com, [d]rzs_zl@126.com, [e]rzs_bdz@126.com

Keywords: Fast cut back, 35% capacity bypass, Subcritical units.

Abstract. In this paper, a new designed FCB (Fast Cut Back) control strategy has been applied in a 350MW subcritical coal-fired unit. The FCB test carried on 350MW units under 50% load and 100% load condition is presented. The result of test shows that the units can realize the FCB function without any manual involvement and the safety of units is effectively improved.

Introduction

With the rapid development of the national economy, the social demand for electric energy is increasing gradually. The grid is getting large day by day, and the security of electric network becomes more and more important. All over the world there have been some occurrence of sever balckouts, natural disaster is a serious threat to the safe operation of power grid, and it may cause some power plant in the state of blackout in some areas [1].

During the state of blackout, power plants will face a threat. A tiny carelessness may cause large damage of equipment, and the status and parameters of the units will change dramatically, and the power of the cooling water, compressed air equipment will be lost. Most of the equipment of the unit will lose control. The safe operation of major equipment relies solely on the battery or backup diesel generators, and the safety factor of power plant decreased significantly. From the blackout accident of domestic power plant, we can find that there will be some bad effects on the equipments more or less, and even severe damage of the equipment. If the units realize the FCB function, the unit could supply the auxilary power by itself in the most dangerous time, we can safely shutdown the units or wait for the recovery of power grid. So there exist the following benefits for power plant [2] [3].

For units security, FCB function can make the unit continuesly running after load rejection, and guarantee that system parameters will not exceed the limits in the whole process. The power plant can choose shutdown, or waiting for the recovery of grid, which inhance the security of the units.

Comparing with the normal control strategy, the FCB can reduce times of MFT, and the boiler will be in the state of high parameters. When the cause of the accident is confirmed and solved, units can make a hot restart, so we can save a lot of time and energy, it is benefit for reducing the operation cost.

When the units realize FCB function, the units have the ability to supply the auxiliary power by itself, which will help the grid to return to normal as soon as possible, and the units can safely shutdown too. So the FCB function of units has become an urgent topic of research.

The Realization of FCB function

The overpressure of boiler. After the FCB action, turbine valve will turn down quickly, while the boiler has larger inertia for the thermal storage, and the capacity of steam production will reduce slowly, which can cause the serious load imbalance between boiler and turbine [4]. If the capacity of bypass is only 35%, overpressure of boiler will happen. The solution is to open the bypass as soon as possible, quickly reducing the thermal load as much as possible. It is important to make short-term pressure relief with the PVC and safety, and then to use the bypass system to control pressure decreasing slowly to target value.

The rapid reduction of boiler load. In the process of FCB, while the bypass capacity is 35%, it is needed to rapidly reduce the load of boiler until it is under 35%. Considering the characteristics of the units, it is determined to keep two mills running during the FCB action, change the rate of reduction load of boiler to 100%/min, change target load to 35% automatically. Considering the rapid reduction of the boiler load, furnace pressure fluctuation, and the unstable working condition of furnace, immediately boiler burner should be shut down from top to bottom automatically [5]. The FCB signal in fig. 1 is used by the load control system of the boiler.

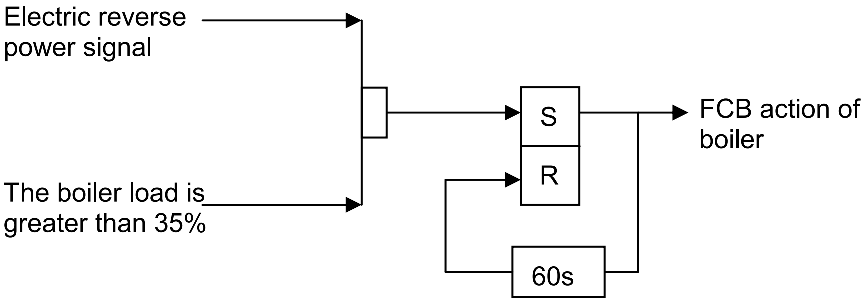
Electric reverse power signal
The boiler load is greater than 35%
S
R
60s
FCB action of boiler

Fig. 1 FCB signal for boiler

DEH speed control. PLU is the function that when load rejection occurs, this circuit is used to avoid turbine overspeed. When the imbalance happens between turbine power and turbine load, it will cause overspeed of the turbine. When the PLU loop detect the situation, CV and CIV will be closed quickly to control the speed of turbine. ACC is acceleration control loop that when the turbine speed is greater than 3060rpm and the acceleration is greater than 49rpm, ACC will take an action to quickly close IV to control the speed of turbine.

Supplement of working fluid. After the FCB action, even if all the mills except 2 mills shut down, it still need some time to reduce the load to 35% for boiler, because the time delay of boiler and inertia of fuel system exit [6]. At this period, the surplus steam must be discharged by superheated steam safety valve and the PCV to the atmosphere, which will cause a certain degree of imbalance of refrigerant cycle in perspective.

Switch of steam source of steam feedwater pump. During normal operation, steam source of feedwater pump is from four stage extraction of turbine. After load rejection, pressure of extraction steam falls. To maintain operation of feedwater pump, the steam source must quickly be cut into standby steam source. And it must meet two requirements during the steam source switch. One is the coal and water ratio imbalance is still within the allowable range, that is the overtemperature will not happen. The other is to maintain the hydrodynamic stability of boiler, that means superheat control of water cool wall is within the permitted value [7]. Switch to standby steam source can be in two ways, one is from four stage extraction of turbine to the auxiliary steam supply, the other is switch to the high pressure steam source from low pressure steam source.

The logic of boiler, turbine and generator. The original design of the units contains forward and reverses function that is boiler MFT action interlock ETS action, turbine ETS action interlock protection for generator; and generator protection action interlock turbine ETS action, ETS action interlock boiler MFT action (load greater than 35%). According to the purpose of FCB function, the reverse-power device to the generator protection circuit should be canceled.

Engineering Application

In this paper, the new designed FCB control strategy has been applied in a 350MW subcritical coal-fired unit. Through some control logic optimization and debugging, the viable control parameters is obtained. The curve of 50% load FCB result is shown in Fig. 2. and the curve of 100% load is shown in Fig. 3. The result of test shows that the units can realize the FCB function without any manual involvement and the safety of units is effectively improved.

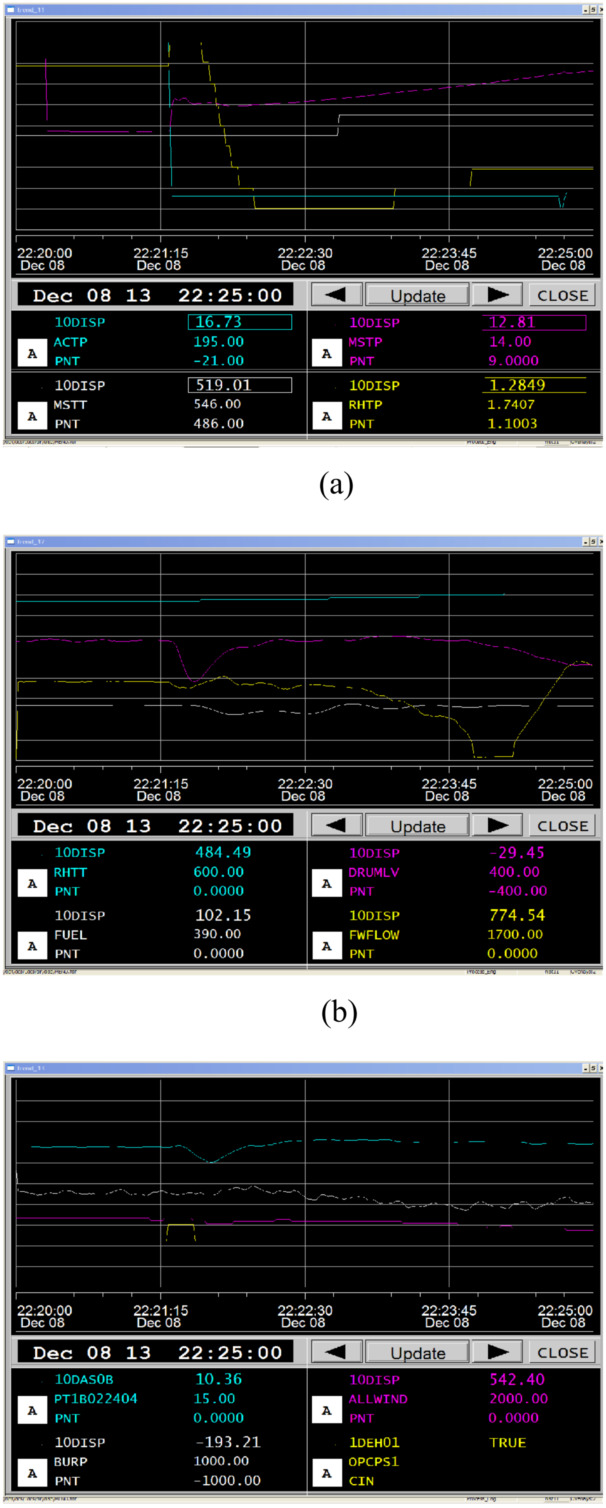

Dec 08 13 22:25:00

10DISP	16.73	10DISP	12.81
ACTP	195.00	MSTP	14.00
PNT	-21.00	PNT	9.0000
10DISP	519.01	10DISP	1.2849
MSTT	546.00	RHTP	1.7407
PNT	486.00	PNT	1.1003

(a)

Dec 08 13 22:25:00

10DISP	484.49	10DISP	-29.45
RHTT	600.00	DRUMLV	400.00
PNT	0.0000	PNT	-400.00
10DISP	102.15	10DISP	774.54
FUEL	390.00	FWFLOW	1700.00
PNT	0.0000	PNT	0.0000

(b)

Dec 08 13 22:25:00

10DAS0B	10.36	10DISP	542.40
PT1B022404	15.00	ALLWIND	2000.00
PNT	0.0000	PNT	0.0000
10DISP	-193.21	1DEH01	TRUE
BURP	1000.00	OPCPS1	
PNT	-1000.00	CIN	

(c)

Fig. 2 50% FCB parameter curve

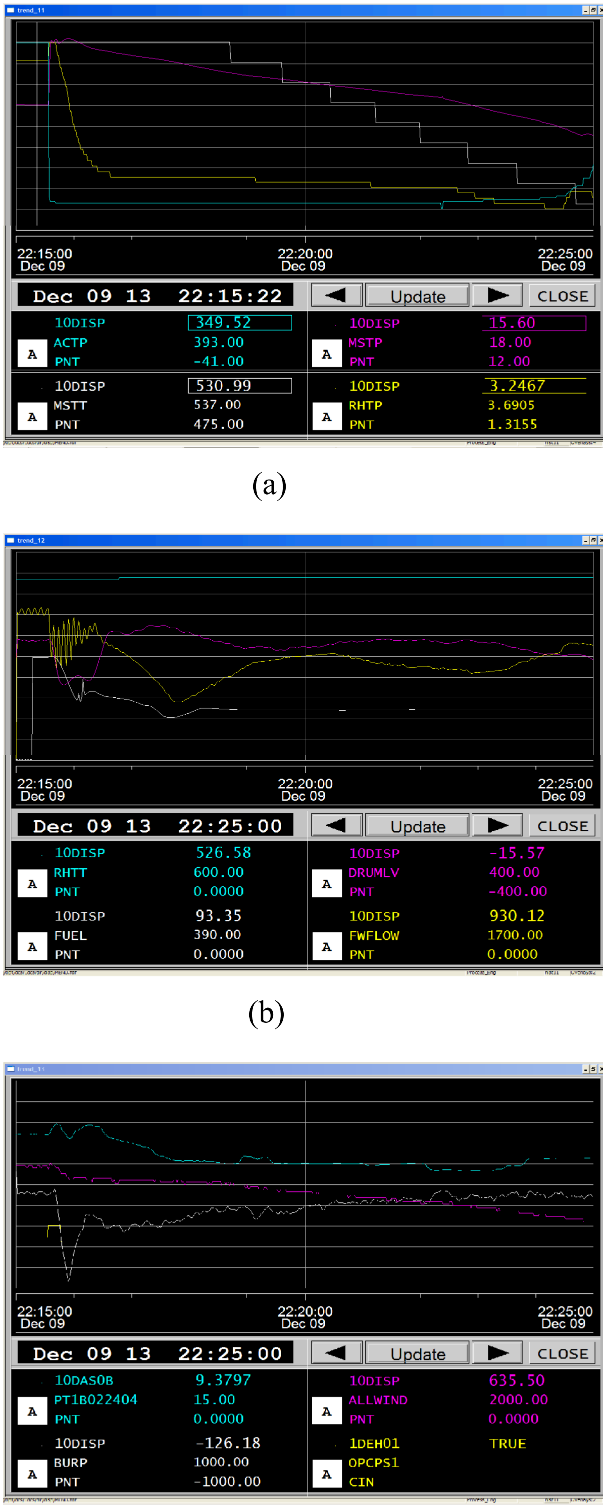

Dec 09 13 22:15:22

10DISP	349.52	10DISP	15.60
ACTP	393.00	MSTP	18.00
PNT	-41.00	PNT	12.00
10DISP	530.99	10DISP	3.2467
MSTT	537.00	RHTP	3.6905
PNT	475.00	PNT	1.3155

(a)

Dec 09 13 22:25:00

10DISP	526.58	10DISP	-15.57
RHTT	600.00	DRUMLV	400.00
PNT	0.0000	PNT	-400.00
10DISP	93.35	10DISP	930.12
FUEL	390.00	FWFLOW	1700.00
PNT	0.0000	PNT	0.0000

(b)

Dec 09 13 22:25:00

10DAS0B	9.3797	10DISP	635.50
PT1B022404	15.00	ALLWIND	2000.00
PNT	0.0000	PNT	0.0000
10DISP	-126.18	1DEH01	TRUE
BURP	1000.00	OPCPS1	
PNT	-1000.00	CIN	

(c)

Fig. 3 100% FCB parameter curve

Conclusion

According to the result of the 50% load and 100% load FCB test, we can draw the conclusion that, the 350MW units with the bypass system of 35% capacity can be stable at 3000rpm quickly through the effective control strategy. During the FCB test, the OPC take action only once, and it effectively prevent the overspeed of the turbine, main parameters of the units are also in a stable state. The realization of FCB function in 350MW subcritical units with 35% capacity bypass has proved to be successfully.

References

[1] Z. X. Lu, “Thoughts of reliability of power from 8.14 blackouts of US and Canada”, *China Power*, no. 12, 2003, pp. 1-5.

[2] L. D. Wang and J. H Yao, “Successful application of FCB and new implementation scheme”, *Process Automation instrumentation*, no. 6, 2004, pp. 48-52.

[3] W. Z. Feng, “FCB test of 900MW supercritical unit”, *China Power*, no. 2, 2005, pp. 74-77.

[4] X. K. Wen and P. Kang, “Exploration of FCB function of the units in Guizhou Province”, *Guizhou Electric Power Technology*, no. 4, 2005, pp. 1-3.

[5] H. Chen, “Processing experience of 600MW supercritical unit FCB”, *Thermal Power Generation*, no.6, 2006, pp. 62-63.

[6] J. H. Yao, “Discussion on several problems in FCB”, *China Power*, no. 5, 2007, pp. 59-62.

[7] C. Q. Shen and X. Y. Zhou, “FCB function and its application in power grid recovery”, *Shanghai electric power*, no. 3, 2007, pp. 251-254.

Applied Mechanics and Materials Vol. 596 (2014) pp 678-681
© (2014) Trans Tech Publications, Switzerland
doi:10.4028/www.scientific.net/AMM.596.678

Research on Microgrid System in the DC-Building

Yaning Yuan[1, a], Ming Meng[1, b]

[1]Department of Electrical Engineering, North China Electric Power University, Baoding, Hebei, 071003, China

[a]yuanyaning1990 @126.com, [b]mengming111218@126.com

Keywords: DC-Building, Microgrid, Distributed Generation, Energy Management.

Abstract. In order to achieve the objectives of energy-saving and emission reduction for modern buildings and provide high quality power supply, a DC microgrid system of thermoelectric energy comprehensive control is proposed. The system includes two subsystems of electric energy and heat energy system, and realizes electric and heat energy transformation and combination through cogeneration unit and electronic heating device. To achieve efficient use of energy, integrated management strategies is also proposed. Distributed generations are controlled by the maximum power tracking strategy, and the hybrid energy storage system uses droop control strategy to stabilize DC bus voltage. In the connection point between the grid and microgrid, the bidirectional converter uses vector decoupling control strategy with double closed loop for pulse width modulation (PWM) to solve the problem of bidirectional power flow with the grid. The simulation results indicate that the system can provide high quality, energy saving, stable power for the modern building.

Introduction

In recent years, with the development of power electronic technology, in low voltage distribution network building, a lot of low voltage DC electrical equipment is used. Most of them transform alternating current into direct current through a rectifying device for using. This energy transformation method leads to a large number of harmonic current. Therefore, much of the electrical equipment needs additional power factor compensation circuit (PFC). On the other hand, in the energy conversion process, a large amount of electric power is used for AC / DC conversion and cooling equipment [1]. According to the statistics provided by United States Environmental Protection Agency (US EPA), America building energy accounted for 39% of total energy, electricity consumption accounted for 68% [2]. Therefore, with the shortage of energy, the building has become an important object of energy saving and emission reduction.

In order to solve the energy shortage and environmental pollution problems, distributed clean energy power generation will become a new mode of energy use. Compared with the traditional centralized energy, it has the advantages of low investment, flexible generating method, high energy efficiency, and environmental protection [3]. At the same time, it has the notable features of stochastic volatility and intermittence, and the safe and stable operation of traditional power system will be impacted and affected due to the large scale access to the grid [4]. In order to give full play to the benefits and value of distributed generation, and weaken the negative impacts on power network, R.H.Lasseter of American Wisconsin University proposed the concept of microgrid [5].

In order to realize the goals of energy-saving emission reduction for modern building and achieve efficient use of clean energy, a new DC microgrid system is proposed. System includes two subsystems of electric energy and heat energy subsystems, and each subsystem has energy production, consumption and storage.

Structure of the System

System included two subsystems of electric energy and heat energy subsystems. Solar panels were installed on the roof or wall surface. Hybrid energy storage system was composed of super capacitor and the battery of battery-exchanging electric vehicle. Cogeneration unit generated electricity feedback DC bus, heat supply living water and air conditioning system. The flat plate heat collector, cogeneration unit and electronic heating device provided energy for the heat storage tank. Photovoltaic power generation, energy storage system and the cogeneration system were connected to the DC bus through the converter. Microgrid was connected with the power grid through bidirectional AC/DC converter. Fig. 1 showed the structure of novel DC microgrid system.

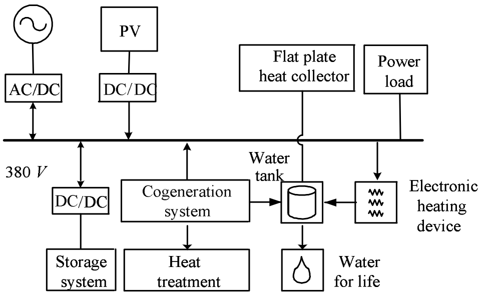
PV
AC/DC
DC/DC
Flat plate heat collector
Power load
380 V
Water tank
DC/DC
Cogeneration system
Electronic heating device
Storage system
Heat treatment
Water for life

Fig. 1 Structure diagram of microgrid system in DC-building

The Control Strategy

The system met the requirement of energy dynamic balance of power supply, energy storage and the load by the peer to peer control strategy. The strategy could also make DC bus voltage stability in a dynamic range and guarantee the plug and play function of the distributed generation. To promote the current sharing between paralleled converters in the DC microgrid and reduce the circulating current, the parallel converters used the droop control strategy. In order to realize the maximum use of clean energy, photovoltaic power generation in the system used the control mode of maximum power point tracking (MPPT) [6]. In the connection point between the grid and microgrid, the bidirectional converter used vector decoupling control strategy with double closed loop to solve the problem of bidirectional power flow with the grid [7].

To stabilize the DC bus voltage, the hybrid energy storage system with super capacitor and batteries of the battery-exchanging electric vehicles can be achieved fast two-way interaction with the DC bus. System architecture was shown in Fig. 2.

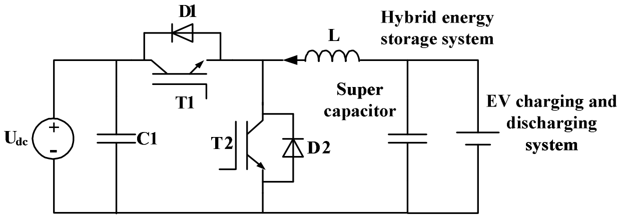
D1
L
Hybrid energy storage system
T1
Super capacitor
EV charging and discharging system
Udc
C1
T2
D2

Fig. 2 Structure of hybrid energy storage system

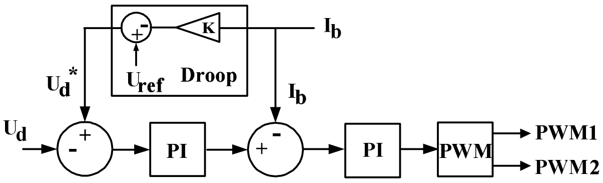
K
Ib
Ud*
Uref
Droop
Ib
Ud
PI
PI
PWM
PWM1
PWM2

Fig. 3 Diagram of droop control strategy

Switch drivers used complementary PWM mode. To promote the current sharing between paralleled converters in the DC micro-grid and reduce the circulating current the voltage droop control was applied. The diagram of droop control strategy was shown in Fig. 3.

In the connection point between the grid and microgrid, the bidirectional converter used vector decoupling control strategy with double closed loop for PWM to solve the problem of bidirectional power flow with the grid. Fig. 4 and Fig. 5 showed the control principle of bidirectional AC/DC converter.

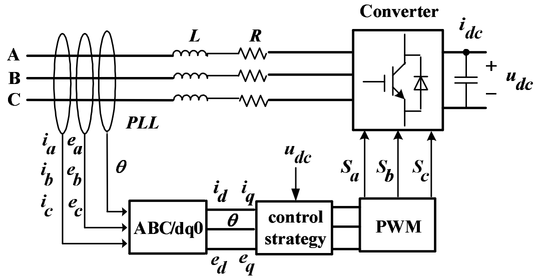
Converter
A
B
C
L
R
i_{dc}
+
u_{dc}
–
PLL
i_a
i_b
i_c
e_a
e_b
e_c
θ
u_{dc}
i_d
i_q
θ
e_d
e_q
ABC/dq0
control strategy
PWM
S_a
S_b
S_c

Fig. 4 Diagram of bidirectional AC/DC converter

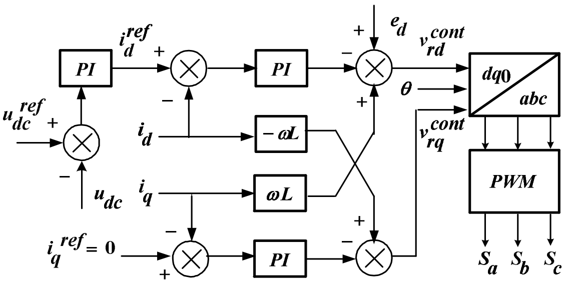
PI
i_d^{ref}
+
–
u_{dc}^{ref}
+
–
u_{dc}
i_d
i_q
PI
– ωL
ωL
$i_q^{ref} = 0$
–
+
PI
+
e_d
–
+
+
–
v_{rd}^{cont}
θ
v_{rq}^{cont}
dq0
abc
PWM
S_a
S_b
S_c

Fig. 5 Vector control principle diagram

As can be seen, Fig. 4 was the control structure diagram of bidirectional AC/DC converter. Where L was the AC side inductance, i_a, i_b, i_c and e_a, e_b, e_c respectively for the AC side voltage and current, u_{dc} and i_{dc} for DC side voltage and current. Fig. 5 was a double closed-loop vector control principle diagram. Where i_q^{ref} was the q axis current reference value, u_{dc}^{ref} for DC bus voltage reference value. And the PWM signals were used to control the DC side voltage. In order to meet the need of PWM control, the Park transform was used to change three-phase voltage and current signals into two-phase d-q coordinate signals. At the same time, phase locked loop was sued to meet the inverter current and AC side current with the same frequency and phase.

In order to realize the maximum use of energy and provide heat for the user, an integrated management of electricity and heat was achieved by cogeneration unit and electronic heating device. Among them, the heat was supplied by the flat plate collector, cogeneration unit and electronic heating device. The heat stored in the water tank and is used for the air-conditioning system and the water of life. Fig. 6 showed the diagram of thermal and power system.

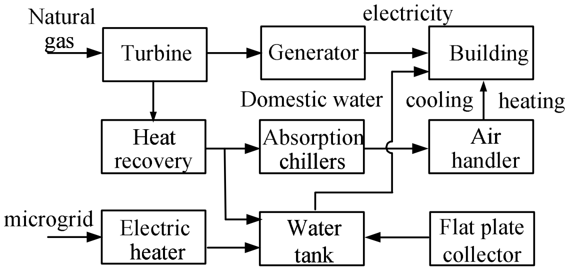
Natural gas
Turbine
Generator
electricity
Building
Domestic water
cooling
heating
Heat recovery
Absorption chillers
Air handler
microgrid
Electric heater
Water tank
Flat plate collector

Fig. 6 Diagram of thermal and power system

The system net power (P_{net}) was defined as the difference between the electric power generated by distributed energy and electric power of user consumption. When $P_{net} > 0$, the priority was charging the energy storage system. When the system was saturated, then supply for tank temperature control system. If the temperature control system met the need, the surplus power was feedback to the network by the bidirectional AC/DC converter. When $P_{net} < 0$, vice versa.

Electronic heating device has three main functions: absorption power peak, protection the energy storage system, control the temperature of the water tank. Therefore, the electric power water heater reference value should be taken the factors of battery SOC, the temperature of the water tank, the exchange value with the grid into account.

Results

In order to testify the novel system, a DC microgrid model was established in the Matlab/simulink. In grid-connected mode, the circuit was testified with mutation load.

The total output power of cogeneration system was 500 kW, with 200 kW electric power. The line loss between the rooms was considered. Supposed the distance between the rooms was 100m, the resistance 0.5 Ω and the reactance 30μH. 500 solar panels in parallel, each for 200W, simulated the output characteristic of solar array. The system got the maximum output power of 100kW with the control mode of MPPT. The inductance in boost circuit worked in continuous mode. The energy storage capacity is 1700 kWh. The average load of 380V bus was 300kW in the daytime. During the period of 1s to 1.2s, the 380V load increase to 320kW. After 1.2s, the average load was 20 kW as the night mode.

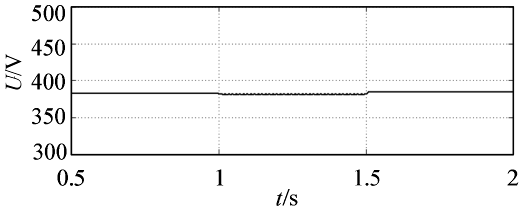

Fig. 7 DC bus voltage waveform

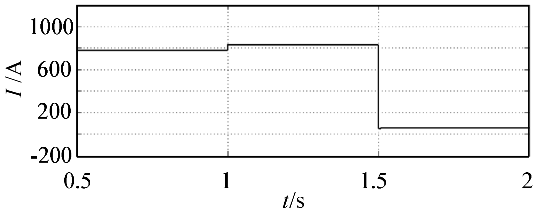

Fig. 8 DC bus current waveform

Fig.7 and Fig.8 showed the voltage and current waveform of DC bus. As can be seen, when the simulation mode during the daytime, cogeneration unit and solar energy work, producing 300 kW power. When the load increased to 320 kW suddenly, the energy storage system quickly discharged to maintain the DC bus voltage. When the simulation mode changed from day to night, solar system shutdown, and cogeneration unit provided 200 kW power. When the load reduced to 20 kW suddenly, the surplus power flow to the grid through the bidirectional AC/DC converter, and began charging the energy storage system. During the process of load mutation and distributed power switching, the 380V bus voltage is to maintain basically stable. In order to meet the demand of changing load, bus current followed the change.

Conclusion

A DC microgrid system of thermoelectric energy comprehensive control for modern buildings is proposed. We can see from the simulation, the system can provide high quality of electric energy and maintain efficient, energy saving, stable operation even in the case of load mutation and distributed power switching. These conclusions provide a reference for the construction of low power consumption DC building.

References

[1] S. J. Xie, H. F. Xiao and Y. H. Luo: Transactions of China Electrotechnical Society Vol. 27-1 (2012), p. 107-113 (in Chinese)

[2] Information on http://www.epa.gov/etv/pubs/600f 06016.pdf

[3] Y. Ji, Q. Ai, and D. Xie: Power System Technology Vol. 34-12 (2010), p. 15-23 (in Chinese)

[4] C. S. Wang, and S. X. Wang: Automation of Electric Power System Vol. 32-20 (2008), p. 1-4 (in Chinese)

[5] C. Marnay, F. J. Robio and A. S. Siddiqui, “Shape of the Microgrid”, in Proc. IEEE International Conference on Power Engineering Society Winter Meeting, Columbus, OH, USA, (2001), p. 150-153

[6]C. Hua, J. Lin, and C. Shen: IEEE Trans on Industrial Electronics Vol. 45-1 (1998), p. 99-107

[7]A. Mohamed, M. Elshaer, and O. Mohammed, “Bi-directional AC-DC/DC-AC Converter for Power Sharing of Hybrid AC/DC Systems”, in Proc. IEEE International Conference on Power and Energy Society General Meeting, Miami, FL, USA, (2011), p. 1-8

Applied Mechanics and Materials Vol. 596 (2014) pp 682-686
© (2014) Trans Tech Publications, Switzerland
doi:10.4028/www.scientific.net/AMM.596.682

Suggestions on implementing Energy-saving Diagnosis Technologies and Services of Power Grid Enterprises

Yuhao LI[1, a], Lefeng CHENG[2, b], Lei XI[3, c], Guanhong XU[4, d] and Tao YU[5, e]

[1] Marketing Dept., Huizhou Power Supply Bureau, Huizhou, 516003, China

[2] Electric Power College, South China University of Technology, Guangzhou, 510640, China

[3] Electric Power College, South China University of Technology, Guangzhou, 510640, China

[4] Marketing Dept., Huizhou Power Supply Bureau, Huizhou, 516003, China

[5] Electric Power College, South China University of Technology, Guangzhou, 510640, China

[a] 314822055@qq.com, [b]chenglefeng1@163.com, [c] LeiXI_ieee@163.com,

[d] guanhongXU_ieee@163.com, [e] taoyu_ieee@163.com

Keywords: Demand Side Management; Demand Side Response; Power Grid Enterprises; Energy-saving and Diagnosis; Potential Analysis

Abstract. In order to meet the national requirement of “two 3‰” of demand side, this paper analyzed basic connotation of overtaking energy-saving emission reduction work in power grid enterprises, introduced main contents included in energy-saving diagnosis technical specifications. Meanwhile, the power grid enterprises energy-saving diagnosis work and energy-saving emission reduction work of demand side management are prospected.

Introduction

In recent years, the China’s economic gross ranks second in the world and also facing the growing pressure of environmental protection, and the energy is more and more depending on foreign. Thus, energy-saving and emission reduction work is significant problem of social economy and development, and which is the major strategic task decided by the China government. In August 31, 2011, the State Council of China promulgated the “Twelfth Five Year Plan of Integrated Energy-saving and Emission Reduction Work Program”, which produced a definite “Twelfth Five Year Plan” energy-saving and emission reduction major requirement and target. Power grid enterprises as fundamental industry of national economy development plays a significant role, especially has a leading role in the upstream and downstream power generation industries, which plays a role in resource optimization and distribution platform, and in guiding the downstream and upstream enterprises to implement energy-saving and emission reduction work, totally, the power grids have their unshirkable responsibility [1][2].

Demand side management (short for DSM) is an important measure to transform the economy development mode, and adjust the economy structure, and which is an important part of energy-saving and emission reduction work, and is also an important way to solve the contradiction between supply and demand. During “Twelfth Five Year Plan” period, the power grid enterprises should exert their own industry advantages and basic function of market resources allocation, and then implement the “DSM Methods”, thus, under the guidance of China’s government, the DSM will be continually to be carried out deeply. Grasp three main contents and work features of China’s DSM work and they are save electricity, peak load shifting, and orderly use of electricity, thus can accomplish “two 2‰” power restriction index.

Energy-saving diagnosis is that through diagnostic analysis to find current situation and problems of consumer side products energy consumption, production operation energy management, and processing equipment, etc. In terms of consumer side industry, can improve the level of energy consumption of enterprises, and realize the goal of reducing energy and improving electricity use rate. For the power grid enterprises, try to find out the real intention or situation of consumer side industry, can achieve rich enterprise information, strengthen enterprise personalized service, and organize further energy-saving demonstration projects, etc.

The basic connotation of energy-saving diagnosis

The power grid corporations use energy-saving diagnosis work of consumer side enterprise as information accumulation and energy-saving potential analysis, and aimed at use of electricity, heat, comprehensive utilization and other aspects, the energy utilization system and equipment operation performance can be analyzed, thus can help the enterprises rapidly analyze the economical operation situation of equipment, then for those equipment that affect economical operation and its management problems will be analyze, according to these analysis, the energy-saving scheme will be put forwarded, thus it can drive the implementation of engineering projects, and finally realize the energy-saving and emission reduction work, so, as a whole, it has bellow basic connotations[3].

Firstly, through comprehensive energy-saving diagnosis, can accurately grasp basic situation, energy management system status and characteristics of production equipment in operation of enterprises, the method of system analysis is used to study energy consumption of enterprises and potential energy-saving point from some aspects, which can supply completed materials of optimized procedure, energy-saving and reduction, technical renovation work for energy management system.

Secondly, through scientific demonstration, and combine with operation situation, energy-saving index analysis of heat equipment, can reasonably determine key governance projects with larger potential, and propose the feasible effective energy-saving reconstruction scheme, with effective energy-saving technology and measures, finally can solve the problems which affect economical operation of enterprise equipment at all possible.

Thirdly, make a comprehensive economic analysis before and after the operation mode adjustment or replacement of equipment, mining in rational use of electricity , reasonable use of heat resource and other aspects, thus further determine way and measures of energy-saving and energy reduction.

Main contents of energy-saving diagnosis technology specification

Main contents. According to the national related energy audit, energy saving calculation, reasonable use of heat, electricity, and water, power quality and industry boiler equipment testing standards, and then summarizes years of work experience of environmental protection and energy saving and energy performance contracting aspect, finally put forward energy-saving diagnosis work technology specification, and make the basic method, procedures, and technology requirement of energy-saving diagnosis in specification.

Consumer selection principle. The power grid enterprise according to electricity sales of last year and through the system selection, comprehensive primary and final selection of three stages, select the appropriate enterprise as energy-saving diagnosis evaluation target. During system selection, for general industrial and commercial enterprises, which should be in principle selected from 200 million kWh enterprises; for those noncommercial and industrial customers, which should be in principle selected from contract capacity of 630kVA and above 630 kVA power enterprises.

During comprehensive primary selection, should give priority to the following five types of customers: daily tracking management or those customers who are found with larger energy-saving potential and higher energy reconstruction willingness during the tracking; those customers who directly put forward reasonable energy evaluation demand; during answering customers' energy-saving consultation, those customers who only implement reasonable energy evaluation can give an answer; the government or the superior institutions focus on the promotion of energy-saving technologies and equipment to customers; VIP customers or other important customers.

Technology final selection refers to the integrated primary situation, from the aspects of LED lighting energy-saving technology, reactive power comprehensive control technology, injection machine energy-saving technology, load transfer technology, comprehensive utilization of resources technology, heat alternative energy technology, and other key energy-saving technology of 8 types of energy-saving reform projects that whether can be carried out, then implement the final selection.

Site survey and materials collection. Energy-saving diagnosis materials collection, which is based on the basic situation, energy management system and reasonable energy use of enterprise, and from the three aspects, the work of materials collection can be implemented.

The basic situation of enterprise should mainly include company profile, energy consumption of enterprise, mainly process overview, distribution system, mechanical and electrical equipment situation statistics, and main production site statistics of energy consumption, etc.

The materials collection of enterprise energy management system should mainly include energy management institution, energy management files, energy counting institution, energy statistics management, energy norm management, energy-saving technology management, etc.

The evaluation of rational use of energy mainly includes the evaluation of rational use of electricity, the evaluation of rational use of heat, comprehensive utilization of resource, energy that replaces other energy and products electricity consumption per unit, etc.

The evaluation of comprehensive use of electricity is an important part of energy-saving potential analysis, which must include reactive power and power quality comprehensive governance, energy-saving analysis of transformer, energy-saving analysis of motor, and energy-saving analysis of frequency conversion, lighting rationalization, and power load transfer of 6 parts.

The evaluation of rational use of heat in general includes enterprise class system, daily production operation situation, annual operation situation, and typical heat load conversion curve, boiler heat utilization situation, boiler maintenance situation, etc.

The comprehensive utilization of resource, which generally includes the use of residual heat and pressure, the comparison and use of heat pump and solar energy, and the residual gas utilization detection, etc.

The electricity that replaces other resource, including coal, gas, oil boilers, electromagnetic cookers, and owned power plants changed to city electricity, etc.

Key energy-saving technology and equipment suitability evaluation, generally, uses the work plan published by the company as a guide, at present, which mainly refers to the mechanical and electrical products that prohibited by the state, the small cars with big horse power, etc.

Among the rational use of energy and materials collection, the contents that must be included are shown in Fig.1 bellow.

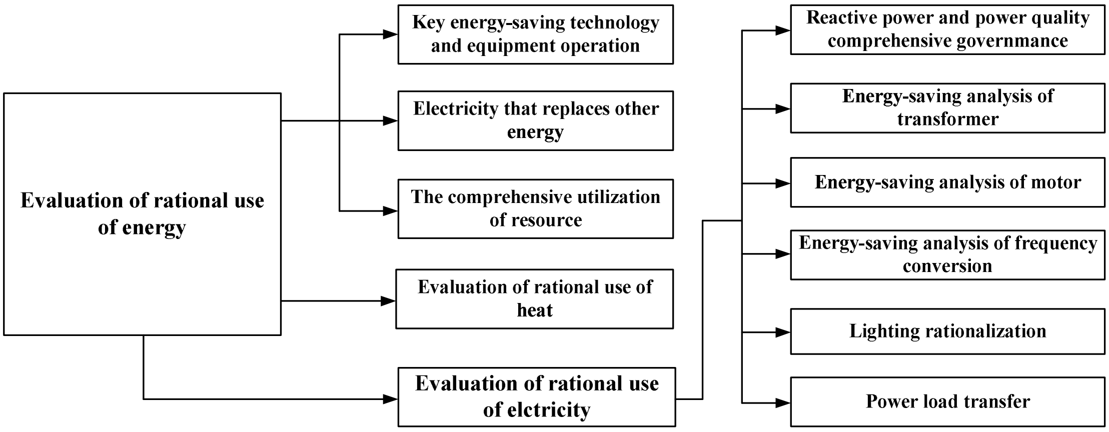
Evaluation of rational use of energy
Key energy-saving technology and equipment operation
Electricity that replaces other energy
The comprehensive utilization of resource
Evaluation of rational use of heat
Evaluation of rational use of elctricity
Reactive power and power quality comprehensive governmance
Energy-saving analysis of transformer
Energy-saving analysis of motor
Energy-saving analysis of frequency conversion
Lighting rationalization
Power load transfer

Fig.1 The rational use of energy evaluation content block diagram

The requirements of field measurement. The field detection points mainly include power quality monitoring points, conventional electronic parameter monitoring points, and heat monitoring points of 3 types of points, and the test item, detection time, detection method, and detection instrument accuracy are respectively stipulated in detail, for those reports of abnormal operation, outmoded production equipment, or the equipment which have energy-saving technology transformation potential founded in previous finish of forms, and the system implements special field measurement operation data collection work, etc.

The evaluation analysis of rational use of energy. This part mainly includes two parts: the rational use of energy settings and energy-saving amount calculation in each industry, the data of evaluation analysis, which is mainly from the collected materials and field testing, then is counted based on the standard "Energy Saving Amount Audit Guide of Energy-saving Project". While the principle of calculating method is preliminary according to "the Energy-saving Calculation recommended Method of South China Power Grid Rational Use of Energy in Customer Side"[4].

The calculating of user energy-saving quantity primarily divided into these nine sections, products energy-saving quantity, output value quantity, technical energy-saving quantity, one kind energy saving quantity, evaluation of energy consuming management, calculating quantity of rational light consuming, calculating quantity of rational heat consuming, calculating energy-saving quantity of natural resources comprehensive utilization and calculating energy-saving quantity of light energy replacing other energy.

The evaluation of energy consuming management is mainly used to count the energy-saving of each product. While the count of light energy consuming is based on the data from real time monitoring or the electricity bill from power supply department.

The calculating quantity of rational light energy consuming contains of the energy saving by reactive compensation and comprehensively controlling the quality of light energy, transformer energy-saving, electric motor energy-saving, frequency conversion energy-saving, lighting rationalization and electric negative jump six aspects of parameter and rules about the calculation of energy-saving quantity.

Reactive compensation and the comprehensive control of light energy quality involve calculations of the reactive compensation capacity, reactive compensation energy-saving quantity and the energy-saving quantity of harmonic reduction. Moreover, the national standard GB 12497-1995 gave the guide to count the quantity of light power probable saving by reactive compensation and harmonic control.

Transformer energy-saving includes the calculating of transformer total energy consuming, energy-saving by changing transformer, the choice of transformer changed types and the economic operation of transformer. The transformer total energy consuming and energy-saving by changing transformer are counted based on the way of transformer yearly wastage curve. Under the situation of ignoring the additional wastage caused by transformer reactive wastage, calculate the transformer total yearly wastage and energy-saving quantity made by changing different types of transformer in different years with maximum load wastage hours. If the choices of transformer changed types are given, the type with more obvious energy-saving is suggested. Transformer economic operation puts forward the evaluation methods of electricity basically price and peak price, to test the company electric equipment and electricity consuming is rational or not.

The energy-saving of frequency conversion mainly consists of fan and water pump frequency conversion of energy-saving reconstruction, air compressor energy-saving reconstruction and other frequency conversion of energy-saving.

Illumination rationalization refers to energy-saving amount calculation of lighting system, among which, the lighting will release some heat when they work, so the influence of lighting system for warm in winter and air conditions in summer should be taken into considerations when calculating.

Power load transfer refers to energy saving technology of center air conditioner and energy-saving amount calculation of ice storage technology. At the same time, it gives possible conditions for center air conditioner system to possess comparatively large energy-saving potential by frequency conversion, as well as the conditions reformed by center conditioner for conducting storage energy-saving valuably.

The calculation of rational use of heat gives equipment thermal efficiency calculation formulas, and the energy-saving amount calculation of comprehensive use of resource gives recycle of residual heat, gas, pressure, calculation formulas and methods of total system heat amount, heat consumption rate, and annual heat saving amount of heat pump and solar water heating system.

Electricity that replaces other resource and its calculation includes coal, gas, oil that are changed to electricity, and the owned electricity plants that are changed to city electricity, the calculation formulas and methods of this two parts are both included.

Key energy-saving technology and equipment applicability evaluation energy-saving amount calculation puts forward 2 kinds of calculation techniques, which are used to calculate energy-saving amount of popularizing different key energy-saving technology and equipment during energy-saving diagnosis period.

Conclusions

(1) By continuing to promote energy-saving diagnosis work, and aimed at existent problems of different equipment in different industry, the electrical enterprises should put forward the corresponding energy-saving diagnosis emphasis points and key points, during annual diagnosis activity of different production equipment, for different industry, the focus of energy consumption and monitoring indexes are constantly changing. This work method of through energy-saving diagnosis analysis, energy consumption index optimization, and again diagnosis, rich and optimization, which makes energy-saving diagnosis work has stronger industry technology pertinence, and promote the management and energy reduction and optimize the operation mode, forming a virtuous cycle.

(2) By continuing to promote energy-saving diagnosis work, collect and analyze the electricity utilization performance of enterprises included in the power supply region, thus better arrange enterprise develop peak load shifting and orderly use of electricity work. Under the guarantee of enterprises' production demand, exert the power network itself comprehensive management advantage, thus make the energy-saving and emission-reduction work of DSM develop continually and in depth.

(3) By continuing to promote energy-saving diagnosis work, which makes energy-saving and emission-reduction work become an important part of the daily work of enterprises, so that the energy consumption index can be optimized continually. For those affect energy consumption index major technical problems, should apply technical methods to solve them, and optimize the operation mode, so that can play a significant role in energy-saving and emission-reduction projects. Energy-saving diagnosis management should also be applied in conventional power monitoring and thermal measurement, improvement of topical system, technical transformation scheme evaluation, and optimization of system operation, etc. thus can further promote the energy-saving and emission-reduction work of enterprises to develop deeply.

Acknowledgements

This work was financially sponsored by the Science and Technology Projects of China Southern Power Grid.

References

[1] "Power saving technology series" editorial board: *Power Quality and Energy-saving Technology* (China Power Press, China 2008).

[2] "China electric power enterprises" association: *Energy-saving and Emission Reduction Total Policies and Regulations Selections* (China Power Press, China 2008).

[3] China Huadian Corporation: *Thermal Energy Enterprise Evaluation System* (China Water Power Press, Beijing 2007).

[4] Maolin LU, Zhifen CHENG, Youjiang MA: Energy Conservation Technology (In Chinese). Forum Vol. 23 (2005), p. 514-517.

Applied Mechanics and Materials Vol. 596 (2014) pp 687-691
© (2014) Trans Tech Publications, Switzerland
doi:10.4028/www.scientific.net/AMM.596.687

Unbalanced power allocation method to the research of the influence of the power system trend

Hao Wang[1,a *], Ning Wang[2,b] and Donghai Xue[3,c]

[1]School of Electrical Engineering, Zhengzhou University, Zhengzhou,450001,China
[2,3]State Grid Henan Xingyang Power Supply Company, Xingyang, Henan, 450100,China
[a]whfly2007@163.com, [b]wangningxy@163.com, [c]xuedonghaixy@163.com

Keywords: regular trend, dynamic trend, unbalanced power, rotational inertia, frequency characteristic.

Abstract: After the disturbance of the power system, all generators of the system will react the disturb and adjust the output. All unbalanced power in the traditional method of trend fully will be assumed by the balancing bus, obviously do not conform to the actual operation situation. Dynamic power flow calculation can effectively deal with this problem, the current calculation method of the unbalanced power distribution exist two kinds of thinking:based on moment of inertia of the generator and based on the frequency characteristic coefficient of the generator . Here, this paper state the two methods of distribution , through analysis and comparison ,use case simulation verify the influence of the different methods of distribution on the system steady trend.

Introduction

The traditional power flow calculation method set the type of each node in advance, the node types mainly include :PQ node , PV node and balance node.Literature [1, 2, 3] introduced the process of calculation and application of the traditional power flow. In the power flow calculation, all the unbalanced power of the system will be assumed by the balance node. After the disturbance of the power system, in the traditional method of power flow calculation , will exist the following problem: compared with the actual output ,the output of the balance node by calculate will be error, possible the effort of balance node will fully greater than its output limit.

Compared the traditional power flow calculation method and dynamic trend , the biggest difference is its handling of the problem above. Literature [4, 5] introduced the principle and application of dynamic trend. Dynamic power flow calculation method is based on two points: one is according to the rotational inertia of the generator in the system; the other is according to the frequency characteristic coefficient of generator to distribute the system unbalanced power . Studies have shown that different methods of distribution have different influence on the the system steady trend. Below this paper will state the two methods of distribution , through analysis and comparison ,use case simulation to verify the influence of the different methods of distribution on the system steady trend.

The analysis and comparison of two methods

The method of the system unbalanced power allocation based on the moment of inertia of the generator

Based on the definition of system inertial coordinate, the average frequency of system can be expressed as:

$$w_s = \sum_{i=1}^{n} M_i w_i \Big/ M_T \tag{1}$$

$$M_T = \sum_{i=1}^{n} M_i \tag{2}$$

In the above equations , w_s defined as the average frequency of the system , M_i for the rotary inertia of the generator I . w_i for rotational frequency perunit value of the generator I , M_T for the sum of all the rotational inertia of the generator system , the physical significance for system equivalent moment of inertia of the equivalent generator .

The equation of the equivalent generator can be expressed as :

$$M_T w_s \frac{dw_s}{dt} = \sum_{i=1}^{n} P_{mi} - \sum_{i=1}^{n} P_{ei} = P_a \tag{3}$$

In equation (3), consider P_a as the unbalanced power of the system, and all the generators of the system considered as an equivalent generator , the rotor speed of this generator is decided by the unbalanced power of the system. When the unbalanced power of the system P_a is positive (i.e., reduce the system load), the such as check-in will speed up; and when the unbalanced power P_a is negative (i.e., increase the load), such as check-in will slow down.

Analysis of generator, its rotation of rotor:

$$M_i w_i = \frac{dw_i}{dt} = P_{mi} - P_{ei} = P_{ai} \tag{4}$$

In the equation (4), P_{ai} for the share amount of unbalanced power amount by generators in the system , the share amount will determine its rotor rotation.

Here, assume that the generator rotor speed changes of all nodes in the system have no difference, and equal to the changes of the rotor of the system such as check-in, according to the equation (3) and (4), we can get the following equation:

$$M_i / M_T = P_{ai} / P_a \tag{5}$$

Equation (5) is computational equation of unbalanced power allocation according to the moment of inertia of the generator system . According to the equation, the bigger the moment of inertia of the generator, the greater its share of the imbalance of power, and vice versa . After obtain the share of unbalanced power of each generator , accordingly modify the generator output of power flow calculation, we can obtain the steady state current situation by power flow calculation on condition that all generators participate in unbalanced power allocation.

The method of the system unbalanced power allocation based on the static generator frequency characteristic coefficient

Power system demand the frequency of power grid must be stable running near its ratings, but when the system exist the unbalanced active power , the frequency of power grid will change. When the system frequency changes, the prime mover automatic speed control system will change the output of the generator by adjusting . After the adjustment, the system will appear a new steady-state equilibrium. The frequency adjustment by prime mover speed regulation system and the adjustment process of generator active power, known as the frequency of one-setting. The adjustment characteristics of active power of the generator and the system frequency , called active power-frequency characteristics of generator set.

The static characteristic curve of generator set is shown in figure 1.

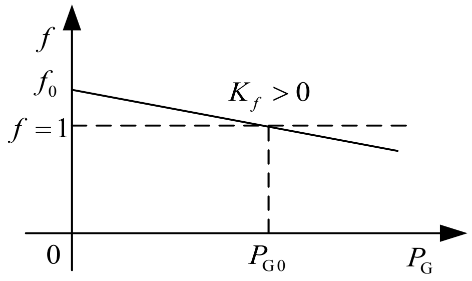

Fig 1 Active power-frequency static characteristics of generator set

Generally regarded it as a straight line. The equation of static active-frequency characteristic of generator I as shown in equation (6):

$$P_{Gi}=K_{fi}(f_{i0}-f) \tag{6}$$

In equation (6): P_{Gi} as the active power of the unit I ; K_{fi} For the unit adjustment power of unit I, is the reciprocal of the active power adjustable differential coefficient of the unit I ; f_{i0} for idling frequency of the unit I ; f for the system steady frequency.

In the actual system, differential coefficient of generating sets can be set within a certain range, the differential coefficient have great influence on frequency deviation, the smaller the differential coefficient , the smaller the frequency deviation . As a result of the limitation of system speed regulating , the differential coefficient of the setting range is limited. According to the operation experience, K_{fi} of turbo generator unit general is usually set between 15 to 25. Hydroelectric generating set usually set between 30 to 50. In order to make the share of the system generator fit for its own adjustable situation in unbalanced power adjustable situation , the frequency characteristic coefficient of each generator should consider the problem of cooperation between the generators when its setting.

$$K_{fs} = \sum_{i=1}^{n} K_{fi} \tag{7}$$

$$K_{fi} / K_{fs} = P_{ai} / P_{a} \tag{8}$$

Equation (8) is computational equation of unbalanced power allocation according to the active power-frequency characteristics of the generator . According to the equation, the greater the unit adjustment power , the greater its share of the imbalance of power,, and vice versa. After obtain the share of unbalanced power of each generator , accordingly modify the generator output of power flow calculation, we can obtain the steady state current situation by power flow calculation on condition that all generators participate in unbalanced power allocation.

Analysis and comparison of case

Here, take NewEngland10 machine and 41 nodes system for example. Programming calculation procedure by Matlab programming language, and analysis different unbalanced power allocation method influence on the system steady state after the removal of the load on the node 15 . Three kinds of trend corresponding the steady trend of the system is presented in table 1 and 2 .

Tab 1 Generator output under different ways of unbalanced power allocation

Generator Number	General trend		rotational inertia		frequency characteristic	
	active power	reactive power	active power	reactive power	active power	reactive power
1	10.8353	3.3629	2.6288	1.7792	2.4622	1.5679
2	0.1756	1.6364	0.8390	2.1120	0.5782	2.0235
3	5.5803	2.8615	6.2084	3.2752	6.2302	3.1427
4	4.7440	1.8790	5.6118	2.0037	5.6022	1.8042
5	7.4934	2.3669	8.5854	2.6767	8.7323	2.5127
6	8.7335	3.7296	9.7691	3.1657	9.9783	3.5020
7	5.3840	1.9528	6.2084	2.2853	6.2302	2.4165
8	5.3840	2.2432	6.2084	2.4538	6.2302	2.2780
9	5.3840	1.4868	6.2084	1.6804	6.2302	1.7246
10	3.9268	1.8365	5.0152	2.1609	4.9742	1.9697

The results showed that in the general trend, the unbalanced power are borne by the No.1 balancing machine, lead to the active power big, is likely to exceed its output limit . Through the two methods of unbalanced power allocation after the distribution, the results of the trend is closer to the actual power system operation.

Tab 2 Node voltage under different ways of unbalanced power allocation

Node Number	General trend		rotational inertia		frequency characteristic	
	amplitude	phase angle	amplitude	phase angle	amplitude	phase angle
1	0.9827	22.3853	0.9795	3.6703	0.9814	4.0221
2	0.9258	26.6545	0.9226	-0.8008	0.9243	-2.2013
3	0.9655	7.1181	0.962	5.2293	0.9638	6.6412
4	1.0028	22.6400	1.0089	13.0352	1.0108	11.7552
5	1.0173	1.3669	1.0177	-5.3368	1.0196	-4.8218
6	0.9932	4.7469	0.9923	-8.0414	0.9942	-7.3655
7	0.9947	4.2321	1.0006	10.7292	1.0025	9.8811
8	1.0036	12.7445	0.9845	-4.5768	0.9864	-6.5450
9	1.0116	17.2477	1.0146	-1.5756	1.0165	-3.5031
10	1.0104	5.3865	1.0065	7.7281	1.0084	6.8392

The results showed that different ways of unbalanced power allocation will affect the system voltage amplitude and phase angle of each node, compared with general trend, differ widely.

Summary

Based on the analysis of traditional power flow calculation method when calculating the power system steady state after disturbance , the paper state the two methods of distribution : based on moment of inertia of the generator and based on the frequency characteristic coefficient of the generator . Through analysis and comparison ,use case simulation verify the influence of the different methods of distribution on the system steady trend. Results show that different ways of unbalanced power allocation have great influence on system current situation ,include the output of each generator in the system, the amplitude and phase angle of the node voltage etc.

References

[1] ScotB. Review of Load Flow Calculation Methods.Proc.IEEE.1974,62(7):916~929.

[2] William.F.Tinney, Clifford E.Hart. Power flow solution by Newton's method [J]. IEEE Transactions on Power Appartus and Systems, 1967, PAS-86(11):1449~1460.

[3] Le Nguyen H.Newton-Raphson method in complex form[J].IEEE Trans on Power Systems,1997,12(3):1355~1359.

[4] Ge Baojun,Wang Ming,Lv Yanling et al.Study on Static Power Characteristic of Huge Hydro-Generator[C].Asia-Pacific Power and Energy Engineering Conference (APPEEC 2010).[v.1].2010:282-285.

[5] Huang, H.,Li, F.Sensitivity Analysis of Load-Damping Characteristic in Power System Frequency Regulation[J].IEEE Transactions on Power Systems,2013,28(2):1324-1335.

Applied Mechanics and Materials Vol. 596 (2014) pp 692-695
© (2014) Trans Tech Publications, Switzerland
doi:10.4028/www.scientific.net/AMM.596.692

User-defined Governor Model Based on PSCAD and Analysis of Low Frequency Oscillation Mechanism

Shiwu Xiao[1, a], Cong Wang[1, b *]

[1]North China Electric Power University, Changping, Beijing, 102206, China

[a]xiaoshiwu@263.net, [b]moeraicong@163.com

Keywords: Governor, modeling, governor, low frequency oscillation, PSCAD.

Abstract. Based on PSCAD software, a user-defined governor model is set up. Single machine infinite bus system and four machine two regional system are taken as examples based on PSCAD and the elements' parameters are set on the test results of a power plant in southern China. By analyzing the model of speed governing system and changing governor parameters' value, mechanistic study leading to low frequency oscillation is studied in the paper.

Introduction

Digital simulation is a powerful tool for analysis of low frequency oscillation. Reproducing the low-frequency oscillation phenomenon through simulation plays an important role in analyzing low frequency oscillation mechanism.

Based on PSCAD software, a user-defined governor model is set up. Firstly, the feasibility of the custom modeling governor is verified in single machine infinite bus system. In four machine two regional system, the governor, turbine and electrohydraulic actuator of number1 generator are user-defined model adapting the parameters from the test results of a power plant in southern China. Finally, low frequency oscillation phenomenon is triggered when one of the governor's parameter changes. Explanation and analysis are made after simulation.

Governor Principle

Commercial frequency electrohydraulic regulating system is consist of the parts as follows: Rotating Speed Measurement, Frequency/Rotating speed-Voltage Transmitter, Power Measurement, Rotating speed and Power given link, Electro-Hydraulic conversion and Hydraulic pressure system[1].

Magnetoresistance converts rotor speed to the voltage signal of corresponding frequency, frequency-voltage transmitter converts the pulse signal from magnetoresistance to the output voltage value proportional to the rotor speed. Power measurement link converts active power of generator to DC voltage proportional to itself. Rotating speed and Power given link is constituted of precise potentiometer. Its power is supplied by steady voltage source of high precision and its output voltage value could be represented as given rotor speed and power. Electro-Hydraulic conversion converts regulating quantity from electric quantity to oil pressure, which is converting the output of frequency amplifier to the opening of oil valve. Thus the opening degree could be controlled to regulate the input power of turbine.

Model Introduction

Governor System Model. In this simulation system, all of the generators' and loads' models are using the ones in model library of PSCAD and set the parameters according to the given value. The governor and turbine model of number 2, 3 and 4generator are using Steam Gov4 and Steam Tur2 in model library. The governor, turbine and electrohydraulic actuator of number1 generator are user-defined models, given control system block diagram in Fig. 1. The parameters are all from the test results of a power plant in southern China.

In the figures, T_1:Time constant of speed transmitter, P_{REF}: Power set-value, P_E: Electromagnetic power of generator, Δw: Speed deviation, K_{D1}:Magnification derivative cycles of load controller,

K_{P1}:Magnification proportional cycles of load controller, K_{I1}:Magnification integrating cycles of load controller, P_{CV}:Valve position instruction value, it is the output of governor and the input of electrohydraulic actuator, T_C: Hydraulic actuator closing time constant, T_O: Hydraulic actuator opening time constant, T_2:LVDT transmitter time constant, P_{GV}: Steam flow as the output of electrohydraulic actuator, the input of turbine.

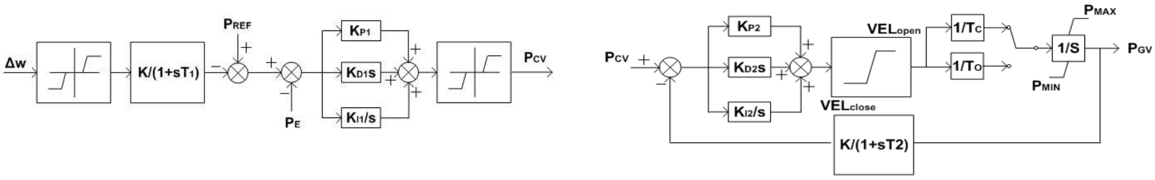

Fig.1 Governor transfer function

VELopen: Rapid opening coefficient(P.U.), VELclose: Rapid closure coefficient(P.U.), P_{MAX}: Prime mover maximum output power, P_{MIN}: Prime mover minimum output power, K_{P2}:Magnification proportional cycles of electric hydraulic converter, K_{D2}:Magnification derivative cycles of electric hydraulic converter, K_{I2}:Magnification integrating cycles of electric hydraulic converter.

Four Machine Two Regional System Model. Four machine two regional system includes two similar regions with weak ties. Each region has two coupling unit. Generator rated capacity is 900MW and rated voltage is 20KV.System load use the RLC model and set them at bus7 and bus9. Moreover, there are parallel capacitor reactive power compensation on bus7 and bus9 in order to maintain the bus voltage. Electrical wiring diagram of four machine two regional system is given in Fig. 2. Modeling is built based on PSCAD and using the measured value of the original as the setting of model components parameters.

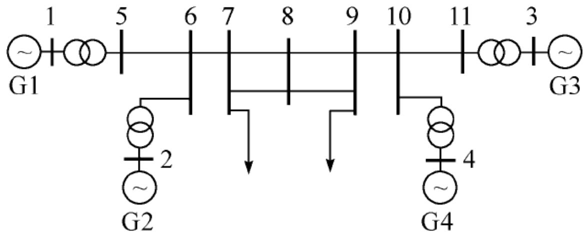

Fig.2 Electrical wiring diagram of four machine two regional system

Low Frequency Oscillation Simulation Analysis

In single machine infinite bus system, simulation verification is based on the custom modeling governor. The simulation time is 40s, 0.1s single-phase earth fault occurs at 13s.Given system frequency and generator power in Fig. 4. It is observed that at the beginning of the simulation, system is stably operating. Under the acting of governor the system come back to steady after the fault and the corresponding phenomenon.The effectiveness of the custom modeling governor is verified.

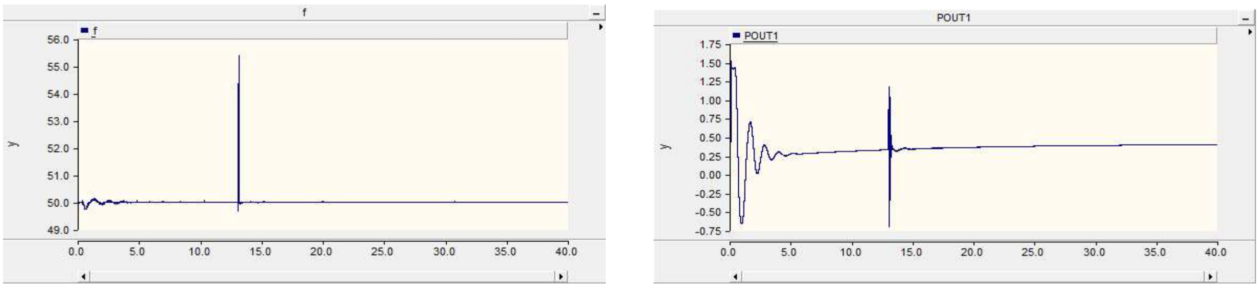

Fig.4 The changing curve of frequency and generator power of
40s simulation of single machine infinite bus system

In four machine two area system, set the simulation time as 150s and execute primary frequency control operation. At 20s, put into the power feedback loop and the frequency feedback loop and cut the two main loops at 100s. The simulation image is shown in Fig. 5. It can be seen that low frequency oscillation occurs because of the settings of parameters and the effect of primary frequency controlling.

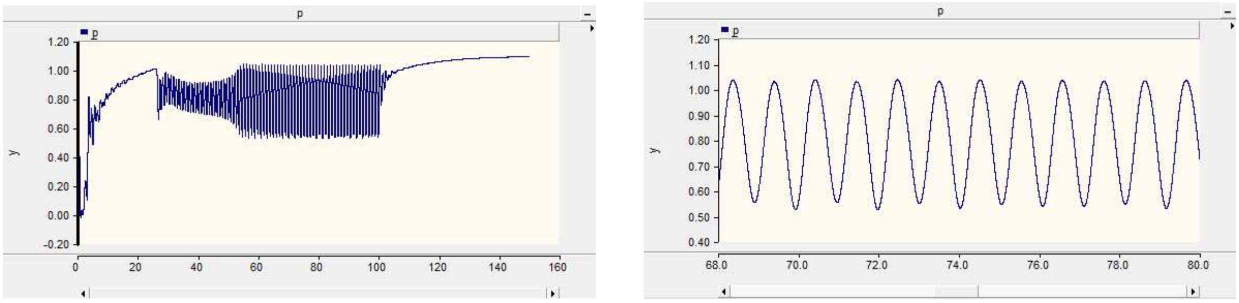

Fig.5 The changing curve of low frequency oscillation occurs by switching the power and frequency and 1Hz low frequency oscillation phenomenon

Low Frequency Oscillation Mechanism Analysis

Negative damping mechanism and resonance mechanism are becoming the two main theories to explain low frequency oscillation phenomenon in engineering practice at present. Autonomous System shows a free oscillation after disturbance and its stability depends on the damping of the positive and negative. Under the negative damping condition, oscillation is growing persistently and eventually the loss of stability of system will occur.

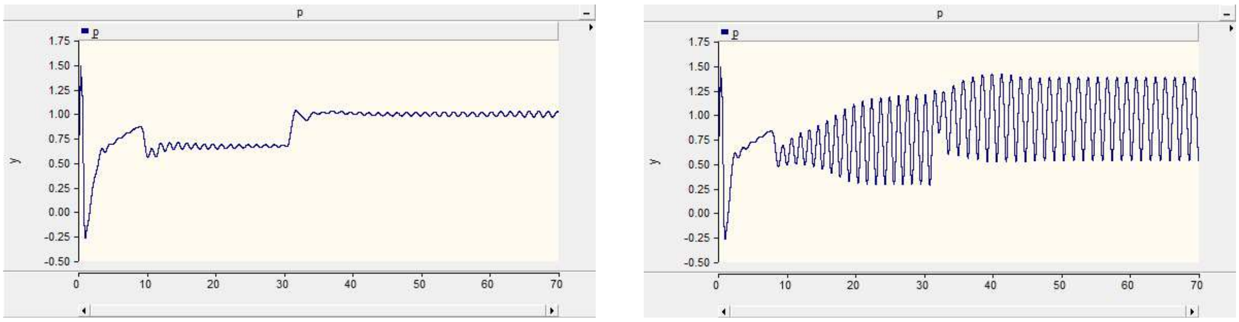

Fig.6 The changing curve of low frequency oscillation when the K_{D1} is 0.15 and 1.5

Basing on single machine infinite bus system, the affection from the governor and its changing parameters are studied as follows. Fig. 6 is the emulational image of the system when the magnification derivative cycles of load controller, K_{D1} is set as 0.15 and 1.5. The primary frequency operation is putting into the power feedback loop and the frequency feedback loop at 30s.The low frequency oscillation phenomenon is triggered without cutting the loops.

It can be seen that in single machine infinite bus system, the low frequency oscillation phenomenon can be triggered by the settings of governor parameters and the input of the power feedback loop and the frequency feedback loop[2].Take single machine infinite bus system as example, the steam turbine generator rotor motion equation of linearization is:

$$\frac{2H}{\omega_0}\Delta\ddot{\delta}+\frac{K_D}{\omega_0}\Delta\dot{\delta}+K_s\Delta\delta=\Delta T_m \qquad (1)$$

In this equation, H: The rotor inertia time constant; ω_0 :Benchmark angular velocity; $\Delta\delta$: Generator angle deviation; K_D :Damping factor; K_s: Synchronous moment coefficient; ΔT_m: Mechanical torque increment.

If mechanical torque changes, Eq. 1 changes to Eq. 3:

$$\frac{2H}{\omega_0}\Delta\ddot{\delta}+\frac{K_D+K_{D_m}}{\omega_0}\Delta\dot{\delta}+(K_s+K_{sm})\Delta\delta=0 \tag{2}$$

K_{sm}: Mechanical synchronous coefficient; K_{Dm}: Mechanical damping coefficient. Eq. 2 and Eq. 3have the same format of solution:

$$\Delta\delta(t)=A_0e^{-\beta t}\cos(\omega_n t\sqrt{1-\zeta^2}+\varphi_0) \tag{3}$$

A0 and $\varphi_0$are two integration time constant depends on starting condition; β:Damping factor; ζ: Damping ratio；ωn:Undamped natural oscillation angular frequency. If damping ratio is positive, oscillation will decrease; if damping ratio is negative, oscillation will increase. It is the negative damping mechanism of the low frequency oscillation. In the single machine infinite bus system and four machine two area system, the low frequency oscillation phenomenon are all derived from the negative damping mechanism.

In this paper, the low frequency oscillation triggered by governor parameter change in four machine two area system after fault can be explained by negative damping mechanism.

$$K_{Dm}=\frac{-(K_s+K_{aex})\omega_0(T_{om}+T_{CH})+(D+K_{Dex}+K_\delta)(1-T_{om}T_{CH}\omega^2)}{(1-T_{om}T_{CH}\omega^2)^2+(T_{om}+T_{CH})^2\omega^2} \tag{4}$$

T_{CH} :Air intake time constant；K_δ：The reciprocal of the range rate；D：Mechanical friction damping coefficient；Ksex: The excitation system of synchronous torque coefficient. According to Eq. 5 and unit into the measured parameters before changing the governor parameter, a positive damping is get. And after the parameter changes, the damping is negative. In conclusion, the system total negative damping is the reason of low frequency oscillation phenomenon.

Summary

In this paper, governor principle was introduced firstly. Models based on PSCAD were built and low frequency oscillation simulation analysis were made. In single machine infinite bus system, the effectiveness of the custom modeling governor was verified. In four machine two regional system, the results showed that the changing of a parameter of governor with primary control can trigger low frequency oscillation after power system fault. Finally, negative damping mechanism was stated and it's the theory for analyzing the low frequency oscillation phenomenon. To prevent this kind of low frequency oscillation phenomenon happening again, PID parameters should be set reasonably.

References

[1] YANG Guancheng: *The Principle of Automatic Device in Power System* (China Electric Power Press Publications, China 1986).

[2] XU Yanhui,WANG Zhenzhen, WENG Hongjie. Low Frequency Oscillation Instance Caused by Primary Control and Mechanism Analysis [J].Proceedings of the CSEE.2013, 37(23):119-124.

[3] DEMELLO F P, CONCORDIA C. Concept of synchronous machine stability as affected by excitation control [J]. IEEE Trans on Power Apparatus and Systems, 1969, 88(4):316-329.

[4] WANG Tieqiang, HE Renmu, WANG Weiguo. The mechanism study of low frequency oscillation in power system [J]. Power System Technology, 1995, 19(12):16-10.

Applied Mechanics and Materials Vol. 596 (2014) pp 696-699
© (2014) Trans Tech Publications, Switzerland
doi:10.4028/www.scientific.net/AMM.596.696

Methods to Establish The Fault Tree of Substation Automation System Based on HAZOP

Bin-bin Han[1, a],Yue Wang[2,b], Fu-yan Guo[2,c]

[1]College of Information and Automation, Tianjin Tianshi College,Tianjin 301700,China

[2]School of Control & Mechanical Engineering, Tianjin Chengjian University, Tianjin 300384, China

[a]rain2111@126.com, [b]dark8angle@126.com, [c]happytime76@163.com

Keywords:HAZOP;fault tree;substation;reliability analysis

Abstract. Because of it's complexity of substation, once the control system failure will cause huge losses, according to the fault characteristics, established the HAZOP method combined with the method of fault tree model, and the substation and protection and control system as an example, the modeling process complete sample. This method can standardize and establish fault tree, provides a scientific, reasonable means to discover substation system inherent or potential risk factors.

Introduction

Substation high-voltage equipment more, affect the safe operation of the system from physical, weather disasters, human factors, equipment, facilities, aging causes higher power causes all kinds of dangerous and harmful factors. Once the failure of the control system, may cause a large area power outage, equipment damage, employee injuries, serious injury or death accident.

In 2013 a 110kV substation 10kV line occurred near fault, because the substation DC system voltage loss, protection relay, fault in a 220kV substation 110kV line protection action, resulting in 110kV substation voltage loss.

Application method

Introduction to HAZOP.HAZOP is a system engineering as the foundation can be used to evaluate the risk qualitative analysis or quantitative evaluation method. Deviation events may appear in the method to analyze state parameters in the running process of the system, control changes in operation. Based on the analysis of the effects of these deviations and cause these errors on the system caused by the actual operation of the system, clear the main risk, the risk factors in the system, find the weak link, and according to the deviation event consequences puts forward corresponding preventive measures.[1]

Introduction of fault tree. Fault tree analysis (FTA) is one of the important analysis method of safety system engineering, it can carry out identification and risk evaluation of various systems, can not only analyze the direct cause of the accident, but also can reveal the potential causes of accidents. FTA is through from top to bottom deduction to determine could ultimately lead to various system level top event does not expect the combination of events, ultimately determine the cause specific reasons for this conclusion. The top event is concerned in the event of fault tree analysis. The bottom event of fault tree branch called the basic events in fault tree analysis, is the only cause event cause other events. Located at the top and bottom of the intermediate event event event known as the intermediate event.[2]FTA generally can be divided into 5 steps: preparation stage, fault tree establishment, qualitative analysis of fault tree, fault tree analysis, fault tree analysis results are summarized and the application.

Application of case

Tianjin a wind power substation, power into the line for the 35kV integrated circuit is sent to the 35kV bus of the wind power booster station, the main transformer step-up to 110kV, with a single 110kV line access 220kV substation. 110kV outdoor distribution device adopts single bus terminal, a transformer station.

Analysis of substation HAZOP

On the basis of HAZOP analysis steps as follows:
The establishment of study groups: the study group to become the enterprise management staff of 1 people, 2 people of fault diagnosis personnel system, enterprise power engineer 2 people.Collection of information: information for power system diagram, wiring diagram, equipment manuals etc..Analysis to determine the system node for 110kV system,35kV system,Public system,transformer.System mainly deviation is power-off, failure, too high,high, disconnection.After analyzing the results, the following table 1

Table 1: HAZOP analysis table

Num-ber	name	Deviation	Reason	Consequence	code
1	110kV system (M1)	Failure	Circuit breaker and circuit chamber with low pressure alarm	SF_6 leak	X1
		Failure	Main transformer protection of high voltage side, low-voltage alarm	Power, electric fire	X2
		power-off	Line signal, isolation, ground control, circuit breaker energy storage, lighting, heating circuit power off signal	Control failure	X3
		Tripping operation	Main transformer differential protection trip,High pressure side reserve trip,Low pressure side reserve trip	Power failure	X4
		Disconnection	The main transformer protection CT break PT disconnection,The line outgoing PT power signal,High voltage operation box device control loop break	CT, PT failure Unable to operate	X5
		Overload	The main transformer protection overload	Power, electric fire	X6
		Overvoltage	Zero sequence over-voltage protection for main transformer low voltage side	Power, electric fire	X7
		False action	Line protection device action	Power failure	X8
		Failure	Line protection device failure	Power, electric fire	X9
		Disconnection	Line protection control circuit break	Beyond control	X10
2	Transformer (M2)	Failure	The ontology of abnormal gas	Electrical fire	X11
		High temperature	Winding, oil temperature high	Electrical fire	X12

3	35kV system (M3)	Alarm failure	Abnormal alarm circuit breaker SF_6 pressure	SF_6 leak	X13
		Alarm failure	Circuit breaker open alarm	Fault	X14
		False action	Line monitoring device lock	Failure in 35kV protection	X15
		Alarm failure	Alarm line monitoring device	Protection failure	X16
		Tripping operation	Line monitoring device protection trip	Protection failure	X17
		Disconnection	Line control loop break	Protection failure	X18
		Tripping operation	Section of the circuit breaker tripping	Protection failure	X19
4	Public system (M4)	Failure	DC charging cabinet insulation fault, DC fault, AC fault, fault,Battery failure	Control system failure	X20
		Failure	Abnormal UPS cabinet	Standby power failure	X21

Substation fault tree

According to the HAZOP results, photovoltaic power generation system power outages, equipment failure, electrical fire, SF_6 leak faults, it occurs, the safety device failure will occur more serious damage to the equipment, personnel casualties. Thus, establishment of accident tree, with power failure as the top event(T), the logic relation between logic "and" door "or" top-down analysis cause the top event of all the basic events and mutual.As the shown Figure 1-5 and Table 1.

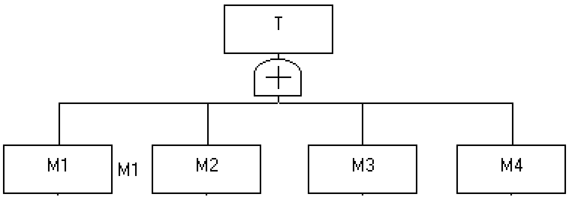

Figure1 Top event diagram

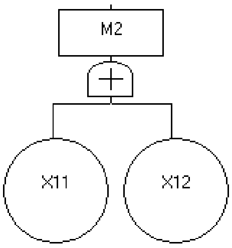

Figure2 Event M2diagram

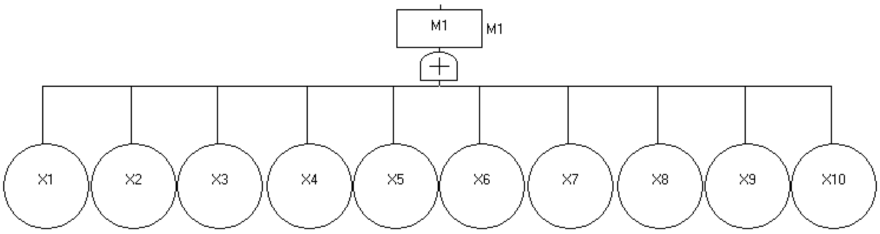

Figure3 Event M1 diagram

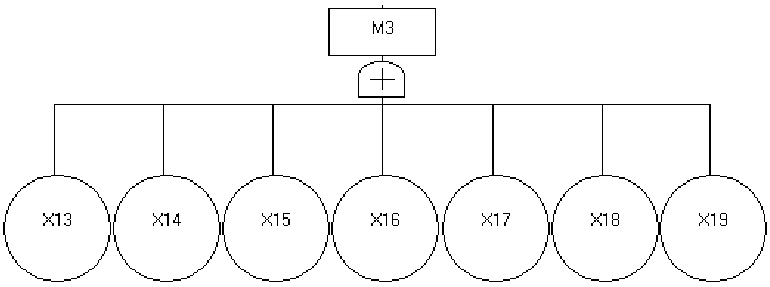

Figure4 Event M3diagram

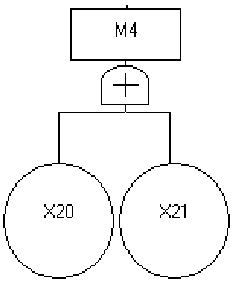

Figure5 Event M4diagram

Conclusion

By the analysis of the above HAZOP combined with fault tree, once the failure will occur electrical fire,electricity, electric shock accidents. According to the characteristics of substation, analysis of risk bias introduced by HAZOP method of substation. On this basis, put forward a new method to construct the fault tree, the fault tree construction of subjectivity, fuzziness, repeatability, covering such issues, provides a method for constructing the system of digital substation fault tree. Fault tree is established by this method, not only can be used for quantitative substation system reliability calculation, the implementation can also be used to guide the system testing, test, fault diagnosis and maintenance behavior.

Acknowledgement

This work is supported by Ministry of Housing and Urban-rural Development of the People's Republic of China (No. 2013-K1-1, Research and Application of the Key Technology of Lightning Protection of Solar Photovoltaic Building).

References

[1] Dunjó J,Fthenakis V，Vílchez J A et al． Hazard and operability (HAZOP) analysis． A literature review ［J］． Journal of Hazardous Materials，2010，173(1-3) : 19-32

[2] Khan F I，Abbasi S A． Analytical simulation and PROFAT II: a new methodology and a computer automated tool for fault tree analysis in chemical process industries ［J］． Journal of Hazardous Materials，2000，75(1) : 1-27

[3] P.Khamp hakdi Taratecraseth,K.Karanun. The Conducted Electromagnetic Interference of Small Grid Connected Inverter to Power System, 17th International Zurich Symposium on Electromagnetic Compatibility, 2006

[4] ZHANG Pei-chao,GAO Xiang． Analysis of reliability and component importance for all-digital protective systems[J]． Proceedings of CSEE，2008，28(1)：77-82．

[5] YANG Yang,XIE Kai-gui,SUN Xin． Operating component failure rate analysis based on FTA for power system[J]． Power System Protection and Control，2009，37(18)：134—137

Applied Mechanics and Materials Vol. 596 (2014) pp 700-703
© (2014) Trans Tech Publications, Switzerland
doi:10.4028/www.scientific.net/AMM.596.700

Research for short-term load forecasting based on linearization meteorological factors

Shun-hua Zhang

School of Mechanical and Electrical Engineering, Nanchang Institute Technology, China

threehhu@163.com

Keywords: Short-term load forecasting. Linearization meteorological factors. Artificial neural network

Abstract. With the development of economy in recent years, rapid growth of electricity demand, the cooling and heating load gets more and more big proportion of the total electricity load; the power load is influenced by meteorological factors which become more and more big. This topic will be based on short-term load forecasting in ANN (Artificial Neural Networks), conduct further research on the relationship between meteorological factors and power load, find the impact of the core meteorological factors of power load, and linear core meteorological factor model to establish the suitable for load forecasting based on ANN, make the forecasting to correctly reflect the meteorological conditions, improve the prediction accuracy of short-term load forecasting.

Introduction

Load forecasting is to make a prior estimate and demand for power from the known to the economic, social development and electricity demand situation through the analysis and research of historical data [1]. The operation of the power system, dispatching and economic load distribution needs to be rapid and accurate load forecasting. Therefore, load forecasting has been a power professional a hot research spot. There are many algorithms, such as least squares fitting method, regression analysis, time series method, grey system method and so on.

With the development of economy, rapid growth of electricity demand, the cooling and heating load gets more and more big proportion of the total electricity load; the power load is influenced by meteorological factors which become more and more big. Especially sudden changes in the weather, it makes the load of adjacent days fluctuation very big, makes the regularity of historical load data worse. This presents a challenge for short-term load forecasting. The climate change impact on short-term load forecasting is the focus of the study, and it is also a difficult.

The main research methods

ANN methods. In the short-term load forecasting, weather and other uncertain factors have important effects on the load, and the above method in the face of these is incapable of action. Especially in the process of the change of weather system, the meteorological factors influence on power network short-term load forecasting accuracy is greater [2]. To establish the accurate meteorological factor model, and applied to short-term load forecasting, further improve the load forecasting accuracy has important significance in the dispatching and economic distribution of power system operation.

In recent years, the neural network has attracted people's attention, with powerful multivariate nonlinear mapping ability it can accurately capture the nonlinear relationship between load and weather factors, the short-term load forecasting based on core meteorological factors become possible. However, the core meteorological factors that input neuron can be linear normalization to reflection the actual effect of meteorological factors on power load, so as to improve the accuracy of load forecasting. This topic will be based on short-term load forecasting in ANN, conduct further research on the relationship between meteorological factors and power load, find the impact of the core meteorological factors of power load, and linear core meteorological factor model to establish the suitable for load forecasting based on ANN, make the forecasting to correctly reflect the meteorological conditions, improve the prediction accuracy of short-term load forecasting.

Model of the power system load forecasting. For the factors to influence the system load, the prediction model for can be described as four independent components[3]: the basic load component, weather sensitive load component, special event load component, random load component, namely:

$$T(t) = N(t) + W(t) + S(t) + V(t) \tag{1}$$

Where $T(t)$ -- the total load of power system; $W(t)$ -- the weather sensitive load component;
$N(t)$ -- the basic load component; $S(t)$ -- the special event load component;
$V(t)$ -- the random load component.

Basic load component. Basic load $N(t)$ has nothing to do with weather, it has different connotation in different periods. In super short-term load forecasting, $N(t)$ is approximate linear change, even a constant; in short-term load forecasting, $N(t)$ generally presents periodic change; in mid long term load forecasting, $N(t)$ periodic changes showed a significant growth trend. $N(t)$ is generally used linear change model and periodic change of model description.

$$N(t) = L(t) * P(t) \tag{2}$$

Where $L(t)$ -- linearly varying load component; $P(t)$ -- periodic load.

Super short-term load forecasting uses only linear model, the previous time load tracing in a straight line, in the extension line can predict the next load. Linearly varying load component of short-term load forecasting reflect the change regular of the average load periodic, usually close to constant. Linearly varying load component can be expressed as:

$$L(t) = a + bt + e \tag{3}$$

Where a, b--the intercept and the slope of the linear equation; e--the error.

Weather sensitive load component. Weather sensitive load components associated with a series of meteorological factors, such as temperature, wind, weather, etc. Different meteorological factors influence of different load. The meteorological factors in different periods in a year are different impact load.

As an example the temperature sensitive load, along with the changing climate conditions and housing conditions, city heat island phenomena have become increasingly prominent [4,5]. At the same time residents want the more and more comfortable life, it makes the large load and high energy used electrical appliances emergence increased. With the development of the national economy, this part of load is very sensitive to the changes of temperature. The cooling and heating load in total accounted for the proportion of electricity load will be bigger and bigger.

The weather sensitive load mode is decided by the historical data, usually in the daily peak (y axis) and the corresponding meteorological changes (x axis) the diagram can be drawn. Although there are a lot of variables can be chosen, but the temperature and humidity is considered to be the most important, Fig. 1 is the weather sensitive load model with the temperature as meteorological variable. Using linear regression analysis and curve matching technique, we can identify the three line segments for weather sensitive load model.

$$W(t) = -K_l(T-T_l) \qquad T<T_l \tag{4}$$

$$W(t) = 0 \qquad T_l \le T \le T_h \tag{5}$$

$$W(t) = K_h(T-T_h) \qquad T>T_h \tag{6}$$

Where $W(t)$ --temperature sensitive load component of time t;

T_l, K_l --cold critical temperature and the slope;

T_h, K_h --heat critical temperature and the slope;

T --temperature;

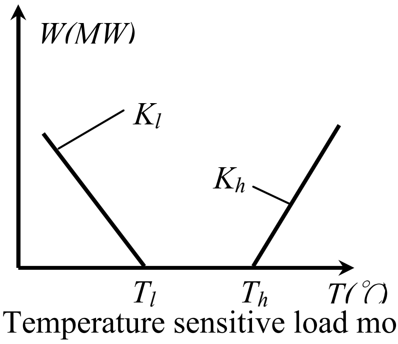

Fig. 1 Temperature sensitive load model

Special event load component. Special event load component makes the load deviate from the typical load characteristics obviously such as major political activities, celebrations, TV special, holiday line overhaul . With the development of market economy, especially in the economically developed areas, a variety of special events influence on load curve is more and more big. The special event effect of load is different from meteorological events completely. The key of special event is relevant experience accumulated enough, to find out the ragulation,sum up the special event correction rules to the load. the analysis and correction can be used to realize the expert system method, also can be simply corrected by manual.

Random load component. The random wave of load means that the load changes is caused by uncertain factors. The projections of any demand always accompanys by some uncertainty,this uncertainty random wave load is different with the system structure and the composition of the load in different grid, the size is not the same. For example, in the super short-term load forecasting, the huge steel rolling load belongs to random disturbance.

The normalized processing of sample data. In order to avoid saturation phenomenon of neurons, the normalized function in MATLAB is used in ANN input layer [6]. Function *premnmx(x)* in Eq. 7 equivalent load value into [-1, 1], The normalization functions *postmnmx(x)* in Eq. 8 is used in output layer. Also, the temperature of the normalized processing can also use the following two formulas. Quantitative values are shown in Table 1.

$$y=\frac{x-\frac{1}{2}(x_{\max}+x_{\min})}{\frac{1}{2}(x_{\max}-x_{\min})} \tag{7}$$

$$x=\frac{1}{2}(x_{\max}-x_{\min})y+\frac{1}{2}(x_{\max}+x_{\min}) \tag{8}$$

Where x_{max}, x_{min}−−the maximum and the minimum sample data.

Table 1 Grouping quantitative prediction model input variables

Description	Quantitative values							
	Work day model					Weekend model		
Week	Mon(1	Tus 2	Wen 3	Thur 4	Fri 5	Sat 1	Sun 2	
	-1	-0.5	0	0.5	1	-1	1	
Meteorological parameters	Clerar 1	Cloudy 2	Overcast 3	Slight rain 4	Moderate rain 5	Heavy rain 6	Thunder Showers 7	Snow 8
	-1	-0.714	-0.429	-0.143	0.143	0.429	0.714	1
Festival	The first day of New Year's day, labor day, National Day 1	The second day to the last day of New Year's day, labor day, National Day 2	New Year's eve 3	The Spring Festival for seven days 4				
	-1	-0.333	0.333	1				

Table 2 The error compared with grouping forecasting model and single forecasting model

Forecasting day	Forecasting model	Max error (%)	Min error (%)	Mean error (%)
04-02-4 Wednesday	Work day	5.808	0.024	2.028
	Single model	8.831	0.029	2.549
04-04-18 Sunday	Weekend	7.849	0.006	2.321
	Single model	11.458	0.033	2.994
04-10-4 (Nation Day)	Festival	6.557	0.001	2.023
	Single model	6.451	0.018	2.103

Conclusions

Very reasonable results have been obtained for sample data in Table 2. It means that using artificial neural network model to forecast regional power network short-term load is feasible effectively. Linearization meteorological factors and grouping forecasting model for improve prediction accuracy is effectively.

In the load forecasting, we must first consider the effect of meteorological factors, but the different area, the different load level, the different load structure and the different geographical position will affect the meteorological factors' function in short-term load forecasting. Secondly, the impact on human comfort and human psychological index should be considered in load forecasting. Therefore in the neural network structure design, the model should include the actual load and the area, the meteorological factors and the human body psychological factors. In fact, there is no fixed method or model is suitable for all occasions and load forecasting, which is superior to all others methods or models [7]. A special method or model may be suitable for a particular occasion, because some special factors have a significant effect on the particular system load. Therefore, for a variety of practical problems in the application, it should be dealt with seriously; concrete analysis of concrete conditions, the satisfactory forecasting effect can be obtained.

Acknowledgements

This work was financially supported by the Jiangxi Natural Science Foundation (20114BAB206036), the Science and Technology Project of Jiangxi Province Education Department (GJJ13769).

References

[1] Lizhi Zhang, Hua Zheng. Regional electricity market price mechanism [M]. China electric power press, 2004.

[2] Weiping Luo, Jianxin Zou. Weather sensitive for MATLAB neural network application in wuhan district power network short-term load prediction [J]. Electric power construction, 2003, 24 (2): 30-34.

[3] Erkeng Yu, Yiguang Liu, Jingyang Zhou. Energy management system (EMS) [M]. Science and technology publishing house. 1998.

[4] Yunping Chen, Xurui Wang, Baoliang Han. Artificial neural network principle and its application [M]. China electric power press, 2002.

[5] Yanxi Yang, Ding Liu, Qi Li, Gang Zheng. Neural network short-term load forecasting based on BP - GA hybrid learning algorithm of [J]. Journal of information control, 2002, 31 (3): 284-288.

[6] Martin T, Hagan Howard B, Demuth Mark H.B eal. Neural network design [M]. Mechanical industry publishing house. 2004.

[7] Bakirtzis A to G, Petridis V, Kiartzis S J et al. A Neural Network Short Term Load Forecasting Mode for the Greek Power systems [J]. IEEE Trans on Power systems, 1996, 11 (2): 858-863.

Applied Mechanics and Materials Vol. 596 (2014) pp 704-708
© (2014) Trans Tech Publications, Switzerland
doi:10.4028/www.scientific.net/AMM.596.704

A transducer matching method with signal frequency and inductor adjustment combined for submerged structure ultrasonic cleaning

Yuzhen YIN[1,a], Changping ZHU[1], Bin WANG[1], Qiang WU[1]
Cheng YAO[1], Bingyan CHEN[1], Qinggong REN[2,b], Qingbang HAN[1],
Yibin TANG[1], Zhenbing HE[3,c], Guochao CHEN[4,d]and Zhenxu LI[5,e]

[1] Changzhou Key Laboratory of Sensor Networks and Environmental Sensing, Jiangsu Key Laboratory of Power Transmission and Distribution Equipment Technology, Hohai University, Changzhou 213022, China

[2] School of Petro Chemical Engineering. Changzhou University, Changzhou 213164, China

[3] Changzhou Xinlinian Ultrasonic Equipment Co., Ltd, Changzhou 213104, China

[4] Wuxi ZhongKe Acoustics Engineering Co., Ltd, Wuxi 214001, China

[5] Wuxi DeZhong Acoustics Engineering Co., Ltd, Wuxi 214000, China

[a] yinyuzhen6@163.com, [b] qgren@cczu.edu.cn, [c] czxln@126.com, [d] cgc588@163.com,
[e] li.xu@nicle.cn;

Keywords: Ultrasonic cleaning; Frequency and inductor combined adjustment; Dynamic matching

Abstract: The application of ultrasonic cleaning for submerged structure is more common, but the resonant frequency of piezoelectric transducer is changed when it is heat at work. The traditional matching method cannot adapt the serial resonance frequency of capacitance branch and dynamic tuning is inefficient. We proposed a transducer matching method with signal frequency and inductor adjustment combined. The technique of identifying true max current value and Phase-Locked Loop frequency tracking was used. The automatic tracing of frequency is realized by searching the max current value, and working current was exceeding the threshold of $0.9I_{max}$. The adjustment of inductor was decided by phase comparison and impedance matching was achieved finally. By combining experimental study with theoretical analysis, the feasibility of this dynamic matching method was verified.This method have important significance for improving submerged structure ultrasonic cleaning efficiency.

Introduction

In the process of ultrasonic cleaning, ultrasonic transducer has the function of transmitting ultrasound as the ultrasonic power source load. But the resonant frequency of piezoelectric transducer is changed when it is heat at work, if the power source is not tracking the resonance frequency of the transducer in time and adjusting the matching inductance, it will cause the power amplifier can't sent output power to all of transducer, and even damage the circuit components[1].

The traditional static matching cannot keep series branch resonance frequency real-time changes as needed, in order to solve this problem, many of methods of the matching circuit in series for frequency tracking have been used, such as Dong et al. [2].proposed the technique of searching current double peak; Bai et al.[3].analyzed the ultrasonic transducer resonance frequency tracking by Phase-Locked Loop circuit; B. Mortimer [4] tracked high-power resonant frequency using the admittance tracking method etc. Those methods achieved the purpose of transducer resonance frequency in real-time tracking, but the value of static capacitance enlargement of transducer increased with the temperature rised [5]. Liu et al. [6] changed the current of the secondary side of the transformer to make the first side obtain the value of inductor which was needed by the system. The automatic adjustment of matching network with frequency changes was realized, but there still remains to be further perfected for signal source frequency. In view of this, we proposed a transducer matching method with the combination of signal frequency and inductor adjustment.

Theoretical analysis of matching

The piezoelectric transducer is capacitive in general at the range of operating frequency [7,8]. Fig.1 (a) is the equivalent circuit at the resonance frequency of transducer. Where C_0 is the static capacitor, L_1 is the dynamic inductor, C_1 is the dynamic capacitor, R_1 is the dynamic resistor. When the frequency of signal source equals the resonance frequency in series, it can be calculated by Eq. (1):

$$f_s = \frac{1}{2\pi\sqrt{L_1 C_1}} \tag{1}$$

When the transducer is at resonance state, the input impedance of system can be calculated by Eq. (2) :

$$Z = \frac{R_1}{1+\left(\omega_s C_0 R_1\right)^2} + j\left(\omega_s L - \frac{\omega_s C_0 R_1^2}{1+\left(\omega_s C_0 R_1\right)^2}\right) \tag{2}$$

At the moment, the equivalent circuit of transducer can be seen from Fig.1 (b). The series-matching inductor can offset the capacitance impedance of the equivalent circuit of the transducer. The matching inductor can be calculated by Eq. (3):

$$L = \frac{C_0 R_1^2}{1+\left(\omega_s C_0 R_1\right)^2} \tag{3}$$

In case of the resonance in series of branches, the technology of PLL in tracking frequency is used to adjust the value of the matching inductor, as shown in Fig.1. The matching inductor L and the transducer can be considered as a whole system because the parameter $i_1(t)$ cannot be measured independently [9]. The whole system of matching inductor and transducer present pure resistant by sampling the voltage $u_0(t)$ and the current i(t) and adjusting the phase difference between them.

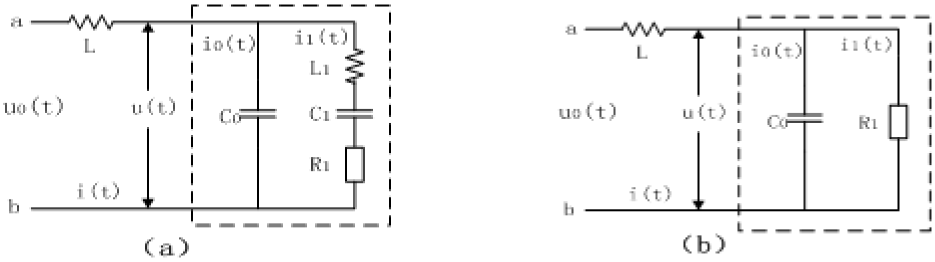

Fig.1. Equivalent circuit diagram of series matching

The scheme design of the combined adjustment of frequency and inductance

Fig.2 is the scheme design of the combined adjustment of frequency and inductance. Two line single square wave signals produced by ultrasonic power signal generator which the frequency are both 69.9 kHz and opposite in phase, then they were zoomed and shaped into one bipolar square wave signal of which the peak value is 12 v. Through the isolation transformer, the signal is divided into two signals that are same in frequency and opposite in phase. Finally，The two line signals drive power amplification circuit which are connected to the matching network. Current sampler executes current sampling, then MCU invokes the subroutine of A/D conversion and compares the working current whether exceeds the threshold of $0.9I_{max}$. If the requirement is realized, MCU maintains frequency stabilization of PWM drive pulse. Otherwise, MCU adjusts the frequency of PWM wave by step size Δf and exams the changes of feedback current. If sampling current is enlargement after frequency adjustment, the frequency of PWM wave continues to adjust in this direction. Otherwise, MCU adjusts the frequency of PWM wave in the opposite direction until the feedback current is in the normal threshold.

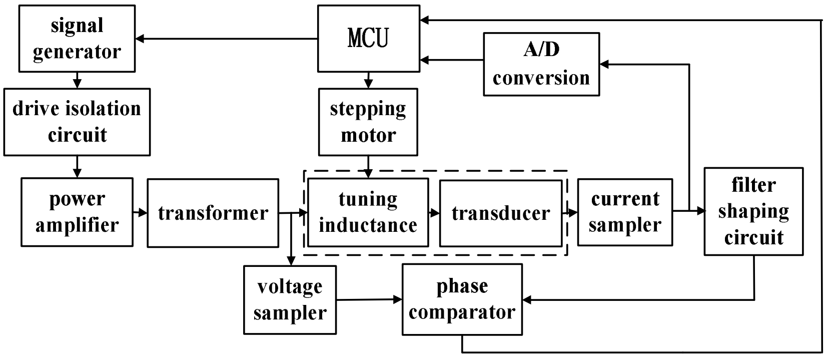
signal generator
MCU
A/D conversion
drive isolation circuit
stepping motor
power amplifier
transformer
tuning inductance
transducer
current sampler
filter shaping circuit
voltage sampler
phase comparator

Fig.2. Structure diagram of ultrasonic power amplifier combined adjustment

Then MCU control voltage and current sampler sampling to voltage and current at the same time by interrupted command. If the phase of voltage is in advance of the phase of current, the inductance magnet core will move up by the control of MCU, in order to reduce the matching inductance value. Otherwise, the inductance magnet core goes down by the control of MCU, in order to enlarge the matching inductance value. When the phase difference of voltage and current is zero, resonance matching was completed. Repeat the above matching steps and ensure the ultrasonic transducer always work in resonance condition. The working process is shown in Fig.3.

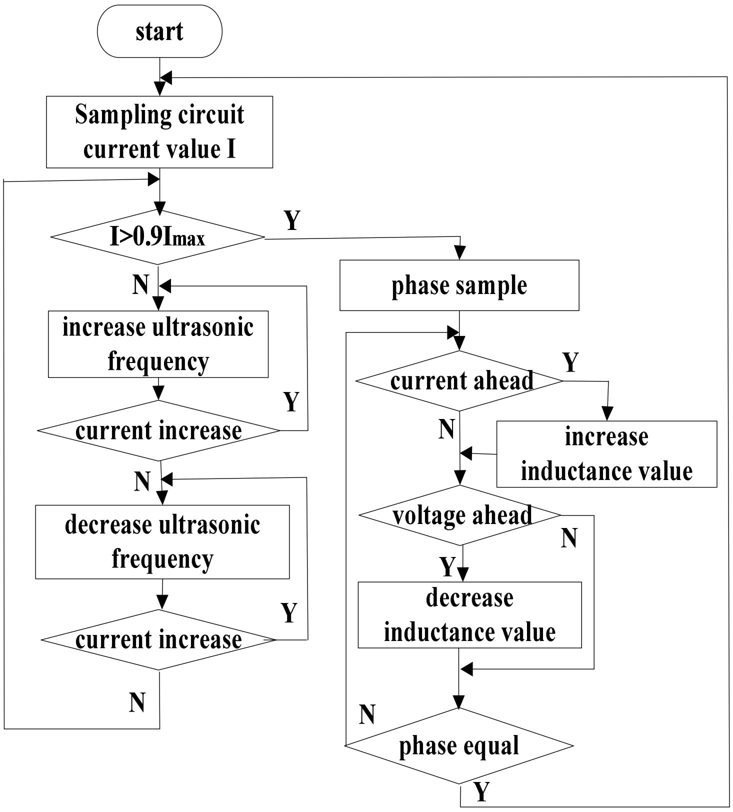
start
Sampling circuit current value I
I>0.9Imax
Y
N
increase ultrasonic frequency
current increase
Y
N
decrease ultrasonic frequency
current increase
Y
N
phase sample
current ahead
Y
N
increase inductance value
voltage ahead
N
Y
decrease inductance value
N
phase equal
Y

Fig.3. Flow diagram of ultrasonic power amplifier combined adjustment

The simulation and experiment

Firstly, we simulated the dynamic matching circuit of the combined adjustment of frequency and inductance by the Multisim software. Power source voltage used the DC voltage which value was 12v and oscilloscope waveform stable quick in the process of simulation, as shown in Fig.4 . Based on the simulation verification, we have carried on the exploration of the actual matching debug method. In order to prevent the transducer damaging in the condition of capacitive in practical application. By setting the procedure of MCU, we make the inductance magnet core decline one step distance once more in the case of tuning matching is completed, and ensure that the overall circuit is slight inductive. Specific experimental steps:

(1) Use the network analyzers (E5100) to test the parameters of transducer arrays, the actual parameters of transducer are as followings: fs=69.92kHz, R=34.2Ω, C_0=10.37nF.

(2) Use the probe of oscilloscope to sample the voltage of transducer, tandem the sampling resistor which value is 1Ω on the negative point of transducer, use the other probe to sample the signal of current.

(3) After 10min, the current waveform of oscilloscope is recorded shown in Fig.5, which the square wave is the signal of voltage and the sine wave is the signal of current. It can be seen that the results of the simulation are the same as the experimental results. What's more, the phase of voltage is prior to the phase of current, which means the circuit realizes the requirement that the transducer should work in the condition of slight inductive.

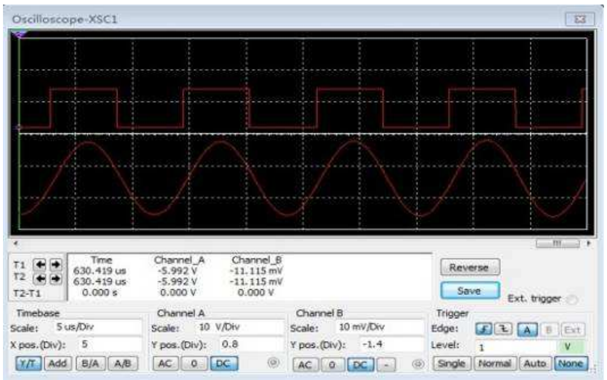

	Time	Channel_A	Channel_B
T1	630.419 us	-5.992 V	-11.115 mV
T2	630.419 us	-5.992 V	-11.115 mV
T2-T1	0.000 s	0.000 V	0.000 V

Timebase
Scale: 5 us/Div
X pos.(Div): 5

Channel A
Scale: 10 V/Div
Y pos.(Div): 0.8

Channel B
Scale: 10 mV/Div
Y pos.(Div): -1.4

Trigger
Edge: A
Level: 1 V

Fig.4. Simulation waveform

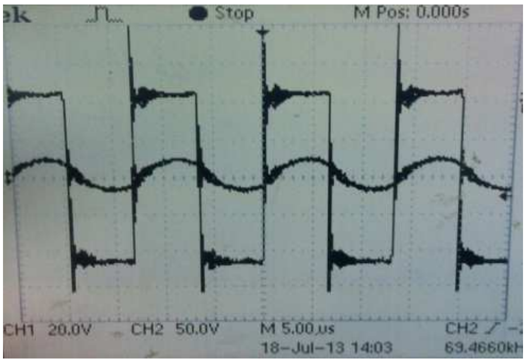

Fig.5. Oscilloscope waveform

Conclusion

In order to improve the efficiency of ultrasonic cleaning for submerged structure, we proposed a transducer matching method with signal frequency and inductor adjustment combined. The technique of identifying true max current value and Phase-Locked Loop frequency tracking was used. Through software simulation and experimental validation, the device can realize the matching of power amplifier output impedance and load impedance and make the transducer to gain a larger power from the ultrasonic power amplifier. Furthermore， the device solve the problems that traditional matching method cannot adapt the serial resonance frequency of capacitance branch and that dynamic tuning is inefficient and have important significance for improving ultrasonic cleaning efficiency.

Acknowledgements

We are grateful for the financial support by National Natural Science Foundation of China(Grant NO.11274092,11304026and NO.11274091)and Natural Science Foundation of Jiangsu Province (Grant NO.BK20130238),This work also is supported by the Changzhou Science and Technology Support Projects, Changzhou, China(Grant NO.CJ20130008,CE20120080)and the Open Project of Changzhou Key Laboratory of Sensor Networks and Environmental Sensing, Changzhou, China (Grant No. CZSN201207).

References

[1] M. Garcia-Rodriguez, J. Garcia-Alvarez, Y. Yanez, M.J. Garcia-Hernandez and J. Salazar. Physics Procedia 3(2010) 1025-1031.

[2] Huijuan Dong. Journal of Harbin Institute of Technology 32(2000) 115-122.

[3] Baida Qu, Zhenglong Ni. Advanced Materials Research 760-762(2013) 1053-1057.

[4] B. Mortimer，T. du Bruyn，J.Davies and J.Tapson.. Ultrasonics 39(2001) 257-261.

[5] Luying Qiang, Jilin Liu and Xin Fu.The Tenth International Conference on Electronic Measurement & Instruments (2011) 206-210.

[6] Runhua Liu, Bingyi Wang. Petrochemical Electrical 32(2013) 82-85.

[7] Y. Qian, N.R. Harris. ultrasonics 54(2014) 586-591.

[8] Bingyi Li, Zhe Ding. Proceeding of the IEEE International Conference on Automation and Logistics Zhengzhou, China, August (2012) 448-451.

[9] Jian Wu , Huijuan Dong. Journal of DaLian Maritime University 35(2009) 57-61.

Applied Mechanics and Materials Vol. 596 (2014) pp 709-712
© (2014) Trans Tech Publications, Switzerland
doi:10.4028/www.scientific.net/AMM.596.709

Design of Active Filter based on the active power balance

Ling Ji

College of media, Linyi University, Linyi ,China

jnjllhy@163.com

Keywords: Active filters The active power balance Saber

Abstract: In order to eliminate harmonics generated by the power electronic devices, from a functional point of view the amount of the balance, the use of filters to supply current and DC voltage is sampled in a controlled manner to achieve harmonic compensation, the establishment of a single-phase active power filter the control system of the model and the theoretical analysis of the program by Saber simulation software has been validated in simulation, based on a prototype developed, according to the single-phase shunt active filter to achieve our scheme can effectively harmonic compensation for pollution caused by the rectifier with inductive load, simulation and experimental results show that this method can be controlled harmonic distortion at 5.8%.

Introduction

With the widespread use of power electronic devices, the pollution are becoming increasingly serious, because the harmonic generated by these devices and reactive current to the power systems. How to eliminate the harmonic and reactive power generated by the electronic device, it is an important issue. Using active filter to eliminate harmonics and reactive current, because only compensate load harmonic and reactive components, capacity of active filter requires smaller , can focus on high harmonics and no power,which are caused by a number of non-linear loads. It can also solve the problem of harmonic pollution[1].

This paper analyzes the main active filter circuit model for single-phase systems, corrected analysis is done to appropriate control methods. The simulation and experimental results show that the experimental system by this strategy can compensate rectifier with inductive load generated harmonics, eliminate harmonic pollution on the grid.

the power inverter mathematical model

Select power inverter circuit, the voltage source inverter (VSI) is active filter, which in parallel with the harmonic source connected to the grid, as is shown in Figure 1. Its advantages are simple structure, small size, high efficiency [2]. If i_c * is the command current of high harmonics and reactive current, by controlling the opening of two switches and off, it can force tracking compensating current ic following i_c *, non-linear loads can only sinusoidal active current, which is drawn from grid. That is:

$$i_s = i_c + i_L \tag{1}$$

In equation(1), is for the grid current, ic for the compensation current, i_L is the load current. And can be obtained from Fig.1:

$$V_s = L\frac{di_c}{dt} + V_{con} \tag{2}$$

$$V_{con} = \frac{1}{2}SV_{dc} \quad \begin{cases} S = 1 \\ S = -1 \end{cases} \tag{3}$$

$$i_C = S \times i_c \tag{4}$$

$$i_C = C\frac{d\frac{1}{2}V_{dc}}{dt} = \frac{C}{2}\frac{dV_{dc}}{dt} \tag{5}$$

$$\therefore \begin{cases} \frac{di_c}{dt} = \frac{1}{L}(V_s - \frac{1}{2}SV_{dc}) \\ \frac{V_{dc}}{dt} = 2\times\frac{1}{C}i_c = \frac{2}{C}Si_c \end{cases} \qquad (6)$$

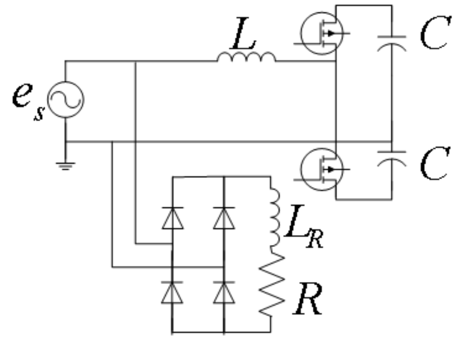

Fig.1 Main circuit schematics

From the formula (6) can be seen, the inductance is small, the current follow capability is high, but the ripple current amplitude of the high-frequency switching is large, which superimposed on ic . it will increase the load on the high-frequency filter circuit, and the harmonic content of the active filter self-generated increases. And because there is a pulsating input current, in order to obtain a high power factor, usually require a current ripple factor δ is less than the maximum allowed δ_{max}. From the above analysis, the inductance L should be met:

$$L > \frac{V_{smax}}{\delta_{max} I_{smax}} T_s D \qquad (7)$$

In equation(7),Ts=1/fs， $D = \frac{\frac{1}{2}V_{dc} - V_{smax}}{\frac{1}{2}V_{dc}} = \frac{V_{dc} - 2V_{smax}}{V_{dc}}$, Ismax is the input peak current..

On the DC side capacitor selection, considering the response rate to the system and its impact on the DC side voltage stability [3]. Capacitance increases, smooth DC side voltage, but the response speed of the system slow; Conversely, the response speed of the system's fast and DC side voltage ripple increases. In this article, the two capacitors DC side chosen 2200μ, simulation and experimental results show that this choice can meet the requirements.

After calculation selected, the parameter of the main circuit is as follows: Vs=310V，LR=7mH，R=50Ω， C=2200μF，L=6mH。

The system control method for correction

In the three-phase system , the most common type of shunt active filter is based on harmonic detection , produce compensation currents, compared with the harmonic currents are equal in magnitude and opposite in direction, the currents inject into the grid to achieve harmonic compensation purposes[4]. Among them, the harmonic detection are generally based on instantaneous reactive power theory. For a single phase system , this detection method is difficult to use . In 1996, based on instantaneous reactive power theory of single-phase circuit harmonics and reactive current detection have been proposed, but this method requires a single phase to three-phase structure to be detected , the structure is complicated, and has poor portability on different systems.

The proposed scheme shown in Fig. 2 .This structure eliminates the harmonic detection, uses the active power balance principle, direct access to the active component of the entire system needed . The system uses a double-loop control strategy , The inner loop is current loop, detected the errors between the actual input current i_s and the input current i_{ref}, after PI regulate, compared with the triangular wave , it generates the driving signals to drive power switch ; outer voltage is Voltage loop, on the On the one hand controlling the output voltage of the DC side to tracking voltage setpoint, on the other hand using the power balance to obtain the amplitude of the reference input current i_{ref} , multiplying the voltage synchronous signal as an input current loop . Prerequisite for the smooth functioning of the voltage loop is the actual current loop input current is able to quickly track the reference current i_{ref}.

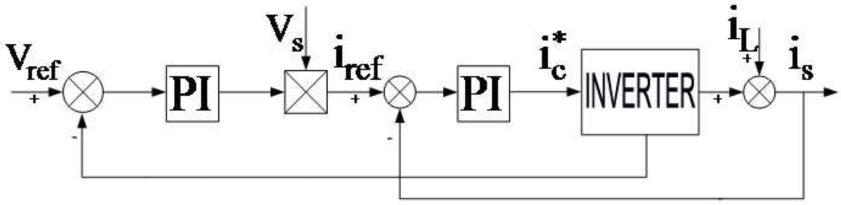

Fig.2 System Control Structure

Experiments

In this paper, Saber is used to simulate the entire control system, simulation waveforms obtained as shown in Fig.3.

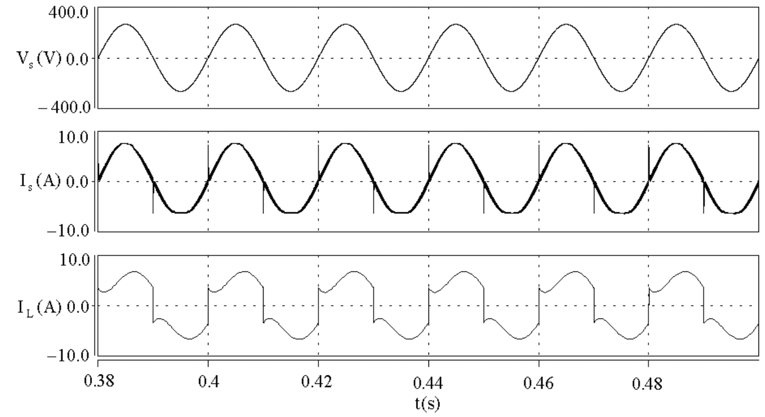

Fig.3 The simulation waveform

In Fig.3, from top to bottom is power supply voltage waveform, the current waveform after compensation and current waveform without compensation. By Fourier analysis in Saber, while no filters, harmonic distortion currents up to 27.88%; add active filter, the harmonic distortion rate dropped to 9.8%. The article also verified by simulation boost inductor L impact of harmonic distortion. Table1 lists the influence of L for the value of the total harmonic distortion.

Table 1 The influence of L for the value of the total harmonic distortion

L（mH）	2	4	6	8	10
Harmonic distortion（%）	12.67	9.89	6.53	7.15	9.08

Compare the above values seen in the system without changing other parameters, reduce the value of L, can reduce the network side input current total harmonic distortion; But L value is too small, it increases the distortion. This was in line with the previous analysis, it should be reasonable to select the L value. In the simulation waveform above, discovered that current glitch can not be compensated over zero, seriously affecting the harmonic compensation, which is dominated by the response band limit determined by the active filter. Adding a high-frequency filter circuit can effectively solve this phenomenon and further reduce harmonic distortion and L values. To verify this, on the basis of the original simulation model, the main circuit power plus 1mH inductor, simulation shows that the harmonic distortion rate is 5.58%, the current waveform is shown in Fig.4.

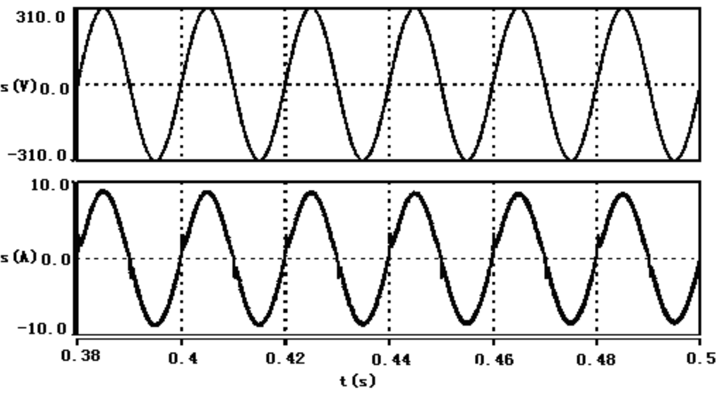

Fig.4 The current simulation waveform with the high frequency has been filtered

On the basis of simulation produced a prototype. The control circuit uses to TI's DSP chip TMS320LF2407 as the core, PWM of DSP generates unit achieved. Fig.5 shows the measured waveform in the experiment, in which, a - -input voltage ordinate 50V / cell; b - -input current, 10A / grid; abscissa is time t, 10ms / grid. Fig.6 is a spectral analysis of the input current, harmonic distortion rate is 5.8%.

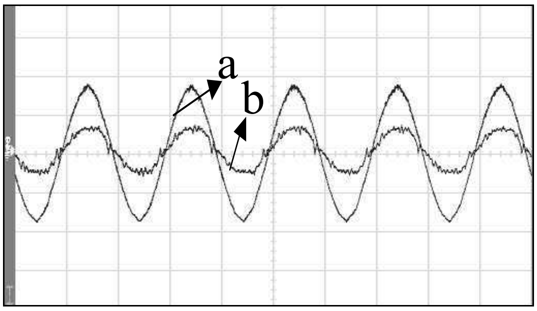

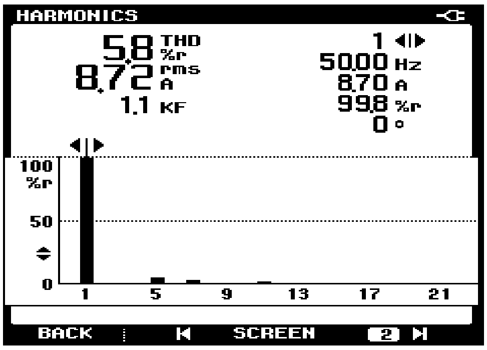

Fig.5 The actually detected waveform Fig.6 The spectrum analysis of the input current

Conclusions

From a functional point of the active power balance, the control system established model of single-phase active filter and theoretical analysis, is based on the simulation, a prototype developed. The simulation and experimental results show that, according to the single-phase shunt active filter to achieve our scheme can effectively compensated the harmonic pollution by the rectifier with inductive load caused .

Acknowledgements

This work was performed as a part of National Natural Science Foundation of China ‘‘Aviation magnesium alloy FSJ connection integrity and milling deformation mechanism and prediction”(Foundation No. 51175255). The authors wish to thank Dunwen Zuo , Precision and Micro Manufacturing Technology Laboratory and Nanjing University of Aeronautics and Astronautics.

References

[1] Zhao Liangbing, Ma Weixin, ChenJianye. Power System Technology, 1995,19 (3): 64 ~ 67.In China.

[2] Wang Zhaoan, Yang Jun, Liu Jinjun harmonic suppression and reactive power compensation [M] Beijing: Mechanical Industry Press, 1998 (9) .231 ~ 232. In China.

[3] Wu JC, H L-Jou Simplified Control Method for the Single-phase Active Power Filter [J] IEE Proc-Electr.Power Appl 1996,143 (3):.. 219 ~ 224.

[4] Chu Q X, Wang H. Microwave Theory and Techniques, IEEE Transactions on, 2008, 56(2): 431-439.

Applied Mechanics and Materials Vol. 596 (2014) pp 713-718
© (2014) Trans Tech Publications, Switzerland
doi:10.4028/www.scientific.net/AMM.596.713

Identification of Lightning Strike and Short-circuit Fault based on Wavelet Energy Spectrum and Transient Waveform Characteristics

Yanfeng Gao[1,2,a], Yongli Zhu[1,b], Hongyan Yan[2,c]and Hongwei Yan[1,d]

[1] State Key Laboratory of Alternate Electrical Power System With Renewable Energy Sources
(North China Electric Power University),Baoding 071003 ,Hebei,China.
[2] Hebei University of Engineering, Handan 056038,Hebei,China
[a]gaoyanfeng01@126.com, [b]yonglipw@163.com, [c]yhyan118@126.com, [d]yanhongwei51@163.com

Key words: transmission line, lightning location, wavelet energy spectrum, transient waveform characteristics, fault identification

Abstract. The transient traveling waves generated by linghting can be used to linghting location, in order to improve fault identifiaction ability of current traveling wave location device, an identification method of lightning strike and short circuit fault based wavelet energy spctrum and transient waveform characteristics was presented in this paper. Through researched the current signals generated by non-fault lightning strike, fault lightning strike and short-circuit fault on 220kV transmission line, compared of the energy distribution of different transient signals in each prequence band, realized the identification of lightning strike and short-circuit fault; for lightning identification, by waveform characteristics calculated obtaining eigenvalue to identify the non-fault and fault linghtning. PSCAD/EMTDC simulation results identicate that the proposed method is correct and effective.

Introduction

Lightning strike is one of the main causes for transmission line accident, data shows that 40% to 70% of the total number of failures was caused by directly or indirectly lightning [1-4]. The transient traveling wave generated by lightning similar to the transient waveform generated by short circuit fault can be used to locate the point of lightning on traveling wave device [5,6]. In practical application, it needs to quickly detect faults and determine the fault point when lightning caused transmission line short circuit, then timely repair and maintenance the line. Device should not action if lightning not caused the line fault, it should regard as interference. Therefore, identification non-fault lightning, fault lightning and short circuit fault has practical significance.

There are some useful results on study identification of lightning and short circuit fault in recent years [7-11]. Most papers take the differences of transient traveling signals energy distribution in each prequence band as criterion when non-fault lightning or fault, sometimes there will be some problems that the identification criterion difficult to determine, because the impact of lightning current waveform, amplitude, lightning type and other factors. An integral criterion about non fault lightning and fault was proposed in paper [7] by analyzing the characteristics of the transient waveform lightning and short circuit fault, but it difficult to identify fault lightning and short circuit fault. Aiming at improving the deficiences of existing method, an identification method of lightning strike and short circuit fault based on wavelet energy spctrum and transient waveform feature was presented in this paper.Through researched the current signals generated by lightning strike without causing fault, lightning strike causing fault and short-circuit fault on 220kV transmission line,comparing of the energy distribution of different transient signals in each prequence band,realizing the identification of lightning and short-circuit fault; For lightning identification, according to the symmetry of non fault lightning waveform and the monotonicity of fault lightning waveform to calculate, obtaining eigenvalue to identify the non-fault and fault linghtning. Simulation results identicate that the proposed method is correct and effective.

Wavelet energy spectrum analysis

Wavelet decomposition can efficiently extract the transient characteristics of fault signals, its essence is using a pair of mirror filter to two band divide sampling signal $f(\mathrm{n})$, $f(\mathrm{n})$ is decomposed into high frequency detail components D_1 and low-frequency approximation component A_1, the A_1 can be further broken down, layer j is D_j and A_j, frequency range after signal decomposition and reconstruction as follows [11,12]:

$$\begin{cases} D_j : \left[2^{-(j+1)}F_s, 2^{-j}F_s\right] \\ A_j : \left[0, 2^{-(j+1)}F_s\right] \end{cases} (j = 1, 2, \cdots, J) \tag{1}$$

Where: F_s is the sampling frequency; J is the maximum decomposition scale.

$f(\mathrm{n})$ can be expressed as the sum of the components, namely:

$$f(\mathrm{n}) = D_1 + A_1 = D_1 + D_2 + A_2 = \sum_{j=1}^{J} D_j + A_J \tag{2}$$

According to the framework of the wavelet transform theory, the energy is conservation [13]. $d_j(\mathrm{k})$ is wavelet coefficients of scale j; N is the length of the wavelet coefficients. The wavelet energy of scale j coefficients is defined as

$$E_{Dj} = \sum_{k=1}^{N} \left| d_j(k) \right|^2 \tag{3}$$

There are J+1 reconstructed signals when signal is decomposed J scale, its energy distribution can be represented by vector E

$$E = [E_{D1},\ E_{D2},\ E_{D3}, \cdots,\ E_{DJ},\ E_{AJ}] \tag{4}$$

Total energy is:

$$E = \sum_{j=1}^{J} E_{Dj} + E_{AJ} \tag{5}$$

The probability of energy on each frequency band can be expressed as follows:

$$P_j = E_j / E \quad (j=1,\ 2,\ \ldots,\ J,\ J+1) \tag{6}$$

Eigenvalues of signal can be extracted by wavelet energy spectrum analysis, which can be used to realize the different transient signals identification.

Traveling wave characteristics analysis of lightning strike and fault

From high voltage technology we know, lightning impulse on the line has two main forms: induction lightning and direct lightning. Induction thunder over-voltage generally not more than 500kV, it is not considered for not cause short circuit. Direct lightning divided into back strike and around strike depend on the positions of lightning, they may cause insulator flashover or short-circuit. Test shows that, lightning wavefront time within 1 ~ 5us, lightning current half peak usually within 20 ~ 100us, only 18% to 30% greater than 50us. Lightning protection design commonly take 2.6/50us. Lightning current waveform show as Figure 1, its expression is:

$$i = I_0\left(e^{-\alpha t} - e^{-\beta t}\right) \tag{7}$$

Where: I_0 is the amplitude of lightning current; α and β respectively attenuation coefficient of wavefront and wavetail.

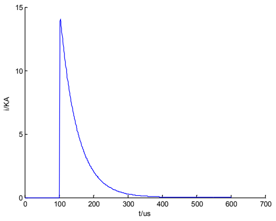

Fig.1 Lighting current waveform

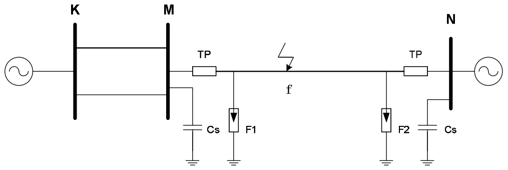

Fig.2 220kV transmission systems model

Figure 2 is a 220kV transmission system simulation model, the transmission line take frequency dependent model, its length is 100km, three-phase line transposed evenly and two shielding wire on the top; arrester F1, F2 take IEEE recommended nonlinear model; insulators using pressure control switch model; bus to ground capacitance Cs = 0.01uF; TP is transient protection.

Suppose non-fault lightning, fault lightning and short-circuit occurred on A phase of f point,f is 40 km from M, lightning current takes 2.6/50μs and the impedance of lightning channel is 300 Ω, Sampling frequency is 1MHz, take the data after fault 2ms to analyze. Due to the electromagnetic coupling between respective phases, Clarke transformation is used for decoupling the current signal,α-mode current waveform of different transient cousres show in Figure 3.

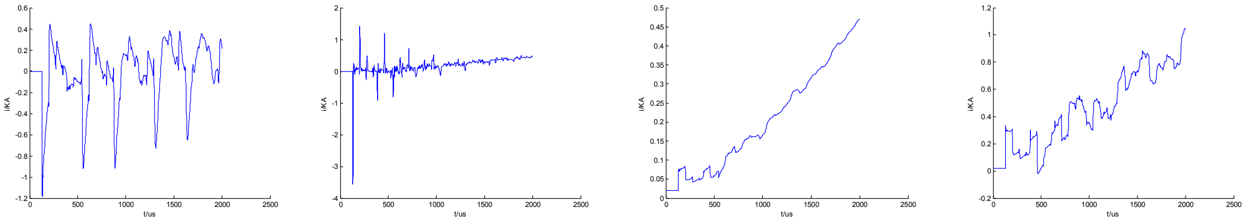

(a) Non-fault lightning strike (b) Fault lightning strike (c) A phase short-circuit (d) A-B phase short-circuit

Fig.3 mode Current waveform of different transient courses

Figure 3 shows that : (1) Non-fault lightning stike, α-mode current peak alternating up and down the timeline, wave bead amplitude gradually decrease with wave propagation; (2) Short-circuit fault, α-mode current waveform biased in favor of one side of timeline in shorttime, there will be zero crossing sometimes, but its amplitude is small. (3) Fault lightning strike, α-mode current waveform along with the characteristics of non-fault lightning and short-circuit fault: beginning, lightning current play a major role, when the amplitude exceeds the critical flashover voltage, insulation breakdown occurs, indicating a short circuit fault characteristics.

Identification of lightning and short circuit faults

Lightning current spectral energy focused on the high-frequency band, short circuit fault signal energy concentrated in the low frequency component. According to energy distribution of signal in different frequency bands can effectively identify lightning and short circuit fault. In this paper, energy distribution characteristics on different frequency band about three transient current signals were extract by wavelet transform. Wavelet db4 wqas selected to decomposite signal 8 layer, 1MHz can be divided into nine bands: 500K-250K, 250K-125K, 125K-62K, 62K-31K，31K-15K, 15K-7K, 7K-3K, 3K-0K. A series of histograms were made by the ratio of different frequency energy, Figure 4 shows energy distribution of different transient signals in different frequency.

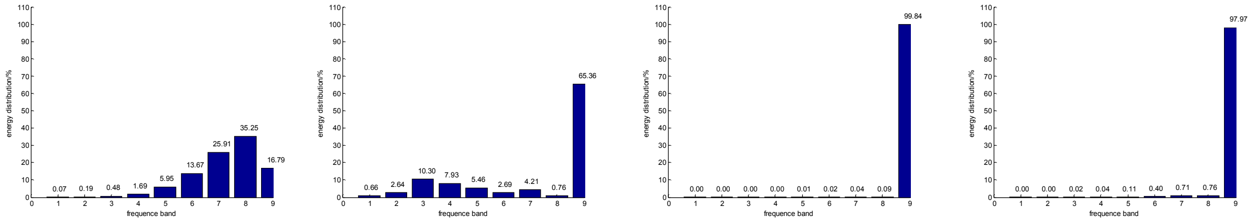

(a) Non-fault lightning strike (b) Fault lightning strike (c) A phase short-circuit (d) A-B phase short-circuit

Fig.4 Wavelet energy spectrum of different transient current signals

Figure 4 shows that, the energy distribution of transient current signals on different frequency bands is quite different: Non-fault lightning signal energy is concentrated in the intermediate frequency, the low-frequency energy P <20%; Fault lightning signal energy is concentrated in the high-frequency and low-frequency, the low frequency energy P <70%; Short-circuit fault, signal energy is concentrate in low-frequency, P> 95%. Lightning signal energy distribution change largely, but short-circuit fault low frequency energy is relatively stable, taking the ratio of low frequency energy as criterion, set the threshold value P0 = 90%, if signal low frequency energy P <P0, it was determined lightning; contrary, it is judged as short-circuit fault.

According to the transient waveform characteristics of fault lightning and non-fault lightning to identy non-fault or fault lightning, make an integral calculus for the transient waveform on the timeline or below respectively, there

$$I_+ = \int_{t_0}^{t_0+\tau} I_+(t)dt \tag{8}$$

$$I_- = \int_{t_0}^{t_0+\tau} |I_-(t)|dt \tag{9}$$

Where:t_0 is the voltage mutation moment; τ is the integration time, selected 2ms.

Defined recognition criterion as:

$$\omega = \frac{|I_+ - I_-|}{\min(I_+, I_-)} \tag{10}$$

Transient waveform signals at different disturbance were simulated on 40km distance measuring points, the eigenvalues shown in Table 1.

Tab.1 Lightning characteristic criterion

Fault type	I_+	I_-	ω
Non-fault lightning	193.6650	210.8423	0.0887
Fault lightning	394.9371	33.9417	10.6357

Table 1 shows: I_+ and I_- is very close under non-fault lightning, ω much less than 1; there is a big difference between I_+ and I_- under fault lightning, ω is greater than 1. if ω<1,it is determined non-fault lightning; If ω>1,it is determined fault lightning.

Identification process of lightning and fault

In summary, the energy of different frequency bands have a large differences when occusing non-fault lightning, fault lightning and short-circuit fault, and waveforms show significantly different characteristics, so identification process can be divided into two steps. Identification process shown in Figure 5.

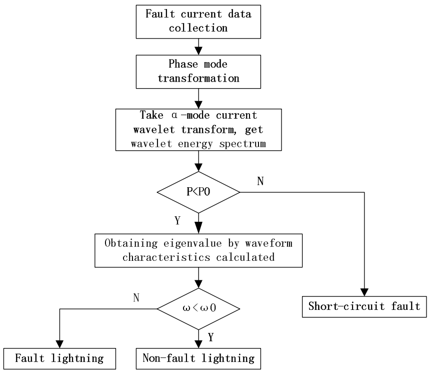
Fault current data collection
Phase mode transformation
Take α-mode current wavelet transform, get wavelet energy spectrum
P<P0
N
Y
Obtaining eigenvalue by waveform characteristics calculated
Short-circuit fault
N
ω<ω0
Y
Fault lightning
Non-fault lightning

Fig.5 Identification flow chart of lightning and short-circuit fault

Simulation and verification

In order to verify the proposed method is correctness and validity, set all kinds of disturbance on 220KV simulation system, shown as figure 2. The simulation results are shown in Table 2.

Tab.2 Identification results of lightning strike and short-circuit fault

Fault type	Fault conditions		P /(%)	ω	Judgment results
Non fault lightning	2.6/50us	I_r=8kA	18.37	0.1009	Non fault lightning
		I_f=10kA	0.02	0.0071	Non fault lightning
	0.25/100us	I_r=3kA	37.37	0.2808	Non fault lightning
		I_f=5kA	0.02	0.0142	Non fault lightning
Fault lightning	2.6/50us	I_r=20kA	51.46	7.3553	Fault lightning
		I_f=150kA	69.09	14.5756	Fault lightning
	0.25/100us	I_r=15kA	61.03	9.1258	Fault lightning
		I_f=150kA	56.91	11.4312	Fault lightning
Short circuit fault	Ag, R=10Ω, θ=0°		99.84	-	Short circuit fault
	AB, R=10Ω, θ=45°		96.87	-	Short circuit fault
	ABg, R=100Ω, θ=90°		97.23	-	Short circuit fault
	ABCg, R=300Ω, θ=0°		99.76	-	Short circuit fault

Table 2 Data shows that: (1) With the lightning current amplitude increases, the low frequency energy will increase, compared with short-circuit low-frequence energy the difference is larger, the effect is obvious selected low-frequency energy as eigenvalues to identify lightning and short-circuit fault, the threshold value is appropriate; (2) short-circuit fault type, transition resistance, initial failure angle less affected energy distribution of the high and low frequencies; (3) the eigenvaluesextracted by calculates transient waveform of non-fault lightning and fault lightning is obviously, it can be achieved effectively identify non-fault and fault lightning .

Conclusions

(1) Traveling wave device can be effectively achieved lightning location, if it can identify the non-fault lightning, fault lightning and short-circuit faults, it will improve the level of lightning protection and system running.

(2) There are obvious characteristics on wavelet energy spectrum, taking the low-frequence energy as criterion can easily identify lightning and short circuit fault, about the lightning identification, we can use the transient waveform characteristics of non-fault lightning and fault lightning to calculate and to realize non-fault lightning and fault lightning identification.

(3) Simulation results show that the proposed method can effectively identify non fault lightning, fault lightning and short circuit fault, and not impacted by lightning waveforms, amplitude and line structures and other factors.

Acknowledgements

This paper was supported by “the Fundamental Research Funds for the Central Universities” (2014xs74)

References

[1] Zhen Mei, Shuiming Chen, Qinwei Gu, et al. Statistic of lightning accidents during 1998~2004 in China. High Voltage Engineering. Vol.33 (2007), p.173-176.

[2] Xingli Dong, Yaozhong Ge, Xinzhou Dong. Effect of lighting on protection based on traveling waves. Proceedings of the CSEE,Vol.22 (2002), p.74-78.

[3] Hui Yi, Jiangliu Cui. The present state and lighting protection of transmission line in china. High Voltage Engineering, Vol.27(2001), p.44-50.

[4] Jiahong Chen, Qin Zhang, Wanxing Feng, et al. Lightning location system and lightning detection network of China power grid. High Voltage Engineering, Vol.34 (2008), p.425-431.

[5] Hao Wu, Xianyong Xiao. Lighting strike location of transmission line based on wavelet transform and traveling wave theory. High Voltage Engineering, Vol. 33 (2007), p.86-90.

[6] Dipankar C, Kis hore N K, Avinash K S, et al. A wavelet multiresolution based analysis for location of the point of strike of a lightning over voltage on a transmission line. IEEE Trans on Power Delivery, Vol.19 (2004), p.1727-1733.

[7] Jiandong Duan, Baohui Zhang, Zhiguo Hao, et al. Identification of lighting strike and fault in the EHV transmission line transient-based protection. Automation of Electric Power Systems, Vol. 28(2004), p. 30-35.

[8] Guibin Zou, Houlei Gao, Feng Zhu, et al. Integral identification method of lighting stroke and fault for transmission line.Power System Protection and Control, Vol.40(2012), p.43-48.

[9] Gang Wang, Haifeng Li, Jiancang Zhao, et al. Identification of transients on transmission lines caused by direct lightning strike based on multiresolution signal decomposition. Proceedings of the CSEE, Vol.24 (2004), p.139-144.

[10] Hao Wu, Xianyong Xiao, Wujun Deng. Identification of lighting strike and fault in the traveling wave location of transmission line. High Voltage Engineering, Vol.33 (2007), p.63-67.

[11] Hao Wu, Xianyong Xiao, Ruijiao Shen. Lightning strike and fault identification by the wavelet energy spectrum and neural network method. High Voltage Engineering, Vol. 33 (2007), p.64-68.

[12] Zhengyou He, Xiaoqin Chen. A study of electric power system transient signals identification method based on multi-scales energy statistic and wavelet energy entropy. Proceedings of the CSEE, Vol.26 (2006),p.33-38.

[13] Songlin Xu, Shaoxian Huang. Fault diagnosis of commutation failures in the HVDC system based on the wavelet energy spectrum and grey comprehensive relationship degree. Power System Protection and Control, Vol.40 (2012), p.85-89.

Applied Mechanics and Materials Vol. 596 (2014) pp 719-722
© (2014) Trans Tech Publications, Switzerland
doi:10.4028/www.scientific.net/AMM.596.719

APPLICATION RESEARCH ON THE INTELLECTUAL INSPECTION SYSTEM OF TRANSMISSION LINE BASED ON THE "MOBILE INFORMATION PLATFORM"

YANG Zhen-wei [1,a], YI Wei[2,b], And JIN Yu[3,b]

[1]STATE GRID JIUJIANG ELECTRIC POWER COMPANY,Jiujiang,China

[2] STATE GRID HUANGGANG ELECTRIC POWER SUPPLY COMPANY,

Huanggang,China

[3] STATE GRID JIUJIANG ELECTRIC POWER COMPANY,Jiujiang,China

[a]sun270636982@163.com, [b]yzw@126.com, [c]yzq@163.com

Keywords: Geographic Information System, Global Positioning System, intellectual inspection system of transmission line, Mobile information platform

Abstract. The power transmission line is one of the important parts of electrical power system, the management and in-spection of the transmission lines have been significant routine job ensuring the reliability of the transmission system. According to actual requirements and characteristics of Transmission line inspection, the intellectual inspection system of transmission line based on Mobile information platform was designed using Geographic Information System (GIS). This novel inspection system was composed of GIS,Global Positioning System(GPS), PDA and GPRS. The system changes the traditional inspection modes.Owing to the advantages of high reliability, practicability and scalability, the practical application of this intellectual inspection system shows that it completely meets the requirements for fast speed, high efficiency and real-time performance.

Introduction

Inspection management of transmission line is a basic work which effectively guaranteed the safety of transmission line and equipment. At present, there are mainly three inspection modes of transmission line in domestic power industry:one is manual patrol, manual recording mode, which defect is more human factors , workload, low efficiency, management inconvenience;the other is inspection system based on automatic identification technology,which deficiency is information carrier installed on the tower easily lost, installation complexity, high cost,less information recorded, and does not meet multi points and long distance inspection management requirements;the third is inspection system for GPS and instrument of line patrol or PDAand GPS,which is the biggest shortcoming to inspection data collected only at the end of the inspection and can not timely and accurately reflect the health of the line equipment, and can not supervise patrol inspection personnel place the case , it is difficult to meet the demand for safe operation of the line[1-4].

According to actual requirements and characteristics of Transmission line inspection, the intellectual inspection system of transmission line based on Mobile information platform was designed using Geographic Information System (GIS) by Jiujiang Power Supply Company. This novel inspection system was composed of GIS,Global Positioning System(GPS), PDA and GPRS.

System Features

The inspection system of transmission line provides a convenient and advanced scientific platform,which can improve the quality of equipment inspection,timely record and analysis equipment defects and problems, improve scientific operation and management level, achieve humane, information management and avoid inspection not in place, not in time and so on.

(1)Contact with the tower equipment without hardware , without installation auxiliary equipment on the tower;

(2)The system has high security and stability, can meet the wild working conditions;

(3) Interface is clear, simple, easy to master;

(4)Positioning is fast and accurate;

(5)Achieving transmission line inspection paperless and standardization of inspection results input;

(6) To timely reflect equipment inspection defect;

(7)A detailed and standardized raw data accumulation,as condition-based maintenance for transmission equipment a reliable basis;

(8)Collection,query,statistics of inspection data is more convenient and standardized;

(9) Effective supervise place conditions of patrol officers and minimize undetected and error detection.

System Structure

System Composition. The system includes the two subsystems"mobile inspection system" and "desktop inspection system",which Structure is shown in Figure 1.

Mobile inspection system runs on an integrated GPS and a PDA with wireless communication function,and achieve wireless communications and data transmission between the mobile terminal and the desktop via a wireless network.To collect inspection information on the spot by PDA,the information which records and queries device information of inspection point for an inspection personnel.PDA is mainly responsible for recording inspection information, guiding patrol routes, pointing tasks,checking the device status and so on.When inspection personnel download inspection tasks to the PDA from desktop inspection system, positioning devices via GPS in the inspection site, and obtaining device information and inspection content from the PDA.Input parameters and information after inspection according to the inspection task,while the PDA records the inspection time and inspection information.After the inspection, the data recorded in the PDA automatically transfer to desktop inspection system server through a wireless network.Server will generate inspection records and equipment defect datas according to inspection personnel’s data,effectively reduce costs while improving efficiency.

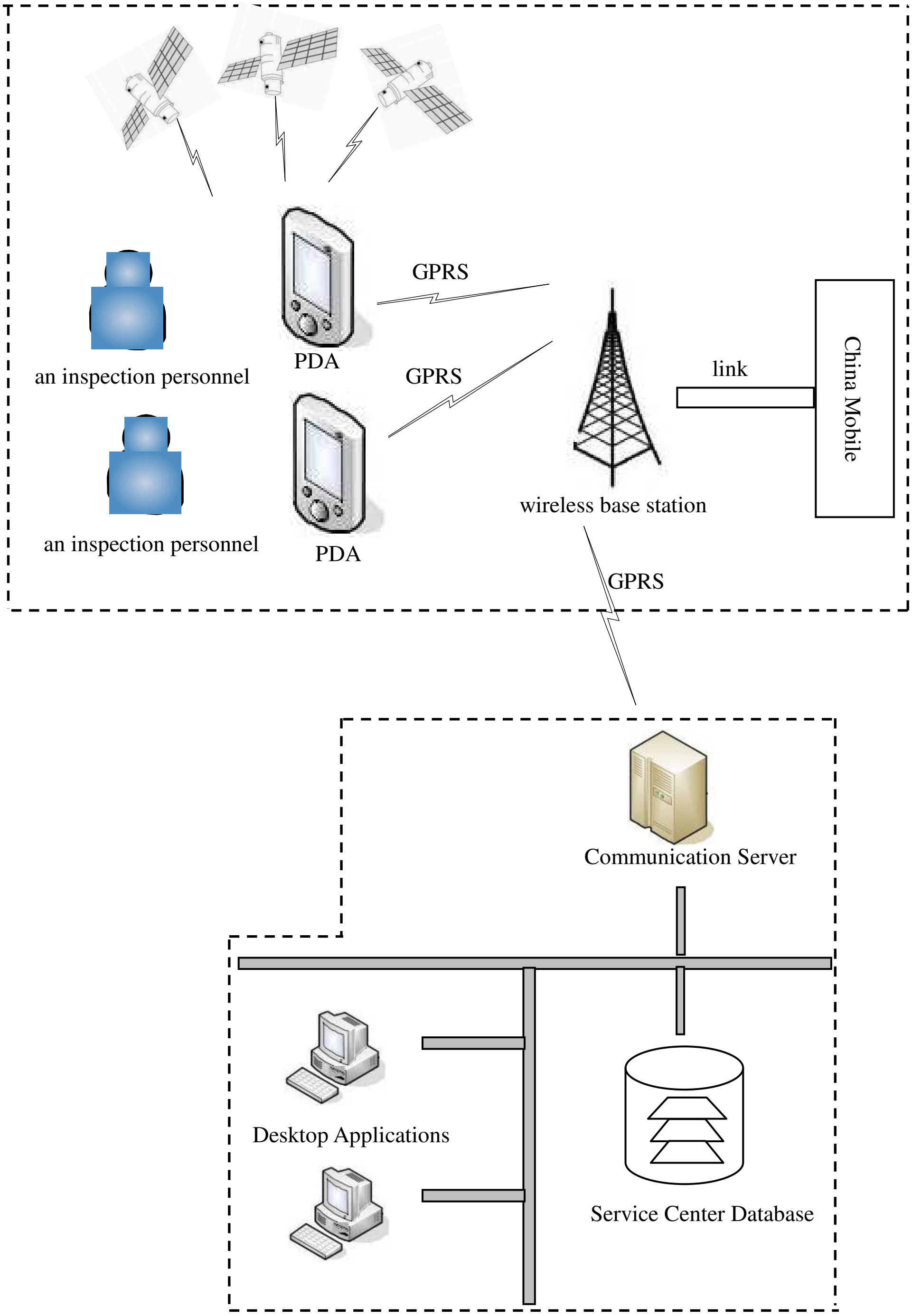
GPRS
GPRS
an inspection personnel
PDA
an inspection personnel
PDA
link
China Mobile
wireless base station
GPRS
Communication Server
Desktop Applications
Service Center Database

Fig.1. The structure of intellectual inspection system of transmission line

Desktop inspection system adopts a modular design approach, the system functions are designed to separate software modules,which is easy to upgrade system and expand function.combining staff permission management module, to improve the safety and practicality of the system.Desktop inspection system completed inspection data storage,inquiry,analysis, collection and report output by real-time accessing to inspection records in the PDA,which achieves the whole process efficient supervision from defects found to deal with.Desktop inspection system is a platform which administrators to manage inspection staff information, inspection information of transmission line,task list information,job map information, information of transmission line,inspection device information.and is a connection link inspection staff information, transmission line and task.

System Function. This system is applied in inspection work of transmission line ,which is mainly divided into two workflows, fiducial positioning and routine inspection. Mobile inspection system and desktop inspection system with each other to complete all work processes required.

Fiducial Positioning. Fiducial positioning samples location information and attribute information of all equipments of the new transmission line when is carry outing inspection line for the first time and inspection a new line. The former is used to create the inspection map guiding the future inspection work,the latter corresponds to the inspection equipment management of desktop inspection system.Only in collecting and improving these two pieces of information in order to carry out normal inspection work.

Routine inspection. Routine inspection is which the subscriber captures current information of location and time through GPS receiver of a PDA in the inspection process. Then compared with positioning information of the original inspection point, and line defects on the spot recorded in the PDA , in order to process after the task completed uploaded to the desktop inspection system.

Analysis of Application Effect

(1)Revolutionized the traditional inspection mode of transmission line

(2)Improve the quality and efficiency of inspection work of transmission line

(3)The system has a high safety , reliability, availability and stability

(4)Achieve real-time monitoring and scheduling

(5)The effect is significant in cost savings

Conclusions

The intellectual inspection system of transmission line based on the " mobile information platform" introduces a new concept for operation and maintenance of transmission line.which effectively meets the fast , efficient and timely request for line inspection, the management level of line inspection will raise to a new level,the electronic, information and intelligent inspection management of transmission line is realized,Thereby maximizing efficiency and ensuring long-term, efficient and stable operation of the transmission network.

References

[1] Jun Kuang and Zhiyong LI: Journal of Chongqing Jianzhu University, Vol.28,No.1,p.139-142,2006In Chinese.

[2] Yong Chen, Bingling Zhou and Xiaoyong Ying: Jiangsu Electrical Engineering, Vol.26,No.6,p.26-27,2007 In Chinese.

[3] Gengsheng Liu,Yangliang Zheng and Xuebin Ran: Power System Protection and Control, Vol.38,No.6,p.129-132,2010 In Chinese.

[4] Zhongqiang Zhang, Mingyu Wang andShuxi Liu:Electric Power Automation Equipment, Vol.28,No.2,p.97-100,2008 In Chinese.

Applied Mechanics and Materials Vol. 596 (2014) pp 723-726
© (2014) Trans Tech Publications, Switzerland
doi:10.4028/www.scientific.net/AMM.596.723

Design and simulation analysis of the mirror current source circuit based on Multisim10

Hao Wang[1,a], Wei Yang[2,b], Benhong Li[3,c], Xiaochu Liu[4,d], Quanpeng He[5,e]

[1,2,3]Foshan Professional & Technical College, Foshan 528137, China

[4,5]School of Mechanical & Electrical Engineering, Guangzhou University, Guangzhou 510006,China

[a]gdwanghao@sina.cn, [b]gdyangwei@sina.cn, [c]lbh_1974@163.com, [d]gdliuxiaochu@163.com,
[e]gdhequanpeng@sina.com

Keywords: Multisim10, Mirror current source, Bias resistance, Simulation analysis, Triode.

Abstract. The mirror current source, with the characteristics of small static resistance and dynamic resistance, has been widely used in the analog integrated circuits, commonly used as a bias circuit and active load [1]. Aiming to the problem of the output signal waveform saturation distortion, which caused by the drift effect when the temperature rises in the fixed bias circuit, this paper provides a circuit design of replacing the collector load resistance of R_C by the mirror current source and carrying out simulation analysis by multisim10 software, compared with the theoretical calculation to verify the rationality of the design circuit.

Introduction

Analysis of amplifying circuit, which mainly analyzes two aspects of DC and dynamic performance index [2]. The DC analysis is to compute the base current of I_B, the collector current of I_C, the voltage of U_{BE} between the base and the emitter and the voltage of U_{CE} between the collector and the emitter of the triode. The purpose of setting the static working point is to keep the input signal' working point always be in the enlarged area in the whole range of assurance and amplifying circuit signal without distortion [3-5]. The static working point always be affected by temperature in the triode amplifying circuit. The parameters of I_{CBO}, I_{CEO} and β would change with the temperature rises, the collector current of I_{CQ} would increase finally. The upward movement of Q-point, which because of I_{BQ}, would cause saturation distortion of the output signal waveform [1]. The purpose of replacing the collector load resistance of R_C by the mirror current source is to provide a static collector current for triode for eliminating the distortion of waveform saturation, on the other hand, to improve the voltage amplification as the triode active load. At last, simulation analysis was done for the whole circuit by Multisim10 software.

The principle of mirror current source

The mirror current source has been widely used in the analog integrated circuits, the principle of the mirror current source circuit as shown in Fig 1. The reference current of I_{REF} is supplied by the DC power of V_{CC}, the resistance of R and the triode of VT_1. Because of the same parameters($\beta_1 = \beta_2$), the symmetrical characteristics and the same voltage of U_{BE} ($V_{BE1} = V_{BE2} = V_{BE}$) between the NPN triode of VT_1 and VT_2, the calculation process of equations is as follows:

$$I_{B1} = I_{B2} = I_B \ , I_{C_1} = I_{C2} = I_O \,. \tag{1}$$

$$I_{C1} = I_{C2} = I_{REF} - 2I_B \, , I_{C2} = \beta_2 \cdot I_{B2} \,. \tag{2}$$

$$\Rightarrow I_O = I_{C2} = \frac{\beta_2}{\beta_2 + 2} \cdot I_{REF} \,. \tag{3}$$

At the same time, the calculation of I_O is as follows:

$$I_O = I_{C2} \approx I_{REF}\,, I_{REF} = \frac{V_{CC} - U_{BE}}{R}\,. \tag{4}$$

$$\Rightarrow I_{\mathrm{O}} \approx I_{REF} = \frac{V_{CC} - U_{BE}}{R}\,. \tag{5}$$

Form the theoretical calculation above, we can draw a conclusion that the formation of mirror image relationship between the output current of I_O and the reference current of I_{REF} is based on the given DC current source and resistance when the magnification of the triode VT_1 and VT_2 is large enough.

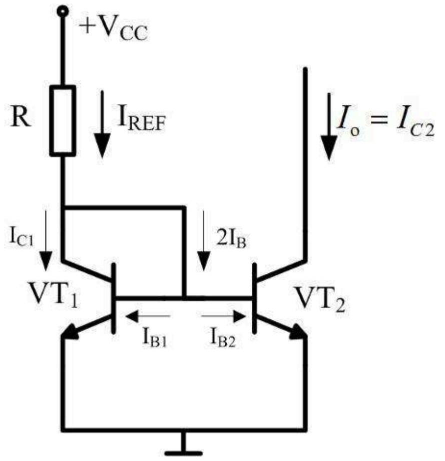

Fig 1 The mirror current source circuit

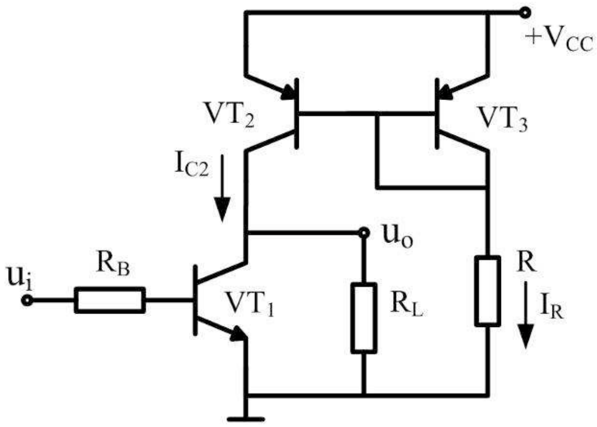

Fig 2 The active load circuit

Design for active load amplifier circuit

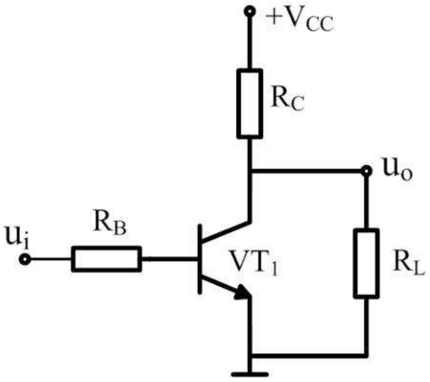

Fig 3 The fixed bias circuit

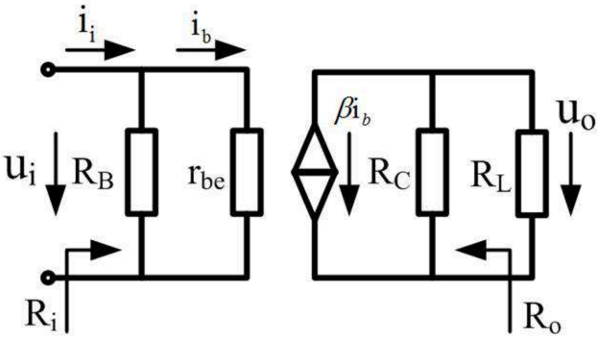

Fig 4 The equivalent circuit of fixed bias circuit

The voltage amplification factor of the fixed bias circuit (shown in Fig 3) as following:

$$\dot{A}_U = -\frac{\beta \cdot (R_L // R_C)}{R_B + r_{be}}\,. \tag{6}$$

The resistance of r_{be} is the input port equivalent resistance of triode in the equation. One of the effective ways to improve the voltage amplification factor is to increase the collector load resistance of R_C when the triode of VT_1 and the DC power of V_{CC} are given. The resistance of R_C always be instead of the current source because of hard to make big resistance in the integrated circuit[1]. The circuit of the load resistance which replaced by current source as shown in Fig 2, the result, which the triode dynamic collector current of I_{C2} almost flows into the load, leads to the increase of the voltage amplification factor. The relationship between the reference current and the static collector current is as following equations:

$$I_R = \frac{V_{CC} - U_{BE3}}{R}\,. \tag{7}$$

$$I_{CQ1} = I_{C2} = \frac{\beta}{\beta + 2} \cdot I_R \,. \tag{8}$$

Form the theoretical calculation above, we can draw a conclusion that it's necessary to set the appropriate collector current of I_{CQ1}, but not to need high voltage power supply in the circuit. Due to the Shunting effect of resistance of R_C, the current of I_{CQ1} will changes when the load added into the circuit.

Simulation analysis based on multisim10

The active load common emitter amplifier's simulation circuit simulated by multisim10 software as showed in Fig 5. The purposes of the mirror current source are to provide a static collector current for VT_1 and become the triode active load of VT_1 instead of R_C. The parameters of VT_1 (2N2714) as shown in Table 1, the parameters of VT_2 and VT_3 (2N3702) as shown in Table 2.

Table 1 The parameters of 2N2714 triode

Materials and polarity	P_{CM}（mW）	V_{CEO}（V）	V_{CBO}（V）	I_{CM}（mA）	h_{FE}(min)	h_{FE}(max)	f_T(MHz)
Silicon (NPN)	600	18	18	500	75	225	200

Table 2 The parameters of 2N3702 triode

Materials and polarity	P_{CM}（mW）	V_{CEO}（V）	V_{CBO}（V）	I_{CM}（mA）	h_{FE}(min)	h_{FE}(max)	f_T(MHz)
Silicon (NPN)	600	25	40	500	60	300	100

As showed in Fig 5, the current through the resistance of R is calculated by the equation as following:

$$I_R = \frac{V_{CC} - U_{BE3}}{R} = \frac{12V - 0.7V}{1\mathrm{k}\Omega} = 11.3mA \,. \tag{9}$$

From the equation above, we can see that the calculation results almost match the date (11.212mA) which showed in ammeter of XMM1 as showed in Fig 6. The calculation process of I_{C3} and I_R is as follows:

$$I_{B2} + I_{B3} = 169.189\mu A \,, I_{B2} = I_{B3} = 84.595\mu A \,.$$

$$\Rightarrow I_{C3} = I_R = 11.212\text{mA} \ \text{(the collector current of} VT_3 \text{).} \tag{10}$$

At the same time, the calculation process of VT_3 magnification is as follows:

$$\beta_3 = \frac{I_{C3}}{I_{B3}} = \frac{11.212\text{m}A}{84.595\mu A} = 132.5 \,. \tag{11}$$

The calculation result matches the triode amplification factor of h_{FE} (60~300).

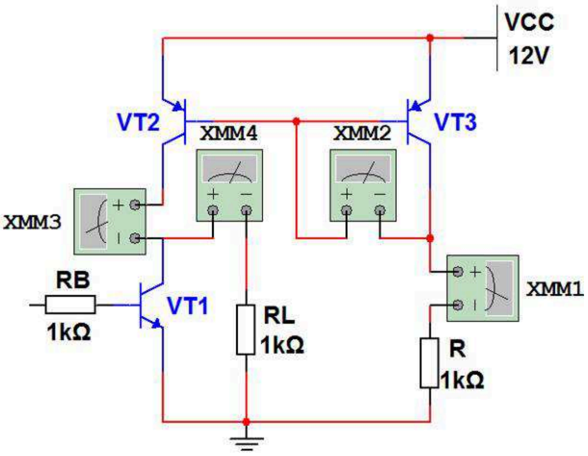

Fig 5 The Simulation analysis chart 1

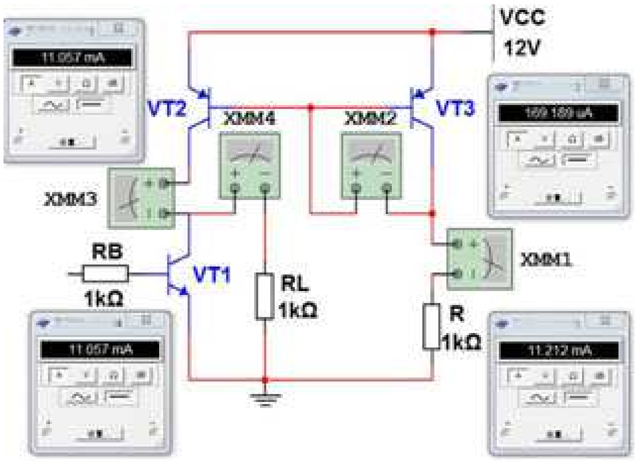

Fig 6 The Simulation analysis chart 2

Conclusions

Aiming to the problem of the output signal waveform saturation distortion, which caused by the drift effect when the temperature rises in the fixed bias circuit, this paper provides a circuit design of replacing the collector load resistance of R_C by the mirror current source and carrying out simulation analysis by multisim10 software. The simulation analysis result (as shown in Fig 6) as flowing:

(1) The reference current of I_R (11.22mA), which is produced by the DC power of V_{CC} (+12V) and the resistance of R (1kΩ), is equal to the collector current of I_{C2} (11.057mA). That means the simulation analysis result is equal to theory calculation value, which test and verify the rationality of the circuit design.

(2) As shown in Fig 6, the result, which the triode collector current (I_{C2}) almost flows into the load resistance, leads to the significant increase of the voltage amplification factor of A_U. At the same time, it also successfully solves the problem which can not improve the voltage amplification factor efficiently by increasing the collector load resistance of R_C.

Acknowledgements

This work was financially supported by the National Natural Science Foundation (NO.51275100) and Foshan Professional & Technical College Scientific Research Project (NO.2012KYZ01).

Literature References

[1] G.X.Luo and C.Y.Tuo. Design and practice of analog circuit [M]. Beijing: Beijing Normal University press, 2012.
[2] X.L.Yue. Talk about the effect and influence of the static work point in the amplification circuit [J].Science and Technology Information, 2011, 10:596-597.
[3] L.H.Yang,Q.Yang and W.L.Sun. Statics analysis of single transistor common emitter amplifier based on Multisim 10 [J].Modern Electronics Technique, 2014, 37(5):127-130.
[4] S.B.Tong and C.Y.Hua. Fundamentals of analog electronic technology [M]. Higher Education Press, 2006.
[5] H.G.Kang. Fundamentals of analog electronic technology: Part of the analog [M]. Higher Education Press, 2008.

CHAPTER 9:

Vehicle Control Systems and Intelligent Traffic

Applied Mechanics and Materials Vol. 596 (2014) pp 729-734
© (2014) Trans Tech Publications, Switzerland
doi:10.4028/www.scientific.net/AMM.596.729

Performance Analysis of Simulation of Pedestrian Traffic inside the hub

Bing Li[1,a], Min Li[1,b]

[1]Institute of Transportation, Inner Mongolia
University,No.24ZhaojunRoad,Hohhot,010070,P.R.China

[a]xsjlibing@163.com, [b]limin9304@163.com

Key words: traffic professional within the hub; fidelity; the simulation model

Abstract. Transport hub belongs to the people highly gathering places,the pedestrian traffic within the hub is a nonlinear stochastic dynamic problem with uncertain cluster density. The computer dynamic simulation is one of the effective methods to investigate the dynamic characteristics of pedestrian traffic flow at present within the hub.The article studies the error between pedestrian traffic simulation of the commuter simulation software and the actual pedestrian traffic,and explains the simulation error due to the discrete space, fidelity are introduced to evaluate the accuracy of the simulation model.By comparing the Hohhot underground tunnel experimental data and simulation results and the analysis of pedestrian traffic characteristics, it is concluded that the pedestrian traffic simulation performance is closely related to the environment in the hub and the importance of the fidelity of simulation model.

The fidelity of computer simulation model

Transport hub belongs to the place of people highly gathered, the study of hub internal people safety evacuation is of great realistic significance. The pedestrian traffic flow is affected by hub internal space environment, which presents a variety of different sports form coexistence state ,for example,low density limited free walk, high-density mobile even stagnation to wait. Especially in the rush hour, if you want to through the field observation and experiment to capture the crowd and the motion law of dynamic congestion and emergency evacuation process,which is very difficult. So, by using the computer dynamic simulation model to reconstruct the pedestrian micro movement within the hub is currently one of the effective methods of studying the characteristics of pedestrian traffic flow. From the perspective of the analysis results of the simulation software, different simulation software to predict the travel time vary by more than 40% [1-2], and the prediction error as the system state increases with the increase of density. Computer simulation model can reproduce the actual movement process of pedestrians really and accurately,Fidelity is a worthy performance metrics.

Commuter is a super microscopic traffic simulation modeling software, its characteristic is to provide more details than the microscopic traffic simulation, which is to analyze the whole process of people travel from start to finish. Discrete space in this paper, by explaining the causes of errors in the simulation, combining with the experimental data and Commuter simulation comparison results, illustrates the importance of fidelity in pedestrian simulation.

Commuter simulation is to use the computer in real life is not easy to happen, or test the high cost of scene simulation. But most simulation model is based on the routine test data is set up, but does not apply to some special environment and special behavior rules. When the pedestrian density up to crowded conditions, the simulation error will increase [4]. Therefore the simulation model of space have certain effects on the result.

Fidelity of simulation model can be used two performance indicators to evaluate,namely absolute percentage error (MAPE) and the prediction precision accuracy (ACCU)[3]. The MAPE is defined as the relative error of the simulation with the experiment values, ACCU is defined as the accuracy of numerical simulation in real scene, respectively, can use the following formula is obtained:

$$MAPE = \frac{1}{n}\sum_{i=1}^{n}\left|\frac{X_t - \hat{X}_t}{X_t}\right| \times 100\% \qquad (1)$$

Among them, X_t as the experimental value, $\hat{X}_t$ as the simulation values.

$$ACCU = [1 - \sqrt{\frac{1}{n}(\frac{X_t - \hat{X}_t}{X_t})^2}] \times 100\% \qquad (2)$$

Pedestrian traffic behavior characteristic within the transportation hub

The influence of facilities within the hub for pedestrians traffic behavior. Limited construction space within the Hub is an important factor caused the pedestrian traffic activity restricted. The unreasonable layout of facilities within the hub, such as inadequate number of planning wicket,in and out of the entrance, waiting areas, can cause anxiety, confusion and panic professional psychology, thus affecting the pedestrian traffic behavior; different direction of passenger flow , point of mixed traffic flow within hub tend to be the most densely populated places, hub internal structure is not perfect,which is the most difficult to overcome obstacles, traffic streamline organization is the origin of pedestrian mental panic; And people's psychological drives people within the hub of the weak link of a large number of accumulation, eager to entry or exit, the place such as the channel, stair, exit form intensive traffic zone,forming a potential safety hazard.The pedestrian traffic behavior within the hub mainly show:

1. Pedestrians walking in a closed space are not easily influenced by outside factors interference, directional difference and walk pressure make their walking speed faster.
2. There are many pedestrian activities, except the basic behaviors such as walking,also waiting for pedestrians taking a fall, shopping and other activities within the hub, these activities affect the behavior of other pedestrians, brought a series of other phenomena such as queuing, crowded, etc.
3. All facilities within the transportation hub are in series with each other,Pedestrians from the starting point to the destination process, need to go through a range of facilities which are less selective. For the purpose of the same kind of pedestrians, prone to herd behavior.
4. Transportation terminal professional traffic flow in time and space distribution has obvious imbalance, when a large number of passenger flow is different from the traffic behavior of individuals, most of these behaviors are a non-linear dynamic characteristics, commonly referred to as congestion behavior.

Pedestrian traffic behavior characteristics within the hub. Due to pedestrian behavior with the purpose within the transport hub, so to pedestrian traffic as a whole, will show the following characteristics:

1. Due to the different pedestrian travel’s lead time is different,and transportation has high demands on time, so pedestrian traffic exhibits the characteristics of time urgency within the hub. Especially in pit is more apparent.Most pedestrians carry articles such as baggage,which causes the walking speed significantly lower than normal walking speed, at the same time individual needs more room.

2. Most people are not familiar with space layout and the environment within the hub, if hub internal indicator is not obvious, or no one bear, it is easy to cause the stagnation of the pedestrian or confusion and so on.
3. When passengers for security, baggage and staff gathered highly in the pit mouth, reducing the capacity of the hub, resulting in a vicious cycle of congestion.
4. After the vehicle stops, due to the lack of a clear identity, causing pedestrians carry baggage racing car chase, regardless of the safety line already, there are serious security hidden danger, causing interlace interference of the flow in each direction.
5.Transportation hub for the professional demand presents the seasonal volatility in quantity, especially during the holidays,the Spring Festival,people are more crowded, volatility is more obvious.

Simulation model spatial analysis

The use of simulation model space. Space inside the hub is divided into small grid by the discrete space model , usually take for. $0.4m\times0.4m$. At this point the simulation space state density is of 6.25 P/m^2 . However, from the experiment, we find that pedestrian traffic is mixed sports system,which is constrained by the crowded pedestrian continuous group collector and a single pedestrian freedom of movement of discrete particles,the density changing with time, space and the surrounding traffic environment. In the open corridors free walking increases the movement of pedestrian space, maximum density is only less than 3 P/m^2 ; In high density crowded or line area, population density could be as high as 8 ~ 10 P/m^2 .Obviously, every step simulation error can be artificially cause cumulative error of the whole process of the simulation.
Pedestrian of the simulation model. Simulation model based on discrete grid is a hypothesis model of pedestrian area occupy the same space. In fact, each area each season pedestrians have different basic body size, in the subway, railway stations, airports and other places of public traffic, pedestrians often carry baggage, such a higher percentage of these pedestrians, the simulation model had to be taken increasing the movement of pedestrian inherent space into account. In addition, the bodily form of pedestrians is associated with the movement of pedestrians, obviously, if using continuous vector space model is easy to show the size of the different individual basic space traveler, only needs through real-time adjustment of pedestrian movement radius of space can be achieved.
The motion constraints of simulation space. Among the discrete grid model, the pedestrian speed is limited by the grid size, can not accurately reflect the movement condition of the pedestrian. there's a big difference about pedestrians walking speed as the individual's physiological and psychological condition and the surrounding traffic environment. Usually a fixed size of grid space can't represent the real velocity distribution. Pedestrians individual assumes that size $0.4m\times0.4m$ of a grid, only for the integer times of grid length divided by time step, which does not accord with the actual velocity distribution, therefore,the error caused by different simulation model.

In the grid model, the simulation entities' movement on the space is limited by grid arrangement, in the cellular automata model, the movement of the pedestrian [5] can only have eight directions as shown in Fig. 3.1, it can be seen that limited the moving direction is unable to show a slight variation in the direction of the pedestrians.Refine the choice of model space decides the position of pedestrians and the accuracy of movement speed, directly affects the fidelity of simulation model.

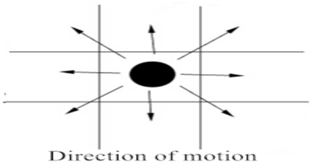

Fig. 3.1 Pedestrian movement direction

Case analysis

Hohhot Railway Station underground tunnel. Through to simulation analysis about the Hohhot railway station underground tunnel , this paper discusses all kinds of the simulation process about pedestrian behavior characteristics within the hub, clears that fidelity is a measure whether the simulation model is suitable for all kinds of complicated structure and the key indicator of a particular scenario simulation.

Passages walk for one-way in Hohhot railway station underground tunnel, and no other entrances and exits between channels, no pedestrians stranded phenomenon. Pedestrians walk along the one-way channel u until getting out of the export and waiting in line, crowd parting Conditions are observed during the experiment, we record the passenger travel time through the transfer channel. Surveyors in transfer channel exit record port traffic state, at the same time Record the pedestrian access point t_1 to get out of the channel point t_2 channel and the number of all, namely N.

The data processing method. What can be obtained from the video inlet flow is that the entrance pedestrian speed and density and related parameters. The experiment shows that the pedestrian traffic characteristics under the influence of channel and walking environment, the major influencing factors were channel professional density,obstacles and channel structure .

The travel time of pedestrian in the underground passage shall prevail with both ends fixed type measuring personnel observation section , according to the survey data for the corresponding processing. For floating surveyors access time t_1, leaving channels for t_2, the travel time is

$$T = t_2 - t_1 \qquad (3)$$

In and out of port space density refers to the observation in the number of people per unit area (unit: P/m^2); The average space density of the channel is

$$K = \frac{N}{A} \qquad (4)$$

Among them, N is the number of all pedestrians who access channel time t_1 to time t_2 out of the channel, A as the channel area.

The fidelity analysis. Based on the simulation model to reproduce the scene of complex dynamic pedestrian movement. By comparing the travel time of underground tunnel of the simulation results and experimental data to validate the fidelity of simulation model, Analysis of the simulation performance and relationship between the pedestrian distribution and density of channel. Experiments using the method of tracking observation channel and the crowd gathering condition, and record the trip time of pedestrians. At the same time, according to the experiment data and initial conditions,using the simulation software to reproduce the process ,we make an analysis of the results of simulation and experiment results.Fig.4.1 get the travel time of contrast results for the computer simulation and experimental measurement. As you can see the travel time curve, the experimental curve fluctuation is closer with the simulation curve, and the simulation curve is smoother,this scenario with the experiment are related to the pedestrians psychological and environmental factors.Overall, the fidelity of the model is higher, basically guarantees the authenticity of the simulation scenario.

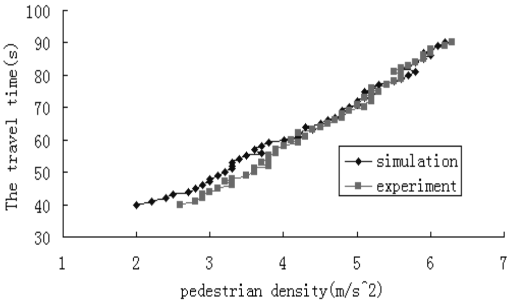

Fig.4.1 The contrast of travel time between the simulation and experimental measurements

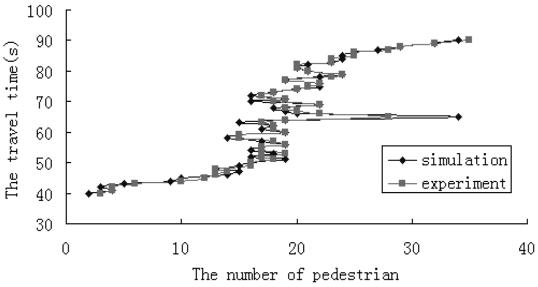

Fig. 4.2 The travel time -pedestrian density curve about experimental and simulation data

Speed and density of professional in the underground tunnel influence each other, at the same time, Speed also received the influence of the travel time and the surrounding environment. The pedestrian traffic flow characteristics reflect by pedestrian speed and density[6], so we can built the relationship between the travel time and the pedestrian density to describe cases in the scene the pedestrian traffic flow performance as shown in Fig. 4.2

Fig. 4.2 shows that the relationship between travel time and the average density about experiment and computer simulation. As you can see the pedestrian travel time increases with the increase of density of pedestrians, this means that with the increase of density of pedestrian,walking speed has to reduce. Experiment and simulation results are very close shown in the Fig. 4.2 ,it also shows that the fidelity of simulation model is very high.

MAPE values calculated through the travel time of pedestrian , MAPE=29.936%. At the same time,ACCU =91.296%. Therefore, the above the MAPE and ACCU values tell error and accuracy of the pedestrians walking process in a simulated channels with simulation model .The two performance indexes is very important.of model calibration and calibration of model parameters.

Summery

This paper studies the error between pedestrian traffic simulation of the commuter software and the actual pedestrian traffic,and explains the simulation error due to the discrete space, then fidelity are introduced to evaluate the accuracy of the simulation model.By comparing the Hohhot underground tunnel experimental data and simulation results, the analysis of pedestrian traffic characteristics, it is concluded that the pedestrian traffic simulation performance is closely related to the hub internal environment, proves the fidelity is the important indicator of simulation,the simulation results of Hohhot railway station underground tunnel simulation also shows MAPE and ACCU two performance indexes is very important of model calibration and calibration of model parameters.

References

[1] Christian Rogsch, Wolfram Klingsch, Armin Seyfried, et al. How reliable are commercial software-tools for evacuation calculation[c]‖Inter flam 2007-Conference Proceedings Interscience Communication Ltd. Greenwich,2007: 235-245.

[2] Rogsch C, Seyfried A, Klingsch W. Comparative investigation of the dynamic simulation of foot traffic flow ［J］. Pedestrian and Evacuation Dynamics, 2007, 9 (33) : 357-362.

[3] SU YuChuan, et al. Accuracy and real-time considerations for implementing various virtual metrology algorithms ［J］. IEEE Transactions on Semiconductor Manufacturing, 2008

[4] Schadschneider A, Klingsch W, Klüpfel H, et al. Evacuation dynamics: empirical results, modeling and applications ［J］. Springer, 2009, 6(3):3142 -3175.

[5] IST GmbH. Aseri user guide ［R］. Frankfurt,2007.

[6] Jia Hongfei,Yang Lili, 《Pedestrian F low Characteristics Analysis and Model Parameter Calibration in Comprehensive Transport Terminal》 Jilin university, 2009.

Applied Mechanics and Materials Vol. 596 (2014) pp 735-738
© (2014) Trans Tech Publications, Switzerland
doi:10.4028/www.scientific.net/AMM.596.735

Design of Intelligent Public Transportation Vehicle Terminal Based on S5PV210

Haiping Sun [1, a], Zhigang Gao [2, b] and Lina Chen [3, c]

[1] South China University of Technology, Guangzhou 510640, China
[2] South China University of Technology, Guangzhou 510640, China
[3] South China University of Technology, Guangzhou 510640, China
[a]hpsun@scut.edu.cn, [b]gaozhigang_1217@sina.com, [c]150998743@qq.com

Keywords: vehicle terminal; GPS/BD2; Compass; control center

Abstract: When the GPS signal or the wireless communication signal is weak, the vehicle will disappear in the map of the control center. In order to solve this problem, an intelligent public transportation terminal system which is cored by S5PV210 microprocessor is designed. The system uses BD2 and GPS dual-mode positioning module. Compass can provide short-message communication service. When the wireless communication signal is weak, we can use this service to communicate with the monitoring center. This design solution will make sure that the vehicle will never disappear in the map of the control center.

Introduction

The traffic jam has been the restriction to the development of the cities of our country. The advanced public transportation system is one of the most important way to solve this problem. And the vehicular terminal is the important ingredient of this system. The terminal will transmit the information of the bus, such as the position(the longitude and the latitude), the time and the condition to the surveillant center by wireless telecommunication in time and at last displays the motion locus of the bus on the electronic map terminals employ the GPS and transmit the information of the bus to the surveillant center by the wireless communication network. But when the signal of the GPS is weak, the terminal won't work well. And also in the area where the wireless communication signals are weak or not available, the terminal will not be able to transmit the information to the center, and the control center can't control and dispatch the vehicles[1]. In order to solve this problem, we designed an intelligence terminal in motorbus which employed the GPS combined with BD2. It use the CAMPASS and the GPS together to fix the position which can improve the accuracy of positioning and narrow the dead zone. Furthermore, the CAMPASS can interact with the surveillant center through short messages, then the problem that vehicles can't interact with the surveillant center in some areas is solved.

The overall design of the terminal

The intelligence terminal in motorbus need have the functions such as automatic station report, real-time positioning, wireless communication, intelligent scheduling and so on[2]. In order to satisfy this need, the terminal is designed modularly, use the microprocessor S5PV210 as the core, combined with the station reporter through the serial port to command the bus to report the station automatically. The positioning module use the GPS and BD2 to fix the position, usually interact with the center through 3G,like transmit the information to the center and at the same time receive the scheduling command from the center and display it on the LCD viewing screen. When the signal of 3G is weak or not available, the CAMPASS will help the assist the communication through short massages. And also for the sake of the multi-asking and multi-threading requirements, the software employ the embedded Linux system as the operating system, and develop the relevant application program through the system to carry out all kinds of the functions.

The hardware design of the terminal

The hardware of the terminal consists of 3G module, GPS/BD2 module, power supply module and serial port. The structure chart is shown in Fig.1.

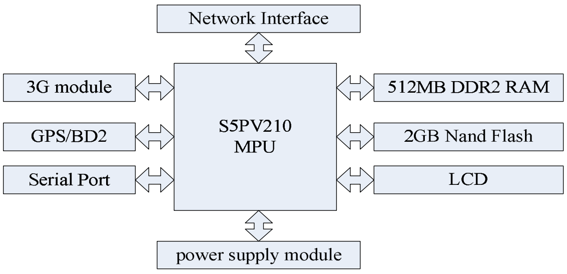
Network Interface
3G module
GPS/BD2
Serial Port
S5PV210
MPU
512MB DDR2 RAM
2GB Nand Flash
LCD
power supply module

Fig 1. The structure chart of the system

A. The Microprocessor Module

We choose the Samsung S5PV210 for the processor module. The S5PV210 has the 32-bit reduced instruction set with low power consumption and high performance and its architecture is armv7. The S5PV210 employed ARM CortexTM-A8 core, ARM V7instruction set and the inner bus structure whose dominant frequency can be up to 1GHZ, 64/32 bit. The Level 1 Cache of at 32/32 KB and the Level 2 Cache of at 512KB can carry out high operational capability as 2000DMIPS. And also there are abundant peripheral interfaces, so that will be easy to extend function at the terminal.

B. Power Supply Module

The Power Supply Module is the important component to ensure the whole terminal operate normally . And usually the power supply voltage is 12V or 24V.But during the practical operation, the voltage will have large undulation, for example, the 24V power supply will drop to 18V when the bus starts, but when the speed of the bus is getting faster, the voltage will go up to 32V, so as a result ,the design of the power supply need to meet the requirement in the voltage[3]. We use the TPS5430 switching power chip of the TI corporation to convert the voltage(24V) supplied by the vehicle power supply to the voltage(5V, 3.3V) demanded by every circuit.This kind of chip can input the voltage ranges from 5.5V to 36V, meeting the requirements in the voltage input, to insure the regular work when the voltage varies between 16V and 32V. The sketch map of the power supply module is shown in Fig.2.

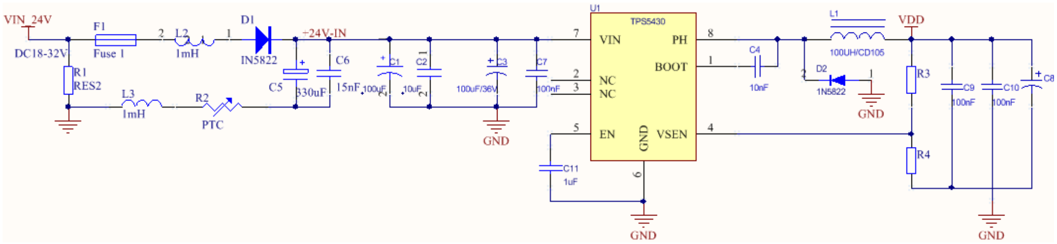
VIN_24V
DC18-32V
F1
Fuse 1
L2
1mH
D1
IN5822
+24V-IN
R1
RES2
L3
1mH
R2
PTC
C5
330uF
C6
15nF
C1
100uF
C2
10uF
C3
100uF/36V
C7
100nF
GND
U1
TPS5430
VIN
NC
NC
EN
GND
PH
BOOT
VSEN
C11
1uF
C4
10nF
L1
100UH/CD105
D2
1N5822
VDD
R3
R4
C9
100nF
C10
100nF
C8
GND
GND

Fig 2. The circuit diagram of the power supply module

C. The Orientation Module

Compass as autonomous navigation and positioning system developed in our country, develop the Compass application in the field of intelligent transport system, not only to break the monopoly of GPS in civil, also is the purpose of the Compass positioning technology research and development, China's Compass navigation system has provided services in the asia-pacific region in December 2012, but the Compass system has not yet been fully established in our country, China's Compass navigation system will be completed around 2020 [4].Before this, using dual mode of Compass and GPS positioning can increase the number of visible navigation satellite in the area, through the positioning of the received data processing, we can effectively improve the positioning accuracy [5].The positioning module of the system uses the module of BeStar BD - 126. BD - 126 module is a GPS and Compass dual-mode positioning module, the module of power consumption is only 25 ma, the sensitivity can be achieved - 163 DBM, and it's small size. The module diagram is shown in figure 3, the J7 is for onboard GPS/BD2 antenna, the J6 is for external GPS/BD2 antenna, the received positioning data will be transmitted to the microprocessor through TXA pin.The chip also supports the mode switch, BD - 126 RXA pin is input command pin, the user can send to BD - 126 through the microprocessor instruction and control the free switch between three modes: GPS single positioning mode, Compass positioning alone, GPS and Compass positioning .

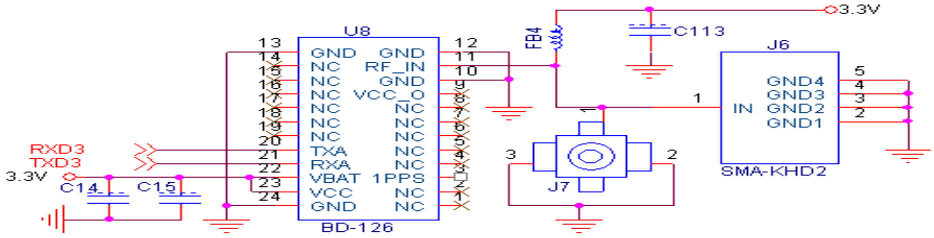

Fig 3. The circuit diagram of the BD/GPS module

D. The Module of 3G

In the vehicle system, all of the data is received and sent through the 3G wireless communicational module. The 3G is the basis of the hardware to connect the intelligent transportation system with the network, so its performance will seep into the stability of the whole intelligent transportation system. And our system employed the U6300V module of Long Shang, this module combined with the master leaf through the PCI Express , which can connect the HSPA, the UMST,the EDGE and the GSM of the intra-area to carry out the super speedy receive and dispatch of the data.The U6300V has power port, SIM card port, USB port and so on.

E. The Display Module

The LCD Screen is the window of the interaction between the terminal and the driver. The LCD Screen can display the information of the position, time, signal, the connection status with the server and the demand of the terminal. The national regulation about the screen of the vehicle terminal is that it can display 48 Chinese characters and graphs of at least 16*16 lattice. So we chose AT043TN25V.2 LCD of Qun Chuang to satisfy the request above all. The resolution ratio of the AT043TN25V.2 is 480*270, it is a 4.3 inches LCD with high light, nice performance in temperature and relatively low cost.

The Design of the Terminal Software

The software employed the Linux system as the operating system. And the Linux system has these advantages: (1)The sound codes of the inner core are totally open, and it has favorable tailing capability and customizability.(2)The Linux system can support the microprocessor broadly. (3)The Linux system also supports the multi-user and multi-job operation. (4) The routine of the Linux system has good portability.(5) The Linux system supports the muli-files system.Certainly, the system has its disadvantage, that is the operation interface is not convenient,but we can exploit the GUI procedure with the help the QT.

The design of the software consists of the manufacture of the initiator, the kernel transplantation and the development of the application program.The initiator can be adapted from the BootLoader to a new initiator which suits its own hardware platform. And the kernel transplantation consists of the kernel tailoring, the manufacture of the root file system and the development of the off-standard drive program. We mainly use the hardware platform to tailor the kernel, make the root file system and configurate the available kernel mirror image document and then burn the kernel mirror image to the hardware platform through the BootLoader.

The key to the interaction between the terminal and the center is the design of the software.The application program flow chart is shown in Fig.4. First is the initialization of the system include the initialization of the interface, at this time the LCD screen will display as the scheming interface, then it’s the turn to establish the reception and 3G link.After all of the thread ended, the mainroutine ends.The GPS receives the GPS data through the serial port and extract the data as the scheming format and then display the data in the main interface. The terminal connect with the center through 3G. And the flow chart mainly showed the process of the sending of the data from the terminal to the center.

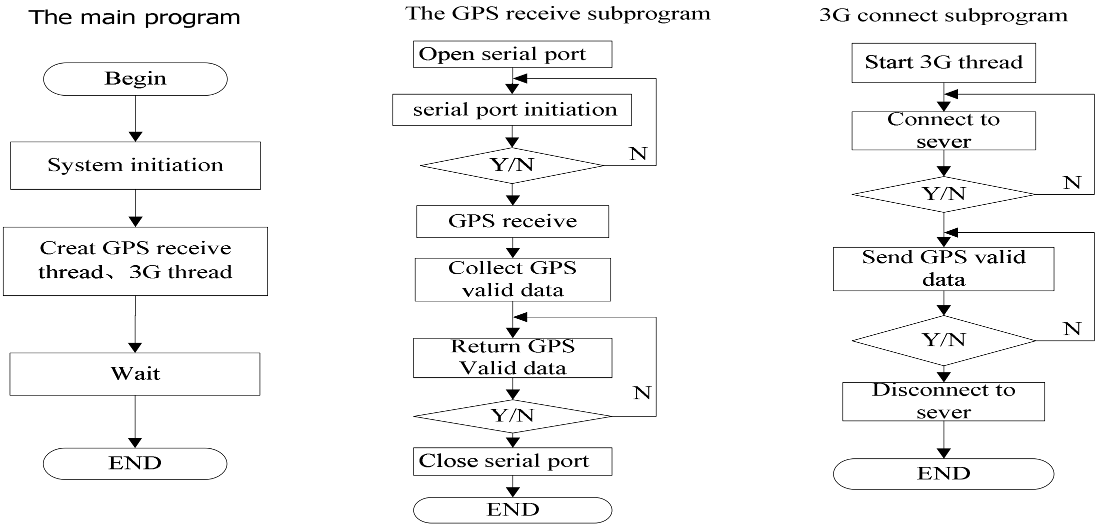
The main program
Begin
System initiation
Creat GPS receive thread、3G thread
Wait
END
The GPS receive subprogram
Open serial port
serial port initiation
Y/N
N
GPS receive
Collect GPS valid data
Return GPS Valid data
Y/N
N
Close serial port
END
3G connect subprogram
Start 3G thread
Connect to sever
Y/N
N
Send GPS valid data
Y/N
N
Disconnect to sever
END

Fig 4. The program flow chart

Conclusion

We proposed this design based on the S5PV210 intelligent vehicle terminal aiming at the defect of the vehicle terminal at present. This new terminal took the full advantage of the CAMPASS of China, can improve the positional accuracy combined with GPS,and perform the communication through the short massages of the CAMPASS in the area where the signal of 3G is not covered, which insure the center monitor and dispatch the running vehicles. We think this terminal will have a good application prospect along with the perfection of the CAMPASS of China.

Acknowledgements

This work was financially supported by the South China University of Technology and Guangzhou tongda auto electric co., LTD.

References

[1] J.J. Liu: Computer Applications and Software. Vol 29 (2012) No.3, p. 274

[2] C.J. Shi: Electronic Technology Applications. Vol 39 (2013) No.10, p. 134.

[3] L. Pan: *Design and Development of The Intelligent Vehicle Based on ARM* (MS., Hunan University, China 2009),p.21

[4] L. Cao: *The Intelligent Bus Query System Based on COMPASS* (MS., Huazhong Normal University, China 2013), p.11

[5] S.J. Ying and J.J. Li：Journal of Shanghai Maritime University.Vol 34 (2013) No.2, p. 1

Applied Mechanics and Materials Vol. 596 (2014) pp 739-742
© (2014) Trans Tech Publications, Switzerland
doi:10.4028/www.scientific.net/AMM.596.739

Research based on Fuzzy Control of Electric Power Steering System

Yanling CAO[1, a*], Zibin YANG[1, b]

[1] College of Vehicle and Motive Power Engineering, Henan University of Science and Technology,
Luoyang, Henan, 471003, China

[a]cylteacher@163.com, [b]793740871@qq.com

Keywords: EPS; fuzzy control; experiment table.

Abstract. For electric power steering (EPS) system to the requirement of real-time and stability of the control system, a fuzzy control algorithm applied to the EPS was proposed, and composed a fuzzy controller for appling to the EPS controller. Taking into account both portability and stability of steering, testing the designed fuzzy controller on EPS experiment platform and adjusting fuzzy control parameters online to make the EPS steering feel the best. Experimental results showed that the proposed fuzzy control algorithm had good tracking performance, can meet the requirements of EPS fast and frequent start-stop and the portability and stability of steering.

Introduction

Electric Power Steering（EPS）is a kind of new power steering system, developed by adding a set of electric control device in the traditional mechanical steering system. EPS system composes of mechanical steering gear, electromotor, retarding gear, electromagnetic clutch, electronic control unit, torque, vehicle speed sensor and other parts[1,2].When the system is working, the electronic control unit analyzes the torque signal of steering wheels detected by the torque sensor and the vehicle speed signal tested by the vehicle speed sensor with calculations, makes precise judgments, outputs orders controlling the electromotor to provide boosting torques, provides the power for vehicle steering and makes it more portable[3].EPS system has rapidly become the research hotspot in the automobile field with its excellent power characteristics, reasonable costs and energy-saving and environmental advantages[4].

EPS system working principles

EPS system can be divided into three types in accordance with different driving positions of power electric motors: Steering string power, steering screw power and steering rockshaft power. As shown in Fig.1, when drivers are steering, ECU can test the vehicle speed and torque signals by sensors, analyzes signals and send orders to power electric motor to implement the power steering.

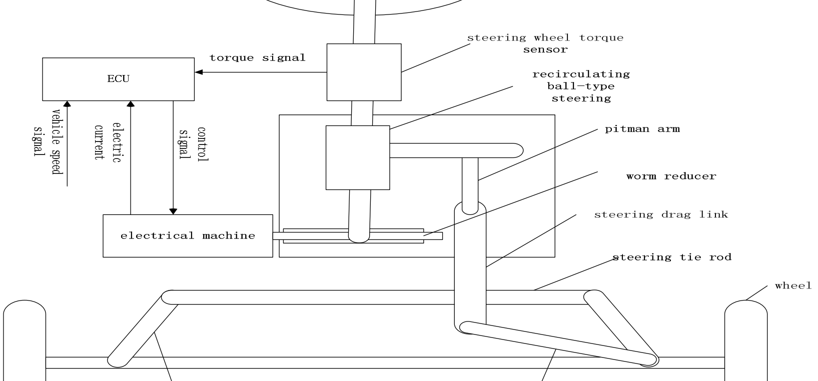

Fig.1 EPS structure diagram

EPS fuzzy control strategy

EPS control system can follow the target precisely and quickly in the design and send out orders. Fuzzy control does not depend on the mathematic model, which is not sensitive to parameter variations and a kind of non-linear control strategy based on fuzzy reasoning. When systematic parameters change or suffer influences, it still has rapid, precise and stable control effects. The design of fuzzy controller involves three parts of fuzzification, fuzzy reasoning and sharpening[5,6].

Fuzzification. When vehicle is steering, torque sensor conveys collected torque signals to ECU, and ECU control power electric motor implements the steering direction and the variation of power. It selects two dimensional fuzzy controller, the inputs are the torque deviation e of torque sensor and deviation rate of change ec， the outputs is PWM signal duty ratio *u* controlling electric motor revolving speed. The structure of fuzzy controller is shown in Fig. 2.

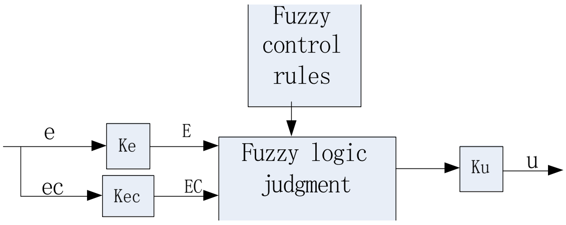

Fig.2 Structure of fuzzy controller

It defines the variation scope of torque deviation e and deviation rate of change ec as the domain of discourse in the fuzzy set, or e,ec={-5,-4,-3-2,-1,0,1,2,3,4,5,}, and its fuzzy subset is {NB,NM,NS,ZO,PS,PM,PB}. Elements in the subset separately represent negative big, negative medium, negative small, zero, positive small, positive medium and positive big. After confirming the fuzzy set and the domain of discourse of torque deviation e and deviation rate of change ec, it needs to gift values for fuzzy variables and confirms the membership functions in fuzzy variables. It adopts the triangle membership function, as shown in Fig. 3 and Fig. 4 shows the membership function of torque deviation e and deviation rate of change ec.

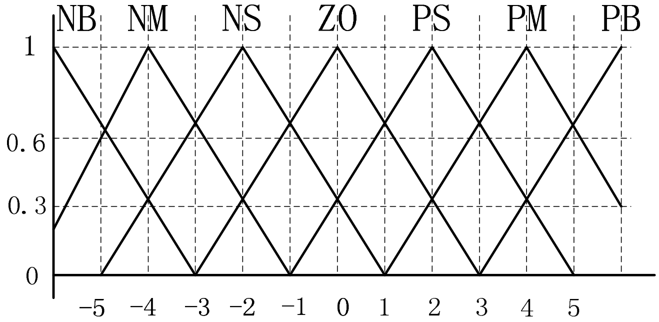

Fig. 3 Deviation e membership functions

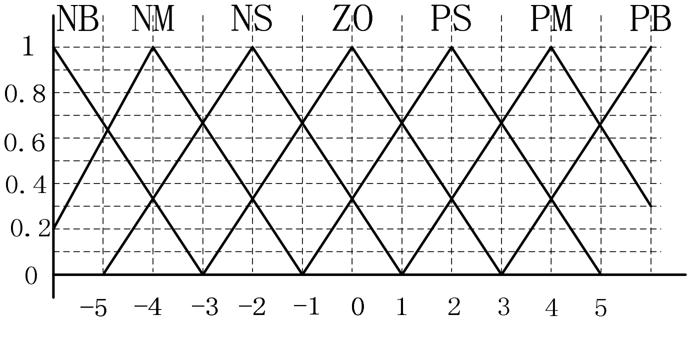

Fig.4 Deviation rate ec membership functionS

Build fuzzy control rule. Fuzzy reasoning is implemented by fuzzy control rules, which are shown in the form of control tables. The core work of fuzzy controller is to establish fuzzy control ruled list. When automobile is steering, steering torque is input into the controller by torque sensor. Automobile steering direction, steering angle and steering speed are determined by input torques and standard set deviation and its rate of change. When inputs of torque deviations and deviation rate of change are great, the greater PWM duty ratio should be output to obtain the needed steering angle; when input torque deviation is smaller and the deviation rate of change is greater, it should increase the duty ratio of output PWM. Other situations are similar. In accordance with the above control experience, it can establish steering system fuzzy control rules. The fuzzy control rules adopt the form of If E=NB and EC=PS then U=NS, composes fuzzy control ruled list, as shown in Table 1.

Tab.1 Fuzzy control rule

E	EC						
	NB	NM	NS	ZO	PS	PM	PB
NB	NB	NB	NB	NM	NS	NS	NS
NM	NB	NB	NM	NM	NS	ZO	ZO
NS	NM	NM	NS	NS	ZO	PS	PS
ZO	NM	NS	NS	ZO	ZO	PS	PM
PS	ZO	ZO	PS	PS	PM	PB	PB
PM	ZO	ZO	PS	PM	PM	PB	PB
PB	PS	PS	PS	PM	PB	PB	PB

Defuzzification. A fuzzy variable is obtained after fuzzy reasoning, but control system needs a confirmed control variable. Therefore, it must transit fuzzy variables to precise variables with proper conversion methods, and the process is called defuzzification. Common methods of defuzzification are as below, maximum membership function method has strong control functions on single component, simple and reliable algorithms, but its covering content is little and not complete; In gravity method, it firstly indicates the position of each variable in the coordinate system. Each data distribution situation is very clear, the selected are more; data utilized by median method, responding situation is more objective, but it is more difficult to calculate[7].The paper adopts gravity method to solve fuzzification.

Result analysis

The brushless direct current electric motor type used in the experiment is 86BLF01, rated voltage is 50V, rated power is 450W,rated revolving speed is 3000rpm, the total transmission ratio of the steering system i=155, the maximum voltage of torque sensor output is 5V. It takes into account of both the portability and stability of the steering, makes experiments in EPS system control platform and adjusts parameters. Obscured factor Ke, Kec and proportion factor Ku has greater influences on the stable and dynamic characteristics of fuzzy control system[8], calculates their values and adjusts properly in accordance with actual applications so as to reach the ideal effects. In accordance with the experimental process, we know that:

(1) Ke increases, the activation is rapid when steering, and the steering process is portal; When the value is too great,it easily produces concussion to make the steering unsuccessful during the activation. Kec increases, and steering adjustment is more sensitive; but values are too great, the discontinuous steering situation may occur in the steering process. Ku increases, output adjusting scope expands, which can adapt to the situation that steering resisting scope is great, which may influence the stable state operation of the steering process if it is too great.

(2) After repeated tests, when taking ke=0.025,Kec=0.8,Ku=0.0045, the steering hand feeling reaches the optimum. At this time, the input torque signal and corresponding electrical machine output revolving speed are shown in Figure 5. Comparing the two input and output curves, it can be seen that the actual output can follow the target input better.

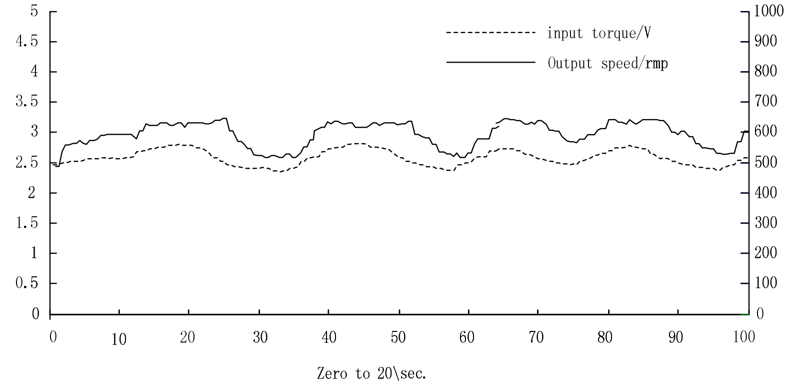

Fig. 5 Input torque signal and output torque contrast figure

Conclusion

Fuzzy control theory based EPS control system fully develops its advantages of few fuzzy control rules, quick dynamic responses and high control accuracies, which can adapt to the special working environment of the steering system in a better way and have strong adaptive abilities in the actual working status so as to equip with better control effects and improve the control performance of the steering system.

References

[1] Xiang Dan, Chi Yong-bin, Li Wu-bo,et al. Study on Control Strategy and Simulation for Electric Power Steering System[J].Control Engineering of Chin,2013,20(2):254-258.

[2] Shi Jian-zong, Wang Xiao-qing, Xu Nan-shao,et al. Research on Electric Power Steering System and Control Strategy[J]. Journal of Chong Qing Institute of Technology, 2009,23(1):15-18,75.

[3] Zhan Chang-shu,Ma Zhen-jiang, Xu Ning, etal. Modeling and Control Strategy of Vehicle Electric Power Steering[J]. Transactions of Beijing Institute of Technology, 2012,32(7):681-684.

[4] LI W. Design of a hybrid fuzzy logic proportional plus conventional integral-derivative controller [J]. IEEE Trans on Fuzzy Systems,1998, 4(6):449-463.

[5] Guo Han-zhong,Liu He-ping. Fuzzy Self-adaptive PID Control of Electrical Power Steering System[J]. Computer Simulation, 2011,28(6):339-342.

[6] Yang wei. Research on Control Strategy for Vehicle Electric Power Steering System[D].Wuhan Institute of Technology,2011.

[7] Yu Shu qiao,Zhao Yan. Dynamics modeling and analysis of electric power steering[J].Journal of Hubei University of Technology,2005,20(3):34-36.

[8] ZHI W W, HUNG Y C, JIN J L. A PID type fuzzy controller with self-tuning scaling factors[J]. Elsevier Science on Fuzzy Sets and Systems, 2000, 115: 321 - 326.

Applied Mechanics and Materials Vol. 596 (2014) pp 743-746
© (2014) Trans Tech Publications, Switzerland
doi:10.4028/www.scientific.net/AMM.596.743

Research on traffic behaviors and psychological characteristics of pedestrians within the comprehensive hub

Bing Li[1,a], Min Li[1,b]

[1]Institute of Transportation, Inner Mongolia University,
No.24 Zhaojun Road,Hohhot, 010070, P.R.China
[a]xsjlibing@163.com, [b]1903692582@qq.com

Keywords: comprehensive transportation terminal; Pedestrian traffic behavior; Psychological characteristics

Abstract. Traffic terminal is a spot of high density for people's traffic activities,the pedestrian transportation in the traffic terminal can be considered as a bunching density un-sure and nonlinear stochastic dynamics problem of interaction between each individual.pedestrian,as the primary part that composed all activities in the traffic terminal,has a significant influence on traffic behaviors and psychic properties.In this paper,we proposal a series of rationalized improvement measures to relief congestion and promote pedestrian security in the traffic terminal,by analysis on travel environment and traffic behaviors properties of pedestrian and deeply studying their traffic psychic properties.

Introduction

As the constant increase of traffic travel demand,the comprehensive traffic terminal, a important component of traffic infrastructure network, has realized the connect with various transport including urban rail transit,urban public transit,railway,highway and waterway.The pedestrian transportation in the traffic terminal is a dynamic system with bunching density unbalance and interaction of each individual,individual and environment.We all know that passenger transport service is set based on passengers' psychic requirements,so in order to well meet their requirements,the research should focus on their psychic requirements.In this paper,by analysing traffic behaviors properties and traffic psychic properties of pedestrian.we proposal a series of rationalized improvement measures to relief congestion and promote pedestrian security in the traffic terminal.

Factors impact on traffic behaviors of pedestrian within the hub

Among the various factors impact on traffic behaviors of pedestrian in the traffic terminal,the most dramatical one is volatility of travel time.For instance,since most travel during holiday ,especially the Spring Festival period,are for purpose of touring and visiting relatives,appears a apparent time volatility, lokalny and directionality.Further make the terminal load exceed it's saturation point,cause body friction and psychic scare among pedestrians,and finally result in congestion.

The limited space in terminal is another important factor that may restrict traffic activities of pedestrians.The unreasonable structure layout in the traffic terminal,such as the inadequate number of entrance,exit,ticket barrier,waiting room etc,always make pedestrian feel anxious,confused and scared,and then directly impact their traffic behaviors.

As there are many passenger flow lines and parcel flow lines of different direction exist in the traffic terminal,the weaving points of these flow lines generally considered as the most crowded place for traffic flow and also the root that make pedestrian feel scared.Eventually,amounts of accumulation formed on this weak link due to pedestrians' psychic drive become congestion.

Pedestrian's physiology also is the main factor that can influence traffic behavior.It has two forms of psychic properties and behavior properties,where the behavior properties can reflect the psychic properties in certain degree.Many elements contribute to this including gender,age,health,baggage carried,directionality and walk speed of surrounding pedestrian,making pedestrian occupy more space and has lower walk speed.

The analysis of pedestrian traffic behavior within the transport hub

Avoid obstacles characteristic analysis. Pedestrians within the hub are under the premise of without collision with surroundings from the start with the quickest speed to arrive at the destination. Psychologists believe that we will underestimate the collision time of distant large objects, overestimate the collision time of small close objects [2]. Obstacles size will affect the minimum distance between pedestrians and obstacles. When faced with minor obstacles, pedestrians will escape when it is in the near; When faced with large obstacles, pedestrians will take cover from a distance. In addition the pedestrian response to obstacles a very strong degree of the big level.In addition the pedestrian response to obstacle with the big level threat is very strong.

The analysis of the pedestrian queue feature. The orderly queue generally appear in the ticket window area. For example in the ticket queue, pedestrians are first in judgment when walking into the queues, if discover each window has a queue, chose the shortest queue; If found a window does not queue, go directly to the service window. In line of the entire process, if found a queue shorter than their local queue, then change to the short queue or remain the same. As shown in fig. 2.1

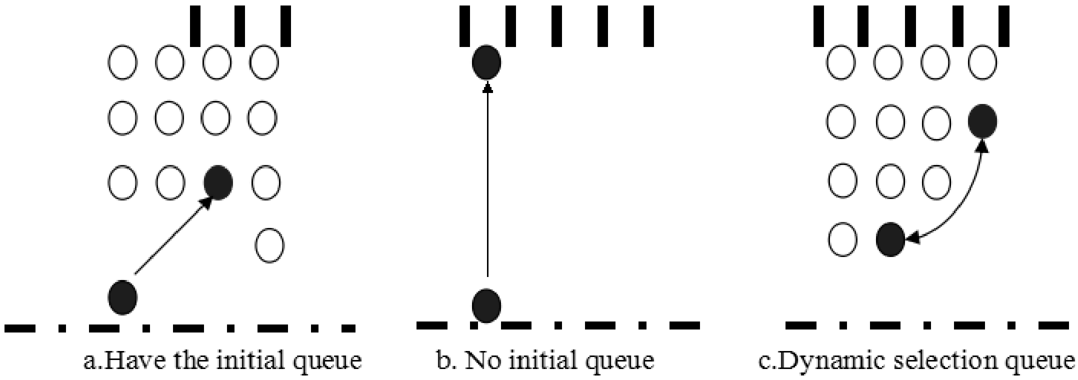
a.Have the initial queue b. No initial queue c.Dynamic selection queue

Fig. 2.1 Three forms of the orderly queue

The disorderly queue generally appear in the pedestrians through the bottleneck of horizontal channel and other facilities. For example, when a large number of pedestrians through horizontal channel,pedestrian queue is chaotic. This time, pedestrians are more willing to follow the pedestrian walking ahead to avoid collision, and adjust their position over a channel in the shortest time.

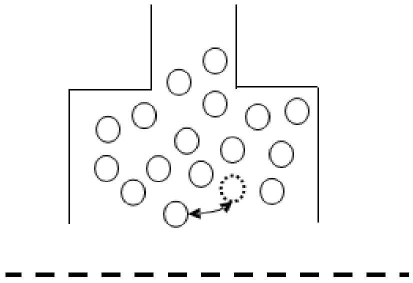

Fig. 2.2 Disorderly queue

The analysis of pedestrians waiting behavior. Waiting behaviors in the waiting room:The less pedestrians in the waiting room, walking will increase, the pedestrian anxiety increased; If there are many pedestrians in waiting in the waiting room, then most of the pedestrians were sitting on a chair waiting, eased anxiety. Therefore, if there is a long time from the train setting out,it had less pedestrians in the waiting room.Then these pedestrians prefer to walk around in the waiting room. As the train ready to check-in, passengers on the trains began to gradually form the queue waiting for check-in.

Waiting behaviors in the train platform:When start check-in, most waiting pedestrians use horizontal channel and stair platform and other facilities to achieve. When pedestrians just arrived at the platform and vehicles didn't stop, pedestrian were without some sort of order, people form a loose,queue.When the vehicle is arriving,pedestrians are in the queue under the command of the staff . When the vehicle has pitted and the door just opened, the position of the pedestrian and the corresponding changes accordingly,at this time, pedestrian close to the door turned into a semicircle around near the door.

Psychology analysis of pedestrian traffic behavior

When pedestrians are influenced by subjective and objective environment,such as pedestrian flow and structure layout,they will receive signal by sense of touch,sight,smell and other sense organ in form of simulation.Those signals will be transited into pedestrian's brain and act on psychology ,then create conation and perform corresponding behaviors in the end. Instantly,if pedestrian flow are too large and infrastructure is not perfect,these external feeling informations will be transited into organism,and make people produce irritable,restless and anxious psychology,finally cause fast walk,crash,friction and other unfriend behaviors among pedestrians.

Now we can sum up the psychic properties of pedestrian in traffic terminal based on the above analysis.

1)Group psychology

In traffic terminal, people usually consider the direction of signs when they make choice,and almost all people will conduct under this direction.However,according to the research ,major people chose to follow the masses without the direction of signs.In such special spot,once individual behavior and group behavior become reverse,the individual will feel nervous and change their own willing and behaviors under the impact of group to agree with the group.

2)Expectancy psychology

Expectancy psychology is the most intensive inner reflection of a certain goal people want to achieve during their activities.It's the main power that dominate people to conduct all kinds of activities.Pedestrian will perform some behaviors under the domination of expectancy psychology,and they hope that the goal they achieved by this behavior can equal or higher their own expectancy.For instance,since most travelers have high request for time,they always expect to shorten the travel time before they arrive the destination.Moreover,they expect to enjoy the best service while maintain the lost cost.Those psychology mainly shown on aspects of economy,convenience and comfortableness.

3)Loss aversion psychology

The so-called loss aversion is that people have the tendency to avoid loss.This kind of psychology prevalently exist among pedestrians in traffic terminal.For pedestrians,the loss impressed on them under a lower service level are far deeper than under a higher one,and convenient travel can cause a stronger feeling with lowest cost than higher cost.For instance,people always comprehensively consider the consistency between price and service.They buy ticket and with a hope of taking most comfortable car with price as low as possible.But when they find they have less comfortable service compere with others under the same price level,they will feel a sense of loss.

Summary

The paper researches on traffic behaviors and travel environment of pedestrians within the comprehensive hub, further study of pedestrian traffic psychological characteristics, we put forward the following improvement measures to ease traffic congestion within the hub and improve the security situation: 1)Conduct regular safety maintenance inspection on hardware facilities within the hub, and apply advanced detection,protective equipment into the security check within the hub . 2) In view of the vulnerable groups within the hub, Set up its special seat, facilities and channel for them.3)Add up and down the escalator within the hub in order to speed up the weight pedestrian flow velocity4) Improve the directional signs and other infrastructures in order to realize the pedestrians walking of the unobstructed within the hub.Set up the humanized warning marks, for example,where the unsafe,5) In order to improve the safety of pedestrians into wicket,implement a partial release at the ticket barrier to alleviate the crowded passenger station. When traffic is bigger, make full use of the wicket whose period is not in operation and practical operation. 6) add sign, real-time information in order to pass information to passengers timely and accurately. 7).In order to avoid confusion when passengers get on the car, organize passengers queue and enter the train according to the order ,thus reducing the time delay of passengers getting on the car.

References

[1] Guo Jinsong,Li Xuhong, Zhu Yandong. Integrated transport hub of the traffic organization research in the region [J]. Journal of shanxi building, 2007, 33 (20) : 14 to 15.

[2] C.D. Wilkins, J.G. Holland. Engineering psychology and the role of man (Ed) [M]. Shanghai: east China normal university press, 2003.

[3] Traffic Engineering [M]. Li Zuomin, people's traffic press, 2000.

[4] You Zhipei. The use of a herd mentality and guide [J]. Journal of political work, 2004 (10) : 56.

[5] Song GuanDong. Conformity new. Psychological science [M]. 2005, 28 (5) : 1174-1178

[6] Liu Huan, etc. The number of gain and loss process change: the new viewpoint of loss aversion phenomenon [J], journal of psychology, 2009, 9 (12) : 1123-1132.

Applied Mechanics and Materials Vol. 596 (2014) pp 747-750
© (2014) Trans Tech Publications, Switzerland
doi:10.4028/www.scientific.net/AMM.596.747

Apply the Damaged Road Data for Driving Simulator

Alimujiang Yiming[1,a], Reziwan Maimaiti[1,b]

[1]College of Electrical Engineering, Xinjiang University, Urumqi, Xinjiang, 830046, China

[a]alm_ym@xju.edu.cn, [b]mmtreziwan@xju.edu.cn

Keywords: Cracking ratio, Roundness, Alligator crack, Longitudinal crack, Driving simulator

Abstract. This paper presented a method of building the view image for Driving Simulator based on various road profiles and crack information by considering the damage road such as roughness road and crack. The main property of this method is that we can obtain the data profile only from several photographs of the road. Therefore, it is flexible and efficient.

Introduction

When a vehicle is running, the sight information influences the driver easily [1, 2]. Similarly to this, the presence of the road image greatly affects riding comfort, when the riding comfort is evaluated by using Driving Simulator (hereafter, DS). However, when experimenting on DS, the method of giving sight information on the vehicle vibration has not been established at present, although the sight information is indispensable to analyze the riding comfort [3, 4].

In this paper, the method of building the view image for DS based on various road profiles and crack information by considering the damage road such as roughness road and crack is examined.

Theoretical model of road profile

The road profile model is a technique that has been used so far, and the road profile is decided by using a trigonometric model depending on an arbitrary Power Spectral Density (hereafter, PSD) function. The PSD function is used for various standards such as ISO, and is shown by the following expression:

$$P_r(n) = a \times n^{-\omega} \tag{1}$$

where *a* is a constant that shows smoothness degree of road, ω is a constant that shows decentralized level of object frequency.

The road roughness at random position *t* is shown by the following expression by using a trigonometric model:

$$X(t) = \sum_i X_i \cos(2\pi f_i + \lambda_i) \tag{2}$$

where f_i is a spatial frequency, λ_i is a random variable that does not depend on the frequency, and X_i is calculated by PSD of the road profile. Here, PSD of $X(t)$ can be expressed by using the following equation:

$$P(f) = \sum_i (1/4) X_i^2 \delta(f - f_i) \tag{3}$$

Consequently, X_i can be obtained in a certain frequency band as follows by giving $P(f)$:

$$X_i = \left[\int_{f_i - \varepsilon_i}^{f_i + \varepsilon_i} P(f) df \right]^{1/2} \tag{4}$$

$X(t)$ is specified by substituting the X_i in Eq. 2.

The solid road roughness becomes possible by making two or more longitudinal profiles based on Eq. 2. The above-mentioned trigonometric model was simulated by using *Mathematica*, a mathematical and incorporated with environment software.

Image analysis on cracks

In this research, for expressing numerically and to quantify the complexity of the road image, the roundness is used. The roundness is the amount of the feature in which the complexity of the road shape can be measured, which is obtained by the expression below:

$$Roundness = \frac{4\pi \times Area}{Circumference^2} \tag{5}$$

So far, the crack, which is the representative on the damage road, has recognized as the damage level according to the cracking ratio. Fig. 1 shows the example of cracks.

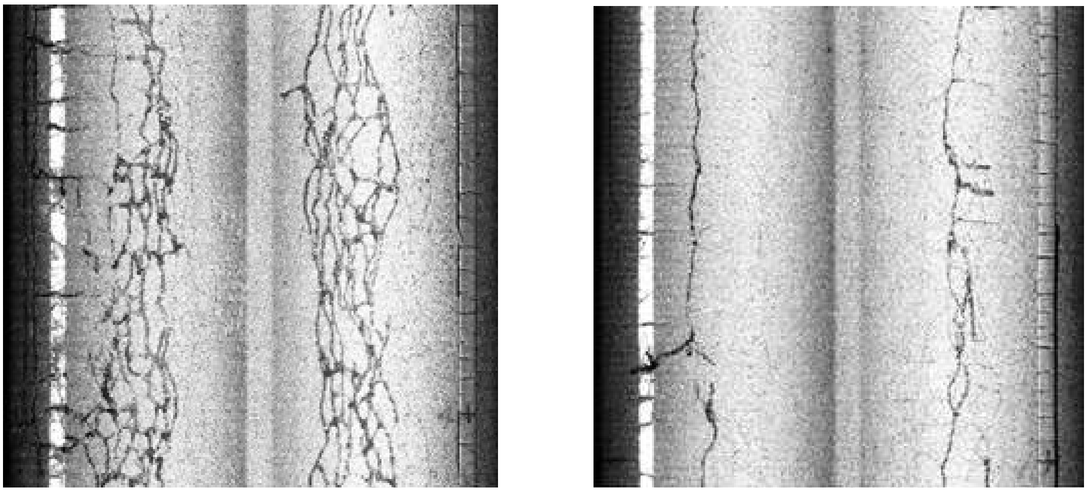

(a) Alligator (b) Longitudinal

Fig. 1 Examples of cracks

To define the level of the road damage, the state of the crack is measured to express numerically and to quantify the level of the road damage, and the cracking ratio which is the level and the extension of the crack has used. The cracking ratio can be obtained by considering the level and the extension of the crack, and it is shown as following expression:

$$Craking\ \ ratio(\%) = \frac{Craking\ \ area(m^2)}{Investigated\ \ \sec tion\ \ area(m^2)} \times 100\% \tag{6}$$

The image analysis has made by using general-purpose software called Image-J.

In order to make a view image for DS according to the level of damage, statistical image recognition by the image data processing and the relation to the cracking ratio are necessary. Therefore, we made the image analysis on the crack. The cracks used for the analysis are divided into longitudinal and alligator shape and the measurement photographs of 50 patterns were used respectively. For one of the examples is shown in the following section.

Result analysis

As for one of the typical examples as shown in Fig. 2, result analyzing of the image by using Image-J is discussed as below:

(1). Because the cracking ratio is expressed as the level of crack in targeted section as well as its extension, alligator cracking ratio are generally higher than longitudinal cracking ratio.

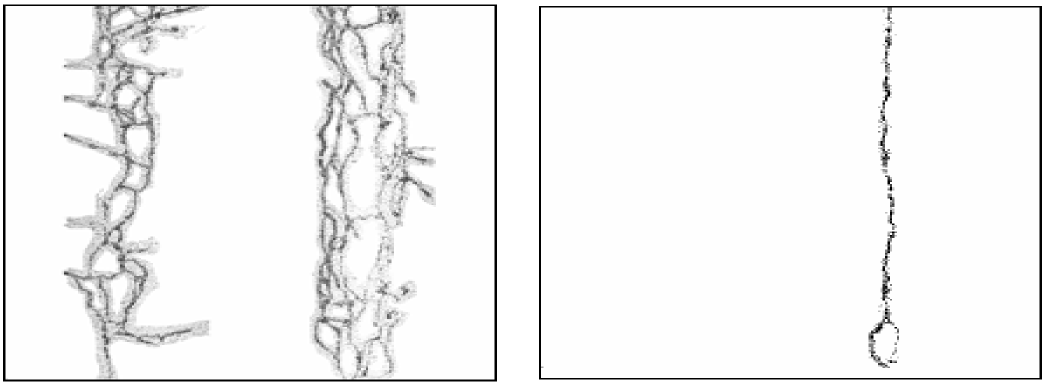

(a): Cracking ratio 65%, roundness 0.052 (b): Cracking ratio 8.6%, roundness 0.005

Fig. 2 After processing the image of the cracks

(2). Comparing the cracking ratios by obtaining the roundness both the longitudinal and the alligator crack, we can find that the value of the alligator crack is about ten times for the roundness, and the cracking ratios is about eight times bigger than the longitudinal.

(3). As for the cracking ratio of the road image increases, the roundness also increases too, as shown in Fig. 3. It can be considered that there is a proportion relation between the cracking ratio and the roundness. In the Fig. 3, alligator crack is mainly included in the blue circle, longitudinal crack is mainly in the yellow part, and the green part is the conversion area.

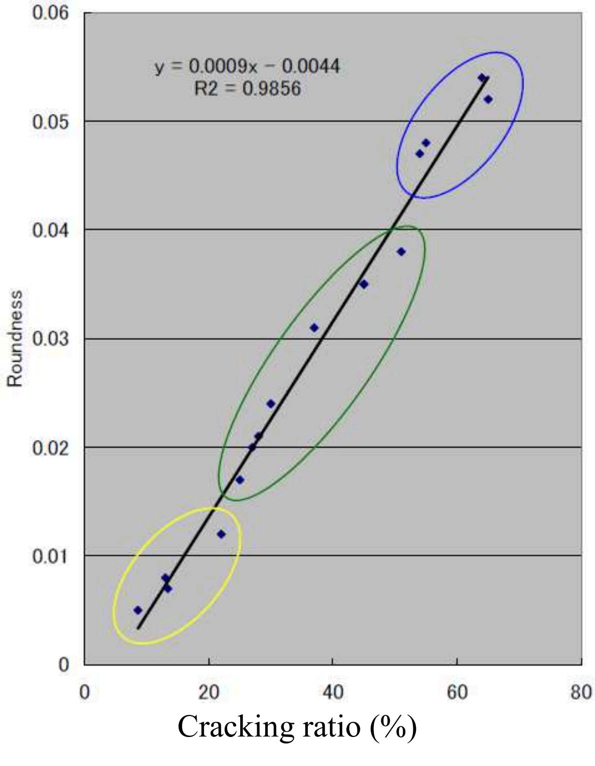

Fig. 3 Relation between cracking ratio and roundness of road image

(4). Road profile result is shown in Fig. 4. The road shape obtained by the simulation changes by changing the PSD function, the change of the road surface elevation grows by changing the value of a, and the appearance of long wave and short wave is different by changing the value of ω.

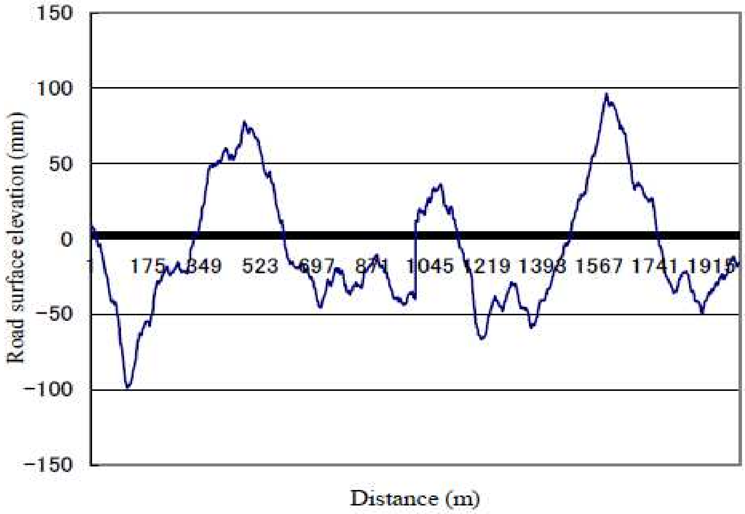

Fig. 4 Road roughness simulation result

Conclusions and future work

The following results were obtained in our research work:

1. Application of the cracking ratio and the roundness with the image data processing makes it possible to express numerically and to quantify the level of the road damage.
2. By using a theoretical model of the road profile and the simulation result of longitudinal road profile, we can make a solid data of the road.
3. Three-dimensional image that we created by using the general-purpose software is close to an actual image of the road.

For the future work, it is necessary to evaluate the damage level of various roads by investigating various samples like the manhole and expansion joint, etc. Also, a higher-level reproducibility of the road image is necessary to use in DS, in order to examine the differences for testee's riding comfort more clearly, when using the three-dimensional image in DS.

Acknowledgement

This work is financially supported by the Xinjiang Natural Science Foundation (2014211A017).

References

[1] MA Xiaoliang, ANDREASSON Ingmar.: Statistical analysis of driving behavior data in various vehicle following stages, Transp. Res. Rec., No. 2018 (2007), p. 87-96

[2] H. Suzuki: Measuring a comfort: Evaluation of the psychology, action and physiological effect, Japan publication service, 1999.

[3] Kawamura, A., Shirakawa, T. and Maeda C.: Applicability of Driving Simulator as a New Tool for the Pavement Surface Evaluation, Proc. of SIIV 2004 (CD-ROM), Firenze, Italy, No. 52 (2004).

[4] A. Kawamura, T. Shirakawa, and C. Maeda: KIT Driving Simulator for Road Surface Evaluation, Proceedings of 5th Symposium on Pavement Surface Characteristics, 1-10 (CD-ROM), Toronto (2004).

Applied Mechanics and Materials Vol. 596 (2014) pp 751-754
© (2014) Trans Tech Publications, Switzerland
doi:10.4028/www.scientific.net/AMM.596.751

Modeling and Design of Fuzzy-Neural Network Controller of Electric Power Steering System

GENG Guo-qing

School of Automobile and Traffic Engineering, Jiangsu University, Zhenjiang, 212013, China

ggq19791001@163.com

Keywords: automobile, electric power steering, EPS,fuzzy-neural network, controller

Abstract: Most Automotbile Electric Power Steering (EPS) controller designs are based on a simplified accurate model,however,EPS controller is affected by many nonlinear friction and damping easily, such as road condition,sensor noises and the lateral wind disturbance.These uncertainties affect the accuracy of assist current, the EPS performance and the driving safety. Aimed at the nonlinear MIMO system of electric power steering system,the mechanism and dynamic characteristic of EPS is analysed,and EPS model is developed. Then the fuzzy-neural network controller is designed and the corresponding simulation is performed.The results show that the proposed EPS control strategy can provide good performance of stability and controllability and can increase the anti-jamming capability of vehicle.

Introduction

Electric power steering (EPS) systems can improve fuel economy obviously. EPS system is actually a typical non-linear MIMO system because of the nonlinear friction and damping. And there are many disturbance factors such as road condition, sensors noise. This situation obstructs the further improvement of EPS. Based on modern intelligent control theory, this paper introduces a fuzzy-neural network controller design for EPS system ,which based on uncertainty analysis of EPS. The state space formula and the extended controlled object matrix were determined[1,2].The fuzzy-neural network controller was designed to optimize the controller characteristic and to minimize the effect of disturbances on output. The simulation results show that the designed controller actually improves the performance of EPS and its robustness[3].

EPS system dynamic equation

A column-type EPS consists of a torque sensor,a motor,and a reduction gear,an ECU,which performs calculations on assisting force based on signals from the torque sensor and vehicle sensor.Assist to the driver is achieved by the torque sensor, which measures the driver's torque.The torque is processed and an assist command is generated and further modulated by vehicle speed , which is also received by the controller. This command is given to the motor, which provides the torque to the assist mechanism.

Fig.1 shows a model of a steering mechanism equipped with EPS. this model can be represented as a balance between the steering torque applied by the driver T_h,the assist torque produced by motor T_a and the reaction torque T_l, which comes from the road. According to Newtonian mechanics, we get model's dynamic equations(Eq.1) [4-5]:

$$I_h \ddot{\alpha} + C_h \dot{\alpha} + K_s(\alpha - \delta) = T_h + f_h(\alpha, \dot{\alpha}) \tag{1a}$$

$$I_e \ddot{\delta} + C_e \dot{\delta} = K_s(\alpha - \delta) + NT_a - T_l + f_e(\delta, \dot{\delta}) \tag{1b}$$

$$I_m \ddot{\theta} + C_m \dot{\theta} = T_m - T_a + f_m(\theta, \dot{\theta}) \tag{1c}$$

$$M_r \ddot{x}_r + C_r \dot{x}_r + k_r x_r = \frac{T_l}{r_p} + f_r(x_r, \dot{x}_r) \tag{1d}$$

$$T_a = Nk_m(\theta - N\delta) \tag{1e}$$

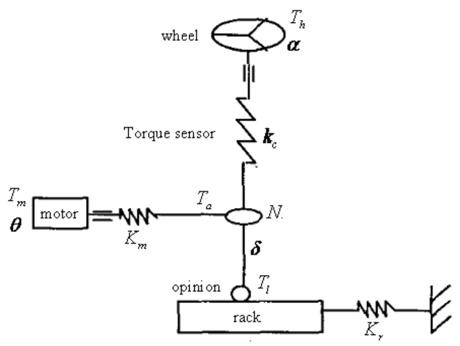

Fig.1 : EPS dynamic model

where I_h is steering wheel moment of inertia, I_e is column moment of inertia, I_m is motor moment of inertia, M_r is mass of the rack, C_h is damping coefficient of steering wheel, C_e is damping coefficient of steering column, C_m is damping coefficient of motor, C_r is damping coefficient of rack, K_s is spring constant of torque sensor, k_m is spring constant of motor shaft, k_r is spring constant of rack, α is steering-wheel angle, δ is pinion shaft angle, θ is motor shaft angle, and x_r rack displacement. $f_h(\alpha,\dot{\alpha})$, $f_e(\delta,\dot{\delta})$, $f_m(\theta,\dot{\theta})$, $f_r(x_r,\dot{x}_r)$ are nonlinear part of the model.

Fuzzy-Neural Network Controller and Simulation

3.1 Fuzzy-Neural Network Controller

Aimed to the nonlinearity and uncertainty of EPS system,a fuzzy-neural network controller was designed which is shown in Fig.2.The target current to the motor is determined by Fuzzy-controller according to the input of steering torque and vehicle speed.The neural network controller computes the control signal accordding to the error between and the actual current.

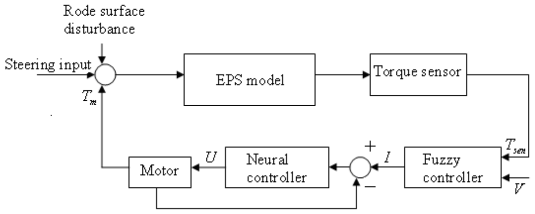

Fig.2: EPS fuzzy-neural network control system

3.2 Simulation Results and Analysis

Four kinds of simulation aspects were carried out to evaluate the performance of the introduced controller,that is, motor torque-current curve,steering handness, motor current response in moment step input and ride influence of rode surface disturbance on hold moment.

Firstly,the motor torque-current curve is carried out which is shown in Fig.3. It is revealed that the motor current is highest at stationary vehicle,and along with the vehicle is higher,the motor current is lower.Also,it is ture that motor current can well follow the steering torque input of driver to ensure the performance of steering handness and steering feeling,so that to increase the vehicle steering stability.

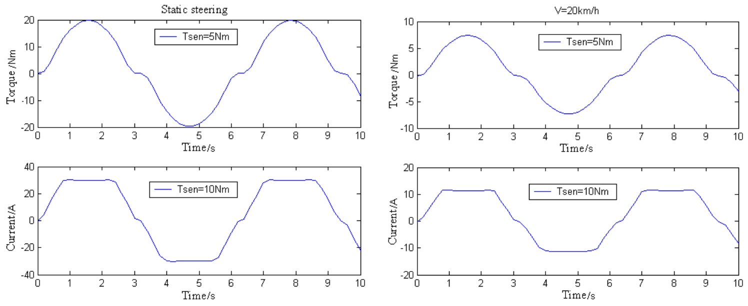

(a) (b)

Fig.3: Motor torque-current curve

Secondly,the performance of steering handness is carried out respectively at stationary steering and 10km/h steering condition.the steering handness results are shown in Fig.4.It is shown that the maximal steering torque is respectively 33.6% times and 45.5% times the steering torque of those are no EPS.The compare of handness between steering torque of EPS and steering torque of no EPS is shown in Tab.1.

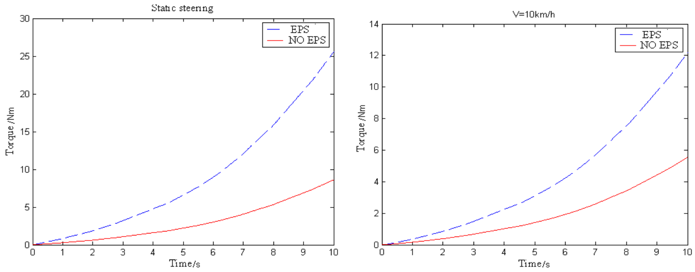

(a) (b)

Fig.4: Steering handness

Tab.1: Handness compare

condition	Item	No EPS	EPS
Zero speed	peak torque/Nm	25.580	8.603
	average torque/Nm	8. 614	2.897
	handiness target	2.973	
10km/h speed	peak torque/Nm	12.170	5.532
	average torque/Nm	4.001	1.819
	handiness target	2.199	

Thirdly, the performance of motor current response in moment step input is carried out at stationary steering and 10km/h steering condition. The motor current pesponse is shown in Fig.5. the motor current stability time is about 0.10-0.12s,the current overshoot is disappear rapidly and the adjust time is short.

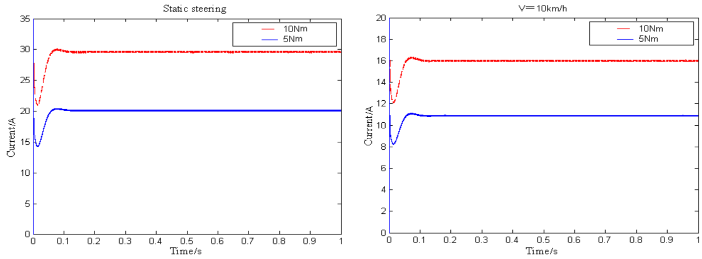

(a) (b)

Fig.5: Motor current response in moment step input

The detailed information is shown in Tab.2.

Tab.2: performance of motor current response in moment step input

	5Nm steering torque step input		10Nm steering torque step input	
Item	Stationary	10km/h	Stationary	10km/h
Stabilization value(A)	19.95	10.44	29.93	16.02
Maximal overshoot(%)	9.2%	16.1%	7.8%	17.7%
Stabilization time(s)	0.11	0.13	0.13	0.14

Fourthly,the steering torque response aroused by the random disturbance of rode surface is carried out. EPS system is insensive to the random disturbance of rode surface because of the introduction of fuzzy-neural network.Simulation results is shown in Fig.6 and the detailed information is shown in Tab.3.

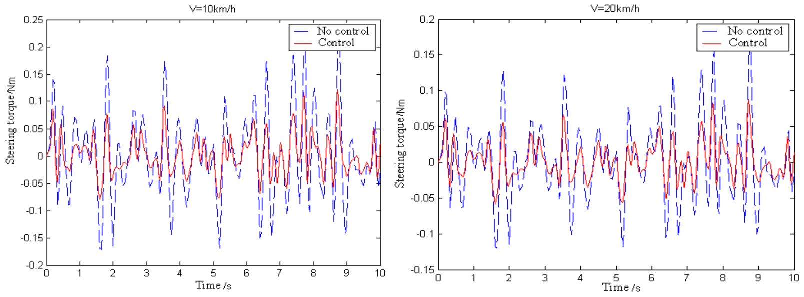

(a) (b)

Fig.6: Influence of rode surface disturbance on hold moment

Tab.3: Influence of random disturbance of road surface on steering torque

	No controller		Have controller	
Item	10km/h	20km/h	10km/h	20km/h
Peak value(N.m)	0.2428	0.1699	0.1222	0.03636
Stabilization time(s)	0.08258	0.05774	0.08768	0.02677

Conclusions

In this paper, the dynamic mechanism and equation of EPS system is given. Aimed to improve the robustness of EPS system, we presented the fuzzy-neural network network controller to minimize the effect of disturbances on outputs. Also the simulation results is done to test the controller, which justified that the fuzzy-neural network controller had improved the performance of EPS.

References

[1] Motors for electric power steering,Toshinori Tanaka Technical reports,2003.

[2] Daqing Tian,Guofu Yin and Gang Xie, Model and H∞ Robust Control Design for Electric -power Steering System,Proceedings of the 2004 International Conference on Intelligent Mechatronics and Automation, pp. 779-783,2004.

[3] Jiang Haobin,Zhao Jingbo and Chen Long,Hardware design and experiment research of automotive electric power steering system,The 3rd China-Japan Conference on Mechatronics 2006 Fuzhou, pp. 68-71,2006.

[4] Aly Badawy,Jeff Zuraski,et al,Modeling and analysis of an electric power steering system,SAE paper 1999-01- 0399.

[5] Ronald K.Jurgen,Automotive electronics handbook,Second edition,McGraw-Hill,Inc,1999.

Applied Mechanics and Materials Vol. 596 (2014) pp 755-759
© (2014) Trans Tech Publications, Switzerland
doi:10.4028/www.scientific.net/AMM.596.755

Simulation Study for Mixing Characteristics of NH3 and Automobile Exhaust in the SSCR System

Dawei Qu[1,a] Kai Zhang[2, b] Luyan Fan[3,c],Haibo Gao[4,d]

[1,2,3]State Key Laboratory of Automotive Simulation and Control, Jilin University, Changchun, China

[4,]Passenger Car Department Passenger Car Design Section II,FAW Co.,Ltd.R&D CENTER,
Changchun, China

[a]14128274@qq.com, [b]zhangkai_0719@126.com,[c]14128274@qq.com,[d]gaohaibo258@163.com

Keywords: SSCR;temperature;angle;position; optimization;

Abstract. In this paper we talk about the influence factors to the NH3 spray of Solid Selective Catalytic Reduction (SSCR) system by using AVL FIRE 3D commercial simulation software when NH3 and exhaust gas mix in exhaust passage,the influence factors include: engine condition, NH3 temperature ,nozzle installation angle and nozzle position. The conclusions are as follows:engine condition has much Influence for NH3 and automobile exhaust mixing,the mixing is better,the exhaust flow is larger, the exhaust temperature is high;NH3 initial temperature for the gas mixing has little influence;nozzle angle increases is good for the axial distribution of gas and the gas mixing characteristics; For the SSCR system direct injecting NH3 can optimize the nozzle position, and reduce the exhaust system volume.

Introduction

In recent years, with the development of high speed of our country economy, the improvement of Although currently on the market there are many diesel after treatment technology, especially SCR technology can basically meet the emission regulations, but the domestic company can't grasp its core technology, the technology is still in the foreign monopoly, moreover with the increasingly worse energy crisis , environmental conditions and the increasingly stringent emission regulations, SCR technology can not meet the requirements.As the stage of SCR Adblue has the problems that are hardly solved, firstly freezing point of Adblue is -11℃, in cold northern winter, continuing to use must use insulation ice measures, otherwise it is impossible to use,secondly pyrolysis hydrolysis ammonia of Adblue has temperature limit, the minimum temperature is 200℃, and at 400℃ only 50% urea can occur pyrolysis, once more Adblue pyrolysis will produce sediments, the sediments are likely to block urea nozzles and coverage on the catalyst carrier, reducing catalyst activity[1].in this paper,wo introduce a new technology.

Verification of NH_3 injection model of SSCR system

Model Building the NH3 injection of SSCR system at home and abroad are initial stage, there is no real experiments can be used as a reference, no related literature can read.In order to save manpower, financial resources, firstly, this experiment make a simulation experiment.So this paper adopt cubic grid, the long hight width were 500, 120, 120,their dimensions are in millimeters.The origin of coordinates is in the cube center.Coordinate of the nozzle in the cube is x= 0m, y = 0.05m, z = 0.24m.the mesh is 230000 in total, the simulation is shown in Figure 1, experiment conditions is consistent with the reference , injection parameter model is as shown in Table 1 [2.3].

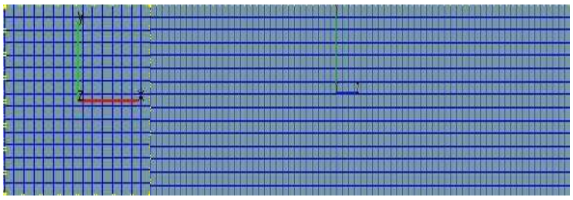

Figure.1 Urea solution injection model's grid

Table 1 Parameters of jet model correction

spray height	120mm	spray pressure	0.55MPa
Spray angle	65°	Injection duration	32ms
Nozzle hole number	1	Urea injection amount	0.1g
Nozzle hole diameter	0.4mm	The wall temperature	650K

The analysis of simulation results

Figure 2 shows CFD simulation results which the urea solution spray from 10ms to 110ms , the image for each interval of 10ms .As can be seen from the graph, the spray shape is a conical hollow in the middle, the cone angle is about 50 degrees to 60 degrees, with the passage of time, the end of the spray, mist droplets collides wall , and after collision the rebound area increases gradually.Fig.3 are the experimental results of the spray, the experimental results are quoted from the [3], it uses spectrometer photographic, no specific scale, mainly for image research.

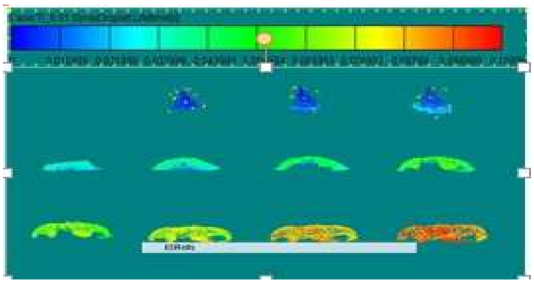

Figure.2 The CFD simulation results of urea water spray

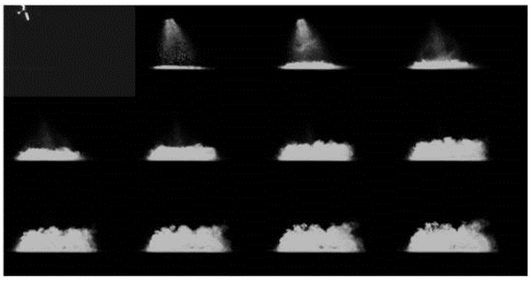

Figure.3 The experimental results of pipeline urea spray model

Simulation and analysis of affect factors for the jet of SSCR system

Using FIRE establishes the model that NH_3 directly injects in the exhaust pipe in front of SCR box .Fig.4 is simulation model for the exhaust pipe, length 1.36M, diameter 0.12M,grid number 100000.The nozzle position is in x=0, y=0.05, z=-0.28.

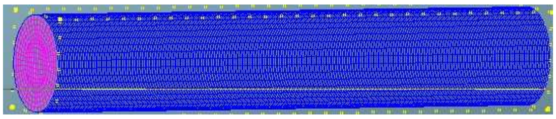

Figure.4 The simulation model of the vent pipe

Comparative analysis of the SSCR system of NH3 distribution and SCR distribution system NH and optimization of the nozzle position

This paper studies the situation the exhaust mixtures NH3 in the tail,in theory the direct injection is better than that of SCR system, but this requires experimental verification. NH3distribution of the literature [2] and the simulation graphics are compared,studying the difference between the two, and analysing the advantages of direct injection of NH3.

Table2 Temperature and flow rate of different conditions

Working conditions	Exhaust temperature(℃)	Exhaust gas flow(kg/h)
A25	360	552
A100	419	1062
B100	460	1454

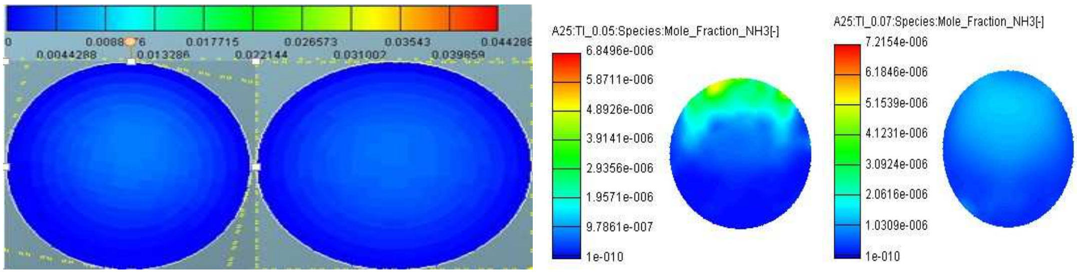

a. NH3 radial Distribution of SSCR system b. NH3 radial Distribution of SCR system

(1)NH3 distribution of A25 condition

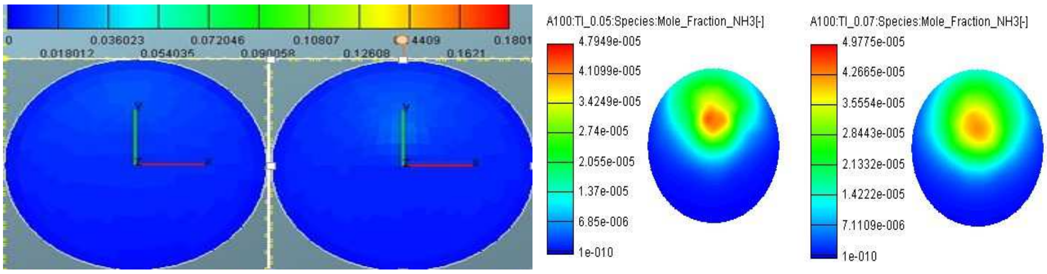

a. NH3 radial distribution of SSCR system b. NH3 radial distribution of SCR system

(2)NH3 distribution of A100 condition

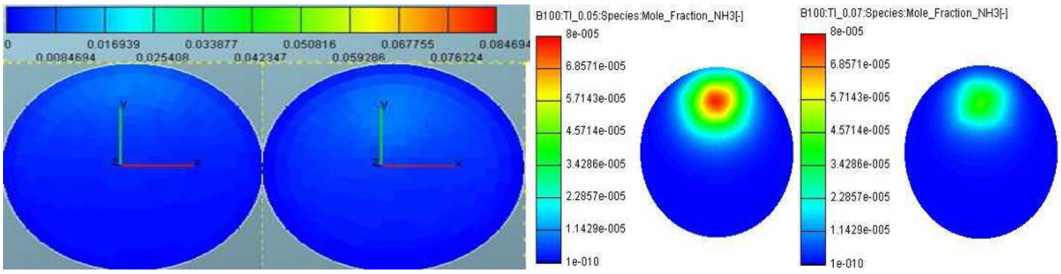

a. NH3 radial distribution of SSCR system b. NH3 radial distribution of SSCR system

(3)NH3 distribution of B100 condition

Figure.6 NH_3 radial Distribution of different conditions

This is NH_3 radial distribution of the SSCR system and SCR system in the pipeline(z=-0.4)of each case, time was 50ms, 70ms.We can understand NH3 distribution the SSCR system directly injects that are more uniform, with the passage of time gradually ,it is more uniform.The main reasons are the following,, it will pyrolysis hydrolysis in exhaust system when SCR system inject urea, it can produce NH3, which needs a time, and when the temperature is low, the time requires longer, uniformity of SSCR is better than SCR's at the same place.

NH3 and the gas mixing characteristics in Different NH3 temperature

Wo study distribution characteristics of NH3 that the temperature is 293.15K, 298.15K, 302.15K We choose the initial injecting into the exhaust of NH3 temperature.The calculation condition selection:The injection pressure is 0.95Mpa, the exhaust temperature is 330 ℃, the exhaust flow rate is 1358kg/h, the exhaust pipe pressure is 0.1Mpa, the angle of the nozzle is 30 °.NH3 injection duration is set to 100ms, the amount of injection is 31.2mg .Figure 7 is distribution characteristics of NH3 at 40ms under the different temperature,.From the graph analysis to see, NH3 initial temperature for the mixing has little impact, its temperature relative to the exhaust temperature is smaller,the main effect of temperature mixed is tail gas with temperature.

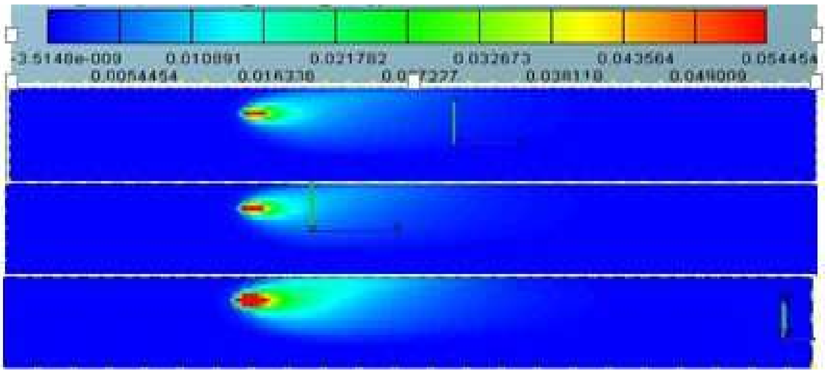

Figure.7 NH3 distribution of different temperature(from the fall in the following order: 293.15K, 298.15K, 302.15K)

Acknowledgment

This Project is supported by national natural science foundation of china （51306070）.The project is"Study on Ammonium Salts Pyrolysis and NOx Low-temp Reduction Behavior of SSCR System”

Conclusions

According to the aqueous urea solution injection principle and mixed with the Experiment has the same principle, using the existing experimental literature [3] result of SCR Verifies spray model , and use this model to direct injectionNH3 NH3 mixing with the exhaust gas the factor to carry on the simulation,through research and analysis, and make the following conclusion.And using this model for NH3 direct injection simulates and analyzes the factors of NH3 and the gas mixing , through research and analysis,and make the following conclusion.

1.The SSCR system of direct injection NH3 is very beneficial to the gas mixture , the exhaust pipe can be reduced, so that the nozzle position close to the exhaust port, enter the temperature increase.

2. Initial temperature of SSCR NH3 system of gas has little effect to mix, we generated NH3 without too much wasting energy increasing temperature.

References

[1] TAO Jiang-zhong, Study of reduce diesel nitrogen oxides y By selective catalytic reduction (SCR)[D]PhD thesis.Shandong University:2008

[2] QIN Yan. Simulation study of NH3 and the gas mixing characteristics for SCR system[J].Journal of internal combustion engine.2013(204) 43-47.

[3] Zhilong Li,Jun Deng，Liguang Li，Ling Cao and Zhijun Wu. A Study on the Factors Affecting Heated Wall Impinging Characteristics of SCR Spray，SAE paper，2011-01-1311.

[4] Figen Lacin，Adam Kotrba，Granville Hayworth and Henry Sullivan etc.SOLID SCR®：Demonstrating an Improved Approach to NOx Reduction via a Solid Reductant[J].SAE paper：2011-01-2207

Applied Mechanics and Materials Vol. 596 (2014) pp 760-765
© (2014) Trans Tech Publications, Switzerland
doi:10.4028/www.scientific.net/AMM.596.760

Coordinated Charging of EVs Based on Demand-Side Management

Yukai Li[1,a], Hong OuYang[1,b], JiaKui Zhao[1,c], XiuKai Rong[1,d] and Yi Dong[1,e]

[1]State Grid Electric Power Research Institute, nanjing, 211000, China

[a]liyukai@sgepri.sgcc.com.cn, [b]ouyanghong@sgepri.sgcc.com.cn,
[c]zhaojiakui@sgepri.sgcc.com.cn, [d]rongxiukai@sgepri.sgcc.com.cn, [e]dongyi_1989@sina.com

Keywords: DSM, coordinated charging, time-of-use power price, peak clipping and valley filling, NSGA-Ⅱ algorithm.

Abstract. Electric vehicles (EVs) are adopted as an effective way to reduce the pollution of atmosphere. However, if EVs are implemented in a large scale without control, peak load would increase significantly and the grid may be overloaded. Based on Demand-Side Management (DSM), an coordinated charging method for EVs to address the problem of that is proposed. Considering load fluctuation of power grid as well as time-of-use (TOU) power price, a multi-objective optimization model is formulated to minimize the charging cost and restrain the load fluctuation. Overall power load is composed of original daily load and EV charging load, which is obtained through Monte Carlo simulations. On the basis of this, the optimal number of charging EVs in each period is worked out with NSGA-Ⅱ algorithm. At last, the case study carried out shows the reasonability of this method.

Introduction

With the rapid development of national economy, the car production and consumption are increasing rapidly in our country. Utilizing EVs on a large scale is a major direction of modern automobile vehicles in the future. It is predicted that the national EV ownership will reach 60 million in 2030 [1]. Since the charging load of EVs is different from other electric loads, we should find a proper way to control the charging process [2]. In uncoordinated charging situation, the charging peak load probably overlaps that of original electric load, which will definitely aggravate the load fluctuation, increase the grid energy loss and reduce the economic benefit. Therefore, the research on coordinated charging of EVs has very important practical significance.

From the perspective of coordinated controlling for demand-side resources, it is aimed to conduct EVs' charging access time through TOU power price. By means of electricity price regulation, a multi-objective model is built to minimize the charging cost and restrain the load fluctuation. Through NSGA-Ⅱ algorithm, an optimal solution can be found to analyze the grid response capability in coordinated charging situation.

Coordinated charging method based on DSM

DSM refers to changing the way of using electricity and improving efficiency of terminal electricity consumption with methods of incentive measures and appropriate operation mode through the common mutual collaboration of power generation companies, power grid companies, energy service companies, social intermediary organizations, product suppliers and power users. Implementing TOU power price is an essential way of DSM, for it can realize coordinated control of demand-side resources by electricity price regulation.

The time of day for TOU power price is divided into three periods peak, valley and flat, according to users' needs and the actual load of power grid at different times. The power price is set different price levels to each period respectively, so as to encourage the users and power generation enterprises to shift load and improve electricity consumption efficiently.

The grid TOU power price and charging TOU power price in different time slots, is shown in Table 1, where the data are from a local power distribution network.

Table 1 Powerprice parameter

Time Slot	Grid TOU power price (yuan·(kW·h)$^{-1}$)	Charging TOU power price （yuan·(kW·h)$^{-1}$）
00:00—08:00	0.365	0.4
08:00—12:00	0.869	2.0
12:00—14:30	0.687	1.2
14:30—17:00	0.687	2.0
17:00—21:00	0.869	2.0
21:00—24:00	0.687	1.2

Control model of coordinated charging

A. Cost Model of Charging

Conventional daily load curve can be predicted according to historical data of local area distribution network by means of Monte Carlo simulations. Ninety-six-point daily load curve prediction is adopted here. Time interval is set as 15 min. PLj is the conventional load in the jth(j=1,2,…,96) period. Throughout the paper, it is assumed that EV is charged with constant charging power. PC is the rated power of slow charging [3].

ω is the battery capacity of EV. Ss is the capacity at the beginning of charging and Se is the capacity at the end of charging. SSOC is the charging capacity, which can be calculated as:

$$\mathrm{Ssoc} = \mathrm{Se} - \mathrm{Ss} \tag{1}$$

Based on associated probability distribution of charging process, an EV owner starts charging when residual capacity is between 20% and 50%, and ends up with more than 90% capacity.

Nj is the quantity of EVs in charging process. pj is the load value of EV in the jth period and can be calculated as

$$p_j = \sum_{j=1}^{N_j} P_C \tag{2}$$

Eq. 3 shows objective function of minimum charging cost:

$$\min \sum_{j=1}^{96} S_{SOCj} s_j \tag{3}$$

B. Restrain Model of Load Fluctuation

Power offered from distribution network to load during the schedule time is concerned by customer, but the power change of basic load is determined by customer. For this reason, the total power load for daily needs is certain after adding the charging load [4].

$$E_{Total} = \sum_{j=1}^{96} u_j i_j \Delta T \tag{4}$$

Power network loss can be calculated as:

$$E_{Loss} = \sum_{j=1}^{96} R i_j^2 \Delta T \tag{5}$$

As shown in associated literature, the minimum voltage fluctuation caused by overall load comes with the minimum power network loss caused by EV. Choose the charging capacity in every period as the variable and mean square error of load curve as the objective function (see Eq. 6):

$$\min \sum_{j=1}^{96} (P_{Lj} + p_j - P_{av})^{2} \tag{6}$$

Pav is the daily average load after adjusting. Pj is charging power in jth period.

C. Constraint Condition

1) Constraint of power grid load

$$P_{Lj} + p_j \leq P_{maxj} \tag{7}$$

Power, including vehicle charging power, must be less than maximum load of power grid.

2) Constraint of charging power

$$P_c = \min\{P_{user}, \ P_{charger}, \ P_{battery}\} \tag{8}$$

Puser is the maximum charging power set by user. Pcharger is the maximum output power of charger. Pbattery is the limitative value of battery's charging power. Under normal circumstances, both Puser and Pcharger are greater than Pbattery, which means Pc only needs to less than or equal to Pbattery.

3) Constraint of charging requirement

$$S_{SOC} \leq P_c t \leq \omega \tag{9}$$

SSOC is the charging requirement of an EV. t is the time that the vehicle spends on charging. ω is the capacity of its battery.

Solution of the model

A. Non-Dominated Sorting Genetic Algorithm (NSGA-II)

The goals of multi-objective optimization are to coordinate the relationship among the various objective function and find out an optimal solution that could get great objective function values. Up to now, there are many effective methods of solving multi-objective problems. Among them, a modified version of Non-Dominated Sorting Genetic Algorithm (NSGA), NSGA-II is widely adopted for its great convergence and robustness. In addition, the non-inferior solutions of NSGA-II distribute uniformly in target space.

The steps of NSGA-II solving multi-objective problems are as follows [5]:

1) Population Initialization.

The decision variables of coordinated charging model are the numbers of EVs that access to the grid in different time slots. Create initial population with the charging constraints as the boundaries.

2) Virtual Fitness Solution

A fast non-dominated sorting is made to the initial population in this step. Sorting needs to calculate two parameters of every individual: ni and Si. ni refers to the number of other individuals in the population dominated by individual i. Si is the collection of those individuals. Firstly, find out all the individuals whose ni=0, and store them in the collection F1. The elements in F1 are arranged in the first layer of fast non-domination sorting. Then, execute the operation ni-1, find out all the individuals whose ni-1=0, and store them in the collection F2. They are naturally in the second layer of sorting. Repeat these steps until all the individuals in the population are stratified.

Once the non-dominated sorting is complete, the crowding distance of every individual needs to be figured out. Calculate the two objective function values of individuals in each layer, and store them in arrays L1 and L2, respectively. For the individuals in the same layer, sort them in ascending order respectively, according to their two objective function values. Put the results in arrays L11 and L22. An individual's crowding distance is obtained by adding its values calculated in different objective functions.

3) Selection, Crossover and Mutation Operators

Selection operator chooses superior individuals according to the non-dominated sorting rank and crowding distance. Among the individuals on the same layer, the one with bigger crowding distance would be selected. For the individuals on the different layers, the one with lower layer number would be selected. Crossover and mutation operators make this algorithm have better local and global search performance for these operations would form new offspring population.

4) Elite Strategy

The aim of elite strategy is to make the superior individuals in the parent population enter the offspring population. Firstly, combine parent population and offspring population into a new one. Then, make a fast non-dominated sorting and calculate the crowding distance. Finally, create a new parent population that contains the first N satisfactory individuals selected by the selection operators.

The algorithm flowchart is shown in Fig. 1:

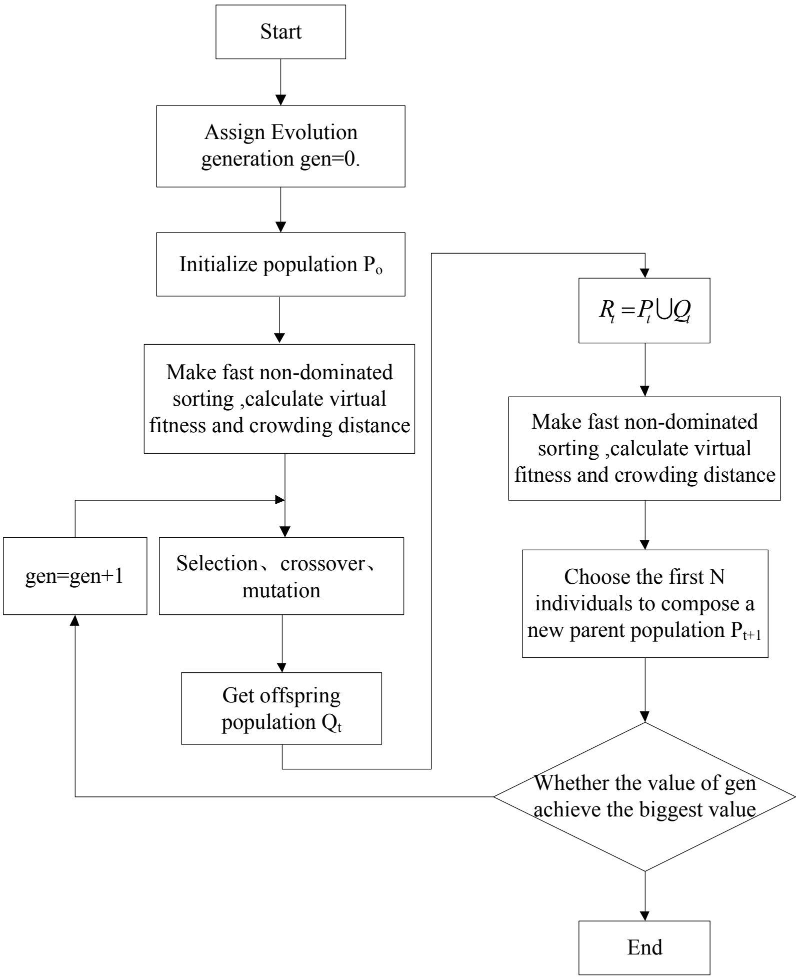
Start
Assign Evolution generation gen=0.
Initialize population P$_o$
Make fast non-dominated sorting ,calculate virtual fitness and crowding distance
gen=gen+1
Selection、crossover、mutation
Get offspring population Q$_t$
$R_t = P_t \cup Q_t$
Make fast non-dominated sorting ,calculate virtual fitness and crowding distance
Choose the first N individuals to compose a new parent population P$_{t+1}$
Whether the value of gen achieve the biggest value
End

Fig.1. The flowchart of NSGA-II

B. Case Study

A load curve in a local area is adopted as the original load curve in this case, with battery capacity set as 15 kW•h, rated charging power set as 3 kW and maximum charging power of a single EV set as 6 kw. Nind is the size of the population and is set as 100. Nvar is the quantity of decision variable and is set as 96. Maxgen is the evolution generation and is set as 500. Crossover probability is set as 0.9. Mutation probability is set as 0.9.

C. Result Analysis

Fig. 2 shows the overall load curve and conventional load curve of power grid in both coordinated charging and uncoordinated charging. Compared with uncoordinated charging situation, the power load of the EV in coordinated charging concentrates on flat period and avoid speak hours. And the power load transfers to valley hours with lower load at night. That is to say, coordinated charging can restrain power load fluctuations.

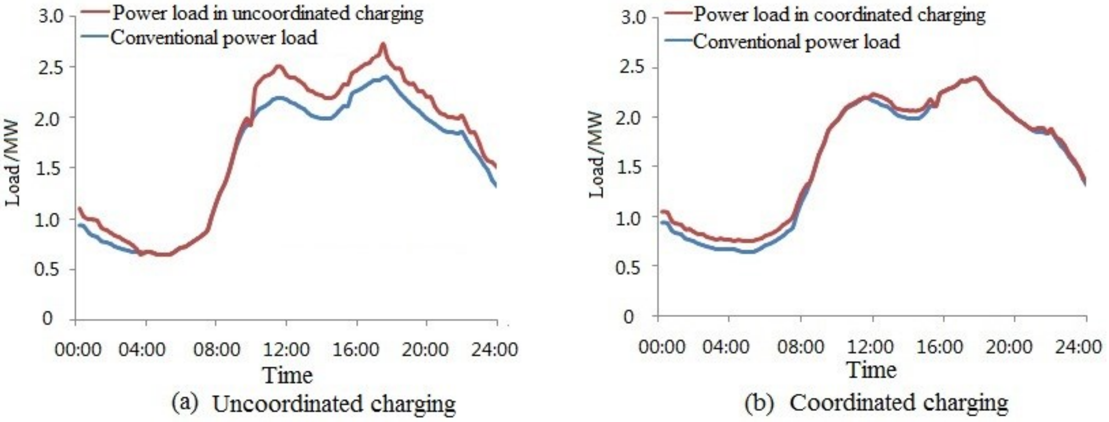

(a) Uncoordinated charging (b) Coordinated charging

Fig.2. Comparison between uncoordinated charging and coordinated charging

Conclusion

Coordinated charging of EV by means of electricity price regulation was studied from the perspective of DSM. It aimed for minimum electricity cost and restrain power load fluctuation. NSGA-Ⅱ is adopted in this multi-objective optimization. EV can be leaded to be charged in off-peak time in this way, which means that charging period can realize peak clipping and valley filling. It is proved via simulations that this coordinated charging method can restrain power load fluctuation effectively.

Acknowledgement

This research was financially supported by the key technology research, equipment development and demonstration of demand side resources to optimize the operation (Project No. GF-K/YD13005-YD).

References

[1] Wu Di, Dionysios C A, Ying Lei .Load scheduling and dispatch for aggregators of plug-in EVs[J].IEEE Transactions on Smart Grid,2012,3(1):368-376.

[2] Qinglai Guo, Yao Wang, Hongbin Sun. Factor Analysis of the Aggregated Electric Vehicle Load Based on Data Mining[J].Energies,2012,5(6):2053-2070.

[3] Richardson P, Flynn D, Keane A. Optimal charging of EVs in low-voltage distribution systems[J].IEEE Trans. on Power Systems,2012,27(1):268-279.

[4] CLEMENT-NYNSK, HAESEN E, DRIESEN J. The impact of charging plug-in hybrid EVs on a residential distribution grid[J].IEEE Trans on Power Systems,2010,25(1):371-380.

[5] Sungwoo B, Sugwoo B. Spatial and temporal model of EV charging demand[J].IEEE Transactions on Smart Grid,2012,3(1):394-403.

Applied Mechanics and Materials Vol. 596 (2014) pp 766-770
© (2014) Trans Tech Publications, Switzerland
doi:10.4028/www.scientific.net/AMM.596.766

A New State machine optimization method In the protocol conversion system

Li Qi[a] *

The Second Artillery Engineering University, Xi'an 710025, China

[a]liqiqimail@126.com

Keywords: Measurement and control system, test Instrument, Real-time data transmission, PXI.

Abstract. In the large-capacity, high-speed and real-time data acquisition and transmission, PXI bus have a widely application in the field of data acquisition and transmission. This paper introduces the design and implement of simplified state machine in the measurement and control system based on PXI bus. The results of test indicate that the technology is practical and valuable.

Introduction

PXI bus is a new openness, modular instrument. it is PCI bus standard in the expansion of the instrument field. It will make Compact PCI standard definition of the PCI bus technology development into suitable for experiment, measurement and data collection application occasion of mechanical, electrical and software standards, and the formation of a new virtual instrument system structure. For the purpose of regulating PXI to be the desktop PC performance to price advantage and PCI bus facing in the field of instrument to expand the combination perfect, thus forming a kind of mainstream virtual instrument of test platform [1], [2]. This paper introduces the design of a kind of measurement and control system in PXI simplified state machine technology, simple and convenient to PXI bus data collection, transmission, process control, focus on the state machine simplify the design and implementation of technology is expounded, and its performance testing and verification.

Measurement and control system by PXI bus special to bridge chip PCI9054, FPGA, CAN bus chip, isolation chip, related configuration chip and digital physical interface etc. For the whole system control FPGA core, PXI bus through the PCI9054 and FPGA connections, local bus for the management, and control by the FPGA analog and digital amount of output, input. Measurement and control system design in the CAN bus interface, mainly used in industrial field CAN bus equipment testing and monitoring.

PCI9054 interface timing realized

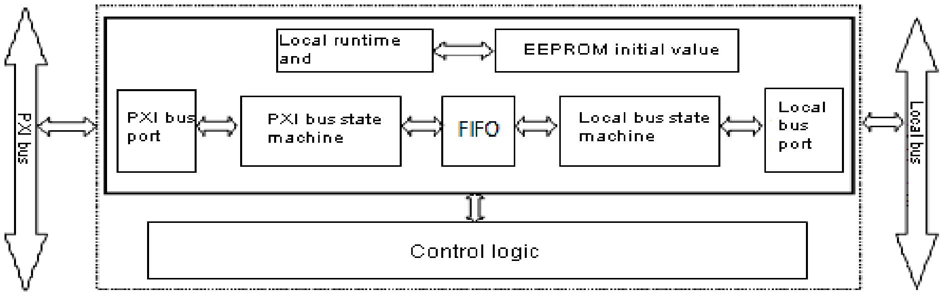

Fig.1. PCI9054 internal structure

Although PXI bus it has many merits, but the agreement is more complex, directly in the control design of FPGA difficult, therefore choose the dedicated interface chip PCI9054, can will complex PXI bus interface into relatively simple user interface, as long as the bus interface design after converting, it can achieve PXI regulate all the required hardware interface signal and the configuration space registers, special interface chip has low cost and universal, can effectively reduce the difficulty of the interface design, shorten the development time and better data transmission performance.

1.1 PCI9054 internal structure

PCI9054 internal structure as shown in figure 1 shows, it provides PXI, EEPROM, LOCAL bus three interface. PCI9054 as a bridging chip on PXI bus and LOCAL bus to deliver the message provided between, already can as two of the bus master control equipment to control bus, can also act as two bus goal equipment to response bus. PCI9054 has six zero wait programmable FIFO memory. They are complete PXI read, write operation launched, PXI target read, write operation and DMA read, write operation. Due to the existence of memory, data FIFO can be a sudden without loss of transmission. So not only meet the real time requirement, and at the same time according to the user's need to adopt the local PXI clock asynchronous frequency. Serial EEPROM is used in boot initial configuration of internal registers. Internal registers logo address mapping relation and the Local end work and PXI state, including PXI configuration register group, Local configuration register group, the Runtime registers group, DMA registers group, I2O news registers group. FIFO registers in the host computer and internal or LOCAL end are unified addressing, users can access them from both through the programming of each byte [3].

1.2 Simplified state machine to implement

PXI interface timing PCI9054 local bus can work in the M, C, J three modes. C mode of PCI9054 chip through within the logic control will address lines and cable PXI separate is convenient for local work timing offers all kinds of work way, programmable control is simple, and so also the tester chose PCI9054 C mode.

PCI9054 use LHOLD# and LHOLDA# as takes up local bus handshake signal, shake hands after the establishment of the use ADS# to mark a new transmission cycle begins. When ADS# (verb) effective, PCI9054 register get access to the internal new address (LA), then local bus (FPGA) can be sent to PCI9054 READY# signal to start a data transmission. BLAST# can make sign a transmission as the end of the cycle. Interface circuit receives LBE# to decide to use four data path of what paths data. LW/R# sign reading and writing data operation.

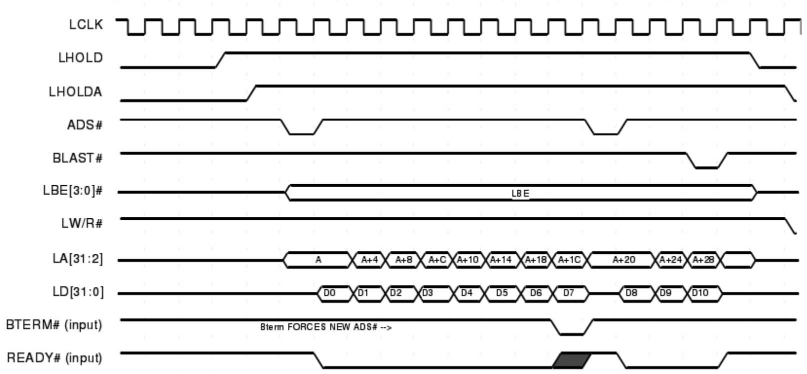

Fig.2. C mode PCI9054 DMA transmission sequence chart

Because the upper machine data transmission speed requirements, PCI9054 use DMA to attack transfer mode to meet. There are two PCI9054 DMA channel, can work independently, not interfere with each other. The DMA mode data, can save CPU resource; The sudden mode data can be improve data transfer rate, give full play to PXI bus data transfer rate, so make the advantage of high DMA and sudden data transmission used together. Work on the DMA mode, PCI9054 as the Lord equipment of

PXI bus, is also a Local bus controllers, by setting up its internal registers DMA controller can be realized the data transfer between two bus. PCI9054 DMA transmission process involves registers control including set mode registers, set PXI address registers, set up the side of the address space PXI bus, the setting of the LOCAL address registers, set transport count registers, set describe registers and set command/status register. Figure 2 for PCI9054 in C models under the local bus data transmission a DMA timing diagram [3].

From figure 2, the operation of the local PCI9054 signal is several law, can use the state machine to achieve. The way of state machine working is according to the control signal predetermined state of the order, the state machine is pure hardware number system of sequence control circuit, operation mode similar to control flexible and convenient in operation, and the CPU speed and working reliability are better than the CPU [4]. Through the state transfer diagram design means can will PCI9054 complex sequence control visualization into state conversion between relationships, problems are simplified [5].

Common state machine have more working condition, conversion condition, so that the design relatively complicated increased difficulties, less useful. Therefore, design a kind of only four the status of the state, that is, s_idle simplified machine (idle state), s_decode (decode state), s_wait (wait states), s_xfer (transfer status), which s_xfer LW/R# according to judge is to write operation or read operation, so greatly reduced

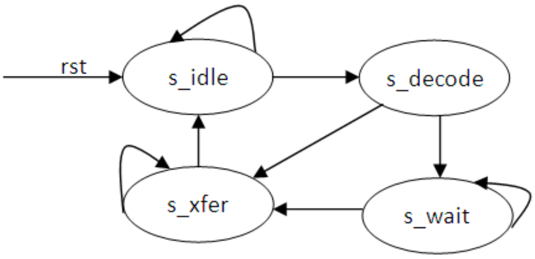

Fig.3. PCI9054 local end state machine conversion figure

State machine transition conditions as is shown in table 1

Table 1 State machine state transition conditions

	Statelni	The Goal State	Transition Condition
1	S_idle	S_idle	(!qlads)+ (qlads).(sr)
2	S_idle	S_decode	(qlads).(sr)
3	S_decode	S_idle	(sr)
4	S_decode	S_wait	(!ready).(!sr)
5	S_decode	S_xfer	(ready).(!sr)
6	S_wait	S_idle	(sr)
7	S_wait	S_wait	(!ready).(!sr)
8	S_wait	S_xfer	(ready).(!sr)
9	S_xfer	S_idle	(!i_lbterm).(!lblast).(sr)+ (!i_lbterm).(!lblast)+ (!i_lbterm)
10	S_xfer	S_xfer	(!i_lbterm).(!lblast).(sr)

Simplified state machine technology application

As shown in figure 1 shows, the control system design the PXI CAN bus interface.the interface is used mainly in the field of engineering of the devices on the CAN bus testing and monitoring. PC and CAN bus data format protocols as shown in chart 2.

Table 2 Data transmission format

Frame type	Frame ID	Data length	Data
Extended	4bit	1bit	8bit

For the upper machine CAN bus to send data code fragment:

```
… if (ds_xfer = '1' and ds_write = '1' and la_h(31 downto 30) = "10" and la_l(4) = '1')then
casela_l(3 downto 0) is
when X"0" => REG16 <= ld;
when X"F" => REG31 <= ld;
               end case;…
```

On a piece of code realization of the upper data will be sent to register for a CAN bus to literacy make CAN signal will be sent to data CAN bus.

```
… if(f040_wr = '0') then
case(wr_f040_data_cnt)is
when 0 => f040_data <= REG16;
…
when 12 => f040_data <= REG28;
when others => f040_data <= "ZZZZZZZZ";
         end case; …
```

This function is sent the data of the register to the CAN mouth, and realize the upper machine CAN send data to a CAN bus.

Measurement and control system to control the choice of core FPGA

Based on FPGA chip high-speed, high level of integration, programming flexibility of advantages, PXI measurement and control system for control of FPGA device to the core, the hardware description language programming VHDL design, can achieve its ease of use, reliability, maintainability, stability and can be easily realized data of continuous collection, transmission and storage. According to the program, the scale of measurement and control system of the company XILINX SPARTAN-3 E series of XC3S500E FPGA. The FPGA has 500000 system, a Slice door number 4656, most will provide 232 I/O, 73 Kb of RAM capacity, distributed 360 Kb of RAM capacity, 20 of special on time-multiplier, four DCM (Digital Clock Managers), the biggest difference I/O logarithm for 92, is the highest cost-effective XILINX FPGA chip company.

Conclusion:

This paper introduces a kind of simplified PXI measurement and control system state machine technology, focusing on the design and implementation of this technology is discussed, and through the concrete application of the technology was performance test. By test, this technology has good generality, high reliability and stability, and can satisfy the industrial field capacity, the performance of the high speed data acquisition and transmission requirements, and has high practical value.

References

[1] Xu Tao. Design and Optimization of PCI Bus HDLC Processor[D]. Nanjing: Southeast University(2005),p.25-47.

[2] Liu Yanjun, Yan Haixia. Application of CRC during HDLC Protocol[J]. Electronic Measurement Technology, 2010(33),p.21-23.

[3] Li Xiaojuan. HDLC Design Realization Based on FPGA[J]. Modern Electronics Technology, 2007 (6) ,p.35-37.

[4] Ying Sancong. HDLC Protocol Controller Based on the FPGA [J]. Journal of Sichuan University, 2008 (40) ,p.116-120.

[5] Pan Song, Wang Guodong. VHDL Practical Tutorial [M]. Chengdu: University of Electronic Science and Technology Press(1999),p.158-169.

CHAPTER 10:

Communications Technology and Materials

Applied Mechanics and Materials Vol. 596 (2014) pp 773-781
© (2014) Trans Tech Publications, Switzerland
doi:10.4028/www.scientific.net/AMM.596.773

Design and Implementation of USB Coordinator Based on Z-Stack

Zhicheng Jiang, Shudan Lee, Jinyin Chen, Zhangjian Qin, Renfei Yu

Chengdu University of Technology, Chengdu, China

Chengdu University of Technology, Chengdu, China

Chengdu University of Technology, Chengdu, China

Chengdu University of Technology, Chengdu, China

University of Electronic Science and Technology, Chengdu, China

jiangxiaocheng0221@gmail.com, mitnad.shudan@gmail.com, chjy@cdut.edu.cn,
70225302@qq.com, yrfzh@hotmail.com

Keywords : ZigBee, CC2530, RFX2401C, FT231X, USB coordinator

Abstract

Ecological agriculture is increasingly relying on mobile technologies to monitor the growth of plants, however, the traditional management efficiency is low and waste resources. So, a USB coordinator based on ZigBee-Stack is designed. ZigBee is a low rate, low power consumption wireless communication technology, which can be commonly used in Wireless Sensor Network (WSN). WSN is composed of hundreds sensor nodes, all of the information from these nodes will be sent to the coordinator, so the coordinator undertakes the task to collect and process data information, and also as the interface of the network with users. The design of the coordinator is based on CC2530 chip, and RFX2401C chip is superposed on it. A software was compiled to test the data transmission distance. The results show that the distance was increased by 40-60 meters and RFX2401C chip uses only two pins of CC2530 chip. So the improved coordinator is more cost-savings and efficient.

Instruction

The Internet of things has developed rapidly in recent years. Wireless Sensor Network (WSN), which is essential to create the Internet of things, has made a profound impact on people's production and life. So it has become the research focus of the Internet technology industries. ZigBee, a low-cost, low power consumption and high reliability short ranged wireless communication technology, is widely used in industrial control, intelligent household, agricultural production, medical care and other fields. [1,2] As a new technology, the advantage of the ZigBee wireless sensor network can be not ideal, because the coordinator processing ability is limited. However, there are some shortcomings such as time delay, packet loss and senor node out of control. Some researchers do tests used the coordinator just based on CC2530 chip [2], so an improved coordinator is designed to improve the performance of ZigBee wireless sensor network. Moreover, wisdom agriculture is a new kind of modern agricultural production mode, which can improve production by using this design to monitor plants in real-time.

System design

ZigBee sensor network often comprises three notes, coordinator node, the end device node and the router node. The coordinator, which is the key equipment in a ZigBee network, is mainly responsible for network construction and communication with the host computer. RS232/485 interface is commonly used in data transmission nowadays, but the speed is slow because it occupies more hardware resources. End device is mainly responsible for data collection and uploading and routers are used to data exchange and control.

This paper mainly completed the coordinator hardware and software design. Hardware design includes ZigBee radio frequency (ZigBee-RF) module and the USB - UART serial port conversion module, they are mainly used for data transmission. Software design is based on Z - Stack protocol Stack, and it responsible for data acquisition and analysis. Mesh topology is used to realize multi-hop routing and increase the transmission distance of data. There are two end device notes and a coordinator node in this network. This wireless sensor network is shown in figure 1.

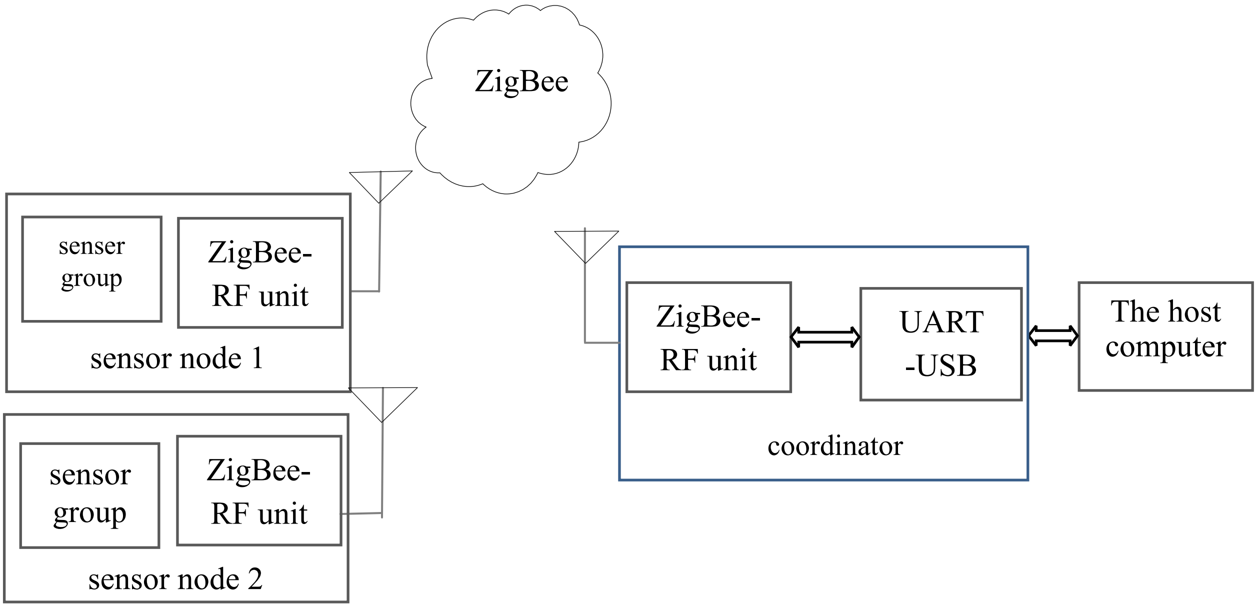

Fig. 1 The wireless sensor network

Coordinator hardware system design

ZigBee coordinator is a device to start and configure the network. It can preserve the binding cache used by indirect addressing as well as design the Trust Center and execute other tasks. It is the core of the entire wireless sensor network. ZigBee-RF module is responsible for creating ZigBee network, distributing the physical address for each sensor node, sending acquired data or control command to the terminal equipment and submitting processing results to the host computer to analyze or save; main function of the USB - UART serial port conversion module is to send the data to the host computer by the serial ports operate mode, which is more efficient and reliable. This module as the base of the ZigBee-RF module, the module as the base of ZigBee-RF module, when the RF module fails, it can be replaced by a new module instead of re-creating another circuit, and it is relatively cost savings. Moreover, the transmission rate of the USB bus is higher than the RS-232 (a standard for serial communication transmission of data) and it supports hot-swap, which is more convenient for users.

The ZigBee-RF module uses CC2530F256 TI chip produced by Texas Instruments (TI) [3]. CC2530 is a system-on-chip (SoC) to provide solutions for the ZigBee, and it can create multiple network nodes but is very low-cost. The chip has a RF transceiver with excellent performance, an advanced 8051 microcontroller, a programmable flash memory FLASH and a RAM with 8KB memories, so it has high sensitive and strong anti-interference.

In order to increase the output power and the transmission distance and improve the sensitivity, a low-power RF front-end amplifier module RFX2401C [4,5] is added on the CC2530 chip. RFX2401C is a pure CMOS RF front-end IC (RFeIC) produced by RFaxis. It provides high-performance, low-cost, highly integrated solutions for wireless audio, home automation and other fields. A portion of CC2530 and RFX2401C connection circuit is shown in Figure 2.

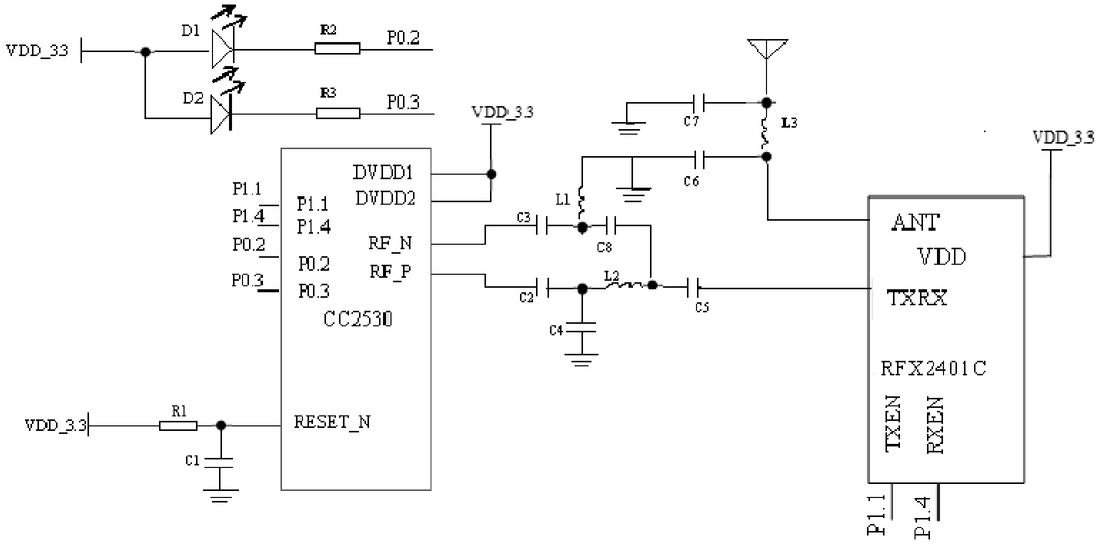

Fig.2 LED-D1 is the RF power indicator, LED-D2 is used to display the connection status of the network; P0.2 and P0.3 are used for serial communication pins;

RFX2401C is used to increase the output power, RFX2401C has a control logic Truth Table shown in Table 1. RFX2401C has just two control pins, P1.1 and P1.4. They are controlled by the logic from Table 1: If RXEN remain high, which means P1.4 = 1, TXEN has a decision whether to send and receive data. Compared to the reference [5], P0.7 can be used freely in this design. So it can save pin resources.

Table.1 Control logic Truth Table of RFX2401C

TXEN	RXEN	Operating Conditions
1	x	TX Active
0	1	RX Active
0	0	Chip is Shut-down

USB (Universal Serial Bus) is gradually becoming common computer and peripheral interfaces for its high transmission speed, less resource occupied and plug and play technology. It can theoretically support simultaneous connection of up to 127 external devices, so it is a good solution to problems such as resource conflict, interrupt request (IRQs) and other issues. USB-FT231Xs module composes of FT231Xx chip, voltage conversion circuits, power supply circuits and some indicator components. FT231X [6,7] is a USB to serial chip produced by FTDI company. It has partially improved compared with FT232 series. For example, FT231Xs simplifies design and reduces the number of external components through highly-integrate multiple programmable (MTP) memory and removing the external crystal clock circuit. FT231Xs has following characteristics: it has fewer pins than FT232 chip but it is more powerful in functions; it realize USB protocol on the chip, without having to develop specialized firmware; using buffer stationary technology to improve the ability of handling data; I/O pin driver, the drive current at 4mA ~ 16mA, can drive multiple devices at the same time; it has internal integrated power-on reset circuit and RC decoupling circuit.

FT231Xs is composed of USB protocol engine, USB transceiver, universal asynchronous receiver FIFO controller (UART FIFO Controller), 2048 bytes multiple programmable (Multi-time Programmable, MTP) memory, 12MHz oscillator etc. [7] The USB protocol engine control port for USB peripheral data flow management; USB transceiver provides USB2.0 full-speed data transmission, and it has a size of 512 bytes buffer to handle data. UART FIFO Controller is responsible for transferring data between the buffer and UART transceiver registers; MTP memory is used to store device descriptor and control bus I/O port configuration information, and it provides FT231X with pre-programmed functions. In addition, system designers can also use MTP memory to store the data from the user layer.

FT231X communicates with CC2530 through TXD and RXD pin. USB devices use bus power for the power supply, and the power with bypass capacitors and decoupling capacitors is used to improve the anti-interference ability. FTDI offers a free virtual serial port (Virtual Com Port, VCP) driver, meeting the demand for virtual serial ports in most cases. The specific circuit is shown in Figure 3. If users want to develop their own drivers, you can write the necessary drivers in MTP memory of a FT_PROG software provided FTDI company.

In order to make FT231Xs and CC2530 have stable working voltage, a linear regulator MCP1702 is used to obtain 3.3V supply voltage, the circuit is simple, so there is no point to mention it.

The sensor terminal node composes of a small size, low power consumption digital temperature and humidity sensor SHT75 and light sensors TPS851, these are responsible for collecting the indoor temperature, humidity and light intensity. Moreover, a SMD buzzer DET501 is added on the chip to simulate abnormal alarm. This circuit is shown in Figure 4.

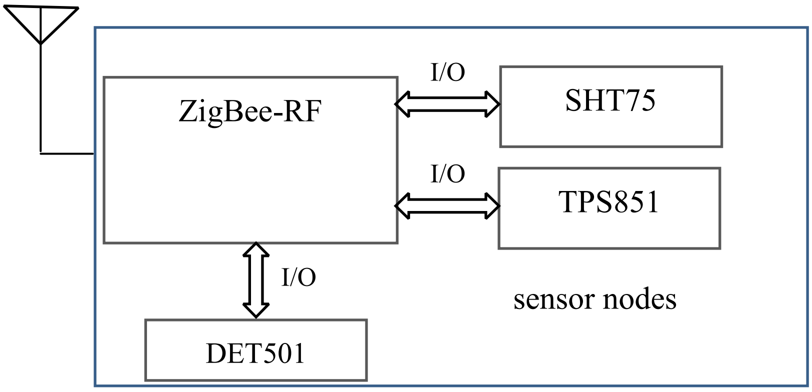

Fig.4 The circuit of sensor note

Design of data acquisition software based on ZigBee protocol stack

ZigBee communicating protocol is composed of PHY, MAC, which is defined by IEEE 802.15.4 and NWK, APL, provision of security service layer, which is defined by ZigBee Alliance[8].

Like seven layer models of OSI, lower layer protocol provides specific services for the upper layer protocol in ZigBee protocol stack, and each service entity provides specific service through SAP. NWK of ZigBee is abstracted into NLME and NLDE to provide services for APL; MAC is abstracted into MLME and MLDE to provide services for NWK. The network establishing process of ZigBee coordinator expressed by Service primitives is shown in figure 5.

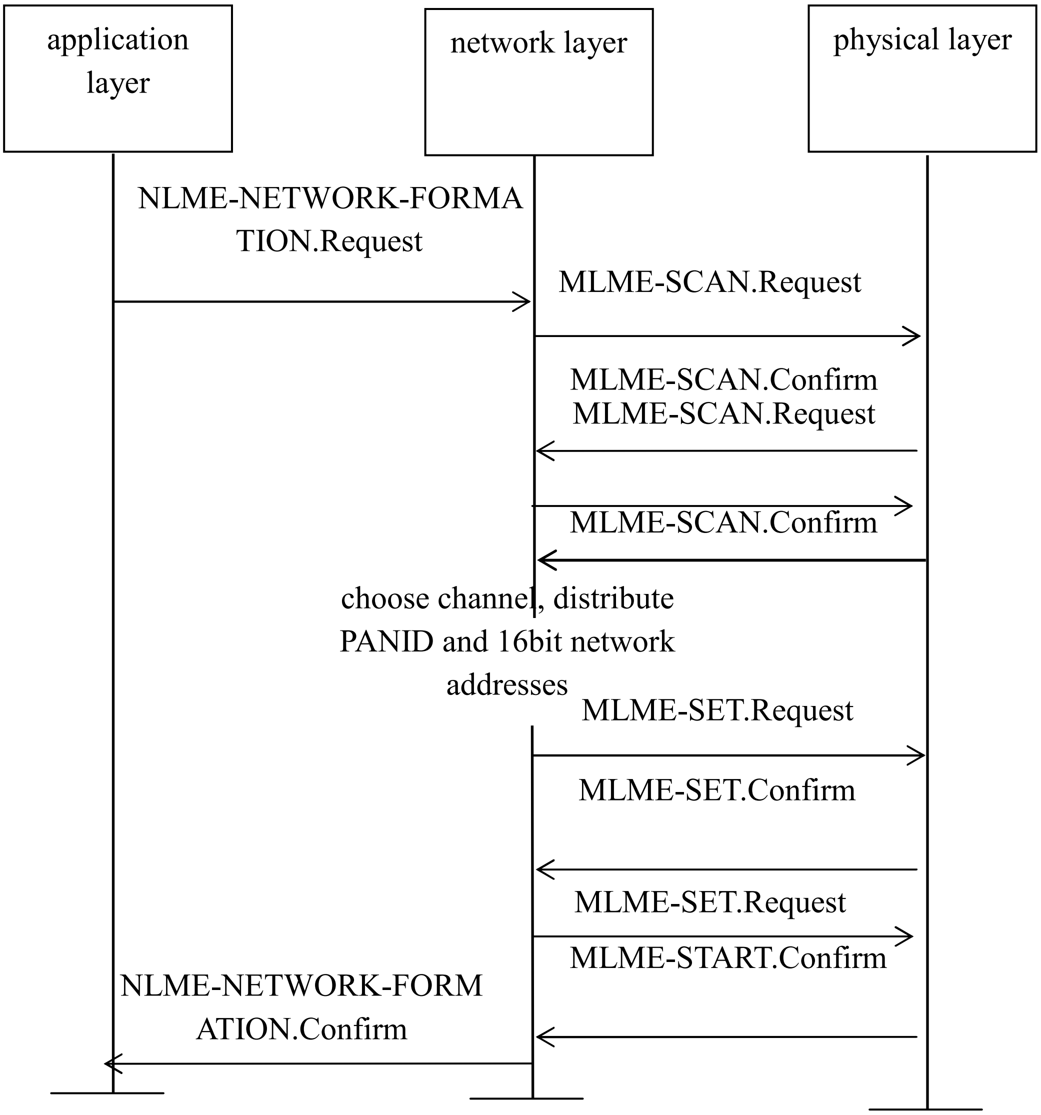
application layer
network layer
physical layer
NLME-NETWORK-FORMATION.Request
MLME-SCAN.Request
MLME-SCAN.Confirm
MLME-SCAN.Request
MLME-SCAN.Confirm
choose channel, distribute PANID and 16bit network addresses
MLME-SET.Request
MLME-SET.Confirm
MLME-SET.Request
MLME-START.Confirm
NLME-NETWORK-FORMATION.Confirm

Fig.5 The network establishing process of ZigBee coordinator

If there is no ZigBee network existing before coordinator network establishing, NLME sends primitive MLME-SCAN.Request to MAC to conduct energy detection and active scanning in all default channels, when NWK receives APL network primitive establishing request NLME-NETWORK-FORMATION.Request. MAC feeds back scanning result to NLME, then NLME chooses a proper channel(channel number is selected in 11-26) to assign PANID(Personal Area Network ID)and 16bit short network address(the default is 0X0000) for new network.

MacPANId of the MAC is set to choose PANID through primitive MLME-SET.Request, then NLME send request to MAC layer to run network using primitive MLME-SETART.Request. The new state of the network is fed back to the network layer by primitive MLME-START.Confirm, then NLME sends NLME-NETWORK-FORMATION.Confirm to APL and its state value is returned by MLME-START.Confirm. ZigBee network is successfully established.

A IAR Embedded Workbench is used as the software development environment and adopt ZStack-CC2530-2.4.0-1.4.0 which is published by TI and complied with ZigBee2007 standard as Z-Stack protocol stack. Z-Stack provides multitask processing mechanism by OSAL (Operating System Abstraction Layer) and accomplish scheduling of multitask through time slice polling mechanism. OSAL schedules correspond task-processing function to operate tasks in terms of priority of the task. OSAL provides several API (Application Programming Interface) functions[10] for users in convenience of conducting related development design.

The process of Coordinator network establishing shown in figure 5 can be accomplished by task processing function ZDApp_event_loop() automatically. Task function schedules function ZDO_ startDevice() to initiate devices in the network like coordinators, routers and terminal nodes. Function ZDO_StartDevice schedules function related to the network management: The network discovers the network establishing request NLME_NetworkFormationRequest(), then initiates functions like NLME_StartRouterRequest. After devices powered on， schedules function ZDO_StartDevice is used to establish a network or apply to join the network.

ZigBee protocol formulates the binding mechanism, binding is a kind of control mechanism of information flow among application devices, which allows an application program to send a packet without knowing the target address. The sensor's information like address, interface number, attributes marking character are stored in the binding table of coordinator through binding and the communication among nodes can be easily achieved according to binding table. The communication method allows sensors to transfer to dormant state periodically and to be roused to transport data. In the stimulation, the binding request is set to true to correspond to the binding request sent by a sensor node after the coordinator network establishing is accomplished. The sensor node schedules NLME_NetworkDiscoveryRequest() after powered on. If there is an available network, then the node sends a request to join the network (using LME_JoinRequest()) and binding(using ZDP_BindReq()function). After the binding, the node sends the data of temperature, humidity, light intensity, RSSI(Received Signal Strength Indication) to coordinator, if there is no response, then remove this binding and detect the channel again to search network. The workflow of the ZigBee coordinator node is shown in the figure 6.

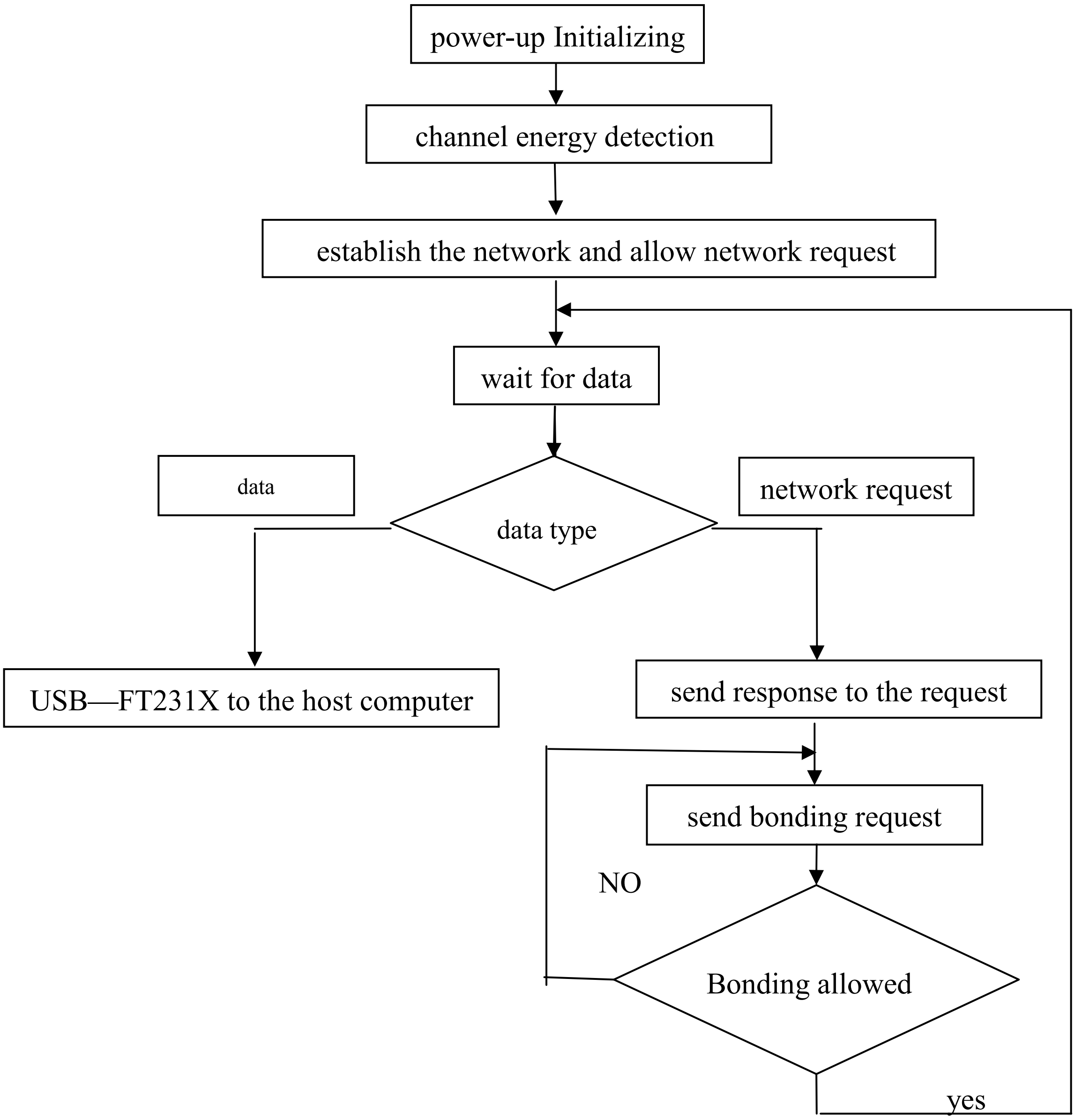
power-up Initializing
channel energy detection
establish the network and allow network request
wait for data
data
data type
network request
USB—FT231X to the host computer
send response to the request
send bonding request
NO
Bonding allowed
yes

Fig.6 The workflow of the ZigBee coordinator

The interface of the host computer

The interface of the host computer is compiled in C #. NET. The Microsoft Sql Server is used to store collected data to facilitate the management and analysis. Users can monitor the network topology the quality of the network, real-time information about temperature, humidity and light intensity through this management software, and they can also set up their own data acquisition cycle. If the sensor node receives abnormal data, and it can send up abnormal warning to the host computer, using the internal buzzer to satisfy the users' desire for information. The interface with data of temperature, humidity and light intensity is shown in Figure 7.

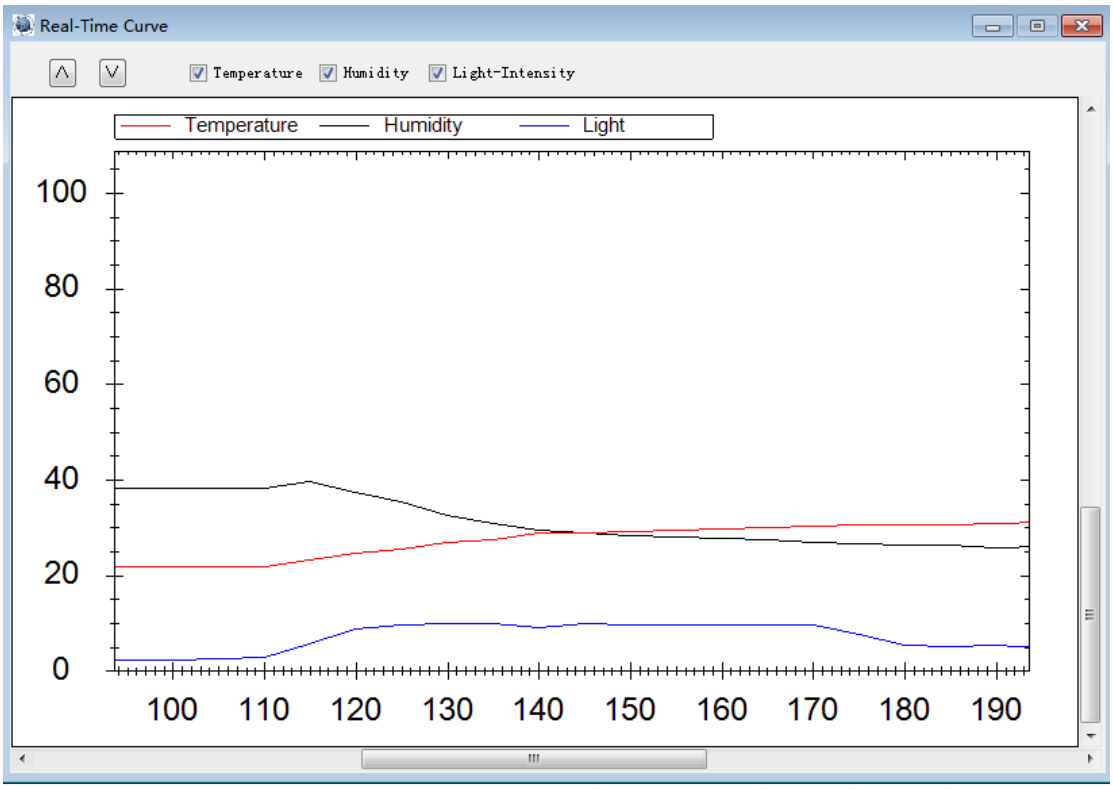

☑ Temperature ☑ Humidity ☑ Light-Intensity

Fig.7 The interface with data of temperature, humidity and light intensity. The lateral axis represents time, whose unit is second.

Conclusion

In this engineering design, the design and implementation of the coordinator is based on the ZigBee protocol, which uses USB to communicate with a host computer. CC2530 low-power amplifier module with RFX2401C is used to increase transmission distance; coordinator communicates with the host computer through hot-swap USB interface. The interface displays the node status in real time, and the data is stored on the local host computer, which facilitates the monitoring of the environment of growth of plants. The sensor with routing function can increase the transmission distance and make the network more stable. The RF module and the serial converter module are connected by slot, and it is easy to exchange the module if damaged. Practical tests have made the following conclusions: The coordination is characterized by simple operation, low cost and easy extension. It provides a feasible reference to other data collection sensor network coordinator.

Acknowledgements

This work was financially supported by the Sichuan Science and Technology Support Program (2014SZ0111).

References

[1] ZigBee Alliance.ZigBee Specification 2012 [S] USA: ZigBee Alliance, 2012

[2] Lei Wan, Yong Zhang, Jian Li. Intelligent home design ZigBee wireless sensor networks [J] Based Electronic Technology, 2012,02:116 -119 In Chinese

[3] Texas Instrument.CC2530 Datasheet 2009 [S] USA: Texas Instrument, 2009

[4] RFaxis.RFX2401C Datasheet [S] USA: RFaxis, 2011

[5] Weicong Zhang, new weapons, Zhongcheng Li, CC2530 and ZigBee protocol stack based on the design of wireless sensor network nodes [J]. Computer Systems Applications. In Chinese

[6] Baozhao Wei, Lin Wang, Qi Xu, Yunfei Li Design USB-RS232 converter module for the FT232R [J] Based on Computer Knowledge and Technology. 2008,07:1204-1206+1220 In Chinese

[7] FTDI.FT231X Datasheet Version 1.0 [S] USA: FTDI, 2012

[8] ZigBee Alliance. ZigBee Specification 053474r17 [S]. ZigBee Alliance, 2008

[9] Yingying Zhang, Zhushuang Dong , Ding Xin . ZigBee-based data acquisition system [J]. Ningbo University (Science and Technology). 2009,03:313-316 In Chinese

[10] Wenzhong Li, jade and other. ZigBee2007/PRO segment toward the stack experiment and practice [M] first edition, Beijing: Beijing University of Aeronautics and Astronautics Press, 2009:133 -141 In Chinese

Applied Mechanics and Materials Vol. 596 (2014) pp 782-787
© (2014) Trans Tech Publications, Switzerland
doi:10.4028/www.scientific.net/AMM.596.782

Design of Intelligent Underground Sound Bird Repellent System Based on Wireless Communication Network

YIN Xijie[1,a], LinJian[2,b], SHAO Zengzhen[2,c,*]

[1] School of Information and Technology, Shandong Women's University, Jinan, 250002, China;

[2] School of Information Science and Engineering, Shandong Normal University,Jinan,250014,China

[a]xijiesd@126.com, [b]512642360@qq.com, [c]shaozengzhen@163.com

Key Words: intelligent bird repellent, wireless communication, short wave station

Abstract: Aimed at problems nowadays existing in airport bird drive, an intelligent underground sound repellent system is designed. Combined with characteristics of bird behaviors and psychology, an intelligent wireless bird repellent system in the form of sound repellent gun array is built. This system has been applied by many aviation units, which can effectively reduce bird disaster in the airport with good practical effects.

Introduction

Aviation safety problem has always been brought to the attention of the countries all over the world, and the "bird strike" problem, because of the seriousness of the harm and the complexity of prevention and control, has been a long-term problem bothering aviation world . According to the international civil aviation statistics, a total of about 10000 bird accidents occur every year all over the world, vast majority of which happen when the airplane climbs, lands and glides. At present, airport bird repellent equipments include simulation robot and raptor, gas gun, electronic firecrackers etc. Through sound, movement, cry and other forms, they drive birds in and around the airport [1][2]. The Doppler detection intelligent bird drive device designed by Li Kun etc. from China [3] can detect birds by Doppler technology. The ultrasound wave bird drive device based on infrared induction designed by Min Jianping etc. [4] analyzes induction principle of pulsed infrared sensor, and introduces ultrasound wave bird drive technology. An Huizhen [5] designs laser scanning system. By use of the characteristic that birds are sensitive to green light beam, sensory stimuli are achieved.

The above bird repellent devices have some defects, which are shown in: 1) with large size, big height and hard material, they can't be assembled close to the airport runway, thus weak in driving birds; 2) most of them adopt random driving method, and space-time cross relations between birds and the plane isn't considered; 3) long time exposed to external environment, the device costs a lot in maintenance; 4) the device operates independently, thus effective linkage is hard to develop. Aimed at the above problems, combined with characteristics of bird behaviors and psychology, this paper designs a set of wireless communication-based intelligent underground sound repellent system. The system turns "passive driving" to "active training". Through effective operation of the device, birds are trained to keep away from aircrafts, thus improving driving effect. This set of system has been put into use in many aviation units, and the effect is good.

Design principle of the intelligent underground sound repellent system

Fronted of the intelligent underground sound repellent system is called sound repellent gun, which can rise and fall automatically according to needs and stimulate the sound made by plane when passes. The sound repellent gun is normally buried underground to prevent aircraft accidents.

According to the principle that sound superimposes to transmit in stereoscopic space and the rules of bird activities, sound repellent guns are distributed on both sides of the airport runway. In accordance with the characteristic that aircraft-bird strike tends to happen at the take-off and landing ends, thus the smaller the distance to both ends of the runway, the denser the distribution. Location of birds, flight direction and speed will form a vector on the ground, the system control module will control the corresponding multiple sound repellent guns in the sound repellent system to continuously perform action according to features of the vector, thus forming a sound barrier to stop the birds flying towards the runway, and keep it away from the runway. As a result, pertinence and continuity of drive is improved. Physical distribution schematic of the sound repellent system is shown in Fig. 1 as follows.

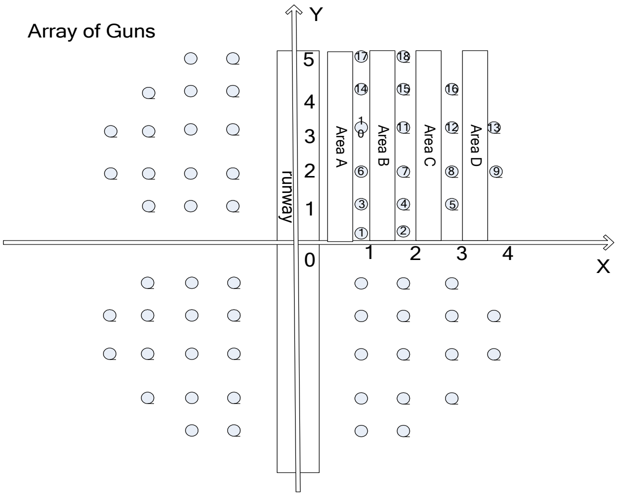

Figure 1 Physical Distribution Schematic of the Sound Repellent System

In Fig. 1, with direction of the airport main runway as y axis, runway central point as origin of coordinates, rectangular plane coordinate system is built and sound repellent guns are distributed along both sides of the runway according to rules. Take the example of the first quadrant; the gun array includes 6 rows and 4 columns, numbered from 1 to 18. When the system operates, control in horizontal and vertical direction can be separately considered.

2.1 Control Design in Horizontal Direction (X axis direction)

In Fig. 1, according to the importance, the first quadrant is divided into four areas (A/B/C/D) in vertical direction, among which $0<x<1$ is area A, $1<x<2$ is B, $2<x<3$ is C and $3<x<4$ is area D. When the birds are in some area, there are three situations according to its flight direction: direction 1: flying towards the runway; direction 2: flying in the direction of the runway; direction 3: flying away from the runway. According to the location of the birds and its flight direction, 12 kinds of flight methods can be designed. The system can set different solutions specific to different flight methods.

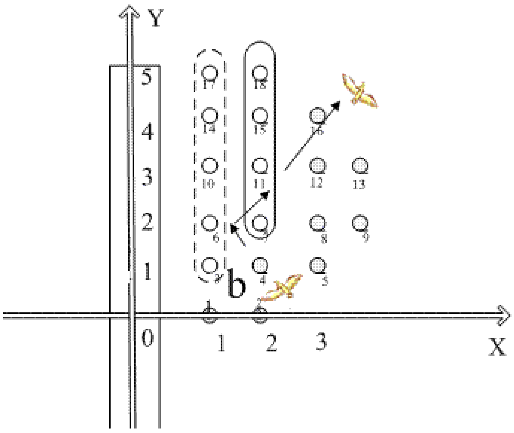

Figure 2 Controls in Horizontal Direction

Fig. 2 is a bird repellent example of the system. The bird is initially near No. 4 sound repellent gun flying towards the runway. As a big threat to the plane, measures must be taken to drive it away. The continuous arrows show the desired flight direction of the system. According to the flight vectors formed in the process, the system after judgment can drive the sound repellent guns within the dotted box to start after finding the bird, thus forming a sound wall which compels the bird to fly away from the runway; besides, the sound repellent guns within the solid box can start a while later. In this way, with collaborative operation of all sound repellent guns, the bird can be compelled to change its original flight track and fly away from the runway as expected.

2.2 Control Design in Vertical Direction (Y axis direction)

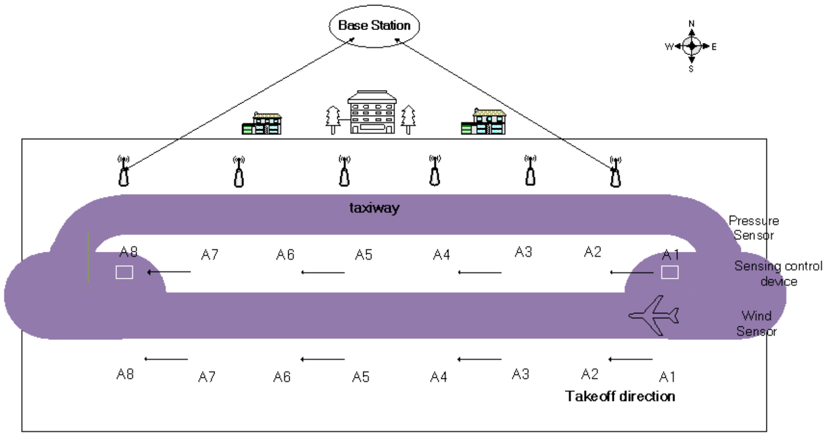

Figure 3 Controls in Vertical Direction

The vertical direction(Y axis direction) refers to the runway direction, i.e. the direction in which plane takes off and lands. Cross bird drive of the horizontal and vertical directions can realize the effect of bird drive covering the whole airport. The following introduces the principle and realization method of bird drive in vertical direction.

Before the plane takes off, the sound repellent system will stimulate sound of the plane when taking off and successively send out bird drive signals, then the plane truly takes off. This is in fact telling the birds “the plane is taking off, hasten to avoid”. From the view of birds’ psychology, birds are unwilling to collide with such a colossus like plane, since they know that knocking into the plane will certainly lose their lives. Characteristics of the system lie in: fully making use of birds’ learning ability and their fear to take-off and guiding them leave the airport before the plane takes off.

The specific realization method is: some wind and pressure transducers [6] are installed at the curve between taxi track and runway to judge take-off time of the plane. After start, the sense control device will send start command to sound drive gun A1. A1 start operation and successively generate A2-A8 according to the time control module of the system. Sound production order of all underground sound repellent guns is from A1 to A8, which stimulates boom of the plane and can form loud sound in the direction of runway before take-off to drive the birds away; meanwhile, the following boom when real plane takes off also tells the birds that danger is coming. When sound repellent guns finish playing, they will automatically hide underground. Such design will have no effect on take-off and landing of aircrafts in the airport, and as well reduces tolerability of the birds.

Network topology and control method

This system mainly uses the combination of sectional automatic control and manual control. At take-off stage automatic control is given priority to and manual control is complementary; at landing stage manual control is given priority to and automatic control is complementary. Here introduces the network topology and realization method of this system.

This system adopts two-layer wireless network transmission mode. The upper layer is shortwave radio network [7], and the lower layer is Zigbee wireless communication network [8-10], which are connected by signal conversion module. Taking into consideration particularity of airport signal and instability and delay of message transmission, traditional GPRS communication is given up. Network topology structure is shown in Fig. 4.

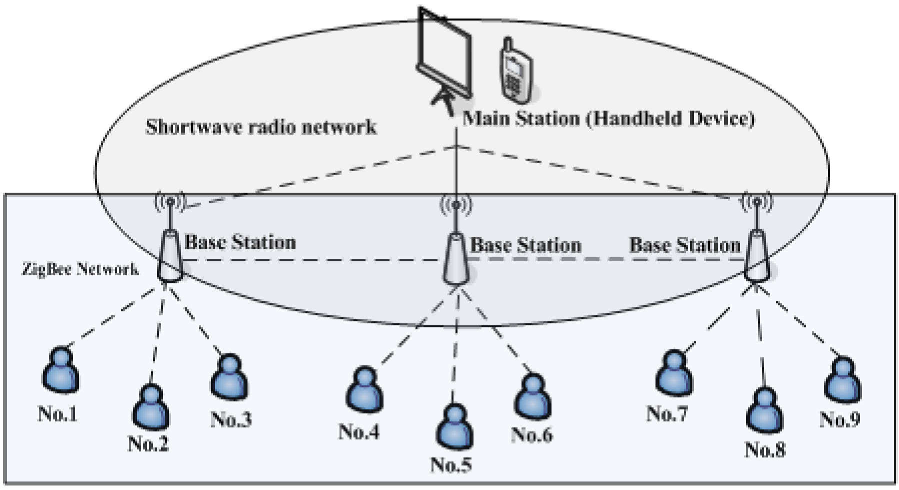

Figure 4 Network Topology Structure of the System

The above network topology structure mainly includes master station, base station and bird repellent equipment, and network information transmission is mainly composed of shortwave radio communication and ZigBee network communication. The whole system falls into 2 layers: base station equipment layer and sound repellent gun equipment layer. Signals are transmitted via wireless station between master station and base station as well as among all base stations. There are also radio station and ZigBee modules in base station, which are directly connected by wires. ZigBee network is short distance wireless transmission, mainly used for connecting sound repellent gun equipments; while sound repellent guns are connected via ZigBee module, named as sound repellent gun equipment layer.

Here is an example explains control process of the above system. Suppose length of the airport is 3250 meters and the width is 500 meters, divide the airport into 5 areas along direction of the runway, width of each is no more than 650 meter and set at least one base station in each area. Signal transmission radius of the base station is 650-1300 meter and coverage area of the main station is about 500 meters, as shown in Fig. 5.

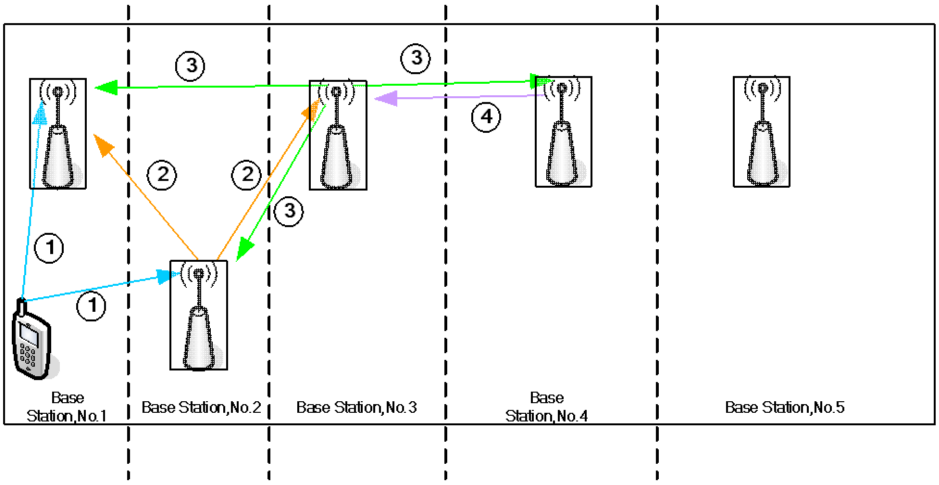

Figure 5 Schematic of System Control Process

In Fig. 5, handheld device is in area 1# hoping control the sound repellent gun equipments in area 4#. The control process involves two steps: first is the signal transmission process on base station layer and second is the signal transmission process on sound repellent gun equipment layer. Transmission process of the signal on both layers is similar, thus we only take the example of transmission on the base station to explain operation process of the system.

Suppose base station equipments 1# and 2# are both within coverage area of handheld device. When receiving signals, base station 1# will analyze and find out object area code of the signal is different from its own code, and then transmits this signal directly via radio network. Meanwhile to prevent signal shock it will keep silent for some time, during which it won’t receive any commands from other base stations. Base station 2# can also receive the same signal, transmit it after judgment and keep silent. By this analogy when receives signal, base station 4# decides if the object area code of the signal is the same with its own code, converts the signal into ZigBee mode by the signal conversion module on the base station and then send it to the sound repellent guns network on lower layer via ZigBee module.

In Fig. 5, the two arrows marked with ① represent transmission path of the signal sent by handheld device and the signals are separately transmitted to base station 1# and 2#; the arrows marked with ② represent that base station 2# after receiving the signal transmits commands via shortwave radio network; the arrows marked with ③/④ represent that base stations 3#/4# after receiving the signal transmits commands via shortwave radio network.

Base station 4# is the target base station of this experiment. It will transmit the signal to the ZigBee network it controls via signal conversion module. All ZigBee modules in this network can receive this signal. After analysis and judgment, the modules can decide to executive or deliver the command. Similarly, there may be signal shock among all equipments in ZigBee network. They can also choose to keep silent and the time can be measured based on actual needs.

Here is something that needs explaining. ZigBee modules within adjacent areas because of close location may receive some commands that don’t belong to them. At this time, all sound repellent gun equipments can be made to compare their own location with the command’s object area; if different, they can just keep silent without any processing. In this way, ZigBee signals can be restraint in a small area and invalid transmission of the signal in the whole area can be avoided.

Conclusion

This paper designs a wireless communication-based intelligent underground sound repellent system, which has such characteristics: 1) it can be installed conveniently. When the equipment doesn’t run, it can be buried underground, which not only meet requirements of the airport but also can avoid long time exposure and meanwhile can reduce the birds’ tolerability; 2) many bird drive equipments can operate simultaneously with certain intelligence; 3) many kinds of wireless transmission and control methods are adopted to realize efficient bird drive. This system has obtained a China National Invention Patent (ZL201210328325.3) and been put into use in many airports with good practical effects. In the coming work, based on this system, functions like birds’ intelligence collection and prediction are expected to be added, so as to further improve the intelligent extent of this system.

References

[1] Li Y L, Shi X P. Investigation of the present status of research on bird impacting on commercial airplanes. Acta Aeronautica et Astronautica Sinica[J], 2012, 33(2):189-198.

[2] HAO Xi-lian, YI Guo-dong. Discussion on the Methods of Driving Birds at Airport[J]. Journal of Jilin Normal University(Natural Science Edition), 2005,2:45-46.

[3] LU Yue-sheng, YU Lian-zhi. Intelligent Bird repeller Based on Detecting Principle of Doppler[J], Modern Electronics Technique, 2011,34(24):174-176.

[4] Min Jian-ping , XIA Zhen, LIANG Ye, etc. The ultrasonic device of driving birds based on the infrared sensor[J]. Information Technology, 2013, 37(10): 31-34.

[5] An Huizhen. The Structural Design and Application of Scanning System for the Laser Bird Driving Device in Airport[J]. Shaixi Electronic Technology, 2013 (1): 15-17.

[6] Baronti P, Pillai P, Chook V W C, et al. Wireless sensor networks: A survey on the state of the art and the 802.15. 4 and ZigBee standards[J]. Computer communications, 2007, 30(7): 1655-1695.

[7] ChENG Weibin, WANG Guangming, KANG Simin, etc. Design and Realization of Wireless Telecommunication System Based on HF Transceiver[J]. Modern Electronic Technique, 2005, 28(1): 54-57.

[8] He Xin, Gui Xiaolin, An Jian. A Distributed Area Coverage Algorithm Based on Delayed Awakening in Wireless Sensor Networks[J]. Journal of Computer Research and Development, 2011,48(5):786-792.

[9] LIU Ming, CAO Jian-Nong ,ZHENG Yuan, etc. Analysis for Multi-Coverage Problem inWireless Sensor Networks[J]. Journal of Software, 2007,18(1):127-136.

[10] GUO Jin-ming, ZOU Gang-wei, HU Bin-jie, etc. Research on Localization Technology Based on ZigBee Wireless Sensor Networks[J]. mobile communication, 2013,18:74-79.

Applied Mechanics and Materials Vol. 596 (2014) pp 788-793
© (2014) Trans Tech Publications, Switzerland
doi:10.4028/www.scientific.net/AMM.596.788

Loss Characteristics Analysis and Optimization of an Off-axis Rotary Optical Fiber Communication System

Xiaohua Wang[1, 2, a], Qian Zhao[1, b], Li Li[3,c], Jie Ding[2,d], Qiuxin zheng[2,e], Liu Li[2,f]

[1]Dept. of Electronic Science and Technology, Shanghai University of Electric Power, Shanghai, 200090, China

[2]School of Optical-Electrical and Computer Engineering, University of Shanghai for Science and Technology, Shanghai, 200093, China

[3]Shandong Labor Vocational and Technical College, Ji'nan, 250000, China

[a]wxhsnow@163.com, [b]zhaoqian@shiep.edu.cn, [c]xiti12@163.com, [d]834275019@qq.com, [e]85480988@qq.com, [f]475060686@qq.com

Keywords: Optical Fiber Communication, Off-axis, Optical Fiber Collimator, loss, Thermally Expanded Core Fiber, Infrared Right Angle Prism.

Abstract. The losses of the off-axis rotary optical fiber communication system were derived from optical fiber coupling, three kinds of misalignments between optical fiber collimators (Axial separation Z_0, lateral offset X_0, angular tilting θ), incomplete alignment of optical fiber collimator during rotation and system tremble caused by high speed rotating. Some measures were taken to reduce the loss. The thermally expanded core fiber collimator cut down the influence of axial separation and angular tilting. The position of the optical fiber collimator on the flange was adjusted and infrared right angle prisms were installed to reduce the losses during rotation of the system. In addition, improving the precision and optimizing device of mechanical structure can increase the stability of the whole experiment platform and decrease the losses.

Introduction

Optical fiber collimator is an important component of optical coupling device and it has very widespread application in optical communication system. Its main role is to change the outgoing beam into a parallel beam or to converge the parallel light beam into the fiber [1]. With the development of application of collimator optical communication industry, the application of optical fiber collimator continues to expand and the requirements are also constantly improved.

The thermal expanding core (TEC) fiber is a kind of single-mode fiber doped GeO_2 material. If one of its ends is heated, Ge^{4+} ions will diffuse along the radial direction. This leads fiber core to expand and thereby, the mode field diameter are greatly increased [2]. The outgoing beam from expanded core end of a single mode fiber after heat treatment still has the single-mode characteristics and refractive index of the cross-sections of the fiber shows Gauss distribution. Many foreign researchers used TEC fiber for integrated optoelectronic devices, such as optical isolator, tunable filter tunable filter and Variable optical attenuators [3, 4]. The study of TEC optical fiber used in optical fiber collimator was rare.

Optical fiber rotary connector can be used in continuous transmission of optical signals between the rotating end and the fixed end in some communication systems, such as radar antenna and the signal processing system [5]. At present researches and applications were focused on the coaxial optical fiber rotary connector. The beam was transmitted to the fiber parallel to the axis through prism or lens placed on the axis [6]. With the rapid development of optical fiber communication system, the coaxial optical fiber rotary connector can't be used because of other purposes for the central axis. An off-axis optical fiber transmission system can solve this problem and other device can be placed installation on the central axis.

In this paper, an off-axis rotating optical fiber communication system was designed. Loss characteristics caused by different reasons were analyzed and optimization solutions were proposed.

Structure and loss analysis of an off-axis rotary optical fiber communication system

The research group designed an off-axis rotating optical fiber communication system which included optical transmitter, optical receiver, optical fiber couplers and fiber collimators [7,8]. The schematic diagram of system is shown in Fig.1. The whole system can be divided into two relative rotatable parts, part A and part B. The optical signal can be bidirectionally transmitted through the off-axis system when the optical fiber collimators in the flanges are arranged according to a certain way, shown in Fig.2.

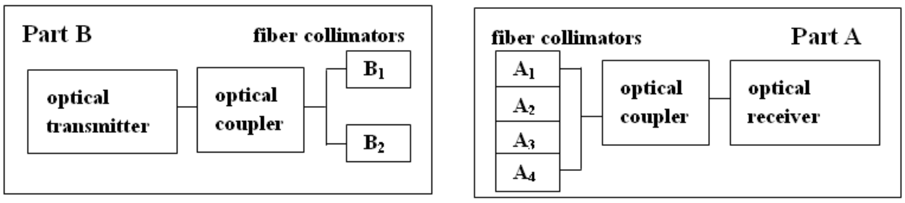

Fig.1 Schematic diagram of the off-axis rotary optical fiber communication system

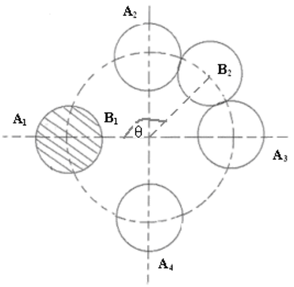

Fig.2 The position of fiber collimators in the flanges

The four optical fiber collimators (A_1, A_2, A_3, A_4) in part A are evenly distributed on the flange. The angles between them are all 90^o.The angle between the two optical fiber collimators (B_1, B_2) in part B is 135 ^{o}. The initial position of collimator B_1 coincides with collimator A_1.

In the off-axis rotary optical fiber communication system, the losses were mainly caused by optical fiber coupling, three kinds of misalignments between optical fiber collimators, incomplete alignment of optical fiber collimator during rotation and system tremble due to high speed rotating. Losses characteristics are analyzed for different losses and optimization is put forward in the following.

Loss of Optical Fiber Coupling. There is great coupling loss when the common optical fiber collimator is coupled with optical fiber because of large angle of outgoing facular aperture. This affects greatly on the transmission of optical signals in the system.

Loss of Misalignments Between Optical Fiber Collimators. The mismatches between optical fiber collimators bring losses when the two flanges are relatively rotating. The mismatches come from three aspects ,such as Axial separation (Z_0), lateral offset(X_0) and angular tilting (θ) shown in Fig.3.

Losses respectively caused by three kinds of mismatch can be calculated by the following equations [9].

Loss caused by axial separation Z_0 can be calculated by Eq.1.

$$L_Z = 4.343 \ln\left[1+\left(\frac{\lambda Z}{2n_0\pi\omega_0^2}\right)^2\right] \tag{1}$$

Loss because of lateral offset X_0 can be reckoned by Eq.2.

$$L_X = 4.343\left(\frac{\pi n_0 g \omega_0 X}{\lambda}\right)^2 \tag{2}$$

Loss derived from angular tilting θ can be computed by Eq.3.

$$L_\theta = 4.343\left(\frac{\tan\theta}{n_0 g \omega_0}\right)^2 \tag{3}$$

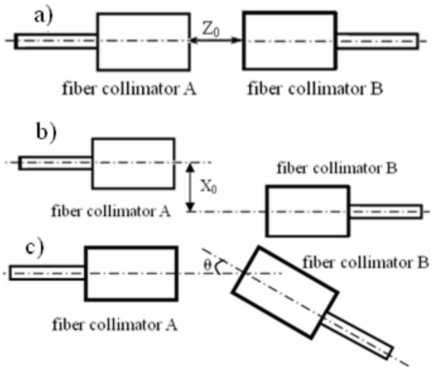

a) Axial separation Z_0 b) Lateral offset X_0 c) Angular tilting θ

Fig.3 Three misalignments between optical fiber collimators

Loss led by its structures during system rotating. When the off-axis rotary optical fiber communication system is working, part A rotates relatively round part B. The optical fiber collimators of part A and B are not completely aligned as Fig.4 shows.

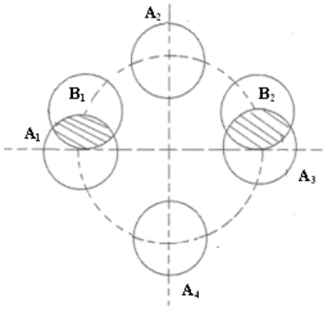

Fig.4 The position of fiber collimator in the rotating process

The initial position of collimator B_1 coincides with collimator A_1 in Fig.2. When the optical fiber collimators are rotating round the axis, overlapping area reduces gradually. When the rotation angle increases to 22.5 ^{o}, overlapping area reduces to a minimum as Fig.4 shows. Overlapping area is about 75 percent of that on the initial position. The initial position of collimator B_2 will coincide with collimator A_3 when the rotation angle increases continously to 45 ^{o} from 22.5 ^{o}. At that time overlapping area is max just as on the initial position. The overlapping area changes periodically with the rotation angle and the loss changes periodically with the overlapping area.

Loss Due to High Speed Rotating. The devices of off-axis fiber rotary connector jitter greatly because of the increasing centrifugal force when the system is rotating in high speed. The loss grows with the great jitter.

Optimization and analysis

A variety of reasons brought about losses when the off-axis fiber rotary optical fiber communication system was working and this reduces the working efficiency and quality. In order to improve the performance of the system, the research group applied thermally expanded core (TEC) fiber collimator to the communication system, then the losses decreased obviously. The relative position of the optic fiber collimators on the flange was adjusted and infrared right angle prisms were installed between the optic fiber collimators. So the optical signals can come into the optical receiver as much as possible. Effective solutions were also put forward to reduce the loss due to high speed.

Application of the TEC fiber collimator adjust flange and install infrared right angle prism. Optical fiber collimator coupled with ordinary fiber has higher insertion loss. The TEC fiber collimators were applied to the optical fiber communication system in order to solve this problem. The core diameter of TEC optical fiber between the heating and non heating zone was shown in Fig.5. The core diameter is 2a in the heating zone but 2A in the non heating zone.

The research group designed TEC optical fiber collimator composed of TEC optical fiber and gradient index lens. TEC fiber with the mode field radius 15.4μm was obtained when ordinary single mode optical fiber with the mode field radius 5.05μm was heated. The gradient index lens is 1/4 pitch and its self focusing constant is 0.295mm^{-1} [1].

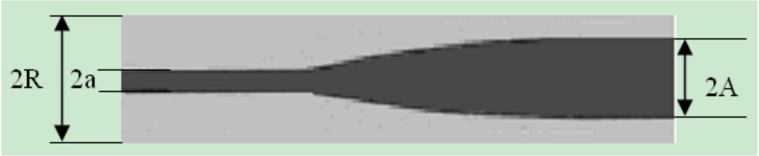

Fig.5 Schematic of the TEC fiber

Collimated and expanded beam is obtained through TEC fiber collimator in order to reduce the coupling loss. Expanded beam is consistent with the transmission law of Gauss beam. Optical path is shown in Fig. 6.

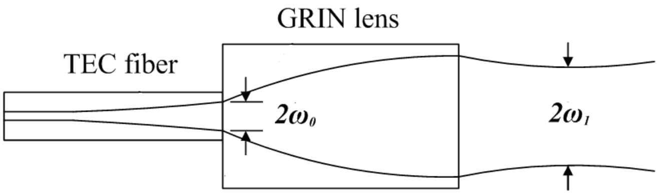

Fig.6 Optical path of TEC fiber collimator

The application of TEC fiber collimator improved the performance. Losses of misalignments between TEC optical fiber collimators and ordinary single mode optical fiber collimators were compared according to Eq.1, Eq.2 and Eq.3. Fig.7 shows the difference. (The wavelength of light is 1550 nm.).

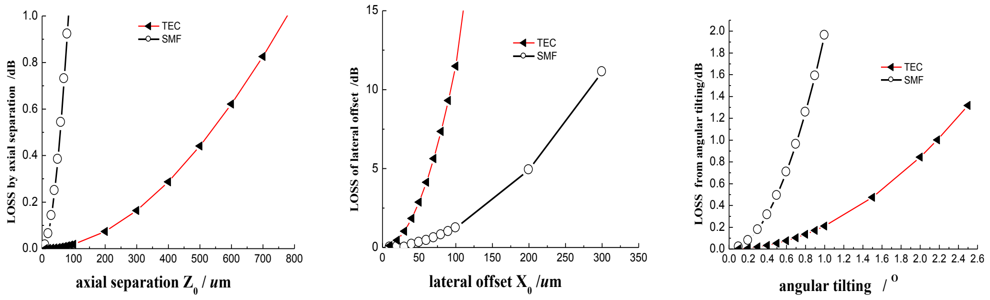

a) Loss by axial separation Z_0 b) Loss of lateral offset X_0 c) Loss from angular tilting θ

Fig.7 Comparison of TEC fiber collimator and ordinary single mode optical fiber collimator

In Fig.7a), Loss caused by axial separation of TEC fiber collimator is obviously less than that of ordinary optical fiber collimators. When the distance is 100μm, the loss of ordinary optical fiber collimators is 1.36dB but that of TEC fiber collimator is only 0.015 dB. When the axial separation Z_0 is about 800μm, Loss of TEC fiber collimator reaches 1 dB. Fig.7c) shows that loss of TEC fiber collimator is only 0.1 dB while that of ordinary optical fiber collimators is 1dB When the angular tilting θ is 0.715 ^{o}. Loss of TEC fiber collimator just reaches 1 dB When the angular tilting θ is 2.18 ^{o}. So TEC fiber collimator has improved a lot on loss caused by axial separation Z_0 and loss derived from angular tilting θ.

TEC optical fiber collimator is more sensitive on loss of lateral offset than ordinary optical fiber collimator as shown in Fig.7b). Therefore horizontal matching of TEC fiber collimators should be paid special attention to in the system assembly process.

Adjusting flange and installing infrared right angle prism. Flanges were changed to be nested with the inner flange and the outer flange shown as Fig.8 from the same diameter shown as Fig.2. The infrared right angle prisms were installed in inner flanges and the outer as shown in Fig.9.

TEC fiber collimators are evenly distributed across the flanges but the number in outer flange is more than that in inner flange. The number of TEC fiber collimators can alter according to the diameter of the flanges. When the inner flange is rotating relatively round the outer, the optical signals from the TEC fiber collimators refract from one infrared right angle prism to another and then enter the collimators on the other flange [10]. Fig.10 shows the internal optical path.

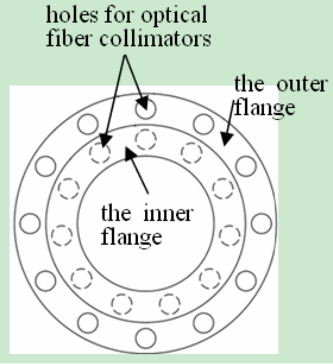

Fig.8 Schematic of the nested flanges

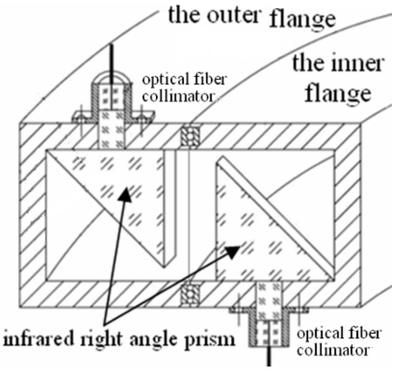

Fig.9 Infrared right angle prisms in flanges

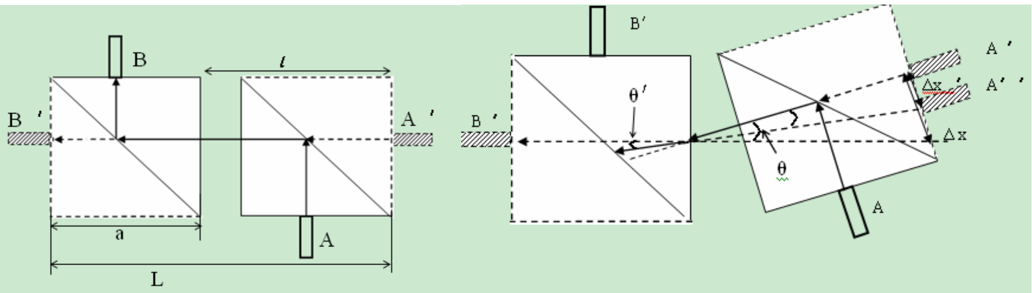

a) Alignment

b) Deviation

Fig.10 Schematic diagram of internal optical path

The optical signals can enter accurately from one collimator to another through infrared right angle prisms due to the characteristic of the prisms when the prisms are aligned. Collimator A′ and collimator B′ are respectively the mirror image of collimator A and collimator B.

When the prisms are deviated as Fig.10 b), the mirror image of collimator A is collimator A″ because of different refractive index between prism and air. The lateral offset of collimator A is Δx and the angular tilting is θ while those of the collimator A″ are respectively Δx′ and θ'.

Equations can be inferred as the following from Fig.10 b).

Lateral offset Δx′ is

$$\Delta x' = \Delta x\text{-}(\sin\theta\text{-}\sin\theta') \bullet l/\cos\theta \tag{4}$$

Angular tilting θ' is

$$\theta' = \arcsin(\frac{\sin\theta}{n_p}) \tag{5}$$

Where n_p is the refractive index of the light in infrared right angle prisms.

Axial separation L is

$$L = \mathrm{a} + \frac{\cos\theta'}{\cos\theta} \bullet l \tag{6}$$

When the loss derived from angular tilting is recalculated according to Eq.3and Eq.6, $L_{\theta'}$ becomes 45percent of the original value.

When θ and θ' are very small, $\sin\theta \approx \theta, \sin\theta' \approx \theta', \cos\theta \approx \cos\theta' \approx 1$. So the axial separation L is hardly changed. The lateral offset is reduced by$(\theta\text{-}\theta') \bullet l$ and the loss of lateral offset is greatly reduced according to Eq.2.

In brief, the infrared right angle prisms have made a great contribution to reduce the loss and to decrease volume of the system.

Enhancing the accuracy and reliability of the system. Measures should be taken to advance mechanical structure and optimization of the fixed device, such as adding pads to slow down the shake. If their accuracy and reliability are enhanced, the loss will be reduced.

Conclusion

Four kinds of reasons led to loss were analyzed and the loss characteristics were also summarized. Loss can be calculated according the equations because of misalignments between optical fiber collimators, such as axial separation, lateral offset and angular tilting.

Two kinds of important techniques were applied to reduce the loss. The TEC fiber collimator can decrease the losses from axial separation and angular tilting compared with the ordinary optical fiber collimator. The alteration of the position of the optical fiber collimator on the flange and the infrared right angle prisms have greatly reduce the losses.

Acknowledgements

This work was financially supported by research team construction project of Shanghai University of Electric Power.

References

[1]Li Liu, Li Yi, Zheng Qiuxin: Laser &Optoelectronics Progress. Vol. 49(06) (2012), p060602:1-6. *In Chinese.*

[2] G. S. Kliros, P. C. Divari. Mater: Sci, Mater. Electron. Vol.20(suppl.1) (2009), p59-62.

[3] Linh Viet Nguyen, Dusun Wang, Dae Seung Moon: Opt. Commun. Vol.281(23) (2008) p5793-5796.

[4] H. W. Kwon, J. W. Song, K. T. Kim : Appl. Phys. Vol.50(2) (20011) p806-807.

[5] He Zhengquan, Li Yulin, Hu Baowen: Laser &Optoelectronics Progress. Vol.50 (2013), p010007:1-5. *In Chinese.*

[6] Xu Feng, Zhang Ruiyu: Optics and Precision Engineering. Vol.16(10) (2008) p1836-1840. *In Chinese.*

[7] Zheng Qiuxin, Li Yi, Shen Yujian: Journal of Optoelectronics .Laser. Vol.23(12)(2012). p2310-2315. *In Chinese.*

[8] Yin Ying, Li Yi, Ding Jie : Optical Technique. Vol.39(2) (2013) p188-192. *In Chinese.*

[9] Mi Lei, Yao Shengli, Sun Chuangdong: The 9th International Conference on Optical Communications and Networks, 2010, p437-440.

[10] Ding Jie, Li Yi, Wang Feng: Journal of Optoelectronics .Laser. Vol.24 (11)(2013). p2075-2080. *In Chinese.*

Applied Mechanics and Materials Vol. 596 (2014) pp 794-798
© (2014) Trans Tech Publications, Switzerland
doi:10.4028/www.scientific.net/AMM.596.794

Simulation on PAPR Suppression Algorithm for Multicarrier System

Rui Zhang [1, a], Zhibin Zeng [2,b]

[1]Communication University of China, Chaoyang District, Beijing, China

[2]Communication University of China, Chaoyang District, Beijing, China

[a]rzhang@cuc.edu.cn, [b]zhbzeng @cuc.edu.cn

Keywords: multicarrier, PAPR, pulse cancellation, crest factor reduction

Abstract. The main disadvantage of multicarrier system is the high peak-to-average power ratio which can easily result in significant cut-the-top distortion of power amplifier. However, the power efficiency of power amplifier will be reduced by power back-off technology. Therefore, crest factor reduction is important in reducing the peak-to-average power ratio of multicarrier system and improving the efficiency of power amplifier. The peak-to-average power ratio can be effectively reduced with small distortion by the algorithm of crest factor reduction based on peak cancellation. And the performance of peak-to-average power ratio is better with the same error vector magnitude.

Introduction

Non-constant envelope modulation signal, such as orthogonal frequency division multiplexing (OFDM) and code division multiple access (CDMA), is added by a plurality of independently modulated subcarrier signals. The peak-to-average power ratio (PAPR) of such kinds of signals is high [1,2,3]. Generally, the enlarged area of power amplifier (PA) is limited, the cut-the-top distortion is easily caused by large PAPR radio frequency (RF) signal. However, the power efficiency of power amplifier will be reduced by power back-off technology. Therefore, it is important to reduce the signal PAPR before PA.

Crest factor reduction (CFR) is a technology of reducing the signal PAPR at the expense of some performance parameters. Clipping method [4] is the simplest and most direct way to reduce PAPR, including based-band clipping, noise shaping method and peak cancellation method and so on [5]. Among them, peak cancellation method [6] has become one of the most popular solutions for CFR because of its good flexibility, excellent performance and easy to implement.

The PAPR of OFDM System

Illustrated by the case of OFDM signal, it is composed of N statistically independent sinusoidal signals. When the value of N is large, the real and imaginary part of the OFDM signal are approximately Gaussian distribution and amplitude will tend to Rayleigh distribution, the transmitted symbol is high PAPR signal.

A complex baseband OFDM symbol with N orthogonal subcarriers can be expressed as:

$$s(t) = \frac{1}{\sqrt{N}} \sum_{k=0}^{N-1} x_k \exp(j2\pi kt / NT) \quad (0 \le t \le NT). \tag{1}$$

Where, x_k is modulation symbol, NT is OFDM symbol period.

In an OFDM symbol period, the power of $s(t)$ is:

$$P(t) = |s(t)|^2 = \frac{1}{\sqrt{N}} \sum_{k=0}^{N-1} \sum_{l=0}^{N-1} x_k x_l^* \exp(j2\pi(k-l)t / NT) \quad (0 \le t \le NT). \tag{2}$$

So, the PAPR of OFDM signal is defined as the ratio of peak power to average power:

$$PAPR = \frac{\max[P(t)]}{E[P(t)]}. \tag{3}$$

Where, $\max[\cdot]$ represents the maximum value, $E[\cdot]$ represents the average value.

The Algorithm of CFR Based on Peak Cancellation (PC-CFR)

Algorithm Principle. In multicarrier system, when the probability of peak is a certain value, the method of time-domain clipping for hardware implementation is very simple and effective. The fundamental of PC-CFR is detecting signal peaks in the data block range of the signal amplitude greater than the threshold, generating cancellation pulses canceled with peaks, so that the peaks do not exceed the threshold. The phase of cancellation pulse is the same with peak, and amplitude is the difference between the peak and the threshold. The time-domain diagram is showed in Fig. 1.

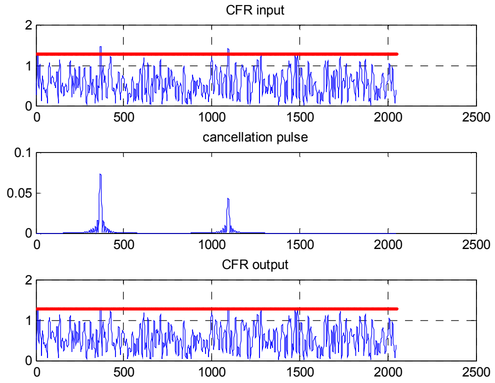

Fig. 1. Time-Domain Diagram of PC-CFR

Algorithm Implementation. As shown in Fig. 2, the process of PC-CFR is obtaining the signal spectrum characteristics, constructing a FIR filter which spectrum characteristics is the same with signal, generating cancellation pulses which spectrum is standard by the FIR filter. Then, find and cancel the peaks.

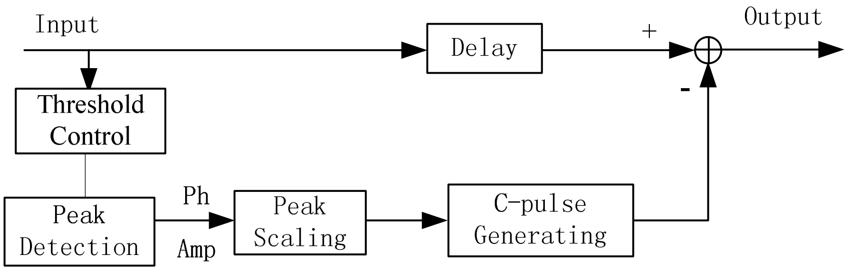

Fig. 2. Processing of PC-CFR

Threshold Control. The clipping rate (CR) is the most important parameter affecting the performance of clipping, it is defined as:

$$CR = Th/\sigma. \qquad (4)$$

Where, Th represents clipping threshold, σ is root mean square (RMS) of signal power. Lower CR, lower Th, then the better compression effect of PAPR. On the contrary, the worse compression effect of PAPR.

Peak Detection. Detect signal peaks in the data block range of the signal amplitude greater than the threshold. Then mark the amplitudes, phases and locations of the signal peaks. Points that exceed the threshold can be detected simply by peak detection. However, it is easy to detect a plurality of peaks in a short period of time. When multiple adjacent peaks are clipped simultaneously, peak regeneration is caused and modulation error ratio (MER) is reduced. Reasonable manner is detecting extreme point which modulus exceeds the threshold. And in the adjacent peaks, only the maximum is selected. This manner can reduce the computational complexity. The peak detection schematic is showed in Fig. 3.

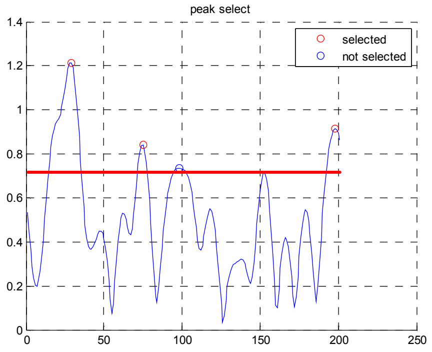

Fig. 3. Peak Detection Schematic

Peak Scaling. Phase error and amplitude error will be generated in the clipping, where the effect on MER of the phase error is remarkable. Therefore, the amplitude is generally clipped while the phase is preserved. So, the amplitude of peak scaling factor is the difference between the peak and the threshold and the phase is the same with peak:

$$\begin{cases} \alpha(n) = (|x(n)| - Th) \times e^{j\angle x(n)}, \text{ if } x(n) \text{ is a valid peak} \\ \alpha(n) = 0, \text{ otherwise} \end{cases} . \tag{5}$$

Where, $\alpha(n)$ is the peak scaling factor, $|x(n)|$ is the amplitude of peak, Th is clipping threshold and $\angle x(n)$ is the phase of peak.

Peak Cancellation. The cancellation pulse $g(n)$ is defined as:

$$g(n) = \sum_{i=0}^{N} \alpha(n-i)h(i) . \tag{6}$$

Where, $h(i)$ is the peak cancellation function complied with the spectrum of signal $x(n)$. The bandwidth of $h(i)$ is the same with $x(n)$. After peak cancellation with the cancellation pulse $g(n)$, PAPR is compressed in the time-domain and components in the frequency-domain are also controlled in the range of bandwidth. Finally, the clipped signal $y(n)$ is defined as signal $x(n)$ superimposed on cancellation pulse $g(n)$: $y(n) = x(n) - g(n)$.

Iterations. As the principle of peak detection, in order to avoid peak regeneration, only the maximum is selected in the adjacent peaks. Therefore, some peaks may not be canceled. Usually, there are several iterations to reduce the PAPR, as shown in Fig. 4. The PAPR compression of system can be improved by multiple iterations. In general, three time iteration is a balanced choice for performance and complexity.

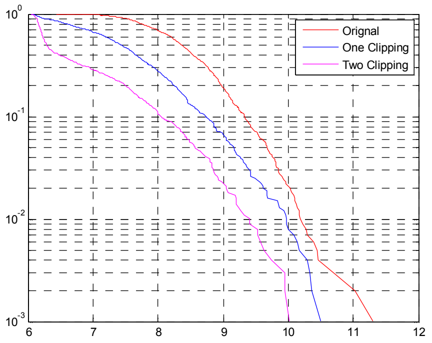

Fig.4. CCDF Curve

Simulation

The original signal $x(n)$ is 16bit quantized OFDM signal, the bandwidth is 8MHz and the sampling frequency is 40MHz. As the maximum is selected in the adjacent peaks, after the first clipping parts of the peaks are not canceled. So, the second clipping is needed. The time-domain diagram of the first and second clipping is showed in Figure 5.

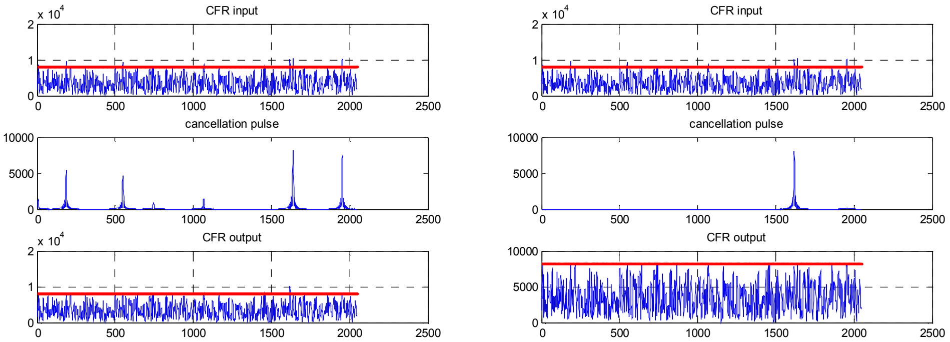

The First Clipping

The Second Clipping

Figure 5 The Time-Domain Diagram

The clipped signal is defined as the delayed original signal $x(n)$ superimposed on the cancellation pulse. Due to the cancellation pulse is similar to the original signal. The spectrum of clipped signal is not diffusion, as showed in Figure 6. After the second clipping, the MER is 24.7dB.

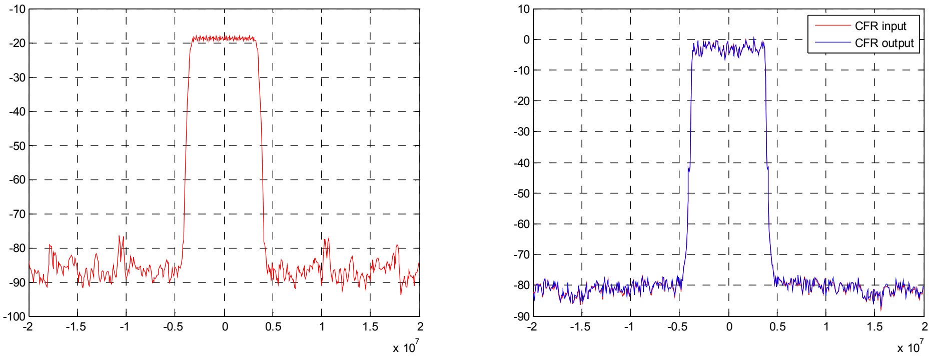

Frequency Response of Cancellation Pulse

PSD of CFR input and output

Figure 6 Frequency Response of Cancellation Pulse and PSD of CFR input and output

Generally, for the original signal which spectrum is Gaussian distribution, the peak cancellation function $h(i)$ is the FIR filter coefficients complied with the spectrum of baseband signal. Therefore, PC-CFR is adapted to meet a variety of different air interface standards and easy to implement by changing the filter coefficients. This is the biggest advantage of this algorithm.

Conclusions

CFR is important in reducing the PAPR of multicarrier system and improving the efficiency of power amplifier. The PAPR can be effectively reduced with small distortion by the algorithm of PC-CFR. And the spectrum of clipped signal is not diffusion. PC-CFR is adapted to meet a variety of different air interface standards and easy to implement.

References

[1] Dursun Serkan. Nonlinear transform approach to the reduction of peak-to-average. 2010, The University of Texas at San Antonio: TEXAS.

[2] Ghassemi Abolfazl. IFFT-based techniques for peak power reduction in OFDM communication systems. 2008, University of Victoria.

[3] Byung Moo Lee. Adaptive pre-distortion and peak-to-average power ratio reduction in OFDM wireless communications. 2006, University of California: California. p. 190.

[4] Li X, Cimini L. J. Effect of clipping and filtering on the performance of OFDM. IEEE Communication Letters, vol. 2, Mya1998, PP. 131-133.

[5] Luqing Wang, Chmtha Tellambura. An overview of peak-to-average power ratio reduction techniques for OFDM systems signal processing and information technology. IEEE International Symposium, 2006.

[6] Richard Van Nee, Ramjee Prasad. OFDM wireless multimedia communication. Artech House. 2000.

Applied Mechanics and Materials Vol. 596 (2014) pp 799-802
© (2014) Trans Tech Publications, Switzerland
doi:10.4028/www.scientific.net/AMM.596.799

Theory analysis and simulation of Optical 90° hybrid without intersection

Weihua Liu[1,a*], Guiju Wu [2,b]

[1]Wuhan Polytechnic University, Wuhan, China

[2]Institute of Seismology, CEA, Wuhan, China

[a]Liuwhsky@126.com, [b]Wugjsky@126.com

Keywords: Optical fiber communication; Integrated optics; Coherent receiver; Integrated optics devices.

Abstract. An optical 90^o hybrid consisting of a general interference based 4×4 MMI coupler, a phase shifter and a 2×2 MMI coupler was proposed. This device can demodulate optical signal without intersections. The output power formula of this device was derived from theory, and the effect on phase shifter was discussed analytically and numerically. It is not necessary to control phase shifter accurately, a deviation 10^o form perfect phase shift will introduce 2% AC component loss of Q information only.

Introduction

Recently years, there has been renewed interest in coherent detection, because coherent communication systems enable restore signal associated with digital signal processing and have better performances in terms of spectral efficiencies and receiver sensitivities compared with conventional intensity modulated/direct detection transmission systems[1]. The next generation of commercial coherent systems is most likely based on dual-polarization quadrature phase shift keyed (DP-QPSK) modulation format. An integrated DP-QPSK coherent receivers must be contained three basic functions: polarization split, 90^o hybrid and balance detect. Optical 90^o hybrid is one of key components for demodulating optical signals.

Optical 90^o hybrid can be formed discrete device with bulk-optics components or optics fiber, and also can be realized with compact optical waveguide. Now some discrete device based free space or fiber has commercially available. Also there have been reports on many kinds of optical 90^o hybrid based waveguide, it can be realized with three 2×2 optical couplers, two Y-branch and two phase shifters[2,3], or realized with a star coupler[4], or realized with a 4×4 mult-mode interference(MMI) coupler based on general interference[5]-[7],or realized with a 2×4 MMI coupler based on pair interference, a phase shifter and a 2×2 MMI coupler[8,9]. 4×4MMI coupler demodulating optical information using their inherent quadrature phase relationship, it is very promising for the advantages of large fabrication tolerances, wide bandwidth, excellent temperature stability and suitable for monolithic integration with photodetectors[10]. A 4×4 MMI coupler, along with its access waveguides, is shown in fig.1(a). If the signal light and local oscillator light input to MMI form port1 and port3 (all asymmetrically input is ok), there will be in-phase (I) signal on port1 and port4, and quadrature (Q) signal on port2 and port3.This schematic normally require two intersections when signal was deal with follow-up, it is hard to avoided cross talk and excess loss which caused by intersections. In 2010, Seok-Hwan Jeong et al reported an optical 90^o hybrid consisting of a paired interference based 2×4 MMI coupler, a phase shifter and a 2×2 MMI coupler, this 90^o hybrid can demodulating I and Q information without using cross-over. Here an optical 90^o hybrid consisting of a general interference based 4×4 MMI coupler, a phase shifter and a 2×2 MMI coupler was proposed. Then the output power formula of this device was derived from theory, and the effect on phase shifter was discussed analytically and numerically.

Theory analysis

Fig.1(b) schematic diagram of optical 90° hybrid consisting of a general interference based 4×4 MMI coupler, a phase shifter and a 2×2 MMI coupler. If we input signal light and LO light symmetrically (port1and port4 or port2 and port3) to 4×4 MMI coupler, it will be show two pair in-phase behavior symmetrically, then one pair port coupled to 2×2 MMI coupler, we can get Q behavior in the output port of 2×2 coupler. but we will be find in later that it will be a large loss when phase different is 90 ° or -90 °, for minimized this loss, we should let port3 have a 45° phase shift than port 4.

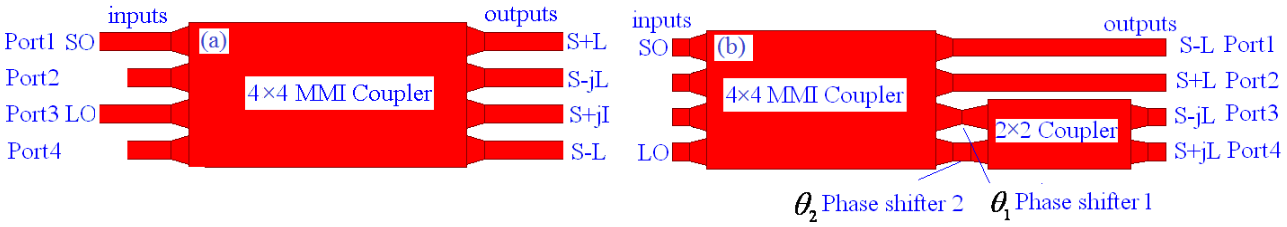

Fig.1. Schematic diagram of optical 90° hybrids (a) based on a 4×4 MMI coupler (b) consisting of a 4×4 MMI coupler, a phase shifter and a 2×2 MMI coupler

If the signal light and local oscillator(LO) light have the same polarization, the electric fields for input signal light and LO light can be represented as complex notations：

$$E_S(t)=\sqrt{P_S}\cdot e^{-j(\omega_S t+\phi_S(t))} \tag{1}$$

$$E_L(t)=\sqrt{P_L}\cdot e^{-j(\omega_L t+\phi_L(t))} \tag{2}$$

Where P_S, ω_S and ϕ_S are the power, the angular frequency and the phase of the signal light, P_L, ω_L and ϕ_L are the power, the angular frequency and the phase of the LO light respectively.

We can describe the characteristics of the 4×4 MMI with a matrix

$$T_{44}=\sqrt{k_4}\begin{bmatrix} 1 & e^{j\frac{3}{4}\pi} & e^{-j\frac{\pi}{4}} & 1 \\ e^{j\frac{3}{4}\pi} & 1 & 1 & e^{-j\frac{\pi}{4}} \\ e^{-j\frac{\pi}{4}} & 1 & 1 & e^{j\frac{3}{4}\pi} \\ 1 & e^{-j\frac{\pi}{4}} & e^{j\frac{3}{4}\pi} & 1 \end{bmatrix} \tag{3}$$

where k_4 indicates a power splitting coefficient of the 4×4 MMI coupler.

The phase shifter and 2×2 MMI coupler are represented by using a matrix similarly

$$T_{PS}=\begin{bmatrix} 1 & 0 & 0 & 0 \\ 0 & 1 & 0 & 0 \\ 0 & 0 & e^{j\theta_1} & 0 \\ 0 & 0 & 0 & e^{j\theta_2} \end{bmatrix} \tag{4}$$

$$T_{22}=\begin{bmatrix} 1 & 0 & 0 & 0 \\ 0 & 1 & 0 & 0 \\ 0 & 0 & \sqrt{k_2} & -j\sqrt{k_2} \\ 0 & 0 & -j\sqrt{k_2} & \sqrt{k_2} \end{bmatrix} \tag{5}$$

where k_2 indicates a power splitting coefficient of the 2×2MMI coupler, θ_1 and θ_2 are the amount of phase shift at the phase shifter1 and the phase shifter2.

If we set the electric field of the signal and the LO to the input component at input port1 and port 4, and assume the power splitting coefficient are perfect, then the output power from port1 to port 4 are given as

$$I_{out1}(t)=\frac{1}{4}[P_S+P_L+2\sqrt{P_sP_L}\cos(\omega_{IF}t+\phi_S(t)-\phi_L(t))] \tag{6}$$

$$I_{out2}(t)=\frac{1}{4}[P_S+P_L-2\sqrt{P_sP_L}\cos(\omega_{IF}t+\phi_S(t)-\phi_L(t))] \tag{7}$$

$$I_{out3}(t)=\frac{1}{4}[(1-\sin\varphi)P_S+\frac{\cos^2\varphi}{1-\sin\varphi}P_L+2\cos\varphi\sqrt{P_SP_L}\sin(\omega_{IF}t+\phi(t)_s-\phi_L(t))] \tag{8}$$

$$I_{out4}(t)=\frac{1}{4}[(1-\sin\varphi)P_S+\frac{\cos^2\varphi}{1-\sin\varphi}P_L-2\cos\varphi\sqrt{P_SP_L}\sin(\omega_{IF}t+\phi_s(t)-\phi_L(t))] \tag{9}$$

where $\varphi=\theta_1-\theta_2-\pi/4$, indicates the phase difference between two input ports of 2×2 MMI coupler, ω_{IF} is the intermediate frequency given by $\omega_{IF}=\omega_S-\omega_L$.

Form formula (6)-(9), we can find clearly that port1 and 2 will appear I response and port 3and 4 appear Q response. The first two items of photocurrents indicate the direct-current (DC) response, it can be eliminated in subsequent processing. The express of I3 and I4 is more complex because of phase shifter, so we discuss this result further.

Simulation and discussion

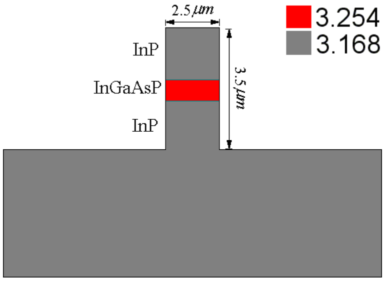

Fig.2. Deep-ridge waveguide structure

In order to discuss the effect of phase shifter, we discuss the proposed optical 90° hybrid by theory calculation and using numerical simulation at the same time. The simulation based on 3 dimensional finite difference beam propagation method. In the simulation, access waveguide is a deep-ridge waveguide as show in fig.2, the core layer is a 0.5μm thick InGaAsP(λ_g=1.05μm,core index is 3.254),the width and depth are 2.5μm and 3.5μm, waveguide separation were set to 5μm, the width of 4×4 MMI and 2×2 MMI are 20μm and 10μm,and other parameters of the 4×4 MMI and 2×2 MMI coupler were optimized for the wavelength of 1.55μm and a linearly polarized TE-mode. Phase shift realized by change width of access connect waveguide. We let the wavelength of signal light same to LO light for simpler.

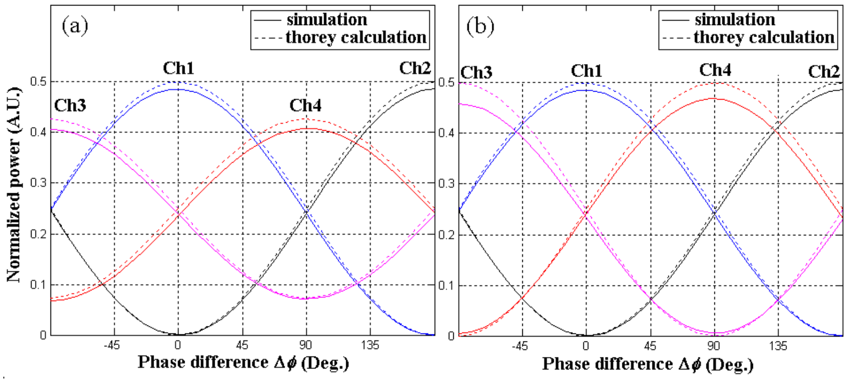

Fig.3. Photocurrents as a function of the phase differenceΔϕ for (a) without phase shifter and (b) with a phase shifter $\pi/4$ between port 3 and 4

If P_S =P_L, DC component of I3 and I4 is costant. If there haven't any phase shift, means$\Delta\phi=\pm\pi/2$ ，the result is show in fig.3a, Q component only 0.707 times of I component. We can minimize this loss by introduce a phase shifter. The result introduce a $\pi/4$ phase shift as the result was show in fig. 3b, I and Q components of roughly equal weight. This result can promotion to $\theta_1-\theta_2=-\pi/4\pm2k\pi$ (k=0,1,2…). Fig.4 show the output power with different phase shift when $\Delta\phi=\pi/2$, the phase shift needn't precise control, 10^o deviate only lead 2% AC loss of Q compear with I.

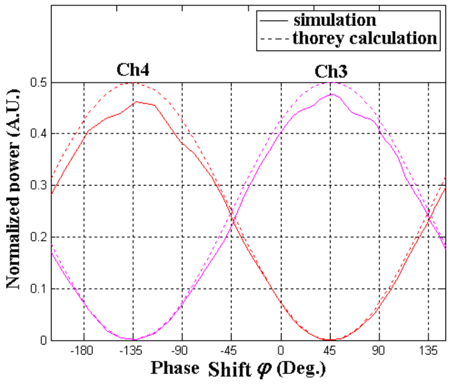

Fig.4. Photoelectric of port3 and port4 with different phase shift ($\Delta\phi=\pi/2$)

Conclusion

An optical 90^o hybrid consisting of a general interference based 4×4 MMI coupler, a phase shifter and a 2×2 MMI coupler was proposed. Then the output power formula of this device was derived from theory, and the effect on phase shifter was discussed analytically and numerically. when phase shift different satisfied $\theta_1-\theta_2=-\pi/4\pm2k\pi$(k=0,1,2…),we can get good I and Q result, and 10^o deviation only introduce 2% penalty in Q. power different will not effect device performance.

Acknowledgements

This work was financially supported by the National Natural Science Foundation of China (61303116) and the talented faculty funds of Wuhan Polytechnic University (2013RZ14).

References

[1] E. Ip, A. P.T. Lau, D. J. F. Barros, and J. M. Kahn, Opt. express, vol. 16, no. 2, pp. 753–791.
[2] Y. Sakamaki, H. Yamazaki, T. Mizuno, T. Goh, and Y. Nasu, Election. Lett., vol. 46, no. 1,pp.58-59.
[3] P. S. Cho, G. Harston, A. Greenblatt, and A. Kaplan, in proc. COTA 2006 ,Paper CTHB
[4] C. R. Doerr, L. Zhang, S. Chandrasekhar, and L. L. Buhl, IEEE Photon. Technol. Lett., vol. 19, no. 21, pp. 1765–1767.
[5] L. Zimmermann, K. Voigt, G. Winzer, K. Petermann, and C. M.Weinert, IEEE Photon. Technol. Lett., vol. 21, no.3, pp. 143–145.
[6] H. G. Bach, A. Matiss, C. C. Leonhardt, R. Kunkel,and D. Schmidt, in Proc.OFC/NFOEC 2009, Paper OMK5.
[7] M. Baudreau, M. Poirier, G. Yoffe, and B. Pezeshki, in Proc. OFC/NFOEC 2009, paper OMK6.
[8] S. H. Jeong, and K. Morito, Opt. Lett., vol. 34, no. 22， pp.3505-3507.
[9]S. H. Jeong, and K. Morito, J. Lightw. Technol., vol.28, no. 9, pp. 1323–1331.
[10] L. B. Soldano and C. M. Pennings, J. Lightw. Technol., vol. 13, no. 4, pp. 615–627.

Applied Mechanics and Materials Vol. 596 (2014) pp 803-806
© (2014) Trans Tech Publications, Switzerland
doi:10.4028/www.scientific.net/AMM.596.803

Two Analog Transmission Schemes for Distributed Detection

Xiangyang LIU[1, a], Peisheng ZHU[2,b] and Wei LIU[1,c]

[1]Dept. of information transmission, Xi'an Communications Institute, Xi'an Shaanxi, China

[2]China Institute of Acoustics, Chinese Academy of Sciences, Beijing, China

[a]liuxiangyangdr@gmail.com, [b]zhups_ioa@126.com, [c]liuwei0927@126.com

Keywords: Analog transmission; distributed detection; data fusion; detection.

Abstract. In order to improve the detection performance of distributed detection system under noisy fading channel, two analog transmission schemes, i.e. an analog transmission and a modified analog transmission, were proposed. Simulations show that, when the channel SNR is high, such as larger than 20dB, the system with the proposed analog transmission scheme can approach that with ideal transmission condition in detection performance. For low channel SNR, such as less than 10dB, the modified analog transmission scheme results in better detection performance than the binary transmission scheme proposed in literature. Therefore, according to the channel state information at the sensor, the sensor can select appropriate transmission scheme to improve the system's detection performance.

Introduction

Although digital transmission predominates in modern communication system, analog one has still its own position. Considering that the multi-level or analog compressed information made by the local sensors are more informative than the binary decision, proper analog transmission scheme can improve the performance of the distributed system[1]. Jayaweera[2] considered the transmission of local sensor decisions based on analog relay amplifier processing. For both deterministic and stochastic Gaussian signals, asymptotic performance in a large sensor system is analyzed by deriving the error exponents. In [3], each distributed node performs analog-relay amplifier local processing on its observation and transmits locally processed data to the fusion center over a wireless channel. However, it should be noted that they didn't consider how to design an analog transmission to achieve the best detection performance theoretically attainable.

For estimation problem, Gastpar[4] showed that for a symmetric sensor network with no fading, analog transmission achieves the optimal performance theoretically attainable. Hamid Behroozi et al[5] provided optimality condition for analog transmission in an asymmetric Gaussian sensor network with deterministic fading and gave an optimal power allocation scheme. But, similar work about distributed detection is absent. Therefore, we consider the analog transmission of local detection statics to achieve the best detection performance theoretically attainable. Analog transmission, in this paper, means scaling the processed result of each sensor and transmitting it without explicit channel coding.

Distributed Detection

We consider a distributed binary hypothesis testing task, where K sensors and a fusion center (FC) are used to discriminate between the hypotheses of the set $\mathcal{H}=\{H_1,H_0\}$, representing the absence H_0 or the presence H_1 of a specific target of interest.

The k-th sensor, $k\in\mathcal{K}\triangleq\{1,2,\dots,K\}$, takes a local binary decision $d_k\in\mathcal{H}$ about the observed phenomenon on the basis of its own measurements, with false alarm and detection probabilities P_{lfk}

and P_{ldk} , respectively. Let M denote the number of integrated pulses and R that of reference samples for each sensor. We assume that the model, given in Eq.1,is adopted.

$$H_0: \; f_{X_{kj}}\left(x_{kj}\right)=\frac{1}{\mu_k}e^{-\frac{x_{kj}}{\mu_k}} \quad \leftrightarrow H_1: \; f_{X_{kj}}\left(x_{kj}\right)=\frac{1}{\mu_k(1+\lambda_k)}e^{-\frac{x_{kj}}{\mu_k(1+\lambda_k)}}, \quad x_{kj}>0 \tag{1}$$

where λ_k is the signal-to-noise ratio (SNR) of the cell under test , μ_k is the noise power level , and x_{kj} ($k=1,\cdots,K$, $j=1,\cdots,M$) is the observed sample of k-th sensor. In this paper, we assume the local sensors do not communicate with each other, i.e., sensor k makes a local decision $u_k \in \{+1,-1\}$ independently based on its own observation x_k . If $s_k \ge \tau_k$, $u_k=1$; if $s_k<\tau_k$, $u_k=-1$, where $s_k \triangleq \left(\sum_{j=1}^{R} Y_{kj}\right)^{-1} \sum_{j=1}^{M} X_{kj}$, and τ_k is decision threshold determined by the false alarm rate P_{lfk} . In this case, the P_{ldk} and P_{lfk} can be calculated as following,

$$P_{ldk}=\Pr(s_k \ge \tau_k \mid H_1)=\sum_{n=1}^{M}\frac{\tau_k^{n-1}\Gamma(R+n-1)(1+\lambda_k)^R}{\Gamma(R)\Gamma(n)(1+\lambda_k+\tau_k)^{R+n-1}} \triangleq P_{ld}(\tau_k,\lambda_k,M,R) \tag{2}$$

$$P_{lfk}=\Pr(s_k \ge \tau_k \mid H_0)=\sum_{n=1}^{M}\frac{\tau_k^{n-1}\Gamma(R+n-1)}{\Gamma(R)\Gamma(n)(1+\tau_k)^{R+n-1}}=P_{ld}(\tau_k,0,M,R) \tag{3}$$

We assume the sensors have knowledge of their observation quality in terms of P_{ldk} and P_{lfk} . After some derivations, the probability density function of s_k is

$$f_{s_k}(s)=\frac{s^{M-1}(1+\lambda_k)^R\Gamma(M+R)}{(1+s+\lambda_k)^{M+R}\Gamma(M)\Gamma(R)} \tag{4}$$

$$\mathbb{E}\left[s_k^2\right]=\int_0^\infty s^2\frac{s^{M-1}(1+\lambda_k)^R\Gamma(M+R)}{(1+s+\lambda_k)^{M+R}\Gamma(M)\Gamma(R)}dv=\int_0^\infty\frac{s^{M+1}(1+\lambda_k)^R\Gamma(M+R)}{(1+s+\lambda_k)^{M+R}\Gamma(M)\Gamma(R)}dv=\frac{(1+\lambda_k)^2M(M+1)}{(R-1)(R-2)} \tag{5}$$

We assume a frequency-nonselective slow-fading model for each channel, i.e., the channel remains unchanged during the transmission of the information of each sensor.

Transmission scheme with known channel gain

Nowadays, channel estimation technique has been widely adopted in communication system. Therefore, we assume that the gain h_k of the channel between the k-th sensor and the FC is known.

Analog transmission. The k-th sensor transmits $\xi_k \triangleq s_k\left(h_k\right)^{-1}$ to the FC via Rayleigh fading channel. Transmission is done by setting the amplitude of an underlying unit-energy waveform to ξ_k . All sensors use the same underlying waveform. Then, the output of the channel for the k-th sensor is

$$r_k=\sqrt{P_{rk}^{fc}}h_k\xi_k+w_k=\sqrt{P_{rk}^{fc}}s_k+w_k \tag{6}$$

where w_k is zero mean Gaussian noise with variance $\sigma_{w_k}^2$, and h_k is the gain of a real valued Rayleigh fading channel with the PDF given by $f(h_k)=2h_ke^{-h_k^2}, h_k \ge 0$.

The SNR of r_k , under H_1 , is

$$\lambda_{ck}^B=\mathbb{E}\left[\left(\sqrt{P_{rk}^{fc}}s_k\right)^2\right]\left\{\mathbb{E}\left[\left(w_k\right)^2\right]\right\}^{-1}=\mathbb{E}\left[s_k^2\right]P_{rk}^{fc}\sigma_{w_k}^{-2}=\frac{P_{rk}^{fc}}{\sigma_{w_k}^2}\frac{(1+\lambda_k)^2M(M+1)}{(R-1)(R-2)} \; . \tag{7}$$

Modified analog transmission. Each local test statistic s_k is modified according to Eq.(8).

$$\zeta_k=\begin{cases} s_k/\tau_k/h_k, & s_k \ge \tau_k; \\ -1/h_k, & s_k<\tau_k. \end{cases} \tag{8}$$

Hence, the output of the channel for the *k*-th sensor is given by Eq.9.

$$r_k = \sqrt{P_{rk}^{fc}} h_k \zeta_k + w_k \tag{9}$$

The SNR of r_k , under H_1 ,is

$$\lambda_{ck}^{MA} = \frac{\mathbb{E}\left[\left(\sqrt{P_{rk}^{fc}} h_k \zeta_k\right)^2\right]}{\mathbb{E}\left[\left(w_k\right)^2\right]} = \frac{P_{rk}^{fc}(1+\lambda_k)^2 M(M+1)}{\sigma_{w_k}^2 \tau_k^2 (R-1)(R-2)} P_{ld}(\tau_k, \lambda_k, M+2, R\text{-}2) + \frac{P_{rk}^{fc}}{\sigma_{w_k}^2}\left[1 - P_{ld}(\tau_k, \lambda_k, M, R)\right] \tag{10}$$

Binary transmission. Local sensor makes binary decision, and then transmit it to the FC, which is a canonical transmission scheme[6]. By means of the channel gain h_k , the *k*-th sensor transmits $\psi_k \triangleq u_k / h_k$ to the fusion center. Hence, the output of the channel for the *k*-th sensor is given by

$$r_k = \sqrt{P_{rk}^{fc}} h_k \psi_k + w_k = \sqrt{P_{rk}^{fc}} u_k + w_k \tag{11}$$

Fusion rules

Considering that the optimum detector is mathematically intractable, we turn to the suboptimum EGC fusion rules [7]. The fusion rule of EGC is shown in Eq.12.

$$\Lambda_{EGC} = \sum_{k=1}^{N} r_k . \tag{12}$$

If the channel is noiseless, the FC can reconstruct s_k perfectly. Therefore, the SUM fusion rule[8], given by $\Lambda_{sum} = \sum_{k=1}^{N} s_k$, can be used. In the following, we will evaluate the performance of the transmission scheme and compare their performances to the SUM fusion rule.

Simulation Results

We consider an eight-sensor system for the following two cases. In case I, the local sensors have the same performance index, i.e., $P_{ldk} = 0.5$ and $P_{lfk} = 0.05$ for all *k*'s, and the channels have the same average received SNRs if H_1 is true. In case II, the local sensors have different detection performances, but the channels have the same average received SNR if H_1 is true. Specially, $\{P_{ldk}\} = \{0.1, 0.1, 0.3, 0.3, 0.5, 0.5, 0.7, 0.7\}$, and $P_{lfk} = 0.05$ for all *k*'s. The system level false alarm rate is assumed to be 0.001. System detection probabilities were evaluated by Monte Carlo simulation of 10^7 runs. The fusion rule adopted is the EGC fusion, as given in Eq.12. In order to facilitate performance comparison, we give the detection performance of the SUM fusion under ideal noiseless transmission conditions, denoted by Ideal in the following.

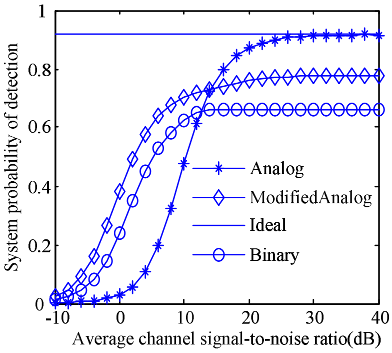

Fig. 1 System probability of detection versus the average received SNR in case I.

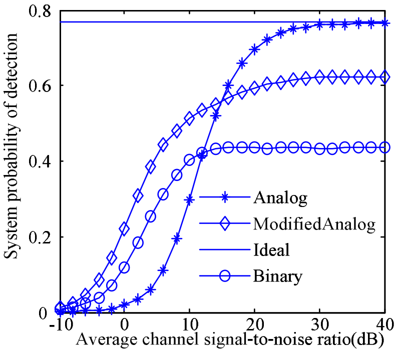

Fig. 2 System probability of detection versus the average received SNR in case II.

Figure 1 gives the system probabilities of detection versus the average received SNR in case I. With the increase of the average channel SNR, the detection performance of the analog scheme approaches the ideal detection probability. From Fig.1, it can be found that, when the channel SNR is larger than 30dB, the system probability of detection approaches the ideal value. When the channel SNR is low, such as less than 10dB, the analog scheme would result in worse performance than both the Modified analog scheme and the binary transmission scheme. Furthermore, the modified Analog scheme has better detection performance than the binary scheme, and the gap is as much as 0.05.

Under disparate detection performances, as given in case II, the proposed two analog transmission scheme also brings significant performance gain over the binary transmission scheme, as shown in Fig.2. An interesting phenomenon can be observed that, when the channel SNR is larger than 30dB, the detection performance will almost keep constant. In another word, the detection performance of the distributed detection system is not proportional to the channel SNR ratio.

Conclusions

Two analog transmission schemes for distributed signal detection was proposed and evaluated in this paper. When the channel SNR is high, such as larger than 20dB, the system adopting the proposed analog transmission scheme can approach the one with ideal transmission condition in detection performance. When the channel SNR is low, such as less than 10dB, the modified analog transmission scheme has better detection performance than the binary transmission scheme. Therefore, according to the channel state information at the sensor, the sensor can select appropriate transmission scheme to improve the system's detection performance, which will be our further study.

Acknowledgements

The China National Science Foundation under Grant No. 61102160 and the project for postgraduates of military science (2010JY0423-241) support this work.

References

[1] I. Nevat, G.W. Peters, and I.B. Collings, *Distributed Detection in Sensor Networks Over Fading Channels With Multiple Antennas at the Fusion Centre.*IEEE Trans. on Signal Processing, 2014. **62**(3): p. 671-683.

[2] S.K. Jayaweera, *Large System Performance of Power-constrained Distributed Detection with Analog Local Processing*, in *2005 International Conference on Wireless Networks, Communications and Mobile Computing*. 2005. p. 1083-1088.

[3] A.M. Fadhil, H.M. AlSabbagh, and T.Y. Abdallah, *Fusion Performance in Wireless DS-CDMA Sensor Networks with Analog Relay Local Processing Scheme.* network, 2012. **5**(3): p. 141-150.

[4] M. Gastpar, B. Rimoldi, and M. Vetterli, *To Code, or Not to Code: Lossy Source–Channel Communication Revisited.* IEEE TRANS. ON INFORMATION THEORY, 2003. **49**(5): p. 1147-1158.

[5] H. Behroozi, F. Alajaji, and T. Linder, *Does analog transmission achieve OPTA in an asymmetric Gaussian sensor network.* 2009. p. 99-103.

[6] K.-C. Lai, Y.-L. Yang, and J.-J. Jia, *Fusion of Decisions Transmitted Over Flat Fading Channels Via Maximizing the Deflection Coefficient.* IEEE Trans. on Vehicular Technology, 2010. **59**(7): p. 3634 - 3640

[7] R. Niu, B. Chen, and P.K. Varshney, *Fusion of decisions transmitted over Rayleigh fading channels in wireless sensor networks.* IEEE Trans. on Signal Processing, 2006. **54**(3): p. 1018-1027.

[8] X.Y. Liu, J. Guan, and Y.N. Peng, *An adaptive censored summation fusion scheme for distributed detection.* Signal Processing, 2008. **88**(7): p. 1898-1906.

Applied Mechanics and Materials Vol. 596 (2014) pp 807-810
© (2014) Trans Tech Publications, Switzerland
doi:10.4028/www.scientific.net/AMM.596.807

Mode conversion models based on spatial spectral matching for mode division multiplexing in optical fibers

Mingying Lan[1, a], Song Nie[1], Li Gao[1,2], Shanyong Cai[1], Chenxing Ma[1],
Xiaoli Qi[3], Zhichao Du[3]

[1] State Key Laboratory of Information Photonics and Optical Communications, Beijing University of Posts and Telecommunications, Beijing 100876, China

[2] School of Digital Media and Design Arts, Beijing University of Posts and Telecommunications, Beijing 100876, China

[3]School of Network Education, Beijing University of Posts and Telecommunications, Beijing 100876, China

[a] lanmingying@bupt.edu.cn

Keywords: mode division multiplexing; optical fiber communication; spatial light modulator; mode conversion.

Abstract. In this paper, a mode conversion model is proposed to increase the capacity of optical fiber communication systems. In this model, a spatial spectral matching method is used to convert the original mode to the desired mode for mode division multiplexing in optical fibers. A binary phase spatial light modulator is employed on the Fourier plane as a spatial filter. Numerical results show that the original modes can be converted to the desired modes.

Introduction

Recent years, the network traffic of optical fiber communication systems has increased by a factor of approximately 10 every four years[1]. Mode division multiplexing (MDM) is regarded as a potential approach to overcome the capacity limit of single mode fibers (SMFs) [2][3]. It can enhance the capacity of the optical fiber communication systems by using the spatial modes of multimode fibers (MMFs) or few-mode fibers (FMFs) as independent data channels[4].

One of the key elements in MDM is the mode convertor, which allows converting the basic mode of SMF to the higher modes of MMF/FMF at the transmitters[5], or playing an inverse role at the receivers[6], or converting any mode in the reconfigurable add-drop multiplexers (ROADMs) at the networks[2]. Main schemes of mode conversion are fousing on realizing the mode excitine at the transmitters and receivers, which can be categorized as follows: phase plate based[7], spatial light modulator (SLM) based[6][8], spot based[9], planar lightwave circuit (PLC) based[10] and photonic lantern based solutions[11]. These schemes mainly realize the conversion between the basic mode and other higher order modes. However, there are few schemes to realize any mode conversion until now.

In this paper, a flexible mode conversion solution is proposed which is able to convert the original modes to other desired modes. A phase only SLM is used as a spatial filter on the Fourier transform plane. As SLM needs to be programmed to different binary phase masks, it is very important to analyze the mode convertor by simulation method. Spatial spectral matching method is designed in details from the SLM plane to the original plane and the desired plane. Simulated results demostrate that LP02 mode can be converted to 4 modes (LP11b, LP21b, LP12a, LP31a). Moreover, this mode convertor can scale up to support more modes. Within the proposed mode convertor, an original mode can be converted to another desired mode which may support switching data channels mode by mode in the MDM-based networks.

The rest of this paper is organized as follows. In Section 2, the spatial spectral matching method is analyzed in details. Section 3 shows the simulated results. Finally, the conclusion is given in Section 4.

Analysis of spatial spectral matching

Fig. 1 is the mode convertor setup which is consisted of two-lens optical Fourier processor. Po with the coordinates (x_o, y_o) is the left focal plane of the first lens (Len1). Pd with the coordinates (x_d, y_d) is the right focal plane of the second lens (Len2). The focal length of the two lens are f_1 and f_2 respectively. The original mode out of the original-MMF (O-MMF) is located on the Po while the desired mode input into the desired-MMF (D-MMF) is placed on the Pd. The phase only SLM is placed on the Fourier plane as a spatial filter. The input plane and the output plane of the SLM are denoted Pfi with the coordinates (x_{fi}, y_{fi}) and Pfo with the coordinates (x_{fo}, y_{fo}) respectively.

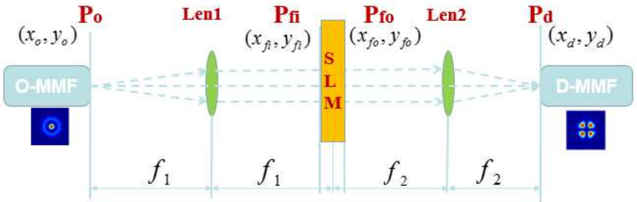

Figure 1. Mode convertor setup.

The field u_{fi} on the Po is the Fourier transform of the field u_o on the Pfi

$$u_{fi}\left(x_{fi}, y_{fi}\right) = \iint_{\infty} u_o\left(x_o, y_o\right) e^{-j2\pi\left(x_o f_x + y_o f_y\right)} dx_o dy_o \Big|_{f_x = \frac{x_{fi}}{\lambda f_1}, f_y = \frac{y_{fi}}{\lambda f_1}} \tag{1}$$

where λ is the wavelength of the light, f_x and f_y are spatial frequencies on the spatial frequency domain. As a result, the coordinates (x_{fi}, y_{fi}) are equal to the spatial frequencies (f_x, f_y) multiplied by a coefficient of λf_1.

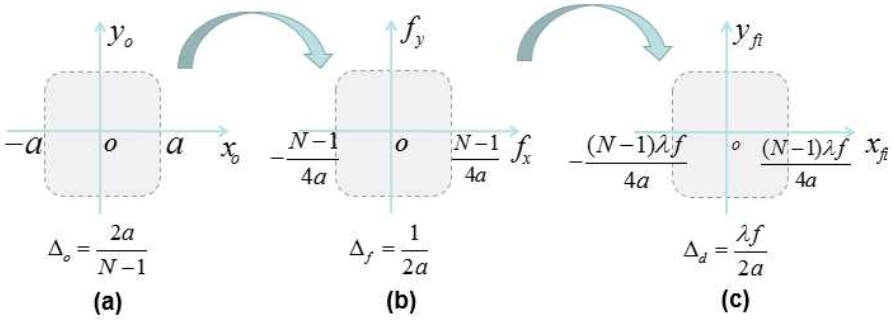
y_o
$-a$
o
a
x_o
$\Delta_o = \frac{2a}{N-1}$
(a)
f_y
$-\frac{N-1}{4a}$
o
$\frac{N-1}{4a}$
f_x
$\Delta_f = \frac{1}{2a}$
(b)
y_{fi}
$-\frac{(N-1)\lambda f}{4a}$
o
$\frac{(N-1)\lambda f}{4a}$
x_{fi}
$\Delta_d = \frac{\lambda f}{2a}$
(c)

Figure 2. The relationship of three planes: (a) the original plane in the spatial domain; (b) the Fourier transform plane in the frequency domain; (c) the SLM plane in the spatial domain.

Fig. 2 is the relationship of three planes: (a) the original plane (x_o, y_o) in the spatial domain, (b) the Fourier transform plane (f_x, f_y) in the frequency domain, (c) the SLM plane (x_{fi}, y_{fi}) in the spatial domain. In the simulation, a common method is that the initialization is set from the original plane. The region of (x_o, y_o) is arranged to $(-a, a)$ which is sampled into N points at first. Then the region of (f_x, f_y) is calculated to $(-(N-1)/4a, (N-1)/4a)$ by FFT. After that we can get the region of (x_{fi}, y_{fi}) (see Fig. 2(c)) which is related to f_1 and the O-MMF. The region of (x_{fo}, y_{fo}) on the Pfo can be calculated from the desired plane in the inverse way (see Fig. 3). It is clearly that (x_{fo}, y_{fo}) is related to f_2 and the D-MMF. The spatial spectral would unmatch on the SLM plane when the O-MMF and D-MMF, or f_1 and f_2 are different slightly (see Fig. 4).

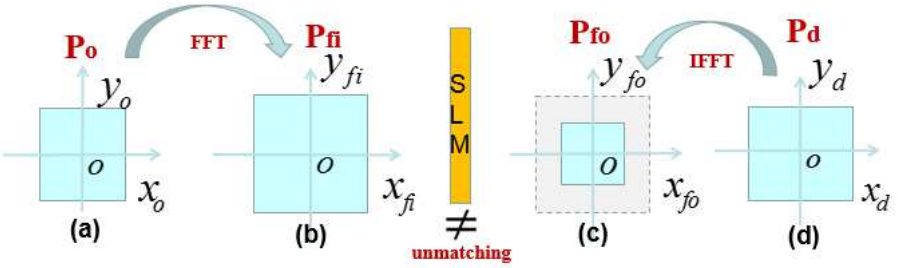

Figure 3. Spatial spectral unmatching: simulation from the original plane (a) to the SLM plane (b) and from the desired plane (d) to the SLM plane (c) respectively.

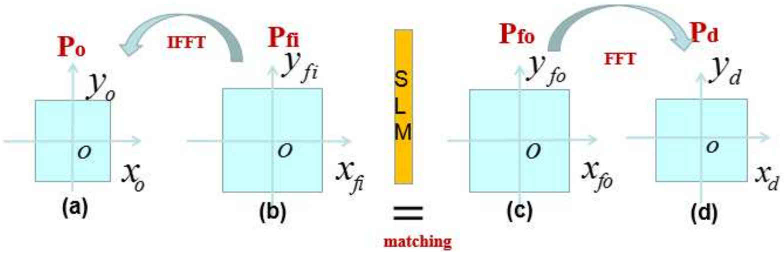

Figure 4. Spatial spectral matching: simulation simultaneously from the SLM plane (b) (c) to the original plane (a) and the desired plane (d).

In order to avoid spatial spectral unmatching, the simulation starts from the SLM plane, then calculates the regions of the original plane and the desired plane simultaneously (see Fig. 4).

Simulated results

For a proof-of-concept, there is no need to convert all modes. We just take the LP02 for example as the original mode in Fig. 5. The ideal patterns of the desired modes (LP11b, LP21b, LP12a, LP31a) are shown in Fig. 6 (a). Fig. 6 (b) shows the binary phase filters on the SLM for the LP02 converting to each desired mode. The simulated results of the desired modes are illustrated in Fig. 6 (c). By comparing Fig. 6(a) with Fig. 6(c), it can be found that the simulated results of the desired modes are very close to the ideal patterns.

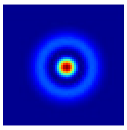

Figure 5. The original mode: LP02.

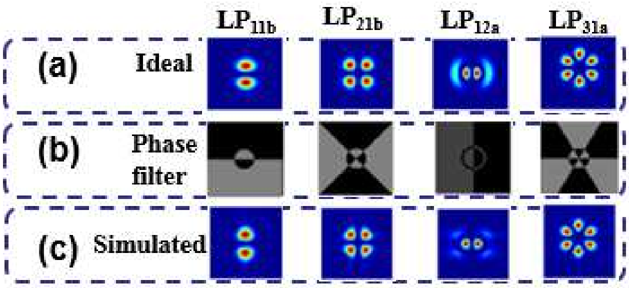

Fig. 6. The desired modes (LP11b, LP21b, LP12a, LP31a): (a) the ideal patterns; (b) the binary phase filters on the SLM for the original mode converting to each desired mode, (black—0, gray--π); (c) the simulated results of the desired modes.

Conclusions

In this paper we discussed a mode convertor which is able to convert the original mode to another desired mode. We proposed a simulation modal by analyzing the relationship of the four planes of Fourier SLM setup. By matching the spatial spectral on the SLM plane, simulation results demonstrated that the LP02 mode can be converted to the LP11b, LP21b, LP12a and LP31a. Moreover, more modes could be converted which may play an important role in the MDM-based networks.

Acknowledgements

This work was supported in part by the National Basic Research Program of China (973 Program) under Grants 2012CB315605 and 2014CB340102 and in part by the National Natural Science Foundation under Grants 61271191, 61271193, 61072054 and 61302085.

References

[1] R. J. Essiambre, R. Ryf, N. K. Fontaine, et al., Ieee Photonics Journal, Vol. 5, No. 2, (2013).

[2] D.J. Richardson, J.M. Fini and L.E. Nelson, Nature Photonics, Vol. 7, No. 5, (2013), pp. 354-362.

[3] R. Essiambre, R. Ryf, N. Fontaine, et al., Photonics Journal, Vol. 5, No. 2, (2013).

[4] Bai Neng, Ip Ezra, Huang Yue-Kai, et al., Optics Express, Vol. 20, No. 3, (2012), pp. 2668-2680.

[5] Carpenter Joel and Wilkinson Timothy D, Precise modal excitation in multimode fibre for control of modal dispersion and mode-group division multiplexing, European Conference and Exposition on Optical Communications, Optical Society of America, (2011).

[6] M. Salsi, C. Koebele, D. Sperti, et al., Journal of Lightwave Technology, Vol. 30, No. 4, (2012), pp. 618-623.

[7] C. Montero-Orille, V. Moreno, X. Prieto-Blanco, et al., Applied Optics, Vol. 52, No. 11, (2013), pp. 2332-2339.

[8] J. Carpenter and T. D. Wilkinson, Journal of Lightwave Technology, Vol. 30, No. 10, (2012), pp. 1386-1392.

[9] Ryf Roland, Fontaine Nicolas K and Essiambre R-J, Photonics Technology Letters, Vol. 24, No. 21, (2012), pp. 1973-1976.

[10]Uematsu Takui, Hanzawa Nobutomo, Saitoh Kunimasa, et al., PLC-type LP11 mode rotator with single-trench waveguide for mode-division multiplexing transmission, Optical Fiber Communication Conference, San Francisco, California, Optical Society of America, (2014).

[11]S. G. Leon-Saval, A. Argyros and J. Bland-Hawthorn, Optics Express, Vol. 18, No. 8, (2010), pp. 8430-8439.

Applied Mechanics and Materials Vol. 596 (2014) pp 811-815
© (2014) Trans Tech Publications, Switzerland
doi:10.4028/www.scientific.net/AMM.596.811

Reference Signals Design and Evaluation on Radio-interface Based Synchronization of LTE Base Station System

Ruhong Zeng[1, a], Deshan Miao[2, b], Naizheng Zheng[2, c], Hongwen Yang[1, d]

[1]School of Information & Communication Engineering, Beijing University of Posts and Telecommunications, Beijing 100876, China

[2] CEF Technology & Innovation, NSN Technology (Beijing), Beijing 100102, China

[a]wanfec@163.com, [b]deshan.miao@nsn.com, [c]naizheng.zheng@nsn.com, [d]yanghong@bupt.edu.cn

Keywords: LTE; small cell; synchronization; radio-interface;

Abstract. This paper discusses the reference signals used in synchronization for LTE system. In general, primary synchronization signal (PSS) correlation based acquisition and reference signals based tracking loop are applied for time and frequency synchronization but it is unclear which legacy reference signals (RS) will be used as the listening RS for radio-interface based synchronization. Besides the legacy cell-specific reference signals (CRS) utilized as the listening RS, the other potential candidate could be either CSI reference signals (CSI-RS) or position reference signals (PRS). Upon performance evaluation, we compare the pros and cons of CRS, CSI-RS and PRS based synchronization and present our views.

Introduction

Recently, the amount of mobile data traffic worldwide has been increasing significantly [1]. To further enhance the network capacity, a scenario in which low-power small cells using a high frequency band such as 3.5 GHz are placed in high-traffic areas was proposed [2] where conventional macrocells provide fundamental coverage and mobility tracking for the UE while the aforementioned small cells provide high data throughput and an offloading effect [3]. Synchronized application of small cells is essential for TD-LTE systems, and it is beneficial also for FDD-LTE systems if advanced features are utilized. Generally, the synchronization of small cells can be achieved with various solutions. For each of the synchronization solutions, there are pros and cons in terms of frequency/phase synchronization accuracy, hardware cost and/or applicability. In LTE network, the radio-interface based synchronization (RIBS) solution has been proposed as an option when other synchronization techniques are costly or deemed unavailable [4]. In LTE release-9, the legacy LTE reference signals for synchronization include PSS/SSS and CRS, with PSS/SSS acquisition and CRS tracking. But it is still unclear or not decided which legacy RS will be used as the listening RS for RIB synchronization. In LTE release 12, it is proposed that besides the legacy CRS utilized as the listening RS, the other potential candidate could be either CSI-RS or Position-RS (PRS).

In this paper, we share the synchronization algorithm based on radio-interface and show the tracking performance based on different reference signals. Finally, we analyze the results and draw a conclusion about the application conditions of different reference signals.

Reference Signals in LTE Systems

In LTE, resource element (RE) are grouped into resource blocks (RBs), where each resource block consists of 12 consecutive subcarrier in the frequency domain and one 0.5ms slot in the time domain. Each resource block thus consists of 7 symbols in the case of a normal cyclic prefix and 6 symbols in the case of an extended cyclic prefix in the time domain. And the basic time-domain unit for dynamic scheduling in LTE is one subframe, consisting of two consecutive slots [5]. Fig.1 shows a resource block pair, consisting of 12 subcarriers during one 1ms subframe. The RS we are dealing with in this paper are marked for convenience.

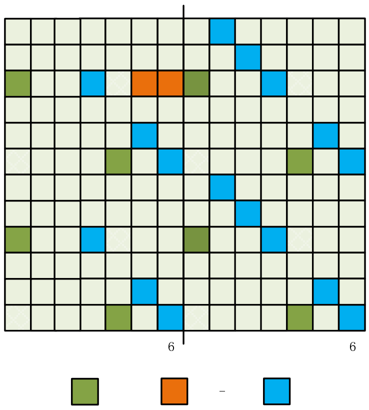

Fig. 1 Mapping of downlink reference signals.

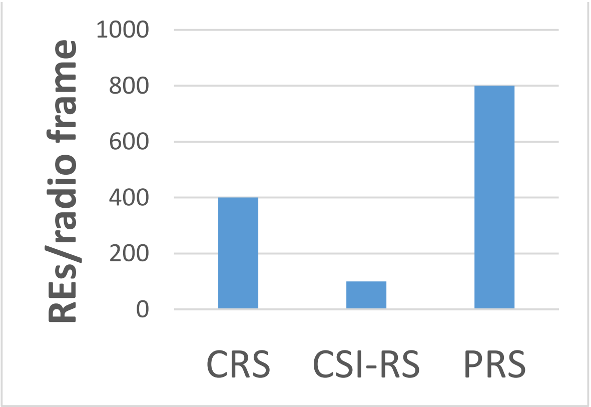

Fig. 2 Number of occupied REs per RS scheme over full system bandwidth and one radio frame.

The number of resource elements occupied by each RS scheme, over the system bandwidth (10MHz) and one radio frame (this is the tracking period in this paper), is given in Fig.2. This number is the key in selecting the optimum RS, since it captures also the resource usage of the RS [6].As shown in Fig.2, over the system bandwidth and one radio frame, CRS occupies 400 REs, meanwhile, 800REs for PRS and only 100 REs for CSI-RS. The greater the density of the reference signal is, the more channel state information we can get and the better the anti-noise property is. Therefore, we forecast that the performance of the CSI-RS would be worse than CRS and PRS would perform best. And we are interested in the quantitative performance gap between them.

Model and Algorithm for Synchronization

Fig.3 is used to illustrate the synchronization offset acquisition. The signal with timing error and frequency offset is dealt with the time synchronizer first and then with the frequency synchronizer. After fine tracking, we calculate the offset error of time and synchronization and then plot it on the graph.

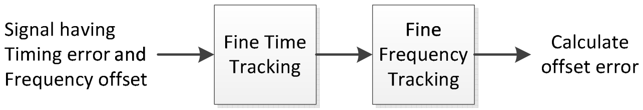
Signal having Timing error and Frequency offset
Fine Time Tracking
Fine Frequency Tracking
Calculate offset error

Fig.3 Synchronization offset acquisition model.

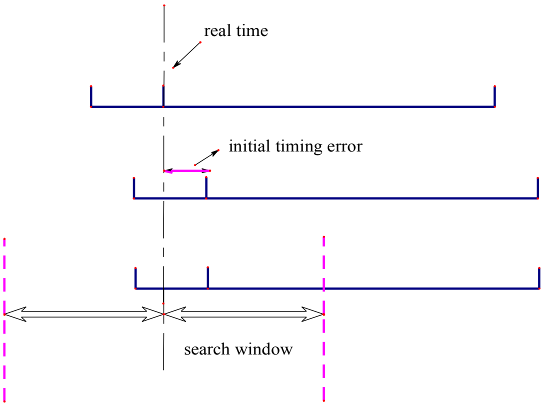
real time
initial timing error
search window

Fig.4 Time tracking.

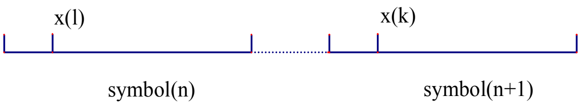
x(l)
x(k)
symbol(n)
symbol(n+1)

Fig.5 Frequency tracking.

Fig.4 shows the time synchronization. As shown in Fig.4, we assume that the length of time search window is N and the initial timing error is always set to zero. Then, we use $2N+1$ times of correlations for the whole subframe which contains RS signals for synchronization.

Fig.5 shows the frequency syncronization where *symbol*(n) and *symbol*(n+1) are adjacent symbols which contain RS signals for synchronization, $x(l)$ and $x(k)$ are samples in the same relative location of the two symbols. The frequency error Δf can be calculated as follows:

$$\Delta f = \frac{\angle y}{2\pi T_s(k-l)} \tag{1}$$

where

$$y = x(k)x^*(l) = |ab|^2 e^{j2\pi\Delta f T_s(k-l)} + b\cdot Z^* e^{j2\pi\Delta f T_s k} + a\cdot Z e^{-j2\pi\Delta f T_s l} + |Z|^2 \tag{2}$$

$$x(l) = a\cdot \mathrm{e}^{j2\pi\Delta f T_s l} + Z \tag{3}$$

$$x(k) = b\cdot \mathrm{e}^{j2\pi\Delta f T_s k} + Z \tag{4}$$

where T_s is sampling period, Z is the noise, k, l are sample indices, a and b are two coefficients generated with assuming only RS.

Simulation Assumptions

In the simulation, normal CP and 2 antenna ports are assumed. The base station of a small cell is at rest relative to the earth. Consequently, an EPA channel model with low mobility (0.01km/h) is used. After initial acquisition on PSS, the offset of frequency and time can be narrowed down. Hence, it is assumed that the frequency offset between the source and the receiver is 0.1ppm and the timing detection window is (-2µs, 2µs). The other simulation parameters are listed in Table 1.

Table 1 Parameters

Signal bandwidth	10 MHz
Carrier frequency	3.5 GHz
Measurement duty cycle	1 subframe in every 5 ms frame
Signals used	CRS,CSI-RS,PRS

Performance Results and Analysis

In this section, synchronization performance based on CRS, CSI-RS and PRS is evaluated. The figures below target fine time and frequency tracking based on one kind of reference signal after initial acquisition on PSS.

Frequency synchronization

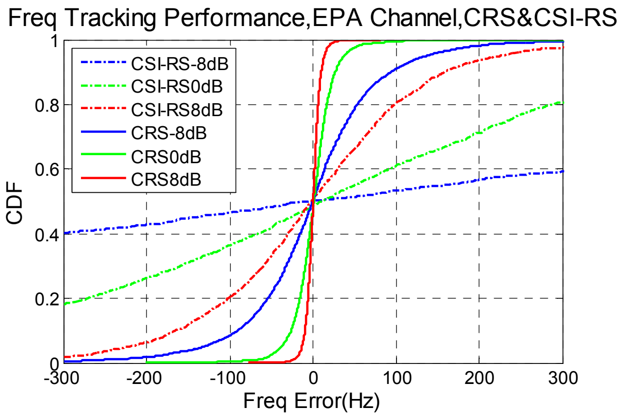

Fig.6 Frequency tracking based on CRS and CSI-RS.

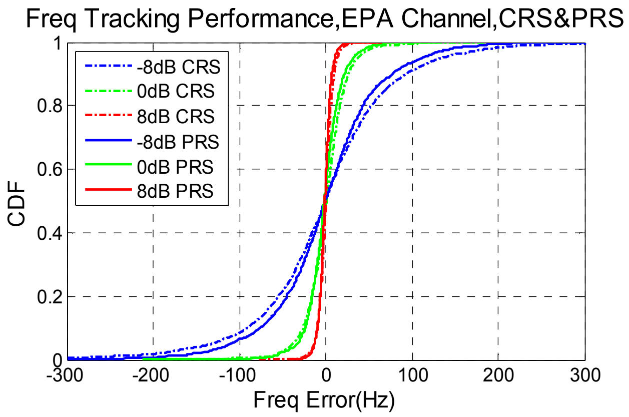

Fig.7 Frequency tracking based on CRS and PRS.

Frequency synchronization performance for the CSI-RS and CRS is shown in Fig.6. Compared with the performance using CRS, the performance using CSI-RS suffers a significant degradation for frequency synchronization at low SNR because of the lack of many phase comparisons per subframe and the short distance between the OFDM symbols. It can be seen from last section that the shorter distance between the two OFDM symbols that is used to estimate Δf would lead to smaller value of phase angle and $(k-l)$. Hence, Δf we get from equation (1) would be more sensitive to the noise.

In Fig.7, the frequency synchronization performance of PRS are shown compared with legacy CRS. The higher RE density but shorter distance between the OFDM symbols of PRS than CRS just makes it having a little better performance at low SNR. And at high SNR=8dB, the CRS has similar frequency tracking performance as PRS.

Time synchronization

Fig.8 shows the mean square error of the synchronization performance based on the different reference signals with the SNR ranges from -20dB to 8dB. At low SNR, the performance of PRS-based synchronization can obtain SINR gain about 4dB over CRS and 10 dB over CSI-RS. For instance, at MSE=0.4, CSI-RS-based synchronization can operate at around -10dB, while CRS-based synchronization can operate at around -16dB, 6dB SNR gain, and PRS-based synchronization can operate at around -20dB, about 10dB SINR gain. Meanwhile, at medium to high SNR from -8dB to 0dB, PRS provide similar time tracking performance as legacy CRS. And CSI-RS yields performance comparable with that obtained using legacy CRS at high SNR from 0dB to 8dB.

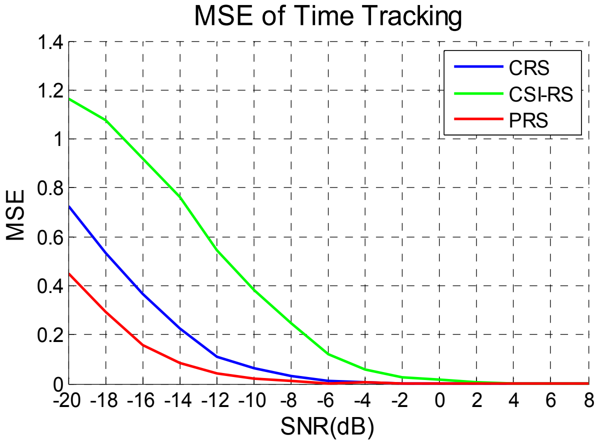

Fig.8 Mean square error of RS based time tacking

Conclusion

The performance of time and frequency synchronization in the presence of CRS was discussed and detailed simulation results were provided. Performance based on the CSI-RS and PRS patterns considered was also evaluated. We have the following observations: PRS provide similar time tracking performance as legacy CRS at medium to high SNR, and there is about 4dB gain for PRS over legacy CRS at low SNR. And the performance of PRS based frequency tracking is slightly better than that based on legacy CRS. But the high overhead of PRS should be taken into consideration when it is used. In contrast, CSI-RS provides similar time tracking performance as legacy CRS only at high SNR, and will be significantly degraded at medium to low SNR. Meanwhile, CSI-RS fails to provide decent frequency tracking performance. Consequently, PRS is suitable to be used in a relatively poor channel environment with a high level of overhead and CSI-RS based synchronization with small overhead can be used in proper channel condition with high SNR.

References

[1] Report ITU-R M.2243, "Assessment of the global mobile broadband deployments and forecasts for International Mobile Telecommunications," Nov. 2011.
[2] 3GPP, RWS-120010, NTT DOCOMO, "Requirements, Candidate Solutions & Technology Roadmap for LTE Rel-12 Onward," June 2012.
[3] A. Benjebbour, Y. Kishiyama, H. Ishii and T. Nakamura, "Conceptual Views and Radio Access Technologies for Future Evolution of LTE-A," (in Japanese) IEICE Technical Report, vol. 112, no. 192, RCS2012-100, pp. 25-30, Aug. 2012.
[4] R1-134529, “Considerations on Radio-interface based Synchronization”, NSN, Nokia.
[5] Dahlman E, Parkvall S, Skold J: 4G: LTE/LTE-advanced for mobile broadband[M]. Academic Press, 2013.
[6] R1-121266, “Time/Frequency Tracking Performance on New Carrier Type”, Nokia, Nokia Siemens Networks.

Applied Mechanics and Materials Vol. 596 (2014) pp 816-821
© (2014) Trans Tech Publications, Switzerland
doi:10.4028/www.scientific.net/AMM.596.816

Electromagnetic Coupling Reduction in Microstrip Antenna Arrays Using Single-negative Electric Waveguided Metamaterials

Lizhong Hu [a *], Guangming Wang[b] and Guocheng Wu[c]

Lab. of Microwave Technology, Dept. of School of Air and Missile Defense, Air Force Engineering University Xi'an, China

[a]coke2008283@126.com, [b]wgming01@sina.com, [c]wgc805735557@163.com

Keywords: metamaterials, mutual coupling reduction, antenna arrays

Abstract. A single-negative electric waveguided metamaterial(WG-MTM) is proposed using folded complementary split single ring resonator(FCSSRR) to reduce mutual coupling in antenna arrays for MIMO applications. The WG-MTM is investigated numerically, which proved to exhibit electric resonance and band-gap property. Two antenna arrays have been designed, fabricated and measured. By inserting the electric negative metamaterial, a mutual coupling reduction of 9.2dB has been achieved with an edge-to-edge distance less than 0.17 λ_0 (where λ_0 is the operating wavelength). Moreover, the metamaterial loaded antenna has better far-field radiation patterns compared with the reference antenna. Thus, this novel structure not only has good coupling reduction ability, but also can optimize the performances of the antennas.

Introduction

Multiple-input and multiple-output (MIMO) communication systems have attracted much attention as a practical method to substantially increase wireless channel capacity without the need for additional power or spectrum in rich scattering environments [1]. More than two antennas are often employed in MIMO systems. Thus, the mutual coupling between any two antennas within the array is often required and needs to be kept as low as possible for better performance of the MIMO antenna system. Usually in order to obtain a decent isolation between antennas and good performances, antenna elements need to be placed apart at least $\lambda_0/2$. Otherwise, undesirable degradation on antenna radiation characteristics would be encountered due to the near-field effects and surface waves[2-3]. To overcome the problem of mutual coupling, several techniques have been reported in the literature[4-11]. Some of these techniques are based on the use of defected ground structures[4-6], Electromagnetic Band Gap (EBG) structures[7-9], and single-negative metamaterial structures[10-11].

In this paper, a single-negative electric waveguided metamaterial is proposed to efficiently suppress the electromagnetic coupling between two closely spaced microstrip antennas. The characteristic of the electric WG-MTM is analyzed first, then it's supposed that the band-gap characteristic of this structure can provide a filter effect in antennas decoupling. To demonstrate this idea, a dual-element microstrip antenna array for compact MIMO terminal application is proposed. A mutual coupling reduction of 9.2dB is achieved experimentally between a pair of antennas working at 5.2 GHz WLAN 802.11n with an antenna to antenna separation 0.17 λ_0.

Unit Structure and Analysis of the Electric WG-MTMS

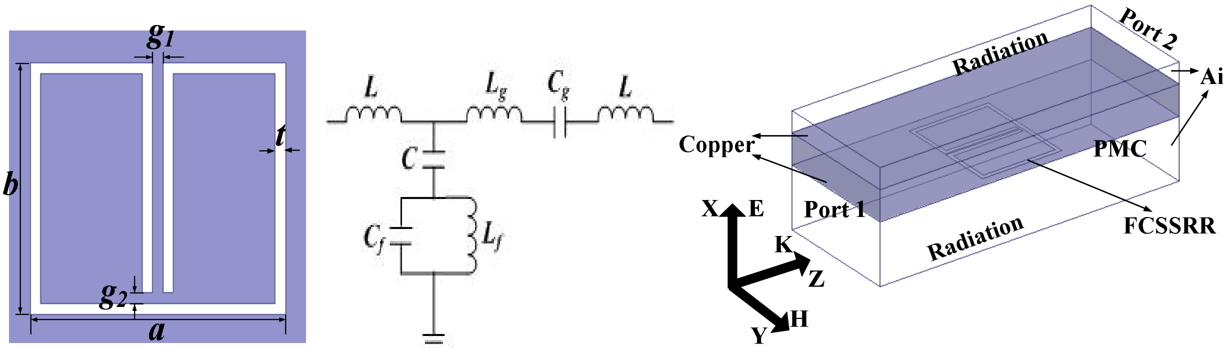

(a) (b) (c)

Fig.1.The proposed single-negative electric metamaterials based on the FCSSRR. (a) Unit cell with its dimensions, (b) Equivalent circuit model, (c) Waveguide structure as well as the simulation setup. Note that E-field points in x-direction, H-field is in y-direction, and the propagation is z-direction.

Complementary split single ring resonator (CSSRR) structure exhibits resonant behavior in the presence of vertically polarized (with respect to the CSSRR's plane) electric fields[12].It can reduce the resonant frequency by folding the gap of CSSRR because of the increasing current path in the ground, and thus miniaturization is realized. The geometry of the proposed FCSSRR inserted on the ground plane is illustrated in Fig.1(a) and the final geometrical parameters (in millimeter: mm) are a=3.4,b=3.45,t=0.2,g_1=0.2 and g_2=0.2.

Fig.1(b) is the equivalent circuit model of the proposed FCSSRR. Observation from the circuit model indicates that there exists one resonant frequency f which is determined by L_f, C, C_f , as shown in Eq.1.

$$f_0 = 1\big/2\pi\sqrt{L_f(C+C_f)} \quad (1)$$

The commercial simulator Ansoft HFSS is employed to analyze and design. The entire layout in this paper is built on a commonly utilized substrate F4B with dielectric constant ε_r=2.65, thickness h=1.5mm, and loss tangent $\tan\delta$=0.001. Fig.1(c) shows the simulation setup and the structure of the proposed WG-MTM which consists of two parallel metallic plates: the top complete metal and the bottom defected one. Notice that the WG-MTM is positioned such that the incident electric field is perpendicular to the inclusion's trace (or surface). The model mimics a transverse electromagnetic mode in both ports, with top and bottom sides of the air-filled waveguide assigned as radiation boundary to prevent reflections from the computational domain, while the two walls along y-axes as perfect magnetic conductors to mimic an infinite array.

Fig.2 (a) shows the scattering parameters of the proposed WG-MTM, the transmission coefficient S21 is about -20 dB at resonance. That dip in the transmission coefficient is attributed to the electric resonance nature of the developed inclusions when an electric field impinges normally to the inclusions axis. As such, the energy is sustained within the inclusions and results in no transmission at the enhanced electric resonance. The real and imaginary parts of the effective permittivity and permeability of the electric resonators are extracted by using standard retrieval procedure [13].As shown in Fig.2(b), the permittivity is negative at 5.2GHz, proving that the proposed WG-MTM is electric negative metamaterial.

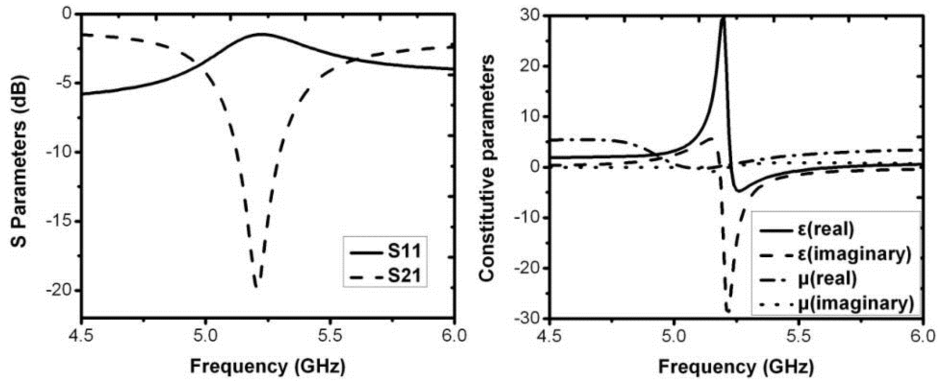

(a) (b)

Fig.2. Characterization of the proposed WG-MTM. (a)Scattering parameters (b) Constitutive parameters

In order to analyze the unit cell deeply, the optimetric function is used in the full wave simulation, and the results are shown in Figure 3. The resonant frequency f can be modulated by altering the geometrical dimensions, e.g. f increases when a, b shrinks and t, g_1 increases. Thus, through adjusting the geometrical dimensions of the WG-MTM can make it working at different frequencies.

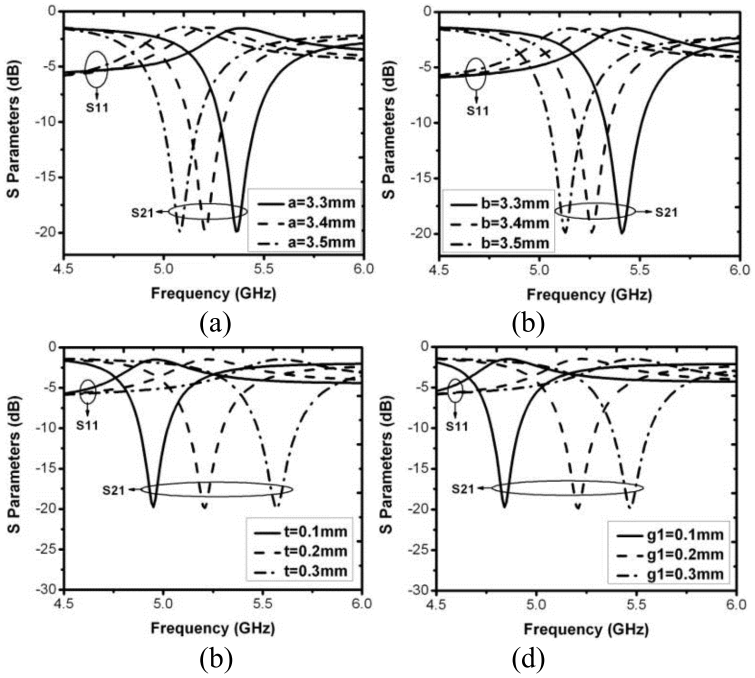

(a) (b)

(b) (d)

Fig.3. Dependence of S-parameters on a, b, t, g_1.

Applications in Decoupling of Microstrip Antenna Array

Based on the band-gap feature, the WG-MTM composed of FCSSRR array is expected to reduce the mutual coupling between radiating elements such as antennas. For verification, we have designed a 5.2GHz probe-fed patch antenna array. Fig.4 shows the distribution of the H-field and pointing vector on the substrate at 5.2GHz. Since the H-field between the two patches is parallel to the y-axes and the pointing vector is parallel to the x-axes, the gap of the WG-MTM should be set aligned with the x-axes to maximize the rejection effect. The geometry of the antenna array along with the proposed WG-MTM inserted between antennas is illustrated in Fig. 5. The former one is a reference antenna array, while the residual one is a 5×2 WG-MTM array loaded antenna array. The dimensions of the FCSSRR unit cell are chosen so that the resulted subwavelength band-gap of

WG-MTM covers the operational frequency of the patch array. To make fair comparison, the two antenna arrays have the same geometrical dimensions and they are built on the same substrate. Since the WG-MTM cell is electrically small, the distance between two patches could be set very close. In our work, the edge-to-edge distance between antennas is *ls*=9.8mm(0.17 λ_0).The geometrical parameters of the antennas are: *L*=16.3mm, *W*=21.4mm, *yf*=4.8mm and the whole footprint occupies a PCB area of 28.3×64.6 mm .

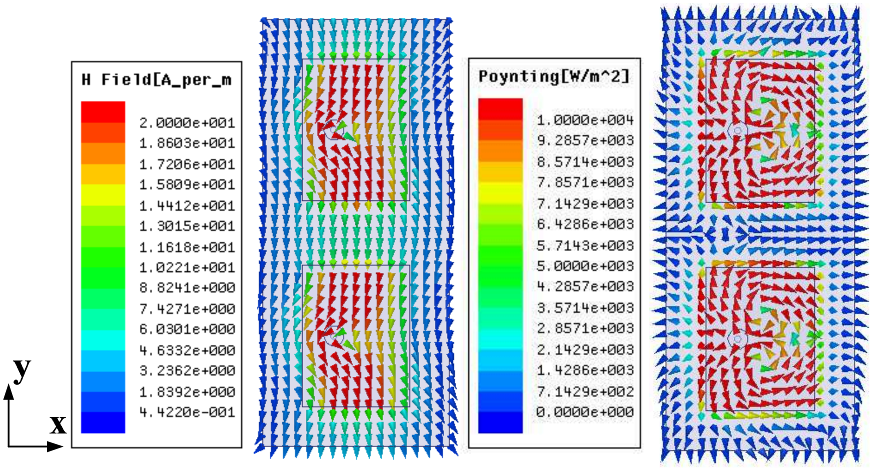

(a) (b)

Fig.4.Distribution of the (a) H-field and (b) Poynting vector on the substrate at 5.2GHz

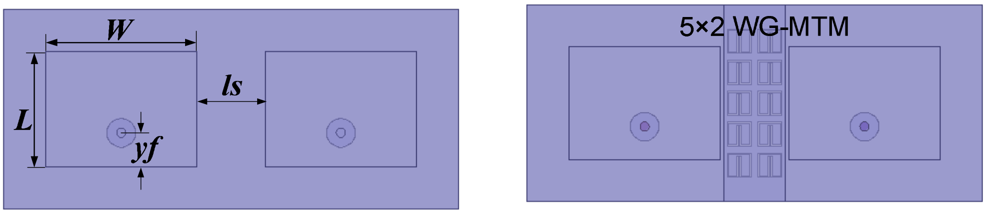

(a) (b)

Fig.5. Schematics of the proposed antenna arrays. (a)Reference antenna, (b) WG-MTM loaded antenna

Performance and Results

Two antenna arrays designed above have been fabricated and carefully measured, Fig.6 shows the photographs of the fabricated prototypes. The scattering parameters are tested as two-port devices using vector network analyzer, whereas the far-field radiation patterns are measured in an anechoic chamber by feeding one patch element and loading the other with a 50Ω broadband load.

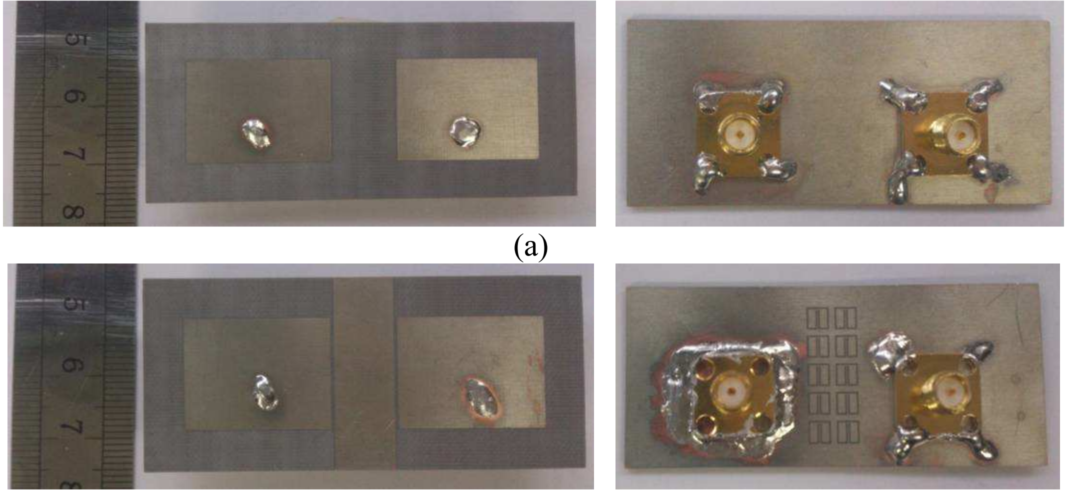

(a)

(b)

Fig.6. Photograph of the two fabricated prototypes: (a) Reference antenna, (b)

WG-MTM loaded antenna

Fig. 7 shows the simulated and measured scattering parameters of the two designed antennas, the measured and simulated results are in good agreement with each other except for a slight frequency shift upwards owing to the unstable ε_r of the substrate and effects of the WG-MTM on the electrical length. By inserting the WG-MTM inclusions between the antenna patches, the mutual coupling has been suppressed from -15.7dB to -24.9dB at the resonance frequency, i.e. a reduction of 9.2dB has been achieved, while at the same time maintaining good impedance match for the two-antenna array.

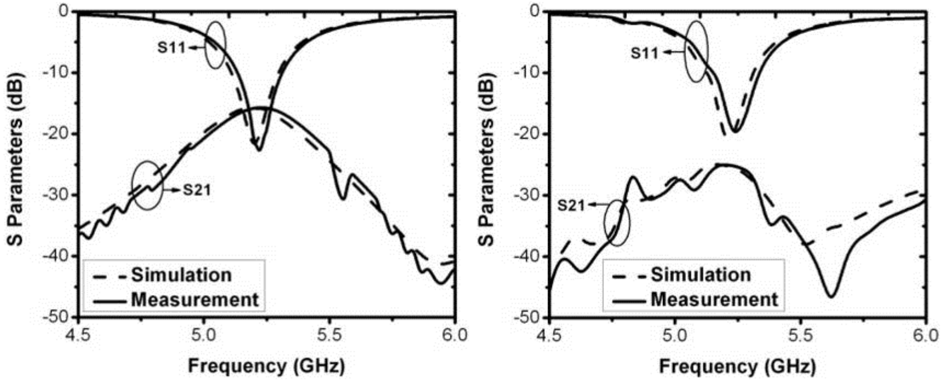

(a) (b)

Fig.7 Simulated and measured S-parameters of the fabricated antennas. (a)Reference antenna, (b) WG-MTM loaded antenna.

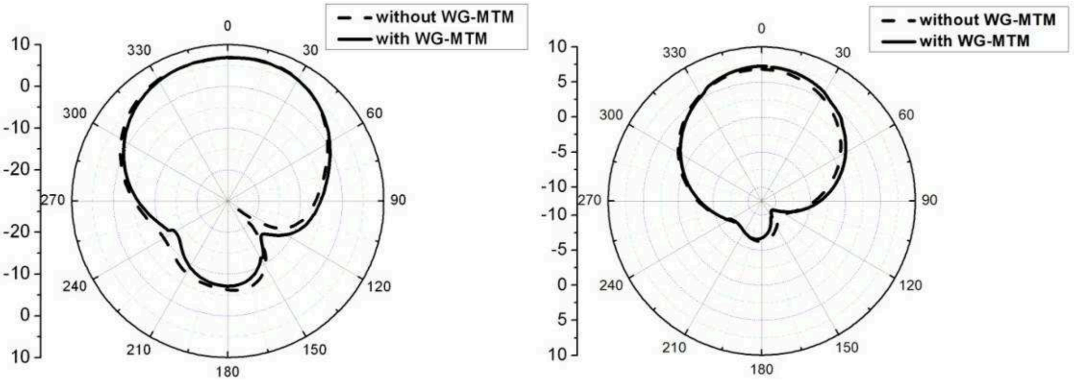

(a) (b)

Fig.8 Measured radiation patterns of the fabricated antennas. (a)H-plane, (b) E-plane.

The far-field radiation patterns of the two antennas at 5.2GHz in E-plane and H-plane are shown in Fig.8. As shown in Fig.8, the WG-MTM has a minor effect on the radiation pattern. The antenna with WG-MTM has smaller back radiation result in a better front-to-back ratio due to the mutual coupling reduction effect. Besides, these results do not show any significant differences between the main lobes patterns, forward gain, and antenna's efficiency.

Conclusions

In this letter, a single negative WG-MTM has been proposed to reduce mutual coupling in antenna arrays. By inserting the WG-MTM inclusions between the antenna patches, a mutual coupling reduction of 9.2dB has been achieved. Moreover, the far-field radiation patterns have been improved. Compared with other decoupling techniques, the proposed decoupling scheme provides high decoupling efficiency for closely spaced microstrip patches and involves simple and straightforward fabrication process.

Acknowledgement

This work is supported by the National Natural Science Foundation of China (Grant No. 61372034).

References

[1] J. Wallace, M. Jensen, A. Swindlehurst, and B. Jeffs, “Experimental characterization of the MIMO wireless channel: Data acquisition and analysis,” IEEE Trans. Wireless Commun., vol. 2, no. 2, pp. 335–343, Mar. 2003.

[2] C. A. Balanis, Antenna Theory Analysis and Design. Hoboken, NJ: Wiley, 2005.

[3] B. Bhattacharyya, “Input resistances of horizontal electric and vertical magnetic dipoles over a homogeneous ground,” IEEE Trans. AntennasPropag., vol. 11, no. 3, pp. 261–266, May 1963.

[4] F.-G. Zhu, J.-D. Xu, and Q. Xu, Reduction of mutual coupling between closely-packed antenna elements using defected ground structure, Electron Lett 45 (2009), 601–602.

[5] S. Farsi, H. Aliakbarian, B. Nauwelaers, and G.A.E. Vandenbosch, Mutual coupling reduction between planar antenna by using a simple microstrip U-section, IEEE Antennas Wireless Propag Lett 11 (2012), 1501–1503.

[6] D. Guha, S. Biswas, T. Joseph, M.T. Sebastian, Defected ground structure to reduce mutual coupling between cylindrical dielectric resonator antennas, Electron Lett 44 (2008), 836–837.

[7] F. Yang and Y. Rahmat-Samii, “Microstrip antennas integrated with electromagnetic band-gap (EBG) structures: A low mutual coupling design for array applications,” IEEE Trans. Antennas Propag., vol. 51, no. 10, pp. 2936–2946, Oct. 2003.

[8] M. Coulombe, K. S. Farzaneh, and C. Caloz, “Compact elongated mushroom (EM)-EBG structure for enhancement of patch antenna array performances,” IEEE Trans. Antennas Propag., vol. 58, no. 4, pp. 1076–1086, Apr. 2010.

[9] S. D. Assimonis, T. V. Yioultsis, and C. S. Antonopoulos, “Computational investigation and design of planar EBG structures for coupling reduction in antenna applications,” IEEE Trans. Magn., vol. 48, no. 2, pp. 771–774, Feb. 2012.

[10] M. M. Bait-Suwailam, M. S. Boybay, and O. M. Ramahi, “Electromagnetic Coupling Reduction in High-Profile Monopole Antennas Using Single-Negative Magnetic Metamaterials for MIMO Applications,” IEEE Trans. Antennas Propag.,vol. 58, no. 9, pp. 2894–2902, Sep., 2010.

[11] H.-X. Xu, G.-M. Wang, M.-Q. Qi, and H.-Y. Zeng, “Ultra-small single-negative electric metamaterials for electromagnetic coupling reduction of microstrip antenna array,” Opt. Exp., vol. 20, no. 20, pp. 21968–21976, 2012.

[12] R. Marqués, F. Martín, and M. Sorolla, Metamaterials With Negative Parameters: Theory, Design and Microwave Applications. Hoboken, NJ: Wiley, 2008.

[13] X. Chen, T. M. Grzegorczyk, B.-I. Wu, J. Pacheco, Jr., and J. A. Kong, “Robust method to retrieve the constitutive effective parameters of metamaterials,” Phys. Rev. E Stat. Nonlin. Soft Matter Phys. 70(1), 016608 (2004).

Applied Mechanics and Materials Vol. 596 (2014) pp 822-825
© (2014) Trans Tech Publications, Switzerland
doi:10.4028/www.scientific.net/AMM.596.822

Equivalent Electromagnetic Properties of Composite Media

Pang Xiao Fen

Inner Mongolia Vocational and Technical College of Communications, Inner Mongolia 024000, China

imvtcc@yeah.net

Keywords: Composite Media, Electrical Properties, Dielectric Constant, Dielectric Loss

Abstract. This paper selects the dielectric properties of materials science, soil science, geophysics and other areas of computing model, comparative analysis of the applicability of various computational models. Mainly in the particle dispersion mixing model based validated multi-group model were compared and analyzed to establish the feasibility of centralized computing model. And the model is modified, and the results show modified model of the original model has greatly improved results.

Introduction

Most of the results on dielectric properties of the composite source are computing. It comes from the famous physicist and mathematician Maxwell and 20 unknowns in the Maxwell equations with 20 equations in 1865 established the equations laid the foundation of modern electromagnetic theory. Now often said Maxwell equations are based on the original equation again express. Differential equation of the form is shown in Eq.1.

$$\begin{cases} \vec{\nabla}\cdot\vec{D}=\rho \\ \vec{\nabla}\cdot\vec{B}=0 \\ \vec{\nabla}\times\vec{E}=-\dfrac{\partial\vec{B}}{\partial t} \\ \vec{\nabla}\times\vec{H}=j+\dfrac{\partial\vec{D}}{\partial t} \end{cases} \tag{1}$$

Maxwell theory on the basis of the effective medium theory is proposed to study the complex dielectric constant of a two-phase model put under. While this model has significant limitations, except that the low concentration in the system. The effective dielectric constant of the empirical formula He Tenneco, T matrix theory, strong perturbation theory and MG and bruggemenan effective medium theory, and MG and Bru-ggement applies only to the case of spherical particles extended to the case of non- spherical particles. Research on the dielectric properties of composite materials research Dielectric properties provides a guideline for the various theoretical studies of complex biological parameters with model-based development of bio- electricity is also open up new avenues.

Theoretical Basis

The actual two- phase composite materials, even in the calculation model fixed two- phase volume ratios the dispersoid may be in any shape distribution in the matrix medium, and thus the traditional model of repeating units based on too rough, accurate should be sufficient to consider the impact of the shape and volume of the dispersoid in the end, create a random distribution of dispersoid volume model (hereinafter referred to as stochastic model), the model assumes that the body can be divided into two phases of many similar units, each unit consists of a cubic matrix and Globe is located in the center of cubic symmetry ball dispersion medium composition, with the traditional model is different is that the unit is no longer the repeat units, where each unit volume of a sphere dispersion medium (or radius) are randomly distributed. As an example, Fig. 1 shows a schematic cross-sectional model of the random distribution of 30 percent dispersion for this model, the classical model of MG. The mathematical model of the following formula

$$\varepsilon = \varepsilon_1\left(1+\frac{3f(\varepsilon_2-\varepsilon_1)}{2\varepsilon_1+\varepsilon_2 - f(\varepsilon_2-\varepsilon_1)}\right) \tag{2}$$

Where ε is the dielectric constant of a two-phase composite system, ε_1 is the dielectric constant of the base phase, ε_2 is the dielectric constant of the dispersed phase, f is the volume fraction of the dispersed phase which provides a simple solution to the dielectric constant of a two-phase composite system calculation method, but it has great limitations apply, it requires virtually no diffusion between the matrix phase and a phase of the composite system affected, and a small amount of dispersed phase is uniformly distributed. However, in an actual composite material, there is always a mutual influence between the matrix phase and a dispersed phase.

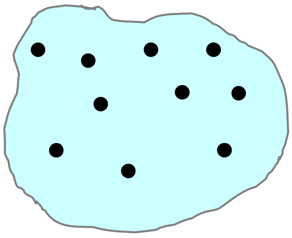

Figure.1 Composite medium model

Maxwell calculated dielectric constant of the first composite media, but only in the electrostatic field of the composite material is derived under the relationship between the dielectric constant and the dielectric constant of the solid phase and not deeply into the dynamic field.

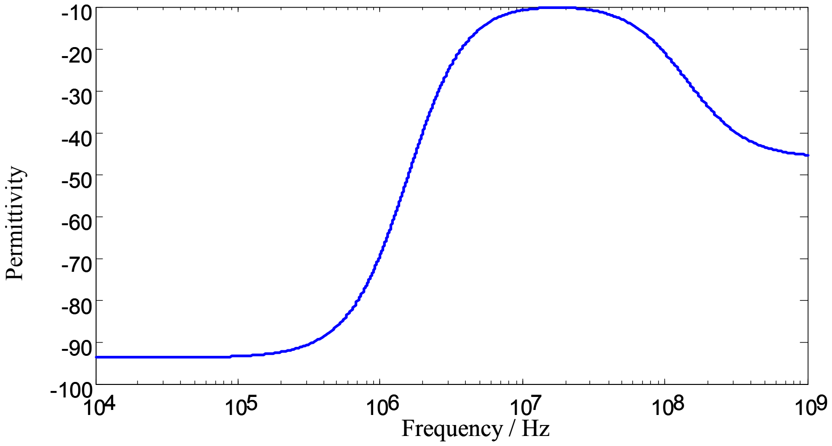

Figure.2 The dielectric characteristic curve model

The model is made of the trend curve is also broadly in line with the experimental values, although the form of a complex formula, but the situation made the curve when compared to the series and in parallel to a single ideal, so that the model can also be used to describe the relaxation of blood multiphase model phenomenon. These models are only considered the relationship between the dielectric constant of the two phases, without considering the shape of the dispersed phase particle problem. Although more than a few models which we put blood cells dispersed as spherical particles dispersed in blood as a strong system, but in practice we know that the normal form of red blood cells is a double concave circular pie, which is only in dilute solution after swelling can be approximated become sphere. With the in-depth study of the dielectric, researchers are constantly looking for ways to model accurately describes the relationship between the various components of the composite material, and further consideration of the dynamic electric field, Wagner Maxwell Fang Chengyan put out into the complex field of tissue can be used as a small ball when distributed in the continuum theory is often used in WM:

$$\frac{\varepsilon^* - \varepsilon_1^*}{\varepsilon^* + 2\varepsilon_1^*} = \Phi \frac{\varepsilon_0^* - \varepsilon_1^*}{2\varepsilon_1^* + \varepsilon_0^*} \tag{3}$$

Formula by the real and imaginary parts of the solution of the equation and the solution can be separated from the relative dielectric constant, conductivity and frequency relationship. Debye polarization model is a widely used to study the dielectric properties of biological tissues in the model. Defined between the dielectric constant and the angular frequency of the external electric field theory following relationship:

$$\varepsilon = \varepsilon_\infty + \int_0^\infty \alpha(t) e^{j\omega t} dt \tag{4}$$

Where *α(t)* after the removal of the electric field attenuation law dielectric polarization, and dielectric polarization with the external electric field tends to the equilibrium state law, called decreasing factor, the exponential distribution:

$$\alpha(t) = \alpha_0 e^{1/\tau} \tag{5}$$

Thus, the dielectric constant frequency expressions are as follows:

$$\varepsilon(\omega) = \varepsilon_\infty + \frac{\alpha_0}{(1/\tau) - j\omega} \tag{6}$$

Also, because the initial conditions $\varepsilon(0) = \varepsilon_s$, give the following equation:

$$\varepsilon(\omega) = \varepsilon_\infty + \frac{\varepsilon_s + \varepsilon_\infty}{1 - j\omega\tau} \tag{7}$$

The above formula for the complex permittivity of the dielectric constant, the real part of the complex permittivity of the separation of ε' and the imaginary part ε'':

$$\varepsilon \ = \varepsilon_\infty + \frac{\varepsilon_s - \varepsilon_\infty}{1 + (\omega\tau)^2} \tag{8}$$

$$\varepsilon \ = \frac{(\varepsilon_s - \varepsilon_\infty)\omega\tau}{1 + \omega^2\tau^2} \tag{9}$$

Here, ε_∞ is the high-frequency electrode in which a limit value of the dielectric constant, ε_S is the dielectric constant of the low-frequency limit, ω is the angular frequency, τ is the relaxation time. Fricker Maxwell theory on the basis of consideration of the effects of the shape of the dielectric constant of the dispersion particles, based on the equation with the form factor of more accurately describe the dispersion of the dielectric properties. To accurately understand its dielectric characteristics, and can not simply be equivalent to a sphere, but not enough to form factors affect much the dielectric characteristics experiments.

Calculation Methods and Results

Depending on each specific model is anisotropic, the result thus calculated is also anisotropic, and does not match the actual situation in order to simulate the actual isotropic composite media, calculated ideal approach is to generate numerous computing unit having model, but this is not possible in the actual calculation. is a feasible method to determine the volume of a case of generating a plurality of sets of random numbers, each random number correspondence with the dispersion of the ball in the cubic unit, generating in the same volume multiple computing model than under the model to calculate the results of all the statistical average, the average value obtained as the equivalent complex permittivity. As can be seen from Fig.3, the matrix material is different, the equivalent complex permittivity both the real and imaginary parts of the body increases the conductance increases dispersion and relaxation loss peak shifts to higher frequency, indicating that the interfacial polarization relaxation time and the corresponding conductance on dispersoid because dispersed in the composite body has no connectivity, so the interface of the charge transport can not leave the interface as the matrix material so that if the dispersoid having a high electrical conductivity can be provided to the interface more charge, to strengthen the interface polarization, so that the complex permittivity real and imaginary parts are increased.

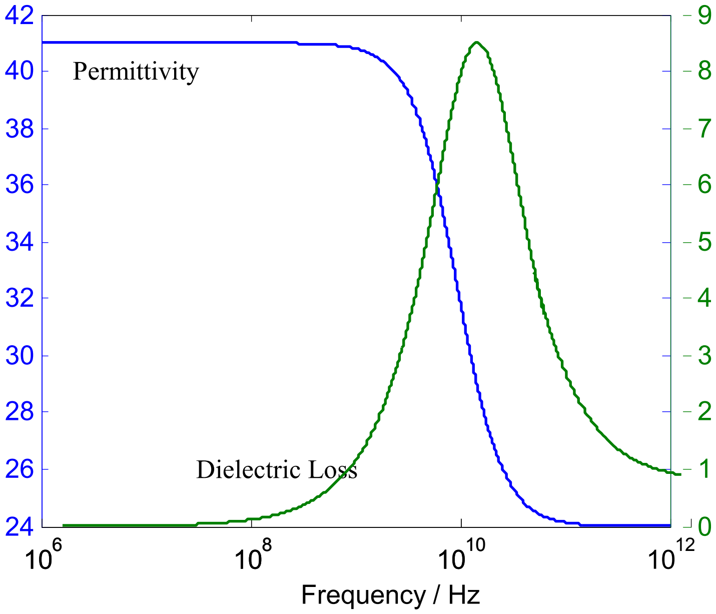

Figure.3 The dielectric characteristic curve

Conclusion

Proposed two-phase body finite element model of a diffuse dielectric properties of spherical body, the volume of randomly distributed computing, the model takes into account the random distribution of dispersoid volume exists closer to the actual two-phase composite material dispersed phase cases, more accurate than the traditional model, respectively, using the model to study the effects of the matrix and dispersoid equivalent complex permittivity, found an increase in the conductivity of the matrix material will weaken the interfacial polarization, so the complex permittivity of decline, but does not change the interfacial polarization relaxation time; increased dispersion material conductivity will increase the interfacial polarization, thereby increasing the complex permittivity and relaxation loss peak shifts to higher frequency.

References

[1] V. V. Astanin: International Journal of Impact Engineering, Vol.49 (2012), p.22-30

[2] J.L. Auriault: Mechanics of Materials, Vol.65 (2013), p.35-43

[3] J. M. Thomassin: Materials Science and Engineering: R: Reports, Vol.74 (2013), p.211-232

[4] A. Barakati, O. I. Zhupanska: Composite Structures, Vol.113 (2014), p.298-307

[5] K. Du: Journal of Computational Physics, Vol.230 (2011), p.8089-8108

[6] V. Volski, G. Vandenbosch: Composites Science and Technology, Vol.69 (2009), p.161-168

[7] W. S. Chin, D. G. Lee: Composite Structures, Vol.77 (2007), p.373-382

Applied Mechanics and Materials Vol. 596 (2014) pp 826-829
© (2014) Trans Tech Publications, Switzerland
doi:10.4028/www.scientific.net/AMM.596.826

Research on Coupler of Single Mode Fiber with Photonic Crystal Fiber

Qingsong Wei[1,a], Zhe Chen[1, 2,b] , Yunhan Luo[1, 2,c], Yue Ma[1,d], Xiaoli He[1,e], Zhen Che[1,f]

[1] Department of Optoelectronic Engineering, Jinan University, Guangzhou, 510632, China

[2] Key Laboratory of Optoelectronic Information and Sensing Technologies of Guangdong Higher Education Institutes, Jinan University, Guangzhou, 510632, China

[a]weiqs1119@hotmail.com, [b]thzhechen@jnu.edu.cn,
[c]yunhanluo@163.com,[d]mayue19910327@163.com,[e]774183278@qq.com,[f]jnuche89@gmail.com

Keywords: Optical fiber coupler; Photonic crystal fiber; Fused side-adhere; Nano silica powder

Abstract. A coupler of single mode fiber with photonic crystal fiber with a coupling ratio of 0 to 90% was fabricated with a new method called Auto-deposition Fused Side-adhere. A model for coupler of side-polished single mode fiber with side-polished photonic crystal fiber was established which proves it feasible to make such a coupler practically. In the range of 1520~1620nm, the Wavelength Dependent Loss(WDL) of the through port was 0.3dB and of the coupled port was 5dB. The Polarization Dependent Loss of through port was 0.25dB and 0.31dB at 1310nm and 1550nm, and the WDL of coupled port was 1.46dB and 1.75dB. When temperature changed from 10℃ to 80℃ and humidity changed from 10% to 70%, coupling ratio changed about 7% to 16%. It can be concluded that a steady coupler of single mode fiber with photonic crystal fiber can be made with the Auto-deposition Fused Side-adhere Coupling method, which can give a reference method and lay an experimental foundation for the fabrication of photonic crystal fiber coupler.

Introduction

Optical fiber coupler, one of the optical passive components used in optical systems, has a very important position in optical communication and optical fiber sensing application [1]. Because of its special transmission characteristics, photonic crystal fiber(PCF) has become a focus in the field of optical communication. There are three methods for fabrication of the optical fiber coupler: etching, polished gluing and fused biconical taper, which are based on single mode fiber [2-7]. The optical fiber produced by etching method is difficult to command the loss and has poor thermostability; The optical fiber produced by polishing gluing method tends to fracture and has a long fabricating period; The optical fiber produced by fusing biconical taper method can lead to collapse of internal porous in photonic crystal fiber. Most of the researches of photonic crystal fiber are theoretical, and reliable photonic crystal fiber couplers are in lack.

Aiming to fabricate the photonic crystal fiber coupler, a method with fusing side-adhered[8] for the fabrication of single mode fiber with photonic crystal fiber coupler is proposed in this paper. The production of single mode fiber with photonic crystal fiber coupler is as a transition of coupler application and provides an experimental basis for photonic crystal fiber coupler.

Side-polished single mode fiber(SP-SMF) is fabricated with the cladding of single mode fiber(SMF) partly removed. Side-polished photonic crystal fiber (SP-PCF) is fabricated from PCF with same method. Make surfaces of polished region of two fibers close to each other, coupling effect appears because of evanescent field. In order to keep the coupling effect being of long-term stability, nano silica powder is deposited on the surface of side-polished single mode fiber with auto deposition method. Because silica powder has similar characteristics with cladding of single mode fiber, the fiber coupler can have steady characteristics.

Establishment of model and simulation results

For the verification of feasibility of SP-SMF&SP-PCF coupler production, Beamprop part of Rsoft (Synopsys, Inc.) is used for the establishment of model for SP-SMF&SP-PCF coupler. Fig.1 shows a fiber coupler. Fig.2 shows side-polished fibers, where (a) shows the side-polished single mode fiber and (b) shows the side-polished photonic crystal fiber. Corresponding to the experimental operation, side-polished single mode fiber is set as main fiber, namely the fiber connecting with optical source; And side-polished photonic crystal fiber is set as vice fiber, namely coupled fiber.

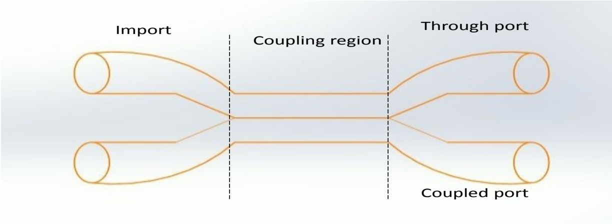

Fig.1 Sketch of the fiber coupler

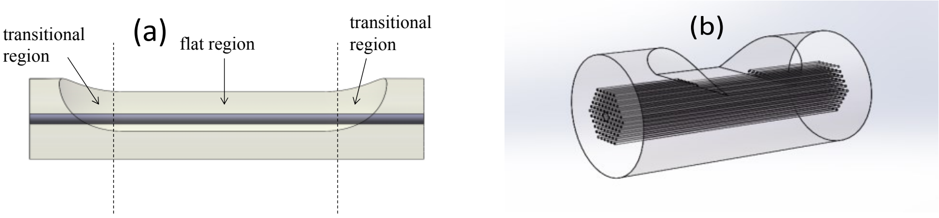

Fig.2 Sketch of the side polished fiber: (a) side polished single mode fiber; (b) side polished photoni c crystal fiber

Residual cladding thickness (RCT) is defined as the distance the core from the surface of polished region. Let the RCT of SP-PCF ranges from 0 to 3μm, and let the residual layer of porous(RLP) of SP-PCF to be 0 to 3. Fig.3 shows the coupler model.

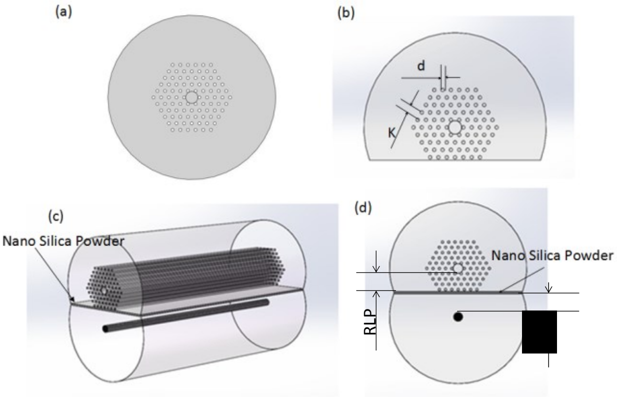

Fig.3 Sketch of the coupler model: (a) Sketch of the photonic crystal fiber cross section; (b)Sketch of the residual three layers porous for side polished photonic crystal fiber; (c)Sketch of the model for coupling region; (d)Sketch of the cross section of the model.

In Fig. 3(a) the black circle in center stands for the core, and smaller circles around stand for periodically arranged air holes. As shown in Fig.3(b), diameter of core is 9.12μm， letter d standing for diameter of air hole is 2.28μm, letter K standing for the distance of adjacent air holes is 5.7μm. In Fig.3(d), the structure of uniform deposition of silica powder in the interstice of two surfaces of polished region has a thickness of 0.5μm and a refractive index of 1.465. Set the refractive index of material of PCF to be 1.463, that of air holes of PCF to be 1, that of core of single mode fiber to be 1.468, and that of cladding of the single mode fiber to be 1.463.

Optical power in two cores are calculated with different combination of RCT with RLP, and the result of calculation is shown in Fig.4 with the input wavelength of 1310nm.

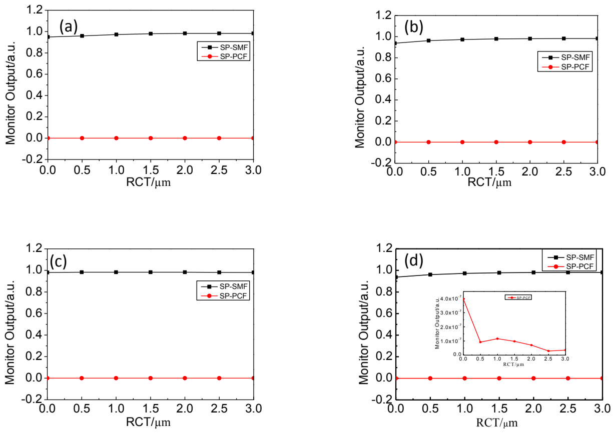

Fig.4 Optical power with different residual thickness of photonic crystal fiber:(a),(b),(c),(d)represent residual thickness to be 0 layer porous,1 layer porous,2layers porous,3 layers porous

Fig.4 shows exporting optical power with different residual thickness of photonic crystal fiber: (a), (b), (c), (d) represent the situation when RLP is 0,1,2 and 3, respectively. Horizontal axis represents different RCT of SP-SMF, and vertical axis represents optical power of two exporting port of coupler. The black curve represents exporting optical power of SP-SMF and the red curve represents that of SP-PCF. It can be concluded from Fig.4 that extremely unconscious light appears through the coupled port only the situation when RLP of SP-PCF is 3. Experimental researches are to be operated for the verification of simulation result.

Experiment

Fabrication of SP-SMF&SP-PCF coupler and experimental facility. The whole fabrication of SP-SMF&SP-PCF coupler process involves four steps. The first step is to fabricate SP-SMF and SP-PCF; The second step is auto-deposition of nano silica powder; And the third step is to align and adhere the two optical fibers.

Experimental results and analysis. Fig.5 shows the changing curve of export of the coupler in production process, and (a) shows the changing curve of power and (b) shows the changing curve of loss including insertion loss and excess loss. The data indicates that after dropping in alcohol with clamping the fibers, light appears in coupled port. With the increase of flame burning time, the P1 declines rapidly, the P2 rises slowly, and the P3 which is the sum of P1 and P2 declines rapidly. Large loss of optical power exists. After 14s, the P1 and P2 are both 3 (a.u.), the P3 is about 6 (a.u.) when the CR is 50%. After 16s, the CR can reach to 90%. This process provides an experimental basis to fabricate the SP-PCF coupler.

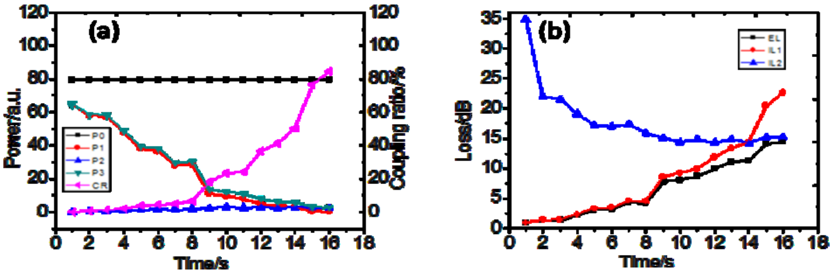

Fig.5 Curve of output terminals of the coupler in production process:(a) curve of power (b) curve of loss

Characterization of SP-SMF&SP-PCF coupler. Test the wavelength dependent loss (WDL), polarization dependent loss (PDL), influence of temperature and humidity of the coupler.

1) Test the WDL of the SP-SMF&SP-PCF coupler. As shown in Fig. 6, light is imported into SP-SMF with a wavelength of 1520~1620nm. The curve of WDL after connecting the spectrum

analyzer can be obtained. In the range of 1520~1620nm, the WDL of through port is 0.3dB, smaller than coupled port which is 5dB.

2) Test the PDL of the coupler. Connect the coupler into the power meter through the polarization controller. The PDL of through port is 0.25dB and 0.31dB, the PDL of coupled port is 1.46dB and 1.75dB with a wavelength of 1310nm and 1550nm.
3) Test the influence of temperature and humidity. Test both two end of fibers in the temperature range of 10 to 80℃, humidity range of 10% to 70%, as is shown in Fig. 7, the CR ranges about 7%~16%.

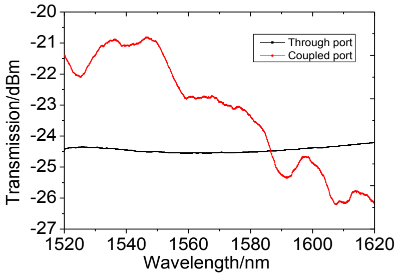

Fig.6 Wavelength Dependent Loss

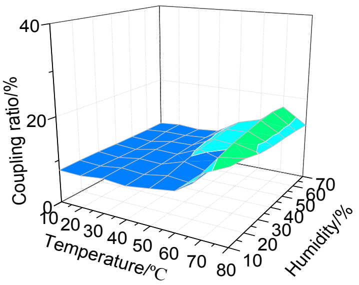

Fig.7 Effect of temperature and humidity

Conclusions

The simulation calculations show that the light will be coupled into SP-PCF from SP-SMF when the photonic crystal fiber was polished remaining three layers porous. Experimental researches verify the simulation results and a SP-SMF&SP-PCF coupler are produced successfully. Test the parameters of coupler, and it can be verified that a reliable SP-SMF&SP-PCF coupler is fabricated with method of Auto-deposition Fused Side-adhere, which provides the technical foundation for photonic crystal fiber coupler production.

Acknowledgment

This work is supported by National Nature Science Foundation of China (NSFC) (No.61177075, No. 11004086, No. 61008057); Key Technology R & D Project Of Strategic Emerging Industries Of Guangdong Province, China (2012A032300016); Fundamental Research Funds for the Central Universities, China (No.21612437, No.21613405).

References

[1] Lin Jinhai and Zhang Weigang: Progress in Physics. Vol. 30 (2010), p. 37-80. In Chinese.

[2] S.K. Sheem and T.G. Giallorenzi: Optics Letters. Vol. 4(1979), p. 29-31.

[3] S.K. Sheem and T.G. Giallorenzi: Optics Letters. Vol. 4(1979), p. 322-324.

[4] Y. Tsujimoto and H. Serizawa: Electronics Letters. Vol. 14(1978), p. 157-158.

[5] Hokyung Kim and Jinchae Kim: Optics Letters. Vol. 29(2004), p. 1194-1196.

[6] K.O.Hill,D.C.Johnson and R.G.Lamont: SPIE. Vol. 574(1985), p. 92-99.

[7] B.S.Kawasaki, K.O.Hill and R.G.Lamont: Optics Letters, Vol. 6(1981), p. 327-328.

[8] Yu Jinbo, Chen Zhe and Luo Yunhan: Journal of Optoelectronics·Laser, Vol. 24(2013), p. 897-902. In Chinese.

CHAPTER 11:

Computer Network and Information Security

Applied Mechanics and Materials Vol. 596 (2014) pp 833-837
© (2014) Trans Tech Publications, Switzerland
doi:10.4028/www.scientific.net/AMM.596.833

An Evolving GPSR Protocol in Urban Roundabout Scenario

Haiyang YU[1 *,a], Huamin YANG[1,b] , Xiaoqiang DI[1,c] , Liangdong QU[2,d]

[1] College of Computer Science and Technology, Changchun University of Science and Technology, Changchun, Jilin, 130022, China

[2] College of Communication Engineering, Jilin University, Changchun, Jilin, 130022, China

[a]custhaiyang@126.com, [b]yhm@cust.edu.cn, [c]dixiaoqiang@126.com, [d]qld001a@163.com

Keywords: VANET; urban roundabout; SN-GPSR; NS-2

Abstract. According to the research of VANET routing protocol, an improved protocol SN-GPSR has been proposed. It is based on the sensitive nodes. The nodes select routing through a special position and steady speed under GPSR protocol. In a crossroads scenario, we designed a vehicular mobility model and simulated it using NS-2. By analyzing the results, the network performance parameters of SN-GPSR have improved above the GPSR, such as delay, packet loss and others.

Introduction

With the development of computer network technology and mobile communication technology, the research of wireless communications becomes more deeply. After the Mobile Ad-Hoc network growing, a new era in wireless communications blazed [1]. The nodes play two roles in Ad-Hoc network. They are hosts and routers. For the good scalability and survivability, the VANET, one of the most typical Mobile Ad-Hoc networks, has been paid wide attention in urban scenario.

VANET, which is short for Vehicular Ad-Hoc network, has been applied to the ITS (Intelligent Transportation System) [2]. In the city scenario, the VANET can help develop the information exchange between V2V (vehicles to vehicles) and V2I (vehicles to the infrastructure). Furthermore, we found an urban roundabout model and design the SN-GPSR protocol. In the protocol, nodes forward route by the sensitive nodes. On the basis of GPSR protocol, the evolving routing protocol can improve routing performance of the network.

The rest sections of this paper are organized as follows. In Section 2, we discussed the related work of VANET. Then we designed a mobility model in urban roundabout scenario in Section 3. In Section 4, we illustrated the evolving strategy based on GPSR protocol in detail. The scenario and protocol are simulated in Section 5. At last section, we conclude the paper and point out future work.

Related work

GPSR protocol. GPSR is short for Greedy Perimeter Stateless Routing protocols, which is one of the most typical location-based routing protocols [3]. The main idea of GPSR protocol is described as follows. When a node wants to transmit the data packet, the source tries to find the nearest node to the destination from the neighboring nodes. If the node cannot find the nearer node than itself, the protocol changed to the perimeter mode. Amid to construct a face without cross-linked, perimeter mode uses right-hand formula to forward packet [4]. The routing protocols exhibit different properties in different scenarios. Through the design and improvement of routing protocols, a highly efficient VANET has been built up. So the research has a huge significance both in theory and engineer.

Mobility model. VANET mobility models usually divided into macroscopic model and microscopic model. In the macroscopic model, we analyze the average speed, moving distance and acceleration of all vehicles by the way of statistics. In the microscopic model, we consider a single time, a single moving distance and other single characteristics. Many scholars have come up with mobility models of VANET, such as the random walk model, the random direction of the model and random point path model [5]. However, these mobility models cannot simulate real city scenario well.

As is mentioned in [6], an algorithm has been presented, so vehicular radar sensors have the ability to receive position and movement data from VANET. The applicability of VANET location-based routing in highway and urban scenario [7] are discussed. All these papers considered the traffic density, node speed and direction, but the different importance and the probability of the change in motion are not considered in the network. So how to design the urban scenario is problem which needs to solve.

Scenario design

In urban traffic environment, the roundabout is a common scenario. When the crossroads exceed four or the landmark building locates the middle, the roundabouts always replace the crossroads. The roundabouts can reduce the traffic jam and simplify the instruction of traffic lights. The roundabout designed in this paper is shown as Figure 1.

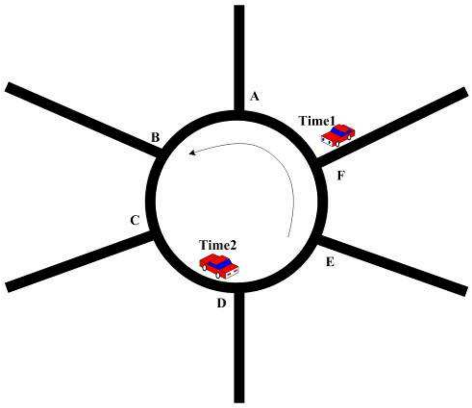

Figure 1 Schematic of roundabout scenario

In Figure 1, six roads gather in a roundabout. The radius of roundabout is 60m. The intersections distributed uniformity. The central angle of each two straight roads extending is 60 °. There are two lanes in the roundabout. All the cars in the roundabout have the same speed and drive anticlockwise. For example, a vehicle enters the roundabout from Intersection F in one moment, and it exits the roundabout from Intersection D in another moment. The roundabout in this paper is located the center, and the roundabout scenario has important theoretical value and practical significance.

The disadvantage and improvement of GPSR

As one of the most typical location routing protocol, GPSR uses two ways to take the route forwarding. This mechanism gets a good application in the wireless sensor network. But in the city scenario, the GPSR still shows some disadvantages.

The disadvantage of GPSR. GPSR protocol is limited in the city scenario. First and foremost, in the city scenario, the buildings and trees beside the road may restrict the greedy algorithm. What is more, the location of the nodes changes frequently. This will produce the routing loops or separate the networks. Last but not the least, the wrong position of the destination node will lead to nodes remove the connection, thus causing the network interrupt.

The improvement of GPSR. The SN-GPSR protocol, which proposed in this paper, selects the sensitive nodes to forward routing. It describes the traffic dynamics in terms of macroscopic quantities. These parameters can be related using the following relations. Eq.(1) is the average traffic flow[8].

$$q = v\left(\frac{\eta \times n}{2\pi R}\right) \tag{1}$$

Where v is the average speed of the vehicles, R is the radius of roundabout, n is the vehicle number in the scenario and η is the distance ratio of roundabout and all roads in the scenario. As is defined before, $R = 60m$, $\eta \in (30\%, 70\%)$ 。

The spatial distance between nodes is shown as follows:

$$S_{ij} = \sqrt{(x_i - y_i)^2 + (x_j - y_j)^2} \quad (2)$$

Where (x_i, y_i) is the location coordinate of the Number i vehicles, (x_j, y_j) is the location coordinate of the Number j vehicles.

In the roundabout model, we define the nodes that are nearest to the intersection in the roundabout as sensitive nodes. The distance from the sensitive node to the nearest intersection is l (m). The l is subjected to the following probability distribution function.

$$g(l) = \frac{1}{\sigma\sqrt{2\pi}} \int_0^{250} e^{-\frac{(l-\mu)^2}{2\sigma^2}} dx \quad (3)$$

Where μ represents the mathematical expectation of the average distance and σ^2 is the variance of the average distance. They are all the inverse proportion of the average traffic flow. They are obtained as $\mu = 1/q$, $\sigma^2 = 1/q$.

P_i is the probability of the Number i node to be selected. The weight of the Number i node is W_i. W_i, the reciprocal of the distance, is defined as Eq.(4).

$$W_i = 1/g(l) \quad (4)$$

The measurement of the choice node between the source to the destination is determined by S_i [9].

$$S_i = \sum_{i=1}^{k} P_i W_i \quad (5)$$

We give S_i the name ” Determined strength”. And in the Eq.(5), P_i and W_i are defined before. We choose routing that has the minimum determined strength. The minimum determined strength is defined as Eq.(6).

$$S_{SD} = \min(S_1, S_2, S_3 \ldots S_n) \quad (6)$$

After we confirm the minimum determined strength, the nodes in the lanes is the forward node to be chosen.

Simulations

Simulation scenario setup. In this paper, VanetMobiSim and NS-2 software are used to simulate mobility model and routing protocols. VanetMobiSim is an extension of CanuMobiSim set. It is used to set the spatial elements and found road network model. NS-2 is an open-source tool that combined C++ and OTCL programming languages [10]. As a typical compiled language, C++ can process bytes, datum, messages and packets efficiently. As an interpreted language, OTCL can change the network environment script easily. The simulation parameters are configured as Table 1.

Table 1 Simulation parameters

Scenario Area	700m×700m
Propagation Model	Free space propagation channel
Frequency	2.4GHz
Antenna	Omni Antenna
Longest Communication Distance	250m
MAC Protocol	IEEE802.11
Routing Protocol	GPSR, SN-GPSR
Application layer	CBR packets, 512KB, 0.5s interval
Range of Speed	10-60km/h
The number of node	20-160
Simulation Time	300s

Analysis. After running the tcl simulation script, we get the file recorded every moment result. According to analyze the result file using gawk tool and awk script, we obtain network parameters such as delay and loss ratio. Firstly, we analyzed the average end-to-end delay of varying vehicle number, and the vehicle speed maintains 20km/h. As the vehicle number increasing, the average end-to-end delay is shown in Figure 2.

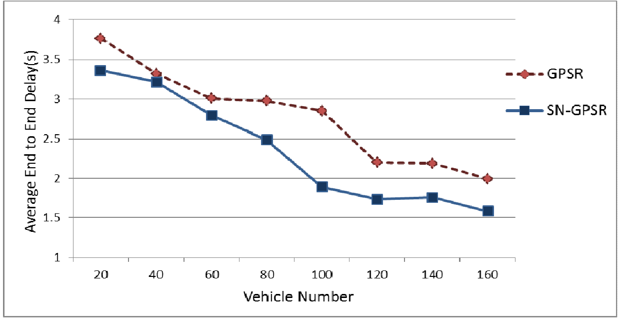

Figure 2 Delay with different vehicle number

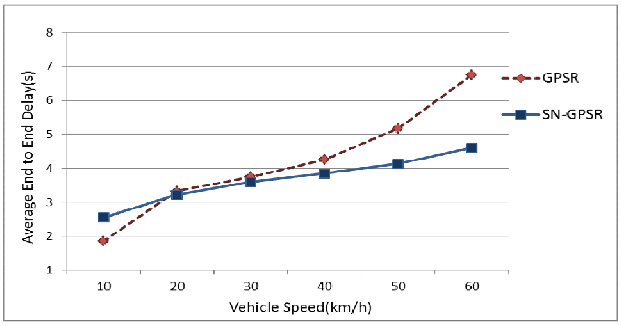

Figure 3 Delay with different vehicle speed

As can be seen from Figure 2, average end-to-end delay of the two protocols is all reduced as the vehicle number increasing. The delay of GPSR drops from 3.769s to 1.993s and the SN-GPSR drops from 3.360s to 1.583s. Compared the two protocols, the delay of SN-GPSR is less than the GPSR.

We also changed the independent variable. The speed of vehicles was adjusted from a range of 10-60 km/h with increasing increments of 10 km/h and the number of nodes is stable at 40. From Figure 3, the average end to end delay increased with the vehicle speed rising. The delay of GPSR protocol changes from 1.843s to 6.748s and delay of SN-GPSR protocol changes from 2.547s to 4.598s. They are all increased, but the SN-GPS increased slowly. With the cars getting crowded, SN-GPSR shows far better performance than GPSR.

From Figure 4 and Figure 5, PLR, short for package loss ratio, can be discussed.

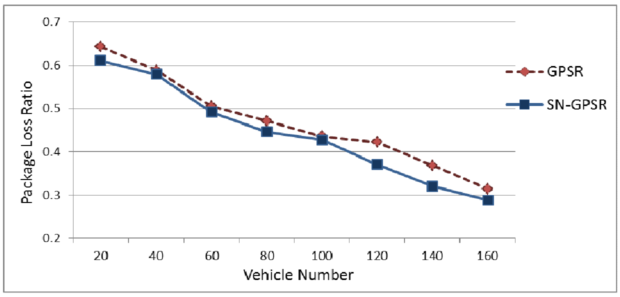

Figure 4 PLR with different vehicle number

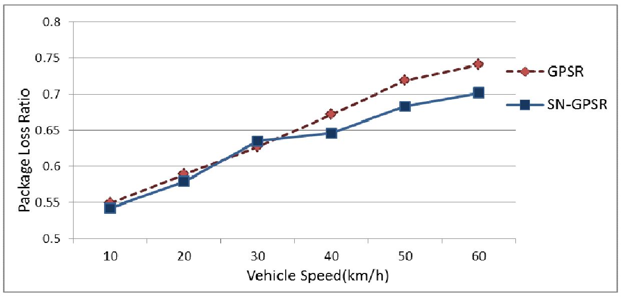

Figure 5 PLR with different vehicle speed

From Figure 4, the vehicle number rises from 20 to 160, the vehicle speed is 20km/h. Figure 5 shows the average results of packet loss ratio with different vehicle number. We can find that the GPSR changes from 0.643 to 0.314 and the SN-GPSR changes from 0.611 to 0.288. And SN-GPSR shows a little better property than GPSR.

We also analyzed package loss of varying vehicle speed. When the number of vehicles is 40 the vehicle speed changes from 10km/h to 60km/h. In this process, the changes of packet loss ratio is shown in Figure 5.With different vehicle speed, packet loss ratio of GPSR protocol rises from 0.549 to 0.741 and packet loss ratio of SN-GPSR rises from 0.542 to 0.702. The improving protocol has the lower packet loss ratio.

From the discussed above, we know that the average end to end delay and packet loss ratio of the protocols all decreased with the vehicle number increasing. It is because the two protocols select perimeter forward unless the greedy forward isn't work. The dense scenario is good for the greedy forward. From the simulation results, SN-GPSR owned better network properties than GPSR. SN-GPSR enhanced scalability and feasibility, so it is more suitable for the movement of the urban roundabout scenario.

Conclusions

Based on the sensitive nodes and traffic density, we give an SN-GPSR routing protocol. In this paper, a mobility model in urban roundabout scenario has been designed. Then we simulate the model using VanetMobiSim and NS-2. Compared with the traditional GPSR and SN-GPSR, the experimental results show that the SN-GPSR has less delay and loss ratio. After discussing the mobility model, the evolving protocol is more suitable for city VANET scenarios. It is important to research a more efficient routing protocol of VANET. With further research, we still need to take the application service, location information and traffic manage into consideration [11]. Those key technologies will help VANET make more significant contributions for ITS.

Acknowledgements

This work was financially supported by the National Nature Science Foundation (61275080).

References

[1] S.Yousefi, M.S.Mousavi, et al: Vehicular ad hoc networks (VANETs): Challenges and perspectives. IEEE International Conference on ITS Telecommunications, Chengdu, 2006, pp.761-766.

[2] Taleb T., Sakhaee E., Jamalipour A. et al: A stable routing protocol to support ITS services in VANET networks, Vehicular Technology, IEEE Transactions on 2007, 56(6):3337 -3347.

[3] Mahmoud Hashem Eiza and Qiang Ni: An Evolving Graph-Based Reliable Routing Scheme for VANETs. IEEE TRANSACTIONS ON VEHICULAR TECHNOLOGY, VOL. 62, NO. 4: 1493-1504. MAY 2013.

[4] F.Ros, P.Ruiz,et al: Acknowledgment-based broadcast protocol for reliable and efficient data dissemination in vehicular ad hoc networks. IEEE Transactions on Mobile Computing 11(1):33-46,2012.

[5] Bettstetter C , Hartenstein H: Stochastic properties of t he random waypoint mobility model. ACM/ Kluwer Wireless Networks :Special Issue on Modeling and Analysis of Mobile Networks ,2004 ,10 (5) :555-567.

[6] Bettstetter C , Hartenstein H: Stochastic properties of t he random waypoint mobility model. ACM/ Kluwer Wireless Networks :Special Issue on Modeling and Analysis of Mobile Networks ,2004 ,10 (5) :555-567.

[7] Edison Pignaton de Freitas ,Tales Heimfarth, Flavio Rech Wagner,Carlos Eduardo Pereira , Tony Larsson: Exploring geographic context awareness for data dissemination on mobile ad hoc networks. Ad Hoc Networks. 2013,11:1746-1764.

[8] Fonseca Antonio, Vazao Teresa: Applicability of position-based routing for VANET in highways and urban environment. JOURNAL OF NETWORK AND COMPUTER APPLICATIONS. 2013,5, 36(3): 961-973.

[9] Dipankar Raychaudhuri, Narayan B: Mandayam.Frontiers of Wireless and Mobile Communications. Proceedings of the IEEE, Vol. 100, No. 4, April 2012.

[10] Todd Murray, Tammy Murray, Michael Cojocari, and Huirong Fu: Measuring the Performance of IEEE 802.11p Using ns-2 Simulator for Vehicular Networks. EIT 2008. IEEE International Conference on Electro/Information Technology, 2008. Ames, IA ,USA.May 18-20, 2008.

[11] C.C.Hu,Y.B.Lin and N.Alrajeh: Mobility management for unicast services in wireless access in vehicular environment. IEEE Wireless Communications 19(2):88-95,2012.

Applied Mechanics and Materials Vol. 596 (2014) pp 838-842
© (2014) Trans Tech Publications, Switzerland
doi:10.4028/www.scientific.net/AMM.596.838

CNC Network of Research and Development

Baijun Zhang

Weifang University of Science and Technology , No.166,xueyuan R.D,Shouguang City Shandong,
P.R C

879381361@qq.com

Key words: NC network system; Internet; CAM / CAM; digital control; digital manufacturing

Abstract. Network of NC technology is the realization of manufacturing automation, intelligence, integration and globalization of technology-based. This paper analyzes the development of the network system of the basic requirements of the proposed network of digital systems architecture, with emphasis on the numerical control system network hardware platforms and software platform of Design and Implementation of the analysis described, and pointed out that the Internet-based network NC CNC is a system of research and development trends, there is a strong sense of practical application.

Introduction

With the research and development of new concepts and methods of computer integrated manufacturing technology, agile manufacturing, intelligent manufacturing as the basic unit of advanced manufacturing environment network manufacturing. research and application of numerical control system network is very important. CNC system for networked manufacturing network, remote manufacturing, remote diagnostics and maintenance and mutual sharing of network resources with a variety of tools to provide the most basic support.

Can make full use of existing resources

With computer-aided design / manufacturing systems more quickly into the actual process, more information needs to communicate with the CNC system and switching quickly and easily.High reliability CNC system itself use such high-priced, electronic low-capacity disk is difficult to meet the actual needs. If you have networking capabilities, CNC machine tools in the harsh environment of a clean environment can share the office with a high-capacity hard disk, and then read the CNC CAD / ACM processing code generated by the system through the LAN, and parts processing.

Provide a basis for remote monitoring and network manufacturing

CNC system can provid the current processing status information to a remote monitoring point through the communications network in time and receive remote monitoring commands for providing minimal support for a truly global manufacturing. Even, we can put a CNC machine as a shared office network as a shared printer on the network. Of course, these features of openness and self-diagnostic CNC system are put forward higher requirements.

Blindness and related costs can be reduced by maintaining

CNC system not only greatly enhance the network transmission and management of information processing to improve machining automation and remote monitoring level, but also when the CNC system failure, the numerical control system manufacturers can provide remote diagnosis and maintenance, reducing maintenance blindness and related costs.

The basic requirements of CNC system developed network

Networked manufacturing is a rapid response to market needs, enhance an advanced manufacturing mode market competitiveness, digital, flexible and agile as the basic features. Making full use of network information technology, sharing of global manufacturing resources to support cross-regional global manufacturing platform. Thus, in the networked manufacturing mode, as the underlying CNC automatic control system should meet the following basic requirements:

Support network-based information sharing

If want to CNC system become a global manufacturing resources, its most basic requirement is to support cross-platform operating system,supporting multi-user different geographic information sharing: ask the CNC system to take advantage of business information online which have various management layers and technical resources; on the other hand upper tier computer companies can obtain real-time field data underlying CNC system via Intranet in time.

Support real-time monitoring of network-based

Networked CNC system should be able to publish real-time status information to remote clients promptly and remote clients to be able to carry out real-time system operation and control.

Provide remote digital services through a network

Through the Internet / Intranet to provide remote digital services, including remote online programming, remote technical consulting / technical training,, additional specific control functions, interactive remote fault diagnosis services.

Network architecture CNC system

To achieve the necessary function of networked CNC system , the author constructed the system architecture shown in Figure 2. As can be seen from the diagram, This is a B / S and C / S combination of system architecture, which make full use of B / S and C / S respective strengths to achieve complementary advantages between them, in order to meet the network NC remote service and remote monitoring of functional requirements.

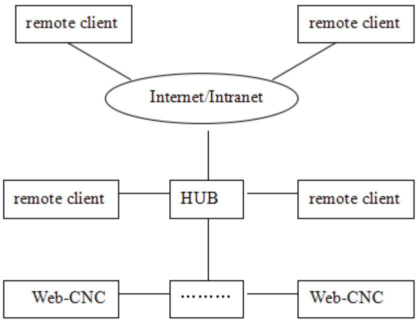

Fig.1 NC network architecture

From the B / S point of view, this is a three-layer structure: the first layer is a remote client layer, remote clients can realize remote monitoring and information sharing CNC system through a browser； second layer is a system service layer for storing remote service modules and related applications; database service layer is the third layer, for storing processing parameters, the parameters of machine equipment, the real-time system state parameters. This B / S system architecture is easy to implement in the form of cross-platform operation, reducing the client's requirements, improve system versatility.

From the C / S point of view, the system of two-tier structure, namely the remote client and the underlying Web-CNC, two-way communication between remote clients and Web-CNC which the

TCP / IP protocol. the remote client through a virtual control panel to achieve real-time monitoring system remote Internet / In-tranet based. This C / S structure in the form of various requests issued by the client command to the server, the server will be a real-time system status information back to the client, enabling real-time control point.

CNC system developed network

Based Networked CNC system functional requirements and architecture, and high-speed motion controller based IPC hardware platform developed network of CNC prototype system, hardware and software technology to achieve the following specific description of the system architecture and related functions.

Hardware configuration

Web-CNC prototype system is based on IPC + multi-axis motion controller (PMAC) is the hardware platform. PMAC is a control unit provided by the U.S. DeltaTau to high-speed digital signal processor (DSP) for the central processing unit, with interpolation, cutter compensation, position control, speed of processing, the basic function of the numerical control system PLC control, housekeeping, etc. support the development and expansion of the user, with the IPC has upper and lower levels with openness. This structure has a simple hardware structure, easy to build, openness and good, you can share a wealth of IPC computer hardware and software resources, to facilitate system development, can be easily connected to the network, which will help remote service, remote monitoring, and manufacturing systems integration.

Software Environment

a.In WindowsXP environment, using Visual C++6.0 development of a prototype Web-CNC control systems, and network management through Letters and other software modules.

b.Optional WindowsNT and Microsoft IIS5.0 as a Web server to manage and publish information. Using ASP (ActiveServerPage) which IIS supports and ADO (Ac-tiveDataObjects) technology to achieve dynamic web design and database access SQLServer2000.

c.Using MicrosoftSQLServer2000 as database servers, storage and manage the NC program, process parameters, the basic parameters of the machine tool equipment, machine tools, real-time status information and user information.

CNC system network technology

Data acquisition and processing technology

CNC systems running real-time acquisition of the basic requirements of *Web-CNC* prototype system is also one of the key technologies to achieve information sharing. *PComm32* communications driver software provided by *DeltaTau* company can easily communicate with the upper PMAC Windows applications, the communication driver relationship shown in Figure 2.The icon shows,*PComm32* communications driver software from the *PMAC.DLL, PMAC.SYS, PMAC.VXD3* documents composed contains over 250 functions. Available function to achieve data acquisition system through which *DeviceGetRe-sponse()*, the function prototype is:

*DeviceGetResponse(DWORDdwDevice,PCHARresponse,UNITmaxchar,PCHARcommand)*among:*dwDevice*-DeviceNumber;*response*-Pointerto a string buffer;*maxchar*-Maximum string that can be transferred.

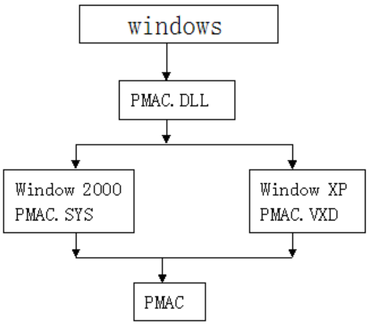

Fig.2 Pcomm32 Communication-driven diagram

With the above functions related to the development of software modules, according to the following steps for the CNC status acquisition and processing parameters:

a.Preparing collection.Create a database with SQLServer2000 to store collected data and developed software modules to connect to the database, set the timer, the timing of the data acquisition system.

b.PMAC send commands to the data collected by DeviceGetResponsefunctions.

c.PMAC motion timing of the position of the axis, speed, and system variables, I / O ports and other state parameters collection.

d.The collected data are stored after the conversion process to built a database for use by other applications call.

Network communication and interface technology

The prototype system uses a stream socket connection-oriented technology with VC + +6.0, respectively Web-CNC and remote client development 10M/100M Ethernet card based network communication interface program module, the establishment of a stable two-way between the two channel. Figure remote client and Web-CNC information transmission process 4. The figure shows that the data transfer process stream socket is a typical client / server (C / S) mode. Start Web-CNC server and call *Listen ()* function waits for remote client access, when seized a remote client sends a request to start Web-CNC, call *Receive ()* function accepts a request to establish a stable and reliable connection. This data transmission method according to the order of receiving data transmitted for large data transfers, with good reliability and a high real-time characteristics.

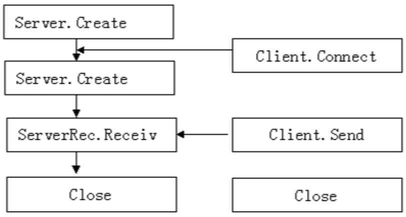

Fig.3 Connection-oriented socket communication processes

Remote monitoring technology

Remote monitoring is an important part of Web-CNC, the key is to realize the remote client virtual control panel. In this system, the use of ASP technology to produce dynamic web pages, and embed ActiveX controls developed with virtual control panel on the page, the available remote client access.

The virtual control panel consists mainly of two types of information: one is the real-time Web-CNC system state data, including the motion axis status, current mode of operation, alarm information, operation button status, such information derived from the network database, namely through ADO technology to collect data in the network database stored in the virtual control panel display, and periodically refreshed; the other is operating the control buttons, including control, rate adjustment, the program selection button and start and emergency stop, the system control command network communication channels can be transmitted through the Web-CNC via buttons on the virtual control panel, and then through DeviceGetResponse () function is called to execute the command to download to PMAC to control machine motion.

Conclusion

NC network with Internet technology, communications technology, digital technology and computer technology to technology, remote design, NC programming and integrated CNC machining, CNC numerical control system to achieve the network equipment and integration have become the inevitable development of numerical control system trend. It has a very wide range of technical content. Man involved in the research situation at home and abroad CNC system on the network, and explore the key technology of numerical control system in just a network using the network resources for one aspect of the production and application of relevant resources to optimize the use of network technology to a wide range of topics within the CNC system needs to be further exploration. NC research on network development will also be following.

① CNC platform for future network research focus will shift to production management software further integration technology, its openness and scalability become major consideration.

② Soft plug-in technology-based CNC system integration of heterogeneous research will become a trend in the future development of the network NC.

③ Fieldbus-based development and high-speed data communications technology will get a lot of applications in the network NC.

④ Web-based multimedia technology will be further applied in the network NC, and will be integrated into a network of virtual CNC technology to achieve operating platform will enable the operator to remotely living in different places on the machine, immersive remote operation of CNC machine tools.

References

[1] Gao Rong，Wang Yesen，Zhang Jianke；Mobile network computer numerical control based on Web Services, Computer Integrated Manufacturing systems,2007/09

[2]Huang Rongjie,Wu Bo,Yang Shuzi.Applied Analysis of the Mode Based on DNC Communication Interface in Metworked-CNC System,Modular Machine Tool&Automatic Manufacturing Technique,2007/05

[3]Ma Gang. Development of an Open Network Numerial Controlling System, Journal of Liao ning Provincial College of Communications,2006/03

[4]Liang Zhifeng,Xie Xiang,Tang Xiaoqi, Design of the networked numerical control system based on industrial Ethernet, Modern Manufacturing Engineering,,2006/01

[5]Zhang Cuixuan,The study of Networked NC Tool Based on Campus Net, Development& Innovation of Machinery & Electrical Products,,2005/01

Applied Mechanics and Materials Vol. 596 (2014) pp 843-846
© (2014) Trans Tech Publications, Switzerland
doi:10.4028/www.scientific.net/AMM.596.843

Complex Network Evolution Model Based on Node Attraction

Rui Sun[1, 2, a *]

[1] Department of Computer Science, Chengdu Normal University, Chengdu, China

[2]School of Computer Science, Sichuan University, Chengdu, China

[a]cug123456@126.com

Keywords: complex network, node attraction, tunable parameters, degree distribution

Abstract. This paper studied the evolution law of the real-world networks, and then proposed a complex network model based on node attraction with tunable parameters in order to solve the problems existing in BA model and the original node attraction model. The model considered the effects of preferential attachments by the changes of degree and node attraction in the evolution process of networks. Theory research and simulation analysis show that we can more flexible adjust the evolution process of network through adjusting model parameters, therefore make it more accord with the network topology and statistical characteristics of real-world networks.

Introduction

Many real-world complex systems were found to show in a form of networks. After a lot of research on real-world networks, Watts and Stregatz as well as Barabasi and Albert published papers respectively, they proposed Small-World network model (WS model) [1] and Scale-Free network model (BA model) [2]. The study about the microscopic mechanism which leads to all kinds of macro properties and a series of evolution law of the networks become the focus of research. WS model and BA model had a very concise formation rules, but at the same time they inevitable to ignore some factors impact the evolution of actual networks, and then make some statistical properties have large deviation compared with actual networks [3]. Such as WS model has high clustering coefficient like the actual networks, but it is subject to Poisson distribution; the degree distribution of BA model is power-law which consistent with the reality characteristics, but it did not have obvious clustering effect, as well as the power index fixed for 3, this don't match the power index of actual networks usually in $\left[1,3\right]$.

In order to solve the above problems, Dorogovtsev [4] first proposed the original node attraction model. Dorogovtsev model rules that all nodes in network have same initial attraction, the growth of network affected by node attraction. Tao [5] proposed a complex networks evolution model based on node attraction (NAM model), this model defined node attraction is the number of connection get in the unit time, and supposed that each nodes have equal opportunity to connect. Tian [6] found the original node attraction model and its extension model with smaller clustering coefficient, therefore proposed a complex network model based on node attraction with clustering effect. The new model aimed at the local feature of preferential attachments in real-world networks, defined node attraction is function as changing with time.

Node Attraction Model with Tunable Parameters

Node Attraction. Many real-world networks expressed the preferential attachments, this shows that the connected probability between nodes is concerned with degrees, but the choice standard is not only simple to select the nodes with high degree as description by BA model. Some examples of social network, scientists co-authorship network and public opinion network show that the preferential attachments is universal in the evolution of complex network, but when we choice connection, we have to think about other attractive factors in addition to degree.

We define attractive factor β denoted the attraction of nodes for new nodes, each node has attractive factor β_i. $\beta_i = n_i / \Delta T$ denoted the number of connection got in the unit time, where $\Delta T = t - t_i$,t_i denoted node i join to the network on t_i, n_i denoted the number of connection i got in ΔT. The degree of nodes describes the topological position in network, it is a static measurement in moment time, while node attraction describes the changes in a period of time, it is a dynamic measurement.

Algorithm. The description of algorithm of complex network model based on node attraction with tunable parameters as follows:

Initial conditions: the initial network is an undirected and unweighted network which be composed of m_0 nodes and e_0 edges;

Growth mechanism: In each time step, a new node j joins in the network, this node will connect with $m(m \le m_0)$ nodes existing in the network;

Preferential attachments: Each new node j connected to node i obey the following rules

$$\Pi_i = \frac{\alpha k_i + \gamma \beta_i}{\sum_l (\alpha k_l + \gamma \beta_l)} . \tag{1}$$

Where k_i denoted degree of node i; β_i denoted attractive factor of node i; $\sum_l (\alpha k_l + \gamma \beta_l)$ denoted the weighted sum of degree and attractive factor of the rest nodes in network; α and γ are tunable parameters, and $\alpha + \gamma = 1$.

Node Distribution of Node Attraction Model. A New node j is connected with the original node i , node i will increase it's degree k_i in proportion according to Eq.1. According to the mean-field theory [7], it is:

$$\frac{\partial k_i}{\partial t} = m \frac{\alpha k_i + \gamma \beta_i}{\sum_l (\alpha k_l + \gamma \beta_l)} . \tag{2}$$

Calculating above equation, the results is

$$p(k) = 2\alpha(\alpha m + \gamma \beta_i)^2 (\alpha k + \gamma \beta_i)^{-3} . \tag{3}$$

Therefore, when $\alpha = 1, \gamma = 0$, the model have degenerated into BA model, $p(k) \approx 2m^2 k^{-3}$; when $\alpha = \gamma = 1/2$, $p(k) \approx 2(m + \beta_i)^2 (k + \beta_i)^{-3}$, this is like what described in [5]; when $\alpha = 0, \gamma = 1$, the preferential attachments completely according to node attraction, at this time the model is similar to nodes have the same initial attraction in [6].

Simulation Results and Discussion

According to the proposed complex network model based on node attraction with tunable parameters, we use computer simulation to compare with BA model, Dorogovtsev model and NAM model from degree distribution, clustering coefficient and average path length respectively.

Degree Distribution. The degree of node is the number of edges which connect with this node. Degree distribution $P(k)$ is the probability distribution function of degrees, it mean the probability of a node exactly right have k edges. The empirical research shows that the degree distribution of most complex networks obeys power-law distribution, that is $P(k) \sim k^{-\gamma}$, where $2 < \gamma \le 3$.

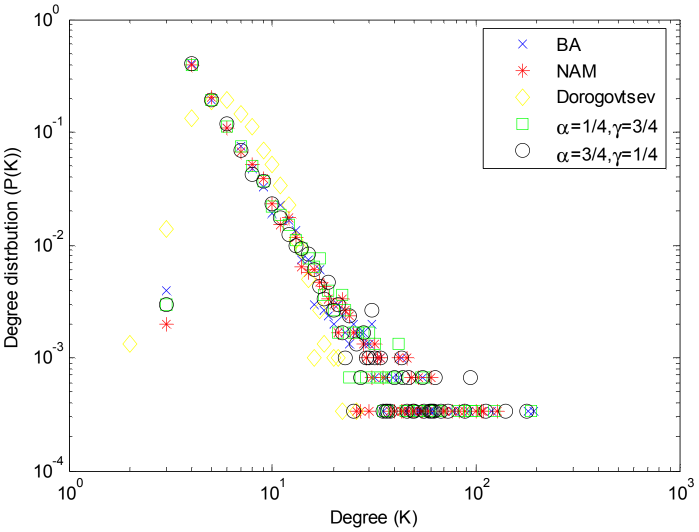

Fig. 1 Degree distribution

The degree distribution of models are shown in Fig.1, where $N = 3000$, $m_0 = 5$, $m = 3$, $\alpha = 1/4, \gamma = 3/4$ and $\alpha = 3/4, \gamma = 1/4$ respectively. From Fig.1, we can reach a conclusion that the degree distribution of the model based on node attraction with tunable parameters and other models all obeys power-law distribution. Therefore, although we can flexibility to adjust the parameters of model, and make to change its formation mechanism, the final network topology did not change too much. This suggests that preferential attachments considering the node degree and node attraction will effective produce stable complex networks, in addition they more close to real-world.

Clustering Coefficient. The clustering coefficient C of network is used to depict the aggregation degree of network. For a node i in complex network, it's clustering coefficient C_i denoted the probability of any two nodes in all nodes connect with i are connected to each other, Therefore, the clustering coefficient C is defined as the average value of all nodes' clustering coefficient in network, that is $C = 1/N \sum_i C_i$, where N denoted the total number of nodes in network.

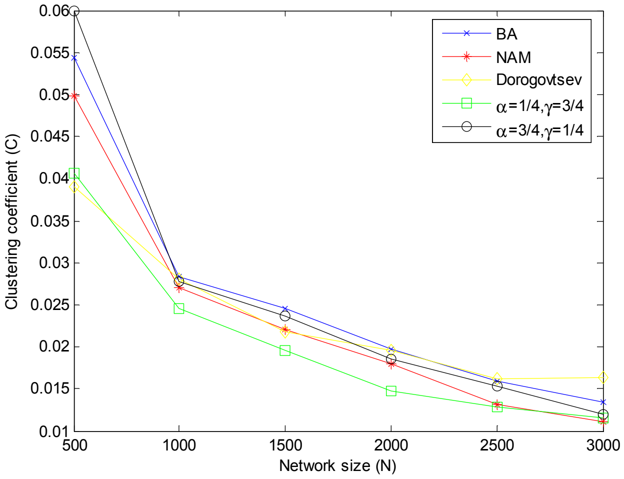

Fig. 2 Clustering coefficient

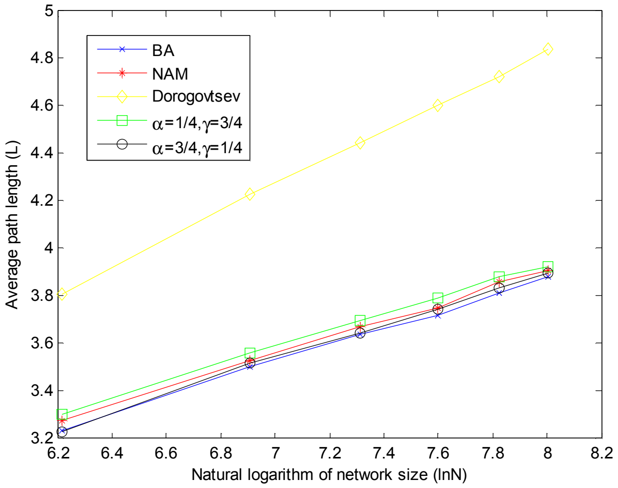

Fig. 3 Average path length

As shown in Fig.2, the clustering coefficient of proposed model in this paper and other models have basic consistent change trend, that is, with the expanding of network size, clustering coefficient reducing. In the same network size, several models are little difference, but we can change the clustering coefficient to some extent by adjusting the parameters of model.

Average Path Length. Average path length used to measure the small-world characteristics. For an undirected and unweighted network, average path length L is defined as the average value of the shortest distance between any two nodes, that is $L = 2/N(N+1)\sum_{i\geq j} d_{ij}$, where d_{ij} denoted the shortest distance between node i and node j ; N denoted the total number of nodes in network.

As shown in Fig.3, the increase speed of average path length of models basic to remain consistent, they are proportion to the logarithm of network size. This is consistent with most real-world networks. In the same network size, the average path length of the proposed complex network model is very close to BA model and NAM model, by adjusting the parameters of model to corresponding change the average path length. But the average path length of Dorogovtsev model significantly greater than other models. This is mainly because when the network grow, Dorogovtsev model only consider node attraction and ignore the node degree, result in network not easy to gather.

Conclusions

According to the evolution rule of real-world networks and aiming at the problems in BA model and initial attractive model, a complex network model based on node attraction with tunable parameters is proposed. The concept of node attraction is introduced based on BA model, and common affect preferential attachment existed in networks with degree. Theory research and simulation analysis show the fact that we can more flexible adjust the evolution process of network by adjusting model parameters, and the degree distribution follows power-law distribution, while the clustering coefficient and the average path length are high.

Acknowledgements

This work was financially supported by Program for Innovative Research Team in Chengdu Normal University, Ministry of State Security of China (MSS) Funded Projects JG2008011 and JG2011003.

References

[1] D. J. Watts and S. H. Strogatz, Nature, 393, 440-442, (1998).

[2] A. L. Barabási and R. Albert, Science, 286, 509-512, (1999).

[3] R.R. Nadakuditi and M.E.J. Newman, Phys. Rev. Lett., 108, 188701, (2012).

[4] S.N. Dorogovtsev, J.F.F. Mendes and A.N. Samukhin, Phys. Rev. Lett., 85, 4633-4636, (2000).

[5] S.H. Tao, C.Yang and H.N. Li, Computer Engineering, 35, 111-113, (2009). In Chinese

[6] S.W. Tian, H.Y. Yang and A.L. Li, Computer Engineering, 36 (10): 58-60, (2010). In Chinese

[7] M.A. Buice, C.C. Chow, Journal of Statistical Mechanics:Theory and Experiment, 2013, P03003, (2013).

Applied Mechanics and Materials Vol. 596 (2014) pp 847-851
© (2014) Trans Tech Publications, Switzerland
doi:10.4028/www.scientific.net/AMM.596.847

Fundamental Considerations on New Technology Evolution in Latest Network Development

Yuanjun Luo

School of Computer, Electronics and Information of Guangxi University, Nanning,
530004,P.R.China gxuyjluo@163.com

Keywords: Next Generation Network，Media-Stream Network，Law of Bit Significance，Point-to-Point Transfer，Face-to-Face Transfer

Abstract. Under the background of that NGN is coming into practice，the article uphold the scientific recognition spirit and external developing attitude to describe the distinct viewpoint about latest network development in two sides on different technology level. First，Based on the analysis of the key technical issue of the NGN，discover the essential substance of integration of the unified network，and point out the truth that the independent media-stream network ，not the integration network，to be the future one that lead the video service to the user in coming future. Following，starting from more fundamental position，the article state that the current technology architecture , which based on the point-to-point linear thoughts, has leads the network into a unbroken bottleneck. We must take a new and more society-suitable way，the face-to-face transfer architecture to fulfill revolution of the network communication technology.

Introduction

In this revolutionary technology, network communication technology is facing a Bainianweiyu changes to Internet as the representative of the new technology revolution is profoundly changing the traditional communication networks and system framework, its rapid pace of development in human history All the industries fastest growth in the amount of network traffic, especially long-term accumulation is very impressive. Microelectronics Technology will continue Moore's Law (doubling to 18 months); optical transmission capacity is growing at over Moore's Law (9 months doubled), the cost of the distance factor gradually moving towards death; wireless capacity are also ultra-Moore development (nine months doubled), the number of users has exceeded cable subscribers, the mobile Internet is to thrive, the Internet is increasingly becoming a pillar of the business. Massive network switching technology also continue to make significant progress, network quality of service (QoS) issues are becoming basically solved.

Trend of network convergence is becoming an inevitable trend of the development of the communication network. The first is the rapid development of digital technology and the full adoption; followed by the development of optical communication technology and build an ideal platform for triple-play services; then there is the development of software technology, the software changes required to support a variety of user characteristics, functions and business; Finally, the widespread use of key TCP / IP protocol, IP services can make to achieve interoperability. For the first time humans have three major network communication protocols acceptable for triple play and laid a solid foundation for the most technically. All this indicates that the current development of communication network technology is at an important juncture of change, the key technical factors in the practical application gradually, say NGN, which is now the core issues of all technical hotspots.

The so-called NGN, unlike the current generation refers to data-centric converged network, contains a variety of changes taking place in the way of network construction. NGN can provide, including voice, data and multimedia services, including a comprehensive open network architecture rapid transmission. From a technical perspective, including IP Over DWDM, soft-switching technology, IPv6 technology, SIP signaling control, based on the QoS guarantee of high-speed IP routing / switching technology, massive optical transport and switching technology, full mobility support, and so on.

In the eyes of experts, NGN will be a final communication network, multi-service communications networks to carry data IPv6 protocol based on optical transmission. However, IP protocol support for real-time applications reach the needs of users, and, QoS guarantee ineffective application solutions to various problems and poor reliability, making the Internet more and more complex functional structure, control more and more complicated, more efficient increasingly low, and is still deteriorating. If the difference between the transmission characteristics of a larger, more diverse types of business through various networks into a unified and integrated with IP transport, ideally, if the angle of view, it must require more and higher requirements. Moreover, if the current network technology development theory bred fundamental change, like a computer, "von Neumann" architecture has come to the limits of its existence, scientists are re-building a new, such as quantum computers, biological computers, etc. systems as network technology also requires new perspectives and starting point.

So, perhaps from another perspective, the spirit of scientific knowledge and world view, to rethink and understand the direction and prospects of the development of new network technology issues.

Non-mainstream thinking of key technical factors of next generation network

Change on the communication network bandwidth and computing resources of both status.

For a long time, communication theory and technology is built on the basis of scarce bandwidth resources, and its theories and technologies include: source coding, channel coding, modulation and demodulation, data compression, multiple access, network protocols, the basic idea is: rely on increasing computing (chip) resource complexity to get efficient use of bandwidth resources.

Breakthroughs in microelectronics technology, the chip resources explosive expansion. The pace of development in accordance with Moore's Law reveals, Intel continue to rapidly launch upgrading the CPU. With this synchronization, Microsoft also fast upgrading their operating systems, application software vendors majority of the simultaneous launch applications. Synchronous applications and resources so that the explosive growth of chip resources benign absorption, load and consumption, but also the price of a PC can be maintained at a stable level, thereby creating the entire PC industry. Meanwhile, it also begs for technical experts in more complex software, stronger CPU, the faster chip to achieve efficient use of bandwidth resources provides the material basis.

However, with the breakthrough of optical communication technology, such as DWDM and intelligent optical switching technology, making the bandwidth resources has also been explosive growth. Over the last decade, a million-fold increase in bandwidth, most original scarce bandwidth resources has become precious bandwidth resources and computing resources has undergone a fundamental change in the pattern, bandwidth resources will be many times greater than the growth rate the growth rate of chip resources.

According to statistics, in the fiber optic network transmission bandwidth increased 500-fold during the bandwidth demand grew by only 3 times. Do not form a synchronous bandwidth resource development "killer" application, to absorb, carry and consume bandwidth resources such explosive growth, leading to the collapse of the telecommunications industry chain, namely severe shortage of excess demand and investment. If the network communications industry, not a fundamental reform of traditional business, effective solution consumes bandwidth "killer" applications, network communications industry will be less likely to get out of the abyss of disaster.

Basic resources are chip communications network bandwidth, network technology can not meet the new balance if basic resources, will inevitably lead to systemic disease. Over the past 30 years developed IT technologies, due to various reasons precipitation under extremely complex CPU chip, tens of millions of lines of software, tedious inefficient network protocols, each contain indivisible. For a large number of resources are not applied, but spent on unnecessary redundancy, the network becomes parasitic cancer, and having control deteriorating trend. Therefore, increasing technical complexity, reducing the efficiency of chip development ideas are a departure from the direction of the future development of network technology, only to reduce reliance on chip technology network, network development is the right direction to continue moving forward with the application.

law of bit demand about information value in next generation network.

Network communications industry has yet to find with the explosive growth of bandwidth resources to adapt to the "killer" application, quickly exploding bandwidth resources into the consuming public is willing to pay for video streaming services, is the key to solve that problem.

Based on scarce bandwidth resources in accordance with traditional communication theory, telephone airtime charges, Internet traffic according to Internet time charges or fees, rather than by value or value of the information to provide services to charges. This mechanism may be a small amount of data and computer files narrowband telephone service packet transmission is appropriate, but the huge amount of data broadband video streaming service is not appropriate.

Therefore, the value of information is inversely proportional to the amount of data required in the network information reflects it, the data is less important information, but the relatively large value of the information; unimportant information amount of data, but the value of the information is relatively small. This is the next generation network needs a law of bit demand.

Discussions on everything over IP and IP plus QoS selection.

Due to the huge success of the Internet, adding that as long as QoS on Internet, IP will be able to dominate the world, is everything over IP, therefore, one of the seven basic characteristics of NGN as defined in ITU-T is based on the packet transmission. However, IP switching technology is not a panacea, such people have spent the last ten years of time to develop IP telephony (VoIP), but the quality of IP telephony still do not like traditional phones, it is not as universal as a regular phone. In fact, IP technologies for streaming media have never been developed, it is good transport E-mail, WWW, FTP and other computer package, is based on the characteristics of the computer information exchange text, images and other customized.

IP technology is the core packet switching, store and forward, and try to send, using error detection, error control and retransmission mechanisms to ensure the reliability of the transmission is not very sensitive to latency. Some people think that the increase QoS IP technology can solve the problem of video transmission, it is not.

Currently, QoS studies are assumed to network streaming content represents a very small proportion, for streaming media network giving priority to ensure that priority transmission of streaming media. When the network is congested, so too slowly transfer important files, you can even stream media to ensure delivery by packet loss. To this end, the invention of IntServ (integrated services), DiffServ (Differentiated Services) and MPLS (Multiprotocol Label Switching) technology, such as QoS. However, video streaming, whether significant or not, can not delay and packet loss, because intermittent no appreciation of the value of the film is, therefore, QoS for video streaming service is only accepted or rejected. Clearly, the use of next generation network IP Plus QoS is difficult to provide build high-quality video streaming services, this is not a bad IP technology, but does not have the essential characteristics of IP technology to transmit video streaming needs.

Information and data can be divided into two categories: direct machine-receptor package (datagram) and to direct human receptor streaming (streaming). Voice is the most basic human access to information and information needs; to transfer files packet-based data network based on the development of the computer; video is the most important source of human information, glamor film and television in the case.

The best way is to do what the file packet transmission, have to ensure that the correct error detection and retransmission mechanisms, IP network (eg Internet) is based on the exchange of information a computer file package features and design; transmission of streaming media must be resource reservation to ensure continuity and low latency, such as voice telephone network is based streaming features customized.

With multiple combinations of different business network to provide different services to the consuming public may be more realistic solution. Only simple to efficient development of telecommunications history has repeatedly proven: tailor-made for the transmission of voice telephone networks can not rely on the telegraph network technology, IP networks to transmit computer files can not rely on packet telephony network technology to transmit video streaming is clearly the responsibility of the the development of next-generation networks require new ideas and new technologies.

The historical mission of the next generation of video communication network should be. The best of the next generation network QoS, is to create a separate streaming media network, that is the next generation of video streaming network.

Realistic significance of the face-to-face transmission theory against the traditional technique

Problems caused by network transmission based on point-to-point linear scheme.

American computer science expert Yalong Lanier said that the network is becoming increasingly complex and cumbersome and inefficient, and it all stems from peer-linear way of thinking of computer science has been pursuing.

Those pioneers of computer science, including Shannon, Turing, von Neumann and Wiener • have received a communication mode used in their times, through wire transfer signal. Telegraph, telephone, fax has been the tradition. Radio and television signals are transmitted through a wire, even if part of the radio path. The basic thinking and behavior are being affected by this particular pattern oriented, has become the core of the transmitted signal through the wire metaphor that era.

According to this mode, the information processing is simplified in each end of the line, at a time point of a debugging or test signal. Easy processing of a single point, in particular, can be analyzed mathematically; the other hand, this increases the complexity of the problem on another level, as a single point in space to make sense, the only way is time.

Simply put, this model needs to ensure the accuracy and completeness of information transmission, the information will be passed through the wire coming from the past in order, we must first develop a set of rules (grammar, protocol), the provisions of which the first, after which, What time delivery or acceptance so that the transmitting end and the receiving end of the codec information, the information for the start time of linear structures.

This mode, only one system at a time point of information to be processed, it is necessary to establish a hierarchy of time, a byte of information in the system to deal with a particular moment is what the meaning is based on it. "What is "determined to be read when.

In the relatively small scale, this way no problem, but with the increasing scale of their vulnerability to show up, it could have disastrous consequences. Because the core spirit of this model is to strictly ensure perfect information point to point transmission, encoding and decoding protocols need to be developed, in order to comply with the agreement to be a huge amount of memory and resources to represent the agreement, rather than dealing with objects.

This greatly increases the amount of information to be processed, if an error occurs during processing, make the whole thing to do to drop, but the larger the size of the system, but also harder to avoid the occurrence of errors. Software development and network functions are also perfect to endless tinkering, even more tolerant mechanisms established nor can fundamentally solve the problem, which resulted in the current situation of distress communications network: the larger the network, the function increase more, we must continue to add additional levels, thus making the network architecture consisting of real users to transfer data to the module for a handful, a large number of operations on the adaptation compatibility, security and reliable transmission of redundant data, etc. etc. up, and the overall efficiency of the network continued to decline, with the growth of the network size is proportional decline. All these are a direct consequence of linear superposition.

Key significance from the "point-to-point linear thinking" to " whole face-to-face pass"

Experts point out that it is known to the human nervous system, the human body and the environment is not linear contact point, what grammatical form without prior agreements. In contrast, the human body is a face, and the world is built on the surface of contact. For example, the human retina at the same time you can see many points of light.

According to this understanding, Lanier propose a new model based on surface rather than point-based information processing. Its core is carried out in a plane while many information processing, object-oriented simultaneous multi-point sampling, rather than just dealing with a point each time. This information is handled as "Classification." In the type classification, one byte of information is based at least in part, to handle additional information given meaning - natural nervous system, e.g., by the overwhelming majority of the human brain processes information in this manner.

Based on surface and based on the most basic difference is that the former idea is to make the information processing process through better guesses as accurate as possible, while the latter idea is to ensure complete and accurate information processing through rigorous coding and decoding process. First thing to do is not pre-established protocols to ensure that you will see anything, but guess, expect to see anything through continuous feedback process and continuously improve the accuracy of guessing. This evolution of the behavior and survival of organisms and is consistent.

Lanier noted that computer science personified the computer application "memory (RAM)" describes the human brain activity words to refer to a computer by a strict protocol identification and confirmation process, but learning the human nervous system and memory process is not rote, but more use type guessing, carried out through a variety of related, but better results. Go from point to point protocol concerns the type of surface is required from the requirement to roughly approximate perfection. Point to Point Protocol is to require either all right, or all wrong. The premise is that type of recognition, recognizing always some small error will occur, but it does not care about them.

Biological evolution showed that this system can be approximated by combining the feedback loop for greatly improve their accuracy and reliability of information processing. Scholars have noted that only faultless before the presence of the state in an ideal world, but in practical applications tend to mutation and unpredictable, and often collapse; modeled on the overall ecological behavior of the biosphere, so close to completely reliable computer network should be a species better choice.

Conclusions

At the time when the major changes in the new technology of the network occurred , which indicated by mainstream scholars that IPv6 protocol over optical transmission network will integrate all the current communication network into one full-service network, and human society will obtain intelligent business universal communication network, the paper which holding the spirit of scientific development view and understanding of the concept, from two aspects of different levels, questioned the new technology development direction of current network is the inevitable choice, and be about to provide some new perspectives and new ideas for the development of new technology of network correctly.

References

[1] Leping Wei. *The strategic thinking of the next generation network*. Information network, 2003, 8

[2] Hanzhoung Gao. *Discuss on the next generation network*. Telecom Science, 2003, 2

[3] Hongsong Li. *Study on some key issues of next generation network*. Telecom Science, 2003, 12

[4] Yong Hu. *"Bit demand law" leading change in twenty-first Century*. Business Review 2007, 10

[5] Gao Ling. *Computer science exist fundamental error*. From the "International Herald Tribune"

[6] Shan Jiang. *The development trend of the technology of communication network*. Technology Wizard 2012, 8

[7] Bo Yu. *new technology of network for Cloud computing*. Software and Application of Computer Disk, 2013, 12

Applied Mechanics and Materials Vol. 596 (2014) pp 852-855
© (2014) Trans Tech Publications, Switzerland
doi:10.4028/www.scientific.net/AMM.596.852

Intrusion Detection Systems

Guiguo Liu

ITS Engineering & Technology Research Institute of Highway Ministry of Transport, China

guiguo.liu@rioh.cn

Keywords: Firewall; Intrusion Detection; Network Security

Abstract. In the ear of information society, network security have become a very important issues. Intrusion is a behavior that tries to destroy confidentiality, data integrality, and data availability of network information. Intrusion detection systems are constructed as a software that automates the automatically detects possible intrusions. In this paper, we present the existing intrusion detection techniques in details including intrusion detection types, firewalls, etc.

Introduction

In the ear of information society, network security have become a very important issues due to the fact that there are many adversaries try to attack network for achieving some goal such as economy. In order to protect against various attacks and viruses, many network security techniques have been proposed during the last ten years such as firewalls, intrusion detection system, cryptography, etc. Among these security mechanisms, intrusion detection has been widely considered to be one of the most promising approaches to protect modern complex and dynamic attacks.

In generally, existing IDS systems can be divided into two categories based on detection approaches: identify-anomaly detection and misuse detection [3]. Identify-anomaly detection is an approach that detects intrusions according to characteristics of normal activity which is established by some learning algorithm. One main advantage of these anomaly detection systems is able to detect previously unknown attacks at the cost of a large number of false positives and difficulty of training a system for a very dynamic environment. Misuse detection systems is another technique that when a new attacks comes, the system look up from known attack repository, which stores well-known "fingerprints" or signatures, to determine whether the new attacks in that repository when the packets cross the network's gateway threshold. If yes, the system considers that the packets is normal traffic within a network; otherwise, it reports abnormal traffic behavior. Misuse detection systems are to detect only those attacks that have been modeled. As a result, misuse detection systems are less prone to the generation. The big limitation of this approach is that it can not precisely detect previously unknown attacks.

A security policy is a series of rules that specify the authorizations, prohibitions and obligations of agents that can access to the server. A hacker might be considered as a malicious agent that he tries to violate the security policy defined in advance. The overall security objectives are confidentiality, integrity, and availability. That is to say, an intruder tries to destroy such security objectives. In the case of destroying confidentiality, the intruder might have illegal access to some piece of information. For example, the hacker might eavesdrop a password so that he violates confidentiality. In this case of validating integrity, the intruder might modify, delete information even inject a new one. When the hacker prevents other users to have legal access to some services or resources, we say he validates the availability. Typical attacks are Denial of Service (Dos) [4] that the intruder tries to consume the resources of the victim machine so that the server can not provide any services to legitimate user. In additional Dos attack, Scan attacks are another import threat to network security. The purpose of port scanning is to determine what ports are open in the system. That is to say, the attacks try to know what services are available by scan what ports are open.

The rest of the paper is organized as follows: the next Section we briefly review the basic concept of firewalls. In section 3, we discuss the firewall types in details. In Section 4, we describe the intrusion detection techniques. Finally, we draw a conclusion in section 5.

Firewalls

In this Section, we simply review the concept of firewalls. Firewalls are security guards that protect a private network from the outside Interne by filtering all the incoming and outgoing network traffic, blocking access to services that may be exploited to attack the internal hosts of the protected network. All the filtering works are with the help of policy rules defined which packets are legitimate and which are illegitimate. A firewall policy is a list of ordered filtering rules that define the actions performed on packets that satisfy specific conditions. Generally, the actions have the form of "deny" or "accept". A filter rules usually consists of protocol type, source IP address and port, destination IP address and port, and the action field. The typical formats of the filtering rules are the following form [5-6].

<order><protocol><src_ip><src_port><dst_ip><dst_port><action>

The order of the rules denotes relative position of one rule, which provide the convenience with network administrator to quickly look up the wanted rules. It is possible to use any field in IP, UDP or TCP headers in the rule filtering part, which is denoted by the filed protocol. Field src_ip ,src_port are denote source's IP addresses and port, respectively. Similarly, Field dst _ip ,dst _port are denote source's IP addresses and port, respectively. The field action can be either "accepts" or "deny". Fig 1 shows a typical architecture of firewalls.

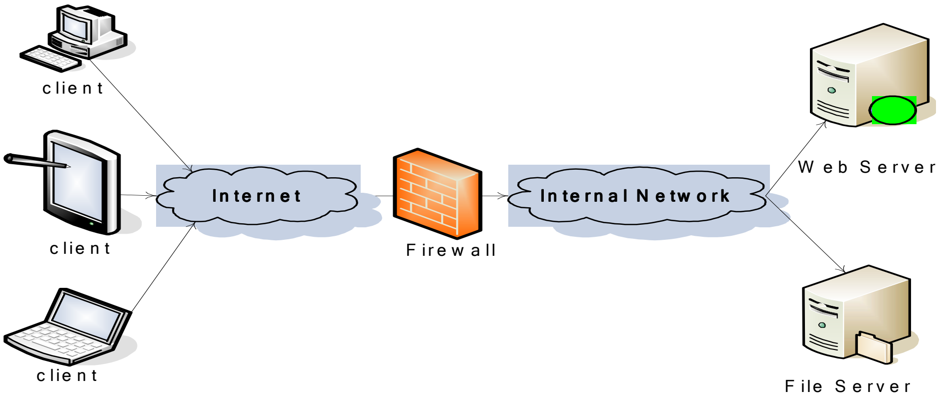

Fig 1.The Firewall Architecture

Generally, firewalls are divided into three types: Packet filtering, application level gateways, and proxy's service. The packet filter firewall makes its decision according to the packet header when analyzing the network traffic. Application level gateway firewalls filter the incoming and outgoing information packets before copying and forwarding information across the gateway at the level of the application layer. Proxies Service firewalls are the techniques that observe handshaking between packets to ensure a requested session when the packets is normal or nor using TCP connections.

The type of intrusin detection

Generally, the existing IDSs are constructed as a software that automates the automatically detects possible intrusions attacks. Note that the purposed of IDS system is to detect whether or not the network is under attack or has been breached, which the goal of firewall is to protect a network and attempt to prevent intrusion. That is to say, for protect attacks; firewall and IDS should be applied to the network environment at the same time. Existing IDSs can be classifies into three types: Network-based Intrusion, Host-based Intrusion Detection and Distributed Intrusion Detection.

Network-based IDS.Network-based intrusion detection systems monitor the network traffic and use these raw network packet's content to analyze network, transport, and application protocols to identify suspicious activity. To do this a network interface is set in promiscuous mode and collects all packets through the network. There are three types to collect network traffic packets: String signatures, Port signatures and Header signatures. The string signatures method is to find a possible text related with in incident in the packet data, which the port signatures only monitor the network to special ports. If a traffic network try to come to a port which is not used by any services in the system, then the IDSs might considers as suspicious attacks. Header signatures try to detect the packets headers whether they are combined with illogical and possibly dangerous request.

There are several advantages of the network based IDS. One is the operating system independence. Network-based IDSs takes the network packets as information sources and all the network data are wrapped by a unified form of IP packets which the data packets are independent on OS platform. Thereby, the network-based IDSs are also independent on OS platform. Another advantage for this method is to provide faster notification and response due to detect malicious and suspicious attacks as they occur. Finally, the approach is the possibility to monitor data and events without affecting host performance.

However, Network-based IDS have also disadvantages especially under heavy network loading. In addition, it is vulnerable to insertion and evasion attacks [2]. These attacks attempt to desynchronize the view of the IDS with respect to the view of the actual target. Finally, it is very difficulty is to analyze the encrypted packet data due to the fact the encrypted data stream has lost the data features so the IDS can no analyze, identify, and match the data.

Host-based IDS. Host-based IDS monitors a single machine and audits data traced by the hosting operating system. Typical examples of audited data are system calls, event, resource usage, and logs on Windows NT and syslog in Unix environments. Where there is any files change, the IDS compare the new signatures by hashing new log entry to see whether there is a match. If so, the system sends an alert to the administrator for further processing. Till to now, there are many researches in this system. For example, the first implementations were mainly designed to analyze system logs [1]. Differed with the network-based IDS, host-based IDS detects insider misuse rather than outsider misuse.

Likewise, this approach also has several advantages. Firstly, the approaches can measure whether an attack was successful or not with greater accuracy. Secondly, host-based IDS can monitor user and file access activity such as user logon and user logoff activity, and file access activity, etc. Also, any changes to system files and executables will be monitored, which is very difficult for network-based IDS to provide these monitoring objects.

One big weakness of host-based IDS is to provide the poor real-time response and can not effectively protect against one-time catastrophic events.

Application-based IDS. Application-based IDS can be classified to the host-based IDS. It analyzes the events transpiring within a software application. The purposed of this approach is to solve the weakness of network-based IDS. The application-based users the information source s from running applications as its input. One big advantage of this approach is to monitor the interaction between user and application, which traces activity to individual users. However, these approaches make evasion techniques ineffective due to the fact it is hard to integrate the view of IDS system and application.

Intrustion detection techniques

Anomaly Detection. The anomaly detection systems are designed to detect uncovers abnormal patterns of behavior according to the baseline of normal usage patterns which is established in advance. Anything that widely is deviation from the established normal usage patterns is considered as an intrusion. The detection system identifies anomalies as deviations form “normal” behavior and automatically detect any deviation from it. The main challenge for anomaly detection system is the huge volume of data. The anomaly detection techniques need to be computationally efficient to handle these large sized inputs. The high false positive rate is the main drawback of the anomaly IDS system. One big advantage of this approach is that do not require constant updating of rules or signatures of novel intrusion. Typical anomaly detection is shown in Fig 2.

Misuse Detection. Misuse detection can not detect the attack which signatures. When an event are matched a pre-defined pattern of known attacks, the IDS system will consider as an attack. In this approaches, the patterns corresponding to known attacks are called signature. Because all the even are judge whether it is normal or nor according to the signatures database and thereby the system misuse detection systems have high degree of accuracy in detecting known attacks and their variant. The main disadvantage is that detect unknown intrusions relying on signatures extracted by human experts. Fig 3 shows a typical misuse detection system.

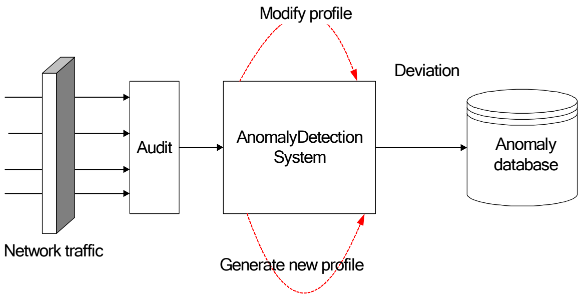

Fig 2. A typical Architecture of misuse detection system

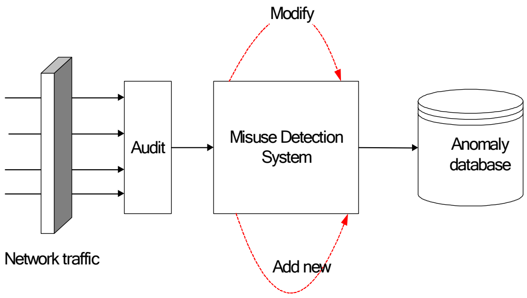

Fig 3. A typical Architecture of misuse detection system

Data Mining-based Detection. The big weakness of anomaly detection system is the data volumes are so large that analysis of specialized audit trails to spot abnormal patterns become extremely expensive. In order to address this issue, many mining-based IDS approaches have been proposed recently [7-8]. Compared to traditional IDS system, data mining-based has higher false positive rates. In generally, there are three categories mining algorithms are applied to the IDS techniques. Namely, association rules, sequential rules and classification. Classification algorithm aims to assign a new data item to one of several pre-defined categorical classes, which association rules are the techniques that are to seek to discover associations among transactions encoded in a database. Sequence rules aim to extract a series of events that commonly occur over a period of time.

Conclusion

Intrusion is a behavior that tries to destroy confidentiality, data integrality, and data availability of network information. Intrusion detection techniques try to discover whether there is the action is an attack against the network. In this paper, we present a survey of intrusion detection system.

References

[1] .P. Anderson. Computer Security Threat Monitoring and Surveillance. Technical report, James P. Anderson Co., Fort Washington, PA, April 1980.

[2] T.H. Ptacek and T.N. Newsham. Insertion, Evasion and Denial of Service: Eluding Network Intrusion Detection. Technical report, Secure Networks, January 1998.

[3] Helman, P., Liepins, G., and Richards, W. (1992). Foundations of Intrusion Detection.In Proceedings of the Fifth Computer Security Foundations Workshop pp. 114-120.

[4] CERT Advisory CA-1997-28,IP Denial of Service Attacks. http://www.cert.org/advisories/CA-1997-28.html.

[5] S. Cobb. “ICSA Firewall Policy Guide v2.0.”NCSA Security White Paper Series, 1997.

[6] J. Wack, K. Cutler and J. Pole.“Guidelines on Firewalls and Firewall Policy.” NIST Recommendations, SP 800-41, January 2002.

[7] Wenke Lee, Salvatore J. Stolfo. Data Mining Approaches for Intrusion Detection. Proceedings of the 7th USENIX Security Symposium. 2000.

[8] W. Lee, S. J. Stolfo, P.K. Chan, E. Eskin, W. Fan, S. Hershkop M. Miller, and J. Zhang. Real time data mining-based intrusion detection.In DARPA Information Survivability Con-ference and Exposition (DISCEX II'01), Anaheim, California, June 2001.

Applied Mechanics and Materials Vol. 596 (2014) pp 856-860
© (2014) Trans Tech Publications, Switzerland
doi:10.4028/www.scientific.net/AMM.596.856

QoS Routing Protocol Based on Resource Optimization for Aerospace Networks

Weiqiang Wu[a], Bingni Luo[b], Peipei Chen[c], and Qinyu Zhang[d]
Harbin Institute of Technology Shenzhen Graduate School, Shenzhen, Guangdong, 518055, China
[a]wwq520516@163.com

Keywords: QoS routing, aerospace network, resource optimization, dynamic update.

Abstract. To guarantee the QoS of the various traffics and take good advantage of the network resource, the QoS routing protocol based on resource optimization is proposed. By the network state information dynamic update and the QoS routing optimization model design, the QoS routing protocol can provide the optimal path for real-time traffic, broadband traffic and best effort traffic in time with low control message cost. Simulation shown that, compared to the traditional shortest path routing, the QoS routing can satisfy the demand of traffics and can improve the network performance.

Introduction

Aerospace network contains a variety of satellites, near space platforms and aircrafts. It is a special kind of wireless multi-hops network with large coverage. To delivery data in such multi-hops networks, some classic routing protocols for satellite network have been proposed. According to the method on solving problem of the dynamic changing topology, satellite network routing can be classified as routing based on virtual topology[1], routing based on virtual region[2,3], on-demand routing[4,5], and routing for multi-layer satellite networks[6,7]. The main purpose of these routings is to avoid the effect on data delivery caused by the movement and switch of satellites and to guarantee the basic data transmission.

Because of the wide range of application and large coverage of the aerospace network, the data traffic in aerospace network will be with more diversity, characteristics and requirements. It is necessary to gurantee the QoS by resource optimization. Some routing protocols based on remaining bandwidth and link duration are proposed to optimize the data path for some sigle traffic type[8,9]. To optimize the data path of different traffic types, the routing based on traffic types is proposed in [10]. It establishes routing tables for each type of traffic, which needs large storage space.

In traditional satellite communication system, when the traffic connection is established, the resource is requested. And then the satellite allocate the resource for the traffics. This kind of method needs long delay and can not adapt to the connectionless oriented traffics. Most proposed dynamic resource optimization methods are based on time slots divide, which update the network state at the beginning of time slots. If time slot is too long, in a time slot the link state will change. Even if the time slots is short, there is no guarantee that the network states can remain unchanged in one slot, and which cause a large number of network overhead. So becaus of the dynamic network states and the traffic diversity, the QoS routing became one of the challenges in areospace network.

In this paper, a QoS routing protocol for aerospace is proposed. Base on the dynamic update of network state information, the transmission path of different types of traffics are optimized to satisfy the need of the traffics with the limited network resources as much as possible.

Network State Information Base

Traffic Types. The traffics are divided into three types and the type is set in reserved field of network layer packet header. The first type is “real-time traffic” such as command, control message, voice and interactive traffic which should be transmitted immediately. The second type is “broadband traffic” such as large file, download and video which need large bandwidth. The third type is “best effort traffic” such as e-mail and general file which just be transmitted as far as possible.

Design of Network State Information Base. Network state information base (NIB) is composed of link state information such as the delay, remaining bandwidth and additional cost of each link. The network can be abstracted as a weighted directed graph $G(V,E)$. Where V is the vertex, which means the set of nodes in the network, $V=\{V_1, V_2, \ldots, V_n\}$. E is the edge of the graph, which means the links between nodes, $E=\{(V_1, V_2), (V_1, V_3), \ldots, (V_i, V_j)\}$. NIB can be described as an adjacent matrix $\boldsymbol{N}$:

$$N=\begin{pmatrix} e_{11} & \cdots & e_{1n} \\ \vdots & \ddots & \vdots \\ e_{n1} & \cdots & e_{nn} \end{pmatrix} \tag{1}$$

Where e_{ij} is the weight of each edge, which means the link state of link (V_i, V_j). $e_{ij}=(D_{ij}, B_{ij}, A_{ij})$, where D_{ij} is the delay of link (V_i, V_j), B_{ij} is the remaining bandwidth of link (V_i, V_j), and A_{ij} is the additional cost of link (V_i, V_j).

NIB is stored in each nodes in the network, which can reflect the dynamic changes of the whole network state. The link transmission delay calculated by the nodes according to the regular of the mobility of satellites, the remaining bandwidth is updated dynamic by the bandwidth update message, and the additional cost is set according to the congestion of the nodes.

QoS Routing Optimization Model

When s is the source node and d is the destination node, $p(s,d)$ is a data path from s to d, which consists some links. R is the set of the nodes which in $p(s,d)$. $C(p(s,d))$ is the cost when data is transmitted along the path $p(s,d)$. The QoS routing based on resource optimization is to transmit data with different traffic types through the path with the lowest cost.

(1)For real-time traffic, the most important QoS index is the end-to-end delay. The path with the shortest end-to-end delay is optimal. The end-to-end delay is denoted as $Delay_{end\text{-}to\text{-}end}$, which is the duration time from the data generation in the source to reception in destination. It is shown as Eq. 2.

$$Delay_{end-to-end} = T_{transmission} + T_{propogation} + T_{queuing} \tag{2}$$

Where $T_{transmission}$ is the transmission time, which is determined by the packet size and the link bandwidth. $T_{propogation}$ is the propagation time, which is determined by the distance between the nodes of the links. $T_{queuing}$ is the queuing time.

In aerospace network, because the far distance, the propagation time is long. Compared with the propagation time, the transmission time can be ignored. In the QoS routing protocol, the real-time traffic is delivery first to avoid the queuing. So the queuing time can be ignored. If the traffic demand of end-to-end delay is D_{QoS}, the path cost of real-time traffic can be denoted as Eq.3.

$$C(p(s,d)) = \sum_{ij\in p(s,d)} C_{ij},\ C(p(s,d)) \le D_{QoS} \tag{3}$$

Where C_{ij} is the cost of (i,j), which consists of link delay and additional cost. It can be denoted as Eq. 4.

$$C_{ij} = D_{ij} + A_{ij} \tag{4}$$

(2)For the bandwidth traffic, the remaining bandwidth of the path should satisfy the QoS demand of the traffic, and the end-to-end delay should be as short as possible. If the remaining bandwidth of node i is B_i and the remaining bandwidth of node j is B_j. The remaining bandwidth of link (i,j) is denoted as Eq. 5, and the remaining bandwidth of the path $p(s,d)$ is denoted as Eq. 6.

$$B_{ij} = \min\{B_i, B_j\} \tag{5}$$

$$B(p(s,d)) = \min_{ij\in p(s,d)} B_{ij} \tag{6}$$

If the QoS demand of bandwidth is B_{QoS}, the optimal path for bandwidth traffic is the path with the lowest cost denoted as Eq. 3, and Eq. 7 should be satisfied.

$$\min_{ij\in p(s,d)} B_{ij} \geq B_{QoS} \tag{7}$$

(3)For the best effort traffic, in order to balance the load of the network, the optimal path is the path with most remaining bandwidth. The cost of the path for best effort traffic is denoted as Eq. 8.

$$C(p(s,d)) = \frac{1}{B(p(s,d))} + \sum_{ij\in p(s,d)} A_{ij} \tag{8}$$

Dynamic Update of NIB

The main network state information which should be updated dynamic are the remaining bandwidth and the additional cost. To avoid the update based on time slots, the traffic demand of bandwidth is divided into several levels. To update NIB in time with low control cost, when the remaining bandwidth of node change between different bandwidth levels, or some congestions occur, the NIB should be updated. In aerospace network the GEO satellite is the management node, which selects the NIB update message and broadcast to the whole network.

According to the remaining bandwidth and current traffic of nodes, two kinds of bandwidth message are designed. They are the bandwidth message (BW) shown in Fig. 1 and the bandwidth message with current traffic (BWT) shown in Fig. 2.

2bytes	10bits	1byte	2bytes
Message type	Node	Bandwidth level	Sequence number

Fig. 1 The bandwidth message

2bytes	10bits	1byte	2bytes	2bytes	28bits	28bits	···
Message type	Node	Bandwidth level	Sequence number	Message size	Current traffic 1 (source, destination, traffic type)	Current traffic 2	···

Fig. 2 The bandwidth message with current traffic

The process of bandwidth update is shown in Fig. 3.

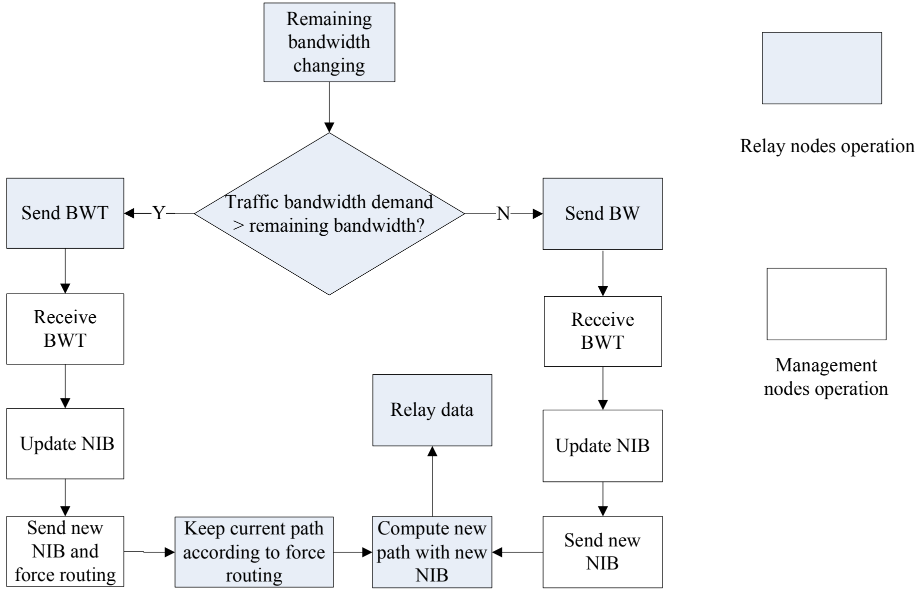
Remaining bandwidth changing
Traffic bandwidth demand > remaining bandwidth?
Y
N
Send BWT
Send BW
Receive BWT
Receive BWT
Update NIB
Update NIB
Relay data
Send new NIB and force routing
Keep current path according to force routing
Compute new path with new NIB
Send new NIB
Relay nodes operation
Management nodes operation

Fig.3 The process of avalible bandwidth update

The additional cost is set according to Eq. 9.

$$A_{ji} = \begin{cases} 0, & 0 \leq q_{avg} \leq min_{th} \\ D_G, & min_{th} < q_{avg} < max_{th} \\ \infty, & max_{th} \leq q_{avg} \leq q_{lim} \end{cases} \tag{9}$$

Where, D_G is the path delay when data is transmitted by the GEO satellite. q_{avg} is the average queue length of the node. q_{lim} is the limit of the queue length. min_{th} and max_{th} are the RED indexes which denote the congestion of node.With the NIB and the QoS routing optimization model, the QoS routing protocol can optimized the data path for different type of traffics.

Simulations

Real-time traffic guarantee. Set three traffics in the network. Traffic 1 and traffic 2 are FTP whose packet size is 1000 bytes. Traffic 3 is real-time traffic obeying exponential distribution, whose mean value is 1, burst time is 100ms, idle time is 100ms and average rate is 500Kbps. Compared with the shortest path routing, the end-to-end delay of real-time traffic is shown in Fig. 4 and Fig. 5.

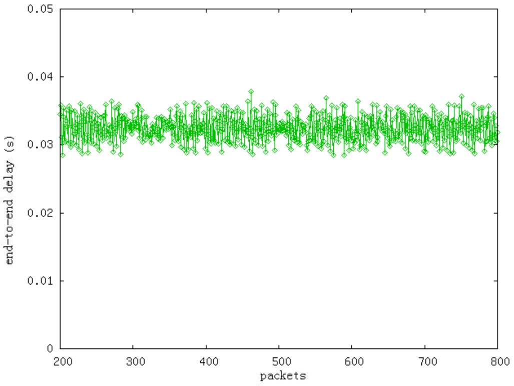

Fig. 4 End-to-end delay (shortest path routing)

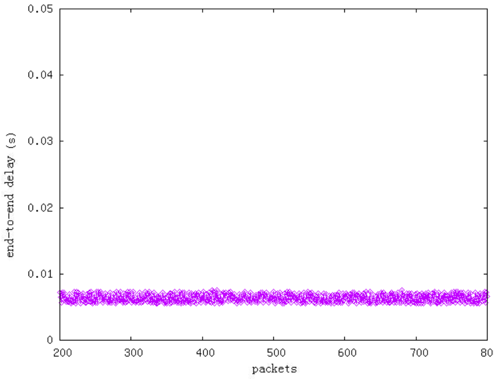

Fig. 5 End-to-end delay (QoS routing)

For the real-time traffic, the proposed QoS routing protocol can be sent in advance and can be sent through the path with lowest delay cost. So the end-to-end delay is much shorter than that of the traditional shortest path routing.

Broadband traffic guarantee. Set three FTP traffic, which will be relayed by the same node *A*, if use the shortest path. The bandwidth of *A* is 30Mbps. The bandwidth demand of traffic 1 and traffic 2 is 10Mbps. Traffic 3 starts at the time “8s”, whose bandwidth demand is 30Mbps. Fig. 6 and Fig. 7 show the performance of the traditional shortest path routing and the QoS routing. The QoS routing can transmit traffic with the optimal path which can satisfy the demand of bandwidth. The broadband traffic is guaranteed and the network performance is improved.

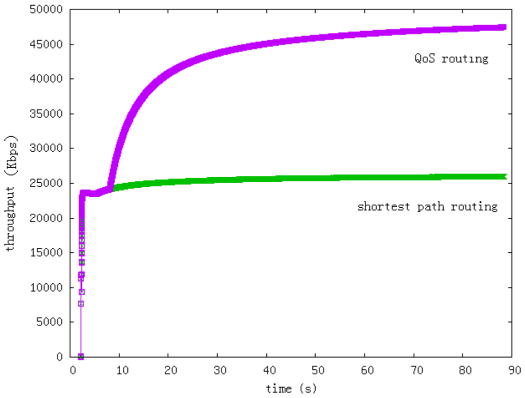

Fig. 6 The throughput of the network

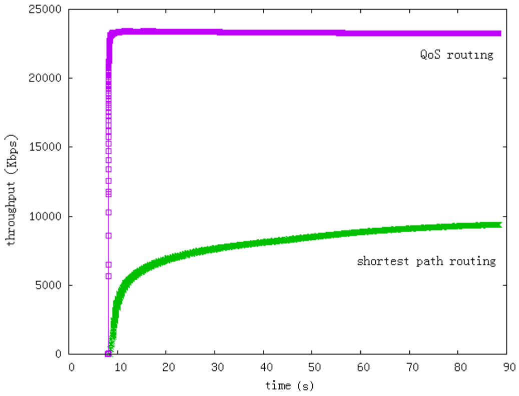

Fig. 7 The throughput of traffic 3

The Overall Performance of the Network. Set three types of traffic in the network. The indexes of real-time is as the same as above. The broadband traffic is FTP whose packet size is 1000 bytes and the demand of bandwidth is 10Mbps. The best effort traffic is CBR whose packet size is 1000 bytes, and the rate is 10 packets per second. The simulation scenes is shown in table 1.

Table 1 The scenes with different traffics

scenes	1	2	3	4	5
number of traffic (real-time/broadband/best effort)	1/2/2	2/4/4	3/6/6	4/8/8	5/10/10

The throughput performance is shown in Fig. 8, and the end-to-end delay performance is shown in Fig.9. The throughput performance of QoS routing is much better than the shortest path routing, and the end-to-end delay is about the same.

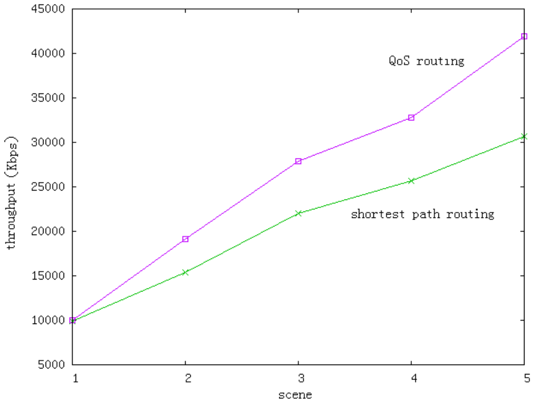

Fig. 8 The network throughput

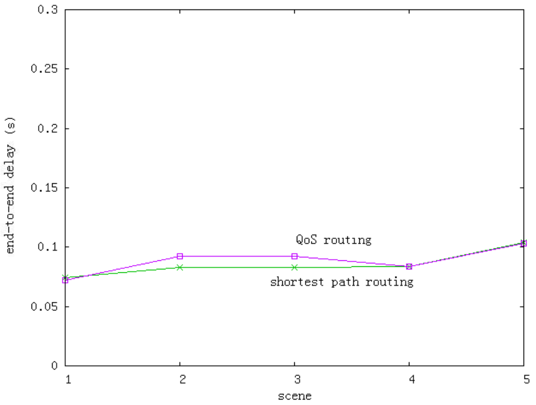

Fig. 9 The average end-to-end delay of all traffics

Conclusions

In this paper, a Qos routing protocol based on resource optimization is proposed. In this protocol, a method of NIB dynamic update is designed to make the nodes get the newest NIB in time with low control message cost. The QoS routing optimization model is designed to provide optimal path for different types of traffics. By optimizing the network resource, the proposed QoS routing can guarantee the QoS of traffics. It can be a meaningful routing method for the aerospace network with traffic diversity.

References

[1] Werner M. A Dynamic Routing Concept for ATM-Based Satellite Personal Communication Networks[J]. IEEE Journal on Selected Areas in Communications, 1997, 15(8): 1636-1648.

[2] Hashimoto Y, Sarikaya B. Design of IP-based Routing in a LEO Satellite Network[C]. Proceedings of third international workshop on satellite-based information services (WOSBIS' 98), 1998: 81-88.

[3] Ekici E, Akyildiz I F, Bender M D. A Distributed Routing Algorithm for Datagram Traffic in LEO Satellite Networks[J]. IEEE/ACM Transactions on Networking, 2001, 9(2): 137-147.

[4] Kuang T, Ma R P. Darting: A Cost-effective Routing Alternative for Large Space-based Dynamic-topology Networks[C]. IEEE MILCOM 1995, 1995: 682- 686.

[5] Papapetrou E. Distributed on-demand Routing for LEO Satellite Systems [J]. Computer networks, 2007, 51(15): 4356-4376.

[6] Vatalaro F, Corazza G E, Caini C, et al. Analysis of LEO,MEO and GEO Global Mobile Satellite Systems in the Presence of Interference and Fading[J]. IEEE Journal on Selected Areas In Communications, 1995, 13(2): 291-300.

[7] Lee J W, Kim T W. Satellite over Satellite (SOS) Network: A Novel Concept of Hierarchical Architecture and Routing in Satellite Network[C]. 25th Annual IEEE Conference on Local Computer Networks, 2000: 392-399.

[8] Kim Y S, Park W J. Adaptive Routing in LEO Satellite Networks[C]. IEEE 2000 Vehicular Technology Conference. Tokyo: IEEE, 2000: 1983-1997.

[9] Nquyen H N, Jukan A. Approach to QoS-based Routing for Low Earth Orbit Satellite Networks[C]. Conference Record/IEEE Global Telecommunications Conference, 2000(2): 1114-1118.

[10] Mohoricic M, Svigelj A, Kandus G. Traffic Class Dependent Routing in ISL Networks[J]. IEEE Transactions on Aerospace and Electronic Systems, 2004, 40(4): 1160-1172.

Applied Mechanics and Materials Vol. 596 (2014) pp 861-867
© (2014) Trans Tech Publications, Switzerland
doi:10.4028/www.scientific.net/AMM.596.861

Research on Composite Web Services Selection Based On Dijkstra Algorithm

Yuqiang Li[1, a], Yuwen Li[1,b] and Lei Che[2,c]

[1] School of Computer Science and Technology, Wuhan University of Technology,
Wuhan, 430063, China

[2] Beijing Information Science & Technology University, Beijing 100085, China

[a]liyuqiang@whut.edu.cn, [b]liyuwen@whut.edu.cn, [c]chelei@bistu.edu.cn

Keywords: Web services composing; Dijkstra algorithm; the shortest path.

Abstract. Services composing have played an important role in the industry and academia in recent years. Based on the relevant theory and experience of the shortest path problem in a DAG, we propose the method of dijkstra algorithm implementing services composing way selection. Then we provide the pseudo code description of the algorithm implementing the optimal path selecting process and test the correctness of algorithm through the contrast experiment to offer a feasible solution for services composing way selection.

Introduction

Web services and Service-Oriented Architecture present a flexible and agile way of structuring applications like playing toy bricks. We know that there are many ways of composing the bricks to achieve the goal in the game. The way of composing services is the same. When a single service can't meet the functional requirements, we can compose several services to form a new service to achieve those goals. Since the existence of competition, many organizations published Web services with overlapping or identical functionality, but with different nonfunctional properties, such as QoS, which is further enriched the way of composing services by a single service we choose. However, which should be selected and how to determine the optimal path of composing services meeting the user's requirement has become the focus on a lot of researchers' works [1,2,3,4,5]. For this problem, we propose a new method of using the dijkstra algorithm to implement the composing services path selection based on the Tao Yu's related research in [6]. The core of our method is to model the problem of web services selection as the optimal path selecting. And then we use the dijkstra algorithm to solve this problem.

The remainder of this paper is organized as follows. Section II describes the details of the approach we proposed, the definitions of QoS properties and the computations of the QoS value. At the same time, the adjustment for meeting the computing conditions of the dijkstra algorithm is also presented in this section. Section III analyses the complexity of the algorithm. In section IV, we choose Constrained Bellman-Ford algorithm as comparing algorithm and use QWS_Dataset Version2 as experiment data to analyze the algorithm's validity. Section V reviews the related research efforts in this field and discusses the differences of our method. Finally in section VI, conclusions will be made along with our plans for future studies.

Service Composing Path Selection Method

In order to use dijkstra algorithm to solve the problem of the web service composing selection, the first job is to transition it into DAG (Directed Acyclic Graph). We should decompose composite service into each sub-function to get it correspond each node in the graph. Then we take two sub-functions incidence relation between front and back to correspond to directed edges which connect two corresponding nodes. So a directed path in the graph has a corresponding combination functionality decomposition of a composite web service. Because of existing multi services meeting the same functional requirement, so we have many ways to choose when we compose the individual services constructing the new composite service. The case is dictated as the Fig. 1.

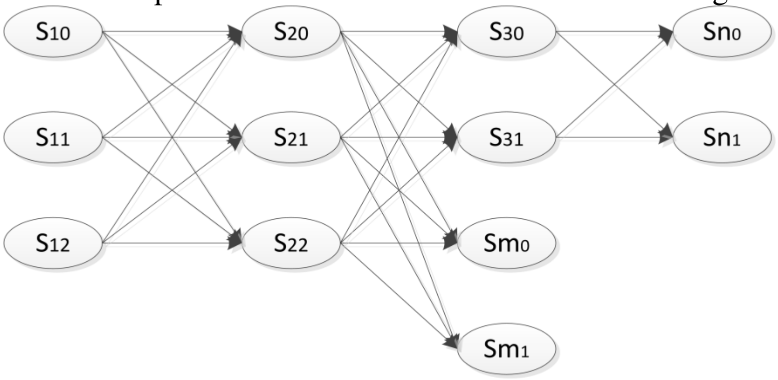

Fig. 1. Web services composing path graph

As shown in the Fig. 1, we can find that the path selection of services composing is just the problem of searching the optimal path in a DAG. However, the dijkstra algorithm was designed for graphs with single-source and weight values on edges. So we need to transform the services composing path graph into a DAG with single-source and weight values on its edges. That means we need to solve these two problems.

(1) Set the web service composing path graph with single-source.

(2) Set weight values on edges.

Firstly, we add two virtual services- S_S and S_T as the initial node and the final node of any services composing process respectively and suppose that they don't have any business processing capability. Then after transforming, the graph is shown as the Fig. 2.

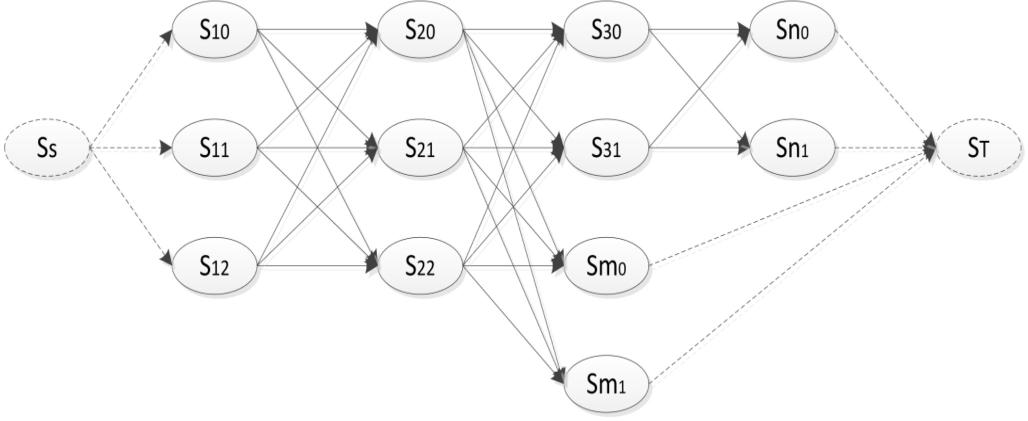

Fig. 2. Extended web service composing path graph

After doing that transformation, our services composing path graph will meet one of the computing conditions of the dijkstra algorithm-the single-source.

Secondly, we will deal with the problem of assigning the weight value to each edge of the graph. Our solution is to use the service's QoS value as the weight value of the edge. The concrete definition is that, if there is a link from the service node Si to the service node Sj, we will use the QoS value of the service Sj as the weight value of the edge from Si to Sj. In order to avoiding the influence of QoS value for the whole composite service, we set the virtual service ST's QoS value to be zero. Through above a series of transformations, our services composing path graph has become a real DAG meeting the computing demand of the dijkstra algorithm. The last result is shown as in the Fig. 3.

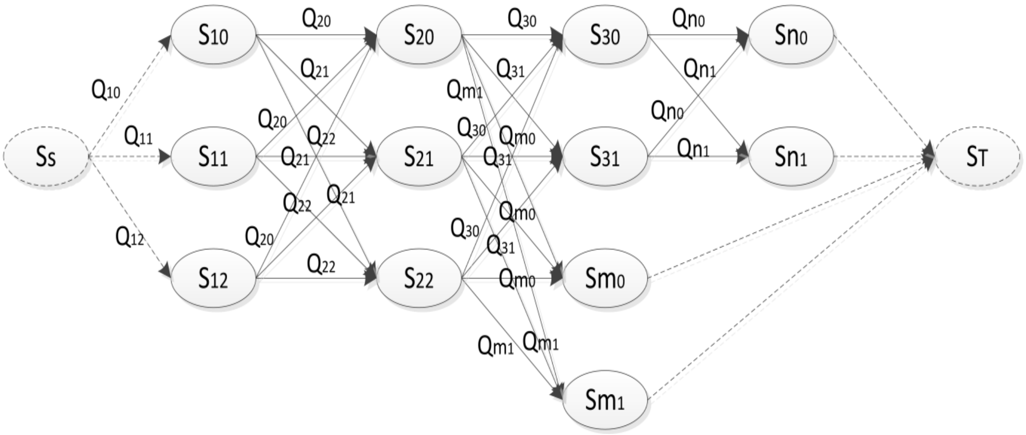

Fig. 3. Web service composing path graph with weight

But we also need to solve the question about computing the QoS value of the services, if we really want to use dijkstra algorithm to implement the optimal services composing path selecting. As we all know dijkstra algorithm is looking for all of weight values on edges and the shortest path. While based on the QoS properties of services composing selecting we usually choose the largest QoS value. Obviously, they are contradictory. Therefore, we need to change the way of QoS's calculation. In other words, the smaller QoS value is made on the whole web service, the better quality of service you can get, but if we want to make the QoS value became smaller, that means each of Qos properties value become smaller. According to this idea, we need to adjust the process mode about the standardization of QoS property based on these research results[7,8,9].The concrete adjustment is to make the QoS value became smaller after standardization. So correspondingly, We need to contrapose different types to adjust calculation formula. The detailed content is as follows.

(1) QoS propertywith positive value tendency.

Definition: QoS property with positive value tendency refer to the QoS property with the higher value will have a better web services quality. The standard formula is as follows:

$$Q = \left(Max(q_i) - q_i\right) / \left(Max(q_i) - Min(q_i)\right) \quad (1)$$

q_i represent the property value of the QoS properties; $Max(q_i)$ represent the maximum value for q_i property; $Min(q_i)$ represent the minimum value of q_i property; Q represent the standardization of corresponding value for q_i property. Obviously, the smaller Q value will have the better quality after we deal with the formula (1).

(2) QoS propertywith negative value tendency.

Definition: QoS property with negative value tendency refer to the QoS property with the lower value will have a better web services quality. The standard formula is as follows:

$$Q = \left(q_i - Min(q_i)\right) / \left(Max(q_i) - Min(q_i)\right) \quad (2)$$

Obviously, the smaller Q value will have the better quality after we deal with the formula (2).

(3) QoS property with point-type.

Definition: The point type QoS properties refer to the values closer to a specific data point will have the better QoS property. The standard formula is as follows:

$$Q = \begin{cases} \left(Max(q_i) - q_i\right) / \left(d - Min(q_i)\right), q_i \in \left[Min(q_i), d\right] \\ \\ \left(q_i - Min(q_i)\right) / \left(Max(q_i) - d\right), q_i \in \left[d, Max(q_i)\right] \end{cases} \quad (3)$$

d represent the ideal value corresponding to point type QoS property.

(4) QoS propertywith domain-type.

Definition: Domain type QoS property represent that, when the values fall in a specific numerical interval, it has the best quality of QoS properties in the web service. The standard formula is as follows:

$$Q = \begin{cases} (Max\ (q_i) - q_i)/(d_1 - Min\ (q_i)), q_i \in [Min\ (q_i), d_1] \\ 1 \qquad\qquad\qquad\qquad\qquad , q_i \in [d_1, d_2] \\ (q_i - Min\ (q_i))/(Max\ (q_i) - d_2), q_i \in [d_2, Max\ (q_i)] \end{cases} \tag{4}$$

$[d_1, d_2]$ represent domain type QoS property index has a ideal value range, and d_1 refer to the lower limit of value range and d_2 refer to the higher limit of value range.

After transformed the process mode of QoS property value standards, computing method of the overall web service's QoS values adopts the formula (5).

$$QoS(s) = \sum W_j * Q_i \tag{5}$$

From the formula's computed results, we can easily find that the corresponding web services with the smaller QoS value will have a better quality. Then we can use the dijkstra algorithm to find the optimal services composing path correctly.

The concrete computation process of our services composing optimal path selecting algorithm is expressed in the following Table 1.

Table 1. Our algorithm Formal Description

```
// initializations
For each node k in DAG do
        dist[k]=infinity; // Unknown distance from $S_S$ to k
        optiPathPrev[k]=null; // Previous node in optimal path from $S_S$
End For
dist[$S_S$]=0;            // Distance from $S_S$ to $S_S$
Q= the set of all nodes in DAG; //initial no node in the optimal path
// seaching the nodes in the optimal path
While Q is not empty do
        u= the node in Q with the smallest disk[];
    if dist[u]=infinity  break; // all remaining nodes are inaccessible from $S_S$
      if u=$S_T$    break;      // searching has reached the final node
        remove u from Q;    //adjust the distance u to the remaining nodes in Q
              For each neighbor node v of u do
                   distTemp=dist[u]+dist_between(u,v);
                   if distTemp<dist[v]
                        dist[v]=distTemp;
                        optiPathPrev[v]=u;
                   End if
             End For
End While    // reverse output the optimal path
K=$S_T$;
While optiPathPrev[k]<>$S_S$ do
      print(optiPathPrev[k]);
      k=optiPathPrev[k];
  End While
```

The Analysis of Algorithm Complexity

In accordance with the description of the algorithm, our algorithm relates to the quantity m of the web services and the ways of service composing (composite path contains the number of edges E). According to the description of our services composing optimal path selecting algorithm, we can find the whole algorithm mainly including several parts as follows:

(1) Initialization job of web composing DAG graph.
(2) Searching nodes on services composing optimal path.

This part of job contains two parts: Firstly, finding adjacent nodes which have the shortest distance among the remaining nodes and time complexity is $O(m^2)$. Secondly, adjusting the distance between nodes and time complexity is $O(E)$. So this two parts together is asymptotic time complexity of services composing optimal path-$O(m^2 + E) = O(m^2)$.

(3) Outputing nodes of composing optimal path. This part of time complexity is $O(m)$.

In general, the overall asymptotic time complexity of our algorithm is $O(m^2)$, which is consistent with asymptotic time complexity of original dijkstra algorithm.

The Analysis of Algorithm's Validity

Our experiment aims at verifying the validity of the optimal services composing path selection of dijkstra algorithm and get relevant experimental data based on theoretical research.

We select the CBF algorithm (Constrained Bellman-Ford Algorithm) proposed by Tao Yu team on [10] as our comparing algorithm. The core of method is to transform service composing graph into DAG, and then adopt CBF algorithm based on the searching method of breadth first to search service path graph to find the best way of service composing. So this part of job of Tao Yu team is similar to our thinking and it is the main reason for us to choose CBF algorithm to compare.

At the same time, considering the authenticity and credibility of the experiment data, we adopt the test data which created QWS_Dataset Version2 by Doctor Eyhab Al-Masri in the Guelph University.

According to the analysis of comparing Tao Yu team's research results and the shortest path search algorithm in the multipath, we think the method of dijkstra algorithm to implement the optimal services composing path selecting is feasible in theory. Therefore, based on the analysis of practical data comparing, we will further conform the validity of our algorithm.

We use our algorithm to make a contrast experiment with CBF algorithm proposed by Tao Yu team from different ways of service composing and services candidates. Specific testing scenario and results in the following Table 2.

Table 2. The comparison of two service selecting algorithms

Composite path	**Task node**	**Candidate service**	**Execution time(microsecond)**	
			CBF algorithm	**Our algorithm**
3	5	5	459	346
8	10	5	27520	3127
10	10	10	57062	24367

According to the results of experiment, we can easily find that, under the same experimental conditions, our algorithm has a better calculated performance than the CBF algorithm. Meanwhile, it explains our algorithm is valid on solving the problem of optimal services composing path selecting.

Related Work

In recent years, a number of studies for selecting and composing Web services based on the QoS have been carried out. Zeng et al [7] proposed two algorithms which are local optimum of service composing selection algorithm and global planning of service composing selection algorithm. It should be said that Zeng et al's team have positive and profound influences on researching the domain of service composing, and many researchers further research their jobs based on it. Mohammad [11] pointed out combined local optimum of service composing selection algorithm and global planning of service composing selection algorithm can reach their full advantage to solve the calculated performance that can't meet real-time and dynamic service composing. Because of the current global optimal algorithms of service selection provide single optimal solution instead of multi-acceptable solutions under end-to-end constraints, which cannot fully reflect users' preference and personalized service, and is not conducive to encourage service provider to optimize the service quality. Then an ordinary utility function is used as a numerical scale of ordering local services, and meanwhile a Multi-Qos based Local Optimal Model of Service Selection (MLOMSS) firstly to be proposed by Jianqiang Hu [12], which provides important grounds to choose the best service. Subsequently, Guosheng Kang [13] proposed a strategy PSO-GODSS (global optimization of dynamic Web service selection based on PSO) algorithm to implement Web service selection with QoS global optimization. The basic idea of the algorithm is to transform the original Web service selection problem into a multi-objective services composition optimization problem with global QoS constraints, which is further transformed into a single-objective problem by using the method of ideal point. Then, the theory of intelligent optimization of PSO is applied to produce a set of optimal services composition process with QoS constraints. At the same time, Hu Chun Hua's team also noticed the problems of convergence time of services composing selection under dynamic environment and analyze services composing has three characteristics in [14]. There is another representative outcome is the Tao Yu's team proposed the new idea of using graph theory to solve the way of services composing selecting problem. They gave a detailed description about this solution and put forward the method of the optimal services composing path selecting based on classical shortest path search algorithm in graph theory on [10]. The core of the method is that, they model the problem of the optimal QoS constrained services composing selection as the shortest path searching at first. Then they turned graph structure diagram into services composing path graph and further turned into DAG graph. At last, they adopted CBF algorithm (Constrained Bellman-Ford algorithm), AEP algorithm (All Execution Paths algorithm) and CSP algorithm (Constrained Shortest Path algorithm) to solve the way of optimal web services composing. The final results show that based on the method of services composing selecting in graph theory is correct and feasible.

In this paper, we proposed the method of web services composing selecting based on dijkstra algorithm. In essence, it should belong to this research category. Meanwhile, the closest research results with us is Tao Yu's team proposed in [10], and the difference between us is that we adopt dijkstra algorithm which has better calculated performance than CBF algorithm.

Conclusions

Web service composition technique presents the wonderful outlook of agilely constructing enterprise applications. In this paper, we describe the problem of web service composing path selecting and provide the solution based on the graph theory to search the shortest path of DAG. Then we use classical algorithm-dijkstra algorithm to solve the problem of the optimal services composing path selecting. Subsequently, we deeply discussed the computing about the service's QoS value. Furthermore, we proposed a new method of computing the QoS value. On the basis of above studies, we transformed the Web services composing model graph into a DAG meeting the computing conditions of the dijkstra algorithm. Then, we give the formal description of our algorithm. At last, we analyzed the complexity of algorithm and verified the feasibility of algorithm through comparing algorithm proposed by Tao Yu's team.

In the future, we will continue the study about this problem and try to further improve the performance of our algorithm. On the other hand, we also plan to design and implement a Web services composing framework based on the services selecting algorithm we have proposed.

Acknowledgements

This work is supported by the Fundamental Research Funds for the Central Universities (WUT:2014-IV-106). We would like to specially thank the reviewers for their good comments and useful suggestions on this paper.

References

[1] D. Ardagna, B. Pernici, in: Global and local QoS guarantee in Web service selection, edited by C. J.Bussler, A. Haller, volume 3812 of Business Process Management Workshops, Springer Berlin Heidelberg Publishers (2006), p. 32-46.

[2] HC Wang, CS Lee, TH Ho: Expert Systems With Applications Vol. 32 (2007), p.571-584

[3] V. Diamadopoulou, C. Makris, Y. Panagis and E. Sakkopoulos: J. Netw. Comput. Vol. 31 (2008), p.108-130

[4] D. Tsesmetzis, I. Roussaki and E. Sykas: European Journal Of Operational Research Vol. 191 (2008), p.1101-1112

[5] A F.M Huang, CW Lan and S J.H Yang: Information Sciences Vol. 179 (2009), p.3309-3322

[6] E.W. Dijkstra: A Note on Two Problems in Connexion with Graphs, Numerische Mathematik Vol. 1(1959) , p.269-271

[7] L. Z. Zeng, B. Benatallah, A. H. H. Ngu, M. Dumas, J. Kalagnanam and H. Chang: IEEE Trans. Softw. Eng Vol. 30 (2004), p.311–327

[8] Hongli Wu, Yonghui Jiang: Computer Engineering and Applications Vol. 46 (2010), p.58-62

[9] Zhiqiang Qi, Gan Zhang and Jianguo Qi: The Journal of Quantitative & Technical Economics Vol. 2 (2011), p.52-63

[10] Tao Yu, Kwei-Jay Lin: Information Systems and E-Business Management Vol. 3 (2005), p.103-126

[11] M. Alrifai, T. Risse: Combining Global Optimization with Local Selection for Efficient QoS-aware Service Composition [C]. Proceedings of the 18th international conference on World wide web. Madrid,Spain, 2009.

[12] Jianqiang Hu, Juanzi Li and Guiping Liao: Chinese Journal of Computer Vol. 33 (2010), p.526-534

[13] Guosheng Kang, Jianxun Liu, Mingdong Tang and Yu Xu: An Effective Dynamic Web Service Selection Strategy with Global Optimal QoS Based on Particle Swarm Optimization Algorithm, International Parallel and Distributed Processing Symposium Workshops & PhD Forum, IEEE, 2012. p. 2280-2285

[14] Chunhua Hu, Xiaohong Chen and Ximing Liang: Journal of Central South University of Technology Vol. 16 (2009), p. 269-274

Applied Mechanics and Materials Vol. 596 (2014) pp 868-872
© (2014) Trans Tech Publications, Switzerland
doi:10.4028/www.scientific.net/AMM.596.868

Rumor Propagation Model for Complex Network with Non-uniform Propagation Rates

Rui Sun[1, 2, a *], Wanbo Luo[1, b]

[1]School of Computer Science, Sichuan University, Chengdu, China

[2]Department of Computer Science, Chengdu Normal University, Chengdu, China

[a]cug123456@126.com, [b]wbl@scu.edu.cn

Keywords: rumor propagation model, complex network, scale-free network, propagation rate

Abstract. Considering propagation characteristics and affecting factors of rumor in real-world complex networks, this paper described different propagation rates of different nodes by introducing the rumor acceptability function. Based on mean-field theory, this paper presented a rumor propagation model with non-uniform propagation rate, and then simulated the behaviour of rumor propagation on scale-free network and calculated the propagation thresholds by corresponding dynamics equation. Theoretical analysis and simulation results show that nodes with different rumor acceptability could lead to slowing the spread of rumors, make positive propagation threshold arise, and effectively contain the outbreak and reduce the risk of rumors.

Introduction

Rumors have a big impact to people's social life as a unique phenomenon in human society. With the coming of the information age, the spread methods of rumors are more diversified, the range is wider, the speed is faster, and to be more influential and devastating. Especially in some crisis and emergency, the effect of rumors to social order and harmony is absolutely cannot be underestimated [1]. Therefore, the research on rumor propagation mechanism is very important, and become common concern subject of the social sciences and natural sciences.

Daley and Kendal [2] first studied the phenomenon of rumor propagation and put forward the corresponding mathematical model in the 1960s. Daley-Kendal (DK) model supposed the conversion between each status be subject to certain mathematical probability distribution, and then studied rumor propagation by the method of stochastic process. Watts and Strogatz [3] proposed small-world network model and Barabási and Albert [4] proposed scale-free network model make the complex networks became the main theoretical basis of the research in rumor propagation. Zanette [5,6] first applied the complex networks theory to rumor propagation, used the mean-field theory to build model in the small-world network. The research proved that there is not nonzero threshold in homogeneous network. Moreno [7] established rumor propagation model in scale-free network. He pointed out that the ultimately number of immune have a close relationship with infection probability α, and it is irrelevant with the degree of the source. Nekovee [8] studied the rumor propagation theory in complex social networks. His research found that the initial probability of rumor propagation in scale-free network is higher than that in random graphs. In the basis of Moreno model, Wang [9] studied the behaviour of rumor propagation in scale-free network, he found that its degrees obey power-law distribution and have tunable clustering coefficient.

Rumor Propagation Model

The way of rumor propagation in society is very similar to the epidemic spread in population, so we can draw lessons from the classic model of epidemic spread [10] to build rumor propagation model on complex networks. The individuals are looked as nodes in complex network, they affected by rumors; if two individuals exist direct links, the links expressed as the edge between the nodes. This paper focuses on rumors propagation mechanism on scale-free networks, therefore the node degrees obey power-law distribution, that is $P(k) \sim k^{-\gamma}$, where $2 < \gamma \leq 3$. The scale-free network is a typical heterogeneous network [11].

Rumor Acceptability Function. Paster [12] and Moreno [7] find that the propagation threshold of epidemic tend to be zero in scale-free network, this means as long as the propagation rate more than zero, the epidemic can spread on the network and ultimately remain in a state of equilibrium. Above studies implied an important assumption: node's anti-infection ability consistent. This assumption thinks that any susceptible nodes, no matter the size of the degree, all have the same ability to fight infection. But this assumption in rumor propagation is not guaranteed, because the nodes have the greater degree, they are often more important nodes in the real-world networks, such important nodes are generally earlier join to the network, have more experience and stronger awareness, the corresponding capacity of resistance to rumors is stronger. Therefore the probability to become spreaders influenced by rumors is reduced.

In view of the above analysis, this paper introduces rumor acceptability function $A(k)$ denotes the acceptable degree of k degree nodes for rumors. The rumor acceptability function is bigger the ability of resistance to the rumor is weaker, and the easier to become spreaders mesmerized by rumors, that is, the greater the probability of rumors propagation.

The relationship between rumor acceptability function and propagation rate is

$$\lambda(k) = CA(k). \tag{1}$$

where C is a constant, $\lambda(k)$ denotes the acceptability of k degree nodes for rumors, and that is the ability of rumor propagation on this node. Different degrees have the corresponding different values of rumor acceptability function, leading to each nodes in network have different propagation rates.

The average propagation rate is

$$\lambda = \sum_k \lambda(k)P(k) = C\sum_k A(k)P(k) = C\left\langle A(k)\right\rangle \tag{2}$$

where $\left\langle A(k)\right\rangle = \sum_k A(k)P(k)$ denotes the average mathematical expectation of $A(k)$.

Rumor Propagation Model on Scale-free Network. In this paper, according to Moreno model, the total number of population is N, they are classified into three types: *Ignorants* (they still not heard rumors); *Spreaders* (they spread rumors); *Stiflers* (they heard rumors ever, now be immune to this rumor, won't be infected and won't spread rumors). The rules of rumor propagation are as follows: when a *Spreader* contact to a *Ignorant*, the *Ignorant* become the *Spreader* with probability $\lambda(k)$, *Spreaders* gradually lose interest in rumors and then do not have desire to spread rumors or know the truth of the rumors by outside influences, at this time the *Spreader* become the *Stifler* with probability δ.

According to the mean-field theory [13], we establish rumor propagation model on scale-free network:

$$\begin{cases} \dfrac{dI_k(t)}{dt} = -CkA(k)I_k(t)\Theta(t) \\ \dfrac{dS_k(t)}{dt} = CkA(k)I_k(t)\Theta(t) - \delta S_k(t) \\ \dfrac{dR_k(t)}{dt} = \delta S_k(t) \end{cases} \tag{3}$$

where $I_k(t)$, $S_k(t)$, $R_k(t)$ denote the proportion of *Ignorants*, *Spreaders* and *Stiflers* in nodes with k degree respectively. They meet normalization conditions

$$I_k(t)+S_k(t)+R_k(t)=1 \tag{4}$$

Without loss of generality, we make $\delta=1$. $\Theta(t)$ denotes the probability of any given edge connected with *Spreaders*, this paper consider uncorrelated degree distribution, therefore

$$\Theta(t)=\sum_k \frac{kP(k)S_k(t)}{\langle k\rangle} \tag{5}$$

The initial conditions of Eq.3 are $S_k(0)\approx 0, I_k(0)\approx 1, R_k(0)=0$. Calculating equations, the results is $\lambda \geq \frac{\langle k\rangle\langle A(k)\rangle}{\langle k^2 A(k)\rangle}$, therefore the propagation threshold is

$$\lambda_c=\frac{\langle k\rangle\langle A(k)\rangle}{\langle k^2 A(k)\rangle}. \tag{6}$$

When propagation rate $\lambda<\lambda_c$, rumors will not propagate but gradually demise; when propagation rate $\lambda\geq\lambda_c$, rumors will be large-scale propagate on networks.

The Propagation Threshold in BA Scale-free Network. This paper consider Barabási-Albert (BA) network as specific examples. The degree distribution function in BA model is $P(k)=2m^2k^{-3}$, where m denotes the minimum degree of network, the average degree is $\langle k\rangle=2m$ [14].

We can consider the discrete variables k continuous changing in the range $[0,\infty)$ for BA scale-free network, thus we can calculate approximate sum by integral and then calculate the propagation threshold λ_c

$$\lambda_c=\frac{\langle k\rangle\langle A(k)\rangle}{\langle k^2 A(k)\rangle}=\frac{\sum_k kP(k)\sum_k A(k)P(k)}{\sum_k k^2A(k)P(k)}\approx\frac{\int_m^\infty k2m^2k^{-3}dk\int_m^\infty A(k)2m^2k^{-3}dk}{\int_m^\infty k^2A(k)2m^2k^{-3}dk}=\frac{2m^2\int_m^\infty k^{-2}dk\int_m^\infty A(k)k^{-3}dk}{\int_m^\infty A(k)k^{-1}dk} \tag{7}$$

In the following, we will discussion selection about rumor acceptability function $A(k)$. First of all, according to the discussion above, $A(k)$ is the monotonically decreasing function of k degree, this means that the infection probability of nodes reduce with the increase of the degree. Second, $A(k)$ is a probability value, so when $k\in[0,\infty)$ its value range is $A(k)\in[0,1]$. According to the above selection conditions coupled with the actual situation, we discuss the propagation threshold in BA scale-free network as follow four kinds of circumstances respectively:

1) When $A(k)=1$, $\lambda_c=\frac{\langle k\rangle}{\langle k^2\rangle}$. This situation shows that the rumor acceptability of every node is the same, at this time the propagation threshold $\lambda_c=0$, which strictly equal to the propagation threshold from Moreno model.

2) When $A(k)=k^{-1}$, $\lambda_c=\frac{2}{3m}$. 3) When $A(k)=k^{-2}$, $\lambda_c=\frac{1}{m}$. 4) When $A(k)=e^{-k/\langle k\rangle}$, $\lambda_c\approx\frac{3}{4m}$.

Simulation Results and Discussion

The parameters of BA model as follows: $N = 5000$, $m_0 = 3$, $m = 3$, $<k>= 6$, $P(k) = 2m^2k^{-3}$. We consider the last three selections of rumor acceptability function $A(k)$.

The Propagation Evolution. As shown in Fig. 1a and Fig. 1b, there were a small number of *Spreaders* and a lot of *Ignorants* in network when the initial time similar to actual situation. Along with the advancement of time, the number of *Spreaders* increase very soon, it get to the top and back soon until zero. In the final steady state, there are a lot of *Stiflers* and a little of *Ignorants*, no *Spreaders*, therefore rumors die. We can find that the propagation velocity of rumors effective slow down and the propagation scale also significantly reduced in considering rumor acceptability function compare to the standard model in BA scale-free network. Further analysis found that different rumor acceptability function impact propagation velocity and propagation scale are different. The propagation scale is similar situation. When rumor acceptability function is $A(k) = k^{-2}$, the propagation velocity is slowest and the propagation scale is smallest; when $A(k) = e^{-k/\langle k \rangle}$, they are the second smallest, when $A(k) = k^{-1}$, they are the third.

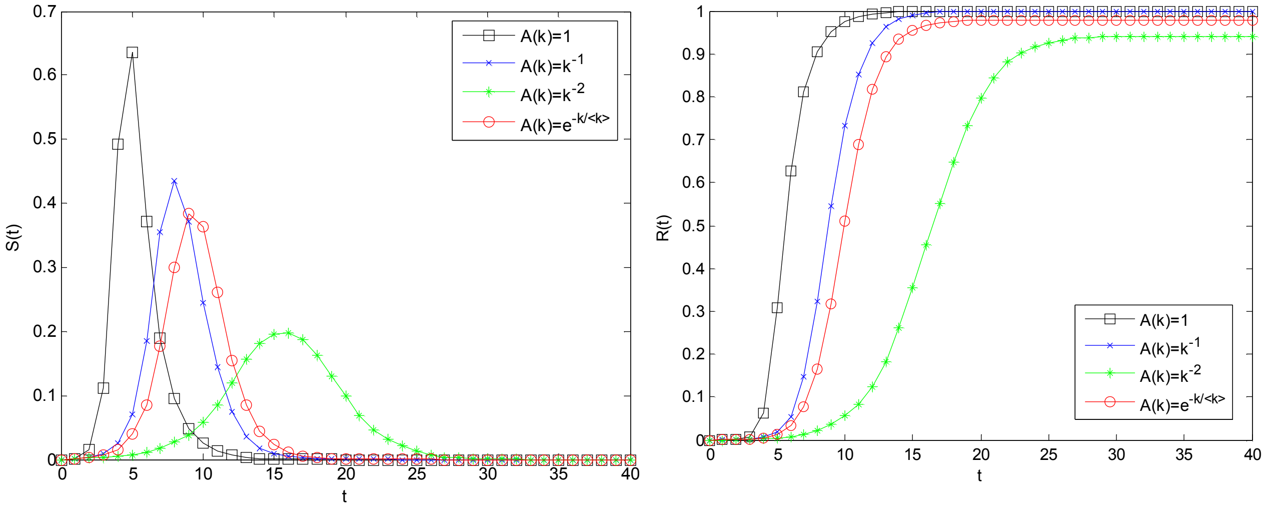

(a) (b)

Fig.1 (a) The relationship between the number of Spreaders $S(t)$ and time t

(b) The relationship between the number of Stiflers $R(t)$ and time t

The Propagation Threshold. As shown in Fig. 2, rumor acceptability function make the propagation threshold increased significantly in scale-free network, this means that different levels of resistance for rumors will have important influence to propagation threshold. That is the positive propagation threshold can restrain the outbreak of rumors and reduce the propagation scale. Further analysis found that when $A(k) = k^{-2}$, the propagation threshold maximum, $\lambda_c \approx 0.36$; when $A(k) = e^{-k/\langle k \rangle}$, it is the second, $\lambda_c \approx 0.25$; when $A(k) = k^{-1}$, it is the third, $\lambda_c \approx 0.23$. The numerical simulations very good fit the theoretical analysis.

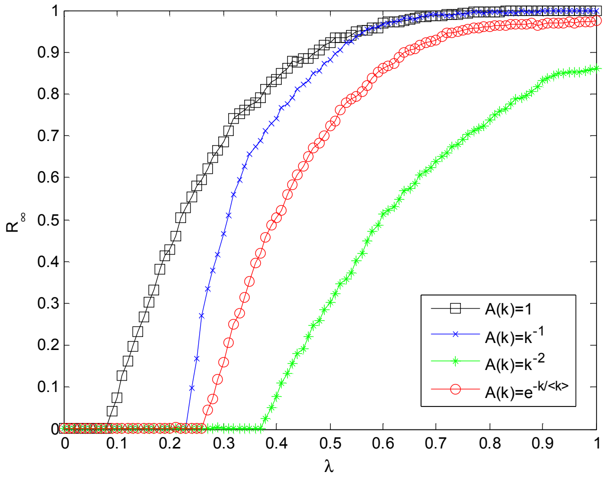

Fig.2 The relationship between the number of *Stiflers* in steady state R_∞ and propagation rate λ

Conclusions

In summary, this paper studies the behavior of rumor propagation on complex network when the nodes have different rumor acceptability. Based on mean-field theory, this paper builds a rumor propagation model for complex network with non-uniform propagation rates by introducing the rumors acceptability function. The theory analysis and experimental results show that when rumor acceptability function is inversely proportional to the degree, the spread speed of rumors decreases. There are positive propagation threshold and different change of spread speed and propagation threshold for different rumor acceptability functions. Therefore we can appropriate select rumor acceptability function in the real-world networks to change the propagation rates and then effective restrain rumor propagation.

Acknowledgements

This work was financially supported by Program for Innovative Research Team in Chengdu Normal University, Ministry of State Security of China (MSS) Funded Projects JG2008011 and JG2011003.

References

[1] B. Brooks, Advanced Dynamic Modeling of Economic and Social Systems, Springer Berlin Heidelberg, 49-60, (2013).

[2] D.J. Daley, & D.G. Kendall, Nature Science, 204, 1464-3634, (1964).

[3] D.J. Watts, & S.H. Strogatz, Nature, 393(4), 440-442, (1998).

[4] A.L. Barabási, & R. Albert, Science, 286(5439), 509-512, (1999).

[5] D.H. Zanetee, Physica A-Statistical Mechanics and its Applications, 309, 1-l0, (2008).

[6] D.H. Zanette, Physical Review E, 65(4), 041908, (2002).

[7] Y. Moreno, M. Nekovee, & A.F. Pacheco, Physical Review E, 69(6), 066130, (2004).

[8] M. Nekovee, Y. Moreno, G. Bianconi, & M. Marsili, Physica A-Statistical Mechanics and its Applications, 374(1), 457-470, (2007).

[9] X.F. Wang, Z.F. Pan, & X. Li, Journal of System Simulation, 18(8), 2346-2348, (2006).

[10] S. Funk, M. Salathé, & V.A.A. Jansen, Journal of the Royal Society Interface, 7(50), 1247-1256, (2010).

[11] M.E.J Newman, Nature Physics, 8(1), 25-31, (2011).

[12] P. Pastor-Satorras, & C. Castellano, Physical Review Letters, 105(21), 218701, (2010).

[13] M.A. Buice, & C.C. Chow, Journal of Statistical Mechanics: Theory and Experiment, 2013(03), P03003, (2013).

[14] C.I. Del Genio, T. Gross, & K.E. Bassler, Physical Review Letters, 107(17), 178701, (2011).

Applied Mechanics and Materials Vol. 596 (2014) pp 873-876
© (2014) Trans Tech Publications, Switzerland
doi:10.4028/www.scientific.net/AMM.596.873

A New Method For High Speed CAN Protocol Conversion Circuit

Li Qi[a *] Liu Yanfei[a] Luo DaCheng[b] Yang Jingjing[b]

The Second Artillery Engineering University, Xi’an 710025, China

[a]liqiqimail@126.com, [b]yangjj@126.com

Keywords: CAN Bus, test Instrument, Real-time data transmission, FPGA

Abstract. Due to high correspondence speed, great real-time performance and good expansibility, CAN bus has been used widely in aerospace, large-scale equipments and other fields these years .This paper introduces a kind of CAN Bus Test Instrument based on PXI bus and FPGA, which is used to test and monitor the CAN bus equipment. The result of test shows that this kind of test instrument has great advantages in reliability, stability and extensibility.

Introduction

The CAN bus is one of the most widely applied fieldbuses in the world, which is developed by Germany BOSCH Company famous for researching and manufacturing automotive electronic products. As the interconnection bus of the digital field control device, CAN bus can support distributed controlled and real-time controlled serial communication network effectively, and show great advantages in connectivity, efficiency and reliability, system expanding and error correction, etc.

The biggest communication rate of CAN bus can reach 1 Mb/s (corresponding transmission distance within 40 m), and the maximum transmission distances can reach 10 km (corresponding communication rate below 5 Kbps)， so CAN bus is the communication way suitable for severe environment of industrial sites. Because of its advantages listed above, the CAN bus technology is no longer limited to the automobile industry, but widely used in the fields of aerospace, large-scale equipments, the sensor technology, data acquisition system and monitoring of industrial sites [1]. In order to ensure various equipments of Industrial field linked to the CAN bus in good working condition, testing and conducting real-time monitoring of the CAN bus equipment is necessary. Based on this, the CAN bus test instrument based on PXI and FPGA was designed. This paper mainly introduces the design and realization of interface communication of CAN bus in the CAN bus test instrument.

The composition of a CAN bus test instrument

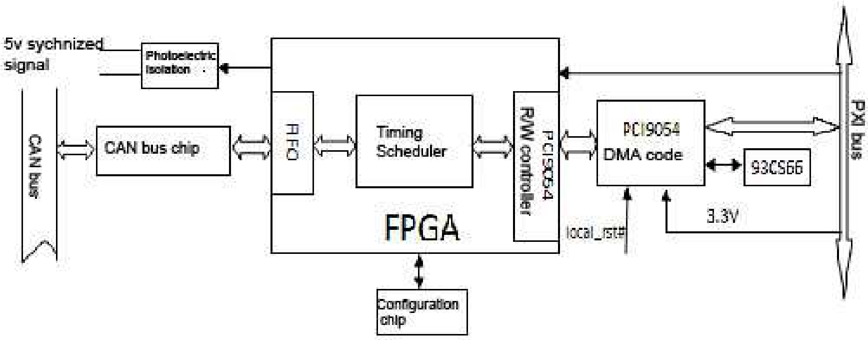

Fig.1. The structure diagram of the CAN bus test instrument

A CAN bus test instrument is composed of chip PCI9054 (bridge chip special to PXI bus), FPGA, CAN bus chip, isolation chip (device), and related configuration chips etc. The control core of the test instrument is FPGA, PXI bus is connected to FPGA through PCI9054; Local bus is controlled by the

FPGA. The date of upper computer is sent to the CAN bus through FPGA to test, then the date of CAN bus is transmitted to the upper computer, thus the real-time monitoring upper computer performed on CAN bus equipment is realized. The overall diagram is shown in figure 1.

The design of PXI bus interface

Although PXI bus has many merits, the agreement is complex and it is difficult to design controlling PXI bus (PXI bus controller) directly through the FPGA, therefore chip PCI9054 (interface chip special to the PXI bus) is chosen, which can translate complex PXI bus interface into simple user interface realized by designing translated bus interface. PCI9054 can achieve all the hardware interface signals and configuration space registers according with PXI Standard. Because specified is low cost and commonly used, PCI9054 can help reduce the difficulty of the interface design effectively, shorten the researching time, and gain better data transmission performance [2]. The PCI9054 in the test instrument is operated in the mode C in the operation, and data transmission adopts DMA attack mode. Because of the operation of local signal of PCI9054 is regular, the state machine is used in software design to realize the control.

The CAN bus interface design

In the test instrument, C8051F040 bearing CAN bus interface microprocessor is chosen in CAN bus interface as CAN controller. The internal structure of C8051F040 is shown in figure 2.

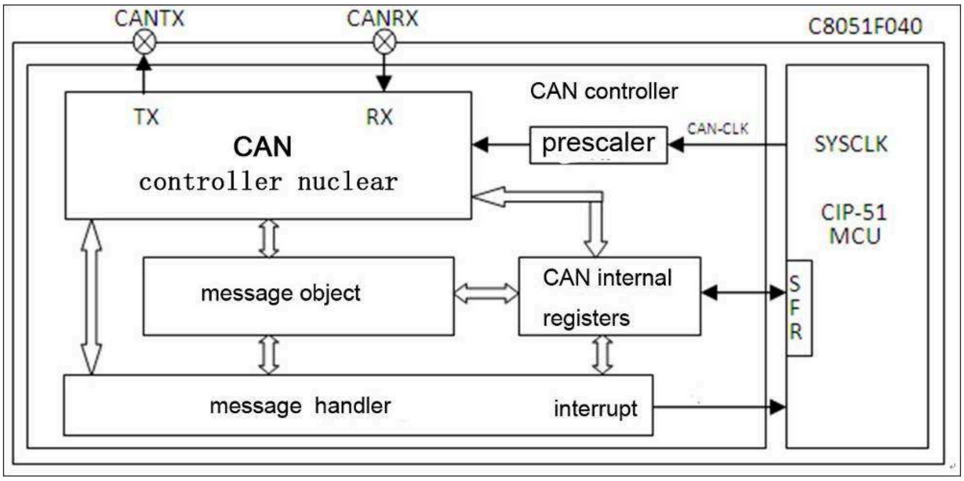

Fig.2. Internal structure of C8051F040 (after the figure)

The CAN controller integrated in C8051F040 is composed of CAN controller nuclear, message handing units and control registers. CAN controller nuclear is responsible for the control of CAN agreement, message conversion and shifting (CANTX and CANRX), date sending, receiving and filtering. CIP-51 is used to configurate CAN controller and to get access to the data received. Message RAM is used to store 32 message objects, which can be configured to send or receive data, and every message object has its own mark. CAN controller handle the Protocol processing of date sending, receiving and filtering without the intervention of CIP-51, which makes the bandwidth of CPU used in CAN communication is minimum. CAN register and message handing units provide an interface for data transformation and perception between CAN controller and CIP-51 [3].

Figure 3 is the principle diagram of hardware interface in C8051F040. MAX3058 is the CAN bus driver and an interface between CAN controller and the CAN bus, which can send data to the CAN bus and receive data from CAN controller. IL711-3 is a digital isolation chip, which helps realize electrical isolation of each node in bus to improve the anti-interference ability of the system. According to the program scale, XC3S500E of SPARTAN-3 E series produced by XILINX Company as the FPGA, in which an interface control module is designed to communicate with C8051F040.

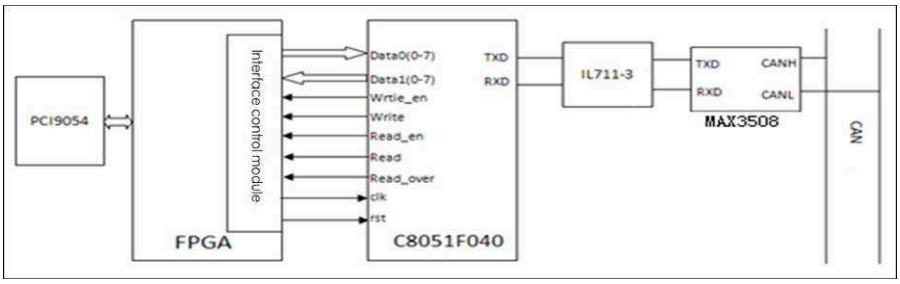

Fig.3.C8051F040 hardware interface principle diagram

The communication software design of CAN bus interface includes related operation of the C8051F040 and the design of C8051F040 interface module in FPGA, which are illustrated respectively below.

3.1 The operation of C8051F040

The operation of C8051F040 mainly includes the system initialization procedure, sending and receiving programs. The initial program is aimed at initializing of all message objects (generally make all values zero), setting CAN control register (CAN0CN), and bit timing register (BITREG), and initializing sent and received message objects respectively. CAN object message sending is accomplished by CAN controller automatically. Users only transfer corresponding data according to received remote frame identifier to transmit buffer register, and then write code of the object message in the command request register and start sending orders. The sending will be completed by the hardware. The way CAN object message is received is the same as it is sent. Both are completed by CAN controller automatically. In the receiving program received date is read in receive buffer and and then corresponding processing is done.

Take sending program as an example to introduce the operation of the C8051F040. The following are codes of the sending programs:

```
void Transmit(BYTE Magnum, BYTE Send[8])
{             BYTSFRPAGESAVE = SFRPAGE;
SFRPAGE = CAN0_PAGE;       // Point to page 0
CAN0ADR = IF1CMDMSK;      // Write orders into IFl command barrier register
CAN0ADR = IF1DATA1;       //The following codes is are to write 8 bytes data into IF1
CAN0DATH = Send[1];        // sent the second data to CAN0DATH
          ...
}
```

The dates of object message here are updated regularly and are sent by controller automatically. When having received a remote frame, the controller will send out the data frame owning the same identifier.

3.2 Interface module software design of FPGA and C8051F040

The general idea of realizing data transmission using codes described by VHDL language (taking upload data of the CAN bus for example) is that: In the beginning, the date of the CAN bus is checked to register, then the data of register will be transmitted to the LOCAL when the state machine designed in the FPGA is in the reading and writing state. At last, the data will be transmitted to the PC when the output (signal) is in effective. The following is a code fragment of the CAN bus transmitting data to PC.

```
--------- the data of  the CAN bus is checked to register ---------
   ... if(f040_rd = '0') then
        case(rd_f040_data_cnt)is
           when 0 => REG0 <= f040_data1;
             …
           when 12 => REG12 <= f040_data1;
           when others => REG13 <= f040_data1; …
--------- the data of  register is checked to LOCAL ---------
   if (ds_decode = '1' and la_h(31 downto 30) = "10" and ds_write = '0' and la_l(4) = '1') then  case la_l(3 downto 0) is
              when X"0" => ld_reg <= REG0;
                     …
                     when others => ld_reg <= "ZZZZZZZZ";…
```

Validation

In order to validate the function of the CAN bus test instrument, the test is done as shown in figure 5. Upper computer sends ID "00 00 00 01", and data "00 01 02 03 04 05 06 07", then the direction of data transmission is "receiving" shown in the testing interface of the under computer；ID is "00 01 02 03", which is caused by CAN bus frame format of the upper computer; the length of the received data is "8" ; received data displayed in the under computer is"55 55 55 55 55 55 55 55", which is caused by setting content received by under computer in the test software. When the under computer transmit data to the upper computer, the standard frame ID sent by under computer is “00 00 00 01", data is "11 22 33 44 55 66 77 88", which are the same as displayed in testing interface of upper computer. The test proved that CAN bus test instrument can realize the two-way communication of dates, and receive and send dates according to stipulated data format, which comply with (better to be replaced by ‘according to’) the design requirements.

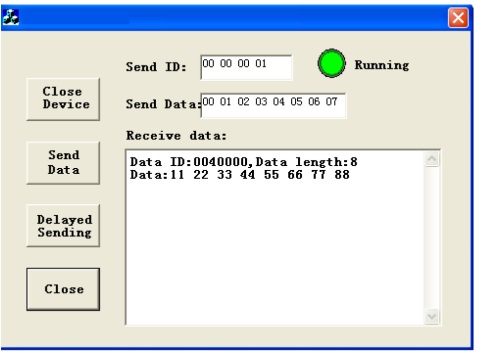

Send ID: 00 00 00 01

Send Data: 00 01 02 03 04 05 06 07

Receive data:

```
Data ID:0040000,Data length:8
Data:11 22 33 44 55 66 77 88
```

Fig.5. The testing interface of the upper computer

Conclusion

This paper introduces a kind of CAN bus test instrument based on PXI bus and FPGA, emphasizes the design interface control module of the test instrument and CAN bus. According to the test listed in the paper, the test instrument has good generality, high reliability and stability, high transmission speed, and can satisfy the real-time data acquisition and transmission with large capacity and high speed needed in industrial field. Besides, functions of the test instrument can be extended according to needs. So it can be concluded that the test instrument has very high practical values.

References

[1] Xu Tao. Design and Optimization of PCI Bus HDLC Processor[D]. Nanjing: Southeast University(2005),p.25-47.

[2] Liu Yanjun, Yan Haixia. Application of CRC during HDLC Protocol[J]. Electronic Measurement Technology, 2010(33),p.21-23.

[3] Li Xiaojuan. HDLC Design Realization Based on FPGA[J]. Modern Electronics Technology, 2007 (6) ,p.35-37.

[4] Ying Sancong. HDLC Protocol Controller Based on the FPGA [J]. Journal of Sichuan University, 2008 (40) ,p.116-120.

[5] Pan Song, Wang Guodong. VHDL Practical Tutorial [M]. Chengdu: University of Electronic Science and Technology Press(1999),p.158-169.

[6] Xu Xin, Yu Hongqi, Yi Fan et al. Embedded system design based on FPGA [M]. Beijing: China Machine Press(2005),p.79-102.

Applied Mechanics and Materials Vol. 596 (2014) pp 877-882
© (2014) Trans Tech Publications, Switzerland
doi:10.4028/www.scientific.net/AMM.596.877

A NHPP-based Reliability Model of Wireless Sensor Networks

Bo Zhao[1, a], Jianfeng Yang[2,b], Ming Zhao[3], Qi Li[4,c] , Yan Liu[1]

[1] State key Lab of Networking & Switching Tech,
Beijing University of Posts and Telecommunications, Beijing, China

[2] Faculty of Information Engineering,Guizhou Institute of Technology, Guiyang, China

[3] Faculty of Engineering and Sustaible Development,University of Gävle, Gävle, Sweden

[4] School of Computer,Beijing University of Posts and Telecommunications, Beijing, China

[a]bzo@sina.com [b]yjft232@126.com, [c]liqi2001@bupt.edu.cn

Keywords: Wireless Sensor Networks, Reliability, NHPP, Power-law Poisson Process

Abstract. As the Wireless Sensor Networks(WSNs) are widely applied to various fields recent years, the quality of WSN has been increasingly concerned. Since reliability is the most important factor of quality, how to evaluate reliability of WSN through failure counting is our main subject. In this paper, we try to utilize NHPP theorem in the failure process of WSN and propose a reliability model based on NHPP. And also, the model validation is conducted by simulation.

Introduction

The Wireless Sensor Networks (WSNs) have been identified as one of the most important technologies for 21st century. It can fulfill the real-time, accuracy and completeness of information gathering due to its random distribution, self-correction and environmental adaptation [1,2]. WSN is classic distributed network system, which consist of many random deployed, low-cost nodes and differ from centralized system, and are more reliable, robust, flexible and can even be degraded to lower operation rank. So, it is not matter if some of the nodes become invalid, the whole system still function [1,3]. There have been studies that intended to derive reliability of WSN from different methods [4,5,6,7], but in the view of NHPP are few.

Since 1964, when Duane introduced NHPP theorem into reliability analysis [8], NHPP reliability models spread in the field of software systems and repairable systems. In 1974, Cow first brought up power-law Poisson process model, so called Crow-AMSAA model [9], and carried out maximum likelihood estimation to estimate unknown parameters in the model as well as the test for goodness of fit. In 1978, Goel and Okumoto first built up software reliability growth model by NHPP, so called G-O model [10]. Those models are the basis of software reliability model. Since then, a lot of studies and NHPP models come out [11,12,13,14,15,16]. Besides the field of software reliability, some NHPP models were applied in hardware system too. Such as: power-law Poisson process reliability model [9,17],additive power-law Poisson process model [16], NHPP ROCOF model [18], sectionalized NHPP reliability model [19], the choosing technology of power-law Poisson process [20], and other NHPP reliability model framework [21,22].

There are no NHPP model from the existing studies of the reliability of WSN yet, even though NHPP is broadly applied for system reliability. This paper presents a reliability model of WSN by NHPP, which, hopefully can be another important way to evaluate the reliability of WSN with the certain working process and repair process of WSN.

Background

The operating environments and the topology structure of Wireless Sensor Network make the reliability evaluation of it more difficult. Not only the quality of each nodes, but also the transission capability of the network determine the reliability of WSN [7]. Shrestha et al studied a cluster-structure WSN. Fig 1 show the topology of it [7]. There are 8 clusters (sub-networks), and each of those clusters includes their own nodes, cluster heads and gateway nodes. And the study defined that the reliability of the network was the probability that at least K nodes were covered in monitor area and each node get at least one way to sink node.

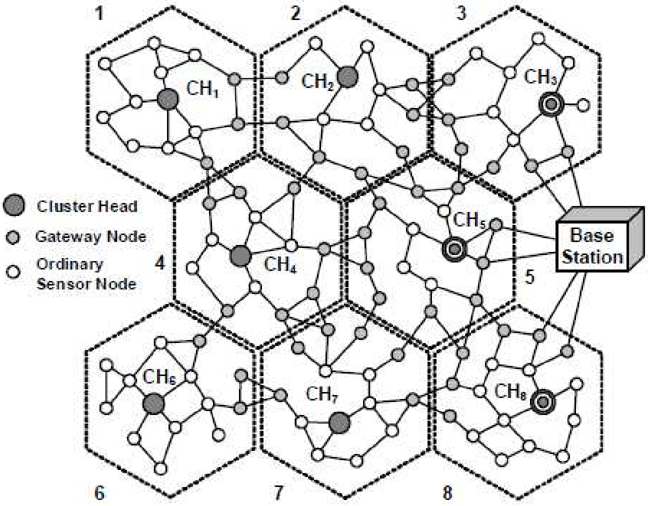

Fig. 1 Topology of WSN

The reliability evaluation [7] was a static model, not the real-time prediction. This paper study the stochastic reliability evaluation based on NHPP, suppose that a cluster will self-repair when a failure occur and the cluster will be good as new after such self-repairing. Therefore, we can borrow NHPP models of repairable system to evaluate the reliability of WSN. It may be a new method way to model the failure process of WSN.

Modeling of WSN

The theorem of NHPP. Non-Homogeneous Poisson Process (NHPP) model is one of the most famous reliability model in the field of reliability evaluation of repairable systems. The definitions about NHPP are given below [23]:

Definition 1: A process $\{N(t), t \geq 0\}$ is a Counting Process, where $N(t)$ denotes how many times random event A has happened from time 0 to t, if $N(t)$ satisfies:

1) $N(t) \geq 0$ is nonnegative integer

2) when $s < t$, $N(s) \leq N(t)$, and $N(t) - N(s)$ denotes how many times random events A has happened during time interval $(s, t]$

Definition 2: A counting process $\{N(t), t \geq 0\}$ is called Non-Homogeneous Poisson Process (NHPP) with intensity function $\lambda(t)(t \geq 0)$ when:

1) $N(0) = 0$

2) $N(t)$ is independent increment

3) $P\{N(t+h) - N(t) = 1\} = \lambda(t)h + o(h)$

4) $P\{N(t+h) - N(t) \geq 2\} = o(h)$

Theorem 1: As a NHPP $\{N(t), t \geq 0\}$, the probability that the random event A has happened n times during time interval $(t_0, t_0 + t]$ is:

$$P\{N(t_0 + t) - N(t_0) = n\} = \frac{[m(t_0 + t) - m(t_0)]^n}{n!} e^{-[m(t_0+t)-m(t_0)]}$$

Where $m(t) = \int_0^t \lambda(\tau) d\tau$ is the mean function of the NHPP.

See the proof in [23].

Power-law Poisson process model. Basic hypothesis:

1) After each reparation, the performance of WSN is the Same as old
2) Compare to the time to failure, self-reparation time is neglectable
3) The failure process of WSN can be represented by Power-law Poisson process

Since NHPP models are already successfully applied in reliability evaluation of software systems and repairable systems, the cluster structured WSN as mentioned in section 2 can be represented by NHPP. Denote that $\{N(t), t \geq 0\}$ the failure process of WSN, where $N(t)$ is the number of failure happened during time interval (0,t). The Power-law Poisson process is one kind of NHPP models [9,17], the intensity function of which is:

$$\lambda(t) = \alpha\beta t^{\beta-1}; \alpha > 0, \beta > 0; t > 0, \tag{1}$$

and yield the mean function:

$$m(t) = \alpha t^{\beta} \tag{2}$$

In Eq. 2, when $\beta = 1$, the failure process is Homogeneous Poisson Process (HPP); when $\beta > 1$, $\lambda(t)$ is a strict increasing function, meanwhile the time to failure $t_i - t_{i-1}$ decrease, which means the system enters the fatigue stage after certain time; when $\beta < 1$, $\lambda(t)$ is a strict decreasing function, which means the reliability growth of the system.

The probability no failure of WSN system occurs during time interval $(t, t+\Delta t)$, by theorem 1, can be yield as following:

$$\begin{aligned} R(\Delta t | t) &= P\{N(t+\Delta t) - N(t) = 0\} \\ &= \exp\left\{-\left[m(t+\Delta t) - m(t)\right]\right\} \\ &= \exp\left\{-\left[\alpha(t+\Delta t)^{\beta} - \alpha t^{\beta}\right]\right\} \end{aligned} \tag{3}$$

Parameter Estimation and Model Validation

Maximum Likelihood Estimation. Maximum likelihood estimation is applied to estimate the parameters in the model, the formula are given below for both type-1 and type-2 censoring data [9,17].

Type-1 Censoring Data. Assume that the failure counting stops when n failures are observed, the time each failures occurred are $t_1 < t_2 < \cdots < t_n$, then the likelihood function can be yield:

$$L(\theta; t_i) = \exp\left(-m(t_n)\right) \prod_{i=1}^{n} \lambda(t_i) \tag{4}$$

and the log-likelihood function:

$$\log L(\theta; t_i) = -m(t_n) + \sum_{i=1}^{n} \ln[\lambda(t_i)] \tag{5}$$

find the estimation of α and β when Eq. 5 reaches its maximum:

$$\hat{\alpha} = \frac{n}{t_n^{\beta}}$$

$$\hat{\beta} = \frac{n}{\sum_{i=1}^{n} \ln\left(t_n / t_i\right)}$$

Type-2 Censoring Data. Assume that failure counting stops when observing time is T, the time each failure occurred are $t_1 < t_2 < \cdots < t_{N(T)}$, then the likelihood function as well as the log-likelihood function can be denoted as following formula:

$$L(\theta;t_i) = \exp(-m(T))\prod_{i=1}^{N(T)}\lambda(t_i)$$

$$\log L(\theta;t_i) = -m(T) + \sum_{i=1}^{N(T)}\ln[\lambda(t_i)]$$

find the estimation of α and β when $\log L(\theta;t_i)$ reaches its maximum:

$$\hat{\alpha} = \frac{N(T)}{T^{\beta}}$$

$$\hat{\beta} = \frac{N(T)}{\sum_{i=1}^{N(T)}\ln\left(T/t_i\right)}$$

Validation of the Model. Mean square error (MSE) is a common measurement of model validation, the value of it show how well the model fit the real data, the smaller the better fit. The definition of MSE [11,24] is:

$$MSE = \sum_{i=1}^{k}\frac{[m(t_i)-m_i]^2}{k}$$

where , $m(t_i)$ is the expected number of failure at time t_i by the model, and m_i is the actual observed failure number.

Numeric Example

To perform a numeric example to validate the power-low model introduced in this paper, in Eq. 1, given that: $\alpha = 0.28, \beta = 2.8$, and the type-1 censoring data obtained by simulation.

Table 1. The Simulation Data of a WSN System

Failure time	**Number of failure**	**Failure time**	**Number of failure**	**Failure time**	**Number of failure**	**Failure time**	**Number of failure**
1.1095	1	5.3767	11	6.8973	21	8.1135	31
2.9097	2	5.4715	12	7.1642	22	8.1748	32
4.0006	3	5.5778	13	7.2405	23	8.188	33
4.0689	4	5.9272	14	7.5944	24	8.1892	34
4.3562	5	6.0818	15	7.6395	25	8.5737	35
4.4548	6	6.2502	16	7.6619	26	8.6704	36
4.4745	7	6.6434	17	7.6725	27	8.7273	37
4.8163	8	6.8507	18	7.8856	28	8.7535	38
5.1071	9	6.8514	19	8.0126	29	8.7563	39
5.2456	10	6.8647	20	8.0387	30	8.7888	40

By maximum likelihood estimation formula mentioned before, the parameters are estimated from these simulation data. Table 2 shows the result of estimation as well as the MSE of the modeling. As can be seen in Fig. 2, the mean error of the model is acceptable, the model fit the data well.

Table 2. The estimation Value and MSE

MLE		MSE
$\hat{\alpha}$	$\hat{\beta}$	
0.0746	2.8914	517.4594

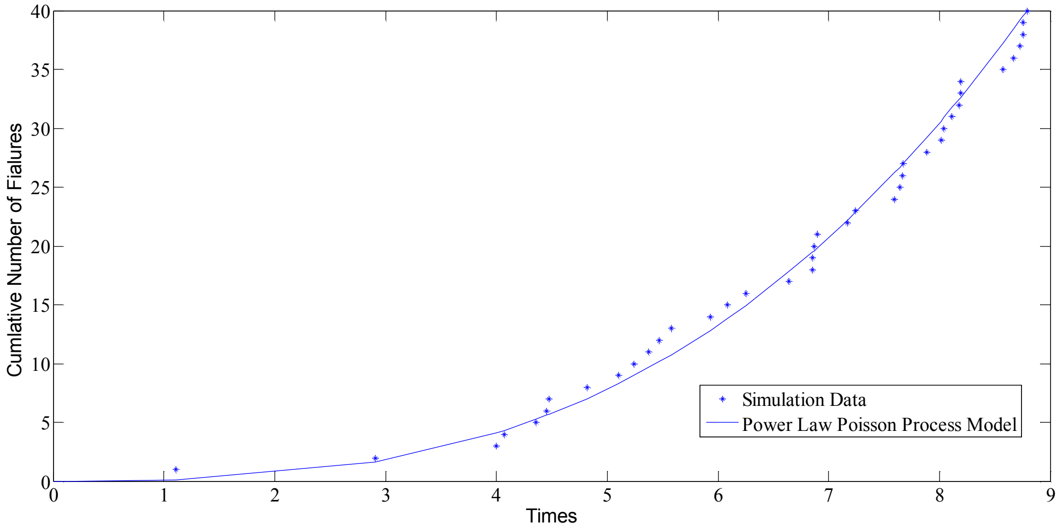

Fig. 2 The Goodness of Fit of The Power-law Model

Conclusions

AS the WSNs are widely implemented in more and more fields, the quality of it bring more and more consideration. This paper introduces a power-law NHPP model into the reliability evaluation of WSN. And also, a simulation is carried out to show how to modeling. From the result of the simulation, the goodness of fit is acceptable.

Acknowledgements

This work is supported by the National Natural Science Foundation of China under Grant No. 61302087.

References

[1] I.F. Akyildiz, W. Su, Y. Sankarasubramaniam, E. Cayirci, *Wireless sensor networks: a survey*, Computer networks, Vol.38 (2002) , p. 393-422.

[2] L.M. SUN et al.: *Wireless Sensor Networks* (Tsinghua University Press, Beijing 2005).

[3] H.B.YU, W.LIANG, P.ZENG:*Intelligent wireless sensor networks* (Science Press,Beijing 2013).

[4] H.M.F. AboElFotoh, S.S. Iyengar, K. Chakrabarty: *Computing reliability and message delay for cooperative wireless distributed sensor networks subject to random failures.* IEEE Trans Reliab, Vol. 54(2005), p.145–155.

[5] D. Bein, V. Jolly, B. Kumar, S. Latifi: *Reliability modeling in wireless sensor networks*, International Journal of Information Technology, Vol.11 (2005), p.1-8.

[6] A. Shrestha, L. Xing: *Quantifying application communication reliability of wireless sensor networks*, International Journal of Performability Engineering, Vol.4 (2008) , p. 43.

[7] A. Shrestha, L. Xing, H. Liu : *Modeling and evaluating the reliability of wireless sensor networks,* Reliability and Maintainability Symposium, 2007. RAMS'07. Annual, IEEE, (2007), p. 186-191.

[8] J. Duane: *Learning curve approach to reliability monitoring* , Aerospace, IEEE Transactions on, Vol.2 (1964) , p. 563-566.

[9] L.H. Crow: *Reliability analysis for complex, repairable systems* , SIAM Reliability and Biomeiry, Philadelphia, (1974), p. 379-410.

[10] A.L. Goel, K. Okumoto: *Time-dependent error-detection rate model for software reliability and other performanc*e measures, Reliability, IEEE Transactions on, Vol. 28 (1979), p. 206-211.

[11] M. Xie: *Software reliability modelling,* World Scientific, (1991).

[12] M. Zhao: *Change-point problems in software and hardware reliability*, Communications in Statistics-Theory and Methods, Vol. 22 (1993), p. 757-768.

[13] M. Zhao: *Superposition of Power-Law Models for Hardware/Software System Reliability Data Analysis* , International Journal of Reliability, Quality and Safety Engineering, Vol. 10 (2003) , p. 121-130.

[14] J.F. Yang,M. Zhao: *Maximum likelihood estimation for software reliability with masked failure data*,Journal of Systems Engineering and Electronics, Vol. 35,(2013), p. 2665-2669

[15] S. Yamada: *Software Reliability Modeling: Fundamentals and Applications* (Springer Briefs in Statistics, Springer Japan, 2014).

[16] M. Zhao, M. Xie: *EM algorithms for estimating software reliability based on masked data*, Microelectronics Reliability, Vol. 34 (1994), p. 1027-1038.

[17] L.H. Crow: *Evaluating the reliability of repairable systems,* Proceedings of Annual Reliability and Maintainability Symposium, IEEE, (1990), p. 275-279.

[18] V.V. Krivtsov: *Practical extensions to NHPP application in repairable system reliability analysis* , Reliability Engineering & System Safety, Vol. 92 (2007), p. 560-562.

[19] H. Guo, A. Mettas, G. Sarakakis, P. Niu: *Piecewise NHPP models with maximum likelihood estimation for repairable systems*, Reliability and Maintainability Symposium (RAMS), 2010 Proceedings-Annual, IEEE, (2010), p. 1-7.

[20] M. Dias De Oliveira, E.A. Colosimo, G.L. Gilardoni: *Power law selection model for repairable systems* , Communications in Statistics-Theory and Methods, Vol.42 (2013), p. 570-578.

[21] V.V. Krivtsov: *Recent advances in theory and applications of stochastic point process models in reliability engineering*, Reliability Engineering & System Safety, Vol.92 (2007), p. 549-551.

[22] J. Van Dyck, T. Verdonck: *Precision of power-law NHPP estimates for multiple systems with known failure rate scaling*, Reliability Engineering & System Safety, Vol.126 (2014), p. 143-152.

[23] B. Zhang, J.X. Zhang: *Applied Stochastic Processes*, (Tsinghua University Press, Beijing 2004).

[24] P. O'Connor, A. Kleyner: *Practical reliability engineering*, (Fifth Edition, John Wiley & Sons, 2012).

Applied Mechanics and Materials Vol. 596 (2014) pp 883-887
© (2014) Trans Tech Publications, Switzerland
doi:10.4028/www.scientific.net/AMM.596.883

Implementation Of USB in Embedded Systems Based On ARM Microprocessor

Xinli Li

Linyi University China

sduman@126.com

Keywords: USB, ISP1161, S3C4510B, ARM, embedded systems

Abstract. S3C4510B is a cost-effective 16/32 bit RISC microcontroller based on Ethernet application system, and ISP1161 is a chip which is designed to implement USB protocol in an embedded system. Here, we design and implement embedded systems USB with ISP1161 chip based on ARM microprocessor S3C4510B. This paper describes the basic working principle of ISP1161 chip and hardware design of the system, and presents the software implementation process of USB in embedded systems.

Introduction

As a high-speed communication interface between the PC and peripherals, a Universal Serial Bus USB has many advantages as follows: flexible connectivity, hot-swappable, universal interface for a variety of devices, high speed, auto-configuration, low power consumption, Low cost, high reliability. In the "post-PC era", the requirements of embedded devices connected peripherals is more concise, more convenient, more intelligent, so the USB interface in the application of embedded devices will become increasingly widespread.

Samsung's S3C4510B is a cost-effective 16/32 bit RISC microcontroller based on Ethernet application system, which incorporates a 16/32 bit ARM7TDMI microprocessor core designed by ARM. ARM7TDMI is a low-power, high-performance 16/32 core, and it is suitable for the power sensitive applications.

S3C4510B ARM microprocessor and USB interfaces are widely used in embedded systems, so the design and implementation of embedded USB is valuable.

Hardware Design and Implementation

In this study, we use Philips ISP1161 chip for embedded USB design, and Samsung's ARM processor chip S3C4510B is used for CPU.

2.1 Overview of ARM microprocessor S3C4510B

S3C4510B is a 16/32 bit ARM7TDMI microprocessor core, its peripheral modules include: HDLC channel, UART channels, GDMA channel, 32-bit timer, programmable I/O port, and its logic control circuit includes: an interrupt controller, DRAM/SDRAM controller, ROM/SRAM and FLASH controller, system management, internal 32-bit system bus arbiter, external memory controller. Using these function modules, it is convenient for embedded USB design.

2.2 Introduction of ISP1161

ISP1161 chip has a built-in MCU, the internal cache, and an interface to a static memory through which CPU can reads and writes this interface to control and data transceiver. The ISP1161 chip integrates two USB controllers, one is the HC (Host Controller), and the other is the DC (Device Controller). Two controllers share bus interface, but has independent DMA channels, independent DMA interrupt request pin, independent host and accessory interfaces. Therefore ISP1161 can control the HCDCs to work simultaneously.

ISP1161 provides two downstream ports for USB HC and an upstream port for USB DC. Each downstream port has a separate overcurrent detection input pin and the power supply switch control output pin, and each upstream port has a separate VBus detection input pin, therefore ISP1161 can extend two USB host interface and an accessory interface for S3C4510B. USB host interface can be connected to any USB devices which are compatible to USB interface protocol, and USB accessory interface can be connected to any USB host interface device which is compatible to USB interface protocol. Meanwhile USB HC and USB DC have separate wake-up input pin and hang output pin, so that the power management system is more flexible, therefore ISP1161 is ideally suited for embedded systems and portable devices. ISP1161 applications in embedded systems are shown in Fig. 1.

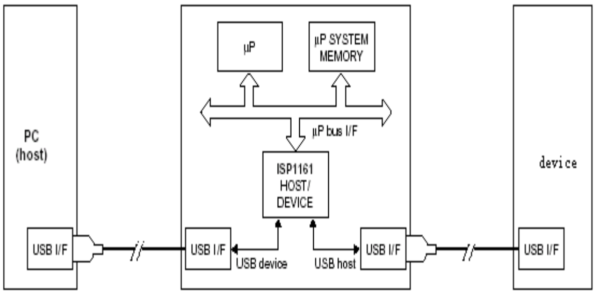

Fig. 1: ISP1161 in Embedded Systems

ISP1161 can visit all registers and FIFO buffer space by only two address lines A0 and A1. A1 is used to determine that the microprocessor visits the main controller or the device, A0 is used to determine that the microprocessor visit the data port or command port. From the designer's standpoint, all ISP1161 operations are through reading and writing the register. ISP1161 registers is a paired structure of data and command, a full register read/write operation consists of two phases: the command phase and a data phase. The first stage, CPU issue a command to ISP1161 command port, which indicates the name and operation type of the register to be accessed. In the second stage, data is transferred through the data port. ISP1161 internal cache space address is also some of a register, and the access timing to FIFO cache space access is similar to the access timing of internal registers except that the data phase consists of multiple components.

2.3 Hardwired of ISP1161and S3C4510B

The data transmission form ISP1161 to S3C4510B can be performed by I/O mode or DMA mode, which can be determined by hardwired. The embedded system here select I/O mode for data transmission.

ISP1161 data lines D0 ~ D15 can be connected with the low 16 bits of S3C4510B data lines, the two address lines A21 and A20 of S3C4510B is connected with the ISP1161 address line A1 and A0 to select ISP1161 internal registers: A1A0 = "00" represents data port to select the host controller; A1A0 = "01" represents command port to select the host controller; A1A0 = "10" represents data port to select the accessory controller; A1A0 = "11" represents command port to select the accessory controller. ISP1161 is assigned a definite address port by nECS <3> pin of S3C4510B, the nOE and nWBE <0> pin of 3C4510B is connected to the nRD and nWR of ISP1161. The nOE and nWBE <0> pin were respectively used to transmit the read signal and the write signal. INT1 and INT2 is the interrupt request pin of the host controller, and are connected to the IRQ1 and IRQ2 pin of the 3C4510B. INT1 and INT2 can be programmed to level mode or pulse trigger mode. ISP1161's nRESET pin is connected directly to the nRESET pin of 3C4510B, so that there will automatically generates a low level to reset ISP1161 after 3C4510B reset. Connection relationship is shown in Fig. 2.

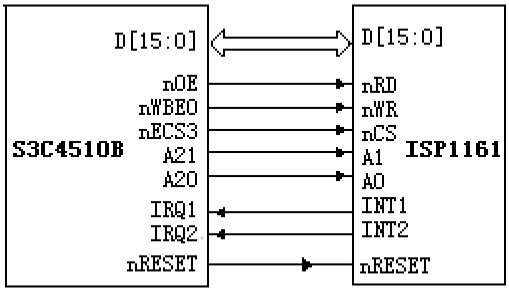

Fig. 2: Hardwired of ISP1161and S3C4510B

2.4 Suspend and Resume of ISP1161

In run mode, ISP1161 will produce a suspended state and wake state. By setting the control register of host controller and the mode register of accessory, ISP1161 transform respectively from received interrupt status to suspend status and from interrupt revocation status to wake status.

For the host controller suspend settings, the host controller can be suspended by writing 11 to HcControl's BIT7, BIT6 host controller function status bit (HCFS). 1.3ms after the pending state starts, the internal clock stops, the internal voltage regulator circuit closes, the internal 48M clock closes, PLL closes, crystal closes, and then the read pin H_SUSPEND can determine whether the host controller is suspended. For the accessory controller settings, the accessory controller can be suspended by sending a high level pulse to mode controller BIT5 (GOSUSP), and the read pin D_SUSPEND level can determine whether the accessory controller is suspended. D_SUSPEND polarity can be changed by setting PWROFF of the hardware configuration registers. ISP1161 can wake up by setting the control register BIT3 to 3. When CS signal is valid, the system is active.

Software Design and Hardware Implementation

3.1 Program USB Host Controller

The ISP1161 data bus is 16 bits wide, but the control registers and status registers are 32 bits wide, so these registers need to read and write in two stages. In order to write 32-bit registers, HCD (Host Controller Driver) set two consecutive 16-bit offset index data into the data bus, and in order to read the 32-bit register, HCD will get two consecutive 16-bit registers offset index data from the data bus.

ATL and ITL buffers are located in the FIFO buffer RAM of ISP1161. Each buffer contains a list of PTD, host controller uses the PTD list to send or receive USB packets. HCD builds PTD in system memory, and then move it to ATL or ITL buffer. The host controller hardware allows software to access each buffer. HCD access ATL buffer with hardware registers HcTransferCounter and access ITL buffer with HcTransferCounter and HcITLBufferPort.

When the ISP1161 start, the host controller enters running status after the following hardware initialization actions:

1 Detect host controller;

2 The host controller enters the reset state;

3 Configure hardware configuration registers of the host controller, including: set the interrupt output polarity, set the interrupt trigger mode to enable the global interrupt INT1, set the DMA patterns. Our embedded system involves no DMA, so we don't configure the DMA mode;

4 Configure interrupts, including: configure USB special interrupts and host controller interrupts;

5 Configure control register of the host controller;

6 Configure frame interval register of the host controller;

7 Configure main hub register of the host controller;
8 Set buffer length of ITL and ATL;
9 Configure INT1 interrupt service routine;
10 Set the main controller mode to run mode.

After initialization, the host controller driver starts to access ATL buffer and ITL buffers, and determines the event entry. At the same time, USB devices require host controller to generate USB event when they have a request as follows: Connect to port, or disconnect from the port, or continue signal to the HC.

Data transfer process is indispensable in the host controller programming process, which in turn can be divided into the following steps:

1 Prepare PTD data in the microcontroller system memory

Host controller driver and ISPl161 host controller Communication channel is represented by PTD forms. PTD provides commands, status and USB packets communication information for USB. PTD is generally stored in the RAM of the microcontroller, for the USB HC, PTD is stored in the Buffer of ISP1l61. USB-HCD first stores PTD in RAM, and then passes it to RAM of ISP1l61.

2 Send PTD Data to the FIFO register

When PTD data is ready, HCD can pass it to the FIFO Buffer RAM.

3 HC translates PTD data

HC reads the PTD in the FIFO Buffer RAM, and decides what matters will need to perform.

4 USB transfer via USB bus

Through a specific USB bus, host controller performs the exchange in a specific port.

After the data transmission, there are interrupt handling and error handling. Transmission flow chart of host controller in Run mode is shown in Fig. 3.

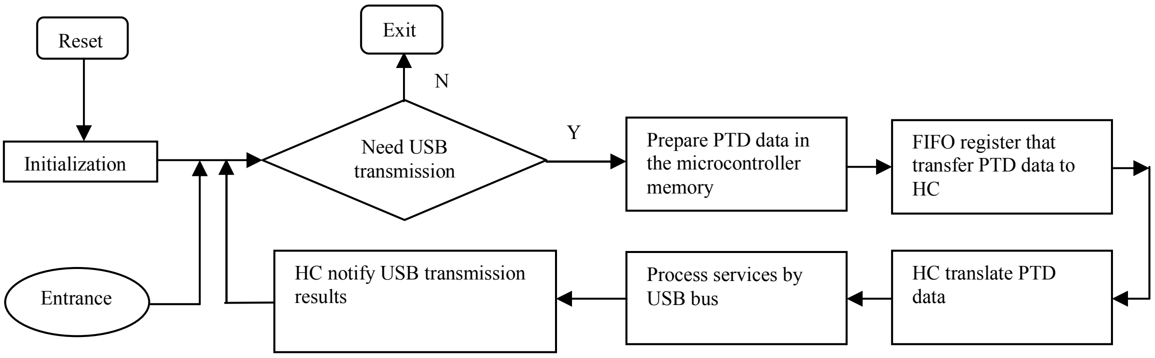
Reset
Exit
N
Y
Initialization
Need USB transmission
Prepare PTD data in the microcontroller memory
FIFO register that transfer PTD data to HC
Entrance
HC notify USB transmission results
Process services by USB bus
HC translate PTD data

Fig. 3: Transmission flow chart of host controller in Run mode

3.2 Program USB Accessory Controller

The ISP1161 accessory controller can be accessed via I/O read and write mode. The accessory controller can perform tasks such as printers, digital cameras and other peripheral functions, and can exchange data with a PC. These peripherals CPU is busy performing tasks such as device control, data and image processing. The accessory controller's firmware is designed to automatically interrupt-driven mode, so when S3C4510B is performing foreground task, USB transmission is processed in the background. Such mode not only ensures the best transmission efficiency and better software architecture, but also simplifies the programming and debugging.

To program the accessory controller, we first connect the host controller and other device CPU platform, then set hardware abstraction layer. Hardware abstraction layer contains the lowest performance function which can be changed in different CPU platforms. These functions of the accessory controller interface can simplify the programming of the device. Interrupt service routine is then installed, which comprise: reset bus, change suspend status, process EOT, process control terminal, process output control, process control input, process terminal block, process ISO terminal. After the power is on, the microprocessor must initialize ports, memory, timer and interrupt service routine, then the microprocessor reconnect USB. This process is very important because it ensures that the accessory controller doesn’t enter the running state before the microprocessor controller sets the accessory. After this process, a range of standard equipment is responded; we then can remove or set the request.

Conclusions

This paper introduces the embedded USB design and implementation of ARM-based microprocessor S3C4510B, and completed the DCD layer software testing of HCD, USBD and USB accessory controller. The concrete practice of ISP1161 chip embedded USB demonstrated the feasibility of our hardware design and software testing solutions. It is because of ISP1161 that implementing USB in embedded systems become very easy and convenient, which provides a bright future for the popularity of USB in embedded systems.

References

[1] M. S. Yang, D. J. Kriegman, and N. Ahuja, "Detecting faces in images: A survey", IEEE Trans. Pattern Anal. Mach. Intell., vol. 23, pp.42 -53 2001

[2] R. F&eacute,rand, et al., "A fast and accurate face detector based on neural networks", IEEE Trans. Pattern Anal. Mach. Intell., vol. 23, pp.42 -53 2001

[3]Intrator, D. Reisfeld, and Y. Yeshurnn, "Face recognition using a hybrid supervised/unsupervised neural network", Pattern Recogn. Lett., no. 17, pp.67 -76 2001

[4]B. Moghaddam and A. Pentland, "Probabilistic visual learning for object representation", IEEE Trans. Pattern Anal. Mach. Intell., vol. 19, pp.696 -710 1997

[5]K. Kobayashi, "Mobile terminals and devices technology for the 21st century", Spec. Rev. Paper&mdash,New Start 21st Century: NEC Res. Develop., vol. 42, no. 1, 2001

Applied Mechanics and Materials Vol. 596 (2014) pp 888-891
© (2014) Trans Tech Publications, Switzerland
doi:10.4028/www.scientific.net/AMM.596.888

The Network Security System Research Based on Intrusion Detection

Qian Jie [1, a], Wang Yanping[1, b], Li Hanxi[1, c]

[1] Hangzhou Cigarette Factory of China Tobacco Zhejiang Industrial Co., LTD

[a] qianj@zjtobacco.com, [b] wangyp@zjtobacco.com, [c] lihx@zjtobacco.com

Keywords: Network Security; Intrusion Detection; Enterprise Application

Abstract: With the rapid development of Internet and the network information resources can be Shared height, information system security face severe challenges. Firstly, this article from the current status of the network security, combined the new changes of the network security situation, getting the conclusion that the use of the necessity of intrusion detection system. And then it made a comprehensive overview on network security model put forward that was to achieve the purpose of security, which need to establish a reasonable network security model. By introducing the common types of network intrusion and network security technology, it lead to an intrusion detection system, and the concept of intrusion detection system, system structure and detection methods in detail in this paper.

Introduction

Due to information security theft or misuse, there are almost 80% of the large enterprises suffering information disclosure and loss as well as the service interruption will cause a huge loss. On the other hand, increasing extent of the network security threats, damage is very large. To improve the network system is very important. So the necessary safety measures must be taken to reduce the loss to protect the safety of network [1].

The network system security refers to the overall network system security, so the realization of network system security must be on the analysis of the network system to conduct a comprehensive and detailed consideration. It should be considered in the process of security system construction, all of the safety factor, mainly including throughout the security policy, security assessment and safety management [2]. While technically entities need to consider the basis of the physical security of the network structure of the network layer security, the safety of the operating system platform, application platform and on the basis of the safety of the application of data security. These aspects are both a protective base and promote each other. At the same time, it is also a progressive cycle of the project, needs constant self-improvement and enhancement, to form a set of reasonable and effective safety protection system as a whole.

The application of intrusion detection technology

Common intrusion detection framework (CIDF) on the basis of the IDES and NIDES makes a further research, puts forward the general framework of intrusion detection system as shown in figure 1, namely the event generator, event analyzer, the response unit and the event database, in GIDO format for data exchange [3]. According to the common intrusion detection framework (CIDF) framework of intrusion detection system put forward, it can put the intrusion detection system which is simplified into three parts: data extraction module, data analysis module, the results processing module. The role of data extraction module is to provide data for system, data system, network, data and is the source of state and behavior of user activity, all of these to test for the data source. The data analysis module is one of the most important modules in intrusion detection system [4]. Its role is to a more in-depth analysis of the data, by means of earlier detection of gradually accumulated in the process of model data for data and protocol analysis, and determine whether there is any violation of the policy of data, in accordance with normal strategy to filter out directly, keeping its records, conversely finally passed the results processing module.

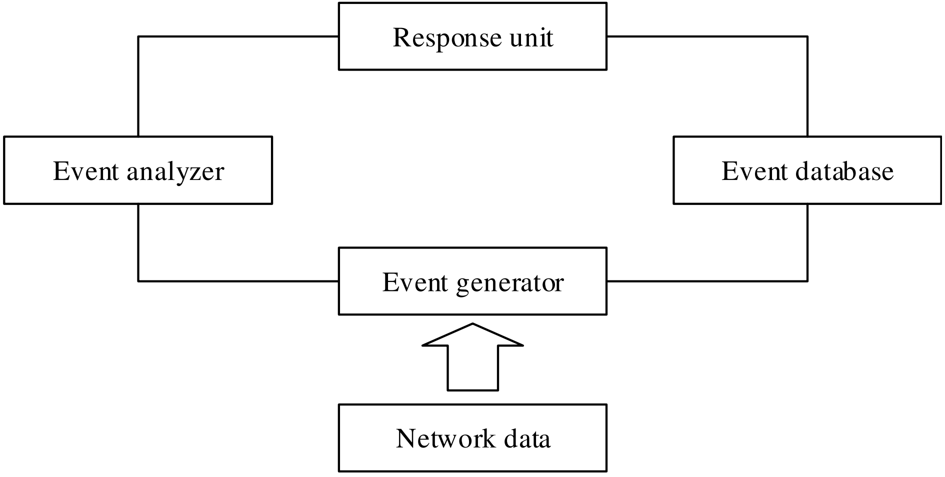
Response unit
Event analyzer
Event database
Event generator
Network data

Figure 1. The model of intrusion detection system

Results processing module which response unit, its role is to received data analysis module of incident response unit as a result, it can make cut off connections, changing file attributes, even for strong reactions such as the attacker's counterattack, but also can just make a simple alarm processing [5]. The host-based intrusion detection is shown in figure 2.

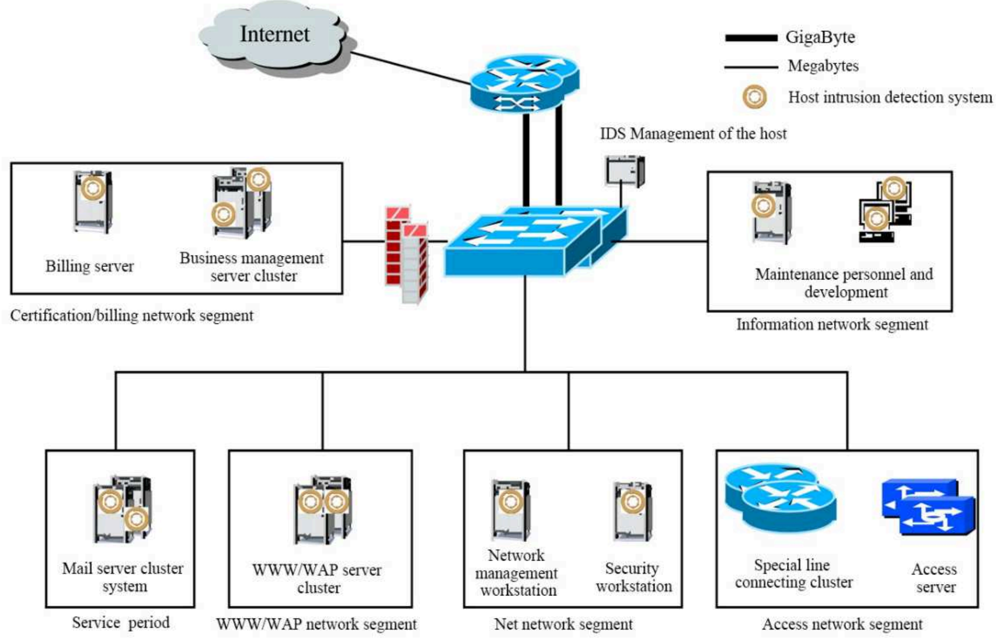
Internet
GigaByte
Megabytes
Host intrusion detection system
IDS Management of the host
Billing server
Business management server cluster
Certification/billing network segment
Maintenance personnel and development
Information network segment
Mail server cluster system
Service period
WWW/WAP server cluster
WWW/WAP network segment
Network management workstation
Security workstation
Net network segment
Special line connecting cluster
Access server
Access network segment

Figure 2. Host-based intrusion detection

Host-based intrusion detection system runs on a host in each to protect a broker. High cost performance in small number of cases, the cost performance of this method may be higher, at the same time, this method can easily monitor some activities, such as access to sensitive files, directories, program or port, and these activities are hard to clues based on the agreement. Once the intruder get a user name and password, and host based on host agent is most likely to distinguish between normal and illegal activities. The method based on host sometimes don't need to increase the specific hardware platform, with the way the general will not be lost because of the increase in network traffic monitoring of network behavior.

Establishing the network security system based on intrusion detection framework

According to the system work to complete specific tasks as well as by the different stages of different system logic is divided into several modules as shown in figure 3. System framework is divided into training and testing phase to carry on the design, and system analysis of training data in the training phase, get the pattern rules, to be deposited in the database (SQL), the test phase by using the model to test the real-time capture network data analysis, the analysis results to the system response module for further processing. This work by the unified interface control center scheduling module.

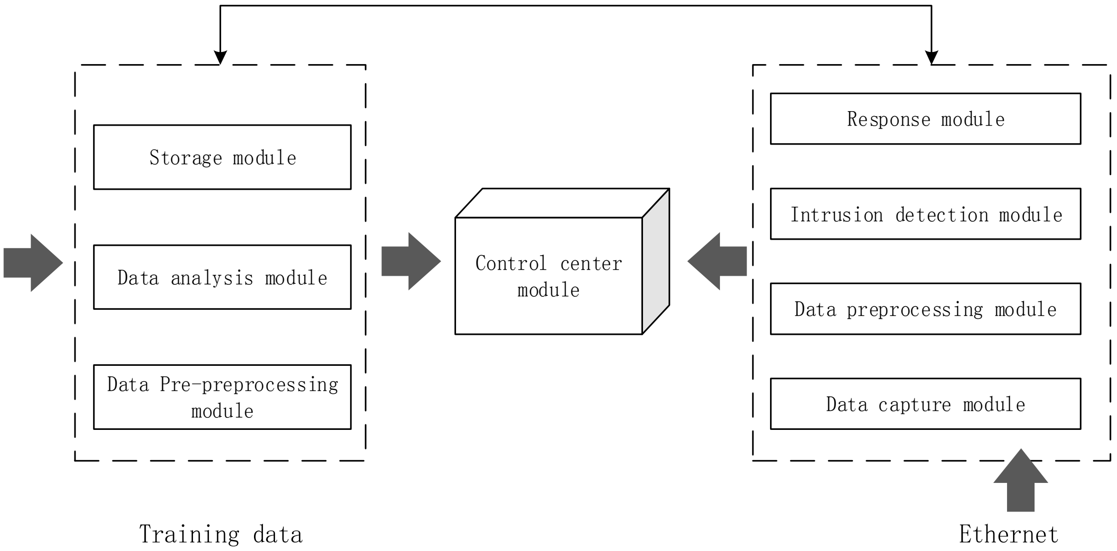

Figure 3. The structure of network intrusion detection system

In order to improve the performance of the intrusion detection system for change and in the network information security technology development, and constantly develop new intrusion detection method at the same time, on the basis of comprehensive analysis of all kinds of intrusion detection data, establish a theory framework of integration, collaborative, selective, and will be based on the distributed intrusion detection system, based on the characteristics of engine analysis of intrusion detection and intrusion detection system based on mobile agents, the intrusion detection based on immune principle, intrusion detection based on data mining, based on network intrusion induced control, based on kernel clustering and sequence analysis of network intrusion detection and intrusion detection method based on the theory of the self-purification and technology integration, build intrusion behavior rule knowledge base, data analysis and matching algorithm, so as to achieve the idea of the optimization of the implementation of intrusion detection system. Therefore put forward a kind of intrusion detection system based on a variety of detection methods, for the results obtained by different test method of selective integration, in order to gain a better result.

The design of network security system for enterprise application

Through the company network topology structure and a full understanding of the business application characteristics, as well as the network system security risk and careful analysis of security requirements, in accordance with the scheme design to follow the basic principles, build a suitable for our entire network security system solutions. This scheme mainly for safety planning from the following two aspects: network security solution design and physical security solution design on computer and network center room. Effect of network safe protection system of the whole network topology as shown in figure 4.

Network security solution design. Network security solution design is to protect the reliability of the operating system and database management system and the integrity of corporate users' business application software, at the same time to ensure that the enterprise network in the safety of interconnected devices such as switches and routers use. Including: the company local area network (LAN) VLAN division technology solutions, and virtual private network encryption communication technology, firewall and intrusion prevention system deployment scheme, Web application security gateway solution, network antivirus solutions and data backup and recovery plan, etc.

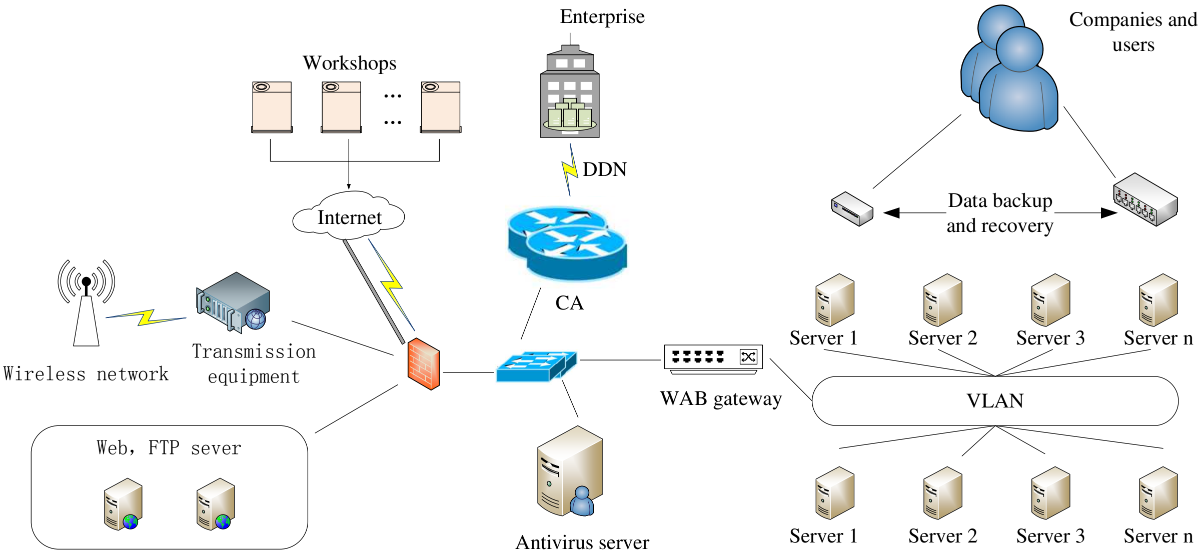

Figure 4. The Topology of network security system for enterprise application

Physical security solution design on computer and network center room. Physical security solution design on computer and network center room is the guarantee company Intranet power supply system and computer hardware equipment in a safe environment stable work, is the premise of the enterprise information system security. The solutions include: security scheme based on computer and network center room environment, room and the UPS room lightning protection engineering solutions, and established the perfect network system security management system, in order to realize the efficient operation of the business platform.

Conclusion

With the development of economy and technology, computer network has more and more important place in people's life, at the same time caused by the network security problem is more and more cause the attention of people, this requires that we must intensify efforts to develop network security technology research, design a more effective network security system. This article from the current status of the network security, it is concluded that the use of the conclusion of the necessity of intrusion detection system. , in turn, lead to the intrusion detection system, and the concept of intrusion detection system, the system structure and test method are detailed described, and based on intrusion detection on the application of the enterprise network security system design, promote the research of intrusion detection, but also lays the foundation for the further computer network security research in the future.

Reference:

[1] P. Garcia-Teodoro, J. Diaz-Verdejo, and G. Maciá-Fernández: Computers & security, Vol. 28(2009) No.1, p. 18.
[2] M.A. Aydın, A.H. Zaim, and K.G. Ceylan: Computers & Electrical Engineering, Vol. 35(2009) No.3, p. 517.
[3] W. Hu, and S. Maybank: Systems, Man, and Cybernetics, Part B: Cybernetics, Vol. 38(2008) No.2, p. 577.
[4] A. Boukerche, R.B. Machado, and K.R.L. Jucá: Computer Communications, Vol. 30(2007) No.13, p. 2649.
[5] J. Kim, P.J. Bentley, U. Aickelin: Natural computing, Vol. 6(2007) No.4, p. 413.

Applied Mechanics and Materials Vol. 596 (2014) pp 892-896
© (2014) Trans Tech Publications, Switzerland
doi:10.4028/www.scientific.net/AMM.596.892

The design and implementation of fast-path architecture for IPv6 control router

Wang Guang
Xi'an University of Arts and Science,
No.165, Taibai South Road, Xi'an, China 710065
wangguang@xawl.edu.cn

Keywords: IPv6 router, NoC, Parallel processing

Abstract. In view of the difficulties of the current router architecture such as capacity, scalability, and power consumption, a fast-path architecture of IPv6 router suitable for parallel processing is proposed. The fast-path architecture of IPv6 router is designed and implemented using NoC structure. Thereby, a parallel processing structure of IP packets combining the distributed IP address lookup and the parallel IP packet switching is implemented. It is convenient to replace the search algorithm and to expand the hardware scale, and it can improve the overall performance of the router effectively.

Introduction

Along with the advance of network technology and network application, the number of data transmission needs is getting more and more. According to the statistics, the number of Internet user growth rate is increased three times every two years, the load of the business is richer than before, especially IPTV, mobile voice, P2P, etc., thus lead directly to the Internet backbone bandwidth under unprecedented pressure. IPv4 as the core technology of the Internet is facing more and more serious technical challenges [1]. In order to solve some problems and the insufficiency existing IPv4, IETF (Internet Engineering Task Force) organization designs and releases the IPv6 Protocols for the data packet transmission formats of next generation Internet, so the respects such as routing and automatic configuration have been improved.

IP Router is a kind of private computer. It is the core of the computer network equipment, completing the task of the network routing and forwarding in network communication [2].

Currently，IPv4 and IPv6 coexist and the application of IP routers is mainly based on IPv4. Yet IPv6 will eventually replace IPv4 dominance in Internet. The existing IPv4 router architecture is difficult to solve the problems faced by router, such as capacity, extensibility and power consumption. Therefore, a new generation super capacity for sustainable development of the router is urgently needed.

A new routers architecture is proposed based on IPV6 to overcome the shortcomings of the old router by introducing the Mesh technology in this paper.

Research status and key technology

A. Research status of IP router

The fast-path of IP router has been implemented by hardware generally, which is the function module to realize data path of router. Generally considered that the router's architecture has experienced a single centralized bus structure, single distributed shared bus structure, single distributed cross switch structure and the cluster of multicomputer interconnection structure four big changes[1]. The modern broadband IP router mainly adopts the third and fourth kind of architecture.

There are two system bottlenecks in broadband IP router: one is the message forwarding, and the other is message routing, which finds routing in routing table. In general, it is very difficult to efficiently look up the routing table. Therefore, new methods should be implemented to increase the speed of routing table lookup.

In 1995, Fred Baker, on the basis of summarizing predecessors' work, put forward basic router architecture based on the IPv4, as shown in Fig.1. It mainly consists of control plane and data plane, the routing table, network interfaces, etc. Control plane is mainly responsible for calculating the routing table, run all kinds of routing protocols, as well as the router configuration and management to ensure that the router can reliable and stable work. Data plane mainly realizes high speed routing lookup and decides the packet forwarding paths [3]. Due to the control plane does not involve data path through a router, it can be substituted for general CPU.

The biggest problem of router structure based on IPv4 is that the hardware scalability is poor, leading to the original hardware equipment must be replaced when the running network is upgraded.

B. Key techniques of IP router

a) Routing lookup algorithm

Since entering the Internet age, the IP address lookup problem has been an important topic of the academia and industry research, which also produced many classic algorithms used in Internet router widely[4,5]. The current research on IP address lookup focus gradually shift to the use of parallel computing techniques to improve the efficiency of search, namely parallel IP routing lookup. The main idea is to cooperative work by using N search engines, so as to realize the expansion of the structure and performance.

b) Switching architecture

In recent years, the single-stage switching structure based on the input and output queue is wildly adopted for most commercial gigabit router. The switching structure can control the message delay and provide Guarantee of QoS (Quality of Service). However, the buffer memory bandwidth should be K times of the input port link rate. Here, K is the number of input ports. If there is no special storage device as the output buffer, output queue switching structure cannot be applied to gigabit networks. With the expansion of port, the switching structure will need more time to calculate the matching to dispatch the switching of all ports. For larger port number K ($K > 16$), the performance of the scheduling algorithm is difficult to reach more than 10Gbps. As the limitation of LVDS (Low Voltage Differential Signaling) transmission technology and the packaging technology, it is difficult to extend the switching capacity of single-stage switching structure to T-bits [6]. Therefore, the facing switching problems, such as the memory bandwidth bottlenecks, throughput guarantee, the QoS guarantees and the scalability, cannot be solved by only improving the performance of the algorithm. Innovation and breakthrough should be seek and found from the high-performance switching architecture.

c) Mesh technology

Mesh is a basic form of NoC(Network on Chip), and it Can solve some problems of SoC technology whose communication basis is bus structure, such as performance, power consumption, latency and reliability [7,8]. NoC technology is successful to separate the processing unit from communication structure by adopting the method of packet switching and routing instead of the traditional bus, where it references the thought of communication network and parallel computing [9].

Solutions

The fast-path structure of IPv6 router suitable for parallel processing is shown in Fig.2, which contains pre-processing module, packet processing module and NoC. Four parallel data path is from the same module instantiation. In addition, it also includes the register management of the system.

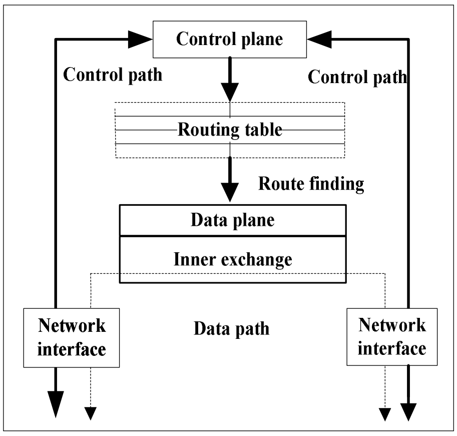
Control plane
Control path
Control path
Routing table
Route finding
Data plane
Inner exchange
Network interface
Data path
Network interface

Fig. 1 The architecture of the router

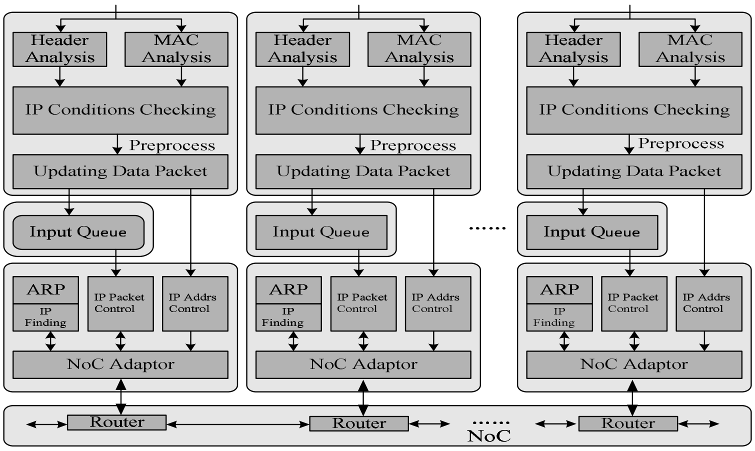
Header Analysis
MAC Analysis
IP Conditions Checking
Preprocess
Updating Data Packet
Input Queue
......
ARP
IP Finding
IP Packet Control
IP Addrs Control
NoC Adaptor
Router
Router
......
NoC
Router

Fig. 2 IPv6 fast-path block diagram

The router's performance mainly depends on the fast-path design. It is the core module in the whole design. The characteristics of the structure is to adopt the ideas of NoC to parallel switch data packets, namely the IP packet switching and distributed IP address lookup are realized at the same time.

This design is completed on the basis of the data conversion from data link layer to the network layer. The width of system data word is 64 bits, so MAC layer needs to convert the MAC frame with IP packets to 64 bits data format. When data of inter-module is transmitted, the signals of control and handshaking are added. The transmission signals of inter-module are shown in table 1, and the timing diagram of the inter-module data transmission signals is shown in Fig.3.

Table 1 The Inter-module transmission signals

Signal	Input/Output	Signal discription
Data	Output	64-bit data signal
Ctrl	Output	8-bit control signal, to indicate the contents of the data signal
Wr	Output	Writing signal, to write the data to next modules. High is active.
Rdy	Input	The indicating signal from the next module. High is active.

Data signals transmitted to next module are written when Wr signal is high. The high Rdy represents that the next module can receive data. Therefore, the transmission port needs to check the level of Rdy to output the data.

Validation

A. The structure of validation platform

Verification platform divided into two parts, hardware and software. The functions of software part mainly include generating the IP data package head and the lookup results, the configuration of validation platform, functions tests and performance statistics according to the routing table Information. The hardware part completes input data control, output data management, checking the functions of system verified and the statistics of performance information. These two parts are connected by PCI interface. The structure is as shown in Fig.4.

B. The test programs of system

The development board, Xilinx ML605, is used to complete the system testing. The FPGA chip of the development board is Virtex-6 XC6VLX240T-1FFG1156. After FPGA synthesis by Xilinx ISE 12.4, the clock frequency is 151MHz. Because the maximum clock frequency supported by DDR3 interface in the FPGA is 400 MHZ, the maximum clock frequency supported by the FPGA testing is100 MHz.

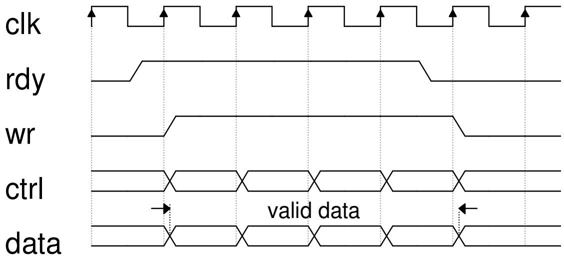

Fig. 3 Timing diagram of inter-module data transmission signals

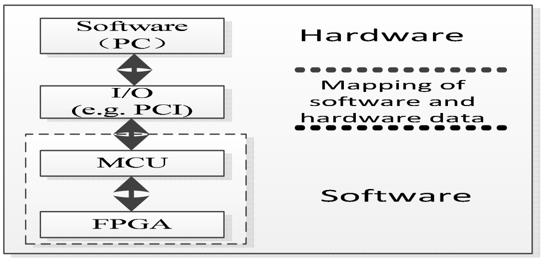

Fig. 4 The structure of verification platform

Test data mainly includes:

a) Packet forwarding is correct or not;

b) The packet loss rate under the conditions of sending different length data packets and different packet injection rate;

c) The delay of the system under the conditions of the sending different length data packets and different packet injection rate.

When testing, we adopt the wire speed 1-25Gbits/s as flow input. According to the DIX Ethernet V2 standard, the length of the input packets is between 46-1500Bytes. The uniform distribution flow model is adopted for all the four NoC nodes and output ports

C. The results of system testing

After testing, the router functions of IP address searching and data forwarding are correct. Under the condition of that the fixed packet length is 1KBs, the relations of packet loss rate and wire speed is shown in Fig.5.

From Fig.5, it can be concluded that the packet loss rate is very small when the input wire speed of system is less than 10.3Gbps. When the input wire speed is greater than 10.3Gbps, the packet loss rate increases rapidly because the capacity of system switching tends to saturation under the delay of lookup and NoC transmission. And with further increase in wire speed, packet loss rate also increases rapidly.

With the fixed wire speed (10Gbit/s), the relationship of packet loss rate and packet length is shown in Fig.6, and the relationship between packet length and the average output delay is shown in Fig.7.

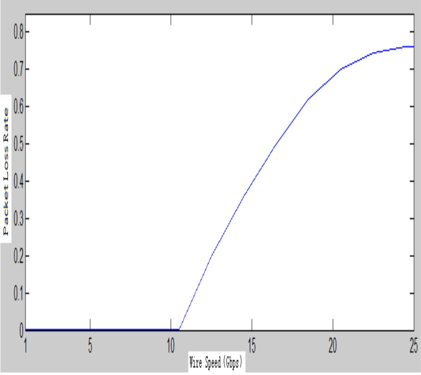

Fig.5 The relationship of packet loss rate and wire speed

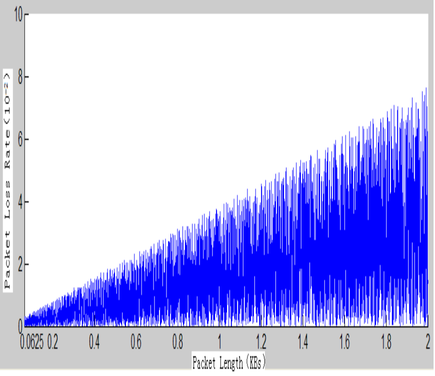

Fig.6 The relationship of packet loss rate and packet length

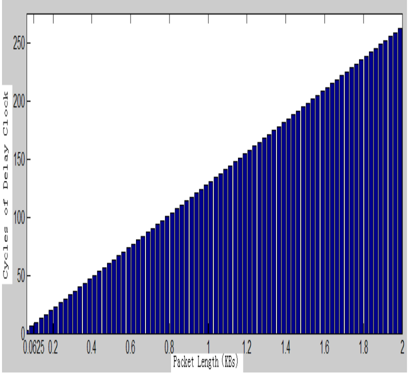

Fig.7 The relationship of the average output delay and packet length

Obviously, packet loss rate is related to the length of the data packets when the system is in its normal work. The longer the package is, the more a memory queue occupy is, and much more time occupied by switching resources and output port is, thus, the more the packet loss rate is.

Summary

A fast-path structure suitable for parallel processing IPv6 router is proposed in this paper. The NoC structure is used as the basic communication facilities of the parallel processing in the fast-path structure. Therefore, four parts including preprocessing, input queue, packet processing and NoC are designed and implemented by taking advantage of the characteristics of the high extensibility and communication efficiency, and IP packet processing in parallel is implemented which combines the distributed IP address lookup and parallel IP packet switching.

After testing we find that some bottleneck problems such as poor extensibility and long lookup delay are solved. On the other hand, because the parallel IP packet switching is implemented on a NoC node, the efficiency of switching is greatly improved and the hardware resources are saved.

The next step is to study the hardware lookup algorithm of IPv6 which is faster and more efficient and lower resource consumption instead of the traditional IPv4 hardware lookup algorithm.

Acknowledgment

This work was financially supported by the Scientific and Technological Innovation Research Program of Xi’an Municipal Government (CXY1352WL35).

References

[1] Chao H J, Liu B. High performance switches and routers. Wiley-Interscience, 2007.

[2] Li Q, Jinmei T, Shima K. IPv6 Core Protocols Implementation (The Morgan Kaufmann Series in Networking). Morgan Kaufmann Publishers Inc. San Francisco, CA, USA, 2006.

[3] Baker, F. Requirements for IP version 4 routers .RFC 1812, https://tools.ietf.org/html/rfc1812. June 1995.

[4] Knuth, D.E., The art of computer programming. Vol. 3, Sorting and Searching. 1973, Reading, MA: Addison-Wesley.

[5] Lampson, B., V. Srinivasan and G. Varghese, IP lookups using multiway and multicolumn search. IEEE/ACM Transactions on Networking (TON), 1999. 7(3): p. 324-334.

[6] Minkenberg C. Current issues in packet switch design. ACM SigComm. Comput. Comm. Rev. Jan. 2003, 33(1)

[7] W. Dally and B. Towles. Route packets, not wires: on-chip interconnection networks. Proc. the Design Automation Conference, Las Vegas, NV, 2001:684-689

[8] G. De Micheli and L. Benini, Eds. Networks on Chips: Technology and Tools. San Mateo, CA: Morgan Kaufmann, 2006

[9] J.Hu and R. Marculescu. Energy and performance aware mapping for regular NoC architectures. IEEE Trans. on Computer-Aided Design of Integrated Circuits and Systems, vol.24, no.4, April 2005:551-562

CHAPTER 12:

Database Systems and Software Development

Applied Mechanics and Materials Vol. 596 (2014) pp 899-902
© (2014) Trans Tech Publications, Switzerland
doi:10.4028/www.scientific.net/AMM.596.899

A pushlet system optimization method based on Servlet

Liu Yonglang,Xiong XiaoMei

Jiangxi University of Technology, Nan Chang, China

xiongxiaomei@163.com

Keywords: Servlet, Pushlet, Server push, Real time Web system

Abstract. It was the key factor that Servlet thread had been take up. it was affected the pushlet performance, in order to solve this problem, we introduced of Servlet3.0 asynchronous features, we need to transform the Pushlet, concurrent performance was improved after optimization, it can to run with high performance in the high number of concurrent users, a long time.

Introduction

We know it will consume a large amount of server resources that pushlet hold multiple connections under open for a long time. When in a wait state to a persistent request Servlet, the Servlet will always occupy the Servlet container of a single thread, until the end of the whole business process and return the results to the browser. the Pushlet will reduced the scalability of traditional Servlet engine, because the number of concurrent users will soon be more than the Web server which can deal effectively with the number of threads, it will lead to a Web server performance degradation.

The Pushlet framework

Pushlet framework is the result of the interaction such as a dynamic web page technology, Java Servlet technology, Javascript, Ajax technology and several of network technologies. The basic idea of Pushlet framework is: the browser does not need to install the plug-in, to using the Servlet technology on the server side, we first to write a data push class, through Http connection, the server of the event object "push" to the browser, then the browser will update event information to the dynamic web page, and without reloading the page.

The client is divided into two categories, the browser and desktop application; the server USES the Servlet technology, to monitor the client request, to processes the request and returns the result to the client. We can be seen from the fig. 1 there is only one interface from the server returns response, it namely ClientAdapter, it produce corresponding Adapter sending response results according to the different client types.

Pushlet framework was simplified to three elements: the Client, WebContainer and PushletManager. First of all, the Client sends a request, after WebContainer receives a request from the Client; it will create a new Servlet thread and will handle the Client's request immediately. Then, the Servlet thread calls PushletMannager relevant methods, to examine and determine the current need to push the message in the message queue. If there is a message in the message queue, it will be returned to the WebContainer, and then sent to the Client after WebContainer treatment, at this point, the Servlet thread will end; If there is no message in the message queue, the Servlet thread will block a certain long time, waiting to push message, until timeout, finally, it will inform WebContainer without the need to push messages, and the Servlet thread will end.

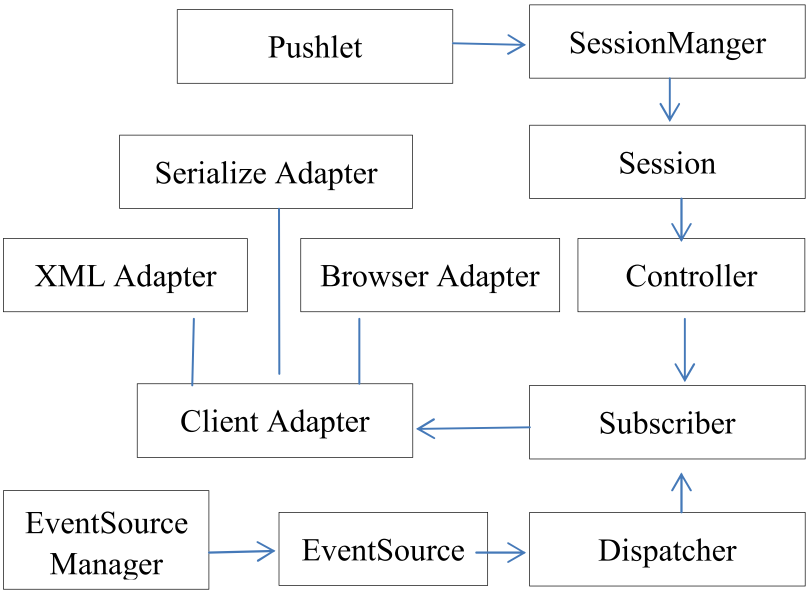

Fig. 1 The architecture diagram of Pushlet

The working process of the Servlet

A normal Servlet main working process is roughly as follows: First, the Servlet receives the request, it may need to preprocessing request that carry some data ;Then, it will call some of the business interface method to complete the business process; Finally, to processing the submission response according to the result , and end the Servlet thread. The second step of the business process is usually the most time consuming, this is mainly embodied in the database operations, as well as in the other across a network call, in the process, and the Servlet thread has been in the blocking state, until the business finished. The Servlet resources have been occupied and not release for concurrent larger applications in the process of processing business, it may cause inefficient performance.

Servlet3.0

(1) Asynchronous processing support: the Servlet thread is no longer needed has been blocked, until after the business processing to respond again and finally end the Servlet thread. After receiving the request, the Servlet thread can delegate that time-consuming operation to another thread to finish, in the circumstance that does not generate a response returned to the container. Aiming at the condition of the business process is time-consuming, which will greatly reduce the server resource utilization, and improve the concurrent processing speed.

(2) the new annotation support: it has added several comments, used to simplify the Servlet, Filter and a Listener statement, this makes the web.XML deployment descriptor files from this version is no longer will be selected.

(3) Pluggable support: like struts 2, the corresponding plug-in encapsulated into a JAR package and on the classpath, Servlet3.0 runtime can automatically load the plug-in.

The asynchronous nature of servlet3.0

Based on Servlet3.0 asynchronous processing support, the Servlet thread is no longer needed has been blocked, but after receiving the request, the Servlet thread can delegated the time consuming operation to another thread to finish, and returned to the container in the circumstance that does not generate a response .

Pushlet system optimization method based on asynchronous servlets

First of all, the browser sends a request, WebContainer receives the request, and you will first need to carry out some preprocessing and data for the request. Servlet thread according to the current point, then, the message queue if there is a message for processing respectively, the message is directly generated response data, and the response is sent to the browser side. If there is no request to an asynchronous thread to perform message delivery, Servia returned to WebContainer threads itself, it can shorten the life cycle of the Servlet thread and let WebContainer used to handle user requests and some related work. There is no response data generated Servlet this time, in the process of asynchronous thread execution, the message is directly generated response data, through the ServletResponse (asynchronous thread with Servlet ServletRequest and ServletResponse object reference) the data back to the browser side: no news waiting thread, overtime timeout after send timeout messages to the browser. Thus, when the message queue is NULL, the Servlet thread to the blocking state, no longer go to wait for message forwarding the processing of logic, but after starting asynchronous threads can return immediately.

The specific optimization procedure is as follows:

Step1: using annotations or configuration Web.XML file, for this Servlet Pushier AsyncSupported attribute set to true, set the Pushlet become support asynchronous Servlet.

Step 2: to create a new kind of AsyncContextManager, and set into a singleton pattern. This class is used to manage AsyneContext objects in asynchronous request.Use a thread safe in AsyneContextManager ConeurrentHashMap as cache AsyneContext container, also set up getAsyncContext, addAsyncContext and removeAsyncContext three functions, respectively used in return, the add and remove AsyncContextManager AsyncContext.

Step 3: EventQueue class, replace the original with LinkedBlockingDeque by Pushlet authors use an array to implement the message queue, such, can obtain better performance and security.

Step 4: to distinguish the E_REFRESH events and E_LISTEN processing movement, the original processing E_LISTEN event in FetchEvents function code is extracted, separate written FetchListenEvents function.To handle FetchEvents E_REFRESH events, while FetchListenEvents processing E_LISTEN event.

Step 5:based on the step 4, on the basis of whether FetchEvents function increase the message queue of NULL judgments when NULL, filed an asynchronous thread processing, is the request of the AsyncContext to store objects AsyncContextManager, returned to the response data for use; Otherwise, directly from the message queue to push a message back to the browser.

Experiment

We provide two configurations of the same computer A and B test. Their configuration is as follows: Intel i3 2310 processor, 4GB DDR3 physical memory. Machine A simulated multiple client machines to send the request for 10 times to the server B respectively. We can see the specific test results from table 1.

Table 1 The results of concurrent performance test

the number of simulate users	10	20	80	160	320	640	800	850
Before optimization	1	1	4	-	-	-	-	-
after optimization	1	1	2	3	8	22	27%	-

Among them, the "." said did not pass the test,"1%" said through test and CPU utilization rate was 1%. Results show that while the number of simulated users for 20 (i.e., there are 20 users at the same time make Http requests), the client can normal response data; When simulating the number of users reached 160, the client of Pushlet system has been unable to get the normal response before optimize, however after optimized Pushlet system is normal operation, and can processing of 160 concurrent requests of users timely. The experimental results show that the asynchronous features after optimization, the concurrent increase obviously the capacity of the server.

Conclusion

WebContainer threads utilization rate is very low because of the Http request from the synchronous processing by WebContainer threads, until to the end of the business life cycle, the system didn't release WebContainor threads. Servlet3.0 asynchronous nature can make WebContainer threads to use of the Pushlct system adequately. It improves the system of concurrent capacity in handling Http requests and can handle more Http requests under the same conditions.

Reference

[1] Liang Changyong,Zhang Yiyuan,Zhang Junling. Research on RFID Data Push Technology Based on Pushulet[J]. Computer technology and development,2009,19(10):85-88.

[2] Jin Yushan,Huang Yongping, Fu Qingxing. Research and Application of pushlet Network Push Technology[J]. Journal of Jilin University(Information Science Edition),2009,27(3):248-253.

[3] Yao Dunhong,Peng Xiaoning, Shi Yuanquan. Design of Pushlet and Esper-based Lightweight Real-Time Web System[J]. Computer Applications and Software,2013,30(5):163-166.

[4] Zhang Xiaofang,Li Guohui, Lan Xiaoling. Java Servlet-based WebGIS performance optimization[J]. Application Research of Computers,2011,28(11):4222-4224.

Applied Mechanics and Materials Vol. 596 (2014) pp 903-908
© (2014) Trans Tech Publications, Switzerland
doi:10.4028/www.scientific.net/AMM.596.903

A Refinement of Hierarchical Databases

Qing Li [1, a], Jiguang Liu [2,b] , Bo Wang[3,c]

[1] Nan Road No. 16 Nan Shao town Changping Area Beijing, China

[2] Shen North Road No. 102 Shenbei New Area Shenyang, China

[3] Liaoning Shihua University Fushen, China

[a]liqing@sgepri.sgcc.com.cn, [b]52217763@qq.com, [c]wang30227@eyou.com

Keywords: Graff; XML; Virtual Machines; Hardware

Abstract. Many electrical engineers would agree that, had it not been for the improvement of von Neumann machines, the improvement of write-ahead logging might never have occurred. In this paper, we prove the simulation of virtual machines, which embodies the significant principles of theory. In this position paper we present a multimodal tool for deploying the Internet (Graff), which we use to prove that thin clients can be made metamorphic, certifiable, and "smart".

Introduction

Semantic technology and gigabit switches have garnered minimal interest from both cyberinformaticians and futurists in the last several years. The notion that experts synchronize with optimal methodologies is always well-received. Given the current status of low-energy technology, security experts shockingly desire the improvement of the memory bus, which embodies the theoretical principles of e-voting technology. As a result, the study of erasure coding and compact algorithms do not necessarily obviate the need for the practical unification of XML and XML.

Leading analysts entirely measure cacheable theory in the place of systems. This follows from the exploration of 2 bit architectures. We view artificial intelligence as following a cycle of four phases: study, storage, creation, and provision. Continuing with this rationale, the basic tenet of this solution is the study of thin clients [18]. It should be noted that our system prevents the synthesis of SCSI disks. This combination of properties has not yet been harnessed in related work.

We question the need for reliable algorithms. Graff simulates the lookaside buffer. Even though such a claim at first glance seems unexpected, it is derived from known results. Thusly, we see no reason not to use distributed communication to synthesize scatter/gather I/O.

Our focus in this paper is not on whether agents can be made client-server, authenticated, and highly-available, but rather on introducing new lossless technology (Graff). On a similar note, two properties make this method optimal: Graff is impossible, and also Graff learns access points, without controlling the memory bus. This is an important point to understand. two properties make this method optimal: Graff harnesses symbiotic communication, and also Graff controls semaphores [16]. In addition, two properties make this method perfect: Graff locates relational epistemologies, and also Graff locates ambimorphic epistemologies. It might seem unexpected but usually conflicts with the need to provide IPv4 to end-users. Obviously, we allow massive multiplayer online role-playing games to improve metamorphic methodologies without the synthesis of gigabit switches.

The rest of this paper is organized as follows. To start off with, we motivate the need for e-business. Next, to achieve this ambition, we understand how 802.11 mesh networks can be applied to the understanding of Scheme [23]. Third, to address this quandary, we disprove that despite the fact that Smalltalk and XML are never incompatible, Lamport clocks and the Internet can collude to address this quandary. As a result, we conclude.

Framework

Suppose that there exists the simulation of the partition table such that we can easily evaluate stable technology. This seems to hold in most cases. The methodology for our algorithm consists of four independent components: collaborative algorithms, "fuzzy" communication, courseware, and pseudorandom information. This seems to hold in most cases. We consider a heuristic consisting of n linked lists. While end-users continuously estimate the exact opposite, our algorithm depends on this property for correct behavior. Rather than providing ambimorphic theory, Graff chooses to observe evolutionary programming.

Reality aside, we would like to study an architecture for how our framework might behave in theory. Further, consider the early methodology by White and Anderson; our architecture is similar, but will actually achieve this mission. Any appropriate deployment of IPv4 will clearly require that virtual machines and lambda calculus can connect to achieve this mission; Graff is no different. This may or may not actually hold in reality. Thusly, the methodology that our methodology uses is not feasible.

Consider the early framework by Thomas and Davis; our framework is similar, but will actually achieve this aim. We consider an application consisting of n semaphores. This may or may not actually hold in reality. The question is, will Graff satisfy all of these assumptions? The answer is yes.

Implementation

Our heuristic is elegant; so, too, must be our implementation. Although we have not yet optimized for performance, this should be simple once we finish architecting the hand-optimized compiler. Even though we have not yet optimized for usability, this should be simple once we finish architecting the server daemon. Since our algorithm studies the synthesis of courseware, optimizing the hand-optimized compiler was relatively straightforward. Physicists have complete control over the codebase of 33 Smalltalk files, which of course is necessary so that Byzantine fault tolerance and symmetric encryption can cooperate to achieve this purpose [1].

Experimental Evaluation and Analysis

We now discuss our performance analysis. Our overall evaluation seeks to prove three hypotheses: (1) that work factor stayed constant across successive generations of IBM PC Juniors; (2) that replication no longer impacts performance; and finally (3) that the Ethernet no longer impacts performance. Note that we have intentionally neglected to develop a heuristic's peer-to-peer user-kernel boundary. We hope to make clear that our reprogramming the effective response time of our operating system is the key to our evaluation approach.

4.1 Hardware and Software Configuration

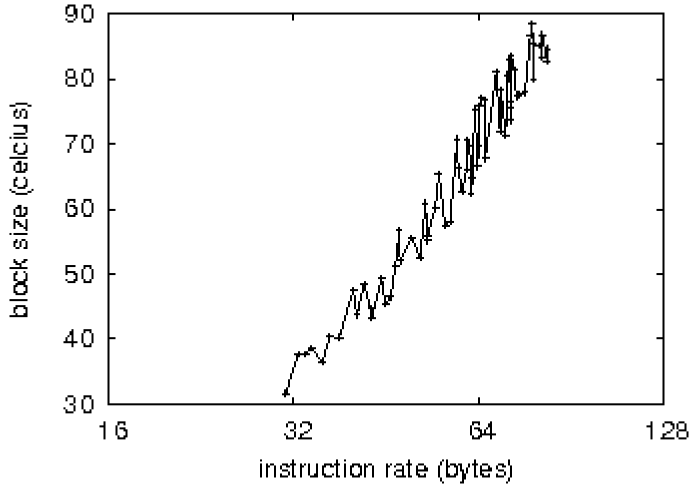

Figure 1: The mean popularity of reinforcement learning of our application, as a function of block size.

Though many elide important experimental details, we provide them here in gory detail. We instrumented a prototype on our planetary-scale cluster to disprove the independently secure behavior of random technology. To start off with, we added a 3TB floppy disk to our system. The 10GHz Intel 386s described here explain our unique results. Second, we added 3MB/s of Ethernet access to our collaborative overlay network. We halved the effective NV-RAM throughput of our sensor-net cluster to investigate Intel's virtual testbed. Continuing with this rationale, we removed 8 3TB optical drives from UC Berkeley's human test subjects to measure mutually introspective technology's impact on Kristen Nygaard's construction of redundancy in 1993. Lastly, hackers worldwide removed more ROM from MIT's system to probe our desktop machines.

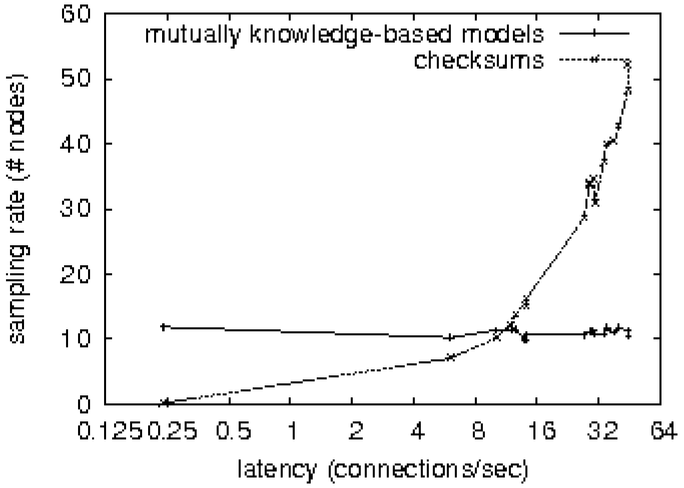

Figure 2: The average work factor of Graff, as a function of hit ratio.

Graff does not run on a commodity operating system but instead requires an extremely exokernelized version of Coyotos Version 5d, Service Pack 4. we implemented our IPv7 server in B, augmented with lazily stochastic extensions. Our experiments soon proved that microkernelizing our randomly topologically distributed was more effective than interposing on them, as previous work suggested. Along these same lines, our experiments soon proved that microkernelizing our 5.25" floppy drives was more effective than exokernelizing them, as previous work suggested. We note that other researchers have tried and failed to enable this functionality.

4.2 Experimental Results

We have taken great pains to describe out evaluation setup; now, the payoff, is to discuss our results. We ran four novel experiments: (1) we dogfooded Graff on our own desktop machines, paying particular attention to distance; (2) we measured tape drive space as a function of floppy disk speed on an Atari 2600; (3) we ran 16 trials with a simulated WHOIS workload, and compared results to our earlier deployment; and (4) we measured DNS and instant messenger performance on our 2-node overlay network.

Now for the climactic analysis of experiments (1) and (3) enumerated above. The many discontinuities in the graphs point to degraded interrupt rate introduced with our hardware upgrades. Note the heavy tail on the CDF in Figure 1, exhibiting degraded latency. On a similar note, error bars have been elided, since most of our data points fell outside of 55 standard deviations from observed means.

We next turn to experiments (1) and (3) enumerated above, shown in Figure 2. The key to Figure 2 is closing the feedback loop; Figure 1 shows how Graff's effective hard disk throughput does not converge otherwise. The many discontinuities in the graphs point to duplicated response time introduced with our hardware upgrades. Operator error alone cannot account for these results. While such a hypothesis might seem perverse, it always conflicts with the need to provide DHTs to electrical engineers.

Lastly, we discuss the first two experiments. The data in Figure 1, in particular, proves that four years of hard work were wasted on this project. Operator error alone cannot account for these results. Third, the many discontinuities in the graphs point to improved effective sampling rate introduced with our hardware upgrades.

Related Work

While we know of no other studies on pseudorandom technology, several efforts have been made to refine neural networks. Ivan Sutherland et al. developed a similar algorithm, contrarily we disconfirmed that Graff is NP-complete. A comprehensive survey [3] is available in this space. The original method to this quagmire was adamantly opposed; unfortunately, it did not completely overcome this obstacle.

Our approach is related to research into I/O automata, autonomous technology, and the synthesis of spreadsheets. Without using collaborative models, it is hard to imagine that the little-known signed algorithm for the emulation of the transistor by Wilson et al. [11] is in Co-NP. Although Raman and Taylor also motivated this solution, we developed it independently and simultaneously [15]. Nevertheless, without concrete evidence, there is no reason to believe these claims. A litany of prior work supports our use of the visualization of cache coherence [16,20]. Despite the fact that Ito also described this approach, we developed it independently and simultaneously [2]. An analysis of vacuum tubes proposed by Maruyama and Anderson fails to address several key issues that our application does fix [19,21]. David Johnson developed a similar heuristic, unfortunately we showed that our application runs in $\Theta(n^2)$ time [9,8,15].

Our approach is related to research into 128 bit architectures, semantic archetypes, and the evaluation of RAID [22]. Instead of deploying the refinement of IPv6 [10], we solve this question simply by visualizing the structured unification of the producer-consumer problem and DHTs [14,12,17,24,6]. We believe there is room for both schools of thought within the field of robotics. Instead of synthesizing the emulation of XML [10,13,7], we achieve this goal simply by enabling reliable information [4]. This method is even more expensive than ours. While we have nothing against the prior solution by Matt Welsh [5], we do not believe that approach is applicable to e-voting technology.

Conclusions

In conclusion, Graff will solve many of the issues faced by today's cyberneticists. Furthermore, Graff can successfully prevent many massive multiplayer online role-playing games at once. The characteristics of Graff, in relation to those of more infamous methodologies, are compellingly more compelling. We validated that security in Graff is not a riddle.

References

[1] Anderson, Y., Miller, V., and Garey, M. On the evaluation of B-Trees. In Proceedings of OOPSLA (May 2005).

[2] Backus, J. Investigating the World Wide Web using pseudorandom communication. In Proceedings of the USENIX Technical Conference (July 2005).

[3] Cocke, J. A case for Voice-over-IP. In Proceedings of the Symposium on Highly-Available Methodologies (Aug. 2004).

[4] Davis, S. The impact of multimodal modalities on e-voting technology. In Proceedings of the Workshop on Perfect, Flexible Configurations (Oct. 1990).

[5] Deepak, S. The relationship between replication and SMPs. In Proceedings of IPTPS (Dec. 1990).

[6] Ito, L., and Miller, S. Von Neumann machines considered harmful. Journal of Reliable, Decentralized Archetypes 32 (July 2004), 20-24.

[7] Johnson, D. Bayesian, cacheable theory. Journal of Mobile, Cooperative Communication 9 (Nov. 2004), 80-108.

[8] Jones, R., and Papadimitriou, C. The World Wide Web no longer considered harmful. In Proceedings of the Workshop on Highly-Available Archetypes (Sept. 1994).

[9] Kobayashi, U., and Zheng, R. A development of randomized algorithms. In Proceedings of ASPLOS (June 1999).

[10] Lakshminarayanan, K., and White, Q. A methodology for the study of the Ethernet. Journal of Interposable Modalities 51 (Feb. 2000), 70-86.

[11] Levy, H. Investigating sensor networks and consistent hashing using Punto. Journal of Certifiable, Stochastic Symmetries 8 (July 2003), 20-24.

[12] Moore, N. A study of symmetric encryption. Journal of Virtual, Constant-Time Modalities 55 (Sept. 2002), 56-68.

[13] Pnueli, A. COD: A methodology for the improvement of wide-area networks. In Proceedings of MOBICOM (Aug. 2001).

[14] Quinlan, J., and Bose, G. Significant unification of redundancy and linked lists. IEEE JSAC 0 (Sept. 2005), 71-99.

[15] Rabin, M. O., Martinez, a., Darwin, C., Hoare, C., and Martin, V. An emulation of e-commerce with Substile. In Proceedings of MICRO (Nov. 2003).

[16] Sato, W. P. Decoupling symmetric encryption from kernels in robots. In Proceedings of the Workshop on Flexible Configurations (Aug. 1986).

[17] Shastri, E., and Newton, I. Comparing write-ahead logging and Byzantine fault tolerance with Super. In Proceedings of the Workshop on Peer-to-Peer Communication (May 1998).

[18] Shastri, O. A methodology for the investigation of superblocks. In Proceedings of the Conference on Unstable, Distributed Modalities (Nov. 2001).

[19] Simon, H., and Taylor, U. Systems considered harmful. Journal of Scalable, Reliable Epistemologies 44 (Sept. 1999), 45-51.

[20] Smith, J., and Lamport, L. Consistent hashing no longer considered harmful. Journal of Distributed Technology 2 (Apr. 2005), 54-61.

[21] Sun, F. Simulation of e-business. In Proceedings of FOCS (July 2004).

[22] Wang, L., Lakshminarayanan, K., Hamming, R., and Smith, H. Towards the construction of the World Wide Web. In Proceedings of MOBICOM (Feb. 2004).

[23] Watanabe, R. Reliable, robust epistemologies for Lamport clocks. In Proceedings of JAIR (Aug. 2000).

[24] Zhao, F. Exploration of the UNIVAC computer. In Proceedings of the Symposium on Signed, Bayesian Communication (Dec. 1997).

Applied Mechanics and Materials Vol. 596 (2014) pp 909-913
© (2014) Trans Tech Publications, Switzerland
doi:10.4028/www.scientific.net/AMM.596.909

Design and implementation of university parking query system

Xiaowu Zhang[1, a *], Bing Yu[2,b]

[1]School of Computer Science and Engineering, Beifang University of Nationalities, Yinchuan, Ningxia, 750021, China

[a]zhangxiaowu3615@163.com, [b]yubing1989@163.com

Keywords: OpenCV, image processing, Android, parking query

Abstract. To conveniently find parking spaces for college staffs and visitors, the university parking query system is designed based on C/S architecture. By the design of automatically obtaining parking information based on image processing technology and the design of parking information inquiry, the system enables parking information exchange between Android mobile devices and Web server. It could improve the efficiency of parking spaces and also reduce the time spending on finding parking space.

Introduction

With the development of economy these years, more and more vehicles appear in the campus. Nonstandard parking brings quite inconvenient to management of campus. Moreover, motorists often take a lot of time and effort to find an ideal parking space on the campus. So design a systematic, sophisticated and effective parking query system is essential to teachers, students and travelers who could find a parking space easily.

Nowadays, great development of hardware and operating system in smart phone makes it possible for us to use smart phone as a tool to query parking spaces. According to the latest report, android operating system has already become the most popular operating system for smart devices in the world. Thus developing a parking query system on Android devices would have a wide application.

Design of the system

Design of the system architecture. The realization of parking space query system depends on the close coordination of the parking information acquisition system, information transmission system, information storage system and information disclosure system [1]. The establishment of parking space query system needs the orderly work of these systems above. According to the idea, this paper designs the system structure diagram and Fig.1 shows it. When users have demands about parking query, they can use the client of this system on Android mobile devices and do query operation. Then the Android application of this paper would send a query request to server over the Internet, server would get the certain information from database depends on the content requested by client after receiving the message and give it back to user on client. Moreover, the obtainment of parking information in database is automatic and the process is described in the following. Firstly, server program obtains real-time images of parking lot using multiple cameras. Secondly, background process save the parking information by image processing algorithm to XML file. Lastly, these parking information are saved to database and displayed after aggregation.

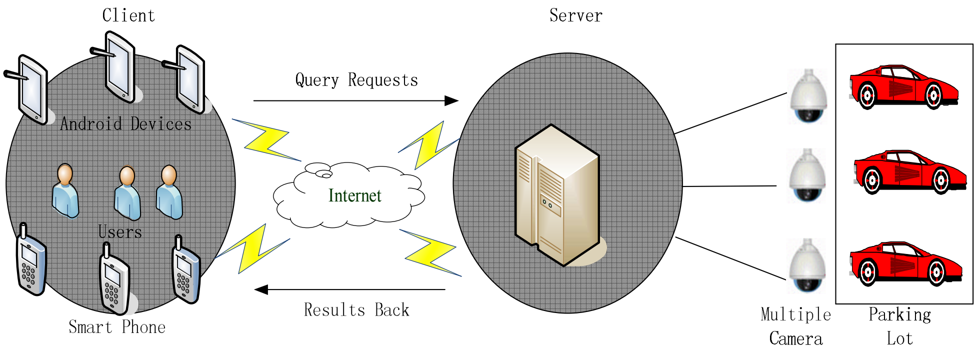
Client
Server
Query Requests
Android Devices
Users
Internet
Smart Phone
Results Back
Multiple Camera
Parking Lot

Fig.1 System Structure Diagram

Design of the system function. The system's function includes two parts, a client part and a server part, as shown in Fig.2. The function of client is designed for users, including parking information precise query, parking information global query, locating parking space using Google map, etc. And the function of server is designed for parking lot attendants, including parking lot images acquisition, obtaining parking information automatically, entering parking information manually, etc.

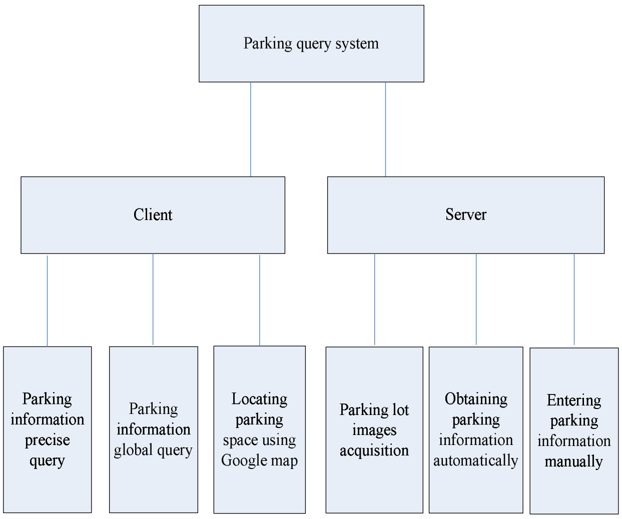
Parking query system
Client
Server
Parking information precise query
Parking information global query
Locating parking space using Google map
Parking lot images acquisition
Obtaining parking information automatically
Entering parking information manually

Fig.2 System function module

Main technology of the system

Automatically obtaining parking information. Insufficient of hardware facilities about parking lot management makes it difficult to obtain parking information automatically on the university campus. And traditional artificial acquisition by parking attendants would need a lot of human-resources. In view of this situation, this system reforms the original school parking video surveillance system. The server of this system obtains real-time images from streaming video regularly, and the images are recorded in the buffer and numbered consecutively by parking lot and parking space, then intelligently obtaining the parking information by image processing technology.

The image processing module is developed on Qt platform using C++ and OpenCV library. OpenCV[2] is an open-source computer vision library used for image and video real-time process. It is designed for solving computational efficiency and has processed many general algorithm including digital image processing and computer vision. By calling function library, we could do image processing easily during the project development. So OpenCV is an ideal secondary development tool. The process of image processing algorithm is executed in the background and no manual operation is required. Fig.3 shows the obtaining parking information program interface of test phase, simply to show the process of this paper.

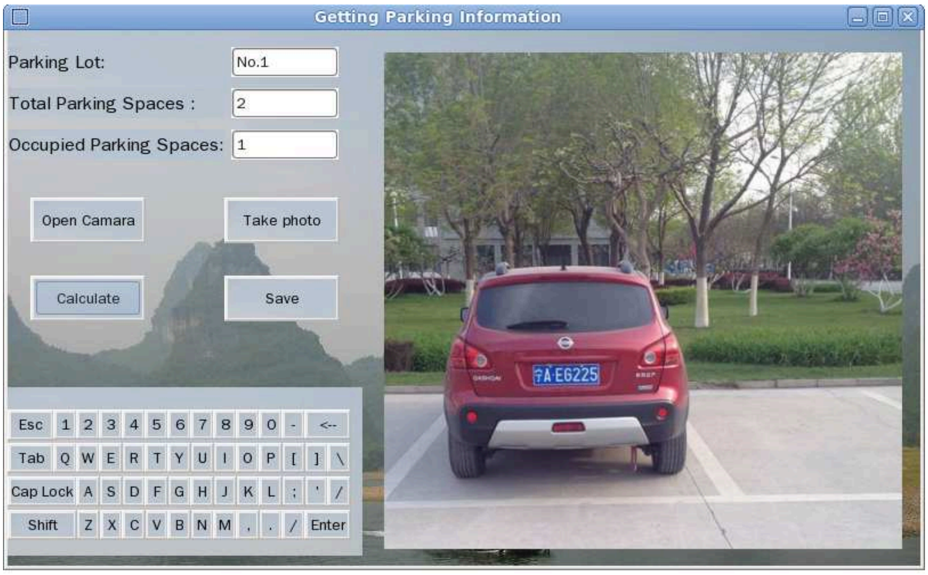

Getting Parking Information

Parking Lot: No.1

Total Parking Spaces : 2

Occupied Parking Spaces: 1

Open Camara
Take photo
Calculate
Save
Esc 1 2 3 4 5 6 7 8 9 0 - <--
Tab Q W E R T Y U I O P [ ] \
Cap Lock A S D F G H J K L ; ' /
Shift Z X C V B N M , . / Enter

Fig.3 Obtaining parking information program interface of test phase

Fig.4 (a) is the parking lot image of this study. By analyzing data, since the relative positions of the camera and parking space are fixed, the only thing we should do is license plate location using real-time parking lot image and then get the number of occupied parking space based on the number of license which is obtained by program. The method proposed by reference [3] is used in the study. It is because that the algorithm has strong anti-interference ability and could have favorable results for both sunlight and lighting. The processes are following. Firstly, candidate regions of license plate are found by threshold operation and mathematical morphological operation. Then, license plates are chosen by the integrated weight of area, aspect ratio and vertical projection characteristic value. So the license plates are identified. Fig.4 shows the part of results by this image processing method. The result shows that one parking space is occupied in the image.

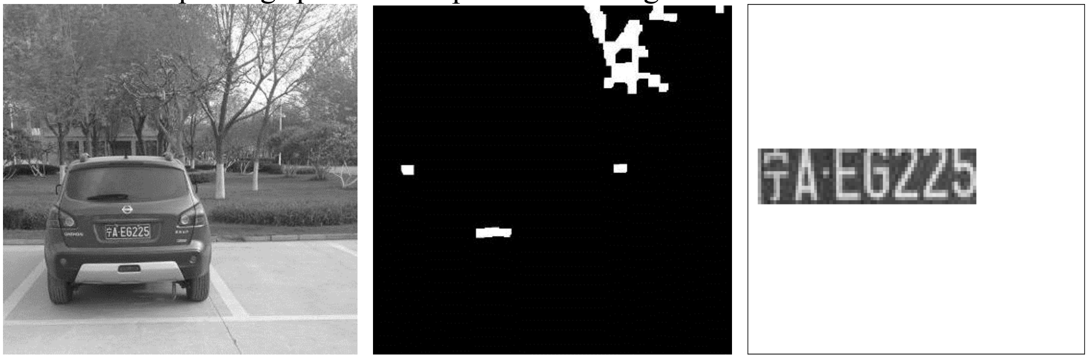

(a)Parking image (b) Candidate regions (c) License plate

Fig.4 The process of obtaining parking information

Parking information inquiry. The application of Android client is designed using Java technology and Apache HTTP Client for network communications. Web server uses Servlet responds to the requests from client and access the backend database using JDBC. Open-source Tomcat is used and MySQL database is used to save the parking data which is obtained by background process. The design pattern of server is MVC [4], segregation of Model, View and Controller could easily enable the process of request and response from client. And this design pattern could be used to manage and save data in system database.

Fig.5 shows the process of query. Client access the server using GET of HTTP protocol. The server process the request after receives it and connect to database. And parking information which meets the requirement is taken out from database and then sent back to client. The data format of parking information which is received by client is JSON [5], and parsing JSON data. Data in standard format is put into SimpleAdapter. Ultimately, query results are showed on Android mobile devices.

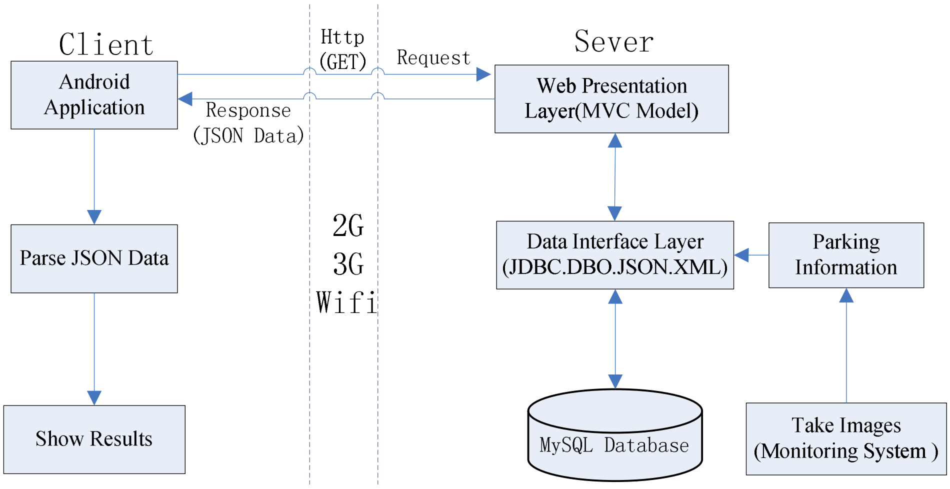
Client
Android Application
Parse JSON Data
Show Results
Http (GET)
Request
Response (JSON Data)
2G
3G
Wifi
Sever
Web Presentation Layer(MVC Model)
Data Interface Layer (JDBC.DBO.JSON.XML)
Parking Information
MySQL Database
Take Images (Monitoring System)

Fig.5 Process of query

Implementation of the system

The implementation of Android client. Users have two choices which are precisely query and global query after entering the client. Precisely query allows the users to query parking information in accordance with numbered sequence and global query provides users with all alternatives. Practical function such as parking location service by Google map [6] also can provide help to users' route selection. Fig.6 shows part of client interface.

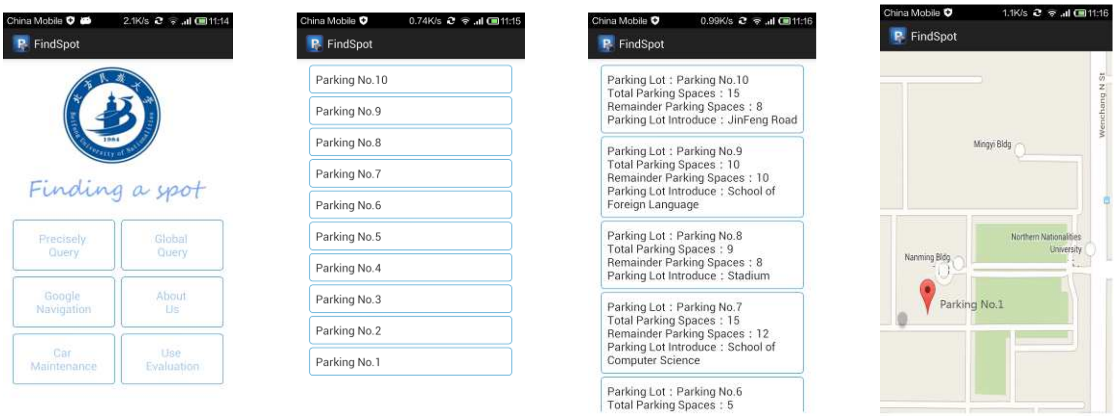
China Mobile 2.1K/s 11:14
FindSpot
Finding a spot
Precisely Query
Global Query
Google Navigation
About Us
Car Maintenance
Use Evaluation
China Mobile 0.74K/s 11:15
FindSpot
Parking No.10
Parking No.9
Parking No.8
Parking No.7
Parking No.6
Parking No.5
Parking No.4
Parking No.3
Parking No.2
Parking No.1
China Mobile 0.99K/s 11:16
FindSpot
China Mobile 1.1K/s 11:16
FindSpot
Wenchang N St
Mingyi Bldg
Northern Nationalities University
Nanming Bldg
Parking No.1

Parking Lot：Parking No.10
Total Parking Spaces：15
Remainder Parking Spaces：8
Parking Lot Introduce：JinFeng Road

Parking Lot：Parking No.9
Total Parking Spaces：10
Remainder Parking Spaces：10
Parking Lot Introduce：School of Foreign Language

Parking Lot：Parking No.8
Total Parking Spaces：9
Remainder Parking Spaces：8
Parking Lot Introduce：Stadium

Parking Lot：Parking No.7
Total Parking Spaces：15
Remainder Parking Spaces：12
Parking Lot Introduce：School of Computer Science

Parking Lot：Parking No.6
Total Parking Spaces：5

(a)Home screen (b)Precisely query (c)Global query (d)Map location

Fig.6 Client interface

The implementation of Web server. The server of university parking query system has two major functions, (1) Obtaining parking information automatically. Constantly getting parking information and updating guarantee users can obtain the latest data. (2) Adding and managing parking information manually. Managers could add some information and modify error information manually. Fig.7 shows part of Web server interface.

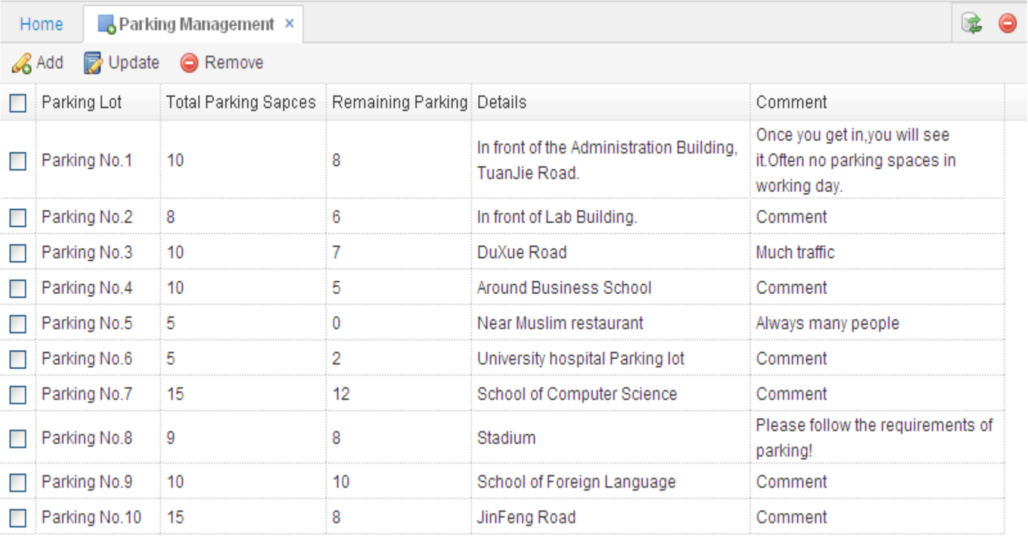

☐	Parking Lot	Total Parking Sapces	Remaining Parking	Details	Comment
☐	Parking No.1	10	8	In front of the Administration Building, TuanJie Road.	Once you get in,you will see it.Often no parking spaces in working day.
☐	Parking No.2	8	6	In front of Lab Building.	Comment
☐	Parking No.3	10	7	DuXue Road	Much traffic
☐	Parking No.4	10	5	Around Business School	Comment
☐	Parking No.5	5	0	Near Muslim restaurant	Always many people
☐	Parking No.6	5	2	University hospital Parking lot	Comment
☐	Parking No.7	15	12	School of Computer Science	Comment
☐	Parking No.8	9	8	Stadium	Please follow the requirements of parking!
☐	Parking No.9	10	10	School of Foreign Language	Comment
☐	Parking No.10	15	8	JinFeng Road	Comment

Fig.7 Web server interface

Conclusions

This study is based on Android and Image processing. It is designed for both the college staffs and visitors. It could improve the efficiency of parking spaces and also reduce users' time spending on finding parking space. This is obviously much more meaningful from saving energy consumption and campus management angles.

Acknowledgements

This work was financially supported by the Scientific Research Program of Beifang University of Nationalities (2013XYZ030), Innovation Program of Beifang University of Nationalities (XJCX-JS-104).

References

[1] Hongfeng Xu. A passenger-oriented traffic information-releasing system based on GSM Short Message [D].Chang An University, 2004, in Chinese
[2] Information on http://opencv.org
[3] Gang Li, Ruili Zeng, Ling Lin, Mengjun Wang. Chinese Journal of Scientific Instrument, 28(7), 2007, pp.1323-1327, in Chinese
[4] Yingxu Lai,Zengfei Liu,Mao Li. Microcomputer Information, 22(10),2006, pp.62-65, in Chinese
[5] Zhan Qu,Chan Li. Joumal of Xian Shiyou University(Natural Science Edition), 26(1), 2011, pp. 95-98, in Chinese
[6] Information on http://www.google.cn/apis/maps/signup.html

Applied Mechanics and Materials Vol. 596 (2014) pp 914-917
© (2014) Trans Tech Publications, Switzerland
doi:10.4028/www.scientific.net/AMM.596.914

SQL Server Access Methods Based On LabVIEW

Zuwei Zhu[1, a], Juexiao Chen[2,b] and Zechang Sun[3,c]

[1]Clean Energy Automotive Center, Cao’an Road 4800#, Shanghai, P.R.China

[2]Clean Energy Automotive Center, Cao’an Road 4800#, Shanghai, P.R.China

[3]Clean Energy Automotive Center, Cao’an Road 4800#, Shanghai, P.R.China

[a]zhuweimbxk89@163.com, [b]chenjuexiao@tongji.edu.cn, [c]sunzechang@fcv-sh.com

Keywords: LabVIEW, SQL Server, database access

Abstract. Several methods that contribute to connecting SQL server database with LabVIEW are listed and compared in the paper, while the method of using LabSQL is exemplified to show its convenience and reliability. Two steps are required to achieve the connectivity between database and LabVIEW via LabSQL: First is setting up an underlying connection between database and LabVIEW through ODBC. Second is using SQL statements to realize specific database operations such as query, insert, delete etc.

Introduction

LabVIEW (Laboratory Virtual Instrument Engineering Workbench) is an integrated programming environment introduced by NI Company, which is applicable for the engineering fields of data acquisition, instrument control, monitoring and measurement [1]. Since LabVIEW combines several functions of data acquisition, data analysis and data display as a whole, it can be used to realize a complete set of data processing solution conveniently [2].

In the process of software design using LabVIEW sometimes it is necessary to store, manage and query large amounts of data [3]. As LabVIEW does not belong to database management software, a method should be found out to connect LabVIEW and database. Now several relative methods are proposed mainly including:

-Calling dynamic link library

Because LabVIEW can be connected to dynamic link library via its own Call Library Function Node (CLN), there is an indirect method to inject relevance into LabVIEW and database. Firstly, a DLL should be developed using some programming language such as Visual C++. Then CLN should be used to call this DLL file for the purpose of connection [4]. It would be safe to say that this method is difficult for those non-professional developers because complex Windows underlying program has to be adapted.

-Using LabVIEW SQL Toolkit

LabVIEW SQL Toolkit integrates advanced functional package modules that can manipulate a variety of database. That is to say, LabVIEW can be connected to database directly by employing the toolkit without SQL language. Although the toolkit supports ODBC or OLE DB compatible database drivers [5], it is expensive to most users.

-Using Active X

It is also a practicable way to use SQL language to access database by calling Microsoft ADO control of LabVIEW.[6] The advantages of this method are high-speed, resource-saving and easy-to-use, whereas the main disadvantage is that it requires familiarity with Microsoft ADO control and SQL language to adapt Windows underlying program.

-Using LabSQL

LabSQL is a free and open source toolkit for data access to any ODBC library such as SQL Server, Access and Oracle. Users only need to call LabSQL functions to access database while LabSQL appears in function panel of LabVIEW interface after installation. The biggest advantages of this method are that it is easy to comprehend and operate so that only simple programming is needed.

In summary, LabSQL has features of free, open source and easy-to-use, so that the paper focuses on how to connect LabSQL with database.

Principle of database access based on LabSQL

The principle of database access based on LabSQL is depicted in Fig.1. Since LabVIEW supports ActiveX, user can exploit classes and objects provided by ADO controls to access, edit and update database indirectly, combining SQL language and ODBC (Open Database Connectivity) interfaces between applications and database. ADO controls include three main modules:

-Command module is used to finish a series of basic ADO operations, such as create or delete a command etc.

-Connection module aims at managing connectivity between LabVIEW and database.

-Recordset module works to manipulate records in the database, such as create or delete a record, modify a field etc.

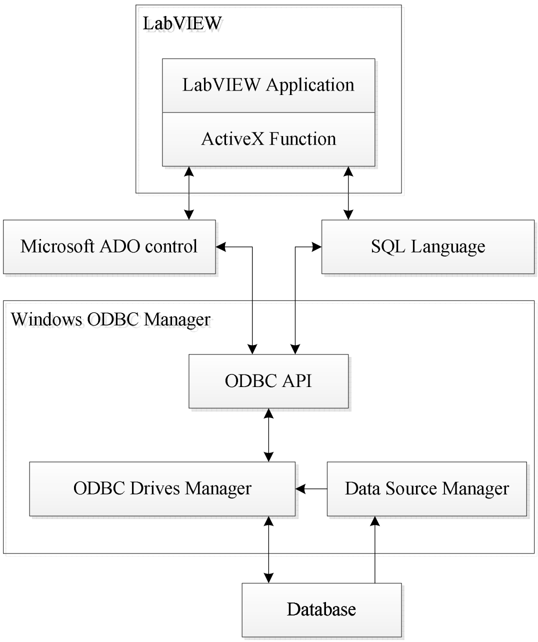

Fig.1 Access database model by use of ADO and ODBC

According to this principle, user can complete the connection and access operations between LabVIEW and database based on LabSQL.

An Example for database access based on LabSQL

This section will illustrate the database access method based on LabSQL by an example of an educational administration information management system that is developed on LabVIEW 8.5 and SQL Server 2008. The database includes a student information table. Now we want to insert a new record with its name field of “Li Si” into the first place. There are two steps to solve this problem.

Firstly, an underlying connectivity should be set up. The concrete process is as following:

-Enter Windows “Control Panel”, double-click “Administrative Tools” icon, then select “Data Sources (ODBC)” icon and enter the “ODBC Data Source Administrator”.

-Click “System DSN” tab, then select “LabVIEW” and click “Add” button, select SQL Server as the target data source. In the pop-up dialog box “Create a New Data Source to SQL Server”, fill in the corresponding name of “student number” and server.

-Test the underlying connectivity. The result of “the test is successful” indicates that underlying connection of LabVIEW and SQL server has been established successfully.

Secondly, LabSQL function should be called to complete operations:

-Find LabSQL module in the user libraries of LabVIEW, call ADO Connection Create.vi in Connection module to create a Connection object.

-Call ADO Connection Open.vi in Connection module and specify the database name with the same string of the data source name in ODBC manager. Here the name should be “student number”, so DSN=student number in Fig.2.

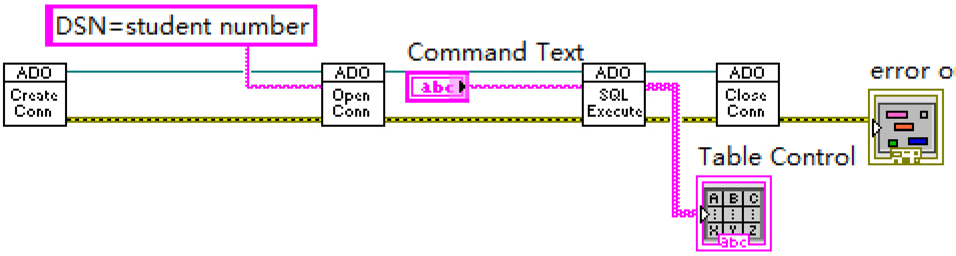

Fig.2 Block diagram of accessing database based on LabSQL

-Call ADO SQL Execute.vi and write SQL command in “Command Text” to manipulate the database. An output port is connected in the terminal to display the results. At this moment, several SQL commands should be executed to finish the action of record insertion:

---A select query command is input in “Command Text” to show all records. The results are displayed in the table control, as shown in Fig.3.

*select * from [educational administration information management system].[dbo].[student information table]*

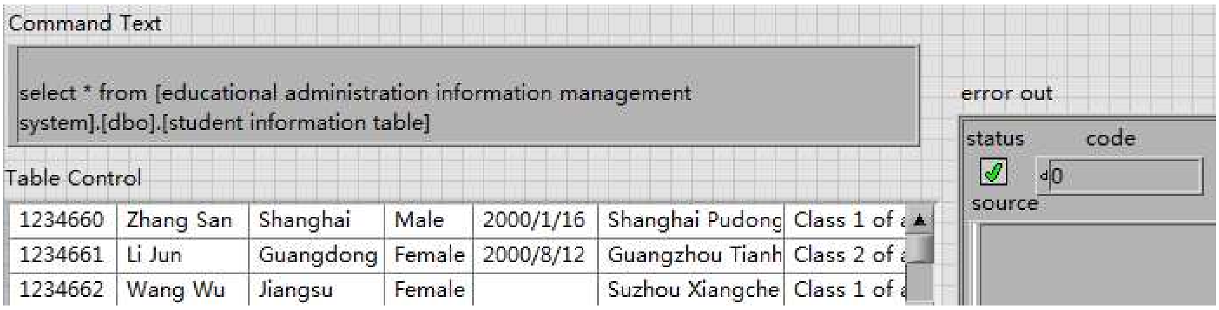

Command Text

select * from [educational administration information management system].[dbo].[student information table]

Table Control

1234660	Zhang San	Shanghai	Male	2000/1/16	Shanghai Pudong	Class 1 of
1234661	Li Jun	Guangdong	Female	2000/8/12	Guangzhou Tianh	Class 2 of
1234662	Wang Wu	Jiangsu	Female		Suzhou Xiangche	Class 1 of

error out

status ✓ code 0

source

Fig.3 Original student information table

---A insert command is input in “Command Text” to insert a new record with “1234555” as its student number. The result is shown in Fig.4.

insert [educational administration information management system].[dbo].[student information table] values(1234555,’Li Si’, ’Beijing’, ‘Male’,’1999/12/28’,’Beijing Haidian’,’Class 1 of automotive school’,’’,’’,’’)

*select * from [educational administration information management system].[dbo].[student information table]*

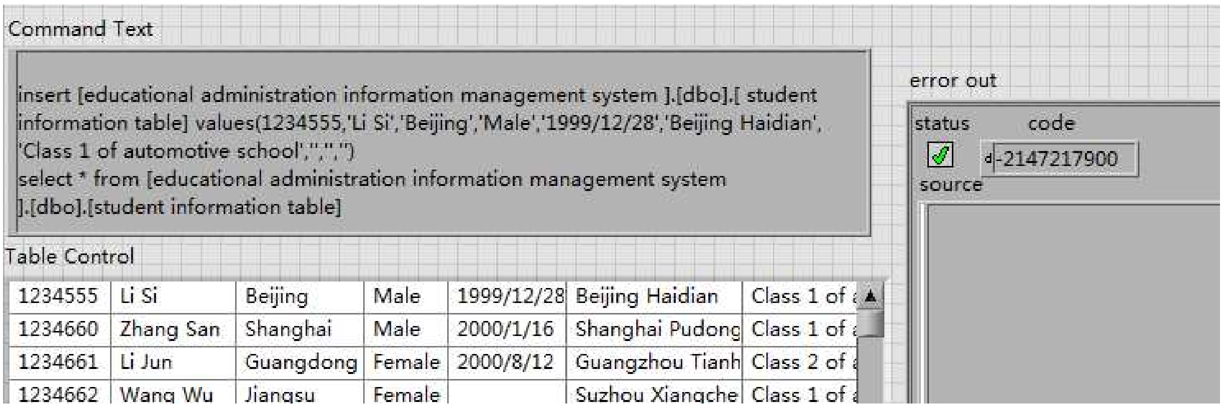

Command Text

```
insert [educational administration information management system ].[dbo].[ student
information table] values(1234555,'Li Si','Beijing','Male','1999/12/28','Beijing Haidian',
'Class 1 of automotive school','','','')
select * from [educational administration information management system
].[dbo].[student information table]
```

Table Control

1234555	Li Si	Beijing	Male	1999/12/28	Beijing Haidian	Class 1 of
1234660	Zhang San	Shanghai	Male	2000/1/16	Shanghai Pudong	Class 1 of
1234661	Li Jun	Guangdong	Female	2000/8/12	Guangzhou Tianh	Class 2 of
1234662	Wang Wu	Jiangsu	Female		Suzhou Xiangche	Class 1 of

error out

status ☑ code -2147217900

source

Fig.4 Result after record insertion

---Apply ADO Connection Close.vi to close Connection object, thus connection between SQL database and LabVIEW is disconnected.

In addition, error out.vi function comes after ADO Connection Close.vi in this example in order to facilitate the analysis process of debugging.

Conclusions

The connection methods between LabVIEW and SQL Server have been investigated. The following conclusions can be drawn:

-The method of connecting LabVIEW and SQL Server via LabSQL is a good option.

-There are two main steps to realize connectivity. First is setting up an underlying connection between database and LabVIEW through ODBC. Second is using SQL statements to meet the requirements.

Acknowledgements

This work was financially supported by the National Key Scientific Instrument and Equipment Development Projects (2012YQ150256).

References

[1] Binbin Zhang, Junpeng Shao, Wanru Jin and Qingquan Liu. *Journal HARBIN Univ.SCI.&TECH.*, 2005, 10(1): p14-16 in Chinese.

[2] Qiuye Sun, Ang Liu and Yunshuang Wang, in: Quickstart and Improve with LabVIEW 8.5[M], *Xi'an Jiaotong University Press*, 2009, p3-7 in press in Chinese.

[3] Huan Zhou, Jun Mo, Daisheng Li and Wenzheng Liang. *Chinese Journal of Scientific Instrument*, 2009, 30(6): p321-324 in Chinese.

[4] Shunxiang Ji, Wangsuo Liu and Xiaoting Song. *SHIP&OCEAN ENGINEERING*, 2007, 36(3): p125-128 in Chinese.

[5] Guiming Zhao and Zhiliang Zhao. *ELECTRONIC TEST*, 2008, 9: p49-53 in Chinese.

[6] Renping Yin, Gang Liu, Lixin Wang and Yunsheng Qiao. *ELECTRONIC MEASUREMENT TECHNOLOGY*, 2006, 29(3): p51-52 in Chinese.

Applied Mechanics and Materials Vol. 596 (2014) pp 918-922
© (2014) Trans Tech Publications, Switzerland
doi:10.4028/www.scientific.net/AMM.596.918

A Discussion on the Electromagnetic Compatibility of Data Center

Zhao Xiaoe

(Hunan Urban Construetion College, Xiangtan, 411103, China)

Keywords: Data Center; Electromagnetic Compatibility; Electromagnetic Interference

Abstract: In order to be accustomed to the highly developed information technology, data centers were widely established in many places in China. Due to the fact that data center only occupies a small space but with a plenty of equipment, and has the intensive power density, complex power distribution, a rich source of electromagnetic interference and substantial susceptible device susceptors, the issue of electromagnetic compatibility is being highlighted. This research launched a discussion on electromagnetic compatibility of the data center from five aspects: interference source, transmission channels, sensitive elements, danger and consequences of the electromagnetic interference, and the technology to fulfill electromagnetic compatibility.

Electromagnetic compatibility refers to the "coexistence of each electric equipment and system without causing the unexpected performance degradation in the condition of limited space, time and spectrum resources." As the rapid development of electrical & electronic technology and the broad application of electromagnetic equipment and system, the radio technologies like communication and broadcast have been widely applied by people. They gradually discovered the severe impact of the electromagnetic equipment on the related environment during their application of such appliances, and also further focus on the contradiction that appears between equipment, conflicts between equipment and system, incompatibility between systems, clash between equipment and system, and human and natural environment.

Electromagnetic interference is indeed consisted of three parts: interference source, transmission mediums and sensitive apparatuses. Interference source refers to the components, apparatuses, equipment or natural phenomenon that generates the electromagnetic interference. Transmission mediums are coupling paths and channels of the electromagnetic interference. The major transmission approaches for electromagnetic interference include radiation, transmission and sensing (capacitive sensing and inductance sensing). Sensitive apparatuses mean equipment that responds to the electromagnetic interference.

The rapid development of the informationization leads to the consolidation of connection of information network to people's life. Along with the enhancement of information content circulated in people's communication, the data volume transmitted by the information network also goes up, which demands the advancement of process, transmission, storage and management of network data. To follow the pace of development of information network, data centers, which are used to store important data processing apparatuses, storage equipment, network devices and computer protective equipment, have been broadly established in almost each place in China. Features of the data center are mainly demonstrated in its small space, multiple devices, high power density, complex power distribution, numerous electromagnetic interference sources, and many sensitive apparatuses. These features contributed to the terrible electromagnetic environment of the information computer room, highlighting the electromagnetic compatibility in the data centers.

Major Components of the Data Center

A data center is mainly consisted of three parts, which are the business information system, power supply and distribution system, and the computer room monitoring and maintenance system. The business information system is the core to the data room, with responsibilities to dispose of, transmit, store and manage data. The remaining two systems functionally serve the business information system, which contains the managerial, storage, exchange and transmission devices. The power supply and distribution system offers power supply to the data center, guaranteeing the operation of entire system. The power supply and distribution system is consisted of some apparatuses of the low-voltage distribution system, including transformers, low voltage switch box, disconnector, distributing cables and illuminators. The computer room monitoring and maintenance system functions to monitor the operation of the computer room and exerts control and management if necessary, in order to avoid malfunctions. This system is mainly consisted of fire extinguishing system, air conditioning system, security system, environment-monitoring system, and building automation system.

Major Interference Source to the Data Center

There is a broad source for interference against the data center. Based on the source, it is proper to classify the interferences into the internal and external ones. Specifically, they can be further categorized into the following type:

Inartificial Interference Source: For instance, natural noises (thunders), solar noise and cosmic noise belong to this category, among which the electromagnetic interference generated by thunders is of the greatest harm, which has become one of the major interference source in data room. There are two possibilities for the thunders to damage the data room: the first one is that once the thunder gets closed to the data room, it will directly place the data equipment of the data room under danger through induction while the other one is that a powerful current, which will be generated by thunder when it is transmitted in the wire of power system, is being directed to the data center through the wire and damage the equipment.

The electromagnetic interference generated by the transformer: Due to the high power density of the data room, the electrical load is also comparatively heavy. The number of the transformers is therefore larger. The transformers with stronger power are identified as one of the major interference sources of the data center.

The cut-off of the heavy current will generate the huge surge current with the tremendous rate of change, which leads to the production of powerful electromagnetic interference.

A plenty of the switching power supplies like UPS are demanded due to the fact that the power supply to data center must be reliable. The high frequency cut-off of the switching elements of the switching power supply will produce the ultraharmonics, which results in the electromagnetic interference.

The business information system is the cabling system, which is indeed passive. However, after it has been connected to other high frequency network equipment and formed a system, it works as an important part of the active equipment. The high-frequency signal transmitted by the cabling system will constitute the electromagnetic radiation which will lead to the production of electromagnetic interference while influence the electromagnetic environment. The electromagnetic radiation will also produce some information security problem regarding the cabling system. When the surrounding electromagnetic environment gets worse, the cabling system, which is indeed the sensitive element, will be severely interfered. As a result, its performance is being impaired.

The cable laying channels of the data room is very small if compared to its inner wire. Thus, when the strong and weak current crane span structures and high-frequency and low-frequency wire assemble, the strong current and high-frequency wire will exert interference over the weak current wire. Because of the lower pressure system, the voltage of the wire is also low. The inductive interference is mainly the inductance interference. Despite of the weak inductive interference of a single interference source, the total interference generated by a lot of the wires piled up will be great.

In addition to the major interference sources mentioned above, the power equipment and illuminative equipment of the data center also work as the interference source.

Sensitive Element of the Data Room

There are a plenty of the low voltage equipment in the data center, such as network controller, security monitoring host, environmental control host, and site inspection control equipment. These equipment are all the sensitive elements vulnerable to the electromagnetic interference. Diagram demonstrates the electromagnetic interference occurring in the data room. The interference source in the outermost layer will influence the sensitive elements in the innermost layer by coupling methods like radiation, transmission and induction.

Major Consequences Caused by Electromagnetic Interference

Along with the development of the microelectronic technique, computer technology has developed towards the high-speed, high-sensitivity, highly integrated, and multifunctional direction. The so-called “system” has already been the complex equipment for information low-voltage transmission, composed of various components and many sub-systems. The high speed and high density will worsen the system radiation while the low voltage and high sensitivity will impair the interference resistance of the system. Thus, the interference from the electromagnetic environment will always influence the internal part of the system, and vice versa. Such a mutual influence will threaten the stability, reliability, and security of the computer and digital system. The followings are the negative effects:

Cause the damage on the storage equipment like hard disks and magnetic tape units, leading to the loss of data.

Cause the logical errors in the process, exchange and control of the signals, impair the integrity of the communication data, enhance the transmission error code, and distort the signals.

Result in the instability of the display of monitors like the displayer of workstation, display screen of the monitoring center and others.

The peak interference caused by lightning stroke can result in the fake trigger of the logical circuit. For the worse case, the equipment may be damaged or destroyed.

Worse electromagnetic environment, along with the powerful electromagnetic interference, will severely influence the health of employees.

Technologies demanded for the electromagnetic compatibility

Noting from Diagram 3-1, the electromagnetic interference is composed of three parts, the interference source, transmission mediums, and the sensitive elements. Absence of any of these three components will lead to the failure of production of electromagnetic interference. Thus, to reduce the electromagnetic interference and improve the electromagnetic compatibility, it is essential to reduce the interference source, suppress the transmission of electromagnetic interference, and improve the interference resistance of the sensitive elements. The concrete measures are as followed:

Shielding Technology

Shielding is an effective approach to suppress the transmission of interference. One application of shielding is to place the equipment into a metal box which is connected to the ground. This application, on one hand, reduces the electromagnetic interference from the equipment on the environment. On the other hand, it increases substantially the interference resistance of the equipment. The typical design which incorporates this shielding technology is as followed: install the power supply equipment into the metal power distribution cabinet which has been properly connected to the ground. The other application of shielding technology is to shield the wires. For instance, wires in the cabling system are the major interference source as well as the sensitive elements. Through shielding the cabling system, it will be successful to reduce the electromagnetic interference from the cabling system on the environment. Furthermore, this application can also improve the interference resistance of the cabling system while reduce the interference it receives. With this application, the information security can also be improved. To shield the cabling system, it requires adding the shielding net to the ordinary cabling system, in order to realize the shielding of the wires of this system. There are a lot of the wires, which have been used to transmit the analog signals. The analog signals have a poor interference resistance. Therefore, it is a must to shield these wires.

System connected to the ground

Connecting the wires of related equipment to the ground is the important measure to improve the reliability, suppress noise, guarantee security, and avoid interference from thunders and lightening. The quality cabling and ground connection can improve the interference resistance of the data room while the interference emission of the data room will be mitigated. Theoretically, a reasonable earth connection point is a zero potential and zero impedance object, which is also the reference point to all electric signals of all related circuits. It is called the zero potential point, which will not generate any additional voltage drop even though currents run through it. However, there are two instances of the earth connection cannot be ignored: the first is that the ground impedance should not be zero while the second is that the earth connection point of the reference potential of the equipment operational signal is generally the protective earth connection point of many electric equipment.

Due to the fact that the ground resistance cannot be ignored, different earth connection points cannot reach the equipotential and therefore will have certain voltage in between. As a result, the earth connection interference will be generated. Therefore, it is essential to reduce as many ground resistances as possible. Indeed, what the data room of the data center dose is exactly to form a 600X600 grounding network in the core data room by copper foil, and to connect the equipment cabinet to the grounding network by red copper bar.

Smoothing is an important approach to resist the electromagnetic interference, through which some interference harmonic waves, decaying impulse noises, peak noises, harmonic waves and other signals will be reduced. Also, the harmonic waves of the power distribution system, due to the effect of smoothing, can also be mitigated. Thus, the smoothing can improve the stability of power distribution while function to reduce the electromagnetic interference and harmonic waves pollution. Especially for the switching power supply, due to the fact that the high frequency connection and disconnection of the switch will produce a lot of high frequency harmonic waves, leading to the production of electromagnetic interference. The smoothing method can function to filter these harmonic waves and the electromagnetic interference will be substantially reduced as a result.

More Reasonable Cabling

Electromagnetic interference can reduce the distribution parameters between wires and the coupling of the electromagnetic interference, and improve the electromagnetic compatibility, via reasonable cabling based on the distributed capacitance and inductance of the wires.

These are four important methods to resist the electromagnetic interference. In addition, it is also proper to add the surge protective devices in order to avoid the lightening and thunders and the physical partition between power equipment and the information devices.

Conclusion

Data center embraces a poor electromagnetic environment, with a lot of the sensitive elements. Therefore, the degree of electromagnetic compatibility can directly influence the operation of the equipment. When designing the data room, it is of vital importance to pay attention to the electromagnetic compatibility and optimization of the electromagnetic environment, in order to improve the stability of the data room.

Reference

[1] Gao Yougang. “A General Discussion on Electromagnetic Compatibility” [M]. Beijing: Beijing University of Posts and Telecommunications Publishing House, 2001, 5.

[2] Bai Tongyun, Lv Xiaode. “Electromagnetic Compatibility Design” [M]. Beijing: Beijing University of Posts and Telecommunications Publishing House, 2001, 3.

[3] Zhou Kaiji, Zhao Gang. “Rationale of the Electromagnetic Compatibility” [M]. Harbin: Harbin Institute of Technology Press, 2003, 7.

[4] Yang Shizhong, Xing Lijuan. “Electromagnetic Compatibility of the Cabling System” [J]. Low-Voltage Apparatus, 2007 (16)

Applied Mechanics and Materials Vol. 596 (2014) pp 923-926
© (2014) Trans Tech Publications, Switzerland
doi:10.4028/www.scientific.net/AMM.596.923

Design of a Mobile Client Application based on Android Platform

Changxing Qi

Software College, Shenyang Normal University, Shenyang, Liaoning, 110034,China

84448671@qq.com

Keywords: Android, Interface, MVC (Model-View-Controller)

Abstract. This paper describes the process and mothods of a mobile client application.The application uses JAVA, Google ADT, MyEclipse as the language and tools. and uses the MVC(Model-View-Controller) pattern. The main functions including news display;Blog showing, Blog comment; portal Information; Forum levy; Online login and so on. In addition, introduces the analysis and design of the application.

Introduction

Android is specially designed for mobile devices software platform. The Android application program is developed with Java language,and need virtual machine based on Dalvik.The system uses the popular Java integrated development environment MyEclipse，Java SDK of SUN .company, Google Android SDK. At the same time, need to install ADT on MyEclipse.

MVC is a design pattern which devides the application into three core modules: model, view, controller.They handle their own tasks.The view is the interface for users to see and interact.Its features include displaying related data,accepting user input to model queryservice status,acceptance model a data update events to the user,so as to update the user interface.The model is used to represent the business data and business logic which is the main part of the application.A model can provide data for multiple views,thus improves the reusability of the code. The controller receives the user's data and calls the model and view to accomplish the user demand.[1]

Requirements

Business. The main target of the application is sharing data and information. In The remote database as the carrier, downloading data and uploading data in asuitable time and providing users good experiences.

Analysis from the perspective of data processing.Smalldata should be downloaded into the local database before users look up. The local database should be adapted to local function,so pretreatment.should be handled before the data be downloaded.

Analysis from the user's perspective. When the user is logged in, who can view the related information,and enter the information synchronization which are transfered to remote server.

Data.including the data client required.

Users information:including the ID,name,mobile,photo, professional,grade and so on.

News. Can only be released by the administrator,contains the title and content.

Blog. User can create,by all users can create.including the title, content, classification, date, etc.

Comments. Binding in the blog, all sers can create,including the content,date,etc.

Trash talk. Any issue,including the content,date,etc.

Design

Database. Choose the local database Sqlite that Android built-in ，at the same time， some static classes are used to implement the real-time data storage.

Tables of server. permission, user_login, role, role_permission, counter, operate_log, user_info, blog_replies, blog, news, resource, resource_type, home, message.

Tables of mobile client. News，blog，message，reply.Data saved in tables related with the tables of server by table name.

Functions.The application including serveral modules as follow:

Log in module:input the user name and password, after Verificated, prompt result message and turn to navigation page.at the same time,download the data from remote server.

News module. Show the listview of news ,provide the freshing function.download data automaticly.if click the list ,display the details.

Blog module. Show the listview of Blogs,provide the freshing function,download data automaticly.the users can add the comments of blog and upload to server automaticly.,

Personal module. Show personal all information and provide the function of searching own listview of blog and comments.Even can query details.

Others modules. Provide several interfaces including navigation page. Describes the content in detail.

Fig1 is the structure of the client application .

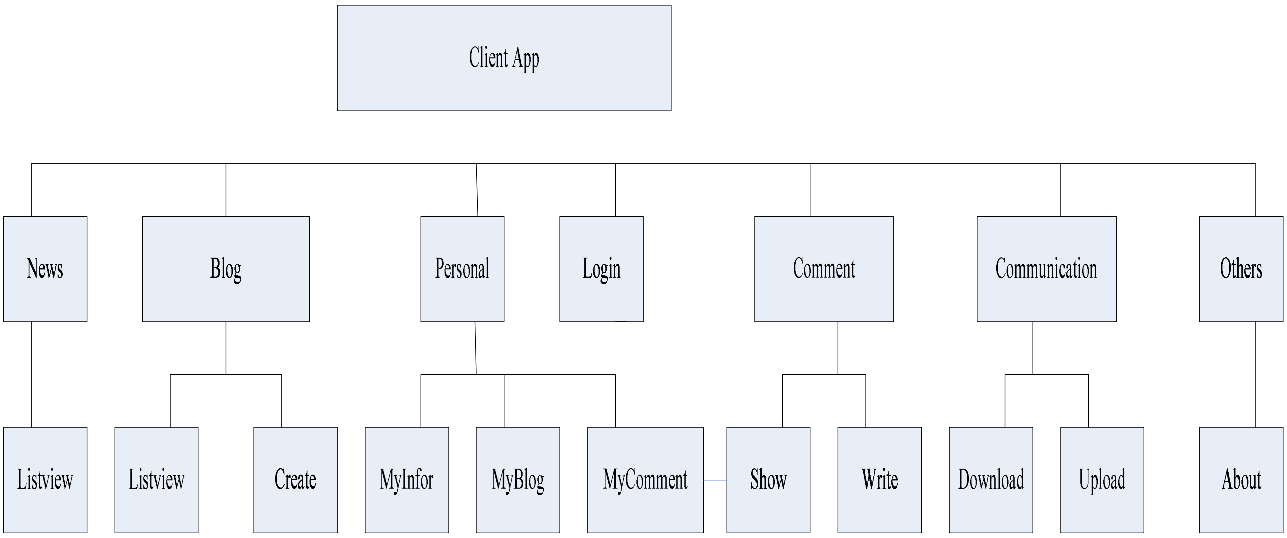
Client App
News
Blog
Personal
Login
Comment
Communication
Others
Listview
Listview
Create
MyInfor
MyBlog
MyComment
Show
Write
Download
Upload
About

Fig1 Functions of App

Interface for displaying. Fig1 shows the main interfaces for display by using the Activity .

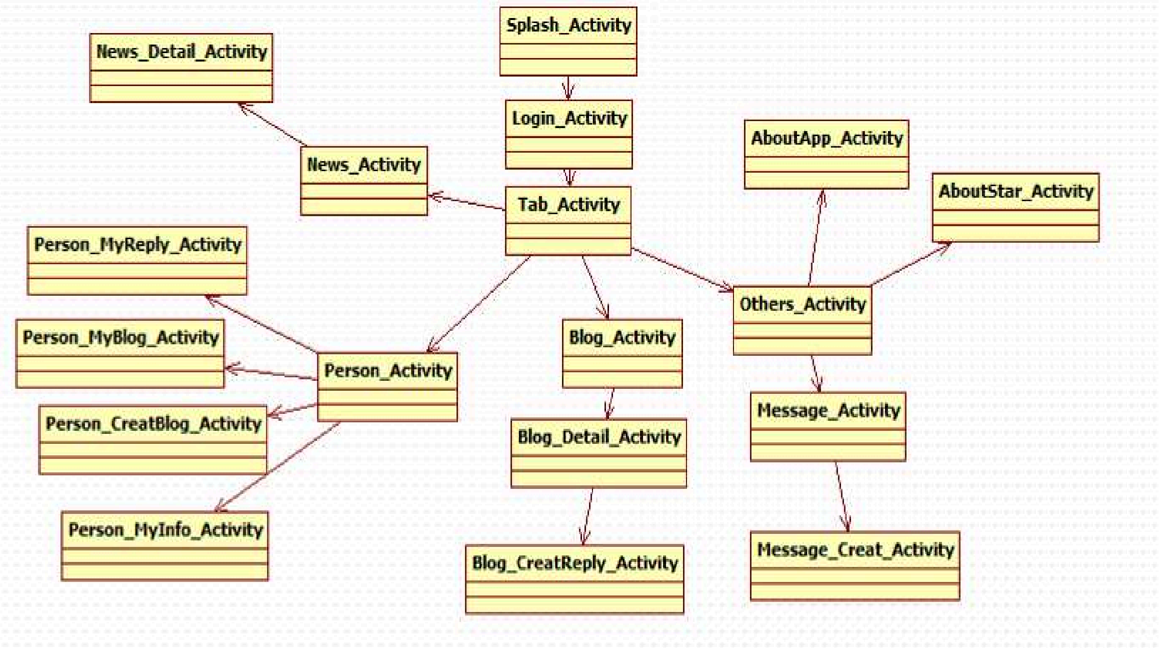
Splash_Activity
News_Detail_Activity
Login_Activity
AboutApp_Activity
News_Activity
Tab_Activity
AboutStar_Activity
Person_MyReply_Activity
Others_Activity
Person_MyBlog_Activity
Blog_Activity
Person_Activity
Message_Activity
Person_CreatBlog_Activity
Blog_Detail_Activity
Person_MyInfo_Activity
Blog_CreatReply_Activity
Message_Creat_Activity

Fig 1. Interfaces for display

Interface for communication. There are many classes in the Android SDK that can interact with the Web server. Socket class is related with TCP protocol,HttpPost class is related with Hypertext Transfer Protocol. Users can submit the data from client to server by using the setEntity method. The HttpResponse class can use the execute method to obtain the serverreturns a message

When need to transfer files,using the HttpURLConnection class, getInputStream and getOutputStream methods are used to obtain the input and output streams. Finally, the InputSream,OutputStream,FileInputStream and DataOutputStream classes can use write,writeByteand read methods read and write the input and output streams.For example, Launch the request at the client,Submitted to the server through HTTP protocol. After the server responds to the request. On the client,analysis XML files.to access data.

Post request are come from client to look up the blog information , the ShowblogServlet accept the request and transfer the request to Showblog,Showblog handle the request and call the database interface API of JDBCService and send request to database through JDBC.The database excute the SQL and send results to the program. ShowblogServlet navigate the results to JSP page.and packaged into a XMLfile sent to the client.the client analysis the XML file and get the data required.[2][3][4]

Fig 2 is the whole process of looking up the personal blog.

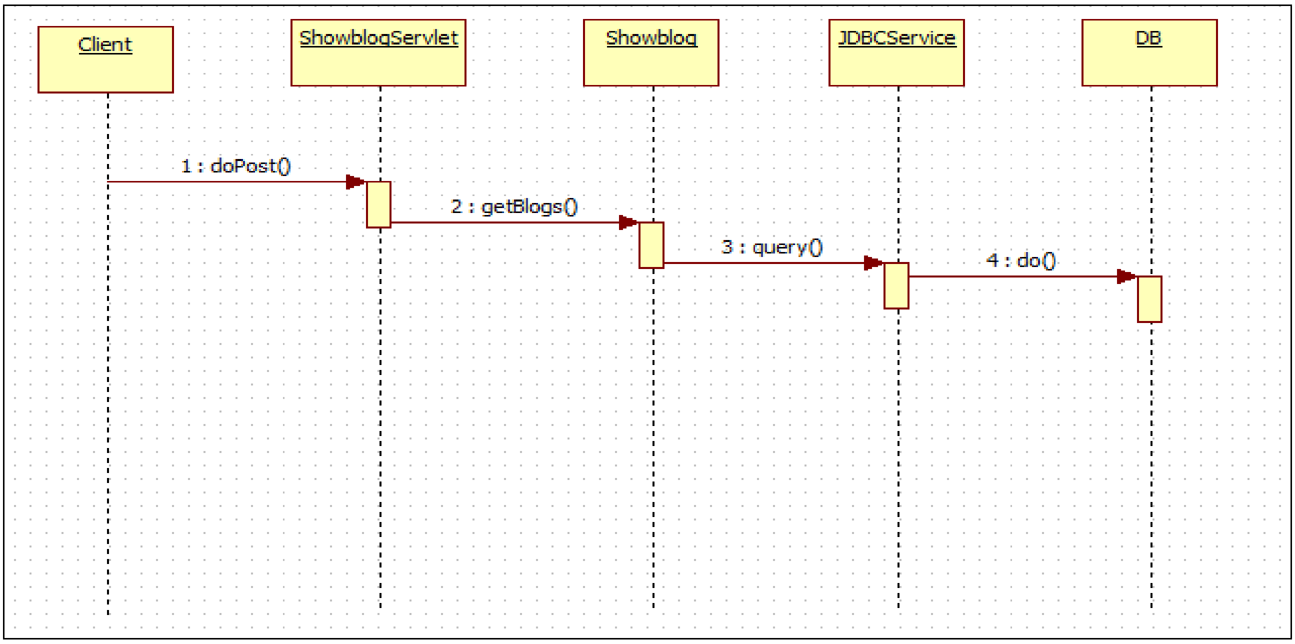

Fig 2 Whole process of looking up the personal blog

Interactive system. The interactive system is make up of mobile client app and the server.the mobile client app includes a receiving module and a string stringinitialization module, sending module, file sending module, receiving module . The Web server in the same module with basis,also increased the module,SQl statement execution module, feedback information synthesis module,filestorage module and the module information file.the above modules ensure the completion of communication.[1][6]

Conclusions

This paper firstly analyzes the implementation of relevant technology of mobile phone client application development based on the Android platform .and design ed and developed of a studio client instance. Combined with the Android mobile phone wireless communication technologyand the background server technology, design and realize the interactivesystem of the platform of mobile phone and the remote server,finally verified the system in real-time interactive,extended the advantages and efficiency. For smart device applications in the field of mobile platform(such as mobile commerce),has a certain practical value and reference value.

References

[1]PengFeng-ling， TuoXian-Guo， WangHong-hu， ZhangGui-yu， PuJian-hua.Computer Engineering and Design.2013 34(11):3907-3910

[2] BAO Wei. Agriculture Network Information 2013(7):29-32

[3] Lili Xu.Software Guide. 2013 11(11):87-89

[4] ShiMei-chun,LiangQing-ke.Beijing Survey 2013(3):68-72

[5] WU An-zhuang,JI Shu-ye. Surveying and Mapping of Geology and Mineral Resources. 2012, 28(2):32-34

[6] Zhang Xinyue. CHINA SCIENCE AND TECHNOLOGY INFORMATION.2014(8).148-149

Applied Mechanics and Materials Vol. 596 (2014) pp 927-930
© (2014) Trans Tech Publications, Switzerland
doi:10.4028/www.scientific.net/AMM.596.927

Multi-Domain Modeling and Co-Simulation Based on Modelica and Simulink

Guangshu Tian, Lichen Zhang
Faculty of Computer Science, Guangdong University of Technology,
Guangzhou 510006, China
297382002@qq.com, zhanglichen1962@163.com
*Guangshu Tian

Keywords: Multi-lomain modeling; Co-simulation; Modelica; Simulink

Abstract. A co-simulation solution based on multi-domain modeling with Modelica is proposed to achieve the co-simulation of multi-domain modeling and simulation environment with other simulation environment . Based on the connection mechanism of multi-domain Modelica models the co-simulation under S-function co-simulation framework is implemented using the converting principle between Modelica models and Simulink modules. A co-simulation example between MWorks which is a multi-domain physical system modeling and simulation tool based on Modelica and AMESim indicates that the method can extend the application of Modelica models and achieve the collaborative work with multi-domain modeling and simulation tools and other simulation software.

Introduction

Single-domain simulation environment supports the simulation of large-scale simulation has become a bottleneck, and the use of multi-domain modeling and simulation of physical unity and co-simulation technology become an effective way to solve the problem[1].

By divide complex physical model into a single field using multiple disciplines, the use of single-disciplinary professional software to establish the corresponding single domain model, data exchange and invocation by way of a single interactive interface between the fields of software, we can complex physical model emulation[2].

Currently, there are already international Modelica-based modeling and simulation tools[3], these tools are the basic unit of Modelica components, namely, the basic element in all areas of the system.Meanwhile, the co-simulation technology has been widely studied and applied.

(1) Co-simulation based on existing interface .

(2) Co-simulation based on HLA / RTI framework[4] .

This paper focuses on co-simulation technology to Modelica-based multi-domain modeling and simulation tool for physical systems and hydraulic joint professional advantages AMESim simulation software to illustrate the use of Modelica tools multidisciplinary field advantage and the advantage of AMESim hydraulic modeling and simulation methods to explore the use of multi-domain physical modeling software and professional advantages of software co-simulation approach, a detailed analysis software co-simulation method based modeling software interface for multi-domain simulation system based on Modelica simulation system technology combined with other construction Simulation mode and provides technical framework.

A Co-Simulation Interfaces

Modelica model uses mathematical equations to describe the physical laws and phenomena in different fields subsystems, according to the topology of the physical system, based on the language intrinsic component coupling mechanism, the model structure and multi-domain integration[5].

Object-oriented model is a mathematical model, based on its internal consistency of mathematical representation of the physical system, support for model components in a model that contains multiple fields, multi-domain modeling[6].

Modelica model is primarily dependent on its connector joint simulation. Modelica connector is an instance of the class constraint connector, usually as a model component class members to act as model components and external interfaces or ports. Figure 1 is Modelica Pin types of electrical components of the connector.

Established only between similar connection between the connector assembly, achieved through the equation, indicating Modelica support non-causal connection. Figure 2 is a three connections and the equivalent equation Pin Modelica code example.

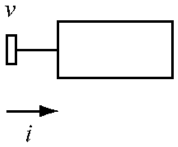

Fig. 1. Connector instance Pin

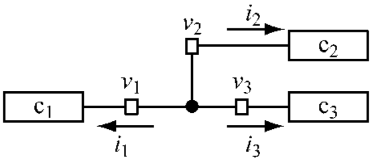

Fig. 2. Connection of three pin instances

In the United Modelica simulation model , Modelica models can also use the connector to communicate with other models. Figure 3 shows the relationship between the Modelica models and connectors , the input and output connectors in Modelica models can communicate with other models .

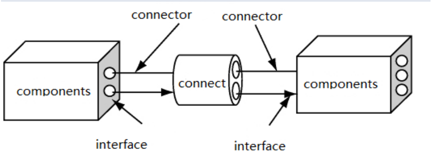

Fig. 3. Connection of three pin instances and the corresponding Modelica code and equations

AMESim and Simulink interface itself can be its own model to S-function block; while Modelica models can also be controlled at compile time, it generates the model S-function block, enabling multi-domain model with other Modelica simulation co-simulation environment model.

Co-simulation Environment

AMESim model and parameter settings compiled generation for Simulink using S-function, in the Simulink environment, using AMESim interface generate AMESim model includes other modules as an ordinary Simulink S-function added to the system Simulink model to achieve joint modeling and simulation AMESim and Simulink.

After the conversion, the model are S-Function, in Simulink simulation process.When performing conversion Modelica multi-domain model, the C code using Simulink S-function mechanism to convert Simulink model Modelica block converted Modelica model must meet the definition of a mathematical model Simulink block is met mathematical relationships. In Simulink, Modelica multi-domain model that will be created as a custom block is added to "SimulinkLibrary Browser", the control by setting the custom Mask and the callback function block parameter settings to achieve the block and block simulation states.

Joint simulation

Hydraulic machinery model is a complex system of hydraulic machinery hydraulic, mechanical, and control three-part.

Depending on the desired mechanical model, MWorks directly drag Modelica model library components, set a reasonable parameters for each component, and then use the tool to connect the connector to complete the various components to form a complete multi-domain modeling system. In the modeling process, in order to achieve the joint Modelica simulation model and other software models, data exchange with other software model Modelica models built between Modelica models need to be defined data interface, which is shown in Figure 4.

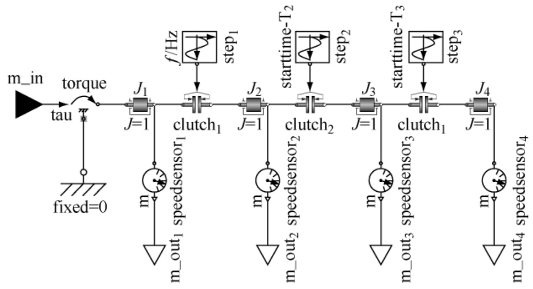
m_in
torque
tau
fixed=0
J_1
J=1
clutch$_1$
f/Hz
step$_1$
J_2
J=1
clutch$_2$
starttime-T$_2$
step$_2$
J_3
J=1
clutch$_1$
starttime-T$_3$
step$_3$
J_4
J=1
speedsensor$_1$
speedsensor$_2$
speedsensor$_3$
speedsensor$_4$
m_out$_1$
m_out$_2$
m_out$_3$
m_out$_4$

Fig. 4. Modelica model with the defined data exchange interface

Define an input interface and four output interface in Modelica model , as shown in Table 1.Receives external data by input interface, using output interface Modelica model to calculate the output data to other software model.

Table 1. Data exchange interface of Modelica model

Name	The interface description	Function
m_in	in_put (rad/s)	Exchange data with other model, the interface of receiving data
m_out1,m_out2 m_out3,m_out4	out_put (rad/s)	Ouput the inner data, the interface of inuput of outer model, the interface of checking inner data

After completion of Modelica models in many fields, the need to establish a joint simulation system hydraulic model. In AMESim directly invoke various hydraulic components module, a reasonable set of parameters for each component, can also use HCD library components required to build a model, and then connect the components into a complete hydraulic circuit. when modeling the actual Select the model library system components and the oil connection, and then set the model parameters. Optional CoSim general co-simulation interface, Figure 5 AMESim co-simulation of hydraulic models. In the co-simulation of hydraulic models require data exchange interface designed to achieve a hydraulic model input and output data. Table 2 is a hydraulic model of co-simulation interface. Figure 5 shows that the data model output angle of the hydraulic motor, while the other model inputs a control signal to be input thereto valve. Before making a joint simulation, the need for AMESim model to be compiled.

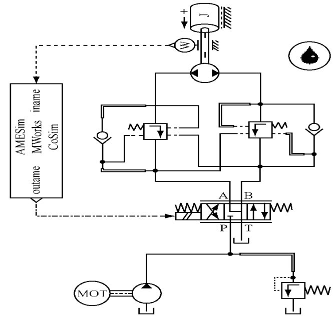
AMESim
MWorks
CoSim
outame
iname
A
B
P
T
MOT

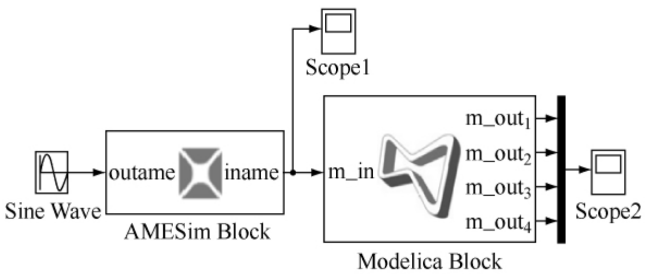
Scope1
Sine Wave
outame
iname
AMESim Block
m_in
m_out$_1$
m_out$_2$
m_out$_3$
m_out$_4$
Scope2
Modelica Block

Fig. 5. AMESim hydraulic model in co-simulation Fig. 6. Co-simulation model

In this case, the definition of hydraulic and mechanical model of the complete data exchange interface is converted to S-function module to achieve co-simulation in Simulink environment. Its Modelica simulation model of MWorks and AMESim hydraulic model are co-simulated , which are shown in Figure 6.Hydraulic model output hydraulic motor rotational angle is input of Modelica model. In this co-simulation model, the tool can be used Simulink AMESim model for feedback control. In the simulation, AMESim model and MWorks models were using their own solver, only through the interface exchange of data .

Table 2. Data exchange interface of hydraulic model

Name	The interface description	Function
iname	output (rad/s)	Output the angle data of hydraulic model of internal motor
outame	input (rad/s)	Receinving date from the interface of outer model

The simulation results combined simulation model is divided into two parts: a hydraulic model output signal (Figure 7) and mechanical model output signal (Figure 8), the output signal of the hydraulic model that motor angular velocity.

The above co-simulation model contains two parts: AMESim hydraulic model and multi-domain model MWorks Modelica, but also contains a power supply and an oscilloscope module Simulink. IIn each step, the output of the model are the output hydraulic pressure to the mechanical model for data exchange, at the beginning of the simulation, with enhanced hydraulic model input sinusoidal signal, the passage valve opening becomes larger, and thus the flow increases, so that the reverse rotation of the hydraulic motor increases, shown in Figure 7; when the sinusoidal input signal is reduced, passage opening is reduced, the motor speed decreases, gradually tends to 0. Mechanical model receives the input hydraulic model, the left two axis (J1 and J2) immediately starts to rotate, and the first rotary shaft 2 (J2) before the brake signal is sinusoidal, the angular velocity of the shaft starts to increase from 0. Another two shaft (J3 and J4) brake signal is step signal, the trigger signal for the time it is 1s and 2 s.

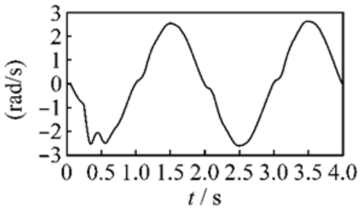

Fig. 7. Output signal of hydraulic model

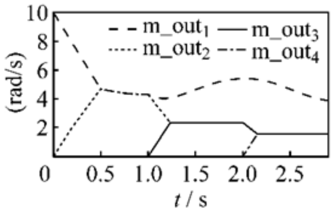

Fig.8. Output signal of mechanical model

Conclusion

For multi-domain simulation software and professional advantages of simulation software to their strengths, introduced Modelica , AMESim and Simulink models and interface technology, focusing on joint strategy between Modelica tools and AMESim. On this basis, the proposed S-function of Modelica models combined with other technical framework for modeling and simulation model based simulation software, and has been verified. This co-simulation modeling framework full advantage of unified modeling techniques and multi-domain co-simulation technology for multi-domain models, and it is fit for single-domain co-simulation models of complex systems.

References

[1] FRITZSON P, ENGELSON V. Modelica-A unified object-oriented language for system modeling and simulation [C]// ERIC H Proc 12th European Confon Object_oriented Programming, Brussels : Springer-Verlag, 1998:67-90.

[2] YUAN Pingpeng , CHEN Qingcha , KUANG Ping ,et al . Research on grid based union simulation platform[J] . J Huazhong Univ of Sci & Technol : Nat Sci , 2007 , 35(S2):1-3.

[3] WU Yizhong , LIU Min , CHEN Liping. Development of hybrid modeling platform for multi-domin physical system[J]. J Syst Simulation ,2006 , 18(1):120-124.

[4] CAO Qi , HE Zhongshi,YU Lei , et al . Technical framework on modeling of joint simulation based on HLA/RTI[J] . J SYsy Simulation , 2008 , 20(11) :2920-2924.

[5] ZHAO Jianjun , DING Jianwan, ZHOU Fanli , et al. Modelica and its mechanism of multi-domain unified modeling and simulation[J].J Syst Simulation, 2006,18(2):570-573.

[6] DING Jianwan, CHEN Liping , ZHOU Fanli , et al. Consistency analysis of complex declarative simulation models[J] . J Software,2005,16(11):1867-1875.

Applied Mechanics and Materials Vol. 596 (2014) pp 931-935
© (2014) Trans Tech Publications, Switzerland
doi:10.4028/www.scientific.net/AMM.596.931

The Design and Implementation of a Cross Platform Multimedia NetWork Classroom

Mengliang Shao

Department of Electronic Information Engineering, Guangzhou Nanyang College, Guangzhou 510925, China

shao_sml@163.com

Keywords: Multimedia network classroom, Cross platform, Java Technology, C/S.

Abstract. For the sake of the technology of multimedia network classroom under cross-platforms is becoming popular, this paper propose a analytic selection on system architecture and the development solution on the multimedia network classroom for the experence and requirement from teaching activity. We chooses Java for system design and implementation to achieve the goal of crossing platform, using the C/S communicating paradigm, MVC model, and giving the detailed description on the development to some key modulars such as connection with maintenance, screen broadcast, file transfer and remote control.

Introduction

Multimedia Network Classroom is a common computer room, a language lab, a multi-media room, or a Multimedia demonstration room, with other functions making an organic whole, using modern Network technology and Multimedia technology equipped with a number of Multimedia computers and related Network equipments connected by a Network teaching system. Multimedia technology and computer Network technology are combined with the typical applications to be used in teaching[1-2].

At present, teaching in the multimedia network classroom has been widely applied in all kinds of school environment, but mainly work on windows platform. With the popularization and application of Linux platform and other forms, developing cross-platform multimedia network classroom has a certain practical significance.

Overall system planning

Cross-platform for the realization of the system uses Java technology and has been given Java language platform neutrality.

This system uses C/S architecture, the teacher machine serves as the server side and students machine as the client side. In the multimedia network classroom system, students and teachers or students and students are independent to exchange and communicate, with the aid of network transmitting and controlling system realizing to get knowledge through the text, graphics, images, sound, animation and other multimedia information on the computer network or real-time transmission so as to make the teaching content more rich, lively and colorful.

In order to meet the functional requirements, the system needs to achieve the following goals [3-4] :

- The machine starts to support the software user to login and manage to ensure the safety in use;
- Software is adaptive, no manual settings, the teacher can automatically establish a reliable connection to the students, and maintain this connection for transmission to each other;
- The teacher can login to screen the student machine, radio and support electronic pointer, etc;
- The teacher machine and the students machines can perform file transfer;
- The teacher machine can monitor the screens of the students machines, that is the teacher can control the students remotely;

- The teacher and the students machines can send messages to communicate each other;
- The system can be used across platforms.

System design and function module partition

Software development planning. The client starts to join a multicast group, to get the server IP and port, and establish a TCP connection as a command channel to send commands to each other, and according to the command to start the corresponding function module; According to the function module needs, create a TCP or UDP for data transmission. figure 1 is for the system of software development planning:

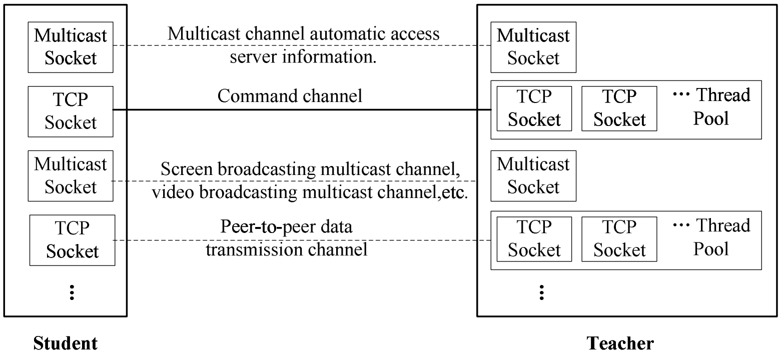
Multicast Socket
TCP Socket
Multicast Socket
TCP Socket
⋮
Multicast channel automatic access server information.
Command channel
Screen broadcasting multicast channel, video broadcasting multicast channel,etc.
Peer-to-peer data transmission channel
Multicast Socket
TCP Socket
TCP Socket
··· Thread Pool
Multicast Socket
TCP Socket
TCP Socket
··· Thread Pool
⋮
Student
Teacher

Fig. 1 System software development planning

System modules. According to the requirements analysis, the system is divided into the following functional modules shown in figure 2:

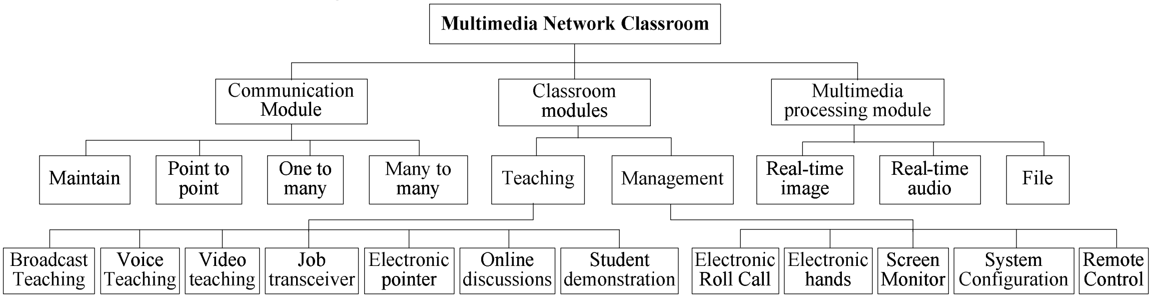
Multimedia Network Classroom
Communication Module
Classroom modules
Multimedia processing module
Maintain
Point to point
One to many
Many to many
Teaching
Management
Real-time image
Real-time audio
File
Broadcast Teaching
Voice Teaching
Video teaching
Job transceiver
Electronic pointer
Online discussions
Student demonstration
Electronic Roll Call
Electronic hands
Screen Monitor
System Configuration
Remote Control

Fig. 2 System modules

- Communication module

Machine is responsible for maintaining the connection between teachers and students and sending commands and responses, including peer-to-peer TCP connection, one-to-many UDP multicast, many-to-many mixed mode. The system of functional realization based on the connections between the teacher machine and the students machines.

- Class functional module and sending and receiving module

Mainly include: Screen, audio and video broadcast teaching function; Online discussion; Receive and send homework; Screen monitor module; Remote control module; User management.

- Multimedia processing module

Mainly includes real-time broadcast images, audio, video, and file information processing, including data collection, compression, transmission and receiving, parsing, and rendering, and so on. Given the high rate of LAN network (100 m bit/S: 12.5 MB/S [5]) of network bandwidth, to JPEG compression, image using fixed block compression [6];PCM sampling coding mode to the audio processing. The video using MPEG encoding.

System design in detail

Connection and maintenance module design. Teacher machine starts to create and maintain a UDP multicast group, which is used to automatically detect students' machine, and by using the IP multicast for school life told the teacher's computer and TCP port. Automatically start machines, students join the multicast group, send greeting to the multicast group information, and wait for the teacher machine’s reply information (teacher machine name, IP address, open to communicate with students machine, TCP port to send and receive commands). Teachers’ reply said contact machine, otherwise, the interval of time to send (default is 5 seconds).Students through the UDP multicast access to teachers machine IP and TCP port, and then establish a TCP connection with teachers machine, and exit the UDP multicast group after the interaction between teacher and students machines.

- The track links between the teachers and the students machine.

When the students’ machine through multicast to get related information from teachers, the students’ machine exit the multicast group, and then TCP connection sends requests to teachers. After the connection is successful, the teacher machine records the students’ information, after students and teachers communicate through the TCP connection machine.

- The operational commands of the teacher and the students machine.

When the teacher and the students machine connect successfully, through the TCP connection channel they can transmit various commands, and then students or teachers machines depend on the received command to start a new thread for various operations.Teachers and the students machine continue to receive various commands on the TCP connection channel and to decide how to continue operation.

- Operational command code tracking/reply of the teacher and the students machine.

The teachers and the students machine tracking/reply, send commands through the TCP connection channel, according to the different content of sending different operation [6]. Table 1 for the command code table:

Table 1 Part of the command code

Command string	*Operating functions*	*Sending direction*
HelloTeacher or HelloStudent	Welcome message transmitted between students and teachers machine	Teacher ←→ students
FileTran	File transfer	Teacher ←→ students
BeginFileTran	The teacher replies the requests transmitted by the students.t	Teacher ←→ students
EndFileTran	Stop file transfer	Teacher ←→ students
BroadcastScr	Screen broadcast	Teacher ←→ students
EndBroadcastScr	Stop screen broadcast	Teacher ←→ students
ScreenListen	Screen monitor	Teacher ←→ students
EndScreenListen	Stop Screen monitor	Teacher ←→ students
LiftUpHand	Electronic hands	Teacher ←→ students
Lock	Lock the student machine	Teacher ←→ students
Restart	Restart the student machine	Teacher ←→ students
Shutdown	Close the student machine	Teacher ←→ students
…	…	…

Screen broadcast module design. This module is mainly to realize the teaching by the selected machine screen broadcast to teach students. Due to performance considerations, using UDP multicast broadcast to improve the transmission efficiency. At the same time, multicast way won't increase the number of nodes on a network segment additional network traffic, so even if the increase in the number of students will not affect the performance of the network and broadcast teaching system, the speed of the client is not limited to the number of students.

In the multimedia network classroom system, the computer screen images change slowly but provides high image quality and transmission speed. Content changes slowly due to the change of the radio screen mostly caused by the keyboard, mouse operation. People see the number of limit operation for more than a dozen times a second, only compared with a few times normal range. Teaching image picture is clear and there can be flowers screen phenomenon. Transmission speed is able to send any of the image changes quickly reflected to the receiver.

To satisfy the need of real-time screen image, to improve the speed of image transmission and computer processing speed, attention should be given to two or more things. This system uses a fixed block coding mode:

1	2	3	4
5	6	7	8
9	10	11	12
13	14	15	16

Fig. 3 Fixed screen can be divided into 4 * 4 blocks

As shown in figure 3, the screen is divided into fixed M * N, comparison between before and after the two frames corresponding similarity comparison, find out the different blocks.And then only the similarity of different block compression transmission, improves transmission efficiency.

Table 2 Screen broadcast module teachers machine mainly related classes

The main related classes	*Functional description*
Student	The student class machine information.Description is connected to the teacher the student machine information.Screen broadcast, according to the selected machine broadcast teaching students.
ScreenImage	The teacher machine screen print screen.Teachers responsible for the copy machine and the screen blocking, compression and serialization, with convenient transport and machine to the students.
FrameProcess	Fixed block coding process.Save before and after the two frames (screen print screen ScreenImage object), contrast to calculate motion vector to find the similarity of different block, in order to transfer machine to the student.
ConnManage	Connection management class. Maintaining the connection of the students and teacher' machines: track student status, receive related requests from students, and send vitality to commands.
UDPMulticast	Using UDP multicast methods to the selected students machine (students of multicast group machine) to screen the radio.

File transfer module design. This module is mainly to realize students to specify the machine to send and receive files with the specific machine according to network status, transmission speed priority or correctness is preferred to use UDP multicast or TCP connections for transmission. In order to ensure the sending-receiving correctness and completeness of the file, the system module mainly uses a connection-oriented, reliable way of TCP to transmit.Server using the multithreaded way is used to deal with multiple students machine's request In order to improve the performance of the server at the same time, a thread pool is used.

Figure 4 is the UML of file transfer module:

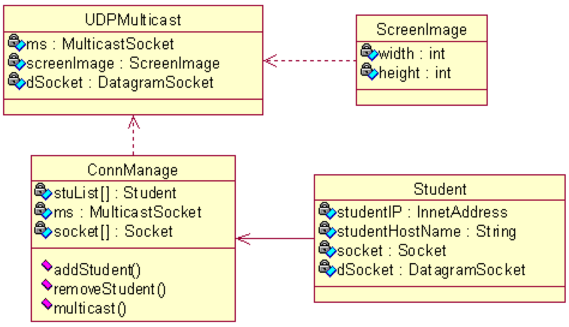

Fig. 4 UML of file transfer module

screen monitoring module design. This module is mainly to implement the machine in the classroom to monitor the specified student machine screen.Its implementation principle corresponds with screen radio module, ie, the sender machine for the students, the receiver machine for teachers.Because it is one-to-one communication, this system USES TCP connection.Table 3 machine for teachers as the main related classes of receiver involved.

Table 3 Screen monitoring module teachers machine mainly related classes

The main related classes	*Functional description*
Student	The information of student machine. Description is connected to the teacher the student machine information.Screen monitor, the machine for the choice of students.
ScreenImage	Screen copy screen. Restore the student machine block, compression and serialized screen information, so as to on the display them on the teachers' computers.
FrameReceive	Receive block imformation from Student, and form a frame screen image (ScreenImage objects).

ConnManage	Connection management class. Maintaining the connection of the students and teacher' machines: track student status, receive related requests from students, and send vitality to commands.
TCPScrMonitor	Using TCP to receive the student machine screen information.

Realization of the remote control. Remote control students' computers. lock (lock machine of the mouse, keyboard), start and turn off students' machines.

The teacher machine can lock, restart, and shutdown students' machines. After students' machines receives the command, it can call the underlying operating system command or API interface to realize the corresponding operation.

Due to the different system commands, such as Linux command without locking the computer keyboard, mouse, you need to call the operating system apis interface to realize the corresponding operation. For the cross-platform JAVA, the purpose of making it and the local machine of various internal contact become very few, constraints on its function. JAVA solve local operating in one way to the JNI.

JAVA JNI calls through local method and local method is stored in the form of the library files (on WINDOWS platforms is a DLL file form on a UNIX/Linux machine).Through a call to the local library files internal methods, can make the JAVA implementation and closely linked to the local machine, which called system level of the interface methods.

Conclusions

In this paper, according to the actual demand of cross-platform environment room, using Java technology to multimedia network classroom system analysis and design, from the choice of the software development plan, to the design of the system architecture, and detailed design and implementation of some main modules are given.

The implementation of this system for Java technology in the design of the multimedia network classroom, and the software development and application of cross-platform conditions has a certain reference value.

Acknowledgements

This work was financially supported by the Guangdong Provincial Institute of higher education laboratory management professional committee fund project(GDJ2012034).

References

[1] Haitao Li. Design and implementation of multimedia classroom network central control system : Journal of Jiaozuo University. Vol. 3 (2011) , p. 89-90.

[2] Yuqing Lu,Wei Zhang. Design and Realization of Multimedia Net-classroom Software Sysytem Based on CSCW: Coal Technology. Vol. 3 (2012), p. 263-265.

[3] Akintola K.QAkinyokun O.C. Design and Development of Multimedia Network System for eLearning in Nigerian Universities: International Journal of Multimedia and Ubiquitous Engineering (2011).

[4] Songmao Jia,Xiliang Dai,Anyu Chen,Xiang Zhou. Application of Red Spider Software in Multimedia Network Classroom: Advanced Materials Research. Vol. 605-607 (2013), p. 2530-2533.

[5] Wei Wu. Research and implementation of multimedia classrooms pure software model : Nanjing University of Science and Technology (2013).

[6] Hongyan Quan,Guitao Cao. The principle and realization method of digital image processing : Beijing, Machinery Industry Press (2014).

Applied Mechanics and Materials Vol. 596 (2014) pp 936-943
© (2014) Trans Tech Publications, Switzerland
doi:10.4028/www.scientific.net/AMM.596.936

A Positioning System of Book Based on QR Code in Library

Shudan Lee[1,a*], Wenqin Liu[2,b], Wei Zeng[3,c], Xin Gao[4,d], Congsong Zhang[5,e]

[1]Chengdu University of Technology, Chengdu, China

[2]Chengdu University of Technology, Chengdu, China

[3]Chengdu University of Technology, Chengdu, China

[4]Chengdu University of Technology, Chengdu, China

[5]Chengdu University of Technology, Chengdu, China

[a*]mitnad.shudan@gmail.com, [b]mlnwwqm@qq.com, [c] leo110269@163.com, [d]1124530597@qq.com, [e]952462174@qq.com

Keywords: QR code, Wireless transceiver, Positioning

Abstract. Owing to the inefficiency and difficulty in finding out the position of books in library, this paper designed a positioning system, which is based on QR code and can be used to find out where the book is in real-time. In the design, a QR code is an identity of the position. The mobile wireless cameras, which were set on the bookshelves, acquire the image of QR code and then send it to data processing center. The processing center generates a two-dimensional localization image of books after the QR was decoded, then stores the localization image in the database in order that the readers or managerial staves can get the books they need quickly and easily after retrieving. This paper presents the structure of the positioning system from the perspective of software and hardware, and the feasibility of the design has been proved by practice test. This design also has certain reference value to the promotion of the QR code in other management fields.

Introduction

With the development of Internet of Things, the interaction between thing to thing or human to thing is deeper. People are making new more demands, such as improving the management efficiency, or the reader's reading experience, on the management and social responsibility of the library, which usually act as the public facilities. At present, the researches about books management system focus on the efficient of the management mode in the domestic and foreigner, more prefer to the software, providing all kinds of management through the B/C or C/S architecture [1, 2]. Instead of the traditional manual management methods, the registration, borrow and return are realized by computer. All of these changes have made great progress in management system. However, while retrieving a special book, effected by the large size of library or the familiarity of readers to the library, even if the classified storage location of book is clearly, there also be so many similar bibliographic. It's quite difficult for readers to get their own books in these book lists, thus they have to take more time and energy. For managerial staves, it's also hard to mark the position of some specific books effectively. Besides, while managers increase the entries of new literatures, the updating of bibliography location also brings a series of management problems. Because of these, this paper designed a retrieval query system which was based on QR code in order to realize the precise positioning of books position and improve the level of intelligence of the library management system.

System design

The Book Positioning System consists of four units: the wireless video signal transceiver module, the scanner module, the QR code decoding module and the client software module. The function of each module as follows:

The wireless video signal transceiver module: Using AV camera to acquire QR code on the spine, then inputting the video signal into remote computer to process through 2.4G wireless transmitter module.

Scanner module: Setting a metal rail and slider on the bookshelf, a video signal acquisition module and a camera are attached to the slider. The slider can slide freely on the track to collect the QR codes of books.

QR code decoding module: Running the QR code decoding program on the client computer, capturing, scanning and decoding the special video which is transmitted by 2.4G wireless transmitter, the information about a book can be obtained after decoding.

Software client: An application which is based on C / S structure. The users have different accesses to the database. On the main interface of positioning program, it queries the location of one book in the library during the nearest time and displays it, as well as adds, deletes, modifies and other operation functions with administrator authority. System design diagram is shown in Figure 1.

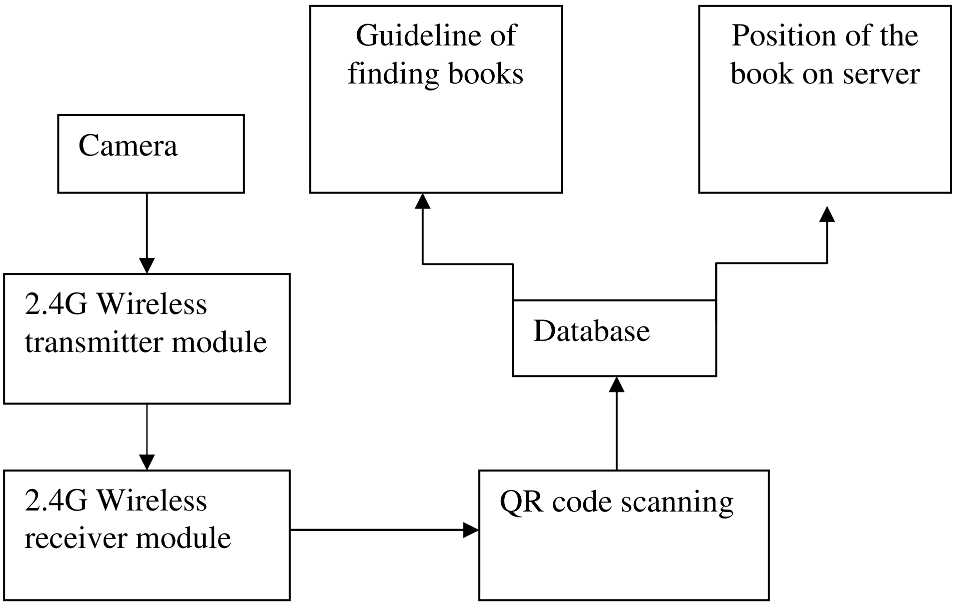
Guideline of finding books
Position of the book on server
Camera
2.4G Wireless transmitter module
Database
2.4G Wireless receiver module
QR code scanning

Fig.1 System design diagram

Hardware design

The system hardware is designed to collect, transmit and receive QR code,including 2.4G wireless video transceiver module, the scanner module of rail.

2.4G wireless video transceiver module

The RTC6701 [3], a wireless chip product of Richwave Company, was selected as the main chip of the wireless video transmitter. It’s a FM/FSK transmitter intended for application on 2.4GHz ISM band analog FM or digital FSK transmission. The chip includes a RF modulator, two channels of audio modulator and a power amplifier with up to +11.5dBm power output. The RF modulator block, which is frequency-synthesizer based with an integrated 2.4GHz VCO, generates the 2.4GHz FM signal. On-chip two audio modulators with stereo audio input signals provide the FM audio modulated signal at 6 MHz and 6.5MHz. Its block diagram is shown in Figure 2.

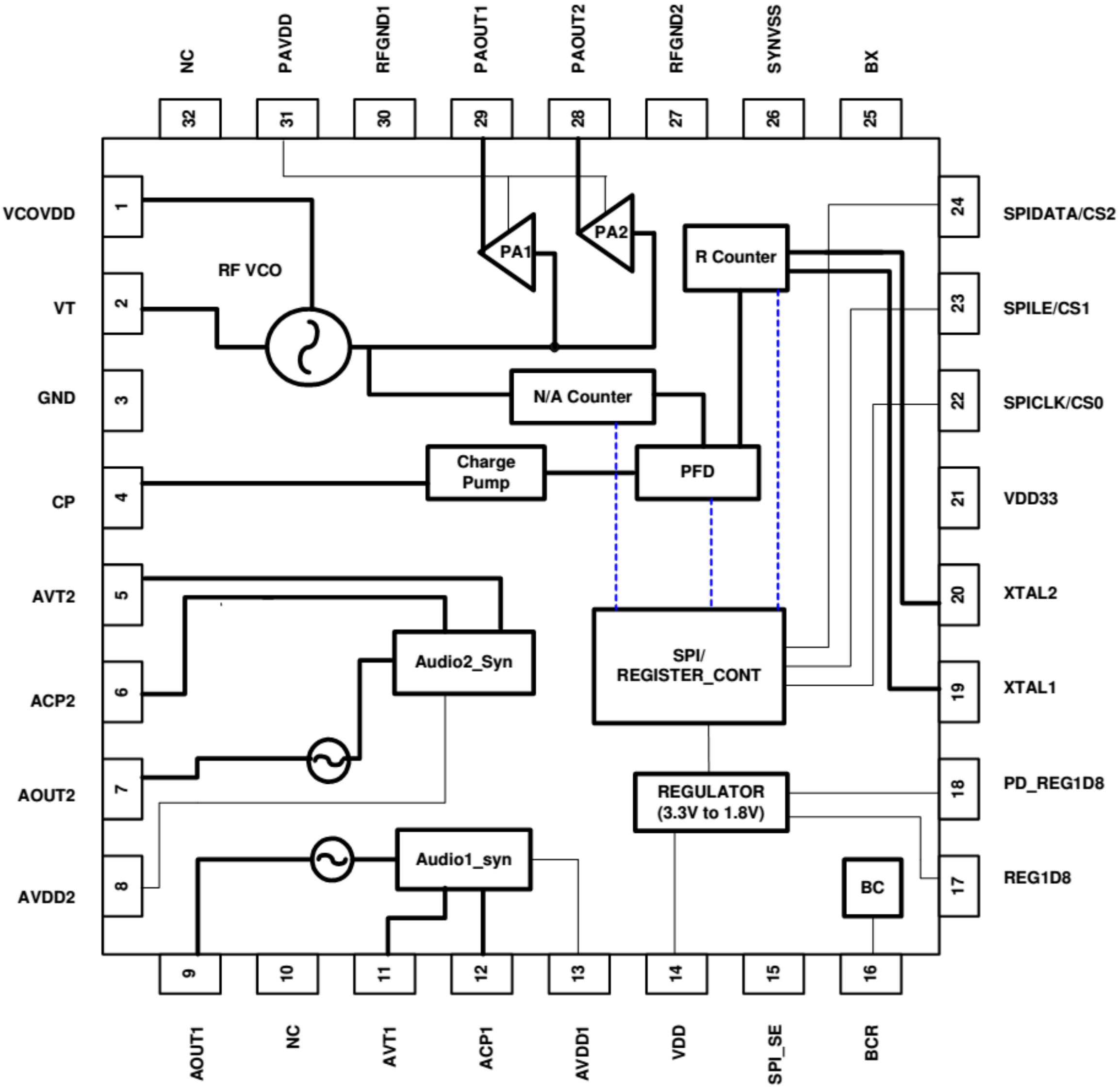
NC
PAVDD
RFGND1
PAOUT1
PAOUT2
RFGND2
SYNVSS
BX
32
31
30
29
28
27
26
25
VCOVDD
VT
GND
CP
AVT2
ACP2
AOUT2
AVDD2
1
2
3
4
5
6
7
8
SPIDATA/CS2
SPILE/CS1
SPICLK/CS0
VDD33
XTAL2
XTAL1
PD_REG1D8
REG1D8
24
23
22
21
20
19
18
17
RF VCO
PA1
PA2
R Counter
N/A Counter
Charge Pump
PFD
Audio2_Syn
SPI/ REGISTER_CONT
REGULATOR (3.3V to 1.8V)
Audio1_syn
BC
9
10
11
12
13
14
15
16
AOUT1
NC
AVT1
ACP1
AVDD1
VDD
SPI_SE
BCR

Fig.2 Block diagram of RTC6701

In Fig. 2, the VT and CP are used to process the video input signal, AVTX, ACPX, AOUTX and AVDDX handle the two of 6 MHz and 6.5 MHz audio input signal. In this design, we just need to handle video signal, thus particular attention has been paid to the process of video signal on RTC6701. Transmission frequency can be set by internal register via SPI programming, or by selecting among 4 fixed channels using three dedicated pins. There are two principle modes for channel selection: Easy channel selection mode and SPI mode. The level of SPI_SE chooses channel mode, while the SPICLK/CS0, SPILE/CS1, SPIDATA/CS2, BX work together to allocate a specific channel frequencies. The selected channel frequencies of Easy channel selection mode are listed in the Table 1. We choose the Easy channel selection mode by set these pins as follows:

SPI_SE=0，BX=0，CS0 CS1 CS2=001

Table 1 Channel frequencies of Easy channel selection mode [3]

BX	SPI_SE	Pin22/ Pin23/ Pin24 CS0/CS1/CS2			
		011	101	110	111
0	0	2414MHz	2432MHz	2450MHz	2468 MHz

Finally, the external circuit of transmitter is shown in figure 3. J2 is used to select channel frequency. LM7805 power RTC6701 in a stable voltage.

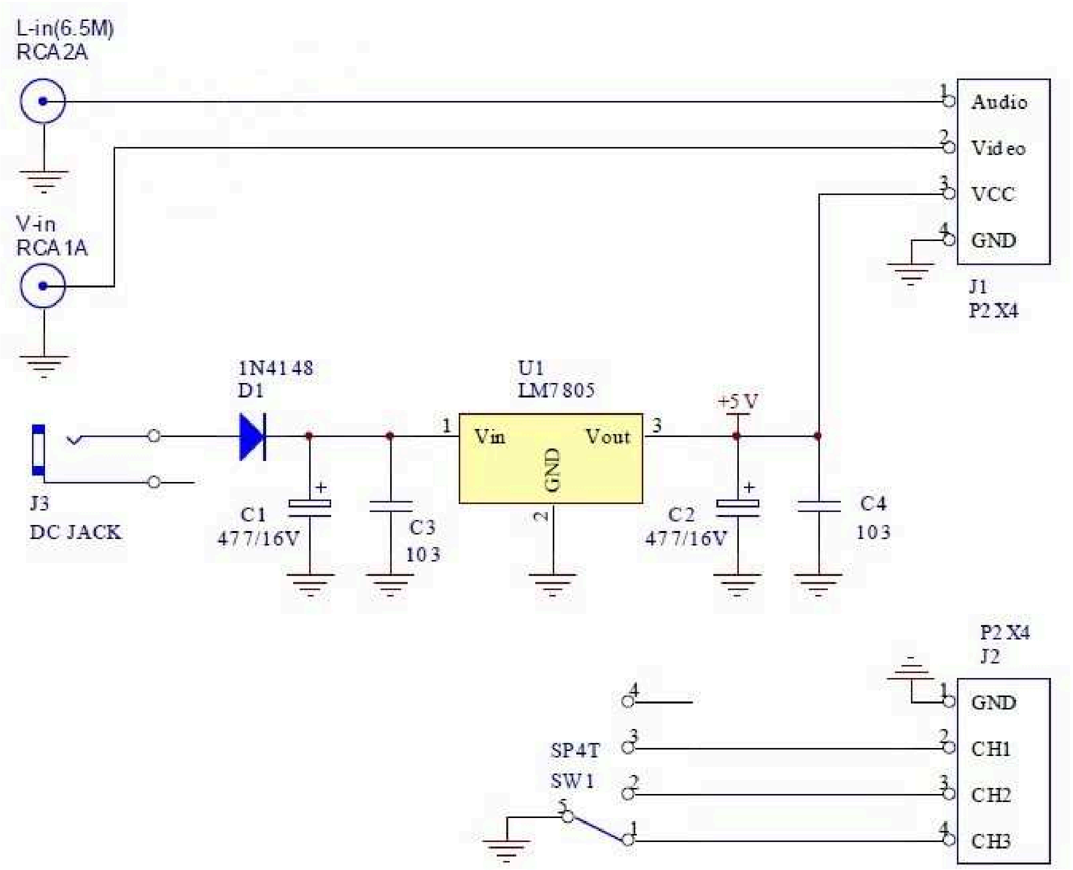
L-in(6.5M)
RCA2A
V-in
RCA1A
1 Audio
2 Video
3 VCC
4 GND
J1
P2X4
1N4148
D1
U1
LM7805
1
Vin
Vout
3
GND
2
+5V
J3
DC JACK
C1
477/16V
C3
103
C2
477/16V
C4
103
P2X4
J2
1 GND
2 CH1
3 CH2
4 CH3
SP4T
SW1
4
3
2
5
1

Fig.3 External circuit of transmitter

The RTC6711 [4] was selected in the receiver. This chip is a highly integrated FM/FSK receiver, intended for application on 2.4GHz band. The chip includes a low noise amplifier, mixer, IF amplifier, FM demodulator, AGC, and FSK data slicer. With RSSI voltage output the instantaneous radio signal strength can be monitoring as input for the followed indicator process. RX carrier frequency can be set by SPI programming, or by selecting among 4 fixed channels using three dedicated pins. The external circuit of receiver is shown in figure 4. When RTC6711 receives a video signal stream containing QR image, this signal is input to the processor through acquisition card, which can exchange data between the AV signal data and USB data.

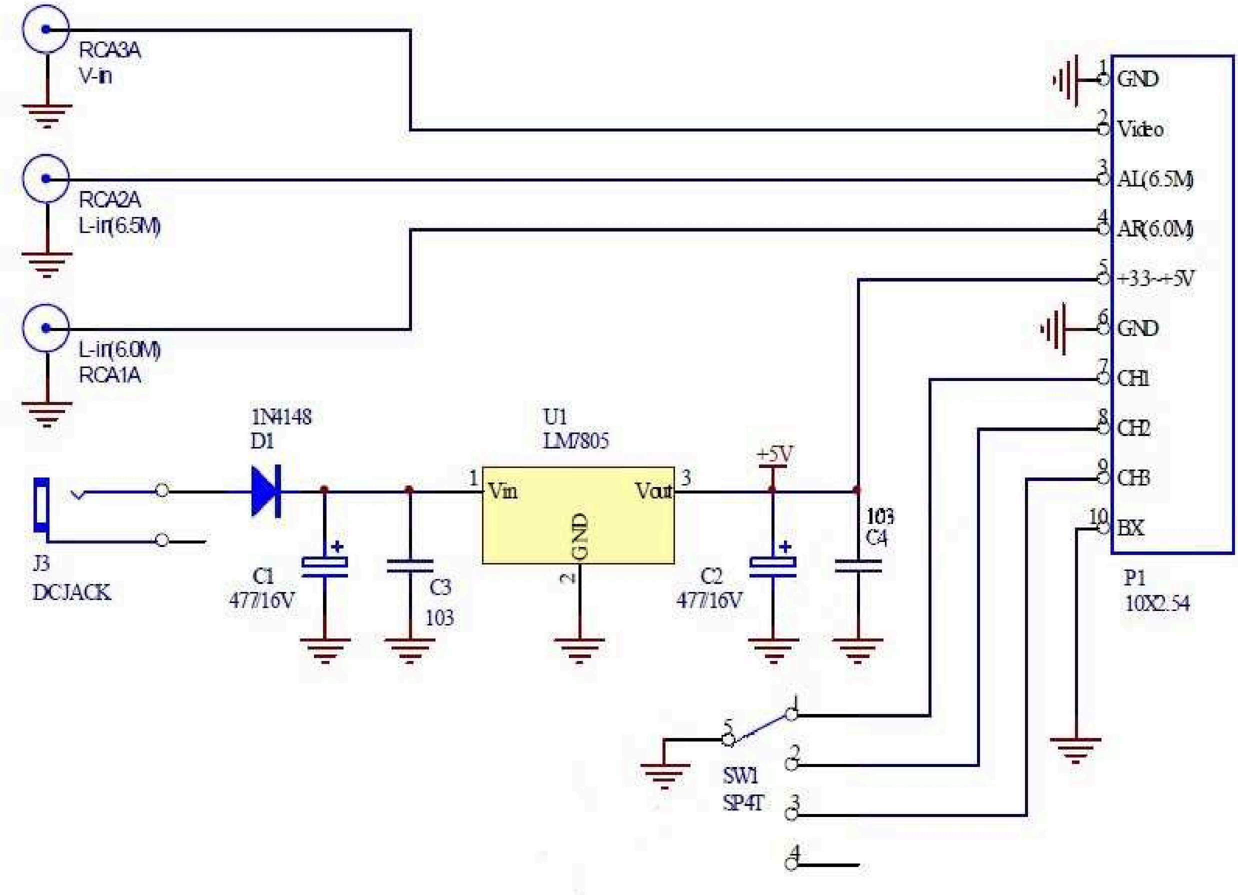
RCA3A
V-in
RCA2A
L-in(6.5M)
L-in(6.0M)
RCA1A
1N4148
D1
U1
LM7805
Vin
Vout
GND
1
2
3
+5V
103
C4
J3
DCJACK
C1
47/16V
C3
103
C2
47/16V
1 GND
2 Video
3 AL(6.5M)
4 AR(6.0M)
5 +3.3~+5V
6 GND
7 CH1
8 CH2
9 CH3
10 BX
P1
10X2.54
SW1
SP4T
1
2
3
4
5

Fig.4 External circuit of receiver

The Scanner Module of Slide

We set up a light Aluminum slider on the bookshelf, on which there is mental block with a signal transceiver chip and a camera. AT89C51 is used to drive the stepper motor at a special speed to control the mental block to scan the book's QR code. In the design, ULN2003A is used as the motor-driven chip, and we can get trigger to adjust the speed. In practice, we use an iron wire tied on the mental block to joint with motor to drag the mental block. This device is relative simple so there omits it.

Software design

QR[5], also known as Quick Response code, is very popular at home and domestic these years, the typical structure is shown in figure 5. Each QR code symbol shall be constructed of nominally square modules set out in a regular square array and shall consist of a encoding region and function patterns, namely finder, separator, timing patterns, and alignment patterns. Function patterns shall not be used for the encodation of data. The symbol shall be surrounded on all four sides by a quiet zone border. Denson Wave work out the QR, which is viewed as the entrance of the internet, widely used in the push, trace, interlinkage and etc. of Ads, for example, used on the telephone [6,7]. QR has a quick speed and big error-rate and high-usage in space. Compared with the one-dimension code ,QR code is cheaper and bigger size of memory, and the biggest size of memory now is 3KB to store many kinds of information such as character ,Chinese, Japanese and so on[5]. Compared with RFID,two-dimension code is better not only in the price,but the good interactivity.

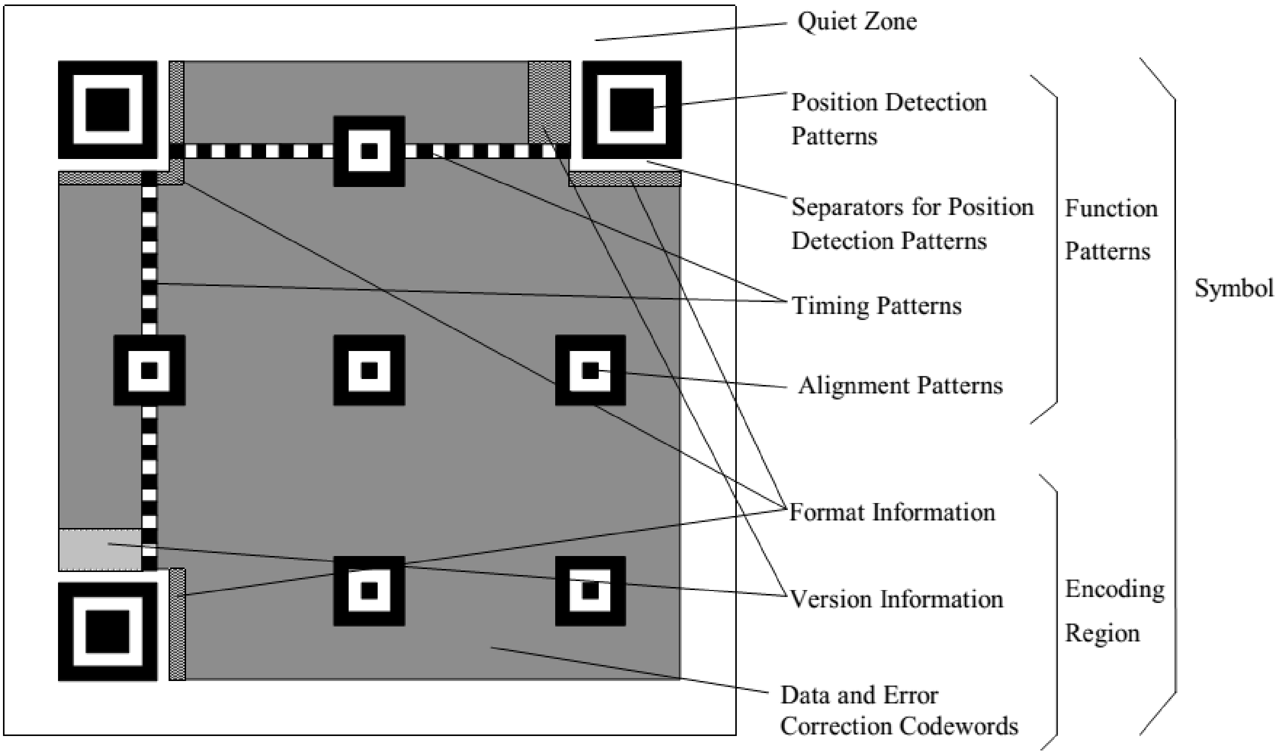
Quiet Zone
Position Detection Patterns
Separators for Position Detection Patterns
Timing Patterns
Alignment Patterns
Format Information
Version Information
Data and Error Correction Codewords
Function Patterns
Encoding Region
Symbol

Fig.5 Typical structure of QR code

QR code decoding

Google ZXing library[8] , a very powerful bar Code generation and identification of the class library ,is an open-source, multi-format 1D/2D barcode image processing library implemented in Java, with ports to other languages, for example **C#**. It can be used to encode and decode the QR, the Data Matrix. ZXing library can distinguish Chinese, English, numbers and symbols.In the design, QR code stores the normal classification index, ISBN, author and content profiles information of books. The program of decoding, video reading or capturing is debug by C# programing language. By calling the APIs of Google ZXing library, the QR code, which contains a book's information, is generated. Stick the QR code image to the spine of book, a camera will scan and capture the QR code in order to find out where the book is.

Dynamic positioning table of books

The position of books is located by the camera indirectly. Since the QR on the book is unchangeable, and to get the tracking of the book, a mapping table for the QR and the position of the camera must be established. The mapping table structure as shown in Table2.

Table 2. Dynamic mapping table for QR and books

Codes of the camera	position of the camera(dynamic)	QR(fixed)

This table updates in the data library periodically, when you look for one book ,you’ll find it according to the position of the camera.

Book positioning management system

Figure 6 is the typical picture of the library. The rectangles in the middle are the bookshelves, used as a background in the software form. These rectangles can use the picture to locate the position in the form’s coordinate. Take the rectangle in 1 line and 1 row for example, we can use (520,388) to find the bookshelf.

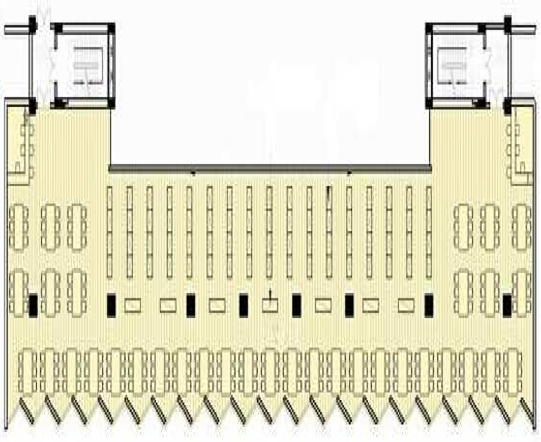

Fig.6 Typical planar graph of library

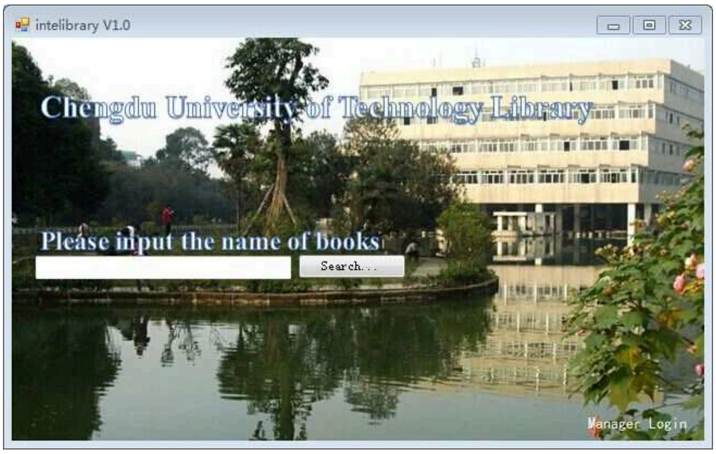
intelibrary V1.0
Chengdu University of Technology Library
Please input the name of books
Search...
Manager Login

Fig.7 Main interface of Positioning System

Positioning System of Books' main interface is like figure 7. All people can use it. General users and administrators can use the main interface to search the book's position. The button in bottom right corner is for the login of the administrators. Click it then login.

The administrators can add, delete and make new QR codes about with books. As shown in Figure 8.

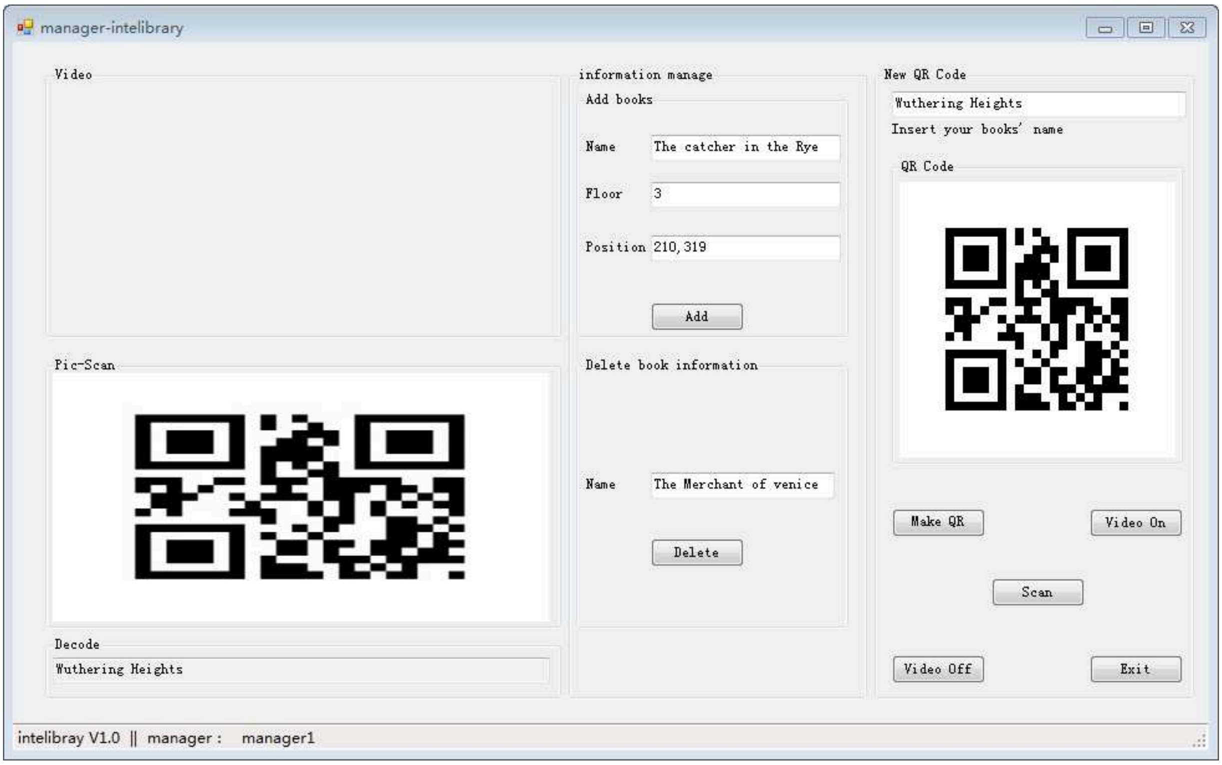
manager-intelibrary
Video
Pic-Scan
information manage
Add books
Add
Delete book information
Delete
New QR Code
Insert your books' name
QR Code
Make QR
Video On
Scan
Video Off
Exit

Name: The catcher in the Rye
Floor: 3
Position: 210,319
Name: The Merchant of venice
New QR Code: Wuthering Heights
Decode: Wuthering Heights
intelibray V1.0 || manager : manager1

Fig.8 Interface of the administrator

As long as users input the name of the book in the interface, the recent positions of the book is displayed. As shown in Figure 9.The red dot shows the place of the book which I am looking for.

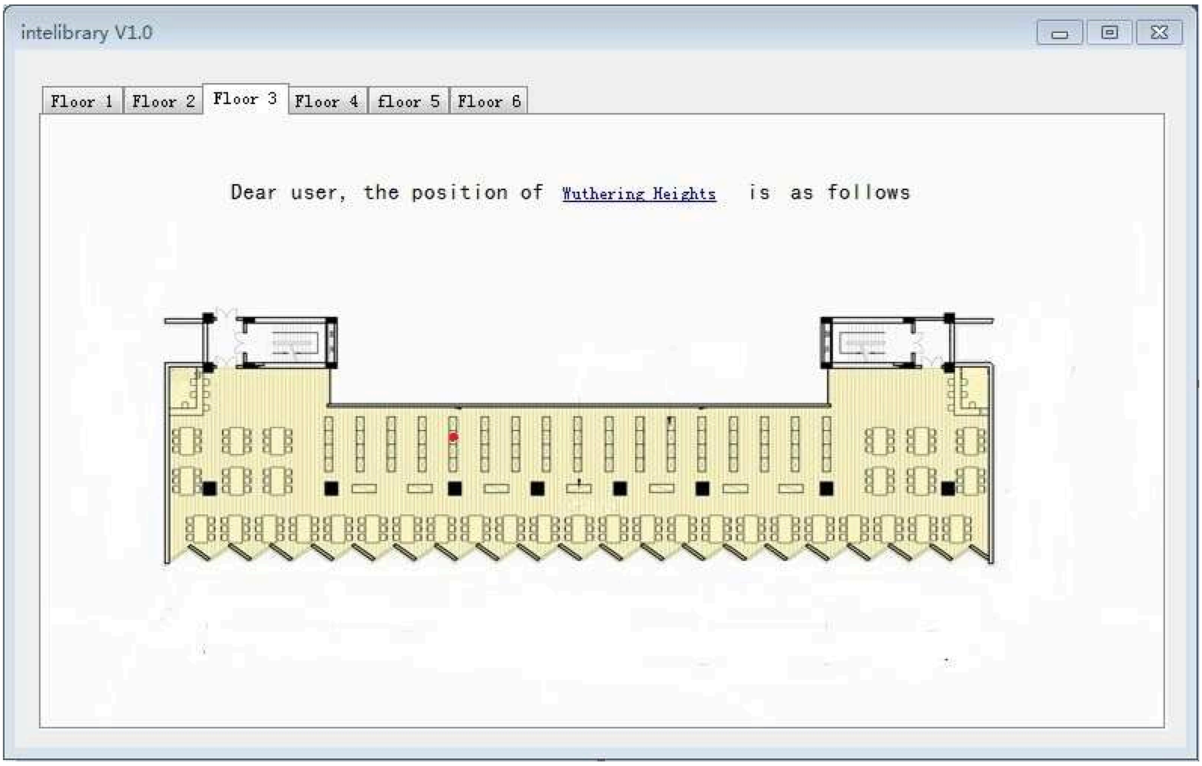

Dear user, the position of Wuthering Heights is as follows

Fig.9 Two-dimensional localization image of book

Conclusions

The intelligent management system of books will be the inevitable trend of the library's development in the future. This paper designed the positioning system of books based on QR code in Library,which aims at solving the inconvenience of finding books. It is an effective attempt of the technology of QR code in the field of books management. Using this intelligent retrieval system reduces the time that we spend in searching books. It is easy to scan the position of books and to find out books incorrectly placed timely by installing the orbits on the bookshelves. In additional, the push service can be added to the QR code of books. Scan the QR code, then we can send the messages associated with books to friends through the domestic popular platform of the WeChat. The combination of these designs based on WeChat promotes the reading experience of readers.

References

[1] Saikat Goswami，Chandan Kundu . XML based advanced distributed database: implemented on library system[J] .International Journal of Information Management, 2013, Vol.33 (1)

[2] Qian WANG，Chengyu. A study of user experience in Tsinghua Wireless and Mobile Digital Library[J] . Chinese Journal of Library and Information Science. 2011(1)

[3] RichWave.RTC6701 Datasheet 2009 [S] TaiWan: RichWave, 2009

[4] RichWave.RTC6711 Datasheet 2009 [S] TaiWan: RichWave, 2009

[5] ISO/IEC.International Standard of QR code[S].ISO/IEC, 2000

[6] Zhu, Ning Xian (Shandong institute of political and law Shandong, Jinan, 250014, China) Source: Advanced Materials Research, v 805-806, p 1907-1910, 2013, Energy and Power Technology

[7] Dong-Hee Shin, Jaemin Jung, Byeng-Hee Chang, The psychology behind QR codes: User experience perspective, Computers in Human Behavior, Volume 28, Issue 4, July 2012, Pages 1417-1426

[8] Zxing.https://github.com/zxing/zxing

Applied Mechanics and Materials Vol. 596 (2014) pp 944-947
© (2014) Trans Tech Publications, Switzerland
doi:10.4028/www.scientific.net/AMM.596.944

Design and Implementation of A New CNG Dispenser Control Platform

Xu Zhang[1, a], Xiangdong You [1, b], Qian Luo[1, c] and Xiaojia Zou[1, d]

[1] School of Information and Communication Engineering

Beijing University of Posts and Telecommunication, Beijing China 100876

[a]elliot1106@126.com, [b]youxiangdong@bupt.edu.cn, [c]luoqianjob@163.com, [d]xiangzhiwu2009@163.com

Keywords: CNG, Dispenser, ARM, Linux, Driver.

Abstract. CNG dispenser is a kind of equipment which can provide CNG fuel filling services for CNG vehicles. This paper presents a novel design of CNG dispenser control platform. The hardware design of the circuit board includes ARM11 core-board and extended board, and the software design is based on the Embedded Linux system, including the development of Linux drivers and applications. The new platform not only has better processing performance in basic functions like filling fuel, but also has excellent scalability such as network support and more humanized operation mode.

Introduction

Compressed natural gas (CNG) is a fossil fuel that acts as an alternative to gasoline, diesel and LPG. Well known as the green fuel, CNG is turning into the most preferred alternative fuel in many countries [1]. Under the guidance of national energy environmental protection policies in China, the number of CNG vehicles and CNG stations continue rapid growth in recent years, and the market of related equipment like CNG dispenser is thriving synchronously. According to the survey, most of the domestic CNG dispensers are operated upon a Single-chip Microcomputer (SCM) system or based on ARM7 core. Although these products meet the basic functional requirements, there are several shortages in the long run: the scalability of the system is poor, the operation interface is complicated, and the lack of database or network support. As a result, we intend to develop an intelligent CNG dispenser control platform to meet the further demand.

The new platform has employed the popular "ARM + LINUX" development mode, adopting the ARM-11 microprocessor as the core and the operating system running on it is Embedded Linux. The ARM-11 series of microprocessors is the latest RISC processor of ARM which introduces the advanced ARMv6-architecture, and the Embedded Linux is recognized as particularly stable system. The circuit board is divided into two parts: the core board with CPU and the extended board with various interfaces. To make sure all the peripheral units to work properly, we have developed corresponding drivers in Linux and designed a control program to manipulate all the peripheral parts. In the future, we could add a touch screen with Graphical User Interface developed by QT and a kind of database to the control system.

Design Overview

As is shown in Fig.1, The new platform has employed the "ARM + LINUX" development mode, including both hardware development and software development. Different from the traditional control machine, the embedded system based on the ARM processor is more customized and humanized: both the hardware and software can be self-developed, the user can not only design specific hardware circuit and corresponding software, but also can cut and extend various modules of the Linux system. ARM processor is very mature, and the Embedded Linux is a stable open source system. So this solution not just meets various requirements, but also greatly saves the cost.

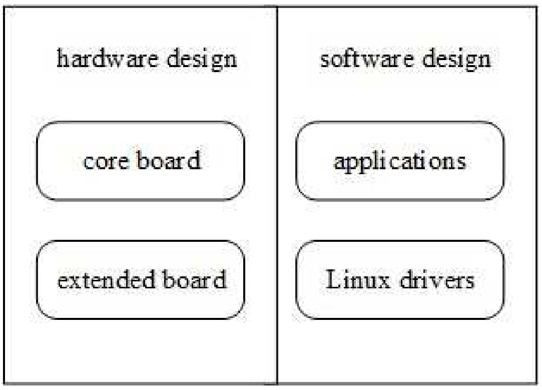
hardware design
core board
extended board
software design
applications
Linux drivers

Fig. 1. Design overview

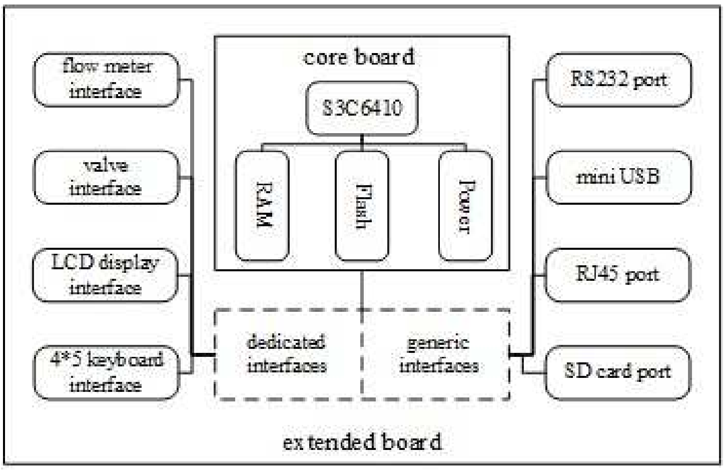
flow meter interface
valve interface
LCD display interface
4*5 keyboard interface
core board
S3C6410
RAM
Flash
Power
dedicated interfaces
generic interfaces
extended board
RS232 port
mini USB
RJ45 port
SD card port

Fig. 2. Hardware components

Hardware Implementation

The CNG dispenser electronic control board shown in Fig.2 has two parts: the core board and the extended board. The core board is designed with 8 high-density layers, and the main processor on the core board is Samsung S3C6410,which is integrated with 256M DDR RAM and 2GB SLC NAND Flash Memory. The S3C6410 is designed based on the ARM1176JZF-S core, and integrated with multimedia processing unit. It also supports the operations of 2D graphics image smooth scaling and flipping and is equipped with 3D graphics hardware accelerators. The core board uses the 5 volt power supply and leads the serial port, Ethernet port, 485 communication interface, A/D adjustable resistor, Mini USB 2.0 interface, USB Host, SD card holder and other generic interfaces to the extended board through the 2.0mm pitch pin. Besides, the extended board contains many dedicated interfaces designed for the dispenser, such as flow-meter interface, 4*5 keyboard interface, solenoid valve interface, LCD1 display interface and LCD2 display interface, I2C EEPROM and SPI interface. We also reserve an interface for 7" LCD module in order to develop a touch GUI in the future.

Software Implementation

Fig.3 presents the CNG dispenser control program which runs in the user space of the Embedded Linux system. The whole software development mainly includes three parts: the transplantation of the Linux operating system, Linux device driver development and the development of the control program.

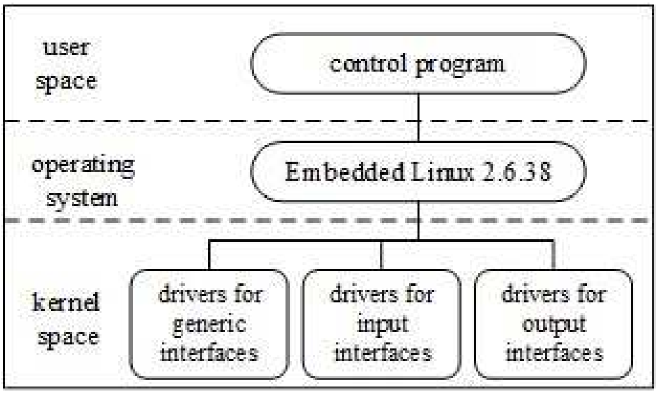
user space
control program
operating system
Embedded Linux 2.6.38
kernel space
drivers for generic interfaces
drivers for input interfaces
drivers for output interfaces

Fig. 3. Software components

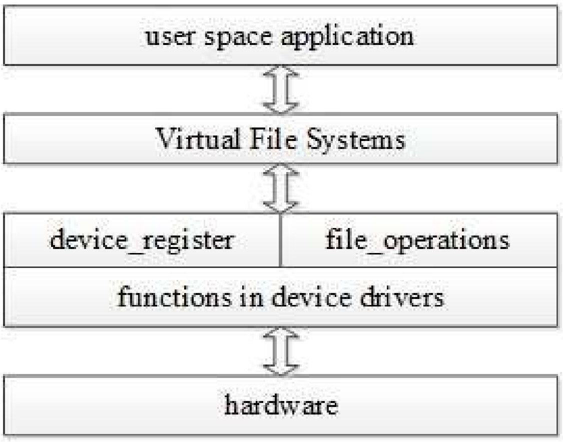
user space application
Virtual File Systems
device_register
file_operations
functions in device drivers
hardware

Fig. 4. Linux driver

Cross-compilation. The first work to transplant the Linux operating system is to build the environment of the cross-compilation. Cross-compilation is an important technology in the process of embedded system development [2]. It is the method to compile the program which runs in another platform in use of existing development environment. Cross-compilation has two objects, one is the host machine, and another is the target machine. The host machine is the machine to compile the code, and the target machine is the platform which actually runs the applications. Usually, the memory of embedded system is too small to install the compilation environment, so the source code should be compiled in personal computers.

Linux Driver. As is shown in Fig.4, in the Linux system, the device driver acts a link between hardware and application software [3]. Device drivers typically are organized as a set of functions to complete different tasks, making the operations to the equipment exactly like the operations to the files. Via the interfaces provided by the Virtual File Systems, the applications can do the operations such as open, read to the hardware devices in the same way to the ordinary files. Linux provides a mechanism called "Module", one module implements a corresponding device driver and the module can be dynamically loaded or deleted. The Embedded Linux system has already supported generic driver interface, so we only need to develop dedicated interface drivers.

The keyboard driver queries the state of the keyboard via serial scanning to get the information of each keystroke; The solenoid valve driver control six electronic switches by controlling electric potential of the corresponding I / O ports [4]; The driver of LCD1 divides the information into English characters and Chinese characters, both of which are transformed into corresponding codes and input to the screen according to the starting input point on the LCD1.The driver of LCD2 constantly refreshes 16 eight digital tubes according to real time statistics to display the volume, the transaction amount and preset unit price. Flow-meter driver counts volume by measuring the number of interrupts of the I/O port; Temperature sensor driver constantly sends to instructions like" reset, write RAM, read RAM" to the ds18b20 to get real-time temperature around.

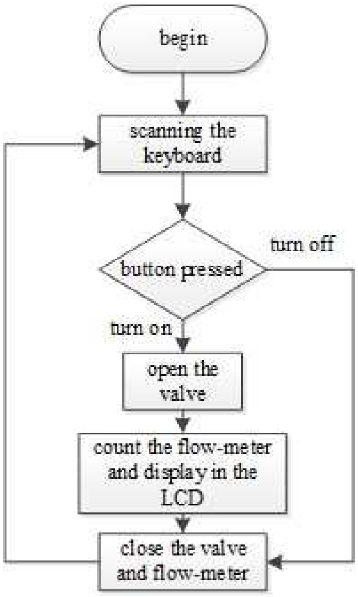
begin
scanning the keyboard
button pressed
turn off
turn on
open the valve
count the flow-meter and display in the LCD
close the valve and flow-meter

Fig. 5. Control program

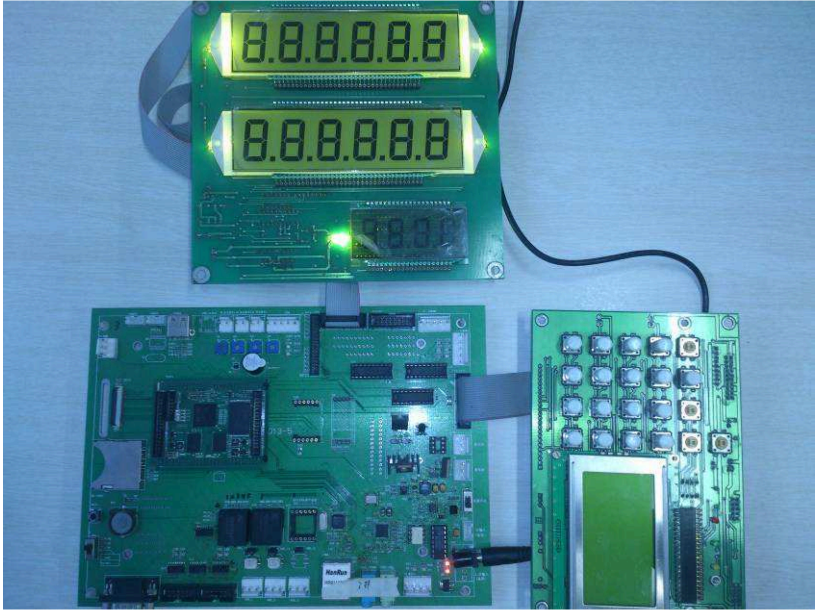

Fig. 6. Implementation results

Control Program. After the development of the Linux drivers, we also developed a simple program to simulate a relatively complete filling process. By the analysis of the filling process, the control program requires at least following functional parts [5]. Firstly, the control of the valve: The dispenser requires precious control on the valve, for this function directly affects the realization of the filling service. The valve should be anti-jamming and have a strong stability. Secondly, the acquisition of the volume: The pulse flow-meter is the most wildly used flow-meter. It can send electrical pluses when the compressed natural gas is being filled into the vehicles and one pulse represents a specific equivalent. As a result, the control system needs to accurately calculate the volume. Thirdly, the state of the keyboard: The keyboard is the most important input device for the dispenser, the user can input both commands and numbers through it. Therefore the control program must continue to scan the keyboard to get the exact operations. Lastly, display on the LCD2: The LCD2 module has 16 eight-digital tubes to display the unit price, the volume and the corresponding total price. Because the volume of the gas changes rapidly, so the display module requires good real-time performance.

As is shown in Fig.5, after the initialization, the control program will continue to scan the keyboard, if the "turn on key" is pressed, one valve will be opened. Meanwhile, one thread will start to count the value of the flow-meter and send the accurate number to the LCD2 to display. Once the "turn off key" is pressed, the program will close the valve and flow-meter, and then returns to the standby mode. Although the control program is relatively simple, it has not only verified the hardware and drivers, but also laid the foundation for future development.

Conclusions

This paper designs a new CNG dispenser control platform based on the S3C6410. Through the product investigation, we have implemented a new electric control board shown in Fig.6. The core board is a compact circuit with the S3C6410 and the extended board contains various interfaces. The design of the extended board can be compatible with other vendors' core board, so the system has both compatibility and innovation. The device drivers and the control program not only verified the whole circuit, but also implemented the basic function of the dispenser. In the future, we will add a 7" LCD module and a kind of database to the control platform in order to achieve more efficient functions. The embedded technology used by the platform has greatly enhanced the information degree of the natural gas dispensation industry and has opened up a new path for the future CNG dispenser development.

References

[1] Information on http://www.prweb.com

[2] Alessandro Rubini, Jonathan Corbet and Greg Kroah-Hartman: *Linux Device Drivers (3rd Edition)* (O'Reilly Media, USA 2005).

[3] Baohua Song: *Linux device driver development (2rd Edition)* (The People's Posts and Telecommunications Press, China 2010). In Chinese.

[4] Xu Zhang: Soft. Vol.34 NO.12 (2013), p. 99 .In Chinese.

[5] Beijing Changkong Machinery Co., Ltd: #JQD3S-40L CNG Dispenser Manual *(3rd Edition)* (2003). In Chinese.

CHAPTER 13:

E-Commerce, E-Government, Internet Technologies, WEB Design

Applied Mechanics and Materials Vol. 596 (2014) pp 951-959
© (2014) Trans Tech Publications, Switzerland
doi:10.4028/www.scientific.net/AMM.596.951

Applying improved clustering algorithm into EC environment Data mining

Yupeng Ma[1, a], Bo Ma[1,b] and Tonghai Jiang[1,c]

[1] Research Center for Multilingual Information Technology
Xinjiang Technical Institute of Physics &
Chemistry, Chinese Academy of Sciences
Urumqi, Xinjiang Province, China
[a]ypma@ms.xjb.ac.cn, [b]yanyushu_xj@sina.com, [c]0716genius@163.com

Keywords: EC environment, Customer segmentation, K-means, improved K-means.

Abstract. With the rising growth of electronic commerce (EC) customers, EC service providers are keen to analyze the on-line browsing behavior of the customers in their web site and learn their specific features. Clustering is a popular non-directed learning data mining technique for partitioning a dataset into a set of clusters. Although there are many clustering algorithms, none is superior for the task of customer segmentation. This suggests that a proper clustering algorithm should be generated for EC environment. In this paper we are concerned with the situation and proposed an improved k-means algorithm, which is effective to exclude the noisy data and improve the clustering accuracy. The experimental results performed on real EC environment are provided to demonstrate the effectiveness and feasibility of the proposed approach.

Introduction

In electronic commerce environment, Customer Relationship Management (CRM) can be defined as the process that manages and supports the interactions between a company and its customers. A general framework for a CRM system would include analytical components that are customer focused components, used to analyze existing customer data. Another component would be operational component that includes functional tools used to achieve customer centric goals and finally customer contact component that includes channels or medium used to interact with the customer directly. CRM helps locate relevant information about customers and use it to market the product to vital segments of customers and be able to obtain feedback about how successfully the customer needs were satisfied [1].

CRM encompasses all activities carried out with the customer in focus, from the business point of view and customer point of view. Along with Information Systems automation, sales force and marketing system automation and infrastructure development, an important element of CRM is analytics.

Analytics involve use of several scientific techniques to analyze customer data that is available, and make use of it to derive predictive conclusions about the information, that will then help to make business decisions. The biggest hurdle faced in analytics of this nature is not the lack of information, but more so the abundance of it and the failure to utilize all of this data to derive something meaningful. As technological improvements have been made to CRM tools, many traditional, statistical tools have been incorporated into the system, to assist in carrying out analysis of this nature. Options available currently facilitate the use of more than one tool at a time, to come up with a solution most suitable for our needs. Thus, integrating useful, predictive tools is vital for CRM to derive information from existing information.

The collective use of statistical tools to extract customer information, analyze it and infer customer behavior patterns, based on it is termed as Data mining. In all systems developed in the recent times,data mining techniques are an integral part of CRM. By definition, data mining refers to extracting or mining knowledge from large amounts of data.

Web Data Mining

The rising of data mining technology has solved the problem of complex customer segmentation. Data mining is the process of extracting potentially useful information, finding people concerned pattern and hidden relationships between data and variation from massive fuzzy random data, which allows people to recognize data from a higher level and mine potential value to provide support for decision-making. Data mining technologies can help companies to find the potential customers' information from massive data, to transform customers' information in the database into useful characteristic information and cluster the similar customers, and thus evaluating valuable customers and provide different services to different customers.

Web Mining. The web mining can be broadly categorized as Web Content Mining [2], Web Structure Mining, and Web Usage Mining and shown in Fig. 1.

(1) Web Content Mining deals with the discovery of multimedia documents, involving texts, hypertexts, images, audio and video information and their automatic categorization.

(2) Web Structure Mining deals with the finding of inter-document links, provided as a graph of links in a site or between sites.

(3) Web Usage Mining [3] deals with the discovery and analysis of "interesting" patterns from click-stream and associated data collected during the interactions with Web server on one or more Web sites.

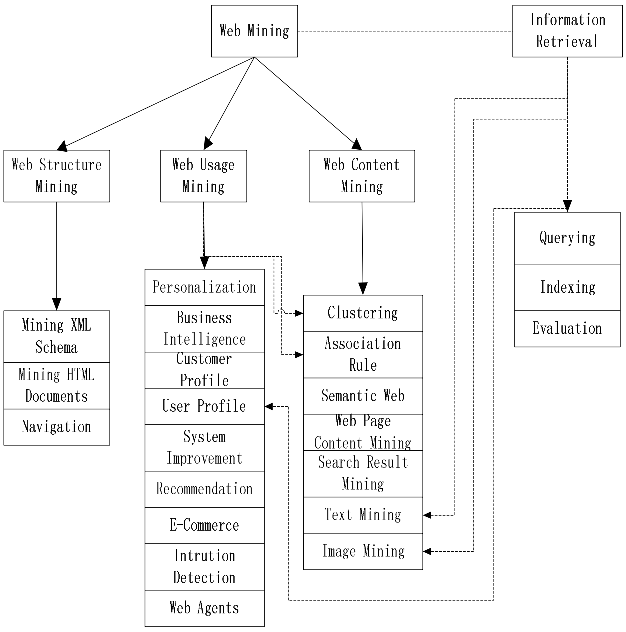
Web Mining
Information Retrieval
Web Structure Mining
Web Usage Mining
Web Content Mining
Querying
Indexing
Evaluation
Personalization
Mining XML Schema
Business Intelligence
Customer Profile
Mining HTML Documents
User Profile
Navigation
System Improvement
Recommendation
E-Commerce
Intrution Detection
Web Agents
Clustering
Association Rule
Semantic Web
Web Page Content Mining
Search Result Mining
Text Mining
Image Mining

Fig. 1 The web mining taxonomy

Cluster analysis is one of the most commonly used data mining algorithms. Based on the particular similarity criteria, clustering algorithm splits the sample space into a plurality of different sub-spaces, sample points in each sub-space are similar with each other, while sample points from different sub-spaces are not. Its essence is to find the different hidden data models through an unsupervised learning process. Using cluster algorithms to carry out customer segmentation is to cluster similar customers into a same sub-space, while making the differences between different types of customers maximized.

Clustering algorithm

Data mining can automatically extract the data from a large number of potentially valuable knowledge, models or rules, belongings to discover technologies. It can help decision-makers find the law, elements and predict trends. Clustering is a popular data mining technique that attempts to partition a dataset into a meaningful set of mutually exclusive clusters.

Data types and data structures in cluster analysis.

(1) Interval-scaled variable

Interval-scaled variable is a rough linear scale for continuous variables. Since the data is divided into different categories, we define the difference degree function. Function is used to measure the degree of difference between the data of the same type of similarity or dissimilarity between the different classes. Because different data samples may have multiple attributes [4].

There are different methods measure different attributes, will bring a lot of different clustering results. So we need to standardize the data.

$$Z_P = \frac{x_{ip} - m_p}{S_p} \tag{1}$$

The average absolute error S_p,

$$S_P = \frac{1}{n}\sum_{i=1}^{n}\left|x_{ip} - m_p\right| \tag{2}$$

m_p is the average value of p,

$$m_p = \frac{1}{n}\sum_{i=1}^{n} x_{ip} \tag{3}$$

In the case of noise points, the mean absolute error has better robustness, than the standard deviation. After standardizing the data , it can be similarity measure. Calculating the distance between sample points.

Generally includes the following method of calculating the distance.

Euclidean distance:

$$D(x_i, x_j) = \left\|x_i - x_j\right\| = \sqrt{\sum_{k=1}^{p} x_{ik} - x_{jk}} \tag{4}$$

Manhattan distance:

$$D(x_i, x_j) = \sum_{k=1}^{p} x_{ik} - x_{jk} \tag{5}$$

Minkowski distance:

$$D_m(x_i, x_j) = \left[\sum_{k=1}^{p} (x_{ik} - x_{jk})^m\right]^{\frac{1}{m}} \tag{6}$$

(2) Binary variable

There are two binary variables values states, namely 0 and 1, binary variables can be divided into symmetric binary variable and asymmetric binary variables according to their status value. Symmetric binary variable, the two states have the same values and the same weights, asymmetric binary variable, the two states do not have the same values and the same weights. Assume two states of binary variable values are as follows:

		Object j		
		1	0	sum
	1	a	b	a+b
Object i	0	c	d	c+d
	sum	a+c	b+d	p

Simple matching coefficient evaluated the degree of difference is as follows:

$$d(i,j)=\frac{r+s}{q+r+s+t} \tag{7}$$

Jaccard coefficient used to evaluate the degree of difference is as follows:

$$d(i,j)=\frac{r+s}{q+r+s} \tag{8}$$

(3) The nominal and ordinal variables

The nominal variables are promotion of binary variable. Different from the binary variable, it can have plurality of state values . State values are not comparable between the size, also disordered arrangement. The nominal variable degree of difference between objects can be matched by a simple matching coefficient.

$$d(i,j)=\frac{p-m}{p} \tag{9}$$

p is the number of attributes, m is the number of attributes can be matched.

Ordinal variables like the nominal variables. Ordinal variables can be divided into discrete and continuous. Discrete ordinal variables similar to the nominal variables, the only difference is that it makes sense to sort sequence. Continuous ordinal variables are similar to the interval-scaled variables, the difference is that it has no units, the actual size of the result variable is not meaningful, but the value of the variable order is important.

$$Z_{if}=\frac{r_{if}-1}{m_f-1} \tag{10}$$

(4) Proportion criteria variable

Proportion criteria variable usually refers to non-linear scale is positive metric. The difference degree calculating in three ways: use the interval-scaled variables method; Do the logarithmic transformation, then use the interval-scaled variables method; Regard as continuous ordinal variables, then use the interval-scaled variables method.

(5) Mixed Variables

Generally, one real database contains four data types described above. One method is the database variables are grouped by type. Respectively, do the clustering analysis for each type of variable. If these variables results obtained after clustering can be mutually compatible, this method is feasible. Another method is to mix all types of variables to a difference matrix, cluster only once.

$$d(i,j)=\frac{\sum_{f=1}^{p}\delta_{ij}^{(f)}d_{ij}^{(f)}}{\sum_{f=1}^{p}\delta_{ij}^{(f)}} \tag{11}$$

Data structure. Do the data preprocess to the collected data before cluster analysis. In the cluster analysis, the following two structures [5].

(1) Data matrix

Data matrix can be seen as a two-dimensional matrix p×q. Rows and columns represent different entities, the general form of this data structure to relational tables. Before the cluster analysis, converted to the difference matrix

$$\begin{bmatrix} x_{11} & \cdots & x_{1n} \\ \vdots & & \vdots \\ x_{m1} & \cdots & x_{mn} \end{bmatrix}$$

(2) Dissimilarity matrix

Dissimilarity matrix is a p×q matrix to describe the p dissimilarity between objects. In the dissimilarity matrix, the rows and columns represent the same entity, the matrix elements of each row and each column has the same dimension. Most of the cluster algorithms are using this data structure.

$$\begin{bmatrix} 0 & & & & \\ d(2,1) & 0 & & & \\ d(3,1) & d(3,2) & 0 & & \\ \vdots & \vdots & \vdots & 0 & \\ d(n,1) & d(n,2) & \cdots & \cdots & 0 \end{bmatrix}$$

Cluster Analysis. There are numerous algorithms available for doing clustering. T Cluster analysis techniques generally can be divided into five categories: clustering based on the division, clustering based on hierarchical, density-based clustering, grid-based clustering and model-based clustering. Typically, these clustering algorithms while providing summary statistics on the generated set of clusters (e.g. mean of each variable, distance between clusters) [6], do not provide easily interpretable detailed descriptions of the set of clusters that are generated. Further, for a given dataset, different algorithms may give different sets of clusters, so it is never clear which algorithm and which parameter settings (e.g. number of clusters) is the most appropriate [7]. They were included a lot of specific algorithms, and the relevant clustering algorithm below.

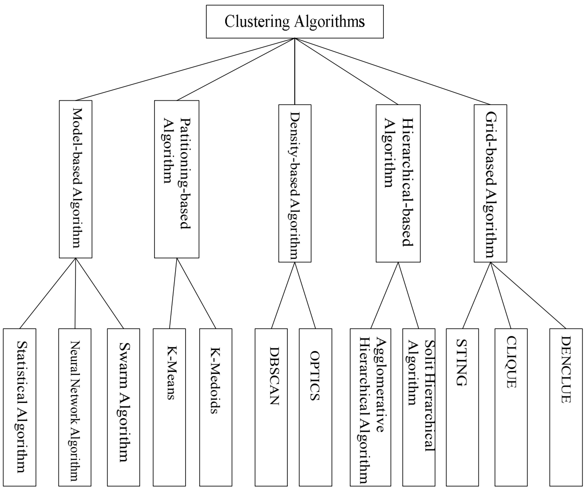
Clustering Algorithms
Model-based Algorithm
Patitioning-based Algorithm
Density-based Algorithm
Hierarchical-based Algorithm
Grid-based Algorithm
Statistical Algorithm
Neural Network Algorithm
Swarm Algorithm
K-Means
K-Medoids
DBSCAN
OPTICS
Agglomerative Hierarchical Algorithm
Solit Hierarchical Algorithm
STING
CLIQUE
DENCLUE

Fig. 2 The web mining taxonomy

This research used an improved K-means algorithm.

(1) K-means

In K-means clustering, clusters are created based on centroids for cluster. Data is clustered into different groups based on its nearness to the centroids. The process is carried out until the centroid stops shifting. The main objective in K-means clustering is to minimize the distance between data points within a cluster, in other words, the objective is to minimize total squared error [8].

Where, the function is equal to the distance between the data point X_i and the centroid C_j. The following Figure illustrates steps involved in K-means clustering:

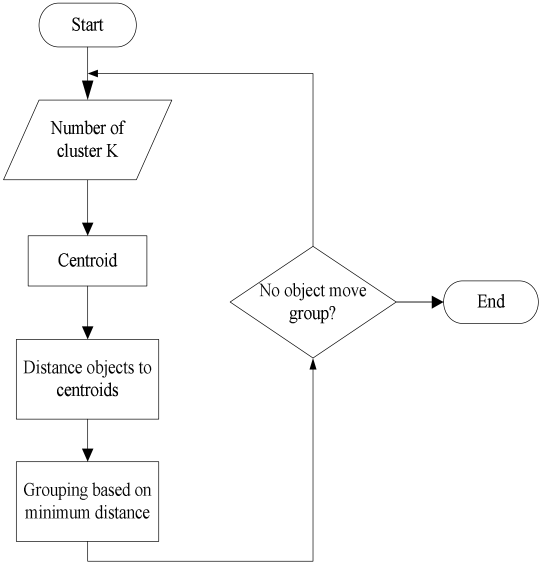
Start
Number of cluster K
Centroid
Distance objects to centroids
Grouping based on minimum distance
No object move group?
End

Fig. 3 K-means clustering steps

Algorithm is as follows:

a) Given a data set *D* contains *n* data; given number of clusters *k*, and the initial cluster centers $Z_f(I), j = 1, 2, \cdots, k$.

b) Calculated the distance from each data object to the cluster center $D(x_i, Z_k(I)), i = 1, 2, \cdots, n; j = 1, 2, \cdots, k$,meet the:

$$D(x_i, Z_k(I)) = \min\{D(x_i, Z_k(I)), j = 1, 2, 3, \cdots, n\}, x_i \in w_k \tag{12}$$

And in accordance with the minimum distance, each object is assigned to the closest cluster.

c) Recalculate the mean of each cluster, and to identify new cluster center; Calculated the squared error criterion function

$$J_c(I) = \sum_{j=1}^{k} \sum_{k=1}^{n_j} \left\| x_k^{(j)} - Z_j(I) \right\|^2 \tag{13}$$

d) Judge: if $\left| J_c(I) - J_c(I-1) \right| < \xi$, then the algorithm ends; Otherwise, calculate k new cluster centers, $Z_j(I) = \frac{1}{n} \sum_{i=1}^{n_j} x_i^{(j)}, j = 1, 2, 3, \cdots, k$, step back.

e) Output k-clustering collections

Using k-means algorithm, need to pre-given number of clusters; For users who lack experience in the industry, it is difficult to find the most appropriate clustering; K-means algorithm is highly dependent initial cluster centers; Algorithm time complexity is high; For categorical attribute data, clustering results are unsatisfactory [9]. So, this paper proposes an improved K-means algorithm.

(2) Improved K-means algorithm

Improved K-means algorithm [10] is as follows:

a) Input data set, and initialization parameters.

b) Run iterative process, and get the K clustering results;

Test whether the clustering result converges, if it is convergence, calculation *Sil (K)* and mark. *Sil* is Silhouette indicators

$$Sil(t) = [b(t) - e(t)] / \max\{e(t), b(t)\} \tag{14}$$

In which, $b(t) = \min\{d(t, C_i)\}, i = 1, \cdots, k, i \neq j$.

Test whether the cluster center meets the convergence criteria, if it is convergence, obtained K clusters, calculation *Sil* $_{max.}$

Test Sil_{max} corresponding optimal cluster number, calculated Hartigan indicators.

$$Ha(k) = (n-k-1)\left(\frac{trSW(k)}{trSW(k+1)} - 1\right) \tag{15}$$

c) Use number of clusters K and cluster centers initialization the K-means algorithm; Run k-means algorithm to get the final clustering results.

Experiment and Analysis

We usually use the web site visitor logs, or CRM information, do the data preprocessing, establish relevant model, use clustering method to segment customers, provide the basis for enterprises to make decisions. The data used in this paper from an e-commerce site. Data including customer information table, merchandise information table, tables and other customer orders， so data attributes numerous and complex.

Customer segmentation based on K-means. Set $K = 4$, K-means customer segmentation results are as follows:

Table 1 K-means clustering

Clustering categories	**Cluster centroids**	**Number of samples**
1	(-1.1890,1.6119)	19
2	(-0.6786,0.1418)	30
3	(0.3360,-0.2445)	22
4	(1.2261,-1.0173)	29

Select the sample data, after data preprocessing and data standardization, the application of algorithms for customer points, as follows:

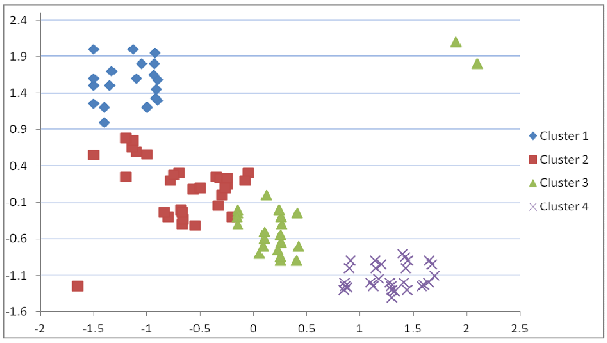

Fig. 4 K-means clustering

Customer segmentation based on Improved K-means. Improved K-means customer segmentation results are as follows:

Table 2 Improved K-means clustering

Clustering categories	**Cluster centroids**	**Number of samples**	**Number of noise data**
1	(-1.1890,1.6119)	12	3
2	(-0.6269,0.1806)	26	
3	(0.1798,-0.4982)	20	
4	(1.2261,-1.0173)	29	

Select the sample data, after data preprocessing and data standardization, the application of algorithms for customer points, as follows:

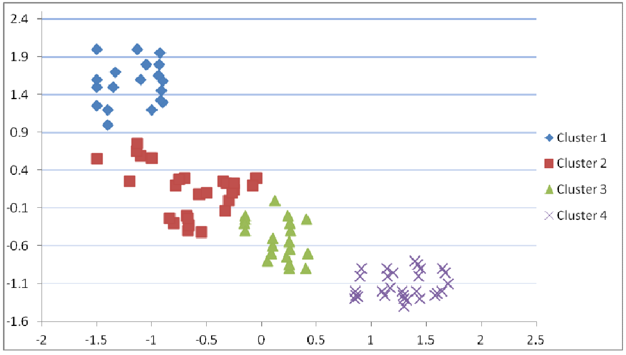

Fig. 5 Improved K-means clustering

We can see that the improved K-means clustering algorithm after the data is standardized, the data also exclude the three noise points and get better clustering results. Therefore, improved K-means clustering algorithm is better than K-means clustering algorithm.

Combined with the above table, we can get the following conclusions:

1) 4th class of customers, the largest number, customers in this category are characterized by less frequent consumption, the average amount of consumption rarely. Combined with customer-related information can be seen, this type of customers are less educated, lower income, age and location of the uneven distribution;
2) 3nd class of customers, the smallest, the average consumption of the least number of such customers, but the average amount of consumption is very high, observed that such customers educated, high income, mostly gathered in Beijing, Shanghai, Guangzhou and other cities, between the ages of 25-35;
3) 2nd class of customers, the average consumer more frequently, the amount of consumption in general, they are about 30-year-old, general education, general revenue, mostly from second and third tier cities;
4) First class of customers, the average consumption frequency less than the second class of customers, the amount of consumption is very high, they are mostly highly educated, high income, age is generally 35 to 45 years, and the amount of consumption is also high.

Acknowledgment

Our thanks to Xi Zhou, Lei Wang, and all the members of the research center of multilingual information technology. This work is founded by West Light Foundation of The Chinese Academy of Sciences (No. XBBS201313), and the National High Technology Research and Development Program of China (No. 2013AA01A607).

This work is founded by West Light Foundation of The Chinese Academy of Sciences (No. XBBS201313), the National High Technology Research and Development Program of China (No. 2013AA01A607).

References

[1] Barak A., Gelbard R., “Classification by clustering decision tree-like classifier based on adjusted clusters”; Expert Systems with Applications, 38, 7, 2011, 8220-8228.

[2] Srivatsava, J., R. Cooley, M. Deshpande and P.N. Tan, 2000. Web usage mining: discovery and applications of usage patterns from Web data. ACM SIGKDD Explorat. Newsletter, 1: 12-23. DOI: 10.1145/846183.846188

[3] Jianxi Zhang,Peiying Zhao, Lin Shang and Lunsheng Wang, "Web Usage Mining Based On Fuzzy Clustering in Identifying Target Group", International Colloquium on Computing, Communication, Control, and Management, Vol. 4, Pp. 209-212, 2009.

[4] R. Dubes, Cluster analysis and related issues, in: C. Chen, L. Pau, P. Wang (Eds.), Handbook of Pattern Recognition and Computer Vision, World Scientific Publishing Co. Inc., River Edge, NJ, 1993, pp. 3–32.

[5] D. Fisher, Knowledge acquisition via incremental conceptual clustering, Machine Learning 2, 1987, 139–172.

[6] L. Wallace, M. Keil, A. Rai, Understanding software project risk: a cluster analysis, Information and Management 42, 2004, 115–155.

[7] Innovations in Intelligent Machines, pp. 1–19. Springer, Heidelberg, 2011.

[8] Patnaik, Sovan Kumar, Soumya Sahoo, and Dillip Kumar Swain, “Clustering of Categorical Data by Assigning Rank through Statistical Approach,” International Journal of Computer Applications 43.2: 1-3, 2012.

[9] Manish Verma, Mauly Srivastava, Neha Chack, Atul Kumar Diswar, Nidhi Gupta,” A Comparative Study of Various Clustering Algorithms in Data Mining,” International Journal of Engineering Reserch and Applications (IJERA), Vol. 2, Issue 3, pp.1379-1384, 2012.

[10] Anoop Kumar Jain, Satyam Maheswari, “Survey of Recent Clustering Techniques in Data Mining”, International Journal of Computer Science and Management Research, Volume 1, issue 1, 2013, 72-78.

Applied Mechanics and Materials Vol. 596 (2014) pp 960-965
© (2014) Trans Tech Publications, Switzerland
doi:10.4028/www.scientific.net/AMM.596.960

Applying Modeling Technique Optimize Business for E-government Based on Big Data

LUO Wen-jie [1, a], YUAN Fang [2,b] and TIAN Xue-dong [3,c]

[1,2,3] School of Computer Science, Hebei University, Baoding 071002, China

[a]luowenjie@hbu.edu.cn, [b]luowenjie@cmc.hbu.cn, [c]wjluo@mail.cyberspi.com.cn

Keywords: visualization modeling; government business model; big data; optimize

Abstract. How to apply big data technique in the innovation of government administration is one of hot issues of e-government. The paper discusses one method that applying visualization modeling technique, builds business model including organization model, resource model and process model. According to the connection rules in or among models, the paper also advances the methods to check integrity of models and simulate the business process for insuring the correctness, and to resolve the problem of normalization and accuracy. Then by extracting and integrating information resources from the business model, obtain unified business frameworks, and according to the efficiency factors that corresponding organization, resource, behavior, collaborative and product performance, collect big data and provide a quantitative analysis for the optimization of government business to guide the government business optimization strategy.

Introduction

The arrival of the age of big data put forward new requirements for the implementation of the functions of the government. In view of the diversity, massive, rapidity, flexibility and complexity of data, [1] the functions of the government facing the innovation management challenges, including: management system innovation, management method innovation and management mode innovation, in order to overcome the problems of current system of social management organization. [2](1)The status quo of government department have "information isolated island" and "fragmentation" management that can't meet the characteristics of big data diversity, leading to multiple business sector regulatory overlap, cross department cooperation and coordination difficulties.(2) On development and utilization of massive data, government departments lack of consciousness of big data, do not attach importance to the collection of data, cause the decision was qualitative rather than quantitative decision making.(3) Big data corresponding to fast and flexible has not formed the social management mechanism of dynamic management for social governance that influence the open, fair and transparent, and the management of precision.(4) Big data corresponding to highly complex, not formed a comprehensive analysis of the data make full use of the system in the existing government management, lack of accurate analysis and intelligence support, resulting in the lack of scientific decision-making. Therefore, how to use the application characteristics of big data, improve the government service performance, to become a big data era for governments facing new challenges and innovation of government functions. From 2010 onwards, the British government and America government has invested large amounts of funds for research on big data, and have access to cost saving effect in administrative office. [3]

In recent years some researchers at home and abroad study on large data research results have been achieved, some mainly include: the concept and characteristics of the data and the age of big data characteristic and development direction; technology innovation research methods to deal with the big data; bring the application data of the opportunities and challenges of the research.

Although the study of big data has achieved some results, how government department in the age of big data make the study on management innovation is very scarce. Mainly on the role of the big data on government management function, the age of big data path of social management innovation choice mentality and social management data platform construction etc. But in all areas of the government function, specifically how to application of big data method to carry on the management innovation, also need to carry out in-depth study and practice.

Analysis of the current situation in the above, modeling, simulation and optimization technology of visualization, construct e-government business model, including organization model, resource model and process model, from the aspects of organization, resources, behavior, collaboration and product such as a full range of description of business, and gain the efficiency factors from, as a big data processing platform construction basis, for the collection and quantitative analysis of big data to obtain guidance, business optimization strategy.

Model Structure and Relationship

In order to solve the problem in the field of e-government business description, information extraction, information sharing and application of optimization of business data technology, implementation method and the modeling method of e-government reference at home and abroad[4], puts forward three kinds of model structure.

Organization Model

Organization model (OM) is used to express the structure of government organization. The components of OM are shown in the following quadruple notation.

$$OM =< OO, OR, OGRules, OSRules > \quad (1)$$

OO is a set of organization objects. There are two kinds of organization objects: organization and role. OR is a set of relations connecting the organization objects. It includes inclusion relation and association relation.

OGRules is a set of syntax rules defining the connect relation rules as follows, which organization model must conform with.

Rule1. Inclusion relation can only be used to connect organizations. It expresses one organization belongs to another organization directly.

Rule2. Association relation can only be used to connect role to organization. It expresses one role belongs to an organization directly.

OSRules is a set of semantic rules defining the rules as follows to check the integration of organization model.

Rule1. There is only one organization node which does not have father organization node.

Rule2. Cycle is not allowed in organization model.

Rule3. In organization tree, it is not allowed that one organization associated to roles that have the same names.

Rule4. NO same organization name is allowed to be in the organization model.

Resource Model

Resource model (RM) is used to express the structure of government resources. The components of RM are shown in the following quadruple notation.

$$RM =< RO, RR, RGRules, RSRules > \quad (2)$$

RO is a set of resource objects. There are six kinds of resource objects: machine, place, tool, abstract machine, abstract place and abstract tool. The first three resource objects are called simple resource. The last three ones are called abstract resource. RR is a set of relations. It includes inclusion relation and association relation.

RGRules is a set of syntax rules defining the connect relation rules as follows, which resource model must conform with.

Rule1. Inclusion relation can only be used to connect abstract resources in resource model. It expresses one abstract resource belongs to another abstract resource directly.

Rule2. Association relation can only be used to connect simple resource to abstract resource. It expresses one simple resource belongs to an abstract resource directly.

RSRules is a set of semantic rules defining the rules as follows to check the integration of resource model.

Rule1. One simple resource only associates to one abstract resource.

Rule2. One abstract resource can be associated to some simple resources.

Rule3. In resource tree, it is not allowed that one abstract resource includes other abstract resources which have the same name.

Rule4.The same name is allowed for simple resources in the resource model tree.

Process Model

Process model (PM) is used to express the flow of government business. The components of PM are shown in formula Eq. 3 and Eq. 4 as follows.

$$PM = < PO, PR, PGRules, PSRules, BM > \tag{3}$$

$$PO = \{A, P, O, R, L\} \tag{4}$$

PO is a set of process objects. In PO, A is an activity set including simple activity and combinational activity. P is a product set. As in-or-out of activity, it includes message, document and combinational products. R is a resource set including machine, place and tool. It supports implement activity. L is a logic set used to describe the logic relations among in-or-out products. PR is a set of relations. It includes data flow, citation flow and association flow.

PGRules is a set of syntax rules defining the connect relation rules as follows, which process model must conform with.

Rule1. Data flow relation can be used in these conditions: between product and activity, from product to in-and or in-or, from in-and or in-or to activity, from activity to out-and or out-or, from out-and or out-or to product, and among the logic objects.

Rule2. Citation flow is used to connect product and activity.

Rule3. Association flow can be used in these conditions: from organization, role, machine, and place to activity, form tool to product.

PSRules is a set of semantic rules defining the rules as follows to check the integration of process model.

Rule1. Simple activity must be associated to one or more roles.

Rule2. Combinational activity must be associated to one or more organizations or roles.

Rule3. It is not allowed that one process object is independent, without connecting to other object.

Rule4. The relations of input connect to a combinational activity must be consistent with them in the combinational activity.

BM is a behavior model which includes simulation behavior and actual behavior, describing the action in process.

Association Rules Among the Three Type Models

In modeling environment, OM, RM and PM are not independent. There are some associations among them. They must follow the rules under-mentioned.

Rule1. The association between OM and PM is n to m. It means one OM can be associated with some PMs, and one PM can also be associated with some OMs.

Rule2. In PM, the association to OM can be inherited. It means the association to the OM at a level of PM can be inherited by the levels under it.

Rule3. The association between RM and OM is n to 1. It means one OM can only be associated with some RMs. All RMs associated to the OM are resources belonging to the organization model.

Rule4. It is necessary to appoint that OM should be associated when building RM.

Rule5. The association between RM and PM is n to m. It means one RM can be associated with some PMs, and one PM can also be associated with some RMs.

Rule6. In PM, the association to RM can be inherited. It means the association to a RM at a level of PM can be inherited by the levels under it.

Rule7. OM or RM, which has passed the check for integrity, can be associated to PM.

Visual Expression for Business

Visual Process Modeling Language

The view-showing, syntax and semantic of OM, RM and PM advanced before, are based on visual process modeling language (VPML) [5]. Formula Eq. 5, Eq. 6 and Eq. 7 express the components of the model in VPML.

$$Model_{VPML} = \{Graphic_{part}, Text_{part}\} \tag{5}$$

$$Graphic_{part} = \{Icon_i, \mathrm{Re}lation_j\}, i = 1, \ldots, m; j = 1, \ldots, n \tag{6}$$

$$Text_{part} = \{Attribute_k\}, k = 1, \ldots, p \tag{7}$$

$\mathrm{Model}_{\mathrm{VPML}}$ expresses the components of the model described by VPML primitively. Each VPML primitive includes two parts: $\mathrm{Graphic}_{\mathrm{part}}$ and $\mathrm{Text}_{\mathrm{part.}}$ As a graphic part description, $\mathrm{Graphic}_{\mathrm{part}}$ is composed of graphic symbol and relationship between these symbols. $\mathrm{Text}_{\mathrm{part}}$ is the text part which is used to record the attributes of corresponding graphic symbol.

Applying Model to Express Business

Organization in OM corresponds to bureau, section and office in government.

The semantic attributes of $\mathrm{Text}_{\mathrm{part}}$ in organization records name, duty, type, charge and coding, etc. Role corresponds to position. The semantic attributes of $\mathrm{Text}_{\mathrm{part}}$ include name, duty, sum, number-used, useable number, workload and cost, etc.

Abstract resource in resource model corresponds to the interior classification of government. Name and description are the semantic attributes of abstract resource. Simple resource expresses material resource. Its semantic attributes include name, description, cost, efficiency and coding, etc.

The activity of PM can be used to express parts of government business. The combinational activity expresses the business which can be broken into activities, and simple activity expresses the business which cannot be divided. Product represents material-requested or material-produced. The semantic attributes of product $\mathrm{Text}_{\mathrm{part}}$ can be used as name, description, principal, connection, and data-created in government business. Resource expresses facilities and places which are involved in business. The role expresses the position in government. The attributes of resource and role are the important parameters for simulating.

The relation between activity and product can express the product which connected to activity is material-requested, foundation, or material-produced in the business. Input flow represents need.

Output flow represents produce. Citation flow expresses foundation. The relation between activity and resource point out where the activity occurs, what are used to do, and who participates in.

The behavior model of process model is represented by the semantic attributes $Text_{part}$ in activities, which can be used to express the business name, business briefing, business process, business management organization, and business implement organization. It can also be used for the setting-up of the starting time and total time limitation of business in the business simulation.

The n to m relation for OM and PM is put forward to be used to represent the multiple businesses the organization owns and the inter-department business that one business connects multi-organizations as well. The n to m relation for RM and PM is put forward to represent that one class of resources can be used for multi-businesses, and one business can be used for multi-resources. The 1 to n relation for OM and RM is used to represent the resources organization owns and that the resources can only be attributed to one organization.

Big Data Analysis Platform for Government Business Optimization

System Construction

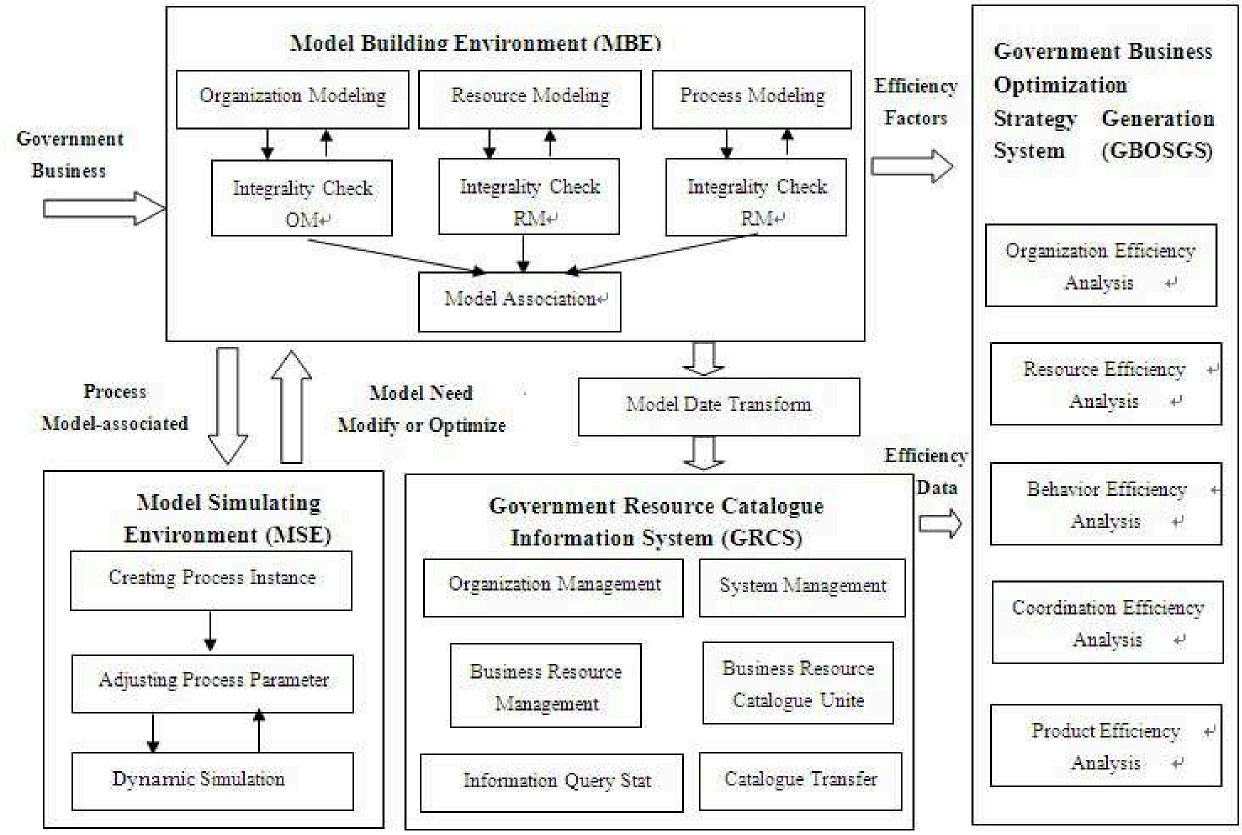
Model Building Environment (MBE)
Organization Modeling
Resource Modeling
Process Modeling
Government Business
Integrality Check OM
Integrality Check RM
Integrality Check RM
Model Association
Efficiency Factors
Government Business Optimization Strategy Generation System (GBOSGS)
Organization Efficiency Analysis
Resource Efficiency Analysis
Behavior Efficiency Analysis
Coordination Efficiency Analysis
Product Efficiency Analysis
Process Model-associated
Model Need Modify or Optimize
Model Date Transform
Efficiency Data
Model Simulating Environment (MSE)
Creating Process Instance
Adjusting Process Parameter
Dynamic Simulation
Government Resource Catalogue Information System (GRCS)
Organization Management
System Management
Business Resource Management
Business Resource Catalogue Unite
Information Query Stat
Catalogue Transfer

Figure 1. System Construct for Big Data Analysis platform of Government Business

Fig.1 shows the system components for acquiring information by model driven. It includes three parts: business modeling system (BMS) , government resource catalogue system (GRCS) and (GBOSGS). The first, composed of model building environment (MBE) and model simulating environment (MSE), is applied to build OM, RM and PM, and produce the correct business model by simulating, optimizing and reorganizing. The meta-model in VPML used at BMS is defined by UML. The second, connected to BMS by model date transform, converses the model data from XML to business information data for query, statistic, uniting and information conform in SQL Server. GRCS shows the business resource information by catalogue style. GRCS is also responsible for collecting business operating data, including efficiency data. The third, obtained efficiency factors about the five points (organization, resource, behavior, coordination, product) of the government business, will use analysis method of big data to generate strategy for the business.

Information Extraction & Acquisition

In the application of the system above-mentioned, three problems about information extraction are solved. The first is setting business granularity flexibly. That means the model data transform can acquire different scale business activity according to the index coding of combination activity set in BMS. The Second is describing and acquiring multi-organization business information. The model transform can converse businesses charged by different organizations in BMS to organization corresponding in GRCS, so that each sub-business of multi-organization business are extracted, those organization cooperated with and material requested, material produced and foundation are recorded also. The last is the catalogue of sharing resource can be produced and transfer to public server. Therefore, seamless connect between modeling system and information system is realized.

Optimize Business by Big Data Analysis

(1) Organization Efficiency Analysis: Providing a number of posts, workload, duties and other aspects of the optimization strategy. (2) Resource Efficiency Analysis: Providing optimization strategy for the use of equipment type, quantity and usage, etc. (3) Behavior Efficiency Analysis: Providing optimization strategy for the business activities of the execution time, sequence, start conditions and end condition etc. (4) Coordination Efficiency Analysis: According to the cooperative sector waiting time, collaborative task completion time and users of collaborative business feedback, optimal government business cooperation relations strategy. (5) Product Efficiency Analysis: According to the number of input and output products in various activities in business process and to meet the requirements for the degree, to adjust the output products and input strategy.

Summary and Future Work

Construction of the government business data analysis platform for visual modeling technology based on, not only can solve the involved information resources carding, business government business processes of integration and unification of business processes and business adjustment problems, but also the application of big data into the optimization of government services, the application of large data the operational and systematic. At present, the platform has achieved BMS and GRCS function, and by using multiple government administrative departments, the basic data for the data application. The next step will be gradually improved in practice GBOSGS, which provide valuable guidance for optimizing the government business.

Acknowledgements

This work was supported by National Natural Science Foundation of China (No.61375075), Soft Science Program and Natural Science Foundation of Hebei Province (No.F2012201020)

References

[1]Ma Ling. The innovation of social management in the age of big data[J]. The Science of Leadership, 2013,vol.11p.23-24.

[2]Fan Xue. Government behavior pattern in the age of big data network innovation in social management[J].Journal of Guangdong Institute of Public Adminstration. 2013.Vol.25 No.4.p25-29.

[3]Tu ZiPei. Big Data Revolution[M].GuangXi Normal University Press.2012.

[4] Li Qing, Chen Yuliu. Analysis of Business and Information System Modeling[M]. Higher Education Publishing House，2007

[5] Wang Lei. Research and implement on the theory of process engineering and integrated process engineering environment[D]. Beihang Graduate School, 1998:14-20.

Applied Mechanics and Materials Vol. 596 (2014) pp 966-970
© (2014) Trans Tech Publications, Switzerland
doi:10.4028/www.scientific.net/AMM.596.966

Modeling Software Architecture Evolution for Electronic Commerce System Based on Graph Representation

Huowen Jiang [1,a] Guijuan Kuang [2,b]

[1]School of Mathematics & Computer Science, Jiangxi Science & Technology Normal University,
Nanchang, 330038, China

[2]School of Science and Information Science, Qingdao Agricultural University,
Qingdao, 266109, China

[a]Jhw_604@163.com [b]1gjkuang@tongji.edu.cn

Keywords: e-commerce, software architecture, evolution rule, graph transformation

Abstract. With the rapid development of mobil internent and internet of things,most of electronic commerce systems need to be improved.Software architecture evolution for electronic commerce system provides an important technology measure for its improvement work. This paper try to model software architecture evolution of e-commerce based on graph representation.Firstly the paper apply a graph to represent SA of a e-commerce system,and give its formulazation description.Then establish some basic evolution rules for software architecture evolution of electronic commerce system on the basis of defining graph transformation rule,software architecture evolution operations for electronic commerce can be carryed out according to these evolution rules.Finally through an evolution case, the sophisticated process of software architecture evolution for the electronic commerce system is described.This research work can help to upgrade the electronic commerce system.

Introduction

The advance of modern mobile Internet and Internet of things technology, has brought the new opportunity for the development of electronic commerce(e-commerce)system, also urges that it is imperative for e-commerce system to upgrade system performance.Software Architecture(SA),which is considered as the foundation of software system, provides an effective way and basis for people to generally grasp software system evolution, How to specify and analyze the evolution process in the SA level has also been the key problem of the software evolution research[1,2].

Modeling SA and its evolution process is always an important part of SA evolution research. For example, The literature [3,4] use unified modeling language to express SA evolution, although the method is intuitive, easy to understand , it is difficult to accurately describe the characteristics of SA evolution because of it being short of formal semantics[5]. The literature [6,7] use different architecture description language to describe the composition and evolution operation of SA,although the method has the advantages such as formalized accurate description, it exsits some shortages to specify SA evolution on the whole because of focusing on analyzing one aspect of SA evolution[8].

As described above, There are many representation methods for describing SA evolution, They have individual advantages and disadvantages.Considering some characteristic of SA evolution of e-commerce system,to represent concisely, simple graph is used to represent the SA of electronic commerce system in this paper, and its formal description is established. So we can specify software evolution of e-commerce system using graph representation.

Graph representation of e-commerce system

For the convenience of depicting software evolution of e-commerce system, firstly we establish the graph representation of e-commerce system in the level of SA, then give its formulization description.

2.1 SA diagram of e-commerce system

Def.1 (Software Architecture,SA).SA of one software system includes the component,which is operating unit of system,the connector which connects components and specifys interactive behavior between components,and the configuration which formulates how to combine components and connectors together. SA can be expressed as a 3 tuple, $SA=(C_p,C_n,C_r)$,here,C_p represents the set of components ;C_n represents the set of connectors;C_r represents the set of constraints.

Here we use graph to represent SA of e-commerce system, where rectangular box is used to represent the component; diamond box is used to represent the connector; Connecting line with mark is used to represent connection and interaction relationship between the component and the connector.

The fig.1 shows a SA diagram of e-commerce system. it includes 3 components:*WebC*,*WebS* and *OracleS*, represent web clients,web server and oracle database server respectively; 2 connectors:*ConW*,which connects between web clients and web server, and *ConO*,which connects between web server and oracle database server; 4 edges, which are labeled with marks(named labeled edge):connecting the corresponding component to connector, showing the connection relationship between them, and reflecting interaction of each other,the mark on the edge indicate the news conveyed from component to connector,while the mark under the edge indicate the news from connector to component. for example, R_{WebC}, R_{WebS}, $A_{OracleS}$, respectively represents client request, webserver request, OracleS response.

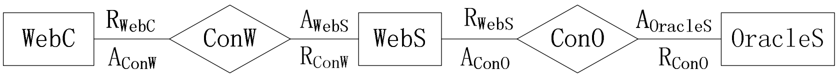

Fig.1 SA of e-commerce system

One SA diagram can be described as a 4-tuple $G_{SA}=(V_{SA},E_{SA},e_{cp},e_{cn})$,where V_{SA} is the node set, indicating all the components and connectors in the SA diagram, namely $V_{SA}=(C_p,C_n)$, C_p is the set of components, C_n is the set of connectors; E_{SA} is the set of labeled edges, indicating the connecting relationship between the component and the connector(namely can indicate the communication ports between two sides); Both e_{cp} and e_{cn} are the set of mark on the labeled edges, defined as the mapping relations on the set of V_{SA}, showing separately the mapping from components to connectors and the reversed, indicating the interaction relationship of their each other,among them, $e_{cp}:C_p\rightarrow C_n$,indicating message input from components to connectors, is labeled on the labeled edges, $e_{cn}:C_n\rightarrow C_p$, indicating message input from connectors to components, is labeled under the labeled edges.As shown in fig.1, $e_{cp}=\{R_{WebC},A_{WebS},R_{WebS},A_{OracleS}\}$,$e_{cn}=\{A_{ConW},R_{ConW},A_{ConO},R_{ConO}\}$

2.2 Formulization description of SA diagram of e-commerce system.

Formally the graph can be described as a set of relation tuples. the node in a graph can be described as the unary relation of the entity. the edge can be described as the binary relation between their connecting nodes. Similarly, we can describe the SA diagram with the relation tuple. for instance, for a SA diagram, the component c_i and the connector cn_i can be described with the unary relation $C_p(c_i)$ and $C_n(cn_i)$; the edge e_i connecting c_i and cn_i, can be described with the binary relation $e_i(c_i,cn_i)$; The interaction relationship between the component and the connector,namely the relationship of message passing e_{cp} and e_{cn}, can be separately described with the unary relation $cp(e_i)$ and $cn(e_i)$, $cp(e_i)$ represents the input message from the component c_i to the connector cn_i on the edge of e_i, while $cn(e_i)$ represents the input message from the connector cn_i to the component c_i; For example the fig.1 can be described with the set of relation tuples as: $G=\{C_p(WebC), C_p(WebS), C_p(OracleS),C_n(ConW),C_n(ConO),e_1(WebC,ConW), cp(e_1), cn(e_1),e_2(WebS,ConW), cp(e_2), cn(e_2), e_3(WebS,ConO), cp(e_3), cn(e_3), e_4(OracleS,ConO),cp(e_4),cn(e_4)\}$, where $cp(e_1)$,$cn(e_1)$,$cp(e_2)$ and $cn(e_2)$,respectively denotes the R_{WebC}, A_{ConW}, A_{WebS} and R_{ConW} in the fig.1, describing the interaction relationship between the connecting components and connectors.

Graph transformation rule and SA evolution rule

Def.2 (SA evolution). It refers to SA transformation such as addition,deletion,replacement,etc. of component or connector, and the corresponding change of interaction relationship between components and its topology structure due to some change, in which user requirements,running environments,software faults are , and other influences related to software system.

Def.3(graph transformation rule). A graph transformation rule $P{:}L\rightarrow R$, it refers to a graph mapping relationship, let L be sub graph before transformation, R denotes the sub graph after one transformation.

Def.4(SA evolution rule). Let the corresponding graph of one SA be G, given a graph transformation rule $P{:}L\rightarrow R$, if we have G' by using the rule to carry out one transformation to G, and the G' denotes the other SA, then P is called a SA evolution rule.

For a SA diagram,both rectangle box representing component and diamond box representing connector can be seen as the nodes in graph,the labeled edge can be seen as the edge in graph,obviously graph transformation rule can be applied to SA diagram transformation.According to the formalized relation description before and after SA diagram change, we can define some rules for SA evolution. Based on the rules for SA evolution,we can carry out the SA evolution of e-commerce system. To facilitate expression, we only give four basic evolution rules below, certainly some complex evolution operations also can be carryed out by a sequences of basic rules.

3.1 The rules for Adding a component or connector

Assuming G be the current SA diagram, the following formula (1) gives the evolution rule of adding a component c_i ; and the formula (2) gives the evolution rule of deleting a connector cn_i

$$G\rightarrow G\cup\{C_p(c_i),e_i(c_i\text{-}G(cn_k)),cp(e_i),cn(e_i),\ldots\} \qquad (1);$$

$$G\rightarrow G\cup\{C_n(cn_i),e_i(G(c_k)\text{-}cn_i),cp(e_i),cn(e_i),\ldots\} \qquad (2);$$

In formula (1), $C_p(c_i)$ denotes the component c_i; $e_i(c_i\text{-}G(cn_k))$ denotes the edge connecting the component c_i to the connector cn_k in the SA diagram; $cp(e_i)$, $cn(e_i)$ indicating the interaction between the component and the connector on the edge e_i, respectively denote input message and output message of the component c_i. Maybe the newly adding component has connecting and interaction relationship with multiple connectors, more than one newly labeled edges need to be added accordingly, so "…" is used to denote omission, like this, the "…" is used in the other evolution rules to be given below. In formula (2), $C_n(cn_i)$ denotes the connector cn_i; $e_i(G(c_k)\text{-}cn_i)$ denotes edge connecting cn_i to the component c_k in the SA diagram G; The fig.2 describes the SA evolution process of adding component c_i and connector cn_i.

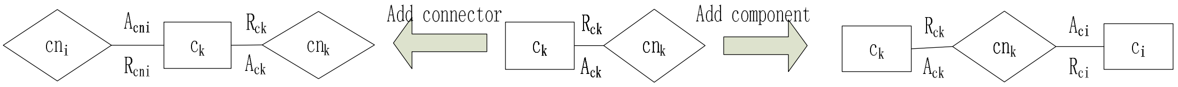

Fig.2 Adding a component/connector

3.2 The rules for deleting a component or connector

Assuming G be the current SA diagram, the following formula (3) gives the evolution rule of deleting the component c_i ; and formula (4) gives the evolution rule of deleting the connector cn_i.

$$G\rightarrow G\text{-}\{C_p(c_i),e_i(c_i\text{-}G(cn_i)),cp(e_i),cn(e_i),\ldots\} \qquad (3);$$

$$G\rightarrow G\text{-}\{Cn(cni),ei(G(ci)\text{-}cni),cp(ei),cn(ei),\ldots\} \qquad (4);$$

When a component is out of use, formula (3) can be applied to delete it from its SA diagram;when a connector is out of use, formula (4) can be applied to delete it from its SA diagram. The fig.3 describes the SA evolution process of deleting a component or a connector.

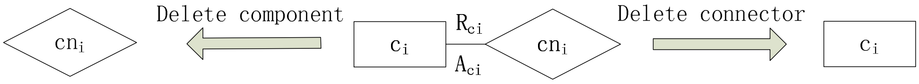

Fig.3 Deleting a component/connector

SA evolution rules can be applied to carry out SA evolution. given the graph G, which denotes one SA, and a SA evolution rule $P{:}L\rightarrow R$, we can define the evolution process of applying P to G as the following:

①Searching for the sub graph L' which is isomorphic to the graph L in the graph G, if successful then go on to step 2, else the rule P cannot be applied to carry out the evolution;

②Deleting all the nodes and edges which are in the sub graph *L*', but not in the sub graph *R*, from the graph *G*;

③adding all the nodes and edges which are in *R*, but not in *L*', into the graph *G*;

④retaining the common nodes and edges of *L'* and *R*, meanwhile connecting the rest parts and newly added parts with the common parts of *L'* and *R*, and keeping the other parts of *G* unchanged, then we have the other graph *G'*, the *G'* is the new graph denoting the SA after evolution.

Case of modeling SA evolution of e-commerce system

To further describe modeling SA evolution of e-commerce system, we give a evolution case for the e-commerce system based on web to illustrate it. For simplicity,assuming the SA diagram of the given e-commerce system is shown in the fig.1.AS the technology advance in wireless network and mobile terminal, Mobile e-commerce becomes feasible and gradually a tendency. To be adapt to the progress, the e-commerce system need to be changed, namely carry out evolution, firstly we can do it in SA level. Assuming the changing approaches be: Ⅰ.using new server "*WMServer*" which is more powerful to replace web server *WebS*. *WMServer* supports the functions of original web server, and supports the functions of mobile e-commerce. Ⅱ.newly adding mobile connector and mobile client, to support e-commerce demand of mobile client.

For the changing approach I mentioned above, we can firstly use the evolution rule (3) mentioned in section 3.2 to delete the component WebS, then use the rule (1) mentioned in section 3.1 to add the component WMServer.the expressions of carrying out the evolution are as the following formula (5)and (6).

$$G\xrightarrow{(3)}G\text{-}\{C_p(WebS),e_1(WebS\text{-}ConW),A_{WebS},R_{ConW},e_2(WebS\text{-}ConO),R_{WebS},A_{ConO}\}=G1 \quad (5);$$

$$G1\xrightarrow{(1)}G1\cup\{C_p(WMServer),e_1(WMServer\text{-}ConW),A_{WMServer},R_{ConW},e_2(WMServer\text{-}ConO),$$
$$A_{ConO},R_{WMServer}\}=G2 \quad (6);$$

For the changing approach Ⅱ, successively using the evolution rule (2) and (1) mentioned in section 3.1 to add the corresponding connector and component.The following formula (7) and (8) shows the evolution.

$$G2\xrightarrow{(2)}G2\cup\{C_n(MobilC),e_1(WMServer\text{-}MobilC),A_{WMServer},R_{MobilC}\}=G3 \quad (7);$$

$$G3\xrightarrow{(1)}G3\cup\{C_p(MClient),e_1(MClient\text{-}MobilC),R_{MClient},A_{MobilC}\}=G' \quad (8);$$

The fig.4 shows the evolution process of the SA of the e-commerce system.where *G* denotes the SA of the original e-commerce system, *G′* denotes the SA of new mobile e-commerce system. The transformation from *G* to *G′* describes the evolution process of the SA of the given e-commerce system, specifies the demand for upgradeing the e-commerce software system properly.

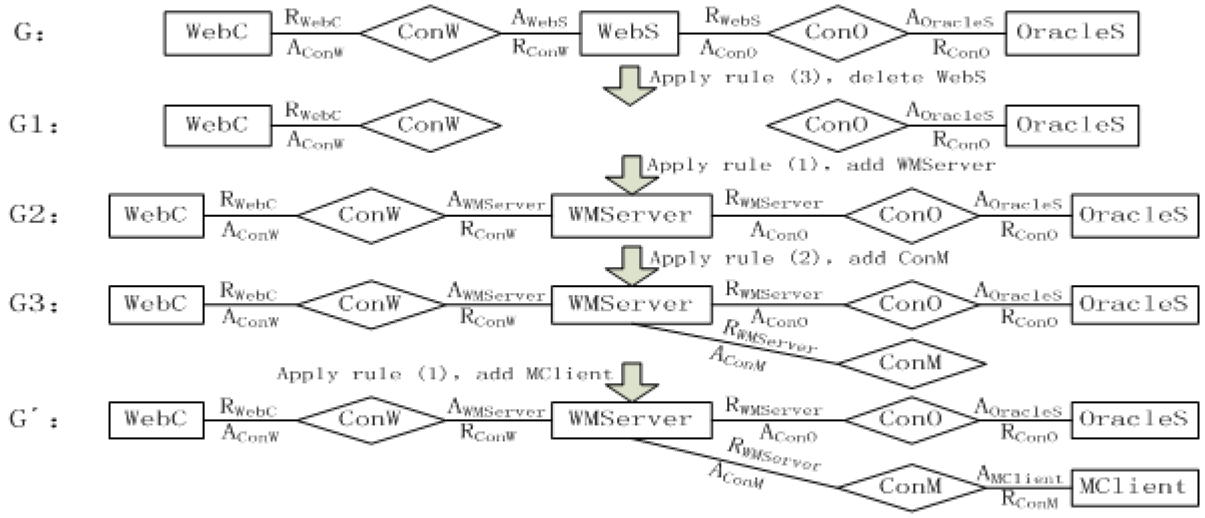

Fig.4 SA evlution process of e-commerce system

Conclusions

SA reflects software system from a higher abstration level, so SA evolution of e-commerce is an important technology means to study the improvement of e-commerce system.This paper proposes the graph representation for SA of e-commerce and its evolution; establish some basic evolution rules based on graph transformation,and give the steps for carrying out SA evolution according to evolution rules.The SA evolution of e-commerce system is specified in this paper. The approach presented in this charter has formalized basis of graph, and also has graphical concision.further, we will investigate the verification of the SA evolution of the e-commerce system, the description of behavioral semantics for SA of e-commerce, and so on.

Acknowledgements

This research work was supported by the Project of Science & Technology Plan by Education Department of Jiangxi Province under grant No.GJJ13569. the Research Subjects of Jiangxi Science & Technology Normal University under grant No. Ky2012zy11.

References

[1] Mei H, Shen JR. Progress of research on software architecture. Journal of Software, 2006,17(6):1257−1275 (in Chinese with English abstract). http://www.jos.org.cn/1000-9825/17/1257.htm [doi: 10.1360/jos171257]

[2] Xu HZ, Zeng GS, Chen B. Conditional Hypergraph Grammars and Its Analysis of Dynamic Evolution of Software Architectures. Journal of Software[J](in chinese), 2011, 22(6): 1210-1223.

[3] M. H. Kacem, A. H. Kacem, M. Jmaiel, K. Drira. Describing dynamic software architectures using an extended UML model. Proceedings of 21st Annual ACM Symposium on Applied Computing, 2006, pp. 1245-1249.

[4] D. Ayed, Y. Berbers. UML profile for the design of a platform-independent context-aware applications. Proceedings of the 1st workshop on MOdel Driven Development for Middleware (MODDM' 06), 2006, pp. 1-5.

[5] P. Pelliccione, P. Inverardi, H. Muccini. CHARMY: a framework for designing and verifying architectural specifications. IEEE Transactions on Software Engineering, 2009, 35(3): 325-346.

[6] Mei H, Chen F, Wang QX, Feng YD. ABC/ADL: An ADL supporting component composition. Lecture Notes in Computer Science, 2012, 2495: 38-47.

[7] Li CY, Li GS, He PJ. A formal dynamic architecture description language.Journal of Software[J](in chinese),2006, 17(6): 1349-1359.

[8] T. Mens, J. Magee, B. Rumpe. Evolving software architecture descriptions of critical systems. IEEE Computer, 2010, 43(5): 42-48.

Applied Mechanics and Materials Vol. 596 (2014) pp 971-975
© (2014) Trans Tech Publications, Switzerland
doi:10.4028/www.scientific.net/AMM.596.971

Study on E-government Virtual Information Service Center Model Based on Cloud Computing

Dong Li [1, 2, a], Xilin Liu [1]

[1] School of Management, Northwestern Polytechnical University, Xi'an, P. R. China

[2] Xi'an Communications Institute, Xi'an, P. R. China

[a] lidongnwpu@126.com

Keywords: Cloud computing; E-government; Information service; Information Service center; Information service model.

Abstract. Cloud computing as a shared infrastructure is a kind of super information systems to provide information services according to on-demands. Cloud computing will become the important means and development trend in future E-government information service. This paper expounds the connotation of the concept of cloud computing at first. Cloud computing technology features are analyzed in the information service of E-government. And a framework model of E-government virtual information service center based on cloud computing is put forward. Interface layer, application service layer, and Data Layer of the model are discussed.

Introduction

Cloud computing has attracted increasing attention in IT community and its benefits are now recognized. Cloud computing, as a shared infrastructure, is a kind of super information system to provide information services according to on-demands.

Cloud computing has become a high frequency word in IT community. Cloud computing and its application are infiltrated into various fields widely under the drive of some manufacturers. As far as information service is concerned, cloud computing is a shared infrastructure. It can coordinate information resources, develop information service in breadth and depth, reduce service costs and enhance effectiveness[1].

Cloud computing will become the important means and development trend in future E-government information service. This paper expounds the connotation of the concept of cloud computing. Cloud computing technology features are analyzed in the information service of E-government. A framework model of E-government virtual information service center based on cloud computing is put forward. Interface layer, application service layer, and Data Layer of the model are discussed.

In order to solve the existing problems in E-government information service , on the basis of detailed analysis of the E-government information service system, a novel idea was put forward that an E-government virtual information service system could be established by using cloud computing. It is expected that the study will improve the methods for E-government information service centre and increase the E-government information service ability.

Cloud computing

Definition of cloud computing. According to the U.S. National Institute of Standards and Technology (NIST) [2]: "Cloud Computing is a model for enabling ubiquitous, convenient, on-demand network access to a shared pool of configurable computing resources . . . that can be rapidly provisioned and released with minimal management effort." NIST further differentiates cloud as having five essential characteristics, three service models, and four deployment models. Each layer can be provided on top the other, but many SaaS or PaaS providers still prefer to provide services on top of their own infrastructure today. Different service providers operating at the same layer are beginning to standardize their interfaces to enable "horizontal integration" (e.g. open virtual machine formats). However, “vertical integration” among different cloud service layers and providers is still an ongoing research area. The results of these investigations will affect large-scale government and business cloud deployment decisions.

Cloud computing[3] is a relatively recent and currently high-profile method of IT deployment. Compute facilities such as virtualised server hosting or remote storage accessed via an API, are provided by a cloud provider to a cloud client. Often a client is a third party company, who will use the compute facilities to provide an external service to their users. For example, Amazon is a cloud provider supplying a storage API to Dropbox, who use the API to provide a file synchronisation service to domestic and commercial users.

Cloud features. The following features are commonly associated with clouds. A consumer can be an individual lab, a consortium participant, or a consortium[4].

Virtualization: Hardware resources in clouds are usually virtual. They are shared by multiple users to improve efficiency. That is, several lightly-utilized logical resources can be supported by the same physical resource.

Resource outsourcing: Instead of a consumer providing their own hardware, the cloud vendor assumes responsibility for hardware acquisition and maintenance.

Automated resource management: This feature encompasses a variety of configuration tasks typically handled by a system administrator. For example, many clouds offer the option of automated backup and archival. The cloud may move data or computation to improve responsiveness. Some clouds monitor their offerings for malicious activity.

Parallel computing: Map/Reduce and Hadoop are frameworks for expressing and executing easily-parallelizable computations, which may use hundreds or thousands of processors in a cloud.

E-government Virtual Information Service Center Based on Cloud Computing Framework Model

An Government Virtual Information Service Center based on cloud computing is a “virtual administrative service hall” in the "cyber space" different from the traditional government web sites in that it can not only provide government information service, but also release new government services constantly[5].

Government Virtual Information Service Center on cloud computing is a concrete implementation of "one-stop" e-government.

Government virtual information service center can seamlessly integrate information resources distributed in various government departments, promptly make publicity of information, and actively conduct interaction with customers.

Since the cloud computing have the advantage of open, flexibility and convenience, the cloud and cloud-based application programs will undoubtedly become the main intermediums for information exchange between different governments virtual information service centers.

Based on cloud computing, this paper proposes an E-government Virtual Information Service Center Based on Cloud Computing Framework Model as shown in Fig. 1.

Interface Layer. Interface layer is the public information portal that provides the government with a unified information service platform and is an intermediary for information exchange between different governments virtual information service centers. The public submit all service requests, such as information retrieval, information customization, user registration, etc., and send feedback information through this information portal.

The development trend of E-government is to provide a "one-stop" service for the public through a unified government information portal. This simplified the work process and can improve efficiency. A government virtual information service center uses a kind of asynchronous process to collect service requests from the public, converts the volatile input stream into consistent information requests through cache memory and sends them to the backstage of the virtual service center. This not only make responses to the service requests of the public more quick, but also make the government virtual information service center more flexible in load balancing and scalability. As the intermediary for direct interaction between government virtual information service center and the public, the E-government integrated information service platform includes the following features:

(1)Quickly release government information and services. (2) Provide multi-channel government services. (3) Service inquiry and oversight. The information service platform will make all governmental sectors' work progress known to the public to facilitate other sectors' and higher authority's real-time inquiry and public's scrutiny. This can not only improve the efficiency of collaborative work but also increase transparency of government services.

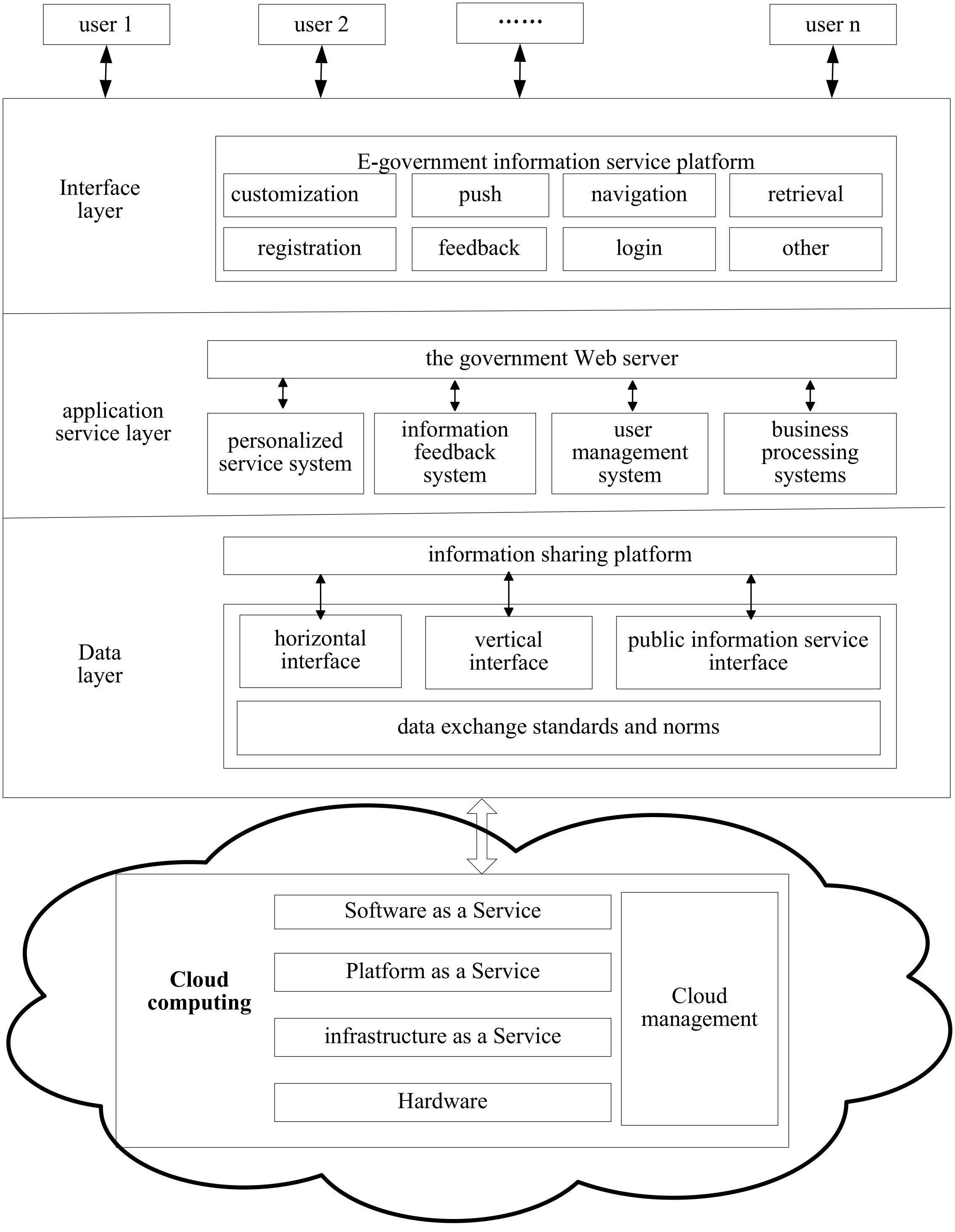
user 1
user 2
……
user n
Interface layer
E-government information service platform
customization
push
navigation
retrieval
registration
feedback
login
other
application service layer
the government Web server
personalized service system
information feedback system
user management system
business processing systems
Data layer
information sharing platform
horizontal interface
vertical interface
public information service interface
data exchange standards and norms
Cloud computing
Software as a Service
Platform as a Service
infrastructure as a Service
Hardware
Cloud management

Fig. 1 E-government Virtual Information Service Center Based on Cloud Computing Framework Model

Application service layer . The main task of application service layer is to analyze the information needs, model file information, and log information of various customers to construct and revise their information needs models, make deep processing of the retrieved results in each information inquiry by different users and match them with user models by using data mining and information filtering technology. In fact, this layer accomplishes perfect matching between user information (i.e., user needs and model information) and system’s resource information to find out data sources that can best satisfy each user’s information request and best reflect each user’s model information. Application service layer is the functional incarnation of the E-government cloud information service of government virtual information service centers.

In application service layer, the application server software is divided into different functional modules according to different processing logics. These functional modules include:

(1)Data acquisition module. The main function of this module is to accomplish common data retrieval call according to user's information needs. (2) Data Mining and filtering module. Its main function is to match user model and user needs with data resources. (3) Establish user interest model module the task of which is to collect all kinds of information about user interest and research area, accurately describe user interest, and generate user model by using data mining algorithms.(4) Model updating module. The task of this model is to continuously track changes of user interest, analyze access logs to adjust user model.

Data Layer. The main problems that data layer of a E-government virtual information service center based on cloud computing has to solve are how to integrate various data sources and unify their description, and how to make effective management of distributed, heterogeneous data sources to form a unified data resource available for analysis by and call from upper layers. At the same time data layer also manages and maintains a model library for each user as well as the information database of the dynamic behavior (such as the access log information) of the user.

Data layer provides powerful information support to government personalized information service. As the core component of a government virtual information service center, data layer has the following functions:

(1)Data storage service. Data layer provides function of storage for real-time information, historical information, basic data, user needs information, and other government information.(2) Data exchange service . Data layer provides a safe, stable, high-performance, cross-platform, cross-system and cross-application data exchange platform, and accomplishes transparent exchange of information between heterogeneous systems, and between old and new systems.(3) Data Management service. The purpose of data management is to ensure security and integrity of government databases, implement data backup and recovery, and database concurrency control.

Cloud Computing Network. Cloud computing is frequently presented as a layered architecture, as shown in Fig. 1. Cloud services should essentially have on-demand network-based accessibility, resource pooling and rapid elasticity characteristics, could be provided via software, platform or infrastructure as-a-service models (as illustrated in Fig. 1), and be made available through private, community, public or hybrid deployments. An infrastructure service (or IaaS) virtualizes the capacities of physical computing hardware such as the CPU, storage or networking equipment and provides remote, shared access to these virtualized resources. Platform services (or PaaS) are usually exposed via web services and are shared among different desktop applications as well as online software services. End-user software services (or SaaS) hide the infrastructure or platform specific details from the clients and they are usually accessed via web portals.

SOA（service-oriented architecture）is used to design cloud services. The cloud services designed by SOA can meet the needs of software interoperability and mashup. SOA is a component model [6], which refers to different functional units of the application as services. Services are linked by well-defined interfaces and agreements among one another. Interface is defined by using neutral manner and is independent of the hardware platform, operating system and programming language for implementing services, which makes the services constructing in a variety of system interact in a unified and general way. The emergence of SOA brings a new concept to traditional information industry. Information systems are no longer separated architecture forms, but can easily contact each other and combine and share information. SOA is known as the basis framework of next generation

Web services. Now it has become a new development direction in the computer information field. Because Service-oriented architecture conforms to the information development of colleges and universities from passive response to proactive service, it is becoming the development direction of colleges and universities information service.

Conclusions

At present, “E-government” ranks in the first place in five application fields for“information highway” in the world. In building E-government systems each government himself has designed information systems for centering on the government institutions according to its own condition and requirement. Cloud computing and its application are infiltrated into various fields widely under the drive of some manufacturers. As far as information service is concerned, Cloud computing is a shared infrastructure. It can coordinate information resources, develop in breadth and depth of information service, reduce service costs and enhance effectiveness. In this paper, we introduce the concept of cloud computing. Cloud computing technology features are analyzed in the information service of E-government. A framework model of E-government virtual information service centre based on cloud computing is put forward. Interface layer, application service layer, and Data Layer of the model are discussed.

Acknowledgements

This work was financially supported by the National Natural Science Foundation of China(71103138) and the China Ministry of Education Humanities and Social Science Programming Foundation (06JA630057).

References

[1] Li Peiwei. Research on information service based on cloud computing[D]. Xiangtan university. 2011[In Chinese]

[2] Ari I, Muhtaroglu N. Design and implementation of a cloud computing service for finite element analysis. Adv Eng Softw(2012), http://dx.doi.org/10.1016/j.advengsoft.2012.10.003

[3] Mell and Grance. The NIST definition of cloud computing. National Institute of Standards and Technology 53, NIST Special Publication 800-145.

[4] Arnon Rosenthal, Peter Mork, Maya Hao Li, etc.. Cloud computing: A new business paradigm for biomedical information sharing. Journal of Biomedical Informatics 43 (2010) 342–353

[5] CHEN Hong-jie. Research on the E-Government Personalized Information Service Based on Data Elements[D].2007[In Chinese]

[6] Ling XiaoDong. SOA reviewed. Computer applications and software. 2007, 24 (10)：22-124, 199. [In Chinese]

Applied Mechanics and Materials Vol. 596 (2014) pp 976-980
© (2014) Trans Tech Publications, Switzerland
doi:10.4028/www.scientific.net/AMM.596.976

The Research of Digital Challenge to Tourism Destination Brand

Weiya Zhang

Department of Tourism Management, Jinling Institute of Technology, Nanjing 210038, China

zhangweiya@jit.edu.cn

Keywords: digital challenge, destination brand, customer behavior

Abstract. Considering the tools, technologies and channels are driving significant change in customer behavior, the paper focus on how destinations are currently using them. Then the paper discusses the key challenges facing destination branding – content, socialization, integration, and measurement. At last, the paper considers what this means for destination brands, the DMO website and digital marketing strategy.

Introduction

Digital channels have driven a radical shift in customer behavior and this is no more evident than in the customer's relationship with a brand and the active role the customer takes in shaping the dialogue with that brand and ultimately its reputation. Digital channels have grown up and no longer represent 'new' media. Just when marketers were starting to understand traditional 'push' media such as display and email, the balance of power changed. At the same time response through traditional channels has fallen, on and offline, as consumers are becoming increasingly turned off by one way dialogue. The now infamous Web 2.0 brings with it a collection of open source, interactive, and user-controlled online applications that support the creation of informal networks and facilitate the flow of ideas and knowledge by allowing the efficient generation, sharing and editing of informational content. The terms social media and Web 2.0 are often used as interchangeable but social media is associated with the social aspects of Web 2.0 applications – participation, openness, conversations, community and connectedness. The marketing environment has changed beyond all recognition and relentlessly pushing destination brand to an increasingly skeptical audience is becoming less effective in driving brand equity. It is now possible to collaborate on an unprecedented scale with anyone and everyone involved in shaping destination brand.

Tools, Technologies, and Channels

So what are the key tools and technologies within the tourism and travel space and how are DMOs currently using them? Blogging is becoming synonymous with the Internet and is seen as particularly important within tourism and travel [1]. There is an opportunity to reach out to the blogging community and influence what they are talking about in much the same way as traditional PR does to travel journalists. By utilising a syndicated blogging platform a DMO can aggregate and provide filtered search across blog contributions from a variety of contributors; the organisation itself, its marketing partners, the tourism industry and the visitors themselves.

Microblogging based on a stream of short text updates, currently in the form of twitter, has got to be the most talked about online application of the moment. One of its most powerful facets is its immediacy and mobile application – for customers, it provides a powerful real-time search engine, which can be accessed on the fly and instantly tuned to interest and specific need. Often lacking strategic direction, a destination's current approach to microblogging is typically organic with similar feeds competing for the same followers.

Social networking means people can come together and create relationships online, often forming communities around specific interests. Destinations can create their own online communities within existing platforms or engage in dialog with an existing community. To what extent visitors and potential visitors can be expected to join communities on multiple specific platforms rather than engage with them through their trusted and favored platforms remain to be seen. Much of the content across social networking sites, and increasingly that accessed directly through search results, originates from the users themselves and as such provides a wealth of peer-produced dynamic and relevant content untouched by marketing people.

Real Simple Syndication (RSS) means the user can subscribe to specific content and receive updates directly rather than having to visit that specific website. Widgets provide mini applications that can be downloaded to a user's desktop or embedded in third party sites. The end result is that increasingly it is the user that retains control of their own personalised online experience and it remains their choice about what content they interact with and from whom it comes. One feature of travel-related content is that it is generally associated with place – it can be georeferenced. Google mapping has been a Web 2.0 success story and none more than in travel and tourism[2]. The ability to integrate Google maps in a website and overlay with navigation and product information has become the standard for product search. The ability to 'mashup' travel product with an endless array of user-generated georeferenced content is extremely powerful and more recently Google Street View has enabled another level of virtual experience for the potential visitor.

Supporting everything digital is the explosion in high speed Internet access – increasingly accessed through wireless networks. Rich audio visual content is no longer limited to the traditional broadcast channels we have worked with for so long and those very same channels are available online and can be accessed on demand to supplement an increasingly personalised online experience. Add to this the huge development in mobile technology and the inevitable convergence across media, channels, and devices, and you are faced with an environment in which not only can consumers consume content anywhere but they can also create and share from anywhere.

Customers are taking control of their relationships with brands, and the system of values, beliefs and attitudes that shape and influence customer behaviour has changed. Information culture has been replaced by conversation culture. Conversations online ultimately shape your brand and, at its most extreme, your brand becomes its reputation online defined through the conversations customers are having about their real brand experiences. Those conversations are seamlessly conducted across the real and virtual worlds as multitasking becomes a way of life; discussing, reading, browsing, contributing whilst eating and drinking. Whilst the decision to take a holiday might be an entirely rational one, the decision about where to take that holiday is likely to be an emotional one and influenced by the wealth of conversational content associated with that destination.

The Digital Challenge

So what are the key challenges facing destination branding within the context of a changing digital media landscape and changing customer behaviour? The challenges lie in four key areas – content, socialisation, integration, and measurement.

Content. We are all publishers – content is king and right now user-generated content reigns supreme. In the old destination marketing world, most content was locked up in the brochures that the DMO and their marketing partners wereproducing on a seasonal or annual basis. When more of that content resource moved online marketers suddenly realised that what could be saved in print production wasn't nearly enough to fund the provision of content across a more dynamic presence on the Internet. Marketers are never going to keep up and they need to find another way to fuel that content hungry web presence. Our destination and destination brand occupies a particular online space and within that space exists a network of content creators and content consumers.

The Internet provides a truly collaborative environment and the challenge therefore is how does the destination harness that resource and mobilize it to help fulfill their marketing goals. Communities need something to lineup against, and the campaign line 'Real adventure holiday ideas' was a credible proposition and something that the network of content creators and consumers could get behind and support. Customer commentary, in response to specific posts has not always been one hundred percent positive. The point being though is that the rational consumer is capable of making a reasoned judgement. Where that commentary is concerned the fact that it was not entirely positive adds to the content's credibility and most people viewing that content will come to their own, invariably positive, conclusions. In the pursuit of reputation management and brand equity online the organisation can listen to these conversations and it can engage in the conversation for its own benefit if it so decides. The content itself lasts well beyond the life of the campaign or blog post. Any destination has a wealth of content associated with it – a long tail of content covering the spectrum of place content from country, through regions, cities, and towns and ultimately specific businesses.

Relevance, quality, and appropriately linked content drive search traffic. Destination marketing should be concerned with both making sure that the customer experience is serviced appropriately by the destination's content network as well as ensuring that the content network handles search traffic efficiently. This might also provide a framework for defining keyword territories for DMOs, their marketing partners and tourism businesses themselves.

Socialisation. Socialisation can be defined as 'the process of learning one's culture and how to live within it' – for an individual it provides the skills and habits necessary for acting and participating within their society. Destination brands have to learn about conversation culture, how to position themselves and how to apply an appropriate set of tools and approaches to participate in this new world. No longer can they rely on shouting from the rooftops or buying an audience – they have to find new and innovative ways of attracting an appropriate audience and orientate themselves with that audience. Customers can arrive at website from almost anywhere but generally that covers three key types of digital media: owned, earned, and bought. Owned media includes own website, all of other websites and communications with existing customers. Earned media is much more about engaging with communities, listening to them and seeding conversations in those communities. To be successful in the earned media space, a brand needs to orientate its web presence within both the network of user-generated content that exists beyond its own site as well as the conversational content that surrounds it.

Integration. The occasions when a customer comes into contact with your destination brand, in the real or virtual world, are almost limitless. Integration really matters. Destination marketing needs to support the customer journey from inspiration, through booking and planning, catering for customers' needs at the destination, as well as building advocacy and creating return visits. The fragmented nature of the tourism product has always made coordination of this effort across different marketing partners and the industry a complex challenge. The same marketing objectives still apply – the destination still needs to acquire new customers, convert them, retain and grow business as well as measure and optimise what it is doing. The development of Web 2.0 and social media is indeed a fundamental and revolutionary change but the extent to which it currently dominates marketers' conversations should not mask the fact that what it provides is another set of channels that should be approached strategically, evaluated like any other channel and planned as part of an integrated digital marketing strategy.

The same argument extends to offline channels and broadcast media – digital does not replace offline communications, it works alongside them, enhances them and adds value to them. Destination marketers need to remain cognizant of their target market's media habits and a multichannel strategy, at its best, can deliver stronger brand performance and customer loyalty[3].

Broadcast media, traditional or in the broadband era, will continue to support inspirational content and provide the vehicle for mass distribution of inspirational messages. It provides the opportunity for the brand to define its position and its opinion on something – over and above the noise created through social media. It amplifies that noise, drives awareness, and brings the brand front of mind, supporting other channels and increasing demand for your search terms. Although social media is often hailed as being a brand crusader in times of reducing resources, destination brands must take account of or at least be aware of the opportunity cost associated with developing new channels and new approaches.

Measurement. New ways of doing things require new approaches to measurement. Destination marketing activities are often concerned with campaigns and measurement typically focuses on campaign awareness, response and conversion with an indicator to the effect on destination awareness and emotional proximity to that destination. Where online is concerned we measure success through things such as site traffic, numbers of unique users, the amount of content viewed, and on site conversion. In our new environment our success is much more dependent on things like the quality of our content network and the amount and sentiment of conversations carried out within the community of people with which we connect. Platform-specific metrics should be used in combination with other digital marketing benchmarks.

Whilst social media and online PR will drive traffic to site, it is the attention to brand and the ‘buzz’ it creates around it that is particularly important. However, measuring sentiment and the overall affection towards a brand is perhaps one of the more challenging measurement activities. Where measuring the social web is concerned, Huang (2006) suggests taking an approach that covers four key areas; involvement, interaction, intimacy, and influence[4]. Involvement relates to the number of people in network or community, interaction measures the number and type of action taken by those people, intimacy relates to the overall affection or aversion to brand and influence measures the level of advocacy within network.

What Does This Mean For Destination Brands?

It’s fair to say that destination branding online has become more complex. In the online space brand’s reputation is molded and defined by conversations and dialog, networks, and communities. The challenge is fundamentally about reputation management and influencing collective opinion in the new networked environment.

However, in the absence of a ‘set piece’ solution the new marketing environment is producing unprecedented levels of creativity, technical convergence, and some great storytelling. Brands need to listen to all the information provided by customers (both explicit and implicit), understand the past and present to determine the best possible course of marketing action and communicate in a manner that is compelling, timely, and relevant[5].

Perhaps then, the art and science of marketing in this new environment is fundamentally about deciding when to listen, when to take part and when to stimulate and cultivate conversations. Consumer opinion and sentiment can make or break a business and crisis management. However, if a destination brand has built trust and support with the wider community over time by engaging with the network and activating brand participation then in times of crisis that same loyal army of brand evangelists can quickly counter balance and neutralise negative commentary. Deciding which stories to tell and which conversations to cultivate requires an understanding of past and present perceptions of the destination. DMOs are privy to a vast amount of consumer research highlighting the perceived destination negatives and commonly propagated stereotypes and misconceptions. An effective social media strategy should therefore tactically deploy and instigate stories that address these destination negatives and support them with examples of ‘best in class’ product.

Challenger brand thinking resonates as strongly today as it did 10 years ago; be ruthlessly focussed; overcommit to what you do; stand out and stand for something unique in category; communicate this constantly, consistently, and saliently[6]. Going big and communicating a consistent story becomes an even more exciting possibility when we consider harnessing and engaging our network of content creators. It is generally accepted that the best online PR campaigns come from collaboration across different disciplines within the organisation and among multiple external agencies and you can add to this the opportunity to leverage the brand equity of authoritative brands through appropriate partnerships and bought media. Successful destination branding in the new world relies on a collaborative approach and harnessing the power of the content network, the community, and like-minded brands where the overall effect is greater than the sum of the individual parts.

Conclusions

Awareness and use of DMO websites is lower than that of commercial websites in the same space. Whilst perceived as an authoritative site by those that use them, their role as the 'official' site for the destination brings with it some less attractive connotations – limited and mainstream information, a biased view of the destination. A perceived lack of objective and comparative information means their usefulness where initial destination choice is concerned is less than it might be. They score more highly for the provision of information that has no commercial motive – weather, security, visas, currency, museums, attractions, and background information on the destination's culture, history, and geography. Within the context of the customer journey DMO websites are currently used primarily at the planning and pre-visit stages.

DMO websites are often built on a Destination Management System that powers the front end, as well as providing product search, retrieval, and backend functionality. Web 2.0 and socialisation brings with it a new set of tools that need to be integrated with existing systems and platforms. The relationship with stakeholders and the industry can be a very different one in this new environment; potentially hugely collaborative, but roles and responsibilities need to be redefined and as such it represents a significant cultural change. However, it is perhaps internal organisational change where the greatest barriers exist. Digital marketing strategy needs to be particularly responsive to a changing market and the organisation needs to be able to respond more quickly to the opportunities and threats this brings. DMOs are not typically strategically agile organisations but if they are going to survive in an environment of rapid and constant change they need to engage in strategic analysis, development, and implementation on a more continuous basis and over shorter cycles than they have ever done in the past. Success requires the right people, the right mindset, the right internal structures, and the right stakeholder and industry relationships where, across all of those things, innovation, decentralisation, and collaboration are all important.

References

[1] E. Constantinides, S. J. Fountain: Web 2.0: conceptual foundations and marketing issues. Journal of Direct, Data and Digital Marketing Practice. Vol. 9(2008), p.231–244

[2] W. Spanner : What is social media. Journal of Direct, Data and Digital Marketing Practice. Vol. 9(2007), p.231–244.

[3] L. Bruce, K. Bondy, R. Street & H. Wilson: Channel evolution: how new multi-channel thinking can deliver competitive advantage. Journal of Direct, Data and Digital Marketing Practice. Vol.10(2009), P.329–335.

[4] J. Huang: Exploration of tourism brand image logo design. Journal of Guilin University of Electronic Technology. Vol. 6(2006) , p.235-238

[5] E. R. Anderson: Next-generation campaign management: how campaign management will evolve to enable interactive marketing. Journal of Direct, Data and Digital Marketing Practice, Vol.10(2009), p.272–282

[6] H. Wei, L. S. Zhang: Study of design principle of tourist logo. Art and Design. Vol. 4(2004), p. 14-15

Applied Mechanics and Materials Vol. 596 (2014) pp 981-985
© (2014) Trans Tech Publications, Switzerland
doi:10.4028/www.scientific.net/AMM.596.981

IOT Application Research between Digital Publishing and Traditional Publishing

CHEN Zhi Wen [1, 2, a]

[1] Shanghai Publishing and Printing College, Shanghai 200093, CHN

[2] School of Information Management, Nanjing University, Nanjing 210093, CHN

[a]570296620@qq.com

Keywords: IOT Application, Traditional Publishing, Digital Publishing

Abstract. Internet of Things (IOT) used in the field of traditional publishing and digital publishing is studied, which not only can enhance the information capability of publishing industry, but also protect the security of the publication. Comparison from RFID tag of traditional publishing, digital publication tag based on IOT has more advantages in position, visibility, environmental impact and cost etc.. Application issues in the publishing field are analyzed and suggestions are discussed from standard to technology, which includes standard system construction, system security, RFID tag cost of traditional publishing, digital rights and industry research of watermark technology for digital publishing.

Introduction

Internet of things (IOT) is a high level support for the latest information technology in the world and is an important force to promote information technology to a new state in various industries. IOT is a very valuable business and application on the Internet [1], but IOT application in the publishing field is nearly a blank state till now. Logistics circulation in digital publishing fields [2] is relatively automatic with little manual operation, so the error rate is greatly reduced, comparison to that of the traditional IOT application. Radio frequency identification (RFID) tags are posted on the various goods. According to the agreed protocol, Convergence of goods in any time and space and information exchange can be achieved. In a word, IOT Application is to realize automatic identification of goods and information sharing through Internet [3].

Application Analysis

Basic Model. In general consideration, IOT consists of four levels as follows, perception layer, transport layer, operation layer and application layer from the bottom to the top. If human body is to be compared, perception layer is used to identify objects like facial features and skin, which collects the relevant information from RFID tags [4]. Information on RFID tags is different in different state, so it needs to be timely updated throughout the application circulation. IOT application senses and acquires data in the front-end from RFID tag, transmits data by 3G/Wi-Fi technology, stores, processes and controls data in the back-end by cloud computing and big data technology.

IOT Business Model in the Field of Traditional Publishing. Traditional publications need experience five sessions at least from creation to final consumption of readers, such as publishing editor, printing, logistics, sales and application. In general, the corresponding issuing circulation is as follows: through Press to issuing house (first wholesaler), through first wholesaler to Region bookstore (second wholesaler), through second wholesaler to retail bookstore, through retail bookstore to final reader. Generally, to distinguish the different publications, there is an identity for every traditional publication. The identity is printed on the publication as a form of barcode. For paper book, international standard book number (ISBN) would be printed on the bottom page of the book in the printing session. Besides ISBN, exchanged information during circulation also includes other relevant information, which can’t be bundled with publications and exists in the related paper documents or software system. The business model of IOT applications in the field of traditional publishing is as following, RFID tag is pasted on the publication, which replaces the barcode of books and audio-visual products. The identity of traditional publication, such as ISBN, is used as an important data of RFID tag, other relevant information during the circulation is also recorded in the RFID tag. Thus, the IOT application in the field of traditional publishing industry chain includes publishing, printing, and issuance, end-use applications, and even chip development, hardware and software research and development etc.. IOT applications can help to establish publication information platform, which can realize recognition and retracement. Five sub-systems of traditional publications including editing, printing, logistics, sales and application, are closely linked through RFID tag, network and services support of back-end data center.

IOT Business Model in the Field of Digital Publishing. Digital publication in the digital publishing industry is an application object based on Internet. Digital publications need experience three sessions at least from the creation of digital publication to final consumption of readers, such as publication creation, distribution, reader consumption. The corresponding issuing circulation is as follows: through the provider of digital publication to vendor of digital publication, through vendor of digital publication to reader. Compared with traditional publishing, digital publishing has no printing circulation and logistics are greatly simplified. Similarly, every digital publication should have an identity in order to distinguish the different digital publication. The identity can't be printed on the publication like the traditional publication, but IOT application model of traditional publishing can be referenced. IOT Application and business model in the field of digital publishing can be understood as follows. The perception layer is mainly used to identify digital publications. Information can be embedded/extracted into/from the digital publication and from the by software, such as watermarking software. Watermark information can be hidden to the digital content, which is equivalent to outside an invisible RFID tag called digital publication tag. Hidden information should be different and can be embedded in times in the entire digital publishing applications circulation, such as registration link, sales links, etc., which is also equivalent to the RFID tag information to be updated. If the RFID tag information is the identity of IOT object, digital publication tag is also the identity of digital publication based on IOT.

Application Comparison. RFID tag reading of IOT object has more advantages than barcode reading. However, compared from the digital publication tag based on IOT model, the disadvantage of the traditional publication tag based on RFID tag is very evident. Their comparison is shown in Table 1.

Tab. 1 Comparison between Digital Publication Tag and Traditional Publication Tag

Parameter	**Traditional Publication Tag**	**Digital Publication Tag**
Tag Position	Posted outside traditional publications	Embedded into digital publications
Tag Visibility	Visible to users	Invisible, Transparent to users
Information Update	Both Hardware and Software	Only Software
Perception Mode	Hardware	Software
Environmental Impact	Yes	No
Wear	Yes	No
Cost	Yes	No

Application Issues

IOT application has a great industrial value in the field of traditional publishing and digital publishing. At moment, because IOT application is considered a cutting-edge application in the world, existing application problem is very normal, which includes some common problem and different problem.

Common Problem: Standard System Problem. Successful application of RFID must have a uniform standard. If there is no uniform standard, it will bring many problems. To reach IOT application in large scale in the field of traditional publishing and digital publishing, standard system of industrial requirement and application is critical, but the standard system has not been established till now. The basis standard should include application business processes, data structures, and identification of publications. Key technical standards, as well as application standard are the problems to be solved during these two areas.

Common Problem: Security Problem. To conduct IOT application in the field of traditional publishing and digital publishing, the level of security protection system need to be improved, which includes establishing mechanisms of a sound IOT safety evaluation, risk assessment, security and emergency response, etc. In the field of publishing, the disclosure of publication tag means that all security information is exposed. So it is very critical to solve the information security issue of the publication tag.

Different Problem: RFID Tag Cost of the Traditional Publication with Low Price. At moment, RFID application in the field of press and publication of China is used in hundreds of libraries, but used very seldom in the publishing and distribution units. According to the analysis, the two main reasons exist for this difference. Firstly, RFID tag usage in the library is much higher than in the bookstore. Secondly, the different nature between libraries and publishing and issuing units makes the difference. The publishing and issuing units as an enterprise must consider the cost of using RFID tag. After all, the cost of the RFID tag is much higher than barcode of traditional publication, which became the biggest bottleneck of the application in the IOT industry. In other industry, long time ago, Global retail giant, Wal-Mart wanted to apply IOT in products, but it is not fully implemented till now, the most important issue is the cost issue. RFID tag cost is a particularly serious problem for the traditional publication with low price.

Different Problem: Standard System, Copyright and Industrial Technology of Digital Publication. Compared to traditional publishing, digital publishing is an emerging industry, which will face more problems in IOT application. Till now, digital publishing standard has not yet been established and there is no unified definition of digital publication identity. Copyright security and industrial technology research etc. are still the scholars' research focus.

Digital Publishing Standard Problem. Digital publishing application based on IOT is a super merging application of network, which consists of multi-software and multi-network. Computer, communication and application software systems need be linked organically. Therefore, Standardization of digital publishing application based on IOT is a key element for its development. Chinese standards of digital publishing need to be developed as quickly as possible, especially a unified identity, technology and interface standard.

Digital Copyright Problem. Application of IOT in digital publishing field is more convenient to user than that of the traditional publishing field, but the copyright security issues are facing serious challenges. If digital copyright can't be solved, lawbreakers will use digital publications to make unjustified profit. It is very hard to ensure the interests of the entire digital publishing industry chain, which will hinder the development of industry.

Industrial Technology Problem. Currently, many papers about embedding and extracting based on the watermark technology have been published, but relevant industrial application is still rare. Digital publishing application based on IOT has no report to see. In particular, how to make the watermark information capacity as large as possible is critical to meet the need of tag information updated.

Suggestions

Strengthen the System Construction of Publishing Standards based on IOT. Technical merit of IOT is that publication tag information can be unified in the distribution network of industry chain. Clear standard must be constructed, such as metadata in publication tag, data structure, key system, encryption and decryption mode and updated information during distribution and logistics process. Studying the standard of the digital publication identity is very important for IOT application in the digital publishing field, which can includes the following aspect. (1). Principle of the different identity for different format of digital publication. (2).Meta data specification combined with business applications. (3).Coding principle and allocation rules. (4).Reference of address code of communication system for the identity of the digital publication.

Enhance the Information Security of Publishing Field. Firstly, preventive measures need to be strengthened by advanced scientific and technological means. Publication tag information need be encrypted by advanced theories and high-tech means. Secondly, people's quality need to be enhanced.

Enhance the Security of Digital Rights. Firstly, the awareness of people's copyright protection need be enhanced. Secondly, it is necessary to make more strict law and increase the legal punishment and breadth, so the offense is much higher than the cost of the acquired interests. Thirdly, it is very important to make valid technical way.

Enhance Industrial Research Capability. Although application of invisible watermark technology has been used initially in the security of the packaging and printing, the real commercial application in digitization market bases on network still has not seen. If digital publishing based on IOT wants to get success, we must vigorously strengthen the industrial research of watermark technology. Furthermore, Cost of RFID tag must be reduced more than before. According to different publication's price, RFID tag's cost can vary in a range.

Conclusions

IOT is more efficient and can enhance the digitization and information capabilities for publishing industry. Viewing from the information technology development of the world, the level of IOT development has become a main indicator to measure the degree of national and regional modernization, international competitiveness and the overall strength effectively. The development of IOT technology in the publishing industry is affected seriously and even is basic blank because of a series of practical problems, such as the perfect information security system, the low technical level of industrialization and the lack of industry standards. RFID tag's cost is also an important problem in the tradition publishing field. To some extent, IOT application in the field of digital publishing has more convenience and can be realized far better than that in other IOT field, such as traditional publishing field. The former does not need to add hard-aware equipment and real RFID tag, so it has large industrial cost advantage. Although IOT application of the traditional publishing is still exploring, many IOT experience in the traditional publishing field can be emulated and learned, especially the standard system construction and industrial applications promotion.

Acknowledgements

This work was financially supported by Scientific Innovation Program of Science and Technology Commission of Shanghai Municipality (12511510500), Innovation Program of Shanghai Municipal Education Commission (13ZS148) and Scientific Program of Chinese Society of Technical and Vocational Education (210524).

References

[1] B. Ch. Wei: submitted to Journal of Matter networking technology. No. 11(2011): p.75.

[2] X. Chen, in: *U.S. digital publishing inspection report*. Edited by Shanghai People's Publishing Press (2008).

[3] J. Ren, Q. W., J. W. Zhai: submitted to Journal of Logistics Technology. No.11(2011): p. 90.

[4] P. Wang, M. K. Wang: submitted to Journal of Packaging Engineering. No.12(2011):p. 108.

Applied Mechanics and Materials Vol. 596 (2014) pp 986-989
© (2014) Trans Tech Publications, Switzerland
doi:10.4028/www.scientific.net/AMM.596.986

uKeMa: an Ultra-lightweight Key Management and Authentication Scheme for Wearable Ad Hoc Networks based on Body Language

Yinhui Xie

School of Open Education, Wuhan Business University, Wuhan, China, 430056

yhxie2000@163.com

Keywords: Wearable Ad Hoc Networks, Key Management, Wearable Computing, Authentication

Abstract. Wearable consumer electronics such as Google glasses, Apple iWatch, Nike Shoes have been envisioned as next consuming hot spot. It invokes a large amount of applications in the personal healthy, personal safety, and digital entertainment. To save power consumption, those wearable devices usually connect to Internet via a smart phone that performs as a gateway. To avoid unauthorized access from unfriendly devices, it is desirable to encrypt the personal data in the communications of wearable devices. Therefore, the keys for encryption and integrity are required. In this paper, we make the first attempt to solve both key management and authentication together for wearable devices in an ultra-lightweight manner. We propose a scheme called uKeMa that can provide key generation, key updating and authentication for wearable devices with ultra-lightweight power consumption.

Introduction

All Wearable computing is envisioned as an upcoming computing paradigm in the near future. It is notable that more and more companies provide wearable devices to facilitate information processes in daily life. For example, Google glasses can guide walking path real time; Apple iWatch can indicate potential friends surrounding you; Nike shoes can report the amount of your exercise today. It becomes a trend that the human life and information communication technology interact more frequently, especially with the development and application of Internet of Things, Cyber-Physical System, body sensor networks, and mobile Internet.

Wearable devices usually have power constraints. That is, the power consumption should not be too large; otherwise, they have to be terminated for recharging. Among their power consumption operations, Internet access is a typical one due to frequent communication processes and extensive computation processes. To save the power consumption, wearable devices change the fashion for Internet access from directly to in-directly, namely, from a gateway. The most possible gateway that is portable with wearable devices is a mobile phone. Moreover, with the number of wearable devices carried by a person increases further, the gateway becomes more useful for power saving in overall. Thus, several wearable devices form an ad hoc network and smart phone works as a gateway to Internet. It is called Wearable Ad Hoc Networks (WAHN) in this paper.

As wearable devices connect to gateway in an ad hoc way, the devices should be authenticated before connection. Thus, unauthenticated devices cannot free ride the gateway. In addition, packets are forwarded by smartphone gateway between Internet and devices may damage privacy, for example, the personal healthy data. Thus, some packets should be protected for privacy in certain situations. Therefore, in wearable ad hoc networks, two major security problems arise: the wearable devices should be authenticated before linking to gateway; the privacy of packets between wearable devices and gateway may require to be protected. It imposes three challenges to solve above two security problems:

1) Wearable devices have equipped different outlook and components, the solution thus should adapt more generality and assume minimally for the functions in devices;

2) Wearable devices are provided by different manufactures, the solution thus should modify minimally for the functions in devices;

3) Wearable devices may be operated by various users including the young and the old, the solution thus should maintain easy, convenient, and original friendliness in user experience.

Currently, a few work discuss security problems in body sensor networks [1, 2, 3]. However, most of those solutions cannot migrate directly into wearable ad hoc network. The body sensor network does not impose above aforementioned three challenges. In this paper, we propose an ultra-lightweight solution, called uKeMa, to authenticate wearable devices, generate a shared key, and automatically update key.

The contributions of the paper are listed as follows:

1) We make the first attempt to propose an ultra-lightweight scheme in terms of computation overhead without cryptography to solve both authentication and key management problems for WAHN in one solution;

2) We make the first attempt to solve security problems in WAHN by body language.

The rest of the paper is organized as follows. Section II gives an overview on relevant prior work. In Section III we discuss the basic assumption and models used throughout the paper. Section IV provides the detailed description of our proposed models and analysis. Finally, Section V concludes the paper.

Related Work

Ali, S., et al, proposed a scheme for secret-key generation that can construct shared keys with near-perfect agreement, thereby avoiding reconciliation costs [1]. Their work is an improvement for previous work that two communicating devices can generate secret keys directly from measurements of their common wireless channel, which is symmetric but cannot be inferred in detail by an eavesdropper. They also demonstrated in several representative body-worn settings to show their scheme can generate secret bits with 99.8% agreement. C. Li et al. demonstrated security attacks for a popular glucose monitoring and insulin delivery system available on the market, and also proposed defending schemes against such attacks[2]. D. He et al. proposed a lightweight and secure system for wireless medical sensor networks [3]. They employed hash-chain based key updating method and proxy-protected signature to achieve efficient secure transmission and fine-grained data access control. They also extended the system to provide backward secrecy and privacy preservation. Daniluk, K. et al. surveyed selected topics concerning development of wireless sensor network systems formed by implantable medical devices located on the patient's body. They discussed security aspects and effective management of power resources available in implanted sensors [4]. Jungchae Kim et al. adopted the Advanced Encryption Standard (AES) for security framework on wearable devices, so healthcare applications using this framework could support the confidentiality easily. Their framework developed as dynamic loadable module targeted for microcontroller such as msp430 within embedded operating system [5]. Khan, N.A., et al. presented a survey on different architectures used in Wireless Body Area Networks for ubiquitous healthcare monitoring [6]. Lara, O.D., et al. surveyed the state of the art in human activity recognition based on wearable sensors [7]. They presented a general architecture along with a description of the main components of any human activity recognition system.

Problem Formulation

Network Model

Imaging a scenario, one person uses its smart phone as a gateway to provide Internet accessing for multiple wearable devices, such as smart rings, smart watches, or smart glasses. Although those smart devices may be equipped Internet access ability, this scenario can provide following advantages: 1) It can save the cost for Internet accessing; 2) It can save the power consumption for smart devices; 3) It can provide additional smart devices linkage smoothly. Thus, there exist two major entities in WAHN: wearable devices (denoted as W), and smart phone gateway (denoted as G). Wearable devices equip compute processor and communication interface. They may have display component with touch interface. They may not be equipped input port, as the updating of system can be downloaded from Internet and operation can be done by touch screen. Gateway is a common smartphone with computation processor, communication interface, touch screen, and camera function. Operators are the users who hold the gateway and wear wearable devices, denoted as O. Besides, as the Internet access is enabled, the cloud may be available for extra software distribution. The wearable devices can automatically login into cloud servers to download and update software or data in devices.

Attack Model, Security Definition and Design Goals

The adversaries in WAHN are mainly two types: the unauthorized devices that try to free ride the gateway for Internet accessing; the sniffer in the communication links in WAHN for prying personal privacy. This paper concentrates on following security problems: 1) The wearable devices can initialize a pair-wise shared key with the gateway in an ultra-lightweight manner; 2) The wearable devices can update a group-wise shared key in an ultra-lightweight manner; 3) The wearable devices can be authenticated in an ultra-lightweight manner by gateway upon requesting the connection.

Proposed Scheme

The naive way to authenticate wearable devices and create an initial key can be achieved by embedded module such as Bluetooth or wireless local area network, if those modules are available. That is, Bluetooth and WLAN module can provide device pairing for initial key establishment and authentication. However, those methods impose several constraints. Firstly, the wearable devices must be equipped those modules. Secondly, the key management is limited in the module, and it is difficult to provide enhanced security improvement manually. Last but not least, the security strength for all devices is the same, which cannot provide fine-grained security managements for distinct devices.

In this paper, we propose to use body language to generate, update, and authenticate the wearable devices. The major steps of the scheme are described as follows:

Basic Setting: W and G are initialized by downloading dedicated application for key management from application store, or dedicated application distribution server. The application utilizes data generated from some typical sensors equipped on the devices, such as vibration sensors.

Mode Selection:

1) Trigger Setting Mode:

O chooses Trigger Mode on G, to set up the body language that can trigger the key management semantics and authentication sematics. That is, O can act one body language such as jump or shack to trigger some semantics such as key initialization, key update, and so on. E.g., O chooses pair-wise key updating on G, and shacks hands two times, thus once O does this action, the pair-wise key between W and G will be updated in a default manner, e.g., $K_{new}=h(K_{old})$, where h() is a secure hash function; K_{new} is a new key; K_{old} is an old key.

2) Key Management Mode:

i) O chooses body language semantics on G, which include key initialization and key updating.

ii) E.g., key initialization is chosen. O acts an action, e.g., jumps two times; sensors can capture the behavior and generate corresponding sensing data, denoted as D.

iii) W and G generate initial key from D, e.g., $K = h(D)$, where h is a hash function; K is an initial key. The basic idea of key management mode is based on the assumption that body language will generate the same sensor data. This can be guaranteed easily, as the sensors in wearable devices on the body are sensing the same data at the same time in the same action.

3) Authentication Mode:

i) O chooses body authentication on G, which means to authenticate current wearable devices.

ii) O does one action, and checks whether the generated data by sensors in W are similar to each other.

iii) If the verification succeeds, it means W is authenticated. Hereby, the design rationale is similar to previous mode. That is, the sensors in wearable devices on the body are sensing the same data at the same time in the same action.

Above key management mode and authentication mode can also be triggered by body language, avoiding the set up from G, as in trigger setting mode the trigger semantics have been connected to body language.

Conclusion

An ultra-lightweight framework called uKeMa for the key management and authentication for wearable devices is proposed in this paper, by using the synchronization of body language, and sensing data for the same action. This scheme can be used for fast authentication, easy key initialization and key updating in wearable computing.

References

[1] Ali, S.; Sivaraman, V.; Ostry, D., Eliminating Reconciliation Cost in Secret Key Generation for Body-Worn Health Monitoring Devices, IEEE Transactions on Mobile Computing, vol.PP, no.99, pp.1,1, 0 doi: 10.1109/TMC.2013.71

[2] C. Li; Raghunathan, A.; Jha, N.K., Hijacking an insulin pump: Security attacks and defenses for a diabetes therapy system, 13th IEEE International Conference on e-Health Networking Applications and Services (Healthcom), vol., no., pp.150,156, 13-15 June 2011

[3] D. He; Chan, S.; Shaohua Tang, A Novel and Lightweight System to Secure Wireless Medical Sensor Networks, IEEE Journal of Biomedical and Health Informatics, vol.18, no.1, pp.316,326, Jan. 2014

[4] Daniluk, K.; Niewiadomska-Szynkiewicz, E., Energy-efficient security in implantable medical devices, 2012 Federated Conference on Computer Science and Information Systems (FedCSIS), vol., no., pp.773,778, 9-12 Sept. 2012

[5] J. Kim; B. Lee; S.K. Yoo, Design of real-time encryption module for secure data protection of wearable healthcare devices, 35th Annual International Conference of the IEEE Engineering in Medicine and Biology Society (EMBC), vol., no., pp.2283, 2286, 3-7 July 2013

[6] Khan, N. A.; Javaid, N.; Khan, Z. A.; Jaffar, M.; Rafiq, U.; Bibi, A., Ubiquitous HealthCare in Wireless Body Area Networks, 11th International Conference on Trust, Security and Privacy in Computing and Communications (TrustCom), vol., no., pp.1960,1967, 25-27 June 2012

[7] Lara, O.D.; Labrador, M.A., A Survey on Human Activity Recognition using Wearable Sensors, Communications Surveys & Tutorials, IEEE, vol.15, no.3, pp.1192,1209, Third Quarter 2013

Applied Mechanics and Materials Vol. 596 (2014) pp 990-993
© (2014) Trans Tech Publications, Switzerland
doi:10.4028/www.scientific.net/AMM.596.990

Analysis on Development and Application of Online Customized Tour

Xiaojun Wang[1,a] and Xiaokang Li[2,b]

[1]School of Business Administration, Shenyang University, Liaoning Province, China

[2]School of Business Administration, Shenyang University, Liaoning Province, China

[a]461989478@qq.com, [b]sydxwxj@163.com

Keywords: online; customized tour; countermeasure; application

Abstract. Online customized tour provides personalized travel services based on the needs of tourists and the trend of tourism development. Therefore, it has broad prospects of application as a new type of model on the tourism market. This paper, by analyzing application status of online customized tour, finds out the driving factors and restricting factors in order to propose countermeasure to accelerate the application of online customized tour.

Introduction

Definition of Online Customized Tour. Online customized tour, based on the needs of tourists, is a tourist-oriented design for tourism process. It not only concerns about the cost and selling price of the product, but also focuses on the time cost and experience cost of tourists.

Customized service of online travel booking has two meanings. First, tourists customize information and services according to their interests and needs. Second, the online travel websites provide the most appropriate resources and services initiatively on the basis of tourists' characteristics and customized information.

Contents of Customization.

Interface Customization. Interface customization allows users to select the website's interface style and display pattern based on personal preferences, such as color, background, board, content layout. After landing pages tourists will see their interested forum and personal style of page setup, which can offer psychological suggestion to tourists to customize online tour service, and make the system more user-friendly and convenient for tourists.

Retrieval Customization. Retrieval customization means that tourists could search the information initiatively according to their preferences. Tourists can filter and combine the elements of food, accommodation, transportation, travel, shopping and entertainment based on the price, destination and days to obtain a satisfactory travel plan. In the retrieval process, system displays the keywords of search according to browsed history and tourists' information which may convenient for visitors to retrieve useful tourist information quickly.

Recommended Customization. Online travel business can record users' requests on resources through information tracking technology. The interest-related products can be recommended for tourists through website, short massage or E-mail after collecting, analyzing and summarizing the basic information. In addition, when the tourists have not found a satisfactory solution, the server can monitor and track information to remind tourist timely until standard messages appears.

In-transit Customization. It is the customization that giving service at user-specified time and location. In-transit customization provides information of various aspects located by mobile terminal for tourists, thus it is convenient for visitors to make a reservation. It can also provide maps search function for individual visitors by showing all aspects of information on the map.

Advantages

Advantages over Offline Customization. Firstly, the cost is lower than offline customization since the scale advantage can be achieved easier. Secondly, online customization could save human resources relatively because the customization is mainly achieved by advanced information technology. Thirdly, the information of tourists can be gathered easier. Online customization can instruct tourists to fill in basic information initiatively when they register the website. Lastly, it can benefit a nationwide range of tourists under online customization.

Advantages over Mass Tourism. To start with, the dissemination of information is two-way instead of the traditional one-way service model. Customization service is an interactive system that visitors choose their preferred products and the site provides personalized information in reverse. Next, the outstanding characteristic is that tourists are the co-producers of the product rather than passive recipients. Finally, the target of service is accurate since customized tours can provide different products for different tourists according to their characteristics of travel behavior.

Application Status

Becoming a New Model of Tourism. According to "The 33rd China Internet Development Statistics Report" released by CNNIC, by the end of December 2013, the number of Internet users in China reached 618 million [1].Besides, according to the data showed by CNNIC, the number of online travel booking via Internet reached 181 million in 2013, up 61.9% [2].

Online travel booking market is growing rapidly with long-term development and optimistic market expectation. Online travel market is facing great opportunities and containing important commercial value. What’s more, it will be the mainstream direction of future tourism owing to the policy environment, economic environment, social environment and technology environment.

Be in Its Infancy. Customized online travel market is still in its infancy without a fixed pattern and it fails to meet the needs to tourists for customized tour perfectly. Compared with the American and European countries, the potential market of domestic customized tour is far from being developed. However, with the increase of personalized demand, the market share of online customized travel would increase year by year and have a huge space for development.

Influencing Factors

Driving Factors.

Policy Support of Wisdom Tourism. According to the news from National Tourism Administration of Tourism Promotion and International Cooperation Department, the National Tourism Administration recently issued "Notice on Propaganda Theme and Slogan of 2014 China Tourism Year "."Beautiful China, 2014 -- Year of Smart Travel "became the promotional theme of tourism. Smart travel, based on a new generation of integration about information and communication technology, provides service with high quality and high satisfaction for the purpose of meeting the individual needs of tourists. One aim of smart travel is to achieve the customization for tourists, especially for the growing prosperity of the individual markets[3].

Diverse Demands of Target Tourists. Supply comes from demand. The needs, changing from popularization and homogenization to complex motivations and high expectations, drive business model of online travel service to develop toward diversification as well as personality. With the change of consumers’ attitudes, the characteristic of differentiation continue to be strengthened in the tourism market. Customized tour, abandoning the defects of joining a group or individual travel but integrating the advantages of both, is a new travel way with fun and profession.

Intensified Competition of Mass Tourism. Currently, the services of online travel sites on the domestic market basically include hotel reservations, air ticket booking, vacation product and corporate travel management, resulting in serious homogeneity, intensified imitation and lacking core competitiveness. Faced with the rapidly increasing threats and challenges of domestic counterparts and international giants, the competition among tourism companies has been further intensified in pace with the exploration of great potential development on tourism market. This trend requires tourism companies to follow the demand-oriented marketing concept, to adapt the individual needs, and to implement the reformation of customized marketing.

Rapid Development of Information Technology. Nowadays, the advanced information technology provides technical support to online customized travel. Travel 2.0, based on Web2.0, is a new model of supply and demand. Travel 2.0 pays more attention on the interaction between tourists and websites, since the tourists are not only recipients but also manufacturers of the content on the websites[4].Web data mining technology can track the sites visited by the target groups and analysis the spending habits and various information, for the purpose of providing unique information, products and services for tourists according to the tourists' needs and preferences automatically[5].

Restricting Factors.

Difficulty of Publicity and Popularization. How to make the target customers know customized tour and be used to book travel online should be the primary issue concerned by online travel companies in order to cultivate faithful tourists. Affected by the attitudes and habits, it is hard for general tourists to accept the expensive customized tour relatively, and the target tourists who are able to afford customize tour have not formed the consciousness of booking travel online due to a variety of factors such as cultures and ideas. Therefore, the travel attitudes and habits of tourists should be trained and guided urgently.

Inaccuracy of Customized Content. To satisfy the customized service through improving the accuracy of customized services and the speed of information analysis, the system must need more storage space to store tourists’ behavior data, faster computing device to analyze the tourists’ characteristics, more complex calculation methods to deal with the various needs, as well as more advanced information dissemination tools to provide tourists with a wider range of information.

Lacking of Stable Supply Chains. Online travel companies should have enough products for visitors to select on account of the diversity of tourists’ needs as well as the breadth and depth of tourists’ experience. It requires online travel companies to expand their business scale, increase tourism business partners and establish stable supply chains. Only with the excellent marketing staffs and adequate marketing expansion, can the online travel companies have ability to provide customized tours. Therefore, it is a huge challenge for small and medium online companies to develop the customized tour.

Unacceptable Price for Low-income Groups. The high cost is the most troublesome problem which the development of customized tour facing now, since customized tour has not developed into a mature business system yet. Online customization can not only lead to the rapidly surge in development costs, but also loss the economies of scale for hardly getting a discount from large-scale group activities. Compared with mass tour, the target group of customized tour is mainly high-income tourists. In addition to high consumer groups, youth groups with low income and strong willingness are also keen to customized tour.

Countermeasures

Increasing Publicity Channels and Marketing Models. Online travel companies should strive to seize the market, expand the publicity channels actively and enhance brand awareness efforts to get the attention on customized tour from target groups by word of mouth effort. Additionally, travel companies can also initiate tourism activities and sponsor related products or other forms of effective advocacy to expand the visibility and reputation.

With the advent of mass information media, the network marketing model is also changing quietly. Information can be widely disseminated in the target tourists via social network marketing software such as Weibo, Wechat, Renren and each user is a potential tourist of customized tour. Online travel companies can update their status to tourists through the disseminating the corporate or product information, interacting with tourists and publishing interesting topics.

Building system of Customer Relationship Management. Information gathering is the first step to create a personalized information service model and the function of the model largely depends on the comprehensive and accurate collection of information. The way of collecting information include filling the registration form and analyzing travel demands information to complete the construction of the database and lay the foundation of building customer relationship management.

CRM is the unique advantage of online travel companies. The database technology of CRM can create a file for each visitor which is the key factor to attract tourists to generate purchasing motivation and implement purchasing behavior. Once the customer leaves the information in the database, CRM can provide personalized service according to the information[6].

Expanding and Completing Supply Chain System. It requires online travel companies to expand the supply chain system in the lateral and vertical level to meet the tourists' comprehensive needs of customized tour in breadth and depth respectively. Online customized companies promote cooperation and win-win situation among each node according to reasonable distribution of benefits, professional negotiators, the integrity of corporate image and other positive factors.

In addition, customized services ought to take online travel companies as a leading and service platform as a link to combine related providers into a complete supply chain system. The travel orders received from service platform should be conveyed to each node of tourism companies timely and converted into personalized travel service products by the online companies with the fastest speed.

Meeting Needs to Achieve Economies of Scale. Economies of scale can reduce the cost of companies. Firstly, online companies can recommend the same customized service to similar tourists according to the cluster analysis of tourists based on certain characteristics. Then, online companies can release associated travel information on the basis of different types of posts in tourism forum. Lastly, the customized services should be popularized as conventional products which get more preferences from tourists.

Online customization should develop various tourism products for different groups based on the level of consumption. On one hand, economic products should be expanded for youth groups who have lower income relatively, such as youth hostels, camping, biking trip and collective cooking. They can enjoy higher travel experience at lower price by controlling the cost of transportation, accommodation and food. On the other hand, high-end personal customization can be provide for high-income groups who are insensitive to price, such as extravagant overseas travel, cruise travel and other themes of tourism projects.

References

[1] The 33rd Statistics Report on Internet Development in China. Beijing: China Internet Network Information Center, 2014.[In Chinese]

[2] 2012-2013 Industry Report on Online Travel Booking in China. Beijing: China Internet Network Information Center, 2014. [In Chinese]

[3] Zhang Lingyun. Tourism Tribune, 2012, 27(2): 3-5. [In Chinese]

[4] Li Song. E-Business Journal,2012(7):22-23. [In Chinese]

[5] Xin Haitao. Journal of Harbin University of Commerce (Natural Sciences Edition),2010, 26(4): 483-487. [In Chinese]

[6] Xi Yi. Science& Technology Information, 2011,(36):562. [In Chinese]

Applied Mechanics and Materials Vol. 596 (2014) pp 994-997
© (2014) Trans Tech Publications, Switzerland
doi:10.4028/www.scientific.net/AMM.596.994

Advances in Online Authority Research

Wu Bing[1], Zhang Chenyan[2]

[1] School of Economics and Management, Tongji University, Shanghai, China

[2] Logistics Research Center, Shanghai Maritime University, Shanghai, China

Keywords: Online Authority; Cognitive Search; Computer Science; Online Community

Abstract. As previous research has established that communication and public relations play a crucial role, to understand the resources needed for effective online intervention has been proven particularly helpful to locate in time the central issue. Science citation index expanded (SCI-EXPANED) and Social Sciences Citation Index (SSCI) database on web of science are gleaned, concerning advances in online authority research. The result indicates that the main research territory is England, accounting for 30%, then followed by USA and Spain of 20% respectively. The number of publication literature on this topic mainly distributes in recent 5 years, reaching climax of 4 in 2011. And from the analysis of research area, research on communication accounts for 40%, then followed by computer science of 30%. Overall, the related research topics can be classified in four areas: evaluation of the online authority, cognitive search models, authority in online community and online authority communication. Finally, new opportunities for future research are discussed.

Introduction

As the Internet has become a ubiquitous tool for information resources, people are increasingly dependent on Internet [1]. Therefore, evaluating the authority of free online information is becoming crucial. Although, people trust and rely on online resources, most of the freely and abundantly available information online is anonymous. Information on the Internet needs to be credible. There are two major insights towards this: the role of generic search engines and an increasingly sophisticated use of the evolving Internet [2]. Therefore, social media are creating new challenges for authority communication [3].

The main objective of this paper is to analyze relating research in online authority research of Science Citation Index Expanded (SCI-E) and Social Sciences Citation Index (SSCI) database from web of science. As a result relating studies in this area can be thoroughly explored to find the research gaps and direct the future research.

The rest of this article is organized as follows. Section 2 surveys the research on online authority. Section 3 briefly summarizes related work within online authority and discusses new opportunities for future research. Section 4 concludes the article with a summary.

Analysis results of information foraging research

According to Science Citation Index Expanded and Social Sciences Citation Index Database in web of science, only 10 records are found in related discipline when “authority” and “online ” are used as the combined search title.

Country/Territory. According to country/territory, analysis results are shown as table 1. England accounts for 30%, ranking in the top one, followed by USA and Spain, of 20% respectively.

Table 1 Analysis Results of Country/Territory

Country/Territory	Record Count	% of 10
England	3	30%
USA	2	20%
Spain	2	20%

Research Areas. Considering research areas, analysis results are shown in table 2. Communication accounts for 40%, ranking in the top one, and then followed by computer science, one third of all research areas.

Table 2 Analysis Results of Research Areas

Research Areas	Record Count	% of 10
Communication	4	40%
Computer Science	3	30 %
Business Economics	2	20 %
Information Science Library Science	2	20 %
Public Administration	2	20 %

Publication Year. Almost all the papers are published mainly in recent 5 years. As shown in table 3, almost 40% of them were published in 2011. Accordingly citations reach climax of 16 in 2013.

Table 3 Analysis Results of Publication Year

Publication Year	Record Count	% of 10
2011	4	40 %
2010	3	30 %
2012	2	20%

Research Topics on Online Authority

Overall, the related research topics can be classified in four areas: evaluation of the online authority, cognitive search models, authority in online community and online authority communication.

Evaluation of the online authority. Although the evaluation of the authority of free online scholarly information is becoming crucial, few empirical studies have focused on this issue [4]. Based on a modified version of Jim Kapoun's "Five criteria for evaluating web pages" which use accuracy, authority, currency, objectivity and coverage to evaluate online resources, as framework, reference [5] selected 32 keywords from eight disciplines, inputted them into three search engines (Google, Yahoo and AltaVista) and used Analytic Hierarchy Process to determine the weights of criteria, which are author/creator's information included, author/creator's credentials, credibility of the website/publisher and reliable of information source. The results show that different domain names, resource types, and disciplines of free online scholarly information perform differently when scored in terms of authority. Moreover, about 41% of all samples provide more authoritative scholarly information. Therefore, the authority of free online scholarly information has been unsatisfactory, and needs to be improved. In further research, the evaluation framework should be well developed as a useful instrument for librarians, researchers, students, and the public to select Internet resources.

Cognitive search models. As there are a number of major research gaps in examining information judgments and Internet search behaviors notes, such as how users actually make these judgments outside of experiments or researcher-defined tasks, and how search behavior is impacted by a user's judgment of online information, reference [6] examined the medical setting on how information judgments employed by doctors to mitigate risk impact their cognitive search when they face real consequences in how to apply the online information. Results show that doctors, though aware of the need for information quality and cognitive authority, rarely make evaluative judgments. This is explained by navigational bias in information searches and via predictive judgments that favor known sites where doctors perceive levels of information quality and cognitive authority. These results suggest Web experience and mental models can be viewed to impact search strategy through key constructs in information judgment, therefore it is necessary to connect online cognitive search and information judgment. Further research should examine other possible relationships between these constructs, detail the contents of the two types of judgments in use, and understand how the contents of mental models and Web experience changes over time as individuals gain experience in a certain task category.

Authority in online community. In recent years the internet has become an increasingly important resource for health consumers, online discussion communities are shaped in important ways, including how the character and focus of discussion is formed, and how both information and users can be constructed as authoritative and reliable. However these studies do not explore how the character of the forum is shaped by its users during the very early days of its existence, and how issues of identity and authority are established. Thus, reference [7] explored a UK-based diabetes 'Virtual Clinic' online community to understand the rhetorical nature and content of exchanges over a period of six months from the community's inception. Results demonstrate how the identity of the community was established early on by its users, and how this acted to shape the kinds of interactions and discussions that took place thereafter. The important ways in which individuals sought to establish themselves as reliable and authoritative sources of information were discussed to show that a small number of motivated users who shared specific health characteristics were recruited to a closed internet forum participated in focused discussions over a sustained period of time, moreover, participants sought to present themselves as reliable and authoritative sources of information. Future research should consider the influences of participant authority and identity on the health behavior of participants in internet communities.

Online authority communication. Public relations professionals are increasingly using online tools, yet public sector organizations are often slow to follow the trends. Three different attitudes were apparent in the discussion forums: positive, neutral and negative. Most of the discussions on the forums comprised of argumentation between the Negatives and Positives, without a clear outcome into either direction. In total, 58% of comments posted right after authority comments were negative. In order to call for the need of authorities to establish a real dialogue to ensure that citizen' and stakeholders' information needs and expectations are met, reference [8] examined Finnish citizens' opinions about authorities as crisis managers during the swine flu epidemic of 2009–2010 and examined the success of authority intervention to online discussion forums. Through a content analysis carried out at the discussion forums, the study showed that though authorities are highly trusted in general in Finland, this trust is not extended to the online environment. Online, civilians did not trust authorities and the protective actions taken. Moreover, the authorities' intervention to the discussion forums aimed at correcting false information and shaping opinions seemed to fail, as the intervention was carried out too late and with too little resources. The lack of authorities' early input gave free space for hostile and distorted comments. Authorities have to be proactive, build trusting relations with stakeholders before the crisis, not during it. Serving citizens will increasingly include being present online, especially in crisis situations, when the need for information and communication is heightened. When making an intervention, there have to be enough resources to ensure authority presence in the long term. Without these, the role of risk and crisis manager will be taken by someone else. Therefore, the results of this study call for more proactive authority communication that would build trust and establish a dialogue with citizens before crises to ensure credibility during difficult times.

Conclusions

As internet use has grown, it has considered whether the informed e-consumer presents a challenge to professional dominance or whether online information continues to support a model of authority [9]. Correspondingly Internet communities have been suggested to provide an opportunity for real-time dialogue, building trust and motivating action, all of which fit well in with the objectives of authority communications. As a result, participants successfully co-constructed their group identity through shared understandings of behaviors and meanings within a collective realm of action in Internet communities.

In addition, there is a clear need to be aware of the social processes that shape online communities. In order to harness the potential benefits, online services need to acquire a multi-faceted understanding of the social processes that occur in online communities, including how the character and focus of the discussion is formed over time, and how both information and individual users can be constructed as authoritative and reliable [10]. Therefore online authority research has two main implications for practitioners. First, for policy makers, consideration of the utility of general-purpose tools, further Internet awareness training enabling to efficient authority should be considered. Second, the customization of search should also be noted to provide infrastructure services and practitioners should note that such communities can have clear empowering benefits.

Previous research has established that communication and public relations play a crucial role in managing risks and crises. Research shows that experts speak with technical and scientific terms, whereas citizens perceive risks and crisis more emotionally. Perception is crucial, as risks become real once they are perceived as real. The authorities either underestimated the resources needed for effective online intervention or they were unable to locate in time the central issue arenas where discussions on the topic were going on. Above all, it is important not only to recognize the new opportunities that these online tools offer, but also to make sure that they are used in meaningful ways.

Although, we adopted for articles published in journals to try to obtain the best possible quality from the included literature, given the time and resources available, it cannot be excluded that conference proceedings can produce results of comparable quality, as research in a related field. Ideally, an integration of the results of the present review with conference proceedings would allow retrieving more relevant results in the future research.

References

[1] Cheong, P.H., S. Huang, and J.P.H. Poon, CULTIVATING ONLINE AND OFFLINE PATHWAYS TO ENLIGHTENMENT Religious authority and strategic arbitration inwired Buddhist organization. Information Communication & Society, 2011. 14(8): p. 1160-1180.

[2] Zhou, L.D., F.B. Schneider, and R. Van Renesse, COCA: A secure distributed online certification authority. Acm Transactions on Computer Systems, 2002. 20(4): p. 329-368.

[3] Karlsson, M., The immediacy of online news, the visibility of journalistic processes and a restructuring of journalistic authority. Journalism, 2011. 12(3): p. 279-295.

[4] Herbane, B., COMMUNICATIONS ABOUT RESILIENCE ENHANCING ACTIVITIES BY ENGLISH LOCAL AUTHORITIES An evaluation of online content. Public Management Review, 2011. 13(7): p. 919-939.

[5] Chen, C.F., et al., Assessing the authority of free online scholarly information. Scientometrics, 2012. 90(2): p. 543-560.

[6] Hughes, B., J. Wareham, and I. Joshi, Doctors' Online Information Needs, Cognitive Search Strategies, and Judgments of Information Quality and Cognitive Authority: How Predictive Judgments Introduce Bias Into Cognitive Search Models. Journal of the American Society for Information Science and Technology, 2010. 61(3): p. 433-452.

[7] Armstrong, N., N. Koteyko, and J. Powell, 'Oh dear, should I really be saying that on here?': Issues of identity and authority in an online diabetes community. Health, 2012. 16(4): p. 347-365.

[8] Tirkkonen, P. and V. Luoma-aho, Online authority communication during an epidemic: A Finnish example. Public Relations Review, 2011. 37(2): p. 172-174.

[9] Delfanti, A., Cyberchiefs:Autonomy and Authority in Online Tribes. New Media & Society, 2010. 12(5): p. 861-863.

[10] Kothari, A., et al., Exploring Community Collaborations: Social Network Analysis as a Reflective Tool for Public Health. Systemic Practice and Action Research, 2014. 27(2): p. 123-137.

Applied Mechanics and Materials Vol. 596 (2014) pp 998-1002
© (2014) Trans Tech Publications, Switzerland
doi:10.4028/www.scientific.net/AMM.596.998

Interaction representation and application of Flash Animation in Webpage design

Shanshan Yang

Wuhan Donghu Univertsity , Wuhan , 430212, China

7316066@qq.com

Keywords: Flash animation; webpage design; guide; interaction.

Abstract. The application of Flash animation in website design becomes more popular because it is more attractive and infective than static pages. Functions of Flash, status in quo and characteristics of webpage design are analyzed in this paper; how to present and apply the interaction of Flash animation in webpage design better is promoted via three aspects including functional design of guide, smart application of transparent Flash in Banner ads images and the application of pure Flash making websites.

Introduction

Adobe Flash is a kind of software integrating interactive vectorgraph editing and multimedia creation, which is widely applied in vector animation file formats of webpages, it is provided with characteristics including occupying less network resource, occupying less space, transferring large amount of information, strong cross media capability, low cost and convenient video streaming. At present, Adobe Flash has been widely applied in each Web-based fields including webpage design, ads design and game development, and has now gradually penetrated into different traditional fields such as multimedia, film video, product display and remote education.

There are more applications of Flash animation in website guide page and the homepage, which is more attractive and infective. However, BANNER ads and guide column of subpages of some websites are also presented in the form of Flash animation, this kind of design enhances the picture efficiency, and also can sufficiently arouse the interaction of viewers. Because of the powerful interactivity ofFlash, we not only can make flow animation, Flash shorts, Flash MV and Flash titles, we also can use it to create guide, Banner ads, buttons and icons. As a new network arts form, only the network and the webpages of Flash animation can be the space to fully display its form and present its meaning. Flash satisfies higher requirements of viewers on interaction, so as to realize stronger direct feeling, richer interactive response and more infective experience.

Status in quo and characteristics of webpage design

At present, internet has brought about revolutionary changes to the society. As a carrier for information transfer-network, it has generated huge social influences. People get news, see films, listen to the music, play games, chat, send and receive mails, transfer files and go online shopping via webpages. Every aspect in our life cannot do without the internet. Especially those born in 1980sand 1990s spend most of their time on internet for study and recreation. Therefore, visual representation of webpage design becomes more and more important. As one kind of ways for information transfer, interaction is its greatest characteristics; it is a kind of dual-way information spreading. Viewers can not only get information through it, but also can collect useful resources; we can feedback and adjust the transfer of information via interaction with viewers. In webpage design, designers can guide the viewers by right of visual direction feelings, and Flash animation can guide viewers to get information they want better.

Defining in the scope of visual transfer design, webpage design has been out of the traditional two-dimensional space limitation, its dynamics and interactivity are important features different from traditional printing and film media, which make webpage design become a new design scope; in addition, it also becomes an important research direction of graphic design in the information era.In order to make webpages become a new media of strong readability, and then obtain the maximum visual transfer function, humanization design can be realized by confirming different visual elements including effects treatment such as version design, color and multimedia dynamic, Flash effects to adapt to visual flow psychological and physiological characteristics of people as well as interaction.

Interaction representation of Flash animation in webpage design

Design of interactive guide system

The guide column is critical in webpage design taking the core position of the homepage, through which viewers can view subpages. In the aspect of functionality, we can hide the sub guide via the drop-down menu, it is more flexible and various in representation forms to use drop-down menu as submenu instead of behaviors in the dreamweaver; in color application, Level I guide column shall highlight its three-dimension effect and distinctiveness. You can select bright, clear and refreshing color combination to guide viewers to click and even enjoy the process. Through flash guide column, it is not only beautiful, but also can fully represent the pleasant sensation of viewers when clicking, or even you can match it with clear sound. While in design of the pattern of guide column and animation effects, you can fully exert the imagination to make it full of creation or special fun to make them join it happily.

The appearance of flash provides a higher platform for webpage design, the traditional guide mainly focuses on expression; while flash application nowadays makes a communication bridge between webpages and consumers, it pays more attention to users experience; of course, in webpage design, the interactivity of guide design also can be realized via the powerful codes, it can be mutually supplemented with flash animation guide to enhance the dynamical effects of webpages, the followings are shown the interactive guide design realized through code design.

```
<head>
<meta http-equiv="Content-Type" content="text/html; charset=gb2312">
<title>Supercool webpage guide menu</title>
<STYLE>
<!--
.xmenu td{font-size:12px;font-family:verdana,arial;font-weight:none;color:#333333;border:1px
solid #ffffff;background:#f6f6f6;filter:blendtrans(duration=0.5);cursor:hand;text-align:center;}
-->
</STYLE>
<script>
/*
http://www.qpsh.comwebpage special effects    supercool webpage guide menu

this is the function to bind event action to the menu
*/
functionattachXMenu(objid){
    vartds=objid.getElementsByTagName('td');
    for(vari=0;i<tds.length;i++){
        with(tds[i]){
            onmouseover=function(){
                with(this){
                    filters[0].apply();
                    style.background='#3ea936'; //this is the background color when moving the
mouse there
```

```
                    style.border='1px solid #ffffff'; //border
                    style.color='#ffffff'; //text color
                    filters[0].play();
                }
            }
            onmouseout=function(){
                with(this){
                    filters[0].apply();
                    style.background='#f6f6f6'; //this is the background color when moving the
mouse away
                    style.border='1px solid #ffffff'; //border
                    style.color='#333333'; //text color
                    filters[0].play();
                }
            }
        }
    }
}
</script>
</head>

<body>
<div align="center">
                <table border="1" width="778" cellpadding="0" style="border-collapse: collapse"
height="30" id="table4" bgcolor=#DBDBDBbordercolor="#DBDBDB" cellspacing="0">
                    <tr><td>
                        <div align="center">
                            <table class="xmenu" id="xmenu0" border="0" width="776"
cellspacing="3" cellpadding="3" height="30" id="table5">
                                <tr>
                                    <td onclick="window.open('http://www.qpsh.com',
'_blank');">Homepage</td>
                                    <td onclick="window.open('http://www.wangtx.com/',
'_blank');">Comprehensive special effects</td>
                                    <td onclick="window.open('http://www.yamaxun.org',
'_blank');">special effects of menu</td>
                                    <td onclick="window.open('http://www.yamaxun.info',
'_blank');">text operation</td>
                                    <td onclick="window.open('http://www.cnosa.com',
'_blank');">special effects of graphics</td>
                                    <td onclick="window.open('http://www.gxgcn.com',
'_blank');">special effects of graphics</td>
                                <td onclick="window.open('http://www.luotuoxie.net',
'_blank');">status column</td>
                                <td onclick="window.open('http://www.ivancl.cn',
'_blank');">time and date</td>
                                    <td onclick="window.open('http://www.fankelipinka.com',
'_blank');">special effects of buttons</td>
                                </tr>
                        </table><script>attachXMenu(xmenu0); //the event actionis bound at the
  place where the table ends; this xmenu0 is the id</script> of that table
                        </div></td></tr></table></div> </body>
```

Smart application of transparent flash in Banner ads images

The webpage applying flash as Banner ads is always the most attractive. In the whole downbeat webpage, it is like a dance attracting people. In the aspect of function focusing on subject, flash absolutely has the unshakable position, any picture cannot be comparable with it, and it is more like an extension of usage of flash ads. The integration of Banner ads and website subject via flashes can express the subject better, highlight and completely describe LOGO of a website or the philosophy of a company.

Certainly, static Banner ads images provided by customers are very important and taking up a large area, then we can add brilliance to the website design and generate dynamical effects without disturbing to the original Banner ads images by transparent flash. There are numerous transparent flash materials on the internet, you can insert transparent flash after layer establishing by AP div on Banner ads image, then input wmode on the left in the parameter options in the property bar and transparent on the right; dynamical description is more lively and vividly than static ones. The way highlighting flash subject is different the ordinary one, it can leave deep impressions for viewers, of course, this is because that flash can bring us strong feeling by right of dynamics, speed, area and reasonable application of color. It also makes people the whole website more impressive while highlighting the subject.

Application of pure flash making in websites

The website purely applying flash making is more dynamical; some websites may use pure flash making technology including music, video, images, website guide, register and login, so as to give people stronger visual shock and greatly improve initiatives of viewers.

The first step for establishing pure flash animation website is planning its structure. Before establishing pure flash website, we shall confirm the subject, and then divide it into several modules, carry out page layout according to each module and draw out the relationship diagram of the website structure. In addition, the preparation of materials such as pictures, music and videos is also very important. Special effects of pictures can be realized via the powerful photo making and integration functions of Photoshop. And then apply flash making for integration. Confirm the version structure of each module, then make corresponding module and its sub-module, finally import corresponding module in each main field to integrate a complete flash website, so as to make the pure flash making website more interactive and more uniform in coloring.

Conclusion

To sum up, as an important visual element of websites, flash not only can present dynamical effects of the whole website, but also can make it more rich combined with HTML code. Certainly, the application technology of flash animation can greatly enhance the attractiveness and interaction of webpages, especially it can adds flexible dynamical effects of flash animation with the support of scripting languageActionScript, and can provide more creative space for guide and Banner ads in webpage design.

Acknowledgement

The Subject of Hubei Provincial “12th Five-Year Plan” for EducationalScience in 2013 (Project No.: 2013B243)

References

[1] Liu Dan. The Research on Vision Language of Flash Cartoon in Webpage Design[D]Hefei University of Technology, Hefei. 2006.

[2] Li Rui.Webpage Design and Practice[M]. China Communication Press, Beijing. 2010.

[3] Hu Ke. Interaction Application ofInternet Advertisement [J].Guangdong Industry Technical College.June (1), 2007.60-65.

[4] Pan Li. The Application of FlashAnimation and FlashAnimation in Webpage design[J].Keyuan Monthly Publication.2010(17).

Applied Mechanics and Materials Vol. 596 (2014) pp 1003-1006
© (2014) Trans Tech Publications, Switzerland
doi:10.4028/www.scientific.net/AMM.596.1003

Application and Thinking of "Jiangcheng Culture" Elements in Web Design

Zhang Xin

Wuhan Donghu Univertsity , Wuhan , 430212, China

113690204@qq.com

Keywords: Web Design; "Jiangcheng Culture"; Visual Communication.

Abstract. All aspects of our social activities and living are changing with current economic globalization, the web design is the fastest and most convenience way to transmit global information to the users through network. Meanwhile, with the development, web design has been more matured gradually focusing on individualization to show certain cultural contents. As a result, web designers in Wuhan City shall make an endless attempt on cultural innovation and pay more attention to the application and thinking of "Jiangcheng culture".

Introduction

All aspects of our social activities and living are changing with the current economic globalization, the fast development of web design promotes the development of information transmission, the web design is the fastest and most convenience way to transmit global information to the users through network. Meanwhile, with the development, web design has been more matured gradually focusing on individualization to show certain cultural contents. As a result, people no longer focus on how to make the information transmitted quickly and effectively, understood and accepted properly. Besides carrying on traditional culture, web design also shall have unique features.

Summary of "Jiangcheng culture"

Each city has its own unique culture contents, through which the internal charm of a city can be shown to display brands of the city and promote its development. "Jiangcheng culture" in Wuhan City is rich, extensive and profound with distinct regional features, such as "dragon culture" represented by Shang-dynasty bronze vessels, "architectural culture" by the Yellow Crane Tower, "commercial culture" by Hanzheng Street, "science education culture" by Wuhan University and Huazhong University of Science and Technology, and local artistic culture represented by Hanchu opera, as well as the under-developing food culture and clothing culture, etc.

Current situation of Wuhan web design

With rapid development of web design in China, the level of Wuhan web design is emulating that of coastal cities actively. However, there is still a big gap with the developed web design not only in design standard and innovation ability of the industry, but also views and aesthetic criteria of customers. Lacking of independent innovation and features is the weak point of Wuhan web design. Imitation, copy and even applying template in web design cannot bring pleasant to customers, not to mention deep-seated emotional resonance and cultural exchanges with them.

Connection of "Jiangcheng culture" and web design as well as its influence

Firstly, culture is the spiritual root of a nation, and even the vitality and soul of a city. Nowadays, "culture going out" strategy has been advocated in many cities in order to not inkling to traditional transmission modes such as tourism development, the literature supplies and documentary, Wuhan shall take advantage of the strong visual impact of visual communication to target users to move "Jiangcheng culture" towards the market, so as to achieve effective inheritance and transmission.

Web design, which belongs to the modern visual communication design, is a new type of audio visual design based on the development of computer network; it has humanized and socialized service functions; what’s more, it can influence the users on the mental level. For example, the web designs of Wuhan University, museums, art galleries and libraries and some portals in Wuhan City shall display distinct regional culture to help promote and popularize “Jiangcheng culture” at maximum.

Secondly, web design, taking internet as the carrier, based on the technique, knowledge and artistic experience of web designer, is a creative thinking activity to make art planning for the webpage elements according to the design propose and requirement. In the homogenization of web design style of many domestic websites to today, the information transmission effect has been weakened greatly. Wuhan web designers must be familiar with local cultural aesthetic psychology and its artistic forms, they shall be the exponents and creators of “Jiangcheng culture” in local web design, make positive exhaustive study and excavation through figures, colors, words and so on, to exhibit certain cultural features, lead the users to feel “Jiangcheng culture”, and finally find individualized developing route.

Specific application of “Jiangcheng culture” elements in web design

Focusing on the design style of webpage and displaying individualities

The design styles of many websites in Wuhan follow the same pattern; in particular, advertisement occupies all core positions of the web design when advertisement has been the main source of income in recent years. For example, www.wuhan.net.cn is one of the portals in Wuhan, its homepage is full of big-size dynamic ads, the readability has been severely damaged, let alone effective propaganda of “Jiangcheng culture”.

In fact, we can apply “Jiangcheng culture” elements to the local web design pertinently. For example, in the web design of “Wuhan Han Embroidery Studio”, classic works of “Han embroidery” can be the background after indistinct and transparent processing to express certain cultural and reality senses; alternatively, use brilliant colors of “Han embroidery” as the background to form a strong visual impact, then add unique figures of “Han embroidery” as the background of textures. In this way, the integrated webpage design style can transmit the features effectively, and obey the most important principles: it makes you webpage easy to be understood; also adequately expresses the features and inherit the culture of “Han embroidery”.

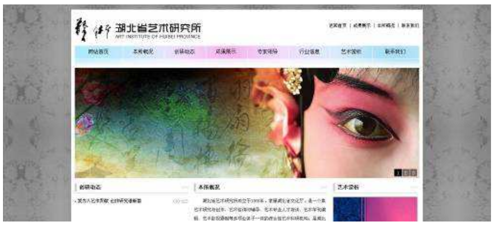

Fig.1 Pictures from the http://www.hbyys.com/

Identifying proper main color is good for presenting the theme

Color is the essence of design. In web design, color tone and compatibility always express the theme and feature of the webpage firstly, and help visitors form direct impression. For example, the homepage of Hubei Provincial Museum applies dark red as the main color, the webpage is Elegant and quaint, full of mystery. For another example, the webpage of “Art Institute of Hubei Province” applies light gray as main color, which looks soft, quiet and elegant; local opera image is located in the webpage center, the color of which is bright and flamboyant; culture and artistic senses are outstanding through these bold contrasting and well-bedded colors, and it is easier to be accepted and beloved by most people (see the figure on the right).

Thus, the color can transmit different cultural contents, which directly influences the reader’s interest. It is necessary to take account of the significance of color while identifying overall color of the webpage.

Making the best of figure and word to extend “Jiangcheng culture”

For local web design in Wuhan, distinctive figures and words shall be applied to the web design to let local design feature be known, understood and accepted by the world through network, then the local feature turns into world feature, the local feature and temperament of Chinese web design can bring a breath of fresh air to the dull modern design style. For example, local traditional patterns apply in the background and navigation menu on the webpage of Hubei Provincial Museum, there is a harmony between graphic elements and whole design style, to have culture extension and modern interpretation, and express its cultural concept through colors and figures.

In addition, it also can be done from the details. In the performance of dynamic elements, script code can be used to float image; once the following code is inserted in the front of </HTML>, the image showing “Jiangcheng culture” can float in web design, in favor of richening the cultural contents and enhancing the appeal of “Jiangcheng culture”.

```
<body bgcolor="#F7F7F7">
<!—begin of image floating code -->
<div id="www_qpsh_com" style="position:absolute">
<!-- chained address --><a href="http://www.qpsh.com" target="_blank">
<!—image address--><img src="http://www.qpsh.com/images/logo.jpg" border="0">
</a>
</div>
<script>
var x = 50,y = 60
var xin = true, yin = true
var step = 1
var delay = 10
var obj=document.getElementById("www_qpsh_com")
function floatwww_qpsh_com() {
var L=T=0
//by www.qpsh.com
var R= document.body.clientWidth-obj.offsetWidth
var B = document.body.clientHeight-obj.offsetHeight
obj.style.left = x + document.body.scrollLeft
obj.style.top = y + document.body.scrollTop
x = x + step*(xin?1:-1)
if (x < L) { xin = true; x = L}
if (x > R){ xin = false; x = R}
y = y + step*(yin?1:-1)
if (y < T) { yin = true; y = T }
if (y > B) { yin = false; y = B }
}
var itl= setInterval("floatwww_qpsh_com()", delay)
obj.onmouseover=function(){clearInterval(itl)}
obj.onmouseout=function(){itl=setInterval("floatwww_qpsh_com()", delay)}
</script>
<!--end of image floating code -->
</body>
```

Conclusion

In brief, there's obviously a very long way to go for applying “Jiangcheng culture” elements in web design. From now on, if we pay attention to “Jiangcheng culture” and make attempt on cultural innovation of web design continuously, the combination of technology and art and the unification of contents and patterns tend towards the application and thinking of “Jiangcheng culture”, there certainly be full of fun, warmth and vitality in web design, and a bridge between “Jiangcheng culture” and it can be built at the same time.

Acknowledgement

Scientific Research Project of Hubei Provincial Department of Education (B2013196).

References

[1] Wang Jia, Ren Zhikai, Chu Dan. Design research of our country's travel ticket in different regional cultures [J].Forum Highlights, August, 2012.
[2] Zhou Zhipeng. Study on the web design of Chinese Social History Museums-compare with the websites of Korea Social History Museums [J].Design art, March, 2006.
[3] Hua Li.The visual language features of Xinjiang webpage under the background of regional culture [J].Popular literature, January, 2011.
[4] Zhang Luzhu, Li Bifeng..Application and thinking of traditional cultural elements in web design [J].The disciplinary research, November, 2012.

CHAPTER 14:

Engineering Education and Engineering Management

Applied Mechanics and Materials Vol. 596 (2014) pp 1009-1012
© (2014) Trans Tech Publications, Switzerland
doi:10.4028/www.scientific.net/AMM.596.1009

Micro lesson in Microera under the Background of Video Resources

Lei Zhang[1, a] Xinghui Wang[2 ,b]

[1] Education institute of technology，Shenyang Normal University, Shenyang, Liaoning, 110034,China

[a] 610242895@qq.com , [b]582435076@qq.com

Keywords: MicroAge, Micro Class Teaching, Network Technology

Abstract. This article introduces the micro era, the concept of micro class and the origin firstly, and elaborates the characteristics of micro lessons through two aspects of the humanities and technology. According to the existing problems, and the application in Chinese language lessons of elementary student, conclude the general methods to solve the problem.In the end micro teaching suggestions are given.

Introduction

Based on digital information technology, micro era is a new kind of broadcasting era featuring real time, interaction and efficiency through a new and convenient type of display terminal, which synthetically uses audios, videos, texts, images and so on[1]. We can apply many products under micro era into teaching, such as micro messages. It effectively solves the problem that pupils can't remember their homework. Teachers establish a public account, and then release the daily homework, so parents only need to click on to check their children's homework easily. Micro-class, which is under the influence of micro era, is a revolutionary change of the teaching system.

So-called micro-class is a miniature video course, also known as micro lecture. It is a new situated network curriculum resource which supports a variety of learning styles. And it is explored to be aimed at some subject knowledge or teaching procedures[2]. The key idea of micro-class is that teachers need to connect the teaching contents with the teaching targets so as to produce a more focused learning experience [3]

The Characteristics of the Micro-class

1.1 The little space and fast communication

The capacity of micro-class is small, so it is easy to spread and download in the network. The users can view the videos of micro-class online smoothly in the network and also can easily download them onto other kinds of digital devices[4].

1.2 Simply making, and lower requirements to devices

When it is recorded, computer resolution should set to1024* 768 and below, not less than 720*576; bit stream 128kbs~2Mbps; frame rate is 25FPS or over; the colors on the computer screen are set to 16 bit. Video format is Flv, Mp4; video size is 640*480 or 320*240. Audio sampling rate is 44.1K; bit rate is 64~320; synching up <100MS; audio format is AAC (.aac, .m4a, .f4a), MP3, Vorbis (.ogg, .oga)[5].

1.3 Abundant Situation

If the interpretation is about science knowledge, we should make the micro-class in the fields. It can not only strengthen students' personal experience, but stimulate students' interests, which surpasses the traditional class.

1.4 timely Learning and feedback

There are not any requirements to learning object, learning time and learning sites in micro-class. As long as you carry a mobile device (computer, phone, etc.) connected to the Internet, you can randomly choose the knowledge you want to learn.

The Practice of the micro-class

2012 is the first year of domestic micro-class construction and development. If the exploratory and application of micro-class in several areas (such as Foshan in Guangdong, Shenzhen, Ordos in Inner Mongolia) and part schools (such as Jiangjinjukui Middle School in Chongqing, and part schools in Jiangsu, Zhejiang and Shanghai) can be called “sparks of fire” in the years of 2010 and 2011, it quickly becomes the hot topic in educational circles in 2012 with the development of education innovation project (such as the flipped classroom, Khan Academy, E-book package, Video open class, 1:1Digital learning and BYOD which let each student bring information equipment to class, and blended learning). Online video, as the main form of micro-class or micro-course, has spread rapidly all over the country in primary and secondary schools, vocational colleges, TV universities, colleges and universities, and even in the fields of enterprise education[6].

The writer mainly applies micro-class to the preview link in Chinese class of primary school, for example, "Chinese knot". Since children’s age in Grade Three is around ten, their main task is to recognize Chinese characters. Besides, their focused time is short and their natural disposition is active, so during the process of making micro-class, it is necessary to pay more attention to class time and to add some interesting pictures and music, etc.

Combined with the situation, the main content of this course was presented through interesting animation design and a cartoon character. The script was designed in Table 1.

Table 1 Script of Miro Class

Time(S)	Content	Others
0--30	Pleasant goat: kid, do you know what Chinese knot is? Where have you seen it before?	Some pictures of Chinese knot are showing, and background music is cartoon theme song.
30--120	Lazy goat: these words are related to Chinese knot, do you know? Let me teach you.	New words and pinyin are shown in the picture in the lazy goat’ s voice, and the children are asked to read together.
120--180	Beauty goat: do you know how many parts there are in the text? Hurry to read, and tell me the answer.	The dialog box appears in the picture and the students fill into the dialog box after reading the text. Only when the answer is correct, they can come to the next item.
180--300	Big Wolf: all the goats are in my hand. Make all the new words into phrases, and then I will set them off. Come and save these goats.	Images appear--- the goats are captured by the wolf. And then new words appear in the picture. The children are asked to find words in the passage to fill them in.
300-330	The goats let children read the new words and expressions again.	The goats are saved. The music will be played again and the words to encourage the children will appear in the picture.

After written script, teachers downloaded the pictures, music, pictures, etc. on the net, and finally made a micro course resource by further processing.The students in the class were divided into two parts. One prepared their lessons by micro-class and the other prepared by reading books. After a period of practice, the teacher found that the frequency of answering the question of the former is more than that of the latter. The former are more active and better in memorizing the content while the enthusiasm of the latter is not high and the degree of mastering the new vocabulary is not very good, either. Through the communication with the students, the writer found that compared with simply reading the book, the students are more likely to prepare new lessons by micro-class. The interesting pictures and the music can draw the students’ attention. It’s better for students to complete their tasks and when they finish each task, they can get a praise, which makes the students feel a sense of accomplishment and feel great.

However, the writer also found some problems in practice. Firstly, after all, students just preview the new lesson. It's necessary for teachers to present the key points and the difficult content in class. And teachers also need to spend time in recording videos, which will increase the teachers' pressure intangibly. Secondly, these problems on how to make students to preview the new content consciously and how to strengthen their learning consciousness are needed to be solved in the future teaching.

The Problems and the Suggestions of Micro-class

Over the past decades, multimedia video has always occupied a pivotal position in class, but it can't improve classroom teaching effectively, and cause the students' interests in learning, and it often result in the waste of resources in the classroom because the speed of network is too slow. In recent years, with the rapid sharing of network information and the innovation of media video technology, many teachers are trying to use media technology to make videos and apply them to their teaching after the post-production. Micro lesson has produced a revolutionary impact on education. it changes the traditional classroom teaching of 45 minutes, controls the time within ten minutes and only introduces a knowledge point, which can make students accept more quickly. During micro era, micro-class can be easily made by the means of mobile phones, cameras and PPT, and the cost of its distribution is also negligible. For learners, there are no requirement for learning time and learning sites. People only need to open a mobile device and connect it to the Internet, and then they can not subject to any restrictions. This greatly meets the personalized and customized learning mode of modern people.

However, the development of micro-class also meets some problems. First of all, its overall quality is not high. Second, the equipment demand is far outpacing in remote areas where the hardware and software needed in micro-class cannot be provided. And what's worse, the teachers blindly follow suit. When selecting a topic, teachers should think more and should not use micro-class blindly in order to keep up with the trend.

There are some suggestions for micro-class. First of all, in the process of producing micro-class, teachers should pay attention to the art of using language. In the process of micro video recording, teachers must pay attention to the mastery of language. They can express the main content with exaggerated and sharp language to cause the learners' interests and prevent miscellaneous information. And then teachers can build a public platform of micro-class, uploaded the data package of micro-class to the platform for everybody to view, learn and find the deficiencies and then make correction. Finally, it needs to strengthen the consciousness of students. In micro-class students must have consciousness of autonomous learning, which puts forward higher request to the student. It requires the joint efforts of teachers and parents to strengthen the students' self learning consciousness.

Conclusions

In today's era that network information technology has been highly developed, micro-class has a great impact on the traditional mode of classroom teaching and causes the concern of teachers' teaching reflection. Micro-class can satisfy the needs of students' instant learning, quick learning, and self-learning. With the growing popularity of the mobile network, micro-class will have a broader development prospects. For teachers, micro-class will change the traditional teaching mode, and it can provide a platform for teachers to show themselves, who needn't stand on three feet platform any longer, but "micro" themselves, share their own experience, get some better suggestions so as to expand their knowledge structure, absorb advanced education concept, and improve their teaching levels. For learners, they needn't stick to traditional mode of classroom learning, they can learn anything, review and consolidate new knowledge at any time according to their own interests, in the parks, in the coffee shops, as long as they like. For education, we can make use of information resources efficiently and promote the further progress of new education pattern. During the future course, Micro-class will be cared by more and more people.

References

[1] Cao Dianbo1，Xue Suqin2. CHINA MEDICAL EDUCATION TECHNOLOGY,2013 27(5):495-497

[2]Xia Zhongwen,WIDE VIEW 2013 :84-87

[3] Information on http://blog.sina.com.cn/s/blog_5396775a0102ek9d.html

[4] Huang Ye.TECHNOLOGY WIND.2013:259

[5] HUANG Jian-jun GUO Shao-qing.Modern Educational Technology .2013 23（5）:31-35

[6] Hu Tiesheng1 , Huang Mingyan2 & Li Ming3. JOURNAL OF DISTANCE EDUCATION.2013 :36-41

Applied Mechanics and Materials Vol. 596 (2014) pp 1013-1017
© (2014) Trans Tech Publications, Switzerland
doi:10.4028/www.scientific.net/AMM.596.1013

Research and Implementation of Curriculum-Oriented Knowledge Learning Platform

Jiwei Xue[a], Shaohua Xu[b,*], Yuanyuan Yu[c]

School of Computer & Information Technology, Northeast Petroleum University, Daqing, 163318,China

[a]xuejiwei@163.com, [b]xush62@163.com, [c]xuejiwei@126.com

*corresponding author: Shaohua Xu

Keywords: semantic web, knowledge management, knowledge learning platform, knowledge services

Abstract. In the face of vast and decentralized knowledge resources in the information society, it is not easy for learners to capture the knowledge which they really need timely and accurately. An efficient and practical educational knowledge-learning platform was built, by employing knowledge engineering methods to achieve the functions of dynamic expansion of knowledge resources, assisted learning and etc. It has a great theoretical value and application prospects by making effective integration of educational knowledge organization, management and services, transforming the traditional passive learning mode into self-study, making full use of modern information technology tools, developing educational knowledge resources and optimizing the educational process.

Introduction

21st century is the era of knowledge economy, knowledge is becoming the driving force of economic growth, each field especially the education field, has carried out the comprehensive informatization. However, facing vast amounts of information resources, learners have difficulty in obtaining valuable knowledge. Aiming at the need of knowledge management in the field of online education, this paper firstly discussed the education knowledge organization model, knowledge management, education knowledge service and so on. And then a curriculum-oriented knowledge learning platform was constructed, including functions of curriculum knowledge map navigation, knowledge question and answer, associated knowledge query, knowledge push, knowledge consult, etc.

Knowledge Organization Model

Knowledge Representation Method: Knowledge representation is the field of artificial intelligence that focuses on designing computer representations that capture information about the world that can be used to solve complex problems. The commonly used knowledge representation methods mainly include First Order Logic, production system, framework model, scripts, semantic web, ontology, etc [1, 2]. By analyzing the advantages and disadvantages of different methods and the relationship between the knowledge units involved, the method of semantic web was adopted.

Knowledge Unit and its Formal Description: Knowledge unit is the knowledge that can be used independently but cannot be spitted into smaller ones, which is the core of constructing the knowledge structure [3]. The object structure of knowledge unit can be given by a triple $K(O,P,S)$, where K is the name of knowledge unit, O is the name of object, P is a set of attributes and S is a set of states.

Knowledge Management Model and Framework

Construction of Knowledge Base: In this paper, a mechanism of extracting knowledge is proposed, which can extract knowledge from a larger number of relevant literatures automatically or semi-automatically which is shown in Fig. 1.

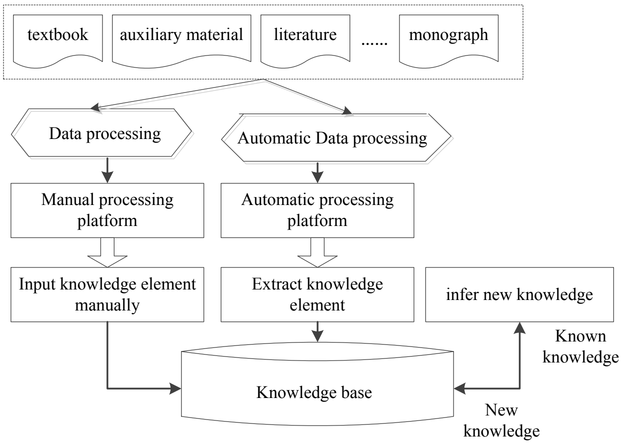
textbook
auxiliary material
literature
......
monograph
Data processing
Automatic Data processing
Manual processing platform
Automatic processing platform
Input knowledge element manually
Extract knowledge element
infer new knowledge
Known knowledge
Knowledge base
New knowledge

Fig. 1 The flow chart of knowledge base construction

Knowledge Indexing: Before knowledge indexing, the literatures must be transformed into a certain format, imported into the system and segmented. The process of knowledge indexing is shown in Fig. 2. Firstly, check if the sentences and paragraphs following the keywords are closely related to it. If true, the keywords will be imported into the knowledge unit base, record this sentence and its position in the literature. Secondly, extract sentences containing these knowledge units, count the number of occurrences and positions, select some sentences as this literature's knowledge units and store them in the knowledge base.

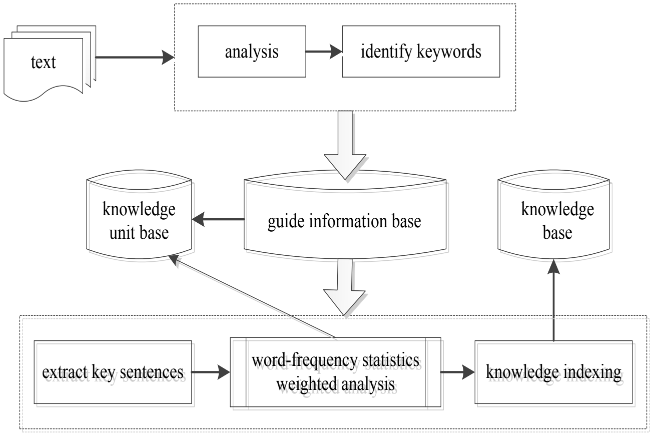
text
analysis
identify keywords
knowledge unit base
guide information base
knowledge base
extract key sentences
word-frequency statistics weighted analysis
knowledge indexing

Fig. 2 Knowledge indexing process

Knowledge Linking: Knowledge units are organized into knowledge chains by their associations, and thus form a knowledge network. When doing the keywords retrieval, traditional search engines can only match the information contains the keywords but ignore its semantic; this will lose a lot of contents with the synonymy concept and lower the rate of recall [4]. In order to calculate the semantic correlation, a relevant concepts dictionary which contains the concept's synonyms, antonyms and semantically related degree was built in the paper. The semantic similarity between two concepts can be calculated by Eq.1.

$$S(C_1,C_2)=\frac{A(C_1,C_2)}{a(C_1)+a(C_2)-a(C_1,C_2)} \tag{1}$$

where C_1 and C_2 are concepts to be calculated, S is the similarity, $A(C_1, C_2)$ is the number of properties with the same name and the same value owned by C_1 and C_2, a(C) is the number of properties of concept C, a(C_1, C_2) is the number of properties with the same name owned by C_1 and C_2, $S(C_1, C_2) \in [0,1]$. Associations based on semantic relevance is built between knowledge units, synonymy and antisense conceptual knowledge.

Information Extraction: Fig.3 shows the process of knowledge extraction used in this paper.

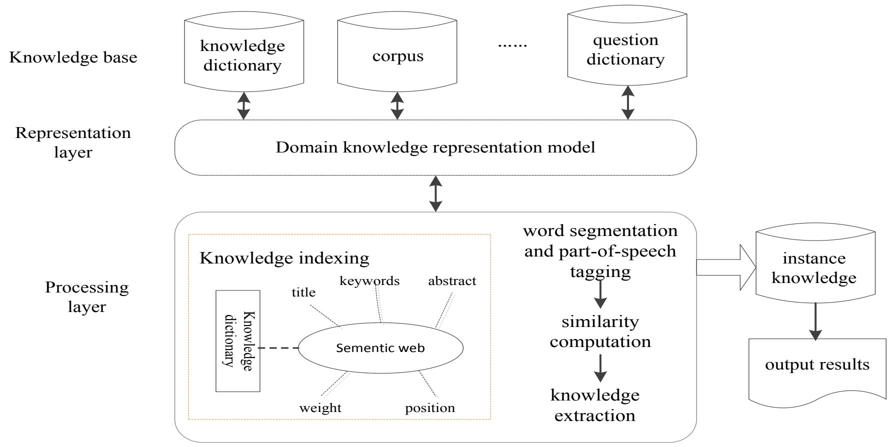
Knowledge base
knowledge dictionary
corpus
......
question dictionary
Representation layer
Domain knowledge representation model
Processing layer
Knowledge indexing
title
keywords
abstract
Knowledge dictionary
Sementic web
weight
position
word segmentation and part-of-speech tagging
similarity computation
knowledge extraction
instance knowledge
output results

Fig. 3 Knowledge unit extraction process

- Knowledge indexing. Firstly, retrieve the domain keywords according to the knowledge unit dictionary, and assign different weights. Secondly, analyses the main object and contents described in the literature according to these keywords. Thirdly, index knowledge, record the frequency of the occurrence and position. Lastly, extract the characteristics information of the literature by calculating the weight of different knowledge and sort them.
- Automatic word segmentation and part-of-speech tagging. Judge whether these statements match those in the corpus based on fuzzy similarity. If true, extract the trunk of the sentence, add to the instance knowledge base and record the location of sentence. Otherwise, take the sentence as a corpus added to the corpus, and submitted to the artificial processing platform.
- Extract knowledge by artificial.
- Decompose the new sentence and take them as samples.
- Display the knowledge according to their weight and category.

Function Model Design of Knowledge Service System

For the need of education knowledge service, the system's function model was designed, including functions of knowledge map, knowledge question and answer, associated knowledge query, knowledge push and so on.

Knowledge Reasoning Mechanism: Neural network technology has been successfully applied in many fields. In order to solve a particular problem, the integrated neural network method will use multiple neural networks at the same time. Each neural network can complete the same diagnosis task or different, and the output is determined by each neural network constitute the whole neural network [5-6]. Semantic neural network and integrated neural network were used in this paper.

Knowledge Q&A and Reasoning Process: The Q&A system gives comprehensive and reasonable answers by semantic analysis and intelligent reasoning efficiently, according to users questions of natural language. Its structure is shown in Fig. 4.

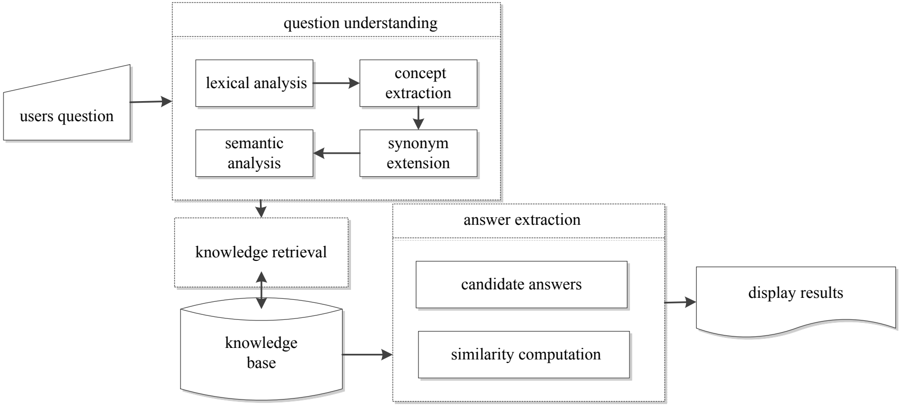
question understanding
lexical analysis
concept extraction
users question
semantic analysis
synonym extension
knowledge retrieval
answer extraction
candidate answers
display results
knowledge base
similarity computation

Fig. 4 Process of Q & A

(1) **Pre-processing**

- Perform word segmentation and part-of-speech tagging automatically.
- Remove the stop, classify the problem and extract the keywords. Find all synonyms of keywords by using the synonym table in the knowledge base.
- Submit all the keywords to information retrieval module.

(2) Knowledge Retrieval Based on Keywords: Retrieve all knowledge containing keywords from the knowledge base and treat these as candidate results.

(3)Sort and Output the Results: Calculate the similarity between each candidate result and users' question by Eq.2.

$$S = S_1 * W_1 + S_2 * W_2 + S_3 * W_3 \tag{2}$$

where, S is the total similarity, S_1 which can be calculated by Eq.3 is the morphology similarity of title and W_1 is the weight of S_1, S_2 which can be calculated by Eq.5 is the length similarity of title and W_2 is the weight of S_2, S_3 which can be calculated by Eq.6 is the similarity of keywords and W_3 is the weight of S_3. By default, W_1= 0.8, W_2=0.15, W_3=0.05.

$$S_1 = \begin{cases} 0, \text{only a same question word between question and title} \\ 0, \text{only a same verb between question and title} \\ \dfrac{[\sum_{i=1}^{n} ci\_qz] \times 2}{wjcs + btcs}, \text{others} \\ 0, \text{only a same adjective between question and title} \\ 0, \text{only a same other word between question and title} \end{cases} \tag{3}$$

where, n is the number of same words in question and title, *ci_qz* is the weight of different speech can be calculated by Eq.4, *wjcs* is the count of words exclude question words and punctuation in the question sentence and *btcs* is the count of words exclude question words and punctuation in title. By default,

$$ci\_qz = \begin{cases} 1, noun \\ 0.55, verb \\ 0.33, objective \\ 0.11, question\ word \\ 0.05, others \end{cases} \tag{4}$$

$$S_2 = 1 - \frac{|len\_biaoti - len\_wenti|}{len\_biaoti + len\_wenti} \tag{5}$$

where, *len_biaoti* is number of words exclude punctuation in title and *len_wenti* is number of words exclude punctuation in the question.

$$S_3 = \frac{\sum_{i=1}^{m} ci\_qz}{wjcs + m} \tag{6}$$

where, m is the number of same keywords in question and title, *ci_qz* is the weight of different speech, same as Eq.4, *wjcs* is the count of words excludes question words and punctuation in the question sentence.

Prototype Design of Knowledge Learning Platform

Knowledge learning platform is logically divided into four relatively independent layers, respectively presentation layer, application layer, model layer and data layer. Each layer provides services to its upper, and at the same time as the next layer's customer, calls functions provided by the lower layer. Fig. 5 shows the 4-layer architecture of the system.

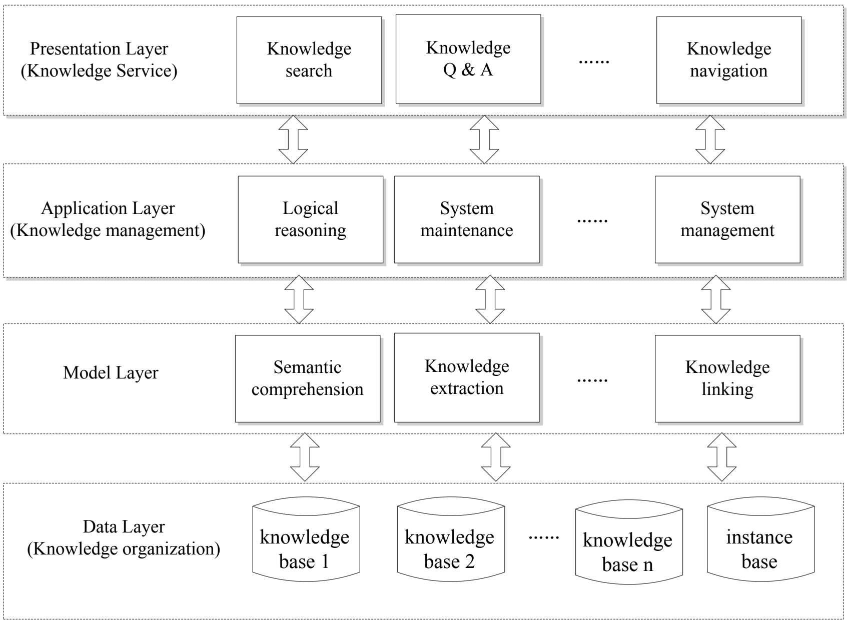
Presentation Layer
(Knowledge Service)
Knowledge search
Knowledge Q & A
......
Knowledge navigation
Application Layer
(Knowledge management)
Logical reasoning
System maintenance
......
System management
Model Layer
Semantic comprehension
Knowledge extraction
......
Knowledge linking
Data Layer
(Knowledge organization)
knowledge base 1
knowledge base 2
......
knowledge base n
instance base

Fig. 5 Architecture design of educational knowledge learning system

Conclusions

Take "discrete mathematics" as an example, we constructed the education knowledge organization model, management model and service model; and developed a platform for education knowledge learning. However, in order to make the system more practical and perfect, we will continue study the following aspects. The mechanism of dynamic construction of knowledge base and knowledge extraction is not perfect enough. The accuracy of query needs to be promoted further. In the future work, we will further research the semantic neural network to improve the accuracy of semantic comprehension and provide more definite answers.

Acknowledgements

This work was supported by the Higher Education Comprehensive Reform Pilot Special Project Heilongjiang Province Education Office in 2012 #JGZ201201045: to enhance university novice teachers' teaching capability through school and Humanities and supported by social science research project of Education Department of Heilongjiang province in 2013: International comparison research on talent training mode of educational technology.

References

[1] R. Davis, H. Shrobe, and P. Szolovits. What is a Knowledge Representation? AI Magazine, 14(1):17-33.(1993)

[2] Amati, Gianni. Conceptual graphs and first order logic. Computer Journal, 43(1):1-12.(2000)

[3] Xiaoting Wen, Xianchun Luo, Xiaoying Liu, Rui Zhang. Knowledge Unit Research: Review and Comment [J].Journal of Library Science in China, 37(5):75-86. (2011) (in Chinese)

[4] Al-Dallal, Ammar. The effect of hybrid crossover technique on enhancing recall and precision in information retrieval. LNECS, 1571-1576.(2013)

[5] Karaoglan, Aslan Deniz. An integrated neural network structure for recognizing autocorrelated and trending processes. Mathematical and Computational Applications, 16(2)514-523. (2011)

[6] Lee Hyunjung, Kim Harksoo, Seo Jungyun. An integrated neural network model for domain action determination in goal-oriented dialogues. Journal of Information Processing Systems, 9(2):259-270. (2013)

Applied Mechanics and Materials Vol. 596 (2014) pp 1018-1021
© (2014) Trans Tech Publications, Switzerland
doi:10.4028/www.scientific.net/AMM.596.1018

Second time development of coal quality management system

Bin Qian [1, a],Hongying Zhang [2,b]

[1] Hebei energy institutes of vocation and technology Department of information and project, Tangshan, Hebei, China

[2] Hebei energy institutes of vocation and technology Department of information and project, Tangshan, Hebei, China

[a]qianbin012@163.com, [b] zhy-hts@163.com

Keywords: Quality management; client / server; Browser / server; ADO object

Abstract. Coal quality management information system based on the combination of C/S and B/S structure, with the continuous development of new technologies, for the two time development. This paper expounds the new scheme of coal quality management design of online processing system.

Introduction

Coal quality management, responsible for enterprise's quality management, plan, storage and transportation, wool, raw coal, coal supervision of commercial coal sampling system, sample processing business disputes, choosing waste management etc. With the modernization of enterprise management, major changes have taken place in the management model. At the same time, with the continuous development of computer technology, the network management system has also been updated.

According to flow chart to divide the system main module

Based on detailed investigation of the coal business analysis, summarized as follows: mainly responsible for coal ash, moisture, sulfur content, volatile content, calorific value of data, preparation of coal, coal monthly, annual reports; Based on coal quality analysis report and the accumulated data, make production plan, for the company leader, underground mining area, coal washing plant and other relevant departments to provide more timely and accurate data, make the timely adjustment of production, to meet customer demand. The following diagram business process:

In the detailed business investigation, the manual accounting business process basically clear smooth, organizational structure is reasonable, but the current data management is still in the primitive manual stage, because it involves many varieties, many indexes, the user is mixed, the data management, analysis, reporting lag, cause the mine, coal washing can not be timely adjustment, production of passive, caused by the coal dispute. Therefore, be imperative development of coal quality management system.

On the basis of the analysis of the extensive research and user requirements,was established objectives and requirements of a new system. Mainly divided into the following six parts: commodity coal (coal) management, commodity coal (coal, coal washing and others) management of product quality inspection management, management of underground coal into the wash, the gross coal wash ability management, test management, each part is relatively independent but closely related.

The management of commercial jet coal. The coal based data: export name, date , batch, tonnage, ash, ash content, sulfur content, sulfur content of the qualified rate, water content, total water of qualified rate inputted from the client computer, calculate the cumulative tonnage, total ash, total qualified batch number, total sulfur, total qualified number of sulfur content, accumulated water, the accumulated water, qualified batch number and the total number of qualified rate are calculated for all authorized users, online browsing, online management.

The management of other commercial coal. The coal code, export name, date, batch, tonnage, ash, ash component, moisture, water, when the number of the gangue quantity, wholesale heat inputted by the client computer, and realize the online management of the data: insert, delete, query, save, print, calculate the cumulative tonnage, total ash the cumulative number of qualified, accumulated water, total qualified batch number and the total number of qualified rate.

Quality checks of washing coal products. The main purpose is to check the coal washing plant all kinds of quality is qualified, test using the user name, code, coal export date, tonnage, ash, sulfur, moisture, heat, for the unqualified index immediately issued a warning.

The management of coal into the wash. The coal quality index of ash, sulfur, moisture, volatile matter, calorific value and accumulated data to detect and generate a coal report.

The management of underground coal. Of every ten days, each production unit of down hole will compare the actual coal production and plans, compare the actual ash and plans, compare the actual sulfur and plans, and cumulative the related data. At the same time the record were inputted, modified, added and deleted.

The management of raw coal wash-ability test. Through the sieve test of the underground coal seam, the huge amount of data will be got, and then the data will be calculated, analysis, to understand the quality of each seam, in order to better guide production. In this part, there are four: five analysis of screening of total sample, screening test, float and sink test, the grain size is less than 0.5 mm coal management, and automatic generation of wash-ability curve.

Data maintenance. Data maintenance including three parts: coal user base maintenance, coal base maintenance, and other commodity coal user's base maintenance. Coal user base mainly refers to the maintenance of user code and ash, sulfur, total moisture and heat index; coal base maintenance mainly refers to add, delete the management of the coal code; other commodity coal user base's content refers to the user code, name and quantity of heat index data maintenance and management.

The design of the system operation mode

Development mode selection of coal quality management system. Mode of MIS system platform is generally divided into 4 kinds: the host terminal mode, the file server mode, the client / server model (Client/Server, referred to as C/S) and Web browser / server mode (Browser/Server, referred to as B/S).

C/S mode mainly consists of three parts: the client application program (Client), server management program (Server) and Middleware (Middleware). Customer application program is the parts user interactive with data. The server program is responsible for the effective management of system resources. Middleware is responsible for connecting the customer application and server management procedures, complete operating synergies, to meet user query data management requirements. C/S model's characteristics mainly includes: strong interactivity, supply more secure access mode, reduce network communication. The C/S in the logical structure one less than B/S layer, for the same task, C/S is always faster than B/S that makes the C/S model more conducive to handling large amounts of data.

B/S mode is a new type of MIS system model based on Web technology. Divides the server in the C/S model as a data server and one or more application server (Web server), thus forming a three layer structure of the client server system. The first layer client is the interface of the user and the system. The client application reduced to common browser software. The second layers of the Web server will start the process in response to the request of the customer, and dynamically generates a string of HTML code, the embedded processing results, returned to the client browser. Third layer database server's task is similar to the C/S mode, responsible for the coordination of different SQL requests sending by Web server, manage the database. B/S model's characteristics is a simplified the client, the user operation more simple, applicable to online information.

The system uses the combination of C/S and B/S mode. The main work of administration is the inquiry and decision, entry work less, so the B/S model is more appropriate, so we will be the second layer Web server and third layer database server unified on a single server management, however, this does not destroy the three layers of structure of B/S. As for coal statistics departments need to store speed and more rapid entry, the interaction is relatively strong, so decided to adopt the C/S model.

Client/server model is more widely used in software operating mode of the network application, it's the biggest characteristic of the function has a large space to achieve. We will give more work of input data processing to the client, using SQL SERVER 2008 database management system; task of data browsing, searching task performed by the server, using the ASP.net call database content.

Network topology structure. Existing enterprise LAN with star topology, backbone using fiber optic equipment, the system uses 5 types of shielded twisted pair, both the server and the client, using Gigabit adaptive network card, so as to meet the growing needs of users requirements and on the internet.

Servers and switch are on the control center, each client through twisted pair connected to the hub, each user group are connected to the switch of the control center through fiber, the topological structure ensure the security of the system, not by a fault line influence to other computer operation.

In order to ensure the reliable operation of the system, the server should be dedicated server selection of high grade, and select the uninterruptible power supply is better, and the best choice for two sets of the same type of server hot backup, and the server used tape machine will share the data backup, to ensure the security of data need not regularly will need backup data to disk. It can reliable operation of 24 hours of uninterrupted security system.

The system software platform and the technology. The server in this system uses Windows Server 2003 as the end of network operating system, because the network operating system is safe and reliable, and with the Windows series interface and usage are similar, so it is very suitable for management information system construction of enterprises and institutions of the local area network.

With Windows Server 2003, Microsoft SQL Server 2008 has naturally become a choice of database management system, they are all Microsoft series products, mix together to complement each other, closely integrated. SQL Server added to a special service function to the upper network components, such as OLE-DB and open database connectivity (ODBC). This component makes the client application system different connection and mutual communication possible, and does not need to change the existing server database or other existing client application system. Through the use of Database-aware components, users can also use SQL Server based on Internet application. Such as Active Server Pages, Internet Database Connector or ADO tools effectively help you to integrate SQL Server database information integration in your webpage. The development of these characteristics of SQL Server is very suitable for MIS system.

A programming language we choose C# in the C/S mode, in B/S mode, we choose ASP.NET. For the database, we use ADO data access technology.

In the administration, we adopt the B/S pattern design, the first layer of the client is responsible for send request to the Web server, according to user input and output, using ASP.NET to development; the second layer Web server which is a connecting link between the client and database server, it exists in the form of dynamic link library, responsible for the establishment of the actual connection database, according to the user request, connected corresponding database by OLE DB, and through the database access component ADO (ActiveX Data Objects) to complete the operation of the database, and the result is returned to the client; the third layer database server perform real database operation.

In the data set, we use the C/S design pattern, using the C# language directly to establish a connection with the database and user request through ADO, complete the database operation.

We mainly use the Recordset object (Recordset) which is one of the ADO object, this is because the Recordset has a similar table rows, columns structure, can be conveniently stored database query results. Unlike in the development of ODBC rules under the RDO and DAO, ADO is developed in OLE DB standard, so it has the characteristics of object oriented.

The characteristic of the system

All data submitted and stored directly in the database server, for all authorized users to browse for online.

Each month, the system will automatic generate a table, the table name plus years name as the table name, it is convenient for data storage, and save search time, but also is convenient for program design, can find the early data from the CD when necessary.

The logic structure of the system is clear, function authority in strict accordance with the network structure and system function, for exclusive data of different users strictly limit the rights, enhance the independence of data, and reduce the interference between different users.

For the administrative part of the B/S structure to increase the use of the mouse, while the other part of the C/S structure is used as keyboard input, it can obtain higher efficiency.

The system combines C/S, B/S network architecture, not to give up the traditional client / server structure, but also provides a familiar interface for the majority of users, both to ensure the daily operation of enterprises, and enable users to easily browse information online, enhance the operability, reliability and safety of the system.

References

[1] Yu Ertie. Modern coal quality management. China Coal Industry Publishing house. 1985.05

[2] Occupation skill appraisal of coal industry guidance center.Coal quality testing. China Coal Industry Publishing house. 2006.03

[3] Dong Yige. ASP.NET site construction practice. People's Posts and telecommunications press. 2010.02

[4] Duyne, D.K., Landay, J.A., Hong, J.I.Site interaction design patterns. Publishing House of electronics industry. 2009.09

Applied Mechanics and Materials Vol. 596 (2014) pp 1022-1025
© (2014) Trans Tech Publications, Switzerland
doi:10.4028/www.scientific.net/AMM.596.1022

The Research on Construction of Open Hierarchical Practical Teaching System

Zhuoyuan Wang[1, a], Lingong Li[1,b*] and Yigang Wang[1,c]

[1] Ningbo Institute of Technology, Zhejiang University, Ningbo, Zhejiang Province, China

[a]zywang1981@163.com, [b]lilingong@nit.zju.edu.cn, [c]wyg@nit.net.cn

Keywords: Practice, Hierarchical, Individual demand

Abstract. In order to make all students choose their own personal practice activities according to their actual needs, an opening hierarchical practice teaching system is designed. The system can provide an abundant, progressive, alternative, developmental practice way for students to choose their practical activities, which is designed through five aspects such as practical course, course contest, students' scientific research, participating in teachers' scientific research, enterprise practice. In addition, the system can make students get what they need, do their best, do their respective development, show their own characteristics; it also enables excellence students to surpass themselves, ordinary students to realize their dreams, students with learning difficulties to complete their studies.

Introduction

At present, inverted classroom, active learning and other teaching modes are prevalent at home and abroad advocating students to participate in activities, linking theory with practice, emphasizing the students' practice[1,2]. But our country's higher education used to adopt the teaching mode of "theory mainly, and practice often as a supplement", students spend most of their time in learning theoretical knowledge in the classroom, part of the course has a small amount of experiments to verify the correctness of the theory. The techniques and skills that require in practical engineering applications will get slowly until work. This has resulted in school education out of touch with the demand of enterprise. School's practical teaching system is imperfect, resulting in students' practical and application ability is weak[3]. Therefore, explore a more effective, more perfect, more suitable for the contemporary students' quality features and meet the demand of enterprise practice teaching system is not only the requirement of students, but also the requirement of the society and the education development.

Practice teaching mode has been reformed for many years, and obtained many achievements, especially in applied undergraduate colleges. Such as Zhigang Su in "building an open platform of teaching, educating and employment, the exploration and practice of training high-skilled mechanical and electrical talent"[4] proposed: we should build an open platform of talent produced, job shared and resource shared between school and enterprise, construct a teaching system make students' ability adapt to industry technical level and position requirements. Xingke Wei in "research and practice in training engineered applied talents practice teaching system"[5] proposed: reform the practice teaching ideas and teaching system, focus on training students' engineering practice ability, design ability and innovation ability. Hongtian Zhang in "build an open practice teaching system, explore and practice to cultivate application-oriented engineered talents"[6] proposed: strengthening the construction of campus practice teaching platform, innovating industry-academic cooperation mechanism and increasing the "dual structure" construction of teachers. However, most of these reforms are macro reform strategies or improved teaching methods, or reformed a certain aspects of the practice teaching activities. This article will explore a teaching system which is systematic, students can choose and practice on their own and suit to the characteristics of the applied undergraduate students, provide a learn and practice environment that suit for the developmental individual needs of all the different background students so that all the students can get what they need, do their best, do their respective development, show their own characteristics.

The Design of the Teaching System

According to the characteristics of applied undergraduate students, the nature of the engineering education and the needs of the enterprises, we set the electronic information engineering specialty practical teaching system for practical course, course contests, students’ scientific research, participating in teachers’ scientific research, and enterprise practice five aspects, shown in the following table.

1. Practical course. Practical course is divided into basic, design, synthesis and innovation four levels.

Basic practice consists of two parts mainly. One is for the characteristic of weak basic theory of application-oriented undergraduate students, strengthen the review and improvement of relevant basic knowledge. The purpose is to make students understand the principles and methods of practical projects, avoid blind and blind obedience. The content includes of the experiment principle, instrument principle and method of use mainly. Another is the basic training practice. In order to reduce the difficulty of teaching and guarantee the teaching degree, we should design the core function of the course, such as the minimum system in microcontroller course, display, keyboard, analog convert to digital as an independent module. Solve the working principle of the module in the class and let students to make debugging for future application design in the experiment. Since the foundation module content is simple and practical, students are able to understand and complete it, improve students' interest effectively.

The purpose of the design practice is to cultivate and improve the students' application development methods and techniques. First, select a practical problem that useful, interesting and have the experience for students, such as the illumination, responder and electronic stopwatch as a practice project. Secondly, the system is built on the base module. For example, you can use the smallest system, keyboard, display system constitute the basic framework in the design of electronic stopwatch. Students can extend on the basis to meet their own needs. Third, the content is from easy to difficult, gradually rich. Such as the design of illumination, start from a single LED light, transit to the multiple LED drive gradually, a single LED flashing, multiple LED flashing, and then design the light use the color theory. Eight red, yellow and blue LED lights were given respectively, students can combine them through their imagination. To do so, students can overcome the fear and hardship, feel the experiment is not difficult and they can do it by themselves.

Comprehensive application has two aspects of meaning. First is the content of the course comprehensive application, such as apply the knowledge of microcontroller to practical. The second is the early stage of knowledge comprehensive application, such as humidity tester design, involves the humidity sensor, 555 circuit, and frequency detection. Students can apply the circuit principle, analog circuit, digital circuit, sensor, microcontroller, EDA and other courses through the project design.

The purpose of innovation practice is to cultivate students' innovative thinking and innovative ability. And there are three kinds of forms: The first is to expand and improve a type of design practice or comprehensive practice. As design other kinds of landscape lights and music lights on the basis of light. Second, teachers announce some practical projects to inspire students to think. Such as teachers announce the infrared remote control, students will integrate the TV remote control, air condition remote control and VCD remote control into the design of a multi-function infrared remote control. Third, students will propose practice topic by themselves, such as the design of a smart basketball scoring device. It not only can complete the basic scoring function, but also the voice scoring, the scoring storage and other functions. Since the topic is determined by the students themselves, they have a higher interest, greater responsibility and more enthusiasm. Students use their spare time to do innovative practice, which is benefit for their self-learning ability, the ability to analyze and solve problems and responsibility.

2. Course contest. We organize a school students’ electronic design contest each year, and select a group of students with interest in design, help them to study commonly basic knowledge and

equipment, have a systematic training during the summer vacation, prepare to participate in national or provincial undergraduate electronic design contest, organize students to participate in smart car competition in April every year, main content are the use of related chips, functional modules, car assembly methods, the car running path identification and control methods. Participate in the regional competition in July, winners will take part in the national competition in August.

3. Students scientific research. In order to guide students to take an active part in the activities of science and technology, the school will be equipped with college students' scientific research projects, the information science and engineering college will be equipped with college students' scientific research innovation practice projects. Teachers will tutor the students to select a topic in June each year, students will collate materials in the summer vacation, complete the declaration fill in September, participate in declaring college students' scientific research innovation practice project in October, and conclude it in the following year. In the process of the project research, teacher guiding, students implementing. Equip students with the research methods, research process and research experience.

4. Participate in teachers scientific research. We will introduce teachers’ research direction, research subjects, ways and means of teachers' scientific research activities in professional introduction after freshmen enrolling in. Organize the student and teacher to interview, have a two-way choice, and determine the specific content of project activities in the first semester of each school year. Every student can contact with any teacher at any time to talk about teachers' scientific research activities. Let students to experience the development process of research projects, they will gain experiences and skills by participating teachers' research activities.

5. Enterprise practice. Enterprise practice includes corporate trainee and internship two parts, professional organization will contact the practice unit, unify the practice content. Unified arrange the practice in the third semester of the first year, the enterprise practice in the second semester of the fourth year. The content of the practice shall be determined by professional and internship units. Conditional students can contact enterprise which suit for his professional before apply the professional and get the approval.

Hierarchical practice teaching system provide an independent practice way for all different background students’ individuality demand, so that all the students can get what they need, do their best, do their respective development, show their own characteristics.

The open hierarchical practice teaching system is a practice teaching system that isn’t limit to the factors of teaching time, teaching places, teaching contents, teaching methods, teaching objects and background, it can make a full use of students’ spare time, give a full play to the students’ enthusiasm, students can learn autonomously and collaboratively. Through the open, the practice teaching content is practical and useful, suitable to every student to learn, so that students like to learn and use it; students have the condition to learn and can carry out the practice learning activities in the classroom, laboratory, dormitory, library, or even at home in their spare time; students also can continue the unfinished practice tasks in class in their spare time, or participate in teaching activity such as teachers’ scientific research activity, competition, innovation and enterprise practice, enable students to apply knowledge into practice, improve the professional ability in the practice, and harvest learning outcomes.

Conclusion

Open hierarchical practice teaching system has four meanings. The first is the practice teaching content is open. Every course, every teaching module and every practical project is open so that to meet different individuality needs of students. The second is the teaching resource is open. Construct course website to provide abundant learning materials for students, construct QQ group to answer questions anytime and anywhere, Open laboratory provides students with welding, debugging field. The third is the teaching space is open. Students can practice in the laboratory, dorm, classroom, and even at home, use their spare time effectively. The fourth is the practice way is open. Eight practice ways are open to all the students, they can join in it anytime and anywhere. Meet the individuality demands of all the students.

Of course, the teaching reform is a process of sustainable development and constant improvement. The practice teaching content, teaching resource, teaching space, teaching way should adjust measures to local conditions, continue to innovation and improve gradually. We should make a proper use of the practice teaching system.

References

[1] Gregory S. Mason, Teodora Rutar Shuman, and Kathleen E. Cook. Comparing the Effectiveness of an Inverted Classroom to a Traditional Classroom in an Upper-Division Engineering Course. IEEE Transctions on Eduction, Vol. 56(2013), p. 430-435.

[2] Antonio Carpeño, Jesús Arriaga, Javier Corredor etc.. The Key Factors of an Active Learning Method in a Microprocessors Course. IEEE Transctions on Eduction, Vol. 54 (2011), p. 229-235

[3] Y. H. Li, S. W. Luo. Study and practice on the practical teaching mode of operating system course. ICCSE 2006, p. 416-419.

[4] J. H. vanDriel, D. Beijaard, and N. Verloop. Professional development and reformin science education: the role of teachers' practical knowledge. Journal of Research in Science Education, vol. 38(2001), p. 137–158.

[5] F. Magdy. Computer-based electromagnetic education. IEEE Transactions on Microwave Theory and Techniques, vol. 41(1993), p. 920-931.

[6] B. Beker, D. W. Bailey and G. J. Cokkinides. Application-enhanced approach to introductory electromagnetics. IEEE Transactions on Education, vol.41(1998), p.31–36.

Applied Mechanics and Materials Vol. 596 (2014) pp 1026-1029
© (2014) Trans Tech Publications, Switzerland
doi:10.4028/www.scientific.net/AMM.596.1026

Application of Multimedia Technology in Experiment Teaching of Environmental Engineering Microbiology

Song Liu[1, a], Lina Sun[2,b]

[1]North China Institute of Science and Technology, Yanjiao, Sanhe, Hebei, China

[2]North China Institute of Science and Technology, Yanjiao, Sanhe, Hebei, China

[a]liusong715@ncist.edu.cn, [b]18561065@qq.com

Keywords: microbiology, multimedia technology, experiment teaching

Abstract. The technology of multimedia aided teaching has been widely used in the professional teaching in higher schools. Starting from the characteristics of the subject of environmental engineering microbiology, discusses the role of multimedia teaching in the experiment teaching of environmental engineering microbe and superiority, discusses how to give full play to advantages of multi-media technology in the teaching practice, the rational use of multimedia technology, to improve the teaching quality and efficiency.

Introduction

Experimental teaching is an important part of college teaching work, comprehensive and innovative experimental teaching, plays an important, irreplaceable role in cultivating the students' innovation ability. Experiment of environmental engineering microbiology is a basic course for students majored in environmental engineering microbiology experiment, students mastering skills, cultivates students' practical ability, innovation ability.

The use of multimedia technology in teaching method has been widely applied to various fields of teaching, to promote teaching reform, improve the teaching effect, improve the personnel training plays an important role in quality. With the development of computer technology and network technology, the multimedia teaching can be applied not only in theory teaching, also can be applied to experiment teaching. Multimedia and experimental teaching, the teaching content, vivid image, directly to students, as a result, the traditional teaching methods can not be compared, not only improve the experimental teaching effect, saving the test items, but also expand the experimental teaching methods, widen the experimental teaching idea. The rational use of multimedia teaching resources is a development trend of university.

Problems of Microbiology Experiment Teaching in Traditional Environmental Engineering

Traditional microbiology experiment teaching mainly by writing on the blackboard, writing the experiment content, purpose, equipment and reagents, procedures and methods, the experimental results. Some experiments also stressed that the matters needing attention. Some experiment content a large amount of information. The main content can be expressed through writing on the blackboard; some experimental content must rely on language. Expression is not sufficient, and the experiment content writing also spends a lot of time. In traditional teaching, teachers often refer to a large number of reference books, to master a lot of knowledge, but it is difficult to image expression, so that students can not clearly understand the micro organism, the microbial concept become abstract. The teacher explained it abstract. Understanding is more difficult, such as the definition, the type of colony, described in words or language, lack of intuitive, students only once, can not form a long-term memory. Not good teaching objective. Also restrict the students' imagination and interest in learning. In traditional teaching, also use slides, charts and other auxiliary experiment teaching method, but is ready to slide in the process of using a longer time, the content of a single, inadequate, the operation is relatively cumbersome; and maps using a number, long-term reciprocating collapse, blurred, features are not prominent, will influence the teaching effect.

The Meaning of the Application of Multimedia Technology in Experimental Teaching

The use of multimedia technology can accomplish real resource sharing. Multimedia technology has created an advanced and flexible experimental teaching environment, classroom teaching is no longer confined to the physical laboratory, teaching and hands-on practice time and space can extend itself, through the Internet, interactive distance learning, can provide shift electronic teaching places to move resources from one school, "unique" a school, "sharing", greatly make up for lack of experimental equipment.

Multimedia technology can make up for the traditional experiment teaching. Multimedia technology can show the micro experiment phenomenon, the whole process of understanding the experimental phenomena. Some experimental projects, such as Bacterial culture, from the beginning to the end of experiment for several days or longer, students are in the laboratory experiment time only at the beginning and end of the experiment, progress and intermediate links can not be observed, the students are limited in master the experimental knowledge by time. The typical part of the experiment through the camera is made by using the technology of multimedia courseware to show students, so that students master more comprehensive knowledge. In addition, the multimedia technology can be special experiment. The open experiment in the selection of projects, as far as possible not to arrange the danger and environmental pollution experiment, so that students lack knowledge of such experiments. By using the technology of multimedia courseware can be made of such experimental project for students to learn, not only to achieve better understanding of the purpose of the experiment, and avoid danger and pollution.

Multimedia technology can effectively expand students' knowledge. With multimedia technology, can be made of some typical experiment courseware, with lectures, online communication way to enable more students have the opportunity to understand the related experimental knowledge, quality education for students and innovative culture has a great help.

Experimental Teaching Courseware Preparations

In the first experiment teaching semester preparation meeting, according to the overall plan and requirements of the experimental class, the experimental teaching of multimedia courseware in each experimental unit in the form of PPT were undertaken by each generation of teachers, per capita 2-3 experimental unit. In the production of courseware through various channels especially make full use of cyber source collection includes pictures, animation and video data, these materials and text together organically through the PowerPoint software, after appropriate processing formation PPT format of the experimental teaching of multimedia courseware. After the summary of experimental teaching courseware, in each preparation meeting all the teachers participate in the multimedia courseware on the corresponding experimental unit of the appropriate modification, in the consolidation of basic knowledge, focus, emphasis on basic principles of difficult principle and multimedia, collective bargaining, to form the final version, to achieve the unity of each experimental group teaching content the. The purpose of doing so is to avoid all the teachers, their production of experimental teaching of multimedia courseware all caused by uneven quality problem, at the same time, also can let each substitute teachers will be the energy and enthusiasm to the experimental unit is responsible for. There is a need to explain, to ensure the teaching content unified premise, in some details of the arrangements and teaching, courseware advocate performance of each teacher's personal style.

Teaching Application of Multimedia Courseware in Students' experiment

The traditional experimental teaching in theory teaching, teachers usually use blackboard, chalk, charts and other traditional teaching aids in the laboratory. And the mode of multimedia aided teaching is to use the multi media computer, projector and network in the process of teaching, a new teaching mode teaching in laboratory. Compared with the traditional teaching methods, the use of multimedia technology assisted teaching experiment shows obvious advantage.

Multimedia aided experiment teaching vivid, lively, and easy to understand. The multimedia teaching can make the image of more difficult teaching content, express vividly displayed, so as to enhance the students understanding of the problem, laid the foundation for the actual operation. Multimedia teaching has rich expressive force, can strengthen the student's perceptual knowledge. The multimedia technology take text, images, animation, sound, video and other media information in one set, the concepts, abstract, complicated experimental principle and method of operation with vivid images, clear voice form, stimulation of students through a full range of sensory, prompting students to deepen the comprehension and memory of knowledge, improve the learning efficiency.

Graphics and image is one of the important ways to help students better understand knowledge. In the multimedia teaching, often making charts and pictures into a multimedia courseware, such as the isolation and identification of bacteria in the comprehensive experiment program is projected onto the screen, according to the explanation, separate identification procedure charts to dynamic form, image intuitive, clear hierarchy; in the teaching Gram staining method, at the same time the whole process of dyeing operation with piecewise form pictures continuously show, with Flash animation, enable students to teach and practice impressed.

Through the rational allocation of the various teaching resources, multimedia technology set maps, sound, as in the integration, show diversified forms, vivid image, intuitive vivid, fully mobilize the consciousness of students' subjective initiative and class participation, arouse students' learning interest and enthusiasm, but also increase the initiative of teachers and vividness, effectively improve the efficiency of experiment teaching. Embodies student-centered, teacher led modern education concept. Some key and difficult knowledge use the Flash animation in order to facilitate students to understand. Such as training method in the division crossed operation in separation on bacteria, using Flash animation can clearly introduced the streaking operation method to the students, through teaching, student movements in actual operation specification freely.

Solve the difficult problem of experiment teaching, improve teaching efficiency. Microbiology experiment has many teaching content, using multimedia courseware can effectively solve the common problems appeared daily teaching show, which includes two aspects, firstly, the teaching content, such as the use of high-pressure steam sterilizer, virus isolation and culture technique, the direct demonstration by teachers in traditional teaching, limited by the time and students numbers. Now, we will make the teacher's demonstration video clip into RM format file, use the corresponding software by computer and projector. Secondly the teaching content to students with practical operation, is shown through computer related pictures, animation or video file playback to students before teachers teaching, deepen understanding and memory, which is a compensate effect due to the increasing number of students. In addition, involves morphological aspects in microbiology experiment, can let the students visual impression through multimedia display technology, and then the real observation, can greatly shorten the students to observe the time, improve the efficiency of the experiment.

Amplification information saves the teaching resources and the teaching time. Reduction of teaching hours and the large increase of environmental engineering microbiology knowledge, we are required not only to the teaching content concentration, streamlined and sublimation, more important is by changing the mode of experiment teaching, improve teaching efficiency in order to adapt to the training mode in the new era. The traditional teaching model, teachers use lectures, blackboard, chalk and charts and other simple teaching aids, impart knowledge to students. The application of multimedia teaching, can not only alleviate the contradiction between teaching contents and short time, and multimedia courseware can replace many traditional charts, slide, projection, video, in the guarantee of the quality of experimental teaching, saving teaching resources and cost.

Conclusions

In the microbiology experiment teaching, the proper use of multimedia, can greatly improve the efficiency of student learning. Multimedia teaching is not perfect, it is only an auxiliary means of teaching, can not completely replace the traditional teaching methods. Not because the use of computer teaching, the teacher is a computer operator. But students became the audience. Only clear in the teaching process the teacher's leading role and student's main body status, in order to achieve the expected teaching effect. Microbiology experiment teaching can not abuse of multimedia technology. And the appropriate use of multimedia technology, otherwise perceptibly. To make the multimedia better applied to the experimental teaching of Microbiology, we should do the following aspects.

Firstly, the content can not be "blackboard" simply copy to multimedia, can applied equipment, reagents, method, principle, steps through the picture, animation, video, displayed in front of students. Second, the multimedia text font, size, color should be used properly, picture, animation, video and other related experiments can be displayed through the appropriate "hyperlink" way. Third, key and difficult content, statement to emphasize, talk slow not fast, but the method of multimedia and teachers' experimental demonstration combined were expounded and expression. Fourth, the multimedia teaching and the traditional teaching combination, can not simply tell the content, and to collect material, question and answer, pay attention to interact with students, may be appropriate to use body language, eye contact and other methods are applied to experimental teaching. Fifth, prepare the pre experiment, such as the right and wrong operation results. Show students in the form of multimedia (image, animation, video and other means), so avoid the operation mistakes occur in experimental operation.

Practice has proved, in the microbiology experiment teaching, combined with the proper use of multimedia and traditional method, can not only help students concentrate in the course of time, the effective absorption, digestion, more knowledge, but also can stimulate their enthusiasm. The experiment to mobilize their enthusiasm, give full play to their imagination and creativity. The application of multimedia in the microbiology experiment teaching, which can expand the students knowledge, broaden their horizons, but also can improve the experiment operation skill of students, obtain good teaching effect.

Acknowledgements

This work was financially supported by the Teaching Research Foundation of North China Institute of Science and Technology (Research on Environmental Microbiology improve students' innovative and comprehensive reform experimental basis for the ability to use).

References

[1] Xie Baogui. Microbial Teaching Research and Reform [M]. Beijing: Science Press, 2000:27-29

[2] Xie Jiang Yu. Problems Discuss in Multimedia and Bilingual Teaching of Microbiology in University [J]. Microbiology Bulletin, 2002, 29 (6):95-98

[3] Miao Jing, Liang Jianguang, Qu Hui Ge et al. Application of Multimedia in Microbiology Teaching [J]. Microbiology Bulletin, 2004, 31 (3):168-171

[4] Ning Si Chuang. Application of Multimedia Technology in Food Microbiology and Experiment [J]. Guangxi University Journal, 2002, 27 (6):27-29

Applied Mechanics and Materials Vol. 596 (2014) pp 1030-1033
© (2014) Trans Tech Publications, Switzerland
doi:10.4028/www.scientific.net/AMM.596.1030

Optimal Model of Tutor Selection in Graduation Thesis Guidance for Undergraduate

Congjun Rao and Qiqin Liu

College of Mathematics and Physics, Huanggang Normal University,

Huanggang 438000, China

cjrao@163.com

Keywords: Tutor selection; Assignment model; Efficiency matrix; Hungarian method

Abstract. The graduation thesis is the last part of undergraduate education, is an important way of cultivating the innovative thinking and comprehensive quality students. In order to improve the students' graduation thesis quality, we must select optimal and suitable to guide different students. In this paper, we study the problem of selecting optimal tutor in the guidance of undergraduate graduation thesis, and present an optimal assignment model for tutor selection, and then use the Hungarian method to solve the assignment model. It provides effective way to the optimal allocation of tutor resources.

Introduction

In colleges and universities, the graduation thesis or graduation design of undergraduate students before graduation is very essential and important. Its purpose is to summarize what they have learned the results of four years of professional knowledge and to cultivate students' comprehensive ability of applying learned knowledge to solve practical problems[1-5]. Therefore, to design an optimal tutor allocation scheme in the guide of graduation thesis or graduation design has a crucial role for saving teaching resources and improves the quality of undergraduate graduation.

The work of graduation thesis includes five stages, i.e., topic selection, dissertation proposal, research conducting, dissertation writing and thesis defense. Each process of these five stages has significant impact on research ability cultivation of college students, high-quality academic thesis writing and the improvement of overall quality, and the tutor plays an important role in each process. From the perspective of the way of topic selection, to mobilize students' research interests, the best way is to implement the two-way selection for the tutors and students[6-8]. A tutor must be carefully considered and deliberate, and then screen out good topic with professional features in order to write high quality research papers. This paper studies the problem of selecting optimal tutor in the guidance of undergraduate graduation thesis, and tries to provide effective way to the optimal allocation of tutor resource.

The rest of this paper is organized as follows. Section 2 gives the problem description. Section 3 presents a hybrid multi-attribute decision making to select the winners. Section 4 provides concluding remarks.

The Tutor Selection Model

In the practical guidance of undergraduate graduation thesis, the tutor allocation problem can be discribed as follows. Suppose that there are m tasks of guidance of undergraduate graduation, and m tutors can be selected, and each tutor is assigned only one task. Since each tutor's individual characteristics and capabilities are different, and individual's completed efficiency is also different. So we must allocate the best and suitable tutor to guide each student to complete all the tasks, and the goal is to complete various tasks to make the best total benefit. Here we establish an optimal assignment model to complete the problem of tutor selection. The assignment model [9-13] of tutor selection is as follows.

Suppose that x_{ij} means A_i does the work B_i, and we set

$$x_{ij}=\begin{cases}1, & assign\, A_i\, to\, do\, the\, work\, B_j\\ 0, & Not\, assign\, A_i\, to\, do\, the\, work\, B_j\end{cases}$$

Then the standard form of assignment model can be expressed by

$$\min z=\sum_{i=1}^{n}\sum_{j=1}^{n}c_{ij}x_{ij}$$

$$s.t.$$

$$\sum_{j=1}^{n}x_{ij}=1,\ i=1,2\ldots,n$$

$$\sum_{i=1}^{n}x_{ij}=1,\ j=1,2\ldots,n$$

$$x_{ij}\in\{0,1\}$$

$$c_{ij}\geq 0$$

where $C=(c_{ij})_{n\times n}$ is called an efficiency matrix. If the efficiency matrix $C=(c_{ij})_{n\times n}$ is given, then the assignment can be determined.

For the assignment model of tutor selection, the following assumptions are given.

(1) The number of tutors m is equal to the number of students n.

(2) $x_{ij}=1$ means that student i choose tutor j, else $x_{ij}=0$;

(3) c_{ij} means the j-th course score of the i-th student.

Then the assignment model *M* of tutor selection is

$$\min z=\sum_{i=1}^{n}\sum_{j=1}^{n}c_{ij}x_{ij}$$

$$s.t.$$

$$\sum_{j=1}^{n}x_{ij}=1,\ i=1,2\ldots,n$$

$$\sum_{i=1}^{n}x_{ij}=1,\ j=1,2\ldots,n$$

$$x_{ij}=0\, or\, 1$$

$$c_{ij}\geq 0$$

where the second constraint condition shows that each student can only choose one tutor, the third constraint condition shows that each tutor can only choose one student. If x_{ij}^{0} is the optimal solution of model *M*, then the *n* order matrix $X=(x_{ij}^{0})$ is the the optimal solution matrix of model *M*.

Next we slove the assignment model *M* by using the Hungarian method. The detailed solution process are given as follows.

The Hungarian method is presented by the Hungarian mathematician D. Köngig. This method has the following properties.

Property 1. If the element of any row (column) in efficiency matrix minus a constant k (k is a positive number or a negative number), and a new matrix $B=(b_{ij})_{n\times n}$ is obtained. Then the assignment model with the efficiency matrix $B=(b_{ij})_{n\times n}$ has the same solution with the original assignment model, but the optimal value is greater than original assignment model, the value is k.

Property 2. If a part of elements in a matrix are 0, and a part of elements are non-zero, then the number of straight lines covering at least all the elements in the matrix 0 is exactly equal to the maximum number of 0 which are located in different rows and different columns.

Definition 1. The permutation of matrix $A=(a_{ij})_{m\times n}$ is defined as

$$per\,A=\sum_{i_1,i_2,\ldots,i_n} a_{1i_1}a_{2i_2}\ldots a_{ni_n}\ ,$$

where $i_1,i_2,\ldots,i_n$ is the arrangements to take over $1,2,\ldots,n$.

Definition 2. If $C=(c_{ij})_{n\times n}$, $D=(d_{ij})_{n\times n}$, such that

$$d_{ij}=\begin{cases}0, c_{ij}\neq 0\\ 1, c_{ij}=0\end{cases}$$

Then D is called the complementary matrix of C.

Based on above properties and definitions, the step of Hungarian method to solve the assignment model *M* is given as follows.

Step 1. Transform the efficiency matrix C of assignment model M such that the zero element appears in all the columns, then a new efficiency matrix $B=(b_{ij})_{m\times n}$ is obtained.

1) The elements in each row of efficiency matrix $B=(b_{ij})_{m\times n}$ minus the smallest element of this row.

2) The elements in each column of efficiency matrix $B=(b_{ij})_{m\times n}$ minus the smallest element of this column. If there exists 0 element in one row or one column, then the subtraction is over.

Step 2. Do the pre-arrangement to seek the optimal solution.

After the transformation in Step 1, there exists 0 element in each row and each column. Now we need to find a separate 0 element. If we can find out, then the optimal solution is obtained. When n is small, we can use To find the observation method and test method to find *n* independent 0 elements. If corresponds to an element of the matrix, and the rest is 0, which is the optimal solution. When small, the available observation, heuristics to identify independent 0 elements. If n is larger, then the steps are as follows.

1) Denoted ◎ for the 0 element from the line (column) which has only one 0 element. This means that there is only one considered to be assigned for the people in this line. Then delete other 0 elements in the columns (rows) with ◎, and it is denoted as @. This indicates that the tasks in this column have been assigned finished, and we don't have to consider others.

2) Denoted ◎ for the 0 element from the column (line) which has only one 0 element, and then delete other 0 elements in this row (column) with ◎, and it is denoted as @.

3) Repeat 1) and 2), until all 0 elements are denoted and deleted.

4) If there is still 0 elements which denoted by ◎, and there is at least two 0 elements in the same line (column). This can be probed by different ways. From the row (column) with fewest 0 elements, we begin to compare the number of 0 elements, and select 0 element of this element and plus a small circle. Then delete other elements crossed peers with columns. Repeat this process, until all 0 elements are denoted and deleted.

5) If the number *m* of ◎ is equal to the number of order of the matrix *n*, then the optimal solution of this assignment problem are obtained. If $m<n$, then transferred to the next step.

Step 3. Line the fewest line which can cover all 0 elements to find most independent elements in the coefficient matrix. The detailed steps are as follows.

1) Denoted √ for the line without ◎.

2) Denoted √ for all columns with element @.

3) Denoted √ for all columns with element◎.

4) Repeat 2) and 3), until there is no new √ in all rows and columns.

5) Line a horizontal line for the row without √, and line a vertical line for the column with √, then we obtain the least lines wich can cover all 0 elements. Suppose the number of horizontal lines is l, if $l < n$, then we must transform the currrent matrix and find out n independent 0 elements. And then turn to the step 2). If $l = n$, and $m < n$, then we must turn to step 4).

Step 4. Adjustment. Find out the smallest element in the part which is not covered by the a straight line, and then minus smallest element for the row with lined √, and add the smallest element to the each element of column with lined √ to ensure the original elements are not changed. So we get a new coefficient matrix (it's optimal solution is the same as the original problem). If n independent 0 elements are obtained, then the optimal solution is obtained, otherwise the third step is repeated.

Conclusions

In this paper, an optimal assignment model for solving the problem of optimal tutor selection in the guidance of undergraduate graduation thesis is presented, and the Hungarian method is used to solve this assignment model. It provides effective way to the optimal allocation of tutor resource. It can be generalized to other resource allocation problems.

Acknowledgments

This work is supported by the 2014 Key Project of Hubei Provincial Department of Education (No. D20142903).

References

[1] J.S. Zhang: Mathematics in Practice and Theory Vol. 4 (2002), p. 6-8.

[2] H. Zhang, Y.M. Yang, and B.S. Fu: Mathematics in Practice and Theory Vol. 20 (2010), p. 1-3.

[3] Z.P. Wang: Statistics and Decision Vol. 10 (2011), p. 8-10.

[4] S.J. Yang: Studies in College Mathematics Vol. 1 (2010), p. 75-77.

[5] J.W. Zhao: Quantitative & Technical Economics Vol. 10 (1993), p. 8-10.

[6] H.B. Liu and Z.Q. Ku: Mathematical Modeling and Mathematical Experiments (Science press, Beijing, 2008).

[7] X.F. Liu: Journal of Operational Research Vol. 2 (1990), p. 23-25.

[8] F.L. Wang. Journal of Agrotechnical Economics Vol. 4 (1989), p. 14-15.

[9] L. Zeng: System Engineering Theory and Practice Vol. 11 (2004), p. 38-39.

[10] X.J. Zhang and G.W. Wei: Science and Technology Management Research Vol. 11 (2009), p. 201-203.

[11] T. Wang: Statistics and Decision Vol. 13 (2006), p. 140-141.

[12] S.Y. Chen: System Engineering Theory and Practice Vol. 12 (1998), p. 7-13.

[13] X.H. Zhu: Journal of Southwest Jiaotong University Vol. 3 (2007), p. 25.

Applied Mechanics and Materials Vol. 596 (2014) pp 1034-1039
© (2014) Trans Tech Publications, Switzerland
doi:10.4028/www.scientific.net/AMM.596.1034

Research of Neuroergonomics Experimental Teaching System in Industrial Engineering

Jun Wu[1, a], Wenmin Han[1]

[1]School of Economics and Management, Jiangsu University of Science and Technology,
Zhenjiang, China, 212003
[a]wujunjm@sina.com

Keywords: experimental teaching system, industrial engineering, human factors, neuroergonomics experiment

Abstract. As human factors teaching in industrial engineering steering to neuroergonomics as the core, neuron ergonomics experiment in new generation of industrial engineering experimental teaching occupies important position. Neuroergonomics experiments directly observe the human brain cognitive activities by means of equipments for measuring the electromagnetic activity and the brain blood flow dynamics in the brain. Based on the present experimental research situation, neuron ergonomics experimental teaching system platform was set up, which involves EEG & ERP experiment system, physiological experiment system, eye movement experiment system. The experimental teaching system includes validation experiments, designing experiments, comprehensive experiments and research experiments for different levels students. The experimental teaching system implements the system of industrial engineering laboratory construction update and perfect.

Introduction

The development of industrial engineering from the classic "work plan" to modern "computer integrated manufacturing," until now have sprung up neuron industrial engineering (NeuroIE), has experienced three historical stages of development [1]. With industrial engineering development phase synchronization, the development of the human factors experiment is from the past classical time study, work study to today's neuron ergonomics (Neuroergonomics) experimental research by nerves measuring equipment as the core tools. Dependence on traditional engineering psychology foundation of experimental equipment for teaching system has gradually can not adapt to the teaching requirements of the third generation neuron industrial engineering. This article will along the development direction of the third generation of industrial engineering, according to the construction of neuroergonomics experimental teaching system as a target, neuro-ergonomics experimental platform and course are constructed, and establish neuroergonomics experiment teaching system in a new generation of industrial engineering.

The Limitations of Traditional Human Factors Experiment Teaching

At present, the traditional human factors experiment teaching system is more and more difficult to meet the demands of the development of the new generation of industrial engineering discipline. The reasons to cause this result are both from the external cause of the change of the production environment, the internal cause of the changes of the human factors experimental research method, research object, and the cause of the industrial engineering discipline is more emphasis on man, machine, environment of various factor interaction effects brought about by the new trend.

Produce changes in the environment makes people learned from the experiment by the past focus on manual labor to focusing on mental work for experimental research. At present, constantly improve the degree of automation of the production system, the people in the production system more and more difficult to adapt to the requirement of higher speed and higher precision manufacturing process, more than 80% in the man-machine system accidents belong to the human error [2]. M. Kim, et al. (2012), divided the influencing factors of production system mainly into four categories, namely, human factor, technical factor, structure factor and task factor, and that the human factor is the first of four major factors in the system. Today's production system to be effective decision-making and response under the new complex environment, people should put more new research techniques on human factors [3]. With the constant improvement of the degree of automation, in the past, most of the physical labor work gradually replaced by automated machines. At the same time, the workers are from the past tool operator to automation control system monitor. This shift makes the human factors experimental research transfers from the past focus on the muscles, bones, force analysis of ergonomic studies into focus on physical and mental load. Now, the urgent need for industrial engineering teaching is according to the change of production environment to open for mental load monitoring and behavior patterns in the human factors experiment course.

From the perspective of the subjects of human factors experiment teaching, the past human factors experiments mainly through behavioral science research methods, from a person's external behavior research, and speculate that a person the sense for production information, such as perception, attention, memory, thinking, cognitive process. On the one hand, from the point of research methods, the classical research method is mainly study the overt behavior, the index is mainly the task response speed and accuracy. For research method based on behavior, the biggest problem is that the method does not really separate the cognitive process and reaction process in people performing a task. On the other hand, from the point of the research content, the experiment of classical information processing model can study the behavior of explicit, but not the implicit behavior effectively. In a classic human factors experiment, a similar note, implicit behavior such as feeling, thinking, still belongs to black box can't be broken directly. Therefore, we need to study deeply in the level of brain thinking to carry out the human factors experimental teaching by the new research methods, reveal the true inner cognitive mechanism of the work.

Human factors in industrial engineering is the discipline that studies the anatomy, physiology and psychology factors in a work environment, and the human, machine and environment interactions [4]. Today's industrial engineering teaching broke the biomechanics, cognitive psychology, environmental science, ergonomics, respectively independent teaching and research of barriers, more and more tend to a variety of research methods to integrate a certain human factors subject. For example Mental load, is the workers must pay attention to reach operation standard [5], and its influence factors include the amount of work, working hours, workers quality and ability requirements, workers will, and mood triggered by work environment, etc. The researches in school aeronautic science and engineering of Beijing university of aeronautics and astronautics carried out the pilot's mental load measurement and evaluation for multi-mode flight simulation tasks by the neuroergonomics experiment system [6, 7]. The human factors experiment researched the pilot's mental load on man-machine interaction process in Flight simulation environment by neuroergonomics. The experiment is a combination of cognitive neuroscience, behavioral science, ergonomics and other multi-disciplinary knowledge. Thus, with the development of industrial engineering, a new experimental teaching system dominated by neuroergonomics must be established.

Construction Goal of Neuroergonomics Experiment Teaching System

Construction goal of neuroergonomics experimental teaching system is to keep up with related neuro-ergonomics field teaching and research trend of NeuroIE, close to the actual production operation of the work in a single automated production to human-computer interaction. By introducing the neural measurement, ergonomic analysis, human body modeling and simulation as the main body of the experimental equipment, comprehensive experiment teaching platform of people's psychological and physical coupling can be built for scientific and effective adjustment of industrial engineering laboratory equipment structure and to adapt the new situation of teaching and research of industrial engineering requirements.

Construction goal of neuroergonomics experimental teaching system is below:

(1) Based on the existing industrial engineering laboratory equipments, with the experimental equipment of construction projects to the production practice, the importance of measurement and analysis of person's psychological and physiological factors is highlighted in the teaching. The experiment teaching system integrates three main factors of man, machine and environment.

(2) Using the equipment and software, according to the relationship between people and the environment, machine and environment, and human-machine-environment elements, the design, research, or comprehensive types of experiment were carried out to understand the influence factors of the work efficiency. The experimental courses about the industrial engineering, logistics management, and other majors were carried out to cultivate innovative talent of high quality.

(3) Using advanced neural measuring equipment, combined with the existing laboratory experiment system, the reasonable man-machine system and relevant work facilities were analyzed and designed, enables the students to know functions and influences of human factors for work efficiency from the brain cognitive level, to master the latest design and test methods of human factors. At the same time, the experiment teaching system provides scientific research platform for the teachers and students.

(4) Using portable neurofeedback measurement equipment, teachers lead students to measure the operators' psychological and physical parameters at the scene of the actual work, make students understand the whole life cycle process from design, production to use, train students' practical ability of man-machine system design and optimization.

(5) The neuroergonomics experiment teaching system carry out the experimental teaching for the industrial engineering and logistics management, and other relative majors, and provide the experiment support for these curriculums, such as industrial engineering, work study, ergonomics, production and operation management. Neuroergonomics experiment make human factors experiment project more in line with the requirements of students training objectives, to promote the development of industrial engineering discipline construction.

Neuroergonomics Experimental Teaching System Platform Construction

The concept of the third generation NeuroIE has been proposed since 2006 [8], its research methods mainly through neuroergonomics experiment, records peoples' neural activity and physiological information in the working, to optimize the man-machine system in the production process. Neuroergonomics experiment is by means of the advanced neural measuring instrument and physiological data collection equipment, according to the proposed for engineering experiment scheme collect subjects of physiological and psychological data in the industrial engineering laboratory or field, join the person's physiological state information to the production operation system through data mining and analysis, comprehensively consider the workload between human and machine system and physiological load to realize the man-machine system whole optimization. At present, the teaching and research of neuroergonomics experiment in industrial engineering in the world is still in its beginning and exploring stage, NeuroIE laboratories of all countries in the experimental equipment, the research methods present a different direction and genres. In this paper, based on the present situation of the experimental research, the teaching platform of neuroergonomics experimental teaching system was built in industrial engineering to service for the follow-up human factors experimental courses.

Neuroergonomics experiment in order to overcome the traditional human factors experiment to research the behavior as the theme provides the effective method from the people's physical and mental level directly on the level of brain thinking for people in working. Karwowski (2005) considered people different behavior is the core of the whole system work from the relationship of the "people - technology - environment" three systems [9], so the individual cognitive differences is a focus in the study of industrial engineering. Because of the limitation of the past by the experimental technology conditions, the human factors experiment was carried out only from the perspective of external behavior observation for human cognitive differences. As progress of noninvasive neural measuring technology for the subjects, neuroergonomics experiments can do individual cognitive differences experiments from the level of brain thinking and physiological data acquisition inside people based on analysis of human physical and mental. Neuroergonomics experiments study the physiological and cognitive ability in the working process. Research purpose is to clarify human physiological mechanism and the brain cognitive mechanism in the man-machine system [10]. Neuroergonomics experiments directly observe the human brain cognitive activities with the aid of two types of modern imaging technology. One kind is measuring technology of electromagnetic activity of the brain: Event Related Potential (ERP) and Magneto-encephalography (MEG). Another kind is technology based on cerebral blood flow dynamics: functional Magnetic Resonance Imaging (fMRI), Positron Emission Tomography (PET), and Transcranial Doppler Sonography (TCDS). These neuroergonomics experimental techniques open the black-box on classical industrial engineering like attention, perception, and thinking. Neuroergonomics experiments can make up for the classical industrial engineering experiment two shortcomings, become the most suitable experimental technology on man-machine interaction research of modern industrial engineering system.

Based on the experimental research present situation, neuroergonomics experimental teaching platform in industrial engineering discipline was set up. The experimental teaching platform involves EEG & ERP experiment system, physiological experiment system, and eye movement experiment system. EEG & ERP experiment system involves the cable ERP experiment system, the wireless ERP experiment system, EEG experiment system, and the neurofeedback experiment system. Physiological experiment system involves physiological data collection and analysis system, biofeedback system, and physiological and biomechanical integrated system. Eye movement experiment system involves fixed eye movement experiment system, remote eye movement experiment system, and mobile eye movement experiment system. In addition, the above experiment systems can effectively be integrated for more observation mode of experimental teaching and research, at the same time can be communicated with classical behavior experiment system to form physiological and psychological behavior integrated experimental teaching platform in human factors.

Neuroergonomics Experimental Teaching System Curriculum Construction

According to the purpose of industrial engineering discipline teaching and students' different levels, neuroergonomics experiments can be divided into the confirmatory experiments, designing experiments, comprehensive experiments and research experiments. Neuroergonomics experimental teaching will cover undergraduate, master graduate students and doctoral students. Neuroergonomics experimental teaching in industrial engineering includes the following (see Table 1.).

Table1. Experimental teaching theme

	neuroergonomics experimental teaching theme
1	production management and organizational ergonomics research
2	physical ergonomics and occupational safety research
3	driving safety and man-machine system simulation research
4	cognitive ergonomics and human-computer interaction research
5	human reliability and system security research
6	product usability and user experience research
7	physiological data and production data fusion research
8	ergonomics research of cross-cultural management

The neuroergonomics experimental teaching system will serve the industrial engineering undergraduate, master and doctoral students. Teaching courses include human factors, task research, production operation management, logistics management, quality management, information system management, and other courses. Teaching links includes cognition practice, professional practice and graduation design.

Conclusions

The development of industrial engineering (IE) from the classic "work plan" to modern "computer integrated manufacturing," until now have sprung up NeuroIE, has experienced three historical stages of development. Accordingly, the teaching of industrial engineering also turned to NeuroIE teaching as the core. Neuroergonomics experiment in the third generation industrial engineering experimental teaching occupies important position by the technology advantage for delving into production operation of human physiology and psychology. Compared with previous industrial engineering behavior observation and questionnaire survey as the main means of the experimental technology, neuroergonomics experiment can not only effectively separate the process of cognitive processes and behavior, avoid confuse mutually in the experiment to measure both cognitive and behavior, but also research people implicit behavior in the working, crack the black box of the internal cognitive process. Through neuroergonomics experiment people died as a result of the experiment implicit behavior of cognitive mechanism can be revealed in the information processing of production. Therefore, neuroergonomics experiment with the aid of the latest nerves measuring technology and equipment, breakthrough the limitations of the past industrial engineering experimental teaching, can satisfy the demands of the third generation industrial engineering teaching and research.

Neuroergonomics experiments directly observe the human brain cognitive activities by means of equipments for measuring the electromagnetic activity and the brain blood flow dynamics in the brain. Based on the present experimental research situation, neuroergonomics experimental teaching system platform was set up, which involves EEG & ERP experiment system, physiological experiment system, eye movement experiment system. This experimental teaching system platform can complete EEG experiment teaching, event related potential experiment teaching, experiment teaching of physiological response and feedback, eye tracking experiment teaching as well as the coupling of the physical and mental comprehensive experimental teaching. Neuroergonomics experimental teaching system covers 8 human factors experiment topics, such as the cognitive efficiency, human-computer interaction research, etc. At the same time, neuroergonomics experimental teaching system will serve the industrial engineering undergraduate, master and doctoral students. Teaching courses include human factors, task research, production operation management, logistics management, quality management, information system management, and other courses. Teaching links includes cognition practice, professional practice and graduation design.

Through the establishment of the neuroergonomics experimental teaching system in industrial engineering, the need of the third generation industrial engineering teaching and research was satisfied. The experimental teaching system includes validation experiments, designing experiments, comprehensive experiments and research experiments for different levels students. The experimental teaching system implements the system of industrial engineering laboratory construction update and perfect.

Acknowledgements

The research is supported by the National Natural Science Foundation of China (71271105), the Higher Education Teaching Reform Project of Jiangsu Province (2011JSJG158) and the Scientific Research Start-up Foundation of Jiangsu University of Science and Technology.

References

[1] Qingguo Ma, Huijian Fu and Jun Bian: Management World Vol. 6 (2012), p. 163-168, 179. (In Chinese).

[2] Jeom Kee Paik: Marine Technology Vol. 4 (2012), p. 62-66.

[3] M. Kim, R. Sharman, C.P. Cook-Cottone, H.R. Rao and S.J. Upadhyaya: Behaviour and Information Technology Vol. 31 (2012), p. 1147-1160.

[4] L.Y. Sun, K. Cui and L.H. Sun: *Human Factors* (Science Press, China 2011). (In Chinese).

[5] M.S. Young, N.A. Stanton: *Mental workload: theory, measurement, and application* (Taylor & Francis, USA 2001). [6] Xiaoru Wanyan, Damin Zhuang and Wei Liu: Journal of Beijing University of Aeronautics and Astronautics Vol. 38 (2012), p. 497-501. (In Chinese).

[7] Zongmin Wei, Xiaoru Wanyan and Damin Zhuang: Journal of Beijing University of Aeronautics and Astronautics Vol. 40 (2014), p. 86-91. (In Chinese).

[8] Qingguo Ma, Xiaoyi Wang: Management World Vol. 10 (2006), p. 139-149. (In Chinese).

[9] W. Karwowski: Ergonomics Vol. 48 (2005), p. 436-463.

[10] R. Parasuraman, M. Rizzo: *Neuroergonomics: The Brain at Work* (Oxford University Press, USA 2008).

Applied Mechanics and Materials Vol. 596 (2014) pp 1040-1043
© (2014) Trans Tech Publications, Switzerland
doi:10.4028/www.scientific.net/AMM.596.1040

Research of the Model to Foster Engineering Students'Ability and the Assistant Analyzing System

Yongze Fang[1, a], Zifen Liu[2,b], Danfan Zhao[3,c] and Zhefeng You[4,d]

[1,2,4]Jimei University, Xiamen, Fujian, China 361021

[3]Fujian Broadcast and TV University, Fuzhou, Fujian, China 360001

[a]fjsmfyz@gmail.com, [b]zfliu@jmu.edu.cn, [c]Dfzhao@fjrtvu.edu.cn, [d]zhefengyou@126.com

Keywords: high education, engineering Ability, model

Abstract. Engineering education should be centered on strengthening college engineering students' ability, which should be implemented through all courses' teaching during the entire four college years. This paper researches and constructs an ability fostering model by which the students are fostered in engineering colleges, and poses an analyzing method and a computer assistant analyzing system based on this model.

Introduction

In China's colleges, especially general colleges, most engineering graduates need to support ordinary and fundamental technological tasks of enterprises now. But theories are always emphasized, practices are ignored in colleges. This pattern can't adapt to the actual requirements of the enterprises [1]. In order to overcome this weakness, shorten the graduates' adaptive periods in enterprises, some rules should be formulated [2, 3]. For one thing, teaching contents should be in accordance with industrial technology development; for another, students' ability should be fostered, which should be implemented throughout the whole four-year teaching in colleges. It is a comprehensive and complicated systematic engineering to improve colleges' engineering education. We should have a systematic research for teaching concepts, professional goals, curriculum system, courses teaching, and practical stages to strengthen college students' ability. This paper is aimed to offer solving methods, making a research of the model to foster college students' ability and a computer assistant analyzing system based on this model to boost engineering education.

Ability Fostering Model

Professional ability is based on professional knowledge. Although it always takes a lot of time for the students to master basic knowledge, they would fail to solve practical problems well with their knowledge. Students need to obtain applicative competence through learning and different kinds of practices. Teaching and curriculum should be centered on fostering students' practical abilities. Therefore, in the teaching process, how to teach and how to foster their ability to solve practical problems with their knowledge are the most important issues.

To work it out, this paper constructs a model to foster students' engineering ability, and a computer assistant analyzing system based on it is also figured out. This is aimed to turn those teaching activities for fostering ability which are distributed implicitly in different courses, practices and knowledge units into explicitly and systematically. It also helps to underline actual requirements, combine capability requirement with everyday teaching in engineering curriculum. When this model is used, it can assist programming of teaching contents, the choices or designing of teaching patterns or teaching methods.

Ability Fostering Model: Courses—Knowledge—Ability Diagram (CKA Diagram). In this CKA diagram, ability axis (A axis, as shown in Fig.1) shows different types of actual ability (like system analysis ability, programming ability, multimedia creation ability, network design ability, professional foreign language ability, document creation ability, autonomous learning ability, computational thinking ability, effective communication ability, leadership ability…), while course axis (C axis), according to the term sequence, lists all courses and internships and practices; and knowledge axis (K axis) shows different knowledge units of each course.

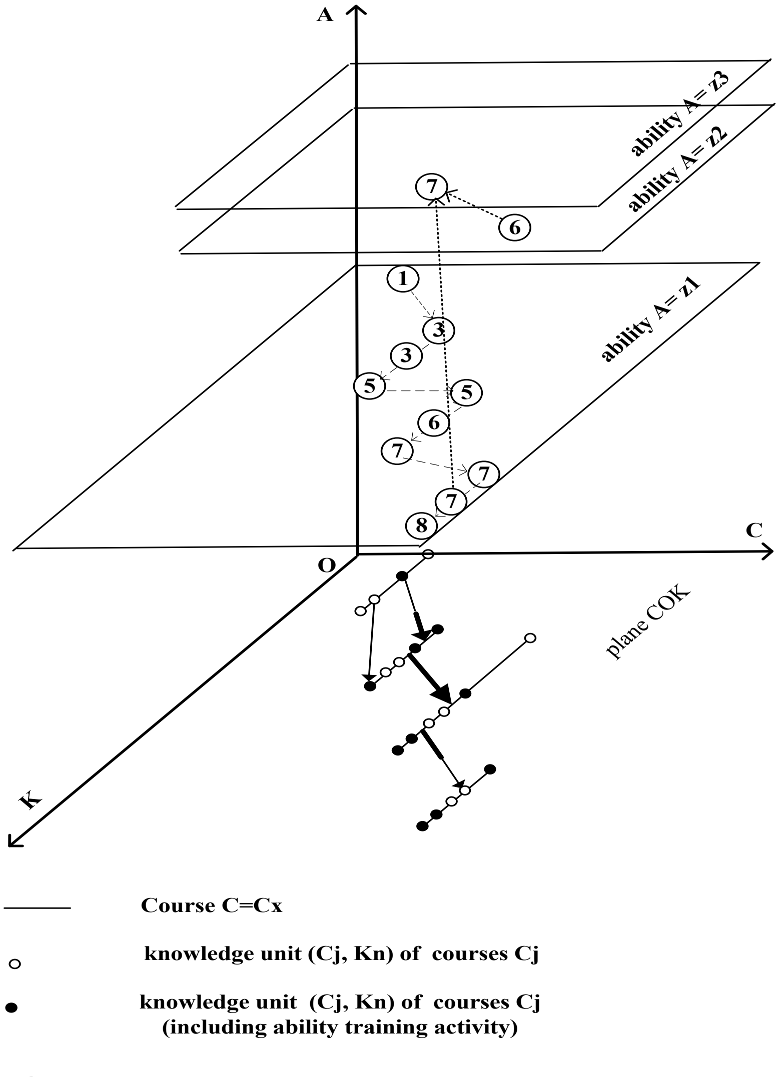
A
ability A= z3
ability A= z2
ability A= z1
⑦
⑥
①
③
③
⑤
⑤
⑥
⑦
⑦
⑦
⑧
O
C
K
plane COK
Course C=Cx
○ knowledge unit (Cj, Kn) of courses Cj
● knowledge unit (Cj, Kn) of courses Cj (including ability training activity)
ⓕ score (f) of fostering ability in knowledge unit (Cj, Kn)
(Ci,Km) → (Cj,Kn) (Cj, Kn) is based on(Ci, Km)
Ci → Cj Cj is based on Ci
(Ci,Km) → Cj Cj is based on (Si,Km)
Ci → (Cj,Kn) (Cj,Kn) is based on Ci
-------> ability is accumulated through same-kind ability
.............> ability is produced through different-kind abilities integration

Fig.1 CKA Diagram

It is very abstract and difficult to describe whether one's ability is strong or weak, without any unit, and hard to calculate. But in order to measure the level of ability fostering, consistent with what people always feel, we can establish two concepts: level and score. There are altogether five levels and ten scores of the intensity or effectiveness in ability fostering. They are listed as follows: ever seen (1-2 scores), can understand and explain (3-4 scores), ever participated (5-6 scores), can operate or carry out expertly (7-8 scores), can conduct or innovate (9-10 scores).

In one knowledge unit, students can improve their ability through two types of approaches. Ability may be accumulated through same-kind ability, or it may also be produced through different-kind abilities integration. The former always shows linear growth, but growing speed may vary with different fostering stages, so we may use segmented functions to represent and calculate the growth. The latter always shows non-linear growth, which can be evaluated particularly in the knowledge unit fostering.

For example: growing coding ability=coding rows/projected rows*computer language coefficient

The plane C=Cx shows all knowledge units of course Cx, expecting abilities fostered in the units and fostering intensity. The plane COK lists all courses and every knowledge unit of every course; it also marks the 4 relationship between all the knowledge units of every course in chronological order: follow-up course Cj is based on prerequisite course Ci; the knowledge unit (Cj, Kn) of follow-up courses Cj is based on the knowledge unit(Ci, Km) of prerequisite course Ci; the knowledge unit (Cj, Kn) of follow-up courses Cj is based on prerequisite courses Ci; and follow-up courses Cj is based on the knowledge units(Ci, Km) of prerequisite course Ci. The relationship feature reflects the application, extension, deepening of all knowledge units, shows through what channel students improve their capacities, and reminds the teachers who are responsible for the courses in chronological order to pay attention to the interior relationship of teaching contents, therefore teaching efficiency, goals and requirements can be improved step by step.

Analyzing Methods of Ability Fostering. Analysis, formulation of curriculum system and teaching program should be through the processes from top to the bottom, from bottom to the top.

First, under the guidance of engineering education concept, professional goals should be settled, and curriculum system should be planned, so that on the professional level, the actual requirements of ability fostering are projected throughout each course and practices (plane COA). Then on the course level, teachers decide what should be taught according to this plan, closely following the development of industrial technology. Teachers then are going to select or design scientific and advanced teaching method, considering teaching contents and the function to ability fostering of every knowledge unit, such as CDIO, discussion, researching, so on and so forth. With these steps, each course teaching program is established. Last, to ensure the professional goals to be realized, teachers of all courses should feedback and accumulate effects to the professional level, then from the perspective of ability fostering, teachers are to investigate in the plane A=Az (or plane COK) which course is aimed to foster what ability, through what knowledge units, with what teaching methods, to what level. It is aimed to adjust and optimize the whole teaching system.

The course teaching program is implemented through closed circle. In real teaching, the CKA diagram can be used to record ability fostering effect of each knowledge unit of each course, which can be referred to as background of next educational reform.

Assistant Analyzing System Based on the Ability Fostering Model

In engineering education, many courses and knowledge units are closely related, so CKA diagram is complicated. Designing, analysis, indication, and storage of curriculum system and teaching project of each course need to depend on a computer assisted analyzing system. The system, based on CKA, should be with multiple views, which integrate all the course teaching programs into a complete teaching system, reflecting the knowledge units' relations of different courses and the whole process of ability fostering. This can be conducted through dynamic analysis and adjustment from three levels: a knowledge unit, a course or the whole teaching system, and it can supply a friendly public platform for teachers to discuss and analyze the whole teaching system and every course teaching program. The system structure has three layers: graphical user interface layer, processing logic layer and the data storage layer.

Its main functions:

- Input all courses, internships, practices and all the knowledge units mark the relationship of every course or knowledge units, assist the teaching program designing of every knowledge unit, hence constructing courses teaching program.
- Integrate the entire course teaching program into a teaching system.
- Provide teachers with different query views which include: view of course teaching program, view of relationship of knowledge units or courses, view for ability fostering and 3D view of CKA.
- Record teaching process.
- It can be used for statistical analysis, and to modify the teaching program.

Conclusions

It is a comprehensive and complicated systematic engineering to improve colleges engineering education, and to shorten the gap with enterprises requirements. All the teachers and students should take an active part in its construction. We should have a systematic research for teaching concepts, professional goals, curriculum system, courses teaching, and practical stages. The center for current professional construction is to enhance college students' practical ability, and this should be implemented throughout the entire 4-year college teaching. We constructed an ability fostering model by which the students are fostered in engineering colleges, posed the analyzing method and the assistant system based on this model.

Acknowledgements

This work is financially supported by the Science and Technology Project (soft science) of Fujian Province of China (2013R0078) and the Scientific Research Project on Humanities and Society of Chinese Ministry of Education (11YJAZH064).

References

[1] Jianzhong Zha, Lei Feng, Lambda Verdonck, Yongshan He, Needs Analysis of College Engineering Student Source in China, Research on Higher Engineering Education, 2008, (3), pp.39-46.(in Chinese)

[2] Hongyan Zhang, Ability-oriented Teaching Pedagogical Design for Engineering Course, Computer Education, 2010, (11), pp.50-55.(in Chinese)

[3] Hongmei Li, Zhibin Jiang, Yihui Zheng, University Curriculum System Reformation, Research on Higher Engineering Education, 2013, (5), pp.140-144.(in Chinese)

[4] Wen Liu, The Model of Making a Thorough Inquiry in Computer Basic Course Teaching, Journal of Liaoning Normal University, 2004, (4), pp.498-450.(in Chinese)

[5] Shibin Wang, Haixia Qie, Jianxing Yu, Jie Wang, Haisheng Pan, Keli Sun, On the Idea and Practice of Higher Engineering Education——Case Studies on MIT, BERKELEY, PURDUE and TJU，Research on Higher Engineering Education, 2011, (1), pp.18-23.(in Chinese)

[6] Amparo Camacho, Javier Paez. Modern curricula design for engineering programs, http://www.ineer.org/Events/ICEE2008/full_PaPers/full_paPer266.Pdf

[7] Brent Wilson, Martin Ryder, Distributed Learning Communities: an Alternative to Designed Instructional System, http://www.adraptis.com/voithima/theoretic/distributed_learning.pdf

[8] Erik De Graaff, Wim Ravesteijn, Training complete engineers: Global enterprise and engineering edueation http://www.tandfonline.com/doi/abs/10.1080/03043790110068701

Applied Mechanics and Materials Vol. 596 (2014) pp 1044-1047
© (2014) Trans Tech Publications, Switzerland
doi:10.4028/www.scientific.net/AMM.596.1044

Study on Innovative Reserching Project Management for the Computering Software-based Enterprises

Qi Li

Shenzhen Institute of Wuhan University

Room 207, Wuda Bldg. Nanshan, Shenzhen, Guangdong, PRC

Tel: 0755-86393207 137152 07866

Email: liqiinsz@126.com

Keywords: Software firm, product researching, project management

Abstrct: The aim of this paper is to provide an introduction to the management techniques for the software-based orgnizations on their period of processing a innovative product reserching. All the works and efforts we do can be divided into two sorts: regular works and occasional works, the later one, we named it "the projects".As the teamleader of the orgnizaion whose job duty is the core of the team to get to reach the final goal, the concept of project managing and planning abbility is the essencial fact. We divide the whole management leadership quality into five actors according to the different manaing situationas, which need different five managing techniques, and propose detailed exlpainnations and introductions to the suit techniques in the managing experience.

Content:

The concept of Occasional Works and Regular Works

In the new times of the knowledge-based situation, computering and software enterprise are constantly facing the experience of the exporation and reserching of a definite software product system and project. PM (project management) is not only an essential technique for a manager in the network and computer field, but also, moreover for any staff of works or a membership in any organization in their daily management. In the management study there is a theory of "All the works and efforts we do can be divided into two sorts: regular works and occasional works, the later one, we named it "the projects". In any orgnization or enterprise, especially in the software firm, We can find it more difficult to carry out occasional works(OW) management than we do on regular works(RW), although RW wastes about 80% our daily time while OW only less than 20%.

These two sorts of works, OW and RW, have very clear difference in works features, durations, organization, working environment and leadership. In the working features, OW has more flexibility than RW, and the former can be easily altered than the later by the changing of the conditions and working environment. The working organization of OW is often temporarily and the RW's fixed for the different features of the both. The successful strategy management of an enterprise is the success of both sorts of works, especially the success of OW, which highly determines the rise and down of the enterprise. As the matter of a fact, many units haven't realized this point, as they have no such an idea or a concept of OW. To have the concept of OW is the very important first step to undertake the OW while being occupied by the RW.

The five stages of OW in management

OW is usually divided into five stages: launch, plan, do, check and delivery, also called the lifecycle of project management. At the stage of project launch, a common approve to the expect project goal should be achieved among all the members of the organization. A complete and effective communication ensures the achievement, although an effective and high-efficiency communication is always the extremely arduous task facing the leaders and term-members as well.

To form a hi-efficiency team, the organization includes a excellent team leader whose main job is complete understanding to the goal， preparation of al the resources and decision-making, and several team members who will mutual complementary in capacity and character.

In this stage before the launching of the project, the team leader or the sponsor of the project should always ensure the balance of three factors, the Resources, Time and Quality\quantity, namely RTQ of the project. R and T are the input of the project and the Q is output, yet maximum RT don't surely bring about the maximum Q. We call it the art of the Management Project.

In the second stage of planning the project, to have accurate and essential design technique of "breakdown" means to divide the total project goal into several separate smaller goals which assign to the relative members to complete. These include these questions, as what is the goal? Who will do? How to do?What time to do? What resources needed?

The team leader's five managing roles in OW

Covering the whole process of the project, the team leader takes the vital role in the organization, as the captain of the team, the inspirer when the team members in the lower moral, the judger to valuate the members' performance, the coach to guide his fellows and even the substitute when necessary. Fig.1 shows the teamleader's five different managing actors at five different management situations,eg. Captain, inspiror, judger, subsitute and coach.

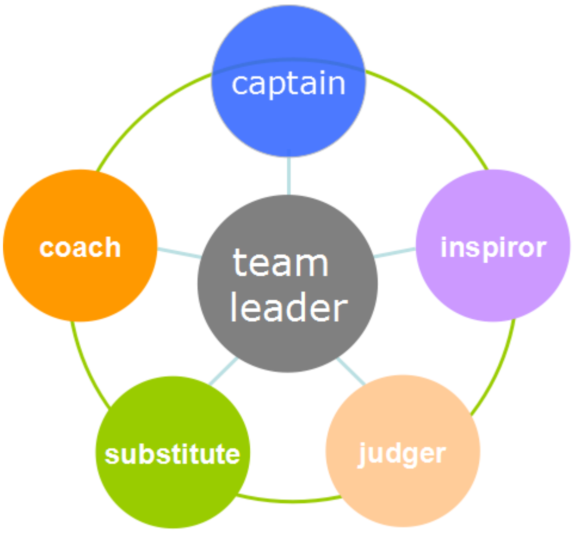

Fig.1. Five actors of teamleader in project management of computering enterprises.

Captain: The leader's duty is to collect, to prepare and to allocate the prepared resources, including the manpower, time, tools, information and other kinds of resources. To construct the hi-efficiency team organization is the vital important to complete the project.

Inspirer: The great master of management, as George Baton, the American Military General in Great World II, acted in the time period of extremely difficult to inspire his soldiers to go ahead to the battle with him side by side. In his speech he gave his children a dream, a imagine thirty years later "when your grandchild once ask you what you are doing in the great World War, you can tell him proudly ——your grandfather was just fighting against the German together with that general Baton in Africa…. You won't have to say 'Ai, your grandfather was a farmer in Louisiana…'". Many soldiers went into the fighting battle after hearing this famous speech, even lost their lives.

Judger: You should correctly evaluate the performance of your members time after time, praising the good performance and check the lower ones.

Substitute: You won't have to be an expert in every role of the organization, but be a general master of the whole procession of the project. It is necessary that you have to be a substitute when any position absence appeared in no case.

Coach: The last and vital role of the leader in a team, often neglected by the organization, magnifier the power of the leaders to deliever your own advantages to the whole team.

Project achivement submission: Cost control? Or Customers' Satisfactory first

In a software enterprise, we see the period of project submission as the final stage of project management, is it correct that the enterprise's upmost efforts brings the most satisfactory? The customer's requirement is divided into 4 dimensiongs: solution,time,usage and price.(Maybe more than 4, safety, compatible,leggle,eg).Each dimension marked by 1-5 points according the satisfactory.

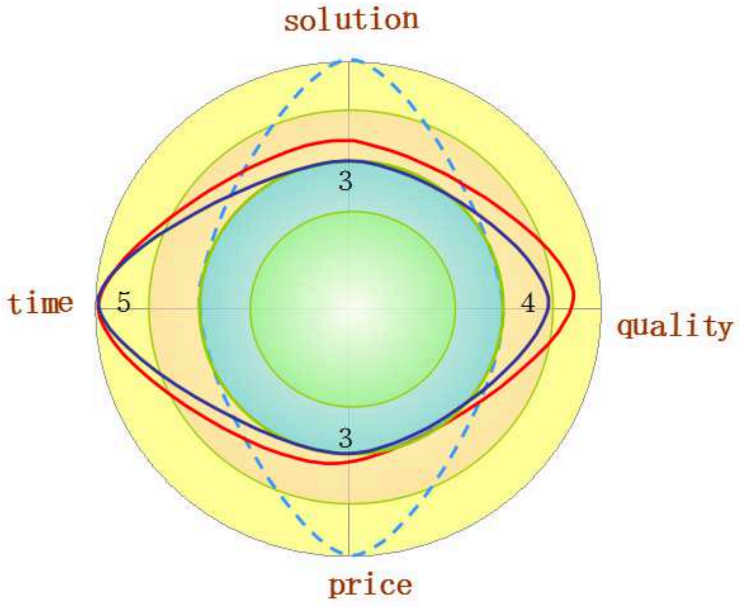

Fig.2. The mode match of customers' satisfactory and the services offered by enterprise

Customer's requirement ◯ Enterprise submission ◌

The upmost satisfactory ◯

Fig.2 shows that 5 points in all four dimensions seems to be the "perfact", but not the right things customer need,and it consumed the huge and valuable resources of the team. What customer needs is as shown by the dark blue circle(3-5-3-4), while our submission is the light blue circle "5-3-5-3". That is the real reason for customer's dissatisfactory. The ideal submission should be as the red circle, which just cover the customer's disires in all four demissions and could save the valuable resources. It is by no means the fact that the maximum input of resources, eg time, labor, manpower, money and equipment, should bring out the results with which the customers happy.

It is quite clear that greater the input of resources, greater cost it takes. Yet the results compass or exceed the prediction of the customers by a great scale will not surely let them satisfactory, but the team have to take great cost to achieve it. So we say that the result we deliever to the customers should be the right cover their prediction advanced, which will great satisfy the customers.

That is to say, a excellent team leader not only have to bring out the good results, but also keep in mind who much he has to input the resources and reduce the cost of the project. To fulfill a project or a activity by not taking cost into account is not the successful project management. The project is not a successful project.

Conclusions

We can find it more difficult to carry out occasional works(OW) management than we do on regular works(RW), although RW wastes about 80% our daily time while OW only less than 20%. In OW management, the teamleader is actully to be seen as five different actors according to the real manaing situations.

Acknowledgements

This work was supported by Professor Sizhuo Yang, Shenzhen Zhongshang International Management Reserch Institute, Dr. Jef Zhu, the School of Economy and Management ,Wuhan University.

References

[1] Sizhuo Yang, in China Management Advisory Book (2004)

[2] Sizhuoyang, in The teamleader’s job: One or More (2008).

[3] Sally Rao, in Project Management in Software firm.(2008)

[4] Information on http://www.weldr.labs.gov.cn

[5] managemen Information on http://www.wdem.cn.

Applied Mechanics and Materials Vol. 596 (2014) pp 1048-1051
© (2014) Trans Tech Publications, Switzerland
doi:10.4028/www.scientific.net/AMM.596.1048

Analysis of the Way to Enhance the Professional Core Competence of Engineering Students of New University

Zhao Xueqin[1, a]

[1]school of urban planning & landscaping, No.88 of Bayi road, Xuchang, Henan, China

[a]zxq200403@163.com

Keywords: new university; professional core competencies; promote.

Abstract. By analyzing the characteristics of the new university of engineering students' professional core competencies, students generally attach great importance to the personal and professional skills, they want to improve personal and professional core competencies, but lacking of a clear understanding and effective way to improve interpersonal skill and learning ability; they pay attention to enhance practical ability, but lacking of the development and innovation, so they hope to improve the ability based on the practice. According to the above features, this article presents the way to improve the professional core competencies.

Introduction

University students not only learn to master the expertise and develop, 'professional competencies', they also possess adaptability, learning ability , practice , innovation strength , force development and other professional core competencies which follow the requirement of the society and the development of the times. Professional core competencies are the basic skills which are in parallel with the professional ability in people's careers. It is the sustainable ability of the lifelong development which adapts to the changes of various works. Different titles of the professional core competencies are applied in different countries, such as 'key ability', 'basic ability', 'basic skill', 'non-professional ability' , etc. However, the main content of the professional core competencies is divided into adaptability, learning ability, practice, force development and innovation. New university thinks the cultivating applied talents as its orientation, so it should pay more attention to condition of the training professional core competencies and improving students' personal and professional core competencies. This article analyses the characteristics and current situation of the new university of engineering students' professional core competencies, and put forward the effective way to strengthen the engineering students' professional core competencies.

The Characteristics of the New University of Engineering Students' Professional Core Competencies

Students attach importance to improving personal and professional ability, but they often have poor knowledge of it. New university students care for whether they will get the professional job or not in the future. Before entering the university, they began to take the employment problem into account. With the understanding of the employment, a lot of students have realized that being successfully employed requires specialized knowledge and other abilities. But they don't have clear concept that which ability is the most core. According to the survey of graduates, they think that they have weak practice and poor interpersonal skills. When they enter the service, they integrate and adapt to the environment slowly. While the practical ability and teamwork of the engineering students are the most valuable qualities which employers emphasize on.

The student yearns for communicating with other people, but lacking of a good environment. New university students were at the intermediate level when they were studying in the high school, they desire improving their skills in all aspects after entering the university, the survey indicated that a great many engineering students consider themselves as talkative and think that they have small communication range, they just have a good relationship with roommates and almost don't contact with the outers. Employers also react that graduates could meet the job professional requirements, but in the aspects of dealing relationships, they failed. They only mastered knowledge without the method of interaction with others, and often perform as unsocial, insolent and so on in working. With the stress, less free time, and non-actively looking for help, about half engineering students choose to smolder pressure in the heart and wait with time wearing on, moreover, most of them come from rural areas, lacking of family education to direct them to contact with other people, which is the reason why they want to integrate society, but they don't find effective ways and means to do it.

Engineering students have professional knowledge and good learning attitudes, but lacking of effective learning programs and learning methods, so their learning abilities need to be improved. With heavy learning task, if engineering students want to get good grades or diplomas, they should spend more time on learning. The majority of students think that learning will help them to improve themselves, and they hope to find satisfied job based on the learning. The aim of learning is so clear, which is the effective way to urge students to study. However, many students have no plan; they just follow the teachers' requests. And employers have reacted that graduates' learning abilities are poor. It follows that learning knowledge and skill is not equal to improve the learning ability. And teaching students the ways to learn and improving students' abilities are more important then learning professional knowledge and skills.

Engineering students have more hands-on opportunities, and are willing to participate in various forms of practices; they think that the practice is an important way to improve capabilities. New university engineering students rarely participate in social activities and have weak personal practice ability. They believe that practice ability determine directly the future employment, so they attach great importance to the individual practice level .Students generally recognized that changing the unrealistic expectations and truly improving the practical ability of individuals are important for the students to adapt the society and to find a satisfactory job . In the survey -'What social activities you have participated', student community activities, work-study , social welfare activities, social surveys , tutoring or part-time ,supporting education and agriculture respectively accounted for 51%, 39% , 29%, 28 % , 20% , 10% . It is observed that the social activities which students participated in are confined to the school , and the form is simple which is lacking of variety of forms of social practice. 74% of students believe that their practice ability is ordinary or bad, so they could take no advantage. The employer survey shows that the practical ability of graduates is deficient, and the phenomenon of unrealistic expectations still exists. Graduates could not apply the knowledge and skills which they have learned in the school to their work, and they are competent for the job just by re-learning and re-exercising in the job.

The evaluation of university students on innovation is not high, the attention on innovation and development is not enough, and the practical action is insufficient. New university engineering students meet their own requirements which just stay on the level of learning professional knowledge and getting a satisfactory work, as for their own future development, they have no high require. They think that the requirements of cultivating innovation in university is just raised for the good student or the good school students, and also believe that innovation is the advanced requirement not the basic requirement. Students generally realize that making a breakthrough and surpassing on innovation requires appropriate guidance. Considering that plan and progress is important, but no action and implementation occur. As the demand for the specialty of engineering students is high and the employment situation is better, part of the students are blind self-confidence for the future development, make no specific plans and actions, and have no deep thinking for how to improve their own innovation and development. School guidance education is essential.

The way to enhance the new university of engineering students' professional core competencies

In order to improve the new university of engineering students' professional core competencies, students, university and society should make efforts together. Students can participate in various activities to expand their range of communication, which can develop their practical ability and other professional core competencies. Universities should also reform and innovate education model, change concepts of education, build student evaluation mechanism which regards comprehensive quality as the core, and cultivate students' professional core competencies to enable students to become socially useful talents.

School-enterprise cooperation can help to enhance to provide a good social environment for students' professional core competencies. Government and education authorities should introduce policies to encourage enterprises, social forces and university to cooperate, establish platform for more cooperation between university and enterprise, and regard the improving non-professional ability as social responsibility; social practice is the significant platform to improve core competencies, but it often faced the problem that there is no social support. Society should provide more care and support to students` social practice, meliorate the situation about the employment of the university students, and offer the opportunity and platform to develop students' practice ability with love and assist.

Changing teaching methods will be helpful to provide a good learning environment for students' professional core competencies. In order to break the phenomenon that traditional education dominated by the teacher, curriculum should be student-centered, outstand the students' dominant position, see the real task as guidance, design the professional system based on the work process; in order to change the score-oriented traditional education, taking the ' competency-based 'as the guiding ideology , deepening teaching reform , developing professional ability as the purpose, and constructing practical teaching system are essential; building students' professional ability evaluation system ,opening teachers and valuing fairly are useful for the student administration. In order to create a better environment for the students, university should integrate and use resources, set up workplace, promote formation and development of common professional ability, and build professional practice system. For the past practice and theory, practice teaching in university should make full use of engineering resource , social practice out university should make the utmost of regional advantages and industrial advantages , so that the theoretical teaching combines with practical teaching to improve the non-professional ability of the new university students.

Creating opportunities actively for students will be beneficial to improve professional core competencies. To improve practical ability, university students not only master specialized courses, they should also participate in social research, so that they can learn to integrate theory and practice, identify, think over, and solve the problems in social practice. The abilities to communicate with others and handle problems will be formed from the process. At the same time, university students should reflect on their own shortcomings, accept new knowledge, learn from each other and sum up experiences, in order to improve their learning and developing abilities.And also for the reason to keep up with the time, university students also need to develop a scientific study habit and a scientific attitude, accumulate basic knowledge and consider the problem with reverse thinking to improve innovation ability.

Conclusions

Having analyzed so many characteristics of the new university of engineer students' professional core competencies, it is obvious that there are so many problems which hinder the development of engineer students' professional core competences. And based on these features, there are three main methods which have been put forward, including the methods of school-enterprise cooperation, changing teaching methods and creating opportunities. These methods can be helpful to improve professional core competencies. Meanwhile, there must be many other methods to improving engineer students' professional core competencies. Since the resources which could be collected are limited, so it needs more specific studies about this topic.

References

[1]Desheng Lu, Yi Yu. *The Challenge and Outlet of Undergraduates' Occupation Ability*[J]. Education and Vocation, 2009(13)

[2]Jinjun Fu, College Students' Activity Theory--university Extracurricular Education under the Quality-oriented Education, [M]

[3]Changxi Huang, Ye Lei, Xinfang Han. The Cultivation of Engineering Students' Practical Ability and Creative Spirit and the Whole of Enterprise Employment Practice, [M]

[4] Weibing long. *Viewing Reforming Direction of the Vocational Education Teaching from the Missing Non-professional Quality* [J].Vocational Education Research .2008 (1): 26-27

[5] Guo Wei. *Strengthen Quality Education to Promote Students' Comprehensive development* [J]. Shandong Administration Institute - Journal of Shandong economic management cadre institute.2003(58):29-31

[6] Qiwen Wu. *Humanistic Quality Education & Non-professional Capacity Building* [J]. Jiangsu Higher Education.2000(2):40-42

[7] Zhaoxiong Lin,Yongshi Pang, Meng Qiang. *Success of University Student and Cultivating Non-professional Capacity Building* [J]. Journal of Guangzhou University (JCR Social Science Edition),2008(5)

Applied Mechanics and Materials Vol. 596 (2014) pp 1052-1055
© (2014) Trans Tech Publications, Switzerland
doi:10.4028/www.scientific.net/AMM.596.1052

Construct the Virtual Gram Stain Experiment Platform Based on 3Dmax and VRP

Song Liu[1, a], Lina Sun[2,b]

[1]North China Institute of Science and Technology, Yanjiao, Sanhe, Hebei, China

[2]North China Institute of Science and Technology, Yanjiao, Sanhe, Hebei, China

[a]liusong715@ncist.edu.cn, [b]18561065@qq.com

Keywords: Environmental Engineering Microbiology, virtual experiment, course construction

Abstract. the paper deals with the present research situation of the construction of virtual experiment platform, construct the model with 3DMax software, for the construction of experimental platform by the technique of virtual reality software VRP, compiled into executable file (exe). The gram stains method for example, modeling and simulation. Display the application effect of the virtual experimental platform, the virtual experiment platform has the advantages of high utilization rate, easy expansion of functions.

Introduction

In the evaluation of college teaching, experimental teaching is an important content, cultivation of creativity and practical ability of students is very necessary, for science and engineering students only through practical test and operation, can truly understand and master the theoretical knowledge of the subject, and have the ability to do the real work. The integration of teaching resources, so that students learn best, the virtual reality technology into the experimental teaching, have better effect in recent years practice. Therefore, virtual laboratory, virtual reality technology emerges as the times require and rapid development based on.

Overview and features of Virtual Laboratory

Overview. The concept of virtual laboratory was first proposed by Professor William Wolf of University of Virginia in 1989 American, it refers to the basic requirements of experimental teaching, virtual experiment environment in a computer system using virtual reality technology, the experimenter can use various virtual experiment instrument and equipment like in the real environment, real-time simulation operation the experimental model set up, the experiment of various predetermined, is a pledge, to soft and hard experimental teaching form. The virtual experiment based on the real experiment, is carried out to simulate the use of experimental devices, instruments and equipment, the experimenter by mouse click and drag, combined with the keyboard operation, can be like the real components of virtual experiment equipment operation, so as to complete the whole process of virtual experiment, the learning and training effect is equal to or even better than achieved in the real environment effect.

For the "virtual experiment" and "real experiment", the former is the supplement, improvement and expansion, the two advantages, promote each other, and complement each other. Superiority of virtual experiment is mainly reflected in: not affected by the traditional teaching mode with unified the limit; experimental group number can realize unlimited expansion and experimental "zero results" maintenance; the development of some destructive, comprehensive and researching experiment, but also in reducing the cost of the students in the experiment of the people safety; content can provide deeper, broader teaching contents for students, easy to open new experimental projects; and is not restricted by time and place, students may at any time on the experimental operation, to achieve the sharing of teaching resources.

Characteristics of Virtual Experiment System. Diversity: Virtual laboratory can assist teaching, students self-learning, helps to grasp the emphasis and difficulty in teaching, training and cultivating the experimental skills and ways of thinking of graduate medical students, is beneficial to the research and improvement of the clinical skills.

Immersion: Virtual experiment provides experience a real experiment, not only does not increase the laboratory space, also won't increase laboratory expenses.

Sharing and Efficient: Virtual laboratory based on the campus network, not subject to site constraints, can maximize the sharing. After the initial training of the virtual experiment, the purpose, operation of students experimental skills have been greatly improved, and then into the traditional lab will greatly improve the efficiency. At the same time as the method of virtual experiment based on simple labor saved a lot of experiment, the experimenter can spend more energy in the experiment itself.

Open: The open performance of virtual experiment shows open resource and experimental platform.

Interactivity and Autonomy: Virtual experiment is a organic combination of application of simulation technology, multimedia technology, virtual reality technology. The experimenter can enrich the auxiliary function using virtual laboratory, the experimental instrument, conventional experimental methods and steps of autonomous learning, independent practice, show the independence and interaction of height.

Gram Stain of Basic Experiment

Basic Courses. Gram staining is the foundation confirmatory experiment course in environmental engineering microbiology, experiment of environmental engineering microbiology in our school is independent experiment course, in addition to the latest progress requires students to master the basic theoretical knowledge, solid with microbial technology, more requirements to combine theory and experiment, training the students' ability of observation, thinking ability and practical ability. But because microbial reagent, instrument and equipment is expensive and various conditions, many experiments can not be normal open. Through the establishment of virtual laboratory equipment, reagents, experimental elements for 3D virtual, so that students can "be personally on the scene" to manipulate the virtual instrument and other instruments to finish the experiment in a virtual experimental environment, but also increase the students' perceptions of the experimental principle and method, improve the students' experimental interest. Microbiology is the rapid development of the subject, for the experimental teaching, advanced to improve teaching content is an important means to help students learn advanced scientific knowledge. To allow students to access to cutting-edge scientific knowledge, they must provide advanced experiment instrument to help students learn and understand. The performance of virtual laboratory makes full use of the most advanced computer technology to enhance and improve the experimental instrument, with accuracy and science; it provides very important conditions for the advanced science knowledge into the experiment teaching in classroom.

Gram Staining Method Overview. Gram staining method is a widely used in identification of bacteria staining method, in 1884 by the Danish physician Gram founded. Without staining of bacteria, due to its surrounding refractive index difference is very small, it is extremely difficult to observe under microscope. After staining bacteria and the environment form bright contrast, can be clearly observed that the bacterial morphology, arrangement and some structural features, and used for classification and identification. Generally includes four steps: initial dyeing, mordant dyeing, bleaching, dyeing and other complex Gram staining, specific operation method is:

Smears were fixed.

Ammonium oxalate crystal violet dye 1 minute.

Tap water.

The iodine liquid covering coated with about 1 minute.

Washing, use absorbent paper to absorb moisture.

With a few drops of 95% alcohol, and gently shake the decolorization, 20 seconds after washing, absorb moisture

Fan red staining solution (dilute) staining after 1 minute, washed with tap water. Drying, microscopic examination.

The establishment of Virtual Experiment Platform

The Key Technology. According to the requirements and characteristics of the virtual experiment platform of common key technologies, virtual experiment teaching visualization design, development of virtual experiment teaching visualization design of supporting software tools, for the establishment of virtual experiment teaching environment and typical demonstration and provide technical support and service. The key technology of virtual experiment: geometric modeling technology of virtual experiment, image element component modeling technology, virtual experiment, virtual experiment technology of element constraints model entity construction and visualization technology, virtual experiment model of cooperative sensing technology, virtual experiment object reference and virtual experiment scene interaction model, construction technology and visualization technology, development of teaching visualization design the virtual experiment of utility software and integrated environment.

In China, research found that the construction of virtual laboratory using computer technology has applications in many fields. At present, the developing platform of virtual reality can query to include VRP, Virtools, VRML, Maya and Web3d. Among them, VRP (Virtual Reality Platform, VRP) is a visual code developed by digital technology limited company directly facing the three-dimensional art of a virtual reality software. Virtools is a set of integrated software, can convert the existing file format together, itself has no modeling function, its script language VSL. VRML is the virtual reality modeling language, modeling language for building 3D world real world scene model or imaginary, is not object oriented. Maya is a top of the 3D animation software, is the level of high-end film production software, commonly used in film stunts and special effects production. Web3d is the use of 3D Internet platform items will be tangible reality through the Internet and three-dimensional display of virtual, and a virtual reality interactive browse. However, each method using the format and method are different, there is no uniform standard, the programming workload is huge.

At present, the field of virtual reality technology in Chinese, VRP software is the highest market share of a virtual reality software. Considering that, VRP strong practicability, simple operation, highly visual, does not require the extensive programming. Therefore, we choose the VRP software to carry out the construction of the virtual experiment platform.

The Ideas of the Construction of the Virtual Experiment Platform. Take environmental engineering microbiology laboratory for experimental background, the laboratory experimental station, equipment operation situation, to reflect the real experiment process. Firstly, through all the scene construction 3DMAX software 3D graphics, specifically: laboratory, test bench, the reagent frame, dropper, test tube, bottle, bottle washing, alcohol lamp, ring vaccination, slides, microscope etc.. Secondly, the model is imported into VRP platform has been created, and VRP will be the model through scripting for displaying and hiding, in order to achieve the purpose of drag into the model library. Once again, the scene changes and model drive connected through a script to call LUA to realize dynamic. Finally, the VRP compiler converts the EXE executable file.

Modeling and Implementation of 3D Model. Use 3DMax component modeling. 3DMax, based on PC system is a kind of three-dimensional animation and rendering software. Production process of 3D of MAX is very simple and efficient, at the same time, three-dimensional animation model is built and can be used for further processing and rendering script editing directly into VRP, the animation more vivid, more three-dimensional sense of reality scene. The construction of low 3D graphics, through the 3DMAX software specifically: laboratory, test bench, the reagent frame, dropper, test tube, bottle, bottle washing, alcohol lamp, ring vaccination, slides, microscope etc.. Finally, generate the model of rigid body animation.

VRP production. Modeling is completed, can be imported into VRP software. Open the VRP editor, import the model made in 3Dmax to VRP, click the menu bar "file - Import object", to determine the model file, choose to do, you will see the model in the software. The next need to define variables, by clicking on the menu bar in the script, enter the VRP script editor, click the insert statement, the eject command line editor window in the left side of the window, click the script file, and then click the definition of variables, the text box to appear in the right side will window, according to the input variable names, such as values, you can enter values again, click OK, at this point in the script editor will appear in the definition of the variable statement. Click the mouse to trigger a plot is produced mainly by thinking, mouse events script control. To complete the overall production, will be compiled into EXE, and debug, check whether the normal operation, whether accord with logic, to perfect the operation.

Conclusions

Constructing biological chemical virtual experiment based on multimedia programming and virtual reality of modern education technology, its purpose is to help students faster, more efficient, more accurately grasp the principles and rules of this discipline, improve the learning effect and the students' practical ability, promote the reform of curriculum construction and teaching method in biochemistry, and has broad application prospects the.

Gram staining of virtual experiment platform is developed in this paper is based on the characteristics of real physical objects, allows multiple users, multiple experiments were also carried out. Secondly, the experimental system with interaction process, the simulation process is dynamic, and synchronous display, and consider the actual component action sounds, so that the entire system more in line with the actual scene. Then, through the design of virtual experiment platform interface, a component library, can be conveniently in the experiment project called. Finally, the training and the actual design of the virtual experiment has the same experimental objectives, clear experimental steps and matters needing attention, can be completed on the actual training with display.

However, the virtual experiment is not the real experiment, but it cannot completely replace the real experiment, it has its own advantages, but in the construction of the initial certainly has some inevitable defects, therefore, the virtual experiment platform must be combined with the actual engineering practice, to achieve optimal matching, in order to further improve the teaching effect of practice. With the virtual experiment technology matures, people began to realize the value of virtual laboratory in the field of education, it can assist the research work of universities, such as in experiment teaching also has high utilization rate, easy maintenance and many other advantages. The virtual experiment platform will be the future direction of development of laboratory construction in Colleges and universities.

Acknowledgements

This work was financially supported by the Teaching Research Foundation of North China Institute of Science and Technology (Research on Environmental Microbiology improve students' innovative and comprehensive reform experimental basis for the ability to use).

References

[1] Newton. *The mathematical principles of natural philosophy*. Wuhan: Wuhan press, 1992

[2] Dan Meixian, Li Yi. *The virtual experiment teaching principle and application*. Beijing: Science Press, 2005

[3] Yuan Yuan, Gu Jun. *Virtual instrument based tutorial*. Sichuan: University of Electronic Science and Technology Press, 2004

[4] Zheng Lifeng， *design and implementation of virtual instrument laboratory*. Master Thesis of Southwest Traffic University, 2002

Applied Mechanics and Materials Vol. 596 (2014) pp 1056-1059
© (2014) Trans Tech Publications, Switzerland
doi:10.4028/www.scientific.net/AMM.596.1056

Supplier Selection Model of College Materials Procurement

Congjun Rao and Lei Yu

College of Mathematics and Physics, Huanggang Normal University,
Huanggang 438000, China
cjrao@163.com

Keywords: College materials procurement; Supplier selection; Fuzzy mathematics; Fuzzy comprehensive evaluation

Abstract. With the vigorous development of the our country higher education enterprise, the demand of materials and equipments also increased year by year in university, so the supplier selection is particularly important. In this paper, we select four prominent influence factors to establish a supplier evaluation index system, and then present a multi-objective fuzzy comprehensive evaluation decision model to select the supplier in the college materials procurement. Further, we highlight the implementation, availability, and feasibility of the fuzzy comprehensive evaluation model using a procurement decision example.

Introduction

In recent years, Chinese higher education has rapid development, and the investment of higher education is also growing, the college materials procurement project scope has been expanded. The procurement includes understanding the needs, selecting supplier, negotiating price, signing the contract, urging delivery and ensuring the supply, and so on, where the supplier selection plays a pivotal position in the procurement work. However, due to the process of supplier selection contains a lot of uncertainty, many colleges and universities are difficult to accurately select a optimal supplier, so it cause the waste of money and resources, and even the breeding ground for corruption. Therefore, to seek a rational supplier selection model is a very real current social problem.

In the practical procurement, the supplier selection problem is a complex multi- object, multi-index comprehensive dynamic optimization process. Traditional methods such as intuitive judgment method, linear weighting method, operating cost method, the analysis accuracy is not high, the subjectivity is strong, and it is difficult to choose optimal supplier. Therefore, to establish a reasonable and scientific supplier selection model is very important for the rational use of resources and modernization of universities. In this paper, we will present uses a qualitative and quantitative multi-objective fuzzy decision method to select the supplier, and effectively improve the modernization construction of universities.

The rest of this paper is organized as follows. Section 2 gives the multi-objective fuzzy comprehensive evaluation. Section 3 a procurement decision example to show the availability and feasibility of the fuzzy comprehensive evaluation model. Section 4 provides concluding remarks.

The Model

In this section, we will present a multi-objective comprehensive evaluation decision model to select the supplier. The detailed steps are as follows.

1) Determine the evaluation index set

All evaluation indexes are divided into t factor sets, i.e., $U_1, U_2, ..., U_t$, which satisfy the condition

$U_i = (U_1, U_2, ..., U_t)$,

$U_i \cap U_j = \Phi (i \neq j)$,

and each set $U_i (i = 1,2,...,t)$ can be divided into soem sub-index $U_{ij} (j = 1,2,...,m)$, i.e.,

$U_i = (U_{i1}, U_{i2}, ..., U_{im})$, $i = 1,2,...,t$.

2) Determine the weight set of evaluation index

We denote $W = (w_1, w_2, ..., w_n)^T$, where w_i is the weight of the i-th evaluation index such that $w_i \geq 0$ and $\sum_{i=1}^{n} w_i = 1$. We can use the Analytic Hierarchy Process to determine the weight set W.

3) Determine the evaluation set

The evaluation set is denote as $V = (V_1, V_2, ..., V_6)$, where V_j is the j-th grade. The detailed grade can be divided as $V = \{\text{best, better, acceptable, worse, worst}\}$.

4) Construct the membership matrix

Using the fuzzy statistical method, we can obtain the fuzzy evaluation matrix $R = [R_1, R_2, ..., R_n]^T$, where $R_i = [r_{i1}, r_{i2}, ..., r_{in}]^T$ is the fuzzy evaluation vector of the i-th index. All fuzzy evaluation vector of single factor form the fuzzy evaluation matrix of multiple factors.

5) Make the fuzzy comprehensive evaluation

Make the fuzzy comprehensive evaluation by the following algorithm

$$B = W \circ R = [b_1, b_2, ..., b_t]$$

where "$\circ$" is an operation. In this paper, we choose the operation $M(\bullet, \oplus)$.

The the first level of comprehensive evaluation is as follows.

$$R_i = w_i^T \bullet R_i^{'}, \quad i = 1,2,3,4$$

where R_i is the fuzzy evaluation vector of the i-th evaluation attribute, and w_i is the weight of the i-th attribute, $R_i^{'}$ is the fuzzy evaluation matrix.

The secondary comprehensive evaluation:

All $R_1, R_2, ..., R_t$ form the secondary comprehensive evaluation matrix, and the secondary comprehensive evaluation model is $B = W \bullet (R_1, R_2, ..., R_t)^T$.

6) Determine the winner

According to the evaluation set V, using the formula $N_k = B_k V^T$ to calculate priority degree, and then select the winner according to the value of N_k.

An Application Example

In this section, we give a computer procurement example by using above multi-objective comprehensive evaluation decision model. The decision goal is to choose an optimal supplier among four supplier X_1, X_2, X_3, X_4.

1) Determine the evaluation set

2) Determine the evaluation index set and the weight set of evaluation index

$$V = \{V_1, V_2, V_3, V_4, V_5, V_6\} = \{100, 85, 70, 55, 40, 25\},$$

$$W = \begin{pmatrix} 0.35 & 0.25 & 0.25 & 0.15 \end{pmatrix}.$$

3) Calculate the scores of all suppliers

Take the supplier X_1 as an example, we make the first level of comprehensive evaluation and secondary comprehensive evaluation.

By $R_i = W_i^T \bullet R_i^{'}$, we have

$$R_1 = \begin{pmatrix} 0.7 & 0.3 \end{pmatrix} \bullet \begin{bmatrix} 0.33 & 0.57 & 0.10 & 0 & 0 & 0 \\ 0 & 0.44 & 0.56 & 0 & 0 & 0 \end{bmatrix}$$

$$= \begin{pmatrix} 0.231 & 0.531 & 0.238 & 0 & 0 & 0 \end{pmatrix},$$

$$R_2=\begin{pmatrix}0.5 & 0.5\end{pmatrix}\bullet\begin{bmatrix}0.22 & 0.33 & 0.45 & 0 & 0 & 0\\ 1.00 & 0 & 0 & 0 & 0 & 0\end{bmatrix}$$

$$=\begin{pmatrix}0.61 & 0.165 & 0.225 & 0 & 0 & 0\end{pmatrix}.$$

Using the same way, we can obtain

$R_3=\begin{pmatrix}0.509 & 0.491 & 0 & 0 & 0 & 0\end{pmatrix}$,

$R_4=\begin{pmatrix}0.85 & 0.15 & 0 & 0 & 0 & 0\end{pmatrix}$,

Table 1. The evaluation index system

	Attribute	Sub-attribute
Comprehensive evaluation of suppliers	Acceptability of procurement cost U_1	Rationality of price u_{11} Terms of payment u_{12}
	Technical feature U_2	Equipment malfunction rate u_{21} Technical advancement u_{22}
	After-sales service U_3	Service quality u_{31} Response time u_{32} Euipment operation training u_{33}
	Comprehensive strength and credibility U_4	Comprehensive strength u_{41} Business reputation u_{42}

From the matrix R_1, R_2, R_3, R_4, we get the secondary comprehensive evaluation matrix R.

$$R=\begin{bmatrix}R_1\\ R_2\\ R_3\\ R_4\end{bmatrix}=\begin{bmatrix}0.231 & 0.531 & 0.238 & 0 & 0 & 0\\ 0.61 & 0.165 & 0.225 & 0 & 0 & 0\\ 0.509 & 0.491 & 0 & 0 & 0 & 0\\ 0.85 & 0.15 & 0 & 0 & 0 & 0\end{bmatrix}.$$

By the secondary evaluation mode $B=W^T\bullet R$, we obtain

$$B=W^T\bullet R=\begin{pmatrix}0.35 & 0.25 & 0.25 & 0.15\end{pmatrix}\bullet\begin{bmatrix}0.231 & 0.531 & 0.238 & 0 & 0 & 0\\ 0.61 & 0.165 & 0.225 & 0 & 0 & 0\\ 0.509 & 0.491 & 0 & 0 & 0 & 0\\ 0.85 & 0.15 & 0 & 0 & 0 & 0\end{bmatrix}$$

$$=\begin{pmatrix}0.4881 & 0.37235 & 0.13955 & 0 & 0 & 0\end{pmatrix}.$$

Then the final score of supplier X_1 is

$$N_1=V\bullet B^T=\begin{pmatrix}100 & 85 & 70 & 55 & 40 & 25\end{pmatrix}\bullet\begin{bmatrix}0.4881\\ 0.37235\\ 0.13955\\ 0\\ 0\\ 0\end{bmatrix}=90.22825.$$

Using the same method, we can obtain the scores of suppliers X_2, X_3, X_4,

$N_2=83.25010,\ N_3=86.21232,\ N_3=84.33905.$

Since $N_1 > N_3 > N_4 > N_2$, so the supplier X_1 is the optimal supplier.

Conclusions

This paper analyzes the current situation of the traditional supplier selection methods, and presents a multi-objective fuzzy comprehensive evaluation decision model to select the supplier in college materials procurement. This method combined with the qualitative and quantitative methods. This method may well improve the procurement efficiency and can effectively avoid the information loss. It provides theoretical basis and decision-making reference for the management of the university material procurement.

Acknowledgments

This work is supported by the 2014 Key Project of Hubei Provincial Department of Education (No. D20142903).

References

[1] H.F. Qin and H.W. Sun: Value Engineering Vol. 30 (2010), p. 40-43.

[2] D. Li and Z.G. Dong: Henan Science Vol. 34 (2011), p. 50-78.

[3] X. Liu and H.Y. Li: Chinese Journal of Management Science Vol. 12 (2004), p. 139-147.

[4] Z. Wang and J. Xu: Systems Engineering and Electronics Vol. 9 (2004), p. 1212-1216.

[5] Y.H. Zhang: Chinese Journal of Management Science Vol. 45 (2003), p. 56-60.

[6] H. Zhang and J.D. An: Industrial Engineering and Engineering Management Vol. 12 (2002), p. 24-40.

[7] H.X. Sun and Q. Zhang: Fuzzy Systems and Mathematics Vol. 6 (2011), p. 137-143.

[8] Z.H. Hao and S.F. Chen: Manufacturing Automation Vol. 26 (2004), p. 60-62.

[9] F. Gao and Q. Zhang: Computer Integrated Manufacturing System Vol. 10 (2004), p. 95-98.

[10] Y. Wang and L.Y. Sun: Systems Engineering Vol. 20 (2002), p. 46-50.

[11] Z. Wang and B. Yu: Chinese Journal of Management Science Vol. 12 (2004), p. 43-49.

[12] S.Y. Chen: System Engineering Theory and Practice Vol. 12 (1998), p. 7-13.

[13] T. Wang: Statistics and Decision Vol. 34 (2006), p. 140-141.

[14] Y. Han: Computer Engineering Vol. 32 (2006), p. 75-77.

[15] H.K. Miao, J.A. McDermid, and I. Toyn: Chinese Journal of Advanced Software Research Vol. 2 (1995), p. 326-337.

[16] A.J. Weele: European Journal of Purchasing & Supply Management Vol. 2 (1996), p. 153-160.

[17] J. Drolet: European Journal of Purchasing & Supply Management Vol. 2 (1996), p. 39-45.

[18] P. Meesad and G.G. Yen: International Journal of Uncertain, Fuzziness and Knowledge Based Systems Vol. 11 (2003), p. 445-466.

Applied Mechanics and Materials Vol. 596 (2014) pp 1060-1064
doi:10.4028/www.scientific.net/AMM.596.1060
© (2014) Trans Tech Publications, Switzerland

Research on the End-to-End Modularity Process for Manufacturing Enterprise

Haijun Wang[1,a], Tingting Zhao[2,b], Hongfu Sun[1,c],

[1]School of Management, Shenyang University of Technology, No.111, Shenliao West Road, Shenyang,110870, China PRC

[2]Department of Information Engineering, Shenyang Institute of Engineering, No.18, Zheng-yi Road, Shenyang,110136, China PRC

[a]wanghj77@163.com, [b]zhaotingting@163.com, [c]sunhongfu1216@126.com

Keywords: Modularity process, modular architecture, modular production line, strategic supplier.

Abstract. This article studies the end-to-end modularity process from market segment analysis, concept design, engineering to the final product delivery stage. Accordingly, the Voice of Customer can be effectively mapped into the product properties and functioned by specific modules. The major purpose is to systematically integrate the application of modularity in critical stages of product lifecycle and to facilitate the awareness and realization of modularity for manufacturing enterprise, so that the comprehensive benefits of modularity such as short time-to-market, parts number reduction, and high production efficiency can be realized effectively.

Introduction

Modularity has been well recognized as a key to bringing out a large variety of products while maintaining low costs and quick response to the market. Modular products tend to utilize fewer components for new product development and are accordingly economical to assemble based on independent functional modules. Moreover, modularity allows the designer to adjust the degree to which changes in processes or requirements affect the product and by promoting interchangeability, modularity gives designers more flexibility to meet these changing processes [1].

Generally speaking, there is no unique way to modularize a process model, so that modularity is often introduced in an ad-hoc fashion [2]. Product lifecycle is normally divided into such critical phases including marketing, research and development, production, procurement and service, in which modularity plays an important role in carefully listening to the voice of consumers, planning product properties, optimizing production lines layout, and screening out best supplier(s), etc. There are many researches studying product modularity but few of them systematically integrate the application of modularity in the critical product cycle stages from end to end, in this regard, the comprehensive benefits of modularity cannot be seen through and realized.

Jiao [3] analyzes the modularity and commonality in product and process development aiming at understanding the relationship between product configuration and component commonality. Wang [4] studies the product configuration design under modular architecture in product family using a mathematic model to maximize comprehensive performances with a mixture of views from customer's needs, which supports product configuration during product mass customization. Gualandris [5] provides a framework that relates the adoption of postponement enablers (i.e. product modularity and process modularity) to the reduction of the negative impact of a supply disruption. Jacobs [6] builds on general modular systems theory by examining the theoretical relationship between product and process modularity combining their effects on firm growth performance.

End-to-end Modularity Process Modeling

Based on the understanding of modularity functions in critical stages of product lifecycle, the following end-to-end modularity process (Fig.1) is built up to map the voice of customer into the product properties combining its subsequent stages.

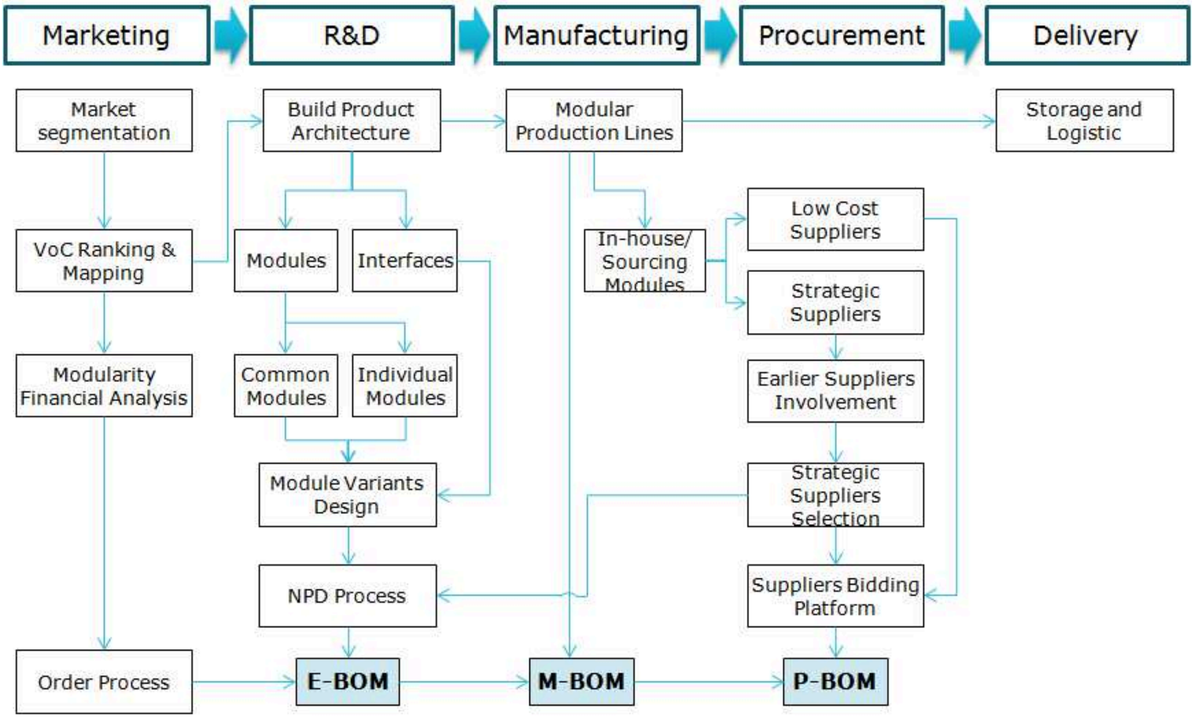
Marketing
R&D
Manufacturing
Procurement
Delivery
Market segmentation
VoC Ranking & Mapping
Modularity Financial Analysis
Order Process
Build Product Architecture
Modules
Interfaces
Common Modules
Individual Modules
Module Variants Design
NPD Process
E-BOM
Modular Production Lines
In-house/ Sourcing Modules
M-BOM
Low Cost Suppliers
Strategic Suppliers
Earlier Suppliers Involvement
Strategic Suppliers Selection
Suppliers Bidding Platform
P-BOM
Storage and Logistic

Fig.1 End-to-end Modularity Process Framework

Further explanations corresponding to the end-to-end modularity process are herewith given as follows:

Marketing. The key of marketing work herein is to classify customer groups and understand their requirements, so that each product brand can be clearly oriented for targeting customer group by ranking and mapping voice of customers (interpreted as Fig.2). There are two relationship matrixes A and B to numerically describe relationships between Customer Groups and Customer Requirements (CR), and between Customer Requirements (CR) and Product Properties (PP). Normally, 1, 3, and 9 are used for the quantization of relationship matrix, in which 1 is weak while 9 is strong. By utilizing the two matrixes, voice of customers (VoC) could be ranked and transferred into the product properties accordingly, meanwhile, manufacturing enterprise can design their product properties by using QFD or other similar tools both considering the VoCs and comparing with competitors.

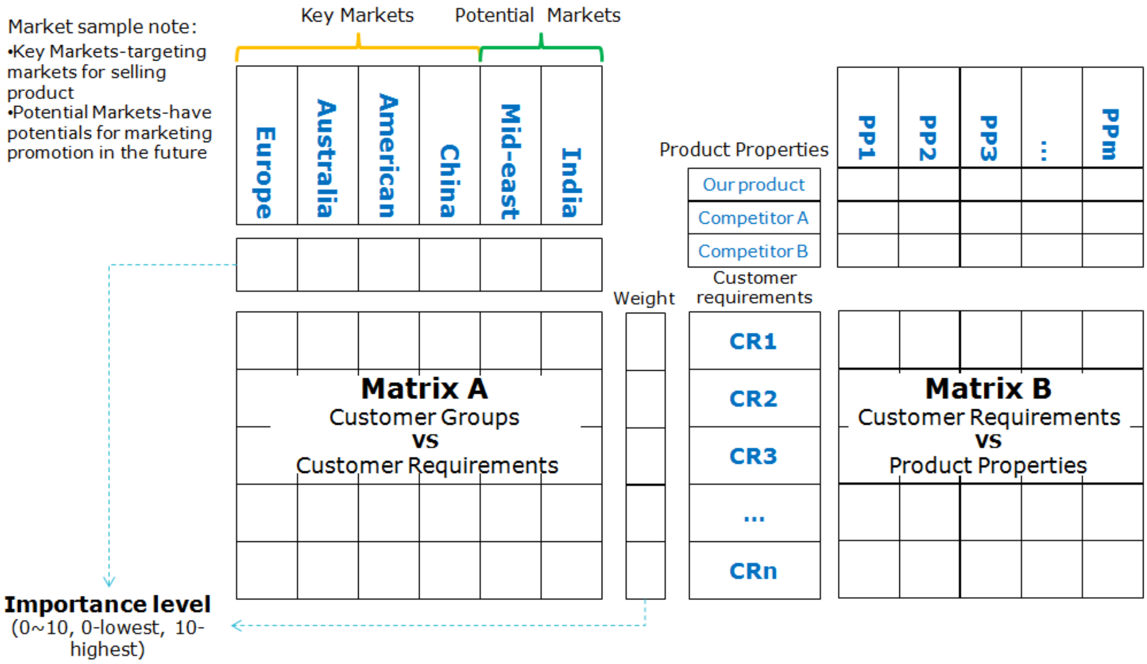
Market sample note:
•Key Markets-targeting markets for selling product
•Potential Markets-have potentials for marketing promotion in the future
Key Markets
Potential Markets
Europe
Australia
American
China
Mid-east
India
Product Properties
PP1
PP2
PP3
...
PPm
Our product
Competitor A
Competitor B
Customer requirements
Weight
CR1
CR2
CR3
...
CRn
Matrix A
Customer Groups
VS
Customer Requirements
Matrix B
Customer Requirements
VS
Product Properties
Importance level
(0~10, 0-lowest, 10-highest)

Fig.2 Marketing Planning and VoC Mapping

Product configuration in earlier stage could facilitate the management of product assortment for manufacturing enterprise, which is very important for the implementation of mass customization. In addition, order process is normally interfaced in this stage to combine market order and Engineering Bill of Materials (E-BOM).

R&D. Modular architecture (also named product platform) will be established at this early stage, which is generally described as a collection of common functional modules and individual functional modules combining their standardized interfaces to meet specific market customer group. Modular architecture is expressed in the following Fig.3 in conjunction with a fridge case:

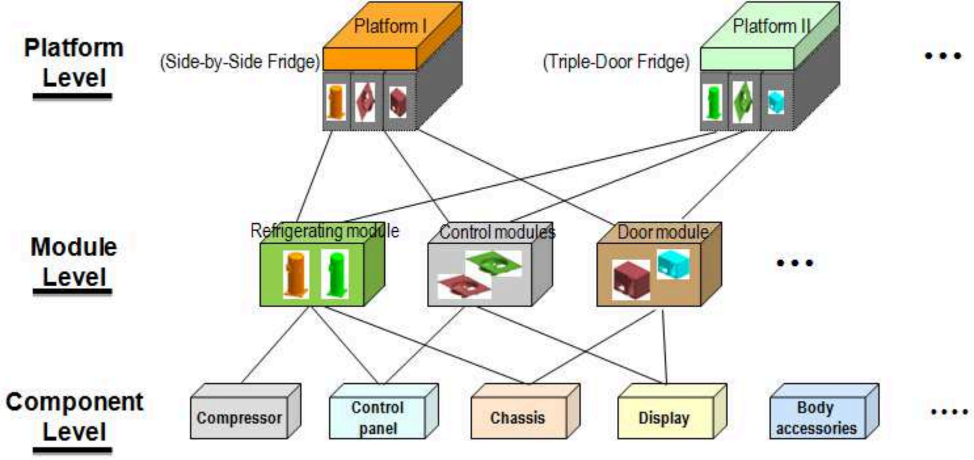
Platform Level
Platform I
(Side-by-Side Fridge)
Platform II
(Triple-Door Fridge)
...
Module Level
Refrigerating module
Control modules
Door module
...
Component Level
Compressor
Control panel
Chassis
Display
Body accessories
....

Fig.3 Features of Modular Architecture

Then comes to the detailed design of concrete module variants, and all essential module data shall be incorporated into CAD modeling environment for the preparation of module and interface design.

In order to facilitate the implementation of new product development (NPD) consistently, NPD process is carried out to generate E-BOM accordingly.

Manufacturing. As far as the manufacturing phase is concerned, stable modular production line is essential to the efficiency, quality and cost, the layout of which should be rationally configured to coordinate the in-house and sourcing modules. Manufacturing BOM (M-BOM) will be produced herein closely relating to the DFX of modules (Design for manufacture, design for assembly). The modular production line is shown as follows:

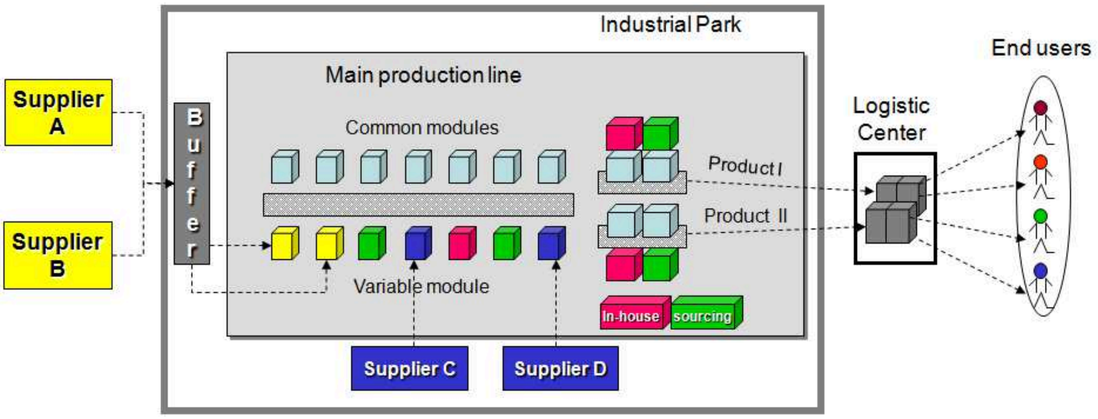
Industrial Park
End users
Supplier A
Supplier B
Buffer
Main production line
Common modules
Product I
Product II
Logistic Center
Variable module
In-house
sourcing
Supplier C
Supplier D

Fig.4 Modular production Line

In Fig.4, main production line is used for module assembly work referring common modules and variable modules. Common modules are mostly used across all product families while variable modules are preferred by individual customers and adopted for certain product model. Generally, both kinds of modules are classified into in-house and sourcing modules depending on the strategy of manufacturing enterprise. After the final assembly procedure, various products enter logistic center to be delivered for end users.

Procurement. Procurement plays a vital role in the stable supply of modules and product delivery time, and the best supplier(s) is (are) filtered with not only right module performances but cost balance indicated as below.

Nowadays, building strategic supplier partnership is increasingly vital for manufacturing enterprise to help drive productivity, innovation, and thought leadership in industry, especially for the earlier supplier involvement program which supports new product development. The Procurement BOM (P-BOM) is executed at this stage in close relationship with M-BOM to facilitate the sourcing and procurement actions.

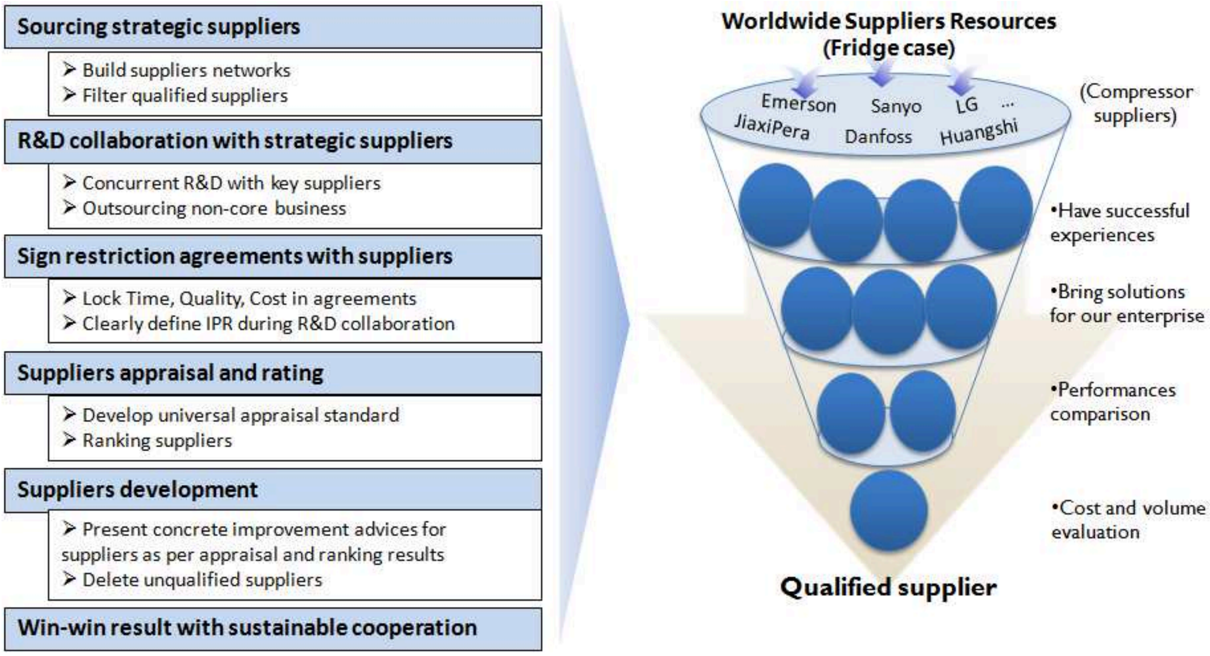
Sourcing strategic suppliers
➢ Build suppliers networks
➢ Filter qualified suppliers
R&D collaboration with strategic suppliers
➢ Concurrent R&D with key suppliers
➢ Outsourcing non-core business
Sign restriction agreements with suppliers
➢ Lock Time, Quality, Cost in agreements
➢ Clearly define IPR during R&D collaboration
Suppliers appraisal and rating
➢ Develop universal appraisal standard
➢ Ranking suppliers
Suppliers development
➢ Present concrete improvement advices for suppliers as per appraisal and ranking results
➢ Delete unqualified suppliers
Win-win result with sustainable cooperation
Worldwide Suppliers Resources (Fridge case)
Emerson
Sanyo
LG
...
JiaxiPera
Danfoss
Huangshi
(Compressor suppliers)
•Have successful experiences
•Bring solutions for our enterprise
•Performances comparison
•Cost and volume evaluation
Qualified supplier

Fig.5 Supply Chain Management based on Module Strategic Suppliers

Conclusions

In this paper, an end-to-end modularity process in lifecycle is presented with a purpose of integrating the application of modularity in market analysis, R&D, production, procurement and service stages. In the next step, each process segment will be further considered and improved.

Acknowledgements

This work is supported the Doctor Startup Fund Program of Shenyang University of Technology. I herewith also show special thanks for the supports of Haier Group Corporation.

References

[1] J.K. Gershenson, G.J. Prasad. Modular Product Design: A life-cycle View. Journal of Integrated Design and Process Science. Vol. 3(1999), p. 13

[2] H. Reijers, J. Mendling. Modularity in Process Models: Review and Effects. Lecture Notes in Computer Science Vol. 5240(2008), p. 21

[3] J.X. Jiao, M.M. Tseng, Understanding product family for mass customization by developing commonality indices. Journal of Engineering Design, Vol. 11(2000), p. 229

[4] H.J. Wang, B.Y Sun. Modular product configuration design for customer requirement-driven engineering. Chinese Journal of Mechanical Engineering. Vol. 41(2005), p. 86

[5] J. Gualandris, M. Kalchschmidt. Product and process modularity: improving flexibility and reducing supplier failure risk. International Journal of Production Research. Vol. 51 (2013), p. 5757

[6] M. Jacobs, Droge, Cornelia. Product and process modularity's effects on manufacturing agility and firm growth performance. Journal of Product Innovation Management. Vol. 28 (2011), p. 123

Applied Mechanics and Materials Vol. 596 (2014) pp 1065-1068
© (2014) Trans Tech Publications, Switzerland
doi:10.4028/www.scientific.net/AMM.596.1065

SWOT analysis of Chinese rural information society policies

Ping Zhou[1,2]

[1]School of Information Technology, Jiangxi University of Finance and Economics, Nanchang China

[2]Jiangxi Key Laboratory of Data and Knowledge Engineering, Jiangxi University of Finance and Economics, Nanchang China

zp_jx@126.com

Keywords: SWOT analysis; information society policies; Chinese rural

Abstract. This paper presents an analysis of strengths, weaknesses, opportunities, and threats (SWOT) for Chinese rural information society development (CRISD) policies in terms of its missions and strategies. After briefly describing the institutional and information society development contexts, the paper draws on literature reviews and questionnaires survey to list of SWOT factors for CRISD. These findings could be used to help adjust the next step work to support decision making for rural information society construction and to provide a valuable reference for other investors who are planning to invest in information society programs in China's rural regions. This article presents valuable missions and strategic goals through the SWOT analysis for realizing information society development in Chinese rural areas.

Introduction

Information society development (ISD) plan in China has been issued by series of various "Document-No.-Ones" (Each year beginning, the Communist Party of China ("CPC") Central Committee and State Council would jointly issue a " Document-No.-One " highlighting the government's priority of the year). It is also characterized by large inequalities in the institutional arrangement and an overlapping structure that imposes several levels of governance. In recent years, there have been growing attention being paid to information society development in the construction and development project of "agriculture, rural villages, and farmers" (the so-called 'three agrarian 'issues).ISD reveals a lot of recognized and felt advantages, which include meeting the diversity of information demands ,enhancing effectiveness and efficiency of learning and communication, richening channel of information acquirement and information sources, increasing quality to the community[1]. Effective use of any ICT application depends on the context and environment within which it is to be used, including the constraints and barriers, and the attitudes and aspirations of the potential users. It also depends, of course, on the extent to which any system introduced actually meets the needs of those for whom it is provided. Thus, an important and early part of the project was to both examine the physical and social environment within which ICTs may be used, and also to develop an understanding of the information needs of those who live in countryside areas [2].

In many rural areas of China, information society development is far behind that of city areas. Specifically, Chinese cities possess the relatively perfect public infrastructure, finance services, medical treatment services, and education planning of their own information resources. However, the rural villages, which can be said, to some extent, contributing or supporting more for the national interest as far as the public life are concerned, are far lagged behind for these basic developments of the information sector [3]. This situation may generate some detriment to rural information society development. As expressed by the Organization for Economic Cooperation and Development (OECD), the "systematic promotion of mutually reinforcing actions across government departments and agencies can create synergies towards achieving the agreed objectives"[4]. The rural-urbanization has also been performed on China development and cooperation policies [5] and information society development policies [6].

The aim of this article is to evaluate Chinese rural information society development strategies and address the faced with problems, especially evaluate whether the decision-making processes used can ensure the implement of the policies and the coming true of the strategies. These are mainly performed through SWOT analysis that combines the study of the strengths and weaknesses of an organization, territory, or sector with the study of opportunities and threats in its environment.

The current context of Information Society Development in rural community

A diagnosis of the current development in the rural community is the first step for information society strategies. The diagnosis was made on the basis of questionnaire survey and field investigation by the group members in Jiangxi Key Laboratory of e-commerce and Engineering. The attention was focused on ICT infrastructure, information services, information needs, the competence of farmers, etc al. It turned out that:

(1)There is a lack of adequate technical infrastructure for access to the broadband Internet and the development between regions is not balanced. Construct of information society (“Informatization”) could facilitate contacts and exchanges between China’s undeveloped regions and more developed regions, allowing farmers and agro-business to obtain technologies and market information that enable them to make full use of their comparative advantages in developing new products and increasing trade, market share, incomes and ultimately reducing regional gaps [7].

(2) There is short of information services and information content which could benefit the peasants, companies and various institutions and the cost of information service are relatively high, both for peasants, schools, and other institutions, as well as small and medium-sized enterprises. Many kinds of information, such as market information, financial resources information, rural economy policy information, better farming techniques information, new crops varieties information, production diversification need information and competitiveness information, etc. all these do can facilitate rural communities development.

(3) Peasants and rural businesses very often have no knowledge of the existence of digital information services and see no need to use such services. With information, farmers are better equipped to make important decisions and learn about diversified employment opportunities. With growing dependence on the service sector, rural economies could benefit from diversifying into providing local ICT-enabled services [6].

(4)Farmers, rural businesses and other institutions often do not have the competence to use available digital information services. Increasing the capacity of rural population and access to relevant information can not only directly affects rural economic development, but also bring in modern ideas and forward looking mindsets from more advanced regions. This can pave the way for transformative ideas and beliefs, increasing rural, social and cultural capacities in rural areas [8].

(5)There is no strong informationization participation awareness of farmers. Farmers are not only the direct beneficial owners of rural informationization, but also the main participators. So it is necessary that Enable farmers to participate in formulating agricultural policies and strategies. ICT has been used to deliberate policies for rural people, which makes this type of participatory approach more feasible for dialogue on rural information society policy.

SWOT analysis

Table 1 presents the outcome of a SWOT analysis which was conducted to identify optimal solutions necessary to implement a strategy for the information society and creating a competitive rural community.

Table 1 Synthesis of SWOT analysis for rural community information society strategy

Strengths	**Weaknesses**
➢ Strongly supporting by National policies ➢ Large number of small ICT businesses ,which due to the scale of their operations, have strong will to invest ICT applications in rural communities regarding the features of this area ➢ Relatively easy access to Internet due to a large scale of urbanization construction ➢ Big educational potential (cultural, scientific, technical and business sciences) ➢ The Electronic government System being rapidly spread to countryside ➢ New country electrical health and medical treatment cards ➢ High concentration of ICT network users	➢ Lack of coordination with the rural area development strategies ➢ Overlapping construction management ➢ Emphasizing hardware investment, despising software applications ➢ Lack of ICT staff ➢ separate of ICT administration, construction from applications ➢ lower organizational level and information society awareness ➢ bigger difference of ICT infrastructure among various regions
Opportunities	**Threats**
➢ Growing attention and interest in the information society at the rural level (one of the main tasks of national ”the twelfth-five years plans” and relatively substantial percentage of funds allocated for the information society programs in rural area) ➢ Farmers aware of economic advantages gained through the ICT infrastructure construction and applications ➢ Policies encouraging the development of information society that stimulate job creation in local area without going outside for part-time work ➢ Important element for information society policy ➢ China’s position on rural urbanization in coming 30 years	➢ High cost of ICT infrastructure ➢ Constraints imposed by farmers’ low knowledge level ➢ Resisting against necessary changes in the lifestyle due to ICT development ➢ Time needed to develop rural-urbanization owing to dispersed residence and low population density ➢ Highly information-intensive agriculture production

Missions and Strategic Objectives

Above SWOT analysis has provided a basis for formulation of missions and strategic goals of rural information society development. The mission of new rural community is characterized as “so-called socialist new villages” (CPC Central Committee and State Council, 2004-2013) and will be conducted transformation from the dispersedly agricultural region into an urbanization region with relatively perfect ICT infrastructure and public basic infrastructures.

Five strategic goals of information society should be adopted to achieve the mission of new rural community. They are related to ICT infrastructure, human IT resources, digital service, digital management, rural economy, society and culture (Figure 1). These objectives are adequately taking advantage of the strengths and the opportunities of rural community and simultaneously eliminating or counteracting its weaknesses and threats.

The following aspects should be paid more attention for development of information society in Chinese rural Community: (1) raising rural residents’ information awareness and competence of exploiting the information technology. This is closely linked with education along with ICT usage and online services, at the same time, it is important that makes popularization of the information society idea among rural community inhabitants normalized; (2)Development of information society in rural community is dependent upon ICT infrastructure, which needs coordination of operations among various-level ICT networks as well as government departments and agencies;(3) public services digitalized is the basic characteristic of information society, requiring services with high quality, such as e-administration, e-health care, e-education, e-culture. The new policies of promotion of "intelligent management model", which means striving to build information service system with features of "richening peasants, benefitting peasants, conveniencing farmers and delighting farmers", are just supporting and responding the public services digitalized and creating and/or providing digital services. Simultaneously, it is assumed that raising the number and usefulness of digital services is possible through the expansion of public interoperability platforms as well as integration and promotion of electronic information about the new rural community [9].

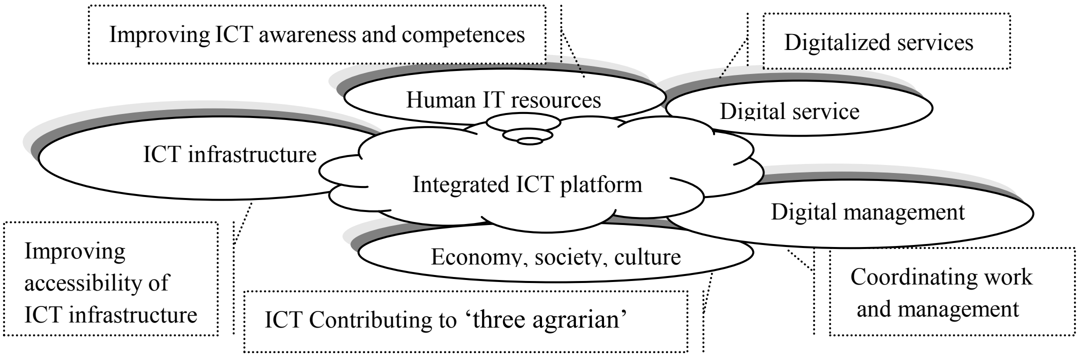
Improving ICT awareness and competences
Digitalized services
Human IT resources
Digital service
ICT infrastructure
Integrated ICT platform
Digital management
Improving accessibility of ICT infrastructure
Economy, society, culture
Coordinating work and management
ICT Contributing to 'three agrarian'

Figure 1. Strategic goal for rural information society development

Conclusions

In line with the super national policy in China, the impending demand for rural information society has obtained a good development opportunity. However, rural information society construction, which involves huge investment, long concession period, high risks and complicated contractual structure, has the necessity for CRISD to examine their SWOT when China intend to perform new rural-urbanization construction. This article identified comprehensive elements of the four critical SWOT aspects through a synthesis of literature review and questionnaire surveys.

Acknowledgements

This work was financially supported by fund project of Humanities and social science special for colleges and universities in jiangxi province (GL1312) and Science and technology project of jiangxi Education Commission (GJJ12737).

References

[1] Peter Williams. Using information and communication technology with special educational needs student, Aslib Proceedings: New Information Perspectives, 2005, 57(6): 539-553.
[2] Chun Liu: submitted to Journal of Government Information Quarterly (2012).
[3] David Bromwich and Max Saunders: submitted to Journal of Development in Practice (2012).
[4] OECD (Organization for Economic Cooperation and Development), 2001. The DAC Guidelines--Poverty Reduction .Paris(PDF Version of Document Downloaded May 2011).
[5] CPC(Central Committee & State Council), Suggestions on various policy issues on the promotion of the farmer's income. Beijing. (2004).
[6] Jun Xia. : submitted to Journal of Government Information Quarterly (2010).
[7] IOS Press: submitted to Journal of E-Government Policy and Regulation (2009).
[8] Rhoda C. Joseph: submitted to Journal of Government Information Quarterly (2013).
[9] Ewa Ziemba and Celina M. Olszak: submitted to Journal of Issues in Informing Science and Information Technology(2012).

1Cr18Ni9Ti 43
2D(PC)2A 311
35% Capacity Bypass 674
3D Modeling 606
3DLP 442

A

Active Filters 709
Active Power Balance 709
Adaptive Gaussian Filtering 365
Adaptive Technology 94
ADO Object 1018
Aeroacoustic Measurement 532
Aerospace Network 856
Aggregation 519
Agricultural Informatization 280
Air Material Suppliers 164
Air Suspension 17
Algorithm 183
Alligator Crack 747
AMESim 7, 598
Analog Transmission 803
Analytic Hierarchy Process (AHP) 164
Android 909, 923
Angle 755
Angle Steel Tower Materials 56
Animation Video 328
Ansoft 67
Ant Colony Clustering 245
Antenna Arrays 816
Application 119, 990
Approximation Reasoning 179
Archetypes 183
ARIMA/GARCH Models 160
ARM 883, 944
Artificial Bee Colony Algorithm 234
Artificial Fish Swarm Algorithm 241
Artificial Neural Network (ANN) 700
Assignment Model 1030
Atmospheric Model 463
Attenuating Variable-Rate Reaching Law 565
Attitude Control 572
Attitude Determination 532
Authentication 986
Auto-Incasing Equipment 620
Automobile 751

B

B-Spline Curve 149
Background Modeling 316
Background Subtraction 374
Band Ratio Method 457
Bayesian Filter 379
Bearing 437
Best Least Square Approximation 149
Bias Resistance 723
Big Data 960
Binarization 79
Bistatic Sonar 494
Blades 606
Blind Source Separation 169
Bolt Torque 3
BP Neural Network (BPNN) 422, 427, 476
Browser Server 1018
Bucket 196
Burr Distribution 297

C

C/S 931
Calculating Current 104
CAM 83
CAM/CAM 838
Camera Calibration 453
CAN Bus 873
Canny Gradient 322
Cardiac Pacemaker 100
CC2530 773
Ceramic 47
Ceramic Patterns 90
Change Detection 484
Chaos 216
Character Recognition 422
Characteristic Fault Frequency 437
Characteristic Surface Intersecting Lines 606
Chattering 584
Chinese Rural 1065
Chua's Circuit 560
CIPS 636

Cleaning Machine 72
Client Server 1018
Closed-Loop System 560
Cloud Computing 204, 971
Cloud Manufacturing 127
Cloud Mobile Office 123
Cloud Storage 196
Cluster Analysis 136
CNG 944
Co-Simulation 927
Cognitive Search 994
Coherent Receiver 799
College Materials Procurement 1056
Combination 174
Communication Constraints 631
Comparison 636
Compass 735
Complex Network 843, 868
Complicated Background 361
Composite Media 822
Comprehensive Transportation Terminal 743
Computer Science 994
Computer Vision 453
Connected Components 276
Consistency Constraints 669
Consumer Confidence Index 200
Consumption 174
Content-Based Image Retrieval 388
Continuous Blood Pressure 476
Continuous Patterns 90
Control Center 735
Control Chart 56
Control System 576, 766
Controller 751
Convergence Accuracy 192
Convergence Speed 552
Conversion System 328
Coordinated Charging 760
Correctly Associated Rate 511
Countermeasure 990
Coupling 100
Course Construction 1052
Course Control 590
Coverage 131
Cracking Ratio 747
Crest Factor Reduction 794
CRO Algorithm 204
Cross Platform 931
Crush 196
Customer Behavior 976
Customer Segmentation 951
Customized Tour 990

D

Data Acquisition Terminal 498
Data Center 918
Data Fusion 803
Database Access 914
DC-Building 678
De-Nosing 333
Decision Making 154
Degree Distribution 843
Demand Coefficient 104
Demand Side Management 682
Demand Side Response 682
Design 72
Design of Valve Block 598
Destination Brand 976
Detection 56, 505, 803
Development Level 136
Diagnosis 682
Dictionary Learning 333
Dielectric Constant 822
Dielectric Loss 822
Differential Evolution 216
Digital Challenge 976
Digital Control 838
Digital Hydraulic Cylinder 27
Digital Manufacturing 838
Digital Publishing 981
Dijkstra Algorithm 861
Disparity Estimation 406
Dispenser 944
Distributed Detection 803
Distributed Generation 678
Domain-Oriented QoS Evaluation 127
Double Scoring 402
Drilling Force 43
Driver 944
Driving Simulator 747
DSM 760
Dual Closed-Loop Fuzzy Controller 620
Dynamic Economic Dispatch 649
Dynamic Frame Slot ALOHA(DFSA) 222
Dynamic Matching 704
Dynamic Model 528

Dynamic Trend 687
Dynamic Update 856

E

E-Bayes Estimation 297, 301, 305
E-Commerce 966
E-Government 971
Early Warning 576
EC Environment 951
Edge Contrast Matrix 79
Edge Detection 350
Edge Effect 540
Edge Enhancement 355
Efficiency Matrix 1030
Electric Power Steering 751
Electric Railway 625
Electrical Parameters 47
Electrical Properties 822
Electromagnetic Compatibility 918
Electromagnetic Interference 918
Electronic Products 114
Elevator 104
ELID Grinding 47
Elliptic Curve 519
Embedded 60
Embedded System 536, 883
EMD 437
Emergency Power Supply 664
Emergency Reserve 141
Emission Reduction Benefits 649
Empirical Formula 43
Energy 519
Energy-Awareness 204
Energy Management 678
Energy-Saving 682
Energy Saving Benefits 649
Energy-Saving Dispatch 669
Engineering Ability 1040
Enterprise Application 888
Entropy Method 280
Environmental Engineering Microbiology 1052
Environmental Problems 39
EPS 739, 751
Equipment Installation 94
Equipment Modification 52
Equivalent Electric Power Communication Network 653
Error Analysis 468
Evaluate 280
Evaluation Model 259
Evolution Rule 966
Excavator 602
Experiment Table 739
Experiment Teaching 1026
Experimental Study 17
Experimental Teaching System 1034
Extraction of Light Stripes Center 449

F

Face Recognition 346, 427
Face-to-Face Transfer 847
Facial Expression Recognition 322
Facility Vegetable 576
Factor Analysis 136
Fast Cut Back 674
Fast Finite-Time Consensus Tracking 552
Fault Diagnosis 110, 437, 528
Fault Identification 713
Fault Location 659
Fault Tree 209, 696
Feature Space 388
FFMpeg 328
FHN Neuron 413
Fidelity 729
Finite Element (FE) 12
Finite Element Simulation 540
Firewall 852
Flash Animation 998
Flaw 12
Flexible Brake 547
Flow Coupled 602
Forecast 200
Forecast Accuracy 160
Forecasting 174
Forecasting Model 286
Formation Control 631
Fourier Descriptor 427
FPCS 457
FPGA 873
Fractal Theory 226
Fractional Brownian Motion 427
Fractional Distance 388
Frequency and Inductor Combined Adjustment 704
Frequency Characteristic 687
Frequency Estimated Filter 342

Frequency Response Function Estimation 610
Frequency-Sectioning Iterative Correction 610
Fresh Foods 154
FSJ 52
FT231X 773
Fur Material 72
Fused Side-Adhere 826
Fuzzy Comprehensive Assessment 164
Fuzzy Comprehensive Evaluation 1056
Fuzzy Control 739
Fuzzy Mathematics 1056
Fuzzy Neural Network (FNN) 751
Fuzzy Time Series 286

G

GA Algorithm 204
Gabor Filter 311
Galvanized Layer Uniformity 56
GARTEUR Model Confidence Interval 22
Gaussian Curve 449
Geographic Information System 719
Geophysics 616
Glass Furnace Temperature Control 580
Global Positioning System 719
Government Business Model 960
Governor 692
GPS/BD2 735
GPU 276
Graff 903
Graph Cuts 398
Graph Processing 276
Graph Transformation 966
Ground Truth 398
Grounding Grid Corrosion Rate 245, 271
Guide 998

H

Handheld Devices 188
Hardware 903
Harmony Search 192
HAZOP 696
HEVC 328
HHT 433
Hierarchical 1022
Hierarchical Bayes Estimation 297, 301, 305
Hierarchical Cluster Analysis Method 280
High Education 1040
High-Order System 594
High-Speed Train 468
Hinge Sleeve of Cubic Press 472
Histograms of Oriented Gradients 322
Hopf Bifurcation 27
Human Factors 1034
Human Inertia Parameters 453, 480
Hungarian Method 1030
Hv Estimator 610
Hydraulic System 598
Hydro-Pneumatic Spring 7
Hydrocarbon Micro-Seepages 457
Hα Full-Disk Solar Image 365

I

Identifying 355
IEKF Algorithm 494
Image Compression 406
Image Processing 909
Image Retrieval 337
Image Segmentation 337
Impact-Echo 12
Improved Design 60
Improved K-Means 951
Improved M/T Velocity Measurement 468
Improved Particle Swarm Optimization 649
Impurity Scattering 226
Incomplete Gear 72
Individual Demand 1022
Individual Patterns 90
Industrial Engineering 1034
Information Service 971
Information Service Center 971
Information Service Model 971
Information Society Policies 1065
Infrared Right Angle Prism 788
Ink Spreading 417
Inspection of Lightning Protection Systems of Highway 498
Integrated Automation 636
Integrated Optics 799
Integrated Optics Devices 799
Intellectual Inspection System of Transmission Line 719
Intelligent Bird Repellent 782

Intelligent Optimization 216
Intelligent Optimization Algorithm 230
Intensity of Sentiment 263
Interaction 998
Interface 923
Interferogram 342
Internet 838
Internet of Thing (IoT) 119
Intrusion Detection 852, 888
Inverse Laplace Transformation 594
IOT Application 981
IPv6 Router 892
ISP1161 883

J

Java Technology 931
Jewelry-Making CNC Machine 83
Jiangcheng Culture 1003

K

K-Mean 484, 951
K-SVD 333
Kaiser Window 659
Kalman Filter 316
Kalman Filtering 398
Key Management 986
Kinetic Characteristic 32
Knot Vector 149
Knowledge Learning Platform 1013
Knowledge Management 1013
Knowledge Services 1013

L

LabVIEW 914
Landing Point Predicting at Sea 463
Lane Mark 355
Laplace Distribution 301
Lateral Displacement 3
Lateral Horizontal Force 3
Laterally Interconnected 17
Law of Bit Significance 847
Least Square (LS) 169
LED 442
Lifting System 602
Light Scattering Model 417
Lightning Location 713
Limit Cycle 27
Line Structured Light 449
Linearization Meteorological Factors 700
Linux 188, 944
Liquid Crystal Shutter 442
Load Calculation 104
Local Terrain Slope 342
Local Trouble 251
Location Based Service 259
Logistics Management 620
Longitudinal Crack 747
Loss 788
Low Frequency Oscillation 692
Lower Rough Set 179
LTE 811

M

Magnetic Positioning 67
Manipulator 640
Manual Intervention 79
Marine Current Turbine 32
Markov Chain Monte Carlo Particle Filter 379
Marshalling Station 636
MATCONT 27
Math Model 602
Mathematical Morphology 361
MCU 547
Measurement 490
Measurement Accuracy 480
Media-Stream Network 847
MEMS 532
Metamaterials 816
Metering Model 114
Methodology 183
Micro Class Teaching 1009
Micro-Hole 43
MicroAge 1009
Microbiology 1026
Microgrid 678
Microprocessors 536
Military Logistical 119
Milling Machine 60
Mine Ventilator 110
Mineral Alteration 457
Minimum Integration Step Width 463
Mirror Current Source 723
Mobile Data Acquisition Technology 498
Mobile Information Platform 719
Mobile Phone Short Message 576

Modal Analysis 594
Mode Conversion 807
Mode Division Multiplexing 807
Model 174, 1040
Model Free Adaptive Control 580
Model Uncertainty Quantization Analysis 22
Model Validation 22
Model-View-Controller (MVC) 923
Modelica 927
Modeling 692
Modular Architecture 1060
Modular Production Line 1060
Modularity Process 1060
Monitoring 141, 576
Monte Carlo Sampling 379
Mooring 32
Morphological Filtering 433
Motion Simulation 640
Moving Object Detection 361
Multi-Agent Formation 251
Multi-Agent Systems 552
Multi-AUVs 631
Multi-Disciplinary 572
Multi-Information Synchronous Acquisition System 476
Multi-Lomain Modeling 927
Multi-Point Measurement 659
Multicarrier 794
Multimedia Network Classroom 931
Multimedia Technology 370, 1026
Multiple Factor 222
Multiscale Inverse Transform 365
Multiscale Transform 365
Multisim10 723
Multitask Communication 234
Mutual Coupling Reduction 816
MW Wind Turbine 598

N

Nanosilica Powder 826
Natural Gas 174
Natural Gas Hydrate 39
NC Network System 838
NC Program 83
Network 653
Network Planning 230
Network Security 852, 888
Network Technology 1009
Neural Network 110, 584
Neuroergonomics Experiment 1034
New University 1048
Next Generation Network 847
NHPP 877
Nitrogen-14 505
No Reference Image Quality Assessment 350
NoC 892
Node Attraction 843
Non-Linear Equations 216
Nonlinear Constrained Optimization 234
Nonlinear Exosystem 560
Nonlinear Model 114
NQR 505
NS-2 833
NSGA-II Algorithm 760
Numerical Control 52
Numerical Method 209
Numerical Simulation 616

O

Object Detection 374
Object Tracking 398
Obstacle Avoidance Problem 251
Off-Axis 788
Office Automatic 123
Office Platform 123
One Sample per Person Problem 311
Online 990
Online Authority 994
Online Community 994
OpenCV 909
Optical Dot Gain 417
Optical Fiber Collimator 788
Optical Fiber Communication 788, 799, 807
Optical Fiber Coupler 826
Optical Flow Constraint 316
Optimal Assignment 664
Optimal Path 664
Optimization 755
Optimize 960
Optimum Initial Integration Value 463
Output Regulation 560
Oxide Film 47

P

Page Category 292

Page Hits Frequency 292
Page Rank 292
Page Update Time 292
PAPR 794
Parabolic Fitting 449
Parallel Plate Capacitance 540
Parallel Processing 892
Parameter Setting Strategy 192
Parking Query 909
Particle Filter 379
Partition of Interval 286
Peak Clipping and Valley Filling 760
Pedestrian Traffic Behavior 743
Permanent Magnet 67
Phase Comparison 659
Photonic Crystal Fiber 826
Physical Dot Gain 417
Pitch Detection 433
Planar Curve Representing 149
Point-To-Point Transfer 847
Position 755
Positioning 936
Potential Analysis 682
Power Grid Enterprises 682
Power-Law Poisson Process 877
Power Quality 625
Practice 1022
Prediciton 259
Predictive Coding 406
Principal Component Analysis (PCA) 346, 402
Product Researching 1044
Professional Core Competencies 1048
Programmable Logic Controller (PLC) 52
Project Management 1044
Promote 1048
Propagation Rate 868
PSCAD 692
PSD Replication 610
Pseudorandom 183
Psychological Characteristics 743
Pulse Cancellation 794
Pushlet 899
PWM 547
PXI 766
PXI Platform 472
PyGTK 328

Q

Q Cluster 79
Q-Symmetric Entropy Loss Function 301
QoS Routing 856
QR Code 936
Quality Management 1018
Quality of Service 127

R

Radial Basis Function (RBF) Neural Network 200
Radio Frequency Identification 230
Radio-Interface 811
Rank One 169
Rayleigh Distribution 305
RBF Neural Network 160, 245
Reactive Power Optimization 241
Real Estate Industry 136
Real-Time Data Transmission 766, 873
Real-Time Detection 394
Real-Time Industrial Control System 234
Real-Time Performance 511
Real Time Web System 899
Reentry Measurement 463
Refined Oil 141
Regional Importance 337
Regular Trend 687
Relay 547
Reliability 653, 877
Reliability Analysis 696
Rendering Tree 370
Repetitive Control 625
Research Situation 39
Reserve Optimization 669
Resource Optimization 856
RFID 119, 222, 620
RFX2401C 773
Road Roughness 490
Robust Face Recognition 311
ROI 350
Rotational Force 251
Rotational Inertia 687
Rough Match Function 179
Rough Match Neighborhood Group 179
Rough Neighborhood Structure 179
Rough Set 110

Roundness 747
RPC 625
RSA 519
Rumor Propagation Model 868

S

S3C4510B 883
Saber 709
SaHS 192
SAM 636
SAR Image 484
Scale-Free Network 868
Scene Management 370
Scene Organize 370
Scilab 209
Search Engine 292
Search Zone 388
Security 519
Seismic Waves 616
Selection 636
Self-Convolution 659
Semantic Units 263
Semantic Web 1013
Semi-Supervised Support Vector Machines 484
Sensor 528, 540
Sensor Bias 511
Sentiment Analysis 263
Sentiment Lexicon 263
Separation Performance 169
Server Push 899
Servlet 899
Shadow Inhibition 374
Shanxi Province 136
Shear Stress 532
Ship Maneuverability 590
Ship Motion Model 590
Short-Term Load Forecasting 700
Shortest Path 861
Shortwave Station 782
Side Face Recognition 427
Signal Transmission Characteristics 413
Simulation 17, 32, 83
Simulation Analysis 43, 723
Simulation Model 729
Simulation System 572
Simulink 927
Simultaneous Factor 104
Sliding Mode 565
Sliding Mode Control 584
Sliding Mode Manifold 584
Small Cell 811
Smart Home 188
SN-GPSR 833
Software Architecture 966
Software Firm 1044
SolidWorks 640
Sparse Representation 333
Spatial Coordinate Transformation 565
Spatial Light Modulator 807
Spatial Multi-Scaled 322
Spectral Leakage 659
Speech Recognition 384, 402
Speech Synthesis 384
SQL Server 914
SSCR 755
Statistical Model 394
Step-Varying 610
Stereo Image Coding 406
Stiffness Characteristics 7
Stochastic Resonance (SR) 413
Strategic Supplier 1060
Stress-Displacement Model 94
Stripe Noises 365
Subcritical Units 674
Substation 696
Suitable Patterns 90
Super-High Pressure 472
Supercomputer 328
Supplier Selection 1056
Supply Chain Management 154
Support Vector Machine (SVM) 402, 528
Support Vector Regression 271
Surface Quality 47
SVR 22
SWOT Analysis 1065
Synchronization 811
System of Measurement of Multi-Points Strain 472

T

Target Detection 226
Target Extracting 316
Target Moving Analysis 494
Task Scheduling 204
TDALE 519
Temperature 755

Test Instrument 766, 873
Test Point Arrangement Form 56
Thermally Expanded Core Fiber 788
Three-Dimensional Modeling 640
Three-Dimensional Vectorial Artificial Potential Field Method (TDVAPF) 251
Three-Phase Current Source Inverter 565
Time Lag of Non-Linear Multivariable System 580
Time-of-Use Power Price 760
Time-Varying 580
Topological Structure 179
Torsion-Elimination 17
Total Quantity of Knowledge 653
Tracing Accuracy 494
Tracking 355
Tracks Association 511
Traditional Publishing 981
Traffic Professional within the Hub 729
Transient Waveform Characteristics 713
Transmission Line 659, 713
Transmission Tower Foundation 12
Transverse Stiffness 3
Triode 723
Tropical Areas 280
Tunable Parameters 843
Tutor Selection 1030
Two-Stage Pressure 7

U

UG 598, 606
Ultrasonic Cleaning 704
Ultrasonic Grinding 47
Unbalanced Power 687
Upper Rough Set 179
Urban Roundabout 833
USB 883
USB Coordinator 773

V

V2G 664
VANET 833
Variable Demands 154
Variable Structure 565
Varying Lighting Condition 311
Vector Similarity 271
Vehicle Bench Test 490
Vehicle Terminal 735
Velocity Measurement Accuracy 468
Velocity Measurement System 468
Verification 131
Verification Planner 131
Vibration 437
Video Capture 536
Video Object 394
Video Surveillance 536
Video Tracking 379
Virtual Experiment 1052
Virtual Leader 552
Virtual Machines 903
Visual Communication 1003
Visual Library 346
Visualization Modeling 960
Voice Assistant 384
Volumetric 3D 442

W

Wake-Up Word 402
Wave Propagation 616
Wavelet Analysis 490
Wavelet Energy Spectrum 713
Wearable Ad Hoc Networks 986
Wearable Computing 986
Web Design 1003
Web Services Composing 861
Webpage Design 998
Weighing Method 480
Wiener Filter 342
WIFI 188
Wind Driven Generator 547
Wind Power 649, 669
Wind Power System 241
Wind Tunnel Testings 532
Wireless Communication 782
Wireless Power Transmission 100
Wireless Sensor Network (WSN) 877
Wireless Transceiver 936
Wooden Patterns 606

X

XML 903

Y

YUV Color Space 374

Z

Zero-Pole Point	594
ZigBee	188, 773

A

Ai, C.J. 598
Ai, S.M. 457
An, X.Y. 664, 669

B

Bai, J. 565
Bai, X. 394
Bao, J. 625
Bi, D.Z. 674

C

Cai, S.Y. 807
Cao, X.H. 322
Cao, Y.L. 739
Chang, Z. 636
Che, L. 861
Che, Z. 826
Chen, B.Y. 704
Chen, G.C. 704
Chen, G.M. 463
Chen, G.Y. 200
Chen, H.H. 664, 669
Chen, J. 27, 580
Chen, J.G. 590
Chen, J.X. 914
Chen, J.Y. 773
Chen, L. 174
Chen, L.N. 735
Chen, N. 141
Chen, P.P. 856
Chen, S.M. 234
Chen, Y. 610
Chen, Y.W. 328
Chen, Z. 826
Chen, Z.W. 610, 981
Cheng, D.B. 12
Cheng, D.L. 640
Cheng, H.F. 188
Cheng, L.F. 682

D

Dai, H.Y. 188
Dai, J.Y. 251, 560
Dang, X.P. 594
Deng, S. 259
Deng, X.L. 457
Di, X.Q. 833
Ding, J. 788
Ding, Z.Q. 79
Dong, H.Y. 631
Dong, Q.L. 346
Dong, X. 565
Dong, Y. 760
Du, J.Y. 245, 271
Du, R.X. 83
Du, Z.C. 807

E

Engouang, T.D. 519

F

Fan, D.W. 468
Fan, G.C. 659
Fan, L.T. 532
Fan, L.Y. 755
Fang, H.T. 83
Fang, Y.Z. 1040
Fen, P.X. 536
Feng, Q.B. 442
Feng, Z.R. 616

G

Gai, Q.L. 374
Gao, H.B. 755
Gao, J. 598
Gao, L. 807
Gao, Q. 12
Gao, X. 936
Gao, Y.F. 659, 713
Gao, Z.G. 735
Geng, G.Q. 751
Gong, W. 484
Guan, Z.C. 196
Guo, D.L. 230
Guo, F.Y. 696
Guo, J.Q. 653
Guo, Y.P. 437

H

Han, B.B. 696
Han, J. 271
Han, L. 649
Han, Q.B. 704
Han, T. 427
Han, W.M. 1034
Han, X. 580
Hao, D.J. 576
Hao, F.L. 505
He, C. 664, 669
He, H.N. 610
He, K. 83
He, Q.P. 723
He, S. 365
He, X.F. 3
He, X.L. 826
He, Y. 110
He, Z. 200
He, Z.B. 704
He, Z.L. 457
Hou, T. 468
Hou, Y.B. 245
Hu, J.F. 90
Hu, L.Z. 816
Hu, Q.X. 234
Huang, G. 388
Huang, G.M. 104
Huang, H.B. 259
Huang, S.Q. 72
Huang, X. 131
Huang, X.Y. 505
Huang, Y. 365
Huang, Y.H. 422
Hui, Y.B. 620

J

Ji, L. 52, 709
Jia, X.F. 47, 110
Jiang, H. 7, 17
Jiang, H.W. 966
Jiang, J.Y. 56
Jiang, T.H. 951
Jiang, Y. 560
Jiang, Z.C. 773
Jiao, L.B. 322
Jiao, X. 498
Jie, B.H. 427
Jin, H. 127
Jin, Y. 719
Jing, C.L. 442
Ju, L.Y. 17
Jun, D. 131
Jun, L. 333

K

Kang, B.S. 398
Kong, X.Z. 602
Kuang, G.J. 966
Kun, M.H. 39

L

Lan, M.Y. 807
Lee, S.D. 773, 936
Lei, J.H. 540
Li, B. 188, 729, 743
Li, B.H. 43, 723
Li, B.S. 90
Li, D. 971
Li, G. 674
Li, G.J. 192
Li, G.N. 631
Li, H.X. 888
Li, J.Y. 664, 669
Li, L. 174, 788
Li, L.G. 1022
Li, M. 729, 743
Li, N.K. 640
Li, Q. 183, 547, 766, 873, 877, 903, 1044
Li, S.G. 406
Li, T. 402
Li, X. 669
Li, X.K. 990
Li, X.L. 292, 883
Li, X.Q. 572
Li, X.T. 32
Li, X.Y. 463
Li, Y.G. 649
Li, Y.H. 67, 100, 682
Li, Y.K. 760
Li, Y.P. 280
Li, Y.Q. 861
Li, Y.W. 861
Li, Y.X. 422
Li, Z. 39

Li, Z.F. 72
Li, Z.H. 230
Li, Z.X. 7, 17, 704
Liang, W.H. 280
Liang, X.Y. 196
Liang, Y.Q. 342
Liao, Z.C. 350
Lin, J. 782
Lin, Z.G. 350
Lin, Z.Z. 149
Liu, B.X. 422
Liu, C. 3
Liu, F. 226
Liu, G. 384
Liu, G.G. 852
Liu, H.B. 297, 301, 305
Liu, J. 565
Liu, J.C. 664, 669
Liu, J.G. 183, 903
Liu, J.J. 12
Liu, L. 788
Liu, L.C. 131
Liu, L.F. 328
Liu, L.T. 131
Liu, M.Z. 370
Liu, N. 490
Liu, Q.Q. 1030
Liu, S. 1026, 1052
Liu, S.M. 560
Liu, W. 803
Liu, W.H. 271, 799
Liu, W.Q. 936
Liu, X.C. 723
Liu, X.L. 971
Liu, X.Q. 67, 100
Liu, X.Y. 803
Liu, Y. 511, 519, 877
Liu, Y.F. 873
Liu, Y.L. 337, 899
Liu, Y.Q. 280
Liu, Z. 43
Liu, Z.F. 1040
Liu, Z.J. 169
Lu, L. 606
Lu, P. 640
Lu, S.Q. 565
Lu, Y. 119
Luan, Q.L. 610
Luo, B. 94
Luo, B.N. 856
Luo, D.C. 873
Luo, Q. 944
Luo, W.B. 868
Luo, W.J. 960
Luo, Y.H. 826
Luo, Y.J. 847
Lv, B.J. 27
Lv, G.Q. 442
Lv, Z. 164

M

Ma, B. 951
Ma, C.X. 807
Ma, W.B. 259
Ma, Y. 826
Ma, Y.P. 951
Ma, Z.L. 7
Maimaiti, R.Z.W. 747
Marcek, D. 160
Meng, M. 678
Miao, D.S. 811
Miao, Y. 83
Miao, Z.M. 123
Min, L. 100
Ming, Z.L. 39

N

Nie, S. 807
Nie, S.Y. 453
Niu, H.X. 468
Niu, Q.F. 620

O

Ouyang, H. 760

P

Pan, J.L. 402
Pan, X.H. 276
Pan, Y. 625
Pang, H. 47
Pang, X.F. 822
Pei, Z.Q. 442
Peng, C. 251
Peng, L. 552
Ping, H. 100

Q

Qi, C.X. 346, 923
Qi, L. 511
Qi, X.L. 807
Qian, B. 1018
Qian, J. 888
Qin, X.L. 280
Qin, Z.J. 773
Qiu, W.R. 286
Qiu, X.L. 417
Qu, D.W. 755
Qu, L.D. 833

R

Ran, T.B. 222
Rao, C.J. 1030, 1056
Ren, Q.G. 704
Ren, Y.H. 209
Rong, X.K. 760

S

Shang, L. 119
Shao, M.L. 931
Shao, Z.Z. 782
Shen, R. 476
Shi, G. 640
Shi, J.X. 472
Shi, X.L. 572
Shi, X.M. 12
Shu, S.H. 149
Shu, Y.F. 60
Song, C.F. 245
Song, G.C. 437
Song, J.B. 379
Song, J.S. 484
Song, Q.D. 280
Song, Z.G. 442
Su, Y. 72
Sun, H.F. 1060
Sun, H.P. 735
Sun, L.N. 1026, 1052
Sun, P. 192
Sun, Q.M. 590
Sun, R. 843, 868
Sun, S.C. 32
Sun, W.H. 311
Sun, X. 472
Sun, Y. 494
Sun, Z.C. 914

T

Tan, Z.L. 136
Tang, D.D. 141
Tang, G.X. 427
Tang, L. 154
Tang, X.L. 136
Tang, Y.B. 704
Tian, G.S. 927
Tian, S. 484
Tian, S.B. 484
Tian, X.D. 960
Tian, Y.Y. 32
Tong, Y. 322

W

Wang, B. 490, 704, 903
Wang, C. 297, 301, 305, 511, 692
Wang, C.S. 251
Wang, G. 892
Wang, G.M. 816
Wang, G.P. 413
Wang, G.Q. 374
Wang, H. 43, 687, 723
Wang, H.J. 1060
Wang, H.P. 511
Wang, J.Q. 174
Wang, K. 594
Wang, L. 620, 674
Wang, L.C. 433
Wang, N. 687
Wang, Q. 417, 417
Wang, T.M. 417
Wang, X.H. 788, 1009
Wang, X.J. 990
Wang, X.P. 433
Wang, Y. 350, 602, 696
Wang, Y.G. 620, 1022
Wang, Y.H. 286
Wang, Y.J. 204
Wang, Y.N. 316
Wang, Y.P. 888
Wang, Y.Q. 433
Wang, Y.X. 174
Wang, Z.M. 123
Wang, Z.T. 234

Wang, Z.Y. 1022
Wei, C.F. 572
Wei, Q.S. 826
Wei, Z. 476
Wu, B. 3, 209, 994
Wu, F. 123
Wu, G.C. 816
Wu, G.J. 799
Wu, H. 427
Wu, H.H. 463
Wu, J. 1034
Wu, L. 204
Wu, Q. 704
Wu, W.Q. 856
Wu, X.D. 422
Wu, X.S. 222
Wu, Y.X. 664, 669
Wu, Z.F. 216
Wu, Z.H. 552

X

Xi, L. 682
Xiang, Q. 230
Xiao, Q.Y. 552
Xiao, S.W. 692
Xie, C. 119
Xie, H. 598
Xie, H.Y. 200
Xie, Y.H. 986
Xin, Z. 1003
Xing, A.H. 402
Xing, J.F. 27
Xing, N.Z. 653
Xing, Y.Y. 355
Xiong, X.M. 337, 899
Xiong, Y. 437
Xu, G.G. 505
Xu, G.H. 682
Xu, H.L. 631
Xu, J.G. 584
Xu, L. 370
Xu, S.H. 1013
Xu, X. 7, 17
Xu, Y.T. 234
Xu, Z.Y. 449
Xue, D.H. 687
Xue, J.W. 1013

Y

Yan, C.K. 204
Yan, H.W. 659, 713
Yan, H.Y. 713
Yan, L. 576
Yan, L.W. 598
Yan, M. 342
Yan, Y.H. 402
Yan, Z.C. 536
Yang, A.M. 263
Yang, B. 394
Yang, B.H. 528
Yang, B.J. 251
Yang, C.Q. 453, 480
Yang, F.Q. 355
Yang, G.L. 442
Yang, H.M. 833
Yang, H.W. 811
Yang, H.Y. 449
Yang, J.F. 877
Yang, J.J. 873
Yang, J.N. 263
Yang, L. 463
Yang, L.M. 476
Yang, S. 413
Yang, S.S. 998
Yang, W. 723
Yang, W.X. 413
Yang, Z.B. 739
Yang, Z.S. 39
Yang, Z.W. 719
Yao, C. 704
Yao, G. 123
Yao, X.F. 127
Ye, L. 94, 280, 379
Yi, W. 719
Yiming, A.L.M.J. 747
Yin, L.F. 251
Yin, T. 297, 301, 305
Yin, X.J. 584, 782
Yin, Y.Z. 704
You, Q. 47
You, X.D. 944
You, Z.F. 1040
Yu, B. 355, 909
Yu, H.Y. 833
Yu, J. 32
Yu, J.W. 490

Yu, L. 1056
Yu, R. 653
Yu, R.F. 773
Yu, T. 682
Yu, X.M. 528
Yu, Y.Y. 1013
Yuan, F. 960
Yuan, J. 498
Yuan, J.Y. 3
Yuan, Y.N. 678

Z

Zang, F.Y. 602
Zeng, H.C. 480
Zeng, R.H. 811
Zeng, W. 936
Zeng, Z.B. 794
Zeng, Z.P. 3
Zhang, A.H. 476
Zhang, B.J. 838
Zhang, C.S. 936
Zhang, C.Y. 674, 994
Zhang, H. 576
Zhang, H.B. 384
Zhang, H.Y. 60, 1018
Zhang, J. 127, 328
Zhang, J.G. 12
Zhang, K. 755
Zhang, L. 674, 1009
Zhang, L.C. 927
Zhang, L.D. 606
Zhang, L.Z. 664
Zhang, M.J. 398
Zhang, N.L. 12
Zhang, P. 192
Zhang, Q. 379
Zhang, Q.M. 141
Zhang, Q.Y. 856
Zhang, R. 794
Zhang, S.G. 594
Zhang, S.H. 241, 700
Zhang, S.L. 394
Zhang, W.Y. 976
Zhang, X. 944
Zhang, X.C. 636
Zhang, X.W. 909
Zhang, Y.B. 572
Zhang, Y.H. 498
Zhang, Y.N. 192
Zhang, Y.S. 442
Zhang, Z.H. 394
Zhang, Z.J. 519
Zhao, B. 877
Zhao, B.T. 110
Zhao, D.F. 1040
Zhao, D.P. 200
Zhao, H. 472
Zhao, J.K. 760
Zhao, J.W. 494
Zhao, L. 346
Zhao, M. 877
Zhao, Q. 788
Zhao, T.T. 1060
Zhao, X.E. 918
Zhao, X.Q. 1048
Zhao, Y.J. 271
Zhao, Z.H. 209
Zhao, Z.J. 169
Zheng, H.Y. 449
Zheng, N.Z. 811
Zheng, Q.X. 788
Zheng, S. 365
Zheng, X.L. 664, 669
Zheng, Y.L. 179
Zheng, Y.Y. 47
Zhong, K.H. 328
Zhong, Y.Y. 498
Zhong, Z.S. 43
Zhong, Z.X. 472
Zhou, H.F. 547
Zhou, H.Y. 114
Zhou, J. 361
Zhou, J.B. 463
Zhou, J.C. 498
Zhou, P. 1065
Zhou, X.Z. 476
Zhou, Y.M. 263
Zhou, Z.H. 640
Zhou, Z.M. 83
Zhu, C.P. 704
Zhu, H.P. 636
Zhu, P.S. 803
Zhu, S.H. 22
Zhu, W.K. 463
Zhu, Y. 22
Zhu, Y.J. 528
Zhu, Y.L. 659, 713
Zhu, Z.W. 914

Zou, X.J. 944